

## Long-baseline laser strainmeter in Kamioka

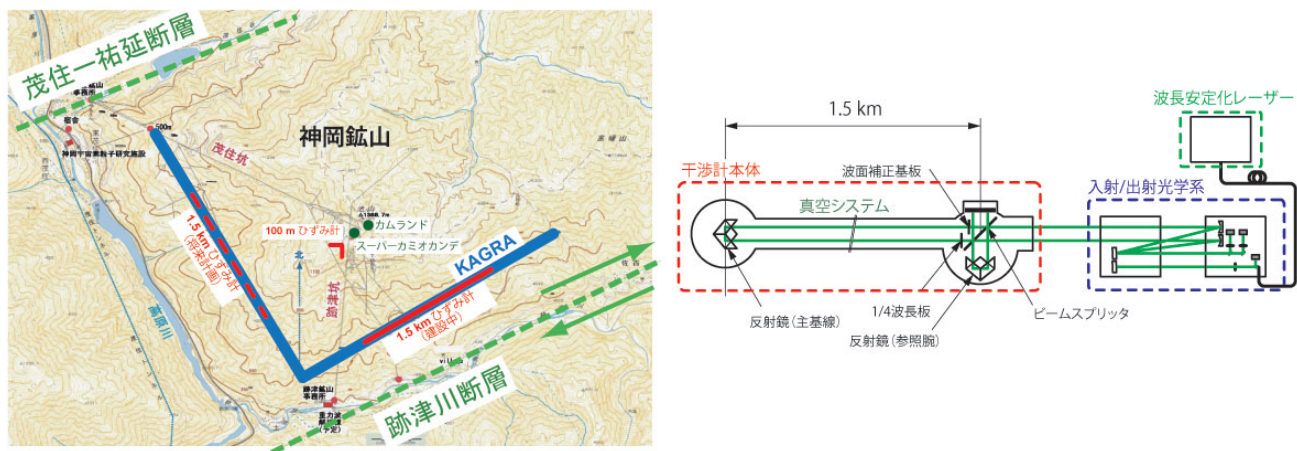
TAKAMORI, Akiteru<sup>1\*</sup> ; ARAYA, Akito<sup>1</sup> ; MORII, Wataru<sup>2</sup> ; UCHIYAMA, Takashi<sup>3</sup> ; OHASHI, Masatake<sup>3</sup> ; TELADA, Souichi<sup>4</sup>

<sup>1</sup>Earthquake Research Institute, University of Tokyo, <sup>2</sup>Disaster Prevention Research Institute, Kyoto University, <sup>3</sup>Institute for Cosmic Ray Research, University of Tokyo, <sup>4</sup>National Institute for Advanced Industrial Science and Technology

In order to facilitate the gravitational-wave astronomy, ' KAGRA project ' has been proceeding under international collaboration hosted by the Institute for Cosmic Ray Research of University of Tokyo. The authors are constructing a long-baseline laser strainmeter with a 1.5 km long baseline in the Kamioka underground site as the part of the project (left figure). It will be the longest baseline laser strainmeter in Japan, and one of the largest instruments worldwide. The longer baseline was opted to achieve the superior sensitivity for the ground strain, more than 10 times better than the currently available 100 m strainmeter. The better sensitivity is anticipated to enable more detailed studies in the ground deformation caused by the fault activities and the Earth ' s free oscillations.

The basic design of the long-baseline strainmeter is adopted from the 100 m strainmeter, consists of the highly asymmetric Michelson interferometer using the Iodine-stabilized laser as the standard of length (right figure). Nevertheless, there are some technical challenges required due to the gigantic scale of the new instrument. The outline of the instrument and the status of R&D will be reported in this presentation.

Keywords: laser interferometer, strainmeter, Kamioka



## Development of software for precise LLR data analysis, Part 2

NAGASAWA, Ryosuke<sup>1\*</sup>; OTSUBO, Toshimichi<sup>2</sup>; SEKIDO, Mamoru<sup>3</sup>; HANADA, Hideo<sup>4</sup>

<sup>1</sup>Graduate University for Advanced Studies, <sup>2</sup>Hitotsubashi University, <sup>3</sup>National Institute of Information and Communications Technology, <sup>4</sup>RISE Project Office, National Astronomical Observatory

We are developing new analysis software for precise determination of lunar orbital/rotational motion and tidal deformation using lunar laser ranging (LLR) observation data.

As the first step of the study, we construct an LLR observation model. This model consists of the lunar orbit and libration obtained from DE430 (provided by NASA JPL), and the other newest physical models compatible with IERS Conventions (2010) such as Earth orientation, solid Earth/Moon tides, and some factors affecting propagation delay. For the purpose of calculating these components precisely, we use the modules of the geodetic data analysis software "c5++" (Otsubo et al., 2011). LLR observation data are provided as normal points. In this calculation, there are 3577 points distributed from June 1996 to July 2013, obtained at Apache Point, Grasse, Matera and McDonald. Comparing the observed and calculated one-way ranges, the mean and the standard deviation of the residuals are about 5.7 cm and 4.8 cm respectively.

The presentation contains the result of the above-mentioned modeling and comparison, and the current status of the software development.

Keywords: lunar laser ranging, analysis software, ephemeris

## Scale parameters of the Earth sensitive to the optical response of spherical SLR targets

OTSUBO, Toshimichi<sup>1\*</sup>; MATSUO, Koji<sup>2</sup>; SHERWOOD, Robert a<sup>3</sup>; APPLEBY, Graham m<sup>3</sup>; NEUBERT, Reinhart<sup>4</sup>

<sup>1</sup>Hitotsubashi University, <sup>2</sup>Kyoto University, <sup>3</sup>NERC SGF Herstmonceux, UK, <sup>4</sup>GFZ Potsdam, Germany

Recent technology upgrades in SLR technique, especially driven by kHz laser ranging systems, make it possible to measure the station-satellite distance at mm precision. The optical response of a sphere-shaped SLR target has been one of the major error factors in measuring the two-way distance, and, following the study on AJISAI, LAGEOS and ETALON (Otsubo and Appleby, JGR, 2003), we look into relatively smaller targets, STARLETTE and its twin STELLA. Based on the detailed optical response simulation adjusted by the actual kHz laser ranging data obtained at Herstmonceux and Potsdam, it is calculated that the standard centre-of-mass correction value for STARLETTE is too small by 3 mm. The impact can be up to 0.5 ppb for the terrestrial reference frame scale and up to 1.7 ppb for the gravity constant (GM) of the Earth.

Long-term worldwide technology upgrades can have a systematic impact on the long-term trend of such scale parameters. As the intensity of photons received at a given detector is reduced, the detection point (timing) goes rearwards and the center-of-mass correction gets smaller as listed in Appleby and Otsubo (LW18, 2013). This can map a non-negligible drift especially in the GM parameter.

Keywords: space geodesy, satellite laser ranging, terrestrial reference frame

## VLBI application for Frequency Transfer and Development of GALA-V System (III)

SEKIDO, Mamoru<sup>1\*</sup> ; TAKEFUJI, Kazuhiro<sup>1</sup> ; UJIHARA, Hideki<sup>1</sup> ; MIYAUCHI, Yuka<sup>1</sup> ; TSUTSUMI, Masanori<sup>1</sup> ; HASEGAWA, Shingo<sup>1</sup> ; HOBIGER, Thomas<sup>1</sup> ; ICHIKAWA, Ryuichi<sup>1</sup> ; KOYAMA, Yasuhiro<sup>2</sup>

<sup>1</sup>National Institute of Information and Communications Technology, Space-Time Standards Laboratory, <sup>2</sup>National Institute of Information and Communications Technology, International Relations Office

NICT is developing the frequency comparison technology using the VLBI as one of the remote frequency comparison technologies. The small broadband VLBI station, which is an important element of this project (Gala-V), is semi-compliant with the specification of the broadband geodetic VLBI system VGOS (VLBI2010 Global Observing System) specifications. Many VLBI observation stations compliant with the VGOS are under development several countries as an international standard specification for the next generation geodetic VLBI. Our Gala-V system is aimed for the comparison of the frequency standard, but of course this is useful for the geodetic observations too.

[broadband feeding development for large diameter antenna]

Most of the VGOS VLBI stations under development are adopting the special optical system so called ring-focus, That is because of wider beam width characteristic of wide frequency band (2-14GHz) feed, currently available. The receiver feed, that has sensitivity about 3 octaves of frequency, has generally wide beam angle, and therefore, existing Cassegrain reflector antenna is difficult to use it. We have been developing a new broadband feed for our 34m antenna. The first test feed become ready and it was mounted on the 34m diameter modified Cassegrain parabola in the end of 2013, and successfully we observed 6.7GHz, and 12.2 GHz emission line of the Methanol maser simultaneously.

[Zero redundant frequency array - Direct Sampler]

The Gala-V system, which is under the development at NICT, is designed to use four bands of the 1 GHz bandwidth with intervals of zero redundancy in the 2-14 GHz frequency range. This enables a fine delay resolution function without uncertainty (Ambiguity), and the precision of delay measurement could be improved by a one order higher than conventional.

In addition to a conventional analog frequency conversion method, we are experimentally adopting a method to acquire specific frequency band with a digital filter with a direct sampler, which acquires data without frequency conversion via a high-speed sampler. If a direct sampling method is established, system components and cost necessary for the system are simplified and reduced.

[development of the broadband signal composition technology]

The VGOS system is targeting to achieve high precision delay measurements by synthesizing 2-14 GHz broadband signal coherently. A new data processing software, which enables estimation of nonlinear phase change caused by the ionosphere and derivation of precise delay from the super broadband signal, and broadband stable phase calibration system are required.

Keywords: VLBI, VGOS, Frequency Comparison

## Ishioka VLBI Observing Facility - Telescope Completion and Setting up the System -

KURIHARA, Shinobu<sup>1\*</sup> ; FUKUZAKI, Yoshihiro<sup>1</sup> ; KURODA, Jiro<sup>1</sup> ; KAWABATA, Ryoji<sup>1</sup> ; WAKASUGI, Takahiro<sup>1</sup>

<sup>1</sup>GSI of Japan

The Geospatial Information Authority of Japan (GSI) proceeded with construction of new VLBI station compliant with the next generation VLBI observing system (VGOS) promoted by the International VLBI Service for Geodesy and Astrometry (IVS). By March 2014, a VLBI telescope with a 13.2-m dish was completed in Ishioka, Ibaraki, now we are going on setting up and testing of the whole system from the telescope through data acquisition system toward. In this presentation I describe the completed VLBI observing facility and progress situation of its setting up and testing.

Keywords: IVS, VGOS

## Development of a new precise positioning technique using multi-GNSS signals

FURUYA, Tomoaki<sup>1\*</sup>; SAKAI, Kazuki<sup>1</sup>; MANDOKORO, Motomu<sup>1</sup>; TSUJI, Hiromichi<sup>1</sup>; YAMAGUCHI, Kazunori<sup>1</sup>; MIYAGAWA, Kohei<sup>1</sup>; YAHAGI, Toshihiro<sup>1</sup>; HATANAKA, Yuki<sup>1</sup>; MUNEKANE, Hiroshi<sup>1</sup>; KAWAMOTO, Satoshi<sup>1</sup>

<sup>1</sup>GSI of Japan

Geospatial Information Authority of Japan (GSI) is developing and standardizing new precise positioning techniques which deal with multiple GNSS constellations, GPS, QZSS, GLONASS, and Galileo, in order to mainly encourage effective surveys at places where are currently difficult to carry out them using only GPS satellites.

In FY 2013, we examined analysis methods to correct Inter System Bias for using single/double differences between GPS and other GNSS. We developed the new analysis software named GSILIB based on RTKLIB developed by Mr. T.Takasu. In addition, we obtained multi-GNSS data in eight cities and evaluated the effects and problems using multi-GNSS signals.

This presentation shows results of FY 2013 and future plans from FY 2014.

Keywords: GNSS, Geodetic survey, ISB

## Notes on the quality of GEONET coordinate solutions

IMAKIIRE, Tetsuro<sup>1\*</sup> ; KAGAWA, Akira<sup>1</sup> ; HATANAKA, Yuki<sup>1</sup> ; MUNEKANE, Hiroshi<sup>1</sup>

<sup>1</sup>GSI of Japan

The routine solutions of geodetic coordinate of observation stations of GEONET, the continuous GNSS observation network operated by GSI, are fundamental data for the studies of crustal deformation and tectonics and widely utilized for a variety of purposes. As GEONET data is available freely, researchers can discuss the crustal deformation or tectonics without carrying out GNSS observation or baseline analysis. However, it should be noted that the coordinates provided by GEONET may include errors caused by various noise sources or factors, such as obstruction of observation signals by trees, multipath caused by site environment or un-modeled tropospheric noise. We present results of evaluation the effects of some of the error factors and introduce ways of examining the quality of coordinate solutions done for crustal deformation monitoring by GSI.

Keywords: GEONET, GNSS positioning, Data quality

## Positioning error estimation due to snow accumulation on GNSS antenna using winter experimental data

YOSHIHARA, Takayuki<sup>1\*</sup> ; MOTOYOSHI, Hiroki<sup>2</sup> ; SATO, Takeshi<sup>2</sup> ; YAMAGUCHI, Satoru<sup>2</sup> ; SAITO, Susumu<sup>1</sup>

<sup>1</sup>Electronic Navigation Research Institute, <sup>2</sup>National Research Institute for Earth Science and Disaster Prevention

In research field of precise positioning using Global Navigation Satellite System (GNSS) such as GPS, it is well known that positioning error is caused by snow accumulation on GNSS antenna [1]. It is important to quantitatively evaluate the error taking account for shape of snow-cap and GPS satellite configuration, which are changing with time past. In this study, we performed two winter experiments in each winter of 2011/2012 and 2012/2013, which enabled us to quantitatively investigate reduction in receiving intensity and propagation delay due to snow accumulation on GNSS antenna. The experimental data was also able to use for positioning error estimation resulted by such effects. We installed a GPS antenna about 50 meters away from weather observational equipment, which measured pressure, temperature, humidity, wind direction and velocity, precipitation, snow depth, etc.), in observation field of Snow and Ice Research Center, National Research Institute for Earth Science and Disaster Prevention (NIED) in Nagaoka, Japan. To observe snow accumulation on GNSS antenna, a photograph of GNSS antenna was automatically took by an interval camera every 10 minutes during winter. To evaluate quantitative effects of snow accumulation on GPS signal measurement, we investigated drop events of snow-cap on GNSS antenna and analyzed gaps of rapid changes in both receiving intensity and carrier phase measurements[2]. Consequently, a snow-cap with a height of 40cm yielded reduction of several dB in receiving intensity (C/N0) and propagation delay of about 4 cm in slant range. We will show relationship between size of snow cap and positioning error based on the experimental data, including simulation analysis with range errors due to snow accumulation and satellite configuration. We will also show evaluation results to use water repellent paint on GNSS antenna radome for mitigation of snow accumulation.

### References

- [1] R. Jaldehag, J. Johansson, J. Davis and P. Elosegui, "Geodesy using the Swedish permanent GPS network: Effects of snow accumulation on estimates of site positions", *Geophys. Res. Lett.*, vol.23, No. 13, pp.1601-1604, June 1996.
- [2] T. Yoshihara, H. Motoyoshi, T. Sato, S. Yamaguchi and S. Saito, "GAST-D integrity risks of snow accumulation on GBAS reference antennas and multipath effects due to snow-surface reflection", *Proc. ION ITM 2013*, no.A1-5, pp.112-120, San Diego, CA, January 2013.

Keywords: GNSS, snow accumulation, positioning error, precise positioning, propagation delay, GPS

## Periodic displacement on continuous GPS observation in coastal area due to long term sea level elevation

OICHI, Kazuyoshi<sup>1\*</sup>

<sup>1</sup>Hydrographic and Oceanographic Department, Japan Coast Guard

Since 1999, Hydrographic and Oceanographic Department carried out continuous GPS observation to survey the crustal deformation at the stations collocated with tidal stations or lighthouse etc. of Japan Coast Guard in south Kanto area. And precise positions in earth centered coordinates of these GPS stations are automatically determined by long baseline analysis from Simosato GPS station. Several stations show significant unexpected annual oscillation in its daily position series. On the other hand, hourly sea level data are available via Japan Oceanographic Data Center from tidal stations of Japan Coast Guard and Japan Meteorological Agency in this area. To eliminate annual oscillation from crustal deformation observation, correlation functions between daily precise position series of GPS stations and sea level height series of tidal stations are calculated. And I tried to evaluate an error from weight variation of sea water on precise GPS observations in coastal area.

Hydrographic and Oceanographic Department continuously observes 30 sec interval data at GPS stations in Izu islands area from 2002. And long baseline analysis from Simosato hydrographic observatory is performed with Bernese GPS Software and IGS final ephemerides. Calculated daily precise positions are utilized for crustal deformation monitoring. However, time series of calculated positions contains unexpected component other than crustal deformation. Particularly, Izu O-Shima station shows significant oscillation in a north-south direction. This oscillation is synchronous with four GPS stations of GSI in Izu O-Shima, and these show annual apparent cycle of expansion and contraction. Some oscillation of local load is suspected as cause of this deformation and move of sea water is considered as major component of these in coastal area. Analyzed positions of these stations are obtained as daily value, thus influence of major component of tide (diurnal or semidiurnal) is negligible, but long term component, for instance, annual change of sea level is inadequately considered. According to the sea level observations at adjacent tidal stations, annual oscillation of sea level shows its amplitude in tens of centimeters, thus long term component of sea water load change is expected as considerable.

To eliminate annual oscillation from GPS monitoring of crustal deformation, I tried to analyze strain caused by load change from sea level elevation. This analysis is performed with the time series of daily precise positions of four GPS stations: Izu O-Shima, Miyake Shima, Kozu Shima, Hachijo Shima, from 2002. Because of Miyake Shima, Kozu Shima and Hachijo Shima stations are collocated with tidal stations of JCG, correlation functions are calculated with time series of sea level in place of stations. And the Izu O-Shima station is collocated with lighthouse, thus analyzed with the Okada tidal station of JMA in Izu O-Shima.

Keywords: GPS, tidal observation, crustal deformation, sea level change, annual oscillation

## Seismic waves detected by 50Hz sampled GNSS observations

KATO, Teruyuki<sup>1\*</sup> ; MIURA, Satoshi<sup>2</sup> ; IKUTA, Ryoya<sup>3</sup>

<sup>1</sup>Earthq. Res. Inst., the University of Tokyo, <sup>2</sup>Grad. Sch. Sci., Tohoku University, <sup>3</sup>Faculty of Science, Shizuoka University

Application of frequently sampled GNSS data is getting increasingly attractive research field, in particular, in the field of seismology (e.g., Larson et al.; 2003, Miyazaki et al., 2004; Yokota et al., 2009; Ohta et al., 2012). As most of GEONET (GNSS Observation NETwork) sites are now archiving 1Hz sampled data, such application research will be more active in the future. Analysis of ground shake may require higher frequency observation such as 5Hz, 10Hz or higher. However, it is known that amplitude and phase of observed ground displacements show fluctuations due to characteristics of data acquisition in the receiver electric circuits (e.g., Ebinuma and Kato, 2012). Thus, we need to be careful in applying such highly sampled GPS data for geoscientific researches.

We have used commercially available GNSS receivers to record 50Hz sampling to tackle above problems. We are introducing a record of ground shake due to an earthquake of 50Hz sampled data. We used three NetR8 (Trimble Co. Ltd.) GNSS receivers and they were established at Shizuoka University (Shizuoka Prefecture) since October 2011, Katono Elementary School (Fukushima Prefecture; KTNO) and Daido-higashi Elementary School (Ibaraki Prefecture; DDHG) since March 2012. We chose latter two locations as they are among the most active aftershock area due to 2011 Tohoku-Oki earthquake (Mw9.0).

About two weeks of 50Hz sampled data are stored in the internal memory of the receiver which are refreshed automatically in the receiver. Data at KTNO and DDHG are remotely archived through internet and data at Shizuoka University are downloaded manually, after a large earthquake occurred. Several data sets due to large earthquakes have been archived so far, all of which registered at least bigger than or equal to JMA Intensity 5- at nearby GPS sites. These data are analyzed using RTNet GPS software.

Among the archived data sets, a seismic wave was detected for the 2013 September 20 Fukushima-Hamadori earthquake, whose hypocentral parameters are as follows: latitude=N37.1deg, longitude=E140.7deg, depth=20km, M5.9, and the biggest JMA Intensity was 5+ at Iwaki, which is nearly immediately below the KTNO site. We used IGS final orbits and estimated the position of KTNO by putting the reference site at Daido-higashi (Baseline distance is about 106km to south) and Shizuoka University (Baseline length is about 308km to south east). Clear seismic wave was obtained for the baseline KTNO-DDHG for three components. Also, clear seismic wave was obtained for the baseline KTNO-Shizuoka Univ., though vertical component was not very clear, probably because the baseline distance was longer.

GNSS antennas at KTNO and DDHG sites are placed at the roof of the school buildings and at the roof of observation hut of Shizuoka University. Therefore, we may have to investigate the effects of swing of the building by comparing the record with nearby recorded strong motion. Moreover, the method of correction for amplitude and phase due to receiver characteristics should be investigated, which is left for future studies.

Keywords: GNSS, high-frequency sampling, GPS, GPS seismology, 50Hz

## Detection of eruption column by using the kinematic precise point positioning

OHTA, Yusaku<sup>1\*</sup> ; IGUCHI, Masato<sup>2</sup> ; UEKI, Sadato<sup>1</sup> ; DEMACHI, Tomotsugu<sup>1</sup>

<sup>1</sup>RCPEVE, Tohoku University, <sup>2</sup>DPRI, Kyoto University

We investigate the ability of kinematic precise point positioning to detect volcanic plumes at Minami-dake of Sakurajima Volcano. In Houlié et al. [1], the authors processed the GPS data obtained during the eruption of Miyakejima volcano, occurred in 2000, and found anomalous values in the ionosphere-free linear combination of the L1 and L2 phase measurements (LC). They related these anomalous values to the path delay effects caused by the presence of a hot volcanic plume; by applying techniques of seismic tomography. Another test was carried out during the eruption of Mt. St. Helens on March 9, 2005, and again the GPS signal showed a clear signature of the volcanic plume presence [2].

In this study, we describe the July 24, 2012 activity at Minami-dake of Sakurajima Volcano. We analyzed the data from 18 continuous GPS stations (3 GEONET sites and 15 Kyoto University sites), which located on the volcano flanks. For the GPS analysis, we used GIPSY-OASIS II version 6.1.4 software [3]. We estimated the post-fit phase residual in the ionosphere-free linear combination for each pair of GPS satellites and ground stations for the detection of eruption column. We applied absolute IGS phase center corrections for satellite and receiver antennas. The wet zenith tropospheric delays and its gradient at all the GPS sites were estimated at all processing epochs (every 30 seconds) under the assumption of a random walk stochastic model. Firstly, we analyze the all of the GPS data in July 21, 22 and 23, 2012 for the reference. Obtained post-fit phase residual of the reference days showed the noise-level for the path delay effects caused by the volcanic plume. This reference post-fit phase residual contained many noise sources such as multipath effects, local atmospheric disturbance, and so on. The noise level of the post-fit phase residual strongly depends on the each GPS satellite and ground station pair. Finally, we analyzed the data of the July 24, 2012. The post-fit phase residual clearly shows large disturbance just after the eruption. For example, the phase residual between SVN34 satellite and GEONET 0720, which located in the east coast of Sakurajima, suddenly increased just after the eruption. The obtained residual amount reached 80mm. It is clearly larger than the noise level measured on the reference days. Furthermore, other GPS satellite and ground station pairs also clearly showed significant amounts of disturbance. These results suggest that the eruption column moved to the westward by the wind after the eruptive event.

[1] Houlié et al. GRL, 2005. [2] Houlié et al. Eos Trans, 2005. [3] Lichten and Border, JGR, 1987.

## Airport survey method for transition to the new CNS/ATM systems in east Mekong area

NAKAGAWA, Yuji<sup>1\*</sup>; OKADA, Kaoru<sup>2</sup>; SHIMADA, Seiichi<sup>3</sup>; SATOMURA, Mikio<sup>3</sup>; SHINDE, Yohei<sup>1</sup>; ITOH, Hirokazu<sup>1</sup>; UKEI, Kazuyuki<sup>1</sup>

<sup>1</sup>Nippo Co.,Ltd., <sup>2</sup>Japan International Cooperation Agency, <sup>3</sup>NIED, <sup>4</sup>Hot Springs Res. Inst, Kanagawa Pref.

The project by the name of "Capacity Development for Transition to the New CNS/ATM Systems in Cambodia, Lao PDR and Vietnam" (Jan.2011-Dec.2015) was officially announced by Japan International Corporation Agency (JICA) on April 2011, and Nippo got the order, after that we got the orders five times for two years. We would like to introduce the procedure of surveying airport coordinates.

The concept of New CNS/ATM System (Communication, Navigation and Surveillance/Air Traffic Management) utilizing satellite technologies was developed by International Civil Aviation Organization (ICAO) in 1991 for globally harmonized implementation in order to cope with the expected increase of air traffic. All the Contracting States of ICAO are required to move from the conventional air navigation systems to the New CNS/ATM Systems in accordance with ICAO Global Plan.

In order to shift air navigation from the ground-based facility use to the satellite use, it is essential to have accurate and updated data of latitude and longitude of airports and air navigation facilities based on WGS-84 coordinates as ICAO Standard. However, in Cambodia, Lao PDR and Vietnam it has not been made known whether airport survey has been conducted, applying long-baseline analysis by using International GNSS Services (IGS) points in accordance with ICAO WGS-84 Manuals (Doc9674 2nd edition).

The purpose of the project is transferring survey method and surveyed airport coordinates in accordance with WGS84 coordinate system.

### Airport survey procedure and recommendation

#### 1.Confirmation of required survey points and facilities

Runway ends, ILS, VOR/DME, control tower, TV antenna, etc.

2.Reconnaissance of Primary Airport Control Station (PACS) and Secondary Control Station (SACS). Installed two PACS survey markers near runway ends and seven or eight SACS survey markers at a regular distance.

3.Set up receivers at two PACS and one SACS and surveyed 24 hours at PACS for three days, at SACS for 1.5 hours simultaneously by differential GPS satellite surveying. (when prepared three receivers. if prepared four receivers, observe two PACS and two SACS simultaneously)

4.Install GPS receivers at other SACS points over lapping the base line on every session.

5.Install total station (TS) at every PACS and SACS and observe each other to verify the coordinates surveyed by GPS receivers.

6.Survey runway ends, radio navigation facilities (ILS, VOR/DME, etc.) and obstacles like control tower, big Buddha stature, tall building. If the obstacle cannot be seen from coordinates known points PACS, SACS, set up receivers at PACS and auxiliary two points in the vicinity of the obstacle.

7.Determine the coordinates of PACS using long baseline analysis software (Bernese) by downloading ultra rapid orbit. Coordinates of SACS using short baseline analysis software.

8.Survey runway ends, radio navigation facility and obstacles by TS using SACS and PACS.

9.We surveyed a fiducial point which has x, y coordinates and above sea level height, and compared the result which obtained by Earth Gravitational Method (EGM) 2008 software in Cambodia. (The result of EGM2008 is higher than our survey by about 80cm, but we could not confirm the accuracy of the height of fiducial point.)

10.Lecture on how to choose the PACS and SACS location, how to use the long baseline software and how to maintain the result data including process of calculation.

Keywords: WGS84, GPS, CNS/ATM, Airport coordinates, East Mekong area

## Vertical deformations revealed by laser scanning surveys in the Muro no mud volcano

TAKAHASHI, Atsushi<sup>1\*</sup> ; FUKUDA, Yoichi<sup>1</sup> ; KUSUMOTO, Shigekazu<sup>2</sup>

<sup>1</sup>Graduate School of Science, Kyoto University, <sup>2</sup>Department of Earth Science

In order to reveal the land surface deformation in the Muro no mud volcano area located in Tokamachi city, Niigata prefecture, we have conducted the laser scanning surveys two times in June and October 2013, using TOPCON Imaging Station IS-301, which can obtain 3D point cloud data by the automatic laser scanning mode without reflector. In the same survey area, Toyama University has been conducting successive leveling surveys at 61 benchmarks so far. We also conducted the height measurements at the benchmarks using the precise ranging mode.

The obtained cloud data have been interpolated on regular grids for the two data sets, respectively, and the surface deformation has been calculated by comparing the gridded data. The obtained result showed a clear concentric uplift pattern in a part of the survey area. We thus modeled the uplift using the Mogi source model. The maximum amplitude estimated from the model was about 1.5 cm and it was almost coincident with the uplift obtained at the nearest benchmark. The result showed that the scanning mode was really beneficial to search for the spatial deformation pattern and the source of the deformation as well, even though its accuracy would be lower than the one of the precise ranging mode.

Keywords: LaserRangeFinder, LaserScanningSurvey, Mud Volcano, Vertical Deformation, Mogi Model

## Asymptotic solutions to the quasi-static spheroidal and toroidal deformation of the SNREI earth

OKUBO, Shuhei<sup>1\*</sup> ; TAKAGI, Yu<sup>1</sup>

<sup>1</sup>Earthquake Research Institute, The University of Tokyo

Asymptotic solutions to the quasi-static deformation of SNREI earth are essential to compute Green's functions, i.e., deformations due to a point load and a point dislocation. So far, only the surface deformations have been presented by previous authors. That is, internal stress/strain fields are not left uncalculated because of lack of asymptotic solutions to the internal deformation fields. In this talk, we present complete sets of spheroidal/toroidal deformations when spherical harmonic degree  $n$  increases to infinity.

Keywords: Internal elastic deformation, Green's function, SNREI earth, Asymptotic expansion

## Evaluation of uncertainty in distance measurement by GNSS surveying instrument and EDM

YOSHIDA, Shigeru<sup>1\*</sup> ; SATO, Yudai<sup>1</sup>

<sup>1</sup>GSI of Japan

GSI has conducted research to establish traceability for distance measurement by GNSS surveying instrument to international standard. The international standard of distance is defined based on speed of light. In order to measure a distance based on the standard, it is necessary to use Electro-optical Distance Meter (EDM) for which the traceability to the standard is established. On the other hand, the traceability for GNSS surveying instrument used in various surveys is not established, because it is difficult and complex to estimate the uncertainty in distance measurement by the instrument. Therefore, we conducted an experiment to compare results of distance measurement by GNSS surveying instrument and EDM on a 2 km baseline.

Although the EDM measurement in this experiment should have been conducted indoors to reduce an affect of meteorological condition change, it was almost impossible to find an indoor 2 km baseline. We therefore divided an outdoor 2 km baseline into 10 short baselines and measured them by EDM. After that, the distance and uncertainty of the whole baseline were estimated from the results of measurements on the short baselines. The 2 km baseline was also measured by GNSS, and the estimated distance and uncertainty was compared to the results of EDM measurements.

The distances and uncertainties estimated by the measurements of EDM and GNSS survey instrument were  $1,999.9828 \pm 0.0014$  m and  $1999.9828 \pm 0.006$  m respectively. As a result of the experiment, we verified that the traceability for GNSS surveying instrument can be established on the 2 km baseline.

Keywords: GNSS surveying instrument, EDM, Uncertainty, Traceability

## Changes of E-W observed by the Quartz-tube Extensometer in the Matsushiro extending after the 2011 Tohoku Earthquake

HASHIMOTO, Tetsuo<sup>1\*</sup> ; FUNAKOSHI, Minoru<sup>1</sup>

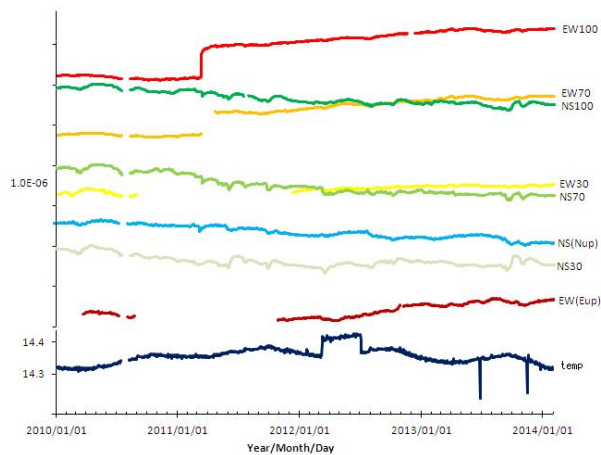
<sup>1</sup>Matsushiro Seismic Observatory JMA

We observed a coseismic step of  $5.8 \times 10^{-7}$  strain in the E-W direction by the quartz-tube extensometer at Matsushiro during the 2011 off the Pacific coast of Tohoku earthquake. After that, an aftereffect of  $0.4 \times 10^{-7}$  strain continued extending in the E-W direction about 1 month. And more, the E-W extension has continued since October, 2011 and it becomes over  $0.5 \times 10^{-7}$  strain. Similar phenomena were observed by superconducting gravity meter in Matsushiro and Kamioka (Imanishi, personal communication). Therefore, we think that these data of the E-W extension indicate true crustal deformation.

Figure shows data of the quartz-tube extensometer, water-tube tiltmeter, thermometer, and the other points of the extensometer. The air temperature in the tunnel heated up  $0.03 \text{ }^\circ\text{C}$  in this range. But the influence of the temperature change hardly caused the extension, because it is very small extension of  $1.6 \times 10^{-8}$  as  $5.4 \times 10^{-7}$  of the temperature response of the quartz-tube. And more, the tiltmeter and the other point data of the extensometer show a similar change, therefore, the change seems to be true. We can catch geophysical phenomena such as the seismic waves (not shown in the figure) of the 2011 off the Pacific coast of Tohoku earthquake, the coseismic step, the aftereffect and continuing extensive change by the one device. This extensive change may indicate a part of crustal upheaval in a geological meaning.

Acknowledgement: We thank Yuichi Imanishi Associate Professor of ERI for teaching us about the continuity of decreasing gravity by the superconducting gravity meters in Matsushiro and Kamioka after the Tohoku earthquake.

Keywords: extensometer, tiltmeter, aftereffect, the 2011 off the Pacific coast of Tohoku Earthquake



## Equatorial flattening of the cylindrical outer core

KAKUTA, Chuichi<sup>1\*</sup>

<sup>1</sup>none

Zhong et al.(2007), showed that the Africa supercontinent was formed after the Pangea(330Ma) in an initially by a spherical harmonic degree-1 form with the Pacific superplume. They suggested that the degree-1 structure is responsible for supercontinent assembly with downwellings(Africa) and upwellings(Pacific). Recent studies show that light elements are transferred from the mantle to the outer core (OC) through the core-mantle boundary(CMB) and that the stably stratified layer are formed in the OC beneath the CMB. The stable layer shows the superadiabatic gradient,  $1 \text{ K km}^{-1}$  and its thermal conductivity is  $150 \text{ W m}^{-1} \text{ K}^{-1}$ . The heat flux is over  $100 \text{ mW m}^{-2}$ . The heat flux of the mantle near the CMB is  $100 \text{ mW m}^{-2}$  in the high temperature region (Perovskite) and  $50 \text{ mW m}^{-2}$  in the low temperature region (Post-Perovskite). The heat flux flows into the low temperature region from the OC. We assume that the OC is a thin cylindrical rotating fluid around the rotating axis. The fluid shows a low frequency motion and the effects of flow pressure fluctuations on the density is ignored (Subseismic Approximation; Smylie and Rochester, 1981). The heat flux in the OC is expressed in the form of the exponential function of the central distance which decreases outward near the CMB. We derive the 1st order variations of the Potential. The azimuthal variation of the potential shows the variation of the equatorial flattening. The maximal value of its variation relative to the mean gravitational potential at the CMB is  $1.1 \times 10^{-5}$  (flattening). This value can be compared with the value of the equatorial flattening of the OC to be  $6 \times 10^{-6}$  obtained by Szeto and Xu(1997).

Keywords: thin cylindrical outer core, heat flux, heat flux in the mantle, potential, variation of potential, equatorial flattening of core

## A bias correction method for improving regularized solution in linear inverse ill conditioned models

SHEN, Yunzhong<sup>1\*</sup> ; XU, Peiliang<sup>2</sup> ; LI, Bofeng<sup>1</sup>

<sup>1</sup>1. College of Surveying and Geo-infomatics, Tongji University, Shanghai 200092, P.R. China, <sup>2</sup>Disaster Prevention Research Institute, Kyoto University, Uji, Kyoto 611-0011, Japan

Geodetic downward continuation and inverse problems are often ill conditioned, and regularization is used for deriving stable and better solutions. However, the regularized estimates of parameters and residuals are well known to be biased. Theoretically the biases of the estimated parameters and residuals can only be computed with the true values of parameters. Since we do not know the true values of parameters in practice, we attempt to improve the regularized estimates by using the regularized estimates themselves to replace the true parameters for estimating the biases and then removing the computed biases from the regularized estimates. Furthermore the biases are also removed from the residuals, and then the variance of unit weight of the observation noises is estimated with the bias-reduced residuals. We derive the analytical conditions for bias correction and show that the bias-corrected regularization performs better than the ordinary regularization in terms of mean squared errors. However, for estimating the variance of unit weight, the biases still need to be full removed from the residuals. We then present the numerical examples of gravity downward continuation to demonstrate the performance of our bias correction method for improving regularized solution. The results show that our bias correction method can successfully reduce the absolute biases of the regularized estimates, and improve the accuracies with more than 5 per cent. Moreover, by removing the biases from the residuals, the derived variance of unit weight is almost unbiased.

**Keywords:** Linear ill-conditioned model, Regularization solution, Bias correction, Gravity downward continuation, Variance of unit weight

## Gravity observation using a superconducting gravimeter at Ishigakijima, Japan (part 3)

IMANISHI, Yuichi<sup>1\*</sup> ; NAWA, Kazunari<sup>2</sup> ; TAMURA, Yoshiaki<sup>3</sup> ; IKEDA, Hiroshi<sup>4</sup> ; MIYAJI, Takeshi<sup>3</sup> ; TANAKA, Yoshiyuki<sup>1</sup>

<sup>1</sup>ERI, The University of Tokyo, <sup>2</sup>AIST, <sup>3</sup>NAOJ, <sup>4</sup>University of Tsukuba

About two years have passed since we started gravity observation by means of a superconducting gravimeter at the VERA Ishigakijima Station, National Astronomical Observatory Japan in 2012, with the main purpose of detecting possible gravity changes associated with the long-term slow slip events beneath the Yaeyama Islands. Up to now, we have experienced three times of events, which took place in May 2012, December 2012 and July 2013. For the two events in 2012, gravity changes possibly associated with the slow slip events were recorded. The July 2013 event was not well recorded because of the damages by the typhoon. In addition, an earthquake swarm near the Yaeyama Islands in April 2013 may have also influenced the observed gravity. The next slow event is expected to take place around February 2014. Modeling and interpretation of the data will be presented in the paper.

Keywords: superconducting gravimeter, slow slip, Ishigakijima

## Various drift rates of gPhone gravimeters obtained from short-term observations at geothermal fields

NAWA, Kazunari<sup>1\*</sup> ; MIYAKAWA, Ayumu<sup>1</sup> ; SUGIHARA, Mituhiko<sup>1</sup>

<sup>1</sup>Geological Survey of Japan, AIST

We carried out short-term but continuous gravity observations using gPhone (spring type) gravimeters at geothermal fields. At hot spring area of Hachijojima, we obtained 1-4 months gravity data using several gPhone gravimeters at different sites and situations of the period between February 2011 and December 2012. Using the obtained data, we calculated and compared temporal variations of the drift rate. As a result, drift rates of gravimeters showed various characteristics according to location and elapsed time from installation. In many cases, it took about a month until initial drift stabilized, that is, drift rate became quasi-constant. Even after stabilized, drift rate of gPhone gravimeters remained a few microGal/day (on the other hand, the nominal drift rate of iGrav superconducting gravimeter is 0.5 microGal/month), although the magnitude of the drift rates were considerably smaller than several hundred microGal/day of CG-3M gravimeters. We will show the result of gPhone-133 replaced from Hachijojima to a geothermal power plant at Kyushu District in March 2013.

Keywords: relative gravimeter, temporal gravity change, Hachijojima, on-land observation

## Gravimetric vertical array observation -the 2013 fiscal year-

TANAKA, Toshiyuki<sup>1\*</sup> ; HONDA, Ryo<sup>1</sup>

<sup>1</sup>TRIES, ADEP

A vertical array of gravimeters (Mizunami Underground Laboratory; MIU) is quite rare in the world, and this method that suppresses rainfall responses and stacks signal from deep part of the crust can contribute to leveling up the potential of gravimetry (Tanaka et al., EPS, 2013). This time (Nov. 2013~Jan. 2014), we have succeeded in getting higher quality data than before with almost same configuration; namely, using two gPhone gravimeters (#130 on the ground, #90 at 300m under the ground). Though blasting for construction works had performed frequently during last year, we can detect sub-microGal responses of rainfall this time in the frequency band from hourly to daily. In the longer band, the sensor temperature of #130 is still shifting slightly, which can affect drifting rate. Here, we describe the four time-series data: data of belowground, (1); data on the ground, (2); sum of the two, (3); difference between the two, (4). We have finally got residual gravity values without tidal and atmospheric responses by using the BAYTAP-G (Tamura et al., 1991), with assuming of linear drift. When it rains, (1) should show gravity decrease, (2) should show gravity increase, (3) should offset the response, and (4) should superimpose the response. Because, only the main part of the Akeyo formation, which overlies an impervious layer from the surface to approximately 80m depth, responds to precipitation (e.g. Tanaka et al., Gcubed, 2006). Actually, we have observed such responses of rainfall. These depend on the way of rainfall; however, it seems that the amplitude of the response of (1) is slightly larger than (2). If so, the infinite slab assumption of a groundwater layer caused by rainfall is unsuitable for this gravimeter layout. On atmospheric correction, (1) and (2) should be almost same, (3) should superimpose, and (4) should offset the response. Actually, we have observed such responses and confirmed that (4) is one-tenth the atmospheric response of that of (1) or (2).

In the future, we will aim to accumulate high quality data, survey the habit of these two gravimeters (i.e. sensor drift, sensor temperature, and tilt response), and finally construct a vertical array including an absolute gravimeter.

**Acknowledgements:** This work is supported by a promotion grant for the establishment of the underground research facility of the Agency for Natural Resources and Energy, Minister of Economy, Trade and Industry. We thank the JAEA for the cooperation of observations (especially Mr. Y. Horiuchi) and our colleagues.

**Keywords:** continuous gravity measurement, gravimeter, inland water, rainfall, atmospheric correction, measuring method

## Huge uplift event of Iwoto: Estimation of gravity change based on the result of gravimeter calibration in Sapporo-Naha

OZAWA, Taku<sup>1\*</sup> ; MIYAGI, Yosuke<sup>1</sup> ; UEDA, Hideki<sup>1</sup> ; NAGAI, Masashi<sup>1</sup> ; FUJITA, Eisuke<sup>1</sup>

<sup>1</sup>National Research Institute for Earth Science and Disaster Prevention

Ogasawara-Iwoto is the volcanic island located to 1200km south of Tokyo. It has a caldera with the diameter of 10km, and its central and southwestern part appears on the sea surface. One of characteristics for its volcanic activity is to have the large uplift rate, and National Research Institute for Earth Science and Disaster Prevention (NIED) has revealed occasional occurrence of huge uplift events and distribution of its crustal deformation (Ukawa et al., 2006). NIED started gravity survey from 1996, and Ukawa (2006) suggested involvement of magma in a huge uplift event. Though continuous subsidence had been observed from early 2003, it rapidly changed to uplift in mid-2006. Its uplift decelerated with time after 2007, but it rapidly re-accelerated in Feb. 2011. According to GNSS observation by NIED and GSI, the amount of uplift from re-acceleration to Apr. 2012 reached 2m. In late April of 2012, discolored water was found around Iwoto, and uplift activity slowed down after that. To investigate crustal deformation and gravity change associated with this event, we carried out GNSS campaign observation and gravity survey. We presented the result of GNSS campaign observation in fall meetings of the geodetic society of Japan and the volcanological society of Japan. We also presented preliminary result for gravity survey, but there was a problem on uncertainty for temporal change of scale factors of used gravimeters (Scintrex CG-3M #284 and #371). To estimate scale factors of their gravimeters, we carried out gravity survey between Sapporo and Naha. In this presentation, we show temporal change of scale factors revealed from this calibration and gravity change of Iwoto estimated using its result.

In gravimeter calibration, we measured gravities at NIED (Bosai-BS), GSI (Tsukuba-GS and Tsukuba-FGS), Haneda airport (Haneda-GS), Chitose airport (Chitose-GS), Hokkaido University (Sapporo-GS), and Okinawa Meteorological Observatory (Naha-GS and Naha-FGS). In estimation of relative gravity, we assumed that the drift rate was constant, and estimated gravities and the drift rate simultaneously. Then we estimated scale factors so that estimated gravities corresponded to those of JGSN96 (Geospatial Information Authority of Japan, Geodetic department, 1997). Since Sapporo-GS was moved to new benchmark, we used gravity measured by GSI. Estimated changes of scale factors from those in 2006 were  $+2 \times 10^{-5}$  and  $-1 \times 10^{-4}$  for #284 and #371, respectively. Temporal changes of scale factors are not orderly, and then obtained scale factor is different significantly from estimated value by the linear approximation. Therefore it indicates that consideration of temporal change of scale factor is important in survey of large gravity difference.

Estimating gravity at the benchmark in Iwoto (IWO101), estimated gravities from #284 and #371 were consistent within 0.027mGal, and its average was decrease of 0.734mGal from that in 2006. Uplift in this period was 3.05m, and then gravity change rate with respect to uplift was -0.241mGal/m. This gravity change rate is in good agreement with that for the 2001-2002 huge uplift event by Ukawa et al. (2006). This result suggests that the huge uplift event from 2006 has been caused by the magma with the similar density to that in the 2001-2002 event.

Acknowledgements. GNSS and gravity surveys were supported by JSDF. A part of survey and analysis for Iwoto was carried out by Ohba Co. Ltd. Gravity calibration was supported by GSI, Hokkaido University, and Okinawa Meteorological Observatory.

Keywords: Iwoto, gravity, scale factor, magma

## Absolute gravity measurements near the Sor-Rondane Mountains, Antarctica

FUKUDA, Yoichi<sup>1\*</sup> ; AOYAMA, Yuichi<sup>2</sup> ; SUGANUMA, Yusuke<sup>2</sup> ; OKADA, Masaki<sup>2</sup> ; DOI, Koichiro<sup>2</sup>

<sup>1</sup>Graduate School of Science, Kyoto University, <sup>2</sup>National Institute of Polar Research

In order to detect the gravity changes due to ice sheet mass changes, Glacial Isostatic Adjustment (GIA) and other effects, we have conducted absolute gravity measurements at Princess Elisabeth Station (PES) near the Sor-Rondane Mountains, Antarctica, as part of the 55th Japanese Antarctic Research Expedition (JARE-55). In addition, the first absolute gravity measurements using a field absolute gravimeter have also been conducted on the Seal rock near the Asuka station, where the gravity reference point (No.26-01) established by JARE-26 is located.

The absolute gravimeters employed were FG5#210 and A10#017, and a relative gravimeter LaCoste #805 was also used for dg/dz measurements and gravity connections. Using DROMLAN (Dronning Maud Land Air Network), we moved to PES with the instruments via Novolazarevskaya from Cape Town in South Africa. The length of our stay in PES was for 18 days from Nov. 29 to Dec. 16, 2013. Belgian researchers have already conducted absolute gravity measurements using a FG5 in North Shelter (NS), a small observation hut built on an outcrop a few hundred meters apart from the main base of PES. One of the main purposes of this project is to monitor long-term gravity changes by means of successive absolute gravity measurements at the same gravity point in NS. Since NS has not enough space for adjusting the gravimeters before measurements, we borrow a room in the main base for the purpose and test measurements as well. We established a tentative gravity point in the room and compared the gravity values measured by A10 and FG5. The result showed the discrepancy was within 2 micro-Gals. This means that A10 was well calibrated. Unfortunately a crucial fault arose in the dropping chamber of the FG5, and it could not be recovered to the last. For this reason, the measurements in NS were carried out using A10. The gravity value on the reference point was calculated to be 982302155.21 micro-Gals with the measured dg/dz of -4.4529 micro-Gals/cm. Although the exact comparisons with the gravity values obtained by the Belgian team have not been completed yet, the gravity values seem to be in agreement within several micro-Gals. Therefore the temporal gravity change would be very small, even if it existed.

The gravity measurements on the Seal rock have been conducted on Dec. 5th and 6th. Since No.26-01 is located near the summit of the Seal rock, where strong wind blows constantly, it is very difficult to conduct absolute gravity measurements even using A10. Therefore a tentative gravity point was set up at the foot of Seal rock, and measurements with A10 were conducted at the point. Then gravity connection to No.26-01 was conducted with the LaCoste gravimeter. The gravity value thus obtained at No.26-01 was 982406.109 mgal with the accuracy of about 15 micro-Gals including the errors due to the gravity connection.

The gravity values of No.26-01 so far obtained were 982405.33mgal by JARE-26 (GSI, 2002), and 982402.817mgal by JARE-27 (Fukuda, 1986). The new value is 0.779 mgal and 3.292 mgal larger than those of JARE-26 and JARE-27, respectively. In JARE-27, two sets of LaCoste gravimeters were employed for the gravity connection between Seal rock and Syowa Station. Since a large discrepancy between the values obtained by two gravimeters was found, Fukuda (1986) applied a step correction of 3.765mGals to the suspected gravimeter. However, judging from the present result, the correction could be applied to the wrong gravimeter. If the correction was applied to the other gravimeter, the difference of 3.292 mgal was set to about 0.5mGals, and it would be likely as the accuracy of the gravity connection. The gravity value of No.26-01 has been used as a reference value for the gravity surveys so far conducted in the Sor-Rondane area. Therefore the revisions of those values should be required from now on.

Keywords: absolute gravity measurement, Sor-Rondane, Antarctica, ice sheet movement, gravity changes, gravity reference point

## Performance of the recoil-compensation mechanism used for a throw-up type absolute gravimeter

SAKAI, Hiroataka<sup>1\*</sup> ; ARAYA, Akito<sup>1</sup> ; TSUBOKAWA, Tsuneya<sup>2</sup> ; EMANUELE, Biolcati<sup>3</sup>

<sup>1</sup>Earthquake Research Institute, University of Tokyo, <sup>2</sup>Shin-ei keisoku, <sup>3</sup>L'Istituto Nazionale di Ricerca Metrologica

Absolute gravimeters can measure gravity acceleration in the accuracy of 8 to 9 digits. They are accurate and useful for many applications, however the apparatus is too bulky and heavy. Therefore, in the field observation, their installation site is limited. As a result, for volcanic observations, a gravity value is usually measured by an absolute gravimeter at a reference point of foot, and then a gravity value of an observation point can be obtained from the gravity difference between a reference point and an observation point measured with a relative gravimeter; such a method is laborious, and requires long time. Furthermore it is hazardous to approach the observation points when the volcano is active. This study is to minimize absolute gravimeter in order to improve these situations. The original point of our new apparatus is to incorporate a recoil-compensation mechanism to improve the measurement accuracy.

In the absolute gravity measurements, we adopted a rise-and-fall method, while conventional absolute gravimeters usually adopt a simple free-fall method. The simple free-fall method has several problems such as bulky mechanism to lift up a test mass, repeated measurements, and long time to take for the preparation. Hence, we developed a throw-up equipment that had no need for lifting up a test mass and could measure repeatedly. This enabled to minimize one of the biggest parts in the absolute gravimeter.

The equipment which we developed this time can throw up the test mass by 3mm in height simply by applying the signal to a piezoelectric element which is incorporated in the expansion mechanism. When the test mass was thrown up, it rotated by an anchoring effect and it may cause the error in the gravity measurement. We applied other piezoelectric elements which separate the stage from the test mass just before the test mass leaves the stage to cut off the anchoring force. At the end of 2012, we carried out a performance test of the throw-up equipment at Esashi Earth Tidal Station in Iwate. At Esashi, we replaced the free fall equipment of the existing absolute gravimeter with the throw-up equipment. As a result, the throw-up equipment was able to detect a gravity change of earth tides. The resolution of the gravity measurement  $\delta g$  was estimated to be  $40\mu\text{gal}$ . However, the absolute gravity deviated from the value expected from the past measurements up to  $\Delta g = 3\text{mgal}$ . This big error was inferred from the recoil effect at the time of throw that induces vibration to the interferometer.

We developed the recoil compensation mechanism of the throw-up equipment to improve the measurement accuracy  $\Delta g$ . Specifically, we put the same piezoelectric element and the expansion mechanism on the other side of the baseplate to which the throw-up mechanism is attached. These expansion mechanisms move symmetric by applying the same signal to the piezos. When the test mass is thrown up, the counter mass fixed by springs is launched downward at the same time to compensate the recoil effect. We could observe the recoil reduction as much as 2.7% of peak acceleration without the compensation mechanism. After performing fine adjustment of the equipment, we plan to conduct gravity measurement by the same method to 2012, and the result and the development status will be reported.

Keywords: absolute gravimeter, throw-up equipment, miniaturization, recoil effect, compensation mechanism, gravity measurement

## Development of a laser-interferometric gravity-gradiometer and its trial operation on the volcanic island of Sakurajima

SHIOMI, Sachie<sup>1\*</sup> ; KAGIYAMA, Tsuneomi<sup>1</sup>

<sup>1</sup>Aso Volcanological Laboratory, Kyoto University

We have been developing a laser-interferometric gravity-gradiometer for volcanological studies. The gravity gradiometer measures differential accelerations between two test masses that are in free fall at different heights. Because its detection principle is based on the differential measurements, measured values are insensitive to the motions of observation points. That is to say, the gravity gradiometer is expected to have a good resolution even when it were used on an accelerating vehicle, such as an airship, or in an active volcanic area. Therefore, the gravity gradiometer could be useful for, for example, resource explorations and studies on volcanic activities.

The gravity gradiometer, to be used on an airship, had been developed at the Institute for Cosmic Ray Research (ICRR) of the Tokyo University from 2009 to 2012. A prototype of the gravity gradiometer was built up and tested at the ICRR. Their laboratory test showed that its resolution of measuring vertical gravity gradients was about a few  $\mu\text{Gal}/\text{m}$  in two second measurements. However, large unexplained disturbances were observed in longer term measurements. In order to understand the sources of the disturbances, the prototype was moved to the Aso Volcanological Laboratory (AVL) of the Kyoto University in July 2012. Since then, its further development, to be used at an observatory in a volcanic area, has been carried out at the AVL.

We will report the current status of the development for volcanological studies and results of trial measurements performed at the Sakurajima Volcanological Laboratory of the Kyoto University, on the volcanic island of Sakurajima, Kyusyu, Japan.

Keywords: gravity gradients

## The two components of postseismic gravity changes and their mechanisms

TANAKA, Yusaku<sup>1\*</sup> ; HEKI, Kosuke<sup>1</sup>

<sup>1</sup>Graduate School of Science, Hokkaido University

The time series analysis of the gravity changes of the three Mw9-class mega-thrust earthquakes (2004 Sumatra-Andaman earthquake; 2010 Chile (Maule) earthquake; and 2011 Tohoku-oki earthquake) gives the strong possibility that the gravity observation separates postseismic phenomena. There are three sensors for earthquake observations: the first sensor is seismographs, the second sensor is GNSS (Global Navigation Satellite System) or SAR (Synthetic Aperture Rader), and the third sensor is the gravity observation. Seismographs cannot be used to catch the signal of postseismic phenomena because they do not shake the ground. GNSS like GPS (Global Positioning System) and SAR catch the signal of postseismic phenomena but they cannot separate those phenomena because the phenomena move the ground with the same polarities. However, the polarities to gravity changes of postseismic phenomena can be different each other. This suggests that the gravity can become the first sensor to catch the separated signals of postseismic phenomena.

GRACE (Gravity Recovery And Climate Experiment), which is the twin satellites launched in 2002 by NASA and keeps on observing the gravity field of the earth, gives the two-dimensional gravity data and the insight into phenomena under the ground when and after earthquakes occur. The results of time series analysis of postseismic gravity changes with GRACE data show that the gravity which decreases coseismically keeps on decreasing for a few months and increases for a longer period; the postseismic gravity changes have two components (short- and long-term gravity changes). This is a new discovery and this also suggests that the gravity observation gets the different postseismic phenomena with different polarities.

The mechanisms of coseismic gravity changes are well known but those of short- and long-term postseismic gravity changes are not clear completely. They are explained with afterslip and viscoelastic mantle relaxation to some extent but each of them has each problem.

Although the mechanisms of postseismic gravity changes have rooms to be discussed, the gravity observation can do what the seismographs, GNSS and SAR cannot do; the gravity observation separates the postseismic phenomena.

## High resolution mapping of ice mass trend in Greenland using GRACE GFZ solution

MATSUO, Koji<sup>1\*</sup> ; FUKUDA, Yoichi<sup>1</sup>

<sup>1</sup>Graduate school of Science, Kyoto University

The gravity satellite mission GRACE has been measuring monthly variations of the Earth's gravity field since its launch in 2002. The GRACE data has updated from RL04 to RL05 in May 2012, and have been provided in the form of spherical harmonic (Stokes') coefficients with degree and order up to 60 (d/o60) from CSR and JPL. In addition, GFZ has provided Stokes coefficients with d/o90 as RL05a product in December 2013. In this study, we examine the measurement error of GFZ RL05a product (d/o90). Then we attempt to delineate a high resolution map of ice mass trend in Greenland by making use of the full Stokes' coefficients.

First, we examine the measurement error. Following the method of Wahr et al. (2006), we derive temporal and spatial variation of the measurement error from error variance matrix of GRACE data. The global average of RL05a error is about 100cm in equivalent water thickness. Because RL04 error is about 300cm, RL05a achieves triple the precision improvement. The temporal variation of error in global average is about 200 cm from January 2003 to July 2003, and reduces to about 100cm afterwards. The spatial distribution shows large error in equatorial region (about 130cm) and small error in polar region (about 40cm). Considering these results, it can be said that the quality of RL05a is especially high in polar region after August 2003.

Next, we derive ice mass trend in Greenland from GFZ RL05a (d/o90) product. Here we apply de-stripping filter (Swenson and Wahr, 2006) to alleviate the noise. In addition, we employ spherical Slepian Basis (Harig and Simons, 2012) to extract ice mass trend in Greenland effectively. In doing so, we can successfully delineate a clear ice mass trend map with about 200 km spatial resolution, which is 1.5 times as high as before. We confirmed very good agreement with ICESat result.

Keywords: Satellite gravimetry, Greenland, Ice sheet mass variation, Space geodesy, GRACE, ICESat

## Establishment of GSIGEO2011 (Japanese geoid model)

KODAMA, Tokuro<sup>1\*</sup> ; MIYAHARA, Basara<sup>1</sup> ; KAWAWA, Hiroshi<sup>1</sup> ; KUROISHI, Yuki<sup>1</sup>

<sup>1</sup>GSI of Japan

Geospatial Information Authority of Japan (GSI) established Japanese geoid model "GSIGEO2000". The model has enabled a translation from ellipsoidal heights to orthometric heights in GNSS survey for triangulation points, which are positional reference for surveys in Japan. As a result, the model greatly has contributed to realize efficient control point survey. In order to expand utilization field of geoid model to height determination of third-order benchmarks by GNSS satellite positioning, GSI has established new Japanese geoid model "GSIGEO2011" and reported here.

GSIGEO2011 has established as a hybrid geoid model of a gravity geoid model and observed geoid height data. New Japanese gravity geoid model, JGEOID2008 (Kuroishi, 2009), is adopted as the base model, and least square collocation method is adopted to fit the model to observed geoid height data obtained at over 750 GNSS-based control stations all over Japan. In order to utilize for height determination of third-order benchmarks, residuals between the model and input observed geoid heights are set to 2cm in standard deviation. JGEOID2008 is greatly improved at reduction of local systematic errors which are contained in older gravity geoid models. Therefore, short wavelength components in geoid are well described and fit to observed data, and as a result, the accuracy of the hybrid model is improved.

The 2011 off the Pacific coast of Tohoku Earthquake caused huge crustal deformation in an wide area around eastern Japan. GSI urgently conducted control point surveys for restoration and opened the result for eastern Japan. GSI also conducted geoid surveys for GNSS-based control points which is located in an area experienced huge crustal deformation, and the results have been utilized for the input geoid heights data of GSIGEO2011. Therefore, GSIGEO2011 is consistent with the revised survey results in eastern Japan.

GSI has published newly established GSIGEO2011 and tired to realize height determination of third-order benchmarks by GNSS survey referring GNSS-based control points which have orthometric heights. This challenge is expected to drive further improvement in efficiency of survey procedure in Japan.

Keywords: GSIGEO2011, Geoid model, survey results

## The Japan Gravity Standardization Net 2013 (JGSN2013)

YOSHIDA, Kenji<sup>1\*</sup>

<sup>1</sup>GSI of Japan

Geospatial Information Authority of Japan (GSI) have established new gravity standardization net, the Japan Gravity Standardization Net 2013 (JGSN2013), from the latest absolute and relative land gravity data which covers Japanese islands. GSI already established and published the Japan Gravity Standardization Net 1975 (JGSN75), which is consistent with the International Gravity Standardization Net 1971 (IGSN71). JGSN75 have been officially referred as Japanese gravity standard.

JGSN2013 have been established by combining gravity data obtained from primary-order absolute gravity survey and first-order relative gravity survey. In Tohoku area, at least one gravity survey was done for each gravity benchmark after the 2013 off the Pacific coast of Tohoku Earthquake. Therefore, the gravity survey data include gravity change caused by the earthquake.

JGSN2013, which is the second Japanese gravity standard net established by GSI, have achieved great improvement in accuracy and special coverage by adopting FG5 absolute gravity meter as an instrument, updating station coordinates to ITRF2008 and modifying tidal correction procedure to more consistent manner through all process. As a result, JGSN2013 have a capacity not only to contribute to monitoring of earth gravity field, which is promoting by GGOS, but also to be registered to international absolute gravity database (AGrav), which is operated as a joint project by IAG IC-WG2.1 and IGFS. The establishment of JGSN2013 is reported in the paper.

Keywords: The Gravity Standardization Net, JGSN75, JGSN2013

## Calibration of the superconducting gravimeter iGrav10 by parallel observation with the absolute gravimeter FG5 #217

SUGIHARA, Mituhiko<sup>1\*</sup> ; NAWA, Kazunari<sup>1</sup> ; MIYAKAWA, Ayumu<sup>1</sup>

<sup>1</sup>AIST

An iGrav superconducting gravimeter (SG) was re-installed in the Farnsworth field, TX for the purpose of studying the effects of CO<sub>2</sub> injection at an enhanced oil recovery (EOR) site in December 2013. Usually the iGrav SG has an ultra-low drift of less than 0.5 microGal / month and a virtually constant scale factor. Empirically, the drift rate looks negligible using the TSoft program. However observed trend contains the drift-like component which is about 0.4 microGal / day. Strictly it is difficult to distinguish real gravity changes from time-varying instrumental drift. We made co-located measurements with the FG5 absolute gravimeter (AG) in middle of December 2013 and middle of January 2014. The gravity differences between the two periods was determined to be +1 +/-2 microGal by the AG measurements, whereas -12 microGal by the SG measurements. The observed drift of the SG was much larger than the specified value, so that the SG was determined to be reset and is improved. Generally it takes at least six months to evaluate such low drift of less than 0.5 microGal / month using co-located measurements with AG. Another choice is parallel SG and SG measurements located in close proximity. We are planning such measurements at the Farnsworth site in 2014. This research is funded and supported by Ministry of Economy, Trade and Industry (METI).

Keywords: Superconducting gravimeter, iGrav, absolute gravimeter, FG5, parallel observation

## Densed gravity survey on the southeastern Kego fault system

NISHIJIMA, Jun<sup>1\*</sup> ; FUJIMITSU, Yasuhiro<sup>1</sup>

<sup>1</sup>Faculty of Engineering, Kyushu University

The Kego fault system is one of the active fault located in Fukuoka city, southwestern Japan. We have conducted densed gravity survey on the southeastern Kego fault systems. One of the purposes of the survey is to reveal the location and detailed shape of the active fault syatem. We have measured gravity value at 721 points using Scintrex CG-3+ and CG-5 gravimeter. The measurement point interval was arranged as about several tens to hundreds meters. The measured gravity values were processed with a series of correction (height, drift, tidal, the free-air, the Bouguer and terrain) in order to obtain a gravity anomaly map. We determined the Bouguer density of 2.47 g/cm<sup>3</sup> using an objective Bayesian approach (Murata, 1993).

According to the gravity anomaly map of the Fukuoka City area that consists of not only our gravity data but also the gravity data of other institutions, the gravitational basement, which has a high density and affects to the gravity anomaly, is thought as Paleozoic Sangun metamorphic rocks and Cretaceous plutonic rocks (Sawara Granite, etc.) (Karakida et al., 1994). And a clear low gravity anomaly extension that has a strike of NW-SE is detected and coincides with the location of Kego Fault confirmed by a trenching survey (Shimoyama et al., 2005).

We will report the result of a three-dimensional analysis using GRAV3D ver. 3.0 (Li and Oldenburg, 1998).

Keywords: Densed gravity survey, active fault, gravity anomaly

## Crustal thickness deduced from a three-dimensional gravity modeling with seismic survey results

FUJIOKA, Yukari<sup>1\*</sup> ; ISHIHARA, Takemi<sup>2</sup> ; OIKAWA, Mitsuhiro<sup>1</sup> ; KANEDA, Kentaro<sup>1</sup> ; NISHIZAWA, Azusa<sup>1</sup>

<sup>1</sup>Hydrographic and Oceanographic Department, Japan Coast Guard, <sup>2</sup>National Institute of Advanced Science and Technology

The Japan Coast Guard (JCG) has conducted multichannel seismic reflection and refraction surveys as part of the Continental Shelf Survey from 1983 through 2008 in the area from the northwest part of the Pacific plate to the Philippine Sea plate. On the other hand, it has also conducted marine gravity surveys in the same area and possesses enormous amount of gravity data. We calculate crustal density distribution by applying the three-dimensional gravity inversion method (Ishihara and Koda, 2007) using these data.

This method has performed in the following procedures: First, an initial density structure model constituting of seawater, sediment, crust and mantle is made by interpolation of seismic survey results with reference to a gravity distribution. Second, gravity anomalies are calculated using the initial model. Mantle Bouguer anomalies are calculated by subtracting a constant, which depends on the regional structure, from the differences between observed and calculated gravity anomalies. Finally, the Moho depths are obtained by inversion analysis to minimize the mantle Bouguer anomalies. We can estimate the crustal thickness distribution in this way.

It confirmed that the above method improves the initial model with the Moho depths due to velocity structure from refraction surveys, and that a more appropriate density structure model can be obtained.

In addition, it is necessary that whole structure depending on a sea area with the effects given by structure, such as a density and/or a thickness of sediment and/or lithosphere, should be considered if the effects of them are large. For example, in the case of the northwest part of Philippine plate, we found that the thickness of the lithosphere depending on its age strongly affects the result of the inversion. Therefore, we used the calculated gravity data after removal of variation for wave length than or equal to 400 km in order to remove effect given by the structure under crust.

We will report these revisions and the crustal thickness distribution in several sea areas. It is expected that gravity determination of the crustal thickness distribution in large sea area gives important clues on tectonic evolution of crust.

Keywords: gravity

## Estimation of the density structure beneath the Kanto District, Japan, by 3-D gravity inversion

EDO, Tatsumi<sup>1\*</sup> ; YAMAMOTO, Akihiko<sup>1</sup>

<sup>1</sup>Graduate School of Science and Engineering, Ehime University

We applied an improved gravity inversion technique by Bear et al. (1995) to rapidly invert Bouguer gravity data in Kanto District, Japan, for a 3-D density distribution as a source of the observed field. The technique estimates the density distribution within the source volume using a least-squares inverse solution that is obtained iteratively by singular value decomposition using orthogonal decomposition of matrices with sequential Householder transformations. The source volume is subdivided into a series of right rectangular prisms of specified size but of unknown density. This discretization allows the construction of a system of linear equations relating the observed gravity field to the unknown density distribution. Convergence of the solution to the system is tightly controlled by a damping parameter which may be varied at each iteration. Application to a gravity data set from Kanto District, Japan, has yielded a geologically reasonable result that agrees with published models derived from interpretation of gravity, magnetic, seismic, and drilling data.

## Collaboratory for the Study of Earthquake Predictability - Global Activities

SCHORLEMMER, Danijel<sup>1\*</sup> ; GERSTENBERGER, Matt<sup>2</sup> ; HIRATA, Naoshi<sup>3</sup> ; JORDAN, Thomas<sup>4</sup> ; LIUKIS, Maria<sup>4</sup> ; MARZOCCHI, Warner<sup>5</sup> ; RHOADES, David<sup>2</sup> ; TSURUOKA, Hiroshi<sup>3</sup> ; WERNER, Maximilian<sup>6</sup> ; ZECHAR, Jeremy<sup>7</sup> ; CSEP WORKING GROUP, The<sup>4</sup>

<sup>1</sup>GFZ German Research Centre for Geosciences, 14473 Potsdam, Germany, <sup>2</sup>GNS Science, Avalon, Lower Hutt, New Zealand, <sup>3</sup>Earthquake Research Institute, University of Tokyo, Tokyo 113-0032, Japan, <sup>4</sup>Southern California Earthquake Center, University of Southern California, Los Angeles CA 90089, USA, <sup>5</sup>Istituto Nazionale di Geofisica e Vulcanologia, 00143 Roma, Italy, <sup>6</sup>School of Earth Sciences and Cabot Institute, University of Bristol, Bristol BS8 1RJ, UK, <sup>7</sup>Swiss Seismological Service, ETH Zurich, Zurich, Switzerland

The Collaboratory for the Study of Earthquake Predictability (CSEP) aims to improve our understanding about the physics and predictability of earthquakes through rigorous and prospective testing of earthquake forecast models. The system-science character of earthquake prediction research demands an open and collaborative structure for experimentation in a variety of fault systems and tectonic regions. CSEP Testing Centers in California, New Zealand, Japan, and Europe are being developed to provide adequate infrastructure for predictability research. CSEP is currently running prospective, automated evaluations of more than 350 models in various testing regions, e.g. California, New Zealand, Japan, Italy, and globally. We present the evolution of CSEP since its inception in 2007 and discuss results from several types of CSEP experiments. Finally, we describe how CSEP is expanding into other areas, including the testing of earthquake early warning systems, geodetic transient detectors, intensity prediction equations, ground-motion prediction models, and other types of hazard models.

Keywords: Earthquake forecasting, Seismic hazard, Statistical seismology, Earthquake statistics, Forecast testing

## One-day earthquake forecasting experiment in Japan after the 2011 Tohoku-oki earthquake

HIRATA, Naoshi<sup>1</sup> ; TSURUOKA, Hiroshi<sup>1\*</sup>

<sup>1</sup>Earthquake Research Institute, the University of Tokyo

An experiment for earthquake predictability in Japan started in 2009 with a framework of CSEP. We have conducted one-day, three-month, one-year, and three-year forecasting experiments with three different regions of Japanese Islands; all Japan including sea area, main lands without sea area, and Kanto area(Nanjo et al., 2011; Tsuruoka et al., 2012). We currently have 160 modes for three regions and four periods. We conducted a retrospect one-day forecast of aftershocks of the 2011 Tohoku-oki earthquake showing that all proposed models failed in consistency tests immediately after the mainshock but in several days some of the models recovered its performance of forecasting (Nanjo et al., 2012). A current method for short-term forecasting has limitation of a period of one-day, which is arbitrarily determined. A shorter time period may be necessary for very intensive seismicity. Seismic activities in Japan have changed very much after the 2011 Tohoku-oki event, which brought us an idea that current forecasting models should be modified. We will present some new results of one-day forecasting experiments in Japan to discuss how to get information about real time earthquake hazard to mitigate earthquake risk. A new method to test performances of a model is also proposed.

Keywords: Earthquake forecasting, One-day forecasting, seismicity, Tohoku-okiearthquake, Statistical seismology

## Prospective evaluation of 3-month testing class of the CSEP-Japan earthquake forecasts

TSURUOKA, Hiroshi<sup>1\*</sup> ; HIRATA, Naoshi<sup>1</sup>

<sup>1</sup>Earthquake Research Institute, University of Tokyo

Collaboratory for the Study of Earthquake Predictability (CSEP) is a global project of earthquake predictability research. The primary purposes of the CSEP is to develop a virtual, distributed laboratory. The final goal of this project is to investigate the intrinsic predictability of earthquake rupture mechanisms.

One major focus of the Japanese earthquake prediction research plan 2009-2013 is testable earthquake forecast models. So, the Earthquake Research Institute joined the CSEP and installed in an international collaboration a testing center as CSEP-Japan for rigorous evaluation of earthquake forecast models.

A total of 160 models were submitted from all over the world. And CSEP-Japan started the prospective experiments from 1 November 2009. The models are currently under test in 12 categories, with 3 testing regions and 4 testing classes of different time spans (1day, 3 month, 1 year and 3 years). We evaluate the performance of the models in the official suite of tests defined by the CSEP (L, M, N, S, R, T and W tests) against authorized catalogue compiled by Japan Meteorological Agency.

CSEP-Japan testing center has conducted over 6-12 rounds tests for 3-month testing classes including 2011 Tohoku-oki earthquake. We will discuss these results of evaluation test of the prospective experiments, and checked the performance of the earthquake models.

Keywords: CSEP, Earthquake Predictability, Seismicity

## Does using Coulomb stress change information create quantifiable improvements in earthquake forecast models?

GERSTENBERGER, Matt<sup>1\*</sup> ; STEACY, Sandy<sup>2</sup> ; MARZOCCHI, Warner<sup>2</sup> ; RHOADES, David<sup>1</sup>

<sup>1</sup>GNS Science, 1 Fairway Drive, Avalon, Lower Hutt, New Zealand, <sup>2</sup>Environmental Sciences Research Institute, University of Ulster, Coleraine, N. Ireland, <sup>3</sup>Istituto Nazionale di Geofisica e Vulcanologia, Roma, Italy

The Darfield, New Zealand earthquake sequence has provided an interesting and active sequence for rigorous testing of earthquake forecast models that include Coulomb stress change information. Coulomb forecast models have long been discussed in the scientific literature as providing useful forecast information during aftershock sequences; however, a challenge that has limited our understanding of their ability is the difficulty in specifying such models so that they are prospective and unbiased. With the Darfield sequence we have the opportunity to use the Collaboratory for the Study of Earthquake Predictability (CSEP) earthquake forecast testing centre, that is already in operation in New Zealand, to develop Coulomb models in such a way. By taking advantage of archived data sets to provide all of the necessary inputs into the models, we are able to pseudo-prospectively test the models within the CSEP testing centre. An initial study by Steacy et al (2013) tested several models with Coulomb information. These models include a hybrid model with STEP (Gerstenberger, 2005), a rate-and-state based model, and several non-Coulomb models. Results of this study indicate that adding Coulomb information that was available 10-days after each main event, to a more traditional Omori-based model, provides a statistically improved forecast, even when attempting to test in an unbiased fashion. The experiment also highlighted significant differences when testing models retrospectively and pseudo-prospectively; these differences are driven by the reduced quality of data available to models in pseudo-prospective tests. Following this study, we are now implementing a larger experiment in collaboration with the European Union funded Strategies and Tools for Real Time Earthquake Risk Reduction (REAKT) project. In this experiment we are testing more than 20 Coulomb and non-Coulomb models within the NZ-CSEP testing centre. These models include hybrid statistical-Coulomb models and pure statistical and Coulomb models. We will discuss both experiments and their implications.

Keywords: Earthquake forecasting, New Zealand, CSEP, Coulomb, aftershock model, Christchurch

## Test of the argument for remote dynamic triggering by small mainshocks

PENG, Wei<sup>1\*</sup>

<sup>1</sup>Wei Peng, <sup>2</sup>Shinji Toda

To understand earthquake interaction and forecast time-dependent seismic hazard, it is essential to determine whether static or dynamic stress change triggers most aftershocks and subsequent mainshocks. Felzer and Brodsky (2006) argued that the observed linear seismic density of small aftershocks with distance from small mainshocks is a product of the decay of seismic wave amplitude. They conclude that even small shocks can dynamically trigger remote earthquakes at distances more than ten source fault dimensions away. Richards-Dinger et al. (2010) counter-argue that the power law decay is an apparent product from independent aftershocks occurring along a large rupture zone or near-simultaneous occurrence in seismic swarms. To test the argument of Richards-Dinger et al. (2010), we use the Taiwanese earthquake catalog of the Central Weather Bureau Seismic Network, whose quality is as good as that in California and Japan. Further, we take an advantage of the absence of major inland earthquakes and significant swarms in the period, 2001-2011.

We follow the methodology of Felzer and Brodsky (2006) for selecting mainshocks using their declustering algorithm, and then seek all shocks that occurred within 5 minutes to make a diagram of linear aftershock density as a function of distance from mainshock. First we select as a mainshock any event that is not preceded by a larger shock within 3 days ( $t_1$ ) and 100 km, and that is not followed by a large shock within 12 hr ( $t_2$ ) and 100 km. The mainshocks and aftershocks are  $2 \leq M < 3$  and  $M \geq 2$  respectively. This yields 706 declustered mainshocks from the 110,157 candidate shocks, but the number of mainshock-aftershock pairs is just 56. We only find four pairs within 50 km distance range (the maximum considered by Felzer and Brodsky), which precludes any regression, while the others located further than 50 km are regarded as background. We then shorten the time period for both  $t_1$  and  $t_2$  to be 1.5 days and 0.25 days, which allows us to regress a power law slope of  $-1.16 \pm 0.45$  for the 35 pairs within the 50-km distance range. The pairs are located mostly along the northern part of the Longitudinal Valley fault zone where small swarm activity and  $M \sim 6$  shocks often occur. We conclude that the much fewer ratios of mainshock-aftershock pairs in the Taiwanese catalog, in comparison to California and Japan, are due to lack of any large rupture and the absence of significant swarms in Taiwan, which supports the argument of Richards-Dingers et al. and renders the possibility that these small shocks are dynamically triggered untenable.

## Prediction performance of empirically defined foreshocks in the Izu region

MAEDA, Kenji<sup>1\*</sup> ; HIROSE, Fuyuki<sup>1</sup>

<sup>1</sup>Meteorological Research Institute

### 1. Introduction

Foreshocks have been thought one of the most promising phenomena to predict large earthquakes. However, as the physical mechanism of foreshocks is not clarified yet, it is very difficult to distinguish them deterministically from background seismicity before a mainshock occurs. Therefore, empirical approach is one of the realistic ways to use foreshock activity as a precursor of a mainshock. We investigate probabilistic features of empirically defined foreshocks and search for the best parameters to define foreshocks which present relatively high performance to predict large earthquakes. Maeda (1996) and Maeda and Hirose (2012) proposed a foreshock definition which gives relatively high performance to predict large earthquakes along the Japan trench. In this study we basically apply the same method to the seismicity in the Izu region where swarm activities related with magma movements are frequently observed, and estimate the prediction performance based on empirically defined foreshock activities.

### 2. Method

The method to search for parameters for foreshocks that present high prediction performance consists of four steps. 1) To eliminate small aftershocks from the original data. 2) To define foreshock candidates as the activities that have number of  $N_f$  earthquakes with magnitude  $\geq M_f$  during the period of  $T_f$  days in the segment of the size of  $D \times D$  degree (latitude  $\times$  longitude). 3) To set the alarm period of  $T_a$  days after a foreshock candidate during which a mainshock is expected to occur. 4) To search for the values of  $T_f$ ,  $M_f$ ,  $D$ ,  $N_f$ , and  $T_a$  which give high prediction performance by the grid search method. The prediction performance is measured mainly by  $dAIC$ , which is defined as the difference of AIC for a stationary Poisson model and a model based on a foreshock activity, and additionally by alarm rate (AR: the fraction of mainshocks alarmed), truth rate (TR: the fraction of foreshock candidates followed by a mainshock), and probability gain (PG: the ratio of mainshock occurrence rate for predicted space-time to background occurrence rate).

### 3. Data and Results

By applying the above method to the earthquakes cataloged by JMA for the period of 1977 - 2013/06 in the Izu region (33.5N, 138.6E - 35.3N, 139.8E), we obtained the best parameters for foreshocks as  $T_f=3$  days,  $M_f=3.0$ ,  $D=0.2$  degree,  $N_f=3$ , and  $T_a=5$  days for the prediction of mainshocks with  $M \geq 5.0$ . The prediction performance is expressed as  $dAIC=473$ ,  $AR=68\%$  ( $=44/65$ ),  $TR=23\%$  ( $=46/196$ ), and  $PG=225$ . We also confirmed that the distribution of interval time between foreshocks and mainshocks is better approximated by a power law like the modified Omori's aftershock distribution rather than an exponential distribution. The 26% ( $=20/77$ ) of mainshocks that occurred within 5 days after the foreshocks have occurred within 4.8 hours after the foreshock. The distance distribution between foreshocks and mainshocks is also found to be better expressed by a power law. If we focus on the specific region of Off Ito (34.8N, 139.0E - 35.1N, 139.3E) where is one of the most active foreshock region, the prediction performance of the same foreshock definition measured by AR and TR, becomes as better as  $AR=100\%$  ( $=18/18$ ) and  $TR=37\%$  ( $=15/41$ ) with  $dAIC=166$ , and  $PG=105$ . As for the Off Ito region, the JMA have been operating an algorithm for predicting the swarm activity basing on the rate increase of volumetric strain observed near the region. When we compare the timing of issuing the prediction information about the swarm activity by the JMA with that of the occurrence of the foreshock defined above, we find that there is not much difference between them. This means that the foreshock activity in this region is strongly related to the crustal deformation before the mainshock.

Keywords: foreshocks, probabilistic prediction, prediction performance, alarm rate, truth rate, Izu region

## Foreshocks and short-term forecasting: comparisons between real seismicity and synthetic catalogs

OGATA, Yoshihiko<sup>1\*</sup>

<sup>1</sup>The Institute of Statistical Mathematics

Some of the statistical characteristics of foreshocks in the Japan Meteorological Agency (JMA) earthquake catalog are similar to those in synthetic catalogs simulated by the space-time epidemic-type aftershock sequence (ETAS) model or even the space-time nonhomogeneous Poisson process. However, they are quantitatively different from each other. Also, the information gain of a foreshock probability forecasting for real seismicity is significantly larger in comparison with that of synthetic catalogs. We discuss the reasons for such differences between the JMA and the synthetic catalogs.

Keywords: Foreshocks, short-term forecasting, JMA earthquake catalog, synthetic catalogs simulated by ETAS model, statistical characteristics of foreshocks, foreshock probability forecasting

## Modelling the effect of fault geometry on earthquake triggering

GUO, Yicun<sup>2</sup> ; ZHUANG, Jiancang<sup>1\*</sup> ; ZHOU, Shiyong<sup>2</sup>

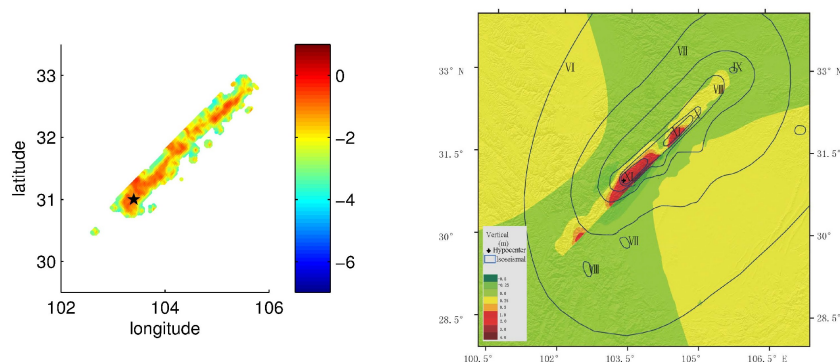
<sup>1</sup>Institute of Statistical Mathematics, <sup>2</sup>School of Earth and Space Sciences, Peking University

This study incorporates the rupture extensions of big earthquakes in the formulation of the Epidemic Type Aftershock Sequence model (ETAS) model, which is a point process model widely applied in the studies of spatiotemporal seismicity, rather than regarding every earthquake as a point in space and time. We apply the new model to the catalog from Sichuan province, China between 1990 and 2013, during which the Wenchuan Mw7.9 earthquake occurred in May 2008. Our results show that the modified model has better performance in both data fitting and aftershock simulation, confirming that the elliptical aftershock zone is caused by the superposition of isotropic triggering effects from each patch of the rupture extension. Also, using the technique of stochastic reconstruction, we found that the direct productivities of aftershocks from each patch on the mainshock fault are positively correlated to the slip distribution. We also confirm that the elliptical aftershock zone is caused by the superposition of isotropic triggering effects from each patch of the rupture extension.

Figure: (Left panel) Reconstruction results of aftershock productivity from each patch of Wenchuan mainshock fault based on the new ETAS model, which considers the rupture extension of large earthquakes instead of regarding all the earthquakes as point source. The values are in the logarithm scale. The Wenchuan mainshock is marked by the black pentagon.

(Right panel) Contour image of the vertical component of the coseismic displacement distribution and isoseismal lines caused by Wenchuan mainshock.

Keywords: earthquake fault, ETAS model, earthquake forecast, aftershock



## History of network detection completeness in Japan

SCHORLEMMER, Danijel<sup>1\*</sup>; HIRATA, Naoshi<sup>2</sup>; ISHIGAKI, Yuzo<sup>3</sup>; NANJO, Kazuyoshi<sup>2</sup>; TSURUOKA, Hiroshi<sup>2</sup>; BEUTIN, Thomas<sup>1</sup>; EUCHNER, Fabian<sup>4</sup>

<sup>1</sup>GFZ German Research Centre for Geosciences, 14473 Potsdam, Germany, <sup>2</sup>Earthquake Research Institute, University of Tokyo, Tokyo 113-0032, Japan, <sup>3</sup>Seismological and Volcanological Department, Japan Meteorological Agency, Tokyo 100-8122, Japan, <sup>4</sup>Institute of Geophysics, ETH Zurich, Zurich, Switzerland

An important characteristic of any seismic network is its detection completeness, which should be considered a function of space and time. Many researchers rely on robust estimates of detection completeness, especially when investigating statistical parameters of earthquake occurrence like earthquake rates. Contrary to traditional approaches, we do not estimate completeness using methods in which the completeness magnitude is defined as the deviation of the frequency-magnitude distribution from the linear Gutenberg-Richter relation. Here, we present a method based on empirical data only: phase data, station information, and the network-specific attenuation relation. For each station of the network we estimate a time-dependent distribution function describing the detection capability depending on magnitude and distance to the earthquake. For each point in time, maps of detection probabilities for certain magnitudes or overall completeness levels are compiled based on these distributions. Therefore, this method allows for inspection of station performances and their evolution as well as investigations on local detection probabilities even in regions without seismic activity.

We present a full history of network detection completeness for Japan and discuss details of this evolution. These results are compared with estimated completeness levels of other methods and with completeness levels in other regions of the World. We present scenario computations showing the impact of different possible network failures. All presented results are published on the CompletenessWeb ([www.completenessweb.org](http://www.completenessweb.org)) from which the user can download completeness data from all investigated regions, software codes for reproducing the results, and publication-ready and customizable figures.

Keywords: catalog completeness, earthquake recording, statistical seismology, earthquake statistics, earthquake forecasting, seismic hazard

## Collaboratory for the Study of Earthquake Predictability & Global Earthquake Model - Testing Center Software Development

BEUTIN, Thomas<sup>1\*</sup> ; LIUKIS, Maria<sup>2</sup> ; MAECHLING, Philip<sup>2</sup> ; MAK, Sum<sup>1</sup> ; SCHORLEMMER, Danijel<sup>1</sup> ; YU, John<sup>2</sup>

<sup>1</sup>GFZ German Research Centre for Geosciences, 14473 Potsdam, Germany, <sup>2</sup>Southern California Earthquake Center, University of Southern California, Los Angeles CA 90089, USA

The Collaboratory for the Study of Earthquake Predictability (CSEP) aims to improve our understanding about the physics and predictability of earthquakes through rigorous and prospective testing of earthquake forecast models. CSEP operates four testing centers in California, New Zealand, Japan, and Europe running prospective, automated evaluations of more than 350 models. These testing centers are the technical infrastructure of CSEP and implement all procedures and protocols for rigorous testing and evaluation of earthquake prediction experiments. These experiments run in various testing regions and comprise forecast periods of one day to many years.

The CSEP testing center software system is the general infrastructure of all CSEP testing centers and is now being used for earthquake early warning systems, geodetic transient detectors, intensity prediction equations, and ground-motion prediction equations. We present the recent developments and introduce the structure of the software system.

Keywords: Earthquake forecasting, Seismic hazard, Statistical seismology, Earthquake statistics, Forecast testing, Software

## Lithospheric stress and deformation, and megathrust prediction

HONG, Tae-kyung<sup>1\*</sup> ; LEE, Junhyung<sup>1</sup>

<sup>1</sup>Yonsei University, Department of Earth System Sciences, Seoul 120-749, South Korea

Lithospheres respond to stress load that is a major cause of earthquakes. Thus, understanding the lithospheric response before and during the megathrusts may allow us to find a way to predict megathrusts. We investigate the lithospheric responses for megathrusts with magnitudes greater than 8.7 since 2000 from precursory and coseismic events. The seismicity presents the cumulation or release of stress before and after megathrust, and discriminative spatial distribution of stress. Normal-faulting earthquakes were increased particularly around large slip regions at shallow depths after the megathrusts, which may be associated with lithospheric rebound and splay-fault development. The earthquake occurrence rate (b value) displays a characteristic slip-dependent feature. The earthquake occurrence rates were decreased with slip amount by forthcoming megathrust due to continuous accumulation of plate-driven stress and tectonic loading around the future rupture planes on slab

surface. The slip dependency of earthquake occurrence rates is enhanced with time until the occurrence of megathrust. The level of seismicity after megathrust is inversely proportional to that before megathrust, yielding the compatible average seismicity before and after megathrust over rupture regions regardless the slip amount of each subregion due to difference of accumulated stress depending the rock properties. It was also observed that the dynamic lithospheric response is highly associated with slip distribution on the rupture plane. Temporal changes of slip-amount-dependent b values are fitted well with an exponential function, suggesting an exponential increase of normal stress with time on locked region until the occurrence of megathrust.

Keywords: lithospheric stress, lithospheric deformation, megathrust, prediction, seismicity

## Global distribution of the earthquake-induced Schumann resonance anomalies

ZHOU, Hongjuan<sup>1\*</sup> ; CAO, Bingxia<sup>1</sup> ; YU, Haiyan<sup>1</sup> ; QIAO, Xiaolin<sup>1</sup>

<sup>1</sup>Harbin Institute of Technology at Weihai, China

Schumann resonance (SR) is a global electromagnetic resonance phenomenon. Recently, SR anomalies before some earthquakes (EQs), which are considered to be concerned with the irregular disturbance of the lower ionosphere above the epicenters, are discovered. Although the examples are limited, we can see that the SR anomalies are usually different for different EQs. This paper concerns with the distinctions of SR anomalies observed at different locations for the same EQ, with the 2011 Magnitude 9.0 Tohoku-Oki EQ in Japan, before which significant SR anomalies have been observed in China, as an example.

Zhou et al. (2013) have found an anomalous SR affect observed at YS and AJ stations of China, associated with the Tohoku-Oki EQ. The anomalies were characterized by an increase in the intensity at frequencies from the first mode to the fourth mode in both magnetic field components, and the abnormal behaviors of the north-south magnetic field component primarily appeared at 0000-0900 UT 3 days prior to the main shock, about 2 h ahead of east-west magnetic field component. The above phenomena are shown in Figures 1 and 2. Figure 1 shows the deviations of the magnetic field amplitudes from the monthly averaged values observed at YS and QJ stations from 1 to 11 March 2011. Figure 2 shows the comparison of the amplitude differences of both magnetic fields on 8 March observed at YS station with 2 standard deviations which is calculated by the spectra over  $\pm 15$  days around 8 March, and the areas where the amplitudes are stronger than 2 standard deviations are marked with white. After the comparative analysis of the disturbed phenomena produced by the selected 10 sites shown in Figure 3 by numerical method with a locally EQ-induced disturbance model of the atmospheric conductivity in the day-night asymmetric Earth-ionosphere cavity, it is concluded that the SR anomalous phenomena before the Tohoku-Oki EQ have much to do with the excited sources located at South America and Asia marked with red circles in Figure 3.

Another 2 observing sites, with Sites 1 and 2 located at ( $N35^{\circ}$ ,  $E137^{\circ}$ ) and ( $N0^{\circ}$ ,  $E110^{\circ}$ ) respectively, are selected besides YS in order to compare the abnormal variations of SR magnetic fields observed at different locations under the same disturbance situation. The same simulation model and method as those in Zhou et al. (2013) are used, and the abnormal variations of both magnetic field spectra of SR observed at 3 sites are shown in Figures 4 and 5, with the source located at SA2 and AS4 as shown in Figure 3 respectively. It is obvious that the differences of the abnormal variations observed at different sites are distinct.

Further, Figures 6 and 7 show the global distributions of the anomalies for the first 3 modes of both SR magnetic field components under the excitation of the source SA2 and AS4 respectively. The color codes stand for the ratio of disturbed amplitude to the regular one, and the regions with green color represent the disturbed ratio lower than 1 and also include the possible nodal points which are the results of the simple model of point sources, while white to dark red colors represent the appearance of SR anomalies. It can be seen that the distribution of SR anomalies is very complicated, and is related to the relative locations of EQ epicenter, lightning currents and the observatories, and of course the EQ-induced disturbance of atmospheric conductivities.

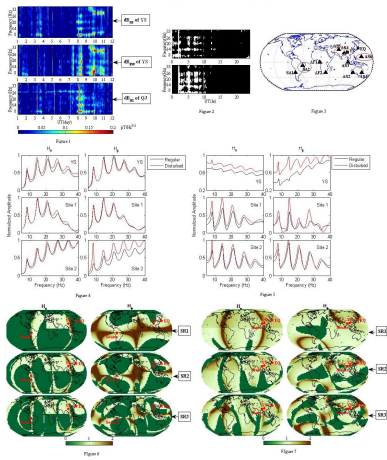
The present simulations are done under the simple models of lightning and disturbed conductivity, which will be improved in the next studies.

**Keywords:** Schumann resonance, Tohoku-Oki earthquake, earthquake-induced Schumann resonance anomalies, day-night asymmetric Earth-ionosphere cavity

SSS01-12

Room:419

Time:May 2 17:15-17:30



## Study on long strike-slip fault model with heterogeneous dynamic stress drops on asperities

OANA, Atsuko<sup>1\*</sup> ; ISHII, Toru<sup>1</sup> ; DAN, Kazuo<sup>1</sup> ; FUJIWARA, Hiroyuki<sup>2</sup> ; MORIKAWA, Nobuyuki<sup>2</sup>

<sup>1</sup>Institute of Technology, Shimizu Corporation, <sup>2</sup>National Research Institute for Earth Science and Disaster Prevention

Oana *et al.* (2013) has established the long strike-slip fault model for a scenario earthquake along the Median Tectonic Line fault zone using the procedure for evaluating the fault parameters by Dan *et al.* (2011), and has simulated the strong ground motions. On that fault model, the dynamic stress drops on the asperities have been homogeneous. However, this is unnatural because the all stress drops on the asperities must be inhomogeneous in the actual earthquakes. How we consider the heterogeneity of the fault rupture is very important subject on the strong motion prediction, because the heterogeneity will have great effects on the spatial distribution of strong ground motions along a fault, especially along a very long fault. The uncertainty of the fault parameters also should be considered into the evaluation of the fault parameters.

In this study, for the strike-slip fault, the procedure for establishing the fault model which takes into account the heterogeneity of the dynamic stress drops on the asperities is examined, and then the spatial strong ground motions are simulated using the fault model based on the procedure. And also, some fault models with the uncertainty of the rupture starting point, the layout of the asperities, and the relationship between the asperity area and the dynamic stress drop on the asperity are established, and then the spatial strong ground motions are simulated using these fault models.

First, the procedure for establishing the fault model to give each asperity the heterogeneous dynamic stress drop is examined. Concretely, first, the probability density distribution of the stress drop is calculated based on the data of the stress drops on the strong motion generation areas of the past earthquakes by previous studies. And then, the procedure is proposed, that gives each asperity the dynamic stress drop corresponding to the frequency of the midpoint of the probability density distribution which is equally divided by the number of the asperity. Here, to satisfy the all relationships among the fault parameters of the asperity model is impossible. So we preceded satisfaction of the relationship formula of the seismic moment, and allowed an error between the obtained short period spectral level and the relationship formula of the short period spectral level. But the error became smaller than about 6 % of the short-period level of the fault model with the homogeneous dynamic stress drops on the asperities. As one of the ideas, we assumed that the relationship between the ratio of the asperity areas and the ratio of the dynamic stress drops on the asperities is random.

Next, for a scenario earthquake along the Median Tectonic Line fault zone, we established the long strike-slip fault model with the heterogeneous dynamic stress drops on the asperities based on the above proposed procedure, and also simulated the strong ground motions by the stochastic Green's function method. As a result, the deviation for the average of the attenuation relation by Si and Midorikawa (1999) of PGA became 0.20 and that of PGV became 0.16. Each deviation is smaller than 0.25, 0.23, which are derived from Si and Midorikawa (1999). It is concluded that this result is relevant, because the attenuation relation is based on a lot of observed records of various earthquakes and sites, while this study targets for the specific earthquake, the local pass, and the local site condition.

Finally, we examined the effect of the uncertainty of the source parameters for the strong ground motions. In the cases of the various rupture starting points, the deviation for the average of the attenuation relation of PGA became 0.23 and that of PGV became 0.21. In the cases of the various layouts of the asperities, those became 0.22 and 0.17, respectively. In the cases of the various relationships between the asperity area and the dynamic stress drop on the asperity, those became 0.20 and 0.17, respectively.

Keywords: Very long fault, Heterogeneity, Strong motion prediction

## Establishing procedure of evaluating fault parameters for predicting strong motions from intra-slab earthquakes with M8

ARAI, Kensuke<sup>1\*</sup> ; DAN, Kazuo<sup>1</sup> ; ISHII, Toru<sup>1</sup> ; HANAMURA, Masaki<sup>1</sup> ; FUJIWARA, Hiroyuki<sup>2</sup> ; MORIKAWA, Nobuyuki<sup>2</sup>

<sup>1</sup>Shimizu Corporation, <sup>2</sup>National Research Institute for Earth Science and Disaster Prevention

For precise prediction of strong motions from intra-slab earthquakes, it is necessary to establish a new procedure of evaluating fault parameters based on the characteristics of intra-slab earthquakes. Although such studies had been conducted by Sasatani et al. (2006) and Dan et al. (2006), procedures of evaluating fault parameters were not fully validated by reproduction of the actual earthquake records. So, Arai et al. (2013) simulated the ground motions of the intra-slab earthquake that occurred off the coast of Miyagi Prefecture on April 7, 2011, and they pointed out the problem of existing procedures of evaluating fault parameters and suggested the ideas to overcome the problem. Hence, in this study, we simulated the ground motion of the intra-slab earthquakes with M8, the 1993 Kushiro-oki earthquake of January 15 (Mw 7.6) and the 1994 Hokkaido Toho-oki earthquake of October 4 (Mw 8.2), using the procedures of evaluating fault parameter proposed by Arai et al. (2013) and we pointed out the problem of the procedure.

In the case of the intra-slab earthquakes of the 1993 Kushiro-oki earthquake and the 1994 Hokkaido Toho-oki earthquake, there was a possibility that the results of evaluation of strong ground motions using the equation of the short period spectral level proposed by Sasatani et al. (2006) or Dan et al. (2006) became too small. So, we tried to use the procedures of evaluating fault parameter proposed by Arai et al. (2013). But, the fault model of the 1994 Hokkaido Toho-oki earthquake was unnatural because the short period spectral level of the earthquake estimated by Morikawa and Sasatani (2004) was too large. For this problem, we developed the new fault model using a method to reduce the fault area while increasing the short period spectral level. We also developed the fault model using a crack model.

We set fault models of the intra-slab earthquakes of the 1993 Kushiro-oki earthquake and the 1994 Hokkaido Toho-oki earthquake, which were derived from the relationships of intra-slab fault parameters by Sasatani et al. (2006), Dan et al. (2006), Arai et al. (2013), and the procedure developed here. And we also set the fault model using a crack model. By using these five fault models, we evaluated strong ground motions by the empirical Green's function method. As a result, in the case of the 1993 Kushiro-oki earthquake, ground motion evaluation results by using Sasatani et al. (2006) and Dan et al. (2006) were smaller than the actual records. On the other hand, ground motion evaluation results by using the Arai et al. (2013), the procedure developed here, and the procedure of using a crack model showed better agreements with the actual records. In the case of the 1994 Hokkaido Toho-oki earthquake, ground motion evaluation results by using Sasatani et al. (2006) and Dan et al. (2006) were smaller than the actual records. And ground motion evaluation results by using Arai et al. (2013), the procedure developed here, and the procedure of using a crack model were larger than the actual records especially in the period of 0.5 seconds or less. This may result from overestimation of the short period spectral level obtained by estimating the S-wave acceleration source spectrum by Morikawa and Sasatani (2004). Actually, the short period spectral level calculated from the fault parameters by Morikawa and Sasatani (2004) is smaller than the short period spectral level obtained by estimating the S-wave acceleration source spectrum. So, we will reconsider the short period spectral level of 1994 Hokkaido Toho-oki earthquake for setting fault models. In this study, we targeted the intra-slab earthquakes of the Pacific Ocean plate. The study on intra-slab earthquakes of the Philippine Sea Plate remains as a future subject.

Keywords: Intra-slab earthquakes, Strong motion prediction, Fault model

## Source effects of the intraslab and interplate earthquakes in Miyagi-ken-oki region based on spectral inversion

KASATANI, Naoya<sup>1</sup> ; KAKEHI, Yasumaro<sup>1\*</sup>

<sup>1</sup>Faculty of Science, Kobe University

Previous studies showed that intraslab earthquakes generate stronger high-frequency waves than interplate earthquakes. For example, Satoh (2004) estimated the high-frequency levels of acceleration source spectra for seven intraslab earthquakes and four interplate earthquakes in Miyagi-ken-oki region. Their result showed the high-frequency level of intraslab earthquake is 3 to 4 times higher than that of interplate earthquake on the average. On the other hand, Katoh et al. (1999) estimated the excitation strength of high-frequency strong motions for intermediate-depth earthquakes based on the peak ground accelerations (PGA). Their result showed the focal depth is a key parameter controlling the PGA amplitudes rather than the difference of tectonic environments, such as intraslab or interplate earthquakes. Thus, the reason for the excitation strength of high-frequency waves of slab earthquake varies among studies, and this problem requires more precise investigation.

In this study, spectral inversion of NIED K-NET strong motion data is done to evaluate source effects of the intraslab and interplate earthquakes in Miyagi-ken-oki region. Then, seismic moments and corner frequencies are estimated from the evaluated source effects, and the high-frequency levels of the earthquakes are determined.

From the comparison between the intraslab and interplate earthquakes, the high-frequency levels of the former are 2 to 3 times higher than those of the latter. On the other hand, from the viewpoint of source depth, a clear trend is found that deeper earthquakes have higher high-frequency spectral levels. Here, it should be noted that the source depths of intraslab earthquakes are systematically larger than those of interplate earthquakes. Additionally, we find no significant difference between the spectral levels of intraslab and interplate earthquakes that have almost the same source depths. This is also seen for the difference between the spectral levels of upper-plane and lower-plane intraslab earthquakes.

Based on these results, we conclude (1) the trend that intraslab earthquakes have higher- high-frequency level than interplate earthquakes is apparent due to the fact that the former have systematically deeper source depths than the latter, and (2) the high-frequency level does not depend on the difference of tectonic environments, such as intraslab or interplate earthquakes, but on the source depth, and deeper earthquakes have higher high-frequency spectral levels. Difference of 4 times is seen between the high-frequency levels of deeper (~80 km depth) and shallower (~30 km depth) earthquakes for the depth difference of ~50 km.

Finally, we pick up two factors, other than source-originated ones, that may effect the evaluation of the high-frequency level: effect of the waveform difference depending on source depth and depth-dependent Q-value structure. These effects are evaluated quantitatively, and we conclude that they cannot bring such biases as can change the above-mentioned trend of the high-frequency level. Thus, we have successfully enhanced the reliability of our interpretation that deeper earthquakes have higher high-frequency spectral levels.

**Acknowledgments:** The strong ground motion data recorded by K-NET, KiK-net, and F-net of National Institute of Earth Science and Disaster Prevention and the hypocenter data of the unified hypocenter catalogue by the Japan Meteorological Agency were used for the analysis.

**Keywords:** spectral inversion, high-frequency level, intraslab earthquake, interplate earthquake, focal depth

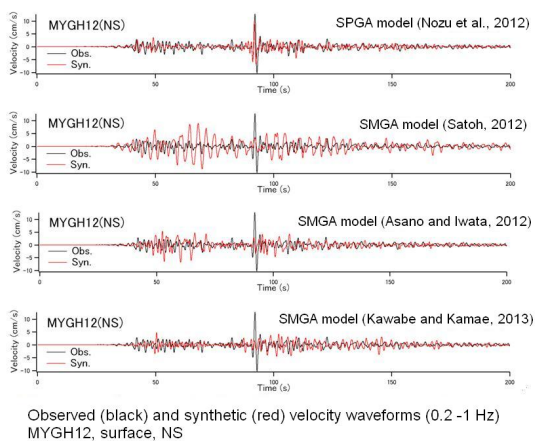
## Comparative study of the performance of source models for the 2011 Tohoku earthquake

NOZU, Atsushi<sup>1\*</sup>

<sup>1</sup>Port and Airport Research Institute

The 2011 Tohoku, Japan, earthquake is obviously the first M9 earthquake which was recorded by dense strong motion networks such as K-NET, etc. Several source models have been proposed to explain strong ground motions from this earthquake. It is significantly important to evaluate the relative performance of these models, especially in the frequency of engineering importance. From engineering point of view, the most striking feature of strong ground motions of the Tohoku earthquake is the generation of strong-motion pulses in the frequency range from 0.2 to 1 Hz observed at many sites along the coast of Miyagi through Ibaraki Prefecture. It is significantly important to consider the generation of such pulses in the strong-motion prediction for mega earthquakes, especially when the prediction is aimed at seismic design of structures. To model strong motion pulses from the Tohoku earthquake, a source model including nine subevents with relatively small size (on the order of several kilometers) was developed (Nozu et al., 2012). The model is called the 'SPGA model'. On the other hand, several 'SMGA models' have been proposed for the same earthquake, in which larger subevents (on the order of several tens of kilometers) are considered. In this study, the errors between the synthetic and the observed ground motions are evaluated for each of these source models. The result clearly indicates that the SMGA model cannot reproduce strong ground motions in the frequency range from 0.2 to 1 Hz, which is characterized by strong-motion pulses. In this frequency range, the performance of the SPGA model is significantly better than the SMGA models. The SPGA model also reproduces the seismic intensity proposed by Sakai et al. (2002), which is in good agreement with the building damage. Based on such results, the author concludes that the SPGA model should be used to calculate strong ground motions for a future mega earthquake as long as the strong motion prediction is aimed at structural safety.

Keywords: mega earthquake, the Tohoku earthquake, source model, strong ground motion, SPGA model, SMGA model



## A pseudo point-source model for off Miyagi intraslab earthquake on May 26, 2003

WAKAI, Atsushi<sup>1\*</sup> ; NAGASAKA, Yosuke<sup>1</sup> ; NOZU, Atsushi<sup>1</sup>

<sup>1</sup>Port and Airport Research Institute

In a recent research, a pseudo point-source model, which is a simplified version of the conventional characterized source model, was proposed and it was verified that the source model can be applied to the 2011 Tohoku earthquake, Japan. In the source model, the spatio-temporal distribution of slip within each subevent is not modeled. Instead, the source spectrum associated with the rupture of each subevent is modeled. For the future application of the source model, it is important to investigate its applicability to other destructive earthquakes.

In this study, the off Miyagi intraslab earthquake on May 26, 2003 is taken as an example, and the applicability of the pseudo point-source model is investigated. It was revealed that the source model can reproduce the waveforms and the Fourier spectra at least as well as the conventional characterized source model.

Keywords: pseudo point-source model, intraslab earthquake, strong ground motion, the 2003 off Miyagi earthquake

## Strong ground motion simulation for the July 23, 2005 northwestern Chiba earthquake by pseudo point-source model

NAGASAKA, Yosuke<sup>1\*</sup>; NOZU, Atsushi<sup>1</sup>; WAKAI, Atsushi<sup>1</sup>

<sup>1</sup>Port and Airport Research Institute

We propose a pseudo point-source model (Nozu, 2012) of the July 23, 2005 northwestern Chiba earthquake. The model is developed for the benchmark test (Hisada *et al.*, 2013) in which various strong ground motion generation methods are compared.

In the pseudo point-source model, detailed spatiotemporal slip distributions within a subevent are not considered. Instead, the source spectrum associated with the rupture of each subevent is specified and it is assumed to follow the omega square model. This model has been applied for some earthquakes and shows good agreement with observations.

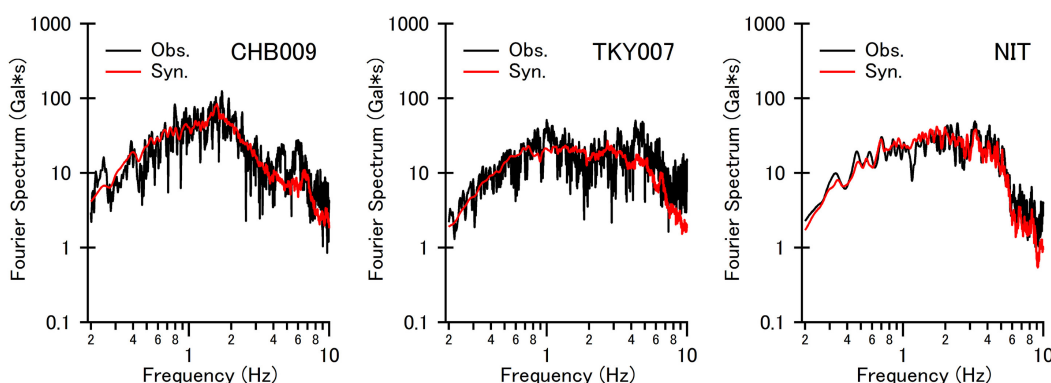
With this simplification, each subevent involves only six parameters, namely, longitude, altitude, depth, seismic moment, corner frequency and rupture time. In addition to these parameters, strike, dip and rake angles of the subevent are considered in this study in order to investigate the effect of radiation pattern while average value has been used in the previous studies. In this study, it is assumed that the theoretical radiation pattern becomes less evident with the increase of the hypocentral distance divided by the wavelength. This means that when the hypocentral distance is large of the wavelength is short, the radiation pattern is close to the average value rather than the theoretical value and vice versa. A new parameter  $Q_R$  is introduced to express this effect that determines how slowly the radiation pattern converges to the average.

The parameters for this particular earthquake are determined as follows. The hypocenter and the mechanism are from Koketsu and Miyake (2005). The seismic moment ( $=9.11 \times 10^{17} \text{Nm}$ ), the density ( $=3.2 \text{g/cm}^3$ ) and the S wave velocity ( $=4.46 \text{km/s}$ ) in the source region are from the F-net. The corner frequency ( $=0.75 \text{Hz}$ ) and  $Q_R (=10\pi)$  are determined so that the synthetic velocity waveforms and the Fourier spectra become consistent with the observations.

The site amplification factor for the K-net or KiK-net sites is from Nozu and Nagao (2005). For other sites (Building Research Institute and UR sites), the site amplification factors are newly determined by using the spectral ratio of the observed records between the target site and neighboring K-net or KiK-net stations. In terms of the Fourier phase information, we pick up 3 earthquakes before the main shock and chose the best one for each site.

As an example of the result, the synthetic Fourier spectra at 3 sites are compared with the observations (see the Figure).

Keywords: pseudo point-source model, benchmark test, the 2005 northwestern Chiba earthquake, radiation pattern, site amplification factor



Comparison of acceleration Fourier spectrum  
(CHB009 and TKY007: K-NET station, NIT: BRI station)

## Three-dimensional grid modeling based on analysis of borehole data

KIMURA, Katsumi<sup>1\*</sup> ; HANASHIMA, Yuki<sup>2</sup> ; NISHIYAMA, Shoichi<sup>3</sup> ; ISHIHARA, Yoshiro<sup>4</sup> ; SEKIGUCHI, Haruko<sup>5</sup>

<sup>1</sup>AIST, Geological Survey of Japan, <sup>2</sup>Smart Solution Corporation, <sup>3</sup>OYO Corporation, <sup>4</sup>Fukuoka University, <sup>5</sup>Kyoto University

The article presents a 3D geologic modeling method and applies it to build a subsurface 3D geologic model in the northern Tokyo and southern Nakagawa lowlands and the adjacent upland area. The modeling method, using borehole data for ground survey consists of (1) the surface modeling of the base of the Chuseki-so (the latest Pleistocene to Holocene incised-valley fill) , which has been improved by interpolating borehole data and (2) the 3D grid modeling of lithofacies and *N*-values constrained by the above surface model. The 3D grid model is very useful for not only geologic expression, but also the ground model of seismic response characteristics, because this can be converted to be S-wave velocity and density models.

Keywords: 3D model, ground, grid model, basal surface of the Chuseki-so, Tokyo lowland, borehole data

## Three-dimensional structure model for modeling strong motion around the Ryukyu arc

FUJIOKA, Akira<sup>1</sup> ; TAKENAKA, Hiroshi<sup>2\*</sup> ; YAMADA, Nobuyuki<sup>3</sup> ; NAKAMURA, Takeshi<sup>4</sup> ; OKAMOTO, Taro<sup>5</sup> ; FUJIWARA, Hiroyuki<sup>6</sup>

<sup>1</sup>Kyushu Univ., <sup>2</sup>Okayama Univ., <sup>3</sup>Kyushu Univ. of Education, <sup>4</sup>JAMSTEC, <sup>5</sup>Tokyo Institute of Technology, <sup>6</sup>NIED

The Ryukyu Islands have frequently been damaged by large earthquakes and tsunamis since ancient times. For instance, in 1771, gigantic tsunamis are occurred from an earthquake and more than 12000 people died in Yaeyama Islands. From the point of view of disaster prevention, it is also important to improve the precision of strong ground motion prediction. Here we build a 3D numerical structure model for modeling of strong ground motion, which includes land and ocean-bottom topographies and a seawater layer as well as subsurface structures of the arc side and the PHS slab, partially based on the J-SHIS model for near-surface structure (NIED) and a slab-top depth model of the PHS (Headquarters for Earthquake Research Promotion, Japan). We then try to improve the near-surface structure model in the islands using our original microtremor surveys. We also conduct numerical simulations of seismic motions for three sub-oceanic earthquakes occurring near the Amami Islands, Okinawa Island and Miyako Island to confirm the applicability of the constructed structure model and to check the improvement of the near-surface model.

Keywords: Ryukyu arc, strong motion, simulation

## 3-D sedimentary layers model and simulation of seismic motions around the Tachikawa fault zone

SAGUCHI, Koichiro<sup>1\*</sup> ; CHIMOTO, Kosuke<sup>1</sup> ; YAMANAKA, Hiroaki<sup>1</sup>

<sup>1</sup>Interdisciplinary Graduate School of Science and Engineering, Tokyo Institute of Technology

Tachikawa fault is one of the most activity faults in the western part of the Tokyo metropolitan area. Strong motion estimation is necessary to know the possible damage due to rupture of the fault considering effects of geological structure. However, a three-dimensional subsurface structural model is not well tuned in the vicinity of the fault.

In this study, we estimated a three-dimensional structure of deep sedimentary layers around the Tachikawa fault zone using Rayleigh wave phase velocity and horizontal-to-vertical spectrum obtained from microtremor explorations and receiver functions from the obtained records of the K-NET, KiK-net and SK-net. And we simulated seismic ground motions around the Tachikawa fault zone using the three-dimensional finite difference method to validate of a three-dimensional structure of deep sedimentary layers.

To accomplish it, we first conducted the array observations of microtremors at 12 sites around the Tachikawa fault. Rayleigh-wave phase velocity at periods from 0.5 to 5.0 seconds was estimated from a frequency-wave number spectral analysis of the microtremors. We next conducted the observations of microtremors at 268 sites on nine lines across the Tachikawa fault zone. Predominant periods of the H/V spectrum clearly indicated differences of subsurface structure across the Tachikawa fault.

Then, we conducted the joint inversion of the phase velocity and the receiver function to a P and S-wave velocity profile based on the simulated annealing method. P-wave velocities, S-wave velocities and thickness of individual layers are inverted very well, and the S-wave velocities of the inverted profile are 0.5, 0.9, 1.5, 2.4 and 3.2km/s. We constructed a three-dimensional structures of the deep sedimentary layers in this area from integrating the 1-D S-wave velocity profiles at all the stations. The basement depth at hanging-wall side of the Tachikawa fault is larger than that at foot-wall side with a difference of about 1.7km in the 3-D model.

Finally, we simulated seismic ground motions around the Tachikawa fault zone using the three-dimensional finite difference method considering three-dimensional velocity structure down to 50km. The results indicate that the maximum accelerations in simulated waveforms were similar to the observed one.

Keywords: Tachikawa fault zone, array microtremor exploration, Rayleigh wave phase velocity, 3-D sedimentary layers model, 3-D finite difference method

## DETERMINATION OF S-WAVE VELOCITY STRUCTURE BY MICROTREMOR ARRAY OBSERVATION IN TEKIRDAG AND ZEYTINBURNU (TURKEY)

KARAGOZ, Ozlem<sup>1\*</sup> ; CITAK, Seckin ozgur<sup>2</sup> ; CHIMOTO, Kosuke<sup>1</sup> ; YAMANAKA, Hiroaki<sup>1</sup> ; OZEL, Oguz<sup>3</sup> ; YALCINKAYA, Esref<sup>3</sup> ; ZANEIH, Hussam<sup>1</sup> ; ASKAN GUNDOGAN, Aysegul<sup>4</sup> ; KAOURU, Kojima<sup>1</sup> ; TOMOHIRO, Tsuchiya<sup>1</sup> ; AKSAHIN, Behiye<sup>3</sup> ; ILKAY, Sena<sup>3</sup> ; SISMAN DERAN, Fatma<sup>4</sup>

<sup>1</sup>Interdisciplinary Graduate School of Science and Engineering, Tokyo Institute of Technology, <sup>2</sup>Japan Agency for Marine-Earth Science and Technology (JAMSTEC), <sup>3</sup>Istanbul University, Department of Geophysical Engineering, Turkey, <sup>4</sup>Middle East Technical Uni., Dept. of Civil Engineering and Dept. of Earthquake Studies, Turkey

The use of environmental vibration recordings (microtremors) is cost effective and easily collected data for site characterization that is a component of microzonation mapping and has become very popular around the world in the last years.

Local site conditions have a major effect on the level of ground shaking. For this reason we carried out microtremor measurements by using circular small array configuration at twenty one locations in Tekirdag, four locations in Zeytinburnu and one location in Yesilkoy. In addition to eight large array measurements for estimating S-wave velocity structures of shallow deeper soil formations for site effect analysis. These sites were selected by considering the different geological units (i.e. recent landfill, clay stone, silt stone, alluvium, lime stone, sand) in the cities. We also collected data on five buildings in Tekirdag in order to understand dynamics properties of buildings.

We estimated the phase velocities of Rayleigh waves at each site from the vertical components of recorded microtremor data by using Spatial Autocorrelation (SPAC) method. Obtained phase velocity dispersion curves are varied from area to area. The obtained phase velocities range from 100 m/s to 750 m/s along the coastline in Tekirdag while, they range from 200 m/s to 500 m/s for Zeytinburnu area.

Genetic Simulated Annealing Algorithm technique was applied for inversion of phase velocities to estimate 1-D S-wave velocity structures beneath the sites. The inverted Vs profiles are not uniformed. The preliminarily results show that similar phase velocity changes have been seen at the low and the high periods on the different geological units along the parallel direction of the coastline. When we check the velocity changes from coastline toward the inland, we can see the different phase velocities on the different geological units.

Keywords: Microtremor, Spac, S-wave velocity, Tekirdag, Zeytinburnu, Turkey

## Characteristics of long-period strong ground motion in the Keihin-area during the 2011 Tohoku earthquake

UETAKE, Tomiichi<sup>1\*</sup>

<sup>1</sup>Tokyo Electric Power Company

The velocity response spectra of 5% damping calculated from the observed data in the Keihin area during the 2011 Tohoku Earthquake had no significant peak at period of around 8 s and had peak over 100cm/s at period of around 3 s. The acceleration seismograms had spindle-shaped envelope and peak accelerations were recorded about 120 s after S-wave on-set. The maximum velocity response at period of around 3 s was recorded in the first half part of waveforms. It is important to realize the difference of wave propagation characteristics between in the first half part and the later part of the waveforms. In this article, the propagation characteristics of long-period strong ground motions during the 2011 Tohoku Earthquake were studied by semblance analysis using the data observed in the Keihin area.

Sixteen strong motion observatories in the Keihin area were used for array analysis. The major axis of the array area is about 18 km and minor axis is about 9km. Distance between adjacent observation points is from 0.6km to 5km. We performed semblance analysis using narrow-band pass filtered waveforms and evaluated the phase velocity for each time sections from the peak point of semblance in slowness plane. The center periods of the filters were 1, 2, 2.5, 3, 4, 5, 6, 7, 8, 9, 10, 12, 15 and 20 s. The length of time window for analysis was 20 s and the time windows were opened every 10 s in wave traces.

The peak semblance values were high for longer period waveforms and were lower value for short period waveforms. The value at period of 1 and 2s were lower than 0.5. The values calculated from large array data were lower than those from small array data. The semblance values in first part of waveform were high but the values in the later part show lower value. The phase velocities in first half part are over 3 km/s for all case. The phase velocities in later part were 1 to 2 km/s and showed the dispersion characteristics. The back azimuths of wave propagation in the first part indicated the epicenter direction but those in later part did not indicate constant direction especially in short period range.

To examine the relation between this dispersion characteristics and underground structure, we calculated phase velocities of surface waves using the underground structure model. The phase velocities evaluated in the first part were faster than phase velocity of the fundamental mode. The phase velocities evaluated for several last time windows in the later part coincided with the phase velocity of the fundamental mode. These characteristics are similar to the results from the data observed the Tokyo lowland area [Uetake (2013)].

Judging from the property of the acceleration waveform and a result of the semblance analysis, the waves caused large response in a period of 2-3 s were more likely to be a body wave not a surface wave of the fundamental mode.

The strong ground motion data used in this study were observed by TEPCO, K-NET of NIED, ERI, JMA, Tokyo Metropolitan office and Yokohama-City. I appreciate these organizations for making the data be available.

Keywords: Long-period strong ground motion, the 2011 Tohoku earthquake, Semblance analysis, Phase velocity, Keihin area

## Characteristics of Long-period Ground Motion in the Osaka Sedimentary Basin due to the 2011 Great Tohoku Earthquake

SATO, Kayoko<sup>1\*</sup> ; IWATA, Tomotaka<sup>1</sup> ; ASANO, Kimiyuki<sup>1</sup> ; KUBO, Hisahiko<sup>1</sup> ; AOI, Shin<sup>2</sup>

<sup>1</sup>Disaster Prevention Research Institute, Kyoto University, <sup>2</sup>National Research Institute for Earth Science and Disaster Prevention

The 2011 great Tohoku earthquake (Mw 9.0) occurred on March 11, 2011, and the largest aftershock (Mw 7.7) occurred in the Ibaraki-oki region, adjacent to south boundary of the mainshock's source region. Long-period ground motions (2-10s) of large amplitude were observed in the Osaka sedimentary basin about 550-800km away from the source regions during both events. We collected the strong motion records in and around the Osaka basin and analyzed the long-period ground motions. The amplitude of horizontal components of the ground motion at the site-specific period is amplified at each sedimentary station and its duration is prolonged. The predominant period is around 7s in the bayside area inside the Osaka basin where the largest pSv among the stations inside the Osaka basin were observed. The pSvs at the bedrock sites surrounding the Osaka basin also have their peak values around 7s.

Then, we focus on the propagation characteristics from the source region to the Osaka basin. We compared the pSvs of 7s at the sedimentary stations in the Osaka basin with those in the Kanto basin. The maximum pSv among the Osaka basin is comparable to the maximum pSv among the Kanto basin whose fault distance is about 500km nearer than the Osaka basin. Moreover, the amplitude of observed pSvs is systematically larger than prediction from the empirical attenuation relationship by Kataoka et al. (2008) at non-sedimentary stations in the region between the Nobi and Osaka basins. The large long-period ground motions in the Osaka basin might be generated by the combination of propagation-path and basin effects.

Thus, we simulate ground motions due to the largest aftershock using the three-dimensional Finite Difference Method (GMS; Aoi and Fujiwara, 1999). The reason we use the largest aftershock is that this event has a relatively small rupture area and simple rupture process compared to the mainshock. The size of the model space is 730km (EW) x 330km (NS) x 100km (Vertical) including the source region and the Osaka basin. A three-dimensional velocity structure model based on the Japan Integrated Velocity Structure Model (Koketsu et al., 2008, 2012) is assumed. The minimum S-wave velocity is 350m/s and the grid spacing in the sedimentary layers is 200m for horizontal direction and 100m for vertical direction, respectively. The minimum effective period in this computation is 3s. We estimated a point source using the long-period ground motions (4-10s) at a station close to the source region (KiK-net CHBH14) and used it for our simulation.

We compared the synthetic and observed waveforms in the periods of 4-10s. As well as the observed ones, the amplitude of synthetic waveforms was amplified and the durations were prolonged at the sedimentary stations in the Kanto basin, the Nobi basin and the Osaka basin. The feature of the attenuation relations in the region between the Nobi basin and the Osaka basin was qualitatively reproduced. At the period of 7s, the amplitudes of synthetic waveforms were little underestimated in the Osaka basin.

Finally, we simulate the ground motion during the mainshock. The model space is 730km (EW) x 400km (NS) x 100km (Vertical). The grid interval and velocity structure model are same as those for the largest aftershock. We assume two point sources based on the two southern SMGAs of the four SMGAs estimated by Asano and Iwata (2012). As a result of the simulation, the synthetic waveforms reproduced the observed ones qualitatively. Therefore, we conclude that the large long-period ground motions in the Osaka basin during both events mainly resulted from the combination of those two SMGAs, propagation-path and basin effects.

### ACKNOWLEDGEMENTS

We used strong motion data recorded by K-NET, KiK-net and F-net of NIED, CEORKA, BRI, JMA, and Osaka prefecture. GMS provided by NIED is used for the computation.

## Long-period ground motion evaluation for the Nankai Trough megathrust earthquakes

MAEDA, Takahiro<sup>1\*</sup> ; MORIKAWA, Nobuyuki<sup>1</sup> ; AOI, Shin<sup>1</sup> ; FUJIWARA, Hiroyuki<sup>1</sup>

<sup>1</sup>NIED

We evaluate long-period ground motions associated with the Nankai Trough earthquakes (M8~9) in southwest Japan. Large interplate earthquakes occurring around the Nankai Trough have caused serious damages due to strong ground motions and tsunami. Such large interplate earthquake potentially causes damages to high-rise and large-scale structures due to long-period ground motions. The long-period ground motions are amplified particularly on sedimentary basins, where big cities have been established. Therefore it is important to evaluate long-period ground motions as well as strong motions and tsunami for the anticipated Nankai Trough earthquakes.

The long-period ground motions are evaluated by the finite difference method (FDM) using “ characterized source models ” and the 3-D underground structure model. The parameters of the characterized source model are determined based on a “ recipe ” for predicting strong ground motion [Earthquake Research Committee (ERC), 2009]. We construct various source models (more than 300 scenarios) assuming various possible source parameters, including rupture area, asperity configuration, and hypocenter location. Each source region is determined by “ the long-term evaluation of earthquakes in the Nankai Trough ” published by ERC. The asperity configuration and hypocenter location control the rupture directivity effects. These parameters are important because our preliminary simulations are strongly affected by the rupture directivity (Maeda et al., 2013). We apply the system called GMS (Ground Motion Simulator) for simulating the seismic wave propagation based on 3-D FDM scheme using discontinuous grids (Aoi and Fujiwara, 1999) to our study. The 3-D underground structure model used in the FD simulation is the Japan integrated velocity structure model (ERC, 2012).

We evaluate the long-period ground motions using the peak ground velocity (PGV) and velocity response spectra (Sv). The simulation shows a large variation of PGV and Sv at a site. The large variation is important to understand the seismic hazard. The variation at the Kanto region, an eastern extension of the source area, seems larger than those at the Nobi and Osaka regions. The scenarios with wider source area have larger PGV and Sv than those with smaller source area. The large number of simulations of this study allows us to select scenarios that correspond to representative (e.g. average and maximum) response spectra at each site.

Keywords: Nankai Trough, long-period ground motion, megathrust earthquake, hazard assessment, GMS

## Long-period ground motion evaluation for the Sagami Trough megathrust earthquakes

MORIKAWA, Nobuyuki<sup>1\*</sup> ; MAEDA, Takahiro<sup>1</sup> ; IWAKI, Asako<sup>1</sup> ; IMAI, Ryuta<sup>2</sup> ; AOI, Shin<sup>1</sup> ; FUJIWARA, Hiroyuki<sup>1</sup>

<sup>1</sup>National Research Institute for Earth Science and Disaster Prevention, <sup>2</sup>Mizuho Information & Research Institute, Inc.

It is important to assess seismic hazard in consideration of uncertainty and occurrence frequency in order to mitigate disasters from future earthquake. Iwaki et al. (2013) examined the influence of the long-period ground motion on uncertainty of asperity (strong motion generation area) or hypocenter location, and the heterogeneity of rupture velocity or slip direction for megathrust earthquakes occurring at the Sagami Trough region. They showed that the asperity or hypocenter location largely affects to the amplitude and predominant period of simulated long-period ground motions. Based on their results, we simulate long-period ground motions by a large number of source models considering the uncertainty of asperity or hypocenter location, and we try to assess long-period ground motion due to megathrust earthquakes occurring at Sagami Trough by evaluating the simulation results statistically.

We set ten source regions containing Taisho and Genroku earthquakes by changing those from Iwaki et al. (2013) referring the model by Central Disaster Council (2013). The range of moment magnitude ( $M_w$ ) is 7.9 to 8.6 and total number of source model is more than 150. We use a "characteristic source model" and source parameters are evaluated by following the method in "Recipe" by Headquarters of Earthquake Research Promotion of Japan. We use a velocity structure model by Earthquake Research Committee (2012) but we revise the topography of the Philippine Sea plate based on recent researches. The long-period ground motions are simulated using a 3D finite difference method with discontinuous grid coded by Aoi and Fujiwara (1999). As long-period-ground motion hazard assessment, we first calculate average and slightly large (i.e. +1 sigma; sigma is the standard deviation) amplitude of peak velocity and velocity response spectrum whose natural period is 5, 7 and 10 seconds respectively on engineering bedrock for every ten source region. And then we integrate them by assuming the "weight" which corresponds to occurrence frequency of each source region.

Although a large number of source models are set up in this study, the uncertainty on the megathrust earthquake occurring at Sagami Trough cannot be covered completely. So it should be required to examine much source models. On the other hand, the source region of magnitude 8-class earthquake at Sagami Trough extends to beneath the metropolitan area. In addition, it is said that the occurrence of the magnitude 7-class earthquake, which does not take in this study, is imminent in southern Kanto region. It is necessary to advance broadband ground motion hazard assessment also including a short-period ground motion.

Keywords: long-period ground motion, seismic hazard assessment, Sagami Trough, megathrust earthquake, GMS

## Empirical ground motion model for long period motions and for long distance -Distance dependent geometrical spreading term

MOTOKI, Kentaro<sup>1\*</sup> ; KATO, Kenichi<sup>1</sup>

<sup>1</sup>Kobori Research Complex Inc.

The GMPEs have been proposed by Sato et al.(2012), Kataoka et al.(2008), and Yuzawa and Kudo(2011). For predictions of long period ground motions on Kanto Plain for the Nankai Trough mega earthquake, the proposed GMPEs cannot be adopted because of the deficiency of applicable distance ranges. In order to establish an adoptable GMPE for long distance, we investigate the distance dependent geometrical spreading term.

We used records for magnitude equal to or greater than 5.0 and distance less than 1000 km. The dataset used in this study is provided by F-net, because of high sensitivity for long period motions and continuous recordings. Since the F-net stations can be regarded as hard rock sites, the site term was not taken into account in the regression.

First, we use a constant geometrical spreading and anelastic attenuation for distance. The regression curve at the 20sec of period decays more slowly than the average of records in the short distance less than 100km, and decays more steeply than records in the longer distance. It implies that the GMPE with a constant geometrical spreading term may underestimate near the source region and in the longer distance.

In the long period range, the dominance of seismic wave changes from the body wave to the surface wave according to the travelling distance, and the slope of the geometrical spreading depends on distance. We will evaluate the geometrical spreading term in the separated distance range to reveal how the geometrical spreading changes.

Keywords: long period motions, long distance, geometrical spreading

## Long-Period Ground Motion Prediction Equations and Their Application to the Magnitude Estimation of Large Earthquakes

IBRAHIM, Rami<sup>1\*</sup> ; SI, Hongjun<sup>1</sup> ; KOKETSU, Kazuki<sup>1</sup> ; MIYAKE, Hiroe<sup>1</sup>

<sup>1</sup>Earthq. Res. Inst., Univ. Tokyo

We developed long-period ground motion prediction equations (GMPEs) for peak ground velocities (PGVs) and peak ground displacements (PGDs) in a period range of 5-30 s. We only used strong motion data of KiK-net downhole stations located in layers of shear-wave velocities equal to or greater than 2000 m/s. We confirmed that the site effects due to surface geology for long-period PGVs and PGDs can be ignored at these observation stations. The dataset consists of 20 earthquakes of  $6 \leq M_w \leq 9.1$  occurred in and around Japan. Two-stage regression analyses were carried out to derive the GMPEs. We fit the data with bilinear regression lines bending at  $M_w$  7.5. Additional factors of focal depth and earthquake type were found to enhance the fitting with the observed data. Our developed long-period GMPEs predict the PGVs and PGDs of crustal earthquakes are larger than those of inter-plate and intra-plate earthquakes. The attenuation coefficients presented in the current study indicate that the long-period PGVs and PGDs increase by increasing depth.

We used the long-period GMPEs developed in this study to estimate the moment magnitude by fitting observed PGVs and PGDs at period range of 5-30 s with GMPEs. We estimated the magnitudes of the same 20 earthquakes and the 2013 Awaji Island earthquake ( $M_w$  5.8) recorded by downhole accelerometers of KiK-net. The results are consistent with the moment magnitudes from the Global CMT project. The method is useful to estimate the magnitude of giant earthquakes such as the 2011 Tohoku earthquake ( $M_w$  9.1). The proposed method can estimate the moment magnitude quickly if information of source area is available.

Keywords: long-period ground motion, ground motion prediction equation, moment magnitude, PGV, PGD

## Evaluation of random errors of displacements and velocities from strong motion records

XU, Peiliang<sup>1\*</sup>

<sup>1</sup>Disaster Prevention Research Institute, Kyoto University

Strong motion accelerographs have been deployed worldwide to monitor the ground shaking of the Earth and the recorded accelerograms have been used to recover the velocities and displacements by integration. In spite of their fundamental importance in seismology and earthquake engineering, few works address the error estimates of the derived velocities and displacements. Although accelerographs have been used to compute velocity and displacement waveforms for more than 80 years, we show that no publications on error estimates of computed velocity and displacement waveforms are correct from the statistical point of view. We show that the error estimates of the velocities and displacements obtained from accelerograms in the earthquake literature approach to zero as the sampling interval of accelerographs tends to zero; these are erroneous from the statistical point of view. As a result, we present a set of formulae to correctly estimate the errors (or variances) of the integrated velocities and displacements from accelerograms. In addition, we also derive the covariances between the velocities and displacements.

Evaluation of random errors of displacements and velocities from strong motion records

Peiliang Xu  
Disaster Prevention Research Institute, Kyoto University  
13, Kyoto 611-0001, Japan  
E-mail: [peiliangxu@dpri.kyoto-u.ac.jp](mailto:peiliangxu@dpri.kyoto-u.ac.jp)

### Abstract

Strong motion accelerographs have been deployed worldwide to monitor the ground shaking of the Earth and the recorded accelerograms have been used to recover the velocities and displacements by integration. In spite of their fundamental importance in seismology and earthquake engineering, few works address the error estimates of the derived velocities and displacements. Although accelerographs have been used to compute velocity and displacement waveforms for more than 80 years, we show that no publications on error estimates of computed velocity and displacement waveforms are correct from the statistical point of view. We show that the error estimates of the velocities and displacements obtained from accelerograms in the earthquake literature approach to zero as the sampling interval of accelerographs tends to zero; these are erroneous from the statistical point of view. As a result, we present a set of formulae to correctly estimate the errors (or variances) of the integrated velocities and displacements from accelerograms. In addition, we also derive the covariances between the velocities and displacements.

## Earthquake detection from strong ground motion observation network in Himalaya, India

MASUDA, Tetsu<sup>1\*</sup> ; KOKETSU, Kazuki<sup>1</sup> ; TAKANO, Kiyoshi<sup>2</sup> ; FURUMURA, Takashi<sup>2</sup> ; OKI, Satoko<sup>3</sup> ; ITO, Takamori<sup>3</sup> ; CHADHA, Rajender kumar<sup>4</sup> ; SRINAGESH, Davuluri<sup>4</sup> ; SRINIVAS, Dakuri<sup>4</sup>

<sup>1</sup>Earthquake Research Institute, <sup>2</sup>University of Tokyo, <sup>3</sup>Keio University, <sup>4</sup>National Geophysical Research Institute

It is an important subject to establish the technical issues and environment of data acquisition and analysis of natural hazards for the disaster mitigation, the first aid and recovery planning. The Indo-Japanese collaborative project on 'Information Network for Natural Disaster Mitigation and Recovery' of 'Science and Technology Research Partnership Sustainable Development International Collaborative Research Program' supported by JST and JICA, Japan initiated strong ground motion observation, crustal movement measurement, and building vibration measurement in Indo-Gangetic plain and foot hills of Himalaya, India.

We started the strong ground motion observation network with deployment of broadband velocimeters and digital equipments at 26 sites near the seismic active region in Himalaya, India by October 2012. The continuous time history of ground motion is digitally recorded with high resolution. Because of the broadband response of the sensor and the high resolution of the recorder, it is expected that the long- period motions or weak ground motions from small local earthquakes and distant earthquakes will be recorded as well as the short-period strong ground motions. It is a necessary task for the seismic data analysis to detect earthquakes using continuous records from the network. In this paper, we present a method developed for fast and precise earthquake detection from continuous records of the network.

The stations of the network are located in the compounds of local schools. The ambient noise is not always low but it changes as well as contains abrupt increases. We developed a detection method with simple algorithm adequate for the noisy circumstances. We compared our detections with the earthquakes reported in the NEIC catalogue. Our results show that the network detected all earthquakes of magnitude 7 or more, more than 90% of magnitude 6.5 through 6.9, more than 50% of magnitude 6.0 through 6.4 regardless of epicentral distances, and more than 80% of magnitude 6 or more from epicentral distances less than 100 degrees.

Several local earthquakes with short S-P times which were not reported in the NEIC catalogue were also detected by the network. Local seismicity is an index of the stress status, and detection of local earthquakes is important to understand the stress distribution in a small region. The preliminary results show that the network will provide data from local and global earthquakes to study the local seismic activity in the Himalayan region, the propagation path effects from the source to the stations, amplification effects at sites, the physical process of the seismic source, and subsurface velocity structure.

Keywords: strong ground motion, observation, network, earthquake detection

## Liquefaction damage expansion caused by the generation of surface waves from base end section

NAKAI, Kentaro<sup>1\*</sup> ; NODA, Toshihiro<sup>1</sup> ; MURASE, Kotaro<sup>1</sup> ; ASAOKA, Akira<sup>2</sup> ; SAWADA, Yoshihiro<sup>2</sup>

<sup>1</sup>School of Engineering, Nagoya University, <sup>2</sup>Association for the development of earthquake prediction

The 2011 off the Pacific coast of Tohoku Earthquake caused liquefaction to occur in reclaimed lands in Urayasu City and in other wide areas of reclaimed land along Tokyo Bay. One of the important characteristic of the observed liquefaction damage is that the level of liquefaction damage was nonuniform spatially, and the variation in the damage levels was large. The difference in damage levels in various parts has often been explained by the presence/absence of past ground improvement and by the difference in the dates of reclamation work. From the boring survey at Urayasu, thin layer of soft alluvial clay is located directly under the liquefiable layer on the inland side where liquefaction damage was small. However, the basement layer is inclining towards coast side and alluvial clay layer is increasing in thickness as approaching to the coast where liquefaction damage was severe. This paper examines the cause of extensive and nonuniform liquefaction damage observed in Urayasu City by focusing attention on the stratum inclination at the deeper part of the liquefiable layer with the use of 2D elasto-plastic seismic response analysis of the multi-layer ground. The analysis code employed in this report was the soil-water coupled finite deformation analysis code GEOASIA (Noda et al. 2008), which incorporates an elasto-plastic constitutive model (SYS Cam-clay model; Asaoka et al. 2002) that allows description of the behavior of soils ranging from sand through intermediate soils to clay under the same theoretical framework.

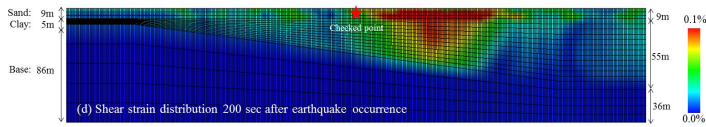
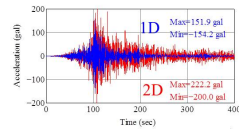
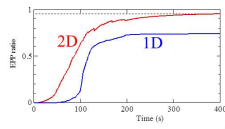
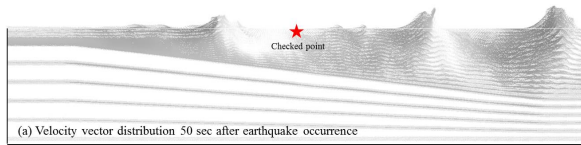
Fig.1 (a) illustrates the velocity vector distribution 50 sec after earthquake occurrence. Only the area around the sloped part is shown in this figure, and the scale in the vertical direction has been magnified by 2 times. Surface waves generate at the base end section of the inclination which shows orbit in a counterclockwise direction with ongoing wave propagation to the right-hand side. Excess pore water pressure ratio at the liquefiable layer is shown, superimposing the result of 1D analysis with same stratigraphic composition at the point. 2D analysis result shows liquefaction (excess pore water pressure ratio is greater than 0.95), even 1D analysis did not liquefy (Fig.1 (b)). In the case of 2D analysis, in addition to the magnitude, duration time of the oscillation increases in subsurface layer accompanied by the generation of surface waves (Fig.1 (c)). Excess pore water pressure ratio of 2D analysis continues to increase for a long period even after the primary earthquake motion. Fig.1 (d) illustrates the shear strain distribution 200 sec after earthquake occurrence. Although shear strains are small in the non-inclined horizontal strata, large strains are produced in the subsurface liquefiable layer. Furthermore, this strain distribution is nonuniform and localized even assuming homogeneous initial conditions for subsurface layer. The nonuniform, localized shear strain are due to the existence of the sloped boundary. In other words, in addition to the vertical component of seismic movement being generated by the stratum slope, multi-dimensional propagation is also exhibited because of complex reflection behavior in the diluvial layer. Moreover, in sloped layers such, the danger of liquefaction is increased compared with the one-dimensional model. The actual liquefaction damage observed in Urayasu City was heavy in the sloped stratum locations where midterm reclamation work had been executed. This behavior resembles the results of the analysis carried out here. The current analysis shows that even in the case of homogeneous geomaterials, stratigraphic nonhomogeneity results in large variations in ground deformation behavior and that such deformation becomes particularly large in sloped strata locations. These things cannot be taken into consideration in one-dimensional analysis and highlight the necessity of performing multi-dimensional effective stress analysis.

Keywords: liquefaction, stratum inclination, surface wave, effective stress analysis

SSS23-19

Room:211

Time:May 1 15:15-15:30



## Relationship between liquefaction occurrence ratio and strong ground motion duration for the 2011 off the Pacific coast

SENNA, Shigeki<sup>1\*</sup> ; WAKAMATSU, Kazue<sup>2</sup> ; MATSUOKA, Masashi<sup>3</sup>

<sup>1</sup>NIED, <sup>2</sup>Kanto Gakuin University, <sup>3</sup>Tokyo Inst. Tech

In this study, We first reorganized the points of liquefaction in the 2011 off the Pacific coast of Tohoku Earthquake and plotted the number of liquefaction points in 250m mesh units, because many areas had not been investigated or were insufficiently investigated, as revealed in the information on liquefaction points disclosed and summarized by December 2011.

Next, using the reorganized liquefaction data, the seismic intensity were calculated and the 'real-time seismic intensity' noted by Kunugi et al.(2008) based on the waveforms recorded by seismographs of K-NET, KiK-net, the Meteorological Agency, and the municipalities and examined the effects of earthquake duration on liquefaction using the data on liquefaction points and the method of Matsuoka et al.(2011) to calculate the liquefaction occurrence, so that the liquefaction occurrence can be examined with consideration of the effect of the duration of seismic motion in the March 11 earthquake.

Keywords: Occurrence of liquefaction, Continuation time of strong ground, Geomorphologic classification, Fragility curve, Regional peculiarity

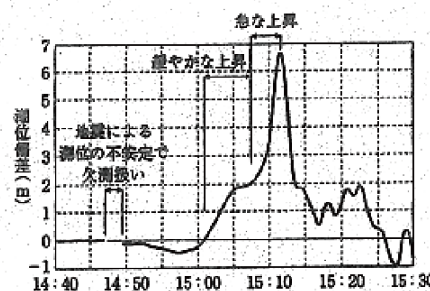
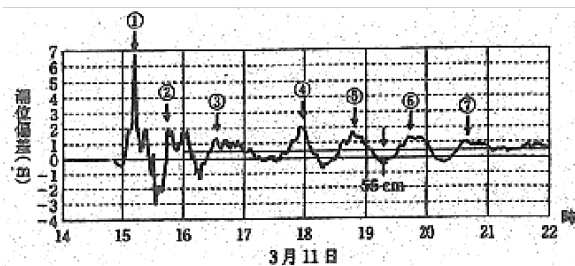
## The Wave Features Theory and Soliton

NISHIZAWA, Masaru<sup>1\*</sup>

<sup>1</sup>none

1. The eye of Writers under the title “ The Great Kanto Earthquake (of 1923) ” correctly spotted, the demolished style difference between the large and small structure.
2. Fourier Spectrum of Earthquake Motion near the observatory forms The Normal Distribution (Gaussian Distribution). And The further near the observatory. And The Sharp shape of Normal distribution mean densely the frequency.

Keywords: Wave Features Theory, Soliton, KDV Equation, Nonlinear waves



岩手県南部沖のGPS波形の記録 (左) と最初の部分の拡大図 (右)  
 国土交通省のデータをもとに作成

Kazuo OIKE  
 『Massive earthquake in Japan archipelago』  
 (Iwanami Library of Science 185, P10)  
 ①: Soliton  
 ②~⑦: Break down of Solitary wave Solitons  
 Reference: Mikio HINO 『流体力学』  
 (Asakura Publishing Co., Ltd. (1992))

## Seismic hazard karte : A Tool for distribution of seismic hazard information with Multi-index

AZUMA, Hiroki<sup>1\*</sup> ; FUJIWARA, Hiroyuki<sup>1</sup>

<sup>1</sup>National Research Institute for Earth Science and Disaster Prevention

### 1. Overview of seismic hazard karte

NIED distributed the "seismic hazard karte(chart)" in July, 2013. An "seismic hazard karte" is what summarized the earthquake hazard information for every point, arbitrary places can be searched and the diagnosis of the earthquake hazard about the place can be drawn up. A result displays many indices, such as various foundation information, hazard curves, etc. about the danger of an earthquake, like the notice of a medical examination by the view format summarized to A41 sheet using many charts and graphs.

### 2. Purpose of Development

It was thought possible to spread the recognition to seismic hazard by using for the user itself the form of diagnosing a certain point with the connection as a starting point, from the investigation by HERP, the argument in a comprehensive sectional meeting, etc. Although the seismic hazard karte was dispatch fundamentally turned to the whole average citizen like other seismic hazard information, when it decomposed into use-cases, it assumed roughly dividing and being used in the following domains. For insurance and real estate, as customer-oriented service data. As the teaching materials which teach the tool for advancing a measure at a workshop or a home to the local resident engaged in disaster prevention educational persons concerned and disaster prevention, and the view of the seismic hazard information on the area. It developed by being that it is easy to carry out use, respectively conscious as a sample of the way of expressing a response using J-SHIS Web API which is open API, and designing to IT persons concerned and developers.

### 3. Distributed Result

There are many echoes from the exhibited beginning and it is thought that effect fixed as one of the how to show the seismic hazard information evaluated across the board by the country was achieved. Nothing new as contents have in the information offered as seismic hazard karte this time, and it is already J-SHIS seismic hazard station offered, was only visualized in a different form. However, receiving a karte "it may be very intelligible. From the thing of having also let the family know who lives in the distance"as a positive thing, many reactions "worth of the possessions affair of our company will be influenced and it will be troubled by it if such a thing comes out" were seen by the negative thing, like when the hazard information is released newly.

### 4.References.

- Seismic hazard karte |<http://www.j-shis.bosai.go.jp/labs/karte/> (Japanese only)
- Manual |<http://www.j-shis.bosai.go.jp/karte-manual> (Japanese only)
- Description |<http://www.yullege.jp/?p=282> (Japanese only)
- J-SHIS Web API |<http://www.j-shis.bosai.go.jp/api-list> (Japanese only)
- Hiroki Azuma, Shinichi Kawai and Hiroyuki Fujiwara, 2013, Development of J-SHIS and Applications Using API, Journal of Disaster Research, Vol.8 No.5, 869-877.

Keywords: Seismic hazard, information tool



## JMA intensity distribution of the 1943 Tottori earthquake derived from immediately conducted questionnaire survey

NAKAMURA, Mariko<sup>1</sup> ; KAGAWA, Takao<sup>2\*</sup> ; NOGUCHI, Tatsuya<sup>2</sup> ; NISHIDA, Ryohei<sup>2</sup>

<sup>1</sup>Okayama City Office, <sup>2</sup>Tottori University

Questionnaire surveys were conducted by university of Tokyo immediately after five disastrous earthquakes in 1940s to evaluate modified Mercalli (MM) intensity scale. The raw data of the surveys had been stored long time without following analyses. We have studied explanation of each item in the Questionnaire sheet and developed the relational expressions between MM and JMA intensity scales. Finally, we derived JMA intensities at 1935 sites in southwest Japan, and estimated JMA intensity distributions with almost same resolution as modern intensity observation network. The distribution map suggests radiation pattern of strike slip fault and effect of surface geology. The result is worth of basic information for earthquake disaster prevention.

Keywords: the 1943 Tottori earthquake, questionnaire survey, JMA intensity scale, modified Mercalli scale

## Mortality in the East Japan Great Earthquake (4) Infants and elderlies should always suffer heavy rate of deaths?

OHTA, Yutaka<sup>1\*</sup> ; KOYAMA, Maki<sup>2</sup>

<sup>1</sup>TRIES, ADEP, <sup>2</sup>Engr. Fac. Kyoto Univ.

With the aim of clarifying age dependency of mortality in earthquakes we have been conducting a series of studies, just employing a simple division of number of deaths over population in age intervals of 5 or 10 years from area to area in devastated region. What we have found up to now is that there are 2 dominant types approximated by the capital U and J letters in English on the 2 dimensional coordinates of X axis as increasing ages and Y axis as mortality. In case of the 2011 East Japan earthquake, the age dependency in terms of J letter type dominates in most of devastated areas, which suggests that the mortality gets heavier with increasing ages but for infants it stays milder. Such result on age-dependency looks to be apart from our general recognition as infants are very much vulnerable in mortality at many disasters. The discrepancy requests further in-depth studies. In order to settle this issue we attempted two different approaches, that is, 1) comparing natural deaths of certain population with number of accidental deaths by an earthquake (Ozaki. 2012) and 2) introducing a way of evaluating the loss of life expectancy as an weighting factor inversely changing with increasing ages.

Consequently, we succeeded to make clear that infants are still very vulnerable in the meaning of bringing heavy rate of deaths.  
Reference

Ozaki; kousei no shihyou, 59, 2012 (in Japanese)

Keywords: East Japan Earthquake, Mortality, Age-dependency, Life Expectancy

## Disaster research in the Toyama Earthquake(1718)

SAKAMOTO, Masao<sup>1\*</sup>

<sup>1</sup>Iida city Museum

### 1,Introduction

Of the destructive earthquakes recorded in Japan over the past approx.1600 years, the only one that caused widespread damage in the southern part of Nagano Prefecture was the Toyama Earthquake of 1718, which had its epicenter at Minamishinano Wada, Iida City. The Toyama Earthquake struck just after 2 pm on August 22, 1718 with a magnitude estimated at 7.0. This earthquake is considered to have occurred along the Median Tectonic Line.

### 2,Survey Results

I identified 35 places where disasters occurred in each prefecture of Nagano Gifu Shizuoka and Aichi. Among these places, a number of characteristic disaster examples are shown as follows.

**(1)Minamishinano Wada,Iida City:** Mt.Moriheizan located close to the epicenter of the earthquake, partially collapsed to form the elevated area called Deyama at its foot. A landslide pushing out from Oshidezawa dammed the Toyama River. **(2)Arakida, Anan Town:** The right bank of the Tenryu River is composed mostly of Neogene strata centered on sandstone and mudstone overlaying granite bedrock. The slope at the place called Kibishima collapsed due to the earthquake and dammed the Tenryu River. **(3)Furujo,Anan Town:** Geologically, this area consists of Neogene sandstone and mudstone. In the Furujo district, landslides occurred in 24 places, and fields with place names that are still in use today were damaged or destroyed in 33 places.**(4)Hisawa,Shimojo Village:** There is an oral tradition stating that the local people saw the collapsed state of mountainsides in the Ina and Akaishi Mountains from this district. **(5)Enshu Yokoyama Town** (Yokoyama Town, Tenryu Ward, Hamamatsu City, Shizuoka Prefecture): A document was found stating that the Tenryu River was stopped at a place called Enshu"Teuna". Currently this place name is not used, but there is a place name "Unna", which is also along the Tenryu River, so it was presumed that this was where the river was dammed.

### 3,Discussion and Consideration

**(1)What this survey shows:** The distribution of the records concerning this earthquake disaster with its epicenter on the Median Tectonic Line in Minamishinano Wada, Iida City is quite one-sided. Records of damage were found only on the west side of a border marked by the Median Tectonic Line running roughly north-south. Because the Akaishi Mountains on the east side of the border had almost no inhabitants, no records of damage from the earthquake were left there. Also, over the course of the nearly three centuries that have passed since the earthquake occurred, the amount of documentary material has been greatly reduced as a result of natural and human causes. **(2)Geological specificity:** The disasters associated with this earthquake can be divided into three types according to geological differences and the disaster distribution. The first type involved large-scale landslides and disasters occurring on basement granite. The second type constituted disasters occurring on Neogene strata centered on Anan Town. The third type of disaster occurred on Quaternary terrace gravels and alluvial fan gravels. **(3)Relation to the Hiei Earthquake:** In 1707, the Hiei Earthquake struck with an estimated magnitude of 8.6, making it one of the largest earthquakes in Japanese history. The Toyama Earthquake, which struck 11 years later, is considered to be an after-shock of the Hiei Earthquake.

---

SSS23-P01

Room:Poster

Time:May 1 18:15-19:30

Keywords: toyama earthquake, the year 1781, earthquake disaster, median tectonic line, hoei earthquake

## A discussion on improvement of calculation technique for questionnaire survey of seismic intensities

SAITO, Ryohei<sup>2</sup> ; YAMAMOTO, Hidekazu<sup>1\*</sup> ; SAITO, Tsuyoshi<sup>1</sup>

<sup>1</sup>Faculty of Engineering, Iwate University, <sup>2</sup>GraduateSchool of Engineering, Iwate University

We compared the seismic intensity from the average intensity with a 1km mesh obtained in the vicinity of the instrumental seismic intensity observation sites. Only in the case of the 2011 off the Pacific coast of Tohoku Earthquake, questionnaire seismic intensities were about 0.5 larger than the instrumental seismic intensities, however, in the cases of other earthquakes, the questionnaire ones were smaller than the instrumental ones. The differences between the instrumental seismic intensity and the questionnaire one are 0.1 to 0.2 at the sites where the instrumental seismic intensities indicate 6 weak. However, at the sites where the instrumental seismic intensities indicate 5 strong, the differences were more than 0.5. Results of the earthquakes of 2008 and 2003 show that the questionnaire seismic intensity is about 0.3 smaller than the instrumental one in the range of 5 weak to 5 strong. Therefore, we compare the method by Inoue et al.(1999) as another method capable in the larger seismic intensity range with the method by Ohta et al.(1998). Inoue et al.(1999) had pointed out that the questionnaire seismic intensity estimated by Ohta et al.(1998) were low in the middle seismic intensity range near about 4.5. They proposed a method capable in large seismic intensity range using the empirical formula to modify the difference without changing the calculating method of Ohta et al. (1979). When questionnaire seismic intensities were calculated using the empirical equation by Inoue et al.(1999), they showed a better correlation with the instrumental seismic intensity for other earthquakes except the 2011 off the Pacific coast of Tohoku Earthquake.

Keywords: Calculation technique for questionnaire seismic intensities, Instrumental Seismic Intensity, Large seismic intensity range

## SATREPS Project on Earthquake and Tsunami Disaster Mitigation in the Marmara Region and Disaster Education in Turkey

CITAK, Seckin ozgur<sup>1\*</sup>; KANEDA, Yoshiyuki<sup>1</sup>; ERDIK, Mustafa<sup>2</sup>; TAKAHASHI, Narumi<sup>1</sup>; OZEL, Nurcan meral<sup>2</sup>; HORI, Takane<sup>1</sup>; HORI, Muneo<sup>3</sup>; KUMAMOTO, Kunihiko<sup>4</sup>; KALAFAT, Dogan<sup>2</sup>; PINAR, Ali<sup>2</sup>; OZEL, Oguz<sup>5</sup>; YALCINER, Ahmet cevdet<sup>6</sup>; NURLU, Murat<sup>7</sup>; TAMIRCAN, Gulum<sup>2</sup>; MIRZAOGLU, Mete<sup>7</sup>; ARIYOSHI, Keisuke<sup>1</sup>

<sup>1</sup>Japan Agency for Marine-Earth Science and Technology (JAMSTEC), Japan, <sup>2</sup>Bogazici University, Kandilli Observatory and Earthquake Researches Institute (KOERI), Turkey, <sup>3</sup>University of Tokyo, Japan, <sup>4</sup>Edogawa University, Japan, <sup>5</sup>Istanbul University, Turkey, <sup>6</sup>Middle East Technical University, Turkey, <sup>7</sup>Disaster and Emergency Management Presidency (AFAD), Turkey

Since 1939, devastating earthquakes with magnitude greater than seven ruptured North Anatolian Fault (NAF) westward, starting from 1939 Erzincan (Ms=7.9) at the eastern Turkey and including the latest 1999 Izmit-Golcuk (Ms=7.4) and the Duzce (Ms=7.2) earthquakes in the eastern Marmara region. On the other hand, the west of the Sea of Marmara an Mw7.4 earthquake ruptured the NAF's Ganos segment in 1912. The only un-ruptured segments of the NAF in the last century are within the Sea of Marmara, and are identified as a "seismic gap" zone. The Sea of Marmara should be focused on through a multidisciplinary research and uncertainty in magnitude, epicenter, recurrence, fault segmentation, and their cross effects should be identified and characterized. To fill the necessity above, a comprehensive multidisciplinary research on earthquake and tsunami disaster mitigation in the Marmara region and disaster education in Turkey in the framework of Science and Technology Research Partnership for Sustainable Development (SATREPS) sponsored by Japan Science and Technology Agency (JST) and Japan International Cooperation Agency (JICA) has been started.

The project is composed of four research groups.

The first is "Earthquake Source Model research" group. Long-term OBS observation, Electromagnetic observation, Seafloor extensometer observation and Trench survey studies will be conducted in order to identify the detailed seismic zone, fault geometry, 3D Velocity structure and reliable crustal deformation beneath the Sea of Marmara.

The second is "Tsunami prediction based on earthquake cycle simulation research" group. In this group earthquake and tsunami occurrence scenarios will be proposed based on especially the research Group 1's outputs and current knowledge on NAF's seismic activities. The outputs will be used for the simulation of strong ground motion, developing of advanced hazard maps and a tsunami early warning system.

The third is "Seismic characterization and damage prediction research" group. This group focuses on modeling of 3D velocity structure, theoretical prediction of ground motion and evaluation of existing structures in the selected urban areas using research outputs of the other groups. Also there will be an attempted of making an urban area model for Istanbul using available data for this area, and to execute earthquake hazard and disaster simulation for various scenarios of a possible earthquake. Improved hazard maps and visual materials for disaster education are expected.

The fourth is "Disaster education using research result visuals from each research" group. In group four, effective use of media in the dissemination of disaster information will be examined and disaster management planning through regional disaster prevention community will be encouraged. as well as, using the research visuals a disaster prevention education program will be conducted through media, web, local communities and schools.

Goals of the project are as follows,

- 1- To develop disaster mitigation policy and strategies based on multidisciplinary research activities.
- 2- To provide decision makers with newly found knowledge for its implementation to the current regulations.
- 3- To organize disaster education programs in order to increase disaster awareness in Turkey.
- 4- To contribute the evaluation of active fault studies in Japan.

Through the project, the research results will be integrated for disaster mitigation in The Marmara region and disaster education in Turkey. The details of SATREPS Japan-Turkey joint research project and latest achievements will be presented.

**Keywords:** sea bottom observation, earthquake disaster mitigation, tsunami disaster mitigation, disaster education, Turkey, SATREPS

## Fragility curves of buildings during the 2011 Tohoku Earthquake using the damage data in the northern Miyagi Prefecture

WU, Hao<sup>1\*</sup> ; MASAKI, Kazuaki<sup>2</sup> ; IRIKURA, Kojiro<sup>3</sup> ; KURAHASHI, Susumu<sup>3</sup>

<sup>1</sup>Graduate School of Engineering, Aichi Institute of Technology, <sup>2</sup>Department of Urban Environment, Aichi Institute of Technology, <sup>3</sup>Disaster Prevention Research Center, Aichi Institute of Technology

Damage ratios in subdistricts of Osaki and Kurihara cities, northern of Miyagi Prefecture are obtained from the damage data provided by the local City Offices. Ground motions in these subdistricts are estimated by use of source model proposed by Kurahashi and Irikura (BSSA, 2013) and underground velocity structures identified from microtremor H/V spectral ratios. The estimated ground motion indices (PGA, PGV,  $I_{JMA}$ , and SI) are used to relate with the damage ratios to construct the fragility curves. It is found that the correlation in small subdistricts is improved, compared with that between the observed ground motion indices and corresponding damage ratios in a wider district.

In addition, we have added some microtremor measurement at plural sites inside each subdistrict, such as Furukawa, and Tajiri, in order to assess the representativeness of ground motions estimated at only one site for the entire subdistrict. We conducted such measurement at or near the preliminary schools inside the subdistricts. The ground motions during the mainshock are estimated with the identified velocity structures from the microtremor H/V spectra ratios. It is found that the variability of ground motions in the Furukawa subdistrict is relatively small. It suggests that the ground motions used for the fragility curves are representative for the entire subdistrict. In contrast, the variability of ground motions in Tajiri is relatively large. It may be caused by the limited numbers of preliminary schools with similar amplification factors.

**Keywords:** Fragility curve of buildings, microtremor H/V spectral ratio, underground velocity structure, representative of ground motions

## The earthquake vibration observation of the Yasuda auditorium using the IT Kyoshin seismometer

ITO, Takamori<sup>1\*</sup> ; TAKANO, Kiyoshi<sup>2</sup>

<sup>1</sup>Keio University, <sup>2</sup>ERI, The University of Tokyo

In order to reduce the seismic disaster, it seems to be the usefulness to investigate the seismic vibration of our familiar buildings such as housing, companies, schools, etc. in small earthquake, examine the weak point and improve the earthquake resistance of these building effectively. For this purpose, we devised IT strong motion seismometer as a new type self install strong motion seismometer.

With this IT Kyoshin seismometer, we continue the vibration observation of some buildings in University of Tokyo from 2006.

The repair work of the Yasuda auditorium will be carried out. We install the IT Kyoshin seismometer and will observe it to confirm an effect of the construction.

We used the high-performance sensor and, in addition to a low cost standard IT Kyoshin seismometer, observed it.

We finish observation before the construction and analyze data now.

After construction was completed, we install the IT Kyoshin seismometer again and are going to compare it.

Keywords: IT Kyoshin (Strong Motion) Seismometer, Structural Health Monitoring

## The effect of torsional and bending vibration on shear-wave velocity extracting from building response by seismic interf

WANG, Xin<sup>1\*</sup> ; MOTOSAKA, Masato<sup>1</sup> ; MASAKI, Kazuaki<sup>2</sup> ; IRIKURA, Kojiro<sup>3</sup> ; HISADA, Yoshiaki<sup>4</sup>

<sup>1</sup>International Research Institute of Disaster Science, Tohoku University, <sup>2</sup>Department of Urban Environment, Aichi Institute of Technology, <sup>3</sup>Disaster Prevention Research Center, Aichi Institute of Technology, <sup>4</sup>Department of Architecture, Kogakuin University

Because shear-wave velocity correlates with the shear rigidity of buildings, the decrease of it is a indicator of the loss of stiffness, which is possibly caused by structural damage or degradation. Therefore, shear-wave velocity identification is intended for use in health monitoring of upper structures excluding the effect of soil-structure interaction. Shear-wave velocity can be extracted from tracing the propagation of a pulse from normalized cross-correlation of the motion between two points based on the view of response as the wave vertical propagation process. In this study, the reference point is the top of the building (virtual source) instead of the base (physical source) which results in the transfer function including the effect of rigid-body rocking. However, for high-rise and eccentric structures torsional motion and bending motion is inevitable. In practical measurement of horizontal motions with single sensors located on the side not the core of the building plane, it is unavoidable to record the torsional response which mixed with the shear-mode motions. Therefore, the effect of torsional response to shear-wave velocity extraction should be deliberated on to avoid erroneous use of the travel time of torsional wave instead of that of shear wave. Furthermore, the extraction of shear-wave propagation from building vibration generally in bending mode is valid or not should be examined.

In this study, firstly a 3D model with eccentricity is used to calculate the horizontal and vertical impulse response to analyze the effect of torsional and bending response to shear-wave velocity extraction. And the method to eliminate the effects of torsional and bending vibrations to obtain the shear-wave propagation with high resolution is presented. Secondly, a practical use of earthquake records measured in a high-rise building to examine the effect of torsional and bending vibration to shear-wave velocity extraction. Thirdly, velocities of shear wave, torsional wave, and bending wave are extracted separately to evaluate the changes of stiffness before and after the Tohoku earthquake for health monitoring.

Keywords: shear-wave velocity of buildings, deconvolution method, torsional response, seismic interferometry, system identification, Tohoku earthquake

## Global "strong" ground motions from the 2013 Sea of Okhotsk great deep earthquake

KUGE, Keiko<sup>1\*</sup>

<sup>1</sup>Dept. Geophysics, Kyoto University

This study presents the characteristics of global ground motions caused by the Sea of Okhotsk deep earthquake (Mw8.3) of May 24, 2013. The earthquake occurred at a depth of 609 km in the subducting Pacific plate, and it is now the largest deep earthquake ever recorded. According to reports in NEIC, the earthquake was felt at very long distances in the world, including Dubai (~76 degrees) and Moscow (~58 degrees). In this study, by using global broadband seismic data from IRIS DMC, we examine ground motions from the earthquake. For the 1994 Bolivia deep earthquake (Mw8.3), which was formerly the largest and were felt in North America, the distant ground motions were examined by Anderson et al. (1995) from the perspective of strong motion seismology. Due to the location, the 2013 Sea of Okhotsk earthquake was recorded by a much better coverage of global stations, compared to the 1994 Bolivia earthquake. This study is an opportunity for exploring the distant "strong" ground motions from the perspective of Anderson et al. (1995).

Peak ground accelerations (PGA) from the 2013 Sea of Okhotsk earthquake decrease as distance increases out to 120 degrees, and have a peak at a distance of approximately 140 degrees. The variation as a function of distance is similar to that of Anderson et al. (1995) for the 1994 Bolivia earthquake. The values of PGA are a few times larger than those from the Bolivia earthquake. At distances between 30 and 80 degrees, PGA are associated with vertical components of direct P waves, and the values of PGA are often in a range from 0.1 to 1 gal. Peak ground velocities (PGV) vary with distance in a similar way to PGA. The values of PGV at distances between 30 and 80 are lower than 0.1 cm/s.

Large PGA at distances between 30 and 80 degrees are observed in the Eurasian continent. The values of PGA in the western part of the continent are larger than those in the eastern part. Because this difference is also observed for PGA of P waves from an outer-rise shallow earthquake near the Kurile trench, it can be attributed to regional structure in the Eurasian continent. PGA from the 2013 deep earthquake are not low in the southern part of the continent, although from a deep earthquake beneath Sea of Okhotsk that has a different focal mechanism from that of the 2013 earthquake, PGA decrease toward the south as distance increases. The focal mechanism of the 2013 earthquake represents that the P wave radiation is the maximum along a ray toward Karachi, Pakistan. This P wave radiation can account for the observations of PGA in the southern part. Global "strong" ground motions from the 2013 Sea of Okhotsk deep earthquake are thus likely to be affected by regional structure and P wave radiation, as suggested by Anderson et al. (1995).

## Relation between smallest microtremor amplitudes and largest seismic amplitudes observed at TRIES seismographic stations

TANAKA, Torao<sup>1\*</sup> ; OKUBO, Makoto<sup>2</sup>

<sup>1</sup>Kyoto University Emeritus Professor, <sup>2</sup>Tono Research Institute of Earthquake Science

In 1999 TRIES, Tono Research Institute of Earthquake Science, started to establish an observation network of seismographic stations in Tono district, the eastern area of Gifu Prefecture, and completed a 10 stations network at the end of the year. The seismographic station TRIES was the first station, and 9 stations, TOGARI, ENA, MIZUNAMI, AKECHI, IWAMURA, NATAKI, MITAKE, TOKI and INUYAMA were established one by one. In order to investigate the correlation between the smallest spectral amplitudes of microseisms and largest seismic spectral amplitudes, we started spectral analysis of microtremors and seismic waves recorded on the same seismograms. By the discrete Fourier transform we calculated the spectral amplitudes and frequencies from the observed microtremors recorded just before the first arrival of seismic waves in the frequency range from 2.0 to 4.0 Hz. Similarly we calculated the spectral amplitudes and frequencies of seismic waves by the discrete Fourier transform in the frequency range from 2.0 to 4.0Hz. We calculated the ratios of the relative amplitudes of the smallest amplitude of microtremors and largest amplitude of seismic waves to those at the station TRIES. By taking the relative amplitudes of micro tremors and largest seismic amplitudes to those at TRIES we can extract the relative site effects caused by the ground soil to those at TRIES. Since the site effect at TRIES is small, the relative largest seismic amplitudes at TOGARI, for example to those at TRIES simply give multiples of the amplitude at TRIES, at each station. Preliminary results show that the smallest amplitude of microtremors will give the spectral amplitudes of the site effect that will amplify the incident seismic waves from the underlain basements.

Keywords: microtremor, seismic waves, discrete Fourier transform, ground soil, largest amplitude, site effect

## A study on model selection methods for ground-motion prediction equations using synthetic data

NODA, Akemi<sup>1\*</sup> ; WU, Changjiang<sup>2</sup> ; SI, Hongjun<sup>3</sup> ; SAIJO, Yusuke<sup>1</sup> ; JIAO, Ning<sup>1</sup>

<sup>1</sup>Kozo Keikaku Engineering Inc., <sup>2</sup>Japan Nuclear Energy Safety Organization, <sup>3</sup>Earthquake Research Institute, University of Tokyo

Numerous ground motion prediction equations (GMPEs) have been proposed for the purpose of assessing seismic hazard. However, a critical problem is that how to select appropriate GMPEs for the application of GMPEs to practical engineering problems.

Recently some model selection methods for GMPEs that evaluate the agreement between observed and predicted data have been proposed. In present study, in order to check the properties of model selection methods, we compare the model selection methods by using artificial dataset generated by a known GMPE. As candidate model selection methods, we have chosen three methods, that is, analysis of root mean square residual (RMR), the log-likelihood method (LLH method, Scherbaum et al., 2009, BSSA) and the Euclidean distance-based ranking method (EDR method, Kale and Akkar, 2013, BSSA). The analysis of RMR is one of the simplest methods to evaluate the difference between observed data and medians of GMPE model. On the other hand, the LLH method quantifies the distance between observed data and GMPEs defined as probability density function (both of median and standard deviation), based on information-theoretic perspective. However, Kale and Akkar (2013) points out the problem that the LLH method may favor GMPEs with larger standard deviations. The EDR method considers not only ground-motion uncertainty of model through standard deviation, but also agreement between the median estimations of models and observed data trend (model bias).

First, we assumed a vertical strike-slip fault with moment magnitude 7.0. We randomly chose 200 sites, whose fault distances are up to 200km. Next, we calculated theoretical PGA and response spectral acceleration for 16 periods using ground motion prediction model of Chiou and Youngs (2008, Earthq. Spectra), which is referred to as CY08 hereafter. And, we generated three kinds of synthetic dataset by adding three types of random noise with (1) zero standard deviation, (2) standard deviation of CY08, and (3) twice the standard deviation of CY08, respectively.

We selected five candidate GMPEs, that is, CY08, Abrahamson and Silva (2008, Earthq. Spectra), Campbell and Bozorgnia (2008, Earthq. Spectra), Zhao et al. (2006, BSSA) and Kanno et al. (2006, BSSA), and ranked the performance of candidate GMPEs for each synthetic dataset. In analysis of RMR that does not account for standard deviations of the prediction models, CY08 is stably ranked the best performing model for all kinds of synthetic dataset. The LLH method basically ranked CY08 as the best performing model for synthetic dataset (1) and (2), but it favored GMPEs with larger standard deviations for synthetic dataset (3). It suggests that the standard deviation of model is emphasized more than the median when we apply the LLH method to poor quality data. In the EDR method, in principle, the parameter to measure the level of model bias of CY08 is not able to be calculated for synthetic dataset (1) that does not have random noise. For synthetic dataset (2) and (3), however, the EDR method ranked CY08 as the best performing model both in the point of view of model uncertainty and model bias.

**Keywords:** attenuation relationship, ground motion predicting equation, root mean square residual, the log-likelihood method, the Euclidean distance-based ranking method

## Seismic hazard assessment using a new ground motion prediction equation

MORIKAWA, Nobuyuki<sup>1\*</sup> ; FUJIWARA, Hiroyuki<sup>1</sup> ; OKUMURA, Toshihiko<sup>2</sup> ; FUJIKAWA, Satoshi<sup>2</sup>

<sup>1</sup>National Research Institute for Earth Science and Disaster Prevention, <sup>2</sup>Shimizu Corporation

In the "National Seismic Hazard Map for Japan" by Headquarters of Earthquake Research Promotion of Japan, seismic hazard is evaluated by the ground motion prediction equation (GMPE) of peak velocity by Si and Midorikawa (1999), and conversion from peak velocity to seismic intensity by using an experiential relation. It is indispensable that earthquakes of moment magnitude (Mw) 9 class take into consideration in the present seismic hazard evaluation. However Si and Midorikawa's (1999) equation is obtained from strong motion records of earthquake up to Mw 8.3. In this study we evaluate seismic hazard by using our new GMPE obtained by using strong-motion database including the records of the 2011 Tohoku earthquake and show the comparison it with the National Seismic Hazard Maps for Japan.

The target strong-motion parameters are peak velocity on an engineering bedrock (here, it is considered as the upper surface of  $V_s=400$  m/s layer), and peak velocity and JMA seismic intensity on the ground. The value on the ground is calculated by using the amplification factor obtained from the average S-wave velocity up to 30 m depth based on the 250m-mesh national geomorphologic classification map.

First, we compare the ground motion distributions calculated from two GMPEs. Here we target following 6 assumed earthquake. (1) crustal earthquake on the Itoigawa-Shizuoka fault zone (Mw7.4), (2) crustal earthquake on the Muikamachi fault zone (Mw=6.6), (3) subduction-zone plate-boundary earthquake at Nankai Trough (Mw=9.1), (4) subduction-zone plate-boundary earthquake at Tokachi-oki region (Mw=8.1), (5) subduction-zone shallower intra-plate earthquake at Chishima trench region (Mw=8.2), and (6) subduction-zone deeper intra-plate earthquake at Chishima trench region (Mw=7.5). Amplification by the deep sediments layers can be obviously seen in our new result of peak velocity distribution. As the result, amplitude in our new result becomes larger in basin region and smaller in mountain region. On the other hand, the influence of the deep sediments is not so remarkable in result of JMA seismic intensity on the ground. The calculated value from our new GMPE is smaller in the distance area (in general 100 km or more) for subduction-zone earthquakes. Midorikawa and Ohtake (2002) pointed out that Si and Midorikawa's (1999) GMPE overestimates the peak values in distant region earthquake whose focal depth is deeper than 30 km. Our results are consistent with them.

Next, we compare the seismic hazard for the megathrust earthquake occurring at the Nankai Trough. Here we use the model in probabilistic seismic hazard maps by HERP (2013).

Moreover, we use the value of variance in the National Seismic Hazard Maps for Japan as it is. The hazard by our new GMPE decreases especially at the distant area as expected from comparison of above-mentioned strong-motion distribution. However, the decrease does not serve in Kanto and Osaka area where amplification by deep sediments is large. On the contrary, JMA seismic intensity is larger when exceedance of probability is lower at some points. This is considered that that the value of the set-up variation is not in agreement for JMA seismic intensity has influenced.

Keywords: seismic hazard assessment, ground motion prediction equation, variance of ground motion

## Ground amplification estimates based on very dense seismic array observation in Furukawa district, Osaki, Japan

GOTO, Hiroyuki<sup>1\*</sup> ; MORIKAWA, Hitoshi<sup>2</sup> ; INATANI, Masayuki<sup>1</sup> ; OGURA, Yumiko<sup>2</sup> ; TOKUE, Satoshi<sup>2</sup> ; HAMASAKI, Shohei<sup>2</sup> ; ZHANG, Xinrui<sup>2</sup> ; SAKKRAWIT, Sripunyaphikhup<sup>2</sup> ; IWASAKI, Masahiro<sup>3</sup> ; ARAKI, Masayuki<sup>4</sup> ; SAWADA, Sumio<sup>1</sup> ; ZERVA, Aspasia<sup>5</sup>

<sup>1</sup>Kyoto University, <sup>2</sup>Tokyo Institute of Technology, <sup>3</sup>Osaki city, <sup>4</sup>aLab Co.Ltd, <sup>5</sup>Drexel University

On March 11, 2011, a huge earthquake hit the eastern part of mainland Japan. The earthquake caused a huge tsunami that killed more than ten thousand people. Structures were also severely damaged over the area of eastern Japan by the tsunami, ground motions, liquefaction, and so on. We focus on the Furukawa district of Osaki City, where severe residential damages occurred downtown. Ground motion records in the downtown area are available at two stations, MYG006 (K-NET) and JMA Furukawa (JMA). The damage level was different between the areas within several hundred meters from the MYG006 and JMA Furukawa stations, which are about 1km away from each other. The severe damages were concentrated within the area approximately 1x1km<sup>2</sup> including the JMA station. This implies that the ground motion characteristics were not uniform in sub-kilometer scale, and the existing two stations are not enough to clarify the damage distribution (Goto and Morikawa, 2012).

In aftermath of the earthquake, we distributed dozens of low-cost seismometers, namely ITK sensor, around the area about 3x2km<sup>2</sup> in the Furukawa district (Goto et al., 2012). The observed data are sent to the remote server through internet connection in real time. The seismometers were installed beside the volunteers' houses. The volunteers can access the interactive information service, namely on-line viewer system. The observed PGA and PGV values show significant spatial variability that may be correlated to the structural damage caused by the major 2011 event.

We assumed one-dimensional horizontally-layered structure just beneath the stations and estimated ground structure by using the records based on the observation. The results indicate that the area where the severe damages were concentrated is related to the area with the thicker surface layers. The distribution is also indicated by the results obtained from gravity anomaly data.

### References

Goto and Morikawa: Ground motion characteristics during the 2011 off the Pacific coast of Tohoku earthquake, *Soils and Foundations*, 52(5), 769-779, 2012.

Goto, Morikawa, Inatani, Ogura, Tokue, Zhang, Iwasaki, Araki, Sawada and Zerva: Very dense seismic array observations in Furukawa district, Japan, *Seism. Res. Lett.*, 83(5), 765-774, 2012.

Keywords: Ground amplification, Furukawa district, Very dense seismic array observation

## Physics-based decomposition of ground amplification using ground transfer function expansion

GOTO, Hiroyuki<sup>1\*</sup>

<sup>1</sup>DPRI, Kyoto University

Amplification of earthquake ground motions at actual deposit sites is an important factor to consider when assessing the risk of an earthquake disaster. In order to identify the amplification properties, several preprocessings such as the Fourier transform are required. I propose a series expansion of the amplification with simple ground transfer functions as a new preprocessing. I define a sequence of transfer functions based on a two-layered structure excluding an internal damping, and a function space spanned by the set of the functions. I mathematically prove that the function space is equal to L2 space. This indicates that all the functions belonging to L2 space, i.e., an arbitrary ground amplification, have a unique series expansion.

In practice, the expansion requires the observed ground amplification. It is directly observable from the spectral ratio of the Fourier spectra at the target site to that at a reference rock site (Goto et al., 2013). When the observations are available, the expansion is applicable even for the site response including a 3D basin effect as the preprocessing, whereas it requires a more precise investigation of what the extracted components physically means for the general cases.

I apply the series expansion to the physics-based decomposition of the amplification. The results indicate that the contribution from the given bases can be represented by the absolute value of their coefficients. The contribution may enable direct quantification of the similarity of models. This property potentially has wide applications, e.g., spatial interpolation of the amplifications from the sites where they are reliably determined, stochastic modeling of the amplification as a mixed state of the fundamental simple states, etc. The detailed application is currently under way.

### References

Goto, H.: Series expansion of complex ground amplifications with a sequence of simple transfer functions, *Earth. Engng. Struct. Dyn.*, submitted.

Goto, H., Kawamura, Y., Sawada, S. and Akazawa, T.: Direct estimation of near-surface damping based on normalized energy density, *Geophys. J. Int.*, 194(1), 488-498, 2013.

Keywords: Ground amplification, Function expansion

## Case study on the wavefield in the 3D structure including sedimentary basin and the effect of source depth on it

ARISUE, Maho<sup>1</sup> ; KAKEHI, Yasumaro<sup>1\*</sup>

<sup>1</sup>Faculty of Science, Kobe University

It is widely recognized that the existence of sedimentary layers has a great influence on the excitation of surface waves. During the 2011 Fukushima-ken shallow inland earthquake (Mw 5.5, depth = 10.6 km), long-period surface wave was observed at a station in the Niigata sedimentary basin, which is over 150 km away from the epicenter, and its duration reached over 100 s. Long-period surface wave was observed also during the 2012 Fukushima-ken-oki deep interplate earthquake (Mw 5.7, depth = 53 km) at the same station, and its duration reached ~100 s. Thus, significant difference was not seen between the surface wave duration in the Niigata basin of these two earthquakes despite of large difference of their source depths. This seems inconsistent with the recognition that surface wave is more efficiently excited by shallower source.

This study investigates the effect of source depth on the seismic wave filed in the sedimentary basin based on the numerical simulation using finite difference method for shallow and deep sources. The calculation area is from off the Fukushima Prefecture to the Niigata basin, and the following three simulations are performed.

In the simulation 1, a simple structure model composed of circular homogeneous sedimentary basin and background two-dimensional structure, two cases of source depths: 5 km and 85 km, and source duration of 3 s are assumed. The result shows the duration of the surface wave in the sedimentary basin is ~50 s for the both shallow and deep sources, and large difference is not seen the two different source depth cases. At the station prior to the basin, wave duration for the shallow source is ~10 s longer than that for the deep source. This difference of 10 s is shorter than the long duration of 50 s in the sedimentary basin, and this can explain the result that large difference is not seen in the basin.

In the simulation 2, a simple structure model composed of circular homogeneous sedimentary basin and background two-dimensional structure, as in the simulation 1, is assumed, and the case study on the material property values of the homogeneous basin is done. Two cases of source depths: 5 km and 75 km, and source duration of 3 s are assumed. The result shows longer duration of seismic waves is seen in the basin for smaller value of S-wave velocity of the basin medium (~125 s for  $V_s = 0.5\text{km/s}$ , ~90 s for  $V_s = 1.0\text{ km/s}$ , and ~40 s for  $V_s = 2.0\text{ km/s}$ ). This is interpreted to be because of larger arrival time difference of S-wave and surface wave for smaller S-wave velocity of the basin.

In the simulation 3, realistic complex three-dimensional structure model is assumed both for the sedimentary basin and for the background structure. We use the three-dimensional model by Koketsu et al. (2012), two cases of source depths: 5 km and 75 km, and source duration of 3 s. Long wave duration of ~90 s is obtained both for the shallow and deep sources. The maximum amplitude at the station is the sedimentary basin is ~2 times (for the deep source) and ~6 times (for the shallow source) larger than that at the station prior to the basin.

Comparing the result of the realistic three-dimensional model case (simulation 2) and that of the simple structure model case (simulation 1), more complex and more continuous wave-packet with long duration is seen in the basin in the former case than that in the latter case. On the other hand, significant difference is not seen in the amplitude and duration at the station prior to the basin, both for the shallow and deep sources. This result suggests the wavefield in the sedimentary basin is mainly affected by the basin structure itself, rather than the structure model of the path from the source to the basin.

Keywords: sedimentary basin, surface wave, numerical simulation, source depth

## Surface wave propagation in the large-scale sedimentary basin: distinct lateral variation of Love wave velocity around m

TAKEMURA, Shunsuke<sup>1\*</sup> ; YOSHIMOTO, Kazuo<sup>1</sup>

<sup>1</sup>Yokohama City University

By detailed analysis of surface waves recorded at dense seismic arrays in Kanto, sudden change of Love wave velocity for frequency of 0.125-0.25 Hz is found at very narrow, 20 km by 20km, region of southern Saitama.

To clarify cause of such sudden change and characteristics of surface wave propagation in thick sediments, we conducted 3D FDM simulations of seismic wave propagation assuming various basement structure (interface between sediments and bedrock) or velocity structure models in the sediments. Our simulations demonstrated that propagation velocity of Love wave is mainly controlled by shallower velocity structure at depth less than 1.5 km, rather than deeper basement structure. Our results were supported by the analysis of sensitivity kernel of Love wave in the sediments.

We constructed S-wave velocity structure in the sediments of Kanto basin using interpolation technique from 14 boreholes VSP measurements and surface wave analysis in this study. To confirm validity of our modeling, we conducted 3D FDM simulations of seismic wave propagation using constructed velocity structure and compared simulation results with observation. Our simulation results well reproduced peak amplitude and propagation velocity of Love wave for frequency of 0.125-0.25 Hz. Our results indicates that realistic modeling of shallower velocity structure and impedance contrast at the sediments-bedrock interface is important for precise evaluation of long-period ground motion in thick sedimentary basin.

### **Acknowledgement**

We acknowledge the National Research Institute for Earth Science and Disaster Prevention, Japan (NIED) for providing the K-NET/KiK-net waveform data. We also use strong motion data from SK-net. The computations were conducted on the Earth Simulator at the Japan Marine Science and Technology Center (JAMSTEC).

Keywords: long-period ground motion, basin structure, numerical simulation, surface wave

## Long-Period Ground Motion Simulation in the Kanto Basin with/without Accretionary Prism

GUO, Yujia<sup>1\*</sup> ; KOKETSU, Kazuki<sup>1</sup> ; MIYAKE, Hiroe<sup>1</sup>

<sup>1</sup>Earthquake Research Institute, University of Tokyo

Large earthquakes in subduction zones generally excite long-period seismic waves. Once these waves enter into basins filled with thick sedimentary layers, they develop and result in largely-amplified long-period ground motions. Such long-period ground motions have caused damage to large-scale buildings during some earthquakes. For the 2003 Tokachi-oki earthquake ( $M_w$  8.3), long-period ground motions with a dominant period of 7-8 seconds were observed in the city of Tomakomai, located on thick sedimentary layers and at a distance of about 250 km from source region. The long-period ground motions triggered the sloshing in many oil tanks, and two of them caught fire (Koketsu *et al.*, 2005). For the 2011 Tohoku earthquake ( $M_w$  9.0), long-period ground motions were observed at a large distance from source region such as the Osaka and Kanto basins, where some tall buildings shook over about 10 minutes (JMA, 2011).

The large earthquakes along the Nankai trough which are expected to occur in the near future can generate long-period ground motions in the Osaka, Nobi and Kanto basins (Furumura *et al.*, 2008). Along the Nankai trough, an accretionary prism composed of soft materials with a thickness of several kilometers lies near the toe of the Eurasian plate. Such prism does not exist at the Japan or Kuril trench. For this reason, in evaluating the long-period ground motions during the large earthquake occurring along the Nankai trough, we should consider the additional effect of accretionary prism on seismic waves. Yamada and Iwata (2005) simulated long-period ground motions for the Kinki region, and concluded that the existence of accretionary prism reduces the amplitudes of direct S-waves and elongates long-period ground motions. In this study, we performed simulations of the long-period ground motions in the Kanto basin for the foreshock ( $M_w$  7.1) of the 2004 off the Kii peninsula earthquake on 5 September at 19:07 (JST) in order to examine the effect of accretionary prism.

In the simulation, we assumed a point source. Except its depth, its source parameter and source time function were the same as those of Yamada and Iwata (2005). We located the source at a depth of about 16 km, which is slightly shallower than that of Yamada and Iwata (2005), to fit it to the depth of the subducting Philippine Sea plate. We used the Japan Integrated Velocity Structure Model (Koketsu *et al.*, 2008, 2012). We calculated long-period ground motions using the finite element method with voxel meshes (Ikegami *et al.*, 2008). The frequency range of the calculation was 0.05-0.3 Hz, and the time duration of synthetic waveforms was set to be six and a half minutes from the rupture starting time. Our simulation model covered an area of 564 km × 198 km and extended to a depth of 61 km. An absorbing boundary with a width of 54 km was also introduced outside the simulation model. According to the velocity structure, the model was discretized by variable voxel meshes with the smallest size of 175 m. We also assumed a velocity structure model without accretionary prism, where the S-wave velocity of accretionary prism (1.0 km/s) is replaced with 3.2 km/s. Then, we calculated waveforms in this model and compared them with those in the accretionary-prism model to examine the effect of accretionary prism.

Our simulation shows that, compared with the velocity structure model without accretionary prism, the long-period ground motions for the accretionary-prism model have smaller amplitudes for direct waves but larger ones for later phases. Our results are consistent with those by Yamada and Iwata (2005). In the accretionary-prism model, the waves trapped in the accretionary prism are continually converted to surface waves, and the incident surface waves to the Kanto basin propagate in the basin. We confirm that this process contributes to the reduction of direct waves and the amplification of later phases in the Kanto basin.

Keywords: Long-period ground motion, Accretionary prism, Nankai trough, Kanto basin

## Semblance analysis for the 2011 Tohoku earthquake using strong-motion and 1Hz GPS data

KUBO, Hisahiko<sup>1\*</sup>; IWATA, Tomotaka<sup>1</sup>; ASANO, Kimiyuki<sup>1</sup>

<sup>1</sup>DPRI, Kyoto Univ.

Source inversion is well used for the analysis of the earthquake source-process. However in the source inversion some assumptions and constraint conditions are used and there are cases where the settings of these affect the result. On the other hand, array analysis can produce the direct image for the seismic-wave radiation. In this analysis, we investigate the seismic-wave radiation characteristics for the 2011 Tohoku earthquake with the semblance array analysis using strong-motion and 1Hz GPS data.

We use not only the strong-motion data recorded by K-NET, KiK-net, and F-net of NIED and JMA but also 1 Hz GPS data recorded by GEONET of GSI. Additional use of 1 Hz GPS data leads to increase the station density and therefore the number of the available arrays increased remarkably compared to previous work (Kubo & Takehi, 2013). Except for F-net data, the strong-motion acceleration waveforms are integrated into velocity waveforms. 1Hz GPS data is converted into displacement waveforms using Kinematic PPP as implemented in RTKLIB Ver. 2.4.2 (Takasu, 2013) and they are differentiated into velocity waveforms. These waveforms are bandpass-filtered from 10s to 25s and resampled with a sampling interval of 0.1s. From the comparison of the observed velocity waveforms for the 2011 Tohoku earthquake at the GEONET and strong-motion stations which distance is less than 3 km, we confirmed that the waveform of 1Hz GPS data matches one of strong-motion data at above period-band.

We use the same method of the semblance analysis in Kubo & Takehi (2013). In this method, we firstly assumed the fault surface model consisting of some subfaults. Then the semblance value for each subfault is calculated assuming spherical-wave incidence when the subfault is the seismic-wave radiation source, and these values are plotted on the fault surface. By doing this analysis with time shift, we can obtain temporal change of the seismic-waves radiation source on the fault surface. The incident waves are assumed to mainly consist of S-wave because the estimated apparent velocity through the semblance analysis assuming plane-wave incidence is approximately 4 km/s and it don't have the dispersion. As the velocity structure model for the calculation of the travel time, we use one-dimensional velocity structure model in Asano & Iwata (2012). In this analysis, we constructed nine arrays at Tohoku and Kanto regions, and estimated the snapshot of semblance images at each array for 250s after the synthetic S-wave onset, which is comparable to the rupture starting time. The time length for semblance calculation is 20s and the time shift is 10s. The semblance value is obtained by averaging the three semblance values of the three-component waveforms.

The semblance images at the arrays north of 39°N are different from ones at the arrays south of 39°N. The images at the former arrays demonstrate that the seismic waves were strongly radiated from off Miyagi up to approximately 150s and that then the seismic waves were continued to be weakly radiated from off Miyagi. On the other hand, the images at the latter arrays demonstrate that the duration time of the seismic-wave radiation from off Miyagi is approximately 100s, that subsequently the radiation source moved to off Fukushima and Ibaraki, and that its radiation continued up to approximately 180s. This image difference indicates that the seismic-wave radiation area for the 2011 Tohoku earthquake extended to south approximately 100s after the rupture start and that off Miyagi radiated the seismic-waves during long time (~200s). We will also investigate the spatial variation for the seismic-wave radiation source along dip direction.

[Acknowledgments] The strong-motion data recorded by K-NET, KiK-net, and F-net of NIED and JMA and the 1Hz GPS data recorded by GEONET of GSI were used for this analysis.

Keywords: The 2011 Tohoku earthquake, Seismic-wave radiation characteristics, Semblance analysis, Strong-motion data, 1Hz GPS data

## Stochastic green function considering 3-D Qs structure-Predicting ground motion of the 2011 Tohoku Earthquake-

NAKAMURA, Ryoichi<sup>1\*</sup> ; UETAKE, Tomiichi<sup>2</sup> ; HIKIMA, Kazuhito<sup>2</sup>

<sup>1</sup>Tokyo Electric Power Services Co.,Ltd., <sup>2</sup>Tokyo Electric Power Company

We have developed a method to simulate strong ground motions by combining the stochastic green function (SGF) and 3-D attenuation effects.

The calculation procedures of our method are as follows.

- (1) To give Source spectra for sub-fault events.
- (2) To calculate basement spectra considering 3-D Qs structure.
- (3) To calculate ground surface spectra by multiplication of the site factors to basement spectra.
- (4) To make time history of ground motions using ground surface spectra and envelope function (Boore, 1983).
- (5) To create main shock ground motion by superimposing the ground motions from sub-fault events considering lapse time: ex. fault ruptures. (Kamae et al.,1991)

In this study, we reproduced strong motions of the 2011 Tohoku Earthquake (M9) by using this method. The fault plane of the 2011 Tohoku Earthquake was divided into 10\*10\*10 element faults planes, and seismic moment of  $M_0=4E+25$  Nm and stress drop 25 MPa are given to the elements uniformly. Target sites to evaluate are ground surfaces of the K-NET and the KiK-net observation stations. The 3-D Qs model and site amplification factors estimated by Nakamura (2009) were used in this study. To show validity of this method, we compared calculation results by using the 3-D Qs model with by a uniform Qs model;  $Q_s=100f^{1.00}$ .

The standard deviation of the logarithmic residual of PGA from the 3-D Qs model is 0.224 and that from the uniform Qs model is 0.231 for the stations with  $PGA > 100\text{Gal}$  and the values are 0.253 and 0.360 respectively for the stations with  $PGA > 1\text{Gal}$ . The difference was more significant for longer epicenter distance area. The response spectra calculated from the uniform Qs model are underestimated in the long distance areas, ex. Kinki and Hokkaido, whereas the response spectra using the 3-D Qs model were well reproduced the observed ones. Seismic wave spreads in deeper part for longer distance travels without attenuating. It is necessary to consider the three-dimensional Qs structure in evaluating the ground motion distribution in a broad area.

We tried to use the complex source model with SMGA. The model with five SMGA segments (Kurahashi and Irikura, 2011) was adopted for calculation. The waveforms calculated from the uniform source model are like spindle shape generally, but the waveforms from the SMGA model are divided into several wave groups of the corresponding to individual SMGA especially for observation points close to the source. The SMGA model could explain well the observed record shape.

Keywords: 3D attenuation structure, Stochastic green function, Qs, 2011 Tohoku earthquake, Depth dependence, Strong ground motion prediction

## Estimation of Strong Motion Generation Area during the 2008 Iwate-Miyagi Nairiku earthquake using broadband strong ground

KURAHASHI, Susumu<sup>1\*</sup> ; IRIKURA, Kojiro<sup>1</sup>

<sup>1</sup>Aichi Institute of Technology

### 1. Introduction

The 2008 Iwate-Miyagi Nairiku earthquake was an Mw6.7 reverse-fault crustal earthquake that occurred at Iwate prefecture, Japan. Surface ruptures associated with the earthquake were found to distribute near the eastern edge of the southern part of the aftershock zone. Strong ground motions were observed at three stations very near the fault area in addition to the Kik-net and K-NET stations. It is important that strong motion generation areas are estimated using broad-band ground motions to find out the source mechanism generating low-frequency ground motions as well as high strong ground motions.

In this study, we attempt to determine the strong ground motion area (SMGA) of the 2008 Iwate-Miyagi Nairiku earthquake using the broad-band ground motions from the earthquake.

### 2. The previous studies of the source model for strong ground motions

We presented the SMGA model of this earthquake by forward modeling using the empirical Green's function method by Irikura (1986) in 2008 and 2013.

The model we presented in 2008 was determined to reproduce the observed waveforms around the fault area of the mainshock. We found the first SMGA was located coinciding with large slip area in the southern part of the fault plane obtained by several authors from the waveform inversion analyses using teleseismic body wave data. We clarified to require one more SMGA in the northern part from the hypocenter. However, we realized that the location and geometry of the fault plane we assumed are not so accurate enough according to the aftershock distribution determined from temporary aftershock observation network deployed just after the occurrence of the earthquake (Okada et al., 2012).

We reanalyzed the SMGA model in 2013 using the fault plane determined by the aftershock distribution from the high dense network. In particular, we attempted to simulate the strong ground motions at IWTH25 located very near the fault plane. We obtained one of the best-fitting SMGA models from which simulated and observed ground motions agreed well including the ground motions at a very-near-field station IWTH25. However, it shall be examined whether this model can explain the broad-band ground motions at other near-field stations.

### 3. Estimation of SMGAs for broadband strong ground motions

In this study, we try to estimate the SMGAs using not only the strong motion records at IWTH25 but other near-field stations, Aratozawa Dam. The observed records at Aratozawa Dam show distinctive strong-motions. This suggests that one of the SMGAs possibly exists near Aratozawa Dam site. On the other hands, the observed records at Aratozawa Dam may have near-field-terms because of very-near-fields from the source area. Therefore, in order to reproduce the mainshock waveform we need to use the empirical Green's functions including the near-field terms, that is ground motion records from an element earthquake occurring very near a source in the fault area. When there is no element earthquake satisfying the near-field condition mentioned above, we use the hybrid Green's functions that have low frequency motions theoretically simulated and high frequency motions empirically obtained. We have no aftershock records at the Aratozawa Dam sites. Therefore, we attempt to simulate the broad-band strong motions at Aratozawa Dam site using only numerically calculated Green's functions to precisely estimate the SMGAs.

Keywords: Iwate Miyagi Nairiku earthquake, Strong Motion Generation Area, broad-band Strong Ground Motion

## Source Model and Strong Ground Motion Simulation for the 2013 Northern Tochigi Prefecture, Japan, Earthquake

SOMEI, Kazuhiro<sup>1\*</sup> ; MIYAKOSHI, Ken<sup>1</sup> ; IRIKURA, Kojiro<sup>2</sup>

<sup>1</sup>G.R.I., <sup>2</sup>A.I.T.

On February 25, 2013, an inland crustal earthquake ( $M_{JMA}6.4$ , Strike-slip type) occurred in the northern Tochigi prefecture, Japan. Strong ground motions with a peak acceleration of  $1225 \text{ cm/s}^2$  and a peak velocity of  $39 \text{ cm/s}$  were recorded at one of the nearest strong motion stations, TCGH07, about 5 km away from the hypocenter. Maeda and Sasatani (2009) showed that a similar large ground motion of  $1100 \text{ cm/s}^2$ ,  $75 \text{ cm/s}$  at HKD020 during the 2004 South Rumoi district, Hokkaido, Japan, inland crustal earthquake ( $M_{JMA}6.1$ , Dip slip type) is mainly attributable to the source effect, short distance from the strong motion generation area (SMGA) and the forward directivity effect. To investigate how large ground motions at TCGH07 from a source's point of view, we estimate the source model based on the two different approaches.

First, we employ the multi-time window linear waveform inversion method (Sekiguchi et al., 2000) by using the 15 strong motion waveforms (0.1-1.0Hz) recorded by K-NET, KiK-net near the source. A finite extent of the fault plane is assumed referring to the aftershock distribution and moment tensor solution determined by F-net. The fault plane is divided into 84 subfaults of  $1.0 \text{ km} \times 1.0 \text{ km}$ . The temporal moment release history from each subfault is expressed by a series of 6 smoothed ramp functions with a rise time of 0.6 sec separated by 0.3 sec. The first time window triggering velocity (FTWTV) was  $2.4 \text{ km/s}$ . The rise time and FTWTV are given by the smallest misfit solution. The weight of the spatio-temporal smoothing constraint value for inversion was determined based on Akaike's bayesian Information Criterion (ABIC). The velocity structure model for each strong motion station is improved by the downhill simplex method (Nelder and Mead, 1965) using the receiver function. The theoretical Green's function is calculated by using the discrete wavenumber integration method (Bouchon, 1981) with the reflection and transmission matrix (Kennett and Kerry, 1979). To validate the improved velocity structure models, we simulate the aftershock records with a point-source approximation.

The derived rupture model has a large slip area whose maximum slip of 0.98 m in the vicinity of the hypocenter. The rupture mainly propagated from the hypocenter toward the shallower northern part. Seismic moment of the estimated model is  $6.67 \times 10^{17} \text{ Nm}$  ( $M_w$  5.8). From the contribution of the large slip area to the synthetic waveforms for TCGH07, we find both the SH-wave radiation pattern from the strike-slip fault source and the forward directivity effect toward TCGH07 mainly yield the large pulse velocity waveform (0.1-1.0 Hz) at TCGH07.

Second, the source model is constructed based on the forward simulations using the empirical Green's function method (Irikura, 1986) in the frequency range 0.3-10 Hz. One rectangle SMGA is estimated to include the rupture start point, i.e., the hypocenter of the mainshock. The rupture of this SMGA mainly propagates from the hypocenter to shallow side for dip direction, and also propagates to the northward for strike direction. The obtained source model explains the observed acceleration, velocity, and displacement waveforms of this event in the broadband frequency range fairly well. As same as the result from waveform inversion (0.1-1.0 Hz), we also see the large pulse velocity waveform is caused by the forward directivity effect toward TCGH07.

Consequently, we concluded that the main factors generating large pulse velocity waveform at TCGH07 are as follows: 1) the SH-wave radiation pattern from the strike-slip fault source and 2) the forward directivity effect along dip direction toward TCGH07.

Keywords: The 2013 Northern Tochigi Prefecture, Japan, Earthquake, Waveform inversion, Empirical Green's function method, Source model, Strong ground motion simulation

## Source process of the Feb. 25, 2013 Tochigi Hokubu Earthquake (M 6.3) [2] -Analyses using Empirical Green's Functions-

HIKIMA, Kazuhito<sup>1\*</sup>

<sup>1</sup>Tokyo Electric Power Company

### \*\*INTRODUCTION\*\*

An M6.3 earthquake occurred in the northern part of Tochigi prefecture on February 25, 2013. A high acceleration strong motion, over 1 G, was observed at the TCGH07 (Kuriyama-west) of KiK-net, which is situated close to the source region. To explain the reason why such strong acceleration was observed, the author has made the studies using the source process analysis and spectral inversion method to separate site and path effects. However, in the source process inversion, it is difficult to calculate accurate theoretical Green's functions in good enough level, because of the difficulty of making accurate subsurface structures. Consequently, the degree of coincidence between observed and calculated waveforms was not so good.

To overcome such the drawbacks in the source process inversions, the author uses the observed waveforms from a small earthquake as empirical Green's functions (EGF) in this study.

### \*\*FAULT MODEL and OUTLINE of ANALYSES\*\*

Tentative analyses are performed with same fault geometry with Hikima (2013, SSJ fall meeting). The fault model was made using the relocated hypocenters, determined by the DD method, and the F-net mechanism solution. The strike direction is NNW-SSE (165 degree in strike, 80 degree in dip). The fault plane is divided in 1km size for the inversion.

The source process is inverted by the multi time window analysis (Yoshida *et al.* (1996), Hikima (2012)). The velocity waveforms, filtered between 0.03 and 1.5Hz, are used in the inversion analyses. The waveforms at TCGH07 are not used in the inversion, because the station is too close from the fault plain. Only the transverse components are used in this study, to weight the S-wave portion of the waveforms. The waveforms from the Mw 4.0 foreshock, which occurred on 15:26, February 25, 2013, are used as EGFs.

### \*\*RESULT\*\*

Tentative result shows a more concentrated slip distribution than the former results by the theoretical Green's functions (Hikima, 2013). The high moment release area is about 4km \*3km. However, the image of the rupture, whose slip propagates to the north, is almost same as former results. The coincidence between observed and calculated waveforms in this study is fairly better than the result by theoretical Green's functions.

Only one result using single EGF has been explained in this abstract. However, many other small earthquakes, which will be candidates for EGFs, occurred in the source area. So the results using other EGFs will be shown and I will discuss the accuracy of resultant slip distributions at the time of the presentation.

Keywords: Source process, Crustal earthquake, Near source, Strong motion, 2013 Tochigi Hokubu earthquake

## Source rupture process of the 2011 Northern Nagano earthquake (Mj 6.7) based on strong-motion records

SHIBA, Yoshiaki<sup>1\*</sup>

<sup>1</sup>CRIEPI

The slip distribution model of the March 12, 2011 Northern Nagano earthquake (M6.7) were estimated by assuming the multiple fault planes model based on the aftershock hypocenters detected from the high-dense seismometer array and the crustal deformation information derived by the interferometry synthetic aperture radar (InSAR). Since the strong-motion record with peak ground acceleration more than 700 gal was obtained at the K-NET station NIG023 near the main shock, it is important to investigate the geometrical relation between the strong motion generation area (SMGA) on the main shock fault and the observation station. Estimated source model displays the largest slip near the K-NET NIG023 and beneath the existing anticlinal structure. The reverse fault motion of this event is considered to contribute the growth of the anticline. On the other hand the secondary fault plane, which was recognized clearly from the crustal deformation data inferred from InSAR, released relatively small or negligible amount of the moment according to our examination. It might have been the deformation caused by the aftershock occurring just after the main shock.

Keywords: 2011 Northern Nagano earthquake, Source process, Strong ground motion, Inversion analysis, InSAR, Anticlinal structure

## Structural analysis of seismogenic fault of the 2013 Mw 5.8 Awaji Island earthquake, NW Japan

LIN, Aiming<sup>1\*</sup> ; KATAYAMA, Shouichi<sup>1</sup> ; RAO, Gang<sup>2</sup> ; KUBOTA, Yasu'uchi<sup>3</sup>

<sup>1</sup>Department of Geophysics, Graduate School of Science, Kyoto University, <sup>2</sup>Department of Earth Sciences, Zhejiang University, China, <sup>3</sup>OYO Cooperation

The 2013 Mw 5.8 (Mj 6.3) Awaji Island earthquake occurred in the southwest Awaji Island, at 5:33, 13 April, 2013, ca.25 km southwest of the epicenter of the 1995 Mw 6.8 (Mj 7.2) Kobe earthquake, southwest Japan. Pre-existing geologic data and focal mechanism show that this earthquake was triggered by an unknown active fault with a thrusting-dominated mechanism at high-dip angle of >70 degree. Interpretations of aerial photographs and 3D perspective images, field investigations and structural analysis of fault rocks, reveal that: i) a new fault, called Yamada Fault here, striking NNW and dipping WSW at a high-angle of 86 degree was found along a topographic lineament developed along the geological boundary between the Mesozoic granitic rocks and the Late-Tertiary-Quaternary Osaka Group composed of interbedded sandstone and mudstone; ii) a main shear zone of the Yamada Fault consists of a fault core that includes a narrow fault gouge zone of <10 cm in width (generally 1~5 cm), a fault breccia zone of <100 cm in width, and a damage zone of 10~50 m in width that is composed of cataclastic rocks and fractures; iii) the foliations characterized by S-C fabrics developed in the shear zone indicate a dominantly thrusting sense, consistent with that revealed by the focal mechanism; and iv) co-seismic surface ruptures occurred locally along the Yamada Fault, which are composed of numerous short fissures ranging from centimeters to several meters in length and concentrated in a zone <5 m. Our findings show that the newly found Yamada Fault is a active fault that probably triggered the 2013 Mw 5.8 (Mj 6.3) Awaji Island earthquake. Therefore, it is necessary to reconstruct the fault model for studying the tectonic activity and paleoseismicity and to reassess the seismic hazard of the active faults for densely populated Awaji Island, northwest Japan.

Keywords: 2013 M 6.3 Awaji Island earthquake, seismogenic fault, active fault, Yamada Fault, S-C fabrics of fault rocks, fault damage zone

## Quasi-cylindrical seismic waveform modeling considering surface topography

TOYOKUNI, Genti<sup>1\*</sup> ; TAKENAKA, Hiroshi<sup>2</sup> ; OKAMOTO, Taro<sup>3</sup> ; ZHAO, Dapeng<sup>1</sup>

<sup>1</sup>RCPEVE, Tohoku Univ., <sup>2</sup>Okayama Univ., <sup>3</sup>Tokyo Tech

An accurate and efficient modeling of regional seismic wave propagation can be achieved by the axisymmetric modeling using the cylindrical coordinates. It assumes the structural model as rotationally symmetric along the vertical axis including a seismic source, and then solves the 3-D wave equation in cylindrical coordinates only on a 2-D structural cross section (i.e., 2.5-D modeling). Therefore, this method can correctly model 3-D geometrical spreading effects and the pulse shape, with computation time and memory comparable to 2-D modeling.

On the other hand, application of the conventional purely axisymmetric approximation is difficult in practice because the structure along the measurement line of the seismic survey is rarely symmetric with respect to the source location. To overcome this difficulty, Takenaka et al. (2003) proposed a "quasi-cylindrical approach". They developed a numerical scheme for seismic exploration using the finite-difference method (FDM). The FDM scheme had then been improved to include an arbitrary moment-tensor point source and the anelastic attenuation for further realistic modeling (Toyokuni et al., 2013, AGU Fall meeting).

In this work, we extended the scheme to treat land and ocean-bottom topographies. We adopted the cell-based staggered-grid FDM, which places the normal-stress components at the center of a unit cell, and applies the 2nd-order FD approximation around the free surface or fluid-solid boundary (Okamoto & Takenaka, 2005; Takenaka et al., 2009; Nakamura et al., 2012). In the presentation, we will show an application of the scheme to the waveform modeling for the volcanic areas in Japan.

Keywords: seismic waveform, finite-difference method, topography, fluid-solid boundary

## Spatial distribution of aftershock decay property beneath Japan Trench

IKUTA, Ryoya<sup>1\*</sup> ; KUWAHARA, Masanori<sup>2</sup> ; MURAKAMI, Hiroki<sup>3</sup>

<sup>1</sup>Graduate School of Science, Shizuoka University, <sup>2</sup>Center of Integrated Research and Education of Natural Hazards, Shizuoka University, <sup>3</sup>Faculty of Science, Shizuoka University

We analyzed the aftershock sequences for individual M6-9 class inter-plate earthquakes and intra-plate earthquakes in Japan Trench for the period between October 1997 and March 2013 using JMA hypocenter catalog (final solution). The purpose is to examine a spatial relationship between the slip zone by the M9 earthquake and activity of aftershock series before the M9 and to understand the mechanism of aftershock. We approximated time variation of the number of aftershock sequences for each earthquake by the modified Omori's Law. Each aftershock sequence was identified from its spatial and temporal distribution. K and P parameters of Omori's Law were obtained by fitting the logarithmic Time-Frequency graphs of the aftershock sequence by linear function. We analyzed aftershock sequences for 44 events and adopted 17 whose K values are larger than 10 as available results because the results with smaller K values than 10 had large uncertainties due to lack of data. The results showed negative correlation between P values and  $M_j$  of the mainshocks. Before and after the M9 earthquake, there was no significant change in the aftershock parameters. However, we found a depth-dependent spatial distribution of aftershock decay property. In the plate boundary, the aftershock sequence lasts for longtime without significant decay in the deeper portion, in contrast that the aftershock decays quickly at the shallower portion. It is known that the deeper part of plate boundary tends to slip aseismically without earthquakes. Taking this slow slipping property into account, our result suggests that the inter-plate frictional property should be responsible to the delay and decay property of the aftershocks.

Keywords: Aftershocks, Modified Ohmori's Law, Tohoku-Oki earthquake, Seismicity

## Location of early aftershocks of the 2011 Tohoku-oki Earthquake using seismogram envelopes as templates

KOSUGA, Masahiro<sup>1\*</sup> ; SAKAI, Yuuka<sup>2</sup>

<sup>1</sup>Graduate School of Sci. & Tech., Hirosaki Univ., <sup>2</sup>Fac. Sci. & Tech., Hirosaki Univ.

The location of early aftershocks is very important to estimate the initial size of mainshock fault, because the aftershock zone generally extends with time. However, the location of early aftershocks is often difficult due to the long-lasting coda wave of mainshock and successive occurrence of aftershocks. To overcome this situation, we developed a location method using seismogram envelopes as templates. During the process of location, we firstly calculate the cross-correlation coefficients between a continuous (target) and template envelopes, and obtain time series of station-averaged cross-correlations for all templates. We then search for templates (initial location) in the descending order of cross-correlations in a time window excluding the dead times around the previously detected events. The third process is the relative event location that accounts for the lag times between actual and template envelopes. We applied the method to the early aftershock sequence of the 2011 Off the Pacific Coast of Tohoku Earthquake (Mw = 9.0). In a time window of 30-minutes just after the mainshock, we could locate 22 events in 8 Hz band by using 96 templates recorded at 33 Hi-net stations. The number of located events by the JMA is 13. Though we should carefully examine the location of detected events, we conclude that the proposed detection method works adequately even just after the mainshock of large earthquake.

Acknowledgement: We thank the NIED for providing waveform data of Hi-net. This work was supported by JSPS KAKENHI Grant Number 23540487.

Keywords: early aftershocks, template, envelope, Off the Pacific Coast of Tohoku Earthquake

## Aftershock distribution in the northern source region of the 2011 Tohoku earthquake by long-term OBSs

SHINOHARA, Masanao<sup>1\*</sup>; YAMADA, Tomoaki<sup>1</sup>; NAKAHIGASHI, Kazuo<sup>2</sup>; MOCHIZUKI, Kimihiro<sup>1</sup>; MACHIDA, Yuya<sup>1</sup>; SHINBO, Takashi<sup>3</sup>; MURAI, Yoshio<sup>4</sup>; HINO, Ryota<sup>5</sup>; ITO, Yoshihiro<sup>6</sup>; SATO, Toshinori<sup>7</sup>; UEHIRA, Kenji<sup>3</sup>; YAKIWARA, Hiroshi<sup>8</sup>; SHIOBARA, Hajime<sup>1</sup>

<sup>1</sup>ERI, Univ. of Tokyo, <sup>2</sup>Kobe Univ., <sup>3</sup>NIED, <sup>4</sup>Hokkaido Univ., <sup>5</sup>Tohoku Univ., <sup>6</sup>DPRI, <sup>7</sup>Chiba Univ., <sup>8</sup>Kagoshima Univ.

The 2011 Tohoku earthquake occurred at the plate boundary and many aftershocks followed. To obtain a precise aftershock distribution is important for understanding of mechanism of the earthquake generation. In order to study the aftershock activity, we carried out extensive sea floor aftershock observation using more than 100 ocean bottom seismometers just after the mainshock. Deployment and recovery of the OBS were repeated, and we obtained the data from OBSs just after the mainshock to the middle of September, 2011. A precise aftershock distribution for approximately three months in the whole source area, with an emphasis on depths of events, was obtained from the OBS data. In the southern source region, an aftershock distribution until September, 2011 was also estimated. Totally urgent OBS observations located 1210 aftershocks (Shinohara et al., 2011, 2012). After the urgent aftershock observation using short-term OBSs, we continued the observation using long-term OBSs to monitor seismic activities in the source area. We deployed 40 LT-OBSs in the whole source region in September 2011 and have completed recovery of the LT-OBSs until November, 2012. In this presentation, we concentrate seismic activities in the northern source region using the data from the urgent aftershock observation and long-term seafloor observation.

We selected events whose epicenter is located below the OBS network from the JMA earthquake catalog, and P and S-wave arrival times were picked from the OBS data. Hypocenters were estimated by a maximum-likelihood estimation technique with one dimensional velocity structures. Thickness of sedimentary layer changes at each OBS site was evaluated and the estimated travel times by the location program were adjusted. We will report precise seismic activities in the northern source region with spatial and temporal variation. From preliminary analysis, seismic activity in off-Miyagi region was still low until the end of the long-term observation.

## A boundary of stress-field orientation in northwestern area of the Kanto plain

YANO, Tomoko elizabeth<sup>1\*</sup> ; TAKEDA, Tetsuya<sup>1</sup> ; SHIOMI, Katsuhiko<sup>1</sup>

<sup>1</sup>NIED

Kanto-Tokai area is particularly important in terms of seismic hazard and mitigating disaster since this area is having high potential to economic and social impacts. Despite the fact, the Kanto region is one of the most seismic active areas due to its complicated tectonics and has an active fault zone, containing Fukaya fault, in northwestern area of the Kanto plain, which has potential to the M8 class earthquake. Many studies and research projects have attempted to understand the seismic activity and stress field. However, reliable and high-resolution catalog is required for the detailed discussion.

We have launched Japan Unified High-resolution Relocated Catalog for Earthquakes (JUICE) project since 2013. Events were relocated using the Double-Difference method for high-resolution hypocenter location to estimate seismogenic layer thickness, to evaluate active faults, and to understand the tectonic processes in Japan. We have completed for the first version of Catalog in the region of Kanto-Tokai area for the shallow (>40 km) earthquakes between M0 and M6.5 from 2001 to 2012. Here, in this presentation, we introduce the result from JUICE focusing on the northwestern area of the Kanto plain that contains a sharp boundary in which pressure and tension axis dramatically change by 90 degrees.

The JUICE catalog clearly shows a band of seismicity from Izu peninsula to the north. This seismic band has a nearly constant width of about 50 km. The focal mechanisms show that strike and thrust type dominate throughout this seismic band continuously, though there exists a area where pressure and tension axis dramatically change within this seismic band. While this “ area ” has been already recognized (e.g. Suzuki, 1989), JUICE helps to draw a precise “ line ” as a stress-field orientation boundary where happened to be close to Fukaya fault.

Bouguer gravity anomaly and seismic exploration data imply structural changes at the stress-field orientation boundary. According to the Bouguer gravity anomaly (Komazawa, 2004), the boundary appears to be associated with the gravity-low zone. The gravity anomalies show a lineation that trends NW-SE, the same direction of the boundary. Seismic profile (Sato et al., 2003) displays changes in basement character showing the pattern of depression beneath Fukaya fault. The shape of depression corresponds to the pattern of seismicity beneath this area, and also the boundary sites beneath the lowest point of the depression.

It appears to split into different regimes at the stress-field orientation boundary. We conclude that it is possible to have major tectonic boundary underneath this northwestern area of the Kanto plain. Moreover, we suggest that Median tectonic line (MTL) is a major candidate underneath this area. MTL runs parallel to the island arc through southwest Japan and divides different geological structures into outer (the forearc side) and inner arc (the backarc side). The trace of MTL disappears on the eastern side of Itoigawa-Shizuoka tectonic line, but Takagi et al. (2006) found an evidence of inner arc materials in the core sample obtained around this area. Therefore we assume that MTL is buried underneath the boundary. This finding may eventually impact on the research relates to hazard of Kanto area.

Keywords: Seismicity and tectonics

## Estimating earthquake swarms in volcanic regions

KUMAZAWA, Takao<sup>1\*</sup> ; OGATA, Yoshihiko<sup>1</sup> ; KIMURA, Kazuhiro<sup>2</sup> ; MAEDA, Kenji<sup>2</sup> ; KOBAYASHI, Akio<sup>2</sup>

<sup>1</sup>The Institute of Statistical Mathematics, <sup>2</sup>Meteorological Research Institute

In the eastern Izu region, earthquake swarms have occurred repeatedly since 1978. These events are known to be triggered by magma intrusions, and the amount of magma intrusion is correlated with volumetric strain of the crust. We show the background seismicity rate is highly correlated with the volumetric strain in this region, with a short time delay. We then discuss the possibility to forecast the seismicity in volcanic regions.

To calculate the background seismicity rate, we used the epidemic-type aftershock sequence (ETAS) model extended for application to nonstationary seismic activity, introduced by Kumazawa & Ogata (2013). The time-dependent rates of both background seismicity and aftershock productivity in the ETAS model are optimally estimated from hypocenter data by Bayesian smoothing method. These rates can provide quantitative evidence for abrupt or gradual changes in shear stress and/or fault strength due to aseismic transient causes such as triggering by remote earthquakes, slow slips, or fluid intrusions within the region.

Keywords: ETAS model, Bayesian smoothing, earthquake swarm, volcanic region, Izu

## Source Characteristics and Coulomb Stress Change of the 19 May 2011 Mw 6.0 Simav-Kutahya Earthquake, Turkey

GORGUN, Ethem<sup>1\*</sup>

<sup>1</sup>Department of Geophysical Engineering, Istanbul University

### Abstract

On 2011 May 19, Simav district of Kutahya province in northwest Anatolia was hit by a moderate size ( $M_w=6.0$ ) earthquake. Centroid moment tensors for 41 events with moment magnitudes ( $M_w$ ) between 3.5 and 6.0 are computed by applying a waveform inversion method on data from the Kandilli Observatory and Earthquake Research Institute broadband seismic network. The time span of data covers the period between 2011 May 19 and 2011 August 22. The mainshock is a shallow focus normal event at a depth of 10 km. Focal depths of aftershocks range from 5 to 20 km. The seismic moment ( $M_0$ ) of the mainshock is calculated  $1.15 \times 10^{18}$  Nm. The estimated rupture duration of the Simav mainshock is 30 s. The focal mechanisms of the aftershocks are mainly normal faulting with a variable strike-slip component. The geometry of focal mechanisms reveals a normal faulting regime with NE-SW trending direction of T-axis in the entire activated region. A stress tensor inversion of focal mechanism data is performed to acquire a more accurate picture of the Simav earthquake stress field. The stress tensor inversion results indicate a predominant normal stress regime with a NW-SE oriented maximum principal compressive stress. According to variance of the stress tensor inversion, to first order, the Simav earthquake area is characterized by a homogeneous intraplate stress field. Eventually, Coulomb stress analysis is performed to calculate the stress transfer and correlate it with the activated region. Positive lobes with stress more than 3 bars are obtained, indicating that these values are large enough to increase the Coulomb stress failure towards NW-SE direction.

Keywords: Aftershock, Coulomb Stress Analysis, Focal Mechanism, Simav earthquake, Stress tensor inversion, Western Anatolia

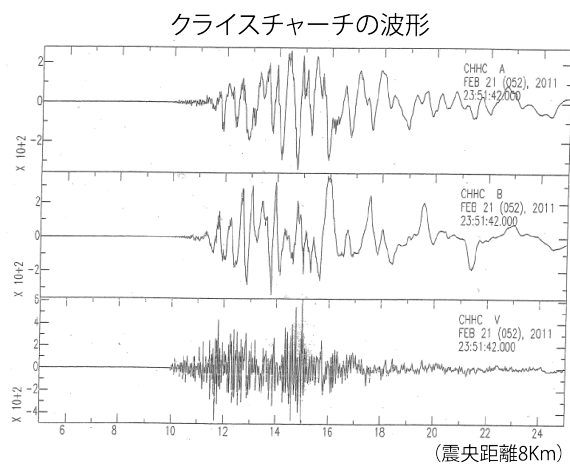
## The Great Kanto Earthquake (of 1923) and YOKOHAMA (1)

NISHIZAWA, Masaru<sup>1\*</sup>

<sup>1</sup>none

1. The reinforced concrete buildings has been completed the leadership factions after The Great Kanto Earthquake (of 1923).
2. The YOKOHAMA Civilization Colour Print was important mediums of the YOKOHAMA exoticim and cultures.

Keywords: The Great Kanto Earthquake (of 1923), Yokohama, Open a port, YOKOHAMA civilization color print, The reinforced concrete building



東西、南北の波の位相は逆転していることは他と同じで、水平方向に建物に対して回転力(又はねじれ)が生じることが判る。

主要動以後の波形は波うっていることは他と同様。しかし、上下動も多少は波うってはいるが、東西、南北に比べると小さい。

## Seismic activity in eastern Japan and the source region after the 2011 off the Pacific coast of Tohoku earthquake

UOOCHI, Akiko<sup>1</sup> ; KUGE, Keiko<sup>1\*</sup>

<sup>1</sup>Dept. Geophysics, Kyoto University

Changes of seismic activity in eastern Japan and the source region were shortly reported after the 2011 off the Pacific coast of Tohoku earthquake (Toda et al., 2011; Kato and Igarashi, 2012). To clarify subsequent changes, we investigated seismic activity in the wide region for two and a half years since the 2011 Tohoku earthquake.

We examined a region in a range of 33.4-42N and 136-145E. The region was divided into small squares with a size of 0.2 degree, and in each square, we computed seismicity rates. First, as the background seismicity, we computed the average number of earthquakes per a year, based on seismic activity for nine years before the 2011 earthquake. Then, to obtain seismicity rates after the 2011 earthquake, we counted the number of earthquake during two periods, respectively, and computed the ratios against the background seismicity. The two periods are 0-1 and 1.5-2.5 years after the 2011 earthquake. We used hypocenters determined by JMA. In regions where large inland earthquakes occurred before 2011, the background seismicity was computed from a period excluding aftershocks. Finally, by plotting the resultant seismicity rates in maps, we searched regions where seismic activity significantly changed. By the same method, we also examined seismicity rates of interplate earthquakes in the source region of the 2011 Tohoku earthquake, based on data selected from the F-net CMT catalog.

Our results show that when two and a half years passed since the 2011 earthquake, seismicity of interplate earthquakes had been lower than the background, throughout the source region of the 2011 Tohoku earthquake except for a region off Iwata. High seismic activities for a year since the 2011 earthquake were found in Iwaki, the middle and northern parts of Akita, the southern part of the Kanto region, and also in regions near active volcanos (Bandai, Nikko-Shirane, Kusatsu-Shirane, Naeba, and Fuji mountains). When two and a half years passed, seismicity in many regions of eastern Japan had been lower than the background, including the activities near Bandai, Naeba, and Fuji mountains. However, activities in Iwaki, the middle and northern parts of Akita, the southern part of the Kanto region, and near Nikko-Shirane and Kusatsu-Shirane mountains continued to be high.

Furthermore, we carefully examined seismic activity in the regions where we detected significant changes of seismic activity. In many regions of eastern Japan, we found that locations of earthquakes and focal mechanisms were changed before and after the 2011 Tohoku earthquake.

Using JMA hypocenters, we also attempted to apply the modified Omori's law for seismic activity after the 2011 earthquake in the regions with significant changes of seismic activity. The modified Omori's law could roughly model the changes of seismic activity in many regions, even when a region is inland, away from the source region. The Omori's regression parameter,  $p$ , was estimated in a range from 0.2 to 1.1. The values ranged between 0.2 and 1.1 in the regions where seismic activity has been high for 2.5 years, whereas they were between 0.8 and 1.1 where high seismic activity for the first 1 year decreased in 2.5 years since the 2011 earthquake. In the southern part of the Kanto region, the value of  $p$  (0.2) was extremely low, compared to the other regions, which implies that the seismic activity decays very slowly. In the regions near active volcanos, the values of  $p$  tended to be high. In the source region of the 2011 Tohoku earthquake, we estimated the values of  $p$  in three regions; a whole source region, an afterslip region, and a region excluding the afterslip region. The values ranged from 1.0 to 1.1, and there was no significant difference in the three regions.

## A statistical feature of anomalous seismic activity prior to large inland earthquakes in Japan

KAWAMURA, Masashi<sup>1\*</sup> ; WU, Yi-hsuan<sup>2</sup> ; KUDO, Takeshi<sup>3</sup> ; CHEN, Chien-chih<sup>2</sup>

<sup>1</sup>Department of Geosciences, National Taiwan University, <sup>2</sup>Grad. Inst. of Geophysics, National Central University, Taiwan,  
<sup>3</sup>General Education Division, College of Engineering, Chubu University

To reveal the preparatory processes of large inland earthquakes, we systematically applied the pattern informatics (PI) method to earthquake data of Japan. We focused on 12 large earthquakes with magnitudes greater than M6.4 (based on the magnitude scale of the Japan Meteorological Agency) that occurred at depths shallower than 30 km between 2000 and 2010. We examined the relationship between the spatiotemporal locations of these large shallow earthquakes and the locations of PI hotspots, which correspond to grid cells of anomalous seismic activity during a designated time span. Based on a statistical test conducted using Molchan's error diagram, we investigated whether precursory anomalous seismic activity occurred in association with these large earthquakes and, if so, studied the characteristic time spans of such activity. Our results indicate that Japanese inland earthquakes with  $M \geq 6.4$  are typically preceded by anomalous seismic activity in timescales of 8-10 years.

Keywords: pattern informatics, seismic quiescence, seismic activation, Molchan's error diagram, stress accumulation, inland earthquake

## Coulomb stress change inverted from the seismicity rate change in southern 2011 Tohoku earthquake's source region

TAKAHASHI, Go<sup>1\*</sup> ; TSUMURA, Noriko<sup>1</sup>

<sup>1</sup>Graduate School of Science, Chiba University

By using the analysis of seismicity rate change, we estimated spatio-temporal evolution of Coulomb stress around the upper boundary of the Pacific plate (PAC) and Philippine Sea plate (PHS) in and around the southern edge of the rupture zone of the 2011 Pacific coast of Tohoku earthquake (Mw=9.0). We used hypocenter catalog of the Japan Meteorological Agency (JMA) for the period between 1998/1/1 and 2013/3/31. Estimated stress change became large just after the 2011 Tohoku earthquake in most of rupture zone. The large stress change estimated from the seismicity reached the southern outside of the contact zone of the PHS and the PAC, while this area is located at outside of the source fault of the 2011 Tohoku earthquake. Moreover, in the October 2011 Boso slow slip event (SSE) initiation area, stress change remained large value after the 2011 Tohoku earthquake.

To estimate the effect of the mainshock and largest aftershock in our inversion result, we calculated Coulomb stress change by simulating the mainshock, afterslip and Mw7.9 aftershock for the 2011 Tohoku earthquake in an elastic half space. From similarity between the result from seismicity rate change and result of forward modeling, most of the stress change pattern in and around mainshock rupture zone after the 2011 Tohoku earthquake might be explained by the effect of the 2011 Tohoku earthquake mainshock, afterslip and the largest aftershock. On the other hand, since the result from seismicity rate change didn't correspond to the result of forward modeling in the October 2011 SSE area, this region was possibly affected by other event or closeness to break strength.

Keywords: stress change, 2011 Tohoku earthquake, aftershock, slow slip

## Spatial distribution of earthquakes off the coast of Ibaraki and the Boso Peninsula after the 2011 Tohoku Earthquake

NAKAHIGASHI, Kazuo<sup>1\*</sup> ; MACHIDA, Yuya<sup>2</sup> ; SHINBO, Takashi<sup>7</sup> ; YAMADA, Tomoaki<sup>2</sup> ; MOCHIZUKI, Kimihiro<sup>2</sup> ; SHIOBARA, Hajime<sup>2</sup> ; SHINOHARA, Masanao<sup>2</sup> ; MURAI, Yoshio<sup>3</sup> ; HINO, Ryota<sup>4</sup> ; AZUMA, Ryosuke<sup>4</sup> ; SUZUKI, Kensuke<sup>8</sup> ; KUBOTA, Tatsuya<sup>4</sup> ; HASEGAWA, Kazuya<sup>4</sup> ; SATO, Toshinori<sup>5</sup> ; TAKATA, Hiroyoshi<sup>5</sup> ; UEHIRA, Kenji<sup>7</sup> ; YAKIWARA, Hiroshi<sup>6</sup>

<sup>1</sup>Kobe Univ., <sup>2</sup>Earthquake Research Inst., <sup>3</sup>Hokkaido Univ., <sup>4</sup>Tohoku Univ., <sup>5</sup>Chiba Univ., <sup>6</sup>Kagoshima Univ., <sup>7</sup>National Research Institute for Earth Science and Disaster Prevention, <sup>8</sup>JAMSTEC

The 2011 off the Pacific coast of Tohoku Earthquake occurred on March 11, 2011, off shore of the northeast Japan region. Many aftershocks occurred following the mainshock. To obtain a precise aftershock activity is important for understanding the mechanism of earthquake generation, and the recovery of plate coupling at a ruptured plate boundary. In order to study the aftershock activity, we had deployed 66 long-term ocean bottom seismometers(LTOBS) off the coast of Ibaraki and the Boso Peninsula from October 2011 to November 2012.

For hypocenter determination, we selected 1606 events whose epicenter catalog which the Japan Meteorological Agency for hypocenter determination. P- and S- wave arrival times were manually picked using the WIN system (Urave and Tsukada, 1991). Hypocenters were determined by the maximum-likelihood estimation technique (Hirata and Matsuura, 1987). The hypocenter location program used in this study is based one-dimensional structure with constant Vp/Vs ratio of 1.73. Because a sedimentary layer below the sea floor generally has a large Vp/Vs value, an adjustment of the station corrections is needed. To obtain the station correction, we used the following method. First, we located the hypocenter using the P- and S-wave arrival times with the assumed station correction values for the velocity structure used. The averaged differences between observed travel time and estimated travel times (O-C times) for each station were then calculated. The averaged O-C times were added to the previous station correction values, and the hypocenters were relocated. We repeated this procedure eleven times. After this procedure, the averaged O-C times were less than 0.1 s for both the P-wave and S-waves. We estimated 458 hypocenter locations with an error of less than 5 km in the horizontal direction and less than 3 km in depth by using LTOBS data.

Most of the hypocenter locations have a depth shallower than 40km. The earthquakes form a plane dipping landward in the study area. Comparing the hypocenter locations with crustal structures obtained by active seismic studies (e.g. Miura et al., 2003). Many events occurred along the plate boundary. We also compared the hypocenter locations with aftershock distribution of the seismic observation conducted immediately after 2011 Tohoku Earthquake (Shinohara et al., 2012). Shinohara et al., (2012) reported that the low seismicity region has seen at the shallow part of the plate interface in the off-Fukushima. On the other hand, our results showed the seismicity is not low at the same region. This difference may reflect the change of stress fields at a ruptured plate boundary.

## Spatial distribution of earthquakes off the coast of Fukushima deduced from a one-year OBS observation in 2013

YAMADA, Tomoaki<sup>1\*</sup> ; NAKAHIGASHI, Kazuo<sup>2</sup> ; SHINOHARA, Masanao<sup>1</sup> ; MOCHIZUKI, Kimihiro<sup>1</sup> ; SHIOBARA, Hajime<sup>1</sup>

<sup>1</sup>Earthquake Research Institute, Univ. of Tokyo, <sup>2</sup>Kobe Univ.

The 2011 Tohoku earthquake (M9.0) vastly changes stress field around the rupture zone, and many aftershocks and other related geophysical phenomenon such as geodetic movements have been observed. The seismicity not only keeps still high rate compared with that before the 2011 earthquake but is important to figure out the time-spacious distribution during the relaxation process for understanding the giant earthquake cycle. Many studies using ocean bottom seismometers (OBSs) [e.g. Shinohara et al., 2011, Nakahigashi et al., this meeting] have been doing since soon after the 2011 Tohoku earthquake in order to obtain aftershock activity precisely. Here we show one of the studies at off the coast of Fukushima which is located on the southern edge of the rupture zone of the 2011 Tohoku earthquake. 12 short-period type [Lennartz 3Dlite] OBSs (SOBS) and 4 broadband type [Guralp CMG 3T] OBSs (BBOBSs) in August 2012 were installed. 20 SOBSs and 4 BBOBSs attached with absolute pressure gauge [Paroscientific Model 8B] were added in November 2012. After one year continuous recording, 36 OBSs were recovered in November 2013. We selected characteristic 1,000 events in the vicinity of the OBS network based on a hypocenter catalog publish by the Japan Meteorological Agency, and extracted the events' data from all available OBS data after time corrections caused by each internal clock. Each P and S wave arrival times, P wave polarity and maximum amplitude were picked manually on a computer display using the WIN system [Urabe and Tsukuda, 1991]. We assumed one dimensional velocity structure that is modification of the result from an active source experiment close to our network, and applied time corrections every station which were estimated from differences from theoretical and observational travel times for removing ambiguity of the assumed structure. Then we adopted the maximum-likelihood estimation technique [Hirata and Matsu'ura, 1987] and calculated the hypocenters. Preliminary results show that intensive activity near the Japan trench can be seen while there was a quiet seismic zone between the trench zone and landward high activity zone.

Keywords: off Fukushima, Aftershock activity, Long-term OBS

## Relation between Seismicity and Stress Change Associated with Interplate Slips off Boso Peninsula: Part 2

HIROSE, Fuyuki<sup>1\*</sup> ; MAEDA, Kenji<sup>1</sup>

<sup>1</sup>Meteorological Research Institute

Hirose & Maeda (2012, 2013, JpGU; 2013, SSJ) investigated a relation between temporal variation of seismicity rate or b-value of the G-R law (Gutenberg and Richter, 1944, BSSA) and stress change associated with slow slip events (SSEs) around Boso peninsula. For example, there are three characteristic stages about seismicity: (S-1) activation during SSE, (S-2) quiescence before 2002 and 2007 SSE, and (S-3) seismicity rate increases after 2007 SSE. On the other hand, b-value repeats a cycle as follows: (b-1) small during and just after SSE, (b-2) gradually increases up to the next SSE.

By considering the correlation of seismicity rate with stress increase and inverse correlation of b-value with stress obtained in laboratory experiments (Dieterich, 1994, JGR; Scholz, 1968, BSSA), they interpreted their result as follows: for (S-1, b-1) during SSE, the slip rate at the edge of SSE on the plate boundary where is seismically active becomes higher (We can confirm it from the distribution of slip deficit and SSE estimated by GNSS data). Then because a strain accumulation rate increases, the stressing rate increases. Thus, seismicity rate increases, and b-value decreases at the same time. On the other hand, for (S-2, b-2) in SSE interval, because the slip rate on the plate boundary becomes lower than that during SSE, the seismicity rate decreases, and b-value increases at the same time. For (S-3) seismicity rate increases after 2007 SSE, the distribution of slip deficit after 2007 SSE is not much different from that before SSE. When we consider a frame of Dieterich (1994), only steady slip rate should become higher without changing of slip deficit rate so that seismicity rate changes under this situation because slip deficit on the plate boundary is independent of the value of steady slip rate (Savage, 1983, JGR). That means the drop of the coupling rate on plate boundary (slip deficit rate / steady slip rate). Therefore, the temporal change of the seismicity and b-value is comprehensively consistent with the perturbation of the slip rate on the plate boundary.

By the way, Boso SSEs had occurred every 4-7 years, but the latest interval of occurrence has a shorter period because those occurred in the end of 2011 and early in 2014. It is considered that the shortening of interval is mainly caused by the influence of the 2011 off the Pacific Coast of Tohoku Earthquake (Mw9.0, hereinafter Tohoku earthquake). We extended data period and investigated whether the same characteristics as before are also seen for the 2014 SSE. As a result, it showed such the same characteristics that (S-1) activation during SSE, (S-3) seismicity rate increases after 2007 SSE, (b-1) small during and after SSE, and (b-2) gradually increase up to the next SSE. On the other hand, (S-2) quiescence before SSE was not recognized because the perturbation of stress caused by the Tohoku earthquake may affect the seismicity.

Keywords: Boso peninsula, slow slip event, b value, stress, temporal change

## Microseismicity around the Nankai trough south off the Kii Peninsula

YAMAZAKI, Akira<sup>1\*</sup>

<sup>1</sup>Meteorological Research Institute

The seismicity around the Nankai trough axis and its southern area, south off the Kii Peninsula, was not well understood, because most previous ocean bottom seismograph observations had been performed at landward from the trough axis. In order to investigate the seismicity around the region, Meteorological Research Institute conducted ocean bottom seismograph observations at around the Nankai trough axis and its southern area from 2005 to 2008, cooperated with Seismology and Volcanology Department, Japan Meteorological Agency (JMA). We conducted four observations, which period was approximately three months, using about ten pop-up type ocean bottom seismographs. As a result, we could detect a microseismic activity, which were not listed in the earthquake catalogue by JMA, around the trough axis.

The features of the microseismic activity are as follows. The depth of the hypocenters distributes around 10km to 25km. Since the depth of hypocenters determined by JMA at the region distributes around 30km to 40km, the true depth of the earthquakes is considered about 20km shallower than that of the JMA. There is a clear lower limit plane of hypocenters, and little earthquakes occur deeper than 25km. As a general tendency, the microseismic distribution has south incline at seaward from the trough axis, north incline at landward. The distribution of the hypocenters is not uniform, and we can detect some seismic clusters, liner arrangements and several seismic gaps of the 20km to 30km in diameter. It seems that seismic segment structures are formed within the Philippine Sea plate.

In general, seismic activity around a trough axis is caused by bending of oceanic plate. Moreover, the activity is affected by somewhat change of interplate coupling status at subduction zone. For instance, it is pointed out that the focal mechanism at outer rise region changes from compressional to tensional tectonic field by occurrence of large interplate earthquakes at subduction zone. We propose a possibility that the temporal change of the microseismic activity around the Nankai trough axis reflects a temporal change of the plate motion or a somewhat change of plate coupling conditions.

Keywords: ocean bottom seismograph, Tonankai earthquake, Nankai earthquake, Nankai trough, microseismicity, Philippine Sea plate

## Repeating earthquake activity along the Izu-Bonin and Ryukyu trenches

HIBINO, Kota<sup>1\*</sup> ; UCHIDA, Naoki<sup>1</sup> ; MATSUSHIMA, Takeshi<sup>2</sup> ; NAKAMURA, Wataru<sup>1</sup> ; MATSUZAWA, Toru<sup>1</sup>

<sup>1</sup>Graduate School of Science Tohoku University, <sup>2</sup>Faculty of Sciences, Kyushu University

There are several subduction systems near the Japanese islands. The 2011 Mw9.0 Tohoku-oki megathrust earthquake occurred at the northeastern Japan subduction zone and revealed a complementary relation between the slip areas for huge earthquakes and small repeating earthquakes (REs). Investigations of REs in other subduction zones and their comparison with Tohoku area are important for revealing generation mechanism of megathrust earthquakes.

We use seismograms from the High Sensitivity Seismograph Network (Hi-net) and Japan Meteorological Agency (JMA)'s permanent seismograph stations from 8 May 2003 to 31 December 2012. We detect RE along the Izu-Bonin and Ryukyu trenches, using similarity of seismogram pairs.

Although, Igarashi (2010) and Yamashita et al. (2012) have already examined RE activity in this region, we mainly follow the method of Uchida et al. (2010) to compare with the REs at Tohoku area. In the method, pair with coherence larger than 0.95 at multiple stations is considered to belong to a repeating earthquake group. We apply this method to the earthquakes along the Ryukyu trench. Along the Izu-Bonin trench, however, the signal-to-noise (S/N) ratios of the waveforms are not so good because of the limited seismic stations at sparsely distributed islands. Therefore, we adopt a coherence threshold of 0.8 and even if S/N ratios of the waveform are good at only one station, earthquake pairs that satisfy the threshold in multiple components are considered as candidates of REs along the Izu-Bonin trench.

Along the Ryukyu trench, we find RE distribution shows two dense bands parallel to the trench axis. This feature is similar to the northeastern Japan subduction zone. We consider the regions between the two bands of REs may have strong interplate locking as suggested at Tohoku.

Along the Izu-Bonin trench, in spite of the non-strict coherence threshold, we find much fewer REs than that in northeastern Japan. Our result suggests that REs are relatively rare along the Izu-Bonin trench and they mainly occur at the shallow part where the Pacific plate contacts with the crust of the Philippine Sea plate.

These varieties in the RE occurrences suggest different interplate locking patterns along these subduction systems.

Keywords: subduction zone, repeating earthquake, Izu-Bonin, Ryukyu, interplate locking

## Ocean bottom seismic observation in the Hikurangi subduction zone offshore the North Island of New Zealand

HAIJIMA, Daisuke<sup>1\*</sup> ; MOCHIZUKI, Kimihiro<sup>1</sup> ; SHIOBARA, Hajime<sup>1</sup> ; YAMADA, Tomoaki<sup>1</sup> ; SHINOHARA, Masanao<sup>1</sup> ; HENRYS, Stuart<sup>2</sup> ; FRY, Bill<sup>2</sup> ; BANNISTER, Stephen<sup>2</sup>

<sup>1</sup>Earthquake Reserch Institute, University of Tokyo, <sup>2</sup>GNS Science

The Hikurangi Plateau which has ~12 km thick crust subducts under the Australian plate in the Hikurangi subduction zone offshore North Island, New Zealand. The plate interface is relatively shallow so that geometry of the plate interface has been revealed in detail by high quality seismic reflection data collected along dense profiles along the margin [Bell et al. 2010]. Distribution of interseismic plate-coupling has been estimated and series of slow slip events (SSEs) have been detected at around the lower limit of the coupling region due to recent installation of dense GPS network over the North Island. In the northern part, along-strike coupling region is narrow and the upper limit extends to near the trench axis and the lower limit is shallow at ~15 km depth. Most of the region of strong interplate coupling is under the sea. We need to conduct seismic observation using ocean bottom seismometers (OBSs) to understand seismicity and hypocentral distribution in detail. SSEs occur at much shallower depth than other subduction zones.

We conducted a passive seismic observation using OBSs for the first time offshore Gisborne to reveal seismicity and low-frequency events accompanying SSEs. We deployed four OBSs in April 2012 and recovered all instruments after 11 months of observation. The northern two instruments were a broadband type and the other southern two were equipped with 1Hz seismometers. Although the recorder of one of the broadband type OBSs recorded only intermittently, good data were obtained from the others. An earthquake swarm occurred to the north of the array in September to November 2012. A large SSE occurred around the Hawke's Bay to the south of the array from mid-February 2013. At first we apply STA/LTA algorithm to this data to detect seismicity. The result shows seismicity was activated accompanying both the earthquake swarm and the SSE. We tried to determine the hypocenters of these events using 4 OBSs and some GeoNet onshore seismometers. We could detect more offshore events than are listed in the GeoNet catalogue owing to higher Signal-to-Noise ratios of the OBS data while most events occurred beneath the seafloor.

Keywords: seismicity, Hikurangi, OBS

## Greenland Ice Sheet Dynamics and Glacial Earthquake Activities

KANAO, Masaki<sup>1\*</sup> ; TSUBOI, Seiji<sup>2</sup> ; TOYOKUNI, Genti<sup>3</sup> ; HIMEMO, Tetsuto<sup>4</sup> ; TONO, Yoko<sup>2</sup>

<sup>1</sup>National Institute of Polar Research, <sup>2</sup>Japan Agency for Marine-Earth Science and Technology, <sup>3</sup>Tohoku University, <sup>4</sup>Seikei University

The Greenland ice sheet and its response to climate change have potentially a great impact upon mankind, both through sea-level rise and modulation of fresh water input to the oceans. Monitoring a dynamic response of the Greenland ice sheet to climate change is a fundamental component of long-term observations in global science. Glacial earthquakes have been observed along the edges of Greenland with strong seasonality and increasing frequency in this 21st century by the data from Global Seismographic Network (GSN). During the period of 1993-2006, more than 200 glacial earthquakes were detected, but more than 95% have occurred on Greenland, with the remaining events in Antarctica. Greenland glacial earthquakes are considered to be closely associated with major outlet glaciers at the margins of the continental ice sheet. Temporal patterns of these earthquakes indicate a clear seasonal change and a significant increase in frequency after 2002. These patterns are positively correlated with seasonal hydrologic variations, significantly increased flow speeds, calving-front retreat, and thinning at many outlet glaciers. These long-period surface waves generated by glacial earthquakes are incompatible with standard earthquake models for tectonic stress release, but the amplitude and phase of the radiated waves can be explained by a landslide source model. The seismicity around Greenland including tectonic/volcanic events was investigated by applying a statistical model to the globally accumulated data. Calculated b values, the Magnitude-frequency-dependence parameter, indicated a slight increase from 0.7 to 0.8 in 1968-2007, implying that the seismicity including glacial events around Greenland become slightly higher during the last four decades. The detection, enumeration, and characterization of smaller glacial earthquakes were limited by the propagation distance to globally distributed stations of the GSN. Glacial earthquakes have been observed at stations within Greenland, but the coverage has been very sparse. In order to define the fine structure and detailed mechanisms of glacial earthquakes, a broadband, real-time network needs to be established throughout the ice sheet and perimeter. The International Polar Year (IPY 2007-2008) was a good opportunity to initiate the program with international collaboration. Then, the Greenland Ice Sheet Monitoring Network (GLISN) was initiated for the purpose of identifying the dynamic response of the Greenland ice sheet to climate change.

Keywords: Greenland, global warming, glacial earthquakes, broadband seismometer, monitoring

## Foreshock activity of the large-scale interplate earthquakes around Japan

TANAKA, Rika<sup>1\*</sup> ; ORIHARA, Yoshiaki<sup>1</sup> ; KAMOGAWA, Masashi<sup>1</sup>

<sup>1</sup>Dpt. of Phys., Tokyo Gakugei Univ., <sup>2</sup>Earthquake Prediction Reserch Center, Tokai University

According to Bouchon et al. (Nature Geosci, 2013), they reported that the number of foreshocks increased towards the mainshock in the interplate earthquakes around North America and Japan. But, the foreshocks were much less frequent in the intraplate earthquakes. We investigate whether such a clear difference is really found between the interplate earthquakes and the intraplate earthquakes around Japan.

Keywords: Foreshocks, Interplate earthquakes, Accelerating seismicity

## Development of Acoustic Frequency Comb technology by ACROSS appropriate for active monitoring of the earthquake field

KUMAZAWA, Mineo<sup>1\*</sup> ; HIGASHIHARA, Hiromichi<sup>2</sup> ; NAGAI, Toru<sup>1</sup>

<sup>1</sup>Nagoya University, <sup>2</sup>University of Tokyo

Acoustic Frequency Comb technology by utilizing ACROSS (Accurately Controlled Routinely Operated Signal System) has been developed since 1994 at Nagoya Univ. and Earthquake Research Institute at Univ. of Tokyo for the active monitoring method of the subsurface structures. It is now being operated routinely in several locations in Gifu, Aichi, Shizuoka, Hyogo and Kagoshima prefectures.

A group of earthquake seismologists wrote in a book "Science of Earthquake Prediction" (UT Press, 2007) as follows: Whereas ACROSS is an indispensable element for earthquake prediction works, there are problems in stability of the instrumentations, methods of data analysis, etc. To resolve the problems raised by them, our own research works are demanded rather than to complain or to criticize.

1. In the current ACROSS transmitters, single force vector  $F$  as frequency-modulated signal is generated by centrifugal force by rotation of a rather small mass  $M$  ( $\sim 100$  kg) with a displacement amplitude  $u$  as constrained by equation of motion;

$$F = M d^2u/dt^2 = -\omega^2 (Mu)$$

The centrifugal force thus generated is transmitted towards the Earth's interiors through a transmitting antenna named 'ground coupler', which is a steel-reinforced concrete block of several meters in size and  $\sim 100$  tons in weight. As specified by the formula above, transmitted force amplitude is proportional to frequency squared, so that signal transmission is difficult in the useful low frequency range. The previous transmitters designed are practically limited for the use above 5Hz. To extend the frequency to the lower span, we propose the use of a linear motion of larger inertia mass  $M$ ,  $100 \sim 100000$  times larger the current transmitter to reduce the frequency by a factor of  $10 \sim 100$ . This could be simply realized by utilizing a large ground coupler as an inertia mass. Quantitative examination of this approach is found to be promising, and we have started the works on the technical realization of this observation system.

2. Low frequency acoustic signal below 1 Hz is useful for the stationary monitoring system covering everything in the whole Japanese Islands, once we build a transmitter array consisting of several tens transmitting stations, since the signal is easily detected up to 100 km distance without any environmental pollution. Local dense array of the signal sensors would provide us with the accurate data set on the swarm of local eigen-modes within the frequency range of the transmitted signals. This approach is the frequency comb interferometry much potential than the seismic daylight interferometry commonly applied nowadays. To make the structural inversion of the data by frequency comb interferometry, we have developed a new forward method named PANW, in which wave equation as a differential equation is converted to arithmetic equation in frequency and wavenumber domain on the basis of the theory of generalized functions.

3. The combined use of observation data by frequency comb ACROSS transmitter array and the data analysis method of frequency comb interferometry by PANW theory is expected to provide us with a potential tool for the practical active monitoring methodology. The contemporary application most relevant is the safety evaluation of artificial constructions such as buildings, tunnels and so on in contact with their subsurface structures.

The prediction and/or control of the earthquakes and volcanic activities will come to be our sound research target after the accumulation of data, our experiences on the 'evolving structural sensitivity' of the materials and its detailed nature at the target zone. Additional essential factor is the associated experimental and theoretical studies on the structural sensitivity of polycrystalline materials containing hydroxyl ions under stress.

We note that the developmental works of this method have been continued for a long period of time by collaboration of so many research workers of a variety of disciplines.

Keywords: Acoustic Frequency Comb, ACROSS, Structure Estimation

## Earthquakes are directed to diversity: An arithmetic seismic activity model

FUJIWARA, Hiroyuki<sup>1\*</sup>

<sup>1</sup>NIED

Seismic activity is diverse. If we use the methodology in which an earthquake generation process is decomposed into individual fundamental processes and they are integrated by assembling a detailed physical model in each process, initial conditions and boundary conditions to be determined become an enormous amount. Therefore, it is difficult to describe the earthquake generation process by finding the solution of one deterministic equation system. In the prediction of seismic activity that has been attempted in recent years, stochastic or statistical techniques have been used. In approaches of stochastic processes theory, characteristics of seismic activities are modeled as probability distributions which are estimated theoretically or empirically. One of the sample path of a stochastic process that is modeled corresponds to the value to be observed. Such an approach is effective to represent the statistical properties of the entire seismic activity, but it cannot be applied to analyze a depth nature of the individual sample path. In this study, we mathematically construct a specific sample path corresponding to the observed value. By showing that they satisfy the statistical nature of seismic activity, we propose seismic activity model based on the idea that different from the stochastic processes approach. A model is proposed for seismic activity due to "number".

We consider a correspondence between earthquakes and prime numbers. We parameterize occurrence time of earthquakes as the prime numbers and magnitude of earthquakes as the interval of prime numbers. Then we obtain a relationship similar to Gutenberg-Richter law. We call the model obtained by this correspondence as "arithmetic seismic activity model". In the "arithmetic seismic activity model", earthquake is equivalent to prime number of prime numbers distribution theory. Earthquake prediction is something equivalent to prediction of emergence of prime numbers. Earthquake is captured as a phenomenon that corresponds to changes in the energy level of the field. Using certain quantum system, we consider to model a field of earthquake occurrence. Considering the Hamiltonian of the field of earthquake occurrence, we set earthquake occurrence as an eigenvalue problem for the Hamiltonian. If we can show that the eigenvalue problem is associated with the zeta function, we can expect to explain the similarity between the distribution of the prime and seismic activity. At present, dynamical system can explain seismic field based on this concept is not known. On the other hand, trying to capture the zero distribution of the zeta function of Riemann in the relationship equivalent to the prime number distribution as an eigenvalue problem of the quantum dynamical system, research on the distribution of prime numbers is progressing. Distribution of prime numbers is related to limits of diversity of "number". Distribution of prime numbers is likely to be associated with critical phenomena. Earthquake can be interpreted as an critical phenomena. For this reason, it is considered that there is a similarity between the prime numbers and earthquakes.

Keywords: Number theory, Prime number, Gutenberg-Richter relation, Earthquake

## Comments on a Bayesian approach to earthquake probabilities of the Poisson model

IMOTO, Masajiro<sup>1\*</sup> ; FUJIWARA, Hiroyuki<sup>1</sup>

<sup>1</sup>NIED

In making national seismic hazard maps for Japan, earthquake probabilities are estimated based on past seismicity with the Brownian passage time model and the Poisson process model. With a small number of past earthquakes, unreliable model parameters produce large uncertainties of estimated values. In the present paper, we discuss a Bayesian approach to the problem for the Poisson model. When  $n$  earthquakes were observed in period  $T_0$ , a Bayesian approach gives the probability that  $m$  earthquakes are observed in period  $T_1$  in the form of a binomial distribution. We compared Bayesian probabilities with those obtained by the maximum likelihood estimate (MLE) for  $n$  less than 5 and found the following significant differences between them. 1) When  $T_1$  is the average interval of the past earthquakes, Bayesian probabilities of at least one earthquake increase 3 to 12% over those of MLE. 2) For a somewhat smaller  $T_1$  than that in 1), the differences become larger. The Bayesian approach presented here could be tested by a simulation study.

Keywords: Earthquake probability, Poisson model, Bayesian statistics, Seismic hazard maps for Japan, Kanto

## Long-term probability for large earthquake along the Nankai trough estimated from an incomplete catalog

OKADA, Masami<sup>1\*</sup>

<sup>1</sup>MRI, JMA

The Earthquake Research Committee of Japan published a report (the second edition) on the long-term evaluation for great recurrent earthquake along the Nankai trough in May, 2013 and newly forecasted the probability for such event in coming 30 years to be 60 - 70%. The giant earthquake may be possible, and the report was socially paid attention to very much. In the calculation of probability the BPT, Brownian Passage Time, distribution model is used in which the distribution parameters estimated with the maximum likelihood method or the time predictable model are plug in directly to the formula of conditional probability. Those are estimated from a few data, but not considered about the bias and uncertainty in them.

The committee explained that an earthquake, the Keicho event (1605) may not occur along the Nankai trough and some qualifying earthquakes are probably missed from the current catalog. In this presentation I will introduce a Bayesian new method with non-informative prior distribution to the parameters in a lognormal distribution for calculating the probability for the coming event from an incomplete catalog, and show the result of about 23 % for the event in the forthcoming 30 years along the Nankai trough

Keywords: Nankai trough, recurrent earthquake, forecast, Bayesian approach, incompleteness of catalog

## Space- temporal stability of the seismic quiescence (4) -Relation of seismic quiescence area and the main shock

YOSHIKAWA, Sumio<sup>1\*</sup> ; HAYASHIMOTO, Naoki<sup>2</sup> ; AKETAGAWA, Tamotsu<sup>3</sup>

<sup>1</sup>Meteorological Research Institute, <sup>2</sup>Meteorological Research Institute, <sup>3</sup>Japan Meteorological Agency

We have been continuing investigation of seismic quiescence phenomena for the purpose of application to earthquake prediction. As a result of re-investigation of the cases for the earthquakes of M7 class in Japan, we found that the distance between the hypocenter of the main shock and the center of seismic quiescence area becomes large with the earthquake magnitude to occur in the detected cases. Based on this scaling law, detectable cases could be newly found in the non-detected ones in the previous investigation.

We applied the method of 'eMAP' which was developed by Aketagawa and Ito (2008) and Hayashimoto and Aketagawa (2010) for detection of the seismic quiescence. For the study we picked up 26 earthquakes that occurred from 1987 to 2011 with the magnitude larger than or equal to 6.7 and the intensity larger than or equal to five in Japan. There were 11 detected cases and 15 non-detected cases in the past investigation (Ota et al.(2009) and Yoshikawa (2012)). In the case of the 1995 Kobe earthquake, where seismic quiescence could not be detected by 'eMAP' in the past investigation, a clear seismic quiescence has been reported by the DPRI of Kyoto University (1995) and the Japan Meteorological Agency (1995). As a result of re-investigation of this case, it became possible to treat it as a detectable case if the following things were considered. Though we have considered as the necessary condition for the precursor that the phenomenon appears in and around the focal area before occurrence of the main shock, we could not recognize as a phenomenon to be connected directly with the main shock because a seismic quiescence appeared in Tamba region approximately 30km distant from the epicenter near the Akashi Channel. And any remarkable quiescence was not detected in the epicenter, since the average seismic activity before the earthquake was too low. It is necessary to make clear the condition to treat the quiescence as a precursor. Then as we re-examined the detected cases, we found that the distance between the epicenter of the main shock and the center of the quiescence area became large with the magnitude of the earthquake to occur. We have reported that there are scaling laws in the size of the quiescence area and the duration of quiescence against the magnitude (Yoshikawa et al., 2013). As the quiescence is supposed to occur in the stress reduction area caused by aseismic slip, the main shock should occur in the periphery of the quiescence area and it is quite natural that the distance between the epicenter and the center of the quiescent area becomes larger obeying the scaling law.

We re-examined other non-detection cases and found that the precursory seismic quiescence can be detected also in the 1987 eastern off Chiba earthquake, the 1994 far-off Sanriku earthquake, the 2000 western Tottori earthquake, and the 2004 south-east off Kii peninsula earthquakes. As a result of this, 16 cases can be considered as detected and 10 cases as not- detected for 26 cases in total.

Keywords: earthquake, quiescence, hypocenter

## Recent anomalous groundwater temperature and water level changes and impending great earthquakes at the Nankai trough

TSUKUDA, Tameshige<sup>1\*</sup>

<sup>1</sup>Japan Women's Univ.

Earthquakes are generated by the anisotropic principal stress regime in the rock medium. In the preparing process of a large earthquake, the medium would be deformed generating regions of contraction and dilatation around the nucleus of the shearing stresses. According to a hydraulic model, pore fluid flow is driven upward to the ground surface through crack systems serving as flowing pipes by high pressure pumps at a deep spot. The change in the quantity of the upwelling hot water from deep underground causes a change of groundwater temperature (Tsukuda et al., 2005).

We have groundwater observation stations for temperature at 12 sites, and for water level at two in the Tokai and Nanki regions, central and southwest Japan, respectively, where are close to the so-called Tokai and Nankai earthquakes. High precision quartz thermometers are installed at Otomi (OT) in Yaizu City and Nakajima (NK) in Shizuoka City. At other stations, platinum resistance thermometers are installed. We use semiconductor pressure sensors for water level. At OT (Yaizu) in the Tokai region, the temperature has been monotonously increasing since the measurement started in 2003. The rate of increase has clearly fallen down since the end of 2012, suggesting weakening of the contraction in the rock medium. At NK (Shizuoka), 14km northeast of OT, the temperature data presented a precursory change from increasing to decreasing trend, one year before the 2009 Suruga-bay earthquake of M6.5 (Tsukuda, 2012). The decreasing rate after the earthquake became much higher than before and had continued till 2012. The temperature changed suddenly into increasing trend since May, 2013. The dilatation of the rock medium under Shizuoka recently changed into contraction. At stations HA and WA in Shionomisaki, Nanki region, Wakayama Prefecture. The long-term trend of the water level is rising, corresponding to the ground subsidence found by levelling and GNSS data (Kobayashi, 2013). The trend of temperature is similarly rising, suggesting contraction of the rock medium under Shionomisaki, the southernmost end of Honshu. At KZ (Kozagawa) in the Nanki region, the temperature is monotonously falling since the observation started in 2002. The decreasing rate is growing during recent two years, suggesting the dilatation turned to be intensified recently.

As mentioned above, the deformations of the rock medium are accelerated under the regions close to the source regions of the great earthquakes at the Nankai trough. For prediction studies for the impending great earthquakes, we should start to conduct detailed and multidisciplinary observations.

Keywords: dilatation, contraction, groundwater temperature, water level, precursor, earthquake prediction

## Two questions related to short- and long-term prediction of the so-called Tokai earthquake

GELLER, Robert J.<sup>1\*</sup>

<sup>1</sup>UTokyo, Earth Planet. Sci.

In the 1970s there was widespread discussion suggesting that a large subduction zone earthquake was imminent in the Tokai district (the so-called "Tokai earthquake"), but the "Tokai earthquake hypothesis" was not stated in a testable form. About 40 years have passed, but no such event has occurred in Tokai. Under those circumstances it seems justifiable to conclude that the hypothesis has been falsified. That does not mean that Tokai is not at risk, just that the risk is not greater than other tectonically similar regions.

Under the Large Scale Earthquake Countermeasures Act (LECA), which was enacted in 1978, an organization for monitoring possible "precursors" and issuing short-term alarms was established. But no reliable precursors have ever been found. LECA should therefore be repealed and the monitoring organization abolished.

Reference:

Geller, R.J., 1997, Earthquake prediction: a critical review, GJI, 131, 425-450.

Keywords: earthquake prediction, Tokai earthquake

## On the sea level changes before the 1946 Nankai earthquake on the Pacific coast of Shikoku, Japan

UMEDA, Yasuhiro<sup>1\*</sup>

<sup>1</sup>Geological Survey of Japan, AIST

### 1. Introduction

The abnormal sea level changes before the 1946 Nankai earthquake (M8.0) were witnessed by the inhabitants, on the Pacific coast of Shikoku, Japan. From a few days before the main shock, irregular tides were witnessed. The fishing boats could not arrive at the ports, because of the low sea level. On the contrary, some boats could arrive at ports. We considered that the abnormal sea level changes were caused by the small tsunamis from a few days before the main shock. The period and amplitude of the small tsunamis seem to have been larger and shorter closer to main shock.

### 2. Period and amplitude of the sea level changes

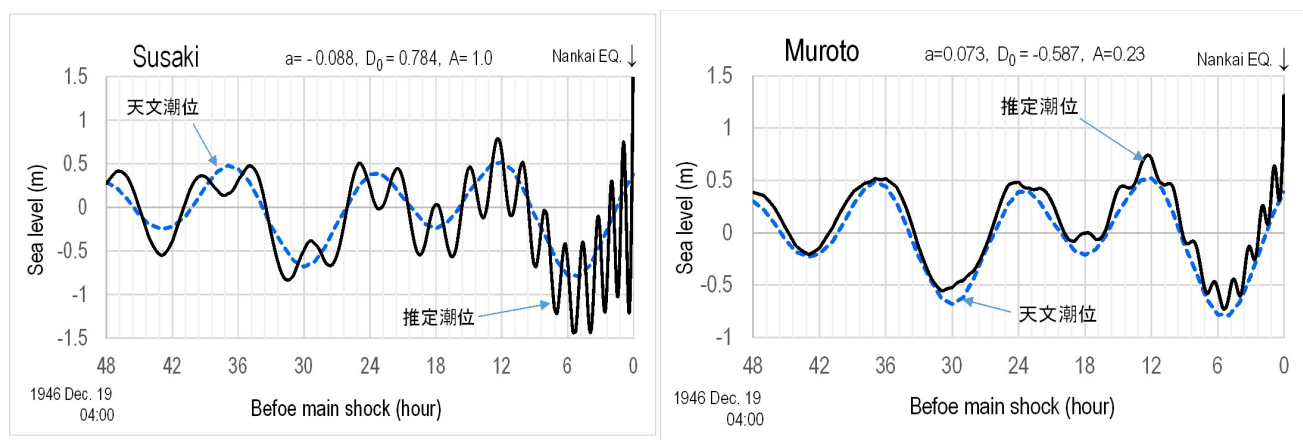
At seven points in the Susaki bay, the sea level changes were observed from

2010 to 2011. The height of tsunami by the 2011 off the Pacific coast Tohoku earthquake was amplified 20 and 8 times compared to that of the Nankai trough of 2300m depth (JAMSTEC) and 100m depth, respectively. The periods of 30-40, 50 and 80 minutes of sea level changes were observed in either case of tsunami, storm or mild weather. The periods of 50 and 80 minutes would be characteristic periods of Tosa bay. We considered that the small tsunamis were generated in the Tosa bay before the 1946 Nankai earthquake.

### 3. Assumed sea level changes

The assumed sea level changes( $f(t)$ ) before the main shock were obtained by the summation of the sea level changes by long term crustal movements( $F_1(t)$ ), small tsunami( $F_0(t)$ ) with the period of 50-80 minutes and astronomical tide( $F_t(t)$ ). That is,  $f(t) = F_1(t) + F_0(t) + F_t(t)$ .  $F_1(t) = a \cdot \ln(t) + D_0$  was adopted by Umeda and Itaba(2013). In view of the summaries by the testimony for the abnormal sea level changes,  $F_0(t)$  was assumed as  $F_0(t) = A \cdot B(t)m[\cos\{\omega \ln(t-t_c) + \phi\}]$ .  $\omega$  and  $\phi$  is frequency and phase angle, respectively.  $A$  is the amplitude ratio at each fishing port when the amplitude of Susaki bay is 1.0. Assumed sea level  $f(t)$  is shown by solid line in figure.  $f(t)$  of Susaki bay is expressed well the witness testimonies, but that of Muroto is not expressed them.  $f(t)$  of Muroto will be improved by considering the short-term and small-scale crustal deformations just before the main shock in the Muroto region.

Keywords: 1946 Nankai earthquake, sea level change, witness testimony,



1946年南海地震の前に小規模な津波が発生していたとして、各地で推定される海水位の変化（黒の実線）と比較のための天文潮位（青の点線）

## Mechanism of generating electric fields just before earthquakes

TAKAHASHI, Kozo<sup>1\*</sup>

<sup>1</sup>none

### 1. Precursory seismic electric fields

We consider that precursory seismic electric fields are generated by the mechanism as follows:(Refer to attached Figure):

- (1) Before earthquakes, micro-cracks run in the source regions (Assumption), and into these cracks pore water pours.
- (2) Uranium compounds, radium compounds and radon, which exist in crystal boundaries, dissolve into the pore water.
- (3) The cracks connect the pore water and spring water, and the radio active materials appear on the surface of source regions.
- (4) The radio active materials ionize the lower atmosphere above the source regions, and the electric conductivity increases there locally and temporarily.
- (5) The ionization increases the current along the trace of cosmic shower between the surface and the ionosphere.
- (6) As the current is pulsating, it radiates wide band radio-waves, which are observed as precursory seismic waves.

For the above mechanism the precursory micro-cracks are indispensable.

### 2. Mechanism generating the current between the surface and the ionosphere

The top of thunderclouds has the voltage up to about 100MV, so the electrons and negative ions flow into the clouds from the ionosphere. As a result, the ionosphere has a few MV. The mechanism, which increases the voltage at the cloud top, will be as follows:

(I) At middle latitudes, in the cloud lower than -10 deg. waterdrops become crystals, and they collide with each other. Then the water film on the smaller crystal, which is negatively charged, moves to the larger crystal, and makes the smaller crystal charged positive. The smaller crystals blow up to the cloud top and make it high voltage.(1)

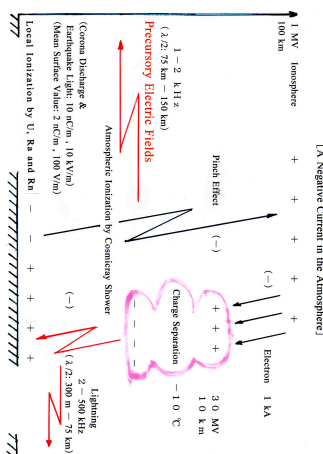
(II) At low latitude, in the cloud no crystal will exist, but electric fields of about 1 kv/m exist, as other areas. So, waterdrops are polarized such as the top is negative and bottom is positive. When they collide, the negative part of smaller waterdrops, which have higher speed than the larger ones, neutralizes the positive charge of the larger waterdrops, and the smaller ones become positively charged and blow up to the cloud top, resulting the high voltage.

In the smoke billowing from volcanos, the lightning is observed. The tephra collide with each, other, and are charged by frictional electricity. By the same reason shown in (II), the charge is polarized and high voltage in the upper part of the cloud is generated. If this high voltage is observed, the explanation mentioned above will be considered to be valid.

### References

- (1) Kozo Takahashi: Mechanism of generating electromagnetic fields just before great earthquakes, Japan Geoscience Union Meeting 2011, S-SS024-13
- (2) Kozo Takahashi: Mechanism of Generating The Earthquake Cloud just before Shallow Great Earthquakes, Japan Geoscience Union Meeting 2010, S-SS012-08

Keywords: precursory seismic electric fields, mechanism of generating thunder, thunder in middle-latitude, thunder in low-latitude, thunder in smoke of volcano



## Relationship between half-graben and high-velocities area at depths of 10 km 7

OISHI, Yukio<sup>1\*</sup>

<sup>1</sup>Atelier Science

There are four oval shaped high velocities areas in Kanto Area .Two of them are in the southern part of Ibaraki prefecture.  
 (after Matsubara Makoto 2005)

These two high velocities areas in Ibaraki prefecture gets larger, the deeper you see. At the depths of about 30km, this huge high velocities mass ,whose shape is donut, almost covers the southern part of Ibaraki prefecture and reaches at the depths of about 50km.

The western half of this huge high velocities area is on The Fourth Plate under Kanto; a part of Philippine Sea Plate(Toda Shinji 2005) at the depths of about 50km.

The eastern half of huge high velocities mass rides on the low velocities and low Poisson's ratio area, that is under beneath Lake Kasumigaura and the Southern of Lake Kasumigaura.( after Matsubara Makoto 2008)

This low velocities and low Poisson's ratio area faces subducting Pacific Plate at the depths of about 70 km.

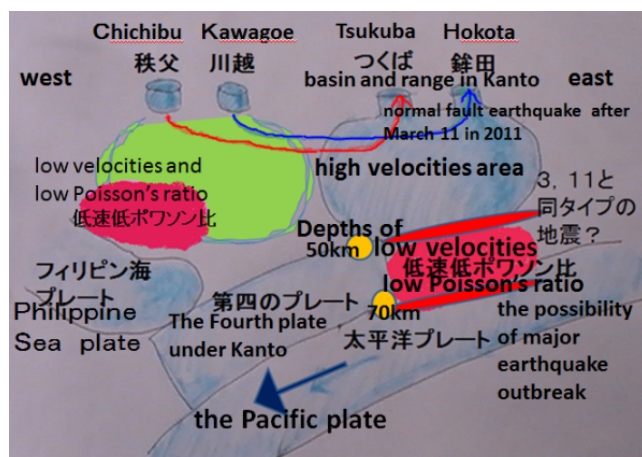
Speaking of the low velocities and low Poisson's ratio area , the similar area exists in the asperity of M9 in 2011 off the Pacific Coast of Tohoku Earthquake; the upper part of the Pacific plate and also exists in Unzen in Nagasaki prefecture from the ground to the depths of about 30km.

**I pointed out the possibility that the flexibility of the existence of the felsic rock or magma developed adherence of asperity of M9. ( Ohishi Yukio 2013)**

**From the above it seems to be necessary to examine the possibility of the major earthquake outbreak underneath Lake Kasumigaura and the Southern Lake Kasumigaura at the depths of about from 50km to 70km.**

There is another view that this low velocities area is not low Poisson's area but high Poisson's area (Nakajima Junichi 2008).

I want to wait for solution.



## Three-dimensional S-wave velocity structure beneath the Naruko volcanic area by ambient noise seismic interferometry

TAMURA, Jun<sup>1\*</sup> ; OKADA, Tomomi<sup>1</sup> ; MATSUZAWA, Toru<sup>1</sup>

<sup>1</sup>RCPEV, Tohoku Univ.

The 2008 Iwate-Miyagi Nairiku earthquake (M7.2) occurred along a fault ranging from the south of Iwate to the north of Miyagi. The focal region of the earthquake is located in the proximity of four volcanoes: Yakeishi-dake, Mt. Kurikoma, Onikobe, and Naruko. To study the positional relationship between the fault and magmatic bodies beneath these volcanoes, several studies have been conducted. Okada et al., (2010) estimated the S-wave velocity structure up to a depth of 40 km from body-wave tomography, and revealed that aftershock regions are distributed escaping the low velocity zones beneath the volcanoes. This study attempts to elucidate the correlation between the shallow structure of the volcanic bodies and aftershock regions in detail, focusing on the Naruko volcano locating in the south of the focal region, by seismic interferometry using cross-correlation analysis from ambient noise. Seismic interferometry is a method based on the fact that a cross-correlation function calculated from particle-motion records at a pair of stations in a wave field is equivalent to a Green's function between the two stations.

In cross-correlation analysis, we used the vertical-component data recorded by an observation network, which is densely installed in the Naruko volcanic region. By spectrum and beamforming analysis, we identified the characteristic of noise dominating in 0.1-10 Hz. The main sources of the noise are due to ocean waves coming from the Pacific Ocean and the Sea of Japan. Targeting the low-frequency range in which surface waves are more dominant than body waves, cross-correlation functions are calculated for each observation day for each pair of stations, and then stacked for 18 months to obtain a Green's function with a high SN ratio. We extract group velocity dispersion curves of Rayleigh waves using the multiple filter technique proposed in Dziewonski et al., (1969). Rayleigh-wave velocity maps from the period of 3 to 10 seconds are then calculated by processing surface-wave tomography based on the method of Barmin et al. (2001). Finally, we estimate the 3-D S-wave velocity structure up to 10 km depth by S-wave velocity inversion.

The structure shows two significant low velocity anomalies in the northwest of Naruko and in the south of Onikobe Caldera between 3 and 4 km depth. These anomalies are presumably magmatic bodies or geothermal water. Compared with the distribution of aftershocks and the fault, we can see that aftershocks do not occur in the low velocity anomaly beneath the Naruko volcano, and aftershock activity stops immediately at the northeast part of the anomaly.

Keywords: seismic interferometry, cross-correlation analysis, ambient noise, tomography

## Three-dimensional velocity structures in the region between Hakone volcano and Tanzawa Mountains, central Japan

YUKUTAKE, Yohei<sup>1\*</sup> ; HONDA, Ryou<sup>1</sup> ; HARADA, Masatake<sup>1</sup> ; SATOMURA, Miki<sup>1</sup> ; MATSUBARA, Makoto<sup>2</sup>

<sup>1</sup>Hot Springs Research Institute of Kanagawa prefecture, <sup>2</sup>Earthquake Research Institute, National Research Institute for Earth Science and Disaster Prevention

Hakone volcano is located in the northern boundary zone of the Izu-Mariana volcanic arc in central Japan, where the Izu Peninsula on the Philippine-sea plate has been colliding into the Japan island arc. There has been fumarolic activity around the Owakudani area, and many intense swarm activities have occurred in the caldera of Hakone Volcano. Previous studies (e.g. Oki and Hirano, 1970; Yukutake et al., 2011) interpreted that the hydro thermal fluid derived from a deep-seated magma beneath Hakone volcano contributes to the occurrence of swarm earthquake. However, there is no evidence to show existence of the hydro thermal fluid and a deep-seated magma. To understand the mechanism of swarm earthquake occurrence and tectonic process around Izu-collision zone, we tried to estimate three-dimensional velocity structure in and around Hakone volcano, by using tomographic inversion of seismic wave velocity.

We used the data of 52 temporary stations installed in and around the caldera of Hakone volcano. We also used the data obtained by the permanent seismic station installed by Hot Springs Research Institute of Kanagawa prefecture, Earthquake Research Institute, National Research Institute for Earth Science and Disaster Prevention, and Japan Meteorological Agency. The double-difference tomography method (Zhang and Thurber, 2003) was applied to the present analysis.

Under Hakone volcano, low  $V_p$  and low  $V_s$  anomaly regions were estimated in the depth range from 6 km to 15 km. Within the low velocity zone,  $V_p/V_s$  is high (1.9) in the 10-15km depth, while that at the 6 km depth is relatively low (1.6). This result suggests that the deep-seated magma body is located in the high  $V_p/V_s$  region, and the low  $V_p/V_s$  region reflects the hydro thermal fluid or volatiles from the magma body. High  $V_p$  and high  $V_s$  regions were estimated under Tanzawa Mountains. The high velocity zone corresponds to a plutonic body of tonalite or hornblende gabbro. A low-velocity wedge was estimated between Tanzawa Mountains and Hakone volcano that corresponds to trough-filled deposits.

Keywords: Three-dimensional velocity structures, Hakone volcano, Tanzawa Mountains

## Continental Moho slanting upwards to the southeast beneath Kii Peninsula and middle layer earthquakes

SHIBUTANI, Takuo<sup>1\*</sup> ; IMAI, Motohiro<sup>1</sup> ; HIRAHARA, Kazuro<sup>2</sup> ; NAKAO, Setsuro<sup>1</sup>

<sup>1</sup>DPRI, Kyoto Univ, <sup>2</sup>Science, Kyoto Univ

We carried out linear array seismic observations in Kii Peninsula from 2004 to 2013 in order to estimate the structure of the Philippine Sea slab and the surrounding area. We performed receiver function analyses for 14 cross-sections including four profile lines in the dipping direction of the slab and two lines in the perpendicular direction so far. We estimated three dimensional shapes of seismic velocity discontinuities such as the continental and oceanic Mohos and the upper surface of the oceanic crust. The results clearly showed that the slab top and the oceanic Moho are dipping northwestwards and that they correspond to the upper surfaces of the low and high velocity layers, respectively. Beneath northern to central Kinki the continental Moho spreads subhorizontally at 35 - 37 km deep, while beneath the Kii Peninsula it shallows southeastwards above the slab, reaching 20 km at the central part and 15 km at the southern shore.

Mizoue et al. (1983) analyzed data from permanent seismic stations which were being developed in the Kii Peninsula at that time, found that the travel time differences between the direct P waves and the Moho reflections or the Moho refractions propagating in the east - west direction became smaller from the northern part to the southern part of the peninsula, and suggested that the continental Moho slanted upwards to the south. They also found out earthquakes in the middle depth which were distinguished from both events in the upper crust and in the Philippine Sea slab, and called them as middle layer events. They pointed out that the middle layer events occurred around the slant continental Moho.

As mentioned above our receiver function analyses successfully estimated the three dimensional configuration of the continental Moho with a high accuracy. The results clearly showed that the middle layer events are located beneath the continental Moho shallowing southeastwards. Usually no earthquake occurs in the depth range equivalent to the lower crust. This is because crustal materials deform plastically at the depth and the strength of plastic flow becomes lower than that of brittle fracture. However, if the continental Moho shallows to the depth, the strength of plastic flow for mantle materials becomes larger than that of brittle fracture. This can be a cause of the middle layer events in the shallow mantle.

Keywords: continental Moho, middle layer earthquakes, Kii Peninsula, receiver function

## Seismic anisotropy within the subducting Philippine Sea slab beneath the central Japan

SHIOMI, Katsuhiko<sup>1\*</sup>

<sup>1</sup>NIED

Subduction of the Philippine Sea slab (PHS) is caused recurrent megathrust earthquakes every 100 to 150 years. Knowledge of slab geometry has been increased by using the recently established dense seismograph networks, but anisotropic feature, which is related to the tectonic stress field and/or rock properties, within the slab is still unclear. To reveal depth-dependent anisotropic feature within the PHS by using teleseismic receiver functions (RFs), we select 100 stations located in the Kii Peninsula and Shikoku, southwest Japan. We choose teleseismic events ( $M > 6.0$ ) from October 2000 to November 2013 for RF analysis, and use seismograms with good S/N. Low-pass filters with  $f_c = 1.0$  and  $1.5$  Hz are applied to estimate RFs. To estimate the orientation of anisotropy symmetry axis at each station, we apply the harmonic expansion method to the RFs (Bianchi *et al.*, 2010; JGR). When we apply this method to the data, we focus at the Moho depth for the CCD stacking and use the seismic velocity model by Matsubara & Obara (2011; EPS).

In the depth range around the slab Moho, the plunge azimuths in the eastern Kii, central and western Shikoku are corresponds well to the dip direction of the slab Moho estimated from the radial RFs only (Shiomi *et al.*, 2008; GJI). At the southern edge of the Kii Peninsula, the plunge azimuths are rotated to clock-wise from the result of Shiomi *et al.* (2008). When N-S directed anisotropic rock exists just above the Moho, this feature can be explained. In the oceanic crust, the plunge azimuths and anisotropic axes correspond well to the dip direction of the slab, and 4-lobed terms are dominant as the Moho deepens to 40 km. This feature is consistent with the NE-SW extension field estimated from the focal mechanisms of earthquakes occurred in the slab. Within the oceanic mantle, plunge azimuths and anisotropic axes are directed to E-W direction. This direction corresponds to the spreading direction of the subducting PHS beneath this area.

Keywords: Philippine Sea slab, Receiver function, Harmonic analysis, Seismic anisotropy

## The receiver function analysis at the area of the Nobi earthquake (II)

IIDAKA, Takashi<sup>1\*</sup>; IGARASHI, Toshihiro<sup>1</sup>; KATO, Aitaro<sup>1</sup>; IWASAKI, Takaya<sup>1</sup>; JOINT SEISMIC OBSERVATIONS, At the area of nobi earthquake<sup>1</sup>

<sup>1</sup>ERI, Univ. of Tokyo

### 1) Introduction

The mechanism of the inland earthquakes is related to the concentration of the strain and accumulation of the stress. It is very important to know the relationship between the stress/strain and fault plane. The 1891 Nobi earthquake is one of the biggest inland earthquakes in Japan. The joint geophysical observations had been done at the area. Based on the results of the previous survey at the Atotsugawa fault region, we found that the lower crust structure and fluid were very important factors to the cause of the inland earthquake. In the Nobi earthquake area, the seismic tomography studies figured out the existence of a low velocity region beneath the fault. The low velocity region continues to the subducting Philippine Sea slab. It can be interpreted that the low velocity region is made by water, which was dehydrated from the subducting slab. It is expected that there is some close relationship between the inland earthquake and liquid released from the subducting slab. We did receiver function analysis at the faults area of the Nobi earthquake.

### 2) Data

The seismic network deployed by the Japanese University Group of the Joint Seismic Observations and the seismic stations belong to the Hi-net were used.

The earthquakes with the epicentral distances from 30 to 90 degs were used. The earthquakes occurred from Aug., 2002 to Mar. 10, 2011.

### 3) Results

It has been suggested that the configuration of the subducting Philippine Sea plate is distorted in the southwestern Japan region. We figured out the image of the subducting Philippine Sea plate using the receiver function analysis.

The cross sections along the longitude of 137.5° E and 137° E suggested the negative and positive receiver function boundaries. We can trace the negative and positive boundaries from shallower part to deeper part. The boundaries are interpreted as the upper boundary and oceanic Moho of the subducting Philippine Sea plate. It was found that the Philippine Sea plate is lying in a horizontal beneath Ise bay to Wakasa bay by the previous studies. Our receiver function results also support the result. We can obtain clear image of the crust and upper most mantle of the area using the spatially high dense seismic array deployed by the joint seismic observation.

Keywords: crust, mantle, Receiver function, Nobi earthquake

## P-wave velocity structure in the forearc region of the southwestern Nansei-Shoto (Ryukyu) Trench subduction zone

NISHIZAWA, Azusa<sup>1\*</sup> ; KANEDA, Kentaro<sup>1</sup> ; OIKAWA, Mitsuhiro<sup>1</sup> ; FUJIOKA, Yukari<sup>1</sup> ; HORIUCHI, Daishi<sup>1</sup>

<sup>1</sup>Japan Coast Guard

We carried out five seismic lines across the southwestern Nansei-Shoto (Ryukyu) forearc region to elucidate variation in crustal structures along the trench. The seismic experiment consists of multichannel reflection seismic (MCS) profiling using 240 ch. and 3000 m long hydrophone streamer and wide-angle seismic refraction profiling using ocean bottom seismographs (OBSs) as receivers. We present the seismic structure related to the Philippine Sea plate subduction in the forearc region of the Nansei-Shoto island arc.

Thick materials with  $V_p$  less than 4 km/s characterize the accretionary wedge at the front of the forearc basin in the oblique subduction area to the southwest of 126 E. On the other hand, P-wave velocity structure beneath the high free-air gravity region in the forearc at 126-128 E reveals that materials with a high velocity of around 4.5 km/s ascend to 2-3 km beneath the seafloor. The subducting Okinawa-Luzon fracture zone was able to be clearly imaged not only in MCS profiles but also in the P-wave velocity distribution to the northeast of 126 E. We will discuss the relationship between the variation in the seismic structure and the characteristic of the regional seismicity.

Many OBSs on the forearc region recorded several reflection signals from the subducting Philippine Sea plate. We tried mapping these signals to estimate the position of the subducting plate.

## Spectral and spatial characteristics of the refined CRUST1.0 gravity field

TENZER, Robert<sup>1\*</sup> ; CHEN, Wenjin<sup>1</sup>

<sup>1</sup>School of Geodesy and Geomatics, Wuhan University

We investigate the density structure of the oceanic and continental crust using the global crustal model CRUST1.0, which has been refined by incorporating additional global datasets of the topography/bathymetry (ETOPO1), the polar ice sheets (DTM2006.0 ice-thickness data) and the global geoid model (GOCO-03S). The analysis reveals that the average crustal density is 2830 kg/m<sup>3</sup>, while it decreases to 2490 kg/m<sup>3</sup> when including the seawater. The average density of the oceanic crust (without the seawater) is 2860 kg/m<sup>3</sup>, and the average continental crustal density (including the continental shelves) is 2790 kg/m<sup>3</sup>. We further compile the gravity field quantities generated by the Earth crustal structures. The correlation analysis of results shows that the gravity field corrected for major known anomalous crustal density structures has a maximum (absolute) correlation with the Moho geometry. The Moho signature in these gravity data is seen mainly at the long-to-medium wavelengths. At higher frequencies, the Moho signature is weakening due to a noise in gravity data, which is mainly attributed to crustal model uncertainties. The Moho determination thus requires a combination of gravity and seismic data. In global studies, gravimetric methods can help improving seismic results, because (i) large parts of the world are not yet sufficiently covered by seismic surveys, and (ii) global gravity models have a relatively high accuracy and resolution. In regional and local studies, the gravimetric Moho determination requires either a detailed crustal density model, or seismic data (for a combined gravity and seismic data inversion). We also demonstrate that the Earth long-wavelength gravity spectrum comprises not only the gravitational signal of deep mantle heterogeneities (including the core-mantle boundary zone), but also shallow crustal structures. Consequently, the application of spectral filtering in the gravimetric Moho determination will remove not only the gravitational signal of (unknown) mantle heterogeneities, but also the Moho signature at the long-wavelength gravity spectrum.

Keywords: correlation, crust, density, gravity, Moho

## Correction of Gravity Measurements Utilizing GSI Maps and its Application in the Southern part of Uemachi Fault Zone

RYOKI, Kunihiro<sup>1\*</sup>

<sup>1</sup>Hyogo Polytechnic Center

### 1. Summary

In Earth science research with some field work, acquisitions of geolocation of the measurement point are essential. Particularly, it is a major burden that the latitude, longitude and altitude of the measurement points are obtained for the various corrections in gravity measurements. These pieces of information can be obtained by geodetic surveying or GNSS surveying in the field. Occasionally, topographic maps of large scale are substituted for these surveying.

On the other hand, the acquisition of geographic information, that has been digitized, into a numerical value has become possible on WWW in recent years. Web browsing service map of GSI, Geospatial Information Authority of Japan, which had been put to the test, was translated to the formal opening to the public on October 30, 2013. The new browsing service is "GSI Maps" (GSI, 2013a). According to the Agreement of GSI Tile Use, it is to be able to take advantage of this service in the academic research (GSI, 2013b). Therefore, it is created that JavaScript applications give information on the measuring position by using GSI Tiles (GSI, 2013c). If combined with some mobile digital devices, information of geolocation is readily available even in the field.

When gravity measurements have been conducted, until now, the authors have been made the most use of the large-scale topographic map as the base map in the southern part of Uemachi Fault Zone. These results were mixed up to base on Tokyo Datum and Japanese Geodetic System 2000. Therefore, they are integrated with the latter in this time.

### 2. Target area

Survey's line of the target has integrated the results by Ryoki (2011), Ryoki and Nishitani (2013) and recent measurements. The length of the survey line is about 9.7 Km. The line lies from Yunagi-cho Izumiotsu to Ibukino Izumi and intersects the some faults included in Uemachi Fault Zone.

### 3. Acquisition of geographic information

Latitude, longitude and altitude of the measuring points were used numerical information provided by GSI. These elements obtained by constructing an HTML application. A JavaScript code has been created to revise some samples of GSI Tile. In general, for the purpose of protecting the system, the string is not transferred directly to the clipboard from a Web browser. However, there is a function to be transferred through JavaScript in the specific browser. On the other hand, in some browsers which not support such a function, the ZeroClipboard library is possible to use to transfer the information (zeroclipboard.org, 2014). Numerical information, transferred to the clipboard, is edited in a spreadsheet application or in an editor software. In this study, an application which is used at indoor after measurement in situ is coded for a batch process. If operated in tablet devices instead to a field note book, numerical information is easily got in the measurement point. Numerical site information is used for various corrections and illustrated the gravity measurement point on the map.

### 4. Result

Formerly, in order to obtain numerical information related to the measurement point, latitude, longitude and altitude had been read using a digitizer from topographic map. But, if using the application proposed in this paper, time required for these operations could be significantly reduced. In particular, as it becomes a constant accuracy of the reading errors of the elevations which determined by GSI Maps, homogeneity of the data could be secured.

### 5. Challenges for the future

It is obvious that the application, which is proposed in this paper, ensures the homogeneity of data and improves the measurement efficiency in a variety of field research that includes geosciences. Development of the system for the operation of the tablet terminal is able to challenge, and it is an aim that an application of the terrain correction have been considered in the future.

Keywords: gravity structure, digital geographic information, JavaScript, Uemachi Fault, field research, efficiency of measurement

## The crustal structures of the subduction of the Philippine Sea Plate in the northern Nansei-Shoto trench

OIKAWA, Mitsuhiro<sup>1\*</sup> ; NISHIZAWA, Azusa<sup>1</sup> ; KANEDA, Kentaro<sup>1</sup> ; FUJIOKA, Yukari<sup>1</sup> ; HORIUCHI, Daishi<sup>1</sup>

<sup>1</sup>Japan Coast Guard

Seismic characters of convergent plate boundaries are reflected in the heterogeneity in the structural evolution, the interior regime as well as external architecture (Kopp, 2013). At the north end of the Nansei-Shoto trench the Amami plateau, which is known as a remnant arc, is subducting, and this causes a landward concave of the subduction axis. The Nansei-Shoto trench was recognized that its seismicity is rather low, but in the past few years, new scientific researches indicated the possibility of a mega earthquake is not so much low. There are needs to grasp the Philippine Sea plate's topography and crustal structure around the sea area of the Amami plateau because they might be constraint conditions how the mega earthquake could happen.

Japan Coast Guard conducted two integrated seismic experiments that combine a wide-angle refraction survey and a multi-channel reflection survey. The first line (line ECr10) was conducted in 2009 and the second line (line ECr11) was carried out in 2012. ECr10 started from the west end of the Amami plateau to the north sea area to the Amami-O-Shima island. ECr11 started from the Kikai basin to the just south of the Yaku Shima Island. A depression on the Nansei-Shoto arc between two seismic lines is well known as a major tectonic boundary of the Nansei-Shoto arc.

The southern end of ECr10 is the west edge of the large Amami plateau. Uyeda(2005) said that there is a local bouguer low anomaly and this means the crust of the Amami plateau should be thicker than the normal oceanic crust. The past seismic survey (Nishizawa et. al., 2009, 2014) reveals that the thickness of the center Amami plateau is approximately 16km, which is obviously thicker than the normal oceanic. The southern end of ECr11 is located on the Kikai basin. The Kikai basin's bouguer anomaly is rather high, this means the possibility that the crust of the Kikai basin should be an oceanic crust. The seismic survey supports the high anomaly because of its thin crust. However the composition of the crust shows the horizontal heterogeneity of its crust and an identification of the middle crust (6.0 - 6.5 km/s layer) exists (Nishizawa et. al. 2009). These characters do not support that the basin is a typical oceanic crust.

We made a comparison of the structure on the Philippine plate between ECr10 and ECr11, by using the seismic surveys results and the precise bathymetric data collected by Japan Coast Guard. Regarding topography, we found many normal faults parallel to the trench direction. Especially there are more faults on the margin of the Amami plateau than of the Kikai Basin. As for crustal structures, the crust of the Amami plateau has a middle crust. The existence of middle crust is along with the past results but not only of the Amami plateau but also of Kikai basin. This means that the subducting margin of the Kikai basin might not be a typical oceanic crust.

Keywords: MCS, crustal structure, subduction, OBS

## Seismic structure beneath Kyushu island, Japan, inferred from S-wavevector receiver functions.

UEDA, Takuya<sup>1\*</sup> ; TAKENAKA, Hiroshi<sup>2</sup> ; MURAKOSHI, Takumi<sup>3</sup> ; OKAMOTO, Taro<sup>4</sup>

<sup>1</sup>Kyushu Univ., <sup>2</sup>Okayama Univ., <sup>3</sup>National Defense Academy, <sup>4</sup>Tokyo Institute of Technology

The underground structure of Kyushu region is characterized by active subduction of the Philippine Sea plate (PHS) beneath the Eurasian plate and several active volcanos, for example, Aso, Kirishima, and Sakurajima volcanos along with the volcanic front, and Unzen volcano located Beppu-Shimabara graben. And also there are very thick sediments at several plains in Kyushu. Therefore the seismic structure beneath Kyushu Island is seemed to be very complicated and it is very important to understand the detailed structure, especially around Moho and the top of PHS. There are many previous researches on seismic structure beneath Kyushu Island. Travel time tomography method is very useful tool for imaging the subsurface structures. In the previous works, a lot of characteristic structures are identified by the tomography for example, low velocity structure beneath volcanic front.

Receiver function analysis is also very useful tool to image the seismic velocity structures. We apply it to image seismic structure on Kyushu area. In this study, we use teleseismic records from Hi-net and F-net seismic stations in Kyushu, which are supplies by the National Research Institute for Earth Science and Disaster Prevention.

If those seismic stations are located at the top or in the sedimentary layer, the records include strong effect of reverberation within the sedimentary layer, which makes the image of the structure unclear. To overcome this problem, we exploit the modified S-wavevector receiver functions (SWV-RFs). The SWV-RFs are derived by deconvoluting the upgoing S-wave component with the upgoing P-wave component of the records. For suppressing the sedimentary layer effect, we apply SWV-RFs for borehole records and move virtually the seismic sensor to the top of the basement layer, and calculate the SWV-RFs at that location [Takenaka and Murakoshi, 2010]. This method needs the structure model from the surface to the sensor location. We employ the Integrated Velocity Structure Model by the Headquarters for Earthquake Research Promotion. We take several cross sections in Kyushu Island to map the calculated SWV-RFs. We then interpret the continental Moho and low velocity regions in the mapped SWV-RFs. It can be seen that characteristic low velocity regions in mantle wedge, some of which may be related to magma. We also model some SWV-RF sections by the 2.5-D finite-difference method to confirm our imaging results.

Keywords: receiver function, crustal structure, top of plate, Kyushu region

## Seismic reflection survey at the Kego fault, Kyushu, Japan

MATSUMOTO, Satoshi<sup>1\*</sup> ; SHIMIZU, Hiroshi<sup>1</sup> ; NAKAMOTO, Manami<sup>2</sup> ; MIYAZAKI, Masahiro<sup>2</sup> ; ABE, Susumu<sup>3</sup>

<sup>1</sup>Institute of Seismology and Volcanology, Kyushu Univ., <sup>2</sup>Faculty of Sciences, Kyushu University, <sup>3</sup>R&D Department, JGI, Inc

Kego fault is one of the active faults in Japan, which located Kyushu Island, Japan. The fault is composed of two major segments; the earthquake fault of the 2005 West-off Fukuoka prefecture earthquake and southeastern part running through central Fukuoka City. We performed reflection survey at the southeastern part of the fault in order to explore detailed structure of the fault. The experiment was carried out on the two profile. One was located at central part of Fukuoka city with length of 1 km for obtaining reflection section shallower than depth of 1 km. Another was for imaging heterogeneous structure in the seismogenic zone beneath the fault, which was deployed 35 km length across southeast end of the fault. After applying seismic reflection processing, we obtain reflection sections for two profiles. The gap of horizontal reflector was found around the depth of 0.6 km in the shallow seismic section at central Fukuoka, corresponding to the Kego fault. The hanging wall of the fault is western side of the fault as geological study suggested. The deep section at the southeastern part of the fault reveals that strong reflective layers exist in the seismogenic zone at the west of the fault. In addition, we found many reflectors at the lower crust beneath the whole area of the profile.

Keywords: Kego fault, seismic reflection survey

## P-wave heterogeneous structure around the Kego fault inferred from reflection analysis for seismic network data

KAMIZONO, Megumi<sup>1\*</sup> ; MATSUMOTO, Satoshi<sup>2</sup> ; MIYAZAKI, Masahiro<sup>1</sup> ; NAKAMOTO, Manami<sup>2</sup> ; SHIMIZU, Hiroshi<sup>2</sup> ; ABE, Susumu<sup>3</sup>

<sup>1</sup>Department of Earth and Planetary Sciences, Graduate School of Sciences, Kyushu University, <sup>2</sup>Institute of Seismology and Volcanology, Faculty of Sciences, Kyushu University, <sup>3</sup>R&D Department, JGI, Inc.

The Kego fault is one of the active fault in Japan, running through the western margin of the Fukuoka plain. On March 20, 2005 the west off Fukuoka earthquake (M7.0) occurred at northwestern extension of the Kego fault. In order to evaluate the effect on the fault by the earthquake, crustal structure is basic information to model the fault condition. This study estimated the subsurface structure around the Kego fault from artificial source used in the reflection survey.

In the survey, vibrator tracks are used as seismic sources at 8 shot points. Sweep time of the source is 24 seconds and sweep frequency range is from 6 Hz to 30 Hz. We recorded the signal from the vibrators at seismic stations deployed by Kyushu University and NIED. Seismic reflection analysis was applied to the data for detecting reflectors beneath the CMP line located between the reflection profile and the station. As simplicity, we processed observed data on the assumption that basement is homogeneous.

We obtained seismic depth sections at CMP lines for the seismic stations. Numerous reflectors in the lower crust are found in the sections; therefore the lower crust is heterogeneous. The reflective zone in the lower crust is from the depth 20 to 32 km in the section, suggesting that the lower limit of the zone corresponds to the Moho discontinuity. Since the section imaged heterogeneous structure across the Kego fault, we compared characteristics of reflectivity between footwall and hanging walls of the fault. The structure of the superficial part is different depending on the place. At the some point CMP lines, there are reflector in the western side, however in the eastern side of the fault it is not so. This difference in reflectivity depends on the cross point between the CMP line and the fault. This suggests that there isn't clear difference in east and west of the fault at other point. Consequently, there might be variation of the structure along the strike of the Kego fault.

Keywords: Kego Fault, Seismic Reflection Profiling

## The seismic velocity structure in the Northern Kinki District using the dense seismic observation

KAIYA, Emi<sup>1</sup> ; KATAO, Hiroshi<sup>1\*</sup> ; SHIBUTANI, Takuo<sup>1</sup> ; IIO, Yoshihisa<sup>1</sup> ; MIURA, Tsutomu<sup>1</sup>

<sup>1</sup>DPRI, Kyoto Univ.

Micro-seismicity in the Northern Kinki District is active. However we do not know the cause and the relation between these seismic activities and crustal structure or active faults around there clearly. In the Northern Kinki District, we are carrying out a dense array seismic observation using 83 temporal stations since 2008. The average station interval at the center of the Tamba plateau is about 5km, so we expect to know the seismic structure beneath this region with higher resolutions than that derived from the permanent stations.

In this study, we estimate high-resolution seismic velocity structure using data from these dense observations. Based on the results of 3D seismic velocity tomography, we discuss about relations between the seismic activities and other geophysical and geological features of this area.

Keywords: Tamba Plateau, Tomography, micro-earthquake, crustal fluid, dense observation, Manten Project

## Seismic attenuation beneath Tateyama volcano

IWATA, Koji<sup>1\*</sup> ; KAWAKATA, Hironori<sup>2</sup> ; DOI, Issei<sup>3</sup>

<sup>1</sup>Ritsumeikan University, <sup>2</sup>Ritsumeikan University, <sup>3</sup>Disaster Prevention Research Institute

Tateyama volcano (Midagahara volcano) locates in southeast Toyama prefecture. Subsurface structures beneath active volcanoes have frequently been investigated using seismic attenuation (e.g., Oikawa et al., 1994; Sudo et al., 1996), and it was reported that there are strong attenuation regions beneath some active volcanoes. The volcanic activity of Tateyama volcano is quite low, and subsurface structure beneath the volcano has not been investigated in detail. Since Hi-net was developed by NIED, the attenuation structure of whole area of Japan has been estimated (e.g., Jin and Aki, 2005; Carcole and Sato, 2009). However, local structure beneath inactive volcanoes is still in question. In this study, we investigated the seismic attenuation beneath Tateyama volcano using seismograms obtained by Hi-net.

In this study, we used seismograms of five Hi-net stations near Tateyama volcano. The seismograms were selected so that epicentral distances from Tateyama volcano were 70 km~140 km, the magnitudes of the earthquakes were larger than 2.5, focal depths were less than 30 km, and signal-to-noise ratios were sufficiently high.

At first, we focused on the two stations which locate opposite sides of Tateyama volcano each other, and compared seismograms whose epicenters were located almost along the line of Tateyama volcano and the two stations. For the seismograms which passed beneath the volcano, S-waves were more attenuated than P-wave. In detail, S-wave attenuation was pronounced in 4~8Hz and 8~16 Hz bands. This feature was seen in all seismograms from northwestern or southeastern sources. On the other hand, seismograms from northeastern or southwestern sources did not show such a feature. There should be a region that preferentially attenuated S-waves beneath Tateyama volcano, and the distribution is heterogeneous.

Also, it should be noted that S-waves passing beneath Tateyama volcano showed clear peak delay, which suggested that there was a region with high scattering attenuation beneath Tateyama volcano.

Keywords: seismic attenuation, volcano, spectral analysis

## Detailed velocity structure along the Nankai trough, off the Kii Peninsula, obtained from DONET data

NAKANO, Masaru<sup>1\*</sup> ; NAKAMURA, Takeshi<sup>1</sup> ; TONEGAWA, Takashi<sup>1</sup> ; KANEDA, Yoshiyuki<sup>1</sup>

<sup>1</sup>JAMSTEC

Along the Nankai trough off southwestern Japan, the Philippine Sea (PHS) plate is subducting to the northwest below the Eurasian plate. Historically, mega-thrust earthquakes have occurred repeatedly along the Nankai trough (e.g., Ando, 1975). Future great earthquakes will cause serious and widespread damage in central and western Japan. The Japan Agency for Marine-Earth Science and Technology (JAMSTEC) installed a network of permanent ocean-bottom observation stations off the Kii Peninsula above the source region of the expected great earthquakes. This is known as the Dense Oceanfloor Network System for Earthquakes and Tsunamis (DONET). Previous studies (e.g. Nakano et al., 2014) revealed that the present seismic activity well overlaps the aftershock region of the sequence of 2004 off the Kii Peninsula earthquakes ( $M_{JMA} = 7.1, 7.4, \text{ and } 6.5$ ). The focal mechanisms of the earthquakes show that the axis of compressive stress in the PHS plate is oriented N-S, almost perpendicular to the direction of plate convergence, indicating a complex tectonic regime in this region. In this study, we investigate detailed seismic velocity structure in this region.

In this region, P-wave velocity ( $V_p$ ) structure is well developed based on repeated seismic surveys, but S-wave velocity ( $V_s$ ) structure is not well known. Therefore, we start from an initial layered velocity structure assuming  $V_s$ , and update it to well explain the travel-time of earthquakes, then obtain three-dimensional velocity structure described below.

1. Estimate average layered structure below the study area.

1.1. An initial layered structure of  $V_p$  is constructed referring to the result of seismic surveys. The  $V_p/V_s$  ratio of each layer is assumed considering oceanic structures. Using this structure, we determine the hypocenter distribution.

1.2. Using the travel-time and initial hypocenters, 3D velocity structure is computed by using the tomoDD program (Zhang and Thurber, 2003).

1.3. The 1D velocity structure is updated by averaging the velocity at each depth.

1.4. Hypocenters are re-calculated based on the updated velocity structure, and the procedures 1.2.-1.4. are repeated until the 1D velocity structure converges.

2. Construction of 3D velocity structure.

2.1. Initial 3D velocity structure representing the subducting plate and oceanic sedimentary layers is constructed based on the study of Nakamura et al. (2011).  $V_p$  is from the result in 1.

2.2. The  $V_p/V_s$  ratio of each layer is obtained by a grid search method, in which minimizes the residual between observed and calculated travel time.

2.3. Site correction is obtained for the best model.

3. Computation of detailed 3D velocity structure.

3.1 Using the velocity structure and hypocenter distribution obtained in 2. as the input, detailed 3D velocity structure is obtained by using tomoDD program. In the computation of travel time, the site correction obtained in 2.3. is included.

The obtained velocity structure shows that the velocity anomaly along the trough anomaly well corresponds to the earthquake distribution. In the oceanic crust, seismic activity corresponds to a region of low-velocity anomaly, while earthquake distribution corresponds to a high-velocity anomaly in the mantle. The obtained structure may help to understand the detailed structure in this region. However, since the used data is from earthquakes immediately below DONET, the resolution of tomography may not be good. We will investigate the resolution and dependence on the initial velocity structures in the future study.

Keywords: Nankai trough, Ocean-bottom seismic observations

## Mechanism of large crustal earthquakes in Kanto and Chubu: Influence of structural heterogeneities

FUJISAWA, Moeto<sup>1\*</sup>; ZHAO, Dapeng<sup>1</sup>; TOYOKUNI, Genti<sup>1</sup>; KITAGAWA, Hiroki<sup>1</sup>; NISHIZONO, Yukihisa<sup>2</sup>; INAKURA, Hirohito<sup>2</sup>

<sup>1</sup>RCPEV, Tohoku Univ., <sup>2</sup>West Japan Engineering Consultants, Inc.

Large inland crustal earthquakes often cause heavy damage to human society. Therefore it is very important to clarify the generation mechanism of the large crustal earthquakes for disaster reduction. It is considered that fluids dehydrated from the subducting Pacific and Philippine Sea slabs affect the nucleation of large crustal earthquakes under the Japan Islands (Zhao et al., 2010). In this study, we focus on the Kanto and Chubu regions, and investigated the cause of large crustal damaging earthquakes ( $M > 6$ ) (Usami et al., 2013; Utsu, 1999) by comparing the earthquake distribution with tomographic images of the crust and upper mantle.

We used high-quality arrival-time data of local earthquakes which occurred during June 3, 2002 to June 26, 2013 compiled by the Japan Meteorological Agency (JMA) Unified Catalogue and those during June 3, 2002 to November 10, 2013 compiled by the Tohoku University Data Base. The local events were carefully selected based on the following criteria. (1) All the events were recorded by more than 20 seismic stations; (2) the uncertainty of hypocentral location is smaller than 4 km; (3) to keep a uniform distribution of hypocenter locations and avoid the event clustering, we divided the study area into small blocks (5 km  $\times$  5 km  $\times$  1 km), and selected only one event in each block that was recorded by the maximal number of seismic stations. As a result, our data set consists of 824,742 P-wave and 627,664 S-wave arrival times from 21,831 events recorded by 877 seismic stations in the study area. We applied the tomographic method of Zhao et al. (1992) to our data set. The grid interval is 0.20 deg. in the lateral direction and 15°30 km in depth, which is the resolution scale of the 3-D velocity model we obtained. The final root-mean-square ravel time residual is 0.287 s for the P-wave data and 0.424 s for the S-wave data.

Our results show significant velocity variations in the crust and upper mantle. The subducting Pacific and Philippine Sea slabs are imaged clearly as high-velocity zones. In contrast, low-velocity anomalies are revealed in the crust and mantle wedge beneath active arc volcanoes, which reflect the source of arc magmatism produced by slab dehydration and corner flow in the mantle wedge. Most of the large crustal earthquakes are located in or around the low-velocity zones in the crust and/or the uppermost mantle. These results suggest that the generation of large crustal earthquakes are affected or controlled by the structural heterogeneities. In particular, fluids play an important role in the nucleation of the large earthquakes.

### References

- Utsu, T., 1999. Seismic Activity. Univ. Tokyo Press.  
Usami, T. et al., 2003. Catalogue of Damaging Earthquakes in Japan. Univ. Tokyo Press.  
Zhao, D., A. Hasegawa, S. Horiuchi, 1992. Tomographic imaging of P and S wave velocity structure beneath northeastern Japan. *J. Geophys. Res.* 97, 19909-19928.  
Zhao, D., M. Santosh, A. Yamada, 2010. Dissecting large earthquake in Japan: Role of arc magma and fluids. *Island Arc* 19, 4-16.

Keywords: seismic tomography, crustal fluid

## Seismic Reflection Survey around the Mouth of Fuji River

ITO, Shinobu<sup>1\*</sup> ; YAMAGUCHI, Kazuo<sup>1</sup> ; IRITANI, Ryohei<sup>1</sup> ; YAMANAKA, Yoshiaki<sup>2</sup> ; ITO, Shun'ichiro<sup>2</sup> ; MURATA, Kazunori<sup>2</sup>

<sup>1</sup>GSI, AIST, <sup>2</sup>Sunco Consultants Co., Ltd

We conducted seismic reflection survey around the mouth of Fuji River in February 2014. Fujikawa-kako fault zone is identified around this area. Shimokawa et. al. (1996) conducted seismic reflection survey in this area, and identified the Iriyamase fault. Shizuoka Pref. (1996) also identified the Nakayama fault. Our purpose of the survey is that we understand structure around both the Iriyamase and the Nakayama fault in more detail than the previous studies. There are two seismic survey lines. A survey line FJK1 is located from the mouth of Fuji river toward Mukaida river along the coastline, and the length of the line is about 3.5km. A survey line FJK2 is located on the right bank of Fuji river and at about 2km north from the coastline, and cross over the Kambara Jishinyama. The length of FJK2 is a little bit longer than 1km. We usedIVI Y2400 as seismic source. Sweep frequency for FJK1 and FJK2 is 10 to 100Hz and 10 to 120Hz, respectively. Sweep length is 12s, and record length is 16s for both lines. We used SG-10 (10Hz of natural frequency) and DSS-12 that is a distributed seismic data acquisition system. Temporal spread length of FJK1 is about 1km. We fixed the spread of FJK2. Geophones are set at intervals of 5 meters for both lines. Some events can be deduced as reflected waves in some samples of shot records for FJK1. However, we are afraid that they are produced by a bank. Soon, we are going to show detailed results.

Keywords: seismic reflection survey, Fuji River

## Depth variation of the P- and S-wave velocities in the Kanto sedimentary basin inferred from seismic interferometry

YOSHIMOTO, Kazuo<sup>1\*</sup> ; SUGAWARA, Yuma<sup>1</sup> ; KAJIKAWA, Kengo<sup>1</sup> ; KOBAYASHI, Manabu<sup>1</sup> ; MASUDA, Kei<sup>1</sup> ; TAKE-MURA, Shunsuke<sup>1</sup> ; HIRATA, Naoshi<sup>2</sup> ; SAKAI, Shin'ichi<sup>2</sup> ; SATO, Hiroshi<sup>2</sup> ; NAKAHARA, Hisashi<sup>3</sup>

<sup>1</sup>Nanobioscience, Yokohama City Univ, Yokohama, Japan, <sup>2</sup>ERI, Univ. of Tokyo, Tokyo, Japan, <sup>3</sup>Geophysics, Science, Tohoku Univ, Sendai, Japan

Information on the seismic velocity structure of the Kanto sedimentary basin is necessary for evaluating the strong and long-period ground motions in the Tokyo Metropolitan area for future large-to-great earthquakes. However, there are few studies on the depth variation of both P and S wave velocities of the sediment, except for the vertical seismic profiling (VSP) measurements at a limited number of deep boreholes. In this presentation, we will report the characteristics of the depth variation of both P and S wave velocities of the sediment on the basis of the seismic interferometry for P and S waves of local earthquakes.

Seismic waveforms of 160 local earthquakes recorded by the MeSO-net were analyzed in this study. The autocorrelation of vertical displacement waveform of P wave and SH displacement waveform from a single event were stacked over all events available at each station, respectively, to obtain the P- and S-wave reflection responses of the Kanto sedimentary basin. We successfully found clear P- and S-wave reflections from the bedrock (seismic basement) at 266 observation points. This result indicates that the P-wave seismic interferometry is effective for the exploration of deep sedimentary basin as well as S-wave interferometry. In our data, two-way travel time between the free surface and the bedrock of P-wave and S-wave (hereafter  $T_p$  and  $T_s$ , respectively) ranges from 0.5 s to 4.0 s and 2.0 s to 8.0 s, respectively. A graph showing  $T_p$ - $T_s$  relation reveals that the trend of its variation is very similar to that reported at Iwatsuki deep boreholes from VSP measurement, even though there is a large scatter of data. Our results indicate that the ratio of P-wave velocity and S-wave velocity of the sediment is approximately 4 at a shallow depth (<0.5 km) and decreases down to 2 or less at a deep depth (>2.0 km) in the Kanto sedimentary basin.

### ACKNOWLEDGMENTS

Data provided by the MeSO-net is gratefully acknowledged. This research was partially supported by the Earthquake Research Institute, University of Tokyo.

Keywords: seismic interferometry, Kanto sedimentary basin, sedimentary structure, seismic velocity structure

## Seismic activity and attenuation structure in fukushima-yamagata prefectural border area

MIYAGKI, Keiichiro<sup>1\*</sup> ; TSUMURA, Noriko<sup>1</sup>

<sup>1</sup>Faculty of Science, Chiba University

In Fukushima - Yamagata prefectural border area, seismicity suddenly became active after off the Pacific coast of Tohoku earthquake (here after we call it 2011 Tohoku earthquake). We estimated distribution and focal mechanisms of earthquakes that occurred in the time period before and after the 2011 Tohoku earthquake to clarify causes of the seismicity activation. We used seismograms which are observed at the Hi-net stations operated by National Research Institute for Earth Science and Disaster Prevention. Earthquakes with  $M \geq 2.0$  in the Hi-net catalogue from July 3, 2002 to March 10, 2011 and from April 1, 2011 to August 31, 2011 were analyzed in this study. As a result, hypocenters which occurred after the main shock were distributed into five clusters they were located at different region from those where earthquakes occurred before the main shock. It is known that there are active faults near the study area. A fault plane estimated from a northwestern cluster's hypocenters shows similar strike and dip of that of an active fault. Further, fault planes estimated from another clusters' hypocenters seems to have a conjugate relationship with the fault plane of the active faults. In addition, we observed that hypocenters in some certain clusters moved to lateral and vertical direction with approximately constant speed. Most earthquakes have the thrust-type focal mechanisms during the study period. Q value is considered to be a sensitive parameter to temperature and existence of fluid in the crust. We estimated  $Q_p/Q_s$  value by taking velocity amplitude spectral ratio between P and S waves to evaluate the affection of magma or fluid to earthquake occurrence. We used 898 spectra of 152 earthquakes which were observed by 9 stations nearby source region to calculate average  $Q_p/Q_s$  value on the ray path by Takaoka et al. (2013)'s method. As a result, ray paths from the hypocenters to stations within 20km showed high  $Q_p/Q_s$  values, while paths from the hypocenters to the far stations showed low  $Q_p/Q_s$  values. This result might indicate that high attenuation region exists in a shallow part nearby source region.

Keywords: Q value, attenuation, In Fukushima - Yamagata prefectural border area, seismicity, off the Pacific coast of Tohoku earthquake

## Crustal and upper mantle structure of East Antarctica, derived from broadband seismic deployments at the International P

KANAO, Masaki<sup>1\*</sup> ; TSUBOI, Seiji<sup>2</sup>

<sup>1</sup>National Institute of Polar Research, <sup>2</sup>Japan Agency for Marine-Earth Science and Technology

Deployment of broadband seismic stations on the Antarctica continent have been an ambitious project to improve the spatial resolution of seismic data across the Antarctic Plate and surrounding regions. Several international collaborative programs were conducted in Antarctica during the International Polar Year (IPY 2007-2008). The Antarctica's GAMBURTSEV PROVINCE (AGAP; IPY #147), the GAMBURTSEV MOUNTAIN SEISMIC EXPERIMENT (GAMSEIS), a part of AGAP, and the POLAR EARTH OBSERVING NETWORK (POLENET; IPY #185) were major contributions in establishing a geophysical network in Antarctica. The AGAP/GAMSEIS project was an internationally coordinated deployment of more than 30 broadband seismographs over the crest of the Gamburtsev Mountains (Dome-A), Dome-C and Dome-F area. The investigations provide detailed information on crustal thickness and mantle structure; provide key constraints on the origin of the Gamburtsev Mountains; and more broadly on the structure and evolution of the East Antarctic craton and subglacial environment. In addition to the PASSCAL observation system by USA, original coordinated systems were developed by Japan (at Dome-F (GM07) and GM06 stations), as well as by other groups in China and France. Regarding Japanese instrument system, the same sensor and data logger as used by US/PASSCAL were utilized, but the electric power supply system and enclosures were developed independently. Data were recorded in MiniSEED format, a commonly accepted international standard, to ease analysis. Logistical and staff support were provided by the US researchers and staff at AGAP-S camp in the installation of the Japanese stations GM06 and GM07. From GAMSEIS and POLENET data obtained, local and regional seismic signals associated with ice movements, oceanic loading, and local meteorological variations were recorded together with a significant number of teleseismic events. In this presentation, in addition to the Earth's interiors, we will demonstrate some of the remarkable seismic signals detected during IPY that illustrate the capabilities of broadband seismometers to study the sub-glacial environment, particularly at the margins of Antarctica. In future, monitoring stations inland ice plateau of Antarctic, such as Dome-F, firmly attribute a crucial role in the Federation of Digital Seismographic Network (FDSN) in southern high latitude.

Keywords: Antarctica, International Polar Year, crustal structure, broadband seismographs, international project

## Seismo-stratigraphy and structure of the Adventure Plateau (Sicily Channel): an example of old data recovery

CIVILE, Dario<sup>2</sup> ; ALP, Hakan<sup>1\*</sup> ; LODOLO, Emanuele<sup>2</sup> ; CENTONZE, Jacques<sup>2</sup>

<sup>1</sup>Istanbul University Department of Geophysics, <sup>2</sup>Istituto Nazionale di Oceanografia e di Geofisica Sperimentale

We present here a seismo-stratigraphic and structural study of the Adventure Plateau, the north-westernmost sector of the Sicily Channel. This bank, where water depths do not generally exceed 150 m, is the shallowest part of the whole Sicily Channel, with relief which sometime rises up to less than 50 m. This analysis is based on a large set of multichannel seismic profiles and well information acquired mostly for commercial purposes in the 70s and 80s. Despite the general poor quality and consistency of the data used, it was possible to draw with sufficient detail the various seismo-stratigraphic sequences, calibrated with well information. The sedimentary sequence crossed by wells in the Adventure Plateau comprises deposits ranging from Triassic to Plio-Quaternary. A broad lithological distinction can be made between the sequences ranging from Triassic to Middle Miocene, predominantly carbonate, and the sequences ranging from Tortonian to Quaternary, predominantly siliciclastic. Moreover, we observe in the wells the presence of various hiatuses, particularly at the top of the Miocene and at the Early Jurassic. Three main structural domains have been identified within the Adventure Plateau: (a) a compressional belt in the N-W part of the bank, deformed during Middle-Late Miocene, and corresponding to the SW-trending offshore part of the Maghrebian Chain; (b) the Adventure foredeep of the Maghrebian Chain, located in the central part of the bank, and filled by over 2000 m of siliciclastic Late-Miocene to Quaternary deposits; (c) the Adventure foreland of the Maghrebian Chain, corresponding to the S-W part of the bank, affected from the Early Pliocene by a strong extensional phase associated to the Pantelleria Graben rifting. The eastern boundary of the Adventure Plateau is part of a broadly NS-trending, lithospheric-scale transfer zone which separates the Sicily Channel into two distinct sectors. This study shows the potential and capability of old data in areas where there is scarce geophysical knowledge. They represent an important source of information, especially for the shallow water areas of the Sicily Channel that are still poorly known in terms of geology and stratigraphy.

Keywords: Sicily Channel, Adventure Plateau, seismo-stratigraphy, synthetic seismograms, structural setting

## Possibility of timelapse survey by seismic interferometry in image domain

SHIRAISHI, Kazuya<sup>1\*</sup>

<sup>1</sup>JGI, Inc.

### (1) Seismic interferometry in image domain

Seismic interferometry (SI) is generally applied in a data domain by crosscorrelating the different seismic traces without information of media for a redatuming or a signal extraction. Then the synthesized virtual source records are processed for a subsurface imaging. The direct subsurface imaging of passive seismic data by interference of extrapolated wavefields based on an imaging condition can be recognized as a SI in the image domain. Although the image domain SI is based on the velocity model for wavefield extrapolation, the fact that both the passive observation data and the velocity model are required for the depth imaging is common in the data domain SI and the image domain SI.

In the SI in the image domain by combining with the principle of a reverse time migration (RTM), arbitrary time-windowed seismic record is propagated forwards from a receiver point which become a virtual source and the same time-windowed records are propagated backwards from other receiver points. If any multiple reflection waves between the surface and the reflection boundaries satisfy the imaging condition, the reflected energy will be focused on those points. Because the seismic records of all receivers in one passive observation are not independent each other, the wavefield extrapolations can be only once in forward and backward respectively. In the data domain SI, however, the forward and backward extrapolations are repeated over all receiver points in a final RTM, because the virtual source records synthesized by the crosscorrelation should be treated independently. Therefore, total computational cost of the image domain SI could be lower than the data domain SI.

### (2) Applicability to a time-lapse study of passive

Passive seismic monitoring or time-lapse survey using permanent observation systems are one of recent research topics. Although high repeatability can be kept in the active seismic survey both on sources and receivers, any repeatability on sources is not guaranteed in the passive seismic survey. In this study, numerical simulation is demonstrated to evaluate the repeatability of the subsurface image and the possibility of extracting a small temporal velocity change by image domain SI with passive seismic data. In this simulation study, simple assumptions with an acoustic wavefield and a same mechanism for all sources are introduced. The passive seismic data for different condition of source distribution or/and velocity perturbation are synthesized, and then the image domain SI is applied for each data set. The repeatability of imaging and the possibility of extraction are measured by some repeatability indexes.

The passive observation records are synthesized using modified overthrust model of SEG/EAGE (15 km x 5 km) with 151 receivers on the surface due to independent 128 sources in the ground (Ricker wavelet with 10 Hz). The sources in the ground are randomly distributed for each model respectively. A velocity change with 10 percent decrease is added in an anticline structure around the center of the model with an elliptical shape (1 km x 0.1 km). A smoothed model from the true velocity model is commonly used for each RTM.

From the simulation study, the global images of the overthrust model are well reproduced in appearance for the different source distributions. However, the repeatability indexes show that the amplitude change due to the source distribution difference is too large to ignore even though the small velocity change can be extracted. Some additional techniques are required to extract only the velocity change without the influence due to the source distribution difference. In addition, there are other difficulties in a real data such as different source mechanism, elastic effects, and some kinds of noises.

Keywords: seismic interferometry, timelapse, reverse time migration

## Temporal changes of P and S wave velocities in NE Japan associated to the M9Tohoku-Oki earthquake from doublets analyses

PACHECO-VIVERO, Karim<sup>1\*</sup> ; NISHIMURA, Takeshi<sup>1</sup> ; NAKAHARA, Hisashi<sup>1</sup>

<sup>1</sup>Geophysics, Science, Tohoku University

Application of seismic interferometry using ambient noise and coda waves of regional earthquakes have shown notable seismic wave velocity decreases associated with the occurrence of the M9.0 Tohoku-Oki earthquake. These analyses can be generally attributed to S-wave velocity changes at shallow structures because these waves are dominant in surface waves. On the other hand, analyses of doublets have also succeeded in detecting temporal changes of direct arrival times of P waves as well as those of S waves. Also, the seismic rays pass deeper portions. However as the medium changes by the M9 earthquake are widely observed in East Japan, it is difficult to separate the observed travel time differences into the effects of hypocenter parameters and the travel time differences caused by the change in the medium beneath the stations. In this study, therefore, we develop a new method to determine temporal changes of P and S wave velocities beneath stations by simultaneously determining hypocenter parameters of doublets. We relate travel time differences of doublets to site factors at each station and the differences of hypocenter parameters. We further give a constraint in which the sum of the differences in origin times of the doublets analyzed is set to be zero, since the doublets are considered to randomly occur. As a result, our inverse problem estimates the model parameters, namely the site factors for P and S waves at each station and the relative locations of hypocenters and origin times of the doublets. Seismic data at 454 stations of the Hi-net seismic network in East Japan are used. We analyze 35 doublets with magnitudes ranging from 3.7 to 4.7 and depths from 30 to 60 km located offshore in East Japan for the period from 2005 to 2013. The seismic data are band-pass filtered between 1-2 Hz and travel time differences of arrival times of P and S waves are measured by applying a cross-spectrum method. The inversion results show that hypocenters of doublets differ by about 0.05 km and 0.12 km at a maximum each other in the horizontal and vertical directions, respectively. Even when we change the data set of doublets, the relative hypocenter locations do not significantly change, which indicates our inversion method is stably determining the hypocenter parameters. For the site factors, we find significant delays of arrival times as large as 0.04 s for the S-waves and about 0.01 s for the P-waves. Time delays are observed mainly at stations located widely in Tohoku region between 37 and 40 degrees in latitude, which are west from the M9 fault zone. The observed spatial distributions of time delays seem not to be well matched with the regions strongly shaken, which are located mostly in the eastern area of Tohoku region, or the regions where seismic velocity reductions at shallow medium are detected from analyses of bore-hole and ground surface records. These discrepancies suggest that the time delays detected from doublets originate from different regions, maybe deeper portions beneath Tohoku region.

Keywords: Tohoku-Oki earthquake, Velocity change, Similar earthquakes, Direct P and S waves

## Estimation for seismic wave propagation property of soil structure based on seismic interferometry

SEIICHIRO, Kuroda<sup>1\*</sup> ; MASUKAWA, Susumu<sup>1</sup> ; TAGASHIRA, Hidekazu<sup>1</sup>

<sup>1</sup>National Institute for Rural Engineering, NARO

Recently seismic interferometry was applied to estimation for seismic response of natural ground but also those of artificial structure like a building. We applied seismic interferometry concept for retrieval of seismic response of a model dike of soil structure like a fill dam. We employed deconvolution interferometry to estimate seismic response in time domain. From the waveforms obtained from deconvolution with the motion in the basement of a model dam, we estimate traveltimes of shear wave propagating through it and its mean velocity. Estimated velocity explain the normal mode of a model dike well. This approach can be applicable to monitor change in seismic response a dike caused by strong earthquakes or its internal water content change.

Keywords: Seismic interferometry, Soil Structure, Dam body, Dike, Shear velocity, Centrifuge test, Fill dam

## Temporal changes of auto-correlation functions associated with the volcanic activity in Hakone volcano, central Japan

YUKUTAKE, Yohei<sup>1\*</sup> ; UENO, Tomotake<sup>2</sup> ; HONDA, Ryou<sup>1</sup> ; MIYAOKA, Kazuki<sup>1</sup> ; HARADA, Masatake<sup>1</sup> ; SATOMURA, Mikio<sup>1</sup>

<sup>1</sup>Hot Springs Research Institute of Kanagawa Prefecture, <sup>2</sup>National Research Institute for Earth Science and Disaster Prevention

Auto-correlation functions (ACFs) of ambient noise are thought to be a powerful tool for searching temporal change of crustal structure associated with strong ground motion, or volcanic activity. In this study, we investigated the velocity changes at Hakone volcano associated with an intense swarm activity.

Hakone volcano is located at the northern boundary zone of the Izu-Mariana volcanic arc in central Japan. Many intense periods of swarm activity have occurred in the caldera. It was noted, in last two decades, that seismic swarms were remarkably prevalent in 2001, 2006, 2008-2009, 2011 and 2013. During the swarm activities, except for that in 2011, crustal deformations related to volcanic activities were detected by the GNSS stations network in and around the caldera of Hakone volcano. In particular, remarkable tilt changes were also detected by the tiltmeters within the caldera in 2001 and 2013 activities. It is interpreted that the crustal deformation was caused by pressure from a Mogi point source or dike at a depth of 7 km and two shallow open cracks in the caldera (e.g. Daita et al., 2009; Harada et al., 2009).

To estimate the velocity changes associated with the 2013 activity, we used the continuous velocity waveforms recorded at the stations of Hot Springs Research Institute, National Research Institute for Earth Science and Disaster Prevention Hi-net, Japan Meteorological Agency in and around the caldera, in the period between January 2012 and December 2013. Filtered trace at the frequency band of 1-3 Hz was used to calculate autocorrelation by one-bit correlation technique. To obtain stable record of the one-day ACF, we stacked the ACFs for time intervals of one week. We obtained fluctuations of the velocity structure by using the stretching method (e.g. Wegler et al., 2009).

The velocity fluctuations at the stations in the caldera show a gradual decrease prior to the swarm activity. The velocity decreases at these stations are consistent with increases in base length detected by the GNSS stations around Hakone volcano. We also found that there was sudden velocity decrease at Owakudani station near fumarolic area just after the beginning of swarm activity and tilt changes. We interpreted the velocity decrease at these stations as a material change or a crustal deformation associated with the volcanic activity.

Keywords: auto-correlation functions, volcanic activity, Hakone volcano

## The roles of dispersion and nonlinear effects in the 2011 Tohoku-Oki earthquake tsunami

SAITO, Tatsuhiko<sup>1\*</sup> ; INAZU, Daisuke<sup>1</sup>

<sup>1</sup>National Research Institute for Earth Science and Disaster Prevention

The present study aims to reveal the roles of the dispersion and the nonlinear effects in the 2011 Tohoku-Oki earthquake tsunami. Tsunami simulations were conducted based on the nonlinear dispersive equations with a high-resolution source model. The result successfully reproduced the waveforms recorded in both near shore and deep sea. The calculated inundation area showed a good coincidence with the actual inundation at the Sendai Plain, the widest inundation area during this event. Conducting sets of simulations using different equations, we obtained the followings insights. Although the dispersion was neglected in most studies, the maximum-amplitude distribution was significantly overestimated in the deep sea if the dispersion was not included. The waveform observed at the station in which the largest tsunami height ( $>2$  m) recorded among deep-ocean stations also verified the necessity of the dispersion. It is well known that the nonlinear effects play an important role for the tsunami inside bays and harbors. Additionally, the nonlinear effects needed be considered for the accurate modeling of the later waves even at the offshore stations. In particular, including nonlinear terms rather than including the inundation was more important for the precise modeling of the waves reflected from the coast.

Keywords: tsunami, dispersion, nonlinear wave, the 2011 Tohoku-Oki earthquake

## Numerical simulation of tsunamis due to a landslide

YOSHIKAWA, Ryo<sup>1\*</sup> ; KAKINUMA, Taro<sup>1</sup>

<sup>1</sup>Graduate School of Science and Engineering, Kagoshima University

Numerical simulation of tsunamis due to a landslide has been performed using a MPS method, where the water surface is indicated based on the spatial gradient of number density of particles. In comparison with the water surface displacements through hydraulic experiments, the calculation results are accurate when the inflow can be assumed as a fluid. The larger the initial potential energy of the inflow is, the larger the tsunami height becomes, although the tsunami height is not large when the initial position of inflow is below the water surface since the initial relative potential energy of the inflow is lower, as well as without impact of plunging. Due to the inflows of the assumed initial values for mass, shape, and velocity caused by a sector collapse of Sakurajima Island, the tsunami height shows more than ten meters in Kagoshima Bay.

Keywords: tsunami, landslide, sector collapse, MPS method

## Point spread functions for earthquake source imaging

NAKAHARA, Hisashi<sup>1\*</sup> ; HANEY, Matthew<sup>2</sup>

<sup>1</sup>Graduate School of Science, Tohoku Univ., <sup>2</sup>U.S. Geological Survey

Recently, various methods such as back-projection method (e.g. Ishii et al., 2005), time-reversal (TR) method (e.g. Larmat et al. 2006), and hybrid back-projection (HBP) method (Yagi et al., 2012) have been proposed and applied for earthquake source studies in addition to kinematic waveform inversions (e.g. Hartzell and Heaton, 1983) . In addition, theoretical relationships among the methods have also been clarified (e.g. Kawakatsu and Montagner, 2008, Fukahata et al., 2013). In this study, we introduce the notion of the point spread function (PSF) into earthquake source imaging, and show that the PSF clarifies the meaning of the earthquake source inversions. Under ideal circumstances in which receivers continuously surround the source, the PSF can be interpreted with seismic interferometry.

Kinematic waveform inversion methods are now standard for earthquake source studies. The observation equations (or forward modeling equations) are based on the representation theorem. According to Claerbout (2001), imaging is defined to be the mathematical process of multiplying adjoint Green's functions with both sides of the observation equation. Fukahata et al. (2013) pointed out that the process is very close to the one used in the HBP method. The source image may be blurred and degraded due to uneven distributions and insufficient number of stations. The degree of blurring and degradation can be expressed by the PSF which is often used in optics. The PSF for the source imaging can be expressed by stacked cross correlations of Green's functions between two source points with respect to receivers on a surrounding surface. If distributions of sources and receivers are discretized, the observation equation can be formulated in matrix form. Source inversion is found to remove the effect of the PSF, but other source imaging methods suffer from the PSF.

Ideal circumstances are considered here to better clarify the meaning of the PSF. It is assumed that stations are continuously distributed so as to surround the source points. For this case, we use source-receiver reciprocity of Green's functions. Then, we can consider the following reciprocal configuration in which sources are surrounding two stations. The point spread function is expressed as the stacked cross correlations of waveforms between the two receivers with respect to the surrounding sources. This configuration is exactly the same as ones in seismic interferometry and therefore we can interpret the PSF based on seismic interferometry. For single-force sources, the PSF is found to be the imaginary part of the Green's function. This fact was already pointed out in terms of TR method (e.g. Fink, 2006). For moment-tensor sources, the PSF is shown to be the imaginary part of the spatial derivative of Green's function with respect to each coordinate of the two receivers. This is a novel finding of this study. It is also suggested that the source image is the integrated version of the true source process when the interpretation based on seismic interferometry strictly holds.

In summary, kinematic source inversion methods can remove the effect of the PSF, but other source imaging methods suffer from blurring and degradation by the PSF. As a result, careful weighting of data is necessary for the source imaging methods. For ideal cases in which receivers surround the sources, the PSF can be interpreted with seismic interferometry with the help of the source-receiver reciprocity of Green's functions. This study will contribute to better understanding of the meaning of source inversion methods.

Keywords: Earthquake source imaging, Point spread functions, Seismic interferometry

## Analysis and application of wave propagation process of sweep signals in attenuative media

MATSUSHIMA, Jun<sup>1\*</sup>

<sup>1</sup>Graduate School of Engineering, The University of Tokyo

The sweep signal is the most extensively used land seismic exploration technique. In conventional data processing using sweep signals, a received trace is cross-correlated with source sweep to convert the extended sweep signal into a pulse signal. For attenuation estimation, a time window is often used to compute the frequencies of the direct-arrival waveforms. Uncorrelated sweep signals are useful in the discussion of harmonics simply because the uncorrelated data are one of the few situations in which we commonly input a nearly pure frequency into the earth. Our previous study proposed a method that enables accurate measurement of ultrasonic attenuation using sweep signals under the assumptions that velocity dispersion can be ignored and the quality factor ( $Q$ ) is not dependent on frequency. This method is independent of the effect of windowing while the windowing effect underestimates the attenuation results due to a spectral leakage effect. In most cases, however, the presence of attenuation is accompanied by velocity dispersion because of causality. The presence of velocity dispersion causes attenuation to be disturbed, although the proposed method is not so sensitive to the presence of velocity dispersion. The present paper elucidates the wave propagation process of sweep signals in attenuative media with velocity dispersion to develop the method which can take the effect of dispersion into account. We obtain a time-scale representation of sweep signals by using the continuous wavelet transform method to perform a time-series analysis of a seismic trace that decomposes the trace into its respective amplitude and phase components in both the frequency and time domains.

Keywords: Seismic attenuation, velocity dispersion, sweep waveform

## 3D numerical simulation of seismic wavefield in inhomogeneous rock samples

YOSHIMITSU, Nana<sup>1\*</sup> ; FURUMURA, Takashi<sup>1</sup> ; MAEDA, Takuto<sup>2</sup>

<sup>1</sup>CIDIR/ERI, The Univ. of Tokyo, <sup>2</sup>ERI, The Univ. of Tokyo

We focus on expanding the applicability of the transmitted waveforms obtained at laboratory experiments to examine detailed medium structure with the aid of novel numerical simulations. For this purpose, we investigate the feature of elastic waveforms in a centimeter class rock sample based on a 3D finite difference method (FDM) simulation. Previously, there were a few ways to approach the later phase of transmitted waveform in a rock sample because the propagation process of the reflected and converted waves generated in a finite-sized rock sample were not figured out. If analyses with entire waveform including the later phases will be possible, it should bring more detailed information on internal medium structure of rock samples.

First, we obtain transmitted waveforms in laboratory with cylindrical Westerly granite sample which horizontal to vertical ratio is 1 : 2. A source transducer is put on the center of the side surface and step voltage is applied to it. Vibration on sample surface is recorded as velocity waveform by laser Doppler vibrometer.

Next, we prepare the simulation model that covers the size of the rock sample. The volume is discretized into 512 x 512 x 1024 grids with an interval of 100  $\mu\text{m}$ . Assuming proportional relationship with X-ray absorption coefficient obtained from micro focus X-ray CT images of the rock sample, we set the density (2.5 - 3.1  $\text{g/cm}^3$ ), P wave velocity (5.0 - 6.0  $\text{km/s}$ ), and S wave velocity (2.8 - 3.5  $\text{km/s}$ ) on each grid. Then, 3D FDM numerical simulation is performed with a single point force which is the same movement with the source transducer of the experiment. Band pass filter with a cut-off frequency of 50 kHz to 2 MHz is applied to the obtained waveforms.

The wavefield obtained from the simulation show that the reflected (PP, SS, PPP, and SSS) and converted (PS, SP, and PPS) waves are generated at the boundary of the sample. As time progresses, waves reflected at the side boundary return to the source area, and waves reflected at the top of the sample propagate through the sample at same time. Thus, we confirmed that waves trapped in the closed medium generate a very complicated shape of the later part of waveforms. Scattering and conversion at mineral grains are also observed due to the heterogeneity of medium, while they have only a limited effect on the simulated waveform in this case.

Radial component of measured and simulated waveforms recorded in the same horizontal plane at the source position are compared. Each phase shape in entire simulated waveform is matched with measured waveform. Two large amplitude phases observed in the measured waveforms are revealed as direct P wave and reflected SS wave from the simulated waveforms. Complex waveform shapes after the arrival of SS wave are indicated to as multiple reflected and converted S waves at the round boundary of the sample.

Keywords: transmitted wave, reflected wave, rock sample, numerical simulation

## Curvilinear grid finite difference method simulation of seismic wave propagation for depth-dependent velocity structure

MAEDA, Takuto<sup>1\*</sup>

<sup>1</sup>ERI, The University Tokyo

I propose curvilinear grid method on large-scale finite difference method (FDM) simulation of seismic wave propagation in depth-dependent structure. The FDM usually uses uniform-sized grid having spatial scale smaller than 6-10 of wavelength. Although it is quite straightforward method and is therefore suitable to large-scale parallel simulation, it is not economical to use homogeneous grid size under depth-dependent structure in regional scale because of wide dynamic range of wavelength. Low-velocity sediment requires fine scale grid, but such smaller grid size also requires very small time-stepping in deeper part to satisfy the stability condition of FDM. To deal with this problem, discontinuous-grid method (Aoi and Fujiwara, 1999; Lee et al., 2008) has been proposed. However, possible numerical instability at a discontinuous surface in the former method (Kristec and Moczo, 2010).

The curvilinear coordinate method can use any non-linear, non-orthogonal coordinate. The uniform-size numerical grid is used along the curved coordinate in the computation domain. On the other hand, we still uses the Cartesian coordinate for expressing physical quantities such as velocity vector and stress tensor. This method has been used to incorporate rough ground surface (e.g., Hestholm, 1999). However the recent study on staggered-grid FDM (e.g., Nakamura et al., 2012) suggest that the rough surface can be expressed by the fine-scale homogeneous grid. So, I use a coordinate whose grid-width gradually and smoothly increases with depth to make ratio between grid-size and wavelength nearly constant. My coordinate transform equation depends on vertical depth only, so that to make the computational loads in coordinate transformation and additional memory requirements relatively small. The rotated-grid staggered grid (RSG) scheme (Saenger et al., 2000) has been adopted to make central finite differentiation possible in all directions under the curvilinear coordinate.

As a test, we implemented this curvilinear coordinate FDM in 2D SH and P-SV systems, with using the Butterworth-shape grid-size increase function. This coordinate has a characteristic depth. Grid size linearly increases with depth at deeper than the characteristic depth. On the contrary, this curvilinear coordinate converges to the Cartesian at the shallow limit. This feature is preferable since one can connect the homogeneous Cartesian grid in the shallower portion to the curvilinear grid system without any boundary conditions. In the numerical experiments, I found that the method is effective and stable even for the coordinate system having large grid-size ratio of up to 10. Extension to the 3D model is quite straightforward, and it makes possible to perform broadband large-scale wave propagation simulations including slow sediment in medium-sized computers.

Keywords: seismic wave propagation, numerical simulation, finite difference method, curvilinear coordinate

## Waveform inversion of seismic reflection data and its application to fault structure survey

WATANABE, Toshiki<sup>1\*</sup> ; KOBAYASHI, Masami<sup>1</sup> ; YAMAOKA, Koshun<sup>1</sup> ; ITO, Taniao<sup>2</sup> ; KANO, Ken-ichi<sup>3</sup> ; ABE, Susumu<sup>4</sup>

<sup>1</sup>Nagoya University, <sup>2</sup>Teikyo Heisei University, <sup>3</sup>Shizuoka University, <sup>4</sup>JGI, Inc.

Seismic waveform inversion (Tarantola, 1984) is a novel technique of imaging subsurface structures. It reconstructs a model of physical parameters that best explains waveforms of observed seismic data by incorporating a nonlinear least-squares inversion. Waveform inversion provides high-resolution model than that from travelttime tomography. Recent development of computational environment accelerates studies on practical application of the method to 2-D/3-D field data.

In this study, we investigate an application of the method, originally developed for crosswell seismic data, to reflection seismic data. The problems are (1) singular nature of sensitivity near sources and receivers at the surface, (2) attenuation of sensitivity in deeper part of the section, and (3) contamination of surface wave. We introduced a weight increasing with depth on the gradient, and near-offset trace mute to reduce the effects of the problems listed above. Using the synthetic waveform data numerically generated from a given structure model, we proved that a clear structure image was successfully retrieved after iteration.

Then, we applied the method to the field data of wide-angle reflection survey acquired in the Fujikawa-kako fault zone - ISTL seismic reflection survey conducted in 2012 (2012FIST)(Ito et al, 2013) to reveal the detailed structure of Omiya fault. Although the reconstructed velocity structure is consistent with the recent interpretation that the Omiya fault is a reverse fault, it was far from convergence due to the insufficient number of seismic sources used in the survey. Problems and requirements for future survey design will be discussed in the presentation.

Keywords: seismic reflection method, waveform inversion, fault structure, non-linear inversion

## Site amplification factor of the Hi-net stations

UENO, Tomotake<sup>1\*</sup> ; SAITO, Tatsuhiko<sup>1</sup> ; SHIOMI, Katsuhiko<sup>1</sup>

<sup>1</sup>NIED

This study estimated site amplification factors of all the Hi-net stations. Employing the coda normalization method and analyzing more than one thousand earthquakes, we obtained the values of all Hi-net sites in the frequency bands of 0.6-1.0 Hz, 1-3 Hz, 2-4 Hz, 2-6 Hz, 4-8 Hz, 6-9Hz, and 8-12 Hz. The site amplification factors were rather small showing that 90 % of the site amplification factors ranged within 20 dB. The site amplification varies from station to station more largely with decreasing the frequency. A correlation between the site amplification factor and the S-wave velocity where the sensor is installed was recognized. The site amplification factor decreases with increasing the S-wave velocity when the S-wave velocity is less than 1.5 km/s. When the S-wave velocity is larger than 1.5 km/s, the correlation disappears. Stations in southwest Japan show smaller site amplification factors, while stations in plains and around the volcanic front in the northeastern Honshu, Japan show larger site amplification factors.

Keywords: Hi-net, Site amplification factor

## Separating body and Rayleigh waves with cross terms of the cross-correlation tensor of ambient noise

TAKAGI, Ryota<sup>1\*</sup> ; NAKAHARA, Hisashi<sup>2</sup> ; KONO, Toshio<sup>1</sup> ; OKADA, Tomomi<sup>1</sup>

<sup>1</sup>RCPEV, Graduate School of Sci., Tohoku Univ., <sup>2</sup>Geophysics, Graduate School of Sci., Tohoku Univ.

We develop a novel method to separate body and Rayleigh waves with the vertical-radial (ZR) and radial-vertical (RZ) components of the cross-correlation tensor of ambient noise. Furthermore, analyzing ambient noise records observed at a seismic array, we validate the method. For the separation, we utilize the difference in polarizations between the rectilinear P and the elliptic Rayleigh waves. Assuming the two-dimensional surface and three-dimensional body waves are the superposition of random uncorrelated plane waves, we derive two fundamental characteristics of the ZR and RZ correlations. One is that, between the ZR and RZ correlations, Rayleigh wave contributions have the opposite signs and P waves have the same signs. The other is that, for both ZR and RZ correlations, Rayleigh wave contributions are time-symmetric and P waves are time-antisymmetric. Accordingly, we can separate P and Rayleigh waves by just taking the sum and difference between ZR and RZ correlations and by just taking the time-symmetric and time-antisymmetric components. This method can be performed (1) without any knowledge of velocity structure, (2) using only two stations with three-component sensors on a ground surface, (3) even in the case of anisotropic wave incidence, and (4) with the quite simple procedure. We consider that the developed method can make better use of three-component observations of ambient noise for evaluating the cross-correlation tensor accurately, for improving deep velocity structure using both of extracted body and surface waves and, more fundamentally, for understanding the composition of ambient noise.

Keywords: ambient noise, seismic interferometry, cross-correlation function, wavefield separation, polarization, body and Rayleigh waves

## Study of high-frequency seismic wave propagation by active-source experiments

TANIMOTO, Toshiro<sup>1\*</sup> ; OKAMOTO, Taro<sup>2</sup>

<sup>1</sup>University of California, Santa Barbara, <sup>2</sup>Department of Earth and Planetary Sciences, Tokyo Institute of Technology

Seismic wavefields generated by resonant shaking experiments of the Millikan Library, on the campus of California Institute Technology (Pasadena, California, USA), were analyzed. Because the resonant shaking frequencies are 1.12 Hz (the east-west direction) and 1.64 Hz (the north-south direction), this active-source experiment can provide opportunities for studying high-frequency seismic wave propagation in Southern California.

Two such experiments for each frequency were analyzed; for the north-south shaking experiments, the harmonic signals were observed up to distance 323 km in one experiment and up to 396 km in another experiment. For the east-west shaking (1.12 Hz), the maximum distance was 200 km but most observations were confined to less than 100 km.

Spectral amplitudes showed a systematic decaying trend with distance in all cases. Numerical simulations indicated that the predominant signals were surface waves. Assuming that all signals were surface waves, we obtained estimates for the parameter  $QU$  for surface waves where  $Q$  is the attenuation parameter and  $U$  is the group velocity (in km/s). There was, however, a major break in the amplitude-distance trend at a distance about 50 km; for data with distance less than 50 km,  $QU = 95 \pm 16$ , where  $U$  is in km/s. For data beyond 50 km, we obtained  $QU = 1454 \pm 226$ . This change in trend must be related to the regions sampled by waves, as the shorter-distance data were dominated by paths in the Los Angeles basins while the longer-distance data did not contain paths in the basin structures.

Through cross correlations between MIK (station in the Millikan library) and a station in the regional network, phase information was also analyzed. For many stations, phase was stable for frequencies between 1.637 and 1.638 Hz which meant that phase is locked between MIK and a station. While it was not possible to estimate phase velocity, because the number of cycles cannot be resolved for high-frequency waves, a stacking approach for multiple-window data allowed us to estimate frequency derivative of phase and group velocity for 25 paths. Group velocity between MIK and network stations are mostly less than 2 km/s. For stations with distance less than 50 km, most group velocity results were about 0.5 km/s or less. Combined with the estimate for  $QU$  from the amplitude-distance data,  $Q$  is estimated to be 190 for distances less than 50 km. This estimate, however, contains uncertainty up to a factor of two as variations in group velocity estimates differ from station to station.

Keywords: Seismic wave propagation, Crustal structure, Active source experiment

## Estimations of seismological structure in the northwestern Pacific using OBS records: Approaches from $>1$ Hz component

TONEGAWA, Takashi<sup>1\*</sup> ; FUKAO, Yoshio<sup>1</sup> ; FUJIE, Gou<sup>1</sup> ; TAKAHASHI, Tsutomu<sup>1</sup> ; KODAIRA, Shuichi<sup>1</sup> ; SUGIOKA, Hiroko<sup>1</sup> ; ITO, Aki<sup>1</sup>

<sup>1</sup>JAMSTEC

Tentative ocean bottom arrays using seismometer, hydrophone and pressure gauge have recently been deployed through many scientific projects all over the world. However, in Japan, a permanent ocean bottom monitoring system, called DONET, is now working, and dense cabled-OBSs (ocean bottom seismometers) have been constructed around the Japan Trench. It seems that, compared to other countries, such environments in Japan potentially give us some advantages for investigating the Earth's interior, seismic activity, and wavefields under the ocean. In order to easily kickoff the use of these records, it would be better to know characteristics of wavefields observed at seafloor.

A large amplitude in the frequency range of 0.07-0.5 Hz can be often seen in the spectrum of noise record observed at seafloor, which is known as microseisms that are generated by wind propagating sea surface. This large amplitude also emerges at land observation. At frequencies longer than 0.02 Hz in the spectrum observed at typical broadband OBS, the amplitude of infragravity wave is strong in the vertical component, and that of tilt effect is dominant in the horizontal component.

In this presentation, avoiding the use of such longer period components, we focus on shorter period components than 1 Hz of records observed at OBSs. We introduce what kind of analyses we can do hereafter with permanent OBS records, which is based on the use of records observed at tentative ocean bottom arrays. In particular, we will introduce ambient noise and receiver function analyses, in which short period components are mainly used.

Keywords: OBS records, short period components, receiver function, seismic interferometry

## Nonlinear radiation of hypocenter and prevision of earthquakes

KIKUCHI, Toshiaki<sup>1\*</sup>

<sup>1</sup>National defence Academy

Hypocenter vibrations have been analyzed using the analysis method based on time reversal. The dynamic model of the hypocenter vibrations based on the results was advocated. In addition, the effectiveness of the dynamic model was confirmed. The activity regions in the hypocenter are presumed using the dynamic model here.

First, the outline of the dynamic model is described. The time-reversal process was executed to the P wave signals received at the observation stations for the earthquake that occurred in the central part of Suruga Bay in August, 2009, and the pulses formed at the position of the hypocenter, that is, time reversal pulse (TRP) was obtained. The TRP corresponds to an equivalent source to which the hypocenter emits. The obtained TRP provided clear orientation dependency. To clarify the origin of the azimuthal dependence, the frequency spectrum of the TRP to azimuth was obtained. The frequency spectrum was greatly changed by the azimuth. Then, the distribution of the maximum amplitude frequency to azimuth was obtained. As a result, the maximum amplitude frequency rises greatly as azimuth moves from west to east and it has descended afterwards. This frequency rise shows the local movement of sources by high speed. The moving direction converged in the direction of Nishiizunishi, Kawazu, and Ito.

The P waves received at these observation stations exhibited a unique behavior. The head part of the wave received in Nishiizunishi was expanded. However, there was no expansion in the head part in the waves received in Ito and Kawazu near Nishiizunishi.

The head's growing in this manner occurs when the progression rate of cracks in an active fault becomes near the velocity of propagation. The pressure that occurs due to the crack is added cumulatively by moving by high speed. That is, the parametric effect occurs in the active fault. Nishiizunishi is a specific point that reflects the feature of this earthquake.

As for the waveform of the aftershock that received at the specific observation station, the head part of the P waves expanded more than that of main shock. Similarly, the expansion of the head part was observed for the precursor earthquake that occurred before the main shock. The dynamic model of hypocenter vibrations has advocated from these results. The point where the narrow beam emitted from an active fault reaches the surface of the earth is called a parametric spot. The head of the pulse to which the head expands is called a parametric head. This model was verified about four earthquakes larger than M5 that occurred from 2012 to 2009 near Mt. Fuji. The effectiveness of the dynamic model was confirmed.

The dynamic model is consistently approved for precursors, a main shock, and aftershocks. Therefore, the dynamic model may be used for the prevision of earthquake.

The precursor earthquakes of the earthquake that occurred in the central part of Suruga Bay in August, 2009 are examined. The receiving waves that accompanied the parametric head in that were observed seven times. These represent evidence that the progress of the crack began to become a high speed in the active fault. Therefore, observing the seismic waves of a slight earthquake at the peculiar parametric spot and examining the change, may foresee a big earthquake afterwards.

Keywords: hypocenter vibrations, dynamic model, time reversal, prevision of earthquakes

## Frequency domain calculation of the seismic wavefield propagating along an ocean trench, with a constant Q attenuation

MITSUHASHI, Yuta<sup>1\*</sup> ; FURUMURA, Mitsuko<sup>2</sup> ; MATSU'URA, Ritsuko S.<sup>2</sup> ; SHOJI, Masahiro<sup>1</sup>

<sup>1</sup>KKE, <sup>2</sup>ADEP

For shallow interplate earthquakes, large long-period later phases are frequently observed at long distance. Simulations using the finite difference, which we have performed, revealed an important effect of seawater on those later phases (e.g. Furumura et al., 2011).

However, attenuation  $\exp(-\pi ft/Q)$  in the finite difference calculation is set to  $\exp(-\pi ft/(Q_o f/f_o))$ , meaning  $Q/f=Q_o/f_o$  is set as a constant, where  $f_o$  is a target frequency of the calculation purpose, and  $Q_o$  is its corresponding attenuation factor, so it causes some problems especially for waves propagating for a long distance.

Then we calculated waves propagating in a 2.5D structure in the frequency domain with FEM to realize Q as a constant instead of Q/f, for both cases with and without seawater. We could confirm the important effect of seawater on later phases as well as the finite difference calculations. Calculated later phases have relative large amplitude for frequencies lower than  $f_o$  in the Q-constant model compared with the Q/f-constant model. It indicates necessity of estimation of difference between realistic Q and modeled one, when we use the finite difference method. In addition, the results reveal large later phases in the case with seawater, which are rarely seen in the calculated waveforms without seawater. It implies overestimation of magnitude of ocean earthquakes obtained from analysis of waves propagating through a long distance along and across an ocean trench, such as the 1911 off Kikai Island earthquake and the 1933 off Sanriku earthquake observed in Honshu.

## Development and extinction of long-period ground motion in thick sediments

TAKEMURA, Shunsuke<sup>1\*</sup> ; YOSHIMOTO, Kazuo<sup>1</sup>

<sup>1</sup>Yokohama City University

To obtain better insights of long-period ground motion in thick sediments, which often cause severe damage of large-scale man-made structures, we analyzed horizontal seismograms recorded by dense strong motion networks in the complex large Kanto basin. We found distinct large amplitude long-period ground motion around northern Kanto, which is caused by Love wave excited at the northwestern edge of Kanto basin. Amplitude of Love wave significantly developed during propagation in thick (>3 km) sediments and then suddenly weakened at region where significant change of basin structure exists.

To clarify causes of such observations, we conducted 3D finite difference method (FDM) simulation of seismic wave propagation. In simulation, we assumed plane SH-wave incident into a realistic basin structure model embedded in a homogeneous half-space background structure, to focus characteristics of Love wave excited at the basin edge. Simulation result in a realistic basin model referred from JIVSM (Koketsu et al., 2008) well reproduced observed Love wave development around the northern Kanto. Another simulation in the model, which is limited to maximum bedrock depth of 3 km, shows no significant difference of simulated waveforms compared with the previous model. Thus, development of surface waves in thick sediments is mainly caused by the deepening of shallower low-velocity layers, rather than the depth variation of bedrock.

### **Acknowledgement**

We acknowledge the National Research Institute for Earth Science and Disaster Prevention, Japan (NIED) for providing the K-NET/KiK-net waveform data. We also use strong motion data from SK-net.

Keywords: long-period ground motion, surface wave, kantou basin, basin structure, numerical simulation

## Receiver function travel time tomography

HIRAHARA, Kazuro<sup>1\*</sup> ; YAMASAKI, Tomona<sup>1</sup> ; ABE, Yuki<sup>1</sup> ; SHIBUTANI, Takuo<sup>2</sup>

<sup>1</sup>Graduate School of Science, Kyoto University, <sup>2</sup>Disaster Prevention Research Institute, Kyoto University

Hirahara et al. (2006) proposed a method of Receiver Function (RF) Tomography which combines travel time tomography using travel times from local and teleseismic events with receiver function analyses. In the method, a 3-D P and S wave velocity structure is estimated together with the velocity discontinuity interfaces, where we add both data of the amplitudes and differential travel times of Ps converted phases in RFs employing Gaussian beam RF synthetics. We found, however, that it is difficult to match the amplitudes of Ps phases to estimate the velocity contrasts between velocity discontinuity interfaces with 2-D undulations.

Here, as a step toward RF Tomography, we are developing a method of RF Travel Time Tomography using only travel times of P and S waves from local and teleseismic events and P-Ps times of Ps converted phases obtained with the receiver function analyses. Abe et al. (2011) developed a method to estimate iteratively geometries of dipping seismic velocity discontinuities with high dipping angles of 30 to 70 degrees from common conversion point stacking of receiver functions, in which the multistage fast-marching method (de Kool et al., 2006) is applied to the ray tracing with refraction at dipping interfaces. The large amplitudes of RFs stacked in 3-D cells are interpreted to the Ps phases converted at the velocity discontinuity interfaces and the differential travel times P-Ps of the corresponding phases are additionally used for the travel time tomography of P and S waves from local and teleseismic events.

In this paper, we do not analyze the actual data but aim at developing the code of RF Travel Time Tomography based on the code of FMTOMO (Fast Marching Tomography) by Rawlinson (2007). First, for a 3-D heterogeneous structure with interfaces of a Moho and a subduction slab, we synthesize travel times of P and S waves from local and teleseismic events, and also Ps times converted at the Moho and the slab top and the oceanic Moho interfaces. Then we investigate the ability of retrieving the 3-D velocities and the undulation of the Moho and the dipping slab interfaces.

Keywords: Receiver function, Tomography, Ps converted wave, Travel time, Seismic velocity discontinuity interface

## Ocean acoustic Rayleigh wave persistently excited by earthquake signals

TONEGAWA, Takashi<sup>1\*</sup>; FUKAO, Yoshio<sup>1</sup>; TAKAHASHI, Tsutomu<sup>1</sup>; OBANA, Koichiro<sup>1</sup>; KODAIRA, Shuichi<sup>1</sup>; KANEDA, Yoshiyuki<sup>1</sup>

<sup>1</sup>JAMSTEC

In the interferometry, the wavefield propagating between two positions can be retrieved by correlating ambient noise recorded on the two positions. This approach is useful for applying to various kinds of wavefield, such as ultrasonic, acoustic (ocean acoustic), and also seismology. Off the Kii Peninsula, Japan, more than 150 short period (4.5 Hz) seismometers, in which hydrophone is also cosited, had been deployed for 2 months on 2012 by Japan Agency for Marine-Earth Science and Technology (JAMSTEC) as a part of “ Research concerning Interaction Between the Tokai, Tonankai and Nankai Earthquakes ” funded by Ministry of Education, Culture, Sports, Science and Technology, Japan. In this study, correlating ambient noise recorded on the hydrophones, we attempt to investigate characteristics of wavefield observed at seafloor.

The observation period is from Sep. 2012 to Dec. 2012. Station spacing is around 5 km. For 5 lines off the Kii Peninsula, the 30 - 40 seismometers are distributed at each line. Sampling interval is 200 Hz for both seismometer and hydrophone. The instruments are located at 100 - 4800 m in water depth. In the processing for the both records, we applied a bandpass filter of 1 - 3 Hz, replaced the amplitude to zero if it exceeds a value that was set in this study. We calculated cross correlation function (CCF) by using continuous records with a time length of 600 s, stacked the CCFs over the whole observation period.

We first aligned only CCFs using two stations with a separation distance of 5 km along lines off Kii Peninsula. As a result, we could detect strong signals in the CCFs that clearly show travel time variation as a function of water depth. The group velocity of the signal gradually changes from 1.3 km/s to 0.7 km/s at water depths from 2000 to 4000 m. In addition to the wave, a relatively weak signal with a group velocity of 1.4 - 1.5 km/s can be seen in the region at water depth of 4,000 m.

We investigated the wavefield by using a numerical simulation with finite difference technique. As a result, all of these signals can be explained by acoustic Rayleigh wave, which has the energy within not only the ocean but also sediment. A case in which vertical forces are located at subseafloor generated the acoustic Rayleigh wave well, and the CCFs using synthetic waveforms match well with the observed ones. However, another one in which vertical forces are located at sea surface failed to describe the observation. This means that the observed acoustic Rayleigh wave in background wavefield would be generated by earthquake signal, not signals due to microseisms. Moreover, we will show that the amplitude of the signals possibly correlates with seismicity distribution, which also supports that the signals are excited by earthquake signals.

Keywords: acoustic Rayleigh wave, ambient noise, correlation analysis

## Modeling inclined cracks in a 2-D finite difference grid

NASUNO, Arata<sup>1</sup> ; KAWAHARA, Jun<sup>1\*</sup> ; SHIINA, Takahiro<sup>2</sup> ; OKAMOTO, Taro<sup>3</sup>

<sup>1</sup>Ibaraki University, <sup>2</sup>Tohoku University, <sup>3</sup>Tokyo Institute of Technology

Seismic scattering due to cracks are often numerically simulated using a boundary integral equation method (BIEM), a finite element method, or a finite difference method (FDM). Among others, the FDM has a great advantage in tractability, though having a limitation that it can treat rectangular grids only. Using the rotated staggered grid that they developed, Saenger et al. (2000, Wave Motion) modeled a crack or cavity as a gather of grid points with zero elastic constants. In contrast, Suzuki et al. (2006, 2013, Earth Planets Space) modeled a 2-D empty crack as a linear array of grid points with zero traction on the basis of a standard staggered grid (Virieux, 1984, 1986, Geophysics). Using this method, these authors successfully simulated seismic wave scattering due to cracks. However, they only treated cracks parallel to grid lines.

Here we extended the method of Suzuki et al. (2006) for modeling cracks with zero antiplane shear traction to the case of cracks inclined with respect to grid lines. Using the idea of the staircase approximation to irregular free surface (Ohminato and Chouet, 1997, Bull. Seis. Soc. Am.), we modeled an inclined crack as staircase-like arrayed grid points with zero antiplane shear traction within a staggered grid. We then simulated a plane harmonic SH wave obliquely incident on the crack until the resultant oscillation of the crack became stationary. We then measured the amplitude of displacement discontinuity along the crack. We also calculated the same displacement discontinuity using a frequency-domain BIEM (Murai et al., 1995, Geophys. J. Int.). It was confirmed that the both results were consistent, irrespective of the crack inclination angle, if the grid spacing was much smaller than the crack length and hence the staircase-shaped crack plane was sufficiently smooth. This implies the validity of the present method of modeling inclined cracks.

Acknowledgments: For the BIEM calculations, we used a code of Dr. Yoshio Murai (Hokkaido University), and used the computer systems of the Earthquake and Volcano Information Center of the Earthquake Research Institute, the University of Tokyo.

Keywords: finite difference method, crack, SH wave

## The recent movement and the future plans of the JMA EEW

NAKAMURA, Masaki<sup>1\*</sup> ; KODERA, Yuki<sup>1</sup> ; TAMARIBUCHI, Koji<sup>1</sup> ; AIZAWA, Koji<sup>1</sup> ; OGAMI, Yoshie<sup>1</sup> ; HIRANO, Kazuyuki<sup>1</sup> ; YAMADA, Yasuyuki<sup>1</sup> ; SAKIHARA, Hirokazu<sup>1</sup> ; URATANI, Junpei<sup>1</sup> ; MORIMOTO, Masahiko<sup>1</sup>

<sup>1</sup>JMA

We sometimes reported our efforts to improve the JMA EEW system and we will make a presentation about the recent movement of the JMA EEW and the future plan to improve the system.

In the case of the 2011 off the Pacific Coast of Tohoku Earthquake (Mw9.0), the warning of the EEW was disseminated 30 s after the Mw9.0 event occurrence, which was 8 s after the first detection. The estimated magnitude was 7.2 at the time and the warning was issued only for Tohoku. We could provide the warning before the arrival of S-waves for all warning areas. However, the actual magnitude was 9.0 and the wide area was ruptured. The under estimate of the magnitude and the extent of the source region caused the under estimate of intensities. Especially, in Kanto, we observed 6-upper, but we could not provide the warning for the public. The warning was provided for the public only once, but the updated information was provided only to the limited users. We issued the EEW totally 15 times for the event. Finally the EEW estimated M8.1 105 s after the first detection. Moreover, aftershocks sometimes occurred simultaneously over the wide region. Then, the system became confused and did not always determine the hypocenter parameters correctly. In 49 days after the main shock to April 28, 2011, 70 EEWs were announced to the public, but actual observed intensities did not exceed 2 at any stations in 17 cases.

To overcome those problems, we will introduce the real-time pseudo seismic intensity by Kunugi et al. (2008), by which we will be able to monitor the extent of the strong motion field (the simplest version of Hoshihara, 2013) and to evaluate the calculated hypocenter parameter. The current JMA EEW system is based on the calculated hypocenter parameter. We have the idea of a hybrid method using the conventional method and the real-time intensities (Kotera et al, 2014). Furthermore, Tamaribuchi et al. (2014) developed a new method to classify multiple concurrent events for EEW. Their approach used the particle filter method and the method estimated location, origin time and magnitude in the probabilistic framework, using trigger time, maximum amplitude, epicentral distance and incident angle of the waveform for the likelihood function. We have a plan to use the method additionally.

Moreover, JMA began to provide long period ground motion information, using the observed waveform at each station, on JMA web site March, 2013 (Aizawa et al., 2014). We have just begun to investigate the long period ground motion forecast aiming at establishing an earthquake early warning for long period ground motion (Ogami et al., 2014).

References: Aizawa et al., 2014, the abstract of this meeting. Hoshihara, 2013, DOI: 10.1002/jgrb.50119. Kotera et al., 2014, the abstract of this meeting. Ogami et al., 2014, the abstract of this meeting. Tamaribuchi et al., 2014, Zisin 2, submitted.

Keywords: EEW, long-period ground motion, JMA, seismic intensity, intensity scale on long-period ground motion, hypocenter determination

## Earthquake Early Warning system combined with real-time ground motion prediction

KODERA, Yuki<sup>1\*</sup> ; YAMADA, Yasuyuki<sup>1</sup> ; HIRANO, Kazuyuki<sup>1</sup> ; MORIMOTO, Masahiko<sup>1</sup> ; HOSHIBA, Mitsuyuki<sup>2</sup> ; NAKAMURA, Masaki<sup>1</sup>

<sup>1</sup>Seismology and Volcanology Department, Japan Meteorological Agency, <sup>2</sup>Meteorological Research Institute

We introduce a hybrid method which is a combined method of the current JMA EEW system and the simplest version of real-time ground motion prediction method. We also report applications of the hybrid method to some cases in which the current JMA EEW system underestimates or overestimates seismic intensity.

The current JMA EEW system (the conventional method) forecasts seismic intensity on the basis of hypocenter parameters estimated from observed seismic waveform. When accurate hypocenter parameters are determined in an early phase, forecast values of seismic intensity in all areas are calculated quickly and long lead times are available in many areas. On the other hand, if estimated hypocenter parameters are inappropriate, the conventional method leads to underestimation or overestimation of forecast values of seismic intensity.

Hoshiba (2013) proposes real-time ground motion prediction method as a method of forecasting ground motion without the use of hypocenter parameters. The real-time ground motion prediction method predicts wave field directly from observed wave field by a boundary integral equation for displacement. This method is expected to robustly forecast accurate ground motion because it utilizes actual wave field information. Forecast of JMA seismic intensity based on the real-time ground motion prediction method can be performed easily by the following algorithm:

(1) Gather real-time pseudo seismic intensities (Kunugi et al., 2013) of observation stations within a radius R from a target station.

(2) Take the maximum value of the real-time pseudo seismic intensities as a forecasted seismic intensity of the target station.

This is the simplest version of real-time ground motion prediction method. The algorithm assumes that a ground motion which causes large seismic intensity propagates within a radius R without attenuation. In this method, a lead time tends to be short because the area where actual wave field information is available is limited to a radius R.

The conventional method and the simplest version of real-time ground motion prediction method have complementary features on earliness and robustness. Therefore, appropriate combination of these methods is expected to become a hybrid method which has both earliness and robustness. We propose a hybrid method as follows:

(1) Take the maximum forecasted value of two methods in ordinary circumstances.

(2) Reject a forecasted value of the conventional method when the conventional method is not consistent with the real-time ground motion prediction method.

We set input data as real-time pseudo seismic intensities of JMA observation stations, output data as forecasted values of seismic intensity meters in Japan and radius R as 30km and apply the hybrid method to some previous earthquake events. In the case of the 2011 off the Pacific coast of Tohoku Earthquake, whereas seismic intensity scales of Kanto region the conventional method estimates are more than one degree smaller than actual, the hybrid method estimates them appropriately with an accuracy of about one degree. In the case of multiple events on April 3, 2011, the hybrid method can avoid overestimation of seismic intensity the conventional method leads to by qualify control of estimated hypocenter parameters of the conventional method. In the case of an earthquake in the northern part of Tochigi prefecture on February 25, 2013, forecasted seismic intensities of the conventional method are one or two degrees larger than actual although the conventional method estimates hypocenter parameters appropriately. The hybrid method also overestimates seismic intensity in consequence of the overestimation of the conventional method.

### Reference:

Hoshiba, M. (2013), *J. Geophys. Res. Solid Earth*, **118**, 1038-1050.

Kunugi, T., S. Aoi, H. Nakamura, W. Suzuki, N. Morikawa and H. Fujiwara (2013), *Zisin* 2, **65**, 223-230. (in Japanese)

Keywords: Earthquake Early Warning, Japan Meteorological Agency, seismic intensity

## Achievement of Faster and More Accurate Earthquake Early Warning System - Combining JMA and Hi-net data -

YAMADA, Masumi<sup>1\*</sup> ; TAMARIBUCHI, Koji<sup>2</sup>

<sup>1</sup>DPRI Kyoto University, <sup>2</sup>JMA

Earthquake Early Warning systems (EEWS) are designed to quickly determine locations and magnitudes of earthquakes and then provide predictive warnings about the arrival time and amplitude of the strong shaking. Current JMA EEWS uses data from two seismic networks: JMA accelerometer network and NIED high sensitive seismometer network (Hi-net). Currently, these two datasets are processed in the different scheme and the results are merged to issue a warning. Combining these two datasets and processing in the same framework should improve the accuracy and speed of the warning.

In this study, we tried to develop a method to use these two dataset in the same framework. A major barrier to do this is that the instrument responses are different in these networks. Hi-net seismometers are velocity-type sensor with the corner frequency of 1Hz, which means that the response of long-period components underestimates ground motions. It also saturates for very large ground motions. We need a special care to use this Hi-net data in the same framework.

We applied time-domain recursive filters to correct instrumental response of Hi-net sensors and adjust them to the response of mechanical seismometers. We successfully developed a method to produce records with the same response to the JMA acceleration data. We evaluated the saturation of the Hi-net data with the data in 2 month after the Tohoku earthquake, and found the effect of saturation was minor. Therefore, we can use Hi-net data and JMA acceleration data in the same scheme theoretically. Speed of the warning improved by 3 seconds in the average for the inland earthquake by combining these two networks.

Keywords: earthquake early warning, Hi-net, saturation, instrument response

## Automatic arrival time picking compared to manual picking (6)

HORIUCHI, Shigeki<sup>1\*</sup>; HORIUCHI, Yuko<sup>1</sup>; IIO, Yoshihisa<sup>2</sup>; TAKADA, Youichiro<sup>2</sup>; SAWADA, Yoshihiro<sup>3</sup>; SEKINE, Shutaro<sup>3</sup>; NAKAYAMA, Takashi<sup>4</sup>; HIRAHARA, Satoshi<sup>4</sup>; KONO, Toshio<sup>4</sup>; NAKAJIMA, Jyunichi<sup>4</sup>; OKADA, Tomomi<sup>4</sup>; UMINO, Norihito<sup>4</sup>; HASEGAWA, Akira<sup>4</sup>; OBARA, Kazushige<sup>5</sup>; KATO, Aitaro<sup>5</sup>; NAKANO, Masaru<sup>6</sup>; NAKAMURA, Takeshi<sup>6</sup>; TAKAHASHI, Narumi<sup>6</sup>

<sup>1</sup>Home Seismometer Corporation, <sup>2</sup>Disaster Prevention Research Institute Kyoto University, <sup>3</sup>Association for the Development of Earthquake Prediction, <sup>4</sup>Research Center for Prediction of Earthquake and Volcanic Eruptions, <sup>5</sup>Earthquake Research Institute, The University of Tokyo, <sup>6</sup>Japan Agency for Marine-Earth Science and Technology

### 1. Introduction

Recent installation of many ocean bottom seismometers increases the number of P and S-wave arrival times to be measured. The number becomes more than the limit that we are able to conduct picking. We have started to develop an automatic system of hypocenter location which is able to locate hypocenter with accuracy compatible to manually picking. Our previous study introduced a method of using the evaluation equation composed of many parameters based on seismological knowledge about how to pick arrival times. We have showed that the method can pick reliable arrival times of P and S waves. We also have introduced the method of hypocenter location which is able to locate hypocenters even at a period of earthquake swarm. The method makes pseudo seismograms whose amplitude become large at P and S wave arrival times and locates hypocenter with applying the semblance technique to the pseudo seismograms. In this paper, we preset the accuracy of P and S wave picking by the automatic system.

### 2. Method

In general, the predominant frequency of S wave is lower than that of P wave. We added the data of time variations of predominant frequency for S wave picking. The predominant frequency is calculated by the similar manner of calculating  $\tau_c$ , which is used widely to calculate magnitude in the EEW system. Firstly, we calculate differential and double differential of horizontal component observed seismograms as follows.

$$V(t) = (u(t) - u(t-dt)) / dt$$

$$A(t) = (u(t) - 2u(t-dt) + u(t+2dt)) / dt^2$$

Then we compute 0.1 second running mean of the absolute value of  $V(t)$ , and  $A(t)$  and calculate the ratio of two running means. We get time variations in predominant frequency from the time change of the reciprocal value of the ratio, though it is required to multiply a constant value. We assume  $dt$  to be 0.02 seconds. We put values of time changes of predominant frequency in the evaluation equation, which is composed of many parameters showing characteristic of seismograms; correspond to the periods between the candidates of arrival times.

### 3. Results

1) Remarkable drop in predominant frequency are found in almost all seismographs at times of S wave arrivals, showing the effectiveness of its usage in the arrival time picking. Same drop is found at P wave arrivals but there are many cases of increase.

2) We copied all available continuous seismic waveform data in Japan for 24 hours on September 3, 2011, and computed hypocenter automatically. Our automatic system locates 1523 events and the number by JMA catalogue is 588 in the same period. The number of automatically picked P waves is 2.6 times larger than that of manually picking by JMA, and S wave 1.6 times larger.

3) We compared P and S wave arrival times picked automatically with those by manually picking. P and S wave time differences are 0.06 and 0.16 seconds, respectively. This value is close to the difference in a case when two operators conduct picking for the same data.

4) We compared origin times estimated by two closed stations both of which have P and S wave arrivals. We select all couple of two stations with station distance less than 30km and compared origin times estimated from P and S wave arrival times. The average origin time differences by the manually picked data and those by automatically are 0.26 and 0.27sec, respectively.

We can conclude from these comparisons that we already developed an automatic system compatible to manually picking.

Keywords: Hypocenter location, Automatic P and S wave picking, Evaluation equation, Semblance, Predominant frequency, compatible to manual picking

## Real-time site correction based on evaluating relative responses to common reference station for wide area network

AOKI, Shigeki<sup>1\*</sup> ; HOSHIBA, Mitsuyuki<sup>1</sup>

<sup>1</sup>MRI, JMA

Hoshiba (2013a, JGR) proposed a method for prediction of ground motion based on real-time monitoring, in which hypocenter and  $M$  are not required. In this method, site amplification must be corrected in real-time manner. Aoki and Hoshiba (2013, AGU) designed the recursive filters for real-time site correction according to Hoshiba (2013b, BSSA), and predicted the JMA seismic intensity of a station by applying this filter to the observed record at the neighboring station, namely exchanging the site amplification factors with each other. In their experiments, in order to consider the effects of the source and propagation in the observed records at adjacent two sites to be identical, the events whose epicentral distances were greater than 100km were selected. Consequently, they show the accuracy of frequency-dependent site correction is better than that of frequency-independent correction using the scalar value, which indicates the average difference in observed intensities at both stations.

In this study, we regard the average spectral ratio, which can be evaluated from the strong motions simultaneously observed at adjacent two stations without the assumptions of attenuation function and source information, as the relative site amplification (RSF) between these two stations. The RSF between distant two stations are estimated by least squares method, combining RSFs of adjacent stations in the network which consists of adjacent station pairs in wide area (Ikeura and Kato, 2011, JAEE). The method is applied to JMA seismic intensity meter network and NIED strong motion seismograph network (K-net and KiK-net including borehole meters), and we can get the RSFs of the stations which almost cover Honshu and Shikoku islands to the common reference station (JMA Tokyo Chiyoda-ku).

The causal digital filters having similar amplitude property to the RSFs are designed according to Hoshiba (2013b, BSSA) and are applied to the waveforms observed in the 2011 Tohoku great earthquake and 2004 Chuetsu earthquake. Site-corrected waveforms can be regarded as the waveforms simulated observing on the sites having the same amplification factor as the reference station. We compare the distribution of seismic intensity with and without site correction. In the distribution of site-corrected intensity on the ground surface, small-scale heterogeneities found on the distribution without site correction vanish and the smooth attenuation of seismic intensity with distance becomes clearer. Before the site correction, the intensity observed in the borehole generally tends to become smaller than that on the ground surface. However the distributions of site-corrected intensities in the borehole are very similar to the distribution of site-corrected intensities on the ground surface. These results indicate that our site correction method applicable to real-time processing works well.

**Acknowledgements:** We make use of the recordings of NIED strong motion seismograph network (K-NET and KiK-net) and JMA seismic intensity meter network.

**Keywords:** Site amplification factor, Spectral ratio method, Real-time processing, Strong motion seismograph network in Japan, Prediction of the ground motion

## Real-time prediction of earthquake ground motion -application of data assimilation and its application to actual data-

HOSHIBA, Mitsuyuki<sup>1\*</sup> ; AOKI, Shigeki<sup>1</sup>

<sup>1</sup>Meteorological Res. Inst., JMA

Aiming at improvement of prediction of seismic intensity in Earthquake Early Warning, we are investigating a new technique for real-time prediction of earthquake ground motion. We have proposed to use data assimilation technique for estimation of current wavefield of ground motion, and then predict future wavefield based on physics of wave propagation. In this presentation, we will show examples of application of the technique to the actual data, such as those from the 2011 Tohoku earthquake and the 2004 Mid-Niigata earthquake.

In the proposed technique, estimation of current wavefield is important. We correct site amplification factors using recursive filtering (Aoki and Hoshiba, 2014), apply band pass filter which is used for JMA seismic intensity (Kunugi et al., 2008), and then estimate envelope of 3-component vector summation of the filtered waveforms. We apply the data assimilation technique to the envelope and then estimate the spatial distribution of strength and propagation direction of ground motion.

The strength and the propagation direction are used as an initial condition, and then wave propagation is calculated. In this presentation, as the physics of wave propagation we will use Radiative Transfer Theory in which wave propagation is simulated by energy propagation based on high frequency approximation. The theory has been used for interpretation of seismogram envelope. We will indicate examples of predictions of 10 and 20s in this presentation.

For application to the 2011 Tohoku earthquake, this method reproduces the strong ground motion which were generated from multiple SMGA, and then propagated into many directions. Strong ground motion, generated at off Fukushima much later than the earthquake origin time, propagated into Kanto region, and then around Kofu and Nagoya. The prediction of 10 and 20s reflects the spatial distribution. In the conventional method based on hypocentral location and magnitude, it was not easy to predict the ground motion for the case of the late rupture.

For case of the 2004 Mid-Niigata earthquake, this method reproduces propagation of strong ground motion from repeated aftershocks. Especially at around epicenter region, strong ground motion repeatedly arrived even when the motion of earlier events still large. In the conventional method, the case of the repeated occurrence of aftershocks was not easy.

The proposed method is expected to be useful for improvement of prediction of seismic intensity in Earthquake Early Warning.

Keywords: Earthquake Early Warning, Data assimilation, Prediction of ground motion, Radiative transfer theory, 2011 Tohoku earthquake

## Investigation for earthquake early warnings of long-period ground motion

OGAMI, Yoshie<sup>1\*</sup> ; AIZAWA, Koji<sup>1</sup> ; SAKIHARA, Hirokazu<sup>1</sup> ; URATANI, Junpei<sup>1</sup> ; NAKAMURA, Masaki<sup>1</sup>

<sup>1</sup>JMA

Sometimes seismic intensity cannot express difficulty of action and indoor situations in high rise buildings properly when severe long-period ground motion occurs. To notify people of such situations and facilitate effective countermeasures, JMA started to provide information on long-period ground motion from March 28th, 2013. And now, we are investigating for an earthquake early warning for long-period ground motion.

There are some techniques for prediction long-period ground motion, and we investigate attenuation relationships of response spectrum because it can calculate at any given seismic parameter and calculate fast.

We investigate following three relationships that they are used for governmental studies, we can get their coefficients and detail information on amplification factors, and they have different equation format or adjustment techniques.

- Sato et al.(2010) and Sato et al.(2012)
- Morikawa and Fujiwara(2013)
- Yokota et al.(2010)

We use earthquakes that earthquake early warnings were issued, their magnitudes are bigger than 5.5, and maximum seismic intensities are 3 or larger, and we calculate absolute velocity response spectrum for seismic parameters of each earthquake early warning information and JMA seismic catalog. Prediction points are JMA seismic stations, K-net stations and KiK-net stations, and prediction element is intensity scale of long-period ground motion.

As a result, every equation represent trend properly. Especially, the probability that intensity scales fall inside the error of +/- 1 is 70 to 80 percent when we use seismic parameters of JMA seismic catalog. But there is a tendency that prediction intensity scale is bigger than one of calculated from real wave form near the epicenter because we use the shortest distance from source faults to observation stations which depend on Mw. In addition, calculated results are affected accuracy of seismic parameters of earthquake early warnings. Therefore there is need to discussion when we issue prediction information and what information number we should use.

Keywords: long-period ground motion, JMA, EEW, attenuation relationship, response spectrum

## Updating of Earthquake Early Warning for Long-Period Ground Motions

IRIKURA, Kojiro<sup>1\*</sup> ; KURAHASHI, Susumu<sup>1</sup>

<sup>1</sup>Aichi Institute of Technology

Introduction: In the present EEW systems developed by the JMA, Japan, hypocenter and magnitude of an earthquake are determined quickly, after which ground shaking strengths such as seismic intensity are predicted based on a ground motion prediction equation and then earthquake warning are sent to public when the seismic intensity are beyond 5-lower. This method might underestimate ground motions for large earthquakes with wide rupture area because source extent produces error in estimating distance from source to site and the effects of rupture directivity prediction are not taken into account. Another problem is that the magnitude and source distance cannot be determined before the rupture terminate. Therefore, lead times of prediction become smaller in disastrous regions as earthquakes become larger. Long-period strong motions related to damage of skyscrapers and large oil-storage tanks are generated only from large earthquakes such as mega-thrust earthquakes. It takes very long time before the rupture terminates. A new idea applying the Kirchhoff-Fresnel boundary integral equation proposed by Hoshiba (2013) will solve the above problem by predicting ground motions at front stations where ground motions do not arrive yet without estimating the hypocenter and magnitude of an earthquake. We attempt to examine the applicability of the front detection method to prediction of long-period strong motions.

Methodology: Ground motion  $u(P,t)$  in the wavefield at location  $P$  and time  $t$  inside a close region is approximated as Kirchhoff-Fresnel Integral.

Equation (1)

In the above equation,  $u(r,t)$  is ground motion at a reference point on  $S$  and  $G(P-r,t)$  is the Green's function between a reference point  $r$  and a target point  $P$ . The above equation is available for the case where the wave length is much smaller than the spatial fluctuation of absolute amplitude of  $u(r,t)$  and  $G(P-r,t)$ , i.e. in high-frequency motions.

When the distance to the source is much larger than  $|P-r|$ , plane wave incidence can be assumed locally around  $P$ . Then,  $u(P,t)$  is approximated as a convolution between  $G(P-r,t)$  and  $u(r,t)$ .

Equation (2)

When the target point is almost aligned along a line connecting the source to the reference point, the crosscorrelation of  $u(P,t)$  and  $u(r,t)$  is approximated as follows.

Equation (3)

$T(P,r,t)$  is the transfer function between the reference point and the target point.  $S(t)$  is defined as the autocorrelation of the source time function  $s(t)$ .

Equation (4)

We can estimate the transfer function when the ground motions from some small earthquakes are obtained at the target point and at the reference point at the same time from (3). The autocorrelation function of the source time function of the small earthquake is estimated in advance, e.g. from the waveform inversion of the source process. When large earthquakes such as mega-thrust earthquakes happen in the subduction zone, we can evaluate long-period ground motions at sites where large shakings do not arrive yet using ground motions at stations already observed closer to the source and the transfer functions calculated in advance.

Keywords: Earthquake Early Warning, Long-Period Ground Motions, the applicability of the front detection method

SSS28-08

Room:312

Time:May 2 12:00-12:15

$$u(\mathbf{P}, t) = \int \frac{1}{v(\mathbf{r})} \cdot (\cos \theta + \cos \theta') \cdot G(\mathbf{P} - \mathbf{r}, t) * u(\mathbf{r}, t) dS \quad (1)$$

$$u(\mathbf{P}, t) = G(\mathbf{P}, \mathbf{r}, t) * u\left(\mathbf{r}, t - \frac{\mathbf{P} - \mathbf{r}}{v} \cos(\theta' - \theta)\right) \quad (2)$$

$$u(\mathbf{P}, \mathbf{r}_\theta, t) * u(\mathbf{r}, \mathbf{r}_\theta, -t) = T(\mathbf{P}, \mathbf{r}, t) * S(\mathbf{r}_\theta, t) \quad (3)$$

$$S(\mathbf{r}_\theta, t) = s(\mathbf{r}_\theta, t) * s(\mathbf{r}_\theta, -t) \quad (4)$$

## Current Status and Issues of the Broadcast Start Condition of Earthquake Early Warning

TAKANO, Kiyoshi<sup>1\*</sup>

<sup>1</sup>III and ERI, the University of Tokyo

In-site broadcasting system is widely used as a means of transmitting of earthquake early warning. But about the current situation of the broadcast start condition, it is determined by the user who introduced it in consultation with providers. For example, if there is a hazardous material in the building, it will be broadcast starting at predicted seismic intensity 3 or more. On the other hand, in the building with no less hazardous materials, it will be broadcast starting at predicted seismic intensity lower 5 or more. The current situation of the broadcast start condition is as described above; the users have determined in consideration of the user environment.

The document, which serves as a reference in the broadcast start condition to determine appropriate, did not exist until the JMA had published guidelines in April 2011. In this guideline, in particular, for the case of in-site broadcasting towards an unspecified number of people, it has been recommended to broadcast suited to the alarm condition of earthquake early warning of JMA.

The alarm condition of earthquake early warning in JMA is, "it is issued for areas predicted strong shaking (seismic intensity lower 5 or more) and for areas where seismic intensity 4 is predicted when if seismic wave were observed at more than two seismic stations and the seismic intensity was predicted to lower 5 or more". And to match in this, mobile phone companies and commercial televisions have broadcast the earthquake early warning in areas where JMA issued an alarm.

At the beginning, we also have set the broadcast start condition of our in-site broadcasting system to match to this alarm condition in JMA. Furthermore, we have operated by setting the "broadcast start condition for giant earthquakes" by using the combination of not only predicted seismic intensity but also predicted magnitude because from the fact that at the time of the Tohoku Giant Earthquake, the predicted seismic intensity at the alarm of earthquake early warning was much lower than the actual.

However in the period of one year from the start of the operation, there were three broadcasting occurred but in those case the real seismic intensity were 2 or 3 and as a result, these broadcasting became the excessive broadcast.

In this opportunity, I would like to report on the results of review for broadcast start condition of earthquake early warning. And I hope to discuss issues for better broadcast start condition and realizing it.

Keywords: Earthquake Early Warning, Broadcast Start Condition, Alarm Condition

## New-development of real-time seismic waveform viewing system feeding from DONET

TAKAESU, Morifumi<sup>1\*</sup>; HORIKAWA, Hiroki<sup>1</sup>; SUEKI, Kentaro<sup>1</sup>; TAKAHASHI, Narumi<sup>1</sup>; SONODA, Akira<sup>1</sup>; MIURA, Seiichi<sup>1</sup>; TSUBOI, Seiji<sup>1</sup>

<sup>1</sup>Japan Agency for Marine-Earth Science and Technology

Jamstec-Ocean seismological database-Integrated byNetwork data (team JOIN) is started since 2012, with the purpose of developing an earthquake research information database through the integration of discrete database, such as real-time earthquake study and lithosphere structure research catalogue. JOIN is consist of three divisions, 1) seismological study using DONET (Dense Ocean-floor Network for Earthquake and Tsunamis) data, 2) sub-structural study for nankai-tonankai earthquake area, and 3) data-management and open to public for oceanographic data acquired JAMSTEC equipment. These can lead not only scientific but practical outreach, consequently, disaster prevention of each local government.

We have developed web-based real-time monitoring system of strong motion and pressure sensor of DONET observatory network, this is user-friendly tool for servant service of disaster prevention department.

Trial operation with the monitoring system is undergoing for a few government close to nankai-tonankai area, aiming full-scale operation which will start from April 2014.

Technical summary of this system will be introduced.

Keywords: DONET, database, real-time trace view, outreach for local government

## Examination of the relative site amplification factor of OBS and their real-time correction: examples of Sagami Bay OBS

HAYASHIMOTO, Naoki<sup>1\*</sup>; HOSHIBA, Mitsuyuki<sup>1</sup>

<sup>1</sup>Meteorological Research Institute

Hoshiba (2013, JGR) proposed a method for real-time prediction of ground motion based on real-time monitoring as the next-generation EEW, in which detection of hypocenter and Magnitude are not required. In this method, site amplification is one of the important factors. Therefore, relative site amplification factor have been evaluated at KiK-net (Iwakiri and Hoshiba, 2011) and at JMA seismic intensity stations (Aoki and Hoshiba, 2013) in the frequency domain. Ocean Bottom Seismograph (OBS) will provide valuable information to grasp ground motion propagation from ocean area. However, it is necessary to correct the site amplification factor of OBS for applying real-time monitoring method. Hayashimoto and Hoshiba (2013, SSJ) reported relative site amplification factor of OBSs at Tonankai region (Tonankai OBS (JMA) and DONET (JAMSTEC)) as a preliminary result. In this study, we evaluate relative site amplification factor of Sagami Bay OBS (NIED, Eguchi *et al.*, 1998, MGR) which is close to land stations, and examine the effects of real-time correction to predict ground motion of land station from OBS.

The averaged spectral ratio of a station-pair from many events can be regarded as the relative site factor when the hypocentral distances to station-pair are much larger than the distance of those stations. In this study, we use the waveform data from the Sagami Bay OBSs and adjacent land stations (K-NET and KiK-net, NIED), and select the dataset with the hypocentral distance which is greater than 100km. We compare Fourier spectra from the waveforms of S-wave portion (20s) on OBSs with those on adjacent land stations as the relative site factors. In examples of the relative site factors of OBSs to KNGH23 (KiK-net borehole station), the amplification factor of the horizontal component is greater than that of the vertical component for frequencies 1-10Hz. We conclude that the site effects of OBSs characterized by such a low velocity sediment layers causes those amplification factors.

In order to examine the effect of frequency-dependent relative site amplification factor, we compare the accuracies of predicted seismic intensity using the spectral ratio with those using the average of seismic intensity (frequency-independent factor). We design the causal digital filter (Hoshiba, 2013, BSSA) having similar amplitude property to relative site factor for the station pair. The filter parameters are estimated and applied for both horizontal and vertical components. And we use the real-time processing of seismic intensity (Kunugi *et al.*, 2008, Zisin 2) to estimate seismic intensity from observed and predicted waveforms. Both of the techniques are applicable in real-time. We consider the RMS of residual between observed and predicted seismic intensities as the accuracy of site correction of each station pair. In the case of prediction of seismic intensities from OBSs data to land stations, the average RMS of frequency-dependent method are smaller than that of frequency-independent method. Similar results are also obtained at pairs of land station. These results indicate that the frequency-dependent site factor is crucial factor to predict seismic intensity from OBS data, and also show that OBS can be used as front stations in the method for prediction of ground motion based on the real-time monitoring.

Acknowledgments: Strong motion acceleration waveform data were obtained from K-NET and KiK-net of NIED.

Keywords: Earthquake Early Warning, Ocean Bottom Seismograph, Real-time prediction of ground motion, Site amplification factor

## Improvement of earthquake early warning system using the extrapolation of wavefield with apparent velocity and direction

SATO, Asuka<sup>1\*</sup> ; YOMOGIDA, Kiyoshi<sup>1</sup>

<sup>1</sup>Global Seismology, Natural History Sciences, Graduate School of Science, Hokkaido University

The present early warning system in Japan utilizes the epicenter information preliminary estimated by P-wave arrival times at stations near an event. The present system is still not effective in the following cases, for example, (a) more than one earthquakes occur nearly simultaneously, (b) a deep event whose wave front propagates in a different manner from shallow ones, particularly with very high apparent velocity on the surface, and (c) a large event ( $M > 8$ ) whose finite fault area cannot be neglected. In order to deal with non-circular wave front expansion of these cases, we propose a new approach based on the extrapolation of the early observed wave field alone without determining an epicenter. The idea is similar to the migration method of exploration seismology. The conventional migration method utilizes the wave field on a given wavefront (e.g., Kirchhoff integral migration). In the early warning system, on the other hand, we can obtain the speed and direction of wave field expansion over the surface. Based on the standard representation theorem with a Green's function, we extrapolate wave field outwards or in the future with not only the observed waveform but also its spatial derivative (normal for the wavefront). This enhances the resolution and reliability in the extrapolated wave field in comparison with the conventional approach with the waveform only.

For the extrapolation of wave fields accurately and reliably, we need a reliable Green function in each case. Since the actual wave propagation of P or S waves is very complex or sensitive to details of 3-D velocity structure between a source to each target point on the surface, we shall consider it in a two dimensional manner only focusing on the practical use of the early warning system, that is, a wavefront propagates on the surface with an apparent velocity of P-wave. These apparent velocities vary for events of various depths in different regions. The velocity of shallow events in Hokkaido is about 7.1km/s while that in Nagano prefecture of central Honshuu island is about 5.5km/s. The velocity strongly depends on focal depth: 7.1km/s for the depth of 10km, and 8.9km/s for the depth 100km. The velocity also varies as a function of epicentral distance, particularly for a deep event. We make a table of apparent velocities in different depths, regions and epicenters so that we can pick up an appropriate Green function (apparent velocity) for the wave field extrapolation when an event takes place. We also explain how to estimate the apparent velocity and propagation direction with several early observed wave forms. One key to apply the wavefield extrapolation in the warning system is the good correlation among the seismograms that are observed early as input data. Nevertheless, correlations are generally poor in high-frequency (about 1Hz) seismograms recorded in Japan such as Hi-net data. To enhance the correlation of P waveforms among adjacent stations, we need to correct the site response of each station promptly. Using both shallow and deep events, we first estimated site effect as a function of frequency for Hi-net stations in Hokkaido. We used a rock site station (ONPH) as a reference station for site correction terms for other stations.

For deep earthquakes, a region of anomalous seismic intensity is seen in the Pacific Ocean side of Japan called 'abnormal seismic intensity', due to a subducting Pacific plate of high velocity and small attenuation. For the earthquake of 590 km deep beneath Vladivostok on 18 February 2010, we examined the direction of P waves propagating in Japan. The apparent velocity is highly anisotropic: fast along the islands but slow perpendicular to them. It is about 7.5km/s in the Souya district in the north of Hokkaido while about 13km/s in the Hidaka district in the south. In our extrapolation scheme, we can model the amplification of waves in terms of abnormal seismic intensity.

Keywords: earthquake early warning system, extrapolation of seismic wave field, migration, apparent velocity, site effect, abnormal seismic intensity

## Early forecasting of aftershocks from seismic energy release rate immediately after the mainshock

SAWAZAKI, Kaoru<sup>1\*</sup> ; ENESCU, Bogdan<sup>2</sup>

<sup>1</sup>NIED, <sup>2</sup>University of Tsukuba

The detection completeness of earthquakes just after a large earthquake becomes very poor because their signals are overlapped each other in seismogram records and are hidden by the large amplitude of coda waves. Currently, the JMA starts to serve the aftershock forecasting at least 24 hrs after the mainshock because long lapse times are necessary before the catalog data becomes available for the forecasting with a certain reliability. Recently, Sawazaki and Enescu (under review) succeeded in estimating temporal change in energy release rate for the mainshock and the early aftershock sequence by using the Hi-net continuous records. In their method, the energy release is not determined for each discrete event, but is estimated as a continuous process like a source time function which sums up energies from all the earthquakes occurring at the same time. Therefore, theoretically there are no missing energies in the energy release rate even just after the mainshock. The estimated energy release rate follows a power-law temporal decay like the modified Omori law from about 40 s after the mainshock, and the deviation of the energy release rate with respect to the temporal regression curve distributes according to a power-law like the Gutenberg-Richter law. Since the current aftershock forecasting is conducted based on these two statistical laws, the energy release rate would be available for the early forecasting of the aftershocks.

We examine the statistical characteristics of energy release rate in the frequency range of 8-16 Hz for three crustal earthquakes took place in Japan. From the energy release rate obtained at the first 1 hr, 3 hrs, and 6 hrs after the mainshock, we estimate the number of energy release rate larger than  $10^8$  J/s (about  $M_W 4/s$ ) occurring within 24 hrs after the mainshock. For the 2008 Iwate-Miyagi Nairiku earthquake, the ratios of the estimated/observed numbers are 24/35, 12/20, and 20/10 for the forecasting at 1 hr, 3 hrs, and 6 hrs after the mainshock, respectively. Likewise, the ratios are 1524/223, 231/99, and 113/50 for the 2004 Niigata Chuetsu earthquake, and 17/59, 8/59, and 30/21 for the 2007 Niigata Chuetsu-oki earthquake. For the Niigata Chuetsu earthquake,  $M_J 5.9$ ,  $M_J 5.8$ , and  $M_J 6.3$  aftershocks occurred in the first 1 hr, while there are no aftershocks larger than  $M_J 5.5$  in the lapse times from 1 to 24 hrs. For the Niigata Chuetsu-oki earthquake, there are no aftershocks larger than  $M_J 5$  in the first 3 hrs, while  $M_J 5.7$  aftershock occurred 5.4 hrs after the mainshock. Such large aftershocks and their secondary aftershocks may change the pattern of aftershock activity, and causes the over- and under-estimations in the forecasting.

Keywords: aftershocks, early forecasting, energy release rate, modified Omori law, Gutenberg-Richter law

## A method to remove non-seismic long-period pulses for improved estimations of automatic centroid moment tensor solutions

SAKAI, Takahide<sup>1\*</sup> ; KUMAGAI, Hiroyuki<sup>1</sup> ; NAKANO, Masaru<sup>2</sup> ; MAEDA, Yuta<sup>1</sup> ; YAMASHINA, Tadashi<sup>3</sup> ; PULIDO, Nelson<sup>4</sup> ; INOUE, Hiroshi<sup>4</sup> ; MELOSANTOS, Arnold<sup>5</sup> ; FIGUEROA, Melquiades<sup>5</sup> ; PUNONGBAYAN, Jane<sup>5</sup> ; NARAG, Ishma<sup>5</sup>

<sup>1</sup>Nagoya University, <sup>2</sup>JAMSTEC, <sup>3</sup>Kochi University, <sup>4</sup>NIED, <sup>5</sup>PHIVOLCS

Non-seismic long-period pulse-like waveforms appear in broadband seismic records when P or S waves arrive (e.g., Delorey et al, Bull. Seism. Soc. Am., 2008). The pulse-like waveforms affect centroid moment tensor (CMT) solutions estimated from waveform inversion, but a method to remove those pulse-like waveforms yet to be established. Broadband seismograph networks were installed in the Philippine and Indonesia region to monitor earthquakes and tsunamis. The pulse-like waveforms appear in those network data frequently. Those data are used for automatic estimations of CMT solutions by SWIFT (Source estimates based on Waveform Inversion of Fourier Transformed seismograms), which was developed by Nakano et al. (Geophys.J.Int, 2008). SWIFT estimates both the CMT and moment function by the use of long-period (50-100 s) waveform data, but sometimes the long-period pulse-like waveforms affect SWIFT solutions. To monitor earthquakes and tsunamis, we have to estimate source parameters rapidly and adequately. In this study, we propose a simple and rapid method to remove long-period pulse-like waveforms from broadband seismic records.

## Japan Meteorological Agency information on long-period ground motion

AIZAWA, Koji<sup>1\*</sup> ; OGAMI, Yoshie<sup>1</sup> ; URATANI, Junpei<sup>1</sup> ; SAKIHARA, Hirokazu<sup>1</sup> ; NAKAMURA, Masaki<sup>1</sup>

<sup>1</sup>Japan Meteorological Agency

An earthquake generates seismic waves with various periods, and earthquakes with larger magnitudes generate stronger long-period ground motions. When the natural period of a high-rise building is close to the predominant period of ground motion, resonance happens and the building is severely shaken longer than surface of the Earth. Today, more and more people spend time in high-rise buildings especially in metropolitan areas. If great earthquake occurs, many people in high-rise buildings will be affected by long-period ground motion.

To notify people of such situations and facilitate effective countermeasures, JMA started to provide information on long-period ground motion from March 28th, 2013. Based on questionnaires to tenants of high-rise buildings, it has become clear that difficulty of people's activities depends on the velocity of floor movement, and we classified the intensity of long-period ground motion into four on the basis of velocity. To get the classification, we use wave forms observed by JMA seismic intensity meters on the surface of the Earth which are automatically sent to the JMA system. To estimate shaking at higher floors from wave forms on the surface of the Earth, we simulate the shaking of buildings by absolute velocity response spectrum of the period between 1.5 and 8.0 seconds which causes a significant resonance of buildings with 45 meters or higher. The information is available on the JMA website, with various kinds of contents such as absolute velocity and acceleration response spectrum.

Keywords: long-period ground motion, strong motion

## Prediction of long-period ground motion intensity for earthquake early warning

DHAKAL, Yadab prasad<sup>1\*</sup> ; KUNUGI, Takashi<sup>1</sup> ; SUZUKI, Wataru<sup>1</sup> ; AOI, Shin<sup>1</sup>

<sup>1</sup>National Research Institute for Earth Science and Disaster Prevention

The 2011 Mw 9.1 Tohoku-oki earthquake caused strong shakings of high rise buildings constructed on deep sedimentary basins in Japan. During the earthquake, many people got into difficulty with their movements inside the high rise buildings even on the Osaka basin located at distances as far as about 750 km from the epicentral area. Japan Meteorological Agency (JMA) has started to provide people with information on intensity of long-period ground motions based on the absolute velocity response spectra ( 1.6 to 7.8 s) of the observed records on the grounds (Aizawa et al., 2013). The intensity scale of long-period ground motions is classified into four: 1, 2, 3, and 4 having spectral values of 5 to 15 cm/s, 15 to 50 cm/s, 50 to 100 cm/s, and more than 100 cm/s, respectively. The spectra were computed at natural periods of 1.6 to 7.8 s using 5% of critical damping. The maximum value of the computed spectra among 1.6 to 7.8 s defines the class of intensity. We have recently constructed empirical prediction equations of absolute velocity response spectra in the period range of 1 to 10s aiming for earthquake early warning application (e.g., Dhakal et al., 2013). The equations use JMA displacement magnitude and hypocentral distance as basic parameters. Earthquakes having JMA magnitude 6.3 or larger and focal depths shallower than 50 km were used. One of the difficulties in empirical prediction of long-period ground motions is to effectively include the effects of local geological structure such as 3-D basin effects in the prediction equations. To simplify this problem, we obtained site correction factors at K-NET and KiK-net strong motion sites as the mean value of the logarithmic residuals. To make predictions possible at sites other than the strong motion observation sites, we derived correction coefficients based on the relationships between the average residuals and depths of deep sedimentary layers, which are available for whole Japan at Japan Seismic Hazard Information Station (J-SHIS). We found that the standard deviations are minimized by corrections using the depth of layer having Vs value of 1.4 km/s.

To define intensity at a site, we obtained the maximum value of the predicted spectra among T=1.6 to 7.8 s using the empirical prediction equations explained above. However, we found that the maximum predicted values were somewhat biased against the observed maximum values. Therefore, we applied an additional correction factor to the maximum predicted values to finally obtain the intensities. When a prediction equation was constructed using the maximum value of the observed spectra as the independent parameter, the additional correction factor was eliminated as the resulting residuals were normally distributed; also, the predicted intensities were almost identical to those obtained based on the regression analysis results for each natural period. In this study, we illustrate and discuss the application of empirical prediction equations for the prediction of JMA intensity of long-period ground motions for earthquake early warning application.

### References

Aizawa K, Kawazoe Y, Uratani J, Sakihara H, Nakamura M (2013), Japan Meteorological Agency information on long-period ground motions, Abstract S41A-2410 presented at 2013 Fall Meeting, AGU, San Francisco, Calif., 9-13 Dec.

Dhakal Y P, Kunugi T, Suzuki W, Aoi S (2013), Attenuation relation of absolute velocity response spectra (1-10s) in Japan - a preliminary analysis. Proceedings: 2nd Intl Symp. on Earthq. Engg, Japan Assoc. of Earthq. Engg., Tokyo, Nov 11-12, vol 2, pp 39-48.

Keywords: Long-period ground motion intensity, Earthquake early warning, Absolute velocity response spectra, Attenuation relations

## Regional Earthquake Early Warning Applications in Marmara Region Based on KOERI Seismic Network

PINAR, Ali<sup>1\*</sup> ; COMOGLU, Mustafa<sup>1</sup> ; ZULFIKAR, Can<sup>1</sup> ; TUNC, Suleyman<sup>1</sup> ; ERDIK, Mustafa<sup>1</sup>

<sup>1</sup>Bogazici University, Kandilli Observatory and Earthquake Research Institute, Istanbul, Turkey

KOERI (Kandilli Observatory and Earthquake Research Institute) operates a seismic network in Marmara Sea region (NW Turkey) consisting of 40 broadband and 30 strong motion inland and OBS stations which has a good topology for regional EEW studies. Data transmission between the remote stations and the base station at KOERI is provided both with satellite and fiber optic cable systems. The continuous on-line data from these stations is used to provide real time warning for emerging potentially disastrous earthquakes.

The Virtual Seismologist in SeisComp3 and the PRESTo regional EEW (earthquake early warning) softwares are the two regional EEW algorithms that have been recently setup at KOERI data center to generate the EEW signal. Onsite EEW application are underway for more than a decade.

The early warning signal is communicated to the appropriate servo shut-down systems of the recipient facilities, that automatically decide proper action based on the alarm level. Istanbul Gas Distribution Corporation (IGDAS) is one of the end users of the EEW signal. IGDAS, the primary natural gas provider in Istanbul, operates an extensive system 9,867 km of gas lines with 550 district regulators and 474,000 service boxes. State-of-the-art protection systems automatically cut natural gas flow when breaks in the pipelines are detected. IGDAS uses a sophisticated SCADA (supervisory control and data acquisition) system to monitor the state-of-health of its pipeline network. This system provides real-time information about quantities related to pipeline monitoring, including input-output pressure, drawing information, positions of station and RTU (remote terminal unit) gates, slum shut mechanism status at 581 district regulator sites. The SCADA system of IGDAS receives the EEW signal from KOERI and decide the proper actions according to the previously specified ground acceleration levels. Presently, KOERI sends EEW signal to the SCADA system of IGDAS Natural Gas Network of Istanbul.

The EEW signal of KOERI is also transmitted to the serve shut down system of the Marmaray Rail Tube Tunnel and Commuter Rail Mass Transit System in Istanbul. The Marmaray system includes an undersea railway tunnel under the Bosphorus Strait. Several strong motion instruments are installed within the tunnel for taking measures against strong ground shaking and early warning purposes. This system is integrated with the KOERI EEW System. KOERI sends the EEW signal to the command center of Marmaray. Having received the signal, the command center put into action the previously defined measures. For example, the trains within the tunnel will be stopped at the nearest station, no access to the tunnel will be allowed to the trains approaching the tunnel, water protective caps will be closed to protect flood closing the connection between the onshore and offshore tunnels.

Keywords: EEW signal, Virtual Seismologist, PRESTo, end users, IGDAS, Marmaray

## Full moment tensor inversion for the 2013 Sea of Okhotsk deep earthquake

HARA, Tatsuhiko<sup>1\*</sup> ; KAWAKATSU, Hitoshi<sup>2</sup>

<sup>1</sup>IISEE, BRI, <sup>2</sup>Earthquake Research Institute, The University of Tokyo

We performed full moment tensor inversion for the May 24, 2013 Sea of Okhotsk deep earthquake, which is the largest deep earthquake (the moment magnitude is 8.3 after the Global CMT solution). Following Kawakatsu (1991), we redefined the diagonal components of the moment tensor, and determined full six component moment tensors. In order to determine the isotropic component independently from the CLVD component, we analyzed long period signals in the period range between 550 and 1000 s following Kawakatsu (1996), and Hara et al. (1995, 1996). We retrieved VHZ channel broadband waveform data from the IRIS DMC. The duration of the time series is five hours. We used the Direct Solution Method (Hara et al., 1991, 1993) to calculate the Green's functions. We considered the 3-D velocity structures of model SAW24B16 (Mégnin and Romanowicz, 2000) and crust 2.0 (Bassin et al., 2000; <http://igppweb.ucsd.edu/~gabi/rem.html>) to calculate synthetic seismograms. We set spatial grids around the PDE hypocenter for possible centroid locations and temporal grids around the centroid time of the Global CMT solution for possible centroid times. We conducted linear moment tensor inversions for pairs of the spatial and temporal grids to investigate the dependence of solutions on centroid location and time. In the preliminary analysis, the isotropic components of the solutions with larger variance reductions and smaller correlation coefficients with the isotropic component and the other moment tensor components are in the range around 2 to 4 per cent (implosive) of the seismic moment of this event. This preliminary result is consistent with Okal (2013), who obtained the implosive isotropic component with about 2 per cent of the seismic moment by the analysis of the normal modes  ${}_0S_0$  and  ${}_1S_0$ , although further evaluation on uncertainty of the estimates obtained in this study is required.

Keywords: deep earthquake, moment tensor, isotropic component

## Estimation of Radiated Seismic Energy from Teleseismic Body Waves

KIUCHI, Ryota<sup>1\*</sup> ; MORI, James<sup>1</sup>

<sup>1</sup>Disaster Prevention Research Institute, Kyoto University

Radiated seismic energy is a fundamental parameter for understanding source physics. Using teleseismic P waves, Choy and McGarr (2002) reported that strike-slip earthquakes in the oceanic lithosphere have high apparent stress (rigidity multiplied by the ratio of radiated energy to seismic moment). However, that estimates may have a large variation, because of the large radiation pattern of nodal arrivals. Therefore, we improved that used method to better correct for radiation pattern. From our result, we find that the strike-slip earthquakes have apparent stress values that are 5 to 8 times higher than dip-slip earthquakes with the oceanic events having slightly higher values than continental events. In addition, using our improved methods, we can estimate the apparent stresses for strike-slip earthquakes with more reliability, since the error of radiated seismic energies becomes smaller.

Keywords: Radiated seismic energy, Apparent stress, Strike-slip earthquake

## Seismic energy estimation of repeating earthquake sequences offshore northeastern Japan

ARA, Masamichi<sup>1\*</sup> ; IDE, Satoshi<sup>1</sup> ; UCHIDA, Naoki<sup>2</sup>

<sup>1</sup>The University of Tokyo, EPS, <sup>2</sup>Graduate school of science Tohoku university

Repeating earthquakes are thought to occur on locked patches, which represent almost time-independent irregularity on the plate interface, to catch up with stable slip on the surrounding interface. Thus, they produce spatial and temporal stress heterogeneity around the source area, which may control the spatial and temporal patterns of seismic energy of repeating earthquakes. We estimate seismic energy for many small to moderate repeating earthquakes that occurred offshore northeastern Japan, to understand the nature of stress heterogeneity and hidden structural irregularity.

Seismic energy reflects dynamic fault motion during an earthquake, while seismic moment is determined by the difference between the initial and final states of the fault. Seismic moment is determined relatively precisely using the low frequency limit of seismic spectra. In contrast, seismic energy has large errors because it is determined from the entire frequency range of seismic spectra, after correcting path and site effects which can be significant especially at high frequencies. Another problem is the size dependence of seismic energy, which has been a matter of debate for two decades in seismological community. A typical question is whether scaled energy (the ratio of seismic energy to moment) is dependent on seismic moment. These problems have to be alleviated to discuss the spatial and temporal variation of radiated seismic energy. Seismic energy must be estimated as precise as possible.

As mentioned, the most serious problem in estimating seismic energy is removing path and site effects. To avoid this problem, the present study adopts an empirical Green's function (EGF) method. We regard the ratio of seismic spectra as the ratio of source spectra, since the seismic spectra of co-located events observed at one station share the same path and site effects. We modify an EGF method with coda waves developed by Baltay et al. (2010), to rigorously evaluate the uncertainty in corner frequencies and the effects of noise.

This method is applied to several repeating earthquakes of magnitude ~2 to 6 that occurred offshore northeastern Japan. We estimate seismic energy for a group of events by calculating the ratios of source spectra using S-coda waves in two horizontal components of Hi-net, National Research Institute for Earth Science and Disaster Prevention. The scaled energy is almost constant or slightly increasing with seismic moment. Nevertheless, the results are still tentative because the estimation of seismic energy is dependent on the assumption of source spectral model, such as the omega-square model, which have not been constrained well.

## Stress drop variations among small earthquakes in the Tohoku-oki region - implications for the 2011 megathrust event

UCHIDE, Takahiko<sup>1\*</sup> ; SHEARER, Peter<sup>2</sup> ; IMANISHI, Kazutoshi<sup>1</sup>

<sup>1</sup>Geological Survey of Japan, AIST, <sup>2</sup>Scripps Institution of Oceanography, UC San Diego

It is important to assess the likely rupture characteristics of future megathrust earthquakes. One approach is to study the spatio-temporal variation of geophysical properties in active subduction zones. We explore this idea by examining stress drops of 1536 small earthquakes (Mw 3.0 - 4.5) shallower than 80 km in the Tohoku-oki region before the 2011 Tohoku-oki earthquake. We estimate stress drops using the spectral analysis method described by Shearer et al. [2006], which isolates source, path, and receiver terms and then applies an empirical Green's function (EGF) correction before computing corner frequencies and stress drops using the Madariaga [1976] model.

We find an overall increase in stress drop with depth, as well as lateral variations in stress drop along strike. Higher-than-average stress drops are found in East Aomori-oki and Miyagi-oki, whereas Sanriku-oki is a moderate stress-drop area. The high stress-drop zone in Miyagi-oki is located just south of the large slip area of the 2011 Tohoku-oki earthquake, and possibly acted as a barrier to further rupture propagation during the event. The Miyagi-oki high-stress-drop zone is located on west of the 1978 Miyagi-oki earthquake rupture area.

Stress drops of earthquakes in the large slip patch of the 2011 Tohoku-oki earthquake are comparable to the mainshock stress drop. Since studies [Hasegawa et al., 2011; Yagi and Fukahata, 2011] indicate that the 2011 Tohoku-oki earthquake released nearly all the stored shear stress, our findings suggest that small earthquakes prior to the mainshock also released a large fraction of the accumulated shear stress. Note that the absolute values of the stress drops of small earthquakes are not well constrained due to assumptions such as the choice of source models, whereas the relative values among the stress drops of small earthquakes are better resolved. Therefore the hypothesis of nearly complete stress drops for the small earthquakes needs to be confirmed by other approaches.

In addition, the frequency dependence of the seismic radiation observed during the mainshock, with proportionally higher frequencies coming from the deeper parts of the fault, mimics the depth dependence we see in small earthquakes in the same region.

These results imply that smaller pre-mainshock earthquakes can provide insights into the fault properties and consequent rupture processes of future megathrust earthquakes.

Keywords: The 2011 Tohoku-oki earthquake, Stress drop, Miyagi-oki, Spatial Heterogeneity of Fault Properties

## Broad-band source image for the 2011 Tohoku earthquake constructed by strong-motion data

KUBO, Hisahiko<sup>1\*</sup> ; ASANO, Kimiyuki<sup>1</sup> ; IWATA, Tomotaka<sup>1</sup> ; AOI, Shin<sup>2</sup>

<sup>1</sup>DPRI, Kyoto Univ., <sup>2</sup>NIED

From the comparison between slip model using long-period (10s $\sim$ ) seismic waves and excitation zones of short-period (0.1-10s) seismic waves, it has been suggested that the 2011 Tohoku earthquake (Mw9.1) has the period-dependent spatial variation on the seismic-wave radiation and this variation would be caused by the spatial difference of slip behavior on the plate boundary (e.g., Koper *et al.*, 2011; Lay *et al.*, 2012). However, their studies were based on the qualitative comparison of the results obtained by different methods, and the quantitative comparison between source models having different period-bands has not been made. Therefore, the construction of the source models at different period-bands by a common method is important to further understand the source characteristics of the 2011 Tohoku earthquake. Kubo *et al.* (2013, Fall Meeting of SSJ) estimated the spatiotemporal slip models for the 2011 Tohoku earthquake on three different period bands (10-25s, 25-50s, and 50-100s). In this study, we estimate the source models for the 2011 Tohoku earthquake on five continuously-different period bands (10-25s, 17-33s, 25-50s, 33-67s, and 50-100s) using strong-motion data, and construct broad-band source image for the 2011 Tohoku earthquake.

The spatiotemporal rupture history is estimated by the kinematic linear waveform inversion using multiple time windows (Hartzell & Heaton, 1983). The Green's functions are calculated by the 3D FDM (GMS; Aoi & Fujiwara, 1999) using a 3D velocity structure model, Japan Integrated Velocity Structure Model Version 1 (Koketsu *et al.*, 2012). Three components of velocity waveforms at 25 stations of K-NET, KiK-net, and F-net of NIED are used in this analysis. Using waveform records at the stations for the middle-size events which occurred in the source area of the 2011 Tohoku earthquake, we confirmed the adequacy 3D velocity structure model at the analyzed period-band.

The source image for the 2011 Tohoku earthquake on the period band of 10-100s is summarized as follows: (1) (1st) Deep rupture off Miyagi rupture at 0-60s toward down-dip mostly radiating relative short period (10-25s) seismic waves. (2) Shallow rupture off Miyagi at 45-90s toward up-dip with long duration radiating long period seismic wave. (3) (2nd) Deep rupture off Miyagi at 45-90s toward down-dip radiating long period (25-100s) seismic waves. The dominant-period difference in the seismic-wave radiation between twice deep ruptures off Miyagi may result from the mechanism that the second rupture is smoother than the first one because small-scale heterogeneities on the fault are removed by the first one. (4) Deep rupture off Fukushima at 90-135s.

The broad-band source model on the period band from 5-100s is under construction and we will report this.

[Acknowledgments] The strong-motion data recorded by K-NET, KiK-net, and F-net of NIED was used for this analysis.

Keywords: The 2011 Tohoku earthquake, Broad-band source image, Source models on different period bands, Source inversion, Strong-motion data

## Foreshocks implying slow slip transients leading to large earthquakes

KATO, Aitaro<sup>1\*</sup> ; OBARA, Kazushige<sup>1</sup>

<sup>1</sup>ERI University of Tokyo

In the recent decades, a growing number of geophysical evidences has clarified that a major fault zone along plate interface hosts not only the unstable fast sliding during rupture of ordinary earthquake, but also slow slip transients without any seismic radiations. Because slow slip transients quasi-statically release the shear stress in the adjacent seismogenic regions, the slow slip transients may have caused stress loading on the nearby seismic patch and might play a role in a slow nucleation process leading to a large earthquake (Beroza and Ide, 2010; Bouchon et al., 2011; Kato et al., 2012). Therefore, it is quite important to reveal interplay between slow slip and unstable fast slip, in order to shed light on the nucleation process of large earthquake.

Here, we explored foreshock activities implying slow slip transients leading up to large earthquakes. We applied the matched filter technique to continuous waveform data around 10 days prior to the past large earthquakes in Japan ( $M > \sim 6.5$ ), and created newly foreshock catalog for each sequence. We found out accelerating seismicity preceding some large earthquakes at plate interfaces and intraplate at time scales of days to hours. These foreshocks were located very close to the initiation point of each mainshock rupture. The increase in foreshock seismicity implies that a fault may begin to slowly slip before large earthquake, as like recognized in the foreshock sequence prior to the 2011 Tohoku-Oki earthquake.

## Similar Characteristics between the earthquake source process and Vere-Jones' Branching model

ZHUANG, Jiancang<sup>1</sup> ; WANG, Dun<sup>2\*</sup>

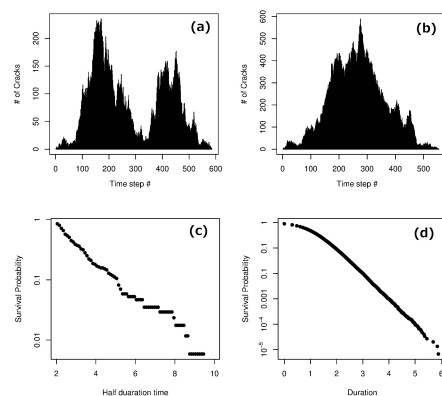
<sup>1</sup>Institute of Statistical Mathematics, <sup>2</sup>Earthquake Research Institute, University of Tokyo

Vere-Jones' branching crack model was developed in 1970s. In this model, the earthquake source is regarded as the results of the total population of crack elements in a critical or near-critical branching process, where the crack does not propagate in a single continuous movement, but through a series of steps. At each step, each crack element simply terminates or generates several other crack elements nearby. Regarding the total number of steps (generation) as the duration time and the total number of crack elements as the total energy released, the following similarities are found between earthquake sources and this model:

1. The distribution of energies is asymptotically a Pareto distribution (power law) for the critical case, or a tapered Pareto distribution (tapered power law, Kagan distribution) for the subcritical case.
2. The duration time of ruptures has a tapered inverse power distribution.
3. The number of crack elements at each generation (time step) show similar patterns of earthquake source time functions.

Figure 1 (a) and (b): Plots of the numbers of crack elements at each time step in two simulation examples. (c): Distribution of half duration times in real earthquake catalog. (d): Distribution of duration times in synthetic catalogs.

Keywords: Branching process, Gutenberg-Richter Magnitude-Frequency Relation, Tapered Pareto distribution, Earthquake source



## Review on Source Type Diagrams

ASO, Naofumi<sup>1\*</sup> ; OHTA, Kazuaki<sup>1</sup> ; IDE, Satoshi<sup>1</sup>

<sup>1</sup>Graduate School of Science, The University of Tokyo

Force system of earthquake is expressed by a symmetric moment tensor, assuming internal forces on a point source, and it has information of characteristic directions, source size, and source type. Although we often assume double couple as the source type, significant non-double-couple component including isotropic component is reported mainly for induced earthquakes or volcanic earthquakes. It is also known that combination of double couples may produce non-double-couple components. For discussion on source types, it is helpful to display them into some visual diagrams.

Since the information of source type has two degrees of freedom, it can be displayed on a two-dimensional flat plane. Although the diagram developed by Hudson et al. [1989] (HPR diagram) is popular, it is inconsistent with the concept of scalar moment [Aki and Richards, 2002]. This problem originates in the projection of a three-dimensional point ( $\lambda_1, \lambda_2, \lambda_3$ ) on a cubic surface, where  $\lambda_1, \lambda_2$ , and  $\lambda_3$  are eigenvalues of moment tensor.

Then, Chapman and Leaney [2012] developed a new diagram by combining spherical projection and stereographic projection (CL diagram). The spherical projection overcomes the problem of the HPR diagram, and the stereographic projection keeps areal density from a spherical surface to a flat plane. This diagram has an advantage that a straight line passing through the center corresponds to the mechanism obtained by combination of an arbitrary mechanism and a double couple, but the diagram is curved shape, and it does not suit for detailed discussions on non-double-couple component when the isotropic component is dominant.

In the present study, we developed another new rectangle diagram that overcomes difficulties of the HPR diagram and the CL diagram simultaneously (AOI diagram). After projecting ( $\lambda_1, \lambda_2, \lambda_3$ ) on a spherical surface, we project it on a cylinder, keeping areal density. This diagram is an orthogonal system of the isotropic axis (the trajectory for varying isotropic component) and the deviatoric axis (the trajectory for varying deviatoric component while keeping its scalar moment). Since isotropic component represents the information from P-wave and deviatoric component represents the information from both P- and S-waves equivalently, the AOI diagram is consistent with the concept of seismogram analyses.

Since there is no source type diagram that is the best at everything, as well as map projection, it is important to use various diagrams taking account of their advantages and disadvantages. In the present study, we also provide examples of projecting a data set on different diagrams, and point out their apparent differences and important considerations.

Keywords: moment tensor, source type diagram, double couple, CLVD, isotropic deformation

## Stress concentration ahead of supershear rupture

FUKUYAMA, Eiichi<sup>1\*</sup> ; XU, Shiqing<sup>1</sup> ; MIZOGUCHI, Kazuo<sup>2</sup> ; YAMASHITA, Futoshi<sup>1</sup>

<sup>1</sup>Nat'l Res. Inst. Earth Sci. Disas. Prev., <sup>2</sup>Centr. Res. Inst. Elect. Pow. Ind.

We report the shear strain field ahead of a supershear rupture. The strain data was obtained during the large-scale biaxial friction experiments conducted at NIED in March 2013. We conducted friction experiments using a pair of meter-scale gabbro rock specimens whose fault area was 1.5m x 0.1m. We applied 2.6MPa normal stress and loading velocity of 0.1mm/s. At the long side of the fault edge, which is parallel to the slip direction, 32 2-component semi-conductor strain gauges were installed at an interval of 50mm and 10mm off the fault. The data are conditioned by high frequency strain amplifiers (<0.5MHz) and continuously recorded at an interval of 1MHz with 16-bit resolution. Many stick slip events were observed and a unilateral rupture event was chosen in this analysis that propagated with supershear rupture velocity. By focusing at the rupture front, stress concentration was observed and sharp stress drop occurred immediately inside the rupture. We found that the stress concentration becomes mild as the rupture propagates and length of the stress concentration area becomes longer. This observation is quite interesting because the rupture propagates at a constant speed close to square root two times the shear wave velocity and thus a longer stress concentration region suggests more energy dissipation. We might speculate that such longer stress concentration area suggests longer plastic region ahead of the rupture (or longer cohesive distance). I.e. The cohesive zone length might be longer as the rupture propagates to maintain constant rupture velocity propagation.

Keywords: Earthquake rupture, Stress concentration, Supershear rupture

## Effects of normal stress on the evolution of AE activities and frictional properties of a fault

IIDA, Takuro<sup>1</sup> ; YABE, Yasuo<sup>1\*</sup>

<sup>1</sup>Graduate School of Science, Tohoku University

To numerically investigate earthquake generations on a plate interface or a fault, we need to know their frictional properties. This study provides a clue to evaluate the frictional properties from spatio-temporal variations of such observations as seismicity and aseismic sliding on the interface of the fault.

We performed frictional sliding experiments using a rotary shear apparatus under a variety of normal stress from about 5 MPa to about 15 MPa. Stepwise change in the sliding rate was imposed to investigate rate dependences of AE activity and friction. Cumulative displacement up to 200 mm was achieved to elucidate their evolutions.

We confirmed similar evolutions of AE activities and friction to those shown by Yabe (2002). That is, the frictional property (rate dependence of friction) of the fault was first the velocity strengthening. The velocity strengthening became weak with an increase in the cumulative sliding. Then, the fault showed the frictional property of velocity weakening. Finally, the rate dependence of friction converged to a constant negative value, when the cumulative sliding reached a critical distance. The  $m$ -value of AE events increased with sliding, when the cumulative sliding distance was smaller than a critical distance. After the critical sliding distance, the  $m$ -value took a constant value. The critical sliding distances of the frictional property and the  $m$ -value were almost the same each other. The rate dependence of the  $m$ -value, which was negative under a small sliding distance, also converged to a constant value of about zero at the cumulative sliding distance.

The evolutions were quantitatively evaluated by applying an exponential-decay function to data that is similar to the function proposed by Wang and Scholz (1994) to express wear processes of a fault. The function well reproduced the experimental data, suggesting that AE activities and frictional properties evolved in association with the wear. The decay distances of evolutions of the AE activities and the frictional properties were equal to each other and in inverse proportion to the normal stress. The latter could be understood by taking into account that the larger the overlap volume of asperities on the fault, the larger the normal stress. Further, when the normal stress was increased, the velocity weakening became weak and the  $m$ -value was decreased.

These results imply that there exists interrelations among seismicity and frictional properties of the fault.

Keywords: frictional sliding, AE activity, frictional property, rotary shear, evolution, normal stress dependence

## Determination of the coefficients of $M_{hdd}$ by a grid search approach

HARA, Tatsuhiko<sup>1\*</sup>

<sup>1</sup>IISEE, BRI

Hara (2007) developed an empirical magnitude formula using durations of high frequency energy radiation and maximum displacement amplitudes using tele-seismic P waves. Recently, Hara (2013), who referred to this magnitude as  $M_{hdd}$ , tried to re-determine the coefficients of the formula using a larger dataset by a linear inversion. The  $M_{hdd}$  calculated by the proposed coefficients better agree with the moment magnitudes from the Global CMT catalog. However, there is slight epicentral distance dependence for their differences. In this study, in order to reduce this epicentral distance dependence, we performed a grid search to determine the coefficients of  $M_{hdd}$  by minimizing both the differences between  $M_{hdd}$  and moment magnitudes and the dependence of their differences on the epicentral distance. The dataset is the same as that of Hara (2013). The search ranges for each coefficient can be set reasonably based on the studies of Hara (2007) and Hara (2013). The preliminary result suggests that it is possible to reduce the epicentral distance dependence using the coefficients obtained by the grid search method.

Keywords: magnitude, high frequency energy radiation, Grid search method

## Wavelet domain inversion for examination of the frequency-dependent characteristics of the seismic wave radiation

SUZUKI, Wataru<sup>1\*</sup> ; AOI, Shin<sup>1</sup> ; SEKIGUCHI, Haruko<sup>2</sup> ; KUNUGI, Takashi<sup>1</sup>

<sup>1</sup>NIED, <sup>2</sup>DPRI, Kyoto University/NIED

Frequency-dependent characteristics of the seismic wave radiation from earthquake sources are important subject for advancing the source physics and the strong-motion prediction. The 2011 Tohoku-Oki earthquake has exhibited particularly distinctive characteristics. The large slip is estimated in the shallow part of the fault from the low-frequency waveforms or geodetic data, whereas the source models derived from the analysis of the higher-frequency seismic data, such as the empirical Green's function modeling or backprojection method, suggest that the high-frequency waves were intensely radiated from the deeper portion. Our previous study (Suzuki et al., 2011) examined the contribution of the significant slip events to the waveform synthesis from the low-frequency waveform inversion results. We found that the sources of the very-low-frequency waves (<0.02 Hz) and higher-frequency waves seem different in the location even in the frequency band used in the waveform inversion. The examination on the frequency dependence in this previous study is somewhat indirect. We have therefore developed the source inversion method that utilizes the wavelet coefficients as the target to fit. This new method is based on the multi-time-window scheme and is linear inversion. The moment rate is directly related to the waveform in each octave band. We have first applied the developed method to 0.01-0.125 Hz strong-motion data of the largest aftershock of the Tohoku-Oki event that occurred in the off Ibaraki prefecture. The preliminary analysis does not suggest the clear frequency dependence for this Mw7.9 event in the analyzed frequency band. As future work, we will extend the analyzed frequency range and also apply to the Tohoku-Oki mainshock.

### References:

Suzuki, W., S. Aoi, H. Sekiguchi, and T. Kunugi (2011): *Geophys. Res. Lett.*, **38**, L00G16.

## Tracing Rupture Process of the 2011 Tohoku M 9.0 Earthquake Using Small Seismic Arrays in China

XUELIN, Shen<sup>1</sup> ; WANG, Dun<sup>2\*</sup>

<sup>1</sup>Key Laboratory of Earthquake Geodesy Institute of Seismology, China Earthquake Administration, <sup>2</sup>Earthquake Research Institute, The University of Tokyo

Back projection(BP) can trace rupture front of large earthquakes. It has been widely applied for better understanding rupture processes of recent large earthquakes. An important result/output from BP is rupture length, which roughly corresponds to the final size of earthquakes given geological environment. Thus it can be used for fast estimate of the size of large earthquakes for the purpose of tsunami warning and disaster evacuation.

Most studies were focused on using data recorded at distances of 30 to 85 degrees to epicenter, in which distance range the first coming wave is direct P wave which ensures a good resolution for the results from BP.

Here we applied several sub China array data to trace the rupture propagation of the Tohoku earthquake to investigate the effect of the other regional phases such as Pn. We tested the effects with seismograms recorded in sub arrays of China seismic array. The results suggest that the overall rupture length can be recovered, though there is some visible disconvergence, especially for those results derived from distant sub arrays.

Keywords: Back projection, Rupture Process, The 2011 Tohoku M 9.0 Earthquake, Small Seismic Arrays in China

## Waveform correlation analysis of small repeating earthquakes using high sampling-rate seismograms

HATAKEYAMA, Norishige<sup>1\*</sup> ; UCHIDA, Naoki<sup>1</sup> ; MATSUZAWA, Toru<sup>1</sup> ; OKADA, Tomomi<sup>1</sup> ; NAKAJIMA, Junichi<sup>1</sup> ; MATSUSHIMA, Takeshi<sup>2</sup> ; KONO, Toshio<sup>1</sup> ; HIRAHARA, Satoshi<sup>1</sup> ; NAKAYAMA, Takashi<sup>1</sup> ; TOHOKU-EQ, Group for the aftershock observations<sup>3</sup>

<sup>1</sup>Graduate School of Science, Tohoku University, <sup>2</sup>Faculty of Sciences, Kyushu University, <sup>3</sup>Group for the aftershock observations of the 2011 Tohoku Earthquake

Repeating earthquake sequence is a series of earthquakes with nearly identical waveforms which occur at the same location repeatedly and they are thought to represent repeated ruptures of small asperities on a fault plane. Since there are many unknown features about asperities such as detailed structures, reproducibility and fluctuation of rupture patterns, it is very important to reveal such features to understand the generation process of interplate earthquakes.

Numerical simulations of the repeating earthquakes with rate- and state-dependent friction laws reveal that stress disturbance caused by postseismic slip of a large earthquake near the repeater can change rupture pattern of the repeater's asperity. Actually, some observations show systematic changes in the magnitudes of small repeating earthquakes immediately after large earthquakes. Such rupture pattern changes will make difference especially in high-frequency components of the waveforms. Therefore, in order to verify the rupture pattern changes of small repeating earthquakes, we have to perform detailed analysis on the differences in high-frequency components of the waveforms.

In this study, we performed 1 kHz sampling-rate seismograph observation at permanent borehole stations along Sanriku coast, Japan for the period from April to November 2011, immediately after the Tohoku-Oki earthquake. We investigate the waveform correlations of small repeating earthquakes using waveform data. We make a pair of earthquakes belonging to the same group of repeating earthquakes and calculate their coherences. The results show that in high-frequency band, there are both high-coherence pairs and low-coherence pairs even in the same repeating earthquake group, although all the pairs show high coherence in low-frequency band. Furthermore, frequency bands in which the coherences are low are nearly the same for all the pairs. These results suggest rupture pattern changes in the asperity.

We also find that earthquakes which show low coherence in high-frequency band for all the counterparts occur immediately after events in the vicinity of the repeater's asperity. This observation implies that rupture pattern changes in the asperity, which make difference in high-frequency components of the waveforms, are caused by stress disturbance due to the nearby earthquakes.

Keywords: repeating earthquake, asperity, high sampling-rate seismogram, waveform correlation analysis, Tohoku-Oki earthquake

## Study on the source process of the largest aftershock of 1923 Kanto earthquake

HONDA, Ryou<sup>1\*</sup> ; KIMURA, Hisanori<sup>2</sup> ; KASAHARA, Keiji<sup>3</sup> ; YUKUTAKE, Yohei<sup>1</sup> ; HARADA, Masatake<sup>1</sup> ; DOKE, Ryosuke<sup>1</sup> ; MIYAOKA, Kazuki<sup>1</sup>

<sup>1</sup>Hot Springs Research Institute, <sup>2</sup>National Research Institute for Earth Science and Disaster Prevention, <sup>3</sup>Association for the Development of Earthquake Prediction

The largest aftershock of M7.5 (Takemura, 1994) occurred at off Boso Peninsula following the 1923 Kanto earthquake. Although the hypocenter have been estimated by previous studies (e.g., Takemura, 1994; Hamada et al, 2001), precise source process have not been estimated yet.

The source region of the largest aftershock is characterized by the region of seismic and aseismic phenomena associated with subduction motion of the Philippine Sea Plate, including slow slip events (SSEs), large backslip events, and repeating earthquakes. Kimura et al. (2009) estimated fault plane of the largest aftershock from geodetic data and they concluded that the fault plane lies within the region of large backslip and the large slip area of the Boso SSE. Estimation of the source process during the largest aftershock is, therefore, important to understand earthquake preparation process around the region.

We set three point sources on the fault plane estimated by Kimura et al. (2009); shallow part (S1), middle part (S2) and deep part (S3). We calculated synthetic seismograms and evaluated the cross correlations between the observed and the synthetic waveforms. We tested the nine hypocenter-asperity combinations using S1, S2 and S3. The combination with the highest value of the average cross correlation is regarded as the best model. We obtained the best score for combination of S2 (hypocenter) and S3 (asperity). This result shows that rupture started from S2 and propagated toward S3.

The observed data used in this study were provided by Kajima Corporation. We are grateful for their kind considerations.

Keywords: 1923 Kanto earthquake, the largest aftershock, source process

## Earthquake source process of the 2013 Santa Cruz earthquake and the tsunami

PARK, Sun-cheon<sup>1\*</sup> ; KIM, Satbyul<sup>2</sup> ; LEE, Jun-whan<sup>1</sup>

<sup>1</sup>National Institute of Meteorological Research, Korea Meteorological Administration, <sup>2</sup>Pukyong University, South Korea

In order to understand the characteristics of large tsunamigenic earthquakes, we analyzed the earthquake source process of the 2013 Santa Cruz earthquake and simulated the tsunami. We first estimated the fault length of about 200 km using 3-day aftershock distribution and the source duration of about 110 sec using the duration of high-frequency energy radiation (Hara, 2007). From these results, we used the initial value of rupture velocity as 1.8 km/s for teleseismic waveform inversions. Teleseismic body wave inversion was carried out using the inversion package by Kikuchi and Kanamori (1991). Teleseismic P waveform data from 28 stations were used and band-pass filter of 0.005 ~ 1 Hz was applied. Our best-fit solution indicated that the earthquake occurred on the northwesterly striking (strike = 290) and shallowly dipping (dip = 15) fault plane. Focal depth and rupture velocity were determined to be 23 km and 1.3 km/s, respectively. Moment magnitude of 7.8 was obtained showing somewhat smaller than the result of previous study (Lay et al., 2013). Slip distribution of the event showed roughly two patches of large slip, one around the hypocenter and the other to the southwest.

Using the slip distribution obtained by teleseismic waveform inversion, we calculated the surface deformations using formulas of Okada (1985) which would be assumed as the initial change of sea water by tsunami. Then tsunami simulation was carried out using Cornell Multi-grid Coupled Tsunami Model (COMCOT) code and 1 min-grid topographic data for water depth. Two DART buoy data were used to verify our simulation. In the presentation, we will discuss more details on the results of source process and tsunami simulation and compare them with the previous study.

Keywords: Santa Cruz, source process, tsunami

## Relationship between the source process of the 2013 Sea of Okhotsk deep earthquake and the thermal structure of the slab

ENDO, Suguru<sup>1\*</sup> ; YAGI, Yuji<sup>1</sup> ; NAKAO, Atsushi<sup>2</sup>

<sup>1</sup>Univ.Tsukuba, <sup>2</sup>Tokyo Institute of Technology

Deep earthquakes occur at depths where, due to the high normal pressures and the prominence of plastic behavior caused by high temperatures, the brittle fracture is difficult to explain. As a consequence, the mechanism of deep earthquakes has been long standing challenge in Earth Science since the early twentieth century. Some mechanisms of deep earthquakes have been suggested and these mechanisms are sensitive to the thermal structure of slabs. Accordingly, the purpose of this study is (1) to infer the source process of the Sea of Okhotsk deep earthquake (Mw 8.3, depth 608.9 km) on 24 May 2013 (UTC) by using the Hybrid Back-projection (HBP) method (Yagi et al., 2012) and waveform inversion (Yagi and Fukahata, 2011) and (2) to elucidate the relationship the source process and the thermal structure in the Kurile slab.

We found that the reactivation of the rupture occurred near the hypocenter. This means that a stress concentration near the hypocenter overcomes the fault strength and reactivates rupture at the hypocenter (Gabriel et al., 2012). We investigated the relationships between our results and the thermal structure of the Kurile slab and found that (1) the main shock started to rupture from the outer portion of the slab (2) the source region of the earthquake extended in a temperature range between 740 °C and 990 °C. This study does not clearly support transformational faulting as a mechanism for occurrence of the Sea of Okhotsk deep earthquake suggested by Zhan et al. (2013) because it is unlikely that metastable olivine exists all over the slab at the depth of the main shock.

Keywords: deep earthquake, HBP method, rupture reactivation

## Focal mechanisms of the triggered tremor beneath the Hinagu fault zone, southwestern part of Japan

MIYAZAKI, Masahiro<sup>1\*</sup> ; MATSUMOTO, Satoshi<sup>2</sup> ; SHIMIZU, Hiroshi<sup>2</sup>

<sup>1</sup>Grad. Sch. Sci., Kyushu Univ., <sup>2</sup>SEVO, Kyushu Univ.

Non-volcanic tremors induced by large amplitude surface wave have been detected all over the world. Most of them are located on and near the plate boundary (Miyazawa and Mori, 2005; Nadeau and Dolene, 2005) and few of them are near volcanoes (Obara, 2012). Chao and Obara (2012, SSJ) found the triggered tremor that located beneath the Hinagu active fault zone, western part of Kyushu Island, Japan. Miyazaki et al. (2013, SSJ) reported that the tremor occurred beneath the seismogenic zone.

In this study, we attempted to estimate focal mechanisms of the tremors triggered by the surface wave of the 2012 Sumatra earthquake. We use the method developed by Hirasawa (1966) that uses the S wave polarization angles. We eliminated the data with low Signal-to-Noise ratio because the angles of waves of tremors were sensitive to background noise.

As a result, we found that focal mechanisms of the triggered tremors were roughly consistent with regional stress field. They could provide constraint for investigating dynamic triggering process of the tremor.

### Acknowledgement

We used the seismic data from Kyushu University, the Japan Meteorological Agency, the National Research Institute for Earth Science and Disaster Prevention and Kagoshima University.

Keywords: triggered tremor, focal mechanisms, Hinagu fault zone

## Spatio-Temporal Variation of Stress Drop Observed at Carthage Cotton Valley Gas Field, Texas

IIDA, Shuhei<sup>1\*</sup> ; KIM, Ahyi<sup>1</sup>

<sup>1</sup>Yokohama City University

Understanding source characteristics of hydraulic fracturing induced microearthquakes is expected to provide a better understanding of the fracturing process and the influence of pre-existing structures controlling the distribution of events. Especially it is still controversial whether the events are associated with volumetric change or not. To address this question, we estimated the source parameters using the empirical Greens function analysis.

Keywords: Stress Drop, Hydraulic Fracturing, Induced Seismicity, Pore Pressure

## Collapse of intraplate earthquake, Separation of accretionary wedge, and Rotation of plate by lateral-fault type

MASE, Hirofumi<sup>1\*</sup>

<sup>1</sup>none

(Refer to the chart)

"Nankai Slab" that subduct from Nankai Trough forms the slope that turned to the northwest and is soaked to the thing that heads eastward. That edge shapes to receive resistance. And, "Nankai Slab" receives the right turning force and weak places collapse. The part that is deeper than that place crawls up and the whole might rotate right. (A), intraplate earthquake of "Nankai Slab", and (B), lateral-fault type earthquake that the boundary with "Tokai Slab" causes, are the Nankai Earthquake(EQ) and the To-Nankai EQ and the Tokai EQ.(this paragraph (1)(2))

Two huge cracks that seem that they relate to the right rotation exist if seafloor topography chart(3) is seen.

Crack(a):This crack starts from the place of about 10km to the east in Cape Daio and lengthens to the south. And, this crack gets to the trough. The trough projects to the south on the west side on the boundary of this place. I think that this crack slips when the upper plate(land side plate, accretionary wedge) greatly moves on the lower plate "Nankai Slab".

Crack(b):This crack is shape of the character of Y off Lake Hamana and reach the trough. "Nankai Slab" and "Tokai Slab" are completely separate in the north from Lake Hamana(7). And, I think in the south this crack leads to the trough while touched. This crack is the one that this plasmotomy reached bottom of the sea and that slips when the whole of lower plate moves with the upper plate put.

Earthquake(B) is the one that Crack(b) slips. It can be said that that Crack(a) slips is intermediate of earthquake(A) and (B).

Dr. Yamanaka proposed in 2004 large and clear source model of the 1944 To-Nankai EQ that eastern edge within the range gets to Omaezaki(4).

That large area of slip is equal to the area of Crack(a) and (b). The 1944 EQ was not only earthquake(A) and everything might have happened. I composed the source process by earthquake(A),(B) and Crack(a),(b) referring to Dr. Yamanaka's (interplate earthquake) source process.

1.Earthquake(A) occurred, and it spread in the direction of northeast along the slab-contour. 2.Separation of the accretionary wedge spread to the southeast and it reached the trough. 3.The separation spread along the trough first and spread along Crack(a) next. 4.(Rotation of upper plate) Crack(a) slipped because the separation was large-scale. 5.(Rotation of lower plate) Crack(b) slipped and earthquake(B) occurred because the environment was in order. The stress occurred in the vicinity of the trough. 6.The Mikawa EQ occurred because of the influence of 4,5. 7.The 2004 EQ occurred and the stress of 5 was absorbed.

Reference literature

(1)Hirofumi MASE(2009)/SSJ2009/P3-64

[http://jglobal.jst.go.jp/detail.php?JGLOBAL\\_ID=200902239527416838](http://jglobal.jst.go.jp/detail.php?JGLOBAL_ID=200902239527416838)

(2)Hirofumi MASE(2010)/JpGU2010/SSS027-P10

[http://www2.jpgu.org/meeting/2010\\_disc2/program/S-SS027.html](http://www2.jpgu.org/meeting/2010_disc2/program/S-SS027.html)

(3)JHOD,JCG/Seafloor Topography of the Plate Boundaries

[http://www1.kaiho.mlit.go.jp/jishin/sokuryo\\_E/sokuryo\\_E.html](http://www1.kaiho.mlit.go.jp/jishin/sokuryo_E/sokuryo_E.html)

(4)Yoshiko YAMANAKA(2004)/Source rupture processes of the 1944 Tonankai earthquake and the 1945 Mikawa earthquake/ERI U-Tokyo

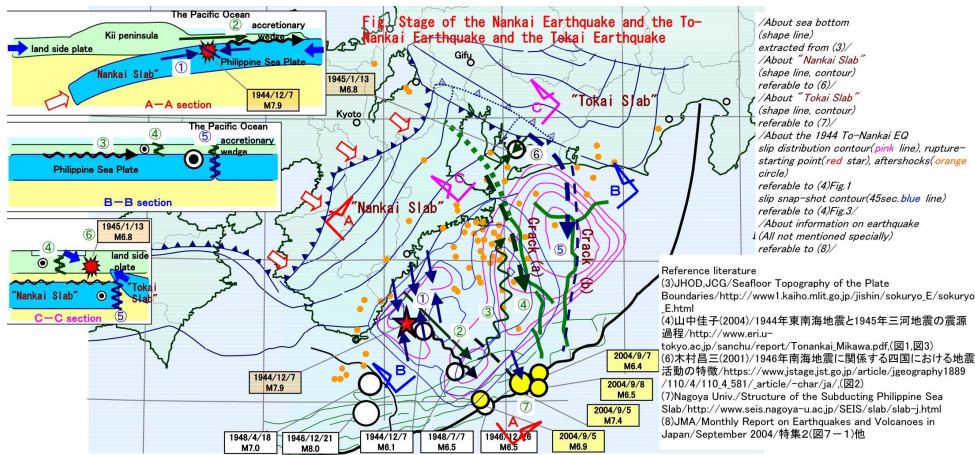
[http://www.eri.u-tokyo.ac.jp/sanchu/report/Tonankai\\_Mikawa.pdf](http://www.eri.u-tokyo.ac.jp/sanchu/report/Tonankai_Mikawa.pdf)

(7)Nagoya Univ./Structure of the Subducting Philippine Sea Slab/ <http://www.seis.nagoya-u.ac.jp/SEIS/slab/slab-j.html>

SSS29-P10

Room:Poster

Time:April 28 18:15-19:30



## Long-term seismic quiescence and activation anomalies preceding to the 2004 Sumatra and the 2005 Nias earthquakes

KATSUMATA, Kei<sup>1\*</sup>

<sup>1</sup>Inst. Seismology and Volcanology, Hokkaido University

I find long-term precursory seismic quiescence and activation anomalies before the 2004 Sumatra ( $M_w$ 9.1) and the 2005 Nias ( $M_w$ 8.6) earthquakes. An earthquake catalog created by International Seismological Center is analyzed between 1964 and 2004, including 1153 earthquakes shallower than 100 km with the body wave magnitude of  $5.0 \leq M \leq 6.0$ . A detailed analysis of the earthquake catalog using a gridding technique (ZMAP) shows that the 2004 Sumatra and the 2005 Nias earthquakes are preceded by not only a seismic quiescence anomaly started in December 1987, but also a seismic activation anomaly started in July 1989. The quiescence and activation areas are located very closely each other between 2S and 6N, which cover the area around the rupture initiation point of the 2004 Sumatra earthquake and the whole area ruptured by the 2005 Nias earthquake. The observed spatial pattern of quiescence and activation can be explained by stress perturbation due to a long-term slow slip event located on the two main shock faults, which is predicted by a numerical simulation [Kato *et al.*, 1997].

Kato, N., M. Ohtake, and T. Hirasawa (1997), Possible mechanism of precursory seismic quiescence: Regional stress relaxation due to preseismic sliding, *Pure Appl. Geophys.*, 150, 249-267.

Keywords: The 2004 Sumatra earthquake, The 2005 Nias earthquake, seismic quiescence, seismic activation, ZMAP, ISC

## Spatial heterogeneity of the frictional property on the Pacific plate off south-east of Hokkaido, Japan

SAITO, Yu<sup>1</sup> ; YAMADA, Takuji<sup>1\*</sup> ; TANIOKA, Yuichiro<sup>1</sup>

<sup>1</sup>ISV, Hokkaido Univ.

The stress drop is an indicator of the difference of the shear strength and the dynamic frictional stress. We analyzed 330 middle-size earthquakes to investigate the spatial heterogeneity of the frictional property on the Pacific plate off south-east of Hokkaido.

Large earthquakes have been occurring repeatedly off south-east of Hokkaido, Japan, where the Pacific Plate subducts beneath the Okhotsk Plate in the north-west direction. For example, the 2003 Tokachi-oki earthquake (Mw8.0) recently took place in the region in 2003. Yamanaka and Kikuchi (2003) analyzed the slip distribution of the earthquake and concluded that the area with a large slip during the 2003 earthquake was mostly overlapped with the area of the 1952 Tokachi-oki earthquake. Miyazaki *et al.* (2004) reported that a notable afterslip was observed at adjacent areas to the coseismic rupture zone of the 2003 earthquake, which suggests that there would be significant heterogeneities of strength, stress and frictional properties on the surface of the Pacific Plate in the region. In addition, some previous studies suggest that the region with a large slip in large earthquakes permanently have large difference of strength and the dynamic frictional stress level and that it would be able to predict large slip areas by analyzing the stress drop of small earthquakes (e.g. Allmann and Shearer, 2007 and Yamada *et al.*, 2010).

We estimated stress drops of 330 earthquakes ( $4.2 \leq M \leq 5.0$ ), using S-coda waves of Hi-net data. The 330 earthquakes were the ones that occurred from June, 2002 to December, 2012 off south-east of Hokkaido, Japan, with the latitude from 40.5N to 43.5N and the longitude from 141.0E to 146.5E. First we selected the closest earthquakes with magnitudes between 3.0 and 3.2 to individual 330 earthquakes as empirical Green's functions. We then calculated source spectral ratio of the 330 pairs of interested earthquakes and EGFs by deconvolving the spectra of S-coda waves. We finally estimated corner frequencies of earthquakes from the source spectral ratios by assuming the omega-squared model of Boatwright (1978) and calculated stress drops of the earthquakes by using the model of Madariaga (1976). The estimated values of stress drop range from  $3.0 \times 10^{(-1)}$  MPa to  $2.0 \times 10^{(2)}$  MPa independent of the seismic moment. Figure shows the spatial distribution of estimated stress drops.

We found spatial difference of estimated values. The average value of stress drop in the afterslip area at the 2003 Tokachi-oki earthquake, where the small displacement was observed, was 1.2 MPa. On the other hand, the value in the source area of the 2004 Kushiro-oki earthquake was 2.0 MPa. In addition, the average values of stress drops in the deeper and shallower parts of the source area of the 1973 Nemuro-oki earthquake were 1.0 MPa and 2.1 MPa, respectively, and the difference was statistically significant. These differences would reflect the spatial heterogeneity of the frictional property on the Pacific plate.

Acknowledgments: We used Hi-net waveform data (<http://www.hinet.bosai.go.jp/>) and the slip distribution of large earthquakes (EIC seismic note; [http://www.eri.u-tokyo.ac.jp/sanchu/Seismo\\_Note/index.html](http://www.eri.u-tokyo.ac.jp/sanchu/Seismo_Note/index.html))

Keywords: Pacific plate, Friction, Spatial heterogeneity, Stress drop

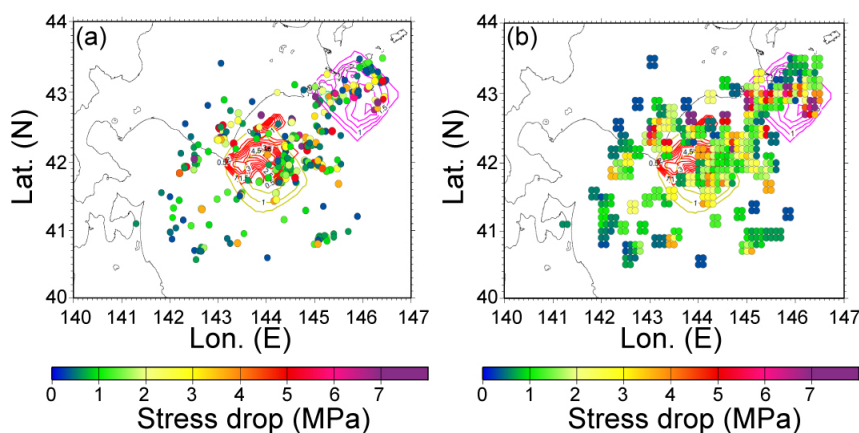


Fig. (a) Estimated stress drops of analyzed 330 middle-size earthquakes ( $4.2 \leq M \leq 5.0$ ). Each circle shows the stress drop for each earthquake. Contours indicate slip distributions of past four large earthquakes off south-east of Hokkaido (EIC seismic note, [http://www.eri.u-tokyo.ac.jp/sanchu/Seismo\\_Note/index.html](http://www.eri.u-tokyo.ac.jp/sanchu/Seismo_Note/index.html)). (b) Spatial pattern of the averaged stress drop. Individual circles indicate averaged values of stress drop for every 0.1 degree, which were calculated from the values of earthquakes in areas with  $0.2 \times 0.2$  degrees.

## Seismically inferred rupture process of the 2011 Tohoku-Oki earthquake by using 3D and 2.5D Green's tensor waveforms

OKAMOTO, Taro<sup>1\*</sup> ; TAKENAKA, Hiroshi<sup>2</sup> ; HARA, Tatsuhiko<sup>3</sup> ; NAKAMURA, Takeshi<sup>4</sup> ; AOKI, Takayuki<sup>5</sup>

<sup>1</sup>Dep. Earth Planet. Sci., Tokyo Institute of Technology, <sup>2</sup>Dep. Earth System Sci. Okayama University, <sup>3</sup>IISEE, Building Research Institute, <sup>4</sup>Japan Agency for Marine-Earth Science and Technology, <sup>5</sup>GSIC, Tokyo Institute of Technology

The March 11, 2011 Tohoku-Oki earthquake (GCMT Mw9.1) generated strong ground motions and large tsunamis, and caused devastating damages in the northeastern Japan. The rupture process of this event provides important clues for understanding the geophysical condition of the generation of mega-thrust earthquakes and the mechanism of the excitation of the large tsunamis.

We analyze "seismic" rupture process of this event by using a non-linear full-waveform inversion method. We incorporate the effect of the near-source laterally heterogeneous structure on the synthetic Green's tensor waveforms because the analysis can result in erroneous solutions if the effect is not considered [1]. Also, in order to increase the resolution we use the teleseismic and the strong-motion seismograms jointly: the distribution of strong-motion station is one-sided and analysis with only the strong-motion records may result in reduced resolution near the trench axis [2]. For the teleseismic P-wave synthetics we use a 2.5-dimensional finite-difference method [3]. For the strong-motion synthetics we use a full three-dimensional finite-difference method that incorporates topography, oceanic water layer, three-dimensional heterogeneity and attenuation. Our simulation is accelerated by GPUs used in parallel [4]: we use the TSUBAME GPU supercomputer in Tokyo Institute of Technology.

In the previous study [5] we used only a single structure model (i.e., a single vertical slice of the 3D heterogeneous structure) to generate all the 2.5D Green's functions. In this paper we have updated the 2.5D structure models. That is, we extracted twenty-three vertical slices from the 3D structure model: each slice was (nearly) perpendicular to the trench axis and was taken along the nodes of the grid that formed the fault plane. By using these new models the 2.5D Green's functions and 3D Green's functions are now "consistent" with each other.

We computed Green's tensor synthetic waveforms for 31 teleseismic and 32 strong-motion components. We used 640 GPUs of the TSUBAME supercomputer for the calculation of each strong-motion synthetics. The inferred slip distribution has large slips near the JMA epicenter with the maximum slip of about 32 m. The amount of slips at the areas close to the trench axis is smaller than that of the land-ward area (i.e., near the JMA epicenter). Inversion results similar to these features have been obtained by previous study [2] but it is remarkable that our joint "seismic" inversion using 2.5D-teleseismic and 3D-strong-motion Green's tensor waveforms resulted in the solution with these features (i.e., land-ward large slips and trench-ward small slips). These features have important implications for tsunami studies because large slips near the trench axis are expected for large tsunamis. In order to verify the solution we will inspect the resolution by using simulations of inversion and the effect of the choice of the Green's tensor waveforms on the solutions.

[1] Okamoto and Takenaka, *Earth Planets Space*, 61, e17-e20, 2009.

[2] Yokota et al., *Geophys. Res. Lett.*, 38, doi:10.1029/2011GL050098, 2011.

[3] Takenaka and Okamoto, in *Seismic Waves, Research and Analysis*, ed. K. Masaki, Intech, 2012.

[4] Okamoto et al, in *GPU Solutions to Multi-scale Problems in Science and Engineering*, ed. D.A. Yuen et al., Chapter 24, 375-389, Springer, 2013.

[5] Okamoto et al., *Seismological Society of Japan, 2013 Fall Meeting*, P1-62, Yokohama, Japan, October 7, 2013.

Keywords: Tohoku-Oki earthquake, rupture process, GPU computing, seismic waveforms

## Seismic velocity and attenuation tomography of the source zone of the 2011 Tohoku-oki earthquake (Mw 9.0)

ZHAO, Dapeng<sup>1\*</sup> ; LIU, Xin<sup>1</sup> ; HUANG, Zhouchuan<sup>1</sup>

<sup>1</sup>Tohoku University, Department of Geophysics

Detailed 3-D P and S wave velocity ( $V_p$ ,  $V_s$ ) and attenuation ( $Q_p$  and  $Q_s$ ) tomography of the crust and upper mantle under the entire Northeast Japan arc from the Japan Trench to the Japan Sea coast is determined (Zhao et al., 2011; Huang and Zhao, 2013; Liu et al., 2014). The suboceanic earthquakes under the Pacific Ocean and the Japan Sea are used in this work and they are relocated precisely using sP depth phases.  $V_p$  and  $V_s$  tomography is determined using a large number of high-quality arrival times, whereas the  $Q_p$  and  $Q_s$  tomography is obtained using a large number of  $t^*$  data measured precisely from P and S wave spectra of local earthquakes. Our results reveal the high-V and high-Q subducting Pacific slab, and significant low-V and low-Q anomalies in the crust and mantle wedge under the volcanic front and the back-arc area. Large megathrust earthquakes ( $M > 6.0$ ) during 1900-2013 including the great 2011 Tohoku-oki earthquake (Mw 9.0) sequence are generally located in high-V and high-Q patches which are surrounded by low-V and low-Q anomalies in the megathrust zone. The high-V/high-Q patches in the megathrust zone generally exhibit large coseismic slips of megathrust earthquakes and large slip deficit on the plate interface. We think that these high-V/high-Q patches represent asperities in the megathrust zone, whereas the low-V/low-Q anomalies reflect weakly coupled areas. These results suggest that structural heterogeneities in the megathrust zone control the interplate seismic coupling and the nucleation of megathrust earthquakes.

### References

Huang, Z., D. Zhao (2013) Mechanism of the 2011 Tohoku-oki earthquake (Mw 9.0) and tsunami: Insight from seismic tomography. *J. Asian Earth Sci.* 70, 160-168.

Liu, X., D. Zhao, S. Li (2014) Seismic attenuation tomography of the Northeast Japan arc: Insight into the 2011 Tohoku earthquake (Mw 9.0) and subduction dynamics. *J. Geophys. Res.* 119, doi:10.1002/2013JB010591.

Zhao, D., Z. Huang, N. Umino, A. Hasegawa, H. Kanamori (2011) Structural heterogeneity in the megathrust zone and mechanism of the 2011 Tohoku-oki earthquake (Mw 9.0). *Geophys. Res. Lett.* 38, L17308.

Keywords: earthquakes, slab, fluids

## A Study on Seismicity before and after the Tohoku Earthquake around its Southern Boundary Using Dense OBS Array Data

NAKATANI, Yukihiro<sup>1\*</sup> ; MOCHIZUKI, Kimihiro<sup>1</sup> ; SHINOHARA, Masanao<sup>1</sup> ; YAMADA, Tomoaki<sup>1</sup> ; HINO, Ryota<sup>2</sup> ; ITO, Yoshihiro<sup>3</sup> ; MURAI, Yoshio<sup>4</sup> ; SATO, Toshinori<sup>5</sup>

<sup>1</sup>Earthquake Research Institute, The University of Tokyo, <sup>2</sup>International Research Institute of Disaster Science, Tohoku University, <sup>3</sup>Disaster Prevention Research Institute, Kyoto University, <sup>4</sup>Graduate School of Science, Hokkaido University, <sup>5</sup>Graduate School of Science, Chiba University

The southern boundary of the 2011 Tohoku earthquake, the source area of the largest aftershock, and a subducting seamount are located around off Ibaraki in the Japan Trench subduction zone. It is important to evaluate the spatial and temporal distribution of seismicity which provides key information about the seismic energy release. However, the seismicity is not well constrained due to a large distance offshore from the onshore network. Therefore, estimating seismic energy release off Ibaraki by using ocean-bottom seismometer (OBS) data is essential to understand the characteristics of the main shock rupture propagation. In this study, we estimated seismicity distribution around off Ibaraki region before and after the 2011 Tohoku earthquake using dense OBS array data.

It is difficult to apply methods that have been designed for on-land seismic stations due to the large ambient noise and effects of thick seafloor sediments. Furthermore, conventional manual picking is difficult because of the occurrence of many aftershocks. We therefore applied a semblance analysis to OBS waveform data with theoretical P-wave travel-time table obtained by the construction of an original 3-D P-wave velocity structure model.

To evaluate the validity of event identification and the accuracy of the epicenter distribution, I conducted comparisons of our epicenters with the JMA epicenters and synthetic tests using theoretical waveforms with several different sets of signal-to-noise ratio and focal depths.

As results of epicenter determination by the semblance analysis, we found that a lot of earthquakes occurred in the vicinity of the frontal region of the subducting seamount after the 2011 Tohoku earthquake. Next, there exists an along-strike density contrast of seismicity, and the inactive region possibly corresponds to the seismically quiet band previously revealed by a seismic observation. Furthermore, we applied the semblance analysis to OBS waveform immediately after the main shock and estimated the spatial and temporal transition of detailed seismicity. We found that the seismicity around the subducting seamount was activated after the largest aftershock rather than between the occurrences of the main shock and the largest aftershock. It puts constraints on the southern boundary of the 2011 Tohoku earthquake.

Keywords: dense OBS array data, seismicity, the southern boundary of the 2011 Tohoku earthquake

## Large shallow slip during the 2011 Tohoku-Oki earthquake: New insights from JFAST and high-velocity friction experiments

UJIIE, Kohtarō<sup>1\*</sup> ; TANAKA, Hanae<sup>1</sup> ; SAITO, Tsubasa<sup>1</sup> ; TSUTSUMI, Akito<sup>2</sup> ; MORI, James<sup>2</sup> ; KAMEDA, Jun<sup>3</sup>

<sup>1</sup>University of Tsukuba, <sup>2</sup>Kyoto University, <sup>3</sup>Hokkaido University

The Japan Trench Fast Drilling Project (JFAST), Integrated Ocean Drilling Program (IODP) Expeditions 343 and 343T were conducted to understand the coseismic deformation mechanisms and dynamics of large shallow slip during the 2011 Tohoku-Oki earthquake. The drill site is located at the toe of the frontal prism near the Japan Trench axis. Observations and analyses of recovered core samples as well as logging-while-drilling data indicate that the plate-boundary fault is highly localized in pelagic clay less than 5 m-thick. The smectite content in pelagic clay is ~78%. The deformations in the plate-boundary fault are marked by distributed shear along anastomosing scaly foliations and localized slip along the boundary between red-brown and dark-brown scaly clays with different fabric orientations. On the microscopic scale, injection structures and mixing of clays of different colors without shear surfaces are observed along the localized slip zone, suggesting fluidization during the localized slip. High-velocity (1.3 meters per second) friction experiments on core samples taken from smectite-rich clay of the plate-boundary fault, show a small stress drop with very low peak and steady-state shear stress. The very low shear stress can be attributed to the abundance of smectite and thermal pressurization effects. Steady-state shear stress is independent of normal stress, and the microstructures after the experiments show evidence for fluidization. These features suggest that the fault material behaved like a fluid during high-velocity shearing due to thermal pressurization of pore fluid. Our results indicate that large shallow slip resulted from coseismic fault lubrication, and the similarity of microstructures between natural and experimental shear zones may represent the fluidization of fault material during earthquake faulting. Seismic slip could be promoted even in plate-boundary faults at shallow depths, as the slip propagates through the smectite-rich fault material.

## Trace element and isotope characteristics of core samples from the Japan Trench Fast Drilling Project (JFAST)

ISHIKAWA, Tsuyoshi<sup>1\*</sup> ; MATSUOKA, Jun<sup>2</sup> ; KAMEDA, Jun<sup>3</sup> ; MORI, James<sup>4</sup> ; CHESTER, Frederick<sup>5</sup>

<sup>1</sup>JAMSTEC, <sup>2</sup>Marine Works Japan Ltd., <sup>3</sup>Hokkaido University, <sup>4</sup>Kyoto University, <sup>5</sup>Texas A&M University

The Integrated Ocean Drilling Program (IODP) Expedition 343 drilled three holes through the plate boundary near the Japan Trench to investigate the cause of very large fault slip during the 2011 Tohoku-Oki earthquake. In this paper, we report trace element and Sr-Nd-Pb isotope compositions of core samples, including plate-boundary fault rocks, recovered from Hole C0019E.

The rocks in C0019E are lithologically subdivided into seven units (Chester et al., 2013): Units 1 to 3, wedge sediments of upper plate; Unit 4, plate-boundary fault; Units 5 to 7, sediments of lower plate. The clay-rich plate-boundary fault rocks (Unit 4) are characterized by elevated concentrations of rare earth elements (REE) and some refractory metals, and are distinct from any other JFAST samples in terms of trace element characteristics. Brown mudstones of the lower plate (Unit 5) show trace element characteristics (e.g. REE pattern) roughly similar to those of the upper plate sediments (Units 1 to 3), but they are still distinguishable from each other. Pelagic sediments in the lower plate (Unit 6) show highly varied trace element compositions with a large Ce anomaly. The Sr, Nd and Pb isotope data show variations that are essentially consistent with trace element characteristics observed for each unit.

The clear relationship observed between lithological units, trace element and isotope compositions and radiolarian ages of the JFAST samples provides a key for understanding the origin of the shallow fault zone of the Tohoku-Oki earthquake and the frontal wedge at the Japan Trench. Geochemical characteristics of the JFAST samples will be discussed along with those of sediments from DSDP site 436, which is a nearby input site, for elucidating the origin of the JFAST rocks and for evaluating coseismic/interseismic processes possibly recorded in the plate-boundary fault rocks.

Keywords: Earthquakes, Fault rocks, Trace elements, Isotopes, IODP

## Paleomagnetic analyses of core samples from the plate-boundary thrust obtained during the IODP JFAST

MISHIMA, Toshiaki<sup>1\*</sup> ; YANG, Tao<sup>2</sup> ; UJIIE, Kohtarō<sup>3</sup> ; KIRKPATRICK, James<sup>4</sup> ; CHESTER, Frederick<sup>5</sup> ; MOORE, Casey<sup>6</sup> ; ROWE, Christie<sup>7</sup> ; REGALLA, Christine<sup>8</sup> ; REMITTI, Francesca<sup>9</sup> ; KAMEDA, Jun<sup>10</sup> ; WOLFSON, Monica<sup>11</sup> ; BOSE, Santanu<sup>12</sup> ; ISHIKAWA, Tsuyoshi<sup>13</sup> ; TOY, Virginia<sup>14</sup>

<sup>1</sup>Osaka City University, <sup>2</sup>China Earthquake Administration, <sup>3</sup>University of Tsukuba, <sup>4</sup>Colorado State University, <sup>5</sup>Texas A&M University, <sup>6</sup>University of California Santa Cruz, <sup>7</sup>McGill University, <sup>8</sup>Pennsylvania State University, <sup>9</sup>Universita di Modena e Reggio Emilia largo, <sup>10</sup>Hokkaido University, <sup>11</sup>University of New Hampshire, <sup>12</sup>University of Calcutta, <sup>13</sup>JAMSTEC, <sup>14</sup>University of Otago

IODP Expedition 343, Japan Trench Fast Drilling Project (JFAST), drilled through the plate-boundary décollement of the Japan Trench, where large slip occurred during the 11 March 2011 Tohoku-Oki Earthquake. In order to reconstruct the deformation of the sediments at the cm scale and less, we conducted paleomagnetic measurements of the core sample from the plate-boundary décollement zone.

The plate-boundary core sample has a scaly fabric and is composed of bicolored clay layers with sharp contacts. We prepared slabs for thin sections across the contacts with typical dimensions of 3x3x5 cm<sup>3</sup> from the core sample. We measured remanent magnetization of 16 slabs. The slabs were subjected to natural remanent magnetization (NRM) measurements in 0.5-1 cm intervals and progressive alternating field demagnetization (AFD) up to 80 mT with a 2G755 pass-through superconducting rock magnetometer at Kochi University.

Typically, two paleomagnetic components were isolated during the AFD of slab samples up to 80 mT. One component ('soft' component) was demagnetized below 20-30 mT, and another component ('hard' component) was not demagnetized even up to 80 mT. For multiple slab samples cut from the same whole-round sample, the hard component generally has a consistent paleomagnetic direction. Contrastingly, the direction of the soft component is not so consistent between adjacent slabs, and even varies within a single slab.

The direction variation of the soft component possibly reflects the cm-scale rotation of competent phacoids during deformation within the slab samples from the plate-boundary thrust zone. The consistency of the hard component directions implies that the hard component was remagnetization during/after the rotation, and was possibly carried by newly-formed magnetic minerals during the deformation.

## Change of permeability caused by 2011 Tohoku earthquake detected from pore pressure monitoring

KINOSHITA, Chihiro<sup>1\*</sup> ; KANO, Yasuyuki<sup>2</sup> ; ITO, Hisao<sup>2</sup>

<sup>1</sup>Graduate School of Science, Kyoto University, <sup>2</sup>DPRI

We have monitored pore and atmospheric pressures at the Kamioka mine in Gifu Prefecture, central Japan since 2005 to study relationship between groundwater and earthquake. Pore pressure decreased after the 2011 Tohoku earthquake (M9.0) occurred on 11 March 2011, which may be attributed to expansion of the crust west of the epicenter or a permeability increase. To evaluate rock permeability changes, we analyzed the Earth tide response of pore pressure before and after the earthquake. Pore pressure fluctuates associated with the meteorological effects, Earth tides and crustal deformation. We assumed that without the change of aquifer conditions tidal response of pore pressure is constant. We compared the tidal response before and after the event. We extracted amplitude and phase lag of M2 and O1 constituents from pore pressure by tidal analysis program, BAYTAP-G. These amplitudes decreased and phases changed after the earthquake. It was in accord with pore pressure decreases. We estimated the hydraulic diffusivity using the poroelastic theory and diffusion equation. If we assume that the poroelastic coefficient is constant, the hydraulic diffusivity increased from 8.9 to 65.0 m<sup>2</sup>/s at the time of the Tohoku earthquake. We also analyzed data before and after the Noto Hanto Earthquake (M6.9) which occurred in the northwestern part of Ishikawa Prefecture, central Japan on 25 March, 2007. The epicentral distance of the Noto Hanto Earthquake from our observation site is 112 km. No hydraulic diffusivity change is detected. The causes of the hydraulic diffusivity change are potentially related to a static and/or dynamic stress change. In order to discuss the difference in hydraulic diffusivity change between the Tohoku and Noto Hanto earthquakes, we analyzed other earthquakes to relate the hydraulic diffusivity changes, and the amount of static and dynamic strain changes.

Keywords: hydraulic diffusivity, pore pressure, Earth tide

## Enigmatic phase lead of pore pressure: 11+ years of ACORK monitoring at the frontal decollement of Nankai Trough

KINOSHITA, Masataka<sup>1\*</sup> ; KANO, Yasuyuki<sup>2</sup>

<sup>1</sup>JAMSTEC, <sup>2</sup>Kyoto Univ. DPRI

For more than 11 years we have been conducting a continuous monitoring of downhole pore pressures at multiple sub-bottom intervals in ODP Holes 808I and 1173B situated landward and seaward of the deformation front in the Nankai Trough off Cape Muroto. We found that the pressure response to the semi-diurnal ocean tide (M2), both amplitude and phase, gradually change during the observed period. The M2 amplitudes at most depths in Hole 808I decay as their phase delay (up to 45 degrees), ONLY IF the amplitude is larger than  $\sim 0.2$  of that for the seafloor. On the other hand, we observe an anomalous phase LEAD (up to -40 degrees) if the relative amplitude is less than  $\sim 0.2$ . We hypothesize that the recorded pore pressure is a combination of two components; one with larger amplitudes and phase-delay and the other with small amplitude and phase-lead. The former can be interpreted as the decrease in formation compliance relative to that of the system, or as the decrease in hydraulic diffusivity around the sensors. The mechanism of the latter variation remain still enigmatic. Existence of gas-rich layer next to the sensor, as suggested by wang and Davis (1996), is difficult to generate such a large phase lead. The predicted earth tide at this site does not coincide with the observed phase. Thermal expansion/contraction caused by the flow within the casing, induced by tidal loading, may cause this phase shift, but a simple thermal/hydrological diffusion cannot explain both the amplitude and phase simultaneously. A complex process including some unknown mechanism may be in operating at Hole 808I.

Keywords: Nankai Trough, ACORK, ODP

## The increase in missing waveform images of the F-net seismographs preceding the 2004 off Kii peninsula earthquake

SUE, Yoshiki<sup>1\*</sup>

<sup>1</sup>No institution affiliation

### 1. Introduction

The F-net is a broadband seismograph network constituted of 73 STS-1 and 2 seismometers. Natural frequency of the seismometers is 120 seconds (STS-2) and longer, thus they can detect long-period ground motion. On its website, waveform images of the stations for a day or an hour are provided. The analyses on their file size have shown long-period vibrations (Sue, 2010).

### 2. Analysis

Variation recorded in waveform images may mean variation of ground motion. Thus operational status of the F-net is investigated. There are two sources on it.

a. Data acquisition trouble log: This is the formal information covering from instantaneous to long-lasting loss of data. Reasons for troubles are shown. While, update of the information is irregular.

b. Missing of waveform images: The website displays the message "Waveform image does not exist". It is surmised that this situation is caused by continuous loss of data exceeding 1 day (Daily plot) or 1 hour (Hourly plot). The reasons are not shown. While update of the information is regular.

So far, analyses on "missing of waveform images" for the 2011 Tohoku earthquake (M=9) has been done (Sue, 2013). As a next step, the 2004 off Kii peninsula earthquake (M=7.4), which occurred on September 5, 2004 at the Nankai trough, is carried out. For details, for the period of about 3 months from June 1, 2004 to September 10, 2004, the F-net stations located in the area between Itoigawa - Shizuoka tectonic line and Okinawa island are investigated (The one in Noto peninsula is excluded).

### 3. Results

Fig. 1 shows the result. During June - first half of July, 2004, which is more than 1.5 month before the main shock, the most frequent number of the image-missing station is 1, and it was stable condition. From last half of July and later, the number varied.

On August 30 and 31, which are 6 and 5 days before the earthquake, there were large increases of the number. Further, arrangement of image-missing stations is mainly in southern part and east coast of the Kyushu island respectively.

On Sept. 4, which is the previous day of the main shock, there were 3 image-missing stations, located from Shikoku island to Kyushu island alongside the Nankai trough (Fig.2).

After the earthquake, number of image-missing station decreased to zero.

The major reasons for missing images are "Network trouble" and "Electric power supply trouble".

### 4. Discussion

Number of F-net station with missing waveform images increases before an earthquake. The phenomena appear not only close to the epicenter, but wide area surrounding it. The phenomena are also observed at the 2011 Tohoku earthquake, thus they may usually appear before a large earthquake. Similar phenomena as shown in this paper might be observed at the anticipated Nankai trough earthquake.

Missing images of all 73 stations happened on 23 to 25 in July (Fig.1). Same phenomena appeared at the 2011 Tohoku earthquake, thus the phenomena may be a sign of unstableness of the F-net system.

It is assumed that increases of the missing waveform images preceding a big earthquake was because the F-net could not withstand possible long-period variation of the earth's surface. "Network trouble" and "Electric power supply trouble" might be causes for such situation. Such phenomena are not observed for the Hi-net seismograph network, probably because of its characteristic (NF = 1 sec).

When the DONET (Dense Oceanfloor Network System for Earthquakes and Tsunamis) detects anomaly, malfunctioning of the F-net may appear at the same time or even earlier.

The area formed by the F-net stations with missing images may have certain relation with magnitude of the earthquake.

### Acknowledgement

The author thanks NIED for using the data of the F-net.

### References

SSS30-11

Room:Main Hall

Time:April 28 14:15-14:30

Yoshiki Sue, 2010, SSJ Fall meeting, D31-12. (In Japanese)

Yoshiki Sue, 2013, The increase in missing waveform images of the F-net broadband seismograph network preceding the 2011 Tohoku earthquake, JpGU2013, S-SS30-P01.

Keywords: F-net, broadband, seismograph network, long period, waveform, Nankai trough

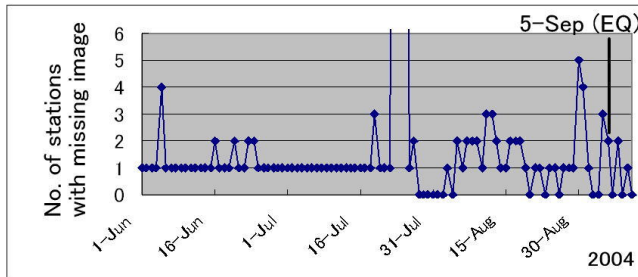


Fig.1. No. of stations with missing waveform images for June 1 to September 10, 2004. No. is 73 on July 23–25. Day is on UT.

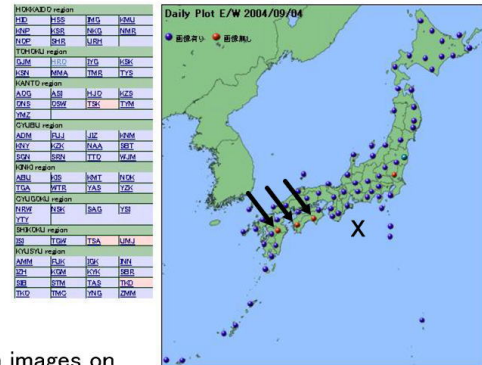


Fig.2. The stations with of missing waveform images on Spetember 4, 2004 (Arrow) and the epicenter (NIED).

## Heat flow distribution along the Nankai Trough: Influence of the structure of the Shikoku Basin oceanic crust

YAMANO, Makoto<sup>1\*</sup> ; KAWADA, Yoshifumi<sup>1</sup> ; GOTO, Shusaku<sup>2</sup> ; HAMAMOTO, Hideki<sup>3</sup>

<sup>1</sup>Earthq. Res. Inst., Univ. Tokyo, <sup>2</sup>Geol. Surv. Japan, AIST, <sup>3</sup>Center Environ. Sci. Saitama

The thermal structure of the Philippine Sea plate (Shikoku Basin) subducting along the Nankai Trough, one of the most important factors controlling the temperature structure around the plate interface, significantly affects physical/chemical processes in the seismogenic zone of subduction earthquakes. Surface heat flow observed on the floor of the Nankai Trough should reflect the thermal structure of the incoming Shikoku Basin. Previous surveys showed that heat flow on the trough floor is extremely high for the seafloor age between 135°E and 136°E (south of the Kii Peninsula), while it is comparable to the value expected from the age in the neighboring area to the east of 136°E. The transition zone from high to normal heat flow lies in the vicinity of the rupture segmentation boundary between the 1944 Tonankai and the 1946 Nankai earthquakes, across which seismicity on the landward side of the trough significantly changes, implying influence of the temperature structure on subduction earthquake processes.

For further investigation of the along-strike variation in heat flow on the trough floor, we conducted heat flow measurements around the Nankai Trough off the Kii Peninsula and off Shikoku in 2011 to 2013. Most of the measurements were made in the area around 136°E, where the high to normal heat flow transition occurs, and on the trough floor to the south of Shikoku, where the existing data were very sparse. 39 new heat flow data on the trough floor allowed us to delineate heat flow variation along the trough. A conspicuous change in heat flow distribution was found at around 136°E. On the west of 136°E, heat flow is extremely high and variable, ranging from 130 to 250 mW/m<sup>2</sup>, while on the east of 136°E, heat flow monotonously decreases eastward from 200 to 100 mW/m<sup>2</sup> in about 50 km with no appreciable scatter. On the trough floor south of Shikoku, west of 134.5°E, no significant change was observed along the trough in spite of westward increase in the seafloor age.

The heat flow distribution described above appears to be correlated with the structure of the Shikoku Basin oceanic crust. The high and variable heat flow area between 134.5°E and 136°E corresponds to the youngest part of the Shikoku Basin which was formed by spreading in NE-SW direction, whereas the neighboring areas with less scattered heat flow, east of 136°E and west of 134.5°E are the older parts formed by E-W spreading. The thickness of the oceanic crust and the basement relief also change around 136°E, in the vicinity of the heat flow transition boundary. Spinelli and Wang (2008) proposed a model for the high heat flow around 135°E that vigorous pore fluid circulation in a permeable layer in the subducting oceanic crust efficiently transfers heat upward along the plate interface. We may infer that the permeability structure of the oceanic crust changes at the transform boundaries between the E-W and NE-SW spreading, which yields variations in vigor and/or pattern of pore fluid circulation, resulting in the contrasting heat flow distributions. Since heat transfer by fluid circulation in the subducting oceanic crust lowers the temperature of the plate interface, the along-strike variation in the trough floor heat flow could indicate corresponding variation in the temperature distribution in the seismogenic zone.

Keywords: Nankai Trough, heat flow, pore fluid, oceanic crust, temperature structure, seismogenic zone

## Reevaluation of temperature at the updip limit of locked portion of Nankai megasplay, inferred from IODP Site C0002 tem

SUGIHARA, Takamitsu<sup>1\*</sup>; KINOSHITA, Masataka<sup>2</sup>; ARAKI, Eiichiro<sup>3</sup>; KIMURA, Toshinori<sup>3</sup>; KYO, Masanori<sup>1</sup>; NAMBA, Yasuhiro<sup>1</sup>; KIDO, Yukari<sup>1</sup>; SANADA, Yoshinori<sup>1</sup>; MOE, Kyaw thu<sup>1</sup>

<sup>1</sup>CDEX/JAMSTEC, <sup>2</sup>KCC/JAMSTEC, <sup>3</sup>DONET/JAMSTEC

Temperature near the updip limit of the locked zone still has large uncertainties due to lack of knowledge about thermal and hydrological properties at depth.

In 2010, the first Long-Term Borehole Monitoring System was deployed at ~900 m below sea floor (mbsf) above the updip limit of seismogenic fault zone in the Nankai Trough off Kumano (Site C0002). Four temperature records show that the effect of drilling diminished in less than 2 years and they all reached thermal equilibrium by 2012. From in-situ temperatures and thermal conductivities measured on core samples, the temperature and heat flow at 900 mbsf are determined as 37.9 °C and 56.1 mW/m<sup>2</sup>, respectively. This heat flow value is in excellent agreement with that from shallow borehole temperature corrected for rapid sedimentation in the Kumano Basin. We use these values to constrain the temperature below 900 mbsf to the mega-splay and plate boundary fault zones.

To extrapolate temperature downward, we use LWD bit resistivity data as a proxy for porosity and the thermal conductivity is modeled from this porosity using a geometrical mean model. Upon integration by the 1-D thermal conduction we included the radioactive heat and frictional heat production. Estimated temperature at the megasplay ranges between 132 to 149 °C, depending on thermal conductivities and radioactive heat. It is significantly higher, by up to 40 °C, than previous 2-D numerical model predictions that can account for the heat flow across the deformation front. The discrepancy may be explained either by increasing the effective frictional coefficients along the fault zones or by introducing a lateral fluid flow along the permeable layers somewhere in the sedimentary layer. Revision of 2-D simulation by introducing our new boundary conditions will also be useful. Ultimately, reaching the megasplay fault and in-situ temperature measurement in the drilled hole is required to understand seismogenesis in the Nankai subduction zone.

Keywords: Seismogenic zone, Nankai Trough, Megasplay fault, Thermal regime, IODP, NanTroSEIZE

## Preliminary Scientific Results of IODP Expedition 348: Ultra-deep Riser Drilling into the Nankai Accretionary Prism

HIROSE, Takehiro<sup>1\*</sup> ; TOBIN, Harold<sup>2</sup> ; SAFFER, Demian<sup>3</sup> ; TOCZKO, Sean<sup>1</sup> ; MAEDA, Lena<sup>1</sup> ; KUBO, Yusuke<sup>1</sup> ; EXPEDITION 348, Scientists<sup>6</sup>

<sup>1</sup>JAMSTEC, <sup>2</sup>University of Wisconsin-Madison, <sup>3</sup>Pennsylvania State University, <sup>4</sup>Chiba University, <sup>5</sup>The university of Tokyo, <sup>6</sup>IODP Expedition 348

The Nankai Trough Seismogenic Zone Experiment (NanTroSEIZE) is a multi-disciplinary scientific project designed to investigate fault mechanics and seismogenesis along subduction megathrusts through seismic imaging, direct sampling, in situ measurements, and long-term monitoring in conjunction with laboratory and numerical modeling studies. International Ocean Discovery Program (IODP) Expedition 348, the latest advance of the NanTroSEIZE project, started on 13 September 2013 and was completed on 29 January 2014. During Expedition 348, the drilling vessel *Chikyu* advanced the ultra-deep riser hole at Site C0002, located 80 km offshore of the Kii Peninsula, from a depth of 860 meters below sea floor (mbsf) to 3058.5 mbsf, the world record for the deepest scientific ocean drilling, and cased it for future deepening. The drilling operation successfully obtained data on formation physical properties from logging while drilling (LWD) tools, as well as from lithological analyses of cuttings and core from the interior of the active accretionary prism at the Nankai Trough. IODP Site C0002 is the currently only borehole to access the deep interior of an active convergent margin.

Preliminary scientific results of Expedition 348 include:

(1) Fine-grained turbiditic mudstones with coarser silty and sandy interbeds, exhibiting steep dips (between ~60 and 90 degrees) are predominant in the prism down to ~3000 mbsf. The biostratigraphic age of the sediments in the lowermost part of the hole is thought to be 9-11 Ma, with an assumed age of accretion of 3-5 Ma.

(2) Slickenlined surfaces, deformation bands and mineral veins are present throughout the drilled interval, while well-developed scaly clay fabrics are increasingly observed below ~2200 mbsf. A substantial fault zone with well-developed foliation was successfully cored from the deep interior of the prism at ~2205 mbsf.

(3) Porosity generally decreases from ~60% to ~20% from the seafloor to 3000 mbsf. However, physical properties including grain density, electrical conductivity and P-wave velocity suggest fairly homogeneous properties in the interior of the prism between ~2000 and 3000 mbsf.

(4) Drilling mud gas analysis during the riser drilling indicates that a source of hydrocarbon gas shifts from microbial origin to thermogenic at around 1700-2300 mbsf.

Lithological and structural characterizations, the style of deformation, and downhole physical properties all indicate a complex structural evolution and will provide unprecedented insights into the mechanical state and behavior of the prism at depth.

Keywords: IODP, NanTroSEIZE, Nankai Trough, accretionary prism

## Levels of frictional heat along deep to shallow parts of the megasplay fault : a Raman spectroscopic analyses of CM

MUKOYOSHI, Hideki<sup>1\*</sup> ; HIRONO, Tetsuro<sup>2</sup> ; MASUMOTO, Hirokazu<sup>2</sup>

<sup>1</sup>Faculty of Education and Integrated Arts and Sciences, WASEDA University, <sup>2</sup>Department of Earth and Space Science, Graduate School of Science, Osaka University

Estimation of frictional heating of deep to shallow portion of ancient megasplay fault is important for understanding of weakening mechanism (e.g., thermal pressurization, melt lubrication) of present plate boundary fault and megasplay fault. In this study, we performed microstructural observation and Raman spectroscopic analyses of carbonaceous materials (CM) in the fault rock of 2.5-5.5 km depth of an ancient megasplay fault (an out-of sequence thrust in the Shimant accretionary complex) and 1-4 km depth of a thrust in the Emi group, Hota accretionary complex. We also conducted heating experiment of CM in host rock of these fault with anaerobic condition (rate of temperature increase: 20 K/min) in order to investigate the effects of fast heating rate like frictional heating during earthquake.

Raman spectrum of CM of both fault is similar to spectrum of 400~600 °C heating experiment of CM. This result shows that both fault had heating history of 400~600 °C by frictional heating. Further examination for effect of shearing to molecular stricter is needed for more detailed evaluation of frictional heating history.

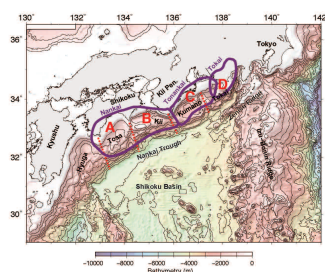
Keywords: ancient megasplay fault, heating experiment

## Upper plate geology controls the rupture area segmentation -A case study of the Nankai Trough

KIMURA, Gaku<sup>1\*</sup> ; HASHIMOTO, Yoshitaka<sup>2</sup> ; KITAMURA, Yujin<sup>3</sup> ; YAMAGUCHI, Asuka<sup>4</sup> ; HAMAHASHI, Mari<sup>1</sup> ; KOGE, Hiroaki<sup>1</sup> ; MORITA, Sumito<sup>5</sup>

<sup>1</sup>Dept. Earth and Planetary Science, The University of Tokyo, <sup>2</sup>Kochi University, <sup>3</sup>Kagoshima University, <sup>4</sup>Atmosphere and Ocean Research Institute, The University of Tokyo, <sup>5</sup>AIST

What controls the earthquake rupture area of megathrust is one of the most fundamental questions in geodynamic research of subduction zone. In the case of the Nankai Trough, Japan, three major controlling factors have proposed so far, surface topography of the subducting plate like seamount, locally strong rigidity of upper plate due to igneous rock composition, and friction property of the plate boundary megathrust including abnormal pore fluid pressure distribution. Such controlling factors are applicable to other subduction zone in general. For example, the topographic high like seamount is proposed to control the location of asperity due to stronger coupling. The topographic-high worked as an asperity contacts with upper plate and rupture could be propagated when the contact breaks. The topographic-high also works as a barrier in the difficult case to be broken. From the geological point of view, plate boundary megathrust in the seismogenic zone must be composed of fault rock in brittle regime because of its temperature range from ~150 °C to ~350 °C, which is cooler than the temperature for the plastic deformation of quartz, feldspar and other rock forming minerals of oceanic crust except for clayey phyllosilicates. In this temperature range, tectonic melange like fault rock with highly pressurized interstitial fluid is expected. Seismic observation showing a reflector with intensive amplitude of negative reflection coefficient suggests a plate boundary fault layer with abnormal fluid pressure. The friction behavior of the fault rock and pore fluid effect is a recent main concern in the subduction zone. The third factor is the mechanical property of the upper plate for the plate boundary megathrust in subduction zone. It is used to treat that the upper plate is a mechanical uniform media saving the elastic energy for theseismic slip along the megathrust. The mechanical property of the upper plate changes for a geological long time scale due to the growth of accretionary prism or tectonic erosion. In addition to such subduction mode of accretion vs erosion, some peculiar tectonic events (e.g. change in convergent direction, some obstacle collision, spreading ridge collision and rapid magmatic accretion etc.) modify the mechanical property of the upper plate and its heterogeneity in space. In the case of the Nankai Trough, a plutonic body is situated beneath the place of epicenter and is suggested to have been functioned as an asperity of 1944 Tonankai and 1946Nankaido Earthquakes. We examined the on-land geology of the Shikoku island and the Kii Peninsula, SW Japan, basement structure and composition beneath the forearcKumano Basin on the basis of recent results of ocean drilling by IODP (Integrated Ocean Drilling Project) and other investigations to infer the geologic composition of the upper plate. As a result we conclude that the key geologic event was middle to late Miocene episodic and rapid growth of forearc crust, mainly due to the magmatic intrusion and extrusion. This event was casued by the eastward migration of the T-T-T triple junction. Such ancient event now controls therupture area of the great earthquake in the subduction zone.



## The research project on the extended Nankai seismogenic zones towards disaster mitigation of the mega-thrust earthquakes

KANEDA, Yoshiyuki<sup>1\*</sup> ; FUKUWA, Nobuo<sup>2</sup> ; FURUMURA, Takashi<sup>3</sup>

<sup>1</sup>Japan Agency for Marine-Earth Science and Technology, <sup>2</sup>Nagoya University, <sup>3</sup>The University of Tokyo

The recurrence of Nankai trough mega thrust earthquakes and tsunamis are the very severe problem to Japan. Therefore, MEXT of Japanese government has implemented the research project during a period from FY2008 to 2012 to evaluate seismic linkage around the Nankai trough mega thrust earthquake seismogenic zones. We have obtained many significant scientific results, such as the extended seismogenic zone, in this previous research project. In the 2013 fiscal year, a new project launched aiming mitigation of disaster caused by the Nankai trough earthquakes in the extended seismogenic zone. This new project is composed of three research fields which are the disaster mitigation research field, observational research field and the simulation research field. According to lessons learned from the 2011 East Japan Earthquake, the disaster mitigation research field are progressing 5 sub-themes which are precise seismic hazard estimation, providing research results to local government/community for disaster measures, investigating recovery and revival methodologies based on social environmental changes, and constructing redundant hazard information database. The observational research field reveals structures of crust and plate, seismicity, and historical tsunami events in the Nankai trough. In the simulation research field, investigations will be conducted for recurrence cycle simulation of mega thrust earthquakes, data assimilation method that improves reliability of the simulation, seismic and tsunami wave simulations for disaster mitigation. We must surely progress each sub-theme at the beginning and finally integrate them for disaster mitigation around the extended Nankai trough seismogenic zones. In this talk, we will introduce the outline of new project and the present progress.

Keywords: Nankai trough seismogenic zone, Seismic linkage, Disaster mitigation

## Ogasawara Bending Slab and Mantle Convection

NIITSUMA, Nobuaki<sup>1\*</sup>

<sup>1</sup>Inst. GeoSciences, Shizuoka Univ.

Ogasawara Slab is not only steeply dipping, but also, bending concentrically and reaching to bottom of upper mantle, which are shown with the hypocenters of 14 May 2013 M7.3 (619 km depth) and 7 February 1998 M6.4 (552 km depth).

Pacific Plate is spreading along East Pacific Rise, and subducting along Japanese Islands down to bottom of upper mantle as slab. If we consider the mass balance in upper mantle on Plate motion with accompanying beneath mantle, the mantle should convect from subduct area toward spreadin area.

The allover concentric bending within the upper mantle realizes overturn of the slab. The slab surface contacts with upper surface of lower mantle where upper mantle minerals change phase for higher pressure. The coldest slab surface in the upper mantle could not change the phase, and might float on the surface of lower mantle toward opposit direction of Plate motion. The return flow of the upper mantle, induced by the floating slab surface, might allow the high speed of the largest Pacific Plate motion.

Izu Slab, north extend of Ogasawara Slab, is bending concentrically above ca. 410km of depth and unbending blow the depth as flat slab. The geometry of the shape from Ogasawara Salb to Izu Salb should intercalate discontinuous part of the slab. Nishinoshima erupted in Nobember 2013 on the slab discontinuous part. The forcal mechanisms on the slab discontinuous part change before and after the East Japan Super Erthquake.

Keywords: Ogasawara Slab, Concentric Bending, Mantle Convection, Upper Mantle Bottom, Nishinoshima Eruption

## Rectified tidal loading: Control on earthquakes manifested by deep tremors

IDE, Satoshi<sup>1\*</sup> ; TANAKA, Yoshiyuki<sup>2</sup>

<sup>1</sup>Department of Earth and Planetary Science, University of Tokyo, <sup>2</sup>Earthquake Research Institute, University of Tokyo

Earthquakes occur due to plate motion, but it remains unclear as to what controls the plate motion. A clue to this problem is provided by a recently discovered cluster of deep tectonic tremors or tiny earthquakes that are occurring in western Japan. Here we demonstrate that tremor activity is strongly correlated with tide levels observed at a nearby station. The correlation is interpreted as representing a nonlinear relationship between stress and slip, which is similar to the rate-dependent friction law. An empirical relationship and observed tide records explain the temporal changes in tremor activity over a period of nine years. The nonlinear fault rheology rectifies oscillating tidal stress and amplifies small changes in tidal amplitude. This mechanism of rectified tidal loading may control temporal changes in plate motion and earthquake occurrence. Remarkably, the background seismicity in the present study area matches the predicted tremor rate obtained from tidal observations over the past 50 years. This mechanism may also explain the weak periodicity of large earthquakes, and is likely to be helpful in probabilistic forecasting of future seismicity.

Keywords: tremor, tide, rectification, slow slip, seismicity, Nankai earthquakes

## Structural mechanics model of plate-interface fracture at subduction zones

EGUCHI, Takao<sup>1\*</sup>

<sup>1</sup>National Defense Academy, Japan

There are unidentified and unveiled properties concerning the physical process of greater inter-plate earthquakes at subduction zones. We, here, present a stochastic fracture model of the plate-interface with dynamic discrete interaction blocks. The stochastic treatment in this study is mainly based on structural mechanics. Here, in the four-dimensional point of view, regarded as significant long-wavelength components of the mechanical inter-plate coupling, we assign several discrete lattice-like blocks being connected each other on a hypothesized plate boundary system. The representative mechanical interaction vector (or tensor) for each discrete block should be variable on the plate boundary system. The total number of the discrete blocks and their nesting pattern should also vary with time during the long-term subduction process with intermittent greater seismic events.

Hereafter, we treat the inter-plate coupling at discrete blocks, using parameters such as failure probability ( $P_{sf}$ ) and safe probability ( $P_{ss}$ ) of the total system of the plate boundary. Here,  $P_{sf} + P_{ss} = 1$ .

The system fracture for the case of parallel connecting blocks is defined as the breakdown of all parallel blocks. Whereas, for the case of a series connecting block system, the system fracture is defined as the failure of one of the series block, or more. The system failure probability of a simple mechanical system being coupled in parallel  $N$  blocks is given as a product of  $p(i)$  from  $i = 1$  to  $i = N$ . Here,  $p(i)$  is the failure probability of the  $i$ -th block of the system. For the case of a mechanical system connected in series  $N$  blocks, the system safe probability becomes a product of  $\{1-p(i)\}$  from  $i = 1$  to  $i = N$ . For a mechanical system composed of both parallel and series blocks, the system failure probability and system safe probability can be estimated with the above definition. Then, we assume that the inter-plate shear coupling of the plate-interface progresses only at discrete blocks of brittle fracture.

We consider two different configuration models for a two-by-four matrix ( $2 \times 4$ ) system of discrete coupling blocks, consist of four columns in the trench-parallel direction and two rows of deep side and a shallow side in the dip direction, as follows.

Configuration model  $A$  is a series-connected system of both the shallower parallel-connected column blocks and the deeper parallel-connected ones.

Configuration model  $B$  is a parallel-connected system of the four columns of the shallower and deeper rows being directly series-connected in the dip direction.

By setting the failure probability,  $p(i,j)$ , of  $(i,j)$ -th block, we can estimate the system failure probability ( $P_{sf}$ ) and system safe probability ( $P_{ss}$ ) for the configuration models,  $A$  and  $B$ . For the configuration models  $A$  and  $B$ , the system safe probability,  $P_{ss}(A)$  and  $P_{ss}(B)$  can be obtained. In the case of  $p(i,j)$  less than 0.5 for all blocks,  $P_{ss}(A)$  becomes larger than  $P_{ss}(B)$ , indicating that the configuration model  $A$  is safer than the model  $B$ . When the representative pattern of the inter-plate coupling changes from the configuration model  $A$  to  $B$ , or vice versa, we should carefully estimate the system probabilities.

We also demonstrated the detailed hypothetical expression form of  $p(i,j)$  by considering the effect of preceding larger seismic ruptures at blocks and the subsequent healing process, etc.

Keywords: subduction zone, inter-plate coupling, structural mechanics, system failure probability, system safe probability

## Seismicity rate variations in subduction zones related to forearc topography

NISHIKAWA, Tomoaki<sup>1\*</sup> ; IDE, Satoshi<sup>1</sup>

<sup>1</sup>Department of Earth and Planetary Science, University of Tokyo

There are clear variations in seismicity among subduction zones worldwide in terms of such as the frequency of earthquake occurrence and maximum earthquake magnitude. These variations have been attributed to differences in tectonic properties in subduction zones, such as relative plate velocity and subducting plate buoyancy. For example, Ide [2013] demonstrate proportionality between relative plate velocity and background seismicity rate — the frequency of seismic events excluding aftershocks. Given that earthquakes occur to release strain in the crust accumulated by relative plate motion, we can intuitively understand this proportionality.

The overriding plate is also an important control on earthquake occurrence in subduction zones. Seismological observations and studies of tectonics have suggested the relationship between forearc topography and frictional properties on the plate interface, such as interplate locking and pore fluid pressure. Given this relationship, variations in forearc topography may reflect differences in frictional properties on the plate interface among subduction zones worldwide. However the relation between forearc topography and variations in seismicity among subduction zones is still unclear. In this study, we compare forearc slope and background seismicity rate in subduction zones worldwide. The forearc slope is based on Smith and Sandwell [1997], and the background seismicity rate is estimated using the epidemic type aftershock sequence (ETAS) model [Ogata, 1988]. We show the correlation between forearc slope and background seismicity rate. Subduction zones with steeper forearc slopes have higher seismicity rates. Furthermore, subduction zones that are outliers of the proportionality between relative plate velocity and background seismicity rate [Ide, 2013], such as Cascadia and South Chile trench, also appear to obey this correlation.

According to the critical taper theory [Davis et al., 1983; Dahlen, 1984], which explains the relationship between forearc topography and frictional properties on the plate interface, and sand box experiments [e.g., Gutscher et al., 1996], steep forearc slope is associated with high basal friction. When we take these studies into account, our results suggest that the seismicity rates are high in subduction zones with steep slopes and high basal friction. This can be explained by considering erosion and accretion processes and geometrical irregularities on the plate interface. Erosional margins tend to have steeper forearc slopes [Clift and Vanucchi, 2004]. Because of thin trench sediments in erosional subduction zones, geometrical irregularities on the subducting plate are not smoothed. Such irregularities may cause high basal friction at the tip of the forearc wedge and steepen the forearc slope. In the seismogenic zone, these irregularities act as numerous small asperities, and these asperities result in many seismic events in the erosional subduction zone. In contrast, accretionary margins generally have gradual slopes. Thick trench sediments smooth subducted seafloor, and it results in low basal friction at the tip of the forearc wedge and the gradual forearc slope. The smoothed plate interface may act as one large asperity in the seismogenic zone, and fewer earthquakes occur in the accretionary subduction zone. Furthermore, these variations in number and size of asperities among subduction zones worldwide may cause differences in megathrust earthquake occurrence.

Our results reveal the relation between forearc topography and seismicity, and suggest that the frequency of seismic events in subduction zones is controlled by not only the mechanical factors such as relative plate velocity and the strain accumulated in the crust, but also the material factors such as erosion and accretion processes, trench sediments, and geometrical irregularities on the plate interface.

Keywords: seismicity rate, subduction zone, forearc topography, erosion and accretion, asperity

## Feasibility of acoustic monitoring of strength drop precursory to earthquake occurrence

KAME, Nobuki<sup>1\*</sup> ; NAGATA, Kohei<sup>2</sup> ; NAKATANI, Masao<sup>1</sup> ; KUSAKABE, Tetsuya<sup>1</sup>

<sup>1</sup>Earthquake Res. Inst., Univ. of Tokyo, <sup>2</sup>Ministry of Education, Culture, Sports, Science and Technology

Rate- and state-dependent friction law (RSF), proposed on the basis of laboratory experiments, has been extensively applied to modeling of earthquake stick-slip cycles. A simple spring-slider model obeying RSF predicts a significant decrease of the frictional strength  $\Phi$  (the state of contact) that is localized within a few years preceding the earthquake occurrence. On the other hand, recent laboratory experiments successfully monitored the history of the strength by simultaneously measuring P-wave transmissivity  $|T|$  across the frictional interface using a 1MHz transducer. This suggests a possibility of earthquake forecast by monitoring the strength of a natural fault by acoustic methods.

The present paper explores the feasibility of such monitoring in the field on the basis of the physics of RSF combined with the linear slip model (LSM) employed in the classical acoustic methodology for monitoring an imperfectly welded interface. The characteristic frequency  $f_c$ , around which  $|T|$  (or reflectivity  $|R|$ ) has a good sensitivity to the interface strength, is shown to be proportional to the strength and inversely proportional to the representative scale of real contacts. For natural faults  $f_c$  is estimated to be 1 to 100Hz, which is practicable in the field. The changes of  $|T|$  and  $|R|$  depend on the ratio of the strength drop to the absolute strength level, the latter of which is not constrained by RSF simulations. Expected changes in wave amplitude in the preslip period would be several percent for strong faults and several tens percent for weak faults, which may be detectable by acoustic methods such as seismic reflection surveys.

Keywords: fault strength, earthquake cycle, rate- and state-dependent friction, precursor, linear slip model, acoustic monitoring

## Semi-quantitative analysis of change in stress state in Chelung-pu Fault, Taiwan

HASHIMOTO, Yoshitaka<sup>1\*</sup> ; TOBE, Kota<sup>1</sup> ; YEH, En-chao<sup>2</sup>

<sup>1</sup>Kochi University, <sup>2</sup>National Taiwan Normal University

Semi-quantitative stress state before and after earthquake in Chelung-pu fault, Taiwan

Stress change caused by earthquake is important to understand size and nature of an earthquake. Detailed waveforms of the 1999 Chi-Chi earthquake were taken along the Chelung-pu fault. In the aftermath of the earthquake, Taiwan Chelung-pu Fault Drilling Project (TCDP) was conducted to take core with the seismogenic fault. In this study, we estimated paleo-stress condition semi-quantitatively using micro-fault inversion method and stress polygon. Then we discuss the relationship between spatial and temporal changes of stress with seismic cycles.

We used Multiple inversion method (MIM) (Yamaji, 2000) and k-means clustering (Otsubo et al., 2006) to estimate paleo-stress. As a result, we obtained four solutions of stress state (c1-c4) from TCDP core. To estimate the range of stress conditions we used stress polygons on the basis of the Anderson theory of faulting as used in Lin et al. (2007). We projected our paleo-stress orientations to the directions of SHmax, Shmin and SV. In addition to that, using stress ratio and a definition that SHmax is larger than Shmin, we can restrict the stress conditions for the paleo-stress in the stress polygons.

Two stress conditions (c1 and c3) were comparable with that from Lin et al. (2007) as a present state and post-seismic condition in normal stress regime. The range of stress condition for c2 is obviously higher than others, and the stress condition is in reverse fault regime. The differences of stress condition possibly indicate the change in stress magnitude in the seismic cycle. Stress drops were estimated as -7.94~2.60MPa for c1 and c2, and 2.71~13.68MPa for c2 and c3. The calculated stress drop is comparable with estimated average stress drop from slip distribution in Chi-Chi earthquake (Ma et al. 2000).

Keywords: stress, micro-fault inversion, stress drop, Chelung-pu fault

## Fluid transport property and diagenetic microstructure of chert in the Mino Belt

YAMAGUCHI, Asuka<sup>1\*</sup> ; TANIKAWA, Wataru<sup>2</sup> ; KAMEDA, Jun<sup>3</sup> ; SHIMIZU, Mayuko<sup>4</sup> ; HAMADA, Yohei<sup>5</sup> ; KIMURA, Gaku<sup>4</sup>

<sup>1</sup>Atmosphere and Ocean Research Institute, the University of Tokyo, <sup>2</sup>JAMSTEC/Kochi, <sup>3</sup>Graduate School of Science, Hokkaido University, <sup>4</sup>Department of Earth and Planetary Science, the University of Tokyo, <sup>5</sup>JAMSTEC/IFREE

Pore fluid pressure along plate boundary megathrust is controlled by both fluid supply and fluid transport property, and it affects on faulting and earthquake mechanics. In the case of subduction zones where relatively old (older than 50 m.y. in age) oceanic plate subducts, oceanic crust is covered with thick pelagic siliceous sediments composed of diatomic and/or radiolarian oozes. In the Japan Trench, Kimura et al. (2012) pointed out that the volume of dehydrated fluid during silica diagenesis from opal-A to quartz through opal-CT is significant compared to that from clay mineral (smectite-illite) transition. However, fluid transport property of siliceous sediments has not been well-understood yet. In this study we conducted both permeability measurement and microstructural/microchemical observation of bedded chert from Inuyama-section in the Mino belt, Jurassic accretionary complex in Japan, as an on-land analog of subduction zone where old oceanic plate subducts.

Initial porosity of chert samples at atmospheric pressure is 0.4 to 2.2 %. Permeability was measured at room temperature under isostatic confining pressures of 5 to 120 MPa, by the steady state flow method with nitrogen gas as a pore fluid. Water permeability was then obtained by using Klinkenberg equation. At effective pressure of 5 MPa converted water permeability is  $10^{-17}$  to  $10^{-19}$  m<sup>2</sup>, decreases with increasing effective pressure down to the ranges of  $10^{-20}$  to  $10^{-21}$  m<sup>2</sup>.

Optical and electron probe microanalyzer (EPMA) analyses show that chert is composed of radiolarian fossils filled with quartz and chalcedony, and red-colored matrix. Red matrix shows ~95 wt.% of SiO<sub>2</sub>, whereas >99 wt.% of SiO<sub>2</sub> are commonly observed from inside part of the radiolarian fossils. Such high concentration of SiO<sub>2</sub> within radiolarian fossils indicates that dissolved silica was precipitated into cavities maintained by radiolarian tests. This process would be related with silica diagenesis, occurring as dissolution-precipitation processes.

Silica mineral precipitation onto pore spaces would contribute to construct characteristic low porosity and permeability of chert. Our result shows that silica diagenesis works as not only a fluid source but also as a process for porosity/permeability reduction in convergent margins characterized by old subducting oceanic plate.

Keywords: subduction zone, diagenesis, permeability, chert

## Mechanical properties of the shallow Nankai Trough accretionary sediments

KANAGAWA, Kyuichi<sup>1\*</sup>; TAKAHASHI, Miki<sup>2</sup>; AZUMA, Shuhei<sup>1</sup>; ITO, Hidenori<sup>1</sup>; INOUE, Atsuyuki<sup>1</sup>

<sup>1</sup>Graduate School of Science, Chiba University, <sup>2</sup>Active Fault and Earthquake Research Center, Geological Survey of Japan

We report the results of triaxial compression and friction experiments of clayey mudstone, silty mudstone, sandstone and tuff samples, which are cored from the shallow (1000-1500 mbsf) Nankai Trough accretionary prism at IODP Sites C0002 and C0009, at room temperature, and confining pressures and pore water pressures close to their in situ conditions.

Triaxial compression experiments at these conditions and an axial displacement rate of 10  $\mu\text{m/s}$  reveal that the failure strength is  $\approx 300$  MPa for a sandstone sample,  $\approx 48$  MPa for a tuff sample,  $\approx 20$  MPa for a silty mudstone sample, and  $\approx 14$  MPa for a clayey mudstone sample. The sandstone, tuff and silty mudstone samples failed relatively rapidly within 20 s, while the clayey mudstone sample failed slowly for  $\approx 40$  s. Another silty mudstone sample did not fail, and deformed ductilely at a strength of  $\approx 15$  MPa. The sandstone sample is strongly lithified by being cemented by calcite, which makes this sample's failure strength very high. The ductilely deformed silty mudstone sample seems not lithified enough to fail. A probable increase in pore pressure during compression of the clayey mudstone sample due to its low porosity ( $\approx 11\%$ ) and permeability ( $\approx 10^{-19}$   $\text{m}^2$ ) in addition to its intrinsic weakness due to the abundance of clay minerals ( $\approx 42$  wt%) likely makes this sample weak and promotes its slow failure. Such failure in clayey mudstone is a possible source for slow slip events observed in the shallow Nankai Trough accretionary prism.

Friction experiments at these conditions and axial displacement rates changed stepwise among 0.1, 1 and 10  $\mu\text{m/s}$  reveal that frictional properties of these samples change systematically according to the content of clay minerals. The content of clay minerals is  $\approx 6$  wt% in the sandstone sample,  $\approx 17$  wt% in the tuff sample, 29-34 wt% in the silty mudstone samples, and  $\approx 42$  wt% in the clayey mudstone sample. Steady-state friction coefficient at the axial displacement rate of 1  $\mu\text{m/s}$  decreases with increasing content of clay minerals, from 0.87 of the sandstone sample, through 0.71 of the tuff sample and 0.53-0.56 of the silty mudstone samples, to 0.25 of the clayey mudstone sample. Slip-dependent frictional behavior also changes from slip hardening to slip weakening with increasing content of clay minerals. Although all samples exhibit velocity-strengthening behavior upon stepwise changes in sliding velocity, the ratio of ( $a - b$ ) value to the velocity dependence of steady-state friction decreases with increasing content of clay minerals, which implies that the friction component decreases while the flow component increases accordingly. Thus, faulting in the shallow Nankai Trough accretionary prism is likely controlled by the content of clay minerals in sediments as well as in fault zones.

Keywords: Nankai Trough, accretionary sediments, failure properties, frictional properties

## Velocity weakening behavior observed for friction of the shallow subduction zone fault material

TSUTSUMI, Akito<sup>1\*</sup> ; NAMIKI, Yuka<sup>1</sup> ; NAKANO, Ryuji<sup>1</sup> ; KAWAI, Tomoaki<sup>1</sup>

<sup>1</sup>Division of Earth and Planetary Sciences, Graduate School of Science, Kyoto University

Recent observations of slow earthquakes along faults within shallow part of subduction zones, for example the very low frequency earthquakes at the Nankai Trough [Ito and Obara, 2006; Sugioka et al., 2012], has demonstrated that faulting there is slow yet seismic; suggesting that frictional velocity dependence along the fault at the shallow portion must be negative. However, previous experimental results have repeatedly shown that velocity dependence of the expected fault zone material is generally estimated to be positive. Here, we present our recent experimental results showing that velocity dependence of the friction of the shallow subduction zone faults are not necessarily be positive.

We have performed a series of rotary-shear large displacement (>150 mm) friction experiments on the following shallow fault simulating material: clayey fault material from the shallow megasplay fault zone within the Nankai accretionary prism, input pelagic siliceous to calcareous sediments to the Costa Rica subduction zone, and simulated artificial gouge of montmorillonite/quartz mixtures (20-40 wt% of montmorillonite). Experimental results reveal that these material do exhibit velocity weakening behavior at a range of velocities from 0.003-0.3 mm/s. Velocity weakening of these material is mostly characterized by a small degree of the friction velocity dependence (the absolute value of (a-b) is typically <0.005).

The SSEs are often described as conditionally stable sliding of faults [e.g., Shelly et al., 2006]. High pore fluid pressure could alter a velocity-weakening fault with a small value of (a-b) to conditionally stable regions by reducing the effective normal stress [Scholz, 1998]. The presented velocity weakening property with a small value of (a-b) could be responsible for generating shallow slow seismic slip events in subduction zones. Textural observation reveals the importance of studying effects of both the clay content and shear-induced deformation textures on the frictional velocity dependence.

Keywords: Nankai Trough, subduction zone, frictional velocity dependence, slow earthquakes

## Frictional properties of simulated faults containing amorphous silica/calcite mixtures

NAMIKI, Yuka<sup>1\*</sup> ; TSUTSUMI, Akito<sup>1</sup>

<sup>1</sup>Graduate School of Science, Kyoto University

Various seismic behaviors such as large earthquakes, episodic slow slip events, or silent earthquakes are observed in subduction zones. Knowledge of the frictional properties of input material to subduction zones would help to understand the complicated seismic behaviors. On the Cocos plate, which subducts beneath the Caribbean Plate at Middle America Trench offshore Costa Rica, input sediments containing clay, silty clay sediments and silicic to calcareous ooze were collected during the IODP expedition 334. We have been studying the frictional properties of the collected input material to the Costa Rica subduction zone. In order to better understand frictional processes of a fault in silicic to calcareous ooze, we have performed a series of friction experiments on a simulated fault gouge containing mixtures of amorphous silica and calcite.

Frictional experiments were performed at a constant slip velocity of  $v = 0.28$  mm/s, and also under a velocity-stepping condition. The silicic to calcareous ooze sample showed the following characteristic behavior. The friction coefficients at 0.28 mm/s showed initial peaks at 0.4-0.6 and subsequent little decrease, followed by a gradual increase to attain a constant friction value at 0.6-0.8. The analogue gouge containing 40-80 wt% of calcite reproduced such frictional behavior well. The experimental samples of the input ooze material required only about 40 mm of displacement to attain constant steady-state friction level. However, the calcite/amorphous silica mixtures needed larger displacement to attain steady-state friction. Furthermore, the calcite/amorphous silica mixtures could not reproduce friction velocity dependence observed for the collected ooze samples. The result suggests the importance of studying effects of grain size distribution and the grain morphologies on the frictional properties of the silicic to calcareous ooze material.

Keywords: subduction zone, frictional experiment, CRISP

## Effect of temperature on frictional behavior of smectite and illite: Implication for the updip limit for seismogenic zone

KUBO, Tatsuro<sup>1\*</sup> ; KATAYAMA, Ikuo<sup>1</sup>

<sup>1</sup>Department of Earth and Planetary Systems Science, Hiroshima University

**Introduction:** Along plate boundary subduction thrusts, the transformation of smectite to illite within fault gouge at temperatures of ~150°C is one of the key mineralogical changes thought to control the updip limit of seismicity. Saffer and Marone (2003) reported illite shale exhibited only velocity-strengthening behavior, opposite to the widely expected, potentially unstable velocity-weakening behavior of illite. They concluded transformation of smectite to illite is not responsible for the seismic-aseismic transition in the updip limit of subduction zones. However, their experiments were limited at room temperature although the updip limit of seismogenic zone is thermally controlled that occurs at temperature around 150°C. Therefore, in this study, we determined the effect of temperature of frictional properties of smectite and illite and discuss whether the smectite-illite transition accounts for the updip limit of seismogenic zone along subduction thrust.

**Experimental methods:** Frictional experiments were performed using a biaxial frictional testing machine at Hiroshima University. The powder materials of clays were placed on the simulated fault surface and two side blocks were placed together to produce a double-direct shear configuration. Normal stress was applied via a hydraulic ram on the side block with 15, 40, 60 MPa, and then, shear stress was applied by advancing the central block downward at a constant velocity. The sample assembly was heated by an external furnace up to 200°C that is monitored by thermocouples located close to the central block. Mechanical data were recorded continuously with a sampling rate of 10 Hz and the frictional coefficient was calculated from the shear force divided by the normal force assuming zero cohesion.

In the frictional experiments, we determined the velocity dependence of sliding friction, which is a key parameter for stable or unstable sliding (e.g., Dieterich, 1979). After steady-state sliding, the loading velocity of 3  $\mu\text{m/s}$  was abruptly changed to 30  $\mu\text{m/s}$  in each frictional experiments to determine the velocity dependence of these clay minerals. We calculated the velocity dependence of sliding friction as follow:

$$(a-b) = d\mu(d \ln V)$$

where a,b is the frictional parameter and V is sliding velocity. The velocity dependence is important to show seismic slip, in which negative values of (a-b) reflect velocity-weakening behavior, whereas positive values of (a-b) reflect velocity-strengthening behavior and thence stable (aseismic) sliding.

**Results and Discussion:** In comparison of steady-state frictional strength of clay minerals, the value of frictional strength of smectite is nearly half as large as that of illite. The effect of temperature on the frictional strength is rather weak, and the steady state friction is slightly increased at high temperatures. Our results suggest that the shear stress required to initiate sliding is much lower for smectite than illite, and smectite could not accumulate much strain energy.

The velocity dependence at room temperature shows always positive at normal stress higher than 40 MPa, which is similar to the results of Saffer and Marone (2003). However, at temperature of 200°C, illite shows negative values of (a-b), suggesting that illite exhibits unstable velocity-weakening behavior. This result explains smectite is potentially aseismic for stable sliding at the subduction thrust, whereas illite becomes seismic due to a negative velocity dependence and unstable sliding at high temperatures. These experimental results indicate that the smectite-illite transition potentially account for the updip limit of seismogenic zone along subduction thrust, which is opposite to the previous results at room temperature.

**Keywords:** updip limit, smectite-illite transformation, effect of temperature, velocity dependence

## Frictional properties of basalt-derived fault rocks and implications for subduction earthquakes

SAITO, Tsubasa<sup>1\*</sup> ; UJIIE, Kohtaro<sup>1</sup> ; TSUTSUMI, Akito<sup>2</sup>

<sup>1</sup>Life and Env. Sci., Univ., Tsukuba, <sup>2</sup>Sci., Kyoto Univ.

Recent seismic reflection surveys in subduction zones such as Nankai Trough suggest that subduction earthquakes mostly occurred along the upper part of oceanic crust composed of basaltic rocks (e.g., Bangs et al., 2009). Hence, frictional properties of basalt appear to be keys for understanding earthquake nucleation and rupture propagation during subduction earthquakes, yet they remain poorly understood. In the Upper Shimanto accretionary complex of eastern Shikoku, basalt and tectonic melange are repeated by thrusts, representing duplex structure associated with underplating (Ikesawa et al., 2005). Underplating-related thrusts develop in basalt and consist of basalt-derived foliated cataclasite and ultracataclasite. Fluidization of comminuted material and mineralogical signatures of frictional heating were reported from a few centimeters-thick ultracataclasite (Ujiie et al., 2007; 2008; Kameda et al., 2011). We examined the frictional velocity dependence at slip rates of 0.0028-0.28 mm/s and high-velocity (1.3 m/s) frictional properties of disaggregated pillow basalt and basalt-derived foliated cataclasite and ultracataclasite. The samples from pillow basalt show velocity-weakening behavior, while those from foliated cataclasite and ultracataclasite exhibit velocity-strengthening behavior. All samples show slip weakening behavior during high-velocity friction experiments, with the samples from ultracataclasite marked by smaller stress drop, slip weakening distance, and fracture energy. The compositions of materials and preliminary microstructural observations suggest that velocity-weakening samples show lower clay content (21 wt.%) and grain-size reduction, while velocity-strengthening samples exhibit relatively high clay content (29-50 wt.%) and clay foliations. Our results suggest that earthquake nucleation likely occurs in subducting basalt, but slip tends to be stable when clays and clay fabrics are formed by hydrothermal alteration and shear deformation, respectively. The results of high-velocity friction tests suggest that earthquake rupture propagates easily through ultracataclasite rather than foliated cataclasite and pillow basalt, which is consistent with the fact that the geological evidence of earthquake faulting was found from the ultracataclasite.

Keywords: subduction earthquakes, basalt, frictional velocity dependence, high velocity friction

## Amorphization of clay minerals by wet and dry grinding

FUJIMOTO, Koichiro<sup>1\*</sup>; FUKUCHI, Rina<sup>2</sup>

<sup>1</sup>Tokyo Gakugei University, <sup>2</sup>Tokyo University

Nanoparticles in fault zones are recently paid much attention since they give significant influences on the frictional properties (Ma et al., 2006). Nanoparticles are considered to be formed not only by mechanical grinding but also by mechanochemical processes. Amorphous nanoparticles were found in Iida-Matsukawa fault, Central Japan (Ozawa and Takizawa, 2007). It is well known that clay minerals are easily transformed into amorphous phase by mechanochemical processes. We conducted pulverization experiments of some clay minerals under both dry and wet conditions to clarify the characteristics of the pulverized materials and the mechanism of amorphization.

We used kaolinite saponite and sericite as starting materials. Pulverization experiments were conducted using planetary ball mill and characterization of run products were conducted by XRD, FT-IR, TG-DTA and FE-SEM. Three minerals were completely transformed into amorphous materials by dry grinding. XRD peaks were weakened but still remain after one day wet drying as for kaolinite and sericite. On the contrary, as for saponite, XRD peaks do not show remarkable change under wet condition. Probably amorphization rate is reduced because impact energy in the ball mill is decreased in the presence of water. Presence of interlayer water affects on the behavior of saponite.

Keywords: clay minerals, kaolinite, sericite, saponite, amorphous

## Fluid inclusion as fossil fluid in seismogenic zone, trap mechanism and interpretations for fault science

SAKAGUCHI, Arito<sup>1\*</sup> ; YANAGISAWA, Kazumichi<sup>2</sup>

<sup>1</sup>Yamaguchi Univ./JAMSTEC, <sup>2</sup>Kochi Univ.

A fluid inclusion, fluid-fill capsule within rigid crystal, preserves density and chemical composition of fluid in deep crust. This records pressure, temperature and other information of the fluid when the fluid trapped. Pore fluid pressure drop due to rapid fluid ejection along the fault was discussed in Kodiak accretionary complex (Vrolijk et al., 1988). CH<sub>4</sub>-H<sub>2</sub>O fluid inclusions are reported at pseudotachylyte bearing Nobeoka Thrust, Shimanto accretionary complex (Kondo et al., 2005). Thermal stretching of fluid inclusions due to seismic frictional heating were found at seismogenic Mugi Melange, Shimanto accretionary complex (Ujii et al., 2008). Though fluid inclusion tells us fluid condition in deep crust, trapping mechanism within crystal is still uncertain. The fluid inclusion is one of crystallographic defect, but general size from sub-micron meter to several mm is much greater than crystal lattice. A crystal tend to growth without large defect, and it seems irregular process to be formed a fluid inclusion. The trap mechanism is significant to interpret the fluid inclusion data.

We succeeded to make artificial fluid inclusion in calcite during hydrothermal experiment. A calcite crystals are nucleated and grown with temperature decrease in autoclave. Fluid inclusions were never formed in simple cooling procedure, but many large fluid inclusions were found at the overgrowth zone formed by re-heating process. Surface condition of artificial calcite of re-heating and overgrowth process were observed using SEM. Etched pattern covers the surface of re-heated calcite crystal. Some depressions are wide shallow and others are small deep. Many growth steps were found on surface of over-growth calcite. The calcite surface may have been advanced with lateral motion of growth steps. This growth step covers most of the etched depressions except small deep one. These small deep depressions are surrounded by new grown surface and became increasingly deep. Some depressions may make large pore within overgrowth zone in this process.

This observation shows that the fluid inclusion were made during overgrowth after surface etching, and this requires temporary solubility change in crystal growth process. The fluid inclusions may record pore-fluid condition after the event of pressure, temperature and/or chemical change in deep crust.

Keywords: Fluid inclusion, trap mechanism, artificial calcite

## New fluid flow mechanism at seismogenic depth in subduction zone

TAKE, Kotaro<sup>1\*</sup>

<sup>1</sup>Dept. of Geosphere. Yamaguchi Univ.

Since pore fluid pressure may concern with seismogenesis, large amount of articles are published for fluid flow research, and -previous researches have been focused only crack flow in deep crust. In general, a pore between sedimentary grain decreases with depth, and fluid flows only within crack in deep crust. This study shows new fluid flow mechanism that doesn't depend on crack in the rocks. This produces new perspective of fluid flow of seismogenic depth in subduction zone.

The Shimanto accretionary complex at SW-Japan, formed at seismogenic depth suffers pressure solution deformation and generally includes brittle failure of web structure and crack-filled veins. The carbonate matrix is lacked in the sediments due to deposition below CCD.

Some sandstones in the late Cretaceous Nonokawa Formation, includes spotted carbonate deposit. This carbonate deposit occurs limited area less than several meters square within sandy layer without crack-filled vein. Microscopic observation shows following features as below.

The spotted carbonate minerals overprint with embayment structure in pressure-solution deformed sandy grains, and these are cut by web structure and crack-filled veins. The fluid may have dissolved the sandy grains, and carbonate minerals were deposited at latest stage of lithification process between pressure solution deformation and brittle failure. These occurrences suggest that fluid can flow with dissolution of rock-forming grains in rigid crust without crack.

Keywords: fluid flow, accretionary complex

## Generation of high-temperature fluid and its spatial distribution in an ancient megasplay fault

MASUMOTO, Hirokazu<sup>1\*</sup> ; HIRONO, Tetsuro<sup>1</sup> ; ISHIKAWA, Tsuyoshi<sup>2</sup> ; TANIKAWA, Wataru<sup>2</sup> ; MUKOYOSHI, Hideki<sup>3</sup>

<sup>1</sup>Department of Earth and Space Science, Graduate School of Science, Osaka University, <sup>2</sup>Kochi Institute for Core Sample Research, Japan Agency for Marine-Earth Science and Technology, <sup>3</sup>Faculty of Education and Integrated Arts and Sciences, Waseda University

An ancient megasplay fault outcrop is identified within Kure region of the Shimanto accretionary complex and has been formed at 2.5 – 5.5 km depth. Recent works show pseudotachylyte produced by frictional melt, fluid-rock interactions at high temperatures (>350 °C) and enrichment of incompatible element concentrations on the fault. However, spatial distribution of pseudotachylyte and high-temperature fluid is not investigated. These informations are important to understand an earthquake is able to produce extensively high-temperature fluid and thermal pressurization. Accordingly, we performed deformation structures analysis and obtained 46 rock samples from the outcrop and analyzed these samples by vitrinite reflectance measurement, powder X-ray diffraction-RockJock mineral composition analyses and trace elements compositions measurement. Therefore, analyses of black gouge samples from the slip zone indicate fluid-rock interactions at high temperatures, whereas footwall sandstone samples that are close to fault gouge indicate enrichment of quartz and decrease of rare-earth element concentrations. These contrasts may be regarded as mobilization of elements derived from seepage of yielded high temperatures fluid within the slip zone.

Keywords: Nankai trough, megasplay fault, Shimanto accretionary complex, fault rocks, fluid-rock interactions, X-ray diffraction

## Multiple damage zone system of an exhumed subduction zone megasplay fault

HAMAHASHI, Mari<sup>1\*</sup>; KAWASAKI, Ryoji<sup>1</sup>; FUKUCHI, Rina<sup>1</sup>; SAITO, Saneatsu<sup>2</sup>; HASHIMOTO, Yoshitaka<sup>3</sup>; HAMADA, Yohei<sup>2</sup>; KITAMURA, Yujin<sup>4</sup>; YAMAGUCHI, Asuka<sup>1</sup>; KIMURA, Gaku<sup>1</sup>

<sup>1</sup>The University of Tokyo, <sup>2</sup>Japan Agency for Marine-Earth Science and Technology, <sup>3</sup>Kochi University, <sup>4</sup>Kagoshima University

More than 90% of the major earthquakes and tsunamis are known to occur at plate convergent margins, along plate boundary faults and megasplay faults. Investigating the mechanical properties and deformation patterns of these megathrusts are important to understand the generation of earthquakes and the dynamics on the subduction plate interface. Large displacement faults contribute to the reduction of steady-state strength at mid-crustal levels, and cause the frictional-viscous deformation at depth. As the candidate for such weak faults, foliated, phyllosilicate-rich fault rocks have been prevalently recognized in many tectonic settings. However, whether foliated fault rocks behave as weak structures in the longer terms and their roles in the strain localization and fault evolution, are poorly understood.

Exhumed fault zones are helpful to constrain fault strength and deformation process of foliated cataclasites formed at upper-midcrustal depths over geological time. One of the well-studied exhumed major fault zones in subduction settings is the Nobeoka Thrust, a fossilized megasplay fault in Kyushu Shimanto Belt, southwest Japan, which exposes foliated fault rocks that were formed under the temperature range of ~180-350 °C (Kondo et al., 2005). During the Nobeoka Thrust Drilling Project in 2011, core samples were retrieved containing both consolidated fault rocks and less consolidated, brecciated fault rocks, preserved from surface weathering and less likely to be drilling-induced. The core samples are expected to provide a different aspect on fault rock strength from previous geological studies on exposed, consolidated outcrops. In the current study, given the unique opportunity to determine the coexistence of cohesive and less cohesive fault rocks in a single fault system, we conduct macroscopic and microscopic structural observation and physical property measurements on the core samples, synthesizing with geophysical logs obtained from the drilling of the Nobeoka Thrust to characterize the damage zone architecture of the fault rocks formed in the frictional-viscous regime along the megasplay fault.

The hanging wall consists of the shale-dominant intervals of dense development of phyllitic cleavages, the sandstone-dominant intervals of disturbed foliations, and the damage zone above the fault core characterized by cataclastically broken phyllite with thick abundant sandstone blocks. The observed density of brittle fractures, breccias, and mineral veins is increased at the sandstone-dominant intervals and near the fault core, whereas brecciated and less brittle/ductile structures are abundant within the shale dominant intervals. The brittle deformation near the fault core may have caused the wearing away of the shale-rich zones by abrasion, and as a result, the sandstone-rich zones that have relatively larger strength, remained and deformed cataclastically near the fault core. On the other hand, the footwall in the drilled range consists of six sets of fracture zones, all of which include a "brecciated zone" intensively broken in the center, sandwiched by a "surrounding damage zone" with abundant cohesive faults, mineral veins, and sandstone blocks. The surrounding damage zone is characterized by the increase in fault and fractures with distance from the fault core, and interestingly associate with the increase in resistivity, P-wave velocity, and density and decrease in porosity. The deformation in the surrounding damage zone is inferred to occur in a strain-hardening manner, strengthening with distance from the fault core. Shear localization may initiate more easily in the sandstone-rich area later forming the surrounding damage zone, and eventually develop an intensively deformed fault core in the center. These insights would enable to reinterpret the deformation processes and weakening mechanisms that occur in foliated fault rocks along the megathrust in subduction zones.

Keywords: subduction zone, megasplay fault, physical property of rock, damage zone, structural observation, rock deformation

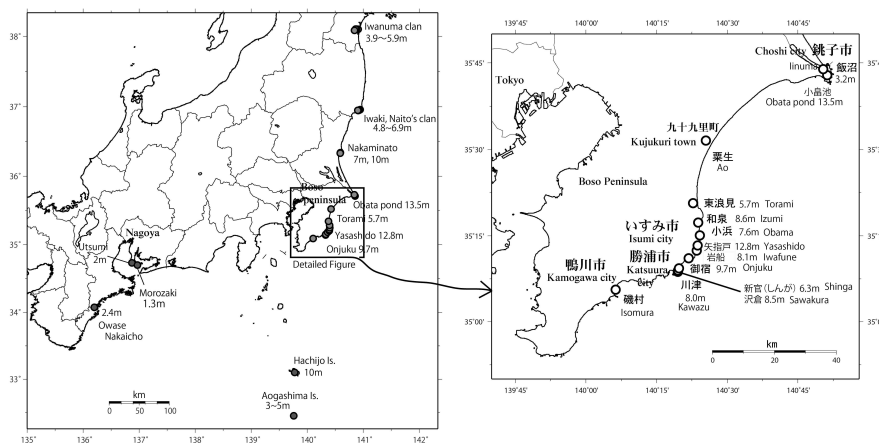
## Damaged coasts of the tsunami of the Enpo Boso-Oki Earthquake of November 7, 1677

YANUMA, Takashi<sup>1\*</sup>; TSUJI, Yoshinobu<sup>2</sup>; HIRAHATA, Takenori<sup>1</sup>; MABUCHI, Yukio<sup>3</sup>; OOIE, Takayuki<sup>3</sup>; OKADA, Kiyohiro<sup>3</sup>; IMAI, Kentaro<sup>4</sup>; IWABUCHI, Yoko<sup>5</sup>; IMAMURA, Fumihiko<sup>4</sup>

<sup>1</sup>Pasco., <sup>2</sup>Fukada Geolog. Inst., <sup>3</sup>Pacific Consultant, <sup>4</sup>IRIDeS, Tohoku Univ., <sup>5</sup>JNES

The Enpo Boso-Oki earthquake of November 7th, 1677 occurred in the sea area of the south east offing of Boso peninsula, Kanto district, Central Japan. The shaking of the earthquake was weak, and no damage occurred due to the shaking. The shaking was felt only on the Boso Peninsula and at Edo (Tokyo). Though the shaking was small, but a huge tsunami hit the coasts of Boso peninsula, and north to Iwanuma city about 20 kilometers south of Sendai. Detailed house and human damage was recorded in "Gyokuro-So", one of the fundamental chronologies of the Tokugawa Government. In Katsuura city on the coast of Boso Peninsula, at Kawazu, Sawakura, and at Shinga villages 47 houses were destroyed, and 7 people were killed in total. Inundation heights of the tsunami at those three villages are estimated at 8.0, 8.5 and 6.3 meters, respectively. At Onjuku fishery village, 30 houses were destroyed and 57 people were killed, and tsunami height was estimated at 9.7 meters. At Yasahido village, where total number of houses was about 30, 25 houses were swept away and 13 people were killed, and tsunami height was 12.8 meters. In Choshi city, sea water rushed into Obata Ike pond. We measure the height of the saddle point separating the pond from the open sea, and we found out that tsunami height was 13.5 meters there. The tsunami height at Iwaki City, Fukushima Prefecture was 4.8 to 6.9 meters. On Hachijo Island, about 300 kilometers south of Tokyo, the residential area of Yato behind Yaene port was flooded by sea water and the inundation height is estimated at about 10 meters. The tsunami wave affected west to Ise Bay, Nagoya City. At Utsumi port in Minamichita town about 25 ships were wrecked due to the tsunami. Tsunami also recorded at Owase city on the south east coast of Kii peninsula. The authors of the present study wish to express their thanks to JNES for its financial support in promoting our research.

Keywords: historical earthquake, historical tsunami, the 1677 Boso-Oki earthquake, metropolitan area, Ise bay, Kii peninsula



---

SSS30-36

Room:Main Hall

Time:April 29 17:30-17:45

## Crustal movement associated with the 1703 Genroku earthquake

NAKANISHI, Ichiro<sup>1\*</sup>

<sup>1</sup>Dept. Geophysics Kyoto University

We analyzed historical documents on the 1703 Genroku earthquake to estimate the crustal movement associated with the earthquake in the Tokyo Bay area, central Japan.

Keywords: 1703 Genroku earthquake, Tokyo Bay, crustal movement

## A Reproduction of 1707 Hoen Tsunami with long rupture duration, referring to 2011 East Japan Pacific Ocean Earthquake

MATSU'URA, Ritsuko S.<sup>1\*</sup> ; ANJU, Akira<sup>2</sup> ; SHOJI, Masahiro<sup>2</sup>

<sup>1</sup>ADEP, ERC, <sup>2</sup>Kozo Keikaku Engineering Inc.

Hoen earthquake in 1707 was the largest earthquake in the Edo period that gave the tsunami damage to a wide area along the Pacific Ocean, from the Izu Peninsula to the Southwest Japan. It was assumed that in Hoen earthquake, the source areas of Ansei Tokai and Nankai earthquakes ruptured subsequently within a very short time [e.g. Usami (2003)], or the source areas of the two earthquakes of Ansei were broken at a time [e.g. Ishibashi (2004)]. However, the recent detailed study of historical records revealed that the crustal deformation and the seismic intensity distribution tell that the western and eastern margins of the Hoen source region did not overlap with the two earthquakes in Ansei [e.g. Matsu'ura (2012)]. Hoen earthquake was the exceptionally huge earthquake, which should be called "Western Japan Pacific Ocean Earthquake" in Edo period.

In order to explain very high tsunami of Hoen in the Western Japan, Aida (1981) set the doubled slip to the source area off the cape Ashizuri. Furumura et al. (2011) even expanded the source area further west towards Kyushu. However, their models cannot match the intensity distribution in Kyushu and arrival times of tsunami to villages along the east coast of Kyushu. We suspect that the commonly used tsunami simulation method does not work for a M9-class huge tsunami like Hoen. The theoretical calculation program of crustal deformation of a rectangular fault in a semi-infinite medium [e.g. Sato and Matsu'ura (1973)], which is widely used for the tsunami simulation, inevitably produces singular margins. When the source area was huge, the singularity should affect coastal areas. When the shallow part near the trench is included in the source area, using the same elastic constants as the deeper part should result in an unrealistic deformation solution for a tsunami simulation.

To avoid these limits to applications of the theory used, we put aside obtaining crustal deformation of the sea floor from a dislocation source model, and calculate tsunami from the model of sea floor upheaval and subsidence, which evolve in time. For a test, we first examine the case of the East Japan Pacific Ocean Earthquake of 2011. In order to avoid the detailed topography along coasts, we only used data from GPS buoys and pressure gauges located offshore. We used the ocean bottom upheaval and subsidence obtained by Saito et al. (2011) as the final crustal deformation of the 2011 huge quake. From the known epicenter, the deformation spreads gradually, with the intermittent of 20 seconds, which was observed by GPS as the stop of movement. Paying the attention for the physical plausibility, the movement starts when the rupture reaches, and continues moving until the rupture reaches the edge of a source area. Since the small smooth subsidence spreads over wide area around the major large upheaval area in Saito's model, most tsunami waveform features were reproduced only from the major upheaval area and the smaller upheaval zone protruding toward Japan Trench.

Then we did for Hoen tsunami. As the source of upheaval, we use the source region proposed by Matsu'ura et al. (2011). The topography in Hoen period, we stripped down claimed lands like the islands of Kansai International airport, and Tenpozan, which are apparently made after Hoen period. We also increased the depth of Sakai port, which had been buried by depositions carried by Yamato River since 1704. Examining tsunami for two cases of hypocenter, one at the east end of the source area near Zenisu, and the other at Kumano-nada, we realized that it is impossible to distinguish a hypocenter from limited tsunami information obtained for historical earthquakes. Even with our rough model, Hoen tsunami can go up to canals in Osaka and in the Lake Ryujin in Hazako, Oita. Our experience tells that we shall leverage the recent high power of ordinary computers for a tsunami simulation and molt to go beyond the 40-year-old theoretical crustal deformation.

Keywords: Hoen Earthquake in 1707, East Japan Pacific Ocean Earthquake in 2011, rectangular source fault model, huge tsunami, historical earthquakes

## Close examination of universality of matter off Miyagi that earthquakes advanced toward the east

MASE, Hirofumi<sup>1\*</sup>

<sup>1</sup>none

I explained how the surrounding of the plate boundary is always compressed(1). I reproduced the Off-Miyagi by the easy experiment(2). I understood earthquakes off Miyagi gradually climbed the slope of the plate boundary. The head within range where small earthquakes occur advanced toward the east gradually and went beyond the hypocenter of 3.11 in November, 2010.(3)

Therefore, the model of off Miyagi is the following. The earthquake of M7 class occurs in several decades by one degree. In every case the hypocenter of it moves east. And, the rear side of it slips to a deep point. The moderate quake guides the earthquake of M7. And, the front of crack is formed. Slip-all-together occurs if the front of crack arrives at a proper place. The feature of this model is to be able to give the answer to the following three large problems at a time. (a)A lot of people think that it is generated repeatedly within the specific range. (b)The cause of the swerve that causes large slip in every case is not discovered. (c)Finally happening is that a shallow part is destroyed at a time.

I want to think about (IC)Off Iwate-Chubu,(IH)Off Iwate-Hokubu,(AT)Off Aomori-Toho,(TK)Off Tokachi referring to (MY)Off Miyagi(Fig.1). The 1968 Tokachi-oki earthquake and the 1994 Sanriku-Haruka-Oki earthquake occurred in (IH)(AT). The coseismic slip distributions on the map of (4) is interesting. Though the rupture starting point and the main rupture zone can be understood of those relation of upper-lower part on slope, both are considerably away. This is a feature and it is necessary to be clarified. I interpret that a main rupture zone is the peak of slip nearest the trench. The 1968 earthquake has two large slip zone. The main rupture zone in the south is located in lower part of the main rupture zone of the 1994 earthquake on slope. I want to pay attention to that. I think the 1968 earthquake went with the earthquake that had to happen ahead of the 1994 earthquake. The earthquakes that occurred in the vicinity in the past(5) have the possibility that there were rupture zones in lower part of the 1968 earthquake or the earthquake that had to happen ahead of the 1994 earthquake on slope. Therefore, I think that (IH)(AT) walks on the road similar to (MY). And, that a shallow part can slips and timing is only waited for. We should think that the earthquake similarly climbs the slope also in region (TK).

Range (39N-40N,143E-144E) in region (IC) is the earthquake-prone zone of small and medium-sized earthquakes after 1923. It is seen that there are a lot of intraplate earthquakes(12). The lower plate always collapses due to the earthquakes and the material overflows up and accretionary wedge will be made. The upper plate relatively becomes long and swells because the lower plate shortens. And, the vicinity of the surface comes into an expansion field. And, steep cliffs are formed and fall because the upper plate surges to the trough. This will explain the geographical features of (IC) shown by (9) and the cause. The expansion field in the vicinity of the surface causes the occurrence of the lateral-fault type(10). The structure of the cliff where the sudden falls easily happen reacts sensitively to peripheral earthquakes. In addition, it has the possibility that is an efficient tsunami generator. This harmonizes with the result of (11).

Reference literature (Details are described to space in the drawing)

(1)MASE(2012) (2)MASE(2012) (3)MASE(2013) (4)NAGAI et al.(2000)/ERI U-Tokyo (5)Wikipedia (9)IZUMI et al.(2012)/JCG (10)NAKAJIMA(1974)/Hokkaido U. (11)ICHIHARA et al.(2013)/JAMSTEC (12)JMA/Monthly Report/June 2004

SSS30-P01

Room:Poster

Time:April 29 18:15-19:30

参考文献

(1) Hirofumi MASE(2012)/The power to form and maintain oceanic basin and island arc / JpGU2012/SCG67-P06 <http://www2.jpgu.org/meeting/2012/html5/session/S-CG67.html>  
 (2) Hirofumi MASE(2012)/Materialization and Experiment of Model of Miyagi Prefecture offing on the 2011 Tohoku-Oki Earthquake/SSU2012/P2-75 [http://globalist.jp/detail.php?GLOBAL\\_ID=2012022271822634851](http://globalist.jp/detail.php?GLOBAL_ID=2012022271822634851)  
 (3) Hirofumi MASE(2013)/Model that harmonizes with the rupture process of (Ide et al.2011) ~Relation between 3.11 and off-Miyagi-earthquakes~/JpGU2013/SSS28-P09 <http://www2.jpgu.org/meeting/2013/session/S-SS28.html>  
 (4) 永井理子・菊地正幸・山中佳子(2000)/三陸における再来大地震の震源過程の比較研究 / 東大震研/JpGU2000/Sa-005 Riko NAGAI, et al.(2000)/Comparative study on the asperities of large earthquakes in Sanriku region/ERI Univ. of Tokyo <http://www.eri.u-tokyo.ac.jp/YOTIKYO/11seikahoukoku/koukai/r11.5fig1.JPG>  
 (5) ウィキペディア (Wikipedia) [三陸沖北部地震/繰り返し発生する地震以外の地震] <http://ja.wikipedia.org/wiki/三陸沖北部地震>  
 (6) 佐竹健治・平田賢治・谷岡勇市郎・山本 滋(2004)/1952年・2003年十勝沖地震の津波波源の比較 - 1952年津波の再検討に基づいて - /産総研/SSU/2004年大会 <http://unt.aist.go.jp/act/fault-eq/seika/meeting/jishin2004/satake.html>  
 (7) 八木勇治(2004)/2003年9月26日十勝沖地震(Mjma 8.0)の破壊伝搬の様子EPS分/建築研 <http://isee.kenken.go.jp/staff/yagi/eq/Japan20030926/japan20030926-j.html>  
 (8) 山中・菊地(2003)/遠地実体波解析9月26日十勝沖地震(Mj8.0)/東大震研/EIC地震学ノートNo.139 [http://www.eri.u-tokyo.ac.jp/sanchu/Seismo\\_Note/030926.html](http://www.eri.u-tokyo.ac.jp/sanchu/Seismo_Note/030926.html)  
 (9) 泉純明・堀内大嗣・西澤あずさ・木戸ゆかり・中田高・後藤秀明・森辺清久・鈴木康弘(2012)/150mグリッドDEMから作成した日本海溝付近の3D海底地形/海峽海洋情報/研究報告第48号 Noriaki IZUMI, et al.(2012)/3D bathymetric image along the Japan Trench based on 150 meter grid DEM/JHOD/JCG <http://www.1.kaiho.mlit.go.jp/GJUTSUKOKUSAI/KENKYU/report/rhr48/rhr48-tr10.pdf>  
 (10) 中島徹(1974)/1968年十勝沖地震の前後における発震機構の変化/北大/地球物理学研究報告 Tohoru NAKAJIMA(1974)/Spacial and Sequential Distribution of Focal Mechanisms before and after the Tokachi-Oki Earthquake of May/Hokkaido U. <http://eprints.lib.hokudai.ac.jp/dspace/handle/2115/14044>  
 (11) 市原寛・浜野洋三・馬場聖三・笠谷貴史(2013)/東日本大地震で発生した津波が巨大化した原因となった場所を特定/海洋研究開発機構/2013年10月8日 Hiroshi ICHIHARA, et al.(2013)/Tsunami source of the 2011 Tohoku earthquake detected by an ocean-bottom magnetometer/JAMSTEC [http://www.jamstec.go.jp/about/press\\_release/20131008\\_2/](http://www.jamstec.go.jp/about/press_release/20131008_2/)  
 (12) 気象庁/地震・火山月報(防災編)/平成16年6月/6月12日岩手県沖の地震/震央分布図、断面図 JMA/Monthly Report on Earthquakes and Volcanoes in Japan/June 2004/6月12日岩手県沖の地震 <http://www.seisvol.kishou.go.jp/eq/gaiko/index.html#monthly> (13) 気象庁/地震・火山月報(防災編)/平成15年10月/特集1/図1-4、平成17年8月/特集1/図8-1,等 <http://www.seisvol.kishou.go.jp/eq/gaiko/index.html#monthly>

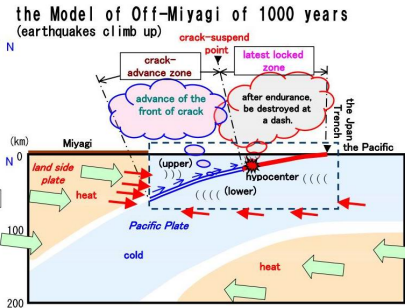
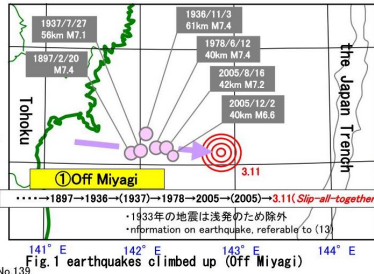


Fig.2 Model cross section intersecting squarely in the Trench and crossing over Miyagi

Explanatory notes		
	Power work by temperature structure of heat-cold-heat	
	Range corresponding to clay lump in the experiment	
	The distribution of power to work by $\alpha$ within $\beta$	

## Diversity of outer-rise earthquakes: As an example of the Off-Fukushima earthquake on 26 October 2013

YOMOGIDA, Kiyoshi<sup>1\*</sup>

<sup>1</sup>Graduate School of Sciences, Hokkaido University

Earthquakes occurring in the outer-rise of a subducting plate are associated with the ruptures of the subduing plate itself, that is, intra-plate earthquakes. Such outer-rise earthquakes have been considered to excite much larger high-frequency than earthquakes in the plate boundary of the subducting and overriding plates, because the outer-rise earthquakes should break a lithospheric part where no peculiar weak zones exist.

A M7.1 earthquake occurred off the coast of Fukushima on 26 October 2013, which was probably associated with the 2011 great Tohoku-oki earthquake. We analyzed broadband seismic waveform data of this event recorded by F-net and other seismic networks. Compared with other large outer-rise earthquakes, the high-frequency component ( $>1\text{Hz}$ ) of all the stations along the Pacific coast of eastern Japan is not abundant although slightly larger than plate-boundary earthquakes of low-angle thrust faulting. In contrast, there was the excitation of several impulsive wave packets of several seconds in period. Since only high-frequency waves are abundant at common stations for aftershocks of this outer-rise earthquake, the above features should not be originated by either propagation path or site effect.

Unlike the other outer-rise earthquakes, the rupture process of this earthquake was unique, relatively smooth with several strong patches on a rather homogeneous fault. The breakout of these patches should have been connected without any complex unbroken areas on the fault in the end, in order to explain the observed waveforms. Although we do not deny the break of a virgin (without any peculiar weak planes) lithosphere in this case, several distinguished large strong patches are likely to characterize the heterogeneity in the fault region of this outer-rise earthquake.

Among recent large outer-rise earthquakes along subduction zones near Japan, we have found another example similar to the Fukushima-oki earthquake: for the M7.0 outer-rise event on 14 March 2012 at the junction between Kuril Trench and Japan Trench, several impulsive waveforms with minor high-frequency waves. The state stress of this subducting Pacific plate should be very complex, which might lead to its non-standard rupture process. We shall need to investigate broadband frequency excitation patterns carefully for large outer-rise earthquakes.

In summary, there should be a wide variety of heterogeneities and/or stress state within a subducting lithosphere, which may be important to consider not only the source process of outer-rise earthquakes but also their tsunami generations.

Keywords: outer-rise earthquake, intra-plate earthquake, high frequency seismic waves, fault rupture, heterogeneity of oceanic lithosphere

## High resolution seismic profiling in the northern Japan Trench axis area

NAKAMURA, Yasuyuki<sup>1\*</sup>; KODAIRA, Shuichi<sup>1</sup>; MIURA, Seiichi<sup>1</sup>; YAMASHITA, Mikiya<sup>1</sup>; FUJIE, Gou<sup>1</sup>; SHIMOMURA, Norio<sup>1</sup>; IWAMARU, Hikaru<sup>1</sup>

<sup>1</sup>Japan Agency for Marine-Earth Science and Technology

Marine geological and geophysical surveys and analysis of their results have revealed that the ruptured area of the 2011 Tohoku earthquake extended up to the vicinity of the trench axis along the plate boundary fault. To investigate the geological structure, especially the faults and the deformation of the sediments, we have conducted reflection seismic surveys in the trench axis area of the Japan Trench off Miyagi and Iwate prefectures. Three seismic cruises have been carried out in 2011 and 2013 along 81 E-W (dip) lines and 17 N-S (strike) lines. We have used 320 or 380 inch<sup>3</sup> cluster air guns and a 1200 m long streamer cable to obtain high resolution seismic data. Surveyed area covers the trench axis area along the trench strike from seaward of the hypocenter of the Tohoku earthquake around 38 N at south, to ~40 N at north. Seismic profiles around 38 N show that the trench axis is located on a graben with sediments which have been deformed by reverse faulting. Similar deformation structure is observed around 40 N, but the trench axis is located on a horst not a graben there. The thickness of the incoming sediments on the Pacific plate typically ranges ~0.3 ? 0.5 s in two way time, however it is reduced down to <0.2 s around 39.5 N where the basement of the oceanic crust shows higher relief and trench inner wall is significantly steep. The thickness variation of the incoming sediments can be traced seaward and corresponded with along strike variation of the structure in the outer rise. These high resolutions seismic data served for the site selection of the JFAST drilling project by IODP and also contributes to the JTRACK proposal for future drilling in the Japan Trench following success of the JFAST.

## Seismic surveys in the ruptured area of the 2011 Tohoku earthquake

NAKAMURA, Yasuyuki<sup>1\*</sup> ; KODAIRA, Shuichi<sup>1</sup> ; KAIHO, Yuka<sup>1</sup> ; NO, Tetsuo<sup>1</sup> ; FUJIE, Gou<sup>1</sup> ; SATO, Takeshi<sup>1</sup> ; YAMAMOTO, Yojiro<sup>1</sup> ; KASAYA, Takafumi<sup>1</sup> ; OBANA, Koichiro<sup>1</sup> ; MIURA, Seiichi<sup>1</sup> ; TAKAHASHI, Narumi<sup>1</sup>

<sup>1</sup>Japan Agency for Marine-Earth Science and Technology

We have conducted seismic surveys in the ruptured area of the 2011 Tohoku earthquake off Miyagi prefecture in 2011 and 2013 using JAMSTEC's R/V Kairei. Three multi-channel reflection seismic (MCS) surveys were conducted in 2011 with R/V Kairei's 7800 inch<sup>3</sup> tuned air gun array and ~6 km long streamer cable. The MCS profiles along 14 E-W (dip) lines and two N-S (strike) lines were acquired during these surveys. Another seismic survey was carried out in 2013 around the JFAST drill site along one dip line and two strike lines. Time migrated sections demonstrated characteristic structure in the Japan Trench subduction zone; the Pacific plate deformed by normal faults (horst and graben structure), frontal prism with seismically transparent or chaotic feature, strong landward dipping reflections corresponding to the backstop interface, "deep sea terrace" in the upper landward trench slope covered with younger sediments mainly deformed with normal faults. Our survey area covers ~150 km in the trench strike direction around the epicenter area, which is rather small compared with the entire rupture zone (400 ? 500 km in the strike direction) of the Tohoku earthquake, however the structure is considerably variable from south to north. We have selected 6 dip lines, including the JFAST dip line, to apply pre-stack depth migration (PSDM). The PSDM sections provide higher quality profiles and interval velocity models in depth domain which are suitable for understanding the structural framework of the Japan Trench subduction zone. In 2013 survey, we also used four ocean bottom seismographs (OBSs) in addition to the MCS system. The P to S converted wave was clearly observed in the horizontal component seismograms, and the  $V_p/V_s$  in the sediment layer around the JFAST drill site was estimated at  $>4.5$ .

## Determination of Three Thermal Properties in Japan Trench Fast Drilling Project (JFAST)

LIN, Weiren<sup>1\*</sup> ; TADAI, Osamu<sup>2</sup> ; FULTON, Patrick<sup>3</sup> ; HARRIS, Robert<sup>4</sup> ; TANIKAWA, Wataru<sup>1</sup> ; KINOSHITA, Masataka<sup>1</sup>

<sup>1</sup>Kochi Institute for Core Sample Research, Japan Agency for Marine-Earth Science and Technology, <sup>2</sup>Marin Works Japan LTD, <sup>3</sup>University of California, Santa Cruz, USA, <sup>4</sup>Oregon State University, USA

The 2011 Mw 9.0 Tohoku-oki earthquake produced a maximum coseismic slip of >50 m near the Japan Trench. Japan Trench Fast Drilling Project (JFAST) as the Integrated Ocean Drilling Program (IODP) Expedition 343 and 343T drilled through the plate boundary fault ruptured during the Tohoku-oki earthquake at site C0019 approximately one year after the earthquake. The most highlighted objective is to detect residual positive temperature anomaly induced by the coseismic frictional heat. To interpret measured temperature anomaly and to calculate coseismic shear stress on the ruptured fault from the temperature anomaly, the full three thermal properties (thermal conductivity, thermal diffusivity and specific heat; only two thermal properties among the three are independent) are necessary. We measured the three thermal properties using four whole round core samples retrieved from borehole C0019E at 177, 697, 802 and 828 mbsf (meter below seafloor), respectively by a transient plane heat source method (also called Hot Disk method). Independently with Hot Disk method, thermal conductivity were also measured by a line heat source method for 45 half core samples using a TEKA half-space probe onboard the D/V Chikyu and by a divided bar technique using 38 crushed core samples (particle samples) in onshore laboratory. The thermal conductivities determined independently by the three methods were consistent each other. Also, the Hot Disk measurements revealed very little anisotropy in thermal conductivity and thermal diffusivity.

Acknowledgments: This research used core samples provided by IODP. We thank all Expedition 343 and 343T scientists and the drilling and logging operation staff on board the D/V Chikyu during expedition 343 and 343T.

Keywords: Thermal Property, JFAST, Thermal conductivity, Thermal diffusivity, Specific heat

## Modeling slow and seismic slips off Tohoku considering low to high speed friction behavior of the shallow plate boundary

SHIBAZAKI, Bunichiro<sup>1\*</sup> ; IKARI, Matt<sup>2</sup> ; NODA, Hiroyuki<sup>3</sup>

<sup>1</sup>International Institute of Seismology and Earthquake Engineering, Building Research Institute, <sup>2</sup>Marum, Center for Marine Environmental Sciences, <sup>3</sup>Japan Agency for Marine-Earth Science and Technology

Ikari et al. (2013) examined low to high speed frictional properties of fault zone material from the shallow plate boundary in the Tohoku region obtained by the IODP Expedition 343 (JFAST). They found velocity-weakening frictional behavior at slip velocities slower than  $10^{-6}$  m/s and velocity-strengthening at higher slip velocities. This frictional property is considered to be a mechanism that causes slow slip events and stress accumulation during the period between slow slip events. We investigate the effects of this frictional property on generation of slow slip events and megathrust events.

We use a rate- and state-dependent friction law with cut-off velocity to an evolution effect to represent this frictional behavior. Based on the experimental results (Ikari et al., 2013), we set the cut-off velocity at  $10^{-6}$  m/s. We also consider dynamic weakening due to thermal pressurization at high slip velocity. We perform three-dimensional quasi-dynamic modeling of slip processes. Numerical results show the occurrence of slow slip events at intervals of several ten years at the shallow plate boundary. During the period between slow slip events, stress accumulation proceeds. When an earthquake nucleates at the deeper region, coseismic slip propagates into this region, which results in larger slip compared to the case where a simple velocity-strengthening friction law is considered.

Ito et al. (2012) detected slow slip events in the Japan subduction zone before the 2011 Tohoku-Oki earthquake. Shallow very low frequency earthquakes off Tohoku were detected by Matsuzawa et al. (2012). In addition, along the shallow plate boundary off Tokachi, sequential activity of very low frequency earthquakes occurs at intervals of several years (Asano et al., 2008). These observations suggest that the transitional friction behavior investigated by Ikari et al. (2013) occurs along the shallow plate boundary off Tohoku.

Keywords: off Tohoku, shallow plate boundary, low to high speed friction behavior, slow slip, seismic slip

## Friction properties beneath the frontal wedge near the Japan Trench: deduction from topographic variation

KOGE, Hiroaki<sup>1\*</sup> ; KODAIRA, Shuichi<sup>2</sup> ; FUJIWARA, Toshiya<sup>2</sup> ; SASAKI, Tomoyuki<sup>3</sup> ; KAMEDA, Jun<sup>7</sup> ; KITAMURA, Yujin<sup>6</sup> ; HAMAHASHI, Mari<sup>1</sup> ; HAMADA, Yohei<sup>4</sup> ; YAMAGUCHI, Asuka<sup>5</sup> ; ASHI, Juichiro<sup>5</sup> ; KIMURA, Gaku<sup>1</sup>

<sup>1</sup>The University of Tokyo, <sup>2</sup>Institute for Research on Earth Evolution Japan Agency for Marine-Earth Science and Technology, <sup>3</sup>Ocean Engineering & Development Corporation, <sup>4</sup>Japan Agency for Marine-Earth Science and Technology, <sup>5</sup>Atomosphere and Ocean Research Institute, The University of Tokyo, <sup>6</sup>Kagoshima University, <sup>7</sup>Hokkaido University

The 2011 Tohoku-oki earthquake (Mw 9.0) produced a fault rupture, extending to the Japan Trench. Deformation and frictional properties beneath the forearc are the keys to elucidate this unusual event.

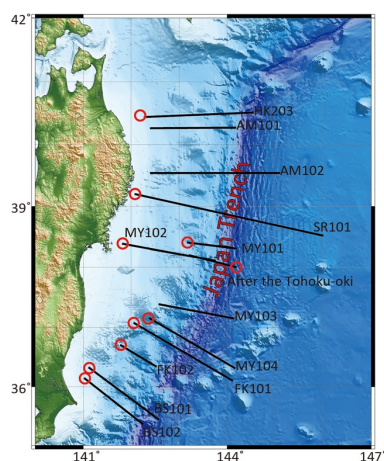
In this study, to obtain frictional properties ( $\mu_b'$ ; the coefficient of effective basal friction), we extracted shape-related parameters from the cross sections of the frontal wedge which are obtained from surveys across the trench that span sporadically along the axis of the Japan Trench. The following two methods were adopted for this study; Critical Taper Theory (CT) and Critical State Theory (CS). Both of the theories are based  $\mu_b'$ . From the Critical Taper Theory, Near latitude 36.1, the taper angles (slope angle + decollement dip angle) has been developed. A possible seamount subduction may differentiate this area. However, near the latitude 38.15 where the largest slip was reported with the 2011 earthquake, the taper angle has also been large without any seamounts. The calculated [or estimated] value of  $\mu_b'$  in this area is larger than that of the other area, suggesting that the larger strain energy was accumulated in comparison with the other wedges.

From the Critical State Theory, the value of  $\omega$  (angle between the basal decollement and backstop interface) becomes smaller toward the north. The results of CS show the increase of the  $\omega$  associate with the increase of the  $\mu_b'$ , suggesting that strain energy is more stored toward the North.

Both results show that the  $\mu_b'$  has decreased after the earthquake. The change in  $\mu_b'$  may be due to the earthquake.

It is possible to know friction properties of before the earthquake and that of after the earthquake with bathymetry.

Keywords: Japan Trench, Critical Taper Theory



## Long-term crustal movement in the Rikuzentakata area, southern Sanriku coast, based on geomorphological/geological featu

NIWA, Yuichi<sup>1\*</sup> ; TODA, Shinji<sup>1</sup>

<sup>1</sup>International Research Institute of Disaster Science, Tohoku University

In the northeast Japan forearc, strain rate estimated based on by geological feature is different from that by geodetic feature. Thus, marine terrace suggests that the Sanriku coast has uplifted at the rate of 1 mm/yr since the late Quaternary. On the other hand, this area has subsided at the maximum rate of 10 mm/yr during the past 100 years based on geodetic data. This disaccord indicates the possibility that the giant mega-thrust earthquake causes the Sanriku coast to uplift. However, the 2011 Tohoku-Oki Earthquake (Mw9.0) was accompanied by subsidence along the Sanriku coast. This fact led us to reexamine long-term crustal movement.

We conducted geomorphological/geological analyses in the Sanriku coast, especially the southern part of the coast, where long-term crustal movement is unknown because of lack of widely distributed Pleistocene marine terrace. In this presentation, we will report preliminary results of consideration of long-term crustal movement in the Rikuzentakata area, southern part of Sanriku coast.

Keywords: marine terrace, southern Sanriku coast, long-term crustal movement, alluvial plain

## Large-scale simulation of coseismic and postseismic crustal deformation using a high-fidelity finite element model

AGATA, Ryoichiro<sup>1\*</sup> ; ICHIMURA, Tsuyoshi<sup>1</sup> ; HIRAHARA, Kazuro<sup>2</sup> ; HYODO, Mamoru<sup>3</sup> ; HORI, Takane<sup>3</sup> ; HORI, Muneo<sup>1</sup>

<sup>1</sup>The University of Tokyo, <sup>2</sup>Kyoto University, <sup>3</sup>Japan Agency for Marine-Earth Science and Technology

Postseismic crustal deformation of a subduction zone earthquake is an essential factor in such studies as interseismic slip deficit rates and stress-field change of the focal area of inland earthquakes. The viscoelastic behavior of the asthenosphere largely affects postseismic crustal deformation. Several studies have used analytical models or three-dimensional (3D) finite element (FE) method to simulate postseismic crustal deformation, considering the viscoelasticity. Yet because of the large computational cost, simulations using a realistic model of crustal structure have not been carried out, despite that detailed crustal data are available. Based on the technique of high performance computing, we performed large-scale finite element simulations using 3D FE models of higher-fidelity (High-fidelity model: HFM) to available crustal data. We used the data of JTOPO30, which was constructed in a 900 m resolution by MIRC (JTOPO30, 2003), for modeling the ground surface and CAMP standard model (Hashimoto et al. 2004) for the interplate boundaries. By using this data, we constructed a one-kilo-meter-resolution HFM with the size of 1700 x 2600 x 400 km, which includes the whole of the Japanese Islands. The model has 30km thick crust and the underlying viscoelastic mantle wedge, where the Philippine Sea and the Pacific plates are subducting beneath the Eurasian and the North American plates. Because the target area was large, we also took into consideration the curvature of the earth. We expect a large degrees-of-freedom in our HFM. Therefore, to compute the time history of the crustal deformation with such a large-scale model, we used the K computer, the fastest supercomputer in Japan.

In the session, we will show the simulation of the 200-year time history of postseismic crustal deformation using the HFM. In addition, by comparing the results of various sizes of temporal and spatial discretization, we will demonstrate that our method can compute the solution with discretization fine enough for numerical convergence.

Keywords: postseismic crustal deformation, high-fidelity finite element model of crustal structure, large-scale simulation

## Tsunami simulation in the Western Pacific Ocean and East China Sea from the hypothetical M9 Nankai earthquake models

HARADA, Tomoya<sup>1\*</sup> ; SATAKE, Kenji<sup>2</sup> ; FURUMURA, Takashi<sup>1</sup>

<sup>1</sup>CIDIR/ERI, the University of Tokyo, <sup>2</sup>Earthquake Research Institute, the University of Tokyo

We computed tsunamis in the Western Pacific Ocean and East China Sea from the hypothetical models of the giant Nankai earthquake proposed by the Cabinet Office of Japanese government (2012). The maximum tsunami heights on the New Guinea coasts, Philippine Islands coasts, and Shanghai coasts in China are about 1.0-5.0 meters, 1.0-7.0 meters, and 0.5-2.0 meters, respectively. They are up to twice large as those computed from the 1707 Hoei earthquake (the largest earthquake along the Nankai trough in Japanese history). The simulation also shows that tsunami heights on the coasts in this area depend on the slip amounts on the Nankai fault.

Responding to the unexpected occurrence of the 2011 Tohoku earthquake, the Cabinet Office of Japanese government (2012) assumed 11 models of the giant Nankai earthquake (Mw 9.1), computed tsunami heights along the Japanese coasts, and estimated the human and economic disasters. The tsunami heights exceed 10 m on the coasts of 13 prefectures, with a maximum height of 34.4 m.

Tsunamis from such a gigantic earthquake may impact the coasts in the Western Pacific Ocean and East China Sea. Harada and Satake (2012, AOGS; 2013, "Tsunami Events and Lessons Learned", Springer) performed numerical tsunami simulations in these oceans by using various fault models of the past Tokai and Nankai earthquakes.

In this study, we carried out the same simulations from the 11 fault models of the M9 Nankai earthquake. Tsunami propagations were computed by the finite-difference method for the non-linear long-wave equations with Coriolis's force (Satake, 1995) in the area of 115-155 deg. E and 8 deg. S to 40 deg. N using the GEBCO 30-second bathymetry data. Initial tsunami heights computed by the Cabinet Office were used. A Manning's roughness coefficient of  $0.025 \text{ m}^{-1/3} \text{ s}$  was assumed for the friction and a computation time step of 1 s is used to satisfy the stability condition of the finite-difference method. We simulated tsunamis for 24 hours after the earthquakes.

We thank the Cabinet Office of Japanese government for providing the hypothetical models of the giant Nankai earthquake.

**Keywords:** sunami numerical simulation, Western Pacific Ocean, East China Sea, maximum tsunami heights, hypothetical M9 Nankai earthquake

## Stress concentration in the C0002 borehole of the NanTroSEIZE Project, Nankai Trough

WU, Hungyu<sup>1\*</sup> ; KINOSHITA, Masataka<sup>1</sup> ; SAITO, Saneatsu<sup>1</sup> ; LIN, Weiren<sup>1</sup> ; SANADA, Yoshinori<sup>1</sup>

<sup>1</sup>Japan Agency for Marine-Earth Science and Technology

Wellbore instability is a major challenge for the engineer evaluating borehole and formation conditions. Instability is especially important to understand in areas with high stress variations, significant structure anisotropy, or pre-existing fracture systems. Borehole (in)stability is influenced by rock strength, structural properties, and near-field principal stresses. During drilling, the borehole conditions also impact borehole integrity. Factors that we can measure in the borehole during with logging while drilling (LWD) to understand these conditions include Mud Weight, mud loss, ROP (Rate of Penetration), RPM (Rotation Per Minute), WOB (Weight on Bit), and TORQ (Power swivel torque value). By observation the resistivity images, we can utilities the significant features under the interactions of effective stresses and formation.

We conducted stress analysis for Site C0002F of the Nankai Trough transect based on riser and riserless drilling data during IODP Expedition 338. Rock strength and basic physical properties, including velocity, density and porosity are obtained from core samples. The borehole shape, determined from LWD resistivity images, indicates that most of drilling occurred in stable environments, however, in a few instances the bottom hole assembly became stuck. We used our stress profile model to evaluate the mud weight required to drill a stable borehole for the measured rock strength and physical properties. Based on our analysis, we constrained the stress magnitude and possible orientation during IODP Expedition 338 by the drilling parameters. The enlargement and collapse in the borehole indicated that mud weight plays the essential role in the drilling.

Keywords: NanTroSEIZE, LWD, Breakout, Drilling, Borehole Instability

## Preliminary results of lithology examined during IODP Expedition 348 in the accretionary wedge of the Nankai Trough

FUKUCHI, Rina<sup>1\*</sup> ; SCHLEICHER, Anja<sup>2</sup> ; MAIA, Ana<sup>3</sup> ; SONG, Chen<sup>4</sup> ; YANG, Kiho<sup>5</sup> ; EXPEDITION 348, Scientists<sup>6</sup>

<sup>1</sup>The University of Tokyo, <sup>2</sup>University of Michigan, <sup>3</sup>Cardiff University, <sup>4</sup>University of Missouri-Columbia, <sup>5</sup>Yonsei University, <sup>6</sup>IODP Expedition 348

International Ocean Discovery Program (IODP) Nankai Trough Seismogenic Zone Experiment (NanTroSEIZE) Expedition 348 took place from 13 September 2013 to 29 January 2014. This expedition was primarily designed to extend riser Hole C0002N to 3600 mbsf (in the event, C0002N sidetrack Hole C0002P was drilled to 3058.5 mbsf). We collected cuttings, core samples, mud gas, and logging data. Here we report the preliminary shipboard lithological results of IODP Expedition 348.

Four lithologic units were identified at Site C0002 based on geological and geochemical characteristics of core and cuttings samples: Unit II (475-512.5 mbsf in Hole C0002M), Unit III (875.5-975.5 mbsf in Hole C0002N), Unit IV (975.5-1665.5 mbsf in Hole C0002N), and Unit V (1665.5-2325.5 mbsf in Hole C0002N, and 1965.5-3058.5 mbsf in Hole C0002P).

Lithologic Unit II is dominated by fine-grained turbiditic deposits. Silty claystone is the main lithology, with subordinate fine-grained sandstone and sandy siltstone. Lithologic Unit III is dominated by silty claystone with trace amounts of very fine loose sand, containing common glauconite grains. Those units are interpreted to be the Kumano forearc basin sediments. Lithologic Unit IV is dominated by silty claystone, with sandstone as a minor lithology. Sandstone cuttings in this unit are generally very weakly consolidated, and occur as disaggregated loose sand. Lithologic Unit IV is divided into five subunits based on sand content and interpreted as the upper accretionary prism sediment. Lithologic Unit V is dominated by silty claystone. Fine-grained and moderately cemented sandstone was a minor component. In Hole C0002P, clay-size content in the silty claystone increases at the depth up to 2625.5 mbsf. The fine silty claystone becomes the dominant lithology from 2625.5 mbsf. This unit is possibly interpreted to be the trench or Shikoku Basin hemipelagic deposits.

Keywords: IODP Expedition 338, NanTroSEIZE, Site C0002

## Physical properties of Nankai accretionary prism sediments at Site C0002, IODP Expedition 348

KITAMURA, Manami<sup>1\*</sup>; KITAJIMA, Hiroko<sup>2</sup>; HENRY, Pierre<sup>3</sup>; VALDEZ, Robert<sup>4</sup>; JOSH, Matthew<sup>5</sup>; EXPEDITION 348, Scientists<sup>6</sup>

<sup>1</sup>Hiroshima University, <sup>2</sup>Geological Survey of Japan National Institute of Advanced Industrial Science and Technology, <sup>3</sup>Aix-Marseille University, <sup>4</sup>Pennsylvania State University, <sup>5</sup>The Commonwealth Scientific and Industrial Research Organization, <sup>6</sup>IODP Expedition 348

Integrated Ocean Drilling Program (IODP) Nankai Trough Seismogenic Zone Experiment (NanTroSEIZE) Expedition 348 focused on deepening the existing riser hole at Site C0002 to ~3000 meters below seafloor (mbsf) to access the deep interior of the Miocene inner accretionary prism. This unique tectonic environment, which has never before been sampled in situ by ocean drilling, was characterized through riser drilling, logging while drilling (LWD), mud gas monitoring and sampling, and cuttings and core analysis. Shipboard physical properties measurements including moisture and density (MAD), electrical conductivity, P-wave, natural gamma ray, and magnetic susceptibility measurements were performed mainly on cuttings samples from 870.5 to 3058.5 mbsf, but also on core samples from 2163 and 2204 mbsf.

MAD measurements were conducted on seawater-washed cuttings ("bulk cuttings") in two size fractions of >4 mm and 1-4 mm from 870.5 to 3058.5 mbsf, and hand-picked intact cuttings from the >4 mm size fractions within 1222.5-3058.5 mbsf interval. The bulk cuttings show grain density of 2.68 g/cm<sup>3</sup> and 2.72 g/cm<sup>3</sup>, bulk density of 1.9 g/cm<sup>3</sup> to 2.2 g/cm<sup>3</sup>, and porosity of 50% to 32%. Compared to the values on bulk cuttings, the intact cuttings show almost the same grain density (2.66-2.70 g/cm<sup>3</sup>), but higher bulk density (2.05-2.41 g/cm<sup>3</sup>) and lower porosity (37-18%), respectively. The grain density agreement suggests that the measurements on both bulk cuttings and intact cuttings are of good quality, and the differences in porosity and density are real, but the values from the bulk cuttings are affected strongly by artifacts of the drilling process. Thus, the bulk density and porosity data on handpicked cuttings are better representative of formation properties. Combined with the MAD measurements on hand-picked intact cuttings and discrete core samples from previous expeditions, porosity generally decreases from ~60% to ~20% from the seafloor to 3000 mbsf at Site C0002.

Electrical conductivity and P-wave velocity on discrete samples, which were prepared from both cuttings and core samples in the depth interval of 1745.5-3058.5 mbsf, range 0.15-0.9 S/m and 1.7-4.5 km/s, respectively. The electrical resistivity (a reciprocal of conductivity) on discrete samples is generally higher than the LWD resistivity data but the overall depth trends are similar. On the other hand, the P-wave velocity on discrete samples is lower than the LWD P-wave velocity between 2200 mbsf and 2600 mbsf, while the P-wave velocity on discrete samples and LWD P-wave velocity are in a closer agreement below 2600 mbsf. The electrical conductivity and P-wave velocity on discrete samples corrected for in-situ pressure and temperature will be presented.

The shipboard physical properties measurements on cuttings are very limited but can be useful with careful treatment and observation.

Keywords: IODP Expedition 348, NanTroSEIZE, accretionary prism

## Effects of frictional heating and comminution on coal maturation

FURUICHI, Hiroyuki<sup>1\*</sup> ; UJIIE, Kohtarō<sup>1</sup> ; SAITO, Tsubasa<sup>1</sup> ; SAKAGUCHI, Arito<sup>2</sup> ; TSUTSUMI, Akito<sup>3</sup>

<sup>1</sup>Life and Env., Sci., Univ. Tsukuba, <sup>2</sup>Sci., Yamaguchi Univ., <sup>3</sup>Sci., Kyoto Univ.

The detection of friction heating on faults is crucial to estimate frictional heat during earthquakes. Recently, vitrinite reflectance (Ro) has been used to detect friction heating along faults. However, the factors controlling increase in Ro on faults remain poorly understood. Moreover, the application of the commonly used kinetic model to the estimation of temperature rise during short-lived thermal events such as frictional heating on faults has not been convinced. Here, we conducted friction experiments on a mixture of 95 wt% clay-rich material from the host rock of the megasplay fault gouge and 5 wt% coal grains from the forearc basin in the Nankai subduction zone at slip rates of 0.15 mm/s-1.3 m/s under dry (room humidity) and wet (water-saturated) conditions. After the experiments, we examined microstructures, Ro and size of coal grains and then compared with those obtained from in and around the megasplay fault gouge. The results show that Ro does not increase by rapid heating alone; grain-size reduction due to comminution is required for increase in Ro. The combination of comminution and heating is the most effective for increase in Ro, possibly due to enhanced mechanochemical reaction associated with an increase in surface area of coal grains. The application of the results to the Nankai megasplay fault gouge is that increased Ro in the fault gouge results from frictional heating and comminution, while that in adjacent to the gouge are mainly derived from comminution. The Ro calculated from the chemical kinetic model is higher than that measured after the experiments. Ro is a useful tool to detect past frictional heating on faults, but the estimation of temperature rise from Ro is problematic; the new kinetics model considering the effects of frictional heating and comminution is necessary to estimate amount of frictional heat.

Keywords: vitrinite reflectance, frictional heating, comminution, Nankai Trough

## Receiver function analysis using OBS data: modeling 3-D structure of the Philippine Sea plate off the Kii Peninsula

AKUHARA, Takeshi<sup>1\*</sup> ; MOCHIZUKI, Kimihiro<sup>1</sup>

<sup>1</sup>Earthquake Research Institute, University of Tokyo

Megathrust earthquakes have repeatedly occurred beneath the southwestern Japan, on the subducting Philippine Sea plate, in cycles of 100-150 years [Ando, 1975]. The rupture boundary of the latest two megathrust earthquakes, the 1944 Tonankai and 1946 Nankai earthquakes, is located at the south of the Kii Peninsula. Although some structural heterogeneity was proposed as factors of the rupture boundary [Mochizuki et al., 1998; Kodaira et al., 2006], the question of why rupture propagation stops there is still open in light of our little knowledge about 3-D geometry of the subducting Philippine Sea plate at offshore region.

In this study, we aim to construct 3-D structure model of the subducting Philippine Sea plate by receiver function (RF) analysis, using data of ocean-bottom seismometers (OBSs) deployed from 2003 to 2007 off the Kii Peninsula [Mochizuki et al., 2010; Akuhara et al., 2013]. These OBSs have three-component velocity sensors with natural frequency of 1 Hz, and their orientations were determined in this study from particle motion of regional P-wave. The difficulty of our RF analysis using OBS data is summarized by the following two factors. The first is that noise is dominant within a low-frequency band ( $1 < \text{Hz}$ ), the most stable band for estimating RFs. The second is that the number of teleseismic events is limited because of short observation periods and low S/N ratio.

To overcome these problems, we calculated RFs with the aid of multi-taper correlation (MTC) method [Park and Levin, 2000]. The method is resistant to spectral leakage and able to estimate frequency-dependent uncertainties for RF, which is suitable for noisy OBS data and for high-frequency analysis. We binned resultant RFs by back azimuths, and computed time-domain uncertainties of the RFs from the frequency-dependent uncertainties estimated by the MTC method, using jackknife resampling within each back azimuth bin [Leahy and Collins, 2009]. This uncertainty estimation makes the following phase identification more reliable, even though the number of teleseismic events is limited.

Our preliminary results show some coherent peaks throughout all back azimuth bins, whose amplitude is larger than one-sigma uncertainties. Some of them have moveout, implying existence of dipping layers, and have arrival times roughly corresponding to the depth of the slab mantle. Although more detailed identification process for these peaks is largely left for our future work, these peaks might be converted phases from the slab mantle.

Keywords: ocean-bottom seismometer, receiver function, subduction zone

## Three-dimensional velocity model for the Nankai Trough seismogenic zone based on structural studies

NAKANISHI, Ayako<sup>1\*</sup> ; TAKAHASHI, Narumi<sup>1</sup> ; YAMAMOTO, Yojiro<sup>1</sup> ; TAKAHASHI, Tsutomu<sup>1</sup> ; OBANA, Koichiro<sup>1</sup> ; KODAIRA, Shuichi<sup>1</sup> ; KANEDA, Yoshiyuki<sup>1</sup>

<sup>1</sup>JAMSTEC

Coseismic rupture area of the great interplate earthquake concerned about its occurrence along the Nankai Trough presumed by government of Japan is now wider to the west, north and south than the former assumption. Although the new estimation is based on seafloor topography, source area of the past largest megathrust event, present seismic activity and so on, structural information has not always been enough reflected yet. In order to estimate precise coseismic rupture area of the Nankai megathrust earthquake, it is necessary to improve a physical model of the Nankai Trough seismogenic zone based on the geometry of the subducting plate and velocity structure model.

Japan Agency for Marine-Earth Science and Technology had conducted the large-scale high-resolution wide-angle and reflection seismic survey and long-term observation from off Kyushu to Tokai between 2008 and 2012. Layered velocity structure models are now obtained along grid two-dimensional seismic profiles from the Hyuga-nada to the Kii channel area. A three-dimensional seismic tomography using active and passive seismic data observed both land and ocean bottom stations had been also performed for the western Nankai Trough.

In this study, we constructed a three-dimensional velocity model of the Nankai Trough with the procedure as follows;

- 1) Sampling the velocity structural information along each seismic profile with interval of ~1km in horizontal, and ~100m in vertical directions
- 2) Preparing the geometry model of each interface included in layered models, e.g., basement, plate boundary, Moho, etc.
- 3) Setting minimum and maximum velocities of each layer based on the velocity models along two-dimensional seismic profiles
- 4) Interpolating sampled velocity information considering layered structure  
(Landmark DecisionSpaceDesktop is used for constructing 3-D modeling)

Previously published layered models are also used to make up for insufficient structural information for the eastern Nankai Trough.

Reliability of the three-dimensional model was confirmed by comparing calculated travel-times with observed travel-times along each seismic profile. We will also try to evaluate the reliability of the model by comparing the hypocenter distribution using three-dimensional velocity model obtained in this study with that determined by three-dimensional seismic tomography using active and passive source data. We will plan to revise our 3D model with additional structural information and construct more precise and detailed model for the entire Nankai Trough area so that the model can be applied to more realistic numerical simulation.

This study is part of 'Research concerning Interaction Between the Tokai, Tonankai and Nankai Earthquakes (FY2008-2012)' funded by Ministry of Education, Culture, Sports, Science and Technology, Japan.

## Seismic observations off Kii Peninsula

YAMAMOTO, Yojiro<sup>1\*</sup>; TAKAHASHI, Tsutomu<sup>1</sup>; KAIHO, Yuka<sup>1</sup>; OBANA, Koichiro<sup>1</sup>; NAKANISHI, Ayako<sup>1</sup>; KODAIRA, Shuichi<sup>1</sup>; KANEDA, Yoshiyuki<sup>1</sup>

<sup>1</sup>JAMSTEC

In the Nankai Trough subduction zone, megathrust earthquakes of M 8 class occur repeatedly. There are three main seismogenic segments (Tokai, Tonankai and Nankai earthquake regions), and these segments have ruptured sometimes simultaneously and sometimes individually. To understand the control factor of the seismic linkage among these segments and Hyuga-nada segments, Japan Agency for Marine-Earth Science and Technology has been carried out a series of wide-angle active source surveys and local seismic observations from 2008 to 2012, as a part of Research concerning Interaction Between the Tokai, Tonankai and Nankai Earthquakes' funded by Ministry of Education, Culture, Sports, Science and Technology, Japan. In this study, we show the results of two local seismic observations off Kii peninsula, the one is in the Kii channel and the other is in the Kumano-nada. The boundary of the Tonankai and Nankai segments is located in this region (Baba and Cummins, 2005), and the existence of the high velocity plutonic rock in the landward plate just beneath Shionomisaki is considered as the control factor of historical rupture variation (Kodaira et al., 2006). Japan Meteorological Agency (JMA) catalogue also indicates the spatial relationship between the seismic activity and seismogenic segments; shallow microseismicity seems to be more active in the Nankai region than in Tonankai region.

The observation in the Kii channel has been performed in FY2010 and was composed of 155 short-term (about 1.5 months) ocean bottom seismographs (OBSs) and 19 long-term (about 10 months) OBSs. First, we relocated the JMA catalogue earthquakes by using three-dimensional velocity model obtained by active source surveys and adding the first arrival time data at OBSs. As a result, the earthquakes near the trough axis were generally relocated 10-20 km shallower than JMA location. Then, we attempt to detect the earthquakes by using long-term OBS records and found the active intraslab seismicity, especially in the up-dip part of the subducted seamount (Kodaira et al., 2000). The observation in the Kumano-nada has been performed in FY2011 and was composed of 150 short-term (about 2.5 months) OBSs and 14 long-term (about 8 months) OBSs. Now we perform the first arrival picking of these data with the seismograph data of Dense oceanfloor network system for earthquakes and Tsunamis (DONET), according to the JMA catalogue earthquake list. We will show the preliminary results of hypocenter distribution in the Kumano-nada at the presentation.

Keywords: Nankai Trough, ocean bottom seismographic observation, seismicity

## Seismic observation and active-source seismic surveys on southern Ryukyu arc

TAKAHASHI, Tsutomu<sup>1\*</sup>; KAIHO, Yuka<sup>1</sup>; ISHIHARA, Yasushi<sup>1</sup>; YAMAMOTO, Yojiro<sup>1</sup>; NAKANISHI, Ayako<sup>1</sup>; OBANA, Koichiro<sup>1</sup>; KODAIRA, Shuichi<sup>1</sup>; KANEDA, Yoshiyuki<sup>1</sup>

<sup>1</sup>JAMSTEC

The Ryukyu arc is an island arc located on southeast of the Eurasian plate. The Philippine Sea plate is subducting north-westward at Ryukyu trench. Many large earthquakes ( $M7\sim 8$ ) occurred on this arc, and some of them generated tsunamis. The 1771 Yaeyama earthquake ( $M7.4$ ) caused a large tsunami of which a maximal height is 30m. For detailed examinations of fault rupture zones and mechanisms of large earthquakes in this arc, it is important to know the seismicity, lithospheric structures and plate geometry. In 2013, Japan Agency for Marine-Earth Science and Technology (JAMSTEC) launched a series of seismic observations and active-source seismic surveys at the Ryukyu arc as a part of research project funded by Ministry of Education, Culture, Sports, Science and Technology, Japan. In FY2013, we conducted refraction and reflection wide-angle seismic surveys and seismic observation on southern Ryukyu arc.

Active source seismic data were acquired on two survey lines. The one is a 480km-long line across the island arc from the south of Ryukyu trench to Okinawa trough. The other is a 100km-long line in Okinawa trough at northwest of Iriomote island. We conducted a refraction survey on the former survey line with 60 ocean bottom seismographs (OBS), and multichannel seismic reflection (MCS) surveys on both lines. Retrieved data shows clear wave trains propagating in the Philippine Sea plate and island arc. Normal faults in Okinawa trough were clearly observed in MCS data.

For seismic observation, we deployed 36 seismic stations including 30 OBSs and 6 onshore stations. All OBSs are equipped with short period geophones. Onshore stations are deployed at Miyako, Tarama, Ishigaki, Iriomote, Kuroshima and Hateruma islands. They are composed of broadband and/or 2Hz seismometers. We also retrieved seismic data from 60 OBSs that was deployed for the active source refraction survey. Observed seismic waves of small earthquakes show path dependences of waveforms that suggest spatial variations of random inhomogeneities and attenuation. For example, OBSs in Okinawa trough did not record clear S-wave for most of earthquakes. However, they observed clear S-wave and long-lasting coda waves for some shallow earthquakes occurred at north of Iriomote and Yonaguni islands. These waveforms suggest strong random inhomogeneities at the shallow part and high apparent attenuation (due to scattering and intrinsic attenuation) at deeper part underneath the Okinawa trough. In this presentation, we outline our observations and notable features of obtained data.

## A plate boundary earthquake model with consideration on submarine active faults

NAKATA, Takashi<sup>1\*</sup> ; WATANABE, Mitsuhsa<sup>2</sup>

<sup>1</sup>Hiroshima University Professor Emeritus, <sup>2</sup>Toyo University

Active faults observed on seafloor along Japan Trench are resultants of repeated large earthquakes. We discuss on the relation between large earthquakes and their source faults based on a detailed active fault map along Japan Trench. Judging from the location and continuation of active faults in the earthquake source area, we consider that one of the extensive thrust faults which extends from off-Sanriku to off-Ibaraki for about 500km, is directly related to the source fault of the 2011 off the Pacific coast of Tohoku Earthquake.

The 2011 off the Pacific Coast of Tohoku Earthquake (Mw9.0) generated large tsunami with massive pulsating pattern of waves (Maeda et al. 2011). A leading hypothesis believed among many seismologists is that rupture of two extensive asperity patches surrounded by stable sliding area on the plate boundary generated the earthquake. One of the asperity patches in depth caused the strong motion and the other near the surface caused fault rupture along the axis of Japan Trench and generated gigantic tsunami. Large displacement ~50m eastward and ~7 to ~10m upward was estimated from comparison of data obtained before and after the earthquake in 2004 and 2011 by multi-narrow beam bathymetric surveys across the trench (Fujiwara et al. 2011). Satake et al. (2011) explained the large tsunami height by simultaneous faulting on two different fault planes that fit with the above-mentioned asperities. Since most of the workers hypothesized without any doubt believed that the earthquake was caused by the fault ruptured up to the trench axis, existence of submarine active fault is rather overlooked so far. However, we consider the large displacement is due to landslide and do not find any extensive fault scarp on the trench axis.

We simulated pattern of seafloor deformation associated with the earthquake using a simple dislocation model for a single fault plane with uniform slip that dips 14 degree in depth and 33.6 degree beneath the tectonic bulge related to the extensive active fault. A result shows that an area of large uplift agrees more or less with the location of tectonic bulge with width of about 20km.

The record of tsunami first wave obtained by the GPS wave gage set on about 200m deep seafloor off Kamaishi on southern Sanriku Coast (Port and Airport Research Institute, 2011). The record suggests that after gradual sea-level rise of 2m during 6 minutes, acute sea-level rise of 4m took place within 4 minutes, and then sea-level abruptly dropped by 4m within 2 minutes. The length of pulsating tsunami wave is estimated about 17km from tsunami propagation velocity at 200m deep sea and total duration of pulsating pattern of tsunami, i.e. 7 minutes. This tsunami wave pattern resembles the pattern of seafloor deformation we calculated above.

We also simulate crustal movement and tsunami height along the Tohoku coast by an earthquake source fault model based the location of the submarine fault with fault-slip deduced from tectonic scarp height that is regarded as cumulative fault-slip. Our simulation explains the observed co-seismic subsidence and large tsunami height along the coast better than many other simulations based on various inversion models.

Based on these observations, we propose active fault model for plate boundary earthquake that large earthquakes are characteristically caused from submarine active faults in the island arc crust that overlap each other above the plate boundary in the narrow sense.

Keywords: plate boundary earthquake, asperity model, active fault model

## The last 6000 years record of tsunami events in the Kaniga-ike pond along the Nankai Trough

MATSUOKA, Hiromi<sup>1\*</sup>

<sup>1</sup>Kochi Univ.

In order to reveal pre-historic record of Nankai Trough earthquakes, we collected 46 vibrocore samples from the Kaniga-ike pond. Stratigraphical study and radiocarbon dating of these samples revealed that sediment of Kaniga-ike pond recorded 17 tsunami events during the last 6000 years. These 17 events repeated almost constant intervals through 300 years. A 2000 years ago event formed remarkable thick tsunami sequence, and also shows an exclusive event in the past 6000 years.

Keywords: Nankai Trough, Tsunami sediment

## Estimate of the contact state of microcrack from the elastic wave velocity measurement

TAMAI, Hayata<sup>1\*</sup>; MUTO, Jun<sup>1</sup>; NAGAHAMA, Hiroyuki<sup>1</sup>; ISHIKAWA, Masahiro<sup>2</sup>

<sup>1</sup>Department of Geology, Graduate School of Science, Tohoku University, <sup>2</sup>Geological institute, Graduate School of Environment and Information Science, Yokohama National Univ

Birch (1960) studied about the relationship between the confining pressure and the elastic wave velocity. It was indicated that the elastic wave velocity increases with the increasing confining pressure because the microcrack is closed at high pressure. The velocity includes the effect of microcracks at low pressure. We must the elastic wave velocity without the effect of microcrack to know the elastic constants of a rock. To do that, it is necessary to know the process of closing microcracks and the contact state of microcrack.

The power-law relation between the elastic wave velocity and confining pressure is expressed with pressure exponent of  $\mu$  (Kobayashi and Kozumi, 1976). They assume that the microcrack has single contact in this model. It is necessary to take account in multiple contacts because the microcracks of a rock have multiple contacts. We applied the single contact model to multiple contacts model with the previous study (Archard, 1953). The microcrack has the point contact, ball contact and plane contact when  $\mu$  is  $2/3$ ,  $3/5$  and  $1/2$  respectively. The microcrack contacts plastically if  $\mu$  is  $<1/2$ . We measured the elastic velocity of rocks with gas medium high pressure apparatus to discuss the effect of the confining pressure.

We measure the velocity with the pulse transmission technique. We set the assembly, composed of a sample between two metal jig pasted piezoelectric transducers, in the pressure vessel. The sample height is about 15-40 mm and diameter is 20 mm. The frequency of transmission wave is 2 MHz. We recorded it  $10^{-9}$ s rate. We measured  $V_p$  and  $V_s$  of the gabbro and granite during pressurization and depressurization to a maximum confining pressure of 200 MPa. The velocity increased drastically with the increase in the confining pressure up to 100 MPa. When confining pressure is lower than about 100 MPa,  $\mu$  of the gabbro and granite is about  $2/3$ , indicating that the contact state of microcrack is point contact. However, under pressure higher than 100 MPa,  $\mu$  becomes under  $1/2$ , indicating that all microcracks are closed plastically in the experiment with gas medium high pressure apparatus. So the velocity at pressure higher than 100 MPa does not include the effect of microcracks. Furthermore, we estimated  $\mu$  of several rocks from previous studies (Birch, 1960, Zimmer et al., 2002). Although  $\mu$  depends on rock type at low pressure, it converges to values smaller than  $1/2$  at high pressure. This indicates that all microcracks are completely closed at high pressure and this result conforms to our experiment. If fluid exists in rocks, the value of  $\mu$  is less than  $1/2$  even at low pressure. Therefore the microcrack with fluid acts as having plastic contact. We revealed the process of closing microcracks with the increasing confining pressure from the elastic wave velocity measurement.

## Frictional properties of the shallow Nankai Trough accretionary sediments

HOSHINO, Koki<sup>1\*</sup> ; OOHASHI, Kiyokazu<sup>2</sup> ; KANAGAWA, Kyuichi<sup>2</sup>

<sup>1</sup>Faculty of Science, Chiba University, <sup>2</sup>Graduate School of Science, Chiba University

We have conducted friction experiments on sandstone, tuff, silty mudstone and clayey mudstone samples cored from the shallow Nankai Trough accretionary prism, using a triaxial apparatus recently installed at Chiba University, at a confining pressure of 37 MPa, a pore pressure of 29 MPa, a temperature of 42 degrees C, and an axial displacement rate of 1 micrometer/s. These pressure, pore pressure and temperature correspond to those supposed at the depth of 1 km below seafloor at IODP Site C0002. The results reveal that frictional properties of these samples change systematically according to the content of clay minerals, in particular of smectite. The content of clay minerals is 6.0 wt% in the sandstone sample, 17.2 wt% in the tuff sample, 34.1 wt% in the silty mudstone sample, and 42.0 wt% in the clayey mudstone sample. Except for the sandstone sample in which smectite is absent, smectite is the most abundant clay mineral in all the other samples, occupying 68-76 wt% of total clay minerals.

Steady-state friction coefficient decreases with increasing content of clay minerals, from 0.83 of the sandstone sample, through 0.74 of the tuff sample and 0.34 of the silty mudstone sample, to 0.27 of the clayey mudstone sample. Slip-dependent frictional behavior also changes according to the content of clay minerals; the sandstone sample exhibits slip hardening, while the other samples exhibit slip softening, which becomes more pronounced with increasing amount of clay minerals.

We will also report the velocity dependence of steady-state frictional strength at this condition as well as how frictional properties of these samples change at deeper conditions up to 5 km below seafloor.

Keywords: Nankai Trough, accretionary sediments, frictional properties

## Effects of shear displacement and fault zone structure on the frictional behavior of montmorillonite-quartz gouge

KAWAI, Tomoaki<sup>1\*</sup> ; TSUTSUMI, Akito<sup>1</sup>

<sup>1</sup>Graduate School of Science, Kyoto University

Recent observation of the low frequency earthquakes in the shallow part of the Nankai subduction zone has demonstrated that faulting there is slow yet seismic; suggesting that frictional velocity dependence along the fault would be negative. However, in a widely accepted model, sediments there is expected to exhibit velocity-strengthening frictional behavior. We have reported that the fault material along the megaseismic fault in the Nankai Trough exhibited both velocity-strengthening and velocity-weakening frictional behavior [Tsutsumi et al., 2011]. Fault zone structures may be important to understand why the samples exhibited different velocity dependence. In this study, we have conducted frictional experiments on artificial gouges composed of montmorillonite and quartz mixtures, in order to understand the relationship between the fault zone structures and velocity dependent frictional behavior.

We examined frictional behavior and fault zone structure of the artificial gouge samples composed of montmorillonite/quartz mixtures. All of the experiments were conducted under water-saturated conditions at 1 to 5MPa of normal stress, with shear displacement of 30 mm to 14 m, using a rotary-shear friction testing machine. Velocity step tests were conducted in a range of velocities from 0.003mm/s to 30 mm/s, in order to examine velocity dependent frictional behavior.

Results of these experiments reveal influences of normal stress and displacements on frictional behavior. Velocity weakening behavior was observed for the mixtures of montmorillonite/quartz = 20/80 and 40/60 wt%, respectively, at large displacement. In velocity-weakening samples, montmorillonite becomes to be finer-grained and is well mixed with quartz in the gouge layer after long shear displacements and at high normal stresses. These observation demonstrates that frictional behavior of the montmorillonite/quartz gouge changes with the development of the deformation structures. It is suggested that fault zone structure is one of the important factors of describing the frictional behavior along faults at the Nankai Trough.

Keywords: montmorillonite, frictional experiment, fault zone structure

## Friction constitutive properties of shallow subduction zone material as estimated from rotary shear friction experiments

NAKANO, Ryuji<sup>1\*</sup> ; NAMIKI, Yuka<sup>1</sup> ; TSUTSUMI, Akito<sup>1</sup>

<sup>1</sup>Graduate School of Science, Kyoto University

In order to understand the dependence of constitutive parameters,  $a$ ,  $b$ , and  $Dc$ , on slip velocity,  $V$ , we conducted experiments by using a rotary shear high velocity friction apparatus. Samples used in this work were collected from the Nankai accretionary prism, offshore from Kii Peninsula, Japan, at Site C0004 during Integrated Ocean Drilling Program (IODP) Expedition 316 [Expedition 316 Scientists, 2009; Tsutsumi *et al.*, 2011], and from the Costa Rica subduction zone, Cocos Ridge, at Site U1381 during IODP Expedition 334 [Expedition 334 Scientists, 2012]. All of the samples from the Nankai accretionary prism are clayey silt, whereas those from Costa Rica can be divided into 2 groups with respect to their composition: one is clayey silt (hereinafter referred to as "Costa Rica Unit I"), the other is silicic to calcareous ooze ("Costa Rica Unit II"). All experiments were carried out at 5 MPa normal stress and 0.0028-2.8 mm/sec slip velocity under wet condition (0.5 g samples with 0.5-0.9 ml distilled water). Moreover, we created a simulation program, which can estimate the values of constitutive parameters and system stiffness,  $k$ , with Levenberg-Marquardt method, supposing the spring-block model.

The results are summarized as the following: (1)  $a$ ,  $b$  and/or  $Dc$  increase with slip velocity; (2) the values are the highest at  $V = 0.028-0.28$  mm/sec; (3) the values are the lowest at  $V = 0.028-0.28$  mm/sec. The reason is not clarified yet, but it is remarkable that, despite the composition, the result of the clayey megasplay fault material from the Nankai accretionary prism resembles the result of Costa Rica Unit II. This implies that, as expected, constitutive parameters depend on not only material but also other conditions. Another remarkable point to be noted is that the values of system stiffness of Costa Rica Unit I decrease by a factor of 10 when compared with the measured apparatus stiffness value. This implies that the mechanical property of the material of Costa Rica Unit I may be more flow-dominated than others. This implies that the mechanical property of the material of Costa Rica Unit I may be more flow-dominated than others. Considering that the samples of the Nankai accretionary prism and Costa Rica contain 20-30 wt%, 60-70 wt% clay, respectively, it is possible that total clay content reflects the gouge behaviour.

Keywords: friction, subduction zone, rate- and state- friction constitutive law, Nankai Trough, Costa Rica

## Physical properties of sediments in reference sites and Frontal prism off Costa Rica: IODP Expedition 344

SAIKI, Ayaka<sup>1\*</sup> ; HASHIMOTO, Yoshitaka<sup>1</sup>

<sup>1</sup>Kochi University

Comparing physical properties in reference and frontal prism sites is key to understand dewatering and lithification processes in subduction zone. Furthermore, it can be evidence for identifying the location of decollement and the underthrusting materials into seismogenic depth. In this study, we examined the physical properties of sediments in reference sites and frontal prism site both from on-board data and from laboratory experiments for velocity and porosity measurements with variation of effective pressure. Finally, we converted on-board porosity to fluid pressure using laboratory experimental data for reference sites and frontal prism site.

We focused on reference sites, U1381 and U1414, and frontal prism site, U1412 in the Integrate Ocean Drilling Program Expedition 344 off Costarica. Laboratory experiments for velocity and porosity measurements were conducted with variation of effective pressure. We kept 1MPa of pore pressure and changed confining pressure stepwise to control effective pressure. We calculated in-situ effective pressure using sample depth, bulk density and assumption of hydrostatic pressure of pore pressure. We obtained velocity and porosity data by 5 steps up to the in-situ effective pressure and 5 steps more up to 10 times of the in-situ effective pressure. Porosity change during experiments was calculated using volume change in pore water volume. We assumed on-board porosity under atmospheric pressure condition. 4 samples from sites U1381 and U1414 were measured so far.

Porosity ranges from about 77% to about 53% during experiments. P-wave velocity ranges from about 1.4 to 1.6 km/s. Velocity-porosity relationships from on-board data and from laboratory experiments are comparable nicely and also represents a good agreement with global empirical model. Because both laboratory data and on-board data shows a similar trend in the velocity-porosity relationship except for data from U1381 Unit II, the physical properties of sediment except for sediments from U1381 Unit II is similar in velocity-porosity-effective pressure relationships. Therefore, the porosity-effective pressure can be applied on most of sediments, implying that we can convert the porosity to effective pressure using laboratory results. We estimated fluid pressure from on-board porosity with depth using porosity-effective pressure relationship obtained from laboratory experiments.

For U1381 Unit I, hydrostatic fluid pressure was estimated although the error was large. Because U1381 is located in reference site, the hydrostatic pressure is expected in U1381. On the other hand, for U1414, lower fluid pressure than hydrostatic pressure was estimated in ~10m intervals in the upper part of Unit II. Hydrostatic pressure was estimated in other interval in U1414. Therefore, fluid pressure was recovered to hydrostatic pressure below the over-consolidated layer. In the over-consolidated layer, porosity decreases quickly with constant grain density, which is comparable with the over-consolidation state. Below the over-consolidated layer, porosity increases with decrease of grain density, although the hydrostatic pressure is estimated. In the interval with increase of porosity, because sediments possibly have different physical property, further laboratory experiments on the sediments are needed. Finally, for U1412, over-consolidated sediments were estimated, which may be due to quick dehydration by frontal accretion.

Keywords: IODP, subduction zone, physical property of sediment, elastic wave velocity, pore pressure

## A structural traverse across the Shimanto belt in western Shikoku, Japan

OOHASHI, Kiyokazu<sup>1\*</sup> ; KANAGAWA, Kyuichi<sup>1</sup>

<sup>1</sup>Graduate School of Science, Chiba University

The Cretaceous and Tertiary Shimanto accretionary complex is largely characterized by imbricated thrust slices of trench-fill and ocean-floor sediments, and is thought as an ancient analog of the Nankai accretionary prism. Recent studies on a thermal structure and fault rock analysis for the Shimanto accretionary complex in the central and eastern Shikoku revealed that it has suffered earthquake faulting along the out-of-sequence thrusts associated with tectonic uplift. However, special distributions of thermal and tectonic structures are remaining unclear since those in the western part of Shikoku are poorly understood. In the presentation, we demonstrate the distributions and details of deformed rocks (e.g. melange and brittle faults), geological structure, and vitrinite reflectance across the Shimanto belt in western Shikoku.

Keywords: Shimanto accretionary complex, Out of sequence thrust, Melange, Vitrinite reflectance, Fault rocks

## Stress estimation of Kure OSTs, Shimanto accretionary complex

KOMETANI, Yusuke<sup>1\*</sup>

<sup>1</sup>yamaguchiuniversity

Stress must be concentrated at front of seismogenic fault during rupture propagation. The level of this stress concentration depends on rupture propagation velocity, fault length, thickness of process zone and strength of host rock. However, few quantitative analysis was reported in natural fault due to difficulty of stress estimation. The calcite-twin piezometer, enables stress estimation from elastic rebounded rock, was proposed based on discrete element method simulation and tri-axial rock experiments (Sakaguchi et al., 2011).

The Shimanto accretionary complex is ancient subduction zone and some fossil seismogenic faults were reported.

Among them, pseudotachylyte bearing Kure OSTs cuts Cretaceous Shimotsui, Nonokawa Formation and Kure Melange. This Kure OSTs is composed of echelon formed small faults with thin damaged zone, and burial depth of the host rock is estimated as below 3 km in depth. We obtained three rock samples, applicable for calcite-twin piezometer. The highest value of estimated stress was approximately 420MPa. This is much higher value than the other seismogenic fault in Shimanto accretionary. The Okitsu Fault, formed deeper depth of approximately 4 km, have suffered lower stress of 350 MPa at fault center (Sakaguchi et al., 2011). This indicates that much higher stress was concentrated at shallow Kure OST than deep Okitsu Fault. We propose two models to make high stress at shallow portion. Long crack length from deep to surface causes high stress concentration at shallow portion. Other model causes high stress due to narrower fault zone than the Okitsu Fault. Stress may tend to concentrate at narrower process zone of Kure OSTs than wide process zone of Okitsu Fault.

Keywords: subduction zone, ancient seismogenic, calcite, twin density

## Paleostress analysis of a subduction zone megasplay fault - An example from the Nobeoka Thrust, Japan

KAWASAKI, Ryoji<sup>1\*</sup> ; HAMAHASHI, Mari<sup>1</sup> ; FUKUCHI, Rina<sup>1</sup> ; HASHIMOTO, Yoshitaka<sup>2</sup> ; YAMAGUCHI, Asuka<sup>3</sup> ; KAMEDA, Jun<sup>4</sup> ; HAMADA, Yohei<sup>5</sup> ; KITAMURA, Yujin<sup>6</sup> ; OTSUBO, Makoto<sup>7</sup> ; KIMURA, Gaku<sup>1</sup>

<sup>1</sup>Dept. Earth and Planet. Sci., Univ. Tokyo, <sup>2</sup>Kochi Univ., <sup>3</sup>Atmosph. Ocean Res. Inst., Univ. Tokyo, <sup>4</sup>Hokkaido Univ., <sup>5</sup>Japan Agency for Marine-Earth Science and Technology, <sup>6</sup>Kagoshima Univ., <sup>7</sup>AIST, Geological Survey of Japan, Inst. Geology and Geoinformation

The megasplay faults in subduction zones, branching from plate boundary thrusts, are thought to have a potential to generate earthquakes and accompanying tsunamis. It is therefore important to understand the fault mechanism of megasplay faults for earthquakes and tsunamis occurring in subduction zones. Paleo-splay faults exposed on land often preserve clear deformation features of the seismogenic zone and provide information on the fault mechanisms at depth. One of the important informations that can be obtained from exhumed faults is paleo-stress field. Here we investigated the Nobeoka Thrust, a fossilized megasplay fault in the Shimanto Belt in Kyushu. The hanging wall is Eocene Kitagawa Group, composed of phyllitic shales. The footwall is Eocene to early Oligocene Hyuga Group, composed of foliated cataclasite originated from sandstone-shale melanges. The thrust has been active during the period of 48-40 Ma [Hara and Kimura, 2008]. The hanging- and the footwall have experienced maximum burial temperatures of approximately 320°C and 250°C, respectively [Kondo et al., 2005]. The existence of klippe apart from the Nobeoka Thrust shows that the Nobeoka Thrust is nearly horizontal in regional scale [Murata, 1991, 1995]. Kondo et al. (2005) described two orientations of slickensides from the outcrop, suggesting the existence of flexural gentle fold in kilometer scale. In addition to the previous studies focusing on outcrops, scientific drilling has performed in 2011 penetrated through the Nobeoka Thrust, and core samples and geophysical logging data are obtained. The cores provide important information for investigating geological features under the ground and have an advantage without surface weathering.

In this study, we analyzed paleo-stress from slip vectors on small faults observed in the cores. Small faults are expected to be less-reactivated. The number of small faults is much larger than that of large faults, accordingly, high statistical reliability is expected. Multiple inverse method (MIM; Yamaji, 2000; Otsubo and Yamaji, 2006) was applied to the small faults. K-means clustering (Otsubo et al., 2006) was applied to stress tensors detected by the MIM for estimating optimal solutions. Preliminary results indicate the presence of solutions with three maximum horizontal stress axes: N85.24°E, N30.07°W and N65.47°E. We examined the formation process of the Nobeoka Thrust based on the results and slickensides on the outcrop. Our results would provide potential insights to the fault evolution of a megasplay fault in subduction zone.

Keywords: Nobeoka Thrust Drilling Project, Subduction zone, Shimanto Belt, paleo-stress, Multiple inverse method

### 3D micro structural observation of pseudotachylyte

HAMADA, Yohei<sup>1\*</sup> ; KIMURA, Gaku<sup>2</sup> ; KAMEDA, Jun<sup>3</sup> ; YAMAGUCHI, Asuka<sup>4</sup> ; HAMAHASHI, Mari<sup>2</sup> ; KITAMURA, Yujin<sup>5</sup> ; FUKUCHI, Rina<sup>2</sup> ; KAWASAKI, Ryoji<sup>2</sup>

<sup>1</sup>Kochi institute for Core Sample Research, JAMSTEC, <sup>2</sup>Department of Earth and Planetary Science, The University of Tokyo, <sup>3</sup>Earth and Planetary System Science Department of Natural History Science, <sup>4</sup>Atomosphere and Ocean Research Institute, The University of Tokyo, <sup>5</sup>Department of Earth and Environmental Sciences, Graduate School of Science and Engineering Kagoshima

Pseudotachylyte, molten fault rock due to dynamic frictional heating, is a strong evidence of seismic fault slip [Sibson 1975]. Recent research reveals pseudotachylytes can be related with dynamic weakening mechanism such as melt lubrication [DiToro et al., 2006]. However, observations of internal structure of pseudotachylyte have been confined to 2D observations with optical-electron microscope. Here we performed X-ray 3D structural observation of natural pseudotachylyte developed close to the Nobeoka thrust which is a major Out of sequence thrust in fossil accretionary prism (Shimanto-belt).

The Nobeoka thrust located in Kyusyu Island, south west Japan, bounding northern and southern Shimanto belt of Cretaceous-Tertiary accretionary complex. The thrust is considered to have been active during 40-48Ma at seismogenic depth of ~11kmsf, experienced maximum temperature of which is 320 C in the hanging wall and 250 C in the footwall. Thus, the Nobeoka thrust is examined that it was major OST in seismogenic zone of accretionary prism (Kondo et al., 2005; Hara and Kimura, 2008; Raimbourg et al., 2009). The pseudotachylyte bearing fault develops in the hanging wall of the Nobeoka thrust with 1 mm of width. Okamoto et al. (2007) reported that carbonate-matrix implosion breccia fill tensile cracks and inner periphery of the fault, interposing pseudotachylyte, based on optical microscopic observation. Though pseudotachylyte cut the implosion breccia, the fault jog consists only of the carbonate-matrix breccia. It may show the fault experienced dynamic pore water pressurizing accompanied by pseudotachylyte generation at its first frictional slip. Therefore, the fault is appropriate to structural investigation of dynamic fault weakening mechanism.

We performed structural observation of this pseudotachylyte with scanning electron-microscope and 3D X-ray microscope. In the electron microscopic observation, we found that fragments of host rock unevenly distributed in the pseudotachylyte. The number of fragments is larger at lower part (footwall-side) than within the center of the pseudotachylyte. We also found open cracks along the fragments arrangement. It is considered to be cooling crack generated due to rapid cooling of molten rock. The 3D x-ray microscopic observation was performed with cylinder sample of 8 mm diameter. The spatial resolution of the x-ray microscope is 1 micro meter, and detailed 3D fault structure was imaged. We focused four planes, A: lower plane of lower fault filling vein, A': lower plane of pseudotachylyte, B: upper plane of upper vein, B': upper plane of pseudotachylyte. The surfaces configurations were extracted and its roughness was evaluated as calculated average roughness, Ra (theta), in each direction. We found that Ra has minimum value in the same direction in each plane, and the lineation strongly develops at the lower planes (A, A').

From the above results, we discussed the faulting process as:

- 1) Start faulting, strain concentrated in the footwall side and pore pressure was raised at the part.
- 2) Hydraulic fracturing by high pore pressure, tensile cracks formation and fluid migration.
- 3) Strength (friction) recovery by draining and formation of pseudotachylyte.

Keywords: pseudotachylyte, 3D micro structure, surface roughness

## Basement structure beneath the Tokyo metropolitan area as revealed with the MDRS method

HORIKAWA, Haruo<sup>1\*</sup>; ABE, Shintaro<sup>1</sup>; YAMAGUCHI, Kazuo<sup>1</sup>; NODA, Katsuya<sup>2</sup>; ABE, Susumu<sup>2</sup>

<sup>1</sup>AIST/GSJ, <sup>2</sup>JGI

We applied the multi-dip reflection surfaces (MDRS) method to seismic data originally acquired by the Tokyo Metropolitan Government, and successfully revealed the shape of basin floor and geological structure above the basin floor. The resultant seismic image is interpreted as rift geometry with imbricated normal faults. Moreover, the active Tachikawa fault seemingly has a high dip angle.

The Kanto region that includes the Tokyo Metropolitan area is located near the boundary between the northeastern Japan and the southwestern Japan, and has complicated tectonic history. Moreover, the region is covered with thick sediment of Neogene to Quaternary. Seismic profiling has contributed to revealing the structure such as concealed half-graben and tectonic history.

The MDRS method is an improvement on the common reflection surface stacking (CRS) method in that the MDRS method can deal with conflicting dipping events. The CRS method can detect subtle reflection events by stacking the data along a specific reflection surface. However, complex geological structure often yields a seismic wave field that contain events from various surfaces with different geometry, and the CRS method has difficulty in resolving such complicated reflection events. The MDRS method seeks subtle reflected events, repeatedly applying the CRS method with various sets of parameters that govern the character of reflection surfaces, and superimposes the derived seismic images with high values of semblance. Consequently, the MDRS method can provide a clear image of such complex geological structure.

Seismic data reprocessed in this study was acquired in the Tokyo metropolitan area. The seismic survey was conducted in order to clarify the depth of the top of pre-Neogene basement and the sedimentary structure above the basement. data processing with the conventional common mid-point stacking was performed in the original survey, and provided an image with vertical offset of the top of the basement that corresponds to the active Tachikawa fault, but it generated a poor image for the overall shape of the basin floor; we can only recognize that the basin floor is not flat.

On the contrary, the MDRS method successfully generated a clear image of the basin floor and the stratification of sediments just above the basin floor. The sediments are in a wedge shape, and contain reflectors with a fanning and upward shallowing of dips. The wedge-shaped sediments are aligned horizontally. We interpret this structure as rift system with imbricated normal faults. In fact, rift system has been recognized beneath the Kanto region that is believed to be formed during the Miocene associated with opening of the Sea of Japan. Moreover, we have newly found that the top of the basement extends further beneath the Tachikawa fault. This suggests that the Tachikawa fault has high dip angle.

### Acknowledgement

The Civil Engineering Center of the Tokyo Metropolitan Government provided the seismic data reprocessed in this study.

Keywords: multi-dip reflection surfaces method, basement structure, seismic reflection survey, common reflection surface stacking

## Seismic velocity structure in Ou backbone range by using a dense seismic array

AOYAGI, Yasuhira<sup>1\*</sup> ; KIMURA, Haruo<sup>1</sup>

<sup>1</sup>Central Research Institute of Electric Power Industry

Ou backbone range is a strain concentration zone with E-W contraction along NE Japan arc, hence forms one of the most active reverse-faulting zone in Japan. Some destructive earthquakes, such as the 1896 Rikuu earthquake (M7.2) and the 2008 Iwate-Miyagi nariku earthquake (M7.2), have occurred there for this century. Fault rupture of the 1896 Rikuu earthquake which occurred along the eastern margin of the Yokote Basin fault zone did not reach all over the fault zone but limited to its northern part. The purpose of this study is to find some crustal structures which could control a termination of fault rupture. In this presentation, we will discuss a property of seismic velocity structure which might terminate the fault rupture of some historical earthquakes based on seismic tomography using a dense arrayed micro-earthquake observation data.

Keywords: Ou backbone range, Seismic velocity structure, Rupture termination, Micro-earthquake observation, Seismic tomography

## Relation between the resistivity structure around Hakone volcano and seismicity induced by the 2011 Tohoku Earthquake

YOSHIMURA, Ryokei<sup>1\*</sup> ; OGAWA, Yasuo<sup>2</sup> ; YUKUTAKE, Yohei<sup>3</sup> ; KANDA, Wataru<sup>2</sup> ; KOMORI, Shogo<sup>4</sup> ; GOTO, Tadanori<sup>5</sup> ; HONDA, Ryou<sup>3</sup> ; HARADA, Masatake<sup>3</sup> ; YAMAZAKI, Tomoya<sup>1</sup> ; KAMO, Masato<sup>1</sup> ; YASUDA, Yojiro<sup>6</sup> ; TANI, Masanori<sup>5</sup>

<sup>1</sup>DPRI, Kyoto University, <sup>2</sup>Volcanic Fluid Research Center, Tokyo Institute of Technology, <sup>3</sup>Hot Springs Research Institute of Kanagawa Prefecture, <sup>4</sup>Institute of Earth Sciences, Academia Sinica, <sup>5</sup>Graduate School of Engineering, Kyoto University, <sup>6</sup>Graduate School of Engineering, Tottori University

Seismicity around the Hakone volcano was activated just after the arrival of surface waves caused by the 2011 off the Pacific coast of Tohoku Earthquake. Most of these triggered earthquakes had similar distribution to prior occasional swarm activities. In order to image electrical properties around such seismic events, we carried out audio-frequency magnetotelluric (AMT) measurements at 39 sites in December 2011 (Yoshimura et al., 2012). In this study, we conducted 3D modeling of dense AMT (Yoshimura et al., 2012) and MT (Ogawa et al., 2012) data, to figure out electrical characteristics around the triggered seismicity. In spite of careful treatments for noise reduction, the effects of noise were still seen on the longer parts of the responses (<1 Hz) at the several measurement sites. Thus we determined to have use of the frequency range from 320 Hz to 1.02 Hz. The full components the impedance tensors at 51 sites in total were inverted using the code developed by Siripunvaraporn et al. [2005]. The model space consists of 64(x-)×46(y-)×36(z-direction; including 7 air layers) blocks. The minimum horizontal size of blocks was 400m×400m. Significant characteristics of the obtained three-dimensional resistivity model are: (1) the most of the triggered earthquakes, which occurred shallower than a depth of 4km, seem to align along edges or areas just inside the relatively resistive block; (2) surface conductive blocks, in which there were very few earthquakes, were observed beneath not only fumarolic areas but geothermal non-active regions.

Keywords: magnetotellurics, three-dimensional resistivity structure, Hakone volcano, triggered earthquake

## Three-dimensional seismic velocity structure around the Neodani fault

NAKAJIMA, Junichi<sup>1\*</sup> ; KATO, Aitaro<sup>2</sup> ; IWASAKI, Takaya<sup>2</sup> ; THE JAPANESE UNIVERSITY GROUP OF THE, Joint seismic observations at the are<sup>3</sup>

<sup>1</sup>Graduate School of Sci., Tohoku Univ., <sup>2</sup>ERI, Univ. of Tokyo, <sup>3</sup>The Japanese University Group of the Joint Seismic Observations at the Area of Nobi Earthquake

The joint research project started in 2007 to enhance our knowledge on the deep structure around the Neodani fault, along which the largest crustal earthquake, the Nobi earthquake (M8.0), occurred in 1891. As a part of the project, 73 seismograph stations were installed around the fault, resulting in a dense seismograph network with a spatial separation of ~10 km.

We performed a travel-time tomography to reveal a detailed 3D velocity structure around the Neodani fault. The tomographic method of Zhao et al. (1992) was applied to arrival-time data of earthquakes (N=3027) that occurred from 2002 to January 2013. The total number of arrival-time data was 248,354 for P waves and 215,034 for S waves. Horizontal grid nodes spaced at intervals of 0.1 degrees were set in the study area and vertical grid nodes were set at intervals of 5°/30.

The obtained results show interesting features in terms of heterogeneity structures beneath the source area of the Nobi earthquake.

1. The lower crust beneath the Nobi plain shows low V<sub>p</sub> and V<sub>s</sub> compared to surrounding areas.
2. A low V<sub>p</sub> and V<sub>s</sub> area is imaged continuously from the Philippine Sea slab and the mid crust beneath the Nobi earthquake.
3. The lower crust beneath the Neodani fault shows an along-fault variation in seismic velocities, with moderate- to high-velocity crust to the southeast and low-velocity crust to the northwest.

## Stress tensor inversion in the Nobi fault area, Central Honshu, Japan

KATSUMATA, Kei<sup>1\*</sup> ; KOSUGA, Masahiro<sup>2</sup> ; KATAO, Hiroshi<sup>3</sup> ; YAMADA, Takuji<sup>1</sup> ; KATO, Aitaro<sup>4</sup> ; THE JAPANESE UNIVERSITY GROUP, The joint seismic observations<sup>4</sup>

<sup>1</sup>Inst. Seismo & Volcano, Hokkaido Univ., <sup>2</sup>Earthquake and Volcano Observatory, Graduate School of Science and Technology, Hirosaki University, <sup>3</sup>Research Center for Earthquake Prediction, Disaster Prevention Research Institute, Kyoto University, <sup>4</sup>Earthquake Research Institute, University of Tokyo

A stress tensor inversion method was applied to 702 focal mechanism solutions in the Nobi fault area, Central Honshu, Japan, which are obtained by using HASH (Hardebeck and Shearer, 2002) that is a method using a first motion polarity of P-wave as data. The study area, 35.3-36.1N and 136.0-137.0E, is gridded with 0.1 X 0.1 spacing in the east-west and north-south directions, respectively. The focal mechanisms are divided into three groups according to the depth of hypocenter: 2-7 km, 5-10km, and 8-13km. From each group the focal mechanisms are selected that the epicenters are located within a radius of 15 km centered at each grid. The SATSI is applied to the data at each group of depth, which is a stress tensor inversion method developed by Hardebeck and Michael (2006). The spatial pattern of stress is obtained at each depth: 2-7 km, 5-10km, and 8-13km. We find that (1) the maximum principal stress ( $\sigma_1$ ) is oriented east-west direction almost all over the study area, and (2) the  $\sigma_1$  direction rotates clockwise by some tens degrees around the Nobi fault.

Keywords: Nobi fault, joint seismic observations, focal mechanism, stress tensor inversion, inland earthquake, active fault

## Strain concentration zone recognized from GNSS data in the San-in region

NISHIMURA, Takuya<sup>1\*</sup>

<sup>1</sup>Disaster Prevention Research Institute, Kyoto University

### Introduction

In the San-in region, southwest Japan, there were many large earthquakes including the 1943 M7.2 Tottori and the 2000 M7.3 Western Tottori prefecture earthquakes in the shallow crust. It is well-known that an active zone of microseismicity exists parallel to the coastline of Sea of Japan. On the other hand, recent geodetic data acquired by the GEONET (GNSS Earth Observation Network) suggest that a rate of contemporary deformation is small in the Chugoku district including the San-in region (e.g., Sagiya *et al.*, 2000). We study a detailed pattern of crustal deformation using the GEONET data to clarify a relation between contemporary deformation and microseismicity.

### Method

We used daily coordinates of the GEONET GNSS stations published by the Geospatial Information Authority of Japan (F3 solution). We fit a function of linear, annual, and semi-annual components to time-series of site coordinates relative to site 950462 (Fukue) to estimate secular site velocities. We also estimate strain distribution at grid points (Shen *et al.*, 1996) and in Delaunay triangles using the site velocities.

### Result

We identify a concentration zone of deformation corresponding to the active zone of microseismicity in an eastern part of the San-in region during April 2005 and December 2009. Distribution of maximum shear strain rate shows that an eastern inland part of the Chugoku district has the lowest strain rate ( $10^{-8}$  yr<sup>-1</sup>) in the Japanese Islands and that the high strain rate ( $10^{-7}$  yr<sup>-1</sup>) is distributed in a band along the coast of Sea of Japan. High strain rate is also observed in a vicinity of the source area of the 2000 Western Tottori prefecture earthquake, which suggests postseismic deformation of the 2000 earthquake is still continuing.

Velocity profile across the active zone of microseismicity shows a velocity component parallel to the active zone (N80°E) has an offset of 2 mm/yr in and around the active zone. Movements across the offset suggest a right-lateral strike slip, which is consistent with a typical focal mechanism of shallow crustal earthquakes in the zone. The 2011 Tohoku-oki earthquake affects crustal deformation in the San-in region. In a postseismic period from January 2012 to December 2013, the strain rate in the San-in region became twice as large as that before 2011.

The deformation can be roughly explained by a right-lateral block motion across the active zone of microseismicity. The used GNSS network is too sparse to estimate a locking depth of a fault between the blocks. A dense GPS array is necessary for more detailed analysis.

### Concluding remarks

Analysis of the GEONET data identifies a strain concentration zone corresponding to the active zone of microseismicity along the coast of Sea of Japan in an eastern part of the San-in region. This zone with a width of ~10 km accommodates right-lateral strike-slip movement of 2 mm/yr, which is concordant with a focal mechanism of shallow earthquakes. The observed strain rate doubled after the 2011 Tohoku-oki earthquake. More detailed distribution of deformation in the strain concentration zone is important to clarify the deformation mechanism. We need to study with both observation and model calculation.

### Reference

- Sagiya *et al.*, PAGEOPH, 147, 2303-2322, 2000  
Shen *et al.*, JGR, 101(B12), 27957-27980, 1996

Keywords: Crustal deformation, Strain concentration zone, GNSS, the San-in region

## HV frictional strength of wet Longmenshan fault gouge and its comparison with the temperature anomaly in WFSD drill hole

TOGO, Tetsuhiro<sup>1\*</sup> ; SHIMAMOTO, Toshihiko<sup>1</sup> ; MA, Shengli<sup>1</sup> ; YAO, Lu<sup>1</sup>

<sup>1</sup>Institute of Geology, China Earthquake Administration

Estimation of frictional strength from temperature anomaly along coseismic fault in a drill hole after a large earthquake has received much attention recently (e.g., J-FAST project in Japan Trench after the Tohoku-oki earthquake. Surface ruptures more than 250 km long formed along existing Yingxiu-Beichuan fault, a major fault in the Longmenshan fault system, during the 2008 Wenchuan earthquake ( $M_w = 7.9$ ). Drilling was conducted at Hongkou in Dujiangyan city, a western part of the fault, as a part of Wenchuan Earthquake Fault Scientific Drilling (WFSD). Temperature monitoring is an important task in the project, and WFSD-1 hole was drilled within one year after the earthquake (fastest drilled hole after a large earthquake in the world). Drilling revealed a large scale fault zone for the depth range of 580~760 m, consisting of cataclasites (about 10 m wide), many thin fault gouge zones and fault breccia (Li et al., 2013, Tectonophysics). Temperature anomaly of only 0.15 degrees Centigrade was recognized at a depth of 590 m along a presumed coseismic slip zone (evidence for coseismic slip zone is not so strong though). Mori et al. (2010, AGU) report friction coefficient less than 0.03 from this temperature anomaly. This friction coefficient was even lower than low friction coefficients (typically 0.05~0.2) at high slip rates, reported in the last two decades.

We have conducted wet gouge experiments on foliated fault gouge containing 25 wt% of water with Teflon sleeve at slip rates to 1.3 m/s and at normal stresses of 1.0~4.8 MPa, and compared the results with those on dry gouge with room humidity. Sample was collected from the Hongkou outcrop (see Togo et al., 2011a, EQS), only several hundred meters from the WFSD-1 drill site. Wet gouge has peak friction coefficient of 0.1~0.36 and steady-state friction coefficient of 0.03~0.14, as compared with 0.65~0.8 and 0.15~0.2 for dry gouge (Togo et al., 2011b, EQS). Wet gouge is substantially weaker than dry gouge, but its frictional strength is still somewhat greater than expected from the near absence of temperature anomaly. However, normal stress expected at the depth of temperature anomaly is expected to be more than twice as high as those of our experiments (experiments could not be done at higher normal stresses due to gouge leak). Both peak and steady state friction coefficients of wet gouge tend to decrease by a power law with increasing normal stresses and the extrapolated steady state friction coefficient at the drilling depth reached from 0.028 to 0.022, which results are consistent with the result by Mori et al. (2010). Thus wet gouge has frictional strength fairly close to that expected from the temperature anomaly.

Wet and dry gouges have completely different deformation textures. Deformed dry gouge is characterized by ultrafine-grained slip zones (typically several to a few tens of microns thick) and weakly deformed gouge. Overlapped slip-zone structures are very common in sheared dry gouge. On the other hand, slight grain-size refinement occurs in wet gouge, and the whole wet gouge zone remains only weakly deformed. We consider that the build-up of pore pressure due to compaction induced and/or thermal pressurization separated grains and suppressed grain crushing in wet gouge.

Keywords: High-velocity friction experiment, Longmenshan fault, Wenchuan earthquake, Frictional heating, Bore hole temperature measurement

## Numerical simulation of shear bands formation in ground due to strike-slip fault

NODA, Toshihiro<sup>1\*</sup>; YAMADA, Shotaro<sup>1</sup>; ASAOKA, Akira<sup>2</sup>; SAWADA, Yoshihiro<sup>2</sup>; KAWAI, Yuta<sup>1</sup>

<sup>1</sup>Nagoya University, <sup>2</sup>Association for the Development of Earthquake Prediction

When a strike-slip fault occurs, flower structures denoting petaloid patterns of shear bands appear inside the ground above the fault, and also the Riedel shear structures showing en-echelon shear bands appear on the surface of the ground. Ueda<sup>1)</sup> conducted model experiments accounting a strike-slip fault and showed evolution process of shear bands inside the model ground using X-ray CT scan system. Also, Sawada and Ueda<sup>2)</sup> numerically simulated evolution of flower structures etc., using a large-deformation analysis where an elasto-perfectly plastic model with the Mohr Coulomb failure criteria was used.

In this study, referring the research work by Sawada and Ueda<sup>2)</sup>, evolution of shear bands was numerically investigated by using a soil-water coupled finite deformation analysis code **GEOASIA**<sup>3)</sup> on which the SYS Cam-clay<sup>4)</sup> was mounted as an elasto-plastic soil model. In the analysis, since the rate-type equation of motion is precisely time-integrated, progressive failure will be analyzed as a nonlinear dynamic problem, and then generation and/or propagation of waves induced by shear bands formation<sup>5)</sup> will also naturally be developed in the analysis. The constitutive model used is capable of describing a wide variety of soils within the same theoretical framework. Here are shown numerical examples in which soil is taken as a non-coupled material with liquid.

First considered was a 3D FE mesh with one element in strike direction of a fault (i.e. y-direction) shown in Fig.1. The right-lateral strike-slip fault was assumed to be located below the three elements at the mid bottom of the ground. As for the boundary conditions, periodic boundary was taken directly above the fault on the x-z planes of the ground, and displacement was applied to the y-direction on the other parts of the x-z planes with a constant rate of  $10^{-6}$ m/s on the opposite side across the fault. Also, x-z and y-z planes were frictionless. In this case, the ground exhibited localization of deformation and the shear bands grow from the bottom in a logarithmic spiral manner ( " flower structures " ). Then, the formation was attributed to plastic swelling behavior of soil element.

Next used were the other 3D meshes with forty elements in the strike direction (Fig.2) so as to investigate evolution of shear bands and effect of homogeneity/initial-imperfection in ground on the evolution. Here, as the boundary conditions, periodic boundary was assumed on the mutually opposite x-z planes and displacement was applied to the nodes located at the bottom with the same rate on the opposite side across the fault, while the same material constants were used. The imperfection was given to some elements directly above the fault by slightly altering a material constant of them. In the imperfection case, flower structures occurred inside the ground, thereafter Riedel shear structures appeared on the surface. The parts of the Riedel shear exhibited more significant upheavals than its surroundings. Furthermore, in the other numerical cases, angle between the Riedel shear and the strike varied with the different material constant.

1) Ueda K.(2003): Evolution of strike-slip fault systems and associated geomorphic structures: Model Test, CRIEPI Rep. No.U03021, in Japanese.

2) Sawada, M. & Ueda K.(2009): Numerical simulation for evaluation of structure zone distribution due to strike-slip fault, CRIEPI Rep.No.N08028, in Japanese.

3) Noda, T. et al.(2008): Soil-water coupled finite deformation analysis based on a rate-type equation of motion incorporating the SYS Cam-clay model, Soils and Foundations, 48(6), 771-790.

4) Asaoka, A.et al.(2002): An elasto-plastic description of two distinct volume change mechanisms of soils, Soils and Foundations, 42(5), 47-57.

5) Noda, T. et al.(2013): Acceleration generation due to strain localization of saturated clay specimen based on dynamic soil-water coupled finite deformation analysis, Soils and Foundations, 53(5), 653-670.

Keywords: strike-slip fault, shear bands, Riedel shear, flower structure, numerical analysis

SSS31-08

Room:502

Time:April 30 16:30-16:45

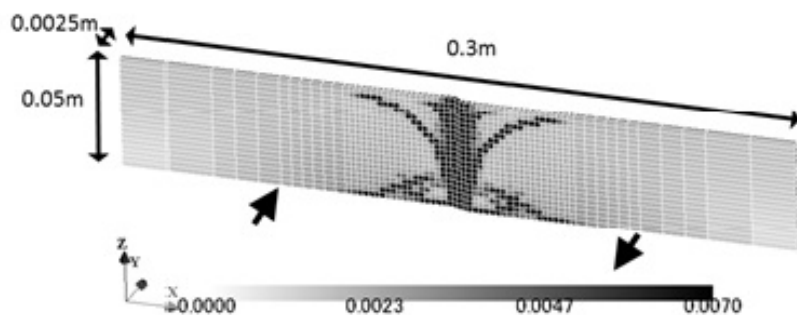


Fig.1. Occurrence of flower structure

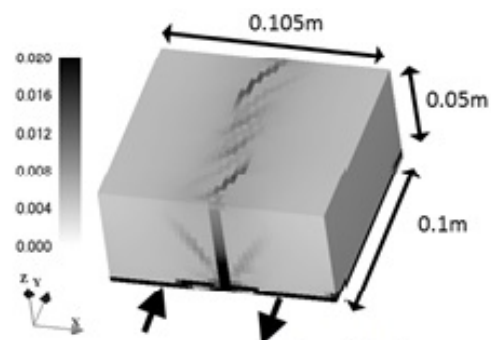


Fig.2. Occurrence of Riedel shear after flower structure, ground with initial material imperfection

## Spatially inhomogeneous stress field in the source area of the 2011 Fukushima Hamadori earthquake sequence

YOSHIDA, Keisuke<sup>1\*</sup>; HASEGAWA, Akira<sup>1</sup>; OKADA, Tomomi<sup>1</sup>

<sup>1</sup>Research Center for Prediction of Earthquakes and Volcanic Eruptions, Tohoku University

After the 2011 great Tohoku-Oki earthquake, many earthquakes occurred near Iwaki, Fukushima Prefecture, including Mw6.8 event of April 11. This 2011 Fukushima Hamadori earthquake sequence is characterized by normal faulting, with T-axis oriented in the NW-SE, E-W and NE-SW directions for events in the northern, central and southern parts of the source area, respectively.

In order to understand the cause of such a remarkable spatial variation of focal mechanisms, we investigated the stress field in the source area of this earthquake sequence. First, we relocated hypocenters of events that occurred during the period from 1997 to 2012 by the double-difference location method. Relocated hypocenters show that events near the 3/19 Mw 5.8 earthquake in the southern area, those near the 3/23 Mw 5.7 earthquake in northern area and those near the 4/11 Mw 5.9 earthquake in central area are aligned along planes dipping westwards corresponding to one of nodal planes, respectively.

Then, we estimated the stress field in the source area of the sequence by a stress tensor inversion of focal mechanisms reported by the National Research Institute for Earth Science and Disaster Prevention and Japan Meteorological Agency. Results show that the stress field is very heterogeneous in space with normal fault stress regime after the occurrences of the main-shock of each part of the source area. In the northern, central, southern and east parts of the source area, the minimum principal stress ( $\sigma_3$ ) axes are oriented in the NW-SE, E-W, NE-SW and NNE-SSW directions, respectively. As a whole,  $\sigma_3$  axis shows the concentric circle-like distribution. In contrast, before the occurrence of the main-shock of each part,  $\sigma_3$  axis is oriented homogeneously in space in the E-W direction.

This observation suggests the possibility that the remarkable heterogeneity in stress field is caused by the static stress change of large earthquakes. We estimated the static stress changes caused by the 2011 Fukushima Hamadori earthquake sequence. A slip model estimated by Hikima (2012) using strong motion waveforms was used for the Mw6.8 earthquake. Furthermore, we made fault models of the 3/19 Mw 5.7, 3/23 Mw 5.8 and 4/12 Mw 5.7 events using hypocenter locations and the scaling relation between moment magnitude, fault length, width and slip amount for estimating their static stress changes.

Spatial distribution of  $\sigma_3$  axis direction of the static stress change is approximately the same as that of the observed stress field after the occurrences of the main-shock of each part of the source area. This strongly suggests that  $\sigma_3$  axis rotated after the 2011 Fukushima Hamadori sequence and the stress magnitude in the focal area before the sequence was smaller than the static stress change (<~several MPa). We estimated the differential stress magnitude assuming that the difference in the stress tensor before and after the earthquakes is equal to the static stress change associated with the large earthquakes. Estimated magnitude of the differential stress was <20 MPa.

Keywords: crustal stress, focal mechanism, weak fault

## To what degree can rocks become weak during deformation?: Fracturing-dissolution-mass transfer-precipitation creep

TAKESHITA, Toru<sup>1\*</sup> ; OKAMOTO, Ayumi<sup>1</sup>

<sup>1</sup>Hokkaido University

The megaquake underneath the Pacific Ocean off the northeast Japan revealed important facts on crustal dynamics of the Japanese island. Among them, a new suggestion on the magnitude of differential stress in the crust is important. After the megaquake, peculiar earthquakes occurred in places, where earthquakes do not frequently occur. A typical example was an earthquake caused by normal faulting near the Iwaki-city, northeast Japan, where the stress field of a weak E-W compression was changed to that of an E-W extension. Based on the facts, Yoshida et al. (2012) estimated that the magnitude of differential stress was on the order of 1 MPa in upper crust. In this presentation, we will discuss the newly arising problems of crustal dynamics in Japanese islands, and also whether or not rocks can be deformed by such low differential stresses (i.e. c. 1 MPa), if this estimate of flow stresses is in fact correct.

We have been studying deformation processes and mechanisms in rocks at brittle ductile transition conditions, which seem to control the strength of upper crust, based on microstructural analyses in naturally deformed rocks. Deformation behaviors at the conditions of brittle-ductile conditions can be observed in metamorphic rocks formed at great depths, because these are elevated from ductile to brittle regions across the depth of brittle-ductile transition. For example, pervasive semi-brittle micro-faulting occurred in quartz schist from the Sambagawa metamorphic rocks at brittle ductile transition conditions. Here, although quartz layers were truncated by micro-faults, very-fine grained dynamically recrystallized quartz grains were also formed along them (i.e. micro-shear zone), suggesting components of ductile deformation. Further, very-fine-grained white mica was formed along the micro-faults, suggesting fluid percolation. With increasing deformation, the density of micro-faults increased, accompanied by the widening of micro-shear zones and associated decrease of the volume fraction of undeformed lenses. Perhaps, dissolution-precipitation creep dominated in micro-shear zones, having led to stress concentration in undeformed lenses, which were subsequently fractured. It is inferred that the rocks became softened with the increasing volume fraction of micro-shear zones.

Similarly, broken and displaced quartz detrital grains are observed in meta-sandstones deformed at brittle-ductile conditions from the Kamuikotan metamorphic rocks, northern Japan. Fibrous overgrowth of quartz occurred between the broken and displaced fragments of quartz, which appears as if these grains themselves restore the original shape. On the other hand, embayment occurred toward quartz grain sides at the boundary between quartz and white mica grains, suggesting dominant dissolution of quartz at this type of boundaries. Further, cataclasites formed along the Median Tectonic Line at the conditions of brittle-ductile conditions in the Cretaceous, and new minerals precipitated from fluids in the space created by fracturing and displacement of protolith forming minerals. The fracturing is accompanied by element migration via fluids, thus the degree increases with increasing degree of fracturing. In conclusion, deformation occurred by dissolution-mass transfer-precipitation assisted by fracturing under the conditions of brittle-ductile transition, by which significant weakening can be generated in rocks.

**Keywords:** differential stress in the upper part of crust, strain softening, micro-fracturing, dissolution, mass transfer, precipitation of minerals

## Detecting the stress condition at a fault from focal mechanism: application to the 2013 Awaji Island earthquake (M6.3)

MATSUMOTO, Satoshi<sup>1\*</sup> ; KATAO, Hiroshi<sup>2</sup> ; IIO, Yoshihisa<sup>2</sup>

<sup>1</sup>Institute of Seismology and Volcanology, Kyushu Univ., <sup>2</sup>Disaster Prevention Research Institute, Kyoto Univ.

One of the approaches used to evaluate potential of an earthquake occurrence is the detection of stress concentration at an earthquake fault. Stress fields in stages for pre- and post-seismic event will be different from one another. However, this change cannot provide information regarding the potential for an earthquake to occur. Here, we propose a detection method for stress conditions that uses focal mechanism data. The condition can be defined both by background stress and by a moment tensor equivalent to the stress concentration. We apply this method to actual focal mechanism data from the Awaji Island earthquake (M6.3), Japan, and show the presence of stress concentration around the earthquake fault before the mainshock. In addition, the regional shear stress is shown to be  $\sim 25$  MPa in the area, implying that the stress level is still high, thus the potential for further seismicity in the area could be high.

Keywords: stress field, earthquake fault, focal mechanism

## A friction to flow constitutive law and its application to a two-dimensional modeling of earthquake cycles

SHIMAMOTO, Toshihiko<sup>1\*</sup> ; NODA, Hiroyuki<sup>2</sup>

<sup>1</sup>Institute of Geology, China Earthquake Administration, <sup>2</sup>JAMSTEC

Establishment of a constitutive law from friction to high-temperature plastic flow has long been a task for solving problems such as modeling earthquakes and plate interactions. A linear combination of friction and flow laws disagrees with experimental data. Here we propose an empirical constitutive law that describes this transitional behavior with good agreements with experimental data on halite shear zones. A complete spectrum of properties including steady-state and transient behaviors can be predicted if friction and flow parameters are known. We show numerical models of seismic cycles of a fault across the lithosphere as an application. Our friction-to-flow law merges brittle-plastic Christmas-tree strength profiles of the lithosphere and rate-dependency fault models used for earthquake modeling on a unified basis. Conventionally strength profiles were drawn assuming a strain rate for the flow regime, but we emphasize that stress distribution evolves reflecting the fault behavior. Previous fault models are revised based on our earthquake modeling. Seismic fault motion is followed by fault creep in the transitional regime and this explains pseudotachylites overprinted by mylonitic deformation, reported at various places in the world.

Keywords: Friction to flow constitutive law, Earthquake cycle modeling, Fault model, Lithosphere rheology, Mylonite, Pseudotachylite

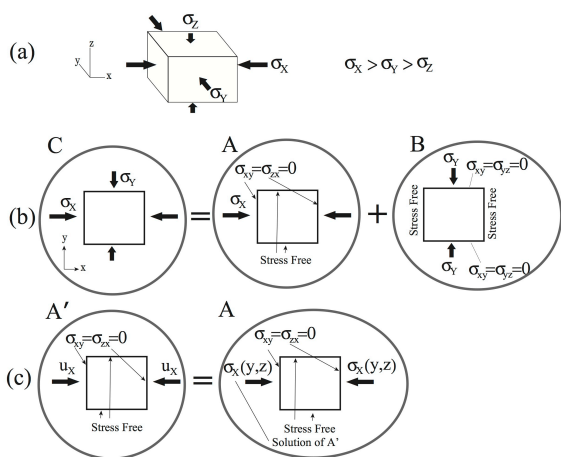
## A consideration about computation of tectonic stress field for inland thrust earthquake

MIYATAKE, Takashi<sup>1\*</sup>

<sup>1</sup>ERI, The Univ. of Tokyo

In the case of pure thrust earthquake, the driving stress system is expected to have been as shown in Fig. 1a. The stress in this figure is tectonic stress; thus, the lithostatic pressure  $\sigma_V (= \rho gh)$  must be added. The tectonic system (Fig. 1a) can be decomposed into two systems (Fig. 1b): A and B. The functional forms of  $\sigma_X$  and  $\sigma_Y$  are unknown. The assumption that that  $\sigma_X$  is uniform in system A causes almost uniform shear and normal stresses on the fault. Strength (peak stress) and dynamic friction can be estimated when  $\sigma_V (= \rho gz)$  is added to the fault normal stress and the resultant normal stress is multiplied by static and dynamic frictional coefficients. Under these conditions, we found a large stress drop in the shallower parts and minimum strength excess at the free surface. This suggests that the earthquake rupture must have started at the surface and that the stress drop must have been the highest at the ground surface. These results can be avoided if the stress  $\sigma_X$  is assumed to increase with depth. The depth dependency is related to variations in elastic constants. The stress field in this region likely originated primarily from plate motions. Therefore, we selected the displacement boundary condition  $u_X = u_0$ , which correspondings to system A' in Fig. 1c. It should be noted that other displacement components were not fixed, but free stress conditions (except the  $\sigma_{xx}$  component) were imposed according. After solving the stress field imposing the above boundary condition, the resultant stress component  $\sigma_{xx}$  was added on the boundary of  $x = \pm L_X$  as a further boundary condition. The solution is the same as the problem in which the boundary condition is imposed. Taking the linear elasticity into account, the target solution can be estimated by superposing solutions A and B in Fig. 1b. System A is equivalent to system A'. The effect of system B on fault normal and shear stress is expected to be negligible, because these stresses are exactly zero for a uniform structure. We estimated such effects in a heterogeneous structure by assuming that the value of  $\sigma_{-Y} = \sigma_{yy}(z)$  on the boundary of  $y = \pm L_y$  is the same as  $\sigma_{xx}(z)$  on the boundary of  $x = \pm L_x$ . We found system B to exert little effect (less than 5%) on the stress components of  $\sigma_{zx}$ ,  $\sigma_{xx}$ , and  $\sigma_{zz}$ . Thus, B had little effect on fault normal and shear stress on the fault plane, where  $\sigma_{xx}(z)$  is the averaged stress component along the y-axis on the corresponding boundaries. Based on the condition of thrust earthquake that  $|\sigma_X| > |\sigma_Y| > |\sigma_Z|$  (Fig. 1a), the above mentioned  $\sigma_{zx}$ ,  $\sigma_{xx}$ , and  $\sigma_{zz}$  were overestimated in our study. Thus, we can ignore the effects of system B.

Keywords: inland earthquake, stress field



## Aftershock activity of the 2008 Iwate-Miyagi inland earthquake suppressed by stress shadow of the 2011 Tohoku earthquake

SUZUKI, Yuhei<sup>1\*</sup> ; TODA, Shinji<sup>2</sup> ; YOSHIDA, Keisuke<sup>1</sup> ; OKADA, Tomomi<sup>3</sup>

<sup>1</sup>Department of Geophysics, Graduate school of Science, Tohoku university, <sup>2</sup>International Research Institute for Disaster Science, Tohoku university, <sup>3</sup>Research Center for Prediction of Earthquakes and Volcanic Eruptions, Tohoku university

The 2011 Tohoku-oki M9 earthquake has increased seismicity rates in many areas in eastern Japan. Several papers already sought the triggering mechanism to static stress change (Toda et al., GRL, 2011), dynamic stress change (Miyazawa et al., GRL, 2011) and pore fluid pressure change (Terakawa et al., EPSL, 2013). In contrast, areas where seismicity rate evidently dropped are restricted to the vicinity of the 2011 rupture zone (Kato & Igarashi, GRL, 2012), the 2004 Chuetsu aftershock zone (Hirose & Toda, SSJ fall meeting, 2011) and the 2008 Iwate-Miyagi inland earthquake aftershock zone (Suzuki & Toda, AGU fall meeting, 2013). Suzuki and Toda (2013) claim that the cause of seismic quiescence is Coulomb failure stress (CFF) decrease due to the 2011 event. However, a small quantity of focal mechanisms prevents them to confirm the mechanism.

In this study, we determine 4106 newly focal mechanisms in the area and develop a model to explain spatio-temporal seismic evolution. To estimate the focal mechanisms, we employ the method of Hardeback & Shearer (BSSA, 2002) using first motion of P-wave, provided by the campaign data by the Group for the Aftershock Observations of the 2008 Iwate-Miyagi inland Earthquake and Japan Nuclear Energy Safety Organization (JNES) in addition to the stationary data from Hi-net and F-net by NIED. Besides, we use F-net moment tensor solutions (VR?80%) and JMA focal mechanisms together with our estimates. Most of the focal mechanisms are strike-slip or thrust fault type and the distribution of ratio of strike-slip type to thrust type is spatially heterogeneous. We find several distinctive seismic clusters from all the distribution. Seismicity in two clusters in southern rupture zone of the 2008 event has been clearly decreased by the 2011 event. We calculate  $\Delta$ CFF on all nodal planes as a proxy for background faults using a Tohoku-oki coseismic slip model given by Iinuma et al. (JGR, 2012) in an elastic half-space of Okada (BSSA, 1992). Apparent friction coefficient,  $\mu'$ , is assumed to be 0.0, 0.4 or 0.8. In the case of  $\mu' = 0.0$ , 80% of  $\Delta$ CFF resolved on all nodal planes are negative and over 50%  $\Delta$ CFF are negative in the case of  $\mu' = 0.8$ . In the distinctive clusters mentioned above, ratios of the negative  $\Delta$ CFF far exceed above overall average.

Seismic response to  $\Delta$ CFF is formulated by Dieterich (JGR, 1994) based on the rate-and state-dependent friction law. The physics-based model can reproduce the empirical Omori's aftershock decay after a stress step controlled by several parameters. In this study, we estimate reference seismic rate from an average number of earthquakes from 2000 to the 2008 mainshock,  $\Delta$ CFF associated with the 2008 mainshock, stressing rate, product of constitutive parameter and normal stress on a fault plane ( $A\sigma$ ) estimated from the aftershocks occurred until the Tohoku-oki earthquake. Using these parameters, we calculate seismic time series from all the calculated  $\Delta$ CFF by the Tohoku-oki earthquake, and then compare the observation with the average of all time-series curves. As a result, the models increase seismicity rate at the Tohoku-oki earthquake, which is inconsistent with the observation. We seek that reasons for mismatch between our model and observation to (i) the paucity of aftershock hypocenter data because of detectability decrease immediately after the Tohoku-oki earthquake, (ii) change in stressing rate due to the post-seismic deformation of the Tohoku-oki earthquake, (iii) reduction of friction coefficient due to fluid injection and/or pore pressure change on fault planes.

**Acknowledgments.** We are grateful to JMA and NIED for hypocenter list and fault plane solutions. We also thank the regional campaign data given by the Group for the Aftershock Observations of the 2008 Iwate-Miyagi inland Earthquake and JNES.

**Keywords:** induced earthquake, static Coulomb failure stress change, rate-and state-dependent friction law, seismic quiescence

## Improvement of gas medium triaxial apparatus derived from thermal fluid analysis

SAOMOTO, Hidetaka<sup>1\*</sup>; SHIGEMATSU, Norio<sup>1</sup>

<sup>1</sup>Active Fault and Earthquake Research Center, AIST

A huge amount of effort has used to be required for trial productions during the development of experimental apparatus. Since such trial productions generally consume vast time period and cost, the reduction of them is now a significant issue. Numerical modeling such as the finite element simulation (FE) is widely used to reduce them in various engineering fields.

Gas medium triaxial apparatus is widely used to determine the mechanical properties of rocks precisely at higher temperature. However, there has been a limitation for the use at the higher temperature in Japan due to the thermal design. In this presentation we plan to improve the gas-medium triaxial apparatus derived from thermal fluid analysis based on the finite element simulation.

Here, the governing equations for thermal fluid analysis consist of the heat conduction equation, the Navier-Stokes equation and the equation of state. By solving those equations simultaneously, we obtain important physical quantities such as temperature distribution, fluid velocity field, delay of heating, etc. The knowledge derived from the computer simulations are: (1) The argon gas flow hardly has any relation with the temperature distribution on solid materials. (2) The temperatures of adiabatic materials placed near the heat sources are below the maximum operating temperature. (3) A large thermal gradient is observed close to the plastic O-ring.

Based on above results, we have attained valuable improvement policies such as replacement of materials, improvement of radiation factor on the copper jig, etc.

Keywords: heat, fluid, Navier-Stokes, equation of state, gas medium triaxial apparatus

## The crustal structure beneath northern Mino region, central Japan revealed by seismic reflection survey

EMOTO, Tomoko<sup>1\*</sup> ; TSUMURA, Noriko<sup>1</sup> ; FUJIWARA, Akira<sup>2</sup> ; ABE, Susumu<sup>2</sup> ; KOJIMA, Satoru<sup>3</sup> ; KANO, Ken-ichi<sup>4</sup> ; OMURA, Kentaro<sup>5</sup> ; TAKEDA, Tetsuya<sup>5</sup> ; ASANO, Youichi<sup>5</sup> ; OBARA, Kazushige<sup>6</sup> ; ITO, Tanio<sup>7</sup>

<sup>1</sup>Chiba University, <sup>2</sup>JGI, Inc., <sup>3</sup>Gifu University, <sup>4</sup>Shizuoka University, <sup>5</sup>NIED, <sup>6</sup>ERI, The University of Tokyo, <sup>7</sup>Teikyo-Heisei University

The Nobi earthquake, the largest inland earthquake in Japan, occurred in 1891 in northern Mino district, central Japan. In that region, most active faults run nearly parallel to the NW-SE trending hinge of megakink structure of the Mino belt (Kano et al., 1990). It is remarkable that the upper surface of the subducting Philippine Sea Plate (PSP) also shows a NW-SE trending broad anticlinal form whose axial zone is deeply situated almost below the hinge of the megakink. However we don't have sufficient information about seismic structure of whole crust and the uppermost mantle beneath this region to discuss influence of subducting plate on surface deformation.

To elucidate the seismic structure, a seismic reflection survey was carried out in October in 2009 (Komada et al., 2010). The survey line intersected at high angle with Neodani faults zone. We applied the seismic reflection method to the shot records of this survey and got seismic profiles of whole crust and the uppermost mantle.

We found reflectors having 2 s duration around 10 s two way travel time (TWT) in the seismic profiles. These waves occurred at TWT 9 - 11 s in the southwestern part of the study area, and at TWT 10 - 12 sec in the northeastern part. Applying depth conversion, the reflectors are located in the depth of 28 - 37km in the southwestern part, and of 32 - 39km in the northeastern part. We can clearly see that the depth of the reflection waves in the southwestern side of the Neodani fault zone are shallower than that in the northeastern side. Further the depth varies just beneath the Neodani fault zone. These feature correspond with the result of velocity analysis in the study area (Emoto et al., 2012).

Those reflection waves are interpreted as a lower crustal lamination by comparing with the result of previous seismic profiles. The geometry of laminated lower crust is consistent with the trend of the displacement on Nodani Fault Zone of Nobi earthquake. The fact might show that the difference of the reflectors depths between the southwestern and the northeastern side is caused by fault displacement and it might reach the whole crust. In southwestern part of study area, the depth of top boundary of the Philippine Sea plate (PSP) was estimated from travel time tomography in the previous studies. Its depth is equivalent in the lower limit of the lower crustal lamination. Then it might show that the crust of the land plate contacts on the subducting PHP beneath the northern Mino district.

Keywords: lower crust, Neodani fault, reflection seismic survey, Philippine Sea Plate, northern Mino region

## Temporary observation of micro earthquakes in the northern Ibaraki prefecture by using commercially-supplied IC recorder

SAITO, Keisuke<sup>1\*</sup>

<sup>1</sup>KEISUKE SAITO, <sup>2</sup>KEI KATSUMATA

In case of estimate focal mechanism solutions by using P-wave first-motion polarity data, a dense seismic observation network is required. In this study we propose a new seismic observation system to record a P-wave first-motion polarity. The system consists of a seismometer with a vertical component that price is approximately ten thousand yen and a commercially-supplied IC recorder that price is approximately ten thousand yen. According to the specification of the IC recorder, the recordable frequency band is from 60 to 3400 Hz. We compare frequency characteristic of waveforms recorded in stations of National Research Institute for Earth Science and disaster Prevention ( NIED Hi-net ) and those recorded by using IC recorder. As a result we find that the IC recorder is able to record seismic waves that frequency band is from about 20 to 3400 Hz.

In this study, we conducted a temporary observation of micro-earthquakes for one month from August to September 2012 in the northern Ibaraki prefecture where many normal-faulting type events occur, and we addressed the effectiveness of the seismic observation system. The 29 seismic stations were deployed along a road so that it allows a deployment of many stations for a short time. After collecting the temporary stations, based on the P-wave first motion polarity, we estimated the focal-mechanisms by using HASH program (Hardebeck and Shearer, 2002). As a result, we obtain the 87 focal-mechanisms for micro-earthquakes occurred in the study area.

To test the accuracy of the focal mechanisms obtained in this study, we compared those with focal-mechanisms determined by Earthquake Research Institute, The University of Tokyo (ERI) temporary stations. We compared focal-mechanisms determined by ERI and Hi-net stations and focal-mechanisms determined by using IC recorder and Hi-net stations. We compare P axis and T axis for focal-mechanisms determined by ERI and Hi-net stations and determined by using IC recorder and Hi-net stations. As a result, nothing is difference of accuracy about focal-mechanisms between determined by ERI and Hi-net stations and determined by using IC recorder and Hi-net stations, because of P axis T axis has almost same distribution on the focal sphere. We conclude that focal mechanisms determined by using IC recorder stations has almost same accuracy as those determined by a traditional three component seismometer.

## Modeling the viscoelastic deformation of the NE Japan arc after the 2011 Tohoku-oki earthquake

SHIBAZAKI, Bunichiro<sup>1\*</sup> ; NAKAI, Yoshihiko<sup>1</sup> ; MUTO, Jun<sup>2</sup> ; IINUMA, Takeshi<sup>3</sup>

<sup>1</sup>International Institute of Seismology and Earthquake Engineering, Building Research Institute, <sup>2</sup>Department of Earth Sciences, Tohoku University, <sup>3</sup>International Research Institute of Disaster Science, Tohoku University

The rheological structure of the Northeastern Japan arc crust and the upper mantle is heterogeneous along and transverse to the arc. Shibazaki et al. (2014) developed a model of the stress state of the Northeastern Japan island-arc crust using a finite element method with viscoelasticity and elastoplasticity. They reproduced several elongated low-stress regions transverse to the arc with viscous deformation that corresponds to hot fingers (high-temperature regions in the mantle wedge). The viscous relaxation process after the 2011 Tohoku-oki earthquake could be affected by the existence of low-viscosity regions caused by hot fingers. A three-dimensional (3D) finite element model was developed to investigate the viscoelastic deformation processes with heterogeneous viscosity distribution after the 2011 Tohoku-oki earthquake. The model considers the realistic crustal and mantle structures, viscoelasticity (Maxwell or Burgers rheology), and coseismic fault slip distribution obtained by Iinuma et al. (2012). For simplicity, only the elastic crust and viscoelastic mantle structure were considered. The westward movement near the trench and eastward movement in the inland region due to viscoelastic relaxation were reproduced, which are consistent with the observations. We also consider the local low viscosity region in the Northeastern Japan arc crust. In this case, extensional viscous strain concentrates on this region. We report the numerical results that take into account the realistic 3D heterogeneous viscosity distribution in the crust and the upper mantle beneath the Northeastern Japan island arc.

Keywords: 2011Tohoku-oki earthquake, NE Japan arc, Viscoelastic deformation

## Rheological phenomena of Zebra fault in South Africa goldmine by the 2011 Tohoku earthquake's surface waves

OKUBO, Makoto<sup>1\*</sup> ; OGASAWARA, Hiroshi<sup>2</sup> ; NAKAO, Shigeru<sup>3</sup> ; MURAKAMI, Osamu<sup>2</sup> ; ISHII, Hiroshi<sup>1</sup>

<sup>1</sup>TRIES, <sup>2</sup>Ritsumeikan Univ., <sup>3</sup>Kagoshima Univ.

The 2011 Tohoku earthquake was a huge earthquake. We can understand again its magnitude by large dynamic-strain observations. In general, fresh rock rupture will relieve  $10^{-4}$  strains at the source. On the other hand the 3.11 had unleashed more than  $10^{-5}$  dynamic strains to almost all of Japan. After these strain state changes, it activated seismic swarm events of Japan. On the other hand, more than  $10^{-7}$  dynamic strains had been also observed at the South Africa Republics distant from 14,000 km epicenter. Ritsumeikan university takes initiative of the projects 'Grant-in-aid : Multidisciplinary monitoring of preparation and generation of earthquakes at M2 sources in South African gold mines' and 'SATREPS: Observational Studies in South African Mines to Mitigate Seismic Risks'. In the project, we can come, we can see, we can observe at proximity micro-seismicity and/or strain field at 1-3 km depths of gold mine.

In this study, we analyzed dynamic strain records of 'Cooke4' mine, which caused by the 2011 Tohoku earthquake. Although static strain changes may be disturbed by mining activity, dynamic strain variations such as teleseismic waves and surface waves have been recorded clearly. We have estimated the strain field variations vicinity of zebra fault from two strain meter combination, and we obtained the result that dilatational strain in the fault and shear strain of both size of fault have changed by passing through the seismic waves. In presentation, we will discuss inactive fault vibration caused by teleseismic waves.

Keywords: Surface waves, Zebra fault, Dynamic strain, SATREPS

## Relationship between ESR signal intensity and grain size distribution in shear zones within the Atotsugawa fault system

FANTONG, Emilia bi<sup>1\*</sup> ; TAKEUCHI, Akira<sup>1</sup> ; KAMISHIMA, Toshio<sup>1</sup> ; DOKE, Ryosuke<sup>2</sup>

<sup>1</sup>Graduate School of Science and Engineering, University of Toyama, 3190 Gofuku, Toyama 930-8555., <sup>2</sup>Hot Spring Research Institute of Kanagawa Prefecture, 568 Iriuda, Odawara, Kanagawa 250-0031, Japan

Shear zones are zones of strong deformation within active faults and constitute significant sources of information on the seismogenic behavior of faults. The Atotsugawa fault system, which is in the Northern margin of the Hida Highland lies within a complex tectonic zone consisting of the Pacific plate, the Philippine Sea plate, the Amurian plate and the Okhotsk plate. This system consists of the Ushikubi fault, the Atotsugawa fault and the Mozumi-Sukenobe fault. The study of deformational fabrics and features within these shear zones can give more clarification on geodynamics of faults. Moreover, seismogenic behavior of a fault depends greatly on fault zone internal structure and fault rock constitutive properties. Although there are many studies on shear zone descriptions and deformational mechanisms, only few relate the description of cataclastic rocks (fault gouge) with Electron spin resonance (ESR) signals, which is based on the detection of paramagnetic defects in minerals produced by natural radiation that have accumulated for a long time and produces a characteristic signal detectable with an ESR spectrometer. By measuring the intensity of these trapped electrons, the rate of comminution and displacement of a fault can be clarified or envisaged. This study therefore focuses on the relationship between grain size distribution (sieve method) and ESR analysis, and rate of deformation with proximity to a slip plane.

Three shear zones from both the Atotsugawa and the Ushikubi fault were investigated. Sieve analysis and photomicrographs from thin sections revealed that grain size becomes coarser away from the slip plane (e.g. Fig.1a and Fig.2) indicating that the effect of displacement is more close to the slip plane. However, an irregular pattern in the grain size distribution was equally observed in some of the shear zones. This could be due to multiple phases of deformation. ESR analysis showed a decreasing trend in the intensity of signals toward the fault plane (Fig. 1b and Fig. 2) indicating that the rate of comminution was more intense towards the slip plane. However, the decreasing trend in ESR signal intensity with proximity to the slip plane was not observed in some of the shear zones probably due to multiple phase of deformation as indicated by the anatomizing faults in the shear zone II of the Ushikubi fault.

Results from ESR analysis suggest that samples closest to a slip plane will have low signal intensity than those further away while grain size distribution analyses indicates that samples closest to a slip plane become finer due to intensive crushing that is always associated with large displacement during fault activities.

Keywords: Active fault, Shear zones, ESR signal intensity, Grain size distribution, Atotsugawa fault system

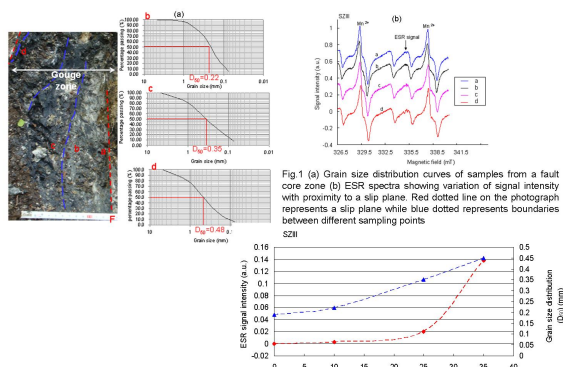


Fig.2: Relationship between ESR signal intensity and Grain size distribution. The intensity of ESR signal increases with proximity to the slip plane. By plotting the  $D_{50}$  of samples taken with proximity to the slip plane, it can be seen that grain size becomes coarser away from the slip plane.

## Physico-chemo-mechanical processes in a slip zone during the 1999 Taiwan Chi-Chi earthquake

HIRONO, Tetsuro<sup>1\*</sup> ; KAMEDA, Jun<sup>2</sup> ; KANDA, Hiroki<sup>1</sup> ; TANIKAWA, Wataru<sup>3</sup> ; ISHIKAWA, Tsuyoshi<sup>3</sup>

<sup>1</sup>Osaka Univ., <sup>2</sup>Hokkaido Univ., <sup>3</sup>JAMSTEC

To investigate the physicochemical processes of minerals during and after slip of the 1999 Taiwan Chi-Chi earthquake, we analyzed the mineral assemblages in the Chelungpu fault by using quantitative X-ray diffraction together with scanning and transmission electron microscope observations. In the primary slip zone, we found markedly low contents of quartz and clay minerals and large amounts of amorphous particles ranging in size from submicrometer to several tens of nanometers. Milling and heating experiments with host-rock samples indicated that these mineralogical changes are due to comminution and frictional heat during slip. Moreover, the changes may affect slip behavior through a mechanism such as thermal pressurization assisted by clay-mineral dehydration. In addition, preservation of a high amount of amorphous fine particles can potentially be used to identify the slip zone of the latest earthquake on not only the Chelungpu fault but also on other faults.

Keywords: mechanochemical, amorphous

## Characterization of carbonaceous materials in the Taiwan Chelungpu fault by micro FTIR-Raman spectroscopies

MAEKAWA, Yuka<sup>1</sup> ; HIRONO, Tetsuro<sup>1\*</sup> ; YABUTA, Hikaru<sup>1</sup>

<sup>1</sup>Department of Earth and Space Science, Graduate School of Science, Osaka University

Coseismic slip during an earthquake induces frictional heating in fault zone. Determination of the temperature recorded in the fault is important for estimating the dynamic shear stress and displacement during the earthquake. Here we performed micro FTIR-Raman spectroscopic analyses of carbonaceous materials from the Taiwan Chelungpu fault, which slipped at the 1999 Chi-Chi earthquake. We also conducted heating experiments and friction experiments and analyzed by FTIR-Raman spectroscopies in order to investigate the effects of fast heating rate like frictional heating during earthquake. Based on the results of analyses, we discuss the capability as new temperature proxy during the earthquake.

Keywords: Taiwan Chi-Chi earthquake, carbonaceous materials, FTIR spectroscopy, Raman spectroscopy

## Frictional properties of ground dolerite gouges at low to high slip velocities

WADA, Jun-ichi<sup>1</sup> ; KITAJIMA, Hiroko<sup>2</sup> ; TAKAHASHI, Miki<sup>2</sup> ; OOHASHI, Kiyokazu<sup>1</sup> ; INOUE, Atsuyuki<sup>1</sup> ; KANAGAWA, Kyuichi<sup>1\*</sup>

<sup>1</sup>Graduate School of Science, Chiba University, <sup>2</sup>Active Fault and Earthquake Research Center, Geological Survey of Japan

We investigated how frictional properties of ground dolerite gouges change according to grinding time. We have ground crushed and sieved grains (smaller than 500 microns) of dolerite using an automated agate mill for 10 minutes, and 6, 12, 24, 36, 48 and 60 hours. Quantitative XRD analyses indicate that amorphous phase is absent in the gouge ground for 10 minutes, but its amount increases up to 40 wt% with grinding time. Gouges ground for more than 6 hours contain abundant spherical grains composed of amorphous nano-particles. Such spherical grains are likely formed by accretion of amorphous nano-particles through their electrostatic attraction and moisture-induced binding, as accretionary lapilli. In fact, thermogravimetric analyses reveal that the amount of water adsorbed increases up to 14 wt% with grinding time in accordance with the amount of amorphous phase.

We have then conducted friction experiments on the ground dolerite gouges using a rotary shear apparatus at room temperature, a normal stress of 2 MPa, and constant slip velocities ranging from 20 micrometers/s to 1.3 m/s. At slip velocities slower than or equal to 1.3 cm/s, temperatures of gouges were lower than 70 degrees C, and steady-state friction coefficients range from 0.59 to 0.75, which tend to be higher for gouges with longer periods of grinding time at the same slip velocity. At the slip velocity of 4 cm/s, temperatures of gouges were over 100 degrees C, and steady-state friction coefficients range from 0.60 to 0.66, the difference of which among gouges with different periods of grinding time was relatively small. At slip velocities faster than or equal to 13 cm/s, however, temperatures of gouges reached higher than 180 degrees C, and steady-state friction coefficients dramatically decreased with increasing slip velocity. In addition, steady-state friction coefficients at the same slip velocity tend to be lower for gouges with longer periods of grinding time.

Such frictional properties of ground dolerite gouges depending on grinding time can be explained by the amount of water adsorbed in amorphous gouge. At slip velocities slower than or equal to 1.3 cm/s, temperatures of gouges were lower than 100 degrees C so that water adsorbed in amorphous gouge was retained. Thus, gouges ground for longer periods of time with larger amounts of adsorbed water likely became stronger in steady-state friction due to capillary bridging between amorphous gouge particles. At the slip velocity of 4 cm/s, temperatures of gouges became higher than 100 degrees C so that dehydration occurred from the amorphous gouge, which resulted in a small difference in steady-state friction among gouges with different periods of grinding time. At slip velocities faster than or equal to 13 cm/s, the moisture production rate from the dehydrated amorphous gouge was likely faster than its leak rate, which resulted in an increase in pore pressure in the gouge layer and hence a decrease in frictional strength. Thus, gouges ground for longer periods of time with larger amounts of adsorbed water became weaker in steady-state friction due to larger increases in pore pressure.

Keywords: dolerite, ground gouge, frictional properties, amorphous gouge, moisture adsorption

## Modelling of the postseismic deformation of the 2011 Tohoku Earthquake based on land and seafloor geodetic observations

IINUMA, Takeshi<sup>1\*</sup> ; HINO, Ryota<sup>1</sup> ; KIDO, Motoyuki<sup>1</sup> ; SUN, Tianhaozhe<sup>2</sup> ; WANG, Kelin<sup>3</sup> ; OHTA, Yusaku<sup>4</sup> ; OSADA, Yukihito<sup>1</sup> ; FUJIMOTO, Hiromi<sup>1</sup> ; INAZU, Daisuke<sup>5</sup>

<sup>1</sup>International Research Institute of Disaster Science, Tohoku University, <sup>2</sup>Victoria University, <sup>3</sup>Geological Survey of Canada, <sup>4</sup>Graduate School of Science, Tohoku University, <sup>5</sup>National Research Institute for Earth Science and Disaster Prevention

On 11 March 2011, the 2011 off the Pacific coast of Tohoku Earthquake (M 9.0, hereafter Tohoku Earthquake) occurred on the plate boundary between the subducting Pacific and overriding continental plates. Terrestrial and seafloor geodetic observations on and around the Japanese Islands has been clearly detecting postseismic deformation associated with the Tohoku Earthquake, although three years have passed since the main shock. Inuma et al. (2013, IAG Scientific Assembly) reported that just considering elastic response to the interplate coupling and postseismic slip on the plate boundary is insufficient to investigate the mechanical process of the postseismic deformation. We must take the inelastic deformation such as viscoelastic relaxation into account.

To tackle this problem, we estimated the displacement due to the viscoelastic relaxation by using a FEM model that includes subducting oceanic slab, difference of the viscosity between the continental and oceanic mantle, and high viscosity at the mantle wedge. The coseismic slip model based on the terrestrial and seafloor geodetic data (Inuma et al., 2012) is used to initialize the viscoelastic relaxation process. After subtracting displacements due to the large aftershocks and viscoelastic relaxation from the original displacement time series data that are measured not only with the terrestrial GPS but also GPS/Acoustic ranging and vertical displacements observed by using Ocean bottom pressure gauges, we estimated the spatial and temporal evolution of the postseismic slip distribution on the plate interface by applying a time-dependent inversion method devised by Yagi and Kikuchi (2003).

The result of FEM calculation shows that westward displacements at seafloor sites are accounted for by viscoelastic relaxation process. However, eastward movements larger than the observed displacements at the most terrestrial GPS stations are predicted by means of the FEM model. Therefore, postseismic slip (or recovery of the interplate coupling) needs account for onshore westward displacement.

One of two areas where normal-fault-type slip distributes is estimated by applying the time dependent inversion analysis to the displacement time series as well as the result of the inversion when we assume a spherical layered structure to calculate the displacements due to the viscoelastic relaxation. But, the locations of the normal-faulting areas are different. When we use the layered structure, the area is mapped inside the main rupture area of the M9 main shock. On the other hand, normal-fault-type slip at a portion of the plate boundary deeper than the coseismic main rupture area is estimated when we calculate displacements due to the viscoelastic relaxation by means of our FEM model. Since such normal faulting areas can be regarded as the patches on the plate boundary where interplate coupling occur, it is essential to estimate the locations and rates of the slip accurately to consider the frictional character on the plate interface. Therefore we need reduce and exclude the dependency of the postseismic slip distribution with respect to the estimation of crustal deformation due to the viscoelastic relaxation. We will examine and improve rheological structure that is included in the FEM model, and will present results of further investigation at the meeting.

**Keywords:** The 2011 off the Pacific coast of Tohoku Earthquake, Postseismic deformation, Viscoelastic relaxation, Postseismic slip, GPS, Seafloor crustal deformation

## Scale dependency of rock friction strength revealed by large scale biaxial friction experiment

YAMASHITA, Futoshi<sup>1\*</sup>; FUKUYAMA, Eiichi<sup>1</sup>; MIZOGUCHI, Kazuo<sup>2</sup>; TAKIZAWA, Shigeru<sup>3</sup>; KAWAKATA, Hironori<sup>4</sup>

<sup>1</sup>NIED, <sup>2</sup>CRIEPI, <sup>3</sup>Tsukuba Univ., <sup>4</sup>Ritsumeikan Univ.

In order to bridge a scale-gap between natural earthquakes ( $\sim 10^3$  m) and laboratory experiments ( $\sim 10^{-2}$  m), we carried out biaxial friction experiments using meter-sized rock specimens. We used a pair of Indian gabbro, whose nominal contact area was  $1.5 \times 0.1$  m<sup>2</sup>. The experiments were conducted under conditions with loading velocities from  $10^{-4}$  to  $3 \times 10^{-2}$  m/s and with normal stress of 1.3, 2.7 and 6.7 MPa. The normal and shear loads were measured with load cells. Hereafter, we refer the shear load divided by the normal load as the friction coefficient. It is well known that the rock friction has dependency on slip velocity at high slip velocity. We observed a similar tendency in the present experiments; the friction coefficient is almost constant ( $\sim 0.75$ ) at low loading velocities ( $10^{-4}$  to  $10^{-3}$  m/s), whereas it falls suddenly at the loading velocity of  $10^{-2}$  m/s approximately. This feature is consistent with the results using small rock specimens whose dimension is on the order of  $10^{-2}$  m (e.g. Di Toro *et al.*, 2011, Nature). It should be noted that the velocity weakening characteristics of rock friction is first confirmed on meter-sized rock. However, we found that the measured friction coefficients show weak dependency on normal stress, which suggests that the slip velocity is not a unique factor controlling the rock friction strength. On small sized rock specimens, dependency of the friction coefficient on work rate was reported; the friction coefficient is almost constant at low work rates, whereas it becomes smaller with approaching to natural conditions (e.g. Di Toro *et al.*, 2011; Mizoguchi and Fukuyama, 2010, Int. J. Rock Mech. and Min. Sci.). We investigated this relationship using the present data, and found a sudden and clear reduction of the friction coefficient at the work rate higher than  $10^{-2}$  MJ/m<sup>2</sup>s. The clear dependency of the friction on the work rate indicates that the weakening property of rock friction is governed by the work rate rather than the slip velocity. Di Toro *et al.* (2011) suggested that the work rate is proportional to a rate of temperature increase on a fault and the heating causes various transitions of rock mineral properties, which leads to the frictional weakening. In the present experiments, similar mechanisms should work and weaken the fault strength. However, we found that the meter-sized rock friction starts to decrease at the work rate one order of magnitude lower than that of the small gabbro specimens. This difference may come from the heterogeneity of the shear stress on the fault. From the point of view, we calculated heterogeneous stress distribution on the simulated fault produced by the present apparatus, and then, we estimated the weakening property of macroscopic friction depending the work rate under the estimated stress condition. We further estimated the weakening property in the case that additional stress heterogeneity was given on the fault surface. The results reveal that stronger stress heterogeneity can make more decrease in the macroscopic friction, which suggests that the rock friction has scale dependency, because such spatial heterogeneity will become strong in larger scale.

Keywords: Rock friction, Biaxial friction experiment, Scale dependency, Work rate

## Graphite-bearing pseudotachylytes in metasediment: Implication for CO<sub>2</sub> degassing by oxidation of graphite

NAKAMURA, Yoshihiro<sup>1\*</sup> ; MADHUSOODHAN, Satish-kumar<sup>2</sup> ; TOYOSHIMA, Tsuyoshi<sup>2</sup>

<sup>1</sup>Graduate School of Science & Technology, Niigata University, <sup>2</sup>Department of Geology, Faculty of Science, Niigata University

Graphite in fault rocks has important role in controlling the redox states in COH fluid, and many researchers have pointed out that the behavior of fluid in pore water or hydrous minerals dramatically change the physical and chemical property of fault rocks. Recently, the CO<sub>2</sub> degassing, from possible biogenic sources, along the faults is monitored in various active faults (e.g. Lewickie and Brantley, 2000). It is expected that the behavior of graphite in fault rocks play a key role about the fluid composition and the physicochemical properties. Here we present a detailed analysis of graphite found in pseudotachylyte and discuss the relationship between graphite and fluid during earthquake activity.

Graphite-bearing pseudotachylyte in Hidaka metamorphic belt, Hokkaido, Japan was examined using SEM, EMPA, and XRD. In pseudotachylyte-bearing cataclasite, melt-induced textures such as biotite microlites, shell textures of Fe-oxide, flow textures, spherulites and vesicles in Fe-oxide are observed. On the basis of microtextures, mineral assemblages of melted and survived minerals, pseudotachylytes are divided into two types; Pst I and Pst II. The matrix of Pst I is composed of sanidine, hematite and vesicles in Fe-oxide, and plagioclase and quartz are remained. These observations suggest that they are solidified from silicate melts by dehydration of biotite at around 700 - 1150 degree Celsius based on the experimental data. In addition, we can also deduce the stability of biotite and graphite in silicate melts of Pst I from the reaction of biotite equilibria on the T-fO<sub>2</sub> plane at 200MPa based on the experimental data of graphite and biotite. Mineral assemblages of sanidine, hematite and volatile in vesicles are stable only in high fO<sub>2</sub> fields, suggesting fO<sub>2</sub> in the range of over 10<sup>-11</sup> at around 700 degree Celsius by frictional melting of Pst I phase. In this phase, graphite in Pst I is unstable and will be converted to COH fluid in silicate pseudotachylyte melts. On the other hand, in Pst II matrix, these phyllosilicates but also quartz, plagioclase and apatite are found to be melted or have formed embayment textures, whereas only zircon has survived. These data indicate that the Pst II has formed at a peak temperature of around 1200 - 1400 degree Celsius by the breakdown of plagioclase, sulfide and apatite. The graphite content in Pst II decrease from 1.5 wt.% to 0.9 wt.% with increasing degree of frictional melting and alter the δ<sup>13</sup>C values, which shows wide range of δ<sup>13</sup>C values between -20.9 and -33.1 permil, when compared with the δ<sup>13</sup>C values of graphite from associated fault rocks and host metamorphic rocks (-24.8 +/- 0.67 permil). These data suggest that the host graphite has been converted to the COH fluids and then a part of fluid deposited graphite are re-precipitated from COH fluid during isobaric cooling and other carbon expelled as COH fluid due to the oversaturated melt.

Thus it is evident that frictional melting and dehydration of sheet silicates during coseismic slip generates CO<sub>2</sub> gas by the oxidation of carbonaceous materials. During the transformation of cataclasite to pseudotachylyte the total carbon content has decreased by about 0.5 wt.%. Assuming a rock density of 2.7g / cm<sup>3</sup>, the fusion of 10<sup>-3</sup> m<sup>3</sup> (i.e. 1mm thickness × 1m<sup>2</sup> fault plane) of cataclasite into Pst II releases 50g of excess CO<sub>2</sub>. The estimation of CO<sub>2</sub> degassing in this study is comparable to those reported by Famin et al. (2008). Thus, not only carbonates but also organic matters, including graphite and carbonaceous materials in crustal rocks, are potential to be a source of CO<sub>2</sub> by frictional melting, and the release of CO<sub>2</sub> into fault planes may drastically change the dynamic properties of flash fluid pressure and frictional properties of fault planes during seismic activity.

Reference: Famin. et al., 2008. EPSL, 265, 487-497. Lewicki. & Brantley., 2000. GRL, 27(1), 578.

Keywords: Graphite, Pseudotachylyte, Carbon isotopes, Frictional melting, CO<sub>2</sub> degassing

## Nanograins and carbonaceous film on a fault surface: an example from a fossil megasplay fault in the subduction zone

KITAMURA, Yujin<sup>1\*</sup> ; KIMURA, Gaku<sup>2</sup> ; KAMEDA, Jun<sup>4</sup> ; KOUKETSU, Yui<sup>5</sup> ; YAMAGUCHI, Asuka<sup>6</sup> ; KAGI, Hiroyuki<sup>5</sup> ; HAMAHASHI, Mari<sup>2</sup> ; FUKUCHI, Rina<sup>2</sup> ; HAMADA, Yohei<sup>3</sup> ; FUJIMOTO, Koichiro<sup>7</sup> ; HASHIMOTO, Yoshitaka<sup>8</sup> ; SAITO, Saneatsu<sup>3</sup> ; KAWASAKI, Ryoji<sup>2</sup> ; KOGE, Hiroaki<sup>2</sup> ; SHIMIZU, Mayuko<sup>2</sup> ; FUJII, Takenao<sup>9</sup>

<sup>1</sup>Dept. Earth and Environmental Sci., Kagoshima University, <sup>2</sup>Dept. Earth and Planet. Sci., University of Tokyo, <sup>3</sup>IFREE, JAMSTEC, <sup>4</sup>Dept. Nat. Hist. Sci., Grad. Sch. Sci., Hokkaido University, <sup>5</sup>Geochem. Research Center, University of Tokyo, <sup>6</sup>Atmosph. Ocean Research Institute, University of Tokyo, <sup>7</sup>Tokyo Gakugei University, <sup>8</sup>Kochi University, <sup>9</sup>SHIMADZU Corp.

Friction on the fault plane controls the behavior of faulting during seismic slip. Recent studies suggest that the frictional process on faults shows scale dependency. It is critically important to observe structures on the fault planes in various scales, especially in smaller scale in the sub-micron range. The roughness on fault planes has long been thought to hold fractal property, however, a recent work observed that a mirror fault plane, when examined up to nanometer-scale, does not obey self-affine roughness. Their observation revealed that the fault surface is coated by grains of several ten nanometers in diameter. In this abstract, we show a detailed observation of a glossy fault plane with striations sampled from drilled core of the Nobeoka Thrust taken by a scientific drilling project, the Nobeoka Thrust Drilling Project (NOBELL).

The NOBELL recovered cores with a total depth of 255 m penetrating the Nobeoka Thrust at 41 m below ground surface. The visual observation of the cores and the wireline log of the borehole clearly differentiate the hanging wall and the footwall. In this study, we analyzed a fault plane just below the Nobeoka Thrust main fault core on which gloss and striation develop using an integrated apparatus of Confocal Laser Scanning Microscope (CLSM) and Atomic Force Microscope (AFM). We also analyzed the sample surface applying Raman spectroscopy, Auger electron spectroscopy (AES) and organic component analysis using CHN coder (Yanaco MT-6).

The sample surface was imaged by the CLSM and AFM in various scale and its topography was obtained. The grains of several tens of nanometers in diameter were observed under the AFM image. This surface shows very flat surface with a height difference of ~80 nm in the imaged square ten micrometers on a side. The X-Z measurement by CLSM revealed an interface of around 1 micrometer below the surface. The interference fringe was observed at the rim of dark area. These facts suggest that the fault surface is covered by a thin film approximately 1 micrometer thick. The result of the Raman spectrometry indicates that the glossy fault plane material is rich in carbon. The organic component analysis of handpicked samples reported carbon fraction. Applying the AES, we recognized carbonaceous material on the true surface.

In conclusion, the questioned sample here appears to have been polished with fault frictional process so intensely that the surface grains comminuted to sub-micrometers and then a thin carbonaceous film developed. Such nanoscale structure observations in combination with the geometrical fractal property and chemical and surface analysis could provide further details of dynamic weakening during seismic slip.

Keywords: Nobeoka Thrust Drilling Project, subduction zone, accretionary prism, Shimanto belt, fault weakening, fault mirror

## Dynamic backthrust branching: role of barriers, and implications

XU, Shiqing<sup>1\*</sup> ; FUKUYAMA, Eiichi<sup>1</sup> ; BEN-ZION, Yehuda<sup>2</sup> ; AMPUERO, Jean-paul<sup>3</sup>

<sup>1</sup>NIED, <sup>2</sup>University of Southern California, <sup>3</sup>California Institute of Technology

Increasing evidence indicates that backthrusts may become active during or after megathrust ruptures in subduction zones, such as in Chile and Sumatra (Melnick et al., 2012; Singh et al., 2011). Previous studies of relevant mechanisms mainly focused on the interaction between forethrusts and the megathrust. Here we investigate through dynamic rupture simulations how backthrusts may be activated by megathrust ruptures in subduction zone environments. Assuming a single backthrust branch that is backward inclined to the compressional side of a continuous main fault, our results show that (1) fast speed and long propagation distance of the main rupture favor the activation of backthrust; (2) the outward propagation of the activated branch rupture interacts with the main fault mainly in the backward direction, while the tapered slip towards the branch end at the junction affects the main rupture behavior around the junction. We further assume an effective barrier for the main fault at the junction, motivated by the previous studies that barriers of various types (e.g. sharp fault bend, fault end, and transition region with increased basal friction) can also generate backthrusts during the long-term quasi-static process. Compared to the case without barrier, one prominent effect of the barrier is to arrest or delay the forward propagation of the main rupture, such that a resultant backward stress lobe as discussed in Xu and Ben-Zion (2013) can load the backthrust branch over a considerable time. This is particularly important for rupture activation along relatively immature backthrusts within sediments, where the nucleation time leading to the spontaneous propagation phase could be long, due to the large effective  $D_c$ , low frictional strength drop, or surface roughness. Indeed, our additional results confirm that the barrier model, although not always necessary, is more favorable for the activation of backthrusts with increased dynamic friction.

Our study has several implications: (i) it agrees with the quasi-static model based on the critical taper theory and limit analysis (Cubas et al., 2013) that an increase of basal friction towards the toe may statistically favor the activation of backthrusts near the up-dip limit of megathrust ruptures; (ii) there are also possibilities that backthrusts can still be activated by a propagating rupture, therefore the dynamic critical taper theory developed by Wang and Hu (2006) needs to be improved. In fact, not only the region near the up-dip limit of the seismogenic zone can be pushed into a critical state, successive region around the propagating rupture front within the seismogenic zone can also be temporarily stressed to failure and may even sustain a failure propagation along preexisting branches; (iii) it provides a specific example of compressional-side antithetic branching that can support the early speculation of fault behavior at junctions (King, 1986; Andrews, 1989).

Keywords: earthquake branching, friction of fault zones, fault barrier

## A possibility of a CM fault thermometer Part 1: Reflectances

OKAMOTO, Shiori<sup>1</sup> ; HOSHINO, Kenichi<sup>2\*</sup>

<sup>1</sup>Fac. Sci., Hiroshima Univ., <sup>2</sup>Grad. Sch. Sci., Hiroshima Univ.

The chemical kinetics of thermal maturation (coalification) of carbonaceous matters (CMs) in the oil and gas windows was well investigated by Burnham and his coworkers (e.g., Braun and Burnham, 1987). Burnham and Sweeney (1989) and Sweeney and Burnham (1990) introduced an activation energy distribution model for their rate law of dehydration and degassing of CMs and presented the correlation between the reflectance of CM in oil (%Ro, in percent) and the extent of the reaction (F) calculated from the rate law. They also noted that the rate law can be applied for heating rates ranging from laboratory conditions (1C/week), igneous intrusions (1C/day), and geothermal systems (10C/100 yr) to burial diagenesis (1C/10 m.y.).

On the other hand, Huang (1996) demonstrated that %Ro increased after a few days heating experiments and estimated a power rate law with  $t$  (second) to the power of 0.078. Muirhead et al. (2012) also examined that R1 ratios of Raman spectra of CMs increased after a few tens-seconds pyrolysis and proposed a power rate law with the power depending on  $T$  (K). However, those power rate laws were obtained from the experiments with bare CM fragments extracted from rocks. The power rate laws may not be applied to CMs in rocks, since we confirmed that the R1 ratios of CMs on surfaces of heated rock samples are larger than those inside the samples (details will be shown in the following presentation, Part 2).

Chips of pelitic rocks collected from the Shimanto accretionary complex were heated in an Ar-purged capsule in an oven. Since the oven takes 18-21 minutes to achieve pre-set steady temperatures and a few minutes for cooling down after heating, the following heating durations are regarded as those of constant temperatures during heating runs. The chips were heated at temperatures, 300, 350, 450, 550, 600 and 750C for 2, 5, 13 and 34 minutes.

Reflectance measurements and Raman spectroscopic analyses were taken for CMs in the chips of which surfaces were scraped off before polishing. The reflectances in air ( $R_a$ , not in percent) of CMs of unheated and heated chips and standards (SiC, GGG, YAG, sapphire and spinel) were obtained by analyzing gradations of G color of 24 bit color microphotographs taken by a reflecting microscope.

Averages of  $R_a$  of CMs in two unheated chips are 0.093 and 0.106, while an average of measured %Ro of the former is 1.99 of which  $F$  (extent of reaction) calculated from the correlation of Sweeney and Burnham (1990) is 0.618.  $R_a$  values of CMs in chips heated below 450C show no significant difference with those in unheated ones. This is consistent with that  $F$  simulated along the  $T$ - $t$  paths of the 300C, 350C and 450C for 34 minutes runs are 0.618, 0.618 and 0.622, respectively.

On the other hand, averages of  $R_a$  of CMs heated at 550C, 600C and 750C for 34 minutes are 0.121, 0.127 and 0.151, respectively, and their respective  $F$  values simulated are 0.742, 0.811 and 0.850. It is interesting that the averages of  $R_a$  for the runs at 750C for 2, 5 and 13 minutes are 1.47, 1.50 and 1.50, respectively. The all simulated  $F$  values for the last three runs are 0.850, the maximum extent of reaction of the rate law.

Although additional heating experiments of rocks with CMs of various initial maturities are needed, we may say from the above results that the CM fault thermometer is quite possible for high temperature faulting.

CM maturations due to heating indicated by Raman spectra will be shown in the following presentation (Part 2).

Keywords: carbonaceous matter, thermometer, fault, reflectance

## A possibility of a CM fault thermometer Part2: Raman spectra

OKAMOTO, Shiori<sup>1\*</sup> ; KOUKETSU, Yui<sup>2</sup> ; SHIMIZU, Ichiko<sup>3</sup> ; HOSHINO, Kenichi<sup>4</sup>

<sup>1</sup>Fac. Sci., Hiroshima Univ., <sup>2</sup>Univ. Tokyo, Grad. Sch. Sci., <sup>3</sup>Univ. Tokyo, Grad. Sch. Sci., <sup>4</sup>Grad. Sch. Sci., Hiroshima Univ.

A possibility of a CM fault thermometer Part2: Raman spectra

OKAMOTO, Shiori, KOUKETSU, Yui, SHIMIZU, Ichiko, HOSHINO, Kenichi

Key words: carbonaceous matter, thermometer, fault, Raman spectra

Parameters of Raman spectra of carbonaceous matters (CMs) have been widely used to estimate geological temperatures (e.g., Beyssac et al., 2002). Huang (1996) and Muirhead et al. (2012) proposed empirical power rate laws for CM maturation represented by reflectances in oil (%Ro) and R1 ratios of Raman spectra, respectively, from pyrolytic experiments of bare CM fragments extracted from rocks and meteorites, respectively.

To investigate a possibility of a fault thermometer by thermal maturations of CMs indicated by their Raman spectra, we conducted heating experiments of pelitic rock samples taken from Aki Group of the Shimanto accretionary belt in Kochi Prefecture, whose diagenetic temperature is estimated as ~180°C by vitrinite reflectances (Kitamura et al., 2014). The samples were heated at temperatures, 300, 350, 450, 550, 600 and 750°C for 2, 5, 13 and 34 minutes (see details in the previous presentation, Part 1).

It was indicated by comparing the spectra of CMs on surfaces of heated samples and those inside the sample that maturations of the former proceeded faster than the latter during heating. Therefore, in order to apply the thermal maturation of CM to a fault thermometer, it is needed to analyze CMs inside the samples.

It should be mentioned that micro-XRD analyses of CMs after the highest and longest heating run show no graphite peak. Hence, the maturation process during the present experiments is not graphitization but coalification.

Raman spectra of CMs show two major peaks, so-called G-band and D1-band peaks. Analytical results of the peaks indicate that certain parameters of Raman spectra of CMs remarkably vary even after low temperature (300 - 450°C) heating runs, whereas reflectances of CMs do not increase (see Part 1). The positions of G-band peak (Gp) and D1-band peak (Dp) tend to shift toward higher wave numbers with increasing heating durations in the all temperature runs. However, they do not shift monotonically with heating temperatures. Their wave numbers increase with the heating temperatures up to 450°C, then decrease at 550°C, and again increase up to 750°C.

Differences between Gp and Dp (Gp-Dp) also vary with heating temperatures and durations. Although they become smaller as the temperature is higher for the longest runs (34 minutes), this temperature dependency could not be seen for the other heating durations.

The ratio of intensity to full width at half maximum of the G-band peak (Gif) and that of the D1-band peak (Dif) decrease with increasing temperatures from 300°C to 450°C and from 550°C to 750°C, but increase from 450°C to 550°C. The both Gif and Dif do not show monotonic change with the heating durations.

As stated in the above, a simple indicator varying monotonically with heating temperatures and durations has not been found yet. However, we conceive that the sensitivities of the above indices of the Raman spectra to the thermal maturation of CM may show their potentials as a fault thermometer. Size dependencies of variations in some of the above indices with heating temperatures and durations and similarities of those of small-grained CMs and rims of large-grained ones also show a possibility to estimate both heating temperature and duration simultaneously by a size dependent thermometer, that is, a thermo-chronometer.

Keywords: carbonaceous matter, thermometer, fault, Raman spectra

## Mineral characteristics of the plate-boundary fault at the Japan Trench

KAMEDA, Jun<sup>1\*</sup> ; SHIMIZU, Mayuko<sup>2</sup> ; UJIIE, Kohtaro<sup>3</sup> ; HIROSE, Takehiro<sup>4</sup> ; IKARI, Matt<sup>5</sup> ; REMITTI, Francesca<sup>6</sup> ; MORI, James<sup>7</sup> ; CHESTER, Frederick<sup>8</sup> ; KIMURA, Gaku<sup>2</sup>

<sup>1</sup>Hokkaido University, <sup>2</sup>University of Tokyo, <sup>3</sup>Tsukuba University, <sup>4</sup>JAMSTEC, <sup>5</sup>University of Bremen, <sup>6</sup>Universita di Modena, <sup>7</sup>kyoto University, <sup>8</sup>Texas A&M University

The rupture and slip of the 2011 Tohoku-oki earthquake (Mw9.0) propagated along the plate-boundary megathrust and caused a huge tsunami. In order to elucidate the physical mechanisms responsible for such unexpectedly large slip of the fault, the IODP Exp. 343, the Japan Trench Fast Drilling Project (JFAST) was carried out one year after the earthquake. It succeeded in recovery of material from the plate boundary shear zone. We have examined how mineralogical properties vary through a depth-section including the plate boundary fault rock.

At the drill site (C0019E) where the large fault slip (>50m) occurred, a plate boundary shear zone was identified around 820 mbsf. X-ray diffraction (XRD) analysis revealed that abundance of smectite is markedly higher within the fault (60-80 wt.%) than in the surrounding host rocks, suggesting the shear zone material had a low intrinsic friction coefficient. Laboratory experiments on these materials demonstrated very low frictional state under various sliding conditions (Ujiie et al., 2013; Ikari et al., submitted)

In comparison, we also examined the mineralogy of reference material recovered on the outer rise of the Japan Trench (Site 436) during DSDP Leg 56. XRD analyses on the continuous series of cores found a marked anomaly in smectite abundance in the topmost ~5m section in the pelagic clay layer. Such a mineralogical feature compares well to that observed in the JFAST cores, and the smectite-rich horizon in the incoming sediments is inferred to be the localized deformation zone (decollement) when it arrives at the Japan Trench.

Keywords: Japan Trench, smectite, pelagic clay, Tohoku-oki earthquake

## Shock compression experiment of olivine- Part 3: pulverization occurred before frictional melting

OBATA, Masaaki<sup>1\*</sup>; MASHIMO, Tsutomu<sup>2</sup>; CHEN, Liliang<sup>2</sup>; ANDO, Jun-ichi<sup>3</sup>; YAMAMOTO, Takashi<sup>3</sup>; UEDA, Tadamasu<sup>1</sup>

<sup>1</sup>Graduate School of Science, Kyoto University, <sup>2</sup>Institute of Pulsed Power Science, Kumamoto University, <sup>3</sup>Graduate School of Science, Hiroshima University

Seismic waves may be generated by a rapid slip accompanied by a rapid drop of shear stress at or near the rupture tip that propagates rapidly. It is an important subject of seismology to identify the material changes occurring at the fracture tip. The inferred slip weakening has been ascribed to (1) frictional melting and lubrication, (2) thermal pressurization, (3) flash heating and melting, (4) powder lubrication, and the combinations of those above. High-speed rotary shear friction apparatus has played important roles in formulating the above hypothesis in the past, but in these experiments fault planes are already prepared and the formation of new fault planes cannot be studied. Moreover normal pressure cannot exceed few tens of mega-Pascal because of the instrumental limitation.

We performed a series of shock compression experiments using a keyed powder gun at Kumamoto University in order to investigate the focal mechanics of deep earthquakes. We used a single crystal of forsterite (Fo 94; shaped in a diskette of diameter 12 mm and thickness 3 mm nearly perpendicular to the olivine c-axis). The olivine disk is mounted in a steel capsule. Flyer speed was 1.5 km/s; applied pressure, 31 GPa; and shock wave velocity, ca. 7 km/s; particle velocity, ca. 1 km/s. After the shock experiment the capsule is recovered from the gun and cut perpendicular to the disk plane and polished thin sections were prepared for optical, SEM and TEM observations.

Many shear planes were generated. Olivine shows wavy extinctions and locally cataclastic texture. Shear planes (i.e., fault) are typically sharp and show up to 0.5 mm displacement. The TEM observation of the fault wall where 'spongy material is attached' revealed that the wall has a zonal structure as follows. Well inside the wall are developed densely spaced and tangles [001] screw dislocations. Outer 2-5 micron zone is polycrystalline olivine of average grain size 200-300 nm. The outermost rim is an aggregate of semi-rounded small olivine particles (ca. 200 nm) mounted in a matrix of glass of olivine composition, indicating that melting of olivine occurred here. It is important to note that the same dislocation structure remained in these olivine nano-particles. It is inferred from these structure that polygonization and pulverization of olivine has occurred before melting began near the fault wall (within a few microns). Such pulverization is possible at running fracture tip, where stress and strain rate are the highest (Reches and Dewers, 2005). The whole process occurred in a short duration of the order of 0.5 microsecond. The fracturing was probably propelled by the rapid sweep of shock waves running through the sample in our experiment. Apart from the role of the shock waves, the situation is considered to be analogous to natural earthquakes. Present experimental result sheds light on the long-lasting controversy on the formation of pseudotachylytes.

Reference: Reches and Dewers (2005) Gouge formation by dynamic pulverization during earthquake rupture. *EPSL* 235, 361-374.

Keywords: shock compression experiment, olivine, frictional melting, pulverization, fault, earthquake

## High-velocity frictional behaviors of dolerite under controlled pore-water pressure

TOGO, Tetsuhiro<sup>1\*</sup>; SHIMAMOTO, Toshihiko<sup>1</sup>; MA, Shenli<sup>1</sup>; YAO, Lu<sup>1</sup>

<sup>1</sup>Institute of Geology, China Earthquake Administration

High-velocity friction experiments on rocks with or without gouge have been conducted mostly under dry conditions and demonstrated dramatic weakening of faults at high velocities (e.g., Di Toro et al., 2011, *Nature*). Recent experiments under wet conditions (e.g., Ujiie and Tsutsumi, 2010, *GRL*; Faulkner et al., 2011, *GRL*) revealed very different behaviors from those of dry faults, but those experiments were done under drained conditions. Experiments with controlled pore pressure  $P_p$  are definitely needed to determine mechanical properties of faults under fluid-rich environments such as those in subduction zones. Thus we have developed a pressure vessel that can be attached to our rotary-shear low to high-velocity friction apparatus (Marui Co Ltd., MIS-233-1-76). With a current specimen holder, friction experiments can be done on hollow-cylindrical specimens of 15 and 40 mm in inner and outer diameters, respectively, at controlled  $P_p$  to 35 MPa, at effective normal stresses of 3-9 MPa, and at slip rates of 60 mm/year to 2 m/s. An effective normal stress can be increased by about 10 times by replacing a 10 kN pneumatic actuator with a 100 kN hydraulic actuator. We report an outline of the experimental system and preliminary high-velocity experiments with controlled pore pressure on Shanxi dolerite.

High-velocity friction experiments were performed on hollow-cylindrical specimens of Shanxi dolerite at effective normal stresses of 0.13-1.07 MPa and at slip rates of 1, 10, 100 and 1000 mm/sec. Nitrogen gas and water were used of the pore fluid and compared the frictional behavior. In the  $N_2$  tests an axial force was kept at 1 kN and the nitrogen gas pressure was increased in steps from 0 to 5 MPa to change an effective normal stress. In the wet tests the specimens were soaked in distilled water in the vessel and  $P_p$  was applied by nitrogen gas in a similar manner as in the dry tests. Nitrogen gas acted as buffer to prevent an abrupt change in the pore-water pressure during experiments. The steady-state friction coefficient of dry dolerite increased from 0.3-0.35 at 10 mm/s to 0.55-0.8 at 100 mm/s and then decreased down to 0.2-0.6 at 1000 mm/s. The results are quite similar to those of dry granite tested under similar conditions (Reches and Lockner, 2010, *Nature*). However, the steady-state friction coefficient of dolerite under a pore-water pressure decreased monotonically from 0.4-0.8 at 1 mm/s to 0.3~0.5 at 1000 mm/s, and the strengthening from 10 to 100 mm/s disappeared with a pore-water pressure. We plan to conduct more experiments with controlled pore-water pressure and to do textural and material analysis of specimens to gain insight on the weakening mechanisms.

Keywords: High-velocity friction experiment, Pore-water pressure

## Re-evaluation of frictional heat recorded in the dark gouge of a megasplay fault at the Nankai Trough

MASUMOTO, Hirokazu<sup>1\*</sup>; HIRONO, Tetsuro<sup>1</sup>; ISHIKAWA, Tsuyoshi<sup>2</sup>; KAMEDA, Jun<sup>3</sup>; YABUTA, Hikaru<sup>1</sup>; MUKOYOSHI, Hideki<sup>4</sup>

<sup>1</sup>Department of Earth and Space Science, Graduate School of Science, Osaka University, <sup>2</sup>Kochi Institute for Core Sample Research, Japan Agency for Marine-Earth Science and Technology, <sup>3</sup>Graduate School of Science, Hokkaido University, <sup>4</sup>Faculty of Education and Integrated Arts and Sciences, Waseda University

Because a megasplay fault branching from the deep subduction boundary megathrust in the Nankai Trough is thought to be the source of large tsunamis associated with past Tonankai earthquakes, investigation of the heat signal due to frictional slip recorded in the fault is important for estimating the earthquake slip parameters. We performed X-ray diffraction and infrared spectroscopic analyses of a megasplay fault-rock sample and re-examined previously reported trace-element and isotope compositions, but observed no specific change related to high temperature ( $\geq 250$  °C). In addition, although a qualitative increase of the illite content in illite/smectite mixed-layer minerals within the slip-zone sample was previously reported, our kinetic evaluation of illitization, taking into consideration the coseismic temperature change due to frictional heating and heat conduction, revealed that the illitization reaction hardly progresses at temperatures under 250 °C. Alternatively, we suggest that the illite content in mixed-layer minerals might increase progressively via a comminution – dissolution – recrystallization process during multiple past slips. Accurate assessment of the slip behavior of the megasplay fault could be efficiently obtained by drilling to penetrate the fault zone at a deeper depth of approximately 1.5 km, where records of high temperatures would be detectable.

Keywords: NanTroSEIZE, Tonankai earthquake, fluid-rock interactions, trace elements, X-ray diffraction, infrared spectroscopy

## Roughness of fault surfaces over a length-scale range from nano- to millimeters.

KISHIDA, Minori<sup>1\*</sup>; MIZOGUCHI, Kazuo<sup>2</sup>; TAKAHASHI, Miki<sup>3</sup>; HIROSE, Takehiro<sup>4</sup>

<sup>1</sup>Hiroshima University, <sup>2</sup>Central Research Institute of Electric Power Industry, <sup>3</sup>Geological Survey of Japan, AIST, <sup>4</sup>Kochi, JAMSTEC

Geometric complexities of faults are first-order effects that complicate the mechanics of earthquakes and faulting. Here we report on the topographic roughness measurements on two natural fault surfaces with a continuous length-scale range from 1 nm to 3 mm. The fault surfaces observed in this study include (1) the Corona Heights fault in the Castro Area of San Francisco, that has been studied mineralogical and microstructural in detail, and (2) the Itozawa fault in Fukushima prefecture, a normal fault moved just after the 2011 Off the Pacific Coast of Tohoku earthquake. Both fault surfaces exhibit shiny slickensides on which various length and width of slickenlines are observed.

In order to measure fault surface topography with a scale range from 1 nm to 3 mm, we performed line-measurements both parallel and perpendicular to the slickenlines using two scanner devices; a confocal white-light scanning microscope (measurable range: 0.15 ~3000  $\mu\text{m}$ ) and a scanning probe microscope (1 ~50000 nm). The topographic properties of the measured surfaces were expressed either as a Hurst exponent ( $H$ ) which are calculated from power spectrum density (PSD) of topography data. As a result, the Corona Heights fault and the Itozawa fault exhibit a consistent geometrical property, a linear behavior on a log-log plot where axes are PSD and spatial length scale. A slope of the log-log plot,  $H$ , of the Corona Heights fault and the Itozawa fault shows  $H_N = 0.73 \pm 0.010$  perpendicular to the slickenslide and  $H_P = 0.81 \pm 0.012$  parallel to it, and  $H_N = 0.87 \pm 0.013$  and  $H_P = 0.94 \pm 0.014$ , respectively. Smaller  $H_P$  than  $H_N$  is often reported, that interpreted as surface roughness in the slip direction becomes less pronounced selectively with progressive displacement (e.g., Sagy et al., 2007). Therefore, almost no difference between  $H_P$  and  $H_N$  in the observed fault surfaces could imply that both faults may be relatively immature due to less total displacement, or otherwise  $H_P$  and  $H_N$  are undifferentiated with displacement in the length-scale range from 1 nm to 3 mm. Candela et al., (2012) measured roughness of thirteen earthquake fault surfaces and suggested that the fault geometry can be expressed as a single geometrical description (i.e., single  $H$ ) over a range of scales from 50  $\mu\text{m}$  to 50 km. Our data, at least  $H_N = 0.81$  perpendicular to the slickenlines, is consistent with their universal  $H_N = 0.81 \pm 0.04$  even for lower length-scale range. Hence, the geometric complexity of fault surfaces in nature can be maintained over length-scales from nano- to kilometer and be described as the single Hurst exponent.

Keywords: fault surface, roughness, fractal, Hurst exponent

## Evolution of fluid transport property by diagenesis in basaltic rocks from the Shimanto belt, Southern Shikoku

TANIKAWA, Wataru<sup>1\*</sup>; YAMAGUCHI, Asuka<sup>2</sup>; KAMEDA, Jun<sup>3</sup>; TADAI, Osamu<sup>4</sup>; HATAKEDA, Kentaro<sup>4</sup>; KITAMURA, Manami<sup>5</sup>

<sup>1</sup>JAMSTEC/Kochi, <sup>2</sup>Atomosphere and Ocean Research Institute, The University of Tokyo, <sup>3</sup>Graduate School of Science, Hokkaido University, <sup>4</sup>Marine Works Japan Ltd., <sup>5</sup>Hiroshima University

Large slip displacement was observed at shallow portion of the plate boundary fault during 2011 Tohoku earthquake, and this slip has contributed to cause large tsunami. The large displacement was probably caused by dynamic fault weakening at shallow boundary fault, or reduction of fault strength at middle to deeper portion by pore pressure generation. Pore pressure can be generated by chemical dehydration, fluid influx from deeper crust or pore volume reduction associate with permeability reduction at a large subduction plate boundary. In this study, we investigate the change of fluid transport property for basalt during diagenesis process at Nankai Subduction zone.

We collected basalt brocks in the Cretaceous Shimanto accretionary complex of Japan from Okitsu-Kozurutsu site and Kure site in Kochi, Japan. Porosity and P-wave velocity of each basalt at atmospheric pressure are 1.4 % and 2.1%, and 6.4 km/s and 5.9km/s, respectively. We found a slight difference of S-wave velocity for basalts. Permeability was measured by using N<sub>2</sub> gas as a pore fluid, and calculated by steady state gas flow method. Permeability was measured at room temperature and under confining pressure that were increased from 1 to 160 MPa in steps.

Gas permeability was decreased with an increase of differential pore pressure at a same confining pressure. This pore pressure dependence implies the Klinkenberg effect, therefore we converted gas permeability to water permeability using the Klinkenberg equation. We did not find a variation of permeability at the lowest effective pressure of 1MPa, and permeability shows from 10<sup>-15</sup> to 10<sup>-16</sup> m<sup>2</sup>. Permeability in all basalts decreased with an increase of effective pressure, and reaches from 10<sup>-18</sup> to 10<sup>-21</sup> m<sup>2</sup>. Basalt from Kure site shows the lowest permeability of 10<sup>-21</sup> m<sup>2</sup> at 100 MPa, and permeability of basalt from Okitsu site shows the largest value of 3×10<sup>-19</sup> m<sup>2</sup>. Permeability reduction with an increase of effective pressure in most samples is described by the power law equation where exponent ranges from -2 to -3. The permeability reduction for the highest permeable basalt was expressed by the theoretical relation that is based on the Hertzian contact theory (Gangi, 1978). Fractures are apparently developed in this sample, therefore the reduction in permeability is influenced more by fracture asperity rather than pore structure.

The permeabilities of basalts in this study are smaller than permeability of basalt in fault zone at Okitsu site (Kato et al., 2004), Juan de Fuca and Tonga-Kermadec (Christensen and Ramanantsoandro, 1988). At present, we did not see clear relationship between the permeability and diagenesis. Most of basalt rock shows very low permeability, therefore they have higher potential to generate a pore pressure by dehydration reaction or influx from depth during subduction at Nankai Trough.

Keywords: permeability, fluid pressure, diagenesis, subduction zone, Nankai Trough earthquake, basalt

## Effects of thermal cracking on elastic wave velocities and Poisson's ratio of basalt, gabbro and granite

NISHIMURA, Kaya<sup>1\*</sup> ; UEHARA, Shin-ichi<sup>1</sup> ; MIZOGUCHI, Kazuo<sup>2</sup>

<sup>1</sup>Faculty of science, Toho University, <sup>2</sup>Central Research Institute of Electric Power Industry

Marine seismic refraction studies have found that there are high Poisson's ratio regions ( $>0.35$ ) in oceanic crust at subducting plate. Christensen (1984) performed laboratory measurements of compressional and shear wave velocities ( $V_p$  and  $V_s$ , respectively) of basalt, which is one of major rocks in oceanic crust, and estimated Poisson's ratio, and suggested that observed high Poisson's ratio can be explained by high pore pressure. This distribution of high pore pressure have been concerned because it should influence fault mechanism of plate boundary at subduction zones. Christensen (1984) used intact rock for the measurements. But there are probably dense cracks near faults in nature. Therefore, to investigate  $V_p$ ,  $V_s$  and Poisson's ratio for fractured rock is important to evaluate distribution of high pore pressure regions by using seismic studies. This study reports the results of measurements of  $V_p$  and  $V_s$ , and estimations of Poisson's ratio for thermally cracked gabbro, basalt and granite, which are major rocks in oceanic crust and continental crust. Rock specimens were heated at 100 °C, 300 °C, 500 °C and 700 °C to thermally crack them. We performed measurements at atmospheric pressure and dry condition. We also measured  $V_p$  and  $V_s$  for water-saturated specimens of gabbro and basalt heated at 700 °C, and compared the results with those under dry condition to investigate the effect of pore fluid on  $V_p$  and  $V_s$ .

As results, specimens heated at higher temperature tended to have slower  $V_p$  and  $V_s$ . Density of the specimens was also decreased as heating temperature was increased, and especially the density change was clear from 500 °C to 700 °C. This imply that clack density of specimens was increased with increasing temperature, and this might be the reason why  $V_p$  and  $V_s$  were decreased. Poisson's ratios obtained in this study (0.05-0.25) were lower than the observed high Poisson's ratio.  $V_p$  and  $V_s$  for water-saturated specimens were generally faster than those for dried specimens, but output signals tended to be smaller and therefore improvements of the measurements systems and methods to analyze the signals should be necessary.

Keywords: Poisson's ratio, Elastic wave, High pore pressure, Basalt, Gabbro, Granite

## Frictional property of rocks in the Izu-Bonin-Mariana Forearc under high temperature and pressure conditions

HYODO, Geni<sup>1\*</sup> ; TAKAHASHI, Miki<sup>2</sup> ; SAITO, Saneatsu<sup>3</sup> ; HIROSE, Takehiro<sup>4</sup>

<sup>1</sup>Department of Earth and Planetary Systems Science, Graduate School of Science, Hiroshima University, <sup>2</sup>Geological Survey of Japan-Advanced Industrial Science and Technology, <sup>3</sup>Japan Agency Marine-Earth Science and Technology, <sup>4</sup>Kochi Institute for Core Sample Research, Japan Agency Marine-Earth Science and Technology

The Kanto region lies atop of three tectonic plates: the North American Plate, the Pacific Plate, and the Philippine Sea Plate. In addition, the collision and subduction of the Izu-Bonin-Mariana (IBM) arc into the Kanto region results in a characteristic tectonic setting as compared with other convergent margins. Due to such complicated plate configuration, the different type of earthquakes including seismic slip (e.g., the Kanto earthquake) and aseismic creep (i.e., slow earthquake of Boso peninsula) occurs at the intra-plate and plate boundaries beneath the Kanto region. Moreover, the different type of events seems to take place side by side at almost same depth (probably nearly same P-T conditions). Although many factors including pore fluid pressure and fault topography can control earthquake generation, this study focus on frictional property of incoming materials to be subducted into the Kanto region in order to examine a hypothesis that the different types of slips arise from different input materials. Thus, we have performed friction experiments on rocks that constitute the IBM forearc using a high P-T gas medium apparatus at AIST.

We sampled five rocks (marl, boninite, andesite, sheared serpentinite and serpentinitized dunite) recovered from the IBM forearc by Leg 125, Ocean Drilling Program (ODP Site 784, 786). The rocks were crushed and sieved into 10~50  $\mu\text{m}$  in grain size. Then, the rock powders were sandwiched between saw-cut alumina cylinders and sheared at temperature of 300°C, confining pressure of 156MPa, pore pressure of 60MPa and axial displacement rates of 0.1 and 1  $\mu\text{m/s}$ . The sheared serpentinite and serpentinitized dunite exhibit steady-state friction of 0.55 and 0.35-0.41, respectively and their velocity dependence of friction is positive (velocity strengthening behavior). On the other hand, for marl, boninite and andesite, a periodic stick-slip behavior appears at 1  $\mu\text{m/s}$ . However, contrary to a stick-slip behavior at room temperature in general, rise time of the stick-slip behaviors are quite long (3.9, 9.3 and 10.8 sec, respectively), that could be called as a “ slow stick-slip ”. Similar slow stick-behavior were observed in halite and serpentinite slipped at high temperatures (Noda and Shimamoto, 2010; Okazaki, 2013), but this is first time to recognize this unique slip behavior in sedimentary and igneous rocks. Although it is difficult to discuss the diverse slip behaviors observed at the Kanto region based on our limited experimental results, we will examine the conditions where the transition between stable and unstable sliding appears using the input materials and explore the generation mechanisms of earthquakes at the Kanto region.

Keywords: Friction, Izu-Bonin-Mariana Forearc (IBM), slow earthquake, stick-slip, earthquake

## Temperature-dependent frictional strength of dolerite in a nitrogen atmosphere and its relation to amorphous material

TANAKA, Nobuaki<sup>1\*</sup> ; WADA, Jun-ichi<sup>1</sup> ; KANAGAWA, Kyuichi<sup>1</sup>

<sup>1</sup>Graduate School of Science, Chiba University

Noda et al. (2011, JGR) revealed by rotary shear experiments on dolerite at a normal stress of 1 MPa, a sliding velocity of 1 cm/s and controlled temperatures from room temperature to 1000 °C, that its frictional strength has a negative correlation with the amount of amorphous phase in wear materials as well as a positive correlation with the amount of iron oxides which increases with increasing temperature by oxidation of the iron-bearing minerals. However, oxidation of iron-bearing minerals as observed in their experiments is unrealistic in fault zones at depths due to the paucity of oxygen there.

We therefore conducted rotary shear experiments on the same dolerite at the same normal stress, sliding velocity and temperature conditions with Noda et al. (2011) in a nitrogen atmosphere with the oxygen content of 0.1 %, and compared the results with those of Noda et al. (2011). We collected mechanical data during stable sliding of 20 m after the presliding of 100 m at each experimental condition. Sieved wear materials smaller than 250 μm were then used for quantitative X-ray diffraction analyses.

Steady-state friction coefficient was ~0.47 at room temperature and 200 °C, ~0.7 at 400 and 600 °C, and ~0.9 at 1000 °C. Steady-state was not reached at 800 °C due to intense fracturing of samples. The amount of amorphous phase in wear materials shows a change with increasing temperature similar to that for experiments in the air (Noda et al., 2011); ~65 wt% at room temperature, ~70 wt % at 200 °C, ~70 wt% at 400 °C, ~45 wt% at 600 °C, ~15 wt% at 800 °C, and 0 wt% at 1000 °C. In contrast, the amount of iron oxides does not show a noticeable change with increasing temperature.

Experiments by Noda et al. (2011) in the air showed a negative correlation between frictional strength and the amount of amorphous phase at temperatures lower than or equal to 800 °C. Our experiments also show an overall tendency of increasing frictional strength and decreasing amount of amorphous phase with increasing temperature. However, steady-state friction coefficient differs by more than 0.2 between room temperature and 400 °C, while the amount of amorphous phase differs by only ~5 wt% between these two temperatures. In addition, the amount of amorphous phase differs by ~15 wt% between 400 and 600 °C, whereas steady-state friction coefficient is almost the same at these two temperatures. This implies lack of a direct relationship between frictional strength of dolerite and the amount of amorphous phase in wear materials. Study on what controls the temperature-dependent change in frictional strength of dolerite is now in progress.

Keywords: Dolerite, Frictional strength, Wear material, Nitrogen atmosphere, Rotary shear experiment

## Observation of 2-D rupture propagation for stick-slip events during large-scale biaxial frictional experiments

TSUCHIDA, Kotoyo<sup>1\*</sup> ; KAWAKATA, Hironori<sup>1</sup> ; FUKUYAMA, Eiichi<sup>2</sup> ; YAMASHITA, Futoshi<sup>2</sup> ; MIZOGUCHI, Kazuo<sup>3</sup>

<sup>1</sup>Ritsumeikan University, <sup>2</sup>National Research Institute for Earth Science and Disaster Prevention, <sup>3</sup>Central Research Institute of Electric Power Industry

Pre-slip was expected to occur prior to large earthquakes, since a pre-slip model was proposed by Ohnaka and Kuwahara (1990) based on their rock frictional experiments. The pre-slip accelerates toward an unstable sliding event. However, such phenomena have never been clearly observed for natural earthquakes. Ohnaka and Kuwahara (1990) observed a 1-D strain distribution along a sample surface, and estimated the apparent rupture propagation speed. In addition, the fault was narrow, and the rupture growth might be affected by free surfaces at the edge of the sample, though the free surface effect is not so common for natural earthquakes. Therefore, we closely observed two-dimensional rupture propagation on a wider fault during rock frictional experiments.

We carried out meter-scale rock frictional experiments (Fukuyama *et al.*, 2013), and investigated rupture propagation of stick-slip events and some of their characteristics, using AE (acoustic emission) and strain records. The fault consisted of an interface of two Indian gabbro blocks. Their width and height were 0.5 m, and the length of upper and lower blocks were 1.5 m and 2.0 m, respectively. The arrays of strain gauges and AE sensors were installed within the lower block in order to understand two-dimensional rupture propagation. Twenty four sets of AE sensors and biaxial strain gauges were attached 60 mm below the sliding surface at intervals of 150 mm parallel to the slip direction and at intervals of 75 mm perpendicular to the slip direction. We analyzed time series of strain and AE data, and found stick-slip events accompanied with slow and accelerating strain decrease that propagated at a speed much slower than elastic wave speed.

This study was supported by NIED research project "Development of monitoring and forecasting technology for crustal activity" and JSPS KAKENHI Grant Number 23340131.

Keywords: stick-slip event, rupture propagation, large-scale biaxial frictional experiment

## The experimental study about frictional instability of fault gouges in terms of Rowe's energy ratio

HIRATA, Momoko<sup>1\*</sup> ; MUTO, Jun<sup>1</sup> ; NAGAHAMA, Hiroyuki<sup>1</sup>

<sup>1</sup>Dept. Earth Science, Tohoku University

### 1. Introduction

The stress-dilatancy relationship for granular materials in a dense packing state was introduced by Rowe (1962). He used the energy ratio (K), which was the ratio of rate of energy dissipation in the direction of minimum principal stress to energy supply in that of maximum principal stress. According to the concept, K shall be a minimum and constant value (Rowe, 1962). However, there are many questions about the physical meaning of K. Therefore, the Rowe's law has not been applied much for fault mechanics until now. Nevertheless the stress-dilatancy relation is related to the onset of frictional instability, it has not been clear yet. So, we conducted friction experiments using simulated fault gouges in order to confirm whether Rowe's law can be applied to fault situation or not.

### 2. Methods

The friction experiments using simulated fault gouges were conducted in a gas-medium apparatus. The confining pressure was ranging from 140 to 180 MPa. We used a cylindrical gabbroic forcing blocks (20 mm in a diameter, 40 mm in a length, and cut by a 50 degree from their cylindrical axis) and quartz gouges were sandwiched by them. The sample sustained loading initially and holding at several values of axial stresses at 190, 450, 640 and 800 MPa. The strain rate was  $10^{-3}$  /s. In order to measure strain, three strain gauges were glued onto a gouge layer through the Teflon jacket. Another one was placed to a forcing block in a vertical direction and far from a gouge layer. Data were recorded at 2 MHz.

### 3. Results and Discussion

From our friction experiments, we obtained K of gouges at different confining pressures. K is given by the ratio of rate of energy dissipation in  $\sigma_3$  direction to energy supply in  $\sigma_1$  direction, so it can be represented by the ratio of output energy to input one. We obtained strain of  $\sigma_3$  direction from three strain gauges glued onto a gouge layer. Similarly,  $\sigma_1$  and strain of  $\sigma_1$  direction were obtained from another gauge.  $\sigma_3$  was the confining pressure. Our results showed that the output energy was the linear function of input one. K increased with confining pressure and showed a certain constant value at each loading and holding stage. Moreover, the change in K was remarkable at the final loading stage. In other words, the output energy increased suddenly because gouge particles began to slip. So, the change in K is large under high stress, including just before unstable slip. It matched shear localization (e.g. Logan et al., 1992; Marone, 1998).

Because K is represented by a function of internal friction angle, we suggest that the change reflects the process of microstructural development. It implied that the statistical particle arrangements of gouges changed at each stress level. After gouges become a closest packing state at the peak stress, the grain size reduction (GSR) of gouges occurs leading to the development of shear structure. Under GSR occurrence, K became a new state. From previous study, it is known that the microstructural development has a close relation with frictional instability (e.g. Logan et al., 1992; Marone, 1998; Onuma et al., 2011). During progressive shear, the angle of R1-shear developed in gouges decreases with cumulative slip (Gu and Wong, 1994). Hence, the change in K, that is to say the change in internal friction angle must be connected with not only microstructural development but also frictional instability.

### 4. Summary

From our experiments using simulated fault gouges, we obtained relationships among microstructural development, frictional instability and energy ratio of it. We confirmed that the Rowe's law could be applied to simulated fault gouges. Therefore, we can assess frictional instability in terms of the energy ratio based on Rowe's law. Systematic laboratory observation provides better understanding on energetical or microstructural consideration on the shear localization and seismogenic process.

Keywords: frictional instability, simulated fault gouge, Rowe's minimum constant energy ratio, friction experiments

## Temporal evolution of slip event probability -Case study of slow slip off the Boso Peninsula and the Yaeyama Islands

MITSUI, Yuta<sup>1\*</sup>

<sup>1</sup>Grad. Sci., Shizuoka Univ.

Spatially-isolated slip events (earthquakes and slow slip events) have occurred quasi-periodically especially at plate interfaces (e.g., Nadeau and McEvilly [1997], Matsuzawa et al. [2002], Rogers et al. [2003]). This fact suggests that the concept of simple elastic rebound at the plate interfaces is true at a certain level.

Of course, the recurrence intervals of the slip events have no periodicity in a strict sense. Probably it is because the slip events never repeat in the same pattern. Earthquakes with dynamic processes especially tend to have this trend. In fact, an earthquake event occurred beyond the expected period from the previous earthquake sequence (Bakun et al. [2005]). Moreover, seemingly spatially-isolated events can be strongly affected by nearby huge earthquakes (e.g., Uchida and Matsuzawa [2013]). Thus it is difficult to discuss the event recurrence quantitatively based on deterministic physical models. Researchers alternatively used probability distribution to evaluate the recurrence intervals.

When we examine the event recurrence by the probability distribution approach, one of the most important point is actual event probabilities at the time of event occurrences. There has been little discussion on this point. We address it, focusing on slow slip events with shorter recurrence intervals. We select the Boso-oki slow slip events (Hirose et al. [2012]) and the Yaeyama-oki slow slip events (Heki and Kataoka [2008]). The probability distribution of the event recurrence intervals is the Poisson distribution. We evaluate the event probability as the subtraction of cumulative probability of zero occurrence from 100%. The cumulative probability reverts back to 100% at the time of an event. The mean recurrence interval as a parameter of the Poisson distribution is the sample average from the forepassed events. The above settings allow us to calculate the temporal evolution of the event probabilities off the Boso Peninsula and the Yaeyama Islands. **We can validate the calculated results** by comparing with the actual event occurrences.

In the result off Yaeyama Islands, the event numbers that occurred at a stage with the smaller probability than 50% are five out of the total numbers twenty six. About 80% of the events occurred with the event probability  $>50\%$ . Besides, off the Boso Islands, the event numbers during a stage of the smaller probability than 50% are two out of the total numbers five. The two events followed the 2011 Tohoku earthquake. This fact may reflect the effect of the stress perturbation due to the Tohoku earthquake, as suggested by Hirose et al. [2012]. In summary, few slow slip events occur with the event probability  $<50\%$ , in the probability evaluation based on the Poisson distribution. We additionally find that the event probability at the time of an event off the Yaeyama islands has increased gradually.

Keywords: Repeating slow slip event, Event probability, Statistical approach, Off Boso Peninsula, Off Yaeyama Islands

## Numerical modeling of concurrent occurrence of shallow very low frequency earthquakes and long-term slow slip events

MATSUZAWA, Takanori<sup>1\*</sup> ; SHIBAZAKI, Bunichiro<sup>2</sup> ; OBARA, Kazushige<sup>3</sup> ; HIROSE, Hitoshi<sup>4</sup>

<sup>1</sup>National Research Institute for Earth Science and Disaster Prevention, <sup>2</sup>Building Research Institute, <sup>3</sup>Earthquake Research Institute, University of Tokyo, <sup>4</sup>Research Center for Urban Safety and Security, Kobe University

Concurrent occurrences of shallow very low frequency earthquakes (VLFs) and long-term slow slip events (SSEs) are found in the Bungo channel (Hirose et al., 2010, Science). This region is located at the western rim of the area where a large slip of megathrust earthquake is expected. Thus, the understanding of such behaviors will help us to reveal the preparation process of megathrust earthquakes. We aim to numerically reproduce the concurrent slip at the shallow VLFE and the long-term SSE region.

In our numerical model, a subducting plate interface is modeled as a flat plane within a semi-finite elastic medium. Frictional stress on the plate interface is given by a rate- and state-dependent friction law with cut off velocities (e.g., Matsuzawa et al., 2010, JGR). To reproduce long-term SSEs, a region with a cutoff velocity of  $10^{-6.5}$  m/s and low effective normal stress is assumed below the depth of 10 km. In terms of shallow VLFs, result of rock experiments shows that velocity-weakening and strengthening behaviors are found at low and high slip velocity, respectively (Saito, et al., 2013, GRL). In addition, it is estimated that a radius of shallow VLFs is 5-10km from seismic data analysis (Ito and Obara, 2006, GRL). Based on these results, we assume circular regions for VLFs with a cutoff velocity of  $10^{-4}$  m/s and a radius of 6 km. In addition, we pose a stable sliding region beside the long-term SSE region, as more stable sliding behavior is expected in the Hyuganada region where shallow VLFs frequently occur even in the period without long-term SSEs. In this study, some cases are calculated to examine the effect of the distribution of frictional parameters. Model 1 is a model based on the above assumptions. Model 2 is a model without a stable sliding region beside the long-term SSE region. In Model 3, the top of the long-term SSE region is set to the depth of 18 km.

In the numerical results of these three models, recurring slip at shallow VLFE and long-term SSE regions are reproduced. Concurrent occurrence of shallow VLFs and long-term SSEs are reproduced in Model 1 and 2, while the concurrent occurrence is not clear in Model 3. In addition, slip events at the VLFE region are also found during the period without long-term SSEs in Model 2, while most of slip events at the VLFE region are found with long-term SSEs in Model 1. Our results suggest that the top of the long-term SSE region are close to the VLFE region, and the model with stable sliding region beside the long-term SSE region (Model 1) is more preferable to reproduce observed results than the model with fully locked surrounding region (Model 2).

Keywords: very low frequency earthquake, slow slip event, numerical simulation, Bungo Channel

## Spatio-temporal afterslip distribution of the 2011 Tohoku-Oki earthquake considering visco-elastic response

SUZUKI, Syota<sup>1</sup> ; ITO, Takeo<sup>1\*</sup> ; SATO, Kachishige<sup>2</sup> ; HYODO, Mamoru<sup>3</sup>

<sup>1</sup>Graduate School of Environmental Studies, Nagoya University, <sup>2</sup>Faculty of Education, Tokyo Gakugei University, <sup>3</sup>Japan Agency for Marine-Earth Science and Technology

### 1. Introduction

The 2011 off the Pacific coast of Tohoku Earthquake with a moment magnitude ( $M_w$ ) of 9.0 occurred at 5:46 (UTC) on March 11, 2011 along the boundary between the subducting Pacific Plate and the overlying plate. Since large earthquake are likely to produce stress concentrations in neighboring region along the plate boundary, the mainshock might have been trigger afterslip. It is very important to determine the detail of spatio-temporal distribution of afterslip, in order to understand the characteristic of friction relationship on the plate boundary. In this study, we estimate spatio-temporal afterslip distribution using visco-elastic Green's function (GF).

### 2. Method

We make GF using 3D finite element method (FEM) with a grid model for the Hokkaido and Tohoku regions. The model space and assumed subsurface structure for the 3D-FEM have a dimension of 2600 km (in the ESE direction) x 1500 km (in the NNE direction) x 400 km (depth) and typical subsurface structure consist of four sub-regions, i.e., upper crust, lower crust, upper mantle, and Pacific plate. The numbers of node and cell of 3D-FEM mesh are 3,205,950 and 3,121,200, respectively. For the calculation, we use the Pylith version 1.9.0, which is designed for simulating lithospheric deformation. In order to estimate the distribution of afterslip, we assume subfaults on the plate interface in and around the co-seismic slip zone of the 2011 Tohoku-Oki event. In inversion, we impose the smoothness constraint on the slip distribution. We estimate co-seismic and spatio-temporal distributions at the same time, considering visco-elastic response, derived from GEONET and seafloor observations.

### 3. Results and discussion

We obtain the co- and post-seismic slip distributions. The maximum slip of the 2011 event is about 60 m close to the Japan Trench. Estimated afterslip distribution is complementary to co-seismic slip distribution and also historical source regions. Amount of afterslip is about 2m, and the cumulative seismic moment is 8.06, considering visco-elastic response during 2.5 years after event. In case of only considering elastic response, amount of after slip is about 4m. There is no slip off Fukushima prefecture only considering visco-elastic response. And, our result can explain seabottom observations. i.e., Miyagi-Oki1 site move to west about 38 cm during 2 years after event. The effect of visco-elastic response is too large. In inversion for afterslip distribution from geodetic data, it must be consider to visco-elastic response due to relaxation in upper mantle.

Keywords: Afterslip, Visco-elastic response, FEM

## Vertical displacement in Naruko Volcano area following the 2011 Tohoku earthquake deduced from precise leveling survey

TSUKAMOTO, Yuya<sup>1\*</sup> ; SUGIYAMA, Kenichi<sup>1</sup> ; FUJITA, Wakana<sup>1</sup> ; WATANABE, Keitaro<sup>1</sup> ; WATANABE, Kosui<sup>2</sup> ; TAKAHATA, Akihiro<sup>2</sup> ; MATSUOKA, Moe<sup>2</sup> ; GOTO, Akio<sup>3</sup> ; OHTA, Yusaku<sup>2</sup>

<sup>1</sup>Fac. Sci., Tohoku University, <sup>2</sup>Grad. School Sci., Tohoku University, <sup>3</sup>CNEAS, Tohoku University

Large subsidence accompanied the 11 March 2011 Great East Japan Earthquake along the Pacific coast. GEONET data have indicated that the subsidence goes down westward (<http://www.gsi.go.jp/common/000059956.pdf>). In a summer field seminar by the Division of Earth and Planetary Material Science, Tohoku University, we made precise leveling survey for 10km on the second-order leveling route along the National Route 47 (from benchmark number 047-064 to 047-074; hereafter indicated as BM64, BM74 etc.) which locates along the east to west in Naruko area, Miyagi prefecture, to detect the vertical crustal deformation of this area. We performed the leveling twice (23-28 August, 2011 and 19-25 August, 2013) using bar-code leveling rods (Leica CPCL3) and an electronic digital level (Leica DNA03). By comparison with the data by Geospatial Information Authority of Japan in 2009, we acquired the change of difference in elevation at each benchmark against the westernmost BM64. We conducted round-trip survey between each benchmark and re-measured when the residual error did not meet the first-order leveling, except the segments between BM66 and BM68 in 2011 and between BM72 and BM74 in 2013 due to the fixed seminar schedule.

Contrary to our expectation before the leveling, we found all benchmarks subsided against BM64 and the degree of subsidence increases westward. At the 2011 leveling 5 months after the earthquake, benchmarks BM66, 68, 70, 72, and 74 subsided 13.0mm, 21.4mm, 81.7mm, 91.1mm and 113.9mm, respectively. This subsidence continued further with decreasing the amount, 8.5mm, 16.2mm, 23.7mm, 41.9mm and 46.2mm between 2011 and 2013, respectively. Obtained displacement pattern along the leveling survey between 2011 and 2013 is almost similar pattern with the 2009 and 2011 one.

Ozawa and Fujita (2013) and Takeda and Fukushima (2013) showed local depressions on some major volcanic areas in Tohoku region by In-SAR analysis. They explained the depressions by the east-west extension of hot and soft medium under the volcanoes. Our research route locates on one of that volcanic area and our leveling result is consistent with their previous studies. In contrast, their analysis just focused on the coseismic displacement. In our analysis, we found not only subsidence during the coseismic stage but also the subsidence in the postseismic stage. Particularly, it is worth noting that the subsidence increases remarkably between BM68 and BM70, which is inferred to cross the rim of Naruko caldera.

### Acknowledgement

We appreciate Ryohei Kobayashi and Emi Hara who joined the leveling survey in 2011.

Keywords: Great East Japan Earthquake, Naruko caldera, precise leveling survey, subsidence

## Postseismic gravity changes after the 2011 Tohoku earthquake recorded by superconducting gravimeters

IMANISHI, Yuichi<sup>1\*</sup> ; TAMURA, Yoshiaki<sup>2</sup> ; NAWA, Kazunari<sup>3</sup> ; IKEDA, Hiroshi<sup>4</sup>

<sup>1</sup>ERI, The University of Tokyo, <sup>2</sup>NAOJ, <sup>3</sup>AIST, <sup>4</sup>University of Tsukuba

Continuous gravity monitoring by means of superconducting gravimeters is revealing significant effects of the 2011 Tohoku Earthquake on surface gravity in Japan. Two stations of superconducting gravimeters, Matsushiro and Kamioka, both in the main island of Japan (Honshu), are indicating gravity decreases at similar rates of approximately 10 microgal per year after the 2011 event, and this trend is still going on. Since Matsushiro and Kamioka are relatively far from the earthquake source region (epicentral distances being 420 km and 490 km, respectively), the postseismic crustal uplifts of the stations recorded by GPS are too small to account for the observed gravity decreases. Therefore, the observed gravity changes are likely to reflect ongoing changes in the density of the earth material, maybe associated with a viscoelastic flow of the asthenosphere. Data from Mizusawa, another SG station in Honshu, will also be presented in the paper.

Keywords: superconducting gravimeter, 2011 Tohoku earthquake, postseismic gravity changes, viscoelasticity

## Pressure Source Model Inferred from Crustal Deformation Preceding Seismic Swarm in 2013 beneath Tarumae Volcano

KOSHIROMARU, Takuma<sup>1</sup> ; MURAKAMI, Makoto<sup>1\*</sup>

<sup>1</sup>ISV, Hokkaido University

Tarumae-volcano is an active volcano with an altitude of 1,041 m located in the southwestern part of Hokkaido. In past 350 years, three major magmatic eruptions occurred, i.e. Plinian eruptions in 1667 and 1739 and dome forming eruption in 1909. Volcanic activity in recent years is restricted to gas emission or volcanic earthquake activity at the shallow part of the volcano. A spherical source model for inflation/deflation sequence is inferred at shallow depth beneath the summit dome by campaign GPS observations by the Meteorological Agency. No sign of crustal deformation is found at the deeper depth of the volcano by continuous GPS observation in a regional scale either by the Geographical Survey Institute nor the Meteorological Agency. Thus, until now, a crustal deformation which suggests fluid activity beneath the Tarumae-volcano at deeper depths had not been detected.

In July, 2013 swarm seismic activity started at the depths of between 2-5 km about 2 km to the west of summit dome. In addition a crustal deformation preceding the swarm was identified at several observation sites. The size of the change was at about 1 micro radian or micro strain level. Because the change appeared commonly at several stations around the volcano, it is highly likely that the strain and tilt change is resulting from a activity of a source at a depth beneath the volcano. A spherical inflation source was inferred from the observation data. The estimated position is at the m.s.l. depth of 4.2 km and about 1.3 km to the NNW of the summit horizontally with inflation volume of  $3.4 \times 10^5 \text{ m}^3$ .

Since the position and time of activation of the source are close to those of seismic activity, it is likely that there is some geodynamic relationship between swarm seismicity and crustal deformation. In our presentation we also discuss possible relationship between them.

Keywords: Crustal Deformation, Active Volcano, Swarm Earthquake, Tarumae Volcano

## Campaign GPS for detection of the volcanic deformation on and around Mt.Meakan and Mt.Tokachi

WADA, Sayaka<sup>1\*</sup> ; MORI, Hitoshi, Y.<sup>1</sup> ; OKUYAMA, Satoshi<sup>1</sup>

<sup>1</sup>Hokkaido University, Institute of Seismology and Volcanology

Mt. Meakan is an active volcano located in the eastern Hokkaido, Japan. It made phreatic eruptions in 1996, 1998, 2006 and 2008. Mt. Tokachi is one of the famous active volcanoes sits in the central Hokkaido. In the recent 100 years, three major magmatic eruptions took place in 1926, 1962 and 1988-1989.

In this presentation, we will discuss the results of the campaign GPS on and around Mt. Meakan and Mt. Tokachi. Each broad area GPS observation had begun at Mt. Meakan in 2006 and at Mt. Tokachi in 2007, respectively. The campaign GPS observations have made for several days to weeks in each year for Mt. Meakan at 8 sites, and that for Mt. Tokachi at 12 sites.

We used the data of our campaign observations after the 2008 eruption for Mt. Meakan and since 2007 for Mt. Tokachi. We also used the data of several sites operated by JMA (Japan Meteorological Agency) at the same time. Analyzing these data, annual movements at those points were estimated. These movements included deformations of the regional tectonic moving, and of the coseismic step of Tohoku-oki earthquake on March 11, 2011. For making corrections of these non-volcanic deformations, we used the continuous data of GEONET sites by Geospatial Information Authority of Japan (GSI) around the volcanoes. Using the GEONET data from 2007 to 2013, the regional tectonic and the seismic deformations were estimated by linear approximation in space. To elucidate the volcanic deformation, seasonal variations should be taken into consideration. The discussion about estimated volcanic deformation will be made, with the corrections about the regional deformation, the coseismic step and the after slip of 2011 Tohoku-oki earthquake, and the seasonal change.

### Acknowledgements

In this study, JMA, Sapporo District Meteorological Observatory furnish their observation data to us. We would like to express our gratitude to them. Also, we used the data of GEONET sites of GSI with thanks.

Keywords: campaign GPS observation, volcanic crustal deformation, Mt. Tokachi, Mt. Meakan

## Crustal deformation associated with the unrest of Zao Volcano

MIURA, Satoshi<sup>1\*</sup>; NISHIMURA, Takeshi<sup>1</sup>; OHTA, Yusaku<sup>1</sup>; YAMAMOTO, Mare<sup>1</sup>; DEMACHI, Tomotsugu<sup>1</sup>; TACHIBANA, Kenji<sup>1</sup>; OHMI, Katsuya<sup>2</sup>; SHINOHARA, Eiichiro<sup>2</sup>

<sup>1</sup>Graduate School of Science, Tohoku University, <sup>2</sup>Sendai District Meteorological Observatory

Mt. Zao (1,841 m) is an active volcano located in northeastern Japan and having histories of phreatic or phreato-magmatic eruptions in the last 2 ka. Unrest of Zao volcano started in January, 2013 with a volcanic tremor (JMA, 2013) followed by activated seismicity mainly in the lower crust and very long-period seismic events (VLP) up to today. Since the number of volcanological observatories within a distance of 10 kilometers from the volcano was limited at the time of beginning of the unrest; two continuous GPS sites and two sites equipped with borehole seismometers and tiltmeters, Tohoku University has built up 4 sites with broadband seismometers, 5 sites with continuous GPS, 1 site with shallow borehole tiltmeter, and 2 sites with a Proton magnetometer.

Using the new broadband network, we detected some VLPs with dominant period of about 10 sec, and revealed the source of the VLPs is located at a depth range of 2-4 km beneath the crater lake, from where the recent eruptions occurred since ~600 years ago. There were, however, no significant surface phenomena such as steam explosion, ash effusion, and so on associated with the VLPs, except for precursory tilt signals about 5 minutes preceding a few major events.

We deployed dual-frequency GPS receivers at 5 new stations and the data are transmitted to the university using cellphone network for continuous observation (Demachi et al., 2011). The data are processed using the precise point positioning strategy (Zumberge et al., 1997) of GIPSY-OASIS II ver. 6.1.2 with IGS08 precise ephemerides and GMF mapping functions (GMF, Boehm et al., 2006). Since the wide area of northeastern Japan still suffers the long lasting postseismic deformation following the 2011 Tohoku-oki earthquake (M9.0), we try to extract volcanic deformation related to the unrest of the volcano using spatial and temporal filtering. Even though no distinct deformation has been recognized in the continuous GPS and tiltmeters at present, we may detect cm level variation of the shape of the mountain.

### Reference

Boehm et al. (2006), GRL, 33, L07304, doi:10.1029/2005GL025546.

Demachi et al. (2011), Abstract for JpGU2011.

Japan Meteorological Agency (2013), [http://www.seisvol.kishou.go.jp/tokyo/STOCK/kaisetsu/CCPVE/shiryo/127/127\\_no06\\_2.pdf](http://www.seisvol.kishou.go.jp/tokyo/STOCK/kaisetsu/CCPVE/shiryo/127/127_no06_2.pdf)

Zumberge et al. (1997), JGR, 102, 5005-5017.

Keywords: GPS, Ground Tilt, Volcanic deformation, Volcanic activity

## The acceleration episode of the back-arc rifting in the Izu-Bonin Arc possibly triggered by a remote earthquake in 2004

ARISA, Deasy<sup>1\*</sup> ; HEKI, Kosuke<sup>1</sup>

<sup>1</sup>Department of Natural History Sciences, Faculty of Science, Hokkaido University

The Izu-Ogasawara (Bonin)-Mariana Island arc lies along the convergent boundary between the subducting Pacific plate (PA) and the overriding Philippine Sea plate (PH) in the western Pacific. Nishimura (2011) found that the back-arc rifting goes on behind the Izu arc by studying the horizontal velocities of GNSS stations on the Izu Islands. Here we show that this rifting has accelerated in 2004 using GNSS data at stations such as Aogashima, Hachijojima, Mikurajima, Shikinejima, and Nijima (we excluded stations in the Miyake Island because of the volcanic deformation).

The back-arc rifting behind the Izu islands can be seen as the increasing distance between stations in the Izu Islands (they are located to the east of the rifting axis) and stations located in the stable part of PH, e.g. Minami- and Kita-Daito islands. We found that their movement showed clear acceleration around the third quarter of 2004. Such an accelerated eastward movement could be interpreted not only as the acceleration of the back-arc rifting, but also as the trenchward movement of the arc due to a slow slip episode at the PH-PA boundary.

We first rule out the second possibility by constraining the onset time of the acceleration episode, and by correlating it with other inter-plate earthquakes in the PH-PA boundary. There was an inter-plate earthquake occurred on May 29, 2004 (M6.5) at the PA-PH boundary just to the south of the Boso-oki triple junction. However, the time series clearly lacked the jump which should mark the onset of the eastward slow movement. Moreover, the additional velocity vectors do not converge to the epicenter, and the onset time that minimizes the post-fit residual is significantly later than May. We therefore conclude that the accelerated eastward movement started in 2004 was not due to the afterslip of the interplate earthquake in May.

We found that the onset time coincides with the occurrence of the September 5, 2004, Kii-Hanto-oki, September 5, 2004, earthquake (M7.4), which occurred in the PH slab subducting at the Nankai Trough off the Kii Peninsula. We found that the accelerated movement vectors of these islands are almost parallel with each other, and perpendicular to the rift axis. We hypothesize that the seismic wave radiated from the epicenter of this earthquake dynamically triggered the acceleration of the back arc opening in the Izu Arc.

Keywords: GPS, GNSS, Izu-Bonin Arc, time series, back-arc opening, acceleration

## Subsurface structure and slip pattern of the Median Tectonic Line, SW Japan inferred from GPS displacement rate field

EDAGAWA, Nobuko<sup>1</sup> ; TABELI, Takao<sup>1\*</sup> ; ICHITANI, Shozui<sup>2</sup> ; NAKAMURA, Yasuhiko<sup>2</sup>

<sup>1</sup>Fac. Science, Kochi Univ., <sup>2</sup>Grad. School Int. Arts Sciences, Kochi Univ.

The Median Tectonic Line (MTL) is the longest arc-parallel fault system in southwest Japan. Its right-lateral strike-slip motion is originated from oblique subduction of the Philippine Sea plate at the Nankai Trough, separating the Nankai forearc sliver (the outer zone) from the inner zone of southwest Japan. The deformation of the forearc sliver is characterized by interseismic contraction in the direction of the plate convergence (NW-SE) and long-term westward block movement along the MTL. In addition the MTL itself has a potential to generate a large inland earthquake in the future. Therefore it is important to understand subsurface structure and current slip/locking pattern of the MTL fault plane.

From dense GPS campaign measurements along a traverse line across the MTL, we have made it clear that a transition zone of the relative motion between the outer and inner zones is located 20-30 km north of the surface trace of the MTL (Tabei et al., 2002). To interpret the transition zone, we used a northward-dipping MTL fault plane which was revealed by seismic reflection survey (Ito et al., 1996) and assumed that its upper part was locked and a stationary right-lateral slip was occurring at depth. However, the concept of a pure strike-slip on an inclined fault plane seems somewhat unrealistic. In addition linear distribution of earthquakes aligned 20-30 km north and parallel to the MTL seems inconsistent to the hypothesis of the dipping MTL fault plane because most of them show a right-lateral slip on a nearly vertical fault plane. Unfortunately station distribution of the nationwide continuous GPS network is rather sparse in the north of the MTL because of the existence of the Seto Inland Sea. In this area we have deployed supplementary three GPS stations and collected continuous data since November 2010.

We propose a kinematic model of the transition zone. The model consists of several vertical right-lateral faults in a hanging wall above the northward-dipping MTL fault plane, which are close and parallel to each other. Distributed slip deficits on this parallel fault system may block the relative motion between the outer and inner zones and act as a broad shear zone as a whole. In this study we assume four parallel faults with different widths and depths from surface. Integrated displacement field from relative block motion and slip deficits on these faults is consistent with that derived from a strike-slip on an inclined fault.

We check the effect of the 2011 Tohoku-Oki earthquake on the deformation field of southwest Japan. We compare two displacement rate fields before (Jan. 2006 - Dec. 2009) and after (Mar. 2011 - July 2013) the earthquake. After the earthquake, additional wide-area displacements of 1-4 cm/yr trending to the source region (extension) have been superposed on the original compressional deformation field due to the subduction of the Philippine Sea plate. No significant change has been recognized in the latter.

Keywords: Median Tectonic Line, Nankai Trough, GPS, Deformation

## Continuous GPS observation in northern part of Nansei Islands

NAKAO, Shigeru<sup>1\*</sup>; YAKIWARA, Hiroshi<sup>2</sup>; HIRANO, Shuichiro<sup>2</sup>; GOTO, Kazuhiko<sup>2</sup>

<sup>1</sup>GSSE, Kagoshima Univ., <sup>2</sup>NOEV, Kagoshima Univ.

GEONET, which is a nationwide GPS observation in Japan cover on all over Japan. However, there is a GEONET site in Toshima-mura which is located in northern part of Nansei Islands. This region is defined the boundary between Northern and Central part of Ryukyu arc (Nishimura et al., 2004). It is not clear that where is the boundary because there is almost no GPS site. Goto (2013) concluded that the great earthquake occurred in 1911 is the interpolate event in this region. We set up the continuous GPS in islands of this region due to observe crustal deformation in this region.

In Akuseki Island (AKSK), Takarajima (TAKR) and Kuchinoshima (KCHI), continuous GPS (CGPS) observation started in March 2007, July 2007 and September 2010, respectively. CGPS set up on Gajyajima (GJYA) and Ujishima (UJIS), where is a deserted island, in May 2009. CGPS in Yokoatejima (YKAT) started in September 2013. Data is recorded at CGPS sites. Electric power system at GJYA, UJIS and YKAT is composed of batteries and photovoltaic cells.

Bernese GPS Software ver. 5.0 are used with IGS precise ephemerides and IERS rotation parameters. We also estimated tropospheric delays every hour and their horizontal gradients every six hours.

The short-term repeatabilities are from 1.6 to 3.0 mm in horizontal component and from 6.5 to 7.9 mm in vertical components. These observation is expected to make contribution to resolve rigid movement and crustal deformation in this region.

## The detection of crustal deformation associated with earthquake swarm in Tanzania observed by SAR

HIMEMATSU, Yuji<sup>1\*</sup> ; FURUYA, Masato<sup>1</sup>

<sup>1</sup>Graduate School of Science, Hokkaido University

The East Africa Rift Valley is one of the divergent plate boundaries can be seen on the land surface. The area undergoes middle-class earthquakes and eruptions due to the existing faults and volcanoes.

An earthquake swarm occurred in the Northern Tanzania in July 2007 including the largest earthquake with Mw5.9 and lasted for approximately two months. According to the Global CMT solution, eight  $M > 5$  earthquakes occurred during the earthquake swarm and all of them were reported to be caused by normal fault. One week after the start of the swarm, an effusive eruption began at Mt. Oldoinyo Lengai located near the epicentral region, and a major ash eruption was observed by the time when swarm was terminated.

Biggs et al. (2009, 2013) also detected the crustal deformation associated with the earthquake swarm and Mt. Oldoinyo Lengai eruption, using mainly ENVISAT/ASAR C-band SAR data. In these interferograms, however, the ground displacements at some deforming areas were uncertain because of the difficult of phase-unwrapping. Also, these datasets were acquired only along the descending track, and the 3D deformation fields were unclear. Therefore, we used the L-band ALOS/PALSAR data obtained at both ascending and descending track to detect the detailed crustal deformation.

The purpose of this paper is to elucidate the mechanism of crustal deformation associated with the earthquake swarm in Tanzania in 2007 by interferometric synthetic aperture radar (InSAR).

By using InSAR data for ascending and descending track and the azimuth-offset data, we determined the 3D displacement. The results show a subsiding region along the NE-SW direction that are sandwiched by two horizontally deforming regions toward NW and SE directions. These spatial variation patterns are consistent with the expected direction, where the East Africa Rift Valley is expanding. In addition, the azimuth-offset data reveals slightly southward displacement in sediment area.

The ground at the subsiding region indicated ~62 cm subsidence and ~33 cm horizontal displacement toward SSE. The two-lobe pattern in eastern and western half each moved several centimeter upward and ~50 cm in NW-SE direction horizontally.

In order to describe the ground displacement in detail, we estimated a fault source model assuming slip distribution in a homogeneous elastic half-space. Considering the complexity of the fault geometry, we derive a non-planar fault source model with triangular dislocation elements. Based on the result captured by InSAR and the observed area is in tension field, we propose two fault segments. The model indicates dip-slip and strike-slip displacement with maximum slip of about 1 m and 75 cm at 2-4 km depth.

Derived slip distribution can well explain the spatial variation pattern acquired by InSAR. The amount of moment release inferred from the model (Geodetic Moment: GM) exceeds that of the earthquake swarm (Seismic Moment: SM), and the ratio (SM/GM) is 37.2 percent. The ratio indicates that significant aseismic crustal deformation contributes to GM.

Some interferograms also detected the crustal deformation associated with Mt. Oldoinyo Lengai eruption during the earthquake swarm. We will also discuss the relationship between the earthquake swarm and the volcanic eruption of Mt. Oldoinyo Lengai.

Keywords: InSAR, Crutal deformation, East Africa rift valley, Earthquake swarm, Continental techtonics, Tanzania

## Coseismic Deformation Detected by SAR and Fault Source Modeling of the 2009 Cinchona Earthquake (Mw6.1), Costa Rica

UMEMURA, Shutaro<sup>1\*</sup> ; FURUYA, Masato<sup>1</sup>

<sup>1</sup>Department of Natural History Sciences, Hokkaido University

A shallow earthquake with magnitude 6.1 (Mw) occurred in Costa Rica, Central America, on 8 January 2009. This earthquake, called Cinchona earthquake, accompanied with many landslides and caused around 20 fatalities. In the proximity of epicenter, there is the Angel-Vara Blanca fault that has a strike NNW-SSE. Montero et al. (2009) inferred the fault as the earthquake source fault. After 4 days of the earthquake occurrence, Poas volcano located 6 km to the west of the epicenter erupted (Volcanic Explosivity Index 1) after a quiescence of one year. This volcano had remained dormant for a decade after 1996 and became active since 2006. As the 1st step to study the possible relationship between earthquake and volcanic eruption, we detected the coseismic deformation by using the ALOS/PALSAR data and created fault models to explain the data.

In this study, we used ascending (path 162, frame 190) and descending (path 465, frame 3410) data of ALOS/PALSAR. To correct for the topography effect, we used the digital elevation model of ASTER GDEM. We analyzed the SAR data with GAMMA software. In the interferogram processing, we removed the atmospheric noise. We calculated the Green's function by triangular dislocation elements using Meade (2007) scripts.

The detected interferogram indicated that the maximum coseismic LOS (Line of Sight) changes were 20cm for ascending and 22cm for descending track, respectively. We derived the fault source model that could explain the LOS changes by trial-and-error approach. The estimated strike/dip angle of the fault were 133/65, and the rake angle at the center of fault was -163 degree. The difference of fault parameter from Angel-Vara Blanca fault suggested that the previously unknown fault worked. We calculated the pressure change caused by fault movement. This indicated positive change (compression) under the Poas volcano.

Keywords: InSAR, Coseismic Deformation, Fault Source Model, Costa Rica

## An acceleration event of creeping slip detected by precise leveling survey at the central part of the Longitudinal valle

MURASE, Masayuki<sup>1</sup> ; MATSUTA, Nobuhisa<sup>2\*</sup> ; LIN, Cheng-hong<sup>3</sup> ; CHEN, Wen-shan<sup>4</sup> ; LIN, Jui-jen<sup>3</sup> ; NISHIKAWA, Yuka<sup>4</sup> ; WADA, Erika<sup>1</sup> ; KOIZUMI, Naoji<sup>5</sup>

<sup>1</sup>Department of Geosystem, College of Humanities and Sciences, NIHON University, <sup>2</sup>Graduate School of Environmental Studies, Nagoya University, <sup>3</sup>Institute of Earth Sciences, Academia Sinica, <sup>4</sup>National Taiwan University, <sup>5</sup>The National Institute of Advanced Industrial Science and Technology

Precise levelling surveys were conducted across the central Longitudinal Valley Fault, eastern Taiwan, to understand the deformation of the transition zone between the stable fault creep area and the locked area, which maybe correspond to an asperity. In order to investigate the surface relationship between the fault creep area and the geological condition of the transition zone, we established levelling routes in the Yuli, and Chike-san areas. The Yuli area forms the geological boundary of the Lichi Melange Formation, which is composed of chaotic mudstones containing numerous exotic blocks of various sizes and lithologies. Along the Yuli route, located on the Lichi Melange, an uplift rate of 30 mm/yr was detected during the period 2010-2013, suggesting that aseismic fault creep might be continuing with long-term stability. Along the Chike-san route, located on no Lichi Melange, a vertical deformation rate of 8 mm/yr, 40mm/yr, and 20mm/yr were detected in the period 2010-2011, 2011-2012, and 2012-2013, respectively.

The creep slip distribution was estimated by using a two-dimensional single-fault model proposed at Chike-san in the period 2012-2013. Large slip rates were estimated at 4-5 km of the fault plane. At the previous periods 2010-2011 and 2011-2012, relatively large slip rates were estimated at two parts of the fault plane-one at a depth of about 1.5 km and another at a depth of 4-5 km-. We believe that the acceleration event of creeping slip was continued at the depth of 4-5 km in the period 2012-2013. The northern limit of the stable creep area may be the Yuli area. The episodic creep event occurred in the transition zone between the stable fault creep area and the asperity area. The boundary between the stable creep area and the episodic creep area is consistent with the geological boundary of the Lichi Melange Formation.

Keywords: Taiwan, Longitudinal valley fault, precise leveling survey, aseismic creep motion

## Internal stress changes due to point dislocations in a spherical earth

TAKAGI, Yu<sup>1\*</sup>; OKUBO, Shuhei<sup>1</sup>

<sup>1</sup>Earthquake Research Institute, The University of Tokyo

A simple and complete theory about internal deformations due to point dislocations in a homogeneous half-space was proposed by Okada (1992). This theory has been used by many researches to estimate Coulomb stress changes due to an earthquake and has contributed to understanding of seismology. Although a homogeneous half-space is a first approximation of the earth, global deformation like broad stress changes due to a great earthquake have to be calculated in a more realistic earth model, spherically symmetric earth model. Sun and Okubo (1993) succeeded in calculating surface displacements and gravity changes due to point dislocations in a spherically symmetric earth model. However, internal stress changes and displacements have never been calculated because there exist some difficulties to realize the calculation in spite of early proposal of a fundamental method (Takeuchi and Saito, 1972). In this research, we propose a strategy to realize the calculation of internal deformations and present some computational results.

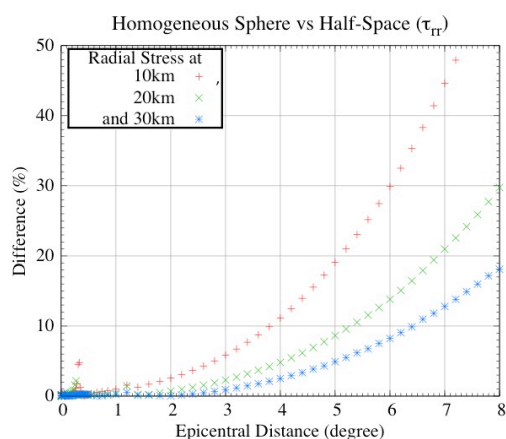
We shall

- i) outline the strategy to calculate internal deformations,
- ii) compare the stress changes in a homogeneous sphere with those in a half-space which were already solved and
- iii) show the results in a stratified earth model such as PREM.

Our study shows that significant difference between a homogeneous sphere and a half-space model occurs when epicentral distance exceeds several hundreds kilometers. For example, epicentral distances at which difference of radial stress changes in two models reach 10% are 4, 5 and 6.5 degrees at observation depth at 10, 20 and 30, respectively (Figure). Angular distance of 4 degrees, which is 400km, roughly equals the length of fault that is thought to have slipped in the 2011 Tohoku-Oki earthquake.

Figure. Difference of radial normal stress changes due to a vertical-strike slip at depth of 32km in two models, a homogeneous sphere and a half-space. The horizontal axis is epicentral distance and vertical axis is difference between the two models in percentage. Red, green and blue points indicate observation depth of 10, 20 and 30km, respectively.

Keywords: internal stress change, spherically symmetric earth, point dislocation, stratification



## Continuous measurements of ocean bottom crustal movements based on GPS-acoustic system using GPS buoy

IMADA, Naruyuki<sup>1\*</sup> ; TERADA, Yukihiro<sup>2</sup> ; SAKAUE, Hiromu<sup>3</sup> ; TADOKORO, Keiichi<sup>4</sup> ; KATO, Teruyuki<sup>5</sup>

<sup>1</sup>Hitachi Zosen Corporation, <sup>2</sup>Kochi National College of Technology, <sup>3</sup>None, <sup>4</sup>Graduate School of Environmental Studies, Nagoya University, <sup>5</sup>Earthquake Research Institute, the University of Tokyo

We report the results of experiments of continuous measurements of ocean bottom crustal movements using GPS buoy and acoustic system.

We have developed a GPS buoy system for the early detection of tsunami. The system uses a buoy that is freely floating on the sea, tied to the sea bottom using an anchor, equipped with a GPS sensor at the top of the buoy. The system enables us to estimate the position of the buoy in a few centimeter accuracy.

On the other hand, Spiess (1985) and other researchers have developed the GPS-acoustic system for estimating the ocean bottom position in sub-decimeter accuracy. However, these systems have used owned or chartered vessels to measure the position of ocean surface, so that the measurements have been only intermittent. After the 2011 Tohoku-oki earthquake of Mw9.0, it has been recognized that continuous monitoring of ocean bottom crustal deformation is very important. Thus, we got an idea in that the GPS buoy could be used for the continuous monitoring of the ocean bottom crustal movements, if an acoustic system is equipped at the GPS buoy.

Based on this idea, we started experiments using our GPS buoy, which is located off Muroto Peninsula, western Japan, in the year of 2013. After a preliminary experiment in March 2013, we made an experimental observation from August to October of 2013. Three transponders were placed around the buoy and the equipment of sound sender/receiver at the side surface of the buoy. The water depth of the site is about 700meter and the ocean bottom transponders are placed so that the distances among these are in the same scale. We will report the results including noise characteristics of data, daily repeatability of estimated ocean bottom position, effects of swinging buoy, etc.

Currently, 15 GPS buoys have been established around the Japanese coasts. Augmentations of the acoustic system in these GPS buoy network will provide a powerful tool of monitoring ocean bottom crustal movements as well as tsunamis. Further requirements to GPS buoys are to be placed farther offshore, say, more than 100km from the coast. Recent developments of the GPS buoy system, including a newly developed algorithm, PPP-AR (precise point positioning with ambiguity resolution), clarified this requirements. However, still another problem of how data at the buoy placed far offshore is transmitted to land in real-time manner is still to be solved. For such problem of a newly designed high capacity data transmission system using a dedicated satellite system will be necessary. Our current experiment will provide an important data for designing a specification of such satellite system.

Spiess, IEEE Trans. Geosci. Remote Sens., 23, 502-510, 1985

## Movement of a fault arised by a pumping or a spring water and its understanding by poroelasticity -a case of NNW fault-

ISHII, Hiroshi<sup>1\*</sup> ; ASAI, Yasuhiro<sup>1</sup>

<sup>1</sup>TRIES, ADEP

Tono Research Institute of Earthquake Science (TRIES) has developed a borehole stress meter for continuous observation and multi-component borehole instruments. At the present time about 15 borehole stations are in operation. We have investigated crustal movements and behavior of underground water by using data obtained from borehole observations. The depth of the deepest borehole is 1030 m.

Near TRIES, JAEA (Japan Atomic Energy Agency) is constructing deep boreholes with diameters of 4m and 6.5m. And depth is about 500m at the present time. The boreholes are 40m apart and connected by stages. NNW fault is running beside the 6.5m borehole. We are investigating a relationship between water flow and geophysical observations by using experiments of pumping water and spring water.

The main results obtained are as follows:

1. Water level of TGR350 borehole station decreases by pumping water and spring water. Data of the strain meters installed at 350m depth indicate right lateral movements of NNW fault.
2. Data of the strain meters installed at 350m depth indicate left lateral movements of NNW fault in case of recovery of water level.
3. Strain meters installed shallower depth (165m) and extensometers installed in sedimentary layer do not indicate such fault movements.
4. We have considered a mechanism explaining the phenomena by using poroelastic understanding.

We will present the details of observations and analyses.

Keywords: Deep borehole observation, Fault movement by spring and pumping water, Groundwater flow, Understand by poroelasticity, Continuously observable stressmeter

## Construction of Syobasama crustal activity observatory ?Installation of Ishii-type borehole stressmeter?

ASAI, Yasuhiro<sup>1\*</sup> ; ISHII, Hiroshi<sup>1</sup>

<sup>1</sup>Tono Research Institute of Earthquake Science, Association for the Development of Earthquake Pred.

Large changes in the pore pressure in Toki granite have produced by the excavation of underground facilities of Mizunami Underground Research Laboratory (MIU) and drilling well for hydraulic tests in MIU (e.g. Asai and Ishii, JpGU2013). We have observed remarkable stress/strain/tilt variations associated with the pore pressure changes at borehole observation site TRIES, STG300 (on the north-east side of the fault), Togari(TGR350/TGR165), STG100, STG200 (south-west side), respectively within 500m of the MIU.

In this area the NNW trending sub-vertical (normal) fault is exists (e.g. JNC, 2003 and 2004). Pore pressure changes occurs in the south-west side of the fault, its impact were observed in water level/pressure record of the same side, and were also observed in stress, strain and tilt record. On the other hand, its impact were not seen in the water level/pressure record of the north-east side of the fault, but its impact were observed on stress, strain and tilt record. Pore pressure change occurs in the north-east side of the fault are similar to those of the south-east side. This observation results indicate that fault has impermeability and elastic deformation of the rock caused by pore pressure change extends over the fault.

In order to clarify the relationship of groundwater level changes to crustal strain changes at Syobasama observation site which is located approximately 1km northwest of MIU, Tono Research Institute of Earthquake Science has constructed the new borehole depth of 110 m and installation of Ishii-type borehole stress meters is scheduled in February 2014. We will present the details of construction of Syobasama observatory, and result of continuous stress observation with groundwater records.

Keywords: Pore pressure change, Elastic deformation, Mizunami Underground Research Laboratory, Ishii-type borehole stress meter

## Post-seismic crustal movements of the 11 April Mw6.6 Fukushima Hamadori earthquake based on GPS observations

HORI, Kayako<sup>1\*</sup> ; AOKI, Yosuke<sup>2</sup> ; KATO, Teruyuki<sup>2</sup> ; MIYASHITA, Kaoru<sup>1</sup>

<sup>1</sup>Graduate School of Science, Ibaraki University, <sup>2</sup>Earthquake Research Institute , The University of Tokyo

Tohoku earthquake on March 11, 2011 (Mw9.0) was accompanied by a vigorous aftershock activity. One of the aftershocks occurred on April 11, 2011, nearby Iwaki city, Fukushima Prefecture, and was called as Fukushima-Hamadori earthquake (Mw6.6; Depth=5km). The focal mechanism of the earthquake was a normal fault. Co-seismic crustal movements due to the earthquake observed by GPS observation was amounted to about 30cm to northeast direction at Iwaki site.

Crustal deformations associated with the Fukushima-Hamadori earthquake is obtained by InSAR and the data were used to construct detailed fault slip models by the previous studies (Kobayashi et al.,2013 : Fukushima et al.,2013). However, it has not been possible to measure the postseismic deformations using the SAR because the ALOS satellite has terminated its operation in immediately after the Fukushima-Hamadori earthquake. Thus, the postseismic crustal movements has been observed only by the GPS observations. Therefore, we aim to elucidate the mechanism of postseismic deformations due to the Fukushima-Hamadori earthquake using the GPS data in this study.

In this study, it was assumed that postseismic crustal deformations were caused by a slip in the vicinity of the fault. We used earthquake fault geometries employed by previous studies (Kobayashi et al.,2013 : Fukushima et al.,2013). As the GPS data is including large postseismic displacements due to the main shock since the March 11, first, we removed the postseismic transient displacements from GPS data using a postseismic slip model of the main shock (Fukuda et al., 2013). The obtained residual displacements after April 11, 2011, are considered as postseismic displacements due to the Fukushima-Hamadori earthquake. We, then, estimated slip distribution on the fault plane based on the residual displacement field. We will discuss estimated results in our presentation.

## Coseismic slip distribution for the 2011 Tohoku-Oki earthquake with topographic corrections

GOSHIMA, Hitoshi<sup>1\*</sup> ; MIYAZAKI, Shinichi<sup>1</sup>

<sup>1</sup>Graduate School of Science, Kyoto Univerisy

Seismological study (Ide et al., 2011) revealed that the rupture of the 2011 Tohoku-Oki earthquake extended to the Japan Trench (i.e. free surface). Since the depth of the trench is about 8km, it is not appropriate to use green functions for elastic half-space media as given by e.g., Okada (1992). When we employ green functions for the half-space, it is not possible to satisfy the following two conditions simultaneously; (1) the updip limit of the rupture is ~8km deeper than the ground surface, and (2) the rupture extends to the free surface (i.e. the trench). If the condition (1) is satisfied, the rupture extends to ~8km at depth, not to the free surface. On the other hand, if the condition (2) is satisfied, the depth of the trench must match to the ground surface. The maximum discrepancy in between predicted ground displacements for the condition (1) and (2) is 5% in horizontal, and 15% in vertical component. Thus, it may be important to take the topography into account in green functions.

In this study we applied the topographic correction on green functions as proposed by Williams and Wadge (2000). Segall (2010) suggests that this method is applicable to approximately incorporate the earth sphericity into green function for observation sites within about 600km from the dislocation. Combining those two corrections, we are able to calculate corrected green functions for spherical earth with topography. Although this method gives only approximate green functions, it helps us to investigate the dependence of green functions on topography and fault geometry.

Then we use the corrected green functions for the inversion of coseismic slip distribution for the 2011 Tohoku-Oki earthquake. In the inversion we use the following data set: GEONET F3 solutions obtained by the Geospatial Information Authority of Japan (GSI), the ocean bottom deformation data by the Japan Coast Guard (Sato et al., 2011), and that of Tohoku University (Kido et al., 2011; Ito et al., 2011). Then the inversion result is compared with the half-space solutions.

Keywords: crustal deformation, the 2011 Tohoku-Oki earthquake, topography, sphere

## Secular change of permeability estimated by using the variations of groundwater discharge

MUKAI, Atsushi<sup>1\*</sup> ; OTSUKA, Shigeaki<sup>2</sup>

<sup>1</sup>Faculty of Informatics, Nara Sangyo University, <sup>2</sup>Faculty of Humanities and Sciences, Kobe Gakuin University

Secular change of permeability causes the variation of the atmospheric pressure admittance of groundwater discharge. We estimated the permeability of the surrounding crust by using the groundwater discharge observed at Rokko-Takao station during 12 years from 2001 to 2012. The estimated secular change of permeability contained the short term variations for about a year as well as the gradual decrease. It is considered that the gradual decrease of permeability was caused by the closure of the cracks, which were opened in the 1995 Hyogoken Nanbu earthquake, due to the accumulation of mud and the crustal stress. On the other hand, the short term variations of permeability suggest the temporary re-open of the cracks due to the earthquake ground motions.

The Rokko-Takao station is located in Kobe, the southern Hyogo prefecture, and passes through the fracture zone of Manpukuji fault. At this station, the significant increase of groundwater discharge was observed just after the 1995 Hyogoken Nanbu earthquake (Fujimori et al., 1995). This suggested that the many cracks were opened in the fracture zone around the station by the ground motion of the earthquake. Mukai and Otsuka (2009) estimated the elastic properties by using the tidal strains observed at the station and reported that the Young's modulus of the surrounding crust showed the secular increase. This suggested that a part of cracks were closed by the crustal stress and the accumulation of mud and the strength of the fracture zone had been recovering.

Mukai and Otsuka (2013) estimated the variations of permeability due to the 2011 Tohoku earthquake by using the atmospheric pressure admittances of the groundwater discharge observed at the station under the assumption of one-dimensional model about groundwater migration. The permeability just after the earthquake increased by about 1.9 times just before the earthquake and decreased to the level about 1.3 times just before the earthquake in 10 months. This suggested that even the small ground motions due to the teleseismic waves could cause the outflow of the mud and the temporary re-open of the cracks in the fracture zone.

In this study, we estimated the secular change of permeability around the station during 12 years from 2001 to 2012 by using the procedure of Mukai and Otsuka (2013). The permeability estimated by using the atmospheric pressure admittances of the groundwater discharge showed the secular decrease by about 50% in 12 years. This result agrees to the secular increase of Young's modulus estimated by using the tidal strain and is considered that the gradual decrease of permeability was caused by the recovering of the fracture zone, in which the cracks were opened in the 1995 Hyogoken Nanbu earthquake.

Keywords: fracture zone, permeability, groundwater discharge, strain change

## Vertical crustal deformation in Boso Peninsula from 1966 to 2001 deduced from leveling and sea level data

KOBAYASHI, Akio<sup>1\*</sup>

<sup>1</sup>Meteorological Research Institute

Leveling data and sea level data for the period from 1966 to 2001 in Boso Peninsula, Japan, were investigated to characterize unsteady vertical deformation. We estimated the steady vertical deformation rate at each GEONET GNSS station using the daily coordinates for the periods from January 1997 to January 2011 avoiding the period of the large earthquakes.

First-order leveling surveys have been conducted repeatedly every one or several years since 1966 in Boso Peninsula. We determined crustal displacements by comparing leveling data from successive surveys. We subtracted subduction-related steady component derived by the GNSS from the distribution of vertical crustal displacements during periods between leveling surveys. If any episodic events have not occurred, they should show little spatial variation around zero vertical displacement. Unsteady vertical deformation was not seen in the period from 1966 to 2001 except the land subsidence by pumping industrial water and natural gas brine.

Keywords: Boso Peninsula, crustal deformation, leveling, sea level

## 2014 Boso slow slip

OZAWA, Shinzaburo<sup>1\*</sup>

<sup>1</sup>Geospatial Information Authority of Japan

### Introduction

The GPS network detected transient crustal deformation on the Boso peninsula in 1996, 2002, 2007, and 2011. The detected transient displacements subsided for approximately 10 days. Rupture process and slip area are similar among the past four Boso SSE. The recurrence intervals of Boso SSE are 6.4, 4.9, 4.2 years from 1996. Under this circumstance, the anticipated slow slip event started from January 1 2014. This recurrence interval of 2.2 years is the shortest one compared with the previous 4 slow slip events. In this research, we estimate spatio-temporal evolution of the 2014 Boso slow slip and compare it with those in 1996, 2002, 2007, 2011.

### Data and analytical procedure

Trend and annual components which are estimated for the period between 2009 and 2011 are removed from the raw time series. The detrended crustal deformation in 2014 shows southeastward movements with 1 cm maximum movement in the Pacific coastal area.

We employed time dependent inversion to the detrended crustal deformation associated with the 2014 Boso SSEs. We used EW, NS, and UD components of crustal deformation at approximately 40 GPS sites relative to Yasato station. The plate geometry of the upper surface of the Philippine Sea plate is based on Nakajima and Hasegawa [2006]. The fault geometry is composed on the B-spline and slip on the fault is also composed of superposition of B-spline function. As a boundary condition, we set 0 slip on the edge of the fault geometry.

### Results and Discussion

The results show that the slow slip started offshore of the Boso peninsula and expanded to the south over time. The estimated moment magnitudes are 6.4, while those area 6.4 in 1996, 6.5 in 2002, 6.5 in 2007 and 6.6 in 2011. The 2014 Boso SSE ruptured an area similar to those of the four Boso SSEs. The recurrence interval is 6.4 year from 1996 to 2002 events, 4.9 years from 2002 to 2007 events, 4.3 year from 2007 to 2011, and 2.2 years from 2011 to 2014 events. The five events do not seem to be slip predictable nor time predictable. Though the 2011 event shows the largest magnitude among four cases, recurrence interval from 2007 event is the shortest. We cannot rule out a possibility that the Tohoku earthquake may have affected the occurrence of the 2011 event. In fact, dCFF increased near the rupture area of the Boso peninsula from the Tohoku earthquake [Hirose et al. 2012]. However, it remains unclear the reason why recurrence interval change drastically from 4.2 to 2.2 years for the 2011 and 2014 events, since dCFF does not change so much from 2011 and 2014. Another interpretation of shortening of recurrence interval is based on a scenario proposed by several simulation studies in which recurrence interval of slow slip events become shorter as occurrence of large earthquake nears. If this is the case, it is quite important to monitor crustal deformation on and around the Boso peninsula..

Keywords: Boso peninsula, slow slip

## Estimation of frictional parameters in afterslip areas by assimilating GPS data :The 2003 Tokachi-oki earthquake

KANO, Masayuki<sup>1\*</sup> ; MIYAZAKI, Shinichi<sup>2</sup> ; ISHIKAWA, Yoichi<sup>3</sup> ; HIYOSHI, Yoshihisa<sup>3</sup> ; ITO, Kosuke<sup>3</sup> ; HIRAHARA, Kazuro<sup>2</sup>

<sup>1</sup>ERI, Tokyo Univ., <sup>2</sup>Kyoto University, <sup>3</sup>JAMSTEC

Seismological and geodetic observations have revealed that various aspects of fault slips are determined by frictional properties on the interface. Kano et al. (2013) developed an adjoint data assimilation method to estimate frictional parameters from synthetic in-situ slip velocity data and found by numerical experiments that all frictional parameters are constrained if both acceleration and deceleration phases are observed. Additionally, we found that synthetic surface displacement data also have the ability to constrain frictional parameters in the areas where slip is well resolved. Following their study, we then applied the method to an actual case of the 2003 Tokachi-oki earthquake. Given reasonable initial conditions of simulation variables, estimated frictional parameters are well constrained if two conditions above are satisfied. Our results imply that the adjoint method we developed is useful to investigate and understand fault frictional properties.

Keywords: afterslip, adjoint method, frictional parameters, GPS, earthquake cycle

## Crustal deformation of the northeastern margin of the Izu Collision Zone inferred from GPS observations

DOKE, Ryosuke<sup>1\*</sup> ; HARADA, Masatake<sup>1</sup> ; SATOMURA, Mikio<sup>1</sup> ; MIYAOKA, Kazuki<sup>1</sup>

<sup>1</sup>Hot Springs Research Institute of Kanagawa Prefecture

Izu Collision Zone is characterized by the collision between Izu Peninsula and Tanzawa Mountains, and Philippine Sea Plate also subducts beside this zone. Because of these complicated plate geometries, a number of historical earthquakes occurred in the northeastern margin of this zone. Additionally, there are a lot of active faults in the marginal area of the collision zone.

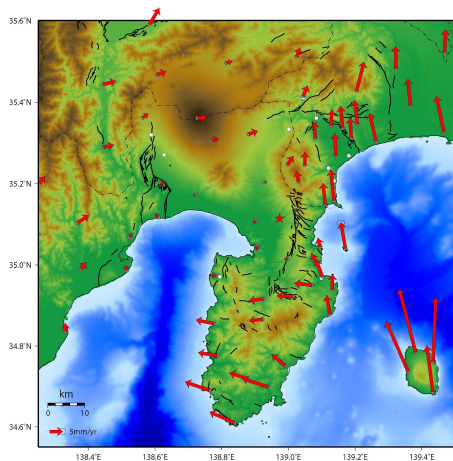
It is important to describe the steady state of crustal deformation in the Izu Collision Zone, in order to clarify mechanisms of earthquakes occurring in this area. In this study, we examined crustal deformation of the northeastern margin of Izu Collision Zone by using the datasets of GEONET sites (coordinate F3) and our original GPS sites.

Based on the displacement velocity vector diagram and profile, we can point out the following characteristics of crustal deformation there.

- 1) Remarkable northward crustal displacement vectors were observed in the eastern area of the Kita-Izu fault zone.
- 2) A shear zone with North-South trend was detected in the area between Kita-Izu fault zone and Ashigara Plain. Width of its zone was estimated about 15-20 km. Average shear strain rate in this zone was about 0.47 micro-strain per year.
- 3) Such remarkable crustal displacement vectors were not observed in the western area of the Kita-Izu fault zone.

This shear zone may be a transition zone between the collision and the subduction blocks on the Philippine Sea Plate, caused by the displacement gap between the blocks.

Keywords: GPS, crustal deformation, Izu Collision Zone, Kita-Izu fault zone



## The wind velocity correction of the precipitation to use for the rainfall correction of the volumetric strainmeter

KIMURA, Kazuhiro<sup>1\*</sup>

<sup>1</sup>Meteorological Research Institute

The rainfall correction of the volumetric strainmeter has the sensitivity that can judge quality of the precipitation data.(Kimura et al., 2013) In the observation of the rain gauge, it is well known that a capture rate of the rainfall decline at the time of a strong wind. We try the rainfall correction of the volumetric strainmeter in consideration of wind velocity dependence. As a result, the strainmeters at the slope of the big mountain or near the river where had a long basin area is improved the rainfall correction. This is not influence of the capture rate of the rain gauges, it is caused by the fact that altitude dependence of the precipitation is remarkable as a strong wind.

For the rainfall correction of the crustal movement data such as the volumetric strainmeter, it is necessary to consider it about the rainfall at high altitudes in addition to the precipitation around the observation station.

Keywords: strainmeter, rainfall correction, wind velocity, altitude dependence of the precipitation

## The change except the sudden contraction of the Higashiizu staraimeter with the seismic activity east off Izu Peninsula

KIMURA, Kazuhiro<sup>1\*</sup> ; KIMURA, Hisao<sup>2</sup>

<sup>1</sup>Meteorological Research Institute, <sup>2</sup>Japan Meteorological Agency

The sudden contraction strain change of the Higashiizu staraimeter with the seismic activity east off Izu Peninsula is well known. These changes were clear for anyone, but the Higashiizu staraimeter couldn't detect the long-term change that Murakami(2006) pointed out by the GNSS data until now. However we became able to remove the seasonal change by the rainfall from the strainmeter data by using the rainfall correction(Kimura et al., submitted). After reviewing the Higashiizu strainmeter data using the rainfall correction, this data detect the interesting change with the seismic activity east off Izu Peninsula.

Keywords: Strainmeter, seismic activity east off Izu Peninsula, Higashiizu

## Characteristic strain distribution following the 2011 Tohoku earthquake based on the kinematic PPP analysis

HIRATA, Yuichiro<sup>1\*</sup> ; OHTA, Yusaku<sup>1</sup> ; OHZONO, Mako<sup>2</sup> ; MIURA, Satoshi<sup>1</sup>

<sup>1</sup>Gradual School of Science, Tohoku University, <sup>2</sup>Faculty of Science, Yamagata University

The 2011 off the Pacific coast of Tohoku Earthquake (March 11, 2011, M 9.0) generated widespread coseismic deformation. The slip on the plate boundary is larger than the 10 m in widely (e.g. [1]). Ohzono et al [2] found inhomogeneous strain distribution caused by the coseismic step of the 2011 Tohoku earthquake. They extracted the residual strain distribution, which is estimated by comparison between the expected coseismic displacement by a simple rectangular faults model and the observed coseismic displacement in the Tohoku area. Ozawa and Fujita [3] found the local deformation around the Akita-Komagatake, Kurikoma, Zao, Azuma, and Nasu volcanoes caused by the 2011 Tohoku earthquake based on the ALOS/PALSAR and GPS data. They suggested that the coseismic extensional deformation concentrates in the soft medium under a volcano and that this deformation has caused local deformation with subsidence based on the FEM modeling. These previous studies, however, used the daily coordinates time series of the GPS observation. Thus, these previous studies result might be contained early postseismic displacement following the 2011 Tohoku earthquake. Based on these backgrounds, we tried to extract the pure coseismic deformation by the kinematic Precise Point Positioning (kPPP) approach.

We estimated every 1 seconds coordinates time series of the 1,208 GEONET by the GIPSY-OASIS II software version 6.1.2. We defined the "pure" coseismic displacement, which is coordinate difference between just before the origin time and 600 seconds after the event. We averaged from 500 to 700 seconds after the event for eliminating short-term fluctuation of the time series. Based on the estimated "pure" coseismic displacement, we estimate the dilatation strain distribution by method of the [4]. We also estimated strain distribution in the early time period after the 2011 Tohoku earthquake, which estimated coordinate difference between coseismic displacement by the daily coordinate (e.g. difference between 10 to 12th March, 2011) and "pure" coseismic displacement by the kPPP analysis.

As a result, we found the characteristic local expansion in and around the Mt. Gassan, which located in Yamagata prefecture. We also found the characteristic contraction in and around Mt. Zao even though this obtained strain amount is smaller than the noise level determined by the kPPP time series. We also estimated strain distribution of early postseismic between mainshock and 15th March for the understanding the spatiotemporal development of strain distribution. The area of the expansion is clearly larger than the 12th March in and around the Mt. Gassan. Furthermore, the contraction area around the Mt. Zao clearly changed to expansion between just after the mainshock and 15th March.

In the presentation, we will discuss more detail characteristics and its interpretation of the obtained strain distribution.

[1] Inuma et al., (JGR, 2012), [2] Ohzono et al., (EPS, 2012), [3] Ozawa and Fujita, (JGR, 2013), [4] Shen et al., (JGR, 1996)

Keywords: strain, 2011 Tohoku earthquake, postseismic deformation, kinematic PPP

## Convergence of the Philippine Sea Plate in Mindanao, the Philippines

NAKAMURA, Yasuhiko<sup>1\*</sup>; TABELI, Takao<sup>2</sup>; OHKURA, Takahiro<sup>3</sup>; KIMATA, Fumiaki<sup>4</sup>; TERESITO C., Bacolol<sup>5</sup>; ENDRA, Gunawan<sup>6</sup>

<sup>1</sup>Grad. School Int. Arts Sciences, Kochi Univ., <sup>2</sup>Fac. Science, Kochi Univ., <sup>3</sup>Aso Volcanological Laboratory, Kyoto Univ., <sup>4</sup>Tono Research Institute of Earthquake Science, <sup>5</sup>Philippine Institute of Volcanology and Seismology, <sup>6</sup>Grad. School of Environmental Studies, Nagoya Univ.

Tectonics of the Philippines Archipelago is characterized by westward subduction of the Philippine Sea plate at the Philippine Trench in the east ( 5.8 - 7.0 cm/yr), eastward subduction of the Sunda plate at the Manila Trench in the west ( 3.3 - 3.6 cm/yr), and left-lateral strike-slip movement of the Philippine fault inland. Under the SATREPS project "Enhancement of earthquake and volcano monitoring and effective utilization of disaster mitigation information in the Philippines" we have conducted yearly GPS campaign measurements in the eastern part of Mindanao since March 2010. The main purpose of the observation is to make clear the plate locking distribution at the Philippine Trench and slip/locking pattern of the Philippine fault in order to estimate earthquake generation potential in Mindanao.

We occupied 15 sites in the eastern Mindanao and collected continuous data for successive three to six days on March 2010-2013. Collected data were processed with Bernese software ver.5.0 together with the data from global IGS station (PIMO near Manila) to obtain coordinates and displacement rates based on ITRF2008. The displacement rates were then converted to those with respect to the Sunda plate. Moreover we used previous displacement rate data obtained in the central and western Mindanao from the 1997-2003 campaign measurements to cover the whole of Mindanao.

The resulted displacement rate field shows that west-northwest motions are dominant due to the convergence of the Philippine Sea plate from the east but their spatial decay with increasing distance from the trench is not significant. Even the full locking of the Philippine Trench plate interface down to the depth of 80 km can explain only 29 percent of the observed displacement rate at the maximum. Thus we need to introduce remarkable rigid block rotations to interpret the deformation pattern of Mindanao. As a result of the estimate of pole position and angular velocity of the block rotation, deformation field of Mindanao cannot be reproduced by a rotation of single block. Considering the Philippine fault as a block boundary, it is natural to introduce multiple blocks into Mindanao. Unfortunately current station coverage and density are not enough to resolve elastic deformation due to plate locking at the trench and rigid motions due to multiple block rotations.

Keywords: Philippine Trench, Philippine fault, GPS observation, Mindanao

## Slip deficit rate distribution and its temporal changes along the Japan islands

HIGUCHI, Shun<sup>1\*</sup> ; KOKETSU, Kazuki<sup>1</sup> ; YOKOTA, Yusuke<sup>2</sup>

<sup>1</sup>Earthq. Res. Inst., <sup>2</sup>Japan Coast Guard

The Japan islands are located along several plate boundaries, where the oceanic plates are subducting beneath the continental plates. Due to this subduction, slip deficits are being generated and strain is being accumulated in coupled zones of the plate boundary so that many large earthquakes have occurred. Therefore, in order to reveal the generation mechanism of large earthquakes at the plate boundaries, it is necessary to clarify slip deficit rate distributions. In addition, as seen in long-term slow slip events, there are significant temporal changes in the slip deficit rate distributions. In this study, we determined the slip deficit rate distribution along the whole Japan islands for each year from 1996 to 2010 (the observation period of GEONET operated by GSI before the 2011 Tohoku earthquake) using the inversion method, and compared each other to investigate their temporal changes.

For calculating the deformation fields in Japan, we used the daily coordinates of F3 solutions. We obtained daily time series data considering the movements of the continental plates against reference frame and removing the offsets and postseismic effects due to nearby earthquakes. We then derived horizontal rate fields in Japan for each year by least-squares fittings. For reflecting the geometry of the plate boundaries, we used the plate model (Baba et al., 2005) incorporated in JIVSM (Koketsu et al., 2012). The Green's functions were calculated using the frequency-wavenumber method (Zhu and Rivera, 2002). We performed slip deficit inversions using the method of Yoshida et al. (1996).

The slip deficit rate distributions derived from the inversions were consistent with the previous study and the plate convergence rates. In addition, known long-term slow slip events were found in the temporal changes of the slip deficit rate distributions. Furthermore, we can see the temporal changes in the Hokkaido and Kanto regions, which suggest variations of plate coupling in these regions. The zones of large slip deficit rate in the distributions look corresponding to the source regions of past megathrust earthquakes. These correspondences are significant not only in Earth science but also in seismic hazard assessments.

Acknowledgement: We would like to thank Geographical Survey Institute for geodetic data recorded by GEONET.

Keywords: the Japan islands, crustal deformation, GPS, slip deficit, megathrust earthquake

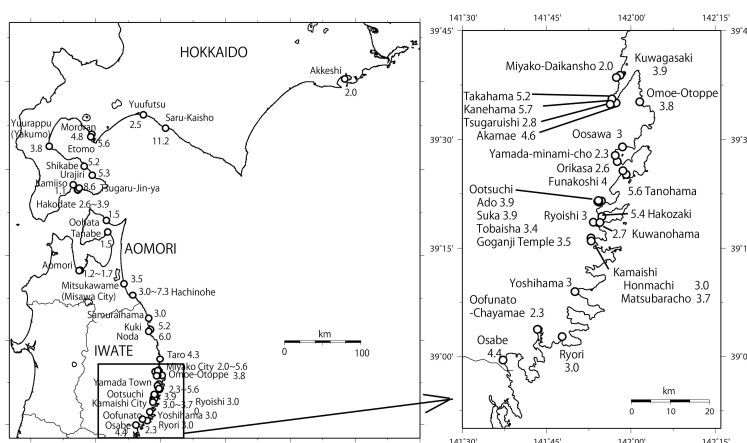
## Height Distribution of the tsunami of the Ansei North Sanriku-Oki earthquake of August 23, 1856

TSUJI, Yoshinobu<sup>1\*</sup> ; MABUCHI, Yukio<sup>2</sup> ; OKADA, Kiyohiro<sup>2</sup> ; KUROYANAGI, Yosuke<sup>2</sup> ; OOIE, Takayuki<sup>2</sup> ; KURIMOTO, Masashi<sup>2</sup> ; KINAMI, Takahiro<sup>3</sup> ; HORIE, Takehito<sup>4</sup> ; HASHIMOTO, Keisuke<sup>4</sup> ; SASAKI, Takayuki<sup>4</sup> ; IWABUCHI, Yoko<sup>5</sup> ; IMAI, Kentaro<sup>6</sup> ; IMAMURA, Fumihiko<sup>6</sup>

<sup>1</sup>Fukada Geolog. Inst., <sup>2</sup>Pacific Consultant, <sup>3</sup>Kubiki Techno., <sup>4</sup>Alpha Hydraulic Eng. Consultant, <sup>5</sup>JNES, <sup>6</sup>IRIDeS, Tohoku Univ.

A large earthquake occurred in the sea area between Aomori coast, most northern district of Honshu, and Hidaka coast, Hokkaido, on 23rd August, 1856 (3rd year of Ansei era) . This earthquake is a one of the series of the plate boundary earthquakes at the joint point of the Japan and the Kuril trenches, where the 1968 Tokachi-Oki earthquake occurred. The 1677 Enpo North Sanriku-Oki earthquake is considered also as the same typed one. The tsunami of the 1856 North Sanriku-Oki earthquake hit the coasts of Sanriku districts, the north east part of Honshu, and the pacific coast of Hokkaido. As the total number of victims of the tsunami was only 38 people in all, and it was considered not to be a large natural hazard. So it did not become a lecture for tsunami hazard in the time of the 1896 Great Meiji Sanriku tsunami. The diary kept by a priest of Kokutaiji Temple at Akkeshi in east Hokkaido records that human disturbance broke out there, and tsunami height was estimated at 2.0 m. At Saru-Kaisho office in Monbetsu town, Hidaka district, a strong tide came in front of the building of the office, where sea water rose up to the height of 11.2 meters. At Etomo village in Muroran city, sea water invaded into the residential area (height: 5.6m). On the pacific side of Hakodate peninsula, sea water flooded up to the fort of Tsugaru Clan "Tsugaru-han Jin'ya" where the ground height is 8.6 m. At Same fishery port in the central area of Hachinohe city, residential area was flooded up to 7.3 meters height. At Kanehama village in Miyako city, which is located at the innermost point of the V-shaped bay, inundation height was 5.7 meters. As for the coasts of south part of Iwate Prefecture Tsuji et al.(1995) conducted survey. Together with this result, we have the distribution map of the tsunami height as the figure. The authors of the present study wish to express their thanks to JNES for its financial support in promoting our research.

Keywords: historical earthquake, historical tsunami, Sanriku coast, Hokkaido, Japan trench



## Reexamination of 1945 Mikawa earthquake disaster (1) Detailed distribution of earthquake victims

KIMATA, Fumiaki<sup>1\*</sup> ; MATSUTA, Nobuhisa<sup>2</sup>

<sup>1</sup>Tono Research Institute of Earthquake Science, Association for the Development of Earthquake Predict, <sup>2</sup>Earthquake and Volcano Research Center, Graduate School of Environmental Studies, Nagoya University

Iida (1978) organized the Mikawa earthquake disaster under the cooperation of Aichi prefecture, and clarify the whole picture of the disaster. However, he could not discuss the disaster in community level precisely. For example, 46% of 1200 houses were collapsed in Hukuji village, Hazu-gun in 1944 ToNankai earthquake, and additionally 67% of left 650 houses were also collapsed in 1945 Mikawa earthquakes one month later. The reason of strong damages in Hukuji is not discussed enough until now.

It is very important to make clear whole picture of the earthquake disaster in history and in near future as national government. As the earthquake disaster remains a rare event, detailed research of the historical earthquake disasters needful to understand the following disasters. In the presentation, we would like to discuss the disaster of the Mikawa earthquake in local community level.

### 1. Discussion on characteristic disaster based on earthquake victim distribution

Earthquake fault shaped S was appeared in the ground surface at the Mikawa earthquake. However recent researches of fault geomorphology and ground deformation based on geodesy point out two main faults striking with NNW-SSE direction, and an E-W striking fault is tear fault caused by slips on two faults. Additionally, dominant rupture should be occurred at Fukodu fault located in east. The total  $M_0$  estimated by ground deformation is the earthquake moment of  $1.6 \times 10^{19} \text{Nm}$  ( $M_w 6.7$ ), and the third four of the released one is by slip of Fukodu fault. In our presentation, we discuss earthquake disaster with the local community level based on two N-S striking earthquake faults.

#### 1) Katahara: compact cluster of dead located close to Fukodu fault

Katahara town of Hoi-gun (then-9300 people and 1887 houses) located just on Fukodu fault, lose 227 people and 319 completely destroyed houses (15.2% collapse rate). In the town, the damages are different in each street corner. Numbers of dead and completely destroyed houses within the town are shown as bar charts and color scale in 59 neighborhood blocks. The dead are limited in the narrow zone of 1 km wide along the earthquake fault. There are some communities with no collapsed house, which are located 1 km distance from the fault. Dead are corresponding to 73 % of completely-destroyed houses, and some blocks closing the fault show the rate over 90%. Precisely, people are attacked by strong seismic waves during the hours of sleep, and they had no time to evacuate to outsides from houses. There are many blocks to have no dead and no collapsed houses, which are locating more 1 km far from the fault.

#### 2) Fukuji: Decentralized dead far from fault in river plain

On the one way, Fukuji village (then-673 houses), Hazu-gun locating 5 km southwestward from the Yokosuka Fault, one of main faults, lost 162-350 peoples and 400 houses completely. In one month before, the village also attacked by 1944 ToNankai earthquake, lost 21 people and 550 houses completely. They lost 1000 houses by earthquakes in 1200 houses for one month. The numbers of the dead are shown in each block in Fig.1B.

The dead distributions are obviously different with that in Katahara. They lost many people in almost all blocks in the village. The collapse rate of ToNankai earthquake is by far the worst in Aichi prefecture, because, second worst is 21.3% in Tomiki village, Chita-gun. The Fukuji village is just located in river plain with Yahagi and old-Yahagi rivers. An exist of thick alluvial formation caused the large damages in Fukuji.

The dead by Mikawa earthquake are caused by two reasons. One is there are very strong shaking at the blocks located immediately above the fault, and second is amplitude shaking by alluvial formation in river plain. The former is a case of Katahara and later is a case of Fukuji.

Keywords: Mikawa earthquake, Fukodu fault, Yokosuka fault, earthquake disaster, seismic victim, collapse rate

## Interpretation of an illegible old stone inscription by SfM image analysis at Itsukushima shrine, Nojimizaki

SUZUKI, Hinako<sup>1\*</sup> ; UCHIYAMA, Shoichiro<sup>1</sup> ; INOUE, Hiroshi<sup>1</sup>

<sup>1</sup>National Research Institute for Earth Science and Disaster Prevention (NIED)

This study shows that interpretation the illegible old stone inscription by structure from motion (SfM) image analysis. The stone monument built in 1927 for memorial on the 1923 Taisho Kanto Earthquake, the inscribed capitals can hardly read. We captured 158 photographs on the surface of the stone, and processed by SfM to generate 3 D model of it. As a result, illegible capitals became clear on the 3 D model, so visible coated contamination removed by SfM. It is effective method to archive stone inscriptions.

Keywords: structure from motion (SfM), stone inscription, interpretation, historical natural hazard, Nojimizaki



## The Evidence of the Uplift associated with the Kanto Earthquakes inferred from the Marine Terrace in the Alluvial Valley

KIM, Haeng yoong<sup>1\*</sup> ; MANNEN, Kazutaka<sup>1</sup> ; SASAGE, Kazuo<sup>2</sup> ; KUMAKI, Yohta<sup>3</sup> ; MATSUSHIMA, Yoshiaki<sup>4</sup>

<sup>1</sup>Hot Springs Research Institute of Kanagawa Prefecture, <sup>2</sup>PASCO, <sup>3</sup>Senshu University, <sup>4</sup>Kanagawa Prefecture Museum of Natural History

Recurrent giant earthquakes at the plate boundary along the Sagami Trough have been considered as one of the greatest threat of the Tokyo Metropolitan area. At the southwestern tip of the Miura Peninsula, in south of Tokyo, the tide gauge station records the coseismic uplift amount of 1.4 m and the interseismic subsidence amount of 0.3 m in and after 1923 earthquake, respectively. It is effective to reveal evidences of the past coseismic uplift to know the future earthquake.

Wave-cut benches which emerged in 1923 are widely distributed along the rocky coast. Higher wave-cut benches, good indicators of coseismic uplift prior to 1923, are also recognizable. It is, however, often difficult to spatially compare one another due to the erosion.

We investigated the distribution of the tidal-flat deposits and the 1923 wave-cut benches at two small bays in the southwestern and southern parts of the Peninsula. The aggradation of the coastline associated with the 1923 uplift was identified by the comparison between the 1:25,000 topographic maps before and after the 1923 earthquake. Observations of outcrops and drilling cores at the 1923-formed marine terrace showed that the tidal-flat deposits consist of shelly sand and gravels. The elevation of tidal-flat deposits indicates the coseismic uplift in 1923 and the interseismic subsidence after 1923. The uplift amount was estimated approximately 0.9 m and 2.1 m at the southwestern and southern parts of the Miura Peninsula, respectively. The uplift amount inferred from the tidal-flat deposits is concordant with that inferred by the wave-cut benches.

Keywords: Kanto Earthquake, Paleo-earthquake Record, Alluvial Valley, Microlandform, Tide-zone Deposits, Miura Peninsula

## Coseismic uplifts of the southern Izu Peninsula and the coastal area of Shimizu Plain

KITAMURA, Akihisa<sup>1\*</sup> ; KOBAYASHI, Konatsu<sup>1</sup> ; OHASHI, Yoko<sup>2</sup> ; YOKOYAMA, Yusuke<sup>2</sup> ; MIYAIRI, Yosuke<sup>2</sup>

<sup>1</sup>Shizuoka University, <sup>2</sup>The University of Tokyo

We examined coseismic uplift events in the coastal area of the Shimizu Plain, and at the southern end of the Izu Peninsula. On the basis of lithologies, fossil contents, and radiocarbon dating, we identified geological and paleontological evidence for abrupt changes in depositional environments related to coseismic uplift associated with the AD 1854 Ansei-Tokai earthquake. We estimated a maximum coseismic uplift of 1.2 m and post-earthquake gradual subsidence of ca. 0.6 m. Radiocarbon dating of the emerged sessile assemblages at the southern end of the Izu Peninsula, central Japan suggest that at least four coseismic uplift have occurred in the area, during 3387-2485 cal yr BP, AD 570?820, AD 1000?1270, and AD 1430?1660.

Keywords: Coseismic uplifts, southern Izu Peninsula, Shimizu Plain, Holocene, Ansei-Tokai earthquake

## Former shoreline height and Active Faulting around Obama Bay, Fukui, Central Japan

WATANABE, Mitsuhsisa<sup>1\*</sup>

<sup>1</sup>Toyo Univ.

I examined the distribution of marine terrace surface assigned to the oxygen isotope stage 5e along the coast around Obama Bay, Fukui Prefecture, central Japan. The marine surface is recognizable on the western and southern coast of Obama bay, which indicates only southwestern coast has progressively uplifted. There is no marine terrace surface along the NE coast of the bay. This strongly suggests that an active fault divides the bay just on the extension of the FO-A fault and the Kumagawa fault. The FO-B and FO-A fault are left-lateral active fault trending NW-SE direction. The Kumagawa fault trending WNW-SES direction display the same vertical displacement as them and SW hanging-wall uplift. These active faults composing of an extensive active fault ca. 65-km long across Obama bay displaying distinct trace jog close to the mouth of the bay (Nokogiri-zaki point). Height distribution of the former shoreline on the marine terrace surface shows the uplift pattern in this area. Comparing the uplift pattern with calculated displacement based on the dislocation theory, the fault model mentioned above explains the general features of the crustal deformation.

Keywords: marine terrace surface, former shoreline, submarine active fault, caclulated displacement, Obama bay

## Comparison of the fault zones of the fault activity terminated until the Early Pleistocene and the active fault

OHTANI, Tomoyuki<sup>1\*</sup> ; KONO, Masahiro<sup>1</sup> ; KOJIMA, Satoru<sup>1</sup>

<sup>1</sup>Gifu Univ.

In the active fault surveys without younger sedimentary layers, it is desired that the new method is developed to assess the fault activity using the fault rocks in the basement rocks. To achieve this, it is important to understand the characteristic features of the fault zones not only active faults, but also the faults terminated their activity recently. We studied the fault zone of the Median Tectonic Line (MTL) in Yoshino, Nara, and compare its results with those of active faults.

The MTL is the active fault in the west of the central part of the Kii peninsula, in which the fault activity is terminated recently in the east. In this eastern area, Okada and Togo (2000) show the fault which terminated its activity until 300 ka in the active fault maps. Sangawa and Okada (1977) reported an exposure of fault zone that makes a border of the Early Pleistocene Shobudani Formation and the Cretaceous Izumi Group, and that is covered by the Middle Pleistocene Gojo Formation unconformably. Based on the sedimentary ages of their formation, the MTL in this area is terminated until 1 to 1.2 Ma. The fault exposure reported by Sangawa and Okada (1977) is covered by concrete presently, we studied the fault exposure 13 km east away from the previous exposure.

In this exposure, the fault gouge zone with ca. 1 m thickness strikes E-W. The Izumi formation is in the northern side of the fault zone, in which no exposure in the southern side. The Izumi Formation in this exposure is mainly mudstone. Bedding plane is subhorizontal in the host rock, in which foliation is subvertical in cataclasite near the fault gouge. Composite planar fabric in foliated cataclasite indicates the uplift of the southern side.

The powder X-ray diffraction and X-ray fluorescence analyses were performed using the samples from this fault exposure. The results of the powder X-ray diffraction analysis shows disappearance of mica and formation of chlorite in the foliated cataclasite close to the fault gouge, and decomposition of plagioclase and formation of calcite in foliated cataclasite and fault gouge. The altered minerals indicate a remarkable alteration in foliated cataclasite rather than fault gouge. Smectite is not detected in fault gouge and cataclasite.

The results of the X-ray fluorescence analysis show the increase of TiO<sub>2</sub>, Al<sub>2</sub>O<sub>3</sub>, MgO, K<sub>2</sub>O and P<sub>2</sub>O<sub>5</sub> toward the fault gouge and the decrease of CaO, Na<sub>2</sub>O and MnO in foliated cataclasite and fault gouge. The decrease is especially in foliated cataclasite rather than fault gouge.

The studied feature is compared by that of the active faults. In the active fault zone, the latest fault gouge is characterized by the formation of smectite and concentration of Mn. Smectite is the mineral formed under lower temperature. Mn deposits under the oxidized condition. These are consistent with recent near-surface condition of the active fault zone. The studied fault zone would be displaced in the deeper part because its activity has been terminated and present surface exposure should be exhumed from 1 to 1.2 Ma to present. Mn is difficult to concentrate in the deeper reduction condition.

Keywords: Early Pleistocene, fault zone, active fault

## Analysis for deformation structures, mineral composition, and elemental composition in the Atera fault

KATO, Naoki<sup>1\*</sup> ; HIRONO, Tetsuro<sup>1</sup> ; ISHIKAWA, Tsuyoshi<sup>2</sup> ; KAMEDA, Jun<sup>3</sup> ; OHTANI, Tomoyuki<sup>4</sup>

<sup>1</sup>Department of Earth and Space Science, Graduate School of Science, Osaka University, <sup>2</sup>Kochi Institute for Core Sample Research, Japan Agency for Marine-Earth Science and Technology, <sup>3</sup>Department of Natural History Sciences, Graduate School of Science, Hokkaido University, <sup>4</sup>Department of Civil Engineering, Gifu University

The Atera fault is an active fault extended 70 km along southern — central Gifu Prefecture, Japan, which is considered to slip at 1586 Tensho earthquake based on the field outcrop and trenching survey by previous researches. However, the seismic slip behavior along the fault has been understood. In this study, we performed the field observation on the Tase outcrop of the Atera fault, microscopic observation, X-ray diffraction, trace element analysis by using ICP-MS for investigating the deformation structure, mineral assemblage, and geochemical anomaly in the Atera fault. We will present their preliminary results.

Keywords: Active fault, Fault gouge, Trace element

## Deformation simulations by the discrete element method controlling basement motions by the dislocation solutions

KUSUMOTO, Shigekazu<sup>1\*</sup> ; ITOH, Yasuto<sup>2</sup>

<sup>1</sup>Grad. Sch. Sci. Eng. Res., Univ. Toyama, <sup>2</sup>Grad. Sch. Sci., Osaka Prefecture University

In previous studies on deformation of sedimentary layer due to fault motions within the basement by means of the discrete element modeling, the basement has been treated as rigid body. In this study, we attempted to control motions of the basement by dislocation analytical solutions based on the elasticity in order to discuss the deformation field of the sedimentary layer in connection with fault parameters.

As a result, we found tilt of deformed sedimentary layer which did not appear in the rigid basement model. And, shapes of deformed sedimentary layer around the fault tip were different from rigid basement model, and even in the elastic basement model it was shown that their shapes will be varied by the fault parameters selected in the modeling.

Since sedimentary layers deform by following to shape of deformed basement, and the basement controlled by the dislocation analytical solutions deforms by the fault parameters, it was shown that not only shape of deformed sedimentary layers but trishear and its propagation processes will be able to be discussed in connection with the fault parameters. In the future, we will accumulate some know-how on practical analyses method by applying our modeling procedure to interpretations of topography, geological structures and seismic survey data, and we would like to hasten quantitative discussions on tectonics and/or forming processes of geological structures.

Keywords: Discrete Element Method, Dislocation analytical solutions, Displacement of sedimentary layer, PFC

## The reproductive experiments of stratum deformation on the trench for the Kushibiki fault using numerical experiments

ANDO, Koichi<sup>1\*</sup>

<sup>1</sup>Tokyo Metropolitan University Department of Geography

### Introduction

The Quaternary regional stress field in eastern-central Japan tend to be east and west compaction force. Therefore, a number of thrust faults develop in this area. These faults sometimes indicate complex features, such as back thrusts or branches above 3 km depth.

It is considered that seismic waves are generated by fault activity below 3 km depth. Therefore, indirect earthquake surface faults which branch off from a earthquake source fault not generate seismic waves. Additionally, earthquake surface faults which directly connect to a earthquake source fault specify crustal movements around these faults. Therefore, we must distinguish between indirect earthquake surface faults and faults which directly connect to a earthquake source fault.

According to the approach of foam rubber models and dynamic lattice model simulations, it is known that a fault slip velocity accelerates toward a ground surface (e.g., Oglesby *et al.*, 2000; Ma and Hirakawa, 2013). According to numerical calculations which base on dynamic models, peak slip velocities of thrust faults with dip angles of 30-45 degree are 2.5-4.0 m/s (e.g., Oglesby *et al.*, 2000; Ma and Hirakawa, 2013). On the other hand, according to the numerical calculation, the peak slip velocity of the back thrust which was the indirect earthquake surface fault from the 2008 Iwate-Miyagi Nairiku earthquake in Japan was 0.05 m/s (Ando and Yamazaki, 2013). Therefore, we may be able to distinguish between indirect earthquake surface faults and faults which directly connect to a earthquake source fault, from peak slip velocities. Thus I estimated the peak slip velocity of the Kushibiki fault which is considered as indirect back thrust of the Fukaya fault, from numerical experiments.

### Relation between the Kushibiki fault and the Fukaya fault

Sugiyama *et al.* (2009) described that the Kanto-heiya-hokuseien fault zone is active fault zone which intervenes between the Kanto mountain terrain and the Kanto plain with NW-SE strike. The Kanto-heiya-hokuseien fault zone which is SW dipping thrust consists chiefly of fault groups along the Fukaya fault and the Fukaya fault.

The Hirai-Kushibiki fault zone which is considered as back thrust of Fukaya fault except the Hirai fault, consists of the Hirai fault, the Kushibiki fault and Kamikawa fault. In addition, the Kushibiki fault is bedding fault of Neogene sediments which have a dip angle of about 20 degree (Sugiyama *et al.*, 2009b; Shintani *et al.*, 2009).

### Methods

In this study, I performed numerical experiments about stratum deformation by faulting of the Kushibiki fault, and these experiments were executed by SDSSC (Strata Deformation Simulation System using CIP method) Ver 4.09. The model which feeds into SDSSC is modeled by the stratigraphy, the dip angle and the unit displacements from drilling surveys (Sugiyama *et al.*, 2009b) and trenching study (Shintani *et al.*, 2009).

Numerical experiments were performed with taking into account the erosional vacuity and the sedimentation for stratum by the faulting at the trenching area, and the peak slip velocity was estimated by comparison between experimental results and trenching results.

I adopted CWFS (cohesion weakening and frictional strengthening) model (Hajiabdolmajid *et al.* 2002) as the deformation characteristic about the stratum.

### Result and Discussion

I estimated the peak slip velocity of the the Kushibiki fault at 1-1.5 m/s. Therefore, this conclusion leads to the suggestion that the peak slip velocity of the indirect back thrust is slower than the thrust faults.

### Acknowledgement

For this study, I have used the computer systems of the Earthquake and Volcano Information Center of the Earthquake Research Institute, the University of Tokyo.

Keywords: Kushibiki fault, earthquake surface faults, back thrust, fault slip velocity, numerical experiment, CIP method

## Spatial Variation on Recurrence-time Distribution of Paleearthquakes and Its Influence for Long-term Forecast

NOMURA, Shunichi<sup>1\*</sup> ; OGATA, Yosihiko<sup>2</sup>

<sup>1</sup>Graduate School of Information and Engineering, Tokyo Institute of Technology, <sup>2</sup>The Institute of Statistical Mathematics

The Earthquake Research Committee (ERC) of Japan performs and publishes the long-term forecast of major paleoearthquakes in Japan. The ERC adopts renewal processes assuming that the recurrence intervals of paleoearthquakes are independently and identically distributed as the BPT (Brownian Passage Time) distribution. When applying this model, we need to estimate the mean and coefficient of variation (CV) on recurrence times. The estimation error in CV occasionally affect so much on the long-term forecast. However, while the mean parameter can be estimated with a certain precision from only the number and approximate ages of historical activities, the estimates of CV parameter have quite large errors without plentiful and accurate data. So the ERC assumes a common estimate for all active faults in Japan to ensure a certain reliability for the estimate. But as the historical paleoseismic data are accumulated by investigations, some active faults show significantly large variation in recurrence times.

Renewal processes with the BPT distribution are based on a physical model that assumes a cyclic mechanism where stress on a fault surface is accumulated by tectonic forces until an earthquake occurs that releases the accumulated stress to a basal level. In this model, the mean recurrence time represents the rate of stress accumulation by tectonic motion and the CV implies the strength of stress perturbation caused by nearby seismicity. Therefore, these parameters are supposed to have regional trends as seen in the analysis of Nomura et al. (2011). In our study, we estimate the spatial variation of these parameters on the BPT distribution in Japan and apply it to the long-term forecast on the active faults with very few historical data. In addition, we compare our forecast with the forecast by the ERC to discuss the influence of parameter estimation on earthquake prediction.

Keywords: long-term forecast, BPT distribution, renewal process, coefficient of variation, spatial model

## Spatial distribution of faults and folds in the offshore extension of the western margin fault zone of the Takada plain

ABE, Shintaro<sup>1\*</sup> ; ARAI, Ryoyu<sup>2</sup> ; OKAMURA, Yukinobu<sup>1</sup>

<sup>1</sup>AIST, <sup>2</sup>KGE.Co.,Ltd

We carried out a marine geological investigation on an offshore extension of the western margin fault zone of the Takada plain. The main purpose of this study is to clarify the total length of the fault zone and characterization of recent faulting. The western margin fault zone of the Takada plain is west dipping reverse fault, and the total length of this fault zone is 30 km from land to sea are based on the existing material.

We conducted 31 lines of high-resolution multichannel seismic reflection survey to recognize the detailed structure of the faults and folds. The reflection profiles depict the geological structure with extremely clear images.

The reflection profiles showed that the geological structure of the offshore area is characterized by the fold belt along the northern margin of the sedimentary basin that is formed in front of Takada plain. The shape of the fold is asymmetric weakly, and suggesting the fault related fold that has been deformed by west or north west dipping blind reverse fault as with land. This fault related fold zone is continuous to the Northern Kashiwazaki-oki Anticline from the Naoetsu-oki fault while changing asymmetry on the way. The North Kashiwazaki-oki Anticline is an active structure that has been pointed out the relevance of the source fault of the Chuetsu-oki earthquake.

Keywords: The western margin fault zone of the Takada plain, offshore, fault, fold, active structure, high-resolution seismic reflection survey

## Geologic structures and their activities around junction of main part and southern part of the active eastern boundary f

KOMATSUBARA, Taku<sup>1\*</sup> ; SATO, Tomoyuki<sup>1</sup> ; KOU, Yoshihide<sup>1</sup> ; OZAKI, Masanori<sup>1</sup> ; KOMATSUBARA, Junko<sup>1</sup>

<sup>1</sup>Institute of Geology and Geoinformation, Advanced Industrial Science and Technology

A 130-km-long N-S trending active fold and thrust zone (eastern boundary fault zone of Ishikari lowland) occurs in the Ishikari lowland and off the Yufutsu plain. This fault system is one of the boundary faults between the Kuril arc and the Northeast Japan arc. This fault system consists of east-dipping thrusts accompanying with fault-related folds. This fault system is subdivided into two parts with gap and echelon arrangement around the Yufutsu plain. The main part is 72 km-long and its mean vertical displacement rate is larger than 0.4 m/ky since the late Pleistocene. The south part is 86-km-long and its mean vertical displacement rate is 0.2-0.3 m/ky since the late middle Pleistocene. The southern part of this fault zone includes discontinuous structures such as short-axis anticlines and short monocline in the terrestrial part. This discontinuity of geologic structure would be related to irregularity of basement rocks underlying the southern part of Ishikari Lowland.

Keywords: Eastern margin fault zone of Ishikari Lowland, fold and thrust belt, active fault, mean displacement rate, geographical information system

## Revisited most recent paleoearthquakes along the ISTL active fault system, central Japan

KONDO, Hisao<sup>1\*</sup> ; TANIGUCHI, Kaoru<sup>1</sup> ; SUGITO, Nobuhiko<sup>2</sup>

<sup>1</sup>AIST AFERC, <sup>2</sup>Hosei University

The ISTL active fault system, central Japan, is well-known as one of the most hazardous fault systems based on the previously-reported paleoseismological works. Since the first paleoseismic trench survey was performed in 1980s, the number of paleoseismic sites becomes over 44 sites along the 150-km-long fault system, that is the highest density on active fault zone in Japan. In those studies, the timing of the most recent paleoearthquake had been reported around 1200 y.B.P., and the events had been longly estimated to be correlated with one multi-segment earthquake either 762 A.D. or 841 A.D. historical earthquakes. On the other hands, the recent result of geoslicer survey at the middle section of the ISTL indicate that the most recent event occurred around 2300 y.B.P., contradicting with the correlations with the historical earthquakes. Thus the most recent earthquakes on the ISTL is still ambiguous, therefore, we carried out systematic paleoseismic surveys around the largest segment boundary, Lake Suwa segment boundary, at the middle of the ISTL active fault system. The Lake Suwa segment boundary is structural Quarternary basin formed by left fault step-over between left-lateral strike slip faults. At three paleoseismic sites inside of the Suwa basin, we revealed the most recent events occurred a few thousands years before ~1200 y.B.P. and those are not correlatable with the historical earthquakes. These data indicate that the most recent earthquake along the ISTL did not rupture through the Lake Suwa segment boundary. In addition with this, the compiled timing of the most recent event along the entire the ISTL suggest that spatial clustering of the most recent earthquake. One large earthquake ruptured between the Kamishiro fault and the Gofukuji fault or possibly up to the Okaya fault, and another event ruptured between the Kamanashi-Yama faults and the Shimotsutaki fault. These two events will be correlated with either the 841 A.D. and the 762 A.D. earthquakes along with more reliable historical document surveys. Furthermore, this paleoseismic scenario during the most recent earthquake cycle do not deny the possibly that the larger multi-segment earthquake rupturing through the Lake Suwa segment boundary. In fact, paleoseismic event occurred between 2000 y.B.P. and 2300 y.B.P. was identified at the sites on the Gofukuji fault, the Okaya fault, and the Chino fault. Since those faults have left-lateral-strike slip component forming the pull-apart basin, the 2000-2300 y.B.P. event might have ruptured through the Lake Suwa segment boundary. To be testified this possibility, further investigation on the slip per event around the segment boundary is necessary.

Keywords: active fault, paleoearthquake, historical earthquake, ISTL active fault system

## High resolution seismic reflection profiling across the Kurehayama fault, Otokawa Line, central Japan

ISHIYAMA, Tatsuya<sup>1\*</sup> ; KATO, Naoko<sup>1</sup> ; SATO, Hiroshi<sup>1</sup> ; KOSHIYA, Shin<sup>2</sup> ; TODA, Shigeru<sup>3</sup> ; KOBAYASHI, Kenta<sup>4</sup> ; TERUI, Kyoko<sup>2</sup> ; KONDO, Shiori<sup>3</sup> ; YAMAUCHI, Koichi<sup>1</sup> ; SHIORI, Abe<sup>1</sup>

<sup>1</sup>Earthquake Research Institute, University of Tokyo, <sup>2</sup>Department of Civil and Environmental Engineering, Faculty of Engineering, Iwate University, <sup>3</sup>Aichi Educational University, <sup>4</sup>Department of Geology, Faculty of Science, Niigata University

We collected and processed shallow high-resolution seismic reflection data in order to resolve shallow structures and to understand structural linkage between active faults and folds recognized at ground surface and deeper, complicated fold and thrust structures along the Kurehayama fault, Toyama Prefecture, central Japan. We deployed more than 800 seismic channels, 10-Hz geophones, and Enviro-Vib (IVI, Inc) as a seismic source along about 8-km-long seismic line. Common midpoint stacking by use of initial velocity analysis successfully illuminates subsurface geometries of active fault-related fold to 1.5 two-way time in time section and up to about 1.5 km in depth section. Detailed seismic reflection analyses including refraction and residual statics, migration, deconvolution, and time-space variant bandpass filters, and depth-conversion by use of stacking velocities enable to obtain subsurface depth section of these active structures.

## Active faults in and around the Yoshinogari Heritage

KAGOHARA, Kyoko<sup>1\*</sup> ; YOSHIDA, Haruka<sup>2</sup> ; SOEDA, Yoshio<sup>3</sup> ; OKADA, Shinsuke<sup>4</sup> ; MATSUTA, Nobuhisa<sup>5</sup> ; TODA, Shigeru<sup>6</sup> ; IMAIZUMI, Toshifumi<sup>7</sup> ; NAGAOKA, Shinji<sup>8</sup>

<sup>1</sup>Faculty of Education, Yamaguchi University, <sup>2</sup>non, <sup>3</sup>West Japan Engineering Consultants, Inc., <sup>4</sup>International Research Institute of Disaster Science, Tohoku University, <sup>5</sup>Disaster Mitigation Research Center, Nagoya University, <sup>6</sup>Aichi University of Education, <sup>7</sup>Graduate school of Science, Tohoku University, <sup>8</sup>formerly Nagasaki University

The normal faults are distributed around the boundary line of between Saga Plain and Sefuri Mountains (The Research group for Active tectonics in Kyushu, 1989, etc.). Shimoyama (2010) suggested that this normal fault zone relatively uplift the north side block, based on the displacement of boundary between Aso-4 and Mitagawa Formation. According to the Regional evaluation of the active fault (Kyushu), the Headquarter of Earthquake Research Promotion evaluated that the normal fault zone (Saga Heiya Hokuen Fault Zone) can be traced about 22 km from Ogi City to Yoshinogari Town, based on the feature of gravity anomaly and tectonic geomorphology. However, the distribution and activities of active fault are not understood well. Yoshinogari Heritage, one of the Japan's important heritages, is on a terrace that is formed by Aso-4 pyroclastic flow deposits. Many relics during the Paleolithic era and Early-modern era have been excavated from here. Especially, it is famous for moat-surrounded settlements of the Yayoi period. The prospered moat-surrounded settlements were abandoned in the late third century. In the Nara period, Kando (ancient road) and government agencies which extend to Hizen Province (Saga and Nagasaki Prefecture) from Dazaifu, were established in the northern Saga Plain including the Yoshinogari Heritage. Yoshinogari Heritage and surrounding areas are regions where the civilizations of the many periods remain. Therefore, in this area that records man's activity for a long time, it is expected that influences of fault activities on civilizations can be known. To clarify the time and spatial relationships between active faults and ruins, we described the distribution map on active faults and ruins in and around the Yoshinogari Heritage, based on interpretation of topography using large-scale maps, aerial photograph, 5m DEM and results of field and archaeological surveys, and also conducted several very shallow seismic reflection profiles across clear tectonic scarps.

Keywords: Normal fault zone, Saga Plain, Yoshinogari Heritage, DEM, Very shallow seismic reflection profiling

## Study on great palaeoearthquakes and the decline of the Sanxingdui and Jinsha civilizations, Sichuan basin, China

LIN, Aiming<sup>1\*</sup> ; RAO, Gang<sup>2</sup> ; WANG, Maomao<sup>1</sup>

<sup>1</sup>Department of Geophysics, Graduate School of Science, Kyoto University, Kyoto 606-8502, Japan, <sup>2</sup>Department of Earth Sciences, Zhejiang University, Hangzhou 310027, China

The ruins of ancient civilizations damaged by large palaeoearthquakes, which have been reported worldwide, are often used as surface markers for Holocene tectonic and palaeoseismic events. Previous studies have demonstrated that recurring palaeoearthquakes have caused repeated soil liquefaction at the same site, leaving a record in both sediments and ancient ruins; such records can reveal a great deal about earthquakes that occurred prior to human-recorded observations or measurements<sup>5?10</sup>.

The Sanxingdui civilization, which developed on the Sichuan Plain, central China, during the Bronze Age (ca. 4800 years ago), flourished from ca. 4200 to ca. 3500 years ago until its sudden disappearance ca. 3200 years ago. Subsequently, the Jinsha civilization arose in the area around Chengdu city, ca. 40 km southwest of the Sanxingdui site, but it too suddenly disappeared ca. 2500?2200 years ago. It has been speculated that floods or regime changes might explain the collapse of both civilizations, but no solid evidence for such causes has so far been reported.

In this study, to search for a link between palaeoearthquakes and the abrupt unexplained falls of the Sanxingdui and Jinsha civilizations, we investigated the liquefaction induced by great palaeoearthquakes that occurred repeatedly in the past 5000 years on the Sichuan Plain, central China, in the region of the former Sanxingdui and Jiasha civilizations. Here, we present evidence that great palaeoearthquakes may have caused the collapse of both the Sanxingdui and Jinsha civilizations, as the cultures flourished in the periods during ca. 4200?3500 years and ca. 2800?2300 years ago, respectively, on an active fault zone of the Longmen Shan Thrust Belt (LSTB) that triggered the 2008 Mw 7.9 Wenchuan earthquake. Field observations, archaeological evidence, and radiocarbon dating reveal that at least four great palaeoearthquakes have induced liquefaction in wide areas around the Sanxingdui and Jinsha civilization sites during the past 5000 years, with an average recurrence interval of ca. 1000 years. We suggest that palaeoearthquakes occurring ca. 3300 and ca. 2200 years ago caused the fall and disappearance of the Sanxingdui and Jinsha civilizations, respectively, by causing extensive damage to infrastructure and manufacturing facilities, as well as numerous deaths.

Keywords: palaeoearthquake, Sanxingdui civilization, Jinsha civilization, Yangtze River civilization, Longmen-Shan Thrust Belt, Sichuan Basin

## Active thrusting beneath an alluvial terrace in the southern Longmen Shan range front, Sichuan basin, China

WANG, Maomao<sup>1\*</sup> ; LIN, Aiming<sup>1</sup> ; JIA, Dong<sup>2</sup> ; SHAW, John<sup>3</sup>

<sup>1</sup>Department of Geophysics, Kyoto University, <sup>2</sup>Nanjing University, <sup>3</sup>Harvard University

The devastating 2008 Mw7.9 Wenchuan earthquake, China, demonstrates that the central and northern parts of the Longmen Shan are currently active. However, evidence for active faulting and folding in the southern Longmen Shan remains poorly documented. In this paper, we define the structural geometry, fault kinematics, and seismic hazard of the Qiongxian thrust fault system (QTF) along the southern Longmen Shan range front by integrating deep and shallow seismic reflection data and geomorphic observations. The QTF is a 50-km-long, N-S-trending set of faults and associated folds that exhibit geomorphic evidence of Quaternary surface deformation. Geomorphic observations and seismic reflection data reveal that these faults dip steeply to the east and merge at depth with a blind, west-dipping thrust ramp. The trend and reverse sense of slip along the QTF indicates that the structure accommodates east-west crustal shortening. Based on uplift of stratigraphic horizons across the fault zone, we define a late Pliocene to early Pleistocene fault slip rate of 0.2-0.3mm/yr, and a middle Pleistocene to present rate of 0.4-1.2 mm/yr on the west-dipping thrust ramp. This ramp soles to a basal detachment in the Triassic section at a depth of 4.5-5.5 km. To the west, this detachment steps down onto a blind, northwest-dipping thrust termed the Range Front Thrust. A rupture of the QTF in combination with the Range Front Thrust could generate a Mw7.8 earthquake with average displacement of 5.7m. This type of earthquake source poses significant hazards to the adjacent, highly populated Sichuan basin.

## Identification of Fault Displacement and Stratigraphic Correlation of Black Soils based on Radiocarbon Ages

YASUE, Ken-ichi<sup>1\*</sup> ; HIROUCHI, Daisuke<sup>2</sup> ; SAITO-KOKUBU, Yoko<sup>1</sup> ; MATSUBARA, Akihiro<sup>1</sup> ; FURUSAWA, Akira<sup>3</sup>

<sup>1</sup>Japan Atomic Energy Agency, <sup>2</sup>Shinshu University, <sup>3</sup>Furusawa Geological Survey

In order to clarify the stratigraphic correlation around the fault and the timing of faulting event, we carried out radiocarbon dating of the black soil sampled from the trench wall of the Atera Fault. Black soils were sampled at an interval of 3-6 cm along the vertical direction on both the hanging wall and footwall located approximately 50 cm away from the fault plane. Sample preparation and radiocarbon dating were carried out in the JAEA-AMS-TONO of Tono Geoscience Center, JAEA. Calendar years were obtained by calibrating <sup>14</sup>C age using OxCal 4.2.3 (Bronk Ramsey, 2013) with IntCal13 atmospheric curve (Reimer et al., 2013).

The dating results show that the soil ages vary from 4,000 to 2,000 years with depth of the sampling points. Black soil was deposited at approximately constant rate each at both sides of the fault in 4,000-2,000 years ago. This indicates that the fault didn't move during this period. In the upper part, there is no variation in ages of black soils including the gravel with depth. This suggests that sedimentation rate was faster. One of the causes that the sedimentation rate around the fault suddenly changes is fault displacement. It is thought that this fault move in about 2,000 years ago. About this timing, it is necessary to consider in behavioral segments of the Atera Fault zone in detail.

In addition, we are going to present results of the volcanic ashes analysis and radiocarbon ages of the lower part.

Keywords: radiocarbon dating, C-14 age, black soil, Atera fault, timing of faulting event

## SEM observation on the active fault surface

TANAKA, Shiro<sup>1\*</sup> ; KAMACHI, Takao<sup>2</sup> ; KANII, Takehiro<sup>3</sup> ; MIZOGUCHI, Kazuo<sup>1</sup> ; NAKATA, Eiji<sup>1</sup>

<sup>1</sup>CRIEPI, <sup>2</sup>KEPCO, <sup>3</sup>NEWJEC

SEM observation of the fault surface was attempted in order to clarify the feature of the fault plane of active fault. The sharp plane of cutting other structures in outcrop was judged to be the latest activity surface, and the block sampling of the latest surface was carried out. After identifying the continuity of the fault plane by observing the internal structure of the sample in detail using helical X-ray CT, the samples for SEM observation were prepared. As a result of observation on the latest activity surface with a stereomicroscope and a scanning electron microscope, the following features have been identified. (1) A slickenside and striations are observed on the latest fault surface. (2) The fault plane is formed of the crushed fine-grained particles, and the dumpling-like structure where fine-grained particle was covered with paste-like clay is observed as a feature. (3) Growth of euhedral minerals formed by diagenesis in deep such as illite and chlorite, were not observed on the latest fault surface.

Keywords: active fault, fault surface, clay minerals

## Examination of evaluation method for fault activity based on an observation of fault zone - 1. Selection of outcrops -

KAMETAKA, Masao<sup>1\*</sup> ; OKAZAKI, Kazuhiko<sup>1</sup> ; NAKAYAMA, Kazuhiko<sup>2</sup> ; SESHIMO, Kazuyoshi<sup>2</sup> ; AOKI, Kazuhiro<sup>2</sup> ; TANAKA, Yoshihiro<sup>2</sup> ; SHIMADA, Koji<sup>2</sup> ; SHIMOGAMA, Kota<sup>1</sup> ; INADA, Noriyuki<sup>1</sup>

<sup>1</sup>Dia Consultants, <sup>2</sup>Japan Atomic Energy Agency

The activity of a fault is normally evaluated by observing the displacement/deformation of strata which cover the fault. However, it is difficult to evaluate the activity of a fault which exists only in the basement rock without any overlying strata. In such a case, the fault activity needs to be judged carefully through a comprehensive approach to geomorphology, geology and present/past stress fields. Items in analyzing a fault zone include observation of the fault plane, width of fracture zone, color, hardness, magnetic susceptibility, form of fractured material, mineral and chemical composition analysis, dating, etc. Since some of these items have uncertainties in quantification and reproducibility, a method for evaluating fault activity by analyzing the fault zone in the basement rock is yet to be established. The authors have been carried out the observation and analysis of the fault zone to establish more scientific method of evaluation of fault activity.

In order to do the survey of certain active fault, we should study the outcrop of fault which give a displacement/deformation to the overlying certainly younger formations, and should observe the extension of fault from the overlying formations to the basement rocks. On the other hand, in order to do the survey of the fault zone of certain non-active fault, we should study the outcrop of fault which is covered by the old enough formations from the evaluation point of view.

We selected the outcrops which fulfilled the above-mentioned conditions through literature, then we decided the study outcrops through geological survey. The study area are limited in granite-bearing area, because granite show generally homogeneous and simple structure, is widely distributed in land, and well documented about fault rocks.

Examples of outcrops of active fault are one of the Gosukebashi Fault (Loc. 5 of Maruyama et al., 1997, Active Fault Res.) and one of the Rokko Fault (Loc.1 of Maruyama and Lin, 2002, Tectonophysics) in the Rokko Mountains, southern Hyogo Prefecture.

The fault zone of the Gosukebashi Fault appears in the Rokko Granite at the upperstream of the Gosuke-Dam site. Sand and gravel beds are bounded with granitic fault zone in the upper part of the outcrop. The fault zone consists of thick fault gouge in black and brown color, foliated cataclasite and granitic cataclasite.

At the western Funasaka, the Rokko Granite is in contact with rhyolitic volcanoclastic rocks of the Arima Group and overlying gravel beds through the Rokko Fault. The fault zone of the granite are remarkably altered and composed of brown fault gouge, foliated cataclasite and granitic cataclasite. The fault zone of the rhyolite is composed of black Fe-Mn-bearing layer, rhyolitic cataclasite and damaged rhyolite.

An example of non-active fault was selected from the fault which does not effect the strata of higher terrace deposits. Higher terrace deposits surrounded by badlands of weathered granite are well developed around the Rokko Horai-kyo in the northern Rokko Mountains. The fault including relatively thick gouge which is overlain by the deposits was selected for this survey, and is named the Rokko Horai-kyo Fault. For keeping the safety against the rock fall, the survey has done in the lower extension of granitic slope from the unconformity. The fault zone appears in the weathered granite, and composed of brown gouge, with black Fe-bearing layer and cataclasite.

The observation of fault zone (evaluation of fault plane, in-situ measurements of color and hardness), striation analysis, observation of fault structure by slabs, sections and SEM samples, mineral composition (XRF) and chemical composition (ICP-MS) analysis, mechanical and physical tests were done at the fault zones of these 3 faults. In this paper, the outline of this study and the results of geological survey are described. The details of the observation results of fault zones are explained in another paper (Okazaki et al., 2014, Abst. JpGU).

Keywords: active fault, evaluation method of fault activity, Rokko Mountains, Gosukebashi Fault, Rokko Fault, fault zone

## Examination of evaluation method for fault activity based on an observation of fault zone - 2. in-situ experiments -

OKAZAKI, Kazuhiko<sup>1</sup> ; KAMETAKA, Masao<sup>1\*</sup> ; NAKAYAMA, Kazuhiko<sup>2</sup> ; SESHIMO, Kazuyoshi<sup>2</sup> ; AOKI, Kazuhiro<sup>2</sup> ; TANAKA, Yoshihiro<sup>2</sup> ; SHIMADA, Koji<sup>2</sup> ; SUZUKI, Kazushige<sup>1</sup> ; SHIMOGAMA, Kota<sup>1</sup> ; INADA, Noriyuki<sup>1</sup>

<sup>1</sup>Dia Consultants, <sup>2</sup>Japan Atomic Energy Agency

In order to establish a method for evaluating fault activity based on observation and analysis of fault zone in the basement rock, a comparative study has been carried out at outcrops of active and non-active fault. Of the three outcrops selected in the Rokko Mountains situated in southern Hyogo Prefecture, two were of an active fault and one of non-active fault. They are: the outcrop of Gosukebashi Fault at the upperstream of Gosuke-Dam site (GSB) and the outcrop of Rokko Fault at the western Funasaka (FSW) for active fault, and the outcrop of Rokko Horai-kyo Fault overlain by higher terrace deposits (HRK) for non-active fault (Kametaka et al., 2014). This paper focuses on an evaluation method which is relatively brief and easily enforceable at the outcrops, and describes the suitability of making a morphological observation of the fault plane and conducting in-situ experiments on hardness and color.

Fault plane of the active fault seems to be well continued, smooth surface and cut the older texture of the fault zone. To describe these features objectively and quantitatively, we measure 1) the relationships between the fault plane and the older texture, 2) the continuity of the fault plane, 3) planarity of the fault plane, 4) semi-quantitative observation using guideline of ISRM (Rock Net Japan, 1985, ISRM Guidelines), 5) arithmetic average toughness based on the authorized photograph. The results indicate that the fault plane of GSB and FSW show good continuities and well cut the older texture, while that of HRK show discontinuous part and poorly cut the older texture. The planarity, surface roughness and waviness, of the fault plane are well in GSB and poor in HRK, and partly poor in FSW possibly caused by the texture of alteration. The fault plane in the basement rock show relatively better planarity than that between basement rock and gravel beds. The arithmetic average toughness leads quantitative evaluation of fault plane, though there are some soluble problems about forming of outcrops and recognition of fault plane.

It qualitatively said that the fault gouge of an active fault is possibly soft and that of a non-active fault gouge is possibly hard and consolidated (Kimura, 1981, Jour. Japan Soc. Eng. Geol.). To quantify the hardness of intrafault materials, in-situ experiment of needle penetration test has been done. The result indicates that the fault gouge of GSB, FSW and HRK show 0 kN/m<sup>2</sup>. The altered cataclasite and weathered granite (damaged granite) of rock surface even show low value, while they show higher value at 20 cm below the surface. On the other hand, the fault gouge of the underground indicates still low value.

Fault gouge of an active fault possibly show reductive color and that of a non-active fault possibly show oxidative color (Research Core for Deep Geological Environments, AIST, 2012, GSJ Open File Rep.). To quantify the color of intra-fault materials, color measurements (Lab color) were done by using portable soil color meter. The results indicates that the fault gouge of GSB show low a\*value and low-middle b\*value, that of FSW show high a\*value and very high b\*value, and that of HRK show low-middle a\*value and low-high b\*value. The fault rocks around the fault gouge show intermediate value between fault gouge and non-deformed granite, indicating color change associated with weathering pass of granite.

In this paper, we show the specific contents of each measurement, and discuss about the validities of evaluation methods of the fault activity.

Keywords: active fault, evaluation method of fault activity, Rokko Mountains, Gosukebashi Fault, Rokko Fault, fault zone

## Active faults and topographic surfaces on the stereoscopic topographic map

IMAIZUMI, Toshifumi<sup>1\*</sup> ; MIYAUCHI, Takahiro<sup>2</sup> ; KAGOHARA, Kyoko<sup>3</sup> ; OKADA, Shinsuke<sup>4</sup> ; SHIRASAWA, Michio<sup>5</sup> ; YOKOYAMA, Ryuzo<sup>5</sup> ; SASAKI, Tatsuya<sup>6</sup>

<sup>1</sup>Graduated School of Science, Tohoku University, <sup>2</sup>Graduated School of Science, Chiba University, <sup>3</sup>Faculty of Education, Yamaguchi University, <sup>4</sup>International Research Institute of Disaster Science, Tohoku University, <sup>5</sup>Yokoyama Geo-Spatial Information Lab., <sup>6</sup>OYO Corporation, Database Business Department

Thematic topographic maps have developed by the progress in analysis using digital elevation model (DEM) and have made clear representation possible.

We made digital stereoscopic topographic maps in scale 1:25,000, by using 5m mesh DEM data arranged by Geospatial Information Authority of Japan (GSI) . These 3D maps have same information, mode, scale and interval 10m contour, comparing to Quadrangle topographic sheet map.

We demonstrated the overlapping active fault line (Nakata and Imaizumi, edit 2002) on these 3D maps, in order to easily interpretation of the location of fault line, fault feature, evidence of faulting and displacement of faulting from professional and educational viewpoints.

Keywords: Active fault, Topographic surface, Stereoscopic topographic map, Interpretation of topographic map

## Genetic algorithm-based displacement extraction technique for LiDAR dataset

SAOMOTO, Hidetaka<sup>1\*</sup>; MARUYAMA, Tadashi<sup>1</sup>; KONDO, Hisao<sup>1</sup>

<sup>1</sup>Active Fault and Earthquake Research Center, AIST

Owing to recent progress of aerial survey with laser transmitting device, we can easily obtain detailed digital elevation model represented by point cloud data. This model is applicable to many purposes such as active fault detection, quantification of bluff lines, and extraction of ground displacement caused by an earthquake.

Although some methods for seismic displacement extraction from point cloud data have been proposed, we need more robust and powerful method in terms of noise immunity. In this study, we propose a new method based on the RBF (Radial Basis Function) interpolation and the GA (Genetic Algorithm) for the seismic displacement detection and then conduct a series of inquests including the parameter setting, the evaluation of noise resistance, and the comparison among four optimization techniques: GA, L-BFGS-B, Nelder-Mead, and COBYLA.

The results of considerations revealed that: (1) the size of unit for pattern matching should be set to 24 m square for the point cloud divided into 1 m grid; (2) the proposed method stably detect the correct displacement even under ill-posed condition; (3) the combination of the RBF and the GA is well suited for this problem because the objective function appearing in this study possesses extreme multimodality, suggesting that we should not use the optimization method based on gradient information.

Keywords: genetic algorithm, interpolation, LiDAR, displacement, optimization

## Geologic structures around the coastal area of the southern part of the active eastern boundary fault zone of Ishikari I

SATO, Tomoyuki<sup>1\*</sup> ; KOMATSUBARA, Taku<sup>1</sup> ; KOU, Yoshihide<sup>1</sup>

<sup>1</sup>Institute of Geology and Geoinformation, Geological Survey of Japan, AIST

A 130-km-long N-S trending active fold and thrust zone (eastern boundary fault zone of Ishikari lowland) occurs in the Ishikari lowland and off the Yufutsu plain. This fault system is one of the boundary faults between the Kuril arc and the Northeast Japan arc. We surveyed around the coastal area of the Yufutsu plain based on the marine high-resolution seismic-survey and the database of land borehole cores. As a result, two active anticlines (Yufutsu anticline and Hamaatsuma anticline) were recognized. These anticlines can be correlated to the anticlines described as a part of the active eastern boundary fault zone of Ishikari lowland (AIST, 2007). The trend of the Yufutsu anticline was N-S despite The Headquarters for Earthquake Research Promotion reported the trend was NW-SE. The Hamaatsuma anticline continued to the Mukawaoki anticline and the southern end of the fault zone extend to the southern end of the Mukawaoki fault which is concerned to the Mukawaoki anticline.

AIST(2007)Activity survey of the eastern boundary fault zone of Ishikari lowland. Working papers. H18-8, 35p.

Headquarters for Earthquake Research Promotion(2010) Evaluation of the eastern boundary fault zone of Ishikari lowland (revised). 34p.

Keywords: Active eastern boundary fault zone of Ishikari lowland, Seismic survey, Quaternary, Hokkaido, Coastal area

## Seismic reflection survey across the northern part of the Western Boundary Fault Zone of the Yamagata Basin

OKADA, Shinsuke<sup>1\*</sup> ; IMAIZUMI, Toshifumi<sup>1</sup> ; KAGOHARA, Kyoko<sup>2</sup> ; ECHIGO, Tomoo<sup>3</sup> ; YAGI, Hiroshi<sup>4</sup> ; MATSUBARA, Yoshikazu<sup>5</sup> ; MIWA, Atsushi<sup>5</sup> ; KOSAKA, Hideki<sup>6</sup>

<sup>1</sup>IRIDeS, Tohoku Univ., <sup>2</sup>Yamaguchi Univ., <sup>3</sup>Geo-Research Institute, <sup>4</sup>Yamagata Univ., <sup>5</sup>OYO Corporation, <sup>6</sup>Kankyo Chishitsu Company Limited

The Western Boundary Fault Zone of the Yamagata Basin borders the western margin of the Yamagata basin and is traceable for about 60 km. In the northern part of this fault zone (from Sagae to Ooishida area), subparallel traces of the active fault distribute in the western side of the basin. At the center of the basin, Kawashima-yama located as a tectonic bulge and its western side the Mogami river incise and meander in the fault zone. Along the eastern side of the Kawashima-yama, syncline is indicated as a frontal deformation by Ikeda (2002) and Imaizumi (2001).

To reveal the subsurface structure and tectonic evolution of this fault zone, we carried out two lines (Line A and Line B) of seismic reflection survey from September to October 2013. The Line A has a length of 4.11 km and started from Saigo area to Oomaki via. Kyouei bridge. The Line B has about 3.75 km length and started from Taruishi area to Goten along the Taruishi river. The source used in this survey was an Enviro Vib (IVI Inc.). Sweep length was 16 sec and sweep frequency range beginning at 10 Hz up to 120 Hz. The receiver was GS-20DX (natural frequency, 10 Hz; Geospace Inc.). The source and receiver spacing was 10m, with 192 ch geophones used for each recording. We selected the Geode (Geometrics) for the recording system and its sampling rate is 1 msec.

We thank to students of Tohoku University and Kanazawa University for their assistance in our survey. This work was supported by project research of the International Research Institute of Disaster Science (IRIDeS), Tohoku University.

### [References]

- Ikeda et al., 2002, Atlas of Quaternary Thrust Fault in Japan, Univ. of Tokyo Press, 254pp.  
Imaizumi et al., 2001, Active Fault Map in Urban Area, Geographical Survey Institute.

Keywords: active fault, seismic reflection survey, the Western Boundary Fault Zone of the Yamagata Basin, subsurface structure, Murayama City

## Very shallow seismic surveys of the Shionohira earthquake fault appeared at the Fukushima-ken Hamadori earthquake

YAMAGUCHI, Kazuo<sup>1\*</sup> ; ITO, Shinobu<sup>1</sup> ; KANO, Naomi<sup>1</sup> ; YAMANAKA, Yoshiaki<sup>2</sup> ; ITO, Shunichiro<sup>2</sup>

<sup>1</sup>AIST,GSI, <sup>2</sup>Suncoh consultant

In the southern part of the Fukushima-ken Hamadori area, seismicity increased after 2011 Tohoku earthquake and an M7.0 earthquake occurred on April 11th, 2011. Remarkable surface ruptures appeared along active faults by this earthquake. We conducted very shallow seismic surveys to reveal subsurface structure of the surface rupture down to 20 m in depth.

The survey line is located along a road in the Shionohira of Iwaki city. The displacement of the surface rupture is 2m east-side-up and 0.4m left lateral at the cross point of the survey line. The road was fixed and flat at the survey time.

The survey menus were S-wave survey and P-wave survey. Survey instruments and specifications are as following. Seismic source: S-wave/SWG-5(Suncoh), P-wave/10kg hammer, receiver: S-wave/GS20DM(Oyo Geospace, 28Hz), P-wave/GS11D(OyoGeospace, 4.5Hz), recorder: DSS-12(Suncoh), line length: 191m, source interval: 1m, receiver interval: 1m, stack number: 1-5, spread: S-wave/192ch fixed, P-wave/96ch landstreamer. The data quality was good because of low traffic noise.

The data were processed by S-wave refraction, S-wave reflection, P-wave refraction and surface wave methods. S-wave tomography and P-wave tomography analyses were applied and confidence of resolution and dependency to primary model were estimated. P-wave data were processed by inversion of phase velocity dispersion and S-wave velocity structure was obtained. S-wave data was processed by CMP stacking method and time section, migrated section and depth section were obtained.

According to S-wave velocities by S-wave refraction and surface wave methods, velocity layers below 0.7 km/s is thick to the west of the fault and thin to the east of the fault. Strong reflector between sediments and basement is deep and continuous to the west of the fault, shallow and uneven to the east of the fault and steps are recognized around the fault. The basement rises between this step and 135m of the survey line. This corresponds to the part of high Bouguer anomaly of 0.06 mgal.

Keywords: Fukushima-ken Hamadori earthquake, Itozawa fault, Shionohira fault, subsurface structure, very shallow seismic survey

## Pit excavation along the Tachikawa fault at Sayama Shrine Site

ISHIYAMA, Tatsuya<sup>1\*</sup> ; HIROUCHI, Daisuke<sup>2</sup> ; SATO, Hiroshi<sup>1</sup> ; SUZUKI, Takehiko<sup>3</sup> ; KOBAYASHI, Kenta<sup>4</sup> ; KORIYA, Yorihide<sup>5</sup> ; OMATA, Masashi<sup>5</sup> ; SHIBATA, Tsuyoshi<sup>6</sup>

<sup>1</sup>Earthquake Research Institute, University of Tokyo, <sup>2</sup>Department of Education, Shinshu University, <sup>3</sup>Faculty of Urban Environmental Sciences, Tokyo Metropolitan University, <sup>4</sup>Department of Geology, Faculty of Science, Niigata University, <sup>5</sup>Crearia, Inc., <sup>6</sup>Aero Photo Center

We excavated a 10-m-long, 2-m-deep pit across the hypothesized south-facing topographic scarp on along the Tachikawa fault. Preliminary results include clear evidence of accumulated, west-facing monoclonal folding of underlying conglomerates, predicted by the topographic scarp. Asymmetric ductile shear zone exposed on the bottom indicate nature of significant sinistral strike-slip component of faulting, rather than a simple reverse faulting. Future works include establishing stratigraphy based on radiocarbon dating and tephrostratigraphy.

## Geological structure interpreted from two boring cores beside the Tachikawa Fault Zone, Tokyo, NE Japan

SUZUKI, Takehiko<sup>1\*</sup>

<sup>1</sup>Tokyo Metropolitan University

In order to clarify the accurate position and activity of the Tachikawa Fault Zone, which possibly cause an earthquake under Tokyo in future, survey on the Quaternary sediments with tephrochronological method is effective. We conducted an all-core boring (TC-12-1) survey at Enoki in Musashi-Murayama City in 2012, where a relative subsidence will be occurred at its activity. By this result, we pointed out the evidence of deformation in altitudes of Middle Pleistocene gravel bed base, and also found a tephra layers estimated its age to be at 1.63 Ma. In this study, an additional all-core boring (TC-13-1) survey in relative uplifting side was carried out. The following are preliminary report of TC-13-1 core survey. Site of all-core boring (TC-13-1) with the length of 90 m is ca. 300 m northwest of Tachikawa Fault Zone of which the altitude is 109.50 m. Sediment with a depth 0 to 28.65 m is composed of coarse gravels with diameters 3 to 10 cm (max. 20 cm). Upper part of this gravel bed is equivalent to the fluvial terrace deposits of Tachikawa 2 Surface, and lower one is most likely to be the gravel bed identified as Middle Pleistocene sediment in the survey of TC-12-1 in 2012. Altitude of the base of this gravel bed (80.85 m) is higher than that of TC-12-1 (71.97 m), suggesting the evidence of fault activity with uplifting of east side. Sediment with a depth 28.65 to 90.00 m is composed of the alternation of silt (mudstone), sands, and gravels, and is correlative to the Kazusa Group of Lower Pleistocene. Five cycles of sedimentation composed of upper consolidated silt to mudstone and lower gravel bed were recognized. Also, shell in mudstone of 67.15-68.00m in depth and tuffaceous mudstone layers were found. We will examine theses sediments in detail. This survey was financially supported by Ministry of Education, Science, Sports, and Culture (Intensive Survey and Observation on the Tachikawa Fault Zone).

Keywords: Tachikawa Fault Zone, Underground geology, Boring core, Musashi-murayama

## Examination of tectonics of the Shinano River basin, Niigata and Nagano prefectural border.

TAKAKUWA, Kensuke<sup>1\*</sup>

<sup>1</sup>Department of Geology, Faculty of Science, Niigata University

In Niigata and Nagano, the trend of a general structure has a NNE-SSW strike called what is called the direction of Niigata. Moreover, it is thought that the trend of an active fault has the direction of Niigata similarly. However, the western Tokamachi fault belt continuous from Tokamachi city to Niigata and Nagano prefectural border contains in the south the Miyanohara fault which is an ENE-WSW strike(Headquarter of Earthquake Research Promotion 2010).

The Shinano River syncline which has in Tokamachi a NNE-SSW strike which exists in Shinano River and parallel being crooked in Tsunan-cho, and becoming an E-W trend.(Shimazu and Tateishi 1993. And Takeuchi et al 2000).

However, the exact position and a posture are not specified.

That is, it was not necessarily confirmed based on detailed investigation, the structure of the area is the direction.

The tectonics of the area has many questions as mentioned above. It inquired for the purpose of solving the tectonics of the area.

It was able to ask for the exact position of the Shinano Kawamuki slant continuous to a the area as a result of investigation. Moreover, Chikumagawa anticline and hokushin syncline was newly authorized in the area.

Moreover, the sectional view over the Miyanohara fault in this research was compared with Sega (2012MS) in a Tokamachi basin west marginal fault belt. When done so, it turned out that the form of folding is alike. Therefore, it is thought that a Tokamachi basin west marginal fault belt and the Miyanohara fault are the same postures. Therefore, these connect and it is thought that the western Tokamachi fault belt is constituted. Moreover, the form of folding is alike also around hirataki. Therefore, the southernmost end of the western Tokamachi fault belt may be extended further west.

Furthermore, small fault method which used the Multiple Inverse Method was conducted. A result, it turned out that the small fault is recording two or more times of transcurrent fault type stress.

Horizontal gap stress is as conformable as the earthquake mechanism of aftershock of the northern Nagano earthquake in 2011,3,12.

Therefore, it is possible that Japan of those days was also placed by the same stress-ization as the present after the offing earthquake of the Tohoku earthquake.

## Tectonic geomorphology around the eastern piedmont of the Myoko volcano and their tectonic implications

TAJIKARA, Masayoshi<sup>1\*</sup> ; MIZUMOTO, Tadaki<sup>1</sup> ; MATSUDA, Tokihiko<sup>1</sup> ; TSUTSUMI, Hiroyuki<sup>2</sup> ; GOTO, Hideaki<sup>3</sup> ; NAKATA, Takashi<sup>3</sup>

<sup>1</sup>ERC, ADEP, <sup>2</sup>Kyoto Univ., <sup>3</sup>Hiroshima Univ.

The Myoko volcano group is located in the south of Takada plain, and its eastern piedmont is intermontane trough (hereafter, referred as the Myoko trough) between the Nishi-kubiki Mountains and the Higashi-kubiki Hills. The Myoko trough is located from the south of the Takada plain to the north of the Nagano Basin. The Takada-heiya-toen fault, Takada-heiya-seien fault, and the Nagano-bonchi-seien fault are located along the eastern margin of the Takada plain, the western margin of the Takada Plain, and the western margin of the Nagano Basin, respectively (Nakata and Imaizumi, 2002). Based on detailed analysis of areal photographs, we newly mapped active faults and tectonic landforms in the Myoko trough. we describe evidences of recent activity and discuss the property of these tectonic landforms and their tectonic implications. Newly mapped active faults and tectonic landforms are distributed almost continuously from the southern edge of the Takada-heiya-toen-fault to around Fujisato village in the Shinano town. Based on these distributions, we judged that newly mapped active faults constitute a part of the Takada-heiya-toen fault, and that the length of the Takada-heiya-toen fault may be elongated from 26 km to max. 55 km. However, active faults in the Myoko trough and the Nagano-bonchi-seien fault are distributed in parallel at distance of 13-14 km. Therefore, these two faults may be converged at depth of 6-7 km, and the southern part of the Takada-heiya-toen fault may be a backthrust of the Nagano-bonchi-seien fault.

Keywords: Takada plain, active fault, air photo, Myoko volcano group, Takada-heiya-toen fault

## Investigating the role of the Itoigawa-Shizuoka tectonic line in the evolution of the Northern Fossa Magna rift basin

PANAYOTOPOULOS, Yannis<sup>1\*</sup> ; HIRATA, Naoshi<sup>1</sup> ; SATO, Hiroshi<sup>1</sup> ; KATO, Aitaro<sup>1</sup> ; IMANISHI, Kazutoshi<sup>2</sup> ; KUWAHARA, Yasuto<sup>2</sup> ; CHO, Ikuo<sup>2</sup> ; TAKEDA, Tetsuya<sup>3</sup> ; ASANO, Youichi<sup>3</sup>

<sup>1</sup>Earthquake Research Institute, the University of Tokyo, <sup>2</sup>Geological Survey of Japan, AIST, <sup>3</sup>National Research Institute for Earth Science and Disaster Prevention

The Itoigawa-Shizuoka tectonic line (ISTL) fault system is considered to have one of the highest probabilities for a major inland earthquake occurrence in the whole of Japan. It is a complex fault system with the dip directions of the local fault segments changing from north to south between an east-dipping low-angle thrust fault, a strike slip fault and a west-dipping thrust fault. The tectonic relations between the different parts of the fault system and the surrounding geological units are yet to be fully explained. This study aims to reveal the juncture of the northern and central parts of the ISTL and investigate its contribution towards the shaping of the Northern Fossa Magna rift basin. We conducted 3 deployments of 1 or 2 linear arrays of seismic stations across the central and northern ISTL regions and observed local micro-earthquakes for a period of 3 years. Each deployment recorded continuous waveform data for approximately 3 months. Using arrival times of 1193 local earthquakes, we jointly determined earthquake locations and a 3D velocity model, applying the tomography method. We were able to image the regional crustal structures from the surface to a depth of 20 km with a spatial resolution of 5 km. Subsequently, we used the obtained 3D velocity model to relocate the background local seismicity from 2003 to 2009. The juncture of the northern and central parts of the ISTL was well constrained by our results. The depth extension of the northern parts of the ISTL fault segments follows the bottom of the Miocene Northern Fossa Magna rift basin (NFM) and forms an east-dipping low-angle fault. In contrast, the central parts of the ISTL fault segments are estimated to lie along the eastern boundary of the Matsumoto basin forming an oblique strike slip fault.

Keywords: Itoigawa-Shizuoka tectonic line, tomography

## Mapping of active faults in the area around the southern segment of the Itoigawa-Shizuoka Tectonic Line, central Japan

SANO, Mikako<sup>1\*</sup> ; IIDA, Kenta<sup>2</sup> ; LIN, Aiming<sup>1</sup>

<sup>1</sup>Department of Geophysics, Graduate School of Science, Kyoto University, <sup>2</sup>Institute of Geosciences, Faculty of Science, Shizuoka University

It is well known that tectonic-related topographic features that develop around active faults record displacements during large-magnitude earthquakes, and that tectonic-related topographic studies are essential for developing a historic and/or paleoseismic perspective of the locations, magnitudes, recurrence intervals, and slip patterns of seismogenic faults. Therefore, it is important to recognize and identify active faults and tectonic-related topographic landform features for studying the present activity of active faults to assess the seismic hazard in a densely populated region.

This study focuses on the mapping of active faults in the area around the southern segment of the Itoigawa-Shizuoka Tectonic Line (ISTL), central Japan. Although previous studies have reported the presence of some active faults in this area, the detail distribution and geometric features of active faults are still unclear. In this study, we identified the active fault traces using perspective maps made from the digital elevation model (DEM) data with 5-m-contours and stereo-examination of aerial photography and conducted field investigations. Interpretations of perspective topographic maps, field investigations, and structural analysis of fault zones reveal that i) many fault traces are newly found, which formed a deformation zone of up to ~100-500 m in width; ii) the active fault traces show more irregular shape than that previously reported, curved around boundary between the mountains and basin, indicating the lower dip-angle thrust fault structures; iii) the active faults developed along the southern sector of the ISTL are found to be extended to the south at least ~25 km longer than that reported previously.

The findings of this study show that the detail mapping of the active faults can provide new insights to study the tectonic activity and fault nature of active faults and to reassess the seismic hazard for the densely populated area around the ISTL.

Keywords: active fault, fault mapping, Itoigawa-Shizuoka Tectonic Line (ISTL), fault trace, fault geometry, thrust fault

## ESR dating of the Shimotsuburai and Hoozan faults in the Itoigawa-Shizuoka Tectonic Line Active Fault System

FUKUCHI, Tatsuro<sup>1\*</sup> ; TANAKA, Mami<sup>1</sup> ; KITTA, Takuto<sup>1</sup> ; IMAI, Noboru<sup>2</sup>

<sup>1</sup>University of Yamanashi, <sup>2</sup>AIST

The Shimotsuburai fault, which is located in the south part of the Itoigawa-Shizuoka Tectonic Line (ISTL) Active Fault System, displaces the lower terrace deposits formed at about 20 kaBP. The trenching survey at the Tozawa outcrop revealed that the latest fault movement occurred at 1,550 ± 70 yBP - 2,350 ± 60 yBP (Toda et al., 2000). Along the fault plane of the Shimotsuburai fault, black injection veins are distributed forming complex networks and a part of the black veins is injected into the fault gouge or lower terrace deposits. Kano et al. (2004) proposed that this black intrusion veins are crushing-originated pseudotachylyte formed at 30-40m or less in depth at the time of the latest fault movement. On the other hand, the Hoozan fault is distributed about 6km west of the Shimotsuburai fault. At the Dondokozawa outcrop, fault gouge is hardly recognized besides cataclasite and mylonite. This suggests that the Hoozan fault may not have moved since its formation in Neogene to early Quaternary, and that the main activity of the ISTL may have shifted to the Shimotsuburai fault (Koyama, 1990). The Gofukuji fault located at the northwest extension of the Hoozan and Shimotsuburai faults may cause a Magnitude 8-class large earthquake, and besides its activity may have increased after the 2011 Tohoku-oki earthquake (M9.0). When the Gofukuji fault moves in the future, it is unclear whether or not its southeast extension would also move operating together. It is important to exactly assess the activity of the Hoozan fault as well as the Shimotsuburai fault. We thus carried out XRD (X-ray diffraction) and ESR (electron spin resonance) dating of fault rocks collected from the Shimotsuburai and Hoozan faults.

As a result of XRD analysis, smectite is detected from the Shimotsuburai fault gouge at the Tozawa outcrop, and smectite and a chlorite/smectite (C/S) mixed layer mineral from the black injection vein just on the fault plane, while besides illite chlorite and C/S are respectively detected from the black and gray gouges of the Hoozan fault at the Ishiutoro-gawa outcrop. In general, the formation depth of clay minerals tends to increase in order of smectite, C/S, chlorite and illite. Therefore, the result from the XRD analysis suggests that the Hoozan fault was much more active at deeper positions. As a result of ESR dating, strong signals of the Al and Ti centers are detected from quartz in the Shimotsuburai fault gouge and black injection vein however these centers show the tendency of saturation implying that the resetting by frictional heating did not work. Since the Al and Ti centers can be completely reset at about 300-350 degree C (Fukuchi, 2004), the result from the ESR dating shows that the frictional heat temperature did not rise so much at the time of the latest fault movement. On the other hand, the quartet signals intrinsic to montmorillonite are detected from the gray gouge of the Hoozan fault, and give the age of 2.8-3.2 ± 0.4 Ma. The chlorite/smectite mixed layer is considered to be formed at about 130-200 degree C (Yoshimura, 2001), so that its formation age may be estimated as 2.2-3.3 Ma assuming the upheaval rate of 2 mm/y and the geothermal gradient of 30 degree C/km. This formation age is consistent with the ESR age obtained from the gray gouge.

### References

- T. Fukuchi (2004) ESR dating of fault movement, Fukadaken Library 63, 45p.
- K. Kano et al. (2004) J. Geol. Soc. Japan, 110, 779-790.
- A. Koyama (1990) J. Geosci. Osaka City Univ. 33, 1-47.
- S. Toda et al. (2000) Zishin (Bull. Seism. Soc. Japan), 52, 445-468.
- T. Yoshimura (2001) Clay Minerals and Alteration, Chigakusosho 32, 293p.

Keywords: electron spin resonance, ESR dating, Itoigawa-Shizuoka Tectonic Line, active fault system, pseudotachylyte, clay mineral

## The SEM observation on the latest active fault plane - the Atera Fault, Tase, Gifu prefecture-

NAKATA, Eiji<sup>1\*</sup> ; UETA, Keiichi<sup>1</sup> ; AIYAMA, Kotaro<sup>2</sup> ; SIGEMATSU, Yasumune<sup>3</sup> ; OTSUKA, Yoshiharu<sup>3</sup>

<sup>1</sup>Central Research Institute of Electric Power Industry, <sup>2</sup>Dia Consultants Co.,Ltd, <sup>3</sup>Kansai Electric Power Co.,Inc.

To evaluate of seismic activity of fault, we performed mineralogical and morphological studies by SEM on the latest fault plane of the Atera fault. On the results of SEM observation, authigenic minerals do not crystallize on the whole shear planes including the latest active fault plane.

Study area is outcrop along the Tase path, Gifu prefecture (Toda et al., 1994). Granitic rock (hanging wall) is thrust on the late Quaternary sandy formation including a lot of conglomerate and humus soil layer. The Atera fault consists on gouge: 3 - 20 cm thickness.

There are two light grayish green gouge zones: 3 - 10 cm width each, including dark brownish gouge: about 3mm width. The sharpest shear zone, which is straightly brownish gouge, distributes in the gouge of hanging wall side. This gouge continues under the humus soil (440y B.P. Toda et al., 1994). This sharp zone was confirmed by X ray CT observation collected mass samples from the outcrop. Another dark brownish gouge zone runs parallel in the light grayish green gouge zone distributed the footwall side, converged into the sharpest shear zone at the central parts of the outcrop. At the footwall side, clayish sandy sediments were intruded into the light grayish green gouge with ductile deformation toward the left direction.

SEM observation was performed for the whole shear planes to be able to identify. For the dark brownish gouge zone, the observation was performed for the bottom, top, and sharp plane. On the results, authigenic minerals do not crystallize on the whole planes. Clay mineral (smectite) aggregates to form small clay ball (0.2 micron diameter), which covered the small particles as the paste (Kamachi et al., 2014).

Column shape? minerals (halloysite?) only coexist with Mn, Fe elements in the brackish lens zone including rhyolite and hexagonal biotite originating the foundation rock mass of the footwall side.

The results of this study show that authigenic minerals crystallized under the a few hundred degrees (clay and zeolite) do not confirm on the Atera fault plane to active after about 8400y B.P.

Reference; Toda et al.,(1994)Zisin,47,(1994),73-77. Kamachi et al.,(2014)JpGU2014.

Keywords: Atera, fault, latest plane, SEM

## Sand boiling traces at the Netsuno ruin in Ishikawa Prefecture and the Morimto-Togashi fault zone

HIRAMATSU, Yoshihiro<sup>1\*</sup> ; KOZAKA, Yutaka<sup>2</sup>

<sup>1</sup>Kanazawa University, <sup>2</sup>Hakusan Tedorigawa Geopark Promotion Council

Sand boiling traces detected at an archaeological site provides important information to reveal historical seismicity. In the Bunyudo ruins located at the central part of the Tedori-river fan, Hiramatsu and Kozaka (2013) detected sand boiling traces, which are the evidence of liquefaction, and discussed its relation to the activity of the Morimoto-Togashi fault zone. We report here sand boiling traces detected by an excavation survey of the Netsuno ruin, near the Bunyudo ruins, in 2013.

In the Netsuno ruin, we observe four sand boiling traces on the plane on which traces of vertical caves housing and Tsukikage wares of the late Yayoi period (1800-1900 years ago) were found. The sand boiling traces consist of ash gray sand with a diameter less than 1 mm. The largest trace has the maximum width of 20 cm and the length of about 2 m. This trace extends from a sand layer between a gravel layer and a silt layer located about 50 cm below the plane on which the traces are observed. Furthermore, this trace does not penetrate into a black soil layer above the plane that deposited from the late Yayoi period to the early Heian period. The observed traces are likely to have been covered by the black soil layer after the boiling on the ground surface at the time, implying that the formation age of the traces is from 1800-1900 to about 1100 years ago.

The Togashi fault is located near the Netsuno and the Bunyudo ruins, and, together with the Morimoto and the Nomachi faults, constitutes the Morimoto-Togashi fault zone of which a the total length is 26 km. No active fault has been reported around the Netsuno and the Bunyudo ruins. We, therefore, consider that the sand boil traces detected at these ruins are possibly formed by the activity of the Togashi fault or of the Morimoto-Togashi fault zone. An excavation survey at the Umeda area located at the northern part of the Morimoto fault revealed that a fault movement occurred about 1800-2000 years ago. A ruin where the surface displacement caused by the fault movement was observed is formed in the late Yayoi period. This period is the same as those of the Netsuno and the Bunyudo ruins. We, thus, conclude that the latest event of the Morimoto-Togashi fault zone is likely to be occurred 1800-1900 years ago.

Keywords: strong motion, the Morimto-Togashi fault zone, liquefaction, geopark

## Offshore active faults of the Mikata and Nosaka fault zones in Fukui Prefecture, revealed by high-resolution seismic pro

INOUE, Takahiko<sup>1\*</sup> ; SUGIYAMA, Yuichi<sup>1</sup> ; SAKAMOTO, Izumi<sup>2</sup> ; TAKINO, Yoshiyuki<sup>2</sup> ; MURAKAMI, Fumitoshi<sup>1</sup> ; HOSOYA, Takashi<sup>3</sup> ; USAMI, Takuya<sup>4</sup>

<sup>1</sup>AIST, <sup>2</sup>Tokai University, <sup>3</sup>Corporation of Chuokaihatu, <sup>4</sup>Sogo Geophysical Exploration Co,Ltd

The Mikata and Nosaka fault zones are located in coastal and shallow sea area off Mihama, Fukui Prefecture. National Institute of Advanced Industrial Science and Technology (AIST) and Tokai University conducted, as part of MEXT 2013 nearshore active fault survey project, a high-resolution multi-channel seismic survey using Boomer and a 12-channel streamer cable, acoustic profiling survey using parametric sub-bottom profiler and shallow-sea drilling survey, in order to clarify distribution and activity of the Mikata and Nosaka fault zones. We present mainly about the results of the high-resolution multi-channel seismic survey.

The most remarkable reflection surface in the seismic profiles is the ravinement surface that truncated evenly the lower sediment. Holocene sediments cover this surface and the sediments become thinner toward offshore.

In seismic profiles across the fault zones, flexure-like deformation in the Holocene sediments continue in the N-S direction in the Mikata fault zone and in the NW-SE direction in the Nosaka fault zone along faults shown by Komatsubara et al. (2000). The deformation in the Holocene sediments has been growing by displacements of an underlying active fault. The vertical offset of the flexure on the ravinement surface is larger than those on other reflectors in the sediments covering the ravinement surface and these offsets decrease upward. This growing deformation indicates that faults are reactivated several times in the last 10000 years. At the Mikata fault zone, vertical displacement of ravinement surface is about 11 meters. Based on the formation age of the ravinement surface presumed by sea level change in the world, we estimate the mean vertical slip rate at about 0.9 m/ky. On the other hand, at the Nosaka fault zone, vertical displacement of the erosional surface is about 8 meters. We obtained core samples reaching to the erosional surface at the Nosaka fault zone. We will compare in detail the seismic profiles with sedimentation ages obtained from the cores, in order to estimate vertical slip rate of the Nosaka fault zone. Event history, latest event and slip rate of the Mikata and Nosaka fault zones are further examined, incorporated with advanced analysis of seismic survey data and core samples.

Keywords: Offshore active fault, the Mikata fault zone, the Nosaka fault zone, high-resolution seismic survey, Event history

## Offshore active fault survey "Mikata fault and Nosaka fault zones". Result of high-resolution stratigraphic survey.

YAGI, Masatoshi<sup>1\*</sup> ; SAKAMOTO, Izumi<sup>1</sup> ; TAKINO, Yoshiyuki<sup>1</sup> ; FUJIMAKI, Mikio<sup>2</sup> ; TAJIMA, Tomoko<sup>1</sup> ; INOUE, Tomohito<sup>1</sup> ; SUGIYAMA, Yuichi<sup>3</sup> ; INOUE, Takuhiko<sup>3</sup>

<sup>1</sup>School of Marine Science and Technology, <sup>2</sup>COR, <sup>3</sup>Active Fault and Earthquake Research Center

The 26km long Mikata fault zone is extending from Kaminaka to Wakasa Bay. The fault zone consists of fault A, Hiruga fault, Mikata fault and Kuramitouge fault. The fault zone is estimated to cause M7.2 earthquakes (The Headquarters for Earthquake Research Promotion, 2002).

The 31km long Nosaka fault zone is extending from Nosaka Mountains to the Wakasa Bay. This fault zone consists of fault B, Nosaka fault and Nosaka southern fault. Fault B displaced the Holocene deposits and the vertical displacement rate is estimated to be about 0.8m/thousand years which are proposed by The Headquarters for Earthquake Research Promotion, 2002. Mikata fault and Nosaka fault zones show horizontal converges a single fault in the continental shelf.

Tokai University performed high-resolution stratigraphic survey to confirm a formation, distribution, and displacement of crust around the coastal area of the Mikata fault and Nosaka fault zones at Wakasa Bay in 2013. Transparent layer with poor internal reflection was observed as the surface layer in this survey area. This transparent layer is defined to as layer A. Layer A is ranges in thickness between 8 and 0 meter generally increase toward west. Displacement of the layer A is about 10m in most. Below layer A, sediments characterized by several reflections. First, we confirmed tilted reflection toward the Nosaka fault in the faults horizontal convergence section. Second, we confirmed progradation pattern reflection inclines to the offshore in the around Mikata fault.

Mikata fault and Nosaka fault are represented as a significant step in the seabed. The west side layer A is thicker than others. In the layer A, faults have not displaced surface sediments in this region. But several characteristic formations are which shows activities of fault has confirmed in sediments below layer A. The analysis still going on, the studies including the boring data will show more detail.

Keywords: Wakasa Bay, Mikata fault zone, Nosaka fault zone

## Drilling survey of the seaward extension of the Mikata and Nosaka fault zones off Mihama Town, Fukui Prefecture

SUGIYAMA, Yuichi<sup>1\*</sup> ; INOUE, Takahiko<sup>1</sup> ; MURAKAMI, Fumitoshi<sup>1</sup> ; SAKAMOTO, Izumi<sup>2</sup> ; TAKINO, Yoshiyuki<sup>2</sup> ; NAGATA, Takahiro<sup>3</sup> ; HOSOYA, Takashi<sup>4</sup> ; USAMI, Takuya<sup>5</sup>

<sup>1</sup>AIST, <sup>2</sup>Tokai University, <sup>3</sup>Dia Consultants Co., Ltd., <sup>4</sup>Chuo Kaihatsu Corporation, <sup>5</sup>Sogo Geophysical Exploration Co., Ltd.

AIST and Tokai University conducted, as part of MEXT 2013 nearshore active fault survey project, high-resolution acoustic reflection surveys and shallow-sea drilling survey across the Mikata and Nosaka fault zones off Mihama Town, Fukui Prefecture. We present the major results of the drilling survey. For the N-S-trending Mikata reverse fault zone, a 4-m-deep core was extracted from the 51-m-deep sea bottom on the western (downthrown) side. For the NW-trending Nosaka strike-slip fault with a reverse component, 27m- and 12m-deep cores were obtained from the 12m-deep sea on the SW (downthrown) and NE (upthrown) sides, respectively. We compiled geologic columns at scale of 1: 10 and conducted magnetic susceptibility measurement, radiocarbon dating, volcanic ash analysis, and diatom and pollen analyses.

Regarding the Mikata fault zone, obtained radiocarbon ages are proportional to the depth, reaching 6,180 to 6,010 and 6,380 to 6,260 cal.yBP at a depth of 3.8m. The average sedimentation rate during the recent 6ky is calculated at 0.6 m/ky. Acoustic reflection surveys have revealed several continuous reflection surfaces displaced by the fault, including the probable base of the postglacial deposits. We are trying to identify faulting-event horizons, using height difference of each reflection surface across the fault. Because drilling survey was unable to determine the age of each reflection surface, we are making efforts to estimate them, extrapolating possible depth-age curves of the postglacial deposits.

The deposits extracted from the both sides of the Nosaka fault zone are divided into the following stratigraphic units based on lithofacies and radiocarbon ages: A1 (<ca.6ka), A2 (ca.6-7.3ka), A3 (ca.7.3-7.5ka), B1 and B2 (ca.7.5-8ka), C (ca.8-10ka) and D intercalating 30-ky-old AT tephra. A1 is subdivided into the upper part (<ca.4ka) and the lower part (ca.5.5-6ka). While the basal surface of B2 shows 5m height difference across the fault, that of the lower A1 represents 1.7m difference across the fault. The lower A1 also shows drastic change in thickness from 1.1 m on the downthrown side to 0.2 m on the upthrown side. These suggest that faulting occurred twice; in the periods post-C/pre-A (8-6ka) and post-lower A1/pre-upper A1(ca.5.5-4ka). Faulting history and slip per event are further examined, incorporated with analyses of acoustic reflection survey data.

Keywords: Mikata fault, Nosaka fault, active fault, acoustic reflection survey, sea drilling

## The fault gouge along the Ikoma active fault zone

MITAMURA, Keisuke<sup>1\*</sup> ; OKUDAIRA, Takamoto<sup>1</sup> ; MITAMURA, Muneki<sup>1</sup>

<sup>1</sup>Graduate School of Science, Osaka City University

The characteristic of the topography of Middle Kinki is reflected as an alternation arrangement of a mountainous district and the basin of north-south characteristics. Ikoma mountains share the Osaka plain and the Nara Basin. The NNE-SSW-N-S trending Ikoma active fault zone is recognized as a high-angle reverse fault under the E-W compressional stress field in the Quaternary Japan. However, from the rock mechanics point of view, high-angle fault is favorable as normal fault formed under extensional stress regime. The high-angle reverse faults may be resulted from the reactivation of the high-angle normal faults (inversion tectonics). In this study, we examined some fault gouge zones along the Ikoma fault zone (Katano and Ikoma faults).

We found three fresh outcrops of mesoscopic fault zones developed along the Ikoma fault zone at Kuraji of Katano City, Kiyotaki of Shijonawate City and Imoriyama of Shijonawate City. In these fault zones, fault gouge with the width of 5-20 cm can be observed. We collected some oriented samples and made thin sections parallel to the striation and normal to the fault plane. In the samples, many dark seams develop parallel to the main fault plane (striation) to form a distinct foliation within the fault gouges. Many fragments with various sizes are observed and their long axis aligned oblique to the fault plane. The parts where edges of the fragments meet the dark seam the edges tends to be rounded, suggesting that the formation of the dark seam was associated with material transportation due to pressure solution. The fragments with high aspect ratios tend to align oblique to the fault plane, suggesting the rigid-body rotation caused by non-coaxial shear deformation. The asymmetric structures, i.e., preferential orientation of the long axis of fragments, drag folds and shear lenses indicate the top-down-sense-of-shear. Furthermore, fractal dimensions of the fragments in samples near the main fault plane are higher than in samples at the margin of the fault gouge.

Consequently, we found the lines of evidence indicative of normal fault movement in the fault gouges associated with the Ikoma active fault zone, suggesting that the N-S striking Ikoma fault zone is recognized as a high-angle reverse fault under the E-W compressional stress regime are of reactivation of the preexisting high-angle normal faults that may be formed under extensional stress field.

Keywords: Ikoma fault zone, active fault, tectonic inversion, fault gouge, internal structures, fracture zone

## Subsurface density structure in Southern Osaka Plain based on gravity and magnetic anomalies

INOUE, Naoto<sup>1\*</sup> ; KITADA, Naoko<sup>1</sup> ; TAKEMURA, Keiji<sup>2</sup>

<sup>1</sup>Geo-Research Institute, <sup>2</sup>Beppu Geothermal Research Laboratory, Institute for Geothermal Sciences, Graduate School of Science,

Geomorphological, geological and geophysical surveys have been carried out in the Osaka plain for the highly precise construction of a model to predict strong ground motion. In recent years, many seismic surveys were performed in the south of the plain. The outline of the basement configuration was estimated from the relationship between gravity anomaly and the depth of the basement. The depth of the basement inferred from the gravity anomaly was shallower than that from the seismic and micro tremor surveys at several points in the Osaka plain. The difference is considered the variation of density contrast due to some local distribution of the volcanic rocks. The magnetic anomaly indicates higher value at these points. The density structure was discussed from the gravity anomaly in consideration of the high magnetic anomaly area.

Keywords: gravity anomaly, magnetic anomaly, density structure, Osaka plain

## Age and horizontal offset of the latest faulting event on the Okamura fault of the MTL fault zone in central Shikoku

IKEDA, Michiharu<sup>1\*</sup> ; GOTO, Hideaki<sup>2</sup> ; TSUTSUMI, Hiroyuki<sup>3</sup> ; KONDO, Hisao<sup>4</sup> ; NISHIZAKA, Naoki<sup>5</sup> ; OHNO, Yuki<sup>5</sup> ; TSUYUGUCHI, Koji<sup>6</sup> ; KOBAYASHI, Shuji<sup>1</sup>

<sup>1</sup>Shikoku Research Institute Inc., <sup>2</sup>Hiroshima University, <sup>3</sup>Kyoto University, <sup>4</sup>AIST/AFERC, <sup>5</sup>Shikoku Electric Power Co. Inc., <sup>6</sup>Yonden Consultants Co. Inc.

In general, information about fault offsets along active faults is one of the important factors to estimate faulting behavior in seismogenic zones. However, it is challenging to determine the information about fault offsets. So far, the average slip-rate and the amount of a single-event offset are obtained only 30 and 6 points on the Median Tectonic Line active fault zone (MTLAFZ) in the Shikoku area (200 km-length), respectively (Tsutsumi and Goto, 2006).

We conducted a trench survey for the Okamura fault which is a part of the MTLAFZ in order to determine the latest faulting event age and the fault offset. The Okamura fault is distributed in a range of 30 km on the central Shikoku. The survey point, Hagioi point, locates on a central part of the Okamura fault. The amount of the fault offset at the latest faulting event is estimated to be below 5.7 m (Tsutsumi et al., 1991). However, this is just one data about fault offset on the Okamura fault. Moreover, the latest event age of the Okamura fault has not been sufficiently constrained by some previous research results; 4-7th century (Okada et al., 1998), 1090-960 yBP (Ehime Prefecture, 1999) and after 16th century (Goto et al., 2001).

The main two results of this trench survey are as following. The latest faulting event age is estimated to be after AD 1490, consisting with after 16th reported in Goto et al. (2001). Moreover, the amount of fault displacement at the latest faulting event is estimated to be below 7.5 m. This value is consistent with the trend of the surface offset information that the surface slip associated with the latest event is greater than 5 m between the Zunden and Okamura faults, and decrease gradually to the east and west.

In taking hypothetical consideration, the fault offset 7.5 m is greater than 5.7 m (Tsutsumi et al., 1991) at 5 km away from this survey site. The recurrence interval (938-1500 years) calculated on the basis of average slip rate (5-8 mm/y) and the fault offset 7.5 m is consistent with the value (1245-1620 years) from the paleoseismological data (Morino and Okada, 2002; Okada et al., 1998). Therefore, the survey result might indicate variety of fault offsets along the Okamura fault, however this fault offset 7.5 m contains estimation errors. Since the fault offset becoming larger toward the fault end is unreasonable, this survey site might not locate on near the end of the Okamura fault and but near the asperity region.

Keywords: latest faulting event age, fault offset, Median Tectonic Line active fault zone, Okamura fault

## Seafloor exploration at off Kochi Prefecture for coseismic subsidence during hysterical Nankai earthquakes

TANIKAWA, Wataru<sup>1\*</sup> ; TOKUYAMA, Hidekazu<sup>2</sup> ; MURAYAMA, Masafumi<sup>2</sup> ; YAMAMOTO, Yuhji<sup>2</sup> ; EBIHARA, Shu<sup>3</sup>

<sup>1</sup>JAMSTEC/Kochi Kore Center, <sup>2</sup>Center for Advanced Marine Core Research , Kochi University, <sup>3</sup>Nippon Kaiyo ltd.

Paleoseismic trenching study and tsunami deposit analysis on land has been performed to understand the historical earthquakes and the scale of disasters caused by the earthquakes. Paleoseismic records are probably stored in seafloor sediments near the coast as well, though the seafloor researches were rarely performed.

In ancient documents, the great Hakuho Earthquake (684 A.D.), that had been classified a Nankai earthquake, had caused large subsidence near the coast and submerged a small village named "**Kuroda-gori**". In addition that, ancient artificial buildings and artifacts were found at off Kochi Prefecture from Aki city to Cape Ashizuri cape. However the relationship between the ancient foundation and the historical Nankai earthquake is not well understood.

Here, we investigate the seafloor foundation at off Kochi Prefecture based on marine seismic profiling and diving. We collect artifacts and sediment core samples from seafloors, and perform chemical and age analyses using them. We then evaluate the coseismic uplift and subsidence process and a magnitude scale of earthquake during paleo-Nankai earthquakes. We begin seafloor exploration at two sites, off-Tochi site and Nomi bay site in Kochi area. We introduce preliminary results of seafloor research on March 2014 and our future plan.

### Acknowledgement

We appreciate the technical support by Nippon Kaiyo ltd..

Keywords: Hakuho earthquake, earthquake foundation, Nankai Trough earthquake, coseismic uplift and subsidence

## Fault activity of the Kokura-higashi fault and the Fukuchiyama fault zone in northern Kyushu Island, Japan

YOSHIOKA, Toshikazu<sup>1\*</sup> ; TANIGUCHI, Kaoru<sup>1</sup> ; HOSOYA, Takashi<sup>2</sup> ; YAGI, Tatuya<sup>2</sup>

<sup>1</sup>Active Fault and Earthquake Research Center, AIST, <sup>2</sup>Chuo Kaihatsu Corporation

The Kokura-higashi fault is an active fault extending in NNE-SSW direction with west-side-up vertical displacement. The Fukuchiyama fault zone consists of the Tonda and Fukuchiyama faults extending in NNW-SSE direction with also west-side-up vertical displacement. Both are located in the northern Kyushu Island. The Earthquake Research Committee evaluated that the probability of the earthquake occurrence in the future on the Kokura-higashi fault and the Fukuchiyama fault zone are unknown or ambiguous because of the lack of paleoseismological data. We carried out a trench excavation study and boring surveys in four sites with total 20 cores on these faults.

A trench is excavated across a reverse scarp along the estimated fault trace of the Tonda fault in the Fukuchiyama fault zone. On the trench wall, steeply inclined sandstone and mudstone of the Paleogene Ashiya Group and overlaid gravel and silt layers are cropped out. However, no clear fault is observed in between bedrocks and sediments.

Based on arrayed boring surveys at the Shii and Shindoji site on the Kokura-higashi fault, a few meters differences in depth of the bedrocks are recognized.

Faults are observed in the cores from the arrayed boring surveys at the Ikeda and Horita sites on the Fukuchiyama fault zone.

Keywords: Kokura-higashi fault, Fukuchiyama fault, Tonda fault, Fukuoka Prefecture, Kyushu Island, active fault

## Revised fault model of the 1771 Yaeyama tsunami, southwest Ryukyu

NAKAMURA, Mamoru<sup>1\*</sup>

<sup>1</sup>Faculty of Science, Univ. Ryukyus

The 1771 Yaeyama tsunami (Meiwa tsunami) has been the largest and devastating tsunami in the Ryukyu Trench since about 300 years. The maximum runup height was about 30 m and 12000 people were dead by the tsunami. Although this tsunami is important for estimating the maximum tsunami in the Ryukyu Trench, the fault model has been unsolved. Then we estimated the source fault model of this tsunami.

(1) The maximum runup heights were 30 m near the southeast coast of Ishigaki Island, 15 m at Tarama Island, 15 m at Irabu Island, and 18 m at south coast of Miyako Island (Goto et al., 2011). The runup height at south coast of Miyako Island was estimated to 10.5 m from the old document "Kyuyo". However, folklore (Goto et al., 2011) and the inundation area estimated from the old document "Otoegaki" (Kato, 1988) showed the runup height were about 20 m.

(2) Tarama Island is formed by the coral middle terrace at the height of 10-14 m. The tsunami reached at the villages (Nakasuji and Shiokawsa) which were located at the center-to-north of the Island. The estimated runup heights in these villages were about 15 m. Since the hill, whose height is 30 m, is located at the north of the villages, the tsunami will have inundated about 1.5-3.0 km from the south or east coast. Shimoji Island is also formed by the middle coral terrace at the height of 10-20 m. Although the Island was uninhabited at that time, the terrace was inundated by the tsunami, and the soil was stripped by the tsunami inundation, and cattle and domestic animals drown by the inundation (Shimajiri, 1988). These suggest that the wide area of the Tarama and Shimoji Island are inundated by the tsunami.

Using these data, we re-construct the fault model of this tsunami. We employed intraplate earthquake and landslide (Miyazawa et al., 2012), interplate earthquake (Nakamura, 2009), and splay fault (Hsu et al., 2013) models.

First, in the case of intraplate earthquake and landslide model, calculated runup heights were consistent with the observed ones. However, the calculated inundation area is limited within about 500 m from the shore at Tarama Island.

In the case of splay fault model, we set the western part of fault at the 125.5E based on Hsu et al. (2013). The calculated tsunami heights were smaller than the observed in the Ishigaki Island. The inundation area is limited within 500 m from the shore at Tarama Island.

Finally, we set the interplate earthquake model, which is revised the model of Nakamura (2009). We set the fault length, width, slip, and dip to 200 km, 70 km, 20 m, and 12 degrees, respectively (Mw8.6). In this case, the calculated runup heights were almost consistent with the observed ones except southeast coast of Ishigaki Island. The calculated inundation area is 1.5 km from the shore at Tarama Island. Then we added the local patch at the south of Ishigaki Island. The length, width, and slip of the patch is 40 km, 30 km, and 40 m (total Mw=8.7). Then we could reproduce the observed runup heights.

Keywords: tsunami, Ryukyu Trench, interplate earthquake, historical tsunami

## Systematical deflections and offsets of stream channels along the left-lateral strike-slip Kunlun Fault

YAN, Bing<sup>1\*</sup> ; LIN, Aiming<sup>2</sup>

<sup>1</sup>Graduate School of Science and Technology, Shizuoka University, <sup>2</sup>Department of Geophysics, Graduate School of Science, Kyoto University

During the past two decades, the integration of geologic, geomorphic, seismic, and geophysical information has led to increased recognition and understanding of the tectonic significance of geomorphic features caused by strike-slip along active strike-slip faults. Tectonic landforms developed along active strike-slip faults are mainly characterized by systematic deflections and offsets of streams which are regarded as reliable displacement markers useful for reconstructing the long-term activity of active faults. It has been demonstrated that stream offsets have resulted from repeated large strike-slip earthquakes. The study of tectonic geomorphology will provide a new insight into the seismic activity, longevity and structural evolution of active strike-slip faults.

The Kunlun Fault is a typical active strike-slip fault zone extends for ~1200 km in the northern Tibetan Plateau that has triggered the 2001 Mw 7.8 Kunlun great earthquake. In this study, we present evidence for the systematical sinistral deflection and/or offset of the stream channels and valleys of the upper Yellow River drainage along the eastern intramontane segment of ~400 km of the fault zone. Topographic analysis of 3D perspective images constructed using Digital Elevation Model (DEM) data, high resolution Google Earth images and 15-m-resolution Landsat Enhanced Thematic Mapper (ETM+) images reveals the following: (i) various amounts of sinistral offset have accumulated on the tributary stream channels, valleys, and gullies of the upper Yellow River; (ii) the eastern intramontane segment of Kunlun fault accumulated sinistral offset amount for at least 12 km; (iii) the linear relationship between the between the accumulated offset amount and the upstream length from the deflected point to valley head of the stream involved can be reliable indicator of long-term slip rate.

The findings of this study support that the Kunlun Fault is a left-lateral strike-slip that partitions deformation into the eastward extrusion of the Tibetan Plateau to accommodate the continuing penetration of the Indian plate into the Eurasian plate.

Keywords: Kunlun Fault, left-lateral strike-slip fault, stream channel, systematical deflection, Tibetan Plateau, eastward extrusion

## On the generalization of the SPAC method and the development of a CCA method

CHO, Ikuo<sup>1\*</sup>

<sup>1</sup>National Institute of Advanced Industrial Science and Technology

### Introduction

Microtremor array methods refer to techniques for estimating subsurface velocity structures from the dispersion of Rayleigh-wave phase velocities obtained through array analysis of microtremors. Methods for analyzing Rayleigh-wave phase velocities include two major constituents: the spatial autocorrelation (SPAC) method [Aki, 1957] and the frequency-wave number spectral (FK) method [Capon, 1969]. SPAC method excels the FK method in the overall analysis efficiency, when account is taken of the requisite number of seismic sensors and the breadth of the wavelength ranges eligible for analysis [Okada, 2003]. The SPAC method, in addition, is intrinsically usable with a two-sensor seismic array [Aki, 1957], a potential that has received reappraisal during the past decade. Given this context, the SPAC method in recent years has not only come to be used more often, but has also seen progress in theoretical studies of its applicability.

### Generalization of the SPAC method and the development of a CCA method

In our case, Cho et al. [2006] generalized the Aki's theory following Henstridge[1979], describing generic formulae to analyze a circular array of three-component microtremors on the basis of the theory of stationary random processes. The generic theory provided a basis for constructing various methods to efficiently analyze Rayleigh- and Love-wave phase velocities, Rayleigh-wave ellipticities, and power partition ratios of Rayleigh to Love waves. It also provided a theoretical foundation to examine applicability conditions and optimal observation durations for two-sensor SPAC methods.

The centerless circular array (CCA) method [Cho et al., 2004] represents one method on the basis of the generic theory to analyze phase velocity of Rayleigh waves. The CCA method is characterized, among other things, by its applicability to an array of three seismic sensors in irregular configuration. It is also characterized by superior analytic performance in long-wavelength ranges. Methods have been proposed to evaluate noise levels, which can negatively impact its analytic performance, in terms of signal-to-noise (SN) ratios and to compensate for the effects of noise.

In the first half of the presentation, the above history will be described after a simple explanation of the general features of microtremor array explorations.

### Development of miniature array analyses for shallow surveys

In the second half, the situation on the miniature array analyses based on the CCA method will be reported. "Miniature array analyses" involves 15-min microtremor measurement sessions using very small seismic arrays, 1 m or less in radius, to obtain the dispersion of Rayleigh-wave phase velocities corresponding to depths of several tens of meters, and sometimes more than 100 m, beneath the surface. In addition to this feature, the analysis results are accompanied with quality control factors. In the last year, we dealt with the following problems so as to put the miniature array analysis into practical use: (i) What is an appropriate way to deal with analysis results of limited quality and dubious reliability in general? (ii) What is a better way to pursue the efficiency of surveys, including the step of estimating subsurface structures after the dispersion curve is obtained?

In the presentation, I will report the solution for this problem on the basis of the experience, the automatization of the analysis procedure (Cho et al., 2014; Senna et al., 2014), and a plan to release a new BIDO package (<https://staff.aist.go.jp/ikuo-chou/bidodl.html>) to draw 2D S-wave sections by miniature array analysis.

**Acknowledgement** The outcomes in the first half were obtained in the collaborative investigation with Dr. Taku Tada and Prof. Yuzo Shinozaki. Those in the second half were obtained in the collaborative investigation with Dr. Shigeki Senna and NIED, and through discussions with the members of the microtremor working group.

Keywords: Microtremor, velocity structure, surface waves, phase velocity, exploration method, array

## Detection of Rayleigh wave and Love wave detection from microtremor array measurements

OHORI, Michihiro<sup>1\*</sup> ; CITAK, Seckin<sup>2</sup> ; KUBO, Atsuki<sup>3</sup> ; OISHI, Yusuke<sup>3</sup> ; TAKAHASHI, Hirokazu<sup>3</sup> ; YAMASHINA, Tadashi<sup>3</sup>

<sup>1</sup>University of Fukui, <sup>2</sup>Japan Agency for Marine-Earth Science and Technology, <sup>3</sup>Kochi University

Microtremor array measurements are considered to be one of the most practical ways to explore the S-wave velocity structures for the seismic hazard evaluation. As seen in many articles (e.g. Horike, 1985), the Rayleigh-wave dispersive characteristics have been derived from vertical components to model the S-wave velocity structures. On the other hand, the detection of Love-waves from horizontal components seems to be limited in very few literatures (e.g. Yamamoto, 2000), because horizontal components of microtremors are composed of the Love-waves and the Rayleigh-waves and the separation of two different kinds of surface waves is usually considered to be difficult.

As representative methods to analyze the microtremor array records, the FK spectral method proposed by Capon (1969) and the spatial autocorrelation (SPAC) method by Aki (1957) have been used. Both methods have been extended to treat three-component data and detect the Love-wave as well as the Rayleigh-wave: the FK spectral method by Saito (2007) and the SPAC method by Okada and Matsushima (1990) and Yamamoto (2000), respectively. It is considered to be significant to apply these extended methods to observed data in various test fields. In our previous study, we carried out microtremor array measurements at Takasu area in Kochi city, south-west Japan on November 2010. We used two circular arrays with radii of 50 m and 100 m simultaneously, and successfully detected dispersive characteristics of both Rayleigh-waves and Love-waves in a frequency range between 1.2 to 3.8 Hz (Ohori et al. 2013). In analyses of observed array records, we used two kinds of the FK spectral methods: Capon's technique (1969) applied to vertical component and Saito's one (2007) to horizontal components.

To make a better understanding about characteristics of microtremors for the targeted area and obtain surface wave dispersive characteristics in more higher frequency range (up to 6Hz), we additionally conducted a few smaller array measurements on March 2013, using 4 sets of three-component portable seismometers which compose a circular array with a radius varying step-by-step from 50 m to 25 m and 12.5 m. In our study, results from newly observed data are reported and discussed. Phase velocity results were obtained from FK spectral method for vertical and transverse components. We also applied the SPAC method (Yamamoto, 2000) and compared the estimated phase velocity results from the SPAC method with those from the FK spectral method. The SPAC method provided that the energy power ratio of Love-waves in horizontal components distributed within 40-70% in a frequency range between 1.4 to 6 Hz.

Keywords: microtremor array measurements, FK spectral method, SPAC method, Rayleigh-wave, Love-wave

## Estimating composition of ambient noise from three-component records at Tono array

TAKAGI, Ryota<sup>1\*</sup>; NAKAHARA, Hisashi<sup>2</sup>; KONO, Toshio<sup>1</sup>; OKADA, Tomomi<sup>1</sup>

<sup>1</sup>RCPEV, Graduate School of Sci., Tohoku Univ., <sup>2</sup>Geophysics, Graduate School of Sci., Tohoku Univ.

Ambient noise methods have become common tools to explore and monitor subsurface structure. However, effective uses of ambient noise should stand on the knowledge of a nature of ambient noise. In order to reveal the composition of ambient noise quantitatively, we extend the SPAC method to body wave incidence. Applying the extended SPAC method to the observation at Tono array, northeast Japan, we shows a good agreement between the theoretical cross spectra and the observed cross spectra. By fitting the theoretical cross spectra to the observed cross spectra, we estimated the composition ratio of Rayleigh, Love, and P waves. The characteristics of the composition ratio show a significant change at 1 Hz. While the P wave composition in total power is 5-15% and the lowest one below 1 Hz, the P wave composition suddenly increases above 1 Hz and reaches 50% and the highest one in those of the three wave modes. The change at 1 Hz is attributed to attenuation of high-frequency surface waves because the decay rate of the absolute value of power spectra of surface waves gets steeper around 1 Hz as compared with the constant decay of P wave. We also examine the temporal variation of the composition of ambient noise. Whereas power spectrum of each mode shows long-term and short-term temporal variations coincident with offshore significant wave height, the ratio between power spectra varies little with time. The constant composition ratio suggests that the mechanism and the source-receiver distance are stable in time. Accordingly, near coastal region is a possible region of the dominant source of the observed ambient noise. For applications of ambient noise, we should take account of the composition of ambient noise.

Keywords: ambient noise, SPAC, three-component array observation

## Toward Earthquake Ground Motion Prediction using the Onshore-Offshore Ambient Seismic Field in Subduction Zones

VIENS, Loic<sup>1\*</sup> ; MIYAKE, Hiroe<sup>1</sup> ; KOKETSU, Kazuki<sup>1</sup>

<sup>1</sup>Earthquake Research Institute, University of Tokyo

Ground motion prediction is critical to evaluate the seismic hazard specially in high seismicity areas as Japan. A source of particular concern is the complex geological structures as sedimentary basins which can trap and amplify seismic waves. It has been proved by Prieto and Beroza (2008) that reliable phase and amplitude of the impulse response functions can be extracted by deconvolution of the ambient seismic field recorded by two on-land stations without any pre-processing. This approach has the great advantage to predict accurate ground motion of moderate earthquakes at periods longer than 4 s without the need of any external information about the velocity structure. However, this method allows only to recover relative, rather than absolute, amplitudes. To retrieve the corresponding Green's functions, impulse response amplitudes need to be calibrated using records of an earthquake which happened close to the "virtual" source. Moreover, as surface-to-surface Green's functions are extracted, some mismatches are observed between Green's functions and the earthquake records. This feature is due to the fact that depth and focal mechanism of the event are not taken into account. Despite of these disadvantages, accuracy of the predicted ground motion is high and such long-period ground motion investigation is critical to carried out seismic hazard assessment for high-rise buildings, bridges, or oil tank having long-period resonance. In this study, we use this technique in subduction zones to extract vertical-to-vertical component of the Green's functions between seismic stations located on the ocean bottom and on-land Hi-net stations. The target region is located in the Tokai/Tonankai areas where two submarine cable-based sea-bottom seismographic observation systems have been deployed by the Japan Meteorological Agency (JMA). We use one month of noisy data recorded in January 2013 to compute the Green's functions. The choice of these data is motivated by a strong signal-to-noise ratio of the causal part of the Green's functions during this period. We validate this approach by comparing computed Green's functions with offshore moderate earthquake ( $M_w \sim 5$ ) records in the Nobi sedimentary basin where the Nagoya city is located. As megathrust earthquakes are expected in this area, we extrapolate our results to predict magnitude  $M_w \sim 6$  or larger earthquake ground motions using the scaling law of seismic spectrum developed by Aki (1967). These results are finally compared to long-period ground motion prediction equations to evaluate their validity.

Keywords: Ground motion Prediction, Ambient seismic field, Subduction zones, Low frequency, Deconvolution

## Review of study on microtremors and application for subsurface structure modeling

SUZUKI, Haruhiko<sup>1\*</sup>

<sup>1</sup>OYO

The study on microtremors start by Kanai(1954). In his study, the relation between the subsurface structural model and the predominant period.

The method of the spectral ratio of two sites are devised. The influences source and path is removed.

From the 1980s, using spectral ratio between horizontal and updown component the subsurface structural model was estimated(Arai and Tokimatsu,2005). They assumed the microtremor consists by surface waves. On the other hand Nakamura(1988) assumed the microtremor consists by the SH waves.

H/V spectral ratio is using earthquake damage assumption investigations. Using H/V spectral ratio and phase velocity of Rayleigh wave, R/V spectral ratio of earthquake ground motion, the subsurface structural model from several meter to several kilometer depth are estimated in the Kanto area.

Keywords: Microtremors, Spectral ratio, S-wave structural modeling

## Geological Interpretation of a Liquefied Area by 'i-Bido': A Case Study in Urayasu City, Japan (2)

SATO, Shinji<sup>1\*</sup>; HIGASHI, Masashi<sup>2</sup>; HIGUCHI, Shigeo<sup>3</sup>; INADA, Akira<sup>3</sup>; ITO, Akihide<sup>4</sup>; IWAMOTO, Hiroshi<sup>5</sup>; KAMIKASEDA, Satoshi<sup>6</sup>; KAWASAKI, Kenichi<sup>7</sup>; KUSUNOKI, Keiko<sup>8</sup>; SHINADA, Shoichi<sup>2</sup>; SUENAGA, Kazuyuki<sup>9</sup>; WATANABE, Takumi<sup>3</sup>; SENNA, Shigeki<sup>10</sup>; FUJIWARA, Hiroyuki<sup>10</sup>

<sup>1</sup>Chishirodai high school, <sup>2</sup>JAPEX, <sup>3</sup>No affiliation, <sup>4</sup>Chiba-kita High school, <sup>5</sup>Kanto Natural Gas Development Co., Ltd, <sup>6</sup>NTC Consultants Co., Ltd., <sup>7</sup>Chiba-nishi High school, <sup>8</sup>Urayasu high school, <sup>9</sup>Earth System Science Co., Ltd., <sup>10</sup>NIED

The Great East Japan Earthquake that occurred in 2011 off the Pacific coast of Tohoku caused the formation of two long cracks (crack 1 and crack 2) at Urayasu High School in Chiba Prefecture, Japan. Iwamoto et al. (2014) classified the survey area into different parts by examining the reclamation history and found the following three areas: A, 'Kaimenka-tochi'\*; B, reclaimed land from dredged seabed deposits; and C, the embankment and its surrounding zone. Crack 1 was situated between areas A and B, and crack 2 was between areas B and C.

Based on the investigation, the authors conducted micro-tremor observations at the three reclaimed land areas and Alluvial area. These measurements were conducted to reveal the area's geophysical aspects and to extrapolate three-dimensional data of the subsurface geology from two-dimensional data. At each measurement position, the results of micro-tremor observation were analyzed to give H/V spectra and the relationship between the site's geology and physical data. Field measurements of micro-tremors were performed with JU310, which was designed by the National Research Institute for Earth Science and Disaster Prevention. Measurements and analysis were performed using the i-Bido system (Senna et al., 2011), named after the Japanese word for micro-tremor, which was designed by the same institute.

Analysis revealed that the micro-tremors in areas A, B, and C had clear peaks at 1 Hz or slightly higher. This result corresponds to the impedance ratio at the boundary between the Holocene and Pleistocene deposits. Additionally, the micro-tremors observed at area B, which contains land reclaimed in 1965-1971, had peaks from approximately 4-5 Hz. These peaks were not observed or were unclear in areas A and C. For both crack 1 and crack 2, the peak was clear on one side but not on the other. The interval across a crack was only a few meters; therefore, these peaks depend on the impedance ratio between the silt bed, which was reclaimed by dredging from the seafloor, and the Holocene deposits. Additionally, the Nd-value\*\* of the silt bed was 0, as determined by a survey of the subsurface geology.

The analytical results determined using i-Bido supported the physical aspect put forth by Iwamoto et al. (2014) as the reason and mechanism by which the two cracks formed. Each frequency peak also showed the individual geological unit in the reclaimed bed, further supporting Iwamoto et al. (2014). The i-Bido system was very useful for analysis of the relationship between the site's geology and physical characteristics and for extrapolation of three-dimensional data from two-dimensional data. The authors hope that the methods discussed here will aid the progress of disaster prevention.

\* 'Kaimenka-tochi' means land below sea level literally. Before reclamation, it was located in front of seashore, and it was in the possession of the private owner. and was used to reed cultivation etc.

\*\*Nd-value is brought by Dynamic Cone Penetration Test, which has the following conditions: a slide hammer with a weight of 5kg falling through a distance of 50cm, and diameter of 2.5cm cone. The number( i.e. Nd-value) of blows needed for the cone to penetrate each 10cm is recorded.

### Acknowledgements

The authors are very grateful to Mr. Toshio NAKAYAMA of visiting researcher of NIED, who supported them for using i-Bido system.

### References:

Hiroshi IWAMOTO, Masashi HIGASHI, Shigeo HIGUCHI, Akira INADA, Akihide ITO, Satoshi KAMIKASEDA, Kenichi KAWASAKI, Keiko KUSUNOKI, Shinji SATO, Shoichi SHINADA, Kazuyuki SUENAGA, and Takumi WATANABE (2014) Recent Geological Interpretation of Liquefied Area: A Case Study in Urayasu City, Japan(1). Japan Geoscience Union Meeting 2014.

Shigeki Senna, Hiroki Azuma(NIED), Yuuko Murui(MSS Corp), and Hiroyuki Fujiwara(NIED) (2011) Development of micro-tremor survey of observation system i-bidou, etc. The 124 th SEGJ (Society of exploration geophysics of Japan) Conference. 346-348.

Keywords: liquefaction, crack, micro tremor, i-Bido, Urayasu, reclaimed land

SSS35-06

Room:502

Time:May 2 16:15-16:30

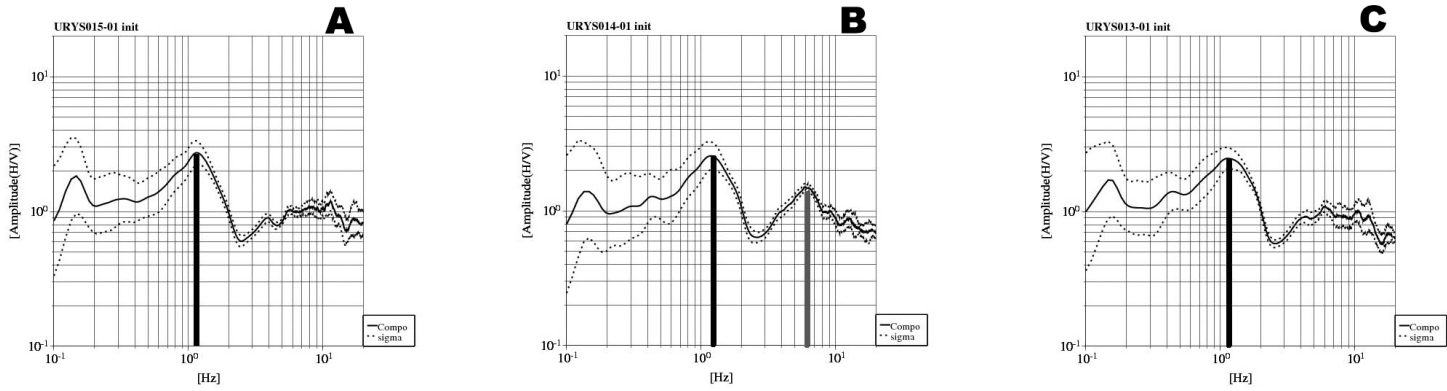


Fig.1 H/V Spectra of A, B, and C Areas

## H/V Spectral Ratios for Both Microtremors and Earthquake Motions and Interpretation based the Diffuse Field Theory

KAWASE, Hiroshi<sup>1\*</sup> ; MATSUSHIMA, Shinichi<sup>1</sup>

<sup>1</sup>DPRI, Kyoto University

Horizontal-to-vertical spectral ratios (HVRs) of microtremors have been traditionally interpreted theoretically as representing the Rayleigh wave ellipticity or just utilized a convenient tool to extract predominant periods of ground. However, based on the diffuse field theory (Sanchez-Sesma et al., 2011) microtremor H/V spectral ratios (MHVRs) correspond to the square root of the ratio of the imaginary part of horizontal displacement for a horizontally applied unit harmonic load and the imaginary part of vertical displacement for a vertically applied unit load at the same position.

The same diffuse field concept leads us to derive a simple formula for earthquake HVRs (EHVRs), that is, the ratio of the horizontal motion on the surface for a vertical incidence of S wave divided by the vertical motion on the surface for a vertical incidence of P wave with a fixed coefficient depending on the bedrock wave velocity (Kawase et al., 2011). The difference of EHVRs from MHVRs comes from the fact that primary contribution of earthquake motions would be of plane body waves. Traditionally EHVRs are interpreted as the responses of inclined SV wave incidence only for their coherent S wave portions.

Before the advent of these compact theoretical solutions, EHVRs and MHVRs are either considered to be very similar/equivalent, or totally different in the previous studies. With these theoretical solutions we need to re-focus our attention on the difference of HVRs.

To that end we have compared HVRs at several dozens of strong motion stations in Japan. When we compared observed HVRs we found that EHVRs tend to be higher in general than the MHVRs, especially in higher frequencies than their fundamental peaks. As previously reported, their general shapes share the common features. Especially their fundamental peak and trough frequencies show quite a good match to each other. However, peaks in EHVRs in the higher frequency range would not always show up in MHVRs. When we calculated theoretical HVRs separately at these target sites, we found that the underground structures that are optimized for EHVRs would not explain perfectly MHVRs.

So we invert underground structures which can explain both EHVRs and MHVRs at the same time based on the different theoretical formula. Using the hybrid heuristic algorithm primarily based on the GA method with generation-dependent probability, we successfully obtain the detailed S-wave velocity structures for these investigated sites. The proposed method using HVRs is quite robust to obtain S-wave velocity structures that can be used quantitative simulation of strong motions at the target sites.

Keywords: microtremors, strong motion, diffuse-field theory

## The Effect of the Basin Edge to the Directional Dependent Horizontal-to-Vertical Spectral Ratios of Microtremors

MATSUSHIMA, Shinichi<sup>1\*</sup>; DE MARTIN, Florent<sup>2</sup>; KAWASE, Hiroshi<sup>1</sup>; FUKUOKA, Yuri<sup>3</sup>; SANCHEZ-SESMA, Francisco<sup>4</sup>

<sup>1</sup>DPRI, Kyoto University, <sup>2</sup>Risk and Prevention Division, BRGM, <sup>3</sup>School of Engineering, Kyoto University, <sup>4</sup>Institute of Engineering, UNAM

Based on the diffuse field theory (Perton et al., 2009), Horizontal-to-Vertical (H/V) spectral ratios of microtremors (or ambient noise) correspond to the square root of the ratio of the imaginary part of horizontal displacement for a horizontally applied unit harmonic load,  $\text{Im}[G_{11}]$  and/or  $\text{Im}[G_{22}]$ , and the imaginary part of vertical displacement for a vertically applied unit load,  $\text{Im}[G_{33}]$ , where both the loads and receivers are at the same point on the free surface (Sanchez-Sesma et al., 2011). This theory can be applied to a site where the subsurface structure cannot be considered as sufficiently flat, horizontally layered (i.e.,  $\text{Im}[G_{11}] \neq \text{Im}[G_{22}]$ ), and lateral heterogeneity exists, and the H/V spectral ratio of microtremors can be derived by the square root of the  $\text{Im}[G_{11}]$  and/or  $\text{Im}[G_{22}]$  and  $\text{Im}[G_{33}]$  (Matsushima et al., 2014).

The authors have shown that by using a numerical method such as the 3-D Spectral Element Method (SEM) (e.g., De Martin, 2011) to calculate the Green's functions from 3-D wave propagation analysis using a 2-D basin structure, it is possible to qualitatively simulate the significant directional dependency that can be seen in H/V spectral ratios of microtremors observed at sites on Uji campus, Kyoto University. The NS/UD has higher peak amplitude and EW/UD has higher peak frequency. The H/V spectral ratios derived from numerical analysis using Green's functions calculated for a simple 2-D basin model with one layer over bedrock show that the observed H/V spectral ratios are qualitatively simulated (Matsushima et al., 2014). Also, Matsushima et al. (2014) has shown that the shape of the H/V spectral ratio is distorted at sites close to the basin edge. This is an indication that if we observe microtremors at several sites close to the assumed basin edge, there may be possibility to identify the shape of the basin edge in detail.

In this study, we focus on the effect of the basin edge to the H/V spectral ratios and study the relation between the basin edge shape and the difference between NS/UD and EW/UD by simulating the H/V spectral ratios at sites close to the basin edge by numerical calculation. We consider a simple 2-D basin model with one layer over bedrock and change the shape of the basin edge. Also, we made microtremor observation for two line arrays orthogonal to the 2-D basin in Uji and found that the observed H/V spectral ratios show the characteristics assumed from the numerical analysis.

From these results, we can see that the condition of the basin edge changes the H/V spectral ratios drastically at sites close to the basin edge. If we accumulate the relation between the shape and condition of the basin edge to the shape of the H/V spectral ratios in two orthogonal horizontal directions, we will be able to use the information from the observed H/V spectral ratios of microtremors to determine the basin edge shape.

### References

Matsushima S, De Martin F, Hirokawa T, Kawase H, Sanchez-Sesma FJ (2014): The Effect of Lateral Heterogeneity on Horizontal-to-Vertical Spectral Ratio of Microtremors Inferred from Observation and Synthetics, *Bulletin of the Seismological Society of America*, 104(1):doi: 10.1785/0120120321

Perton M, Sanchez-Sesma FJ, Rodriguez-Castellanos A, Campillo M, Weaver RL (2009): Two Perspectives on Equipartition in Diffuse Elastic Fields in Three Dimensions, *Journal of Acoustical Society of America*, 126(3):1125-1130

Sanchez-Sesma, FJ., Rodriguez M, Iturraran-Viveros U, Luzon F, Campillo M, Margerin L, Garcia-Jerez A, Suarez M, Santoyo MA, Rodriguez-Castellanos A (2011): A theory for microtremor H/V spectral ratio: Application for a layered medium, *Geophysical Journal International Express Letters*, 186(1):221-225 doi: 10.1111/j.1365-246X.2011.05064.x

Keywords: Microtremor, H/V Spectral Ratio, Diffuse Field, Heterogeneity, Velocity Structure

## Sophistication of microtremor methods to survey shallow structures, PartI: Development of automatic reading algorithms

CHO, Ikuo<sup>1\*</sup> ; SENNA, Shigeki<sup>2</sup> ; FUJIWARA, Hiroyuki<sup>2</sup>

<sup>1</sup>National Institute of Advanced Industrial Science and Technology, <sup>2</sup>National Research Institute for Earth Science and Disaster Prevention

We have been seeking an efficient way to maximize the potential of the microtremor methods for shallow surveys. It is considered that a practical approach has been gained in the observation by the development of portable seismometers (Senna, 2006, 2012) and by the finding of the full usability of the data obtained by a miniature array (radius <1 m), optionally together with a small irregular-shaped array (radius less than 10 m) consisting of three seismometers (Cho et al., 2013a).

As an efficient way to infer an S-wave velocity structure, we consider that a classical, simple profiling method (SPM), where a dispersion curve is directly converted into an S-wave velocity structure (e.g., Heukelom and Foster, 1960), is a good scheme from a view point of simplicity, thus, the balance between the efforts and the information to be extracted. It is true, however, that we frequently like to increase to resolution. Facing this dilemma, we suggested a simple tool "H/V depth conversion" (Cho et al., 2013). We found that the use of an H/V depth conversion followed by a simplified inversion method (SIM) of Pelekis and Athanasopoulos (2011) can in fact increase the resolutions (e.g., Senna et al., 2013; Yoshida et al., 2013).

The current problem is to further promote the efficiency in the data processing procedure. A visual reading of analysis results, which we take at the current time, is time consuming to deal with a vast amount of microtremor data, now obtainable by a streamlined observational procedure. The reproducibility and biases constitute other kinds of problem of visual reading.

To address this problem, we invented the following automatic-reading algorithms. We applied them to observed data consisting of multiple arrays along a measurement line. As the results, natural images of two-dimensional S-wave velocity sections were obtained, not considerably different from the one obtained by visual readings (Senna et al., 2014).

### *Automatic readings of phase velocities*

Let us suppose that multiple dispersion curves have been obtained by either multiple arrays or multiple analysis methods (i.e., nc-CCA, CCA, and SPAC methods) at a single observation point. In the first step, apply the following procedure to each dispersion curve. (i) Divide the frequency range used for analyses into equally-spaced intervals (bins) in a logarithmic scale. Take an average of phase-velocity data in each bin. (ii) Exclude the results from the analyses either when the wavelengths relative to an array radius lie out of the range defined a-priori for each method or when they exceeds the analysis limits having been evaluated by the use of an array with a sensor at the center point. Also, exclude the results when they seem to align in a line passing through the origin.

An automatic reading is obtained for each bin by averaging all values left after the procedure (ii). Readings are deleted, however, when they seem to align in a line passing through the origin.

### *Automatic readings of peak and troughs of an H/V spectrum*

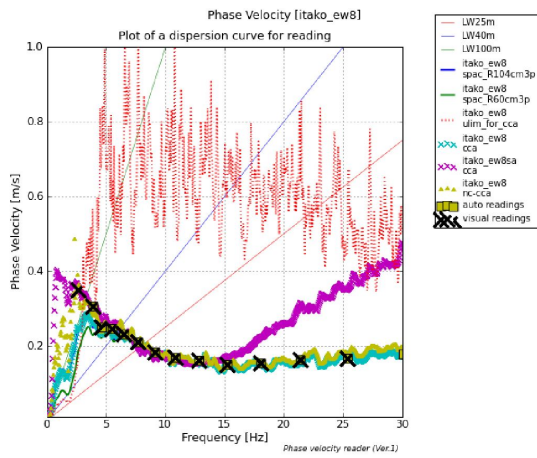
First, an H/V spectrum obtained at a single observation point, or an average spectrum if there are multiple spectra as a representative value, is smoothed using a spectral windows having a frequency-dependent window width. Peaks and troughs of the spectrum are searched from the lower side of the frequency range by using the derivatives. We search pairs of a peak and a trough to stabilize the analysis result: A pair is excluded from the reading results when the difference in either frequency or H/V ratio between a peak and trough is smaller than a threshold. Also, a pair is excluded when a peak (trough) value is smaller than that of an anterior peak (trough). The peak and trough of each pair, thus obtained, are used for the depth conversion, and the resulting depths are averaged to be the representative depth obtained by an automatic reading.

Keywords: Microtremor, velocity structure, surface waves, phase velocity, expolation method, array

SSS35-P01

Room:Poster

Time:May 2 16:15-17:30



## Sophistication of microtremor methods to survey shallow structures, Part2 : Application of automatic reading algorithms

SENNA, Shigeki<sup>1\*</sup> ; CHO, Ikuo<sup>2</sup> ; FUJIWARA, Hiroyuki<sup>1</sup>

<sup>1</sup>NIED, <sup>2</sup>AIST

We have been seeking an efficient way to maximize the potential of the microtremor methods for shallow surveys. It is considered that a practical approach has been gained in the observation by the development of portable seismometers (Senna, 2006, 2012) and by the finding of the full usability of the data obtainable by a miniature array (radius less than 1m), optionally together with a small irregular-shaped array (radius less than 10 m) consisting of three seismometers (Cho et al., 2013a).

As an efficient way to infer an S-wave velocity structure, we consider that a classical, simple profiling method (SPM), where a dispersion curve is directly converted into an S-wave velocity structure (e.g., Heukelom and Foster, 1960), is a good scheme from a view point of simplicity, thus, the balance between the efforts and the information to be extracted. It is true, however, that we frequently like to increase to resolution. Facing this dilemma, we suggested a simple tool 'H/V depth conversion' (Cho et al., 2013). We found that the use of an H/V depth conversion followed by a simplified inversion method (SIM) of Pelekis and Athanasopoulos (2011) can in fact increase the resolutions (e.g., Senna et al., 2013; Yoshida et al., 2013).

The current challenge is to further promote the efficiency in the data processing procedure. A visual reading of analysis results, which we take at the current time, is time consuming to deal with a vast amount of microtremor data, now obtainable by a streamlined observational procedure. The reproducibility and biases depending on analyst constitute other kinds of problem of visual reading.

To address this problem, Cho et al. (2014, thismeeting) invented automatic-reading algorithms. In this study we test their algorithm by applying it to observed data to compare the results with those obtained with visual readings. Our method of observation and analysis is described in the following.

### 1. Observation

Observation duration is set to 15 minutes irrespective of the array shape, where either miniature arrays with a radius of 60 cm or irregular-shaped arrays with radii about 3 to 10 m are used.

### 2. Automatic analyses and readings of phase velocities and H/V spectra

The selection of the data portions and the spectral analysis are automatically executed by using the software BIDO. Cho et al. (2014)'s algorithms are used for automatic readings of phase velocities and H/V spectra.

### 3. Inferring 1D S-wave velocity structures and constructing 2D sections

A dispersion diagram, represented by the relation between the wavelength,  $L$ , and phase velocity,  $V_r$ , is converted into a 1D S-wave structure having the relation between the depth,  $D$ , and S-wave velocity,  $V_s$ , where relations  $V_s = V_r/0.92$  and  $D = 0.375L$  are used (SPM). The resulting 1D structures are spatially interpolated to obtain a 2D section, where H/V depth conversions are overdrawn.

The above procedure from 1 to 3 is fully automatically executed. Incidentally, this study include no examination on SIM because no automatic algorithm has been developed yet because of the robustness problem.

We applied the above procedure to microtremor data obtained along survey lines in four different areas with variable geological environments (e.g., Itako City, Hadano City, Kashiwa City, Urayasu City). As the results, natural views of 2D S-wave velocity sections are obtained in all cases, similar to those obtained by visual readings. Furthermore, resulting velocity sections are consistent with other kinds of subsurface structural data (i.e., geological sections, N-value distributions, the 3D soil model of Senna et al. (2013)). We consider that, needing further improvement, Cho et al. (2014)'s algorithms can provide us with acceptable results at the first stage of automating the analysis procedure.

Keywords: Microtremor, velocity structure, surface waves, phase velocity, array, underground structure model

## Future Initiatives of development of microtremor survey observation system

SENNA, Shigeki<sup>1\*</sup> ; FUJIWARA, Hiroyuki<sup>1</sup>

<sup>1</sup>NIED

The microtremor observation has treated till today as physical investigation information, including the structure model creation for strong motion prediction of the researcher and engineer , etc.

If microtremor observation can observe easily and the observed data can be easily transmitted to a database with information on that observation point, it can expect that the number of collection of observational data will increase explosively in the future because an amateur can also observe, and the advancement of structural model and prediction of seismic strong motions will be attained by leaps and bounds.

It will become an unprecedented thing which leads to grasp of detailed damage distribution, and the improvement in accuracy of real-time earthquake information from the above.

Keywords: microtremor, survey observation system, cloud system, big data

## Estimation of phase velocity of Rayleigh wave using linear array

ZHANG, Xinrui<sup>1\*</sup>; MORIKAWA, Hitoshi<sup>1</sup>

<sup>1</sup>Tokyo Institute of Technology

Since the spatial autocorrelation (SPAC) method has been proposed by Aki (1957), the observation using a circular array of evenly spaced sensors and a central sensor becomes a commonly used measurement technique in the microtremor survey method (Okada, 2003). However, in practice, the strict arrangement of sensors required by the method is difficult to conduct because of the limit of real environment. In order to slacken the requirement of the arrangement, Chavez-Garcia et al. (2005) discussed the validity of performing the SPAC method with a linear array. However, the conclusion of this research is result-based and is not backed by theoretical demonstration. Aki's autocorrelation coefficient could be alternatively seen as the azimuthal average of CCFs (Okada, 2003; Shiraishi 2006). A CCF consists of the Bessel function and an error term which varies with the azimuth of sources. By taking the azimuthal average, the error term vanishes and direct  $J_0(kr)$  can be obtained. The discrete formula of the CCF offers the possibility of extending the original SPAC method. In this research, we develop the solution by controlling the error term in CCF which can obtain directly the phase velocity instead of using records of sensors in a line instead of azimuthally arranged ones.

Under the assumption: 1) Only the fundamental mode is dominated. 2) Different sources are not correlated, the real part of discrete formula of CCF could be expressed as (Shiraishi, 2006). If we neglect the terms of order larger than 6, we can obtain:

$\text{Re}(\gamma_{pq}) = J_0(kr) - 2J_2(kr) \sum \lambda_l \cos 2\theta_l + 2J_4(kr) \sum \lambda_l \cos 4\theta_l$ . It can be seen that there are only three unknown variables  $kr$ ,  $\sum \lambda_l \cos 2\theta_l$  and  $\sum \lambda_l \cos 4\theta_l$ . It is required of at least three sensors (3 different intervals) to solve the 3 unknown variables theoretically. The three sites need to be in a line to make the three CCFs share the same unknowns. Because of the coupling variables and non linear functions, we use the genetic algorithm and particle filter to solve out the optimum solution.

In order to confirm the validity of this new theory preliminarily, the simple wavefield composed of unidirectional plane wave is used to examine the accuracy of estimating phase velocity obtained from a linear array with 3 sensors. The distances between adjacent sensors ( $r$  and  $0.5r$ ,  $r=30\text{m}$ ) are set to be different so that we can have totally 3 different CCFs to solve out the optimum solution. Except for the analytical simulation, we also applied a field test to examine the availability of the new method. We have applied field test to confirm the availability of the method. Observation was conducted on 23 October 2013 at the parking lot of Zoorasia Yokohama Zoological Gardens (ZRS) in Yokohama city of Japan. We deployed 7 seismometers (KVS-300, moving speedometer) constituting two linear arrays. The two linear arrays forms an angle of 60 degree so that the SPAC method could be applied for confirmation.

In the analytical simulation, we confirmed the availability of the new method. The sensitivity of CCF with respect to phase velocity depends on the direction of linear array. When the sensitivity is low, the estimation will be bad. Hence, it is better to use at least two linear arrays forming an angle (90 degree is the best). In the field test in Yokohama, we applied both the SPAC method and the new method using 7 speedometers. Both SPAC method and the new method show good match with the theoretical dispersion curve. The new method shows narrower effective scope and shows some unstability in both low and high frequency range. Through both simulation and field test, the availability of the new method has been confirmed. This new method makes the arrangement of sensors easier which needs only two linear arrays with a non-strict angle. In the future, we will study more about improving the inversion technique and the application of linear array.

Keywords: SPAC method, linear array, coherence complex function, particle filter

## Estimation of Subsurface Structure using Microtremor Observation in Ogasawara Iwo-To Island

MURAKOSHI, Takumi<sup>1\*</sup> ; KOMORI, Etsuro<sup>1</sup> ; SHIMADA, Masaki<sup>1</sup>

<sup>1</sup>National Defense Academy

Ogasawara Iwo-To island is an active volcanic island which is located on the southernmost part of Izu-Ogasawara arc. The microtremor observation was carried out during the period from December 18 to 21, 2013 in Ogasawara Iwo-To island. The microtremor measurements were performed at 54 sites as 3-component seismometers for horizontal-to-vertical spectral ratio (HVSR) analysis. The obtained HVSRs of microtremor are used to determine the dominant frequencies of vibration of the subsurface structures beneath several recording sites in Ogasawara Iwo-To island. The H/V peak period varies from 1.1 to 3.5 sec.

For using the SPAC method of microtremor, the circular-array microtremor data were recorded by 6 seismometers distributed along the circumferences of two circles as well as a seismometer deployed in the center at two sites in the center of the island. The phase velocities and the S-wave velocities of the subsurface structures down to a depth of several km were estimated at each site from the microtremor data by using the SPAC method.

Keywords: microtremor, Ogasawara Iwo-To Island, subsurface structure

## Determination of Subsurface Structure of the Mt. Daisen area in Tottori Prefecture by Microtremor and Gravity Survey

NOGUCHI, Tatsuya<sup>1\*</sup> ; KAGAWA, Takao<sup>1</sup> ; YASUNAGA, Harunobu<sup>1</sup> ; ISHIGO, Masaharu<sup>1</sup> ; KOASAKA, Shuhei<sup>1</sup>

<sup>1</sup>Tottori Univ.

Earthquake damages occurred by the earthquake that occurred at the Middle West of Tottori in 1983 , 2002 and the 2000 Western Tottori earthquake in Mt.Daisen area of Tottori Prefecture. It is supposed that the damage influenced the subsurface structure. It is important that the information of subsurface structures is obtained for prediction of ground motion in the area. Microtremor and gravity surveys were carried out in the plains of the shore part and Mt.Daisen area. S-wave velocity models are obtained at the array observation 3 sites and predominant period distribution at 3-components observation newly. The gravity anomalies were obtained by gravity survey data newly.

## Estimation of inter-station Green's functions using microtremor array data

HAYASHIDA, Takumi<sup>1\*</sup> ; YOSHIMI, Masayuki<sup>2</sup>

<sup>1</sup>International Institute of Seismology and Earthquake Engineering, BRI, <sup>2</sup>Geological Survey of Japan, AIST

The seismic interferometry technique is used to evaluate seismic velocity structure beneath two observation sites [e.g., Ma et al. (2008); Yamanaka et al. (2010); Asano et al. (2012); Hayashida et al. (2014)]. The technique can be applied under the assumptions of non-stationary and uniform distribution of microtremor (ambient noise) sources and it is important to investigate whether the data satisfy the conditions. The array observations of microtremor [Yoshimi et al. (2012)] were conducted at 13 sites in Niigata prefecture, Japan. The surveys were carried out for more than 10 days per site and each array consists of three equilateral triangular arrays whose radii range from several hundred meters to several kilometers. Here we used the data to estimate inter-station Green's functions with the seismic interferometry technique. The stacked cross-correlation functions (CCFs) of microtremor showed coherent and dispersive wave trains in frequency ranges between 0.4 and 1.0 Hz for the small array, 0.2 and 0.7 Hz for the middle array and 0.1 and 0.6 Hz for the large array. The wave trains derived for each array correspond well to each other regardless of azimuth angles, showing the effect from the abnormal microtremor source can be negligible in this study. We also calculated theoretical Green's functions from the estimated S wave velocity structures with the spatial autocorrelation (SPAC) method for each site, assuming 1D velocity structure. The agreements between the calculated Green's functions and the derived CCFs from the seismic interferometry are generally good, especially at lower frequencies. Our results suggest that a combination of velocity structure estimation with surface-wave phase velocity (conventional array methods) and velocity structure validation with Green's function (seismic interferometry technique) provides better estimations for S wave velocity structures.

### Acknowledgements:

We used the microtremor array data observed in a research project funded and supported by Japan Nuclear Energy Safety Organization (JNES).

Keywords: microtremor, seismic interferometry, Green's function, group velocity, SPAC method

## Seismic basement structure estimated from seismic interferometry and microtremor analysis

KOIZUMI, Ryo<sup>1</sup> ; SAWADA, Akihiro<sup>1</sup> ; HIRAMATSU, Yoshihiro<sup>1\*</sup> ; THE GROUP, Aftershock observation<sup>2</sup>

<sup>1</sup>Kanazawa University, <sup>2</sup>the group for the joint aftershock observations

Recently, seismic interferometry has been considered to be a powerful tool for subsurface structure survey. Seismic interferometry is a method that produces pseudo reflected waveform data by computing the autocorrelation function (ACF) of seismic waveform record. In this study, we estimate the seismic basement structure beneath the northwestern Noto Peninsula from seismic interferometry and microtremor analysis. We examine the reliability of seismic interferometry and microtremor analysis by comparing those results with the results from gravity anomalies and a reflection seismic survey (Sato et al., 2007) in this area.

For seismic interferometry, we use waveform data of the aftershocks of the 2007 Noto Hanto earthquake at 44 seismic stations which are located in the northwestern Noto Peninsula. We apply high-pass filter of 2 Hz to SH component of displacement waveform and set a time window of 10 s after the arrival of S wave to calculate ACF. We make the average ACF by stacking all ACFs at each station. For microtremor analysis, we performed microtremors observation at 44 points where the stations for the aftershock observation were located and calculate H/V spectrum at each station. We estimate the basement structure in the analyzed area by assuming two-layer structure from ACF and H/V spectrum.

For the ACF analysis, it is difficult to identify the dominant peak of ACF for most stations. Especially, we cannot estimate the basement depths where the basement depths estimated from the reflection seismic survey (Sato et al., 2007) are shallower than 100 m. Finally, we obtain the basement depths at 14 of 44 stations. On the other hand, for the microtremor analysis, we can estimate the basement depths at 35 of 44 points. This indicates that the seismic interferometry with ACF is not an effective approach to estimate the basement depths in the northwestern Noto Peninsula.

We compare the basement depths estimated from ACF, H/V spectrum and gravity anomaly each other. These estimates are approximately coincident each other and shows that the basement depth of the Kuwatsuka block is shallower than that of the Saruyama block. Coseismic uplift was observed in the Kuwatsuka block at the 2007 Noto Hanto earthquake. Therefore, the results of this study is coincident with the hypothesis that the activity of active faults on seafloor near the coast causes the uplift of the Kuwatsuka block and makes its basement depth shallower (Hiramatsu et al., 2008).

**Acknowledgements:** We are grateful to the group for the joint aftershock observations of the 2007 Noto Hanto Earthquake for the use of waveform data and to NIED for the use of the instrument of microtremor observation. We thank Dr. Shigeki Senna for helpful advice.

**Keywords:** auto correlation function, H/V spectrum, gravity anomaly, geological block structure, the Noto Peninsula

## Retrieval of Green's function in a 3D inhomogeneous medium with nonisotropic source distribution using interferometry

CHIMOTO, Kosuke<sup>1\*</sup> ; YAMANAKA, Hiroaki<sup>1</sup>

<sup>1</sup>Tokyo Tech.

Seismic interferometry is known to retrieve Green's functions in an elastic homogeneous medium with isotropic source distribution (e.g., Wapenaar and Fokkema, 2006), and is applied to estimate velocity structures using long time series of ambient noises (e.g., Shapiro and Campillo, 2004). However, the realistic noise field might be an inelastic inhomogeneous medium with nonisotropic source distribution, and thus the reliability of retrieval of Green's functions using seismic interferometry should be examined.

We study on the reliability of seismic interferometry in a 3D inhomogeneous structure model of Kanto basin with nonisotropic source distribution. The numerical study on seismic interferometry was conducted by using 3D FDM. We cross correlated the surface responses at two sites with multiple surface sources. We used Yamanaka and Yamana (2006) for the 3D inhomogeneous model of Kanto basin. Nonisotropic source distribution was made by using sources located only on the sea area. We investigated the influence for the cross correlation functions by comparing with that in a homogeneous medium or isotropic source distribution.

In a case of homogeneous medium with isotropic source distribution, we see slight difference between the cross correlation function and Green's functions, but the surface wave component was well retrieved and surface wave velocity compares well with the Green's function. The slight difference might have been caused by the approximations in seismic interferometry (e.g., Kimman and Trampert, 2010). The cross correlation function showed symmetry for positive and negative lagtimes. In a case of homogeneous with nonisotropic source distribution, the cross correlation function shows asymmetry whose surface wave cannot be seen in positive lagtimes. However, the cross correlation functions in negative lagtime compares well with that retrieved with isotropic source distribution, and it showed good agreement in terms of group velocity. These indicate the influence of source distribution on seismic interferometry would be large as indicated in numerous studies (e.g., Tsai, 2010).

In a case of a 3D inhomogeneous model of Kanto basin, the cross correlation function showed asymmetry even with isotropic source distribution. That is, an inhomogeneity complicates wave propagations and then make apparent source distribution non-isotropic even with the isotropic case. Specifically, larger amplitudes in negative lagtimes than that in positive lagtimes indicate that eastern sources became large apparently. Considering the Kanto basin model, Kanto mountains located in western part and Pacific Ocean located in eastern part, where have thick sediment layers, the eastern sources would have excited surface wave significantly, which caused apparent nonisotropic source distribution. Due to asymmetry in the cross correlation function, it does not match with the Green's function. Group velocities also show asymmetry, however, they agrees to that of Green's function. In a case of a 3D inhomogeneous model with nonisotropic source distribution, the cross correlation function shows asymmetry and show less agreement with the Green's function. However, the group velocity shows agreement.

As a result, the retrieval of Green's function using seismic interferometry is strongly influenced by source distributions. Moreover, an inhomogeneity affect to source distribution, it would also be the problem. In a realistic case, therefore, to understand how much isotropy is satisfied is important. Because understanding the source isotropy is tough, it is important to examine the influence considering with realistic applications. However, on group velocity estimations as many applications, the reliability showed good in this study, suggesting the high possibility for reliable applications in seismic interferometry.

Keywords: Seismic interferometry, Green's function, inhomogeneous, isotropic source, 3D FDM

## Estimation of subsurface structure by high density microtremor observations in Kochi Plain

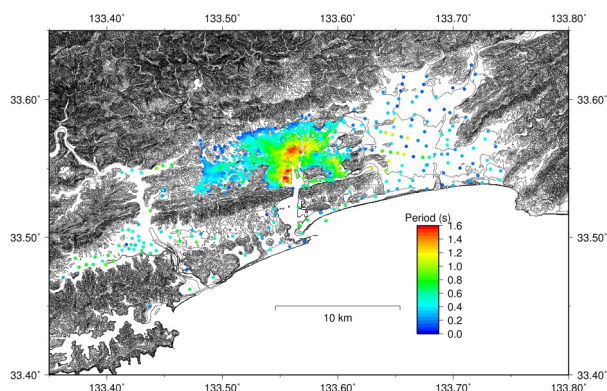
OISHI, Yusuke<sup>1\*</sup> ; KUBO, Atsuki<sup>2</sup> ; TAKAHASHI, Hirokazu<sup>3</sup> ; YAMASHINA, Tadashi<sup>2</sup>

<sup>1</sup>Studies in Science, Graduate School of Integrated Arts and Sciences, Kochi University, <sup>2</sup>Kochi Earthquake Observatory, Faculty of Science, Kochi University, <sup>3</sup>Faculty of Science, Kochi University

Kochi Plain is located around source region of the great Nankai Earthquake. Strong ground motion is expected in this area, because soft subsoil is widely deposited in Kochi Plain. In this study, we investigate H/V spectra of microtremor in the Kochi Plain. Microtremor study with single station is cheaper, quick and easier way than sampling boring core. It is convenient to reveal horizontal variation of soil/basement structure. We append 213 measurements in addition to previous reported 1041 measurements (Oishi et al., JpGU 2013, SSS35-P02). In total 1254 measurements are used to H/V spectral analysis. Figure shows distribution map of dominant periods by H/V spectral analysis based on microtremor observations in Kochi Plain. In perspective, dominant periods of H/V spectra around northern Urado-Bay region are longer than other regions. According to soil/basement model using boring data, the bedrock depth at this region is especially deep but boring which reaches the bedrock is limited. In contrast, H/V spectral analysis is useful to grasp the extent of region with deep soil/basement boundary. Dominant periods of H/V spectra around western part of Kochi Plain are relatively shorter than Urado region. The damaged areas of the past 2 (1854 and 1946) Nankai Earthquakes match with areas where the dominant period is long and/or the amplification factor is large. High density observations in this region show clear local variations. These are not reflected on current hazard maps or seismic intensity estimation maps. Using H/V spectral analysis based on high density microtremor observation, we are detecting patterns of soil/basement structure which has not be grasped using only boring core data.

Acknowledgement: We thank to Tadashi Hara and Nobuaki Kitamura, Kochi University and NEWJEC Inc. for providing their data.

Keywords: microtremor, H/V spectral ratio, subsurface structure, Kochi Plain



## Recent Geological Interpretation of A Liquefied Area: A Case Study in Urayasu City, Japan (1)

IWAMOTO, Hiroshi<sup>1\*</sup> ; HIGASHI, Masashi<sup>2</sup> ; HIGUCHI, Shigeo<sup>3</sup> ; INADA, Akira<sup>3</sup> ; ITO, Akihide<sup>4</sup> ; KAMIKASEDA, Satoshi<sup>5</sup> ; KAWASAKI, Kenichi<sup>6</sup> ; KUSUNOKI, Keiko<sup>7</sup> ; SATO, Shinji<sup>8</sup> ; SHINADA, Shoichi<sup>2</sup> ; SUENAGA, Kazuyuki<sup>9</sup> ; WATANABE, Takumi<sup>3</sup>

<sup>1</sup>Kanto Natural Gas Development Co., Ltd, <sup>2</sup>JAPEX, <sup>3</sup>No affiliation, <sup>4</sup>Chiba-kita High School, <sup>5</sup>NTC Consultants Co., Ltd., <sup>6</sup>Chiba-nishi High School, <sup>7</sup>Urayasu High School, <sup>8</sup>Chishirodai High School, <sup>9</sup>Earth System Science Co., Ltd.

At Urayasu High School (Urayasu City, Chiba Prefecture), where one of authors worked, the 2011 Great East Japan Earthquake caused the formation of two large open cracks from which large amounts of sand and water erupted as a result of soil liquefaction (Kusunoki et al., 2011). The objectives of this study were to investigate both the cause and the mechanism of this phenomenon. The site is located on reclaimed land, and a survey of the site's subsurface geology was carried out by hand auger boring and simple dynamic cone penetration testing to observe the stratigraphy of the reclaimed bed. Aerial photographs of the different stages of the reclamation were also used for analysis.

The survey area was the school grounds, which are located several hundred meters from the former seashore. Holocene deposits were situated at a depth of approximately 3-4 m. Two large open cracks formed in the ground: crack '1' in the NNE-SSW direction and crack '2' in the WNW-ESE direction. Beneath the cracks, we found row of piles from the original ground reclamation work. These rows of piles had been laid underground, and the reclaimed bed consisted of sand and silt. The cracks appeared to be due to the difference in vibrational characteristics between the opposite sides of each crack. Also, the facies of the reclaimed bed were notably different on the opposite sides of each crack. In the cross section of crack '2', the Nd-value\* was very large on the northeast side (Nekozane River side) but relatively smaller on the southwest side. In the cross section of crack '1', the facies of the reclaimed bed from approximately 2 m above to the top of the Holocene deposits were sandy on the western side relatively large Nd-value, but on eastern side mainly formed of silty material recorded almost 0.

Analysis was conducted using aerial photographs and revealed that both cracks '1' and crack '2' were located on the same discontinuity in the reclamation work history, both spatially and temporally. Therefore, the survey area contained three sections of reclaimed land demarcated by the two cracks. Moreover, a fourth section consisted of Holocene deposits. Chronologically, the survey area contained (a) 'Kaimenka-tochi' \*(Urayasu City, 1985), (b) reclaimed land composed of sand and silt dredged from the seabed, and (c) the surrounding embankment. The reclamation process differed between areas (a) and (b). Area (b) was the widest and was typical of reclaimed land. Area (c), in contrast, was not constructed by dredging sand and silt from the seabed. Crack '1' was located between areas (b) and (c), and crack '2' was located between areas (a) and (b).

Therefore, the occurrence of these cracks seems attributable to discontinuities in the reclamation history. This case shows that recognizing the geological and historical processes of both the Holocene deposits and the reclaimed land is an important aspect of disaster prevention.

\*Nd-value is brought by Dynamic Cone Penetration Test, which has the following conditions: a slide hammer with a weight of 5kg falling through a distance of 50cm, and diameter of 2.5cm cone. The number (i.e. Nd-value) of blows needed for the cone to penetrate each 10cm is recorded.

\*\*'Kaimenka-tochi' means land below sea level literally. Before reclamation, it was located in front of seashore, and it was in the possession of the private owner. and was used to reed cultivation etc.

### References

KUSUNOKI Keiko, HIGASHI Masashi, HIGUCHI Shigeo, INADA Akira, ITO Akihide, IWAMOTO Hiroshi, KAMIKASEDA Satoshi, KAWASAKI Ken-ichi, and SUENAGA Kazuyuki (2011) Ground Damage on Man-made Land caused by The 2011 off the Pacific coast of Tohoku Earthquake- Wooden Pile Lines indicate artificial land failure-, The 65 th Annual Meeting (Aomori) of the Association for the Geological Collaboration in Japan.

'History of Urayasu City'(1985). Urayasu City, 64-66.

Keywords: liquefaction, crack, dynamic cone penetration test, Urayasu, reclaimed land

## Development of analysis strategy for continuous total geomagnetic field data around Mt. Fuji

ABE, Satoshi<sup>1\*</sup> ; MIYAHARA, Basara<sup>1</sup> ; MORISHITA, Hitoshi<sup>1</sup> ; KOBAYASHI, Katsuhiko<sup>1</sup> ; TOYOFUKU, Takashi<sup>1</sup> ; KOYAMA, Takao<sup>2</sup> ; OGAWA, Tsutomu<sup>2</sup>

<sup>1</sup>GSI of Japan, <sup>2</sup>Earthquake Research Institute, The University of Tokyo

Geospatial Information Authority of Japan (GSI) has conducted continuous total geomagnetic field observation at Fuji Yoshida observation station (FUJ), which is located the northeast mountainside of Mt. Fuji, and Fuji-City observation station (FJI), which is located at the southern bottom of Mt. Fuji, since 2000. These stations were established in order to enhance observation infrastructure to monitor low-frequency earthquakes underneath Mt. Fuji which had rapidly increased since October 2000. Additional continuous observation in the northwest mountainside of Mt. Fuji had also been started by utilizing electrical power and communication line of Remote GNSS Monitoring System (REGMOS) at Fuji Oniwa. Furthermore, Earthquake Research Institute, the University of Tokyo has conducted continuous total geomagnetic field observation at Fuji Yoshida (FJ1) and continuous geomagnetic observation at Yatsugatake (YAT). These data are also available and useful to monitor and understand geomagnetic variation around the Mt. Fuji.

Although GSI has been monitoring total geomagnetic field difference between the station at the bottom, FJI, and the stations at the mountainside, FUJ and REGMOS, it is almost impossible to identify variation truly caused by volcanic activities because total geomagnetic field around volcanoes can be fluctuated by both volcanic activities and locally unique geomagnetic variation as well as earth's main magnetic field and external magnetic field variation. Therefore, GSI tries to extract volcano-induced total geomagnetic field variation from the observation data around Mt. Fuji by principal component analysis, and develop monitoring strategy by principal component analysis of total geomagnetic fields around Mt. Fuji.

Keywords: Total geomagnetic field, Mt.Fuji, principal component analysis

## Classification of tsunami dynamo phenomena in terms of ocean depths

MINAMI, Takuto<sup>1\*</sup> ; TOH, Hiroaki<sup>1</sup>

<sup>1</sup>Graduate School of Science, Kyoto University

Conductive seawater moving in the geomagnetic main field drives an electromotive force and induces secondary electromagnetic (EM) fields. This effect is well known as "oceanic dynamo effect" and has been investigated for many years, especially for low-frequency phenomena such as tides and steady oceanic flows. However, it was recently found that tsunamis are also significant sources of the oceanic dynamo effect. Toh et al. (2011) reported tsunami-induced EM field data observed at the northwest Pacific seafloor EM station (NWP) at the time of the 2006/2007 Krill tsunamigenic earthquakes. Ever since, many events associated with the oceanic dynamo effect by tsunamis, hereafter called "tsunami dynamo effect", have been reported (e.g., Manoj et al. 2011; Suetsugu et al., 2012; Ichihara et al., 2013). To explain the tsunami dynamo effect, most of the preceding studies adopted analytical approaches in the frequency domain (e.g., Tyler, 2005). However, it is difficult to understand how EM fields are generated by tsunami propagations, although analytical solutions are very useful and handy.

In order to understand the tsunami dynamo effect more physically, we compared analytical solutions and results of numerical simulations using solitary waves, and revealed that tsunami dynamo phenomena can be classified according to the influence of the diffusion term in the induction equation for the magnetic field. In tsunami dynamo phenomena, the ocean depth has a dominant influence on the diffusion term. When the ocean depth is shallow enough, the diffusion term is large and comparable with the source term, while the self-induction term is small. In this case, the self-induction effect cannot attenuate the magnetic field induced by the coupling of the oceanic flows ( $v$ ) and the geomagnetic main field ( $F$ ), namely  $v \times F$ . We can understand this case mostly by the Ampere's Law. On the other hand, when the ocean depth becomes deeper, the self-induction effect gets larger and reduces the amplitude and causes delay in phase of the magnetic field induced by  $v \times F$ . Especially for the ocean depth deeper than 5000 m, the amplitude is attenuated to approximately 70 percent and the phase is delayed by more than 70 degrees compared with the magnetic field due to  $v \times F$ , which can be understood by analogy with "Frozen Flux". As for the case of the tsunami dynamo phenomena reported by Toh et al. (2011) as well as Minami and Toh (2013), we can regard the phenomena as the self-induction dominant case because the ocean depth at the observation site, NWP, is approximately 5600m. This is consistent with the fact that sea level changes observed at the two DART sites in the vicinity of NWP are in phase with that of the vertical component of the magnetic field observed at NWP. In addition, our analysis using analytical solutions revealed that magnitudes of the tsunami-induced magnetic field have maximum peaks around the ocean depth of 2000m, when the tsunami height is fixed to 1m. This is because the self-induction and the diffusion effect, which vary differently according to the ocean depth, balances around that specific depth. These results are important because they enable us to predict how EM fields are induced by tsunamis in a variety of ocean depths, even though the number of observed examples of tsunami dynamo phenomena is limited at present. It is possible that our results are applied to tsunami early warning or mitigation of tsunami hazards in the future.

In the presentation, we will report the methodology of our classification of tsunami dynamo phenomena and discuss how tsunami-induced EM fields vary according to the ocean depth. We will also discuss how the ocean depth influences on the recently found initial rise (Minami and Toh, 2013) in the horizontal magnetic component observed prior to tsunami arrivals.

Keywords: tsunami, dynamo, solitary wave, seafloor observation, finite element method

## Electric conductivity of earth's medium derived from earthquake-excited electromagnetic signals

TSUTSUI, Minoru<sup>1\*</sup>

<sup>1</sup>Kyoto Sangyo University

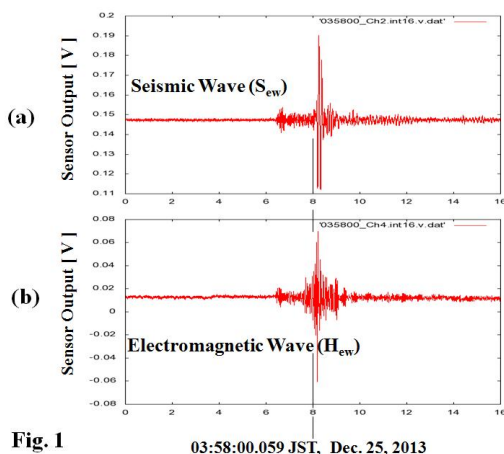
We have been observing electromagnetic (EM) pluses excited by earthquakes, using tri-axial electromagnetic sensors installed in a deep borehole of 100 m in depth. We simultaneously captured waveforms of EM pulses in the borehole and of seismic waves installed near the borehole. We have confirmed that the detected EM waves were co-seismic ones readily generated by piezo-electric effect in earth's crusts [1].

We detected an EM pulse in the borehole when an earthquake of M3.0 occurred at 10 km depth and at 5.4 km north of the EM observation site at 03:57 on Dec. 25, 2013. Figure 1 shows waveforms of (a) east-west component ( $S_{ew}$ ) of the seismic wave, and of (b) east-west component ( $H_{ew}$ ) of magnetic field of the EM pulse. The waveform of the  $S_{ew}$  wave shows an impulsive amplitude at the arrival of its S-wave, which is because the earthquake hypocenter was close to the EM observation site. On the other hand, the waveform of  $H_{ew}$  shows that its amplitude was increasing from about 1 sec prior to the S-wave arrival, and after that it was decreasing.

The amplitude change of  $H_{ew}$  can be explained as follows: Since the electronic conductivity of the earth's medium is large, the amplitude of an EM wave shows an exponential decrease as a function of the distance, in which the decay rate is so-called Skin depth. Since the source of EM pulse was propagating with the S-wave velocity, the amplitude of the EM wave measured at the EM observation site is exponentially increasing as time goes on, and after the S-wave arrival it is exponentially decreasing. Therefore we obtained the Skin depth  $\delta$  for the frequency of 20 Hz and the electronic conductivity as 850 m and 0.0175 S/m, respectively.

[1] M. Tsutsui, submitted to IEEE Geoscience, Letters, 2014.

Keywords: seismic wave, electromagnetic wave, observation in the earth, skin depth, electric conductivity



## Electrical conductivity structures of volcanic areas: a proxy for volcanic gas fluxes

KOMORI, Shogo<sup>1\*</sup>; KAGIYAMA, Tsuneomi<sup>2</sup>; FAIRELY, Jerry<sup>3</sup>

<sup>1</sup>Institute for Earth Sciences, Academia Sinica (Taiwan), <sup>2</sup>Aso Volcanological Laboratory, Kyoto University, <sup>3</sup>University of Idaho

The efficiency of degassing of volcanic gases in magma is one of the key parameters controlling the explosive potentiality of the eruption and the diversity of the volcanic activity. Therefore, to evaluate the mass flux of volcanic gases is important in considering the constraint conditions of the activity. When volcanic gases are dissolved into the pore water of an aquifer, the aquifer has a high electrical conductivity (E.C.); this is because that the pore water conductivity is increased due to the high-salinity and temperature, and that the surface conductivity of rock matrices is also increased due to hydrothermal alteration. Therefore, the spatial extent of the high E.C. region could be related to the abundance of the mass flux of volcanic gases. We have developed the method to estimate the mass flux of volcanic gases using the E.C. structure of volcanic areas as follows.

[Effect of exposure temperatures on the surface conductivity of rock matrices]

There has already been some quantitative formula about the effect of temperature and salinity on the E.C. of the pore water. On the other hand, it has been known that temperatures are closely related to the generation/stability of smectite, which makes a great contribution to the increase of E.C. However, their effect on the surface conductivity has not been understood quantitatively. We performed the E.C. measurements using drillcore samples obtained from drilling projects, to estimate the surface conductivity. Results showed that the relation between surface conductivities and the temperatures to which the rock matrices have been exposed well corresponds to generation/stable condition of smectite. Thus, the surface conductivity could be represented as relatively simple function of exposure temperatures, and the formula could be incorporated into the modeling of dissipation of volcanic gases (Komori et al., 2010, 2013).

[Simplified model for the dissipation of volcanic gases and its application to Unzen volcanic area]

In Unzen volcanic area, there are various geophysical and geochemical studies to understand the formation process of hot springs associated with magma degassing and the magmatic activity. Ohba et al. (2008) proposed three-stage magma degassing; the first magma degassing occurs at the depths of 4-6 km. Correspondingly, the pressure sources are estimated at the similar depths (Kohno et al., 2008). In addition, the high temperature region greater than 200 °C are present above the sources (NEDO, 1988), which corresponds to the high E.C. region inferred from TDEM surveys (Srigutomo et al., 2008).

Based on the above background, we developed the simple model of volcanic gases dissipation into the aquifer at the area, to estimate the mass flux of volcanic gases. The model assumes the isotopic physical properties and the simple geometry of the aquifer. The temperatures and salinity of the pore water are distributed by the simulated flow regime, which is the consequent of the injection of the thermal waters formed by the mixing between volcanic gases and groundwater. Their distributions are converted to the pore water and surface conductivities; which are then converted to the bulk E.C. Results showed that the spatial extent of the high E.C. region is essentially controlled by the volcanic gases flux and rainfall recharge (Komori et al., under review).

[Possibility of effective magma degassing]

The above model was applied to the E.C. structure of the area. The estimated volcanic gas flux was  $10^{4.8 \pm 0.5}$  t/yr, yielding the CO<sub>2</sub> flux ( $10^{3.1 \pm 0.5}$  t/yr) and the magma input rate ( $10^{0.1 \pm 0.5}$  million t/yr). These values are consistent with other petrology, geochemical and geophysical evidences. Our result suggests that the magma is steadily releasing the volcanic fluids into the aquifer. This effective degassing might lead to the decrease of water content of magma, and be one of the reason of the recent effusive volcanism like dome-forming eruptions (Komori et al., under review).

Keywords: Bulk electrical conductivity, Pore water conductivity, Surface conductivity, Volcanic gas fluxes, Unzen volcanic area

## Audio frequency magnetotelluric imaging and tectonic activity evaluation of the Cimandiri Fault, West Java, Indonesia

FEBRIANI, Febty<sup>1\*</sup> ; YAMAYA, Yusuke<sup>2</sup> ; HATTORI, Katsumi<sup>1</sup> ; WIDARTO, Djedi S.<sup>3</sup> ; HAN, Peng<sup>1</sup> ; YOSHINO, Chie<sup>1</sup> ; NURDIYANTO, Boko<sup>4</sup> ; EFFENDI, Noor<sup>4</sup> ; MAULANA, Iwan<sup>4</sup> ; GAFFAR, Eddy<sup>5</sup>

<sup>1</sup>Chiba University, <sup>2</sup>National Institute of Advanced Industrial Science and Technology, <sup>3</sup>Upstream Technology Center, <sup>4</sup>Indonesian Geophysical, Meteorological, Climatological Agency (BMKG), <sup>5</sup>Research Center for Geotechnology, Indonesian Institute of Sciences (LIPI)

The tectonic activity around the Cimandiri fault zone, Pelabuhan Ratu, West Java, Indonesia, has been analyzed for 30 years (1973-2013). The subsurface electrical resistivity structure close to the Cimandiri fault has been also investigated by twenty five audio-magnetotelluric (AMT) sites. The AMT exploration was carried out during two weeks, from July 27, 2009 to August 8, 2009. The sites were distributed on two lines along about 13 km x 6.5 km profile. There are two profiles of the AMT: (1) the A-A' line of the AMT which is perpendicular to the fault (2) the B-B' line of the AMT which is parallel to the fault. Two-dimensional modelling using the code developed by Ogawa and Uchida 2-D inversion has been applied in the AMT data. The result of tectonic activity analysis shows that the Cimandiri fault is the active fault. The subsurface electrical resistivity structure of the Cimandiri fault zone is characterized by (1) the A-A' and B-B' lines present a conductive zone (1-100  $\Omega$ m) from the surface up to the depth of 1 km, which is possibly associated with quaternary volcanics. At the surface, there are also some very conductive spots (1-5  $\Omega$ m) which are indicating the existence of the marine sediments in the study area. (2) The gradual conductive-resistive (500-1,000  $\Omega$ m) zone at the depth of 1-3.5 km overlays above a low resistivity zone (10-100  $\Omega$ m). This low resistivity zone may reflect the combined influences of a fluid network and the presence of the young and less compact sediments with the 500-1,000  $\Omega$ m zone as a cap rock that defines the upper boundary of the low resistivity zone (10-100  $\Omega$ m). Finally, the result of both methods presents that the Cimandiri fault is the strike-slip fault.

Keywords: audio frequency magnetotelluric, subsurface electrical resistivity structure, 2-D inversion, Cimandiri Fault, Indonesia

## Robust magnetotelluric inversion

MATSUNO, Tetsuo<sup>1\*</sup> ; CHAVE, Alan<sup>2</sup> ; JONES, Alan<sup>3</sup> ; MULLER, Mark<sup>3</sup> ; EVANS, Rob<sup>2</sup>

<sup>1</sup>National Institute of Polar Research, <sup>2</sup>Woods Hole Oceanographic Institution, <sup>3</sup>Dublin Institute for Advanced Studies

A robust magnetotelluric (MT) inversion algorithm has been developed on the basis of quantile-quantile (q-q) plotting with confidence band and statistical modelling of inversion residuals for the MT response function (apparent resistivity and phase). Once outliers in the inversion residuals are detected in the q-q plot with the confidence band and the statistical modelling with the Akaike information criterion, they are excluded from the inversion data set and a subsequent inversion is implemented with the culled data set. The exclusion of outliers and the subsequent inversion is repeated until the q-q plot is substantially linear within the confidence band, outliers predicted by the statistical modelling are unchanged from the prior inversion, and the misfit statistic is unchanged at a target level. The robust inversion algorithm was applied to synthetic data generated from a simple 2-D model and observational data from a 2-D transect in southern Africa. Outliers in the synthetic data, which come from extreme values added to the synthetic responses, produced spurious features in inversion models, but were detected by the robust algorithm and excluded to retrieve the true model. An application of the robust inversion algorithm to the field data demonstrates that the method is useful for data clean-up of outliers, which could include model as well as data inconsistency (for example, inability to fit a 2-D model to a 3-D data set), during inversion and for objectively obtaining a robust and optimal model. The present statistical method is available irrespective of the dimensionality of target structures (hence 2-D and 3-D structures) and of isotropy or anisotropy, and can operate as an external process to any inversion algorithm without modifications to the inversion program.

Keywords: Inversion, Probability distribution, Magnetotellurics

## Preliminary report of self-potential observation during a water injection experiment at 1800 m depth in Nojima fault

MURAKAMI, Hideki<sup>1\*</sup> ; HIGA, Tetsuya<sup>2</sup> ; SUZUKI, Takeshi<sup>2</sup> ; YOSHIMURA, Ryokei<sup>2</sup> ; GOTO, Tada-nori<sup>3</sup> ; KAWASAKI, Shingo<sup>4</sup> ; OUCHI, Yuhei<sup>5</sup> ; YAMAGUCHI, Satoru<sup>6</sup>

<sup>1</sup>Natural Sciences Cluster-Science Unit,Research and Education Faculty,Kochi University, <sup>2</sup>Graduate School of Science,Kyoto University, <sup>3</sup>Graduate School of Engineering,Kyoto University, <sup>4</sup>Disaster Prevention Research,Kyoto University, <sup>5</sup>Faculty of Science, Osaka City University, <sup>6</sup>Graduate School of Science,Osaka City University

We report self-potential variations during 2013 water injection experiment at 1800 depth in Nojima fault, which is a surface earthquake fault of the 1995 Hyogoken-nanbu earthquake (Mw6.9). The 2013 water injection test started in 15 September and ended in 29 September. Fresh water was injected into the fault system through the open hole part of the borehole (1800m depth). Average injection rate was 20 liter/min and pressure was 5 MPa. Self-potential variations around the 1800m borehole were very smaller than those in the previous water injection experiments (1997, 2000, 2003, 2004, 2006, and 2008) at 540m depth and self-potential variations did not appear clearly to correspond to the operation of the water injection. The previous water injection experiments have been repeated in the same conditions. The observed variations during the experiments have the following features: 1) self-potential variations appeared to correspond to the operation of water injections; 2) the negative voltage appeared around the water injection borehole, and 3) the magnitude of self-potential variations decreased with increasing distance from the borehole. And the self-potential variations in the previous experiments have become larger every experiment. These features suggest that the observed variations were caused by the streaming potential and the permeability around the open hole part of the borehole (540m depth) has decreased. If the line source model to explain the self-potential variations associated with the water injection is correct, the small self-potential variations observed this experiment may suggest that the permeability of the fault fracture zone at 1800m depth is larger than that around the fault at 540m depth.

Keywords: Nojima fault, 1995 Hyogoken-nanbu earthquake, self-potential, water injection experiment, streaming potential

## Long-term variation of geomagnetic transfer function in Japan

TAKEDA, Masahiko<sup>1\*</sup>

<sup>1</sup>Data Analysis Center for Geomagnetism and Space Magnetism, Kyoto Univ.

Time variation of geomagnetic transfer function in Japan was studied for long period of since 1985. Most of the long-term variation is common at most observatories, and some of them are due to the solar activity. However, different behavior of the variation was found at some observatories, which may be caused by time variation of the local conductivity structure in the earth.

Keywords: geomagnetism, transfer function, long-term variation, induced current, locality

## Numerical simulations for the electrical prospecting of the rock samples

SUZUKI, Takeshi<sup>1\*</sup> ; YOSHIMURA, Ryokei<sup>2</sup> ; OSHIMAN, Naoto<sup>2</sup>

<sup>1</sup>Graduate School of Science, Kyoto University, <sup>2</sup>Earthquake Hazards Division, Disaster Prevention Research Institute, Kyoto University

For the purposes of oil explorations and surveys of active faults, electrical and electromagnetic methods are powerful tools to reveal the underground properties, since the resistivity images have high sensitivity to the existences of the fluid. Obtained resistivity images are interpreted in relation to the porosity of rock and its connectivity with several mixing laws. In order to verify the applicability of such interpretations, we plan to carry out high-density electrical soundings for hand size rock samples whose other geological characteristics are well known.

As the first step of laboratory experiments, we made numerical simulations to estimate the optimal electrode arrangement and the scale of detectable anomalies. In this presentation, we will report the results of numerical simulations and the future plans of laboratory experiments.

Keywords: rock experiments, electrical conductivity, numerical simulations

## Volcano-Loop observation at Kusatsu-Shirane volcano

HINO, Yuta<sup>1</sup> ; OGAWA, Yasuo<sup>2\*</sup> ; KANDA, Wataru<sup>2</sup> ; HASE, Hideaki<sup>2</sup> ; SEKI, Kaori<sup>1</sup>

<sup>1</sup>Department of Earth and Planetary Sciences, Tokyo Institute of Technology, <sup>2</sup>Volcanic Fluid Research Center, Tokyo Institute of Technology

We have made successful measurement of time domain electromagnetic signals using transmitting and receiving loops at the same location. This system is being planned to work for monitoring the volcano vent.

The test measurement was conducted in the Kusatsu-Shirane volcano where detailed resistivity structure is known by audio-magnetotelluric method. The stepwise waveform was used and off-time response was measured using a transmitting and receiving loop both with 33m radius. The induced voltage was measured from the 0.1ms to 30ms. The observed voltages as a function of time in logarithm were inverted using Occam's algorithm and the model resistivity and resolution of the model were investigated. We also compared the result with those obtained by magnetotelluric method and found that the upper surface layers which have 1d structure are consistent with volcano loop results. We plant to use the system for repeated measurements or continuous monitoring the volcano in the future.

Keywords: Electromagnetic induction, time domain, loop, volcano, monitoring

## Electrical conductivity structure beneath the Gomura Fault (Kyotango, Kyoto)

OUCHI, Yuhei<sup>1\*</sup> ; YAMAGUCHI, Satoru<sup>2</sup> ; MISHIMA, Toshiaki<sup>2</sup> ; ODA, Yusuke<sup>2</sup>

<sup>1</sup>Department of Geosciences, Osaka City University, <sup>2</sup>Department of Geosciences, Graduate School of Science, Osaka City University

Fault zone architecture and related permeability structures form primary controls on fluid flow in upper-crustal, brittle fault zone. As the electrical resistivity of rocks is sensitive to distributions of fluids, the magnetotelluric (MT) method can be a powerful tool in investigating the fault zone architecture.

The Yamada Fault is located in Kyoto, Japan. The Yamada Fault zone consists of the main part of the Yamada Fault zone and the Gomura Fault zone. The Gomura Fault zone extends over 34 km and can be grouped into the Gomura Fault, the Chuzenji Fault and so on. The Gomura Fault appeared as a result of 1927 Tango earthquake.

In order to delineate subsurface structure of the fault, we made an audio-frequency magnetotelluric survey at 12 stations along the transect (4 km) across the surface trace of the Gomura Fault. The MT response function was obtained at each station, using remote reference processing. After dimensionality analysis by Phase Tensor method (Caldwell et al., 2004; Bibby et al., 2005), two-dimensional inversions for TE and TM modes were carried out, using the code of Ogawa and Uchida (1996).

The model is characterized by two resistive zones and four conductive zones. The most significant conductive zone is recognized beneath the surface trace of Gomura Fault with a width of more than 650 m and located in a depth range of 0.45-1 km. It is noteworthy that the conductive zone beneath the Gomura Fault is comparable in width to the damage zone determined by geological survey.

**Keywords:** The Gomura Fault, electrical resistivity structure, Magnetotelluric(MT), Damage zone

## A Summary report on the investigations of an electrical resistivity structure beneath Chugoku and Shikoku regions, south

SHIOZAKI, Ichiro<sup>1\*</sup> ; UTO, Tomofumi<sup>1</sup> ; YOSHIMURA, Ryokei<sup>2</sup> ; OSHIMAN, Naoto<sup>2</sup> ; KUBO, Atsuki<sup>3</sup> ; MURAKAMI, Hideki<sup>4</sup>

<sup>1</sup>Graduate School of Engineering, Tottori University, <sup>2</sup>Disaster Prevention Research Institute, Kyoto University, <sup>3</sup>Kochi Earthquake Observatory, Faculty of Science, Kochi University, <sup>4</sup>Department of Applied Science, Faculty of Science, Kochi University

The purpose of this study is to estimate crossing and longitudinal electrical resistivity structure sections in the southwest Japan arc in order to clarify the relation between the deep crustal low resistivity region and seismic activities. Therefore, based on the investigation research of the electrical resistivity structures in Japan arc and the southwest Japan arc, in Sanin region, it is important to clarify the relation between earthquake occurrences out of the strain concentration zone, volcanoes not having eruption records for a long time and crustal fluid, and to find the structural heterogeneity in the inland earthquake occurrence area, the inland seismic gap (beneath the third class and quaternary volcano) and deep low frequency earthquakes. In Shikoku region, it is also important to find the relation between the occurrence pattern and structural locality of crustal earthquakes and deep low frequency earthquakes and the fluid supposed to be supplied from ocean plate subduction.

Our research group has shown that there is a clear relationship between resistivity and seismicity in the Sanin and Shikoku regions. We investigated deep crustal resistivity structures in the measurement lines that traverse a linear seismic activity area along with the coastal part of Japan Sea. As the result, in the eastern part of San-in region, it was found that a conductive area exists in the deep crust part under the seismic region, which is a resistive area, along with the seismic activity area stretching nearly in the east and west direction

However, Ozaki et al. (2011) showed that the crust has generally a high resistivity in the earthquake occurrence region in the middle-west part of Tottori pref. (2002, Mj5.3). This observation fact conflicts with the model advocated by the group including the author that has studied electrical resistivity in Sanin region. That is, there is a possibility that the deep low resistivity area beneath the Sanin region does not exist in series. Assuming that inland earthquakes occur because of local stress concentration caused by heterogeneity beneath a seismic activity band (Iio, 2009), the heterogeneity should be clarified by a spatial and structure analysis, and a more detailed surfacial structure data should be completed hereafter.

On the other hand, in the Shikoku region, the same investigation was carried out mainly in the outer zone, the south side of MTL and the result suggested that a remarkable conductive area should exist in the upper crust of the outer zone, and that the conductive area in the central and western part should have a clear relation with the non-seismic area.

These studies suggest that high conductivity (low resistivity) is possibly caused by the existence of deep crustal fluids, which probably play an important role in the inland earthquake occurrence mechanism of these regions. As one of the possible interpretations of water supply system, it is thought that the fluids in the deep crust are supplied from the subducting Philippine Sea plate by means of the dehydration processes. However, the existence of the plate is not thoroughly identified in the geological inner zone of the southwestern Japan Arc. Therefore, in order to grasp a whole tectonic setting, from the fore to the back arc side in the southwestern Arc, quantitative discussions based on the wideband MT survey covering whole these regions should be required. Consequently, for making the island arc crossing structure section in the southwest Japan arc, an additional structure investigation in the unmeasured area, the area of Setouchi as the main area is required to clear the northern edge of Philippine Sea plate.

In this presentation, the summary report on joint structure analysis result in Chugoku and Shikoku regions and key features of spatial resistivity distributions in these regions, using the recent data acquired in the Setouchi area incorporated in the existing data, will be shown.

Keywords: electrical resistivity, Chugoku and Shikoku regions, heterogeneity

## Electrical resistivity features of the back-arc areas in the NE Japan subduction zone

ICHIHARA, Hiroshi<sup>1\*</sup> ; TADA, Noriko<sup>1</sup> ; BABA, Kiyoshi<sup>2</sup> ; KASAYA, Takafumi<sup>1</sup> ; ICHIKI, Masahiro<sup>3</sup> ; KAIDA, Toshiki<sup>3</sup> ; OGAWA, Yasuo<sup>4</sup>

<sup>1</sup>JAMSTEC, <sup>2</sup>ERI, University of Tokyo, <sup>3</sup>Tohoku University, <sup>4</sup>Tokyo Institute of Technology

Electrical resistivity in the crust and upper mantle depends on the pore-fluid distribution, salinity, and connectivity of fluid-filled rock pores. Thus imaging of resistivity distribution based on magnetotelluric surveys gives us fundamental information about fluid distribution of subduction zones. Marine magnetotelluric survey is important to understand dynamics of the NE Japan subduction zone because dehydration of subducting Pacific plate occurs under the Japan Sea. In this study, we discuss resistivity distribution around back-arc areas in the NE Japan subduction zone based on the marine MT data.

We collected natural EM signals with ocean bottom electro-magnetometers (OBEMs) in the eastern Japan sea area between April and August 2013 by MR13-02A and NT13-18 JAMSTEC scientific cruises. In addition, 3 land MT stations were settled in islands in the Japan Sea (Tobishima, Awashima and Sado islands) between April and October 2013. These recorded time-series data were converted to a frequency-domain impedance tensor based on the BIRRP program [1]. The remote reference technique [2] was applied in the data processing using horizontal magnetic field data from Kakioka Station in the period range between 10 and 20000 seconds. As results, high-quality MT responses and geomagnetic tippers in both the trench and back-arc areas.

We calculated phase tensors [3] based on MT impedances by this and previous studies [4] to discuss re-sistivity distribution beneath the back-arc area. The phase tensor ellipse indicates high  $\Phi_{max}$  (>65 degrees) and  $\Phi_{min}$  (>50 degrees) in the long periods (>8000 seconds). Large  $\beta$  of phase tensor and large amplitude of geomagnetic transfer function are also shown. These features cannot be explained with bathymetry and sediment effects based on the 3-D forward modeling [5]. Thus strong three-dimensionality and deep conductor possibly distributed beneath the Japan sea. In order to discuss detailed resistivity structure, 3-D inversion approaches are required by using a newly developed 3-D MT inversion code for marine data to treat complicated ocean bottom and land topography [6].

**References:** [1] Chave, A. D. and D. J. Thomson, *Geophys. J. Int.* 157, 988-1006 (2004); [2] Gamble, T. D. et al., *Geophysics*, 44, 53-68 (1979); [3] Caldwell, T. G et al., *Geophys. J. Int* 158, 457-469 (2004); [4] Toh, H. et al., *Geophys Res Lett*, 33, L22309 (2006); [5] Baba, N. et al., *Geophys. J. Int* 158, 392-402 (2002); [6] Tada, N. et al., *Earth Planets Space*, 64, 10051021 (2012).

Keywords: back arc, NE Japan subduction zone, magnetotelluric, OBEM, phase tensor

## Conductivity structure beneath the fault segment gap in the Yamasaki fault zone, southwest Japan (2)

ODA, Yusuke<sup>1\*</sup> ; YAMAGUCHI, Satoru<sup>1</sup> ; MURAKAMI, Hideki<sup>2</sup> ; KATOH, Shigehiro<sup>3</sup> ; UYESHIMA, Makoto<sup>4</sup> ; MISHIMA, Toshiaki<sup>1</sup> ; OUCHI, Yuhei<sup>5</sup>

<sup>1</sup>Department of Geosciences, Graduate school of Science, Osaka City Univ., <sup>2</sup>Natural Sciences Cluster-Science Unit, Kochi Univ., <sup>3</sup>Division of Natural History, Hyogo Museum of Nature and Human Activities, <sup>4</sup>Earthquake Research Institute, The University of Tokyo, <sup>5</sup>Faculty of Science, Osaka City University

### Abstract

The Yamasaki fault zone (YFZ) of southwest Japan is a typical strike-slip fault system consisting of the Nagisen fault, the main strand of YFZ, and the Kusadani fault. The main strand of YFZ extends for over 79km and is divided into northwestern (NW) and southeastern (SE) groups based on their latest seismic activity. The NW group consists of the Ohara, Hijima, Yasutomi and Kuresaka-touge faults, and the SE group consists of the Biwako and Miki faults. The maximum magnitudes of the earthquakes generated by the NW and SE groups are estimated to be 7.7 and 7.3, respectively. Simultaneous activation of both fault groups is also pointed out to be as large as  $M = \sim 8.0$  (The Headquarters for Earthquake Research Promotion, 2013).

The subsurface structure beneath the fault segment gap between both groups will be the key information for assessing the possibility of such large earthquake.

To infer the structure, we carried out Audio-frequency Magnetotelluric (AMT) survey at 11 sites along a transect between the NW group and the SE group and showed the two-dimensional resistivity model along the transect based on MT impedances. This model is characterized by three conductive zones. They locate beneath the points where the transect crosses the extension lines of the surface trace of the Yasutomi, Kuresaka-touge, and Biwako fault. We thus concluded that the Yasutomi and Kuresaka-touge faults are extended to southeast and the Biwako fault is extended to northwest further than the recognized terminals of their surface trace.

In this presentation, we show the improved resistivity model which is determined by not only MT impedance but tipper vectors.

Keywords: conductivity structure, active fault, Yamasaki fault system, Magnetotellurics

## Electrical Resistivity Imaging at Western Turkey by Wideband Magnetotelluric Method

TUNCER, Mustafa kemal<sup>1\*</sup> ; CENGIZ, Ozlem<sup>2</sup> ; TANK, Bulent<sup>3</sup> ; TOLAK-CIFTCI, Elif<sup>4</sup> ; KAYA, Tulay<sup>5</sup> ; OGAWA, Yasuo<sup>6</sup> ; HONKURA, Yoshimori<sup>7</sup> ; MATSUSHIMA, Masaki<sup>8</sup> ; OSHIMAN, Naoto<sup>9</sup> ; CELIK, Cengiz<sup>10</sup>

<sup>1</sup>Istanbul University-Turkey, <sup>2</sup>Bogazici University-Turkey, <sup>3</sup>Bogazici University-Turkey, <sup>4</sup>Bogazici University-Turkey, <sup>5</sup>Tokyo Institute of Technology, Japan, <sup>6</sup>Tokyo Institute of Technology-Japan, <sup>7</sup>Tokyo Institute of Technology-Japan, <sup>8</sup>Tokyo Institute of Technology-Japan, <sup>9</sup>Kyoto University-Japan, <sup>10</sup>Bogazici University-Turkey

The westward migration of large magnitude earthquakes along the North Anatolian Fault Zone indicates that a major event may take place at and around the Marmara region, following the Izmit (Mw7.4) and Duzce (Mw7.2) earthquakes that took place in 1999 in northwest Turkey. For this reason many studies were conducted around Marmara sea, west of these events. These studies focused mostly on the northern part of this area because of the high damage risk near Istanbul, but the similar potential is also present for the southern Marmara. In order to investigate the upper crustal electrical resistivity structure at this location, wide-band magnetotelluric data were collected at sixteen sites forming two parallel profiles. These profiles were constructed to cross the southern branches the North Anatolian Fault. Following the application of Groom and Bailey decomposition that has been applied to remove the surplus features and to deduce the appropriate geo-electric strike direction which is an important requirement for two-dimensional interpretation, an inversion algorithm developed by Ogawa and Uchida (1996) was utilized to develop electrical resistivity models. These models pointed out a relatively complicated shallow (surface-to-5 km) structure which may be associated with the presence of crustal fluids, but below these depths the electrical resistivity is more uniform with only a deep conductor appearing beneath the northern ends of the two profiles. The known faults in the survey area correlate well with the features characterized in the final geo-electric models. A resistive-conductive boundary between Manyas - Karacabey basin and Bandirma-Karadag uplift on the western and Uluabat uplift and Mudanya uplift on the eastern profiles may be associated with the South Marmara Fault.

Keywords: North Anatolian Fault, Fluids, Electrical resistivity, Magnetotellurics, geo-electric models

## Installation of a Vector Magnetometer for a Ground-based Tsunami Early Warning

KAWASHIMA, Issei<sup>1\*</sup> ; TOH, Hiroaki<sup>2</sup> ; YOSHIMURA, Ryokei<sup>3</sup> ; FUJII, Ikuko<sup>4</sup> ; OOGI, Junpei<sup>4</sup> ; ABE, Satoshi<sup>5</sup>

<sup>1</sup>Graduate School of Science, Kyoto University, <sup>2</sup>Data Analysis Center for Geomagnetism and Space Magnetism, Graduate School of Science, Kyoto University, <sup>3</sup>Earthquake Hazards Division, Disaster Prevention Research Institute, Kyoto University, <sup>4</sup>Kakioka Magnetic Observatory, Japan Meteorological Agency, <sup>5</sup>GeoSpatial Information Authority of Japan

Conductive sea water moving in the geomagnetic main field generates electromagnetic variations by a physical process called the oceanic dynamo effect. This effect at the time of tsunami passages was recently detected on the seafloor in the northwest Pacific (Toh et al., 2011) and on Easter Island (Manoj et al., 2011). The tsunami-induced electromagnetic field is expected to contribute to existing global tsunami warning systems.

We are carrying out a project that aims to observe geomagnetic variations associated with tsunami passages by ground-based real-time observations. This project requires a pair of geomagnetic observation sites for clear detection of tsunami events. The geomagnetic coast effect and the external field due to ionospheric and/or magnetospheric disturbances can be removed by taking real-time differences between a coastal and an inland geomagnetic sites. We installed a vector magnetometer at Umaji located in the middle of Muroto Peninsula, where artificial electromagnetic noises are very small. This location is selected as a counterpart of the existing observation site at Muroto located at the tip of the peninsula, which is operated by Geospatial Information Authority of Japan (GSI).

In this presentation, we will make a progress report on our ground-based tsunami warning system consisting of a pair of vector magnetometers. This system is intended to detect the geomagnetic field variations induced by tsunamis at the time of Nankai/Tonankai earthquakes.

Keywords: Geomagnetism, Tsunami

## The several Records of tsunami induced magnetic field obtained by the JMA Chichijima observation station(CBI).

TATEHATA, Hidee<sup>1\*</sup> ; HAMANO, Yozo<sup>2</sup>

<sup>1</sup>JMA, <sup>2</sup>JAMSTEC

Through the geomagnetic field, electrically conducting seawater movement generates electric fields and currents in generally. Furthermore, the current induces secondary magnetic fields. Our Chichijima geomagnetic observation station (CBI) is located on the solitary island in the Pacific Ocean. Addition this, located the tsunami observation station (Futami tide gauge) that is subject to the JMA. We are able to obtain concurrent tsunami and magnetic data because the distance between these observation points is only 1 km. So, this Chichijima Island is suitable in order to research tsunami induced magnetic fields research. We have investigated in CBI data (samples taken every 1 second) and Chichijima Futami tide gauge data (every 15 seconds) from 1995 to 2013, finally obtained 9 events tsunami induced phenomena. The many of the signal of these events is small, but three of them has clear record, the 2011 off the Pacific coast of Tohoku Earthquake Tsunami (2011/3/11 M9.0), The 2010 Chile earthquake (2010/2/27 M8.8) and 1996 the Irian Jaya Earthquake Tsunami (1996/2/17 M8.1). The other events are weak, but their magnetic signals are detectable enough. it may be worth worldwide renown that so many induced magnetic phenomena have been found in one observation station Chichijima (CBI). In the low solar activity periods, the induced magnetic signal may be detectable, if the half tsunami amplitude is 20cm or over. Some of these events might have been disturbed and dismissed due to magnetosphere substorm, even though the induced magnetic field was enough to detect. Each of above-mentioned three examples has over 1 m tsunami height, and clear induced magnetic record. Especially, in spite of weak magnetosphere substorm, the record of the 2011 off the Pacific coast of Tohoku Earthquake Tsunami is very clear. So, on 1 m or more-high tsunamis, it is safely said that the induced magnetic fields is detectable definitely. These induced magnetic field records will be one of mediation between the geomagnetic science and the tsunami disaster prevention science.

Keywords: tsunami, Induced magnetic effects, chichijima

## Geomagnetic total intensity variations associated with vertical crustal movement in the eastern part of Izu Peninsula

SASAOKA, Masahiro<sup>1\*</sup> ; OGAWA, Tsutomu<sup>2</sup>

<sup>1</sup>Kakioka Magnetic Observatory, Japan Meteorological Agency, <sup>2</sup>Earthquake Research Institute, University of Tokyo

In order to detect geomagnetic changes associated with the earthquake swarm and anomalous crustal activities, continuous observations of the geomagnetic total intensity have been conducted in the eastern part of Izu Peninsula. The continuous data of the geomagnetic total intensity were utilized after an analysis of removing the effect of external magnetic field from those data during 2010 - 2012. An association between the geomagnetic field variation and the vertical crustal movement was examined comparing the day-to-day variation of the geomagnetic total intensity with that of the geodetic height measured by GPS (Global Positioning System). It is found that the day-to-day variation in the geomagnetic total intensity shows each seasonal change on the quiet seismic period during 2010 and on the relatively active seismic period during 2011 and shows no significant change on the quiet seismic period during 2012, though the day-to-day variation in the vertical crustal movement shows seasonal changes during 2010 - 2012. It is inferred that the hydrothermal activity related to the Dec. 2009 earthquake swarm caused by magma injection had been lasting up to less than two years and the hydrothermal movement associated with the vertical crustal movement had caused the seasonal changes in the geomagnetic total intensity during 2010 - 2011. This suggests the observed variations of the geomagnetic total intensity were not directly associated with seismic faulting. The continuous observation of the geomagnetic total intensity is expected to have a monitoring advantage in predicting the course of the earthquake swarm activity in the eastern part of Izu Peninsula.

Keywords: eastern part of Izu Peninsula, geomagnetic total intensity, crustal movement, hydrothermal activity

## Validity of using space approximation in calculating EM variations generated by the piezomagnetic effect

YAMAZAKI, Ken'ichi<sup>1\*</sup>

<sup>1</sup>Kyoto University

Variations in the magnetic field generated by the piezomagnetic effect, which is referred to as the piezomagnetic field, has been discussed in a framework of magneto-statics, in which temporal variations are totally ignored. This treatment is valid for quasi-static processes, but possibly invalid for dynamic processes including fault ruptures. The earlier works by the author has demonstrated that, when the temporal variations in the EM field is considered, finite conductivity of the Earth's crust alters the feature of the piezomagnetic field. However, consideration of the temporal variations in the EM field makes estimation of the piezomagnetic field complicated, even in a simple two-layered model which consists of the Earth's ground with finite conductivity and the air as a perfect resistor.

The problem will be largely simplified if the situation is approximated by a finite space model with a uniform electrical conductivity.

In the present work, variations in the EM field generated by the piezomagnetic effect are compared for two situations: finite space and semi-finite space models with finite conductivity, assuming the source of the piezomagnetic field is two-dimensional. It is demonstrated that, for some situations, the simpler model provides a good approximation of the expected piezomagnetic field.

Keywords: piezomagnetic effect, electromagnetic field, electrical conductivity, infinite space, semi-infinite space

## Testing paleointensity determination using Wilson method

FUKUMA, Koji<sup>1\*</sup>; SHCHERBAKOV, V. P.<sup>2</sup>; SHCHERBAKOVA, V. V.<sup>2</sup>

<sup>1</sup>Dept. Env. Sys. Sci., Doshisha Univ., <sup>2</sup>Borok Geophysical Observatory, Russian Academy of Sciences

The classical Thellier method still remains most reliable for paleointensity determination, but requires a quite demanding and rarely satisfied condition; a natural remanent magnetization (NRM) must be completely replaced by a laboratory thermoremanence (TRM) at every temperature interval. If a significant amount of multidomain grains is present, this condition is not satisfied and resulting in erroneous paleointensities as obtained from curvatures seen on the Arai diagrams.

A single-step heating method, which sounds quite primitive as adopted in early times (e.g., Folgheraiter [1899]) but is essentially still alive as in the Shaw method, escapes from the strict condition posed on the Thellier method. The Wilson method, being a sort of single-step heating methods, was developed a half century ago (Wilson, 1961 & 1962); comparison of high-temperature continuous thermal demagnetization curves, measured for a natural remanent magnetization (NRM) and then a thermal remanent magnetization (TRM) acquired in a known laboratory field, yield a paleointensity. The reason why the Wilson method was rarely used for paleointensity studies is that magnetization needs to be measured at elevated temperature. Yet this method has a great advantage of being extremely quicker than the other paleointensity methods. If using a modern automated high-temperature magnetometer, we can complete a Wilson measurement within one hour for a 1-cc cube.

We performed testing paleointensity measurements based on the Wilson method for 27 1-cc cubes of basalts and scorias of the 1983 eruption in Miyakejima (the expected field of 45.1 microT). A 1-cc cube was heated in air at the rate of ~40 deg.C per minute along with measuring three-component NRM at elevated temperature using a Orion three-component vibrating sample magnetometer at the Borok Geophysical Observatory. When the magnetization is decreased less than 1 percent of the initial value, heating was stopped and then total TRM was imparted during cooling down in the magnetic field of 45 microT. The total TRM was also continuously demagnetized in the same way as NRM.

We did find nicely straight lines on the NRM-TRM diagrams for 85% of measured samples, indicating that the shapes of unblocking temperature spectrum are essentially unchanged for NRM and TRM. We obtained the expected field intensity of 45.1 microT for the about half of the samples. The Thellier method for the sister samples also gave the expected field, but some of the samples did not. For the another half, the gradients of NRM-TRM lines significantly deviated from unity to higher or lower values. This means that thermal alteration (NOT including domain alteration) increased or decreased TRM capacity but did not appreciably changed unblocking temperature spectrum. Such a kind of alteration is not detected on NRM-TRM diagrams, therefore it is possible to give erroneous paleointensities.

Although the Wilson method is quick and robust even for samples containing multidomain grains, we need to take caution that thermal alteration is not necessarily detected from the linearity on NRM-TRM diagrams. This caution should be exercised for other kinds of single-step heating methods.

Keywords: paleointensity, Wilson method, Thellier method, high-temperature magnetometer

## Microscopic observation of titanomagnetite grains during paleointensity experiments of volcanic rocks

TANAKA, Hidefumi<sup>1</sup> ; YAMAMOTO, Yuhji<sup>2\*</sup>

<sup>1</sup>Faculty of Education, Kochi University, <sup>2</sup>Center for Advanced Marine Core Research, Kochi University

Titanomagnetite (Tmt) grains, some partially maghemitized, of various oxidation levels were microscopically observed under reflected light as a function of temperature step in a Königsberger Thellier Thellier experiment in air. The reflected light microscopy indicated that the brownish colour of homogeneous Tmt turned blue at  $\sim 300$  °C. This false blue colour was caused by submicron scale rugged stripes on the surface, according to scanning electron microscope observations, which was made after the final heating step. The typical grey-to-bluish colour of maghemitized parts of Tmt grains turned to a brownish colour at  $\sim 300$  °C, indicating inversion of titanomaghemite to a mixture of magnetite and ilmenite (Ilm) or haematite (Hem). Although these observations were from Tmt grains on the sample surface, oxidation must have proceeded similarly within samples because the surface changes in the Tmt grains were highly correlated with behaviour of data points on Arai plots. Alterations in Tmt after heating at 610 °C in air for increasing times from 10 to 500 min were evaluated by reflected light microscopy and scanning electron microscopy at the end of the experiment. Mottled patches gradually emerged in the Tmt grains during subsequent heatings. However, the formation of new Ilm lamellae was not observed, even after the final 500 min heating. In conclusion, the alteration of Tmt during laboratory heating in air at  $\sim 600$  °C is likely not due to the typical high-temperature oxidation that forms trellis-type Ilm lamellae. Below  $\sim 400$  °C, the process should be closer to low-temperature oxidation. On the other hand, maghemitized parts of Tmt grains invert instantaneously at 300 °C, and a trellis-type structure with Hem lamellae soon emerges when heated at 610 °C.

## Archeointensity trend between 8th and 11th century in Okayama

KITAHARA, Yu<sup>1\*</sup> ; YAMAMOTO, Yuhji<sup>2</sup> ; HATAKEYAMA, Tadahiro<sup>3</sup> ; TORII, Masayuki<sup>4</sup> ; KAMEDA, Shuichi<sup>5</sup>

<sup>1</sup>Graduate School of Integrated Arts and Sciences, Kochi University, <sup>2</sup>Center for Advanced Marine Core Research, Kochi University, <sup>3</sup>Information Processing Center, Okayama University of Science, <sup>4</sup>Faculty of Informatics, Okayama University of Science, <sup>5</sup>Faculty of Biosphere-Geosphere Science, Okayama University of Science

This study presents three new archeointensity estimated from Sayama-area (Bizen city, Okayama prefecture), for the period of 8th to 11th century. The baked-earth samples (archaeological artifacts) we used in this study were collected from old kilns (part of floor and wall) of Sue wares. These kilns were found during the course of five excavations which were conducted under an archaeological project (see Archaeological lab, Okayama University of Science, 2012; 2013) aiming to trace development-history of ceramics production activity in Sayama-area between Nara and Heian-era. If we adopt the archeological chronology based on the Sue-mura type (e.g. Nakamura, 2006), the Sayama-Shin-ike kiln and the Sayama-Higashiyama kiln were estimated to be under operation during last half of 8th century (? 775±25 year), and the Sayama-Higashiyama-Oku kiln to be at around 10 century (? 900±50 year) (See Archaeological lab, Okayama University of Science, 2012; 2013).

Various rock magnetic and stepwise thermal demagnetization experiments revealed that (1) the samples are generally resistant to laboratory heating, (2) shape anisotropy is small, and (3) main magnetic carriers are Ti-poor titanomagnetite with high blocking temperature. Archeointensity measurements were done by using the IZZI Thellier method (double heating method; Yu & Tauxe, 2005). We applied this method to 19 specimens from 15 samples of the Shin-ike kiln, 10 specimens from 10 samples of the Higashiyama kiln, and 19 specimens from 9 samples of the Higashiyama-Oku kiln. After applying a set of very strict criteria, averaged archeointensity (with one standard deviation) is obtained as follows: 61.6±4.4  $\mu$ T for the Shin-ike kiln (N=4), 51.8±6.5  $\mu$ T for the Higashiyama kiln (N=8), and 49.8±9.8  $\mu$ T for the Higashiyama-Oku kiln (N=9). These values are not contradicted from the ones obtained by the Tsunakawa-Shaw method (Tsunakawa and Shaw, 1994; Yamamoto et al., 2003) though they are preliminary. Our new data show general agreement with the most recent archeointensity compilation in Japan (Yoshihara et al., 2003) and confirm the rapid intensity decrease at ~600 AD on average.

Keywords: Archeointensity, IZZI-Thellier method, Tsunakawa-Shaw method, Old kilns of Sue wares

## Absolute paleointensity determinations of welded tuffs: Correlations between relative and absolute paleointensity data

FUJII, Satomu<sup>1</sup> ; MOCHIZUKI, Nobutatsu<sup>2\*</sup> ; HASEGAWA, Takeshi<sup>3</sup> ; OKADA, Makoto<sup>3</sup> ; SHIBUYA, Hidetoshi<sup>1</sup>

<sup>1</sup>Department of Earth and Environmental Science, Kumamoto University, <sup>2</sup>Priority Organization for Innovation and Excellence, Kumamoto University, <sup>3</sup>Department of Earth Science, Faculty of Science, Ibaraki University

Absolute geomagnetic paleointensities (APIs) have been estimated from igneous rocks, while relative paleomagnetic intensities (RPIs) have been reported from sediment cores. These two datasets have been treated separately, as correlations between APIs and RPIs are difficult on account of age uncertainties. We present a procedure for directly correlating APIs with RPIs of a RPI stack. Correlations between APIs and RPIs were conducted with virtually no associated age errors using both tephrochronologic correlations and RPI minima. Using the stratigraphic positions of tephra layers in oxygen isotope stratigraphic records, we directly compared the RPIs and APIs reported from welded tuffs contemporaneously extruded with the tephra layers. In addition, RPI minima during geomagnetic reversals and excursions were compared with APIs corresponding to the reversals and excursions. The comparison of APIs and RPIs at these exact points allowed a reliable calibration of the RPI values. In this study, we applied the Tsunakawa-Shaw method to 21 welded tuffs to increase API dataset. We obtained mean paleointensities for 16 of the 21 welded tuffs. Since eight of the 16 welded tuff units were correlated with the oxygen isotope stratigraphy, they can be added to the API data used in the correlation procedure. Combining these API data with the reported data, we correlated API data with RPIs from the PISO-1500 stack and SINT-800 stack. For 13 correlation points, RPIs of the PISO-1500 stack showed a linear relationship with virtual axial dipole moments (VADM) calculated from the APIs, indicating that the PISO-1500 stack has a linear relation to the axial dipole moment. On the other hand, RPIs from the SINT-800 stack has a trend with VADM and the correlation coefficient is lower than that of the PISO-1500 stack. The correlation procedure with increased API data can contribute to constraining the relation between RPI of a RPI stack and API and calibrating a RPI stack to absolute values.

Keywords: absolute paleointensity, relative paleointensity, tephra, oxygen isotope stratigraphy, welded tuff

## Rock magnetic study of the North Atlantic sediment during late Pliocene and early Pleistocene

SATO, Masahiko<sup>1\*</sup>; OHNO, Masao<sup>1</sup>; HAYASHI, Tatsuya<sup>2</sup>; KUWAHARA, Yoshihiro<sup>1</sup>; MIYAGAWA, Chizuru<sup>1</sup>; FUJITA, Shu<sup>1</sup>; KITA, Itsuro<sup>1</sup>

<sup>1</sup>Kyushu University, <sup>2</sup>Mifune Dinosaur Museum

As the ocean is a major component in the climatic system, it is crucial for palaeoclimatic study to understand the past evolution of the thermohaline circulation. The North Atlantic Ocean is one of the most important sea areas because newly formed deep water mass is redistributed to the global ocean from there (Broecker et al., 1991). In order to recover the past change in deep ocean circulation at the North Atlantic Ocean, a variety of proxies have been studied. However, the change during Pleistocene and Pliocene is still poorly understood.

In this study we conducted rock magnetic measurement of deep-sea sediments recovered from IODP Site U1314 on the Gardar Drift, to investigate the past change in bottom current flows at the North Atlantic Ocean. Since a coercivity of magnetic mineral varies sensitively with its state such as chemical composition, grain size, grain shape, stress, and so on, coercivity spectra can be used as a proxy for the constituent spectra of the sediment.

The samples were collected at 16 - 50 cm resolution from 199.3 to 262.5 mcd of the core, which corresponds to the age between 2.22 and 2.75 Ma according to the age model by Hayashi et al. (2010). Rock magnetic properties were measured for these samples using a MicroMag 2900 Alternating Gradient Magnetometer. The isothermal remanent magnetization (IRM) acquisition curve was obtained by the application of stepwise-increasing uniaxial fields to the sample at 30 steps from 1 mT to 1 T. The ratio of IRM acquired in a back-field of 0.1 T to that in a forward-field of 1 T (S-ratio) was also measured for all samples.

In order to reveal constituents of the sediment, decomposition of coercivity spectra were conducted. The IRM acquisition curve was normalized by the IRM intensity at 1 T and then the first derivative of the curve was calculated with respect to log<sub>10</sub> field (hereafter referred to as IRM gradient curve). The least square fit was performed so as to decompose the IRM gradient curve into linear combination of two end-members. Two end-member components were calculated by averaging the IRM gradient curves of selected samples. Samples with low S-ratio (<0.57) and younger than 2.4 Ma were chosen for component 1. Samples with high S-ratio (>0.88) and during MIS100, which were associated with the ice rafted debris, were chosen for component 2. These components were distinctly different from each other; coercivity distribution of component 1 was magnetically harder than that of component 2.

In consequence of the decomposition, the fitting error was significantly small for all samples, indicating that North Atlantic sediments in the Garder Drift during late Pliocene and early Pleistocene are explained by mixing of two end-member components. The fraction of two components periodically changes with time and agrees well with the LR04  $\delta^{18}\text{O}_{\text{benthic}}$  stack (Lisiecki and Raymo, 2005): the high-coercivity component dominated during interglacial periods, and the low-coercivity component dominated during glacial periods.

On the basis of the elemental ratio of potassium to titanium (K/Ti), Grutzner and Higgins (2010) reported change in proportion of sources of sediment at Site U1314 during the last 1.1 Ma. They demonstrated that Ti-rich basaltic material transported by the Iceland-Scotland Overflow Water and K-rich particle (continental rock like) derived from the other source dominated during interglacial periods and glacial periods, respectively. Our result is consistent with their result because high-coercivity and low-coercivity components are interpreted as the fine-grain titanomagnetite of Icelandic sources and the coarse-grain magnetic mineral of continental sources, respectively. Therefore the change in fraction of two end-member components represents change in fraction of bottom currents, and the bottom current flow patterns similar to those during the last 1.1 Ma might prevail at the North Atlantic Ocean during late Pliocene and early Pleistocene.

Keywords: North Atlantic Ocean, Deep-sea Sediment, IRM acquisition curve, Bottom current flow

## Magnetic properties of REY rich red clay near Minami-Torishima in the Pacific Ocean

YAMAZAKI, Toshitsugu<sup>1\*</sup> ; USUI, Yoichi<sup>2</sup> ; SHIMONO, Takaya<sup>3</sup>

<sup>1</sup>AORI, University of Tokyo, <sup>2</sup>JAMSTEC, <sup>3</sup>University of Tsukuba

Red clay accumulates slowly on the seafloor deeper than CCD in mid-latitudes. Paleooceanographic and paleomagnetic studies were limited so far because red clay does not yield microfossils that can be used for precise age estimation and sedimentation rates were extremely low, less than a few meters per million years. However, red clay has attracted interest since Kato et al. (2011) reported that red clay rich in REY (rare-earth elements and yttrium) distributes widely in the Pacific Ocean. In this paper, we present magnetic properties of red clay cores obtained from the seafloor near Minami-Torishima during the R/V Kaiei KR13-02 cruise. From these cores, extremely high REY contents were reported (Fujimoto et al., 2013, JpGU; Suzuki et al., 2013, JpGU). We will discuss a possible relationship between REY content and magnetic properties.

It is known in red clay that magnetostratigraphy can be established back to only ~3 Ma, and this also holds for the KR13-02 cores. However, noisy but rather coherent inclinations were obtained throughout the cores even where polarity reversal patterns were obscure. Although a possibility that these directions are of magnetic overprint cannot be excluded, the observed inclinations are not much lower than that expected from the GAD model at the present latitude. This may suggest that the sediments including the intervals of high REY content are not very old, possibly Eocene to Oligocene or younger in age, and that they deposited in the northern latitudes not very far from the present sites. This result is not consistent with the idea that the high REY content is influence of hydrothermal activity along the East Pacific Rise. The cores showed a common magnetic susceptibility variation pattern, and a peak of REY content occurs just below an interval of high magnetic susceptibility. The REY peak coincides with a sharp upward decrease in the ratio of ARM to SIRM, which indicates an increase of the mean magnetic grain size and/or an increase in the proportion of detrital to biogenic magnetic mineral component. These results suggest that the increased REY concentration may have occurred in association with a paleooceanographic event.

Keywords: red clay, REY, rock magnetism, environmental magnetism, Pacific, Minami-Torishima

## A method for measuring rapid magnetization change in high field using a pulse magnetizer: A new rock magnetic approach

KODAMA, Kazuto<sup>1\*</sup>

<sup>1</sup>Center for Advanced Marine Core Research, Kochi University

Pulse magnetizers have frequently been used in rock magnetic studies for the convenience of the production of high magnetic field without the need for a large electromagnet, enabling the rapid acquisition of isothermal remanent magnetization (IRM) for short (*c.*  $10^{-2}$  sec) period of time. Because the demand for high field is limited as much as 10 T for rock magnetism, the pulse magnetizer can be compact and low-cost, and several commercial systems are available for the purpose of imparting IRM. We propose in this study a new method for measuring the dynamical behavior of magnetization in pulsed high-field, a new cost-effective system comprised of a fast broad-bandwidth digital oscilloscope and a newly designed coil system. We show examples of such dynamical behaviors from a set of natural samples, and discuss these results in comparison with conventional rock magnetic analyses.

Keywords: rock magnetism, pulse magnetic field, magnetic hysteresis

## Paleomagnetic study of the Holocene volcanic rocks and tephra from post-caldera central cones of Aso Volcano

ABIRU, Takuya<sup>1</sup> ; SHIBUYA, Hidetoshi<sup>2\*</sup> ; MOCHIZUKI, Nobutatsu<sup>3</sup> ; YATO, Takanori<sup>2</sup> ; MIYABUCHI, Yasuo<sup>4</sup>

<sup>1</sup>Faculty of Science, Kumamoto University, <sup>2</sup>Department of Earth and Environmental Sciences, Kumamoto University, <sup>3</sup>Priority Organization for Innovation and Excellence, Kumamoto University, <sup>4</sup>Faculty of Education, Kumamoto University

We have conducted a paleomagnetic study on Holocene volcanic rocks and tephra from post-caldera central cones of Aso Volcano. Paleomagnetic sampling was made at 25 sites of seven units. Nineteen out of 25 sites gave reliable mean paleomagnetic directions that had a 95% confidence circle of lower than 5 degree. Different sites from a few lavas, which had been treated as a single unit in the geological map of Aso Volcano (Ono and Watanabe, 1985), gave distinct mean directions at 95% confidence level. For Kishimadake lava, Ojodake lava, Nakadake young volcanic edifice, two different mean directions were obtained from multiple sites. These differences in mean directions indicate that multiple flows were extruded with a temporal gap of more than 10 or 100 years. We also found that Kamikomezuka scoria, two sites of Kishimadake lava, two sites of Ojodake lava gave identical mean directions at 95% confidence level. The concordance of the mean directions suggests that the multiple vents erupted simultaneously, in a time interval of the order of 10 years, and these lavas were extruded over a wide area of the post-caldera central cones. In this study, we also made paleomagnetic measurements on tephra layers in a section. Oriented samples were collected from 22 layers of a tephra section, 4km NNE of Nakadake volcano (Miyabuchi and Watanabe, 1997). Seventeen of the 22 layers gave mean paleomagnetic directions that had a 95% confidence circle of lower than 5 degree. Most of the N6 layer, and N5 and N4 layers give an identical direction, which suggests these layers were formed in a short period of several tens of years. A tephra layer record a same direction of a lava flow, which suggests a simultaneous formation of the tephra layer and lava flow.

Keywords: Aso Volcano, paleomagnetic direction, volcanic rock, tephra

## Paleomagnetic secular variation record for the last 7000 years observed in piston cores from the Ichinomegata Maar

ANRAKU, Kazuhiro<sup>1\*</sup>; HAYASHIDA, Akira<sup>2</sup>; HARAGUCHI, Tsuyoshi<sup>3</sup>; YAMADA, Kazuyoshi<sup>4</sup>; SHINOZUKA, Yoshitsugu<sup>5</sup>; GOTANDA, Katsuya<sup>6</sup>; YONENOBU, Hitoshi<sup>7</sup>

<sup>1</sup>Graduate School of Science and Engineering, Doshisha University, <sup>2</sup>Department of Environmental Systems Science, Doshisha University, <sup>3</sup>Department of Geosciences, Graduate School of Science, Osaka City University, <sup>4</sup>School of Human Sciences, Waseda University, <sup>5</sup>Faculty of Environmental Earth Science, Hokkaido University, <sup>6</sup>Faculty of Polycy Informatics, Chiba University of Commerce, <sup>7</sup>Graduate School of Education, Naruto University of Education

The Ichinomegata is a maar lake located in Oga peninsula, Akita Prefecture. Thin-wall core samples (IMG06) obtained in 2006 provided a Holocene paleomagnetic secular variation (PSV) record through measurements of natural remanent magnetization (NRM) of u-channel samples. In this study, we collected the piston-core samples (IMG13P-1 and IMG13P-2) from the center of the lake, and measured magnetic susceptibility, anisotropy of magnetic susceptibility (AMS) and natural remanent magnetization (NRM) of 7cc cubic samples. According to correlation between IMG06 and the piston cores based on lithological and magnetic susceptibility data, both IMG13P-1 and IMG13P-2 cover the last 7000 years. Stepwise AF demagnetization of the NRM showed that high intensity NRM decayed toward the origin linearly in most samples, so we determined the directions by applying the principal component analysis. We excluded some by evaluating inclinations of minimum axis and shape parameters  $q$  of AMS ellipsoids. Excepting some intervals that probably disturbed in coring, inclination and relative declination are showed consistent variations between IMG13P-1, IMG13P-2 and IMG06 cores. Therefore, we argue that the sediments of the Ichinomegata Maar are suitable for PSV studies. The paleomagnetic record from the Ichinomegata Maar shows a good similarity with the archeomagnetic secular variation from southwest Japan (Shibuya, 1980) and the PSV record from Lake Biwa (Ali et al., 1999), implying a great importance in regional reconstruction of the PSV record in Japan.

Keywords: Paleomagnetic secular variation, remanent magnetization, magnetic susceptibility, Ichinomegata Maar

## Thermomagnetic characteristics in the Hikageyama lava: searching a paleomagnetic record of the Laschamp excursion

NISHIYAMA, Hiroto<sup>1\*</sup> ; HAYASHIDA, Akira<sup>2</sup> ; SAWADA, Yoshihiro<sup>3</sup> ; DANHARA, Tohru<sup>4</sup> ; KAWANO, Shigenori<sup>5</sup>

<sup>1</sup>Sci. Environ. Math. Model., Grad. Sci.&Engi., <sup>2</sup>Dept. Environ. Sys. Sci., Doshisha Univ., <sup>3</sup>Shimane University, <sup>4</sup>Kyoto Fission-Track Co., Ltd., <sup>5</sup>Tochigi Prefectural Museum

In the JpGU 2013 Meeting, we reported a paleomagnetic record from the Hikageyama lava. Among the 9 sites, 4 sites in the eastern part of the Hikageyama yielded consistent site mean directions characterized by shallow inclinations and easterly deflection. These site mean directions provide virtual geomagnetic poles (VGP) at around 50 N and 100 W. It can be assumed therefore that the Hikageyama dacite recorded anomalous geomagnetic field at the time of the Laschamp excursion. In addition to the above record, stepwise thermal (TH) demagnetization revealed that the above 4 sites yielded consistent site mean directions.

Thermomagnetic analysis revealed that most samples are composed of a single phase Curie temperature, suggesting magnetite as a remanence carrying mineral. And, the above 4 sites are classified into two groups. One (HKG-9, 10) shows a single phase, similar to the above. The other (HKG-11, 12) shows two phases, suggesting titanohematite and hematite. According to TH demagnetization results, one has two or three NRM components remanence. The other has a single component, which showed highly stable remanence which cannot be demagnetized at peak alternating field of 100 mT as previously reported. We will report these components discussion together with the thermomagnetic results.

Keywords: Rock magnetism, Hikageyama lava, Geomagnetic excursion, Laschamp excursion

## Electromagnetic core-mantle coupling and length-of-day variation in numerical dynamo models

TAKAHASHI, Futoshi<sup>1\*</sup>

<sup>1</sup>Tokyo Institute of Technology

Exchange of angular momentum between the core and the mantle is likely to be responsible for the decadal variations in the length-of-day (LOD). If the changes in the angular momentum of the mantle are balanced by the opposite changes of the core, some coupling mechanisms between the core and the mantle should be invoked. Here we examine the electromagnetic (EM) coupling as a possible mechanism of angular momentum exchange. We use numerical dynamo simulations to investigate the mechanism to explain the LOD variations with respect to time including the decadal time scale. In numerical dynamo models, we impose a uniformly electrically conducting layer of about 200 km-thick on the mantle side of the core-mantle boundary corresponding to the D'' layer. The electric current associated with the dynamo-generated magnetic field can flow in the conducting layer and the Lorentz force can yield a net EM torque with respect to the rotation axis. The electrical conductivity of the layer is varied from 200 - 500 S/m in dynamo models. The LOD variations can put some feedback effects on flows in the core through the changes in the angular velocity, which emerge as a change in the effective Ekman number and the Poincare force. Influences of such a feedback are also included in numerical models. The Ekman number adopted as a nominal value is  $10^{-4}$ . We have obtained the EM torque resulting in typical angular velocity variation of the order of  $10^{-6}$  relative to the nominal angular velocity in a time scale of the magnetic diffusion time. Much smaller changes in shorter time scale are also observed. Based on the findings in the present study, it is suggested that the EM core-mantle coupling in a likely range of the conductance within the D'' layer is a promising mechanism to yield LOD variations in decadal to longer time scale.

Keywords: dynamo, electromagnetic core-mantle coupling, LOD variation, D'' layer

## Influence of surface displacement on fluid motions induced by Joule heating in the inner core of the Earth

TAKEHIRO, Shin-ichi<sup>1\*</sup>

<sup>1</sup>Research Institute for Mathematical Sciences, Kyoto University

The elastic anisotropy of the earth's inner core as revealed by recent seismic observations is considered to originate from the alignment of texture formed along the solidification of the core or alignment of the preferred orientation of crystals by plastic deformation of fluid motions. The depth dependency of the anisotropy is difficult to explain by the solidification mechanism, whereas the various factors driving fluid flows in the inner core considered thus far do not appear to yield sufficiently strong stresses for generation of the elastic anisotropy. Takehiro (2011) proposed Joule heating of the magnetic field penetrating diffusively from the inner core boundary (ICB) as a possible source of inner core flows. His specific calculation in the case of toroidal magnetic field with the horizontal structure of spherical harmonics  $Y_2^0$  showed that downward flow in the equatorial region and upward flows in the polar region are induced by the Joule heating. This flow field has non-zero radial velocity component at the ICB, causing mass exchange between the inner and the outer core. This feature is a result of the constant normal stress boundary condition at the ICB, and it is implicitly assumed that the phase change occurs instantaneously at the ICB. However, the actual speed of the phase change is finite. If the speed of the phase change is slow enough, the ICB would be deformed and the surface displacement is induced by the non-zero radial velocity at the ICB. This surface displacement may prevent inner core flows due to the buoyancy force originated from the density contrast between the inner and the outer cores. Therefore, in this study, we investigate influence of surface displacement on fluid motions induced by horizontally heterogeneous Joule heating in the inner core. We examine the extent of development of the surface displacement and modification of flow field of the inner core.

The difference of the governing equations from those of Takehiro (2011) is the boundary conditions at the ICB. Temperature disturbance at the ICB coincides with the melting temperature which varies depending on the surface displacement. The normal component of stress equates with buoyancy induced by the surface displacement. The toroidal magnetic field and surface displacement with the horizontal structure of  $Y_2^0$  is given. The flow fields are calculated numerically for various amplitudes of the surface displacement with the expected values of the parameters of the cores.

The results show that, when the surface displacement is the order of 0.01–0.001m or less, the flow and stress fields are similar to those of Takehiro (2011), where the surface displacement vanishes. As the amplitude of the surface displacement is increased, counter flows from the polar to the equatorial regions come to emerge around the ICB, while the flow in the inner regions is directed from the equatorial to the polar regions in the inner region and non-zero radial component of velocity at the ICB still exists. When the surface displacement is about 0.14–14m, radial component of velocity at the ICB vanishes, the surface counter flows becomes stronger than the flow in the inner region, and the amplitude of the stress field near the ICB dominates that of the inner region, which might be inconsistent for the elastic anisotropy in the inner core.

Reference: Takehiro, S., 2011: Phys. Earth Planet. Inter., 184, 134–142.

Keywords: anisotropy of the Earth's inner core, magnetic fields in the Earth's outer core, flows in the Earth's outer core, inner core boundary of the Earth, dynamo action in the Earth's outer core

## Paleomagnetism of the Znp-Ohta tephra in eastern Honshu: relative tectonic rotations at local and regional scales?

HOSHI, Hiroyuki<sup>1\*</sup> ; FUTAMURA, Sho<sup>2</sup>

<sup>1</sup>Aichi University of Education, <sup>2</sup>Futagawa Minami Elementary School

We present paleomagnetic data suggesting relative tectonic rotations in eastern Honshu since 3.9 Ma. Samples were collected from a widespread ash bed, called the Znp-Ohta tephra, at three localities. One is the Tomioka locality located to the east of the Abukuma Mountains, where the ash bed (local name = SF4.5 tephra) was sampled at three sites. The other two are the Miyobara and Kohsaka localities on the Boso Peninsula, where the ash bed (local name = An85 tephra) was sampled at three sites at each locality. Stepwise demagnetization was performed on all specimens, and the principal component analysis was applied to the demagnetization data to extract characteristic remanent magnetization (ChRM) components. At Tomioka, site-mean ChRM directions were determined at all sites. They are tightly clustered after tilt correction and have a southerly direction of reverse polarity. Interestingly, the direction is deflected significantly counterclockwise with respect to the direction of the correlative tephra at Chita in central Honshu (Hoshi & Deguchi, 2013). At Miyobara and Kohsaka, the locality-mean ChRM directions are significantly different to each other. The paleodeclination of Miyobara is similar to that of Tomioka, and the paleodeclination of Kohsaka is almost identical to that of Chita. The difference in paleodeclination between Miyobara and Kohsaka seems to be related to the difference in the general geological trend of Neogene strata on the Boso Peninsula, suggesting relative rotation on the peninsula. Our results imply that in eastern Honshu, relative rotations have taken place at local and regional scales since the Pliocene.

Keywords: eastern Honshu, paleomagnetism, Pliocene, relative rotation, tectonics, Znp-Ohta tephra

## Past continental shape inferred from GPS data

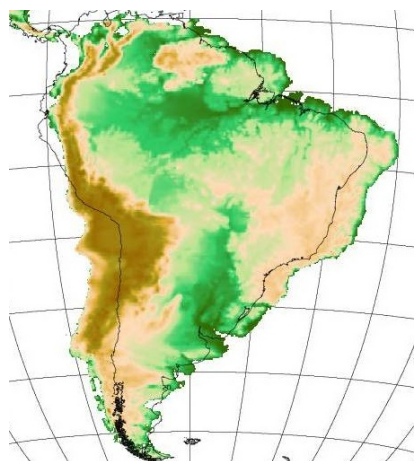
KAWAI, Keigo<sup>2</sup> ; KATO, Tadayoshi<sup>2</sup> ; HARADA, Yasushi<sup>1\*</sup>

<sup>1</sup>Department of Marine and Earth Science, Tokai University, <sup>2</sup>Department of Marine Mineral Resources, Tokai University

Kono et al.,1985 analyzed paleomagnetic data around Andes and showed past shape of the south American continent about 50Ma and figured the Andes mountain range were more linear shape than at present. We tried to reconstruct the 50Ma shape of the south American continent from the current crustal motion of GPS data. Plate motion vectors observed from space geodesy including GPS, can comparable with plate motions of geological time scale. Gordon, 1993 showed VLBI plate motion (time scale of years) and NUVEL-1 plate motion (3 million years mean motion) are in great harmony with each other.

We applied a method of Harada and Kato(AGU Fall Meeting 2012), and calculated about 50Ma shape of the south American continent (figure below). The shape of the Andes mountain range were linear and in good harmony with the result of Kono et al.,1985. We conclude, thus, decades scale GPS data can compare with plate deformation of ten thousands years.

Keywords: GPS, Past continental shape, Deformation of plates



## Problems related to the past motion of the Philippine Sea Plate

TAKAHASHI, Masaki<sup>1\*</sup>

<sup>1</sup>Geological Survey of Japan, AIST

Plate motion through geological time is reconstructed based on the correlation of marine magnetic anomaly patterns and/or hot-spot track analysis. But the past motion of the Philippine Sea Plate cannot be clarified because the plate is surrounded by convergent plate boundary (trench) and it has no hot-spot track. Therefore the paleomagnetic approach is the only method to reconstruct the past location and motion of the plate. However this method contains unacceptable problems that the paleomagnetic declination does not indicate the total rotation of the plate around its Euler pole in most cases. The paleomagnetism has been thought as an effective tool to reconstruct the Philippine Sea Plate motion, but actually it is impossible to clarify the past motion of the plate by paleomagnetic method.

Keywords: tectonics, paleomagnetism, Philippine Sea Plate

## Environmental rock-magnetism of red clay in the South Pacific Gyre during the Cenozoic: relation with rare-earth content

SHIMONO, Takaya<sup>1\*</sup> ; YAMAZAKI, Toshitsugu<sup>2</sup> ; SUZUKI, Katsuhiko<sup>3</sup>

<sup>1</sup>Graduate School of Life and Environmental Sciences, University of Tsukuba, <sup>2</sup>Atmosphere and Ocean Research Institute, The University of Tokyo, <sup>3</sup>Institute for Research on Earth Evolution, Japan Agency for Marine-Earth Science and Technology

Red clay occupies ~40% of the global ocean floor. Paleooceanographic and paleomagnetic studies of red clay were limited so far because red clay does not yield microfossils that can be used for precise age estimation and sedimentation rates were extremely low, less than a few meters per million years. However, red clay has attracted interest since Kato et al. (2011) reported that red clay rich in REY (rare-earth elements and yttrium) distributes widely in the Pacific Ocean. Among the cores studied by Kato et al. (2011), especially REY-rich mud (2110 ppm at the maximum) of ~40 m thick occurs below 13.5 m below seafloor (mbsf) at the Deep Sea Drilling Project (DSDP) Site 596 at the western edge of the South Pacific Gyre. However, the core sections have large gaps, and rock- and paleomagnetic studies were not conducted. In 2010, Integrated Ocean Drilling Program (IODP) Expedition 329 Site U1365 occupied at almost the same position as Site 596. Continuous pelagic red clay cores of ~76 m thick was recovered above the basaltic basement of ~100 Ma in age.

We conducted an environmental magnetic study using the Site U1365 cores to investigate long-range climatic and paleooceanographic changes during the Cenozoic. We also investigate a relation between magnetic properties and REY of the red clay. On the basis of rock magnetic analyses and transmission electron microscopy, magnetic mineral assemblages are dominated by bacterial magnetites (magnetofossils) throughout the cores (Yamazaki and Shimono, 2013). In the uppermost several meters, terrigenous maghemite probably transported as eolian dust increases. High REY mud (2470 ppm at the maximum) of ~40 m thick occurs below 8 mbsf. The variation pattern of REY content is similar to that at Site 596. The ages of the Site U1365 cores were transferred from those of Site 596, which is based mainly on a constant Co-flux model at Site 596 (Zhou et al., 1992), by inter-core correlation using magnetic susceptibility and REY variation patterns. Paleomagnetic stratigraphy is available for the uppermost several meters at Site U1365.

We discuss a possible relationship between REY content and magnetic properties. The REY peak coincides with a sharp upward decrease in the ratio of  $\kappa_{ARM}$  to SIRM, which indicates an increase of the mean magnetic grain size and/or an increase in the proportion of detrital to biogenic magnetic mineral component. A peak of REY content occurs just below an interval of high magnetic susceptibility. These characteristics are similar to those of red clay cores near Minami-Torishima (Yamazaki et al., 2014, JpGU). This suggests that the increased REY concentration may have occurred in association with a common paleooceanographic event. Eolian dust supply may have increased since ~30 Ma. The Eocene/Oligocene (E/O) transition (~34 Ma) is known as the time when major ocean gateways (the Drake passage and Tasmanian gateway) opened and the Antarctic Circumpolar Current was formed (Scher and Marting, 2004, 2006; Stickley et al., 2004). The onset and increase of dust supply in the South Pacific may have occurred after this time. Northward movement of Australia continent to an arid region (middle-latitude) may have also contributed an increase of dust supply. Hyeong et al. (2013) suggested that phosphatization on the Mid-Pacific mountains took place between 36 and 12 Ma, and it peaked at the E/O transition. They connected the results to paleo-deepwater circulation. A REY peak occur near the E/O transition at Site U1365, which may be related with the phosphorus budget.

Keywords: Red clay, REY, South Pacific Gyre, Cenozoic, Environmental Magnetism

## Regional differences in magnetic properties of topmost sediments of the Northern Lake Biwa

ISHIKAWA, Naoto<sup>1\*</sup> ; ISHIKAWA, Kanako<sup>2</sup>

<sup>1</sup>Graduate School of Human and Environmental Studies, Kyoto Univ., <sup>2</sup>Lake Biwa Environmental Research Institute

Rock-magnetic investigations have been performed on topmost sediments above about 30 cm below sediment surface (bss) cored in summer (June to July) and winter (November to December) at eight sites with different water depth, where dissolved oxygen (DO) content in bottom water and its seasonal variation are different, in the first depression at the North Basin of Lake Biwa in order to reveal early diagenetic effect on magnetic properties of the sediments.

Low-temperature magnetometric results indicate that a partially-maghemitized magnetite is a principal magnetic mineral in the sediments. Warming curves from 6 to 300K of isothermal remanence (IRM) imparted at 6K in 1T after zero-field cooling show a remarkable decrease of IRM between 90 and 120K, which is regarded as a suppressed Verwey transition of magnetite. The amount of IRM decrease between 90 and 120K increase downcore at all site, implying the dissolution of maghemite skin covering magnetite. The IRM decrease is more slightly remarkable in the sites with shallower water depth. The degree of maghemitization may be lower in the site. Samples from sites with deeper water depth below about 70m show another IRM decrease between 20 and 30K with the inflection point at about 29K. The IRM drop disappears in samples with hydrochloric acid treatments. These low-temperature IRM behaviors may imply the presence of ferro-rhodochrosite. The IRM drop is detected in samples above about 18 cmbss, and the samples in two zones of 0-3 cm-bss and 6-15 cm-bss show the IRM drop more clearly. The IRM drop is more remarkable in samples with deeper water depth. The occurrence of the magnetic mineral with the characteristic low-temperature magnetic behavior seems to be influenced by the DO values and its seasonal change.

As common characteristics in downcore changes of magnetic properties, the downcore decrease of magnetic coercivity is observed in the uppermost sediments above about 10 cm-bss, and the amount and grain size of magnetic minerals subsequently decreases and increases downcore below 10cm-bss, respectively. These changes are considered to be associated with the dissolution of maghemitized magnetite by the early diagenetic effect. The presence of magnetic minerals with finer grain size and higher magnetic coercivity in the sediments above 10 cm-bss is more remarkable in sites with deeper water depth.

Keywords: rock magnetic property, Lake Biwa, topmost sediment, early diagenesis

## Magnetic properties of the sediments and suspended solids in the sea surface water at the Hiroshima bay station.

KAWAMURA, Noriko<sup>1\*</sup>

<sup>1</sup>Japan Coast Guard Academy

Suspended solids (SS) in sea water are consisted of planktons and insoluble particles, and are an indicator of transparency. SS particles adsorb and incorporate metallic ions. Iron is a metallic ion, and an essential element for phytoplankton. It is supplied from river to sea as bivalent or trivalent ions, and exists as iron compounds as organic complexes in sea water. Aeolian dusts are consisted of SS, and also consists of iron compounds. They will deposit on seafloor, and be sediments as the climatic record. It is important to investigate the distribution and mode of iron compound in SS for the present and past environmental studies. This study aims to diagnose magnetic minerals in SS. Enough amount of SS sample for magnetic measurements are collected by magnetic separation from seawater at the Hiroshima bay station. 4 L of seawater is filtrated, and the particles above 0.45 um in diameter are recovered for XRF analysis. The amount of magnetic particles in sea surface water shows relatively high values from April to July in the bay. The maximum value is found at the station, which is located near an iron works (the supply source). The particle is opaque minerals and looks like needle. The values of IRM imparted at 0.3 T and 2.5 T are not stable. It suggests that SS has strong anisotropy. Results of thermo-magnetometry indicate that magnetic carriers of SS samples are mainly magnetite, and goethite and hematite is also recognized. Magnetic minerals in the sediments at the station are magnetite, hematite, and greigite. It is implied that goethite present in the sea surface water and it may be dissolved on sea floor.

Keywords: Suspended solids, Iron compounds, Goethite

## Paleomagnetic study of the turbidite sediments around the Daini Atsumi Knoll

TAMAKI, Machiko<sup>1\*</sup> ; SUZUKI, Kiyofumi<sup>2</sup> ; EGAWA, Kousuke<sup>3</sup>

<sup>1</sup>Japan Oil Engineering Co., Ltd., <sup>2</sup>Japan Oil, Gas and Metals National Corporation, <sup>3</sup>National Institute of Advanced Industrial Science and Technolog

This study is a part of the program of the Research Consortium for Methane Hydrate Resource in Japan (MH21 Research Consortium)

Keywords: Paleomagnetic study, Paleomagnetostratigraphy, Anisotropy of magnetic susceptibility, Paleocurrent analysis, turbidite sediments, Dainii Atsumi Knoll

## Emplacement mechanism of marine volcanoclastic sediments (IODP Site U1397, 1398) based on rock magnetic properties

SAITO, Takeshi<sup>1\*</sup>; KATAOKA, Kyoko S.<sup>2</sup>

<sup>1</sup>Faculty of Science, Shinshu University, <sup>2</sup>Research Institute for Natural Hazards and Disaster Recovery, Niigata University

Large numbers of marine volcanoclastic sediments with various origins were recovered from the sites U1397 and U1398 during IODP Expedition 340. They were most likely derived from volcanoes on Martinique and possibly from Dominica, Lesser Antilles volcanic arc. Some volcanoclastic units were transported and deposited as turbidites, some were as thin tephra fall deposits and others show both characteristics. They contain various amounts of bioclastic component, pumice and lithic fragments and hemipelagic mud clasts. Therefore, these volcanoclastic sediments are suitable for investigating transport and emplacement mechanisms of volcanic materials and the resultant sedimentary and petro-facies in marine settings. This study focuses on magnetic minerals in the marine volcanoclastic sediments and carried out rock magnetic measurements.

Thermomagnetic measurements showed almost reversible curves and induced magnetization decayed to almost zero below 580 °C, suggesting little contribution of maghemite or hematite. Two Curie temperatures (T<sub>c</sub>) with 350-400 °C and 500-550 °C indicate that the main magnetic carriers are Ti-rich titanomagnetite and Ti-poor titanomagnetite. The proportion of low-T<sub>c</sub> titanomagnetite in central and bottom part of thick turbidite units was larger than that in hemipelagic sediments and in the topmost part of turbidite units, suggesting Ti-rich titanomagnetite is derived from volcanic events. Tephra fall deposits also showed large contributions of Ti-poor titanomagnetite, resulted from large amount of volcanic materials. On the other hand, thin turbidite units showed small contributions of Ti-poor titanomagnetite. This suggests that thin turbidite units are derived from diluted flows which contain few heavy Fe-bearing magnetic minerals.

Magnetic susceptibility and hysteresis measurements showed that heavy and large magnetic minerals in most thick turbidite units were concentrated at the lower part of the unit. Samples from the topmost and bottom part of turbidites showed higher degrees of anisotropy than those from the central part, indicating strong influence of suspension settling at the topmost part and shearing at the bottom part. Bottom parts of fall units contain heavy and large magnetic minerals, whereas upper parts of fall units contain fine magnetic minerals. On the other hand, in thin turbidite units such features cannot be observed and hysteresis parameters and susceptibility values were almost concentrated. Probably thin turbidite units did not experience segregation of specific particles during transportation and settling under the relatively calm condition.

These preliminary results suggest that magnetic minerals are useful indicators of volcanic events and rock magnetic approaches can identify various types of depositional processes about marine volcanoclastic sediments.

Keywords: turbidite, fall deposit, marine sediment, titanomagnetite, magnetic mineral

## Paleomagnetic direction of the Tomikusa Group in southern Nagano Prefecture and its tectonic significance

SAKO, Kazuki<sup>1\*</sup> ; HOSHI, Hiroyuki<sup>1</sup>

<sup>1</sup>Aichi University of Education

We report here a new paleomagnetic direction from Early Miocene (18-17 Ma) sediments of the Tomikusa Group in southern Nagano Prefecture, and discuss the formation of curvature of the Median Tectonic Line (MTL) in central Honshu. Sedimentary rock samples collected from 24 sites were demagnetized stepwise, and site-mean directions were determined for 23. Rock magnetic experiments suggest that the main magnetic minerals are magnetite and maghemite. The site-mean directions pass a reversal test, indicating primary remanent magnetization. The overall mean direction with a northerly declination is indistinguishable from the Early Miocene reference direction derived from the Asian continent. This comparison suggests no significant rotation in the study area with respect to the continent since 17 Ma. The mean declination is deflected about 15 deg counter-clockwise with respect to the strike of the nearby MTL. The same angular relationship is also found in other sedimentary basins in central Honshu (Ichishi in Mie Pref., Chita Peninsula in Aichi Pref., Shitara in Aichi Pref., and Chichibu in Saitama Pref.). Thus we conclude that the MTL was straight in the late Early Miocene (18-17 Ma).

Keywords: paleomagnetism, Tomikusa Group, Median Tectonic Line, Miocene, rock magnetism, tectonics

## Rock magnetism and its petrological characterization of fossil *Porites* coral frameworks in Ishigaki island, Japan

KUMAGAI, Yuhō<sup>1\*</sup> ; NAKAMURA, Norihiro<sup>1</sup> ; SATO, Tetsuro<sup>1</sup>

<sup>1</sup>Graduate school of Earth Science, Tohoku University.

Radiocarbon (<sup>14</sup>C) is produced by the cosmic rays in the atmosphere and is utilized for analysis of the past sun activity. But the Earth's geomagnetic field also controls radiocarbon variability, suggesting that a strong field would shield the planet from high energy charged particles. This mimics lower sun activity. Also, the short-term (in decadal or centennial scale) movement of the geomagnetic pole to the low latitude, such as geomagnetic jerk, could lead to an increased cosmic ray flux impinging on the terrestrial atmosphere and thus to a higher <sup>14</sup>C production rate. Therefore, in order to study the past sun activity from the <sup>14</sup>C production rate, we need to know the movement of geomagnetic pole position, its field strength and the variability of radiocarbon production during decadal to centennial periods. Many researches, which aim to reveal the paleomagnetic secular variation (PSV), have been performed using datasets obtained from volcanic rocks, sediment, and fired kilns. The some reconstruction models of geomagnetic dipole moment are also established from these data sets. But there are few recorders that can be used for the reconstruction of PSV in a decadal or centennial scale. Here we propose an alternative candidate of fossil coral frameworks as a possible paleomagnetic recorder for PSV research. The coral framework has an advantage in reconstructing both the radiocarbon variability and the geomagnetic field, although usual corals show extremely weak intensity of remanence and its low stability. However, it is shown that our recently-ceased coral framework samples from Ishigaki island possess a remanence intensity of 10<sup>-5</sup> -10<sup>-4</sup> A/m and a single-domain like stability from Lowrie-Fuller test. We prepared the standard 1-inch core samples cut parallel to the growth direction of coral *Porites*, including coral's growth bands for a ten to several tens of years. Our thermal and AF demagnetization experiments of oriented coral samples show that a characteristic remanence direction is parallel to the present Earth's magnetic field with some fluctuations. On the other hand, some samples exhibit different remanence directions from the present geomagnetic field with a calcite peak of X-ray diffraction analysis. The presence of calcite indicates that the meteoric diagenesis which changes aragonite coral frameworks into calcite affect the direction of initial magnetization. To constrain the remanence carriers, we are conducting a first order reversal curves (FORC) measurement and petrologic observations by a Schottky field-emission scanning electron microscope (FE-SEM) of acid-treated residuals of our corals. Our results suggest that *Porites* coral framework samples provide a role as a potential use for paleomagnetic recorder for annual to decadal scales with careful examination of calcite content.

Keywords: fossil *Porites* coral frameworks, paleomagnetism

## Effect of thermal expansion on Neel's relaxation nomograph of magnetite and its agreement with the radiocarbon age

SATO, Tetsuro<sup>1\*</sup> ; NAKAMURA, Norihiro<sup>1</sup> ; GOTO, Kazuhisa<sup>2</sup>

<sup>1</sup>Earth Science, Tohoku University, <sup>2</sup>International Research Institute of Disaster Science (IRIDeS), Tohoku University

Age gap between the paleomagnetic viscous dating and the radiocarbon age of tsunamigenic boulders in Ishigaki Island is focused. Recent researchers have conducted radiocarbon dating to label tsunami age, being able to calibrate the paleomagnetic viscous dating. These ages should be the same for the initial tsunami event. In the paleomagnetic viscous dating, time-temperature relation assuming Neel's single domain (SD) theory of magnetite is used. This monograph shows the older remagnetized component in nature can be erased by the higher temperature in the laboratory, and younger is its reverse. Thus, we can predict the age acquired the secondary magnetization by calculating demagnetization temperature and heating time. Our viscous dating results sometimes represented that the unblocking temperature of viscous components for tsunamigenic boulders is higher than the temperature predicted from Neel's relaxation theory of single domain magnetite, suggesting the older age than the one determined from the calibrated radiocarbon age. Previous numerous studies confirmed that the departure from Neel's theory is attributed to the presence of multi-domain magnetite. However, Lowrie-Fuller test, FORC (first order reversal curves) experiments and Low-temperature demagnetization of tsunamigenic boulders confirmed the presence of single domain magnetite. To solve this problem, we consider the thermal expansion of magnetite during stepwise thermal demagnetization process and propose a modified time-temperature relation to be able to fill the age gap. Currently, thermal expansion coefficient of magnetite is reported by some researchers (e.g. Nikolaev and Shipilin, 2000; Levy et al, 2004). If magnetite volume is bigger than initial volume during thermal demagnetization, unblocking temperature should indicate higher value under the assumption of constant coercive force. To confirm this hypothesis, we conducted stepwise thermal demagnetization to a boulder emplaced by 1771 Meiwa tsunami (242 years ago) and compare them to our new modified time-temperature relation.

Keywords: thermal expansion, Neel's theory, single domain, viscous remanence, blocking temperature

## Rock magnetic study of single zircon crystals sampled from river sands

SATO, Masahiko<sup>1\*</sup> ; YAMAMOTO, Shinji<sup>2</sup> ; YAMAMOTO, Yuhji<sup>3</sup> ; OKADA, Yoshihiro<sup>4</sup> ; OHNO, Masao<sup>1</sup> ; TSUNAKAWA, Hideo<sup>4</sup>

<sup>1</sup>Kyushu University, <sup>2</sup>The University of Tokyo, <sup>3</sup>Center for Advanced Marine Core Research, Kochi University, <sup>4</sup>Tokyo Institute of Technology

Geomagnetic field paleointensity data provide critical information such as thermal evolution of the Earth (Stevenson et al., 1983). Also a state of geomagnetic field closely relates to a surface environment (Kulikov et al., 2007). It is pivotal to know the variation of geomagnetic field intensity throughout the history of the Earth. Until now we have not yet obtained, however, enough data to resolve billion-year-scale geomagnetic field variation (Tauxe and Yamazaki, 2007) and need to obtain more paleointensity data.

In this study we focus on a paleointensity experiment using single zircon crystal. Since river sand originates in rocks widely distributed in river basin, detrital zircons in the sand have various ages (Rino et al., 2004). Therefore if the geomagnetic paleointensity can be measured using the single zircon crystal, we will probably obtain paleomagnetic data enough to resolve the long-term geomagnetic field variation.

Zircon crystals used in the present study were sampled from sands of the Nakagawa River, Tanzawa Mountain. The Nakagawa River flows along bodies of tonalite, which is a representative rock of the continental crust. Using coarse-grain single zircon crystals with weight of about 0.1 mg, a suite of rock magnetic measurements were conducted: low-temperature demagnetization (LTD) and stepwise alternating field demagnetization (AFD) of saturation isothermal remanent magnetization (SIRM), and low-temperature cycle using an Magnetic Property Measurement System (MPMS).

SIRM intensities of the single zircon crystals vary four orders of magnitude ranging from  $1 \times 10^{-12}$  -  $2 \times 10^{-9}$  Am<sup>2</sup>, and especially a few percent of the grains have strong SIRM larger than  $1 \times 10^{-10}$  Am<sup>2</sup>. The zircon crystals contain nearly pure magnetite (Fe<sub>3</sub>O<sub>4</sub>), and they are in both single-domain (SD) and multidomain (MD) states. The SD magnetite contained in the zircon crystals has the potential to record the paleomagnetic information. The existence of MD magnetite suggests that stepwise-demagnetization after LTD treatment is an efficient approach for paleomagnetic measurement. Taking into account the relation between SIRM intensity and thermoremanent magnetization (TRM) intensity for magnetite (e.g., Yu, 2010), TRM of single zircon crystal may be measured with a high-sensitivity magnetometer such as a SQUID magnetometer.

Now we plan to sample river sand at the Mississippi River and to conduct rock magnetic measurements of the zircon crystal collected from the sand. On the basis of the rock magnetic studies for the zircon crystals from the Nakagawa River and the Mississippi River, we will discuss the feasibility of the paleointensity experiment using single zircon crystal.

Keywords: Zircon, Rock magnetic study, Paleointensity

## Development of the Japan Archeomagnetism Database

HATAKEYAMA, Tadahiro<sup>1\*</sup>

<sup>1</sup>Information Processing Center, Okayama University of Science

Here we will report the online service of Japan Archeomagnetism Database which is developed since 2012. Now the database includes about 700 site archeodirection dataset, and we are working to add new data from the backyard stocks which has uncertainty about the independent archeological chronology. Therefore we have to confirm that with searching the dating in the original excavation reports.

Moreover we have added new archeomagnetic data from the archeological archives. More than 100 archeomagnetic data have been manually discovered in the reports.

Now we are also providing a paleomagnetic direction at the Far-East region calculated from the Japanese geomagnetic secular variation models.

Keywords: Archeomagnetism, Database, Geomagnetic secular variations

## Medium scale crustal structure based on magnetic and gravity anomalies in the eastern part of Hokkaido, Japan. -part 2

MORIJI, Rie<sup>1\*</sup> ; NAKAGAWA, Mitsuru<sup>1</sup>

<sup>1</sup>Geological Survey of Japan, AIST

The Pacific coast of the eastern Hokkaido (from Kushiro to Nemuro Peninsula) is characterized by high gravity and high magnetic anomalies. However, it was difficult to get a suitable model due to gravity anomalies on land and aeromagnetic anomalies. We sampled basalts in this area and measured densities, natural remanent magnetization, susceptibilities and other magnetic properties. These results were presented in Japan Geoscience Union Meeting 2007. Moreover, new gravity and magnetic anomaly maps of offshore of cape Ochiishi were published by GSJ, AIST (2012). We picked up profiles and modified previous models. Data including new profiles suggested similar models to previous studies.

Keywords: magnetic property, magnetic anomaly, gravity anomaly, Nemuro, Hokkaido

## Seismogenic shear-induced thermal turbulence in Nojima fault gouges: micro-textural and rock magnetic considerations

NAKAMURA, Norihiro<sup>1\*</sup> ; FUKUZAWA, Tomohiko<sup>1</sup>

<sup>1</sup>Dep. Earth Science, Tohoku University

Nojima fault gouges exhibit a characteristic flow microtexture of laminated slip zones, billow-like wavy folds and turbulent disordered structures. Power spectral analysis of the wavy folds indicates that the geometry roughly obeys a power-law of -1.9, agreeing well with the previously measured value of Kelvin-Helmholtz (KH) turbulence in natural environments. The well-known example of KH instability is a cloud that the cloud-atmosphere interface becomes an unstable vortex sheet that rolls up into a spiral. The instability occurs at the interface between two fluids of different densities shearing at different velocities (Thorpe 2005). The KH wave in Nojima fault gouges was found along a slip plane in a blackish cohesive gouge (pseudotachylyte-like gouge), resulting in the presence of instability at the slip interface during ancient earthquake or creep. Thin section observations showed the blackish cohesive gouge consisted of granular materials for both sides of the interface and the KH wave occurs in a denser granular material along an earthquake-originated sharp slip plane. Our scanning Magneto-Impedance magnetic microscope observation shows the KH wave dense layer is only magnetized in isothermally-magnetized thin section, revealing the production of magnetic mineral in KH wave. Because the Nojima fault gouge contains iron-carbonate (siderite), the thermal decomposition of siderite produces magnetite more than 400 °C. Therefore, we suggest that the KH wave is generated through KH instability in a high-temperature (>400 °C) granular dense layer with different densities and different slip velocities. This result suggests that shear-induced thermal turbulence in the fault gouge plays an important role to weaken a frictional strength during earthquake slip dynamics.

## Analyzing the early 19 century's geomagnetic declination in Japan from Tadataka Inoh's Santou-Houi-Ki.

TSUJIMOTO, Motohiro<sup>1\*</sup> ; OMOTANI, Akitoshi<sup>2</sup> ; INUI, Takaaki<sup>3</sup> ; MIYAUTI, Satoshi<sup>4</sup>

<sup>1</sup>Japan Cartographers Association, <sup>2</sup>San-in System Consultant, <sup>3</sup>Matsue Municipal comitee of property, <sup>4</sup>Studyies of Inoh's map and writing Assoc

Santou-Houi-Ki national treasure of Japan recorded by cartographer Tadataka Inoh in 1800-1816, is 67 volumes ledger consist of approximately 200,000 magnetic compass land survey azimuth data accuracy of 0 degree 05 min, from eastern coast of Hokkaido to Yakushima Isl in western Japan. We continue the work of analysis that stopped after only analysis in 1917, which done about the survey data at known position of the retirement home of Inoh at Fukagawa in Edo (Tokyo) in 1802-1803.

(1)It is able to change Japan as one of the most concentrated area of accurate geomagnetic declination data in the world, in early 19th century, from insufficient area of data, and supply new data to northeast Asia by analysis of Santou-Houi-Ki.

The total number of analyzed points exceeded 178, and the outline isogonic line in Japan archipelago and the distribution of the declination in every15 minutes in western Japan coast in those days, begun to appear.

(2)Compare the isogonic Atlas by Gauss and Weber (hereinafter Gauss Atlas) consisted of observed data in 1828-1830, with the analysis from Santou-Houi-Ki, the foundational structure of isogonic lines in Japan archipelago is roughly similar. But we recognize the contradiction to reverse with secular variation in Northern Kyushuu area and Tsushima Island. There are no observed data in Japan in the table supplemented with Gauss isogonic Atlas. The recorded observational data in Gauss Atlas in East Asia were inland area from Pekin to Eastern Siberia, Ohotsk, Kamchatka etc. From the analysis of Santou-Houi-Ki, we recognize the magnetic declination supposed as the local geomagnetic anomaly in southern coast of eastern Hokkaido. The isogonic line of declination in surrounding area of Japan in Gauss Weber's Atlas had drawn by calculated estimates, on a matrix of 5 degree in latitude and 10 degree in longitude, one cell of this matrix is 500km long. Therefore the analysis of Santou-Houi-Ki becomes very important. Today it is very important to verify with the isogonic map of Andrew Jackson et al Gufm1 by NOAA (1800-1815).

(3)Procedure and advantage of interdisciplinary and simultaneous analysis of Santou-Houi-Ki across geomagnetism, cartography, and local history. 1.It increase precise evidence to verify the azimuth and the name or short description of the reference point or the target points recorded in Santou-Houi-Ki, with not only the survey diary by Inoh or Inoh map or the survey map of today, add historical local map, historical local source material, the old survey map by former Japan imperial army. 2. Use the recreation software of scenery or digital map of GSI Japan to grasp the outline of particular latitude and longitude of the reference point and target points and real azimuth. 3. Calculate the average of remainder as the declination, to deduct the magnetic azimuth recorded in Santou-houi-Ki from the real azimuth. 4. The important point is to calculate backward the precise position of the reference point should be adjusted to the position, where all of the declination values from the magnetic survey azimuth to different targets at the reference point are approximately equal to each other, to use the consecutive formula of Excel for speed up and keep accuracy. 5. Use GPS transmitter at the reference point to investigate longitude and latitude, and recalculate the position under 0 second in latitude and longitude, minute accuracy declination, more detail and accurate than traditional study. 6.It is able to find areas or points of local geomagnetic anomaly, or to restore the precise position of survey reference point by Tadataka Ino, accuracy of less than second in latitude and longitude, or the objective point of survey in accuracy second where the valuable in local history, including disappeared constructions or big tree etc.

Keywords: declination, Inoh, SantouHouiKI, Reference point, interdisciplinary

## Slab dehydration, intermediate-depth earthquakes, and arc magmatism: A review of seismological observations

NAKAJIMA, Junichi<sup>1\*</sup>

<sup>1</sup>RCPEV, Graduate School of Sci., Tohoku Univ.

We review recent seismological observations beneath the Japanese Islands and show important roles of geofluids on seismogenesis at intermediate depths and arc magmatism.

Seismicity in the subducting crust of cold slabs is most active at depths of 70-90 km, where seismic velocity in the crust abruptly increases, suggesting that high pore pressures generated as a result of dehydration reactions in the crust facilitate intermediate-depth seismicity. In contrast, seismicity is almost absent in the subducting crust of warm slabs like Cascadia and Nankai. The aseismic crust may be explained by slow dehydration rates in warm slabs, which cannot increase pore pressures effectively.

Magmatism beneath the arc has been discussed in terms of the heterogeneities in seismic velocities together with geochemical and petrological constraints. We recently developed simple but useful method to estimate seismic attenuation structures and applied it to waveform data in NE Japan. Seismic attenuation provides additional insights into ongoing magmatic processes in subduction zones, because higher-temperature environments or the existence of fluids may have different effects on seismic attenuation from on seismic velocity. The obtained results show that a depth profile of  $Q_p^{-1}$  in the back-arc mantle is explained by attenuation expected for a two-dimensional (2-D) thermal model. However, an inclined high-attenuation zone observed in the back-arc mantle wedge, which is interpreted as an upwelling flow, shows higher attenuation than that calculated from the 2-D thermal model. The higher seismic attenuation is probably caused by the concentration of partial melt in the upwelling flow. Our results further imply the breakdown of hydrous minerals in a hydrous layer above the Pacific plate at a depth of ~120 km.

Keywords: dehydration, pore pressure, eclogitization, seismic attenuation

## Imaging mantle melting processes and the effect of water beneath island arcs and backarc spreading centers

WIENS, Douglas<sup>1\*</sup> ; WEI, S. shawn<sup>1</sup>

<sup>1</sup>Washington University, St Louis, MO, USA

We use arrays of land and ocean bottom seismographs to image melting processes in the Mariana and Tonga-Lau mantle wedges. Both regions show arc volcanism, active backarc spreading, and a gradient in mantle water content going from slab to backarc spreading center. The Lau backarc in particular shows a gradient in inferred mantle water content as the spreading centers approach the arc and slab in the south. Water contents range from near-MORB conditions in the Central Lau Spreading Center (CLSC) to high water content for the Eastern Lau Spreading Center (ELSC) and nearly arc-like for the Valu Fa Ridge (VFR).

For both Mariana and Lau we find significant slow velocity and high attenuation anomalies in the upper 100 km of the mantle beneath the volcanic arc and the spreading center. In the Mariana region, the anomalies are separated by a high velocity, low attenuation region at shallow depths (<80 km), implying distinct arc and backarc melting regions, with the anomalies coalescing and possibly allowing material interchange at greater depths. The maximum anomaly in the backarc is shallower (~30 km) than in the arc (~65 km), consistent with geochemical indications on the depth of melt production in these regions. The strongest anomaly beneath the backarc spreading center is narrow (~70 km) and extends from close to the mocho to 80 km depth. Data analyses for the Tonga-Lau project are preliminary, but show similarities to the Mariana images. Extremely low seismic velocity and high attenuation are found in a 100 km wide region beneath the spreading center in the upper 80 km. At deeper depths the anomaly is displaced westward in both velocity and attenuation images, suggesting that partial melting occurs along an upwelling limb of mantle flow originating west of the backarc. 3-D images from Rayleigh wave tomography show a much stronger anomaly along the CLSC when compared to the southern ELSC and VFR. The backarc velocity and attenuation anomalies are stronger in the Lau basin than in the Mariana backarc, perhaps due to higher mantle temperatures inferred from petrology.

Both Q and velocity anomalies are larger than expected for temperature effects based on laboratory-derived relationships, and their configuration is inconsistent with the expected temperature field. In addition, the observed anomalies are roughly inversely proportional to inferred mantle water content, suggesting that water content does not cause the observed large seismic anomalies. However, experimental results suggest that seismic attenuation and velocity are highly sensitive to the presence of even very small amounts of partial melt. Therefore we suggest the high attenuation and low velocity anomalies delineate the melt production regions beneath the ridge axis and volcanic arc, but that only small melt fractions (<1 %) are required to explain the seismic data. Smaller amplitude anomalies beneath the VFR, where large amounts of subduction-derived water are incorporated into the melt, may indicate lower mantle melt porosity due to low melt viscosity and more efficient transport of the water-rich melt, or a different topology of melt in the matrix. A lower melt porosity for aqueous melts is also consistent with the smaller seismic anomaly seen for the water-rich volcanic arc melting regions compared to the backarc melt production zone for both regions.

Keywords: seismic tomography, island arcs, backarc spreading centers, seismic attenuation, mantle fluids, melt generation

## Slab Melting in Subduction Zones

SCHMIDT, Max<sup>1\*</sup> ; MANN, Ute<sup>1</sup>

<sup>1</sup>ETH Zurich, Switzerland

Depending on temperature, slab-to-mantle element transfer in the subarc region may either occur through fluids or melts. In this contribution we present pelite melting experiments systematically varying H<sub>2</sub>O and CO<sub>2</sub> contents and review the presently available information on slab melting. Synthetic pelite model compositions containing variable proportions of H<sub>2</sub>O (0.7-4.4 wt%) and CO<sub>2</sub> (0-4 wt%) was melted at 3-4.5 GPa and 750-1200 °C. The fluid-saturation concentration at 3-8 GPa (i.e. the H<sub>2</sub>O stored in phengite as the only hydrous phase) is 0.8-0.9 wt% H<sub>2</sub>O. We locate the fluid-absent solidus of the H<sub>2</sub>O-pelite system at 3 to 4.5 GPa at 880 °C to 1050 °C about 150-200 °C higher than the wet solidus (3 to 4.5 GPa, 730 to 860 °C). CO<sub>2</sub> increases the fluid-saturated solidus temperature by ~30 °C but leaves the fluid-absent solidus temperature unchanged. For all systems considered, the onset of melting is controlled by phengite and only in the fluid-absent experiments K-feldspar becomes a product of melting (at 3 GPa).

Compiling all available information, we parameterize the amount of melt to be formed as a function of temperature for fluid-saturated and fluid-undersaturated conditions. Melt compositions themselves are meta- to peraluminous high Si-granites (71-77 wt% SiO<sub>2</sub> on a volatile free basis) with low Fe, Mg, and Ca contents and are uniform to ~50% melting when plotted as a function of melt fraction (but not temperature), almost independent of starting compositions. At >2 wt% bulk H<sub>2</sub>O melts are sodic (K/Na=0.2-0.4), while at <1.5 wt% melts are mostly potassic (K/Na=0.9-1.7). Only the fluid-poor H<sub>2</sub>O-CO<sub>2</sub> and the CO<sub>2</sub>-only experiments of Thomsen and Schmidt (2008, EPSL) and Tsuno and Dasgupta (2011, CMP) produce significantly different melts i.e. rather potassic phonolites (Na being increasingly retained in jadeitic cpx with pressure). Near 5 GPa a fundamental change occurs: the H<sub>2</sub>O-silicate solidus comes to an endpoint while in CO<sub>2</sub>-rich systems a carbonatite replaces the silicate melt lowering the solidus temperature by more than 100 °C to 9 GPa.

Regarding the likelihood of sediment melting in the subarc region, only the wet solidus is within reach of the hottest geotherms of the thermal models that predict the highest slab-surface temperatures, i.e. none of the Arcay et al (2007, EPSL) slab surface P-T paths cross the solidus while for Syracuse et al. (2010, G3) about 7 out of 56 modeled slab segments have P-T-paths that may lead to significant melting for H<sub>2</sub>O-saturated pelites at 3-4 GPa. As retention of significant amounts of fluids within a subducting lithology is not an option, flushing with fluids from dehydrating serpentinites would be the only option for achieving significant melting in the hottest subduction zones (at the required P-T conditions, there are no suitable reactions in the mafic crust or the sediments themselves). An alternative option to reach widespread pelite melting would be to dismiss the rigid slab surface concept and allow for sediment diapirs to rise into the hot mantle (Gerya and Yuen, 2003, EPSL; Behn et al, 2011, Nature Geosci.) in which case the pelites could bleed out their incompatible elements completely. Nevertheless, these diapirs are propelled by a density contrast resulting from partial melting and it remains unclear whether they could start rising without melting in the first place.

In conclusion, combining P-T paths, phase diagrams and degrees of melting suggests that significant pelite melting at a rigid slab-mantle interface appears to be a rather rare on present day Earth (and hence much more so for mafic materials), the only option for widespread pelite melting appears to be entrainment of the sediments into the mantle wedge. Removal of CO<sub>2</sub> through melting is utterly inefficient and as subsolidus metamorphic reactions lead to low X<sub>CO2</sub> fluids, most of the subducted CO<sub>2</sub> will be fed into the deep beyond-arc C-cycle.

Keywords: slab melting, H<sub>2</sub>O, CO<sub>2</sub>, pelite

## Diverse magmatic effects of subducting a hot slab in SW Japan: results from forward modeling

KIMURA, Jun-ichi<sup>1\*</sup> ; GILL, James<sup>2</sup>

<sup>1</sup>JAMSTEC, <sup>2</sup>University of California Santa Cruz

In response to the subduction of the young Shikoku Basin of the Philippine Sea Plate, arc magmas erupted in SW Japan throughout the late Cenozoic. Many magma types are present including ocean island basalt (OIB), shoshonite (SHO), arc-type alkali basalt (AB), typical sub-alkalic arc basalt (SAB), high-Mg andesite (HMA), and adakite (ADK). OIB erupted since the Japan Sea back-arc basin opened, whereas subsequent arc magmas accompanied subduction of the Shikoku Basin. However, there the origin of the magmas in relation to hot subduction is debated. Using new major and trace element and Sr-Nd-Pb-Hf isotope analyses of 324 lava samples from seven Quaternary volcanoes, we investigated the genetic conditions of the magma suites using a geochemical mass balance model, Arc Basalt Simulator version 4 (ABS4), that uses these data to solve for the parameters such as pressure/temperature of slab dehydration/melting and slab flux fraction, pressure, and temperature of mantle melting. The calculations suggest that those magmas originated from slab melts that induced flux-melting of mantle peridotite. The suites differ mostly in the mass fraction of slab melt flux, increasing from SHO through AB, SAB, HMA, to ADK. The pressure and temperature of mantle melting decreases in the same order. The suites differ secondarily in the ratio of altered oceanic crust to sediment in the source of the slab melt. The atypical suites associated with hot subduction result from unusually large mass fractions of slab melt and unusually cool mantle temperatures.

Keywords: SW Japan, Volcanic rocks, Geochemistry, Forward model

## Fluids and earthquakes in the Japan subduction zone

ZHAO, Dapeng<sup>1\*</sup>

<sup>1</sup>Tohoku University, Department of Geophysics

Detailed tomographic images are determined for the source areas of large crustal and megathrust earthquakes that occurred in the Japan subduction zone during 1995-2013, thanks to the availability of the dense Japanese seismic network that could locate accurately the mainshocks and aftershocks of those large earthquakes and provide high-quality arrival-time data for tomographic imaging. Suboceanic events are relocated precisely using sP depth phase. Large crustal earthquakes in the forearc region such as the 1995 Kobe earthquake (M 7.2) and the 2011 Iwaki earthquake (M 7.0) might be triggered by fluids that are released from the dehydration of the subducting slab and directly ascend to the crust and enter an active fault zone. In contrast, along the volcanic front and in back-arc areas, the seismogenic layer in the upper crust is thinned and its mechanical strength is weakened because of ascending hot magmas and fluids which are produced by a combination of slab dehydration and corner flow in the mantle wedge. Large crustal earthquakes are apt to take place at the edge portion of the thinned seismogenic layer which exhibits low velocity, high Poisson's ratio, and high electrical conductivity. To clarify the generating mechanism of the 2011 Tohoku-oki earthquake (Mw 9.0) and the induced tsunami, we determined high-resolution tomographic images of the Northeast Japan forearc. Significant lateral variations of seismic velocity are visible in the megathrust zone, and most large interplate thrust earthquakes are found to occur in high-velocity (high-V) areas. These high-V zones may represent high-strength asperities at the plate interface where the subducting Pacific plate and the overriding Okhotsk plate are coupled strongly. A shallow high-V zone with large coseismic slip near the Japan Trench may account for the mainshock asperity of the 2011 Tohoku-oki earthquake. Because it is an isolated asperity surrounded by low-velocity patches, most stress on it was released in a short time and the plate interface became decoupled after the Mw 9.0 earthquake. Thus the overriding Okhotsk plate there was shot out toward the Japan Trench and caused the huge tsunami. Further details of the role of arc magma and fluids in the nucleation process of a large earthquake can be clarified by high-resolution geophysical imaging and multidisciplinary studies of the earthquake fault zones.

Keywords: fluids, earthquakes, Japan Islands, subduction zones, magma, slab

## Silicate solute in aqueous fluids governs trace element and stable isotope behavior in subduction zones

MYSEN, Bjorn<sup>1\*</sup>

<sup>1</sup>Geophysical Laboratory, CIW, USA

Physical and chemical properties of fluids equilibrated with subducting deep crust and overlying upper mantle are saturated in silicate components [1]. These components govern physical and chemical properties of the fluids. For example, the solution behavior of volatile components such as hydrogen, carbon, and nitrogen, which form bonding with silicate components in fluids, will differ from the behavior in pure H<sub>2</sub>O fluids [2]. This can also affect isotope fractionation between fluids and condensed silicate materials.

In pure H<sub>2</sub>O, hydrogen bonding plays a role to temperatures <600 °C at pressures in the 1 GPa-range with a  $\Delta H$  for hydrogen bond formation near 20 kJ/mol. At temperatures less than 600 °C, physical properties of fluids, including density, compressibility, and viscosity, are non-linear functions of temperature, whereas at higher temperature and in the absence of hydrogen bonding, these properties tend to become linear functions of temperature. Solution of silicate components in aqueous fluids changes these relationships. The silica solubility in equilibrium with quartz/coesite reaches >5 mol/kg near 5 GPa and 900 °C with polymerized silicate species, SiO<sub>4</sub>, Si<sub>2</sub>O<sub>7</sub>, and SiO<sub>3</sub> in the fluid. In equilibrium with enstatite and forsterite, the silicate solubility is ~50% less and only SiO<sub>4</sub> and Si<sub>2</sub>O<sub>7</sub> species exist in the fluids. Those variables affect D/H isotope ratios. For example, the fluid/melt partition coefficients for hydrogen, KH, varies by ~40% as a function of variable silicate speciation in fluids in the 500 °C-800 °C/0.5-1 GPa temperature and pressure range. The hydrogen fluid/melt partition coefficient exceeds that of deuterium. Their temperature-dependence also differs so that for the exchange equilibrium of D and H between coexisting water-saturated melt and silicate-saturated aqueous fluid, the  $\Delta H$  is between -4 and -6 kJ/mol. This difference is because in the more silicate-rich fluids (higher proportion of polymerized silicate species), the abundance ratio, OD/OH, is higher in the more polymerized silicate species in the fluid. As a result, increasing pressure, which leads to increasingly polymerization of silicate, will cause the D/H ratio of the fluid will increase. This also means that D/H fractionation between aqueous fluid and condensed silicate increases with increasing pressure.

Interaction between dissolved silicate components and other elements can also affect their solubility and, therefore, their roles as geochemical tracers. For example, in the system rutile+H<sub>2</sub>O, the Ti solubility in the few-GPa-range at ~1000 °C is on the order of 1-100 ppm as compared with thousands of ppm in silicate-saturated aqueous solution [3]. This difference between pure H<sub>2</sub>O and silicate-saturated fluid is related to interaction with the silicate species dissolved in the fluid,  $2M_6Si_2O_7 + 4H_2O + TiO_2 = 4(MH)_2SiO_4 + M_4TiO_4$ , where M is a metal cation. Similar situation likely exist for other nominally insoluble, highly charged elements (e.g., Al<sup>3+</sup>, Zr<sup>4+</sup>, Hf<sup>4+</sup>, P<sup>5+</sup>).

When modeling isotope fractionation and partitioning of nominally insoluble elements between fluid and condensed phases (melts and minerals) in the deep crust and upper mantle of the Earth, the silicate solute concentration and structure in the fluid and the water concentration and structure of silicate melts both can have major effects on the fractionation factors. These factors depend on the element or isotope ratio in question. They also vary with pressure (and likely temperature) because the structure of dissolved silicate in aqueous fluids varies with pressure and temperature.

[1] C. E. Manning, Earth Planet. Sci. Lett. 2004, 223, 1-16.

[2] B. O. Mysen, Lithos 2012, 148, 228-246.

[3] A. Antignano and C. E. Manning, Chemical Geology 2008, 255, 283-293.

Keywords: aqueous fluid, solubility, subduction, stable isotope, structure, fluid property

## D/H intramolecular partitioning in alkali silicate melts: with implications for tracing subduction processes

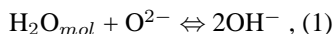
LE LOSQ, Charles<sup>1\*</sup> ; CODY, George<sup>1</sup> ; MYSEN, Bjorn<sup>1</sup>

<sup>1</sup>Geophysical Laboratory, Carnegie Institution of Washington

The D/H ratio is an important probe for studying the cycle of water in the Earth interior in general, and in subduction zones in particular. Indeed, D/H ratios in melt inclusions (MIs) of arc magmas for instance indicate that the  $\delta D$  of subduction fluids is high, near -30 ‰, compared to the  $\delta D$  of the mantle that is near -80 ‰. A possible explanation for these different values is that D/H fractionation during dehydration of the slab in subduction zones enriches the subduction fluids in D, leading to high  $\delta D$  values in subduction magmas. This might be accomplished with hydrogen exchange between the melt and another source enriched in D before entrapment of MIs or a diffusive loss of H from within the inclusion leading to D/H fractionation. However, chemical effects affecting the  $\delta D$  ratio have not been considered because it is usually assumed that D and H have the same chemical and structural properties in silicate melts and glasses.

However, recent results from <sup>2</sup>H and <sup>1</sup>H MAS NMR of Na<sub>2</sub>Si<sub>4</sub>O<sub>9</sub> glasses quenched from melt (equilibrated with fluid at 1400°C and 1.5 GPa) with various amounts of (D<sub>x</sub>H<sub>(1-x)</sub>)<sub>2</sub>O (x = D/[D+H]) lead to the conclusion that D and H isotopes occupy different structural positions in the network. From the <sup>1</sup>H MAS NMR spectra OH<sup>-</sup> groups are distributed in two environments with mean O...O distances close to 0.26 and 0.29 nm in the Na<sub>2</sub>Si<sub>4</sub>O<sub>9</sub> glass. These environments give rise to two strong NMR lines at 16 and 5 ppm respectively. By contrary, <sup>2</sup>H MAS NMR spectra of the same glasses display a strong line at 16 ppm accompanied by a small band near 5 ppm regardless of D/H ratio and total water concentration. This observation leads to the suggestion that OD<sup>-</sup> groups are mainly present in an environment with small O...O distances. In other words, the structural behavior of OH<sup>-</sup> and OD<sup>-</sup> groups in the quenched silicate melts (glasses) differs.

In M<sub>2</sub>Si<sub>4</sub>O<sub>9</sub> glasses, (M = Li, Na or K) with different concentrations of pure H<sub>2</sub>O or D<sub>2</sub>O (from 3.3 up to 17.6 mol%), <sup>2</sup>H and <sup>1</sup>H MAS NMR spectra confirm that by exchanging H with D the intensity of the 16 ppm NMR line increases greatly, whereas the intensity of the 5 ppm line decreases drastically. Interestingly, such a spectral evolution is also observed when increasing the size of the alkali element in the network of hydrous alkali silicate glass. These effects are attributed to steric and electronic effects in the environment of alkali elements, which cause shifts in the equilibrium between H<sub>2</sub>O and O<sup>2-</sup> of the silicate network:



The specific preference of OD<sup>-</sup> groups for small O...O sites is in this mind intriguing, but is not in conflict with previous observations. Indeed, increasing the ionic size of alkali elements lead to promote OH<sup>-</sup> in the small O...O environment. Similarly, it appears that increasing the size of the proton (by substituting H by D) promotes their existence in this small O...O environment. On this basis, we propose that those two observations have a common origin, maybe related to the probability of interaction between H/D and alkali elements depending of their ionic size and/or to molar volume effects related to those ionic sizes.

This large structural-controlled partitioning of D and H in melts, which depends on the melt composition, might be another fractionation process affecting the  $\delta D$  of subduction melts. Consequently,  $\delta D$  values recorded in MIs might be the result of such a structural process and might not reflect the  $\delta D$  of released fluids in the mantle wedge during slab subduction.

Keywords: D/H isotopes, silicate glass, NMR spectroscopy, Raman spectroscopy, Subduction fluids

## Speciation and solubility of F and Cl in coexisting fluids and silicate melts: implications for F and Cl signature in arc

DALOU, Celia<sup>1\*</sup> ; MYSEN, Bjorn<sup>2</sup> ; FOUSTOUKOS, Dionysis<sup>2</sup>

<sup>1</sup>Jackson School of Geosciences, The University of Texas at Austin, <sup>2</sup>Geophysical Laboratory, Carnegie Institution of Washington

The effect of pressure and temperature on the structure of silicate melts coexisting with silica-saturated aqueous electrolyte solutions enriched in fluorine or chlorine in the  $\text{Na}_2\text{O}-\text{Al}_2\text{O}_3-\text{SiO}_2-\text{H}_2\text{O}$  system has been determined. In-situ measurements were conducted with the samples at desired temperatures and pressures in a hydrothermal diamond anvil cell (HDAC) by using microRaman and FTIR spectroscopy techniques. The data were acquired at high temperature and pressure (up to 800°C and 1264 MPa, respectively), and during cooling/decompression to ambient conditions.

The intensity of the Raman bands assigned to stretch vibration of the OH-groups relative to those of coexisting molecular  $\text{H}_2\text{O}$  in silicate melts is lower in the presence of F and Cl. This difference reflects the interaction of F or Cl with  $\text{H}_2\text{O}$  in the melts. With decreasing pressure and temperature (P-T) conditions, SiF complexes are favored in the melt rather than in the fluid, perhaps because of decreasing silicate concentration in fluids with decreasing temperature and pressure. In melts, the solubility of Cl, likely in the form of  $\text{NaCl}_{(aq)}$ , increases with decreasing P-T conditions, whereas the abundance of such complexes in coexisting fluids decreases.

Our experiments data were employed to help model the ascent of a magma-fluid system from the upper mantle to the shallow crust. The information offers particular insights into F and Cl partitioning between and the speciation of F and Cl in melts and magmatic fluids. We suggest that the formation of stable SiF and NaCl complexes and their increasing solubilities during magma ascent explain the late volcanic degassing of F and Cl, compared to other volatile species.

It explains why F and Cl are often undersaturated in arc basaltic magmas (Carroll and Webster, 1994), indicating that they often do not a significant experience a degassing event. In contrast to  $\text{H}_2\text{O}$ ,  $\text{CO}_2$  and S, F and Cl signature in primary arc magmas (arc melt inclusions) can be considered as primary and likely retain information on arc magma sources.

Those results also imply that, while Cl is enriched in aqueous fluids from slab dehydration, F preferentially dissolves in slab melts or supercritical fluids, during flows from the subducted slab into the zone of melting in the mantle wedge. It is therefore expected that at given pressure and temperature, the Cl/F ratio is significantly lower in slab melt and supercritical fluids, than in aqueous fluids. This difference in Cl/F signatures decrease when slab components are dragged down to the deep mantle.

Keywords: Fluorine, Chlorine, silicate melt, aqueous fluid, speciation, HDAC

## The Structure of Water-Saturated Carbonate Melts

FOUSTOUKOS, Dionysis<sup>1\*</sup>; MYSEN, Bjorn O.<sup>1</sup>

<sup>1</sup>Geophysical Laboratory, Carnegie Institution of Washington, USA

The structure of water-saturated Ca- and Mg-bearing carbonate melts under reducing and oxidizing conditions was investigated in a series of hydrothermal anvil cell experiments conducted at 400 - 1100 °C and 442 - 2839 MPa. Equilibria were investigated in the calcite-H<sub>2</sub>O, calcite-CaO-H<sub>2</sub>O, magnesite-H<sub>2</sub>O and magnesite-MgO-H<sub>2</sub>O systems, with redox conditions controlled by Re/ReO<sub>2</sub> and Ti/TiO<sub>2</sub> assemblages. Melting relationships and the C-O-H speciation of the coexisting aqueous fluid and melt were assessed in-situ by Raman vibrational spectroscopy. Hydrous melting of MgCO<sub>3</sub>-MgO occurred at ~850 °C, 1.5 - 2 GPa. In the CaCO<sub>3</sub>-CaO-H<sub>2</sub>O system, melt was formed at 600 - 900 °C and pressures of 0.5 - 1.5 GPa because of melting-point depression imposed by the presence of CaO. The C-O-H speciation of the carbonate melts and coexisting supercritical aqueous solutions was mainly H<sub>2</sub>O and CO<sub>3</sub><sup>2-</sup>, with traces of CO<sub>2(aq)</sub> and CH<sub>4(aq)</sub> in the fluid phase. The melt-fluid H<sub>2</sub>O partition coefficients attained in the Mg-bearing melt (median 0.5) were higher than in the Ca-bearing melt (median 0.3). Under oxidizing redox conditions, dissolved ReO<sub>4</sub><sup>-</sup> was present in all phases, underscoring the enhanced solubility of trace elements and metals in carbonate-bearing melts and carbonatites. In effect, the enhanced solubility of H<sub>2</sub>O along with the ionic nature of the carbonate melts may promote the solvation of ionic species in the melt structure.

From in-situ vibrational spectroscopy, the  $\nu_1$ -CO<sub>3</sub><sup>2-</sup> vibration recorded in the melt spectra suggests the presence of intermolecular interactions between the oxygen of the carbonate ion with water dissolved in the melt. The thermodynamic properties of this water appear to be similar to the supercritical aqueous phase. For example, the estimated enthalpy for the breakage of the hydrogen bonding between water molecules attained values of  $6.8 \pm 1.5$  kcal/mol and  $8.4 \pm 1.3$  kcal/mol in the melt and fluid phase, respectively. The calculated partial molar volume of H<sub>2</sub>O in the melt ( $\sim 48 \pm 6$  cm<sup>3</sup>/mol) is also comparable to the partial molar volume of supercritical water at similar conditions. Interestingly, this value is considerably greater than published partial molar volume values for H<sub>2</sub>O in silicate melts (10-12 cm<sup>3</sup>/mol).

The pressure-temperature melting relationships of the CaO-CO<sub>2</sub>-H<sub>2</sub>O and MgO-CO<sub>2</sub>-H<sub>2</sub>O systems highlight the important role of water and alkali earth oxides on the hydrous melting of the carbonate-bearing subducting oceanic crust. Carbonates present in marine sediments or serpentinized peridotites may melt before complete dehydration at the slab-mantle wedge transition zone, and thus, never reach sub-arc depths. To this end, melting of carbonate minerals at crustal temperatures and pressure can contribute to the volcanic CO<sub>2</sub> flux at the arc through melt/fluid interactions.

Keywords: carbonate melt, aqueous solutions, hydrothermal diamond anvil cell, raman vibrational spectroscopy

## Later phase observations and seismic velocity structure in the subducting crust of the Pacific slab beneath Hokkaido

SHIINA, Takahiro<sup>1\*</sup> ; NAKAJIMA, Junichi<sup>1</sup> ; TOYOKUNI, Genti<sup>1</sup> ; MATSUZAWA, Toru<sup>1</sup> ; KITA, Saeko<sup>2</sup>

<sup>1</sup>RCPEV, Grad. Sch. of Sci., Tohoku Univ., <sup>2</sup>NIED

The subducting crust at the uppermost part of the oceanic lithosphere is considered to play important roles for generation of intraslab earthquakes (e.g., Kirby et al., 1996) and arc-magmatism in the mantle wedge (e.g., Nakajima et al., 2013), because the crust involves a large amount of water in form of hydrous minerals and these hydrous minerals affect seismic velocities in the crust (e.g., Hacker et al., 2003). Therefore, to understand water circulation in the subduction zones and genesis of intermediate-depth earthquakes, it is important to reveal where dehydration reaction of hydrous minerals occurs in the crust. However, it is generally difficult to obtain the detailed velocity variation in the crust because the thickness of the crust is ~7 km.

Later phases, such as mode-converted wave and guided wave, are sensitive to heterogeneous structure in the crust because of their longer propagation paths in the crust, and hence they are very useful to resolve small-scale seismic velocity structure in the crust (e.g., Matsuzawa et al., 1986; Abers, 2005).

At the Hidaka mountain range, middle of Hokkaido, northern Japan, some later phases are reported from earthquakes that occurred in the Pacific slab (e.g., Shimizu and Maeda, 1980). A later phase (Xp phase) recorded in this region has some characteristics: 1) amplitudes of Xp phase are similar to or larger than those of the P wave, 2) Xp-P time lies in a range of 2-10 s and increases with epicentral distances. Shiina et al. (2013, SSJ) discussed the origin of the Xp phase with numerical modeling and interpreted the Xp phase as guided P-wave that propagated in the crust. Moreover, we identified a later phase (Xs phase) that arrives several second after the theoretical initial S waves, and such a phase usually appears in seismograms with guided P-wave. We interpreted the Xs phase as guided S-wave by comparison characteristics of guided P-wave and results of numerical modeling.

In this study, based on these interpretations for later phases that observed in the western part of Hidaka mountain range, we estimated P- and S-wave velocity distributions in the subducting crust beneath the eastern part of Hokkaido. The number of arrival times of guided P- and S-waves picked in this study is 117 records and 56 records, respectively. Then, we obtained Vp of 6.8-7.7 km/s and Vs of 3.5-4.0 km/s at depths of 50-100 km in the crust. The obtained Vp in the crust is similar to that observed beneath Tohoku (Shiina et al., 2013) and lower than that expected for fully-hydrated MORB materials (e.g., Hacker et al., 2003). This result suggests that aqueous fluids may co-exist with hydrous minerals in the crust beneath the eastern part of Hokkaido.

Keywords: subducting crust, later phase, guided wave, the Pacific slab

## Pore fluid geochemistry and carbonates in cores and cuttings from the Nankai accretionary prism

EVEN, Emilie<sup>1\*</sup> ; SAMPLE, James C.<sup>2</sup> ; FUCHIDA, Shigeshi<sup>1</sup> ; IODP EXPEDITION 348, Shipboard scientists<sup>3</sup>

<sup>1</sup>Graduate School of Science, Osaka City University, <sup>2</sup>School of Earth Sciences and Environmental Sustainability, Northern Arizona University, <sup>3</sup>IODP Expedition 348

The recent IODP Exp 348 at Site C0002 has successfully deepened Hole C0002F (Exp 338) down to 3058.5 mbsf, deep into the accretionary prism of the Nankai Trough. During Exp 348, cuttings were collected and analysed from drilled interval of Holes C0002N (875 mbsf- 2325 mbsf) and C0002P (1965 mbsf- 3059 bsf) and limited coring was performed from 2163 to 2218 mbsf in Hole C0002P. The major-element composition of the solid cuttings and the geochemistry of interstitial water in cores was determined. Results provide insights into exchange of elements between minerals and pore water phases, and into geochemical signatures related to lithological changes within the prism. This study reports the main geochemical results from IODP Exp 348.

Interstitial waters were collected using the GRIND method (Wheat et al., 1994), in which core sediments were ground in an agate mill with ultra-pure water. The interstitial water percentage was determined by drying sediments at 60 °C and 105 °C, the former to minimize loss of clay-bound water, and the latter to follow the GRIND procedure used in previous expeditions. Concentrations were interpreted with data corrected for dilution at 60 °C, 105 °C and normalised to chlorinity values. Profiles of carbonates (as CaCO<sub>3</sub>), organic carbon and total nitrogen were determined from cuttings of 1-4 mm and >4 mm sizes and are compared with the observed lithological boundaries. Carbonate veins were observed in a core sample exhibiting a fault zone at ~2205 mbsf, but no increase was observed at the same depth in the carbonates profile.

The GRIND method has limitations in recovering absolute values of dissolved ions in interstitial waters, and yielded very high dissolved-ion concentrations in some samples. But comparison of ions normalized to chlorinity yielded results comparable to what was observed in pore waters at shallower depths of Site C0002. Some of the trend variations in the cuttings profiles of carbonates, organic carbon and nitrogen match the unit boundaries determined by observation of lithological changes in the cuttings. Therefore, it can be suggested to integrate these data when defining geological units.

*Wheat, Boulegue and Mottl (1994) Proc. ODP, Sci. Results, 139: College Station, TX (Ocean Drilling Program), 429-437*

Keywords: Accretionary prism, GRIND method, IODP Expedition 348, Nankai Trough, Pore water

## Solution mechanism of water in depolymerized silicate melts

CHERTKOVA, Nadezda<sup>1\*</sup> ; YAMASHITA, Shigeru<sup>1</sup>

<sup>1</sup>Okayama University, ISEI

It is known that the effect of dissolved water on the viscosity of silicate melts is larger for polymerized melts than for depolymerized melts [e.g., 1, 2]. Direct spectroscopic measurements of melt structure and water speciation at high temperature provide information about the mechanism of water dissolution and its influence on the physical properties of the melts. While *in situ* measurements of water speciation were widely conducted for rhyolitic melts and their analogues [e.g., 3, 4, 5], only limited data are available for depolymerized silicate melts.

We performed high-temperature near-infrared and Raman spectroscopic measurements of hydrous  $\text{Na}_2\text{Si}_2\text{O}_5$  melts (2.3-8.1wt%  $\text{H}_2\text{O}$ ) using externally heated diamond anvil cell (HDAC).  $\text{Na}_2\text{Si}_2\text{O}_5$  composition was chosen as a structural analogue of basaltic melt (anhydrous NBO/T = 1). Experimental pressure was monitored with the pressure- and temperature-dependent Raman shift of  $^{13}\text{C}$  diamond [6]. Near-infrared spectra of the homogeneous liquid phase, observed above 820 degree C, 1.7GPa in the  $\text{Na}_2\text{Si}_2\text{O}_5+2.3\text{wt}\%\text{H}_2\text{O}$  system and above 700 degree C, 1.6GPa in the  $\text{Na}_2\text{Si}_2\text{O}_5+8.1\text{wt}\%\text{H}_2\text{O}$  system, contain absorption peaks corresponding to molecular  $\text{H}_2\text{O}$  (at  $\sim 5200\text{ cm}^{-1}$ ) and structurally bound OH groups (at  $\sim 4500\text{ cm}^{-1}$ ). At 900 degree C and 1.6-1.9GPa the ratio of these peaks height remains approximately constant (2.6-2.2), implying a constant (structurally bound OH)/(molecular  $\text{H}_2\text{O}$ ) ratio for this range of water contents. This observation differs from the regularities reported for more polymerized melts (rapid decrease of OH/ $\text{H}_2\text{O}$  with total water content) [e.g., 4, 7]. At the same time no pressure effect on the ratio of  $4500\text{ cm}^{-1}$  peak height to  $5200\text{ cm}^{-1}$  peak was observed below 2.4 GPa.

### References

- [1] Whittington A., Richet P., Holtz F. (2000) *Geochim Cosmochim Acta* 64, 3725-3736.
- [2] Giordano D., Russell J.K., Dingwell D.B. (2008) *Earth. Planet. Sci. Lett.* 271, 123-134.
- [3] Sowerby J.R., Keppler H. (1999) *Am. Mineral.* 84, 1843-1849.
- [4] Nowak M., Behrens H. (2001) *Earth. Planet. Sci. Lett.* 184, 515-522.
- [5] Shen A.H., Keppler H. (1995) *Am. Mineral.* 80, 1335-1338.
- [6] Mysen B.O., Yamashita S. (2010) *Geochim. Cosmochim. Acta* 74, 4577-4588.
- [6] Mysen B.O. (2010) *Geochim. Cosmochim. Acta* 74, 4123-4139.
- [7] Botcharnikov R.E., Behrens H., Holtz F. (2006) *Chem. Geol.* 229, 125-143.

Keywords: water speciation, hydrothermal diamond anvil cell, near-infrared spectroscopy, Raman spectroscopy

## Effect of the upper mantle structure on the Moho geometry

TENZER, Robert<sup>1\*</sup> ; CHEN, Wenjin<sup>1</sup>

<sup>1</sup>School of Geodesy and Geomatics, Wuhan University

We investigate the effect of the lateral density structure within the upper (most) mantle on the Moho geometry. The gravimetric forward and inverse modeling methods are applied to determine the Moho depths using the gravity data corrected for major known anomalous density structures within the Earth crust. In our numerical experiment we compute and compare the Moho geometry determined using uniform and laterally varying models of the Moho density contrast. The laterally varying model of the Moho density contrast incorporates the information on the upper mantle lateral density structure taken from the CRUST1.0 global crustal model. For the uniform density contrast model, the constant value of the Moho density contrast is determined based on minimizing the spatial correlation between the gravity data and the Moho geometry. Except for the upper (most) mantle, the deeper heterogeneous mantle density structures including the core-mantle boundary zone are not taken into consideration due to the absence of a reliable 3-D density model of the whole mantle. The numerical results revealed that the consideration of the upper mantle density structure improves the fit of the gravimetric solution with the seismic Moho model.

Keywords: crust, density, gravity, mantle, Moho

## Conductivity anisotropy of partial molten peridotite under shear deformation

ZHANG, Baohua<sup>1</sup> ; YOSHINO, Takashi<sup>1\*</sup> ; YAMAZAKI, Daisuke<sup>1</sup>

<sup>1</sup>Institute for Study of the Earth's Interior, Okayama Univ.

Recent ocean bottom magnetotelluric investigations have revealed a high-conductivity layer (HCL) with high anisotropy characterized by higher conductivity values in the direction parallel to the plate motion beneath the southern East Pacific Rise (Evans et al., 2005) and beneath the edge of the Cocos plate at the Middle America trench offshore of Nicaragua (Naif et al., 2013). These geophysical observations have been attributed to either hydration (water) of mantle minerals or the presence of partial melt. Currently, aligned partial melt has been regarded as the most preferable candidate for explaining the conductivity anisotropy because of the implausibility of proton conduction (Yoshino et al., 2006).

In this study, we report development of the conductivity anisotropy of partial molten peridotite in three directions parallel and normal to shear on the shear plane, and perpendicular to the shear plane as a function of time and shear strain. Starting samples were pre-synthesized partial molten peridotite (Fe-free and Fe-bearing systems), showing homogeneous melt distribution. The Fe-free and Fe-bearing partially molten peridotite samples were deformed in simple shear geometry at 1 GPa and 1523 and 1723 K, respectively, in a DIA-type apparatus with uniaxial deformation facility. Conductivity of the partially molten peridotite parallel to the shear direction was initially identical to that normal to shear. However, shear-parallel conductivity increased by more than one order of magnitude after the initiation of shear by piston advancement. Shear-parallel conductivity then stayed constant for the duration of the experimental run. On the other hand, conductivity normal to the shear direction on the shear plane remained constant, whereas conductivity perpendicular to the shear plane decreased gradually after initiation of shear and finally close to that of olivine. Conductivity difference between parallel and normal to shear direction reached one order, which is equivalent to that observed beneath asthenosphere. In contrast, such anisotropic behavior was not found in the melt-free samples, suggesting that development of the conductivity anisotropy was generated under shear stress.

Microstructure of the deformed partial molten peridotite shows partial melt tends to preferentially locate grain boundaries parallel to shear direction, and forms continuously thin melt layer sub-parallel to the shear direction, whereas apparently isolated distribution was observed on the section perpendicular to the shear direction. The resultant melt morphology can be approximated by tube like geometry parallel to the shear direction. This observation suggests that the development of conductivity anisotropy is caused by the realignment of partial melt (forming tube-like melt) parallel to shear direction in the silicate matrix.

In conclusion, the high anisotropy of conductivity in the direction of plate motion can be well explained by anisotropic interconnection of melt in partially molten rocks at the top of asthenosphere, but not hydration of nominally anhydrous minerals. Therefore, our results provide the direct experimental evidence for supporting these geophysically observed high-conductivity anisotropy at the LAB and verify the validity of partial melting hypothesis (Yoshino et al., 2006; Naif et al., 2013).

### References

- Evans, R. L. et al. Geophysical evidence from the MELT area for compositional controls on oceanic plates. *Nature* 437, 249-252 (2005).
- Naif, S., Key, K., Constable, S. & Evans, R. L. Melt-rich channel observed at the lithosphere-asthenosphere boundary. *Nature* 495, 356-359 (2013).
- Yoshino, T., Matsuzaki, T., Yamashita, S. & Katsura, T. Hydrous olivine unable to account for conductivity anomaly at the top of the asthenosphere. *Nature* 443, 973-976 (2006).

Keywords: partial melting, asthenosphere, electrical conductivity, upper mantle, anisotropy, shear deformation

## Surface-wave phase velocity maps of North America with inter-station waveform analysis

HAMADA, Kouta<sup>1\*</sup> ; YOSHIZAWA, Kazunori<sup>2</sup>

<sup>1</sup>Graduate School of Science, Hokkaido University, <sup>2</sup>Faculty of Science, Hokkaido University

The western United States encompasses a variety of tectonic features, including regions with east-west extension, volcanic areas and relatively stable cratonic regions.

In the last decade, the Transportable Array (USArray) has been installed throughout the U.S, and these waveform data have facilitated a variety of tomographic studies in this region using body and surface waves, and ambient noise analysis making the most of the high-density seismic network.

In this study, we have developed a new method of fully non-linear waveform fitting to measure inter-station phase velocities, using the Neighborhood Algorithm (NA) as a global optimizer. This algorithm searches for model parameters to fit two observed waveforms on a common great-circle path by perturbing the phase term of the fundamental-mode Love and Rayleigh waves. We have employed the reliability parameter, which represents how well the waveforms at two stations can be fitted in a time-frequency domain. This parameter is used as a data selection criterion for the subsequent step of phase velocity mapping.

The method has been applied to observed waveform data of the USArray from 2007 to 2010, and we could collect a large-number of phase speed data (over 45000 for Rayleigh and 15000 for Love) in a period range from 30 and 200 seconds, at short distances less than 1000 km. The phase velocity models for Rayleigh and Love waves indicate good correlation on large scales with the recent tomographic maps derived from different approaches for inter-station phase velocity measurements (Foster et al., 2013); e.g., significant slow velocity anomaly in volcanic regions in western Unites States and extremely fast anomaly in the cratonic region in the longer period range, which implies the robustness of such tectonic features as well as the validity of our new measurement technique. The current method can be expanded for the measurements of inter-station higher-mode phase velocities, which will be of great help in enhancing the vertical resolution of the 3-D shear wave models.

Keywords: surface wave, phase velocity, tomography, North America

## Diffusion to dislocation creep transition in the upper mantle inferred from silicon grain boundary diffusion rates

FEI, Hongzhan<sup>1\*</sup>; KATSURA, Tomoo<sup>2</sup>; KOIZUMI, Sanae<sup>3</sup>; SAKAMOTO, Naoya<sup>4</sup>; HASHIGUCHI, Minako<sup>5</sup>; YURIMOTO, Hisayoshi<sup>5</sup>; YAMAZAKI, Daisuke<sup>1</sup>

<sup>1</sup>Institute for Study of the Earth's Interior, Okayama University, Japan, <sup>2</sup>Bayerisches Geoinstitut, University of Bayreuth, Germany, <sup>3</sup>Earthquake Research Institute, The University of Tokyo, Japan, <sup>4</sup>Isotope Imaging Laboratory, CRI, Hokkaido University, Japan, <sup>5</sup>Department of Natural History Sciences, Hokkaido University, Japan

The majority of the dynamical processes in the upper mantle are controlled by creep of minerals. Dislocation creep causes non-Newtonian viscosity and seismic anisotropy whereas diffusion creep causes Newtonian viscosity and no seismic anisotropy. Determination of deformation mechanism in the upper interior is thus essential to understand mantle dynamics. Previous deformation studies on olivine suggested that the shallow regions of the upper mantle should be dominated by dislocation creep and the deeper regions dominated by diffusion creep [Karato, 1992; Karato and Wu, 1993; Hirth and Kohlstedt, 2003]. However, recent study [Fei et al., 2013] demonstrated that those deformation experiments largely misunderstood the creep rate due to the experimental difficulties. Since the creep of olivine is controlled by silicon diffusion, we measured silicon grain-boundary diffusion coefficient in Mg-olivine aggregates as a function of pressure, temperature, and water content. The activation energy, activation volume, and water content exponent are found to be 240-260 kJ/mol,  $1.8 \pm 0.2$  cm<sup>3</sup>/mol, and  $0.22 \pm 0.05$ , respectively. Together with the silicon lattice diffusion data [Fei et al., 2012; 2013], our results predict the diffusion to dislocation creep transition in the upper mantle, which is in contrast with the previously considered model. In the asthenosphere, dislocation creep should dominate because of the high temperature. In the lithosphere, diffusion creep dominates in shallow regions and dislocation creep dominates in deeper parts. The seismic anisotropy jumps at mid-lithosphere discontinuity beneath continents and at Gutenberg discontinuity beneath oceans are caused by the transition from diffusion to dislocation creep. The weak anisotropy in cold lithospheres could be attributed to the fossil anisotropy formed at the spreading ridges. Dominance of diffusion creep in upper lithosphere accounts for the Newtonian rheology suggested by postglacial rebound.

Fei et al., *EPSL* **345**, 95-103 (2012).

Fei et al., *Nature* **498**, 213-215 (2013).

Hirth and Kohlstedt, *Geophys. Monogr.* **138**, 83-105 (2003).

Karato, *JGR* **19**, 2255-2258 (1992).

Karato and Wu, *Science* **260**, 771-778 (1993).

Keywords: diffusion creep, dislocation creep, upper mantle, silicon, grain boundary diffusion, deformation mechanism

## Aluminum incorporation into phase A - a new hydrous silicate in the deep upper mantle

CAI, Nao<sup>1\*</sup> ; INOUE, Toru<sup>1</sup> ; FUJINO, Kiyoshi<sup>1</sup> ; OHFUJI, Hiroaki<sup>1</sup> ; KURIBAYASHI, Takahiro<sup>2</sup> ; YURIMOTO, Hisayoshi<sup>3</sup>

<sup>1</sup>Geodynamics Research Center, Ehime University, <sup>2</sup>Institute of Mineralogy, Petrology and Economic Geology, Graduate School of Science, Tohoku University, <sup>3</sup>Division of Earth and Planetary Sciences, Hokaido University

A new aluminum bearing hydrous silicate was found in the experiments under the deep upper mantle conditions, using phase A ( $\text{Mg}_7\text{Si}_2\text{O}_8(\text{OH})_6$ ) and  $\text{Al}(\text{OH})_3$  as the starting materials. Using electron probe micro analysis (EPMA) and secondary ion mass spectrometry (SIMS), the composition was determined to be very close to  $\text{Mg}_{5.5}\text{AlSi}_2\text{O}_8(\text{OH})_6$ , which contained about 12 wt % of water. Almost pure phase was obtained in the subsequent experiments. The powder x-ray diffraction pattern and transmission electron diffraction patterns showed a hexagonal structure, with an abnormal large c axis. This new phase has similar stability region with phase A. At lower pressure and higher temperature, it breaks down into Chondrodite + Garnet + Brucite + Fluid, while at higher pressure and higher temperature, it breaks down into Al-superhydrous phase B + Garnet + Brucite + Fluid.

Besides, present study shows that phase A coexists with this aluminum bearing hydrous phase, with a small amount of aluminum (<1 wt%) incorporated into phase A structure, which predicts that phase A can preserve only trace of aluminum.

According to Inoue's unpublished data, aluminum can easily incorporate into some dense hydrous magnesium silicates and form aluminum bearing hydrous phases such as phase B, superhydrous phase B, and even perovskite. However, rather than aluminum bearing phase A, the present study shows a small amount of aluminum incorporation into phase A structure, and an appearance of a new aluminum bearing hydrous phase, with the composition very similar to phase A but structure very different from it. Further investigations are needed to clarify these two phases.

**Keywords:** Phase A, Aluminum incorporation, hydrous phase, upper mantle

## Changbai intraplate volcanism and deep earthquakes in Northeast Asia

ZHAO, Dapeng<sup>1\*</sup> ; TIAN, You<sup>1</sup>

<sup>1</sup>Tohoku University, Department of Geophysics

The origin of the intraplate volcanoes in Northeast Asia is considered to be associated with upwelling of hot and wet asthenospheric materials in the big mantle wedge above the stagnant Pacific slab in the mantle transition zone. Among these intraplate volcanoes, Changbai is the largest and most active one, and very deep earthquakes (500-600 km depths) in the Pacific slab under East Asia occur ~300 km to the east of the Changbai volcano. Integrating the findings of geophysical, geochemical and petrologic studies so far, we suggest a link between the Changbai volcanism and the deep earthquakes in the Pacific slab. Many large shallow earthquakes occurred in the Pacific plate in the outer-rise areas close to the oceanic trench, and seawater may enter down to the deep portion of the oceanic lithosphere through the active normal faults which generated the large outer-rise earthquakes. The seawater or fluids may be preserved in the active faults even after the Pacific plate subducts into the mantle. Many large deep earthquakes are observed that took place in the subducting Pacific slab under the Japan Sea and the East Asian margin. At least some of the large deep earthquakes are caused by the reactivation of the faults preserved in the subducting slab, and the fluids preserved in the faults within the slab may cause the observed non-double-couple components in the deep earthquake faulting. The fluids preserved in the slab may be released to the overlying mantle wedge through the large deep earthquakes. Because large deep earthquakes occur frequently in the vicinity of the Changbai volcano, much more fluids could be supplied to this volcano than other areas in Northeast Asia, making Changbai the largest and most active intraplate volcano in the region.

### Reference

Zhao, D., Y. Tian (2013) Changbai intraplate volcanism and deep earthquakes in East Asia: A possible link? *Geophys. J. Int.* 195, 706-724.

Keywords: volcanoes, deep earthquakes, Asia, slab

## Semiconductor diamond heater (SCD): An innovation for ultrahigh temperature experiments in the Kawai cell

XIE, Longjian<sup>1\*</sup> ; ITO, Eiji<sup>1</sup> ; YONENDA, Akira<sup>1</sup>

<sup>1</sup>Institute for Study of the Earth Interior , Okayama University

We developed the semi-conductor diamond heater in the Kawai high pressure cell. The starting material of the semi-conductor diamond heater is born(B)-doped burned-graphite. We succeeded to improve the machinability of the B-doped burned-graphite by decreasing porosity. Following is the motivation and the background of the semi-conductor diamond heater project.

It is important to generate extremely high temperature (~3000 °C) in a large sample volume (~0.1mm<sup>3</sup>) in the Kawai apparatus. X-ray transparency is also desirable for in-situ synchrotron analysis. However, any traditional heater used in the Kawai apparatus so far does not satisfy the both requirements simultaneously.

Semiconductor diamond is a candidate material to generate temperatures higher than 3000 °C with low x-ray absorption. Anton Shatskiy (2009) have generated a temperature of 3500 °C by using the semiconductor diamond heater in a large-volume Kawai-type high-pressure apparatus, although their temperature measurement is questionable from a viewpoint of the power-temperature relation. Furthermore, their semi-conducted diamond heater, made of boron and graphite powders, was not machinable and difficult to control the temperatures. It often became unstable at around 1000~1300 °C and impossible to generate higher temperature.

Systematic experiments have done to improve the performance of the semiconductor heater. We used a machinable block of graphite contain 3 wt.% boron as the starting material for the semi-conductor diamond heater. The graphite-diamond transformation started at ~1000-1200 °C at 15 GPa in the Kawai apparatus. After the transformation, we stably generated temperature to 2000 °C. Activation energy of B-doped diamond is about 0.1 eV, which is much lower than that of pure diamond (5.45eV).

### References:

Anton Shatskiy, Daisuke Yamazaki, Guillaume Morard, Titus Cooray, Takuya Matsuzaki et al. , Review of Scientific Instruments 80, 023907 (2009).

Keywords: Semiconductor Diamond Heater, Ultrahigh Temperature, Kawai Cell

## Recent Global Tomography Models: Where are We Heading for?

TAKEUCHI, Nozomu<sup>1\*</sup>

<sup>1</sup>Earthquake Research Institute, University of Tokyo

Many high-resolution global tomography models have been obtained and we now have consensus about overall features of 3-D heterogeneous structure in the Earth. Majority of models have been obtained by using conventional ray theory which assumes that scale length of lateral heterogeneities is sufficiently large compared with wavelength of seismic waves analyzed.

Primary efforts in recent studies appear to introduce better theories to overcome resolution limits caused by the above-mentioned assumption. The efforts include delay time tomography with finite frequency kernels (e.g., Montelli et al. 2004, *Science*; Obayashi et al. 2013, *GRL*) and waveform tomography with 2-D (e.g, Li and Romanowicz 1996, *GJI*, Panning and Romanowicz 2004, *Science*) or 3-D (e.g, Takeuchi 2007, *GJI*; Takeuchi 2012, *EPSL*) finite frequency kernels. Waveform tomography with further better theories is also becoming feasible (e.g., Lekic and Romanowicz 2011, *GJI*; French et al. 2013, *Science*).

In this presentation, I want to propose another direction to improve resolution: use of a new type of dataset. I will propose to use incoherent part of seismic signals (i.e., scattering waves or coda waves). Scattering waves are sensitive to heterogeneities whose scale length is comparable with wavelength of seismic waves analyzed. Use of such waves therefore should provide new information beyond resolution limit of ray theory. At the time of the presentation, I plan to show feasibility and examples of such analyses to reveal distribution of smaller scale heterogeneities in the subduction zone around Japan.

Keywords: tomography, scattering wave, seismology

## Lattice preferred orientation of stishovite in deformation experiment

XU, Fang<sup>1\*</sup> ; YAMAZAKI, Daisuke<sup>1</sup> ; TSUJINO, Noriyoshi<sup>1</sup>

<sup>1</sup>ISEI, Okayama University

Seismic observations reveal strong negative anisotropy ( $V_{SV} > V_{SH}$ ) at around 550 km depth in the lower part of mantle transition zone (Visser et al., 2008). The mantle tomography indicates the obvious association of this negative anisotropy with the subduction zones (Panning and Romanowicz., 2006). The observed anisotropy can be caused by lattice preferred orientation (LPO) of constituting material when the material is elastically anisotropic. Majorite and ringwoodite, which are the dominant minerals in this region, are nearly isotropic (Chai et al., 1997; Weidner et al., 1984). On the other hand, stishovite, which may occur in significant amounts in this region derived from the delaminated subducting basaltic layer (Karato et al., 1997) and continental crust (Kawai et al., 2012), shows strong elastic anisotropy ( $V_{SV}/V_{SH}$  is as large as 150%) indicated by the acoustic velocities study (Yoneda et al., 2012) on single crystal of stishovite. Therefore, the LPO of stishovite has a high potential to interpret the seismic anisotropy in the lower part of the transition zone and indicate the geometry of mantle flow.

To investigate the LPO of stishovite, deformation experiments on stishovite were conducted in both simple shear and uni-axial geometry. We prepared starting material of polycrystalline stishovite with grain size of  $\sim 10 \mu\text{m}$  at 12 GPa and 1450 °C in a Kawai-type high-pressure apparatus. Then deformation experiments were carried out at 12 GPa and 1600 °C by Kawai-type apparatus for tri-axial deformation (KATD installed at Tokyo Institute of Technology) and deformation-DIA apparatus (SPEED-Mk. II installed at SPring-8). Sintered diamond piston was used in the uni-axial deformation experiment. Shear strain was  $\sim 1.0$  estimated from the rotation of platinum strain maker after deformation. From the change of sample length, uni-axial tension and compression strain were 0.4 and 0.1 respectively. The microstructure and crystallographic orientation of the deformed samples were investigated by SEM with EBSD.

The EBSD results reveal that the [001] direction of stishovite tends to be parallel to the shear direction. (100) plane, though not so obvious, tends to parallel to the shear plane. The slip system is consistent with rutile  $\text{TiO}_2$  (Blanchin and Faisant., 1979), which has the same structure with stishovite. The calculated seismic anisotropy indicates a fast shear wave along shear direction. Polarization anisotropy reported by Visser et al. (2008) can be attributed by a vertical flow and LPO of stishovite in the transition zone. The negative anisotropy along subduction zones in Panning and Romanowicz. (2006) indicates the type A slabs (slabs which penetrate directly into the lower mantle without much deflection in the transition zone) (Karato et al., 2001).

Keywords: stishovite, deformation, LPO

## Phase transitions and mineral chemistry in pyrolite at 1600-2200C across 660-km seismic discontinuity

ISHII, Takayuki<sup>1\*</sup> ; KOJITANI, Hiroshi<sup>1</sup> ; AKAOGI, Masaki<sup>1</sup>

<sup>1</sup>Department of chemistry, Gakushuin University

It is widely accepted that pyrolite is a model rock which represents the chemical composition of the Earth's upper mantle. Because the post-spinel transition in pyrolite occurs at about 23 GPa along mantle geotherm (e.g. Litasov et al. 2005), it has been accepted that the transition is responsible for the seismic 660-km discontinuity. Slow velocity anomalies by global seismic tomography which may indicate mantle upwelling have been found in the transition zone and the lower mantle, and these regions are higher in temperature than average mantle. To elucidate the origin and dynamics of the mantle plume, informations on phase relations in pyrolite are essential. However, few investigations on phase relations in pyrolite have been made at hot-plume temperatures (1800-2200C) (Hirose, 2002; Nishiyama and Yagi, 2003). In this study, we demonstrated detailed phase equilibrium experiments in pyrolite composition at hot plume conditions.

The starting material was prepared as the oxide mixture in pyrolite composition after McDonough and Sun (1995) excluding minor components (MnO, K<sub>2</sub>O and P<sub>2</sub>O<sub>5</sub>). Quench experiments were made at about 20-28 GPa and 1600-2200C for 2-10 hours using a Kawai-type 6-8 multianvil high-pressure apparatus at Gakushuin University. The starting material was packed with pressure calibrants (MgSiO<sub>3</sub> and pyrope) in a Re multi-sample capsule. A LaCrO<sub>3</sub> heater and a W5%Re-W26%Re thermocouple were inserted in a Cr<sub>2</sub>O<sub>3</sub>-doped MgO pressure medium. Phases of recovered samples were identified with microfocus-Xray diffractometer and SEM-EDS.

The mineral assemblages of MgSiO<sub>3</sub>-rich perovskite (Mpv) + magnesiowustite (Mw) + garnet (Gt) + CaSiO<sub>3</sub>-perovskite (Cpv) and Mpv + Mw + Cpv at 1600-2200C are stable at pressure range of 22-24 GPa and above 24 GPa, respectively. The mineral assemblage of ringwoodite (Rw) + Gt + Cpv at 1600C changes to that of Rw + Mw + Gt + Cpv at 1800-2000C, and Rw disappears perfectly above 2200C. From mass balance calculation of analyzed compositions of the phases, we found that Gt content increases with increasing temperature before and after formation of Mpv. We also calculated the densities in pyrolite at each temperature. The density of average pyrolite mantle (1600C) is higher than pyrolite plume (1800-2200C) across 660-km discontinuity due to increase in Gt content with increasing temperature. Therefore, we conclude that hot-plume ascending nearby 660-km discontinuity has positive buoyancy by the phase transitions.

Keywords: post-spinel transition, 660-km seismic discontinuity, mantle plume, pyrolite, post-garnet transition

## Elastic properties of delta-AIOOH under high-pressure: Implications for high $V_S$ anomaly in the mantle transition zone

MASHINO, Izumi<sup>1\*</sup>; MURAKAMI, Motohiko<sup>1</sup>; OHTANI, Eiji<sup>1</sup>

<sup>1</sup>Faculty of Science, Tohoku University

delta-AIOOH is a high-pressure polymorph of diaspore (alpha-AIOOH) and boehmite (gamma-AIOOH) (Suzuki *et al.*, 2000). Since delta-AIOOH is identified to be stable from 20 to 120 GPa, and temperatures up to 2300 K, this phase is considered to be a possible carrier and reservoir of water in subducting cold slab into the deep mantle (Ohtani *et al.*, 2001; Sano *et al.*, 2004; 2008). In order to investigate the effect of composition on seismic velocities in subducting slab, it is important to measure the elastic properties of delta-AIOOH at high pressure.

We have conducted high-pressure acoustic-wave velocity measurements of delta-AIOOH using Brillouin spectroscopy and also explored the chemical bonding of delta-AIOOH by Raman spectroscopy at high pressure in a diamond anvil cell. We obtained sharp peaks from transverse acoustic mode ( $V_S$ ) of delta-AIOOH over the entire pressure range explored up to a pressure of 89 GPa. The peaks from longitudinal acoustic mode ( $V_P$ ) of delta-AIOOH were masked by the diamond shear acoustic modes from 35 GPa. The pressure dependence of the aggregate velocities for the delta-AIOOH at 300 K suggests that the hydrogen-bonding symmetrization with the space group changes from  $P2_1nm$  to  $Pnmm$  occurs during compression above 7 GPa. The shear and adiabatic bulk moduli and their pressure derivatives at zero pressure were determined to be  $K_0 = 192.2(8)$  (GPa),  $G_0 = 158.8(3)$  (GPa),  $(dK/dP)_0 = 3.63(6)$ , and  $(dG/dP)_0 = 1.35(6)$  for the pressures above 15 GPa. Raman spectroscopic measurements have shown that the  $B_1$  mode frequencies of  $P2_1nm$  disappeared around 6 GPa and  $A_g$  mode frequencies of  $Pnmm$  appeared above 5.6 GPa, which also indicates the hydrogen-bonding symmetrization around 6 GPa. These results indicate that delta-AIOOH becomes harder by the hydrogen-bonding symmetrization and probably exists as a phase ( $Pnmm$ ) with the symmetric hydrogen bonding in the mantle transition zone and lower mantle.

Shear wave velocities for delta-AIOOH are larger than those of hydrous wadsleyite (by 30 %), hydrous ringwoodite (by 29 %), and majorite (by 29 %). Those of delta-AIOOH are approximately 7 % below those of stishovite. The delta-AIOOH phase thus found to be one of the hardest phases compared to the minerals of mantle transition zone. The existence of delta-AIOOH may contribute to the cause of high  $V_S$  and  $V_P$  anomalies. Shear velocities for sediment containing delta-AIOOH phase are larger than those of pyrolite (by 10 %) and MORB (by 5 %). The subducting slabs often stagnate at the transition zone before reaching the lower mantle. Particularly beneath Korean peninsula, there is a high  $V_S$  anomaly (~2 %) in the lower part of the transition zone (Zhang *et al.*, 2012). The seismic data under the eastern part of northeast China (NEC) also indicates a slight positive anomaly of  $V_S$  (~1 %), but the  $V_S$  value observed around 600 km depth under NEC is ~1 % lower than that beneath Korea. We explain the difference in the  $V_S$  anomalies beneath the NEC and Korea by the amount of sediment containing the delta-AIOOH phase and the stagnating duration. If sediments stagnate at the transition zone before reaching the lower mantle in this region, we can estimate that the higher  $V_S$  anomaly (~1 %) than NEC would correspond to sediments with 13.4 vol% in stagnant slab. The average oceanic crust subduction rate is estimated to be about 8 cm/yr around Japan. Assuming this estimated rate of subduction, the slab stagnation has lasted for at least 30 million years.

Keywords: delta-AIOOH, Brillouin scattering, Raman spectroscopy, subducting slab, high pressure

## Mechanisms of ultra-deep earthquakes ( $h > 660\text{km}$ ) in a slab penetrating the 660-km discontinuity

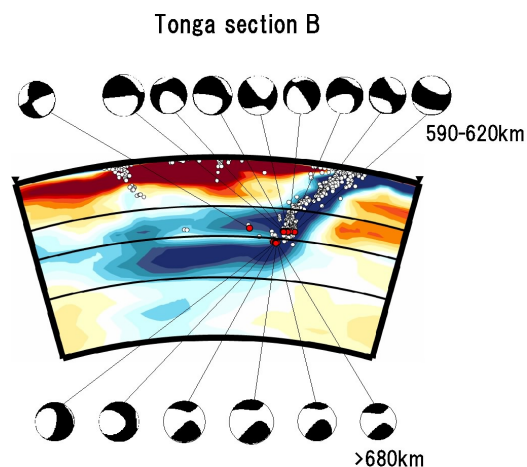
FUKAO, Yoshio<sup>1\*</sup> ; OBAYASHI, Masayuki<sup>1</sup> ; YOSHIMITSU, Junko<sup>1</sup>

<sup>1</sup>IFREE/JAMSTEC

Recent mantle tomography has begun to reveal the characteristic differences between the deep hypocentral distributions associated with stagnant slabs and those associated with penetrating slabs (e.g., Fukao and Obayashi, 2014). We here show that there are differences in focal mechanism as well. Mechanisms of deep shocks within tomographically imaged stagnant slabs (typically in Bonin and Tonga) are characterized by horizontal compression (e.g., Bonnardot et al., 2009). Those within tomographically imaged penetrating slabs (typically in Java and Tonga) are characterized by very steeply dipping compressional axes (e.g., Alpert et al., 2010).

The deepest seismicity is especially active in Tonga, where many shocks occur at depths greater than 660km. Such ultra-deep shocks show in general very unusual mechanisms, typified by nearly vertical tensional axes with a large amount of CLVD component, as demonstrated in Figure 1 (Mechanisms viewed from the side). This figure also shows a remarkable contrast of mechanisms of deepest shocks just above and below the 660km depth. The source region of the ultra-deep shocks ( $h > 660\text{km}$ ) is underlain by the greatly deepened post-spinel phase boundary (Niu and Kawakatsu, 1995) so that the source region is at the pre-spinel state while the underlying portion is at the post-spinel state. This situation along with contortion of the slab associated with its interaction with the post-spinel phase boundary (e.g., Cizkova and Bina, 2013) may explain the mechanism change across the 660km depth as observed in Figure 1. We explore the finer velocity structure and hypocentral distribution in the source region by a technique of differential travel time tomography.

Keywords: mantle dynamics, tomography, deep earthquakes



## A pyrolitic lower mantle with $(\text{Mg,Fe}^{3+})(\text{Si,Al}^{3+})\text{O}_3$ perovskite

WANG, Xianlong<sup>1\*</sup> ; TSUCHIYA, Taku<sup>1</sup>

<sup>1</sup>GRC, Ehime University and ELSI, Tokyo Institute of Technology

To better understand the Earth's lower mantle (LM), thermodynamic properties (TDPs) of LM minerals with Fe and Al dopant should be illustrated more clearly. We have so far reported the TDPs of Fe-bearing MgO, MgSiO<sub>3</sub> perovskite (Pv) and post perovskite. [1-4] We furthermore study the TDPs of Fe- and Al-bearing Pv, where the internally consistent LSDA+*U* method and the lattice dynamics method are applied. Two spin states, high (HS) and low spin state, two substitution sites, Mg and Si site, and several possible distribution configurations are considered. In the LM pressure range, HS Fe<sup>3+</sup> substituted at the Mg site with Al<sup>3+</sup> at the adjacent Si site (Fe-Al pair) is the most stable configuration and tends to distribute homogeneously in LM. Furthermore, negative frequency cannot be observed in the Fe-Al pair-bearing Pv, and Al contributes to middle frequency while Fe mainly to low part due to its heavy mass. This indicates that the Fe-Al pair is vibrationally stable. Incorporation of the pair for geophysically relevant concentrations can increase volume of Pv a little and has marginal effects on the TDPs of Pv except for thermal expansivity and Gruneisen parameter. Simulated densities, adiabatic bulk moduli, and bulk sound velocities show that a composition close to pyrolite is accountable for the reference Earth model.

### References:

- [1] A. Metsue, and T. Tsuchiya, J. Geophys. Res. 116, B08207 (2011).
- [2] A. Metsue, and T. Tsuchiya, Geophys. J. Int. 190, 310 (2012).
- [3] H. Fukui, T. Tsuchiya, and A. Q. R. Baron, J. Geophys. Res. 117, B12202 (2012).
- [4] T. Tsuchiya, and X. Wang, J. Geophys. 118, 83 (2013).

Keywords: First-principles method, Internally consistent LSDA+*U*, Perovskite, Thermodynamic properties, Pyrolite

## Linear analysis on the onset of thermal convection of highly compressible fluids

KAMEYAMA, Masanori<sup>1\*</sup>

<sup>1</sup>GRC, Ehime University

A series of linear stability analysis was performed on the onset of thermal convection in a highly compressible fluid, in order to study the fundamental nature of mantle convection of massive super-Earths in the presence of strong adiabatic compression. We consider the temporal evolution (growth or decay) of an infinitesimal perturbation superimposed to a highly compressible fluid which is in a hydrostatic (motionless) and conductive state in a basally-heated horizontal layer. As a model of pressure-dependence in material properties, we employed an exponential decrease in thermal expansivity and exponential increase in (reference) density with depth. The linearized equations for conservation of mass, momentum and internal (thermal) energy are numerically solved for the critical Rayleigh number as well as the vertical profiles of eigenfunctions for infinitesimal perturbations. The above calculations are repeatedly carried out by systematically varying (i) the dissipation number which measures the effect of adiabatic compression, (ii) the temperature at the top surface and (iii) the magnitude of pressure-dependence in thermal expansivity and reference density.

Our analysis demonstrated that the onset of thermal convection is strongly affected by the adiabatic compression, through modulating the static stability of thermal stratification in the fluid layer. For sufficiently strong adiabatic compression where a sufficiently thick “stratosphere” of stable stratification develops in the layer, for example, the critical Rayleigh number explosively increases with the dissipation number. The explosive changes in the critical Rayleigh number are associated with drastic decreases in the length scales of perturbations both in vertical and horizontal directions. In particular, for very strong adiabatic compression, the vertical motion of fluid is significantly suppressed in a thick “stratosphere”, which narrows the incipient convection in a thin sublayer of unstable thermal stratification. In addition, when the effect of adiabatic compression is extremely strong so that the thermal stratification becomes stable in the entire layer, no perturbation is allowed to grow with time regardless of the Rayleigh number and/or the horizontal wavelength. We also found that the effect of adiabatic compression becomes prominent for higher temperature at the top surface of the fluid layer. These findings may imply the crucial importance of adiabatic compression in understanding the dynamics and evolution of the mantles of massive super-Earths, particularly for those orbiting their parent stars very closely.

Keywords: super-Earths, mantle convection, adiabatic compression, thermal expansivity

## In Situ observation of the Segregation Process of Molten Iron from Partially Molten Silicate using X-ray Radiography

YAGI, Takehiko<sup>1\*</sup> ; GOTOU, Hirotada<sup>2</sup> ; IIZUKA, Riko<sup>1</sup> ; SUZUKI, Akio<sup>3</sup>

<sup>1</sup>Geodynamics Research Center, Ehime University, <sup>2</sup>Institute for Solid State Physics, University of Tokyo, <sup>3</sup>Department of Earth Science, Tohoku University

We have made in situ observation of the segregation process of molten iron from partially molten silicate at 5 GPa and 1800 K using X-ray radiography. Earth's core is believed to have formed by the similar process in the early stage of Earth formation. Although two measure mechanisms, "rain fall" and "percolation", have been proposed for this process, experimental results are still quite controversial. Most of the previous works were made either by the texture analysis of the quenched and recovered sample or by the electrical conductivity measurement. In the present study, an uniform mixture of the powders of Mg(OH)<sub>2</sub>, SiO<sub>2</sub>, and Fe was compressed to 5 GPa at room temperature and then X-ray tomography observation was made with increasing temperature up to 1800 K. Addition of H<sub>2</sub>O component into silicate-iron system reduces the melting temperature of both silicate and iron considerably. The dynamical process of the formation of iron ball at the bottom of the sample chamber was clearly observed. It was proved that this technique is quite useful to study such process in detail.

Keywords: core formation process, molten iron, x-ray, high pressure and temperature

## Influence of majorite on mantle convection

ICHIKAWA, Hiroki<sup>1\*</sup> ; KAMEYAMA, Masanori<sup>2</sup> ; SENSU, Hiroki<sup>3</sup> ; KAWAI, Kenji<sup>4</sup> ; MARUYAMA, Shigenori<sup>5</sup>

<sup>1</sup>GRC, Ehime University and ELSI, Tokyo Institute of Technology, <sup>2</sup>Geodynamics Research Center, Ehime University, <sup>3</sup>Planetary Exploration Research Center, Chiba Institute of Technology, <sup>4</sup>Department of Earth and Planetary Sciences, Tokyo Institute of Technology, <sup>5</sup>Earth-Life Science Institute, Tokyo Institute of Technology

Influence of  $\text{MgSiO}_3$  majorite on the mantle convection has been investigated by using numerical simulations. According to a first principles study (Yu et al., 2011), wadsleyite decomposes to an assemblage of majorite plus periclase with a large negative Clapeyron slope. Since stability field of majorite is limited at high temperature, downwellings are considered to be unaffected by this phase boundary. On the contrary, the upwelling plumes may be significantly modified by this phase boundary. The asymmetry on upwelling and downwelling caused by the phase transitions may induce strong effects on the thermal evolution and the thermal structure of the mantle.

In this study, we performed 2-D numerical simulations on thermal convection of the mantle incorporating majorite stability field. According to our numerical results, very hot upwelling plumes are strongly influenced by the phase transitions related to majorite. The dynamics of these upwellings are controlled by the release and the absorption of latent heat induced by the transitions as well as interruption of currents due to the large negative Clapeyron slope of the transition between wadsleyite and majorite plus periclase.

Keywords: Mantle convection, Majorite, Phase transition

## Rapid lateral variation of P-wave velocity at the base of the mantle beneath the Western Pacific

TANAKA, Satoru<sup>1\*</sup> ; KAWAKATSU, Hotoshi<sup>2</sup> ; OBAYASHI, Masayuki<sup>1</sup> ; NECESSARRAY, Project team<sup>2</sup>

<sup>1</sup>JAMSTEC, <sup>2</sup>ERI, Univ. Tokyo

We examine P-wave velocity structure at the base of the mantle beneath the Western Pacific, where is the western edge of the Pacific Large-Low Velocity Province (LLVP), by using high-quality seismograms that are provided by the NECESSArray project. Forward modeling with the reflectivity method is conducted to explain the variation of P-wave travel times as function of epicentral distance near the core shadow zone after station and ellipticity corrections are applied. Additionally PcP-P travel times are also examined to enlarge the survey area. As a result, a rapid variation of P-wave velocity structure at the base of the mantle is detected. Thin (10 to 60 km thickness) and very low velocity (-2 to -6 %) layers at the base of the mantle are intersected with a 100 km thickness and high velocity (+3%) layer, and a slightly fast layer exists at the north of the region with the thin and low velocity layers. Their spatial separations are typically several hundred kilometers and it would be difficult to explain by only a thermal effect. These observations suggest that very complicated thermo-chemical reactions occur near the edge of Pacific LLVP.

Keywords: P-wave velocity, the base of the mantle, the Western Pacific

## Methods for inversion of body-wave waveforms for localized three-dimensional seismic structure and an application to D''

KAWAI, Kenji<sup>1\*</sup> ; KONISHI, Kensuke<sup>2</sup> ; GELLER, Robert J.<sup>3</sup> ; FUJI, Nobuaki<sup>4</sup>

<sup>1</sup>Department of Earth and Planetary Sciences, Tokyo Institute of Technology, <sup>2</sup>School of Earth and Environmental Sciences, Seoul National University, <sup>3</sup>Department of Earth and Planetary Science, Graduate School of Science, University of Tokyo, <sup>4</sup>Institut de Physique du Globe de Paris

We formulate the inverse problem of waveform inversion for localized 3-D seismic structure, computing partial derivatives of waveforms with respect to the elastic moduli at arbitrary points in space for anisotropic and anelastic media. In this study we minimize computational requirements by using the Born approximation with respect to a laterally homogeneous model, but this is not an inherent limitation of our approach. We solve the inverse problem using the conjugate gradient (CG) method, using Akaike's Information Criterion (AIC) to truncate the CG expansion. We apply our method to invert for three-dimensional shear wave structure in the lowermost mantle beneath Central America using a total of 2154 waveforms at periods from 12.5 to 200 s recorded at stations near the Pacific coast of North America for 29 deep and intermediate-depth events beneath South America. The resulting model shows lateral heterogeneity in the E-W direction which may be associated with a subducted cold slab surrounded by hotter materials with slower velocities. Various tests show that our model is robust.

Keywords: Lowermost mantle, Waveform inversion, Farallon plate

## A magnetic probe into Earth's core and deep-mantle dynamics

SAKURABA, Ataru<sup>1\*</sup>

<sup>1</sup>Department of Earth and Planetary Science, University of Tokyo

It is widely recognized that Earth's core dynamics is an important research subject in understanding the past, present and future states of our planet, firstly because the metallic core is a vast domain accounting for one thirds of Earth's mass and plays a significant role in thermal history, and secondly because it dynamically generates the main geomagnetic field that has historically been observed for several hundred years and geologically recorded in rocks since more than a billion years ago. This review attempts to cover this subject with an attention to general questions: how geomagnetic-field data can be used to advance the deep-Earth science, and what theoretical progresses have been made and could be made. I will deal with some of the following particular topics: (1) various driving sources of convection, such as thermal and compositional buoyancy and inertial forcing (e.g., luni-solar precession); (2) a dynamo without a solid inner core; (3) a dynamo that operates in a part (e.g., an inner part) of the outer core; (4) sensitivity of the geomagnetic field structure (e.g., dipolarity), intensity, and time variations (e.g., reversal frequency) to the above mentioned various parameters.

## Relationship between sound velocity and density of liquid alloy under pressure

TERASAKI, Hidenori<sup>1\*</sup> ; NISHIDA, Keisuke<sup>2</sup> ; URAKAWA, Satoru<sup>3</sup> ; KUWABARA, Souma<sup>1</sup> ; TAKUBO, Yusaku<sup>1</sup> ; SHI-MOYAMA, Yuta<sup>1</sup> ; UESUGI, Kentaro<sup>4</sup> ; TAKEUCHI, Akihisa<sup>4</sup> ; SUZUKI, Yoshio<sup>4</sup> ; KONO, Yoshio<sup>5</sup> ; HIGO, Yuji<sup>4</sup> ; KONDO, Tadashi<sup>1</sup>

<sup>1</sup>Osaka Univ., <sup>2</sup>Univ. Tokyo, <sup>3</sup>Okayama Univ., <sup>4</sup>JASRI, <sup>5</sup>HPCAT

It is important to understand the relationship between sound velocity and density of liquid Fe-alloys under high pressure for obtaining a constraint of the composition of the molten outer core from observed seismic data. We have studied a relationship between sound velocity and density of liquid alloy based on simultaneous measurement of these properties under high pressure and high temperature. Sound velocity was measured using ultrasonic pulse-echo overlapping method and density was measured employing X-ray absorption method combined with X-ray tomography technique. The measured P-wave velocity and density of liquid Ni<sub>75</sub>S both increase with pressure. From these data, adiabatic bulk modulus ( $K_{S0}$ ) of the liquid sample can be well constrained to 29 GPa. It is note that the measured P-wave velocity is found to increase linearly with increasing density. This result provides an important issue in terms of Birch's law for liquid material.

Keywords: Sound velocity, density, liquid, high pressure

## Magnetic-Coriolis waves in convection-driven dynamos: Implications for geomagnetic westward drift

HORI, Kumiko<sup>1\*</sup> ; JONES, Chris<sup>2</sup> ; WICHT, Johannes<sup>3</sup> ; SHIMIZU, Hisayoshi<sup>1</sup>

<sup>1</sup>Earthquake Research Institute, University of Tokyo, <sup>2</sup>University of Leeds, UK, <sup>3</sup>Max-Planck Institute for Solar System Research, Germany

A prominent feature of the geomagnetic secular variation is the westward motion of the non-dipole part of the field, which is significant in the Atlantic hemisphere with timescales of a few hundred years. Potential mechanisms to account for longitudinal geomagnetic drifts are advection due to large-scale zonal flows in the Earth's core as well as propagation of rotating magnetohydrodynamic (MHD) waves, particularly of slow Magnetic-Coriolis (MC) Rossby waves. More commonly the westward motion is thought to reflect zonal flow advection, an assumption that is used when inverting the secular variation signal for the flow at the top of the core. However, recent geodynamo simulations have successfully reproduced longitudinal magnetic drifts and some authors reported that the drift is at least partly a wave propagation.

To assess to what extent waves could play a role in geomagnetic drift, we explore nonlinear simulations of convection-driven MHD dynamos in rotating spherical shells. By performing a tempo-spatial spectral analysis of simulation data, we identify a slow MC-Rossby mode, that follows the dispersion curve predicted by a quasi-geostrophic linear theory. The result indicates that such waves can be excited in the planetary fluid core and that wave propagation may indeed play a role in the magnetic drifts. This gives a framework for further exploration of different wave types, which can provide valuable information about the physical properties in the deep interior fluid core.

## A generating process of the geomagnetic drifting field

YUKUTAKE, Takesi<sup>1\*</sup> ; SHIMIZU, Hisayoshi<sup>2</sup>

<sup>1</sup>None, <sup>2</sup>Earthquake Research Institute, University of Tokyo

The geomagnetic field is comprised of drifting and standing field. The drifting field is the field that drifts westwards nearly steadily over the past several hundred years and the standing field is that stays at the same place. The drifting field has two major characteristic features. When the field is expressed in a spherical harmonic series, the drifting field mainly consists of sectorial harmonics. Secondly the rate of drift is uniform irrespective of the harmonics. This means the drift velocity is non-dispersive.

We here propose a model of the generating process of the drifting field. Because of the non-dispersive nature of the drift velocity, we assume the westward drift is a phenomenon closely tied with material flow rather than a magnetohydrodynamic wave. Furthermore we take it a phenomenon near the surface of the core where the dipole field is dominant.

If the mantle is approximated by an electrical insulator, the electric current in the core normal to the core-mantle boundary must be zero. This provides a strong constraint on the liquid flow near the surface. If we assume infinite conductivity of the core for simplicity, only the sectorial flow is allowed for the toroidal flow, and the meridional flow for the poloidal flow. The sectorial toroidal flow, interacting with the dipole field, induces sectorial poloidal field, whereas the meridional poloidal flow produces the meridional poloidal field. The surface layer, which is rotating westwards as a whole, carries these fields westwards together. Since the rotation of the meridional field is unrecognizable, only the sectorial field is observed as the drifting field.

We present a simplified model that describes the above process.

Keywords: geomagnetic secular variation, westward drift, drifting field, core surface flow

## Electrical resistivity of hcp-Fe under Earth's core conditions

OHTA, Kenji<sup>1\*</sup>; KUWAYAMA, Yasuhiro<sup>2</sup>; HIROSE, Kei<sup>3</sup>; OHISHI, Yasuo<sup>4</sup>

<sup>1</sup>Department of Earth and Planetary Sciences, Tokyo Institute of Technology, <sup>2</sup>Geodynamics Research Center, Ehime University, <sup>3</sup>Earth-Life Research Institute, Tokyo Institute of Technology, <sup>4</sup>Japan Synchrotron Radiation Institute

Iron is the primary component of the Earth's core. Convection of the conductive liquid outer core generates the geomagnetic field, and secular cooling of the core induces growth of the solid inner core and dynamics in the Earth's inside. Synchrotron x-ray diffraction study suggests that iron crystallizes in the hexagonal close-packed structure at the inner core conditions (Tateno et al., 2010). Thus, the electrical resistivity of hexagonal close-packed iron (hcp-Fe) is a key piece of information for estimating the transport properties of the core. We report high temperature electrical resistivity for hcp-Fe to 185 GPa measured in a laser-heated diamond anvil cell. We observed resistivity saturation in hcp-Fe under high pressure and high temperature conditions as predicted in a recent laboratory-based model for the conductivity of the Earth's core (Gomi et al., 2013). The saturation effect is significant in estimating electrical and thermal conductivity of the core, which strongly affect the dynamics and thermal evolution of the Earth.

### References

Gomi, H. et al. The high conductivity of iron and thermal evolution of the Earth's core. *Phys. Earth Planet. Inter.* 224, 88-103 (2013).

Tateno, S., Hirose, K., Ohishi, Y., & Tatsumi, Y. The structure of iron in Earth's inner core. *Science* 330, 359-361 (2010).

Keywords: Electrical resistivity, Earth's core, hcp iron

## Spatial dependence of anisotropic thermal diffusivity and its influence on dynamics in the Earth's core

MATSUSHIMA, Masaki<sup>1\*</sup>

<sup>1</sup>Tokyo Institute of Technology

Small-scale fluid motions in the Earth's core are likely to be highly anisotropic because of rapid rotation of the Earth and a strong magnetic field in the core. We have carried out direct numerical simulations of rotating magnetoconvection to investigate the effect of anisotropic diffusivity on dynamics in the Earth's core, as one of pilot studies. When a computational region is expressed in terms of a rectangular box with periodic boundaries in the three-directions, the prescribed anisotropic thermal diffusivities were found not to influence the character of rotating magnetoconvection, such as kinetic and magnetic energies averaged over the computational region. When a computational region is expressed in terms of a rectangular box with rigid boundary surfaces perpendicular to the gravitational direction, the prescribed anisotropic thermal diffusivities have a significant effect on the character of rotating magnetoconvection; that is, kinetic and magnetic energies can be increased even by a small anisotropy. The degree of increase depends on the direction of anisotropy and the direction of gravity corresponding to location of the computational region. These results suggest that anisotropic thermal diffusivity insignificantly influences dynamics in the bulk of the core, but that it should be effective near rigid boundary surfaces. Therefore, it is likely that anisotropic diffusivity has a more significant effect on MHD dynamos in rotating thin spherical shells. Such an implication can be examined through global numerical simulations of MHD dynamo models with anisotropic diffusivity being variable in the core.

Instead of such a study, we perform further direct numerical simulations of rotating magnetoconvection by prescribing anisotropic thermal diffusivities with spatial dependence; for example, in one case, anisotropic thermal diffusivities are presumed to be effective only near rigid boundary surfaces; in another case, anisotropic thermal diffusivities are presumed to be effective only far from rigid boundary surfaces. Hence this is another pilot study. Kinetic and magnetic energies in the former case seem to be larger than those in the latter case. The result is consistent with that obtained in our previous studies.

Keywords: anisotropic thermal diffusivity, core dynamics

## Can a stably stratified layer interrupt the top-down dynamics of Earth's core?

NAKAGAWA, Takashi<sup>1\*</sup>

<sup>1</sup>IFREE, JAMSTEC

Takashi Nakagawa

In some of previous studies of numerical dynamo simulation with a stably stratified region below the outer boundary, the long-wavelength feature of radial magnetic field can be only found on the outer boundary because a stratified layer can filter small-scale features of radial magnetic field generated in the convective region below the stratified boundary [Christensen, 2006; Nakagawa, 2011]. The existence of the stably stratified region below the core-mantle boundary (CMB) is recently exposed from high pressure mineral physics [e.g. Pozzo et al., 2012] and seismological data analysis [e.g. Helffrich and Kaneshima, 2013].

Regarding the modeling on geomagnetic secular variation from numerical dynamo simulations, the heterogeneous thermal/chemical anomalies at the core-mantle boundary is important for understanding the time-scale of secular variation such as polarity reversals and excursions suggested from paleomagnetic observations [e.g. Olson et al., 2011; Olson et al., 2013] and current observational magnetic field [Aubert et al., 2013]. However, their investigation was not included in the effects of the stably stratified region below the CMB in their dynamo simulations.

Here we introduce several examples of numerical dynamo simulations with both heterogeneous outer boundary prescribed by the CMB heat flux calculated from numerical mantle convection simulations and a stably stratified layer. Preliminary results are found that the large-scale and amplitude of thermal/chemical anomalies induced by the heterogeneous boundary condition, that is, thermal wind type flow, may be trapped at the imposed stratified boundary. This may imply that the geomagnetic secular variations related to the core-mantle coupling may be suggested that the core surface flow would be a key physics.

Keywords: Earth's core, heterogeneity, core-mantle boundary, stably stratified layer, thermal wind

## Sound velocity measurements of liquid Fe-Ni-S alloy at high pressure and temperature via inelastic X-ray scattering

IMADA, Saori<sup>1\*</sup> ; NAKAJIMA, Yoichi<sup>2</sup> ; KOMABAYASHI, Tetsuya<sup>3</sup> ; HIROSE, Kei<sup>4</sup> ; TSUTSUI, Satoshi<sup>5</sup> ; UCHIYAMA, Hiroshi<sup>5</sup> ; ISHIKAWA, Daisuke<sup>5</sup> ; ALFRED, Baron<sup>2</sup>

<sup>1</sup>Department of Earth and Planetary Sciences, Tokyo Institute of Technology, <sup>2</sup>Material Dynamics Laboratory, RIKEN SPring-8 Center, RIKEN, <sup>3</sup>School of Geosciences, The University of Edinburgh, <sup>4</sup>Earth-Life Science Institute, Tokyo Institute of Technology, <sup>5</sup>Japan Synchrotron Radiation Research Institute

The liquid Earth's outer core is mainly composed of Fe-Ni alloy with some amounts (5~10%) of light element(s), such as hydrogen, carbon, oxygen, silicon, and sulfur. Moreover, it has been known that the Mars and Mercury have also liquid (outer) core, although there are less observational data (Dehant, 2003, Margot et al., 2007).

In order to identify the kind and amount of the light elements dissolved in these planetary cores, sound velocity data of iron alloys at high pressure and temperature are important because the seismic wave speeds are the primary observed information in the deep Earth's interior. While sound velocity measurements of solid core materials up to core pressures have been extensively conducted via ultrasonic method, inelastic X-ray scattering (IXS), nuclear resonance IXS, due to its experimental difficulty, there exist few reports on sound velocity measurements of liquid Fe alloys at high pressure (Nishida et al. 2012).

We measured sound velocity of liquid of (Fe,Ni)<sub>3</sub>S up to 30 GPa. Sulfur has been considered to be a major candidate for the light element in the Earth's outer core as well as in the Martian and Mercury's cores (e.g. Lodders and Fegley 1997). We conducted high-pressure and -temperature experiments with an externally-heated diamond-anvil cell (EHDAC). The starting materials were a synthesized or a powder mixture of Fe, Ni, and FeS, with compositions of (Fe<sub>0.83</sub>Ni<sub>0.17</sub>)<sub>3</sub>S, or (Fe<sub>0.64</sub>Ni<sub>0.36</sub>)<sub>3</sub>S. Sound velocity was measured using high resolution IXS at BL35XU, or BL43XU of SPring-8. IXS spectra were collected in the range of the momentum transfer,  $Q=3.2\text{?}6.59\text{ nm}^{-1}$  with a resolution of  $0.45\text{ nm}^{-1}$ . EHDAC was put in a vacuum chamber to reduce the background of the spectra. We will present the sound velocity data of liquid and solid of (Fe,Ni)<sub>3</sub>S and discuss the composition of the terrestrial, Martian, and Mercury's liquid outer core.

Keywords: sound velocity, inelastic X-ray scattering, planetary outer core, liquid iron alloy, High-PT experiment

## Experimental approach to the core-mantle boundary region of Mercury

OKAMOTO, Miho<sup>1</sup> ; URAKAWA, Satoru<sup>1\*</sup>

<sup>1</sup>Dept Earth Sci, Okayama Univ

MESSENGER mission revealed precise moment of inertia parameters of Mercury and its surface chemistry [1, 2]. These data allow to model the internal structure of Mercury, which has a large liquid core with ~2000 km radius and a solid outer shell with ~400 km thickness [3, 4]. As density of solid outer portion is apparently higher than that of the expected mantle silicate, the solid outer layer must include dense materials. Recent models [3, 4] showed that the Mercury's core contains sulfur and silicon as light elements due to high S fugacity and low oxygen fugacity of its interior. Those models presented a solid FeS layer at bottom of solid outer shell of Mercury as a dense layer, which separated from liquid outer core as a FeS-rich liquid due to liquid immiscibility of the Fe-S-Si ternary system. To investigate the FeS-rich layer at the top of Mercury's core, we performed the high-pressure experiments on the Fe-S-Si system using a KAWAI-type multi-anvil apparatus.

Pressure is fixed at 5 GPa corresponding to the CMB of Mercury and temperature is 1800 K, which is 200 K above the liquidus of Fe-S-Si system reported by Sanloup and Fei [5]. Fe-S-Si sample was kept for 30 min at this condition, and then it was quenched into room temperature. Oxygen fugacity of run charges was maintained around 3 log unit below IW buffer. Texture and chemistry of recovered samples were examined by electron microprobe.

We found two immiscible liquids in one run charge, which consist of Fe,Si-rich metallic liquid and FeS-rich sulfide liquid. Sulfur content of metallic liquid ranges 6 to 9 at%, which is higher by ~5 at% than those reported by Morard and Katsura [6]. Differences in texture of recovered samples and run duration between this study and Morard and Katsura [6] suggest that the latter experiments were in disequilibrium state. Our data shows the liquid immiscible region has a narrower extent than the previous estimation and the Mercury immiscible Fe-S-Si core must contain at least 6-9 at% sulfur. The quenched FeS-rich liquid phase consists mainly of crystalline FeS (~90 vol%) and Fe-Si alloy. In the case that FeS-rich liquid contacted with MgO sample container, (Mg<sub>0.8</sub>Fe<sub>0.2</sub>)S crystalline phase coexisted with FeS-rich liquid. Mg-sulfide phase could be made by Fe-Mg exchange reaction between MgO and FeS-rich liquid. In the Mercury core, when FeS-rich liquid ascends to add the bottom of the CMB due to its buoyancy, it makes a stable low density layer. Mg-sulfide phase is produced under low oxygen fugacity and high sulfur fugacity at CMB, and then it incorporates into mantle. This is consistent with the results of X-ray fluorescence spectrometry on the Mercury's surface, which indicates the presence of Mg and Ca sulfides [2].

### References

- [1] Margot JL et al., J. Geophys. Res., 117, E00L09, 2012.
- [2] Nittler LR et al., Science, 333, 1847, 2011.
- [3] Smith DE et al., Science, 336, 214, 2012.
- [4] Hauck II SA et al., J. Geophys. Res.: Planets, 118, 1204, 2013.
- [5] Sanloup C and Fei Y, Phys. Earth Planet. Inter., 147, 57, 2004.
- [6] Morard G and Katsura T, Geochim. Cosmochim. Acta, 74, 3659, 2010.

Keywords: core, CMB, Mercury

SIT03-P01

Room:Poster

Time:April 29 18:15-19:30

## Single crystal elasticity by means of GHz ultrasonics and Brillouin scattering in DAC II

YONEDA, Akira<sup>1\*</sup> ; MURAKAMI, Motohiko<sup>2</sup>

<sup>1</sup>ISEI, Okayama Univ., <sup>2</sup>Department of Earth and Planetary Materials Science, Tohoku University

We have been developing simultaneous measurement of GHz ultrasonics and Brillouin scattering in DAC. At JpGU 2013, we presented fundamental feasibility of GHz ultrasonics in DAC. This year, we will present succeeding progress of it.

Keywords: mantle, DAC, single crystal elasticity, GHz ultrasonics

## Single-crystal elastic property of silicate perovskites

FUKUI, Hiroshi<sup>1\*</sup> ; YONEDA, Akira<sup>3</sup> ; SHATSKIY, Anton<sup>4</sup> ; TSUTSUI, Satoshi<sup>5</sup> ; BARON, Alfred<sup>2</sup>

<sup>1</sup>Graduate School of Material Science, University of Hyogo, <sup>2</sup>Materials Dynamics Laboratory, RIKEN SPring-8 Center, RIKEN, <sup>3</sup>Institute for the Earth's Interior, Okayama University, <sup>4</sup>V.S. Sobolev Institute of Geology and Mineralogy, Russian Academy of Science, Siberian Branch, <sup>5</sup>Research and Utilization Division, SPring-8/JASRI

Information of single-crystal elasticity of silicate perovskite is essential for comprehensive understanding of the lower mantle. We have measured single-crystal elastic property of  $\text{Mg}_{1-x}\text{Fe}_x\text{SiO}_3$  perovskite ( $x = 0$  or  $0.035$ ) by means of inelastic x-ray scattering at the ambient condition. The present results show relatively low values compared to previous reports for the iron free sample. The effect of iron increases both adiabatic bulk modulus and shear modulus. Combining the present results with pressure and temperature derivatives reported in literature, the chemical composition of the lower mantle will be discussed.

Keywords: silicate perovskite, single-crystal elasticity, the lower mantle, inelastic x-ray scattering

## Measurement of thermal conduction of high-pressure minerals at pressures of the transition zone and to the lower mantle

OSAKO, Masahiro<sup>1\*</sup> ; YONEDA, Akira<sup>2</sup> ; YOSHINO, Takashi<sup>2</sup>

<sup>1</sup>National Museum of Nature and Science, <sup>2</sup>Institute for study of the Earth's interior

Knowledge of thermal diffusivity or thermal conductivity of the mantle is vital for study of the dynamics of the Earth. So far thermal diffusivity and thermal conductivity of mantle minerals were measured under high pressure using a pulse-heating method of one-dimensional heat flow. This method is a predominant one for study in deep Earth's materials under pressure because it requires comparatively small amount of samples. It is also applicable to materials with anisotropy in thermal conduction. In addition its measurement yields heat capacity data under pressure.

Thermal conductivity or thermal diffusivity of olivine and garnet increases 3-4 % per 1 GPa, and olivine still reveals anisotropy in thermal conduction under the conditions of the upper mantle. Antigorite, a high-temperature form of serpentine, has low thermal diffusivity and low thermal conductivity which are much lower than those of olivine, whereas talc has high thermal diffusivity and thermal conductivity comparable to those of olivine. All those data were obtained from the measurements at pressures up to 10 GPa and temperatures to 1100 K. An advanced cell assembly was needed to expand the pressure range of measurement.

A new pressure-cell assembly similar to our previous one is designed for a sample of 3 mm in diameter and 0.7 mm in thickness. This smaller cell was applied to pyroxene samples of which sizes were necessarily limited. The measurements were conducted using the Kawai-type apparatus at the Institute for study of the Earth's interior, Misasa. This cell enabled to make measurements of thermal properties at pressures exceeding 15 GPa, which will covers the condition in the mantle transition zone.

We made preliminary measurements by this cell for the garnet sample as a test material. The thermal diffusivity showed slightly lower value (5~10 %) and the thermal conductivity was slightly high (0~10 %) value compared with the previous results by the large cell. The precision of measurements should be improved by well-controlled machining of the cell assembly and by refining the data acquisition system. After that this cell will be used for measurements of wadsleyite, ringwoodite and majorite. A cell assembly of more reduced in size is planned. This cell will be used for measurements of MgSiO<sub>3</sub> perovskite.

Keywords: mantle minerals, thermal diffusivity, thermal conductivity, high-pressure

## Elemental partitioning in the Fe-S-Si system at high pressure and temperature: Implications for the Earth's core

SAKAIRI, Takanori<sup>1\*</sup> ; OHTANI, Eiji<sup>1</sup> ; SAKAI, Takeshi<sup>2</sup> ; KAMADA, Seiji<sup>1</sup> ; MIYAHARA, Masaaki<sup>3</sup> ; HIRAO, Naohisa<sup>4</sup>

<sup>1</sup>Department of Earth science, Tohku University, <sup>2</sup>Geodynamics Reserch Center, Ehime University, <sup>3</sup>Department of Earth and Planetary Systems Science, Graduate School of Science, Hiroshima University, <sup>4</sup>JASRI

It is widely accepted that the Earth's core is mainly composed of iron and contains light elements to account for the core's density deficit. Alloying with light elements significantly affects the physical properties of iron and the arguments on the chemical structure of the Earth's core. Therefore, the melting relation of the Fe-light elements system is the key to clarifying the chemical structure of the core because the inner core has formed by crystallization of the molten outer core. Although there are many candidates for light elements in the core, based on geochemical modeling and high-pressure partitioning experiments, sulfur and silicon are considered to be the major light elements. Despite the importance of the effect of sulfur and silicon on the physical properties of iron, previous studies, including high-pressure melting experiments in the Fe-S-Si system, did not cover the pressure conditions of the core. To better understand the properties of the core, we investigated the melting relations of the Fe-S-Si system under high-pressure conditions corresponding to the Earth's core.

We report on the melting relations in the Fe-S-Si system up to 135 GPa. Melting experiments were performed in the pressure range of 37-135 GPa and the temperature range of 1800-2400 K using a double-sided laser-heated diamond anvil cell. The composition of the starting material was Fe<sub>80.1</sub>S<sub>12.7</sub>Si<sub>7.2</sub> (Fe-8 wt.% S-4 wt.% Si). Melting relations were examined on the basis of quenched textures of the recovered samples and chemical analysis of observed phases. The chemical composition of the coexisting phases in the samples was obtained with an energy-dispersive X-ray spectroscopy (EDS) system attached to the FEG-SEM. We determined the compositions of the coexisting phases and investigated the partitioning behavior of sulfur and silicon between the metallic melt and the coexisting iron alloy.

We consistently found that a quenched melt with a dendritic texture coexists with a solid Fe alloy in the recovered samples, implying that the samples were partially melted under the experimental pressure and temperature conditions. Based on the present results, the partition coefficients of sulfur and silicon between the liquid and solid Fe alloy were determined in the pressure range from 37 to 135 GPa. The value obtained for  $D_{sulfur}$  at 37 GPa was 0.032(28), whereas  $D_{silicon}$  was 4.53(73), which is significantly higher than  $D_{sulfur}$ . The obtained values of  $D_{sulfur}$  were between 0.032(28) and 0.135(35) and those of  $D_{silicon}$  were between 2.63(12) and 5.58(56) in this study. The present results indicate that the solid Fe alloy is silicon rich whereas the metallic melt is enriched in sulfur. We can find that this trend continues up to the core-mantle boundary (CMB) pressure.

The information on partitioning of light elements between the metallic melt and hcp-Fe is the key for clarifying the chemical structure of the Earth's core because the inner core is considered to have crystallized from the liquid outer core during cooling of the Earth. Moreover, previous studies strongly implied that both sulfur and silicon were the plausible candidates for the light elements in the core. Therefore, our experimental results in the Fe-S-Si system offer important clues for understanding the composition of the Earth's core. Based on the present results, if the Earth's core cools down below the melting temperature of the core material, silicon could be preferentially partitioned into hcp-Fe from the Fe-S-Si liquid during crystallization of the inner core. The present data demonstrated that if the Earth's core contains both sulfur and silicon as light elements, the present-day Earth has a sulfur-rich outer core and a silicon-rich inner core.

Keywords: Earth's core, light element, elemental partitioning, crystallization

## Influence of the electrical conductivity heterogeneity at the CMB on the flow and magnetic field in the core

SHIMIZU, Hisayoshi<sup>1\*</sup>

<sup>1</sup>Earthquake Research Institute, University of Tokyo

The effects of electromagnetic induction in the heterogeneous mantle on the observed electromagnetic fields have been studied numerically to investigate possible causes of short time-scale variation known as the geomagnetic jerk. We found previously that the jerk-like magnetic and electric field variations observed at the surface of Earth can be explained by an input of a sudden variation of the toroidal field at the top of the core and large-scale conductivity heterogeneity of which conductivity is about 100 times higher than the background electrical conductivity. In this study, the effect of the heterogeneity on the flow in the core and magnetic field is evaluated by using a simple plane model of a heterogeneous mantle. Preliminary results suggest that the signature of the magnetic field may be detected as a stationary field at the Earth's surface if the heterogeneity is planetary scale, but the penetration length of its effect in the core is much shorter than the length scale of the heterogeneity.

Keywords: geomagnetic field, CMB

## Potassium solubility into the Earth's core at the base of the magma ocean -Implication for the heat source of the core

WATANABE, Kosui<sup>1\*</sup> ; OHTANI, Eiji<sup>1</sup> ; KAMADA, Seiji<sup>1</sup> ; SAKAMAKI, Tatsuya<sup>1</sup> ; MIYAHARA, Masaaki<sup>2</sup>

<sup>1</sup>Department of Earth Science, Graduate School of Science, Tohoku University, <sup>2</sup>Department of Earth and Planetary Science, Graduate school of Science, Hiroshima University

Since the densities of the Earth's inner/outer cores are smaller than pure iron at the core conditions, the core has been thought to include light elements, such as H, C, S, O, Si (e.g., Poirier, 1994). Although the light element(s) in the core has not been decided yet, high-pressure experiments and cosmochemical estimations suggested that Si and O are plausible light elements. The energy causing the geodynamo is derived from the accretion energy at the early stage of the Earth, the latent heat of crystallization of the inner core, the gravitation energy associated with the exclusion of light materials from the inner core, and the radioactive decay of radioactive elements which are potentially present in the core. The Earth's core might contain long-lived radioactive elements such as U, Th, and K. In particular, potassium (K) is more depleted in the mantle than other volatile elements. Thus, potassium may be included in the core. In order to verify the amount of potassium in the core, we have performed potassium partitioning experiments under high pressure and temperature.

We studied partitioning of potassium between aluminosilicate (adularia,  $\text{KAlSi}_3\text{O}_8$ ) and metal containing oxygen and silicon, and partitioning of potassium without light elements (Fe-O, Fe-Si, pure Fe) at pressures up to 50 GPa and 3500 K using a double-sided laser-heated diamond anvil cell. Our results for the pressure, temperature, and compositional effects on the partitioning coefficient of potassium,  $D_K$  (i.e., the content of potassium in metal [wt%] divided by the content of potassium in silicate [wt%]), reveal that the temperature effect is slightly positive but weaker than that reported previously, whereas the pressure effect is negative and oxygen in metal increases the potassium content in metal, although silicon in metal has the opposite effect. According to the effects on potassium partitioning, we estimated that the amount of potassium in the core is less than 32 ppm and that it generates less than 0.14 TW heat in the core. This amount of heat is small compared with the heat flux at the core-mantle boundary (5-15 TW).

Keywords: Potassium, magma ocean, high pressure, high temperature, Earth's core

## Thermal structure of the NE Japan-Hokkaido subduction system: The effects of 3-D slab geometry and oblique subduction

WADA, Ikuko<sup>1\*</sup> ; JIANGHENG, He<sup>2</sup> ; HASEGAWA, Akira<sup>3</sup> ; TAMURA, Yoshihiko<sup>4</sup> ; NAKAJIMA, Junichi<sup>3</sup>

<sup>1</sup>IRIDeS, Tohoku University, <sup>2</sup>Pacific Geoscience Centre, Canada, <sup>3</sup>Graduate School of Science, Tohoku University, <sup>4</sup>Japan Agency for marine-Earth Science and Technology

In this study, we first examine the effects of along-strike variation in slab geometry and oblique subduction on subduction zone thermal structures by comparing 3-D numerical thermal models with a range of generic subduction geometries and parameters with a 2-D reference model. We found that changes in slab dip along a straight margin have modest effects on the mantle flow pattern and thus the thermal field. However, concave and convex ocean-ward margins result in cooler and warmer mantle wedges, respectively, and oblique subduction results in a warmer mantle wedge, compared to the 2-D reference model. We developed a 3-D thermal model for the NE Japan-Hokkaido margin, using a well-constrained 3-D slab geometry model. In general, there is little 3-D effect on the thermal structure of the shallow part (<70 km depth) of the subduction system, where the mantle does not participate in the slab-driven wedge flow. We also found that the 3-D effect is small in the deeper part of the southern half of the system, where the margin is relatively straight and the slab dip does not vary significantly along the margin. These results indicate that 2-D models provide excellent approximations for the thermal structures of the shallow part and the southern part of the subduction system. However, from the northern part of NE Japan to Hokkaido, the mantle flow pattern is affected by the concave ocean-ward margin and oblique subduction, and the wedge is cooler near the NE Japan-Hokkaido junction and warmer in Hokkaido than the 2-D thermal models for the respective regions. We compare the 3-D thermal modeling results with along-strike variations in surface heat flow, arc magma geochemistry, and earthquake distribution in NE Japan and Hokkaido.

Keywords: Tohoku-Hokkaido subduction system, 3-D thermal model, slab geometry, oblique subduction, mantle wedge flow, earthquakes and volcanism

## Effects of a local deepening of slab-mantle decoupling depth on slab surface temperature

MORISHIGE, Manabu<sup>1\*</sup> ; VAN KEKEN, Peter E.<sup>2</sup>

<sup>1</sup>JAMSTEC, <sup>2</sup>University of Michigan

In the subduction zone, we generally observe low seismic attenuation in the forearc mantle. In addition, surface heat flow shows low value in the forearc and a sudden transition to high value in the arc. These observations suggest that the forearc mantle is cold and is not involved in the corner flow in the mantle wedge. We can understand it in terms of slab-mantle decoupling depth ( $D_{dec}$ ). Above  $D_{dec}$ , the mantle does not move with the slab just beneath it. Therefore, it becomes cold quickly due to the cooling from the overriding plate and the slab. Below  $D_{dec}$ , on the other hand, the mantle moves with the slab. It keeps this part of mantle warm by advection of hot material due to the corner flow. Thus,  $D_{dec}$  is a key parameter which strongly affects thermal structure in the subduction zone. Comparison of the observed surface heat flow and the one predicted with 2D numerical model suggests that  $D_{dec}$  does not vary much for each subduction zone and is 70-80km, but in each subduction zone  $D_{dec}$  may show some degree of along-arc variation. One such example is the junction between Japan and Kurile arcs, where the down-dip limit of thrust type earthquake is locally deepened by around 15km. In this presentation, we investigate the effects of a local deepening of  $D_{dec}$  on slab surface temperature.

Toward the goal, we use time-dependent 3D finite element models to compute mantle flow and temperature. Only mantle wedge is treated as a dynamic entity. We use a simple slab geometry and assume a local deepening of  $D_{dec}$  to see its effects. We find that the increase in slab surface temperature at  $D_{dec}$  is larger where we assume a deepening of  $D_{dec}$ , which produces a warmer region there. It is caused by 3D flow in the mantle wedge due to along-arc variation of  $D_{dec}$ . We also calculate surface heat flow from obtained thermal structure, but it does not show significant along-arc variation. These results do not change even when we use a realistic slab geometry which is similar to that of the junction between Japan and Kurile arcs. While the surface heat flow anomaly and deepening of the seismic belt in S. Hokkaido cannot be easily explained by these models, the temperature excursions at the slab surface are significant. These models predict potentially strong variations in the conditions that the fluids leave the slab, which may be visible by various new geothermometers, such as those based on the H<sub>2</sub>O/Ce ratio.

Keywords: subduction zone, slab-mantle decoupling depth, slab surface temperature

## Thermal modeling associated with subduction of the Philippine Sea plate in southwest Japan

YOSHIOKA, Shoichi<sup>1\*</sup> ; JI, Yingfeng<sup>1</sup> ; MATSUMOTO, Takumi<sup>2</sup>

<sup>1</sup>RCUSS, Kobe University, <sup>2</sup>NIED

By constructing a parallelepiped three-dimensional thermal convection model, we investigated temperature, mantle flow and heat flow distributions associated with subduction of the Philippine Sea (PHS) plate in southwest Japan. We proposed new, realistic, and high-resolution temperature field on the plate interface, and attempted to clarify its relationships with the occurrences of megathrust earthquakes, long-term slow slip events (SSE), and low frequency tremors (LFEs). For this purpose, we newly developed a numerical model to deal with subduction of an oceanic plate with 3D arbitrary geometry. We modeled subduction of the PHS plate by using the up-to-date three-dimensional slab geometry, referring to high resolution P-wave seismic tomography and seismic reflection studies. We also used large number of heat flow data such as BSRs, borehole, heat probe, and Hi-net to constrain calculated temperature field, and took account of complicated subduction history in southwest Japan. The results showed that the interplate temperature was lower by approximately 100°C in western Shikoku where a larger true subduction angle exists than eastern Shikoku. Temperature change due to erosion and sedimentation affected surface heat flow with short wavelength. We also found that the obtained interplate temperature in the Nankai seismogenic zone was wider than that in the Tonankai seismogenic zone. The LFEs occurred near the plate interface with temperatures ranging from 350°C to 450°C at depths of 30 to 40 km. The existence of large temperature gradients from the surface to the inside of the PHS plate was considered to be related to the occurrence of long-term slow slip events beneath the Bungo Channel.

## Slab-wedge mantle boundary preserved in the Sanbagawa belt, SW Japan

WALLIS, Simon<sup>1\*</sup> ; MORI, Hiroshi<sup>1</sup> ; NAGAYA, Takayoshi<sup>1</sup> ; KAWAHARA, Hirokazu<sup>1</sup>

<sup>1</sup>Dept. Earth & Planetary Sci., Nagoya Uni.

The Sanbagawa belt of SW Japan is a high-pressure low-temperature subduction type metamorphic belt. The rock types consists of mafic, siliceous and pelitic schists derived from the subducted slab. There are also a series of ultramafic bodies whose origin is disputed: both a slab and wedge mantle origin have been proposed. However, the clear relationship between the distribution of the mantle rocks and metamorphic grade provides strong evidence that they were derived from the wedge mantle. We carried out a detailed study of the Shiragayama body as an example of serpentized mantle from close to the corner of the wedge. Studies of this region can contribute to our understanding of non-volcanic tremor and fluid flow that occurs in these otherwise inaccessible parts of subduction zones.

Keywords: fore arc mantle, subduction metamorphism, slab mantle boundary

## Phenomenology of Episodic Tremor and Slip

OBARA, Kazushige<sup>1\*</sup>

<sup>1</sup>Earthquake Research Institute, UTokyo

Episodic Tremor and Slip (ETS) is a coupling phenomenon composed of continuous weak seismic events and geodetic short-term slow slip event (SSE) in the transition zone between the brittle seismogenic zone and stable sliding regime recognized in southwest Japan and Cascadia. This paper reviews characteristics of ETS and related phenomena to contribute to discussion for subduction process.

ETS is interpreted as a stick slip on the plate interface accompanied by seismic swarm at small patches surrounded by the SSE plane because of coincidence of their sources and linear relationship between the duration of tremor episode and the moment of SSE estimated geodetically for each episode. ETS is distributed in a narrow belt-like zone along the strike of the subducting plate. ETS zone is divided into several segments in which episodes recur at each regular recurrence interval. However ETS is not "characteristic earthquake" because the rupture area and recurrence interval are fluctuated. Sometimes we observe rupture propagation through a couple of segments. The segment is usually bounded by gap which is considered as not a barrier but an easily sliding portion because of the existence of multi-segment migration.

ETS activity has depth dependent property. At the deeper part of the ETS zone minor episode frequently occurs, on the other hand major episode occurs infrequently at the shallower part. Large ETS usually initiates from the deeper part and migrates upward then activates at the shallower part. This might be caused by gradual change in frictional property with increasing the depth. At the downdip edge of the ETS zone tremor episode easily occur due to weak strength and stress concentration from stable sliding zone. Each small episode transfers the stress to the updip side. Finally a small episode can propagate to the updip edge then develop as a large ETS episode.

The activity style of ETS in southwest Japan and Cascadia is very similar; however there are some differences. One is the existence of deep very low frequency earthquake (VLF). In Japan the VLF earthquake is usually associated with ETS but has not been detected in Cascadia. It might depend on the detection capability or difference in inhomogeneity of the plate interface because the distribution of VLF earthquake in southwest Japan is more localized compared to that of tremor.

The other difference is the existence of long-term SSE. It is detected at the updip side of ETS zone in the Bungo Channel and Tokai in southwest Japan but not detected in Cascadia. The long-term SSE with duration from several months to years activates tremor at the adjacent limited region in the ETS zone. On the other hand, the tremor activity at the downdip part is not affected. Similar long-term SSE has been detected in Alaska and Mexico, where tremor activity was recently detected at the downdip side of the source fault of the long-term SSE. The tremor is seems to be activated during the SSE period like as in southwest Japan. The long-term SSE in Tokai is located above the anomalously high  $V_p/V_s$  region in the slab. In Mexico, a ultra slow speed layer was found in the long-term SSE source region. Therefore, the anomalous structure might be a cause of the long-term SSE. ETS and long-term SSE are quite different in the slip velocity. It might reflect the difference in the frictional property. In Tokai, the source region of the long-term SSE and ETS is bounded by the inland Moho discontinuity. Therefore, ETS occurs at the interface between the subducting plate and overlying mantle wedge.

ETS has not been recognized besides in southwest Japan and Cascadia; however ambient tremor has been detected in some regions. We expect that the ambient tremor is triggered by small SSE which is not detected by the current observation. Understanding detail relationship between tremor and SSE based on improvement detection capability is important to reveal the mechanism of ETS.

Keywords: slow earthquake, non-volcanic tremor, slow slip event, subduction zone, plate interface

## Enhancement of slow earthquakes by geometrical irregularity of subducting oceanic crust

KATO, Aitaro<sup>1\*</sup> ; OBARA, Kazushige<sup>1</sup> ; TAKEDA, Tetsuya<sup>2</sup>

<sup>1</sup>ERI University of Tokyo, <sup>2</sup>NIED

Along the worldwide subduction zones, slow earthquakes commonly occur on the deep extension of major tectonic boundary which hosts megathrust earthquake rupture. Slow earthquakes silently release stress to the adjacent seismogenic zone, raising the likelihood of promoting unstable fast slip. However, what controls the transitional variations in fault-slip behaviors from fast to slow modes on the deep extension of megathrust fault remains controversial. Here we use a high-resolution receiver function and seismic tomography illustrated by dense seismic arrays to analyze the structural elements in the subduction complex and fore-arc mantle wedge beneath the Shikoku Island, Japan, where episodic tremor and slow-slip events (ETS) have been most intensive for over a decade.

We find out that deformed oceanic crust with irregularity of surface geometry horizontally lies in the ETS zone, where low seismic velocity zone with high Poisson's ratio that we interpret as high pore-fluid pressure. Step-like discontinuous alignments of intra-slab seismicity support the flat-subduction of the oceanic crust with faulting structure. In contrast, at depths shallower than the ETS zone, the low velocity anomaly within the oceanic crust is weak and dipping towards the NW, implying less amount of high-pressured fluid in the tilting oceanic crust. In addition, lithology of the overlying plate changes to partially serpentinized mantle wedge in the ETS zone. Locally flat-geometry of the subducting oceanic crust combined with the contact of serpentine enhances accumulation of high-pressurized fluids along the plate interface, leading to segregation between slow and fast slip modes at the deep transition zone of mega-thrust fault.

## Deformation experiments on serpentinite at high PT conditions with implications for the mechanisms of slow earthquakes

OKAZAKI, Keishi<sup>1\*</sup> ; HIRTH, Greg<sup>1</sup> ; PROCTOR, Brooks<sup>1</sup> ; KATAYAMA, Ikuo<sup>2</sup> ; TAKAHASHI, Miki<sup>3</sup>

<sup>1</sup>Department of Geological Sciences, Brown University, <sup>2</sup>Department of Earth and Planetary Systems Science, Hiroshima University, <sup>3</sup>Geological Survey of Japan, AIST

To understand the spatial and temporal distribution of earthquakes and deformation in subduction zones, it is important to constrain the rheological properties of metamorphic rocks (i.e., altered mantle, oceanic crust and sediments), and how they evolve during metamorphic reactions following hydration, carbonation and dehydration of the down-going slab. Especially, antigorite (the high-temperature serpentine polytype) serpentinite, the dominant metamorphic phase in hydrated mantle material at the condition of mantle wedge, is the key metamorphic rock to understand the generation mechanism of slow earthquakes and slab-mantle coupling at the plate interface in subduction zones.

Deformation experiments on antigorite serpentinite were conducted within and above the thermal stability field of antigorite using a gas pressure-medium apparatus and a solid pressure-medium apparatus to understand how dehydration reactions influence the mechanical behavior of antigorite serpentinite. At 400 °C, within the stability field of antigorite, antigorite serpentinite shows stable sliding and a positive velocity dependence of shear stress (i.e., friction coefficient). Shear stress increased with increasing confining pressure, while the friction coefficient decreases from 0.55 to 0.37 with increasing confining pressure from 200 MPa to 1500 MPa. These results indicate that antigorite serpentinite deforms by brittle and semi-brittle processes in subduction zones.

During the experiments using a gas pressure-medium apparatus at a confining pressure of 200 MPa and temperatures close to the dehydration temperature of antigorite (450-550 °C), antigorite serpentinite shows a slow stick-slip behaviour, which is characterised by relatively long durations and small stress drops during slip, while this type of behaviour was not observed at higher temperatures when the antigorite becomes completely dehydrated. Stick-slip in this temperature range is consistent with the temperature range where slow earthquakes occur at the corner of the mantle wedge in southwest Japan and Cascadia. The scaling law of slow stick-slip in the antigorite serpentinite gouge is distinct from that of regular earthquakes and a theoretical duration estimated from the apparatus stiffness, but similar to that of slow earthquakes.

We also conducted deformation experiments in which temperature was increased above the thermal stability of antigorite to simulate a prograde metamorphism in subduction zones, similar to the experiments by Chernak and Hirth (2011) but with a general-shear geometry. With increasing temperature from 400 °C to 700 °C during deformation, differential stress decreased and reached 120 MPa. Recovered sample suggest that the strain localizes within shear fractures and limited dehydration occurred during the experiments.

These results suggest that the dehydration of antigorite can form weak zones within the mantle wedge along the plate interface in subduction zones, even if the extent of the dehydration reaction is limited. In addition, slow instabilities of the slip interface can be caused by the dehydration of antigorite within the weak zone in the antigorite serpentinite layer, which can result slow earthquakes.

Keywords: antigorite, serpentinite, semi-brittle flow, slow earthquakes, dehydration, hydrothermal condition

## Metasomatic fault-zone weakening of subduction plate boundary faults

HIRAUCHI, Ken-ichi<sup>1\*</sup> ; SPIERS, Christopher<sup>2</sup>

<sup>1</sup>Shizuoka University, <sup>2</sup>Utrecht University

Fluid influx along faults triggers stress-induced dissolution and precipitation processes, leading to syntectonic growth of weak phyllosilicates. In subduction zones, slab-derived Si-rich fluids may infiltrate into the forearc wedge and transform primary mantle minerals into hydrous phases such as serpentines and talc, changing the mechanical and seismogenic properties of subduction plate boundary faults. However, it remains unclear how frictional strength and sliding stability of the plate boundary faults evolve via Si-metasomatism.

Hirauchi et al. (2013, *Geology*) performed frictional sliding experiments on antigorite (70%) plus quartz (30%) gouges at a pore fluid pressure ( $P_f$ ) of 200 MPa, an effective normal stress ( $\sigma_{eff}$ ) of 200 MPa, temperatures ( $T$ ) of 20, 300, 400, and 500 °C, and sliding velocities ( $V$ ) of 0.1-30  $\mu\text{m/s}$ , using a hydrothermal ring shear machine. At temperatures of 300-500°C, the gouges exhibited a peak friction coefficient ( $\mu$ ) of 0.40-0.62, followed by strain weakening towards a quasi-steady-state  $\mu$  of 0.25-0.47. The weakening was mainly due to the development of through-going, talc-rich boundary shears. The steady-state  $\mu$  of the gouges decreased systematically as the talc-rich layer widened.

At central California, there are several boundary faults that separate serpentinite bodies from shale-matrix melanges of the Franciscan accretionary complex. The serpentinite body is overprinted by anastomosing development of crack-seal veins of talc, serpentine, and calcite, suggesting that intense water-rock interaction took place in connection with faulting. The serpentinite along the faults represents a cataclastic shear zone that records brittle deformation, consisting of angular fragments that are suspended in fine-grained, randomly-oriented talc matrix. Frictional sliding experiments conducted at  $P_f = 40, 80, \text{ and } 120$  MPa,  $\sigma_{eff} = 60, 120, \text{ and } 180$  MPa,  $T = 20, 150, \text{ and } 300$  °C, and  $V = 0.3\text{-}100$   $\mu\text{m/s}$  showed that the serpentinite has friction coefficients that agree with Byerlee's law ( $\mu$  0.6), while the cataclasite is much weaker with friction coefficients as low as 0.2. Examination of the velocity dependence of friction revealed that the serpentinite exhibits both velocity-weakening and velocity-strengthening behavior, whereas the cataclasite is velocity strengthening under all conditions investigated.

Our results demonstrate that in the lowermost part of the forearc wedge, where silica-saturated fluids infiltrate from the dehydrating slab, metasomatically produced talc will form in the intensely sheared serpentinite, causing a much larger weakening effect than expected for serpentines, even if the total amount of talc formed is minor (<10 vol%). The continued reaction with Si-rich fluid will also result in a transition from seismic to aseismic behavior of the plate boundary faults.

Keywords: subduction zone, serpentinite, metasomatism, fault

## Coupled mass transport and serpentinization at crust/mantle boundary: Insights from hydrothermal experiments

OKAMOTO, Atsushi<sup>1\*</sup> ; OYANAGI, Ryosuke<sup>1</sup> ; TSUCHIYA, Noriyoshi<sup>1</sup>

<sup>1</sup>Graduate School of environmental Studies, Tohoku University

Serpentinization commonly proceeds by a supply of water passing through crust, and thus a large mass transport could occur during serpentinization reactions. Especially, silica activity is known as a control of the reaction paths and rate during the hydrothermal alteration of peridotites [1, 2]. However, it is still unclear the role of mass transport on reaction paths, overall hydration rate and volume change during serpentinization. In this study, we conducted two types of hydrothermal experiments on serpentinization. First one is the metasomatic-reaction experiments between olivine (Ol) ? quartz (Qtz) zones as analogue of boundary of mantle and crustal rocks. Second one is the hydrothermal experiments with sintered olivine (analogue of low porosity rock). Both types of experiments were carried out at 250 °C and vapor-saturated pressure (= 3.98 MPa) in alkaline aqueous solution.

In the Ol-Qtz metasomatic experiments (up to 46 days.), composite powders, which was composed of Qtz zone and Ol zone was set in inner tubes and then loaded into autoclave. After the experiments, the mineralogy and H<sub>2</sub>O content of the products were evaluated as a function of the distance from Ol/Qtz boundary. The reaction products after olivine are serpentine (Srp), brucite (Brc), magnetite (Mgt) and smectite (Smc) (instead of talc). The products systematically change from the Smc+Srp to Srp+Brc+Mgt with increasing the distance from the Ol/Qtz boundary. The H<sub>2</sub>O content of the products is low at the Ol/Qtz boundary (i.e., 3.9 wt.% after 46 days), and increases toward the margin of the tube (12 wt.% at ~30 mm from the Ol/Qtz boundary).

The detailed mass balance calculation between 25 to 46 days reveals the characteristic nature of the metasomatic reactions and porosity change as follows. Near Ol/Qtz boundary (Smc+Srp zone), smectite was formed by supply of silica in two ways; hydration of olivine and dehydration of serpentine. In contrast, at the zone far from the boundary (Srp+Brc zone; >20 mm from O/Qtz), the production rate of serpentine and brucite are constant without any silica supply. At the transition zone between Smc+Srp and Srp+Brc zones, a large amount of serpentine is formed by consumption of both brucite and olivine, which results in a largest porosity reduction (~30 %). In the Smc+Srp zone, dehydration and porosity reduction occurs simultaneously, implying a possible raise of fluid pressure. Silica metasomatic reactions causes a significant variation not only in mineral assemblage but also in porosity and fluid pressure, which will characterize the dynamic change of mechanical properties at crust/mantle boundary.

In the hydrothermal experiments of the sintered olivine, the starting olivine aggregate (initial porosity <~10 %, covered by Pt jacket), which was made by hot press at 1200 degreeC, 1 GPa and 4 days, was emplaced in the alkaline water. After 3 days, we recognized the progress of serpentinization reaction to produce serpentine and brucite. An interesting finding of this experiment is that brucite did not formed in pores of the core sample, but it was formed only at the top of the cylindrical core of the sample. This result is quite different from with our previous experiments with using olivine powder (initial porosity is ~50 %) [3], in which brucite and serpentine was formed uniformly. The result of our present study of the sintered olivine suggests that, when the rock porosity is low and volume expansion is difficult, brucite is segregated into open space (c.a. open fracture) during serpentinization; which may also affects on the formation of the local weak zone within the mantle peridotite.

[1] Frost, B. R., & Beard, J. S., 2007. *Journal of Petrology*, 48, 1351-1368.

[2] Ogasawara, Y., Okamoto, A., Hirano, N., & Tsuchiya, N., 2013. *Geochim. Cosmochim. Acta*, 119, 212-230.

[3] Okamoto, A., Ogasawara, Y., Ogawa, Y. and Tsuchiya, N., 2011. *Chemical Geology*, 289, 245-255.

Keywords: serpentinization, hydrothermal experiments, silica metasomatism, porosity change, hydration, mass transport

## Saline fluids recorded in jadeitites in subduction-zone melanges of southwest Japan

MORI, Yasushi<sup>1\*</sup> ; SHIGENO, Miki<sup>1</sup> ; KAWAMOTO, Tatsuhiko<sup>2</sup> ; NISHIYAMA, Tadao<sup>3</sup>

<sup>1</sup>Kitakyushu Mus. Nat. Hist. Hum. Hist., <sup>2</sup>Inst. Geotherm. Sci., Kyoto Univ., <sup>3</sup>Grad. Sch. Sci. Tech., Kumamoto Univ.

Slab-derived fluids play essential roles in mass transfer along subduction-zone channels between the subducting slab and mantle wedge (e.g., Bebout 2013 *Metasomatism and the chemical transformation of rocks*; Spandler and Pirard 2013 *Lithos*). Salinity of such slab-fluids probably affects solubility and fluid-rock partitioning of elements; therefore, it remains to be investigated in various rocks. Jadeitite is a rock composed mainly of jadeite (sodium pyroxene, NaAlSi<sub>2</sub>O<sub>6</sub>) and occurs typically in serpentinite mélanges intercalated to high-pressure and low-temperature metamorphic belts. This curious rock is thought to be the product of direct precipitation from aqueous fluids and/or of fluid-induced metasomatism of a protolith (Harlow *et al.* 2007 *Geology of gem deposits*, Tsujimori and Harlow 2012 *Eur J Mineral*, and references therein). Fluid inclusions are commonly observed in jadeitites, and they may provide information about the fluid composition in subduction-zone mélanges. We determined major components and salinity of fluid inclusions in the jadeitites collected from eight localities in Japan: Omi-Itoigawa (Omi-Renge belt), Oya and Osa (Suo belt), Kochi (Kurosegawa belt), Mie and Tone (Nishisonogi metamorphic rocks), and Shimonita and Yorii (the origin unclear). In all of the studied rocks, primary fluid inclusions consist of a liquid phase and a gas bubble. Raman spectra show the presence of H<sub>2</sub>O liquid and vapor with or without minor CH<sub>4</sub> gas. The freezing point of the liquid phase indicates high-salinity (up to 8 wt% NaCl equivalent) of the primary fluid inclusions. The salinity varies among the localities of the jadeitite. For example, the salinity of the primary fluid inclusions is about  $7.1 \pm 0.1$  wt% NaCl equivalent in the albite jadeitite from Oya and about  $4.6 \pm 1.2$  wt% NaCl equivalent in quartz inclusions bearing jadeitite from Tone. Some jadeitite samples contain secondary CH<sub>4</sub>-rich fluid inclusions along healed microcracks. The presence of minor CH<sub>4</sub> is also reported in the saline fluids inclusions with  $5.1 \pm 1.9$  wt% NaCl equivalent from the Myanmar jadeitite (Shi *et al.*, 2005 *Geochem J*). The present findings suggest that saline fluids with or without CH<sub>4</sub> are common in subduction-zone mélanges in Japan as well as in Myanmar. The reduced conditions can be caused by serpentinization processes. This is contrast to the CO<sub>2</sub>-bearing saline fluids in the peridotite xenoliths from fore-arc mantle wedge (Kawamoto *et al.*, 2013 *PNAS*). The high-salinity of the slab-fluids probably enhances the mobility of elements such as Pb in subduction-zone channels (Keppler, 1996 *Nature*, Shigeno *et al.*, 2012 *Eur J Mineral*).

Keywords: saline fluid, jadeitite, fluid inclusion, serpentinite mélange, subduction zone

## Serpentinite structure above subduction surface: Analysis of a natural example in Sanbagawa metamorphic belt

MIZUKAMI, Tomoyuki<sup>1\*</sup> ; SODA, Yusuke<sup>1</sup> ; YOKOYAMA, Hironori<sup>1</sup> ; HIRAMATSU, Yoshihiro<sup>1</sup>

<sup>1</sup>Kanazawa University

Serpentinization is a key reaction in forearc mantle. Formation of strong schistosity and shear zones under high differential stresses provides anastomosing networks of fluid pathways as well as seismically anisotropic nature in the mantle. Understanding of such structural development is important for both interpretation of seismic analyses and forward modelling of subduction system including thermal structure, material circulation, magma process and slip behaviours of subduction boundaries.

We report results of petrological and structural analyses of layered antigorite (Atg) serpentinite in the marginal part of the Higashi-akaishi ultramafic unit in the Sanbagawa belt. This is a product of hydration of dunite (a rock consisting of almost 100% olivine (Ol)) due to metamorphic fluid from the underlying meta-sediments and meta-basites. Strong shape preferred orientation of Atg and existence of boudinaged layers indicate fluid-rock reaction under extensional deformation.

The layered structure is defined by a centimeter to meter-scale interlayering between Ol-rich and Atg-rich units. The modal amounts of Atg in these units form peaks at 15 vol% and 50 vol%, respectively, showing a bi-modal distribution as a whole. Effects of initial microstructures on the extent of serpentinization are limited: Porphyroclastic and fine-grained dunite, that occupy a large part of the outcrop, are transformed to both Ol-rich and Atg-rich layers although dunite with more than 50 % of coarse Ol grains has been poorly serpentinized. Each Atg layer shows millimeter-scale spaced foliations defined by amounts of Ol and Atg and locally shows a diffusive variation in millimeter to centimeter-scales. Thickness and proportion of Atg-rich layers increase near the contact with crustal rocks.

Reaction for the Atg formation is constrained based on re-distribution of elements among Ol, Atg and opaque minerals. As serpentinization proceeds, Ol is enriched in Fe and Ni owing to their incompatibility in Atg. Taking concomitant formations of minor amounts of magnetite and sulfides into account, the variation of the Ol composition and modal amounts of serpentinization products are quantitatively explained by the following reaction:  $Ol + SiO_{2,aq} + H_2O \Rightarrow Atg$ . This indicates that the development of Atg has been controlled by a supply of silica in aqueous fluids.

We measured thickness of 70 layers for each and, taking the layers with the thickness lower than 200 centimeters, we found exponential relationships in cumulative frequency distributions both for Ol-rich and Atg-rich layers. Relative thickness between neighbouring units  $[d(Ol)/d(Atg)]$  also shows an exponential distribution. We could not find any regular relationships among width and spacing like Liesegang patterns.

It is known that pattern structures appear in reaction-diffusion systems. The above observations strongly suggest that the development of layered structures in Atg serpentinite is controlled by interaction between reaction and material transfer. In this case, potential causes of heterogeneous serpentinization may be diffusional contrast between  $H_2O$  and  $SiO_2$  or permeability contrast between Ol-rich and Atg-rich layers. Scaling analyses of deep low frequency tremors showed that duration-amplitude and size-frequency distributions of tremors in SW Japan can be fit with exponential models rather than power-law models. The seismological observations imply structural heterogeneity with unique scale length. Further examination on the exponential relationships developed in serpentinite may contribute to understand the slip phenomena on plate interfaces.

Keywords: serpentinite, layered structure, reaction-diffusion, exponential frequency distribution, deep low frequency tremor

## Awaruite in serpentinites from Oshima Peninsula, Fukui Prefecture, Japan

YAMAGUCHI, Kai<sup>1\*</sup> ; UEHARA, Seiichiro<sup>2</sup>

<sup>1</sup>Department of Earth and Planetary Sciences, Faculty of Science, Kyushu University, <sup>2</sup>Department of Earth and Planetary Sciences, Faculty of Science, Kyushu University

Awaruite is one of native Ni-Fe alloys, and the compositional range is Ni<sub>2</sub>Fe to Ni<sub>3</sub>Fe. The space group is *Fm3m* or *Pm3m* (e.g., Williams, 1960; Ahmed et al., 1981). Typical grain sizes are 10-300 μm, and grain shapes are typically irregular, anhedral or skeletal. It is found only in the serpentized peridotites and chondritic meteorites (e.g., Ramdohr, 1967; Clarke et al., 1970). In general, awaruite is observed in serpentine vein (Sakai and Kuroda, 1983), and coexist with other metal minerals (Kanehira et al., 1975). This study deals with the characteristic occurrence of awaruite in pseudomorph texture in the Oshima serpentinites from Oshima peninsula, Fukui prefecture, Japan.

All samples were examined with polarizing microscope observation, X-ray diffraction analysis and SEM-EDS analyses. Preparation of TEM specimen and microtexture observation were conducted with an ion milling machine (JEOL EM-09100IS) and TEM (JEOL JEM-2000FX, JEM-3200FSK) in the Research Laboratory for High Voltage Electron Microscopy (HVEM), Kyushu University, Japan. Chemical analyses of microtexture were also examined using JEM-3200FSK equipped with EDS.

Peridotites in this area are partially or perfectly serpentized. Texture of the serpentinite is mesh texture after forsterite and vein texture. Scarcely serpentized enstatite is also observed. Each mesh texture is composed of mesh rim shows optical anisotropy and mesh core shows optical isotropy. The serpentization of mesh texture is strong in close to vein textures. Most mesh rims near vein texture consist of some layers; outer rim, outer-inner rim boundary and inner rim. These rims consist of chrysotile, about 50 nm in width and 2 μm in length, and lizardite, about 300 nm in width and 1 μm in length, and outer-inner rim boundary about 2 μm in width are filled with serpentine fine grains, up to 100 nm in diameter.

A number of awaruite fine grains, 200-300 nm diameter, array along cell boundary, outer-inner rim boundary and rim-core boundary. These awaruite coexist with no other metal minerals; pentlandite, magnetite and etc. In contrast, metal minerals in vein texture are magnetite and minor pentlandite. These results indicate that mesh texture in serpentinite is extremely reductive environment compared with vein texture. The chemical composition of awaruite (average of four analysis) is Ni 73.13% and Fe 26.87%. The cross-section of these awaruite grains is square or rhombic, indicating that these grains are cube or octahedral crystals (fig. 1a). These grains seem to be euhedral from grain shapes, and this is characteristic compared with previous studies (e.g., Rubin, 1991). The SAED pattern recorded along the [001] zone axis shows strong 200, 220 reflections and weak 100, 110 reflections (fig. 1b). This indicates space group of the Oshima awaruite is *Pm3m*, which is ordering phase of *Fm3m* awaruite. Lower symmetry of the Oshima awaruite will be formed lower temperature.

Keywords: Awaruite, Mesh texture, Serpentinite, Microtexture, Serpentine minerals, TEM

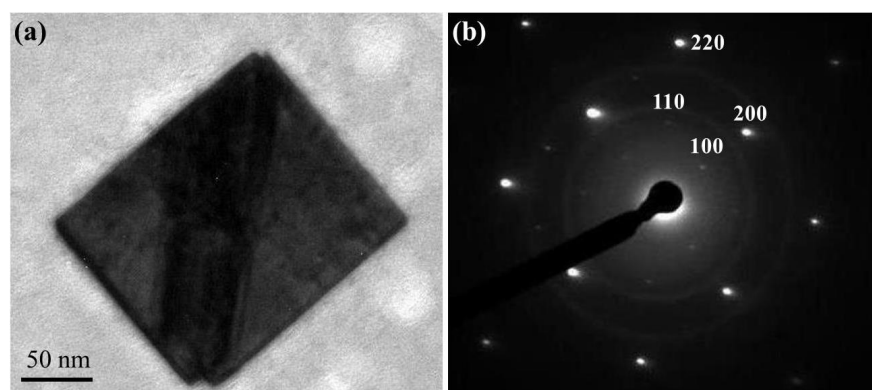


Fig. 1. (a) TEM image of awaruite in mesh texture. (b) The SAED pattern of (a) recorded along the [100] zone axis.

## Antigorite CPO measured by U-stage, EBSD and synchrotron X-rays

SODA, Yusuke<sup>1\*</sup> ; ANDO, Jun-ichi<sup>2</sup> ; URATA, Yoshito<sup>2</sup> ; WENK, Hans-rudolf<sup>3</sup>

<sup>1</sup>Kanazawa University, <sup>2</sup>Hiroshima University, <sup>3</sup>University of California, Berkeley

Foliated antigorite serpentinite with crystallographic preferred orientation (CPO) probably causes shear wave splitting observed at subduction zones (e.g., Katayama et al., 2009). Therefore, the study of type and intensity of antigorite CPO is an important to understand the detail of this phenomenon.

Soda and Wenk (2014) measured CPOs of antigorite serpentinite from the Sashu Fault at the Saganoseki Peninsula, Oita Prefecture, by three independent methods, U-stage (with optic microscope), EBSD and synchrotron X-rays. The obtained antigorite CPOs by three methods are almost same without the fabric strength, maxima of pole figures in multiples of random distribution. The fabric strength decreases in the following order, U-stage >EBSD >synchrotron X-rays, which is probably caused by the characteristics of three methods. Through U-stage measurement, we can obtain the fabric pattern of antigorite CPO mainly from coarser antigorite grains (>30  $\mu\text{m}$ ). In the case of EBSD measurement, we measure antigorite CPO within an area of ca. 0.8 mm  $\times$  0.8 mm. Measurement points of only ca. 30% can be used to make fabric patterns. Residual ca. 70% points are neglect, because the quality of Kikuchi lines from them is too low to identify the orientation. In the synchrotron X-rays method, the result represents the bulk fabric from a volume of ca. 0.5 mm  $\times$  0.5 mm  $\times$  1.0mm.

The serpentinite measured antigorite CPO develops mylonitic structures with a penetrative foliation and lineation (Soda and Takagi, 2010). The antigorite grains show undulose extinction. And their grain boundary is unclear under the microscopy. Mg# (Mg/(Mg+Fe)) of antigorite grains is wide range 0.98-0.88. The BSE images indicate Fe-rich antigorite infilling the grain boundaries and fractures of Mg-rich antigorite.

The same serpentinite has already observed by TEM (Urata et al., 2009). The results indicate that the m-values of antigorite grains, the number of octahedral along the [100] modulation wave, make two groups, high m-value (16-18) and low m-value (13-14). This result suggests that the antigorite are crystallized mainly two stages, which is supported by the variation of Fe contents of antigorite (Fe-rich and Mg-rich). The Mg-rich antigorite grains are main minerals composed of the serpentinite, Fe-rich antigorite grains occupy at the periphery of the others and within the vein. The TEM observation indicates that the Mg-rich antigorite grains are subdivided into sub-grain with 50-100 nm in size, which can be recognized as an undulose extinction under optic microscope.

These microstructures of antigorite grains potentially influence the outcome of CPO measurements. The weaker fabric patterns from the synchrotron X-rays are probably attributed to the fine-grained antigorite crystallized at the deferent stages and to sub-grain. And the U-stage and EBSD measurements focus only the selected grains, which may result in overestimation of elastic wave anisotropy of serpentinite.

### References

- Katayama et al, 2009, Nature 461, 1114-1117.
- Soda and Takagi, 2010, Journal of Structural Geology 32, 792-802.
- Soda and Wenk, 2014, Tectonophysics, in press
- Urata et al., 2009, AGU2009 abstract. MR41A-1858.

Keywords: antigorite, CPO, synchrotron X-ray, elastic anisotropy

## Olivine CPO in non-deformed peridotite due to topotactic replacement of antigorite

NAGAYA, Takayoshi<sup>1</sup>; WALLIS, Simon<sup>1\*</sup>; KOBAYASHI, Hiroaki<sup>1</sup>; MICHIBAYASHI, Katsuyoshi<sup>2</sup>; MIZUKAMI, Tomoyuki<sup>3</sup>; SETO, Yusuke<sup>4</sup>; MIYAKE, Akira<sup>5</sup>; MATSUMOTO, Megumi<sup>6</sup>

<sup>1</sup>Department of Earth and Planetary Sciences, Nagoya Nagoya University, <sup>2</sup>Institute of Geosciences, Shizuoka University, <sup>3</sup>Department of Earth Science, Kanazawa University, <sup>4</sup>Department of Earth and Planetary Science, Kobe University, <sup>5</sup>Department of Earth and Planetary Science, Kyoto University, <sup>6</sup>Center for Supports to Research and Education Activities, Kobe University

Olivine crystallographic preferred orientation (CPO) is thought to be the main cause of seismic anisotropy in the mantle, and its formation is generally considered to be the result of plastic deformation of mantle by dislocation creep. Olivine CPO has been reproduced in laboratory deformation experiments and considerable success has been achieved in understanding the deformation conditions (e.g. stress, temperature and water content) under which different olivine CPO patterns develop. This opens the possibility of mapping conditions in the mantle using seismic anisotropy and has been the subject of considerable study. Here we report an alternative mechanism for olivine CPO without the need for deformation. This process may be important in understanding the seismic properties of mantle in convergent margins.

Metamorphic studies show peridotite in the Happo area, central Japan, formed by the dehydration of antigorite-schist related to contact metamorphism around a granite intrusion. Both field and microstructural observations suggest the olivine has not undergone strong plastic deformation. This was confirmed by TEM work that shows the olivine has very low dislocation densities and lacks low angle tilt boundaries. Such tilt boundaries are general stable even after annealing. These features show that peridotite in the Happo area formed in the absence of solid-state deformation.

The olivine of the Happo peridotite formed dominantly by the dehydration breakdown of antigorite schist. We propose that the olivine CPO formed as a result of topotactic replacement of antigorite by the newly formed olivine. EBSD measurements in samples where both antigorite and new olivine are present and in contact show a very close crystallographic relationship between the two minerals: the *a*-axes are parallel, and the *b*- and *c*-axes are perpendicular. We conclude the strong olivine CPO in the Happo area was inherited from the original CPO of the antigorite. Such a process is likely to also occur in subduction zones where serpentinite is dragged down by plate movement. Topotactic growth of olivine may be an important cause of mantle anisotropy in convergent margins.

Keywords: subduction zones, microstructure, B-type olivine CPO, antigorite, topotaxy

## Cr-rich olivine in deserpentinized peridotite and its implication

ENDO, Shunsuke<sup>1\*</sup>

<sup>1</sup>Institute of Geology and Geoinformation, AIST

Formation of Cr-rich olivine ( $\text{Cr}_2\text{O}_3 > 0.1$  wt %) in the presence of Cr-spinel  $\pm$  pyroxene has been thought to require extremely reducing and/or high-temperature conditions. Indeed, terrestrial olivine is Cr-free except for some high-T occurrences from Archaean komatiites, inclusions in diamonds, and ultrabasic pseudotachylytes. Deserpentinization is an important fluid release process in subduction zones. One of the best studied examples of this process occurs in Cerro del Almirez (SE Spain), where the antigorite-out reaction front ( $\text{Atg} = \text{Ol} + \text{Opx} + \text{Chl} + \text{H}_2\text{O}$ ) at eclogite facies conditions is well preserved. Large elongate olivine crystals (similar to spinifex textures in komatiites) at the reaction front contain abundant exsolution lamellae of Cr-magnetite, and estimated primary compositions of the elongate olivine show high Cr content (0.1-0.4 wt%  $\text{Cr}_2\text{O}_3$ ), leading to a proposal of the spinifex-like textured peridotite being pseudotachylyte ( $> 1600$  °C, Evans & Cowan, 2012), in contrast to the generally held view that the elongate olivine crystallized under ambient subduction-zone T ( $\sim 680$  °C at 1.9 GPa) but high supersaturation conditions.

To better understand the dehydration process of serpentinite in subduction zones, this study focuses on a deserpentinized peridotite from the Eclogite unit of the Sanbagawa belt (SW Japan). It consists of porphyroblastic olivine ( $\sim 70$  vol %,  $\text{Mg}\# = 0.952 \pm 0.004$ ,  $\text{NiO} = 0.37 \pm 0.04$  wt%), antigorite ( $\text{Al}_2\text{O}_3 = 0.3-0.5$  wt%), brucite, zoned Cr-spinel and Ni sulfides. Olivine porphyroblasts contain inclusions of antigorite, brucite, magnetite and Ni sulfides, suggesting that the olivine-forming reaction  $\text{Atg} + \text{Brc} = \text{Ol} + \text{H}_2\text{O}$  took place after serpentinization of a dunitic protolith. Sporadic occurrences of Ni-rich olivine (up to 8.1 wt% NiO) within the olivine porphyroblasts suggest prograde breakdown of Ni-rich sulfides. Zoned Cr-spinel grains are composed of a chromite core, a ferritchromite mantle, and an irregular-shaped overgrowth of Cr-magnetite. The chromite core, being the only primary mineral preserved, shows Cr-rich/Ti-poor compositions [ $\text{Cr}/(\text{Cr}+\text{Al}) = 0.74-0.76$ ,  $\text{TiO}_2 < 0.14$  wt%] indicative of a forearc wedge mantle origin. The Cr-magnetite rim contains inclusions of Cr-rich olivine ( $\text{Cr}_2\text{O}_3 = 0.12-0.70$  wt %,  $\text{Mg}\# = 0.950 \pm 0.004$ ,  $\text{NiO} = 0.37 \pm 0.04$  wt%), in addition to Cr-rich antigorite ( $\text{Al}_2\text{O}_3 = 0.5-3.1$  wt%,  $\text{Cr}_2\text{O}_3 = 0.3-3.9$  wt%), diopside and brucite.

Formation of the Cr-rich olivine inclusions can be explained by dehydration of Cr-rich antigorite that developed around Cr-spinel grains. Slow diffusivity of  $\text{Cr}^{3+}$  compared to the olivine growth rate may have caused disequilibrium Cr incorporation into olivine under low-T conditions just above the  $\text{Atg} + \text{Brc}$  breakdown equilibrium ( $\sim 460-500$  °C). Alternatively, a distinct Cr substitution mechanism ( $\text{Cr}^{3+} + \text{Fe}^{3+} = \text{Mg} + \text{Si}$ ) than that proposed for high-T olivine ( $\text{Cr}^{2+} = \text{Mg}$  or  $2\text{Cr}^{3+} + \text{vacancy} = 3\text{Mg}$ ) could explain the low-T formation of Cr-rich olivine. In any case, the local uptake of Cr in olivine from the Sanbagawa metaserpentinite does not imply very high-T conditions, and this weakens the main basis of the pseudotachylyte hypothesis for the spinifex-like textured peridotite in Cerro del Almirez. The geological record on the causal link between deserpentinization and deep earthquake nucleation remains elusive.

Keywords: Cr-rich olivine, antigorite, dehydration, subduction zone

## Spatial variation in scale length of deep low-frequency tremor inferred from duration-amplitude scaling in western Shiko

HORINO, Kazuki<sup>1\*</sup> ; HIRAMATSU, Yoshihiro<sup>2</sup> ; MIZUKAMI, Tomoyuki<sup>2</sup> ; OBARA, Kazushige<sup>3</sup> ; MATSUZAWA, Takanori<sup>4</sup>

<sup>1</sup>Division of Natural System, Graduate School of Natural Science and Technology, Kanazawa University, <sup>2</sup>School of Natural System, College of Science and Engineering, Kanazawa University, <sup>3</sup>Earthquake Research Institute, University of Tokyo, <sup>4</sup>National Research Institute for Earth Sciences and Disaster Prevention

Slip properties on plate interface vary largely along dip direction from seismic to aseismic slip. At the transition zone at depths of 25-35 km, non-volcanic deep low-frequency (DLF) tremor and short-term slow slip event occur in the Nankai subduction zone. Recent detailed studies (e.g. Obara, 2010) reveal along dip and along strike variations in the occurrence and the migration of DLF tremor in the transition zone. We report here an along dip variation in scale length of DLF tremor inferred from duration-amplitude scaling in the western Shikoku.

A physical process of natural phenomena is reflected by scaling law, for example, frequency of occurrence versus size distribution. Watanabe et al. (2007) reported that a duration-amplitude distribution of DLF tremor shows a better fit to the exponential model rather than the power-law model, which is different from regular earthquakes. We investigate the duration-amplitude distribution of DLF tremor using Hi-net data in the western Shikoku. The procedure of analysis is the same as that of Watanabe et al. (2007).

We focus on the slope of the exponential distribution for the duration-amplitude distribution of DLF tremor. The value of the slope is small in the western area and large in the eastern area. Noting along dip direction, we can recognize a weak variation of the value of the slope. Deeper DLF tremor tends to show a larger value of the slope than shallower DLF. A large value of the slope means a small scale length and vice versa.

Beneath the western Shikoku, the configuration and the age distribution of the subducting Philippine Sea plate changes significantly along the strike, generating a large variation in a thermal structure. Such a variation causes various modes of serpentinization in the hanging wall mantle. The resultant structures due to the different modes are the most likely cause of the detected transition of the scale length.

Keywords: deep low-frequency tremor, scaling law, subduction zone, size distribution, serpentinization

## Lithospheric Rheology and Stress and the Dynamics of Plate Tectonics

ZHONG, Shijie<sup>1\*</sup>

<sup>1</sup>Department of Physics, University of Colorado

Plate tectonics is a kinematic theory that describes relative motions of Earth's surface tectonic plates. However, with the subduction of cold lithosphere into mantle interiors, plate tectonics has profound implications on the thermal and dynamic evolution of planets. Earth appears to be the only planetary body in the solar system that has active plate tectonics. The cause of plate tectonics remains one of the most important unresolved questions in Earth and planetary sciences. The recent discovery of a large population of exoplanets further raises the question on how common plate tectonics is to planetary bodies and what causes plate tectonics. In this presentation, I will discuss two issues that are important to understanding the origin of plate tectonics: lithospheric rheology and stress. Lithospheric rheology is important for understanding crustal and lithospheric dynamics, and the conditions for plate tectonics. For example, numerical modeling studies suggest that plate tectonics emerge from the dynamics of mantle convection when a small coefficient of friction  $\mu$  ( $<0.1$ ) or small yield stress for lithosphere is used [Moresi and Solomatov, 1998]. However, both in-situ borehole stress measurement (to  $\sim 10$  km depth) and laboratory studies suggest that  $\mu \sim 0.6$  [Kohlstedt et al., 1995; Zoback and Townend, 2001]. A recent study that models the seismically observed elastic flexure and seismicity at Hawaiian islands in response to volcanic loading indicates  $\mu > 0.25$  [Zhong and Watts, 2013]. The loading study [Zhong and Watts, 2013] also suggests that lithospheric rheology related to low-temperature plasticity is significantly weaker than laboratory studies [Mei et al., 2010] and that lithospheric stress at Hawaiian islands is 100-200 MPa, possibly largest lithospheric stress on the Earth, given that Hawaiian islands represent the largest uncompensated surface loads on the Earth. These studies highlight the importance to understand the evolution of lithospheric stress and rheology from plate interiors to plate boundaries, in order to understand the cause of plate tectonics. I will also discuss the convection-driven stress in the top thermal boundary (lithosphere). Convection-driven stress scales with Rayleigh number and hence mantle viscosity. A larger mantle viscosity or smaller Rayleigh number leads to a larger viscous stress in the lithosphere in mantle convection models. Some recent mantle convection studies for plate tectonics generation reported  $>500$  MPa stress in lithosphere. It is important to develop independent observable measures to examine the relevance of modeled lithospheric stress. I will discuss possible measures that may be developed and used in this context.

Keywords: Mantle Convection, Plate Tectonics, Lithospheric Stress, Lithospheric Rheology, Brittle Deformation

## 3D numerical modeling of thermal regime and mantle flow associated with subduction of the two oceanic plates

Ji, Yingfeng<sup>1\*</sup> ; YOSHIOKA, Shoichi<sup>1</sup>

<sup>1</sup>RCUSS, Kobe University, <sup>2</sup>Graduate School of Science, Kobe University

Based on a thermal convection model for an arbitrarily curved oceanic plate, we newly constructed a 3D model for subduction of two oceanic plates, and investigated its thermal regime and mantle flow. The 3D parallelepiped modeled domain for numerical simulations is a length of 840 km, a width of 840 km, and a depth of 300 km, with 72\*72\*72 grids, and the total calculation time up to 15 Myr. Geometry of one continental plate and two oceanic plates are prescribed in the simulation. The two oceanic plates subduct with prescribed velocities beneath the continental plate along neighboring two trenches, adjoining with a right angle. The upper oceanic plate and the lower oceanic plate contact each other at their intersection zone. Both of the oceanic plates are assumed to be 30 km in thickness. Giving boundary conditions of adiabatic and permeable walls, half-space cooling and rigid upper surface, and stratified initial temperature condition, we solved equations of mass conservation, momentum, and energy, using the finite difference method (FDM) and Finite Volume Method (FVM). In this study, the dynamical properties of the thermal regime associated with double subduction are investigated in detail. In our numerical simulation for the subducting two oceanic plates, the convergent rate of the upper oceanic plate should be paralleled to the intersection line of the two plates so as to reach a stable and sustainable subduction. Dip angles of the two oceanic plates, obliquity of the lower oceanic plate, and subduction velocity are assumed to be 10 deg, 0 deg ~75 deg, and 5 cm/yr, respectively. As a result of numerical simulation, we found that there are remarkable low temperatures in the inter-slab zone due to subduction of the two cold oceanic plates. We also found that obliquity and relative directions of plate subduction velocities contribute to the obliquity of subduction-induced mantle flow convection adjacent to the two oceanic plates, and spiral mantle convection may be produced by the difference of the obliquity of two oceanic plates.

Keywords: thermal regime, plate tectonics, subduction, numerical simulation

## Mantle flow and overriding plate stress state in 3-D models of thermo-mechanical subduction

HOLT, Adam<sup>1</sup> ; BECKER, Thorsten<sup>1\*</sup>

<sup>1</sup>University of Southern California

The formation of back-arc basins is a fundamental component of plate tectonics, yet the dominant mechanism for their formation, and whether an individual mechanism is dominant over different tectonic settings, is not entirely clear. On top of the classic mechanism of extension being driven by basal tractions due to poloidal return flow, recent numerical and experimental modeling studies have indicated that, for slabs with finite widths, toroidal return flow around slab edges plays an important role. We investigate the relative contribution of poloidal and toroidal flow field components to back-arc extension by examining the overriding plate stress regime in conjunction with the flow field for various model setups. We characterize the velocity field by decomposing it into toroidal and poloidal components at various stages of subduction, and calculating the ratio of the toroidal to poloidal RMS velocities (TPR).

Models are carried out using a thermo-mechanical setup of the finite element code, CitcomCU. We find that the presence of an overriding plate reduces the development of trench curvature, and so 3-D modeling studies that neglect the presence of the overriding plate may be significantly overestimating the rate of development of trench curvature. Within the overriding plate, we observe long wavelength back-arc extensional stresses at a large distance from the trench and more localized forearc compressive stresses. Fixing the position of either the subducting or overriding plate causes the amplitude of back-arc extension to be greater than that for the case when both plates are free. This occurs because, for the fixed overriding plate models, all of the slab rollback is forced to occur at the expense of overriding plate thinning/extension, and for the fixed subducting plate models, increased rollback causes heightened toroidal flow. For all models with significant slab rollback, the poloidal RMS velocity is maximum in the very upper and lower portions of the model whereas toroidal flow is maximum at mid-domain depths due to return flow around slab edges, indicating that slab rollback-induced toroidal flow is focussed at sub-lithospheric depths, where it has the potential to contribute to back-arc extension. Reducing the width of the plate vastly reduces the rate of slab rollback, yet increases the degree of back-arc extension and focuses it closer to the trench. In such models, toroidal flow magnitude is approximately constant throughout the domain resulting in only minor TPR variation with depth, and yet the magnitude of overriding plate extensional stress is large, possibly suggesting an alternate control on back-arc extension.

Finally, we investigate the effect that Byerlee plasticity and a laterally confining side plate has on both overriding plate stress state and the flow field. Including a side plate does not modify the slab dynamics and overriding plate stress state, yet significantly reduces the toroidal RMS velocity component throughout the model, while retaining the systematic variation, which results in uniformly reduced TPR throughout the domain. The inclusion of plasticity, intended to approximate brittle failure, gives rise to elevated forearc compression, due to increased plate convergence, and reduced backarc extension.

Keywords: subduction, mantle flow, slab rollback, overriding plate stress

## Magnetic spectral analysis over the Atlantic Ocean off Portugal

MATSUSHIMA, Jun<sup>1</sup> ; OKUBO, Yasukuni<sup>2</sup> ; ANTONIO, Correia<sup>3</sup> ; UCHIDA, Youhei<sup>2\*</sup>

<sup>1</sup>Graduate School of Engineering, <sup>2</sup>Geological Survey of Japan, <sup>3</sup>University of Evora

Magnetic spectral analysis, which has often been applied to estimate Curie point depths, was used to delineate thermal and crustal structure of the Atlantic Ocean off Portugal. The Atlantic oceanic plate covers the study area deepening eastward and volcanic islands rise in the eastern margin. We used EMAG2, the resolution and the altitude of which are 2 arc minute and 4 km above geoid, respectively. Linear magnetic anomalies are dominant over the study area. They are attributed to the seafloor spreading of the oceanic plate. The magnetic lineation forms a strong directional feature not only in the space domain but also in the spectral domain. Taking the directional feature, we developed a pseudo-one dimensional spectral analysis using two dimensional data sets. The gradient of the power spectrum across the lineation depends on the centroid depth of magnetic layer. The bottom depth is easily calculated by the centroid and the seafloor depth, assuming that the top of magnetic layer corresponds to the seafloor. The bottom of magnetic layer over young oceanic plate deepens with time, because the Curie point depth deepens with time. Taking the relationship, we assume that the bottom of magnetic layer over the Atlantic oceanic plate corresponds to the Curie point depth and delineates a thermal structure. The results of spectral analysis show that the bottom depths over the oceanic plate are deepening gradually from the ridge to Europe. The results correlate well with magnetic isochrons and thermal history of the oceanic plate. The bottom depths over the volcanic islands are anomalously shallow indicating a rise of high thermal structure.

Keywords: Magnetic data, spectral analysis, Curie point

## Subduction Processes and a New Hypothesis for “Top-down Hemispherical Dynamics” of the Earth

IWAMORI, Hikaru<sup>1\*</sup> ; NAKAMURA, Hitomi<sup>2</sup> ; HANYU, Takeshi<sup>1</sup> ; KIMURA, Jun-ichi<sup>1</sup> ; NAKAKUKI, Tomoe<sup>3</sup> ; NAKAGAWA, Takashi<sup>1</sup> ; YOSHIDA, Masaki<sup>1</sup> ; TANAKA, Satoru<sup>1</sup> ; SUETSUGU, Daisuke<sup>1</sup> ; OBAYASHI, Masayuki<sup>1</sup>

<sup>1</sup>JAMSTEC, <sup>2</sup>TITEC, <sup>3</sup>Hiroshima University

Water-rock interactions reduce the rock strength, and possibly produce weak plate boundaries, inducing active plate tectonics. Water-rock interactions may also have geochemical impacts, causing the unique differentiation of the Earth (e.g., formation of granitic continental crust and hydrothermal ore deposits). However, how water actually interacts with the rocks and circulates within the solid Earth to contribute to material differentiation and dynamics has been poorly constrained. In this paper, we present numerical models of water and element transport in subduction zones, as well as global geochemical evidences for water and the associated element cycling in the mantle. Then we compare these geochemical evidences with the geophysical observations and modeling to propose “top-down hemispherical dynamics” for the whole Earth’s interior.

Water-rock interaction may significantly reduce the viscosity of rocks [1], and affects the subduction zone dynamics. Hydrated subducting slabs release water as the slabs are heated up, which hydrates the bottom of mantle wedge just above the subducting slab, to form a serpentinite layer. In this case, the slab-wedge mechanical coupling is reduced, and weakens the wedge corner flow, decreasing the slab surface temperature. The serpentinite layer is stabilized to extend deeper, enhancing mechanical decoupling between the slab and the wedge. This positive feedback has a large impact on the overall thermal-flow structure and magmatism in subduction zones [2]. We compare the model results and the observations such as position of arc magmatism, heat flow and seismic structures to constrain the actual structure and dynamics.

Water may enhance elemental transport once a fluid phase is formed and migrates, which potentially causes specific elemental fractionation. We have constructed two-dimensional models of trace element transport in subduction zones, incorporating (i) slab subduction-dehydration, (ii) fluid migration and its reaction with the convecting mantle, (iii) melt generation and (iv) associated elemental partitioning among the solid, aqueous fluid and melt [3]. This model predicts various trace element abundances in solid, fluid and melt, and shows that significant variability in terms of trace element ratios is produced in subduction zones and can be brought down to the deep mantle. The trace element variability must affect long-term radiogenic isotopic evolution of the mantle (e.g., Sr, Nd and Pb isotopic compositions). Recently, a global isotopic structure has been found based on a statistical analysis of a large geochemical data set including MORB, OIB and arc basalts [4]: the eastern mantle hemisphere is enriched in subducted aqueous fluid components compared to the western hemisphere. Magnitude of the radiogenic ingrowth for the hemispherical structure suggests that it has been mostly developed within the last several hundred million years. These observations can be explained by focused subduction towards the supercontinent (Rodinia, Gondwana and Pangea), which has created the large-scale mantle heterogeneity. A strikingly similar pattern is found for the seismic velocity structure of the inner core [5,6]. Such hemispherical structures may be key to understanding the global dynamics of the Earth. We propose that the focused plate subduction governs the flow and thermal structure of the deep interior, in a “top-down” manner.

References: [1] S. Karato, H. Jung, *Philos. Mag.* 83, 410 (2003). [2] S. Horiuchi, Ph.D. thesis, U. Tokyo (2013). [3] A. Ikemoto, H. Iwamori, *Earth Planet. Space*, in revision. [4] H. Iwamori, H. Nakamura, *Geochem. J.* 46, e39 (2012). [5] S. Tanaka, H. Hamaguchi, *JGR* 102, 2925 (1997). [6] L. Waszek et al., *Nature Geo.* 4, 264 (2011).

Keywords: subduction, water, trace element, isotope, hemisphere, mantle

## Effects of plate-like behavior and material recycling on lateral variation of CMB heat flux

NAKAGAWA, Takashi<sup>1\*</sup>

<sup>1</sup>IFREE, JAMSTEC

We studied the relationship between heat flux across the core-mantle boundary (CMB) and seismic anomalies in the CMB region in numerical mantle convection simulations in a 3-D spherical shell with a simple temperature- and depth-dependent viscosity [Nakagawa and Tackley, 2008]. That study suggested that the relationship between CMB heat flux and seismic anomalies was not simple linear function because of the post-perovskite phase transition and/or compositional heterogeneous structure in the deep mantle. However, in that study, we did not include the complicated rheology that occurred to the plate tectonics-like behavior and the segregation of oceanic crust in the deep mantle because they would be important for regulating the heat flux across the CMB [e.g. Nakagawa and Tackley, 2010].

Here we revisit to investigate the relationship between heat flux across the CMB and seismic anomalies in the deep mantle including plate tectonics-like behavior and material recycling. Preliminary result suggests that the heat flux tends to be more linear relationship with seismic anomalies in the deep mantle including plate tectonics-like behavior and material recycling but the uncertainty of this relationship between two quantities is very strong. The peak-to-peak of lateral variation of CMB heat flux is much larger than that obtained from our previous study. This is still problematic for magnetic field generation caused by geodynamo.

Keywords: CMB heat flux, lateral variation, plate tectonics, material recycling

## Petrology and Geochemical Evolution of Lavas from the Ongoing and Voluminous Puu Oo Eruption of Kilauea Volcano, Hawaii

GARCIA, Michael<sup>1\*</sup> ; PIETRUSZKA, Aaron<sup>2</sup> ; GREENE, Andrew<sup>3</sup> ; MARSKE, Jared<sup>4</sup> ; RHODES, Michael<sup>5</sup>

<sup>1</sup>Dept. Geology-Geophysics, Univ. of Hawaii, <sup>2</sup>USGS, Denver, <sup>3</sup>Dept. Natural Sciences, Hawaii Pacific University, <sup>4</sup>Dept. Terrestrial Magnetism, Carnegie Institution of Washington, <sup>5</sup>Dept. Geoscience, Univ. Massachusetts

The Puu Oo eruption of Kilauea Volcano is one of the longest-lived (31 years and continuing) Hawaiian eruptions. Volumetrically, it is the most significant historical eruption. It has produced over 4 km<sup>3</sup> of lava from several vents along its east rift zone. We have continually monitored the compositional and isotopic signatures of its lavas, which have shown remarkable variations. These variations resulted from diverse crustal and mantle processes including crystal fractionation, magma mixing and storage, assimilation of crust and melting of a heterogeneous plume source. Crystal fractionation is an important process in these lavas based on their wide range of MgO contents (5-10 wt.%) and normally zoned minerals (mostly only olivine). During the first two years, the effects of crystal fractionation were superimposed on hybrid magmas created by mixing two evolved, rift zone-stored magmas with a new, mantle-derived magma. Later lava erupted show no signs of mixing except for one-day, uprift events in 1997 and 2011. Small, systematic variations in Pb and Sr isotopes, incompatible trace element ratios and MgO-normalized (10 wt.%) major element abundances of post-mixing lavas document rapid changes in the parental magma composition unrelated to crustal processes. Lavas erupted between 1985-1998 continued the post-1924 composition trend of Kilauea lavas towards more depleted composition. This trend was initiated by the collapse of summit crater during a period of very low magma supply. Puu Oo lavas showed a systematic temporal evolution towards historical Mauna Loa lava composition from 1998-2003. This trend reversed in 2003 and again in 2008 creating a cyclic pattern of geochemical variations. These reversals in composition are contrary to previous models for geochemical trends during sustained basaltic eruptions. The cyclic variations of Pb isotopic and some trace element ratios during the Puu Oo eruption suggest melt extraction from a mantle source with thin strands of vertically-oriented source heterogeneities. These strands may be 1-3 km in diameter in order to explain the scale of isotopic variations for the Puu Oo eruption. This continuing eruption provides a dynamic laboratory for evaluating models of the generation and evolution of basaltic magmas.

Keywords: volcano, Hawaii, eruption, historical, magma, basalt

## When did the plate tectonics start on the Earth?

MARUYAMA, Shigenori<sup>1\*</sup>

<sup>1</sup>ELSI Tokyo Institute of Technology

Initiation of plate tectonics on the Earth is a key to make life-sustaining rocky planet Earth, because primordial ocean was highly toxic and primordial atmosphere had high XCO<sub>2</sub>. Transportation of huge amounts of CO<sub>2</sub> into mantle by plate subduction depends on pH of seawater and composition of oceanic slab.

Plate tectonics has been proposed from the data set of the ocean-floor, firstly by ocean-floor spreading theory followed by rigid lithosphere. Yet, the oldest lithosphere goes back to only 200Ma, hence demonstration of plate tectonics on the Earth is restricted to the Earth after 200Ma.

Hence, we need to make logical framework of pre-200Ma plate tectonics of the Earth. The principle of Accretionary Complex Geology (ACG) is an only key issue which is centered by Ocean Plate Stratigraphy (OPS). ACG is a technology which separates the subducted oceanic slab from trench turbidites, and offers the MORB, OIB, pelagic sediments, and subduction zone magmatic rocks from the mixture of rock units formed at trench.

Application of this technology to 3.8Ga Isua ACs clarified Early Archean plate tectonics which had different aspects of plate tectonics from the modern plate tectonics, e.g., thickness and composition of lithosphere (Komiya et al., 1999). Specifically, thickness of MORB was 20km which seems to be buoyant to prohibit subduction (e.g., Davies, 1992). But if slab-melting is common, the buoyancy turns to be negative to cause more rigorous slab-pull force at subduction zone (Komiya et al., 2002).

For the Hadean Earth, there are no geologic units remained on the modern Earth, except for zircons with back to 4.4 Ga. Mineral inclusions within the Hadean zircons suggest the host melt with granitic magma. Formation of granitic melts could be most probable for the operation of plate tectonics. But this is logically imperfect, because small amounts of granitic melts can be formed and actually present on the Moon. Conversely, the forward modelling of planetary tectonics could be more important than zirconology. Formation of primordial ocean causes the formation of rigid lithosphere, and hydrous minerals on the slab surface would act as liberated lubricants along Benioff plane. This is plate tectonics and plays even in the state of magma pods remains in the asthenospheric mantle (Sleep et al., 2011). If so, initiation of plate tectonics on the Earth could be back to Hadean Earth, presumably back to 4.4Ga.

## Difference of tectonics and rheological structure between Earth and Venus

AZUMA, Shintaro<sup>1\*</sup> ; KATAYAMA, Ikuo<sup>1</sup> ; NAKAKUKI, Tomoeki<sup>1</sup>

<sup>1</sup>Department of Earth and Planetary Systems Science, Graduate School of Science, Hiroshima University

Venus has been regarded as a twin planet to the Earth, because of density, mass, size and distance from the Sun. However, the Magellan mission revealed that plate tectonics is unlikely to work on the Venus. The plate tectonics is one of the most important mechanism of heat transport and material circulation of the Earth, consequently, its absence might cause the different tectonic evolution between Earth and Venus. Rheological structure is a key to inferring mantle structure and convection style of planet interiors because the rock rheology controls strength and deformation mechanism. In previous study, the behavior of Venusian lithosphere has been inferred from the power-law type flow law of dry diabase. They indicated that lower crust can be weaker than upper mantle, which might result decoupling at the crust-mantle boundary (Moho depth) and mantle convection without crustal entrainment. However, the power-law creep cannot be applicable to infer the rheological structure at Moho depths, because the dislocation-glide control creep (Peierls mechanism) is known to become dominant at relatively low temperatures in materials with a relatively strong chemical bonding such as silicates. In this study, we conduct two-phase deformation experiments to directly investigate rheological contrast between plagioclase (crust) and olivine (mantle) and discuss the difference between these planets in terms of rheological behaviors. Moreover, one-dimensional and two-dimensional numerical calculation is performed to evaluate the influence of the strength contrast on the Venusian tectonics. Our experiments using solid-medium deformation apparatus directly determine the relative strength between plagioclase (crust) and olivine (mantle) without any extrapolating of flow law. The experimental conditions were ranging 2GPa and 600-1000 degrees under dry conditions. The experimental results show that olivine is expected to always be stronger than plagioclase. This result contradicts to that inferred from power-law creep of olivine and plagioclase, suggesting that Peierls mechanism could be dominant deformation mechanism in both olivine and plagioclase at relatively low temperatures. In the case of the Earth, rheological structure of oceanic lithosphere is constrained well by Byerlee's law and power-law type flow law. The oceanic crust and mantle lithosphere are strongly coupled mechanically because the Moho has no strength contrast, so that they could move and subduct together into the deep. In contrast, our experimental results imply that large strength contrast exists at Moho in Venus, resulting decouple of the motion between the crust and mantle lithospheres because the weak lower crust acts as a lubricant. Also one-dimensional numerical calculations show us that the surface velocity becomes more sluggish in the model with larger strength contrast (from two-digit to four-digit difference in viscosity) at Moho. Therefore the crustal part is less likely to be involved to mantle convection when strength contrast gets larger and larger. In fact, two-dimensional simulations suggest that the crustal portion cannot subduct with the mantle lithosphere if the strength contrast exists at Moho

Keywords: plagioclase, olivine, Venus, rheology, plate tectonics

## On the origin of plate tectonics: Thinking outside of the convective box

SOLOMATOV, Viatcheslav<sup>1\*</sup>

<sup>1</sup>Washington University in St. Louis

From the observational point of view, there is no evidence of plate tectonics on other planets in the Solar System. Remote sensing methods for detecting plate tectonics on exoplanets are yet to be developed and are unlikely to be as robust as the surface observations that were conducted for Venus, Mars, and Mercury. The observational constraints on the tectonics of the early Earth are probably the most important clues to the plate tectonics origin and yet, their interpretations remain ambiguous. Some researchers see a very early start of plate tectonics in the data while others do not exclude a relatively late start. From the theoretical point of view, the absence of plate tectonics is easy to explain and can be considered as a normal state of any rocky or icy body. Two decades ago, both the observational data and theoretical studies led to the reversal of the question “why do other planets not have plate tectonics” to “why does the Earth have plate tectonics”. Since then various theories and numerical models focused on the latter question and investigated how plate tectonics began and what conditions are required for plate tectonics to occur on a planet. In most models the starting state of a planet is a non-plate tectonics regime (e.g. stagnant lid convection) which then transitions to plate tectonics. The forces responsible for the transition can be caused by convective motions below the lithosphere and with thermal (e.g. lithospheric relief) and compositional density variations (e.g. continents) near the surface. The role of the factors involved can be complicated. For example, the crust can both hinder and help plate tectonics. The transition to plate tectonics can also be caused by external factors, such as impacts and tidal forces. Similar to the previous, internal factors, these external factors can also either help or hinder plate tectonics initiation. For example, even though impacts are sometimes considered as a possible cause of plate tectonics, they can create conditions that would hinder plate tectonics initiation later on or stop it in case if plate tectonics was previously initiated by other mechanisms. Plate tectonics could also have emerged from a magma ocean, bypassing the stagnant lid regime. In this scenario plate tectonics is a continuation of convection in the magma ocean. As the magma ocean crystallizes, the surface boundary layer, which has little difficulty to recycle in the liquid magma, eventually transforms into tectonic plates as the crystallizing magma ocean undergoes a transition from turbulent convection controlled by melt viscosity to laminar convection predominantly controlled by solid-state creep. Regardless of the origin of the first episode of plate tectonics, the question of how plate tectonics survived and evolved into a relatively stable regime is a challenge for any of these models and may require a combination of many factors such as asthenosphere, surface oceans and volatile cycling.

Keywords: Plate tectonics, Stagnant lid convection, Giant impacts, Magma oceans, Exoplanets

## Estimation of the lithosphere-asthenosphere transition from multi-mode surface waves

YOSHIZAWA, Kazunori<sup>1\*</sup>

<sup>1</sup>Earth and Planetary Dynamics, Faculty of Science, Hokkaido University

The lithosphere-asthenosphere transition (LAT) is a key to the understanding of the present-day plate motion, but its seismological determination is not straightforward unlike material boundaries such as the Moho and core-mantle boundary. Some recent works on the LAT using body-wave receiver functions have revealed evidences for clear converted signals at the bottom of lithosphere, particularly in oceanic region. To the contrary, receiver functions normally do not show clear converted signals from the expected bottom of cratonic lithosphere at about 200 km depth, where surface wave studies indicate fast wave speed anomalies of the thick continental lithosphere.

In this study, we investigate a quantitative way to estimate the depth and thickness of the LAT from S-wave speed models derived from surface waves. Although surface waves are inherently not very sensitive to the sharpness of boundaries due to their long-wavelength features, the depth of LAT can be roughly estimated from the depth of either the negative peak of velocity gradient or the slowest shear velocity beneath the lithosphere. In this study, we consider that the former represents an upper bound of LAT and the latter a lower bound. The thickness (or sharpness) of LAT can be deduced from the differences between the upper and lower bounds.

We have performed synthetic experiments using several types of S-wave models including different smoothness (or sharpness) of LAT. Synthetic experiments using multi-mode surface waves (including up to fourth higher modes) result in a successful recovery of the smooth LAT (with a depth range over 50 km), which is expected at the base of the cratonic lithosphere. However, if we use the fundamental mode only, the recovery is unsatisfactory even for the smooth boundary, and the effects of the sharpness of boundary are almost indistinguishable in the recovered models. Surface waves have less sensitivity to a sharp boundary (with a transition thickness less than 25 km), but our experiments indicate that the estimated depth from the velocity gradient (upper bound of LAT) are found to be coincide well with the depth of sharp boundary, which may indicate the distribution of oceanic LAT can be well represented by the negative peak of vertical gradient in S-wave speed profiles derived from surface waves.

Keywords: lithosphere, asthenosphere, surface wave, higher mode

## Advances in laboratory acoustic emission study

LEI, Xinglin<sup>1\*</sup>

<sup>1</sup>Geological Survey of Japan, AIST, Japan

Acoustic emission (AE) is an elastic wave radiated by rapid cracking in solids. As a technology of nondestructive inspection, AE has a long history of development and has been applied in numerous areas including material sciences, medical sciences and engineering fields. In stressed rocks, macroscopic fracturing is preceded by a very complex pervasive evolution of some pre-failure damage. Thus, studies focusing on both fracture dynamics and pre-failure damage are a subject of interest and can be inferred from AE statistics as the number of AE events is proportional to the number of growing cracks, and the AE amplitudes are proportional to the length of crack growth increments in the rock. In Earth science, since the similarity in size distribution of earthquakes and acoustic emissions (AE) was found in the 1960s, many laboratory studies have been motivated by the need to provide tools for the prediction of mining failures and natural earthquakes. This report aims to draw an outline of laboratory AE studies in the last 50 years, which have addressed seismological problems, with special focuses on some key issues associated with fault nucleation and growth in brittle rocks.

The AE technique, which monitors the spatiotemporal distribution of AE events, is applied to the analysis of the micro-cracking activity inside the sample space, and it can be performed under an artificially controlled pressure, which is very important for the simulation of underground conditions. During the last five decades, a great number of studies were done following developments in experimental technology, AE monitoring technology, and data processing methodology. Fifty years ago, only the hitting time of an AE could be recorded with a single sensor or a small number of sensors. The rock fracture test was performed under simple loading conditions. Later, the number of sensors that could be used in a study increased and thus allowed the determination of the hypocentre of an AE. Developments in transient memory technique in the 1970s through to the 1980s lead to the ability to make a digital multichannel recording of the full waveform of an AE. Hypocentre location was improved greatly by the use of more precise arrival times obtained through waveform analysis. In addition, it became possible to determine the mode of fracture, i.e., the focal mechanism solution of an AE source. In the present day, AE are usually monitored by 16-32 sensors with digital waveform recording at up to a 200 MHz sampling rate and up to a 16 bit A/D resolution. The dead time of a recording is sufficiently short and continuous recording is possible by use of very large amounts of memory. The waveform of most events can be captured with multiple channels, even for the period of dynamic failure in which the AE rate may reach several thousand a second. Rock fracture experiments can be performed under triaxial compression conditions with controlled fluid injection and pore pressure. AE hypocentres are determined with a location error of a few mms. A focal mechanism solution can be determined for individual events or a group of events. As demonstrated by very recent studies progress in laboratory AE study, particularly studies focusing faulting nucleation, is shedding more and more light on earthquake seismology.

By summarising recent results, it can be concluded that the fault nucleation behaviour, including critical size, duration time, and AE productivity, depend on the heterogeneity of the area of weakness of the fault compared with that of the host rock. If the fault is as strong as the host rock then the fracture makes no difference and the rock remains intact. Furthermore, a homogeneous fault or rock mass appears to fracture in unpredictable ways without a consistent trend in precursory statistics, while inhomogeneous faults fracture with clear precursors related to the nature of the heterogeneity.

Keywords: Acoustic emission (AE), Pre-failure damage, Rock fracture, Earthquake, Fault nucleation, Process zone

## Microfracture distributions indicating formation of large-scale cracks in the rock mass ahead of the mining front

NAOI, Makoto<sup>1\*</sup> ; MORIYA, Hirokazu<sup>2</sup> ; NAKATANI, Masao<sup>1</sup> ; MURAKAMI, Osamu<sup>3</sup> ; THABANG, Kgarume<sup>4</sup> ; THABANG, Masakale<sup>5</sup> ; LUIZ, Ribeiro<sup>6</sup> ; YABE, Yasuo<sup>2</sup> ; KAWAKATA, Hironori<sup>3</sup> ; ANTHONY, Ward<sup>6</sup> ; RAY, Durrheim<sup>4</sup> ; OGASAWARA, Hiroshi<sup>3</sup>

<sup>1</sup>Univ. of Tokyo, <sup>2</sup>Tohoku Univ., <sup>3</sup>Ritsumeikan Univ., <sup>4</sup>CSIR, <sup>5</sup>OHMS, <sup>6</sup>SeismoGen

We are monitoring Acoustic Emissions (AEs) down to Mw -4 or less at 1km beneath the ground in the Cooke 4 Mine (previously known as the Ezulwini Mine), where many earthquakes up to Mw 2 are induced by stress concentration due to tabular mining. The network consists of 24 AE sensors and 6 three-component accelerometers. Naoi et al. (2013; Pageoph) made a catalog composed of about 360,000 events by using waveform data obtained for three months, and reported that 90% of them aggregated within 10 m ahead of the mining front at the time.

In this study, we extended the analysis term to 9 months and developed a catalog composed of about one million events. We also applied the double difference algorithm (Waldhauser and Ellsworth, 2000) to them so as to examine spatial distributions of the AEs near the mining front in detail. Travel time differences for relative location were calculated from arrival times automatically read by the program of Horiuchi et al. (2011). To efficiently calculate relative hypocenters for a massive amount of events, we adopted the parallelization method of Hauksson and Shearer (2005), where events in subregions overlapping each other are firstly relocated and then the hypocenters relocated redundantly are averaged to make a single catalog. We succeeded in relocating 96% of the one million events.

The relocated AEs near the mining front exhibited two-dimensional, tabular aggregations with a few tens of meters lateral extent (hereinafter referred to as tabular cluster), rather than a three-dimensional distribution spread more or less uniformly (randomly) over the entire zone of the stope-front activity of 10 m breadth. Each tabular cluster was discernible because they were separated by regions of low AE density. That is, AEs ahead of the mining front basically occur selectively in several discrete tabular zones within a highly stressed volume affected by the mining cavity. The tabular clusters strike parallel to the mining face and dip 60-80°. This resembles similarly large shear fractures along the plane of maximum shear commonly observed by excavation around the stopes (Gay and Ortlepp, 1979; Adams and Jager, 1980; Adams et al. 1981). Ahead of a panel that advanced by 40 m during the analysis period, 10 such tabular zones formed at intervals of 5 m on average.

By the same AE monitoring network, we also have found extremely aggregated (a few tens of centimeter thickness) planar clusters continuous over the cluster's extent, reminiscent of thoroughgoing fracture surfaces. They often coincide with pre-existing geological faults (Naoi et al. 2013; JpGU). In contrast, the AEs of the tabular clusters regularly forming in the mining front were spread over 1-2 m thickness, lacking a dominant aggregation with good continuity. We interpret that the tabular-cluster AEs are microfractures occurring in a formation process of a large-scale shear crack in macroscopically intact rock subjected to high stress ahead of the advancing mining front. Indeed, the activity of tabular clusters gradually increased as the mining front approached and ceased when passed by the front.

Keywords: Acoustic Emission, Induced Earthquake, Rock fracture

## Deformation and acoustic emission of a penetrated granular bed

MATSUYAMA, Kazuhiro<sup>1</sup> ; KATSURAGI, Hiroaki<sup>2\*</sup>

<sup>1</sup>Department of Applied Science for Electronics and Materials, Kyushu University, <sup>2</sup>Department of Earth and Environmental Sciences, Nagoya University

In general, the rheological behavior of granular matter can mimic a certain side of the geophysical phenomena. In this experiment, the plunged granular matter is used to model the deformation and/or fracturing of the geophysical materials.

Penetration resistant force and acoustic emission (AE) from a plunged granular bed are experimentally investigated through their power-law distribution forms. The experimental apparatus used in this study is basically similar to that in our previous works [1,2]. In this experiment, AE measurement is used to approach the grain's-level microscopic behavior in a penetrated granular bed. An AE sensor (NF AE-9913) is buried in a glass beads bed. Then, the bed is slowly penetrated by a solid sphere by using a universal testing machine (Shimadzu AG-100NX). The average diameter of glass beads is varied from 0.4 to 2 mm, and the penetrating sphere's diameter ranges from 10 to 40 mm. During the penetration, the resistant force applied to the sphere and the AE signal are simultaneously measured [3]. The penetration speed (in the order of 1 mm/s) is kept slow enough to focus on the quasi-static regime. In this slow-penetration regime, the resistant force is independent of the penetration speed. Moreover, the resistant force shows power-law relation to the penetration depth. The obtained power-law exponent seems to depend on the size of granular column, i.e., the container's size. By comparing the resistant forces obtained by this experiment and other experiments, we confirm the relation between the resistant force and container's size. The smaller the container is, the larger the power-law exponent of resistant force becomes. This might mean that the slow penetration drag is affected by side wall of the container through force chains.

For AE signal, we observe a lot of (more than 1,000) burst-like AE events in each penetration experiment. We define the size of each AE event by its maximum amplitude. Then we find that the size distribution of AE events obeys power-law that is similar to Gutenberg Richter's law of the earthquakes statistics. However, the measured power-law exponent is not universal in this experiment. It rather depends on experimental condition. Particularly, the size of beads composing the penetrated granular bed affects the result significantly. The small glass beads bed shows larger power-law exponent. This tendency of power-law exponent indicates that the deformation of small-grains-bed is rather plastic, and the deformation of large-grains-bed shows brittle-like behavior. Namely, the emitted acoustic signal relates to the mode of deformation or fracturing. Since the grains network constructed in a small grains bed is dissipative, it also influences the statistics of AE events. The large AE events could be dissipated and screened by a lot of contact points in the small grains bed. This effect is also consistent with the current experimental result. In this study, only the AE events are measured and analyzed based on its power-law distribution. Actually, to characterize the mode of fracturing more precisely, electromagnetic emission (EME) should be also measured. Simultaneous measurement of AE and EME would reveal the details of the mechanics of slowly penetrated granular bed. Although this result is still preliminary to directly compare the power-law exponent with actual geophysical phenomena, the systematic behaviors of the power-law exponents are qualitatively informative to understand the deformation of the granular matter which relates to various geophysical phenomena and is quite different from usual continuum.

[1] H. Katsuragi, *Material, Chem. Eng. Sci.*, 76, 165-172 (2012).

[2] H. Katsuragi, *Phys. Rev. E*, 85, 021301:1-5 (2012).

[3] K. Matsuyama and H. Katsuragi, *Nonlin. Processes Geophys.*, 21, 1-8 (2014).

Keywords: acoustic emission, quasi-static resistant force, granular matter, power law

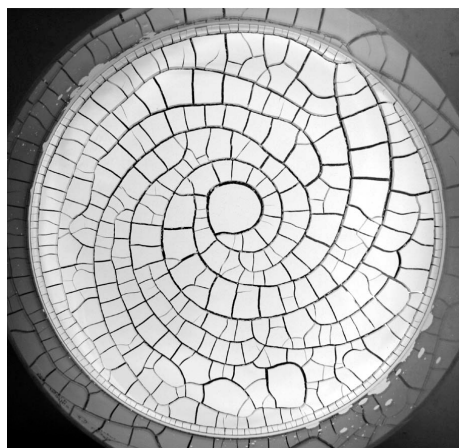
## Variety of memories of clay paste flows which can be visualized as desiccation crack patterns

NAKAHARA, Akio<sup>1\*</sup> ; MATSUO, Yousuke<sup>1</sup> ; OOSHIDA, Takeshi<sup>2</sup> ; OTSUKI, Michio<sup>3</sup> ; KITSUNEZAKI, So<sup>4</sup>

<sup>1</sup>College of Science and Technology, Nihon University, <sup>2</sup>Department of Mechanical and Aerospace Engineering, Tottori University, <sup>3</sup>Department of Materials Science, Shimane University, <sup>4</sup>Graduate School of Human Culture, Nara Women's University

Due to its plasticity, a water-poor clay paste can remember the direction of vibration and flow that it suffered. The memory of flow in clay paste can be visualized as a morphology of crack pattern that appears when the clay paste is dried. When the clay paste remembers the flow direction, desiccation cracks run all parallel to the direction of the flow. Recently, we find that there are some different types of memory of flow, as the direction of crack propagation changes from parallel to perpendicular direction. We would like to discuss on the mechanism of the memory effect of flow.

Keywords: desiccation crack pattern, rheology of clay paste, memory effect of flow



## Precursory Signal of Frontal Thrust Formation: Current status of Large Scale High Precision Sand Box Experiments

HORI, Takane<sup>1\*</sup> ; SAKAGUCHI, Hide<sup>1</sup> ; YAMADA, Yasuhiro<sup>2</sup> ; DOTARE, Tatsuya<sup>2</sup> ; FUKUMOTO, Yutaka<sup>3</sup>

<sup>1</sup>JAMSTEC, <sup>2</sup>Department of Urban Management Engineering, Kyoto University, <sup>3</sup>Graduate School of Agriculture, Kyoto University

In order to find out the mechanism of the three dimensional complex shape formation in sequential thrust and uplift of a accretion prism, we have developed a large scale high precision sand box experimental apparatus since 2011. After a number of modifications in the experimental apparatus and experimental procedure, we finally performed productive runs in July 2013. In specimen preparation, the thickness of a sand layer is controlled with the precision of less than single particle size. As a result, the shape of a frontal thrust became uniformly straight with high reproducibility and no complex shape has been observed since then. However, with such a well-controlled experimental system, we succeeded to detect the precursory signal prior to frontal thrust formation. In this talk, detailed information of the experimental apparatus and our new findings will be given with the scope of applicability of our finding in the field.

Keywords: precursor, earthquake, sandbox experiment

## New modelling devices to enhance the reproducibility of analogue model experiments

DOTARE, Tatsuya<sup>1\*</sup> ; YAMADA, Yasuhiro<sup>1</sup> ; SAKAGUCHI, Hide<sup>2</sup> ; HORI, Takane<sup>2</sup>

<sup>1</sup>Department of Urban Management, Kyoto University, <sup>2</sup>Japan Agency for Marine-Earth Science and Technology (JAMSTEC)

The scaled analogue model experiments have been used for more than 100 years to reproduce the geological development processes in the laboratory scales using the granular material (e.g. dry sand). Recently, we can obtain the small-scale deformation quantitatively by applying digital image analyses. Then, we observed the 'weak shear band' before fault initiation process. However, heterogeneity in the initial model produced by human hand often causes the fluctuation of the experimental results (e.g. fault location, faulting timing and fault geometry).

To solve this problem, we made the experimental device for making the initial model automatically and conducted the experiments to compare the experimental results with the previous method.

We conducted simple convergent experiments. Initial models were made by previous method (human hand) or new method (new device) and experiments were repeated 5 times, respectively.

As a result, while branches of new faults can be seen in the previous method, there are no branches in the new method. In addition, the fluctuation of experimental results was restricted in the new method.

This shows that new experimental device can make the initial model homogeneous and reproduce the same initial model in each experiment.

Keywords: analogue modelling, sandbox, reproducibility, accretionary prism, heterogeneity

## Relaxation processes of granular layer at seismic slip rates and layer thickness.

KUWANO, Osamu<sup>1\*</sup> ; NAKATANI, Masao<sup>2</sup> ; HATANO, Takahiro<sup>2</sup> ; SAKAGUCHI, Hide<sup>1</sup>

<sup>1</sup>IFREE, JAMSTEC, <sup>2</sup>ERI, University of Tokyo

A natural fault has the cataclasite core zone, along which shear deformation concentrates. Rheology of these granular matters thus provides us an important insight in considering the nature of friction on faults from a microscopic point of view. In the past two decades, experiments conducted at sub seismic to seismic slip rates (mm/s to m/s) revealed two remarkable phenomena of high-velocity rock friction; very long critical slip distance ( $D_c$ ) of the order of 1-10m/s and the considerable weakening due to mechanochemical effects by frictional heating [e.g., Di Toro et al., 2011, Nature]. Recently, Chambon et al.[2006, JGR] conducted friction experiment with very large shear displacement experiment on a thick granular layer, and reported significant slip-weakening behavior active over decimetric slip distances. However, the relation between long  $D_c$  observed in a thick granular layer and long  $D_c$  in the high-velocity friction is still not clear. Here, we report on laboratory experiments designed to explore transient responses of a thick granular layer following a step change in slip velocity at seismic slip rates. We use simple particle and choose relatively low normal stress to exclude the possible mechanochemical effects caused by frictional heat. We find that friction coefficient and layer thickness show similar response that is symmetry with respect to velocity changes, and  $D_c$  is of the order of 10m. It appears that these responses are attributed to dynamics of granular matter. We also report how magnitude of the relaxation and  $D_c$  are affected by the layer thickness.

Keywords: high-velocity friction, granular matter, rheology

## Porosity and permeability under effective pressure for the Quaternary Kazusa Group siltstones

MARUMO, Haruna<sup>1\*</sup> ; UEHARA, Shin-ichi<sup>1</sup> ; TAMURA, Yukie<sup>2</sup> ; MITSUHASHI, Shunsuke<sup>2</sup>

<sup>1</sup>Graduate School of Science, Toho University, <sup>2</sup>Faculty of Science, Toho University

The Kazusa group is a geological formation of the middle Pleistocene - Pliocene marine, and widely distributes in middle and northern part of the Boso Peninsula. Mudstones of the Kazusa Group is in the first stage of consolidation (viscous compaction stage), and porosity is 37.9 - 55.5% [1]. In mudstone formations of the Kazusa Group, high porosity anomaly is observed, of which location is consistent with that of natural gas deposits. This high porosity anomaly is suggested to have been generated by an abnormally excess pore pressure. The development process of the high pore pressure is still unknown. Previous studies have discussed the mechanism in connection with production of natural gas, but sufficiently quantitative analyses have not been performed. High pore pressure zone may affect many properties and processes in underground, such as porosity and permeability development in accretionary wedge or sedimentary basins during accretion and depositional process, ground water flows or petroleum migrations in underground, and fault mechanisms. Thus, to elucidate the mechanism of developing the high pore pressure zone is important. We are therefore planning to investigate the mechanism of the high pore pressure zone development by using the 1D model of Tanikawa et al. [2], which include simple deposition and compaction processes. In this study, as the first step of this project, the effective pressure dependences of porosity and permeability were determined for laboratory experiments for siltstone of the Kazusa Group, which are necessary for the modeling.

The measurements were performed using an intra-vessel deformation fluid-flow apparatus at Toho University. The rock samples used in the experiments were collected from outcrops at Umegase Formation, Ota-dai Formation, Kiwada Formation, Ohara Formation and Katsuura Formation of the Kazusa group. The collected samples were shaped into a cylindrical shape about 40 mm in diameter and about 30 mm in height. Distilled water was used for pore fluid and confining pressure was applied by using oil. Permeability and porosity of siltstones were measured at room temperature and under effective pressures from 0 MPa to 35 MPa. To obtain porosity under effective pressure, we measured a volume of water discharged from the specimen when confining pressure was applied. We measured permeability by monitoring flow rate through the specimen under the condition that pore pressure differences at the both side of the specimen is kept constant.

Permeability and porosity ranged from  $10^{-17}$  -  $10^{-18}$  m<sup>2</sup> and to 34 - 42 %, respectively. Permeability and porosity both decreased with increasing effective pressure, and this pressure dependence varies. Based on the results of the experiment, porosity and permeability was expressed in relation to the effective pressure. We have examined the relationship between permeability and porosity.

### References

- [1] Inami, K., Bull. Geol. Surv. Japan 34, 207-216 (1983)
- [2] Tanikawa, W., J. Geophys. Res., 113, B12403 (2008)

Keywords: Kazusa group, porosity, permeability, laboratory experiment

## Rheological properties of mafic schists: Implications for subduction dynamics

OKAZAKI, Keishi<sup>1\*</sup>; HIRTH, Greg<sup>1</sup>

<sup>1</sup>Department of Geological Sciences, Brown University

To understand the spatial and temporal distribution of deformation (e.g., underplating and exhumation of metamorphic rocks) and earthquakes in subduction zones, it is important to constrain the rheological properties of metamorphic rocks (i.e., altered oceanic crust and sediments), and how they evolve during metamorphic reactions following hydration, carbonation and dehydration of the down-going slab. Metamorphism of oceanic crust has stimulated hypotheses on the relationship between intra-slab earthquakes and slab-wedge coupling along plate boundaries in subduction zones. While it is well known that metamorphism has important effects on material fluxes and arc volcanisms at subduction system, it remains unclear how the formation of metamorphic minerals following fluid release influences rheology. Past experimental studies on mafic metamorphic rocks were mostly concentrated on phase equilibrium, thus there are few reports on the mechanical data for these metamorphic rocks.

We conducted triaxial deformation experiments on two mafic schists sampled from the Sambagawa metamorphic belt (Shikoku Island, Japan), using Griggs-type solid pressure- medium apparatus at Brown University. Both mafic schists are mainly composed of amphibole, albite, epidote, and chlorite with small amounts of titanite and phengitic mica. However, there are differences in the peak metamorphic condition (i.e., the maximum PT condition), amphibole composition and mineral abundance of minerals in the two schists. One, which was metamorphosed at greenschist facies (pressure of  $\sim 0.75$  GPa and temperature of  $\sim 400$  °C), has a relatively high chlorite content ( $\sim 12$  %) and actinolite is the dominant amphibole phase. The other, metamorphosed at the epidote-amphibolite facies (pressure of  $\sim 1$  GPa and temperature of  $\sim 520$  °C), has a lower chlorite content ( $< 2$  %) and hornblende is the dominant amphibole phase. Constant strain rate experiments and strain rate stepping experiments were conducted at confining pressures ( $P_c$ ) from 0.76-2GPa, temperatures ( $T$ ) from 300-600 °C and strain rates from  $10^{-5}$ - $10^{-7}$  1/s.

At conditions near the peak conditions of the greenschist ( $P_c = 1$  GPa,  $T = 400$  °C), differential stresses were higher than 1 GPa. The greenschist samples are weaker than the epidote-amphibolite samples under all experimental conditions. Both types of samples exhibit strain rate strengthening; frictional behavior that inhibits earthquake nucleation. Differential stress increased with increasing confining pressure, while friction coefficient decreased with increasing confining pressure and temperature. At  $T = 400$  °C, the nominal friction coefficient ( $\mu$ ) for the greenschist samples was  $\mu \sim 0.34$  at  $P_c = 1$  GPa and  $\mu \sim 0.30$  at  $P_c = 1.5$  GPa; for the epidote-amphibolite,  $\mu \sim 0.48$  at  $P_c = 1$  GPa and  $\mu \sim 0.42$  at  $P_c = 1.5$  GPa. Stress exponents ( $n$ ) for the greenschist samples at  $P_c = 1$  GPa were  $n \sim 26$  at  $T = 300$  °C,  $n \sim 36$  at  $T = 400$  °C and  $n \sim 34$  at  $T = 500$  °C; for the epidote-amphibolite,  $n \sim 31$  at  $T = 400$  °C and  $n \sim 21$  at  $T = 500$  °C. Microstructures of recovered samples showed modest buckling and several localized shear zones. These features suggest that the deformation of mafic schist is accommodated by semi-brittle deformation resulting in strain localization on faults.

We also conducted deformation experiments in which temperature was increased above the thermal stability of chlorite ( $\sim 800$  °C) to simulate a prograde metamorphism in subduction zones. With increasing temperature during deformation, differential stress decreased and reached nearly 0 MPa. This suggests that such reaction-enhanced weakening of metamorphic rocks forms weak fault zones in subducting slab, which might promote detachment of oceanic crust from the subducting slab and allow underplating to forearc crust. The strain-rate strengthening behavior of these materials suggests that such faults would be relatively aseismic.

Keywords: mafic schist, subduction zone, deformation experiment, oceanic crust, semi-brittle deformation, intermediate depth earthquake

## Effect of iron content on the creep behavior of olivine under hydrous conditions

TASAKA, Miki<sup>1\*</sup> ; ZIMMERMAN, Mark<sup>1</sup> ; KOHLSTEDT, David<sup>1</sup>

<sup>1</sup>University of Minnesota

Since iron and hydrogen play important roles in dynamic processes not only in Earth's mantle but also in Mars's mantle, we conducted triaxial compressive creep experiments on polycrystalline samples of olivine,  $(\text{Fe}_{1-x}\text{Mg}_x)_2\text{SiO}_4$ , with  $x = 0, 0.53, 0.77, 0.90$ , and  $1.0$  under hydrous condition. A Paterson-type gas-medium apparatus was used for these experiments. The water contents, determined from Fourier transform infrared (FTIR) spectroscopy analyses of larger  $\text{Fo}_{90}$  crystals embedded in the olivine aggregates, demonstrate that the samples are water-saturated both before and after deformation. The grain sizes of initial and deformed samples were determined using electron backscatter diffraction (EBSD).

Creep tests at 300 MPa confining pressure were conducted at temperatures from 1050 to 1200C at constant stresses in the range 25 to 315 MPa. The values of the pre-exponential term, stress and grain size exponents, and activation energy in the constitutive equation were determined for a wide range of iron concentrations. Samples with high Mg contents are finer grained ( $1-2 \mu\text{m}$ ) than those with low Mg contents ( $10-20 \mu\text{m}$ ). Furthermore, samples with high Mg contents ( $x \geq 0.90$ ) exhibit a stress exponent of  $n = 2$ , whereas samples with low Mg contents ( $x < 0.90$ ) deform with  $n = 3$ . This result is consistent with the dislocation-accommodated grain boundary sliding model of Langdon (1994), which predicts that fine-grained samples that do not contain sub-grains should exhibit  $n = 2$  while coarser-grained samples that do contain sub-grains should exhibit  $n = 3$ . The flow stress decreases with increasing iron content of the olivine samples at constant temperature, strain rate, and grain size. Following the analysis of previous studies (Mackwell *et al.*, 2005; Zhao *et al.*, 2009), we fit our creep data to the following flow law: strain rate =  $A \sigma^n d^{-p} (1-x)^m f_{\text{H}_2\text{O}}^r \exp\{-[Q_0 + \alpha(1-x)] / RT\}$ , where  $A$  is a material-dependent parameter,  $\sigma$  is stress,  $d$  is grain size,  $p$  grain size exponent,  $m$  iron content exponent,  $f_{\text{H}_2\text{O}}$  water fugacity,  $r$  water fugacity exponent,  $Q_0$  activation energy at  $(1-x) = 0$ , and  $\alpha$  a constant. The dependence of strain rate on iron concentration is characterized by two parameters - directly, through the iron content exponent  $m$  and, indirectly, through the term  $\alpha(1-x)$  in the activation energy. The values of  $m$  and  $\alpha$  are determined by the rate-controlling mechanism of deformation and the charge neutrality condition for Fe-bearing olivine.

Keywords: olivine, iron content, creep, rheology, experiments, deformation

## High accuracy measurement of activation energy of creep and electrical conductivity of olivine aggregate

NAKAKOJI, Tadashi<sup>1\*</sup> ; HIRAGA, Takehiko<sup>1</sup> ; MIBE, Kenji<sup>1</sup>

<sup>1</sup>Earthquake Research Institute, The University of Tokyo

It is believed that creep rate of peridotite being major rock in the Mantle is controlled by diffusion of the slowest ion which is  $\text{Si}^{4+}$ . However it is suggested that diffusion of the second fastest ion controls the deformation rate in the system of which not only olivine but it including pyroxene also consists (Sundberg and Cooper (2008)). As seen above, the controlling process has not been understood well. Besides the activation energy being indication for deciding the mechanism is often obtained with a large error range. Therefore, in a case of extrapolating the experimental to the Earth's interior value, the large error will produce a large uncertainty. To solving the two problems, we have conducted the compression experiment and electrical conduction test for olivine simultaneously under a continuously changing temperature.

The sample used for the experiment was synthetic olivine composed of forsterite (90vol %) + enstatite (10vol %), which imitates a material in upper Mantle. To inhibit to grain growth during the experiment, the sample was annealed at 1360 °C for 24 hours in the furnace before the test conducted. During the experiment, the sample was kept loaded at constant stress, 20MPa, and temperature changed from 1360 °C to 1240 °C and then increased from 1240 °C to 1360 °C in order to confirm reproducibility of measurements. Measurement of impedance of the sample was also conducted simultaneously. The sample applied at 20V every ten degree from 1360 °C provided us current response, which was used for measurement of impedance of the sample.

The result of the experimental data provided us viscosity and electrical conductivity of the sample. Viscosity was obtained by the relation of stress and strain rate. Arrhenius plot of reciprocal viscosity shows a linear distribution. This indicates that deformation mechanism of the sample did not change at the applied temperature range in the experiment. Electrical conductivity in the sample was obtained by the resistivity derived from the data by impedance measurement. Assuming that the conduction is thermally-activated process, the relation of conductivity times temperature and temperature shows a linear relation in Arrhenius plot. From each these slopes of lines, Activation energy of  $627 \pm 15$  kJ/mol was obtained about creep and that of  $297 \pm 12$  kJ/mol was obtained about electrical conduction, respectively. This difference of the activation energies indicates that the creep rate and electrical conduction were controlled by different ion or/and different diffusion in the sample.

Sundberg and Cooper (2008) suggested that deformation mechanism is  $\text{Mg}^{2+} + \text{O}^{2-}$  ion diffusion but not  $\text{Si}^{4+}$  diffusion in a case of the sample of olivine + pyroxene. Therefore we compare our result with previous works. Activation energy of lattice diffusion of  $\text{Si}^{4+}$  and  $\text{O}^{2-}$  in olivine are  $\approx 530$  kJ/mol and  $\approx 340$  kJ/mol (Dohmen et al. 2002), respectively and that of  $\text{Mg}^{2+}$  lattice diffusion is about  $400 \pm 60$  kJ/mol (Chakraborty et al. 1994). On other hand,  $627 \pm 15$  kJ/mol was obtained in this study, so that we can infer that lattice diffusion of  $\text{Si}^{4+}$  controlled creep rate. ten Grotenhuis et al. (2004) obtained that activation energy of  $315 \pm 39$  kJ/mol by measuring electrical conductivity of olivine aggregate which has the same composition and almost same grain size of ours, and relation of increase electrical conductivity and decrease in grain size. Consequently, from the grain size is the same one of us, we can infer that grain boundary diffusion of  $\text{Mg}^{2+}$  ion contributed to the conductivity of our sample.

Keywords: olivine, creep, electrical conduction, activation energy, diffusion, polycrystal

## Quantification of grain boundary sliding and grain rotation during diffusion creep of mantle rocks

MARUYAMA, Genta<sup>1\*</sup>; HIRAGA, Takehiko<sup>1</sup>

<sup>1</sup>Department of Earth and Planetary Sciences, Earthquake Research Institute, University of Tokyo

Existence of an anisotropy in the seismic wave velocity in Earth's upper mantle have been known for decades (Tanimoto and Anderson 1984). The seismic anisotropy is often explained by the crystallographic preferred orientation (CPO) of rock-forming minerals, which have anisotropic elasticity. In general, the CPO of olivine produced during dislocation creep is considered to be the primary cause of the anisotropy. Recently, our team showed that the CPO of olivine is produced even during diffusion creep (Miyazaki et al. 2013). However, the mechanism of the CPO development under diffusion creep is still not clear. The purpose of this study is to understand the mechanism in submicron scale by observations of samples surface after the sample deformation where the fine-scale strain markers were imposed.

We used a vacuum sintering technique to synthesize cylindrical samples which were composed of fine-grained forsterite plus 20 vol. % diopside (a combination that we denote Fo80Di20) and forsterite plus 35 vol. % enstatite (En). We polished the lateral side of the sample. Subsequently we imposed grooves on such surface with using a focused ion beam. These marker lines were parallel to the compression axis of sample deformation. We conducted uniaxial compression creep experiments at atmospheric pressure, temperatures of 1300oC and strain rates of  $10^{-5}$  -  $10^{-4}$  s<sup>-1</sup>. After the compression creep experiment, we observed the marker lines under scanning electron microscope (SEM) with field emission gun (JEOL 6500F installed at Nano-Manufacturing Institute, University of Tokyo) to observe how the markers were displaced after the deformation. Such observations allow to quantify the amount of grain boundary sliding and grain rotation due to a plastic deformation of the sample.

We succeeded to observe the marker lines after the deformation. Significant grain boundary sliding was detected from the offsets of the markers at numbers of grain boundaries. No distortion of the markers within the grains was found indicating the absence of intragranular deformation process such as a glide of dislocations. We quantified the grain rotation finding that the rotation angle increases with strain. The average angles in the sample of Fo80Di20 with strain of 3%, 7% and 14% were 1.2°, 3.9°, 6.5°, respectively. We also found larger rotation angle of the grains in Fo80Di20 than in Fo65En35. Fo80Di20 is composed of anisotropic grains of Fo whereas Fo65En35 has isotropic grains, which may explain the difference in the grain rotation between the samples. The shape of anisotropic grains is crystallographically controlled resulting in a development of longer and straight grain boundaries. We assumed that grains were easier to glide at such boundaries resulting in development of CPO during diffusion creep (Miyazaki et al. 2013), which is an modified model of grain rotation during grain boundary sliding creep (Beere 1978). Our present result seems to support our CPO model.

Keywords: grain rotation, grain boundary sliding, CPO, creep

## In-situ observation of crystallographic preferred orientation of olivine deformed in simple shear: Implications for the

OHUCHI, Tomohiro<sup>1\*</sup> ; NISHIHARA, Yu<sup>1</sup> ; SETO, Yusuke<sup>2</sup> ; KAWAZOE, Takaaki<sup>3</sup> ; NISHI, Masayuki<sup>1</sup> ; MARUYAMA, Genta<sup>5</sup> ; HIGO, Yuji<sup>6</sup> ; FUNAKOSHI, Ken-ichi<sup>7</sup> ; SUZUKI, Akio<sup>8</sup> ; KIKEGAWA, Takumi<sup>9</sup> ; IRIFUNE, Tetsuo<sup>1</sup>

<sup>1</sup>Geodynamics Research Center, Ehime University, <sup>2</sup>Department of Earth and Planetary Sciences, Kobe University, <sup>3</sup>Bayerisches Geoinstitut, University of Bayreuth, <sup>4</sup>Earth-Life Science Institute, Tokyo Institute of Technology, <sup>5</sup>Graduate School of Science, University of Tokyo, <sup>6</sup>Japan Synchrotron Radiation Institute, <sup>7</sup>Research Center for neutron Science and Technology, <sup>8</sup>Department of Earth and Planetary Materials Science, Tohoku University, <sup>9</sup>Photon Factory, High Energy Accelerator Research Organization

The characteristics of the seismic anisotropy vary depending on the types of crystallographic preferred orientation (CPO) of olivine. Therefore, the pattern of the seismic anisotropy has been interpreted by taking into account the water- and pressure-induced fabric transitions of olivine in recent studies (Jung and Karato, 2001; Ohuchi et al., 2011). The fabric strength of olivine aggregates is also important when we evaluate the magnitude of the seismic anisotropy in the upper mantle. In the upper mantle, the steady-state fabric strength of olivine is expected to be achieved due to long time-scales of flows.

The dependency of the fabric strength of olivine aggregates on strain has been evaluated in only limited numbers of experimental studies (e.g., Bystricky et al., 2000). Bystricky et al. (2000) showed that total shear strains higher than 4 are needed to achieve the steady-state fabric strength of olivine (D-type fabric) at 0.3 GPa and 1473 K. However, it has been difficult to evaluate the detailed process of the development of fabrics because fabrics of recovered samples have been evaluated. Recently, we have developed experimental techniques for in-situ simple-shear deformation experiments using a D-DIA apparatus. In this paper, we briefly show that our recent experimental results on in-situ observations of stress, strain, and fabric developments in olivine samples.

Simple-shear deformation experiments on olivine aggregates at pressures  $P = 2-3$  GPa, temperatures  $T = 1290-1490$  K, and shear strain rates of  $3E-4$  s<sup>-1</sup> were performed using a deformation-DIA apparatus installed at SPring-8. Shear strain (up to 5) was measured by the rotation of a platinum strain-marker, which was initially placed perpendicular to the shear direction. Differential stress, generated pressure, and CPO patterns of olivine samples were determined from two-dimensional X-ray diffraction patterns using software (IPAnalyzer, PDIndexer, and ReciPro: Seto et al., 2010; Seto, 2012). The CPO patterns of olivine in the recovered samples were also evaluated by the indexation of the electron backscattered diffraction (EBSD) patterns.

A-type olivine fabric was developed under dry conditions. The fabric strength increased with strain ( $<2$ ), and steady-state fabric strength was achieved at shear strains about 2. The [010] axes strongly concentrated to the shear plane normal and its concentration increased with strain. Preferential alignments of the [100] and [001] axes were developed through increase in strain, though concentrations of the [100] and [001] axes were weaker than those of the [010] axes. Development of B-type olivine fabric was observed under wet conditions (~700 ppm H/Si). The fabric strength of B-type sample continuously increased with strain (up to 3). As same as the case of A-type samples, concentrations of the [010] axes were stronger than those of other axes in the B-type sample. Because the concentration of the [010] axes efficiently increases at strains larger than 1, seismic anisotropy (e.g.,  $V_{SH}/V_{SV}$ ) at shear strains = 1 is quite similar to that under the steady-state conditions.

Using the CPO data of the steady-state A-type fabrics,  $V_{SH}/V_{SV}$  of the asthenospheric upper mantle is estimated to be 1.027 (note that 70 vol.% of preferred-orientated olivine grains and 30 vol.% of random-orientated orthopyroxene grains are assumed in the calculation). This value is consistent with the global one-dimensional model reported by Visser et al. (2008). The  $V_{SH}/V_{SV}$  of the asthenospheric upper mantle is expected to have higher values in the case of B-type fabric (e.g., 1.035), which is harmonious with the global one-dimensional model reported by Panning and Romaniwics (2006). Our results show that seismic anisotropy in the upper mantle is mostly explained by the steady-state olivine fabrics (A- and B-types), and other effects (e.g., shape-preferred orientation of melt, CPO of other minerals) would be limited.

Keywords: olivine, crystallographic preferred orientation, in-situ observation, seismic anisotropy

## Simultaneous observations of dehydration and AE activities during the deformation of antigorite at high pressures

IWASATO, Takuya<sup>1\*</sup>; KUBO, Tomoaki<sup>1</sup>; HIGO, Yuji<sup>2</sup>; KATO, Takumi<sup>1</sup>; KANESHIMA, Satoshi<sup>1</sup>; UEHARA, Seiichiro<sup>1</sup>; IMAMURA, Masahiro<sup>1</sup>

<sup>1</sup>Kyushu Univ., <sup>2</sup>JASRI

Intermediate-depth earthquakes are seismic activities at depths of 60-300 km, where subducting plates deform plastically rather than brittle failure. Because dehydration embrittlement (Raleigh and Paterson, 1965) may not work for serpentinite at pressures more than ~2 GPa, it is important to understand the mechanisms of shear instability at higher pressure. To conduct simultaneous observation of dehydration reaction, plastic flow and shear instability, we developed an in-situ observation system combined with synchrotron monochromatic X-ray and AE 6-6 system (multiple acoustic emission measurement for multi-anvil 6-6 type system) using Deformation-DIA (D-DIA) apparatus. Using this system, we carried out antigorite deformation experiments up to ~4.5 GPa and ~850 K including the condition of the antigorite dehydration to talc and forsterite.

Deformation experiments were conducted at high pressure and high temperature using a 1500-ton uniaxial press (SPEED Mk. II) with a D-DIA type guide block installed at BL-04B1, SPring-8 (Katsura et al., 2004; Kawazoe et al., 2011). 50 keV monochromatic X-ray were used to measure two-dimensional X-ray diffraction (2D-XRD) patterns and X-ray radiography images, which give reaction kinetics, differential stress, and strain. We developed MA 6-6 type system (Nishiyama et al., 2008) to monitor shear instabilities by AEs from maximum six piezoelectric devices positioned between first and second stage anvils. AE waveforms were recorded in trigger mode using six-channel 8-bit digital oscilloscopes at a sampling rate of 50MHz. Starting material of polycrystalline antigorite cylinder (1.7 mm in diameter and 2.7 mm in length) cored from high-temperature serpentinite (Eigami, Nagasaki, Japan) were first compressed at room temperature, then heated at constant load, and finally deformed with constant strain-rate mode. In some runs, dehydration occurred during heating or deformation. Microstructures of recovered samples were preliminarily observed by optical microscopy.

A total of ten deformation experiments of polycrystalline antigorite were conducted at 1.1~4.5 GPa, 300~850 K, and strain rates of  $3.4\sim 6.7 \times 10^{-5} \text{ s}^{-1}$ . AEs were frequently generated from the sample during the cold compression. Relatively large AEs were also detected when heating the sample to 673 K, while AE activities became zero at higher temperatures. During the constant strain-rate deformation, the flow stress reached steady state at the sample strain of more than 5%, and no stress drops were observed until the final strain of ~30-40%. These flow behaviors and the flow strength are almost consistent with the previous study (Hilaret et al., 2007). We also detected AEs during the deformation stage although the frequency was lower compared to the cold compression and heating stages. The AE activities during the deformation became large at lower temperature and larger strain conditions. Optical microscopic observation revealed that some faults are present in the antigorite samples recovered from each stage. On the other hand, we observed dehydration reaction from antigorite to talc-like phase during the deformation at 800 K. The reaction was very slow and only one AE event was detected at the strain of ~25%. Because the faults were only observed in the relict antigorite region, the AE was possibly originated from antigorite. At higher temperature of 850 K, complete dehydration quickly occurred before the deformation. No AEs were detected during the dehydration and the following deformation of dehydrated materials to more than 30% strain. No faults were observed in the recovered sample. Our simultaneous observations of reaction and AE activities showed that the AE is not generated by dehydration of antigorite at more than ~2 GPa. Instead, the unstable fault slipping that generates AEs occurs during heating and deformation of antigorite without dehydration.

Keywords: Acoustic emission, In situ X-ray observation, deformation-DIA, antigorite, dehydration, stress and strain

## Seismic attenuation measurement by cyclic loading under high pressure and temperature

YOSHINO, Takashi<sup>1\*</sup> ; YAMAZAKI, Daisuke<sup>1</sup> ; HIGO, Yuji<sup>2</sup> ; FUNAKOSHI, Ken-ichi<sup>3</sup>

<sup>1</sup>Institute for Study of the Earth's Interior, Okayama Univ., <sup>2</sup>JASRI, <sup>3</sup>CROSS

The estimation of the mantle structure using seismic tomography method has been advanced by understanding of the detailed velocity structure of the Earth interior. On the other hand, Brillouin scattering in the DAC at very high pressure, X-rays inelastic scattering, sound velocity measurement of ultrasonic range in the large press is also improved. These developments can be expected this time as a further declaration of a picture of a more detailed Earth interior. However, as compared to the frequency band of MHz to GHz region, the frequency range of the seismic waves propagating through the earth interior is much lower. We should noted that it is greatly affected by the attenuation of seismic waves. Because the materials are not in a perfectly elastic body, energy loss inside the materials occurs in the wave propagation because of presence of grain boundaries, dislocations, and defects. Thus, seismic attenuation occurs as a function of frequency.

The attenuation of seismic waves (the determination of the  $Q^{-1}$ ) of mantle material under high pressure has not been reported until recently mostly because it is an experimental quantification is very difficult. Temperature effects and particle size effects were reported for the first time systematically for olivine aggregates at high temperature under low pressure. However, for this system the upper limit of the generated pressure is low because it is a torsion test performed in the gas pressure. So the study of pressure -dependent and high-pressure mineral is difficult. The other group using the D-DIA type press having two differential ram measured  $Q^{-1}$  combining an in-situ observation and radiation uniaxial periodic vibration test. This system expands a possibility of experimental determination of  $Q^{-1}$  at much higher pressure. In Japan, the DIA type press was installed at SPring8 (D-DIA). Recently we started the measurement of  $Q^{-1}$  under high pressure using in situ image acquisition of the high time and spacial resolution at short period of oscillation cycle.

In this paper, some experimental developments for measuring seismic attenuation at high pressure and results of cyclic loading tests are introduced. Time resolved images of the sample and reference material obtained by a synchrotron X-ray radiography provide their strain as a function of time during cyclic loading. Attenuation is determined as the tangent of the angle of phase lag between the strain of the sample and the strain of the reference material. A newly installed short period sinusoidal cyclic loading oil pressure system enable us to determine minimal strain of the sample in a wide frequency range from 2 to 0.01 hertz on olivine aggregates at 1 GPa and up to 1673 K. The detectable minimum strain is around  $5 \times 10^{-5}$ . Several test experiments exhibited resolvable  $Q^{-1}$  ( $10^{-2}$ ) above 1273 K. The results are generally consistent with previously reported data.

Keywords: seismic attenuation, high pressure, oscillation, Q value, shear modulus

## Viscoelastic property of antigorite

YAMAZAKI, Daisuke<sup>1\*</sup>

<sup>1</sup>Okayama University

Seismological data reveals the structure and dynamics combined with mineral physics. For example, the velocity structures from observations are interpreted using the elastic properties of constituting minerals obtained from the laboratory measurements. Because the minerals in the earth is not perfect single-crystal but they contain a certain amount of defects (vacancy, dislocation, grain boundary), the viscoelastic relaxation is taken place by the viscous motion of the defects during the propagating the seismic waves with the frequency of  $10^{-4}$ -10 Hz. Serpentine can be considered to be one of the candidate for the source of the fluid in the wedge mantle. In the present study, therefore, we examine the viscoelastic property of serpentine (antigorite) under uppermost mantle conditions by means of high pressure experiments.

Fine-grained polycrystalline antigorite (a few micrometer of grain size) sintered at 3 GPa and 550 degree C for 4 hours was used as a starting material for the attenuation experiment. We conducted the experiments by using D-DIA press with a short-period cyclic loading system, which was recently installed at BL04B1, SPring-8, Japan. D-DIA, which is a single stage of six-anvil compression device, applied pressure by forcing each of the six anvils to advance on the cubic pressure medium with a main ram. After pressure reaching to the target value of 1 GPa by the pumping the main ram, a sinusoidal stress and strain was applied by advancing and withdrawing the upper and lower anvils operated by the short-period cyclic loading system with the frequency between 0.01-2 Hz at 1 GPa and 500-750 degree C. At high temperature ( $> \sim 650$  degree C), dehydration is expected. The strain was monitored directly from X-ray radiography of sample located in the pressure medium through the anvil gap during cyclic loading. In the present study, single crystal of forsterite was placed next to the sample along the stress axis of the sample and it can be used as the standard to estimate the stress by recording the X-ray radiography images displaying the lengths of standard and sample simultaneously.

The time lag of strain of sample against that of standard provided us the quality factor,  $Q$ , to be 5.4, 4.8 and 4.4 for the periods of 5, 10 and 20 s, respectively, at 600 degree C. Present preliminary results shows the temperature dependence of  $Q^{-1}$ . At 500 degree C,  $Q^{-1}$ s are  $\sim 0.5$  log unit lower than those at 600 degree C. The present values is  $\sim 2$  order of magnitude lower than that of olivine aggregates. The shear modulus was estimated to be 15-25 GPa in our experimental condition, which is much smaller than the shear modulus without attenuation (38.5 GPa). The large reduction in shear modulus due to attenuation was previously reported in the case of olivine.

## Experimental study of anelasticity of a polycrystalline material near the melting temperature

YAMAUCHI, Hatsuki<sup>1\*</sup>; TAKEI, Yasuko<sup>1</sup>

<sup>1</sup>Earthquake Research Institute, University of Tokyo

Rock anelasticity is important to interpret seismic wave velocity and attenuation structures in the upper mantle. By using organic polycrystalline borneol ( $C_{10}H_{18}O$ , melting temperature = 204.5 °C) as an analog to mantle rock, McCarthy et al. (2011) measured Young's modulus and attenuation  $Q^{-1}$  as functions of frequency  $f$  ( $=10^{-4}$  - 2 Hz), temperature  $T$  (20-50 °C) and grain size  $d$  (3.3 - 22 micrometer). They also measured viscosity, and calculated the Maxwell frequency  $f_m$ . When the obtained  $Q^{-1}$  spectra were plotted as functions of the frequency normalized by the Maxwell frequency  $f_m$ , all  $Q^{-1}$  spectra obtained for various temperatures and grain sizes collapsed onto a nearly single curve. Moreover, data from olivine aggregates (Gribb and Cooper, 1998; Tan et al. 2001; Jackson et al. 2002) collapsed onto the same master curve as borneol, demonstrating the universality of anelastic behavior. However, experimental frequencies normalized by the Maxwell frequency of the samples were lower than  $5 \times 10^4$ , which is considerably lower than those of seismic waves in the upper mantle ( $f/f_m = 10^6$ - $10^9$ ). Therefore, whether the Maxwell frequency scaling is applicable to the seismic waves or not is an open question.

Takei et al. (in preparation) measured anelasticity of organic polycrystalline borneol at lower temperatures (0-20 °C) and higher frequencies ( $10^{-4}$ -50 Hz) than McCarthy et al. (2011). They also investigated the effect of chemical composition on anelasticity, by using the samples made of high-purity borneol and borneol + diphenylamine ( $(C_6H_5)_2NH$ ) (eutectic temperature = 43 °C). Before obtaining these data, our experimental methodology and data quality were much improved. When the obtained  $Q^{-1}$  spectra were plotted as functions of the frequency normalized by the Maxwell frequency, the  $Q^{-1}$  spectra collapsed onto a nearly single curve at  $f/f_m < 10^4$ , but significantly scattered at  $f/f_m > 10^4$ , where the spectra have a broad peak and the scattering is caused by the variation of the peak amplitude and width with temperature, grain size and chemical composition. Therefore, the simple Maxwell frequency scaling is not applicable to the seismic waves in the upper mantle. They found that seismic attenuation predicted from the data of high purity samples and those of the borneol + diphenylamine samples under low temperature conditions is too low to explain the seismic attenuation in the upper mantle ( $\sim 0.01$ ). In other words, enhancement of attenuation near the melting temperature is important to understand high  $Q^{-1}$  in the upper mantle.

In this study, we measured anelasticity of borneol + diphenylamine system at various frequencies ( $2 \times 10^{-4}$  - 50 Hz) and temperatures (20 - 46 °C), and obtained the detailed behavior of anelasticity near the melting temperature (43 °C). The result obtained so far show that the change of viscosity and anelasticity near the melting temperature is not discrete but continuous. This result is somewhat different from our previous understanding that physical properties abruptly change when melting starts beyond the solidus. We will further obtain systematic data for various grain sizes and melt fractions.

Keywords: anelasticity, seismic attenuation

## Experimental study of bulk and shear viscosities of partially molten rock analogue

SUZUKI, Ayako<sup>1\*</sup> ; TAKEI, Yasuko<sup>1</sup> ; WATANABE, Shun-ichi<sup>2</sup>

<sup>1</sup>Earthquake Research Institute, University of Tokyo, <sup>2</sup>Hydrographic & Oceanographic Dept, Japan Coast Guard

Deformation of partially molten rock is controlled by two independent viscosities: shear viscosity for shear deformation and bulk viscosity for compaction/decompaction. Bulk viscosity and its ratio to shear viscosity,  $h_b/h_s$ , play an important role in melt segregation dynamics in the upper mantle (Katz, 2008). However, that value has not been well constrained theoretically nor experimentally especially at small melt fractions. Most numerical studies have used the theoretically predicted value of  $h_b/h_s = \sim f^{-1}$ , where  $f$  is the melt fraction. Takei and Holtzman (2009a) theoretically obtained a constant value of  $h_b/h_s$  by taking into account a diffusion creep mechanism. The discrepancy between two models is significant at small melt fractions. There has not been experimentally determined value of  $h_b/h_s$  because very few experimental studies have been done about bulk viscosity although shear viscosity has been measured extensively. To discuss the validity of these models based on the experimental data, it is highly important to measure both bulk and shear viscosities by using the equivalent samples. In this study, we measured experimentally these two viscosities as functions of melt fraction using a partially molten rock analogue.

Samples were polycrystalline aggregates of borneol-diphenylamine binary with eutectic temperature of 316K, which has a quite similar equilibrium microstructure to olivine + basalt system (Takei, 2000). Initial melt fraction can be controlled precisely by the concentration of diphenylamine because of its simple eutectic reaction. Before deformation experiments, samples were annealed at 320K for  $\sim 100$  hours in a sealed capsule to make those grain size large enough ( $\sim 0.030$  mm), resulted in negligible grain growth during the successive deformation tests at the same temperature.

To measure bulk and shear viscosities, we carried out two separate experiments. For bulk viscosity, compaction experiments were performed under the diffusion creep regime. A cylindrical sample was compacted uniaxially in a rigid sleeve ( $e_{zz} < 0$ ,  $e_{xx} = e_{yy} = 0$ , where  $e$  is the strain). Melt was squeezed out from the partially molten sample into porous metals which contact with the sample at the top and bottom ends until melt fraction becomes nearly zero. Evolution of melt fraction in the sample was calculated from the sample length measured with digital gauge. Apparent viscosities as a function of melt fraction were proportional to  $\exp(-af)$  with  $a = \sim 30$  at  $f > 4\%$ , which is quite consistent with the olivine + melt systems (Renner et al., 2003). At  $f < 3\%$ , deviation of the viscosity from the exponential curve occurs, suggesting the possible effects of permeability and change of rate limiting process of the volumetric creep (Takei & Holtzman, 2009b). For shear viscosity, uniaxial deformation experiments were performed without a horizontal confining pressure ( $s_{zz} < 0$ ,  $s_{xx} = s_{yy} = 0$ , where  $s$  is the stress). Melt fraction was nearly constant during the test. Deformation tests were conducted with some constant load steps under the diffusion creep regime. Apparent viscosity is evaluated from the stress and the strain rate at steady state.

From the two apparent viscosities obtained independently, we can calculate each bulk and shear viscosities as functions of melt fraction. We will test the predictions of models and discuss the possible viscosity ratio of the partially molten rocks in the upper mantle.

### References:

- Katz RF (2008) J.Petrol., 49, 2099-2121.
- Renner J, Viskupic K, Hirth G, Evans B (2003) G<sup>3</sup>, 4, doi:10.1029/2002GC000369.
- Takei Y (2000) JGR, 105, 16665-16682.
- Takei Y, Holtzman BK (2009a) JGR, 114, doi:10.1029/2008JB005850.
- Takei Y, Holtzman BK (2009b) JGR, 114, doi:10.1029/2008JB005851.

Keywords: viscosity, bulk viscosity, shear viscosity, partial melt

## Role of Mg-O grain-boundary diffusion in rheology and grain-growth in the Earth's mantle

NISHIHARA, Yu<sup>1\*</sup> ; NISHI, Masayuki<sup>1</sup> ; MARUYAMA, Genta<sup>2</sup>

<sup>1</sup>Geodynamics Research Center, Ehime University, <sup>2</sup>Earthquake Research Institute, University of Tokyo

Material and heat transports in the Earth highly depends on rheology and grain-growth kinetics of the constituent materials. Although rheology and grain-growth in single phase aggregate have been studied extensively, knowledge of those in multi-phase system is still limited. Sundberg and Cooper (2008) pointed out the importance of a creep mechanism in which strain is produced by Mg-O grain-boundary diffusion accompanied with reaction at olivine-orthopyroxene phase boundary in the Earth's upper mantle. Tasaka and Hiraga (2013) showed that grain-growth in forsterite-enstatite two-phase system is rate-limited by growth of secondary phase through Mg-O grain-boundary diffusion. These reports suggest that Mg-O grain-boundary diffusion plays important role both in rheology and grain-growth. Recently, our group reported Mg-O grain-boundary diffusion coefficients in forsterite and MgSiO<sub>3</sub> perovskite (Maruyama et al., 2013; Nishi et al., 2013). In this study, theoretical model using our Mg-O grain-boundary diffusion data are compared with available rheological and grain-growth data, and importance of these mechanisms are discussed.

Flow-law were calculated for Mg-O grain-boundary diffusion creeps accompanied by reaction at forsterite-enstatite phase boundary (upper mantle) or accompanied by grain-growth of periclase (lower mantle) using Coble's (1963) equation and results by Maruyama et al. (2013) and Nishi et al. (2013). The derived flow-law for the upper mantle shows ~3 orders of magnitude faster strain-rate than that of creep experiments by Tasaka et al. (2013) which suggests this mechanism is not realistic. Although no comparable creep data was reported for the lower mantle, the derived flow-law shows faster strain-rate than that by Si lattice diffusion creep that was assumed in Xu et al. (2011) and the mechanism is a possible candidate deformation mechanism in the most part of lower mantle.

Grain-growth in the forsterite-enstatite two phase system was studied by Tasaka and Hiraga (2013) experimentally and it is already shown that grain-growth in this system is rate-limited by growth of secondary phase through Mg-O grain-boundary diffusion. Based on the same manner as Tasaka and Hiraga (2013), grain-growth law was calculated for the lower mantle assemblage MgSiO<sub>3</sub> perovskite-periclase system using Ardell's (1972) theory and Nishi et al.'s (2013) results. Derived grain-growth law was generally consistent with the grain-growth data in MgSiO<sub>3</sub> + MgO system reported by Yamazaki et al. (1996). Yamazaki et al.'s results can be explained by initial rapid growth from metastable texture and subsequent normal grain-growth which is rate-limited by Mg-O grain-boundary diffusion. Based on this interpretation, grain-size in the lower mantle is estimated to reach several hundred micro meter by 10<sup>6</sup> years.

Keywords: Upper mantle, Lower mantle, Rheology, Grain-growth, Olivine, Mg-perovskite

## Relationship between Skempton's coefficient and diagenesis of the Quaternary Kazusa Group siltstones

MITSUHASHI, Shunsuke<sup>1\*</sup> ; UEHARA, Shin-ichi<sup>1</sup> ; MARUMO, Haruna<sup>2</sup> ; TAMURA, Yukie<sup>1</sup>

<sup>1</sup>Faculty of Science, Toho University, <sup>2</sup>Graduate School of Science, Toho University

Skempton's coefficient  $B$  is one of fundamental properties of sediments and rocks.  $B$  is defined as the change in pore pressure per unit change in total stress applied under undrained conditions. To reveal the evolution of  $B$  of sediments and sedimentary rocks during diagenesis is critical for some processes relating to geophysics and geology, such as mechanisms of developing abnormal pore pressure in sedimentary basins (Tanikawa et al., 2008). However, how  $B$  depends on diagenesis is still not clear. To understand the dependency, we evaluated  $B$  based on porosity measurements under effective stress for siltstones collected from various formations in the Quaternary Kazusa Group. We also tried to measure  $B$  directly, and compared the results with  $B$  values obtained from measurements of porosity.

We used siltstones of Umegase, Otadai, Kiwada, Ohara and Katsuura Formations of the Kazusa Group as the samples for the experiments. The specimens from the samples were 30 mm in diameter and 40 mm in length. The laboratory experiments were performed using an intra-vessel deformation fluid-flow apparatus at Toho University, at room temperature and under confining pressures from 2 MPa to 35 MPa. Distilled water was used for pore fluid. From the results of the porosity measurements under effective pressure, we estimated the compressibilities of the rock on the assumption that volume change of the rock at effective stress change equals to the pore volume change, and calculated  $B$  from the results. In the direct measurements of  $B$ , we measured pore pressure changes when confining pressure were applied under undrained conditions.

The results of  $B$  estimations from porosity measurements indicated that  $B$  tends to decrease with increasing burial depth. But,  $B$  of Ohara siltstones was somewhat higher than other samples despite Ohara Formation is relatively lower in the Kazusa Group. This is probably because siltstones at Ohara Formation were not consolidated enough as compared with those at other formations due to some reasons such as developing abnormal pore pressure. Results indicated that the dependency of  $B$  on effective pressure is not simple.  $B$  was not simply decreased with effective pressure increases, but  $B$  was increased at some range of effective pressure, which mostly reflected that the compressibility was increased at the transition from overconsolidation to normal consolidation state.  $B$  depends on both compressibility and porosity, and in the case of the Kazusa Group siltstones, the behavior of compressibility has greater effect on  $B$ . Thus,  $B$  is decreased as a grade of diagenesis increases because compressibility is decreased. The values of  $B$  measured directly tended to be higher than  $B$  estimated from measurements of porosity. This is probably because a period between step changes of effective stress was not enough for the rocks to reach steady state.

Keywords: Skempton's coefficient, diagenesis, Kazusa Group, porosity, compressibility, laboratory rock experiment

## Effects of pore pressure changes on frictional behaviors of talc

UEHARA, Shin-ichi<sup>1\*</sup>; OKAZAKI, Keishi<sup>2</sup>; SHIMIZU, Ichiko<sup>3</sup>

<sup>1</sup>Faculty of Science, Toho University, <sup>2</sup>Department of Geological Science, Brown University, <sup>3</sup>Faculty of Science, The University of Tokyo

Since the discovery of low frequency earthquake, several classes of physical mechanisms have been proposed to explain this events. Several models and geophysical observations have suggested that the overpressurized fluid along the subducting plate interface have an important role in triggering such events. In addition, the existence of hydrous minerals along the plate boundary at fore-arc wedge may also be important for the seismogenic properties of the slab-mantle interface. Especially, serpentine minerals are generally expected to be the main hydrous mineral present in the fore-arc minerals, and the existence of serpentine in the wedge mantle has suggested by seismological studies. However, talc may also be important in fault mechanism at the plate boundary in the fore-arc wedge mantle, because slab-derived fluids are likely to lead replacement of serpentine by talc at the slab-mantle interface in the fore-arc wedge mantle, and talc is one of the weakest minerals that constitute natural fault zones. However the quantitative influences of pore pressure on the frictional properties of talc are not well constrained. We conducted friction experiments using pre-cut samples of talc with controlling pore pressure  $P_p$  and confining pressure  $P_c$  adopting several kinds of stress paths during an experiment.

Cylindrical samples of talc (Gvangjsih, China), 20 mm in diameter, were cut at an angle of  $30^\circ$  to the sample axis. The sliding surfaces were ground with carborundum (#400). A small hole (3 mm in diameter) through the center of each piece ensured adequate communication of the water between the pre-cut surfaces with the rest of the pore pressure system. The specimen was loaded by a triaxial apparatus and sheared under an axial displacement rate of  $1 \mu\text{m/s}$ . We used water as a pore fluid. All measurements were performed at room temperature. Experiments were conducted under several paths of  $P_c$  (up to 110 MPa) and  $P_p$  (up to 100 MPa). During steady axial loading, either  $P_c$  or  $P_p$  was changed stepwise.

The stepwise changes of effective normal stress  $\sigma (= \sigma_t - P_p$ , where  $\sigma_t$  is total normal stress) resulted in a linear elastic response of shear stress followed by a transient evolution of friction. In the case that  $\sigma$  was decreased, friction coefficient  $\mu$  was temporally increased and then decreased back to steady state, and the normalized transient change of  $\mu$  to the logarithm of normalized amplitude of  $\sigma$  change ranged from 0.2 to 0.28, which is comparable to that for quartz and Westerly granite reported by previous studies (Linker and Dieterich, *J. Geophys. Res.*, 1992; Hong and Marone, *Geochem. Geophys. Geosyst.*, 2005). While in the case that  $\sigma$  was increased ( $\mu$  was temporally decreased then increased), the values were smaller (less than 0.12, and negative in some cases), which means that a transient change of  $\mu$  was less dependent on a change of  $\sigma$  than that for quartz and granite, which may reflect ductile deformation of contacts on fault surfaces during the evolutionary transition.

This frictional property might cause slow slip phenomena. After an initiation of a fault slip, possibly triggered by an increase of pore pressure, partially undrained conditions on the slip surface may cause dilatancy hardening, and therefore  $\sigma$  may be increased during the slip. The results of this study suggest that, in the case that a fault plane is covered by talc, the temporal decrease of  $\mu$  following an increase of  $\sigma$  might be smaller than the case that fault planes are covered by other ordinary minerals. Consequently, a frictional resistance might act more effectively than faults covered by other ordinary minerals and an acceleration of fault slip rate might be mitigated, and therefore a slip rate might be smaller than regular earthquakes.

This research is supported by Grant-in-Aid for Scientific Research on Innovative Areas, KAKENHI.

Keywords: talc, friction experiment, pore pressure, low frequency earthquake

## Sintering experiments on fine-grained polycrystalline orthoclase

OHIRA, Akane<sup>1\*</sup> ; ISHIKAWA, Masahiro<sup>1</sup>

<sup>1</sup>Graduate school of Environment and Information Sciences, Yokohama National University

K-feldspar is one of the major mineral components of granitic rocks and a wide variety of metamorphic rocks. Its deformational behavior is important for establishing the overall rheology of continental crust. The creep strength is influenced by various factors such as mineral species, grain size and pores. Therefore control of these factors in polycrystalline minerals is essential for rheological experiments. In order to make dense polycrystalline orthoclase, we have carried out sintering experiments.

We prepared submicron mineral powders from a single crystal of orthoclase ( $K_{0.83}Na_{0.17}Al_{1.04}Si_{2.96}O_8$ ). As a result of X-ray fluorescence (XRF) analysis,  $ZrO_2$  (<5.65wt.%) which is considered to be contamination from a mill was detected. We formed cylindrical compacts from fine-grained mineral powders by uniaxial dry pressing at room temperature and pressure of 20MPa. Sintering was carried out using a tube furnace at temperature of 970 °C for 4 hours, achieving a vacuum condition of  $\sim 4.1 \times 10^4$  Pa. We also compared the sintered body with a sample sintered at atmospheric pressure using muffle furnace at the same temperature and the time. Sintered bodies were observed using scanning electron microscope (SEM), and analyzed by XRF and X-ray diffraction (XRD).

As the result of vacuum and atmospheric pressure sintering, we obtained sintered bodies with volume reduction of 52.2% and 44.5%, and porosity of 0.15 and 0.17, respectively. SEM images showed that densification process was advanced by both vacuum and atmospheric pressure sintering. We confirmed that crystal structures (Al/Si order-disorder) were not changed from compacts by XRD patterns.

In this study, we found that dense submicron polycrystalline orthoclase can be made from fine-grained powders by either of vacuum and atmospheric pressure sintering, and confirmed that orthoclase does not cause order-disorder phase transition by a sintering for 4 hours.

Keywords: submicron, orthoclase, sintering

## Doping effect on high-temperature creep of polycrystalline anorthite

YABE, Kosuke<sup>1\*</sup> ; KOIZUMI, Sanae<sup>1</sup> ; HIRAGA, Takehiko<sup>1</sup>

<sup>1</sup>Earthquake Research Institute, The University of Tokyo

Rheological properties of lower crust are considered to play important roles on the cause of inland earthquakes. Previous studies on creep properties of polycrystalline anorthite indicate that the polycrystalline anorthite will deform under diffusion creep at temperature condition of 400 to 1000C and grain size of <100 um where such conditions are identified in mylonites which are of lower crust origin. Therefore, it is important to know a precise strength of polycrystalline anorthite during diffusion creep.

Previous studies have shown the influence of grain size, temperature, stress, and water content on the strength of polycrystalline anorthite. It is well known that a small amount of impurities segregated at grain boundaries has a significant effect on the strength of polycrystalline oxides. We have shown that our pure anorthite aggregate, which was synthesized using the technique that could minimize the contamination of impurities, had two orders of magnitude larger strength than anorthite aggregates used in previous studies. In this study, we examine the effect of doping a small amount of MgO on high-temperature creep of anorthite aggregates.

MgO-doped anorthite aggregates were fabricated from nano-sized powders of CaCO<sub>3</sub>, Al<sub>2</sub>O<sub>3</sub>, SiO<sub>2</sub>, and Mg(OH)<sub>2</sub>, all of which have <50 nm in diameter, and vacuum sintering of the powders. We controlled the amount of Mg(OH)<sub>2</sub> powders to obtain anorthite doped with 1wt% of MgO. Constant load tests were performed at temperatures ranging from 1150 to 1380C, stresses from 10 to 120 MPa, and confining pressure of 0.1 MPa. We measured Arithmetic mean grain size of specimens by microstructural observations using scanning electron microscopy (SEM) before and after creep tests.

Grain sizes of the specimens were 1~2um before and after the creep test. Log stress versus log strain rate showed a linear relationship where its slope gave a stress exponent, n of 1, indicating that samples were deformed under diffusion creep. MgO-doped anorthite aggregates exhibited more than one order of magnitude weaker than pure anorthite. We obtained activation energy, Q of 702 kJ/mol which was higher than that of our pure anorthite. The difference in strength between pure and MgO-doped anorthite was attributed to the presence of a small amount of MgO which was probably segregated at grain boundaries.

Keywords: polycrystalline anorthite, diffusion creep, effect of doping

## Synthesis of textural polycrystalline forsterite using colloidal processing in a strong magnetic field.

KOIZUMI, Sanae<sup>1\*</sup> ; HIRAGA, Takehiko<sup>1</sup> ; SUZUKI S., Tohru<sup>2</sup> ; SAKKA, Yoshio<sup>2</sup>

<sup>1</sup>Earthquake Research Institute, University of Tokyo, <sup>2</sup>National Institute for Material Science

It is well known that the crystallographic preferred orientation (CPO) of minerals is commonly produced in the Earth's interior. Thus, it is important to understand the physical properties of the mineral aggregates that exhibit CPO. However, silicate minerals are often feeble magnetic and have small anisotropic susceptibilities so that it is difficult to apply a magnetic field effectively to rotate the mineral particles. Tendency of finer particles to spontaneously agglomerate due to strong attractive interactions (van der Waals forces) add further difficulty. We used a technique of slip casting in a high magnetic field (12T) to align certain crystallographic axis of mineral particles. For the particles to rotate easily in the solvent under a strong magnetic field, we improve the method of deflocculating. To control the surface potential of the particles, we applied various types of polymer modification. Vacuum sintering of the powders that were composed of the aligned particles was expected to produce a polycrystalline material aggregate that exhibits CPO. The resultant materials were characterized by X-ray powder diffraction (XRD), secondary electron microscope (SEM) and Electron Backscatter Diffraction (EBSD).

The specimen exposed to a strong magnetic field exhibits preferential A-axis alignment to the magnetic direction. Those synthetic specimens allow us to examine the effect of CPO on the physical properties of the earth's materials in future room experiments.

Keywords: forsterite, polycrystalline, magnetic field, orientation, CPO

## Grain growth experiment on pyrolite material under lower mantle conditions

IMAMURA, Masahiro<sup>1\*</sup> ; KUBO, Tomoaki<sup>1</sup> ; KATO, Takumi<sup>1</sup>

<sup>1</sup>Kyushu Univ.

Grain size is a key parameter for understanding viscosity of Earth's mantle. Grain growth rate is one of important factors controlling the grain size. Especially, it is indispensable to examine grain growth kinetics in multiple phases because the grain growth rate of major phase drastically changes with the proportion of secondary phases (e.g., Hiraga et al., 2010). In the lower mantle, Mg-perovskite is major phase, and ferro-periclase, Ca-perovskite, and majoritic garnet are present as secondary phases (e.g., Irifune, 1994; Nishiyama and Yagi, 2003). The previous grain growth experiment (Yamazaki et al., 1996) in the two-phase system of MgSiO<sub>3</sub> perovskite and MgO periclase using Mg<sub>2</sub>SiO<sub>4</sub> forsterite as a starting material suggests that the grain growth rate is too slow to explain the lower mantle viscosity constrained by geophysical observations. This inconsistency may arise from effects of the eutectoid transformation prior to the grain growth process (e.g., Solomatov et al., 2002). It is also necessary to examine effects of the chemical composition that affects the proportion of secondary phases and diffusivity. Here, we report preliminary results of the grain growth experiment on pyrolite material under lower mantle conditions.

High-pressure and temperature experiments were conducted using a Kawai-type multi-anvil apparatus (QDES) installed at Kyushu University. Starting material is a powder with pyrolite composition that was used in the previous phase equilibrium study (e.g., Irifune, 1994). We conducted annealing experiments at 25-28 GPa and 1600-1800 °C for 6-600 min. Chemical compositions, microstructures and grain sizes of recovered samples were examined using a FE-SEM with an energy-dispersive analytical system.

Four phases of Mg-perovskite, Ca-perovskite, ferro-periclase and majoritic garnet were present in recovered samples annealed at 25 GPa and 1600-1800 °C. The normalized grain size distribution in the recovered samples showed Gaussian-like shape and the largest grain size is smaller than three times of the mean grain size, suggesting that normal grain growth occurred. The grain growth rate is faster than that of the previous study (Yamazaki et al., 1996). Preliminary analysis of the kinetic data of Mg-perovskite obtained showed the smaller grain growth exponent of 4.3 than that reported in the previous study. On the other hand, three phases of Mg-perovskite, Ca-perovskite and ferro-periclase were present at higher pressure of 28 GPa and 1800 °C, in which the volume fraction of Mg-perovskite increased compared to the four-phases experiment. While the microstructure and the grain size distribution in the three-phase assemblage was similar to those of the four-phase assemblage, the grain size was larger probably due to the smaller proportion of the secondary phases. Our preliminary results provide some insights into the grain-size evolution in the lower mantle and suggest that further quantitative grain growth data with possible lower mantle conditions are needed.

Keywords: lower mantle, multi-anvil, pyrolite, grain growth

## Grain boundary diffusion of noble metal elements in mantle composites

MATSUO, Naoya<sup>1\*</sup>; HIRAGA, Takehiko<sup>1</sup>

<sup>1</sup>Eartuquake Research Institute, The University of Tokyo

So far, it is not clear whether Earth's core and mantle have been chemically isolated through geological time. It has been believed that highly incompatible elements such as siderophile elements in the mantle minerals have not been moved from the core to the mantles so that the elemental abundance of highly siderophile elements (HSEs) in the core and mantle were determined when both were separated. Although HSEs are refractory, amounts of HSEs are very little in the mantle (Wood, 2006) so that these elements are expected to be highly concentrated in the core relative to the silicate mantle. However, a recent study has shown that incompatible elements can be concentrated and quickly diffuse at grain boundaries (Hiraga et al., 2004). If HSEs can diffuse from the core to the mantle, the concentration of HSEs in the mantle can change through Earth's history. Therefore, HSEs can be a good tracer to detect the chemical interaction of the core and the mantle.

We conducted grain growth experiments on Au particles in forsterite (Fo) aggregates at 1 atmosphere pressure and temperature of 1360 °C. We prepared several sintered bodies which were made by dispersing 10vol% Au particles in Fo aggregates and then annealed for several hours. We observed these bodies using a scanning electronic microscope. In the result, Au particles changed their shape from spherical to polygonal. This is due to a balance of interfacial tensions between Au and Fo phases. Further, average grain size of Au particles was found to increase with time. Based on these observations, we conclude that Ostwald ripening of grains, by which Au atoms move from small particles to larger ones to minimize entire interfacial energies of the system, occurred in our experiment. Grain boundaries as diffusion paths should be responsible for Au diffusion. In this case, grain growth of Au particles will follow the relationship of  $d^4 - d_0^4 = kt$ , where  $d$  is the average grain size of Au particles after annealing,  $d_0$  is the initial average grain size,  $k$  is the grain growth coefficient, and  $t$  is annealing time. Using the average grain size of each body, we calculated  $k$ . In addition, we estimated the interfacial energy of the system from the shape of Au particles and calculated the product of concentration of Au particles at grain boundaries,  $c$ , and diffusivity of Au atoms at grain boundaries,  $D$ .

Keywords: grain boundary diffusion, grain growth, core-mantle interaction

## The effect of partial melting on the mantle viscosity and electrical

SUEYOSHI, Kenta<sup>1\*</sup>; HIRAGA, Takehiko<sup>1</sup>

<sup>1</sup>Earthquake Research Institute, University of Tokyo

In this study, in order to know the change in mantle viscosity and electrical conductivity during partial melting, which corresponds to decompression melting of ascending mantle beneath mid-ocean ridge, mantle analogue sample was synthesized and used to measure its viscosity and electrical conductivity under atmospheric pressure and high temperature conditions. The sample has lherzolite composition of olivine (50%), orthopyroxene(40%) and clinopyroxene(10%) with addition of 0.5 vol% spinel. Constant force was applied to the sample under increasing the temperature where its range includes sample solidus. Sample viscosity and the electrical conductivity by the impedance measurement were calculated for every temperature. We particularly examined how viscosity and conductivity change when the sample transforms from melt-free to melt-bearing system. Temperature ranged from 1100 to 1390 °C, which resulted in the change of melt fraction ( $\phi$ ) from 0 to 0.09, where the melt composition becomes enriched in clinopyroxene component as the temperature increases.

We observed a continuous and gradual reduction of sample viscosity with increasing temperature. The effect of the increasing melt fraction on the sample viscosity should have been added to the viscosity change simply due to thermally activation process. There is a linear relationship between measured  $1/T$  and  $\log(1/\eta)$ , which goes well with the previous proposed empirical expression of flow law that, which is an function of melt fraction.

Analyzing the observed viscosity change with temperature with this law, the apparent activation energy of 970 kJ/mol is obtained at a temperature range of 1220 °C to 1340 °C and the effect of increasing melt fraction on sample viscosity roughly corresponds to the activation energy of  $\sim$ +35 kJ/mol. The activation energy on the melt free system is estimated to be 935 kJ/mol. This value is close to the activation energy of the dislocation creep of orthopyroxene and clinopyroxene indicating that the sample viscosity was essentially controlled by deformation of pyroxenes.

Electrical conductivity did not change dramatically when the experimental temperature reached and exceeded the sample solidus. Grain size dependency on the conductivity was observed at all temperature conditions indicating that the conductivity is simply determined by grain boundary conductivity even at higher melt fraction condition, probably due to fine grain size of the samples. Compared with previously reported grain boundary conductivity in the melt-free forsterite system, grain boundaries in our sample have 3 to 4 times higher conductivity indicating that the pyroxene grain boundaries have a large effect on the bulk sample conductivity in our experiment.

In this study, it was demonstrated that previously proposed empirical flow law as a function of melt fraction can approximate the viscosity change of the mantle during its transition from melt-free to melt-bearing. Taking into account of the incremental rate of melt fraction with temperature and the connectivity of intergranular melt in the mantle highly depend on the volume fraction of the pyroxenes and spinel phases, mineral mode in the mantle should have substantial effects on the mantle rheology and electrical conductivity during mantle melting.

Keywords: rheology, lherzolite, melt, viscosity, electrical conductivity

## Stress calibration of Griggs-type deformation apparatus with solid salt assemblies

KIDO, Masanori<sup>1\*</sup> ; MUTO, Jun<sup>1</sup> ; NAGAHAMA, Hiroyuki<sup>1</sup>

<sup>1</sup>Department of Earth Sciences, Tohoku University

Mechanical properties of rocks and minerals can be quantitatively studied by deformation experiments under high-temperature and high-pressure conditions relevant to the Earth's interior. There are several types of deformation apparatus using different confining media such as gases, liquids or weak solids (e.g., Tullis and Tullis, 1986). Liquid medium apparatus have the disadvantage that they cannot be used for temperatures above 500 °C because of prevention from alteration of oil at high temperature. Solid medium apparatus can provide us high pressure safely and stably for a long time. However, stress accuracy is not high due to frictional forces between pressure medium and load piston or samples (e.g., Tullis and Tullis, 1986). Gas apparatus has most accurate stress measurement because of the usage of internal load cell; thus measured stresses do not include frictional forces. However, experiments are restricted to confining pressures less than 200 MPa in Japan due to safety issues on the usage of high-pressure gas. Therefore, solid medium apparatus is necessary for generating high temperature and high pressure required to investigate rheological behaviors of rocks and minerals in lower crust or uppermost mantle.

Recently, comparisons of mechanical results obtained for metals at the same confining pressure, temperatures and strain rates deformed in a Griggs apparatus with solid salt assemblies (SSA) and a gas apparatus provide calibration for Griggs apparatus with SSA (Holyoke and Kronenberg, 2010). This calibration law allowed differential stresses to be measured accurately to within  $\pm 30$  MPa. However, we have not been able to reproduce elastic, yielding and post-yield behaviors because the calibration law was obtained by the comparison of strengths at 5% strain of mechanical results. Calibration law for measured stresses using Griggs apparatus in all deformation behaviors are required for revealing detailed rheological behavior of rocks and minerals.

In this study, we performed axial compression experiments on high-purity nickels to measure differential stresses using a Griggs apparatus with SSA at Tohoku University. Samples were given by Drs. Holyoke and Kronenberg. Experimental conditions were confining pressures of 300 and 1200 MPa, temperatures of 600, 700, and 800 °C and strain rates of  $2 \times 10^{-4}$ ,  $2 \times 10^{-5}$  and  $2 \times 10^{-6}$  /s. Measured differential stresses agreed with results of the former study within  $\pm 30$  MPa under the identical confining pressure of 300 MPa. However, differential stresses were larger with confining pressure. We analyzed obtained mechanical data of nickels based on the high temperature viscoelastic constitutive law developed by Shimamoto (1987). We made the master curve which normalized temperature and strain conditions. In the same way, we also made the master curve from mechanical data of nickels using a gas apparatus (mechanical data are from Holyoke and Kronenberg, 2010). Master curves were made of mechanical data of the identical material between Griggs apparatus and gas apparatus under normalized temperature and strain conditions. Therefore, difference in master curves is thought to be derived from apparatus and assembly. We derived calibration law for Griggs apparatus from difference in master curves. Applying this calibration law to differential stresses of nickels obtained using Griggs apparatus with SSA, it became possible to reproduce gas apparatus's differential stresses not only steady state but also elastic, yield and post-yield behaviors within the systematic error of  $\pm 30$  MPa. However, the error was  $\pm 70$  MPa when the calibration law was applied to the mechanical data of carbonate rock. Moreover, unlike gas apparatus, measured differential stresses using Griggs apparatus tend to become larger with confining pressures. Therefore, it is necessary to investigate the effect of confining pressures on measured stresses in the calibration law.

Keywords: rheology, deformation experiment, calibration of Griggs-type apparatus

## Preliminary experiments on in-situ stress-strain measurements of Ca-Pv and Mg-Pv up to 23 GPa

TSUJINO, Noriyoshi<sup>1\*</sup> ; YAMAZAKI, Daisuke<sup>1</sup> ; YOSHINO, Takashi<sup>1</sup> ; SAKURAI, Moe<sup>2</sup> ; NISHIHARA, Yu<sup>3</sup> ; HIGO, Yuji<sup>4</sup>

<sup>1</sup>ISEL, Okayama Univ., <sup>2</sup>Tokyo tech., <sup>3</sup>GRC, Ehime Univ., <sup>4</sup>JASRI

In order to discuss mantle dynamics in the Earth's interior, knowledge of viscosity of the Earth's lower mantle, which is the highest of the whole mantle, is important. Viscosity models of the Earth's lower mantle were reported by geophysical observations. However, observation values of viscosity have large variety (2~3 order magnitude). Although determination of viscosity of lower mantle minerals by high pressure experiments is needed to understand mantle dynamics, stress-strain relationship for MgSiO<sub>3</sub>-perovskite (Mg-Pv) and CaSiO<sub>3</sub>-perovskite (Ca-Pv), which are principal minerals of the Earth's lower mantle, are not reported due to difficulty of high pressure deformation experiments. In this study, we tried in-situ stress-strain measurements of Ca-Pv and Mg-Pv up to 23.0 GPa.

In-situ uniaxial deformation experiments were conducted using a deformation DIA apparatus (SPEED-Mk.II) as Kawai-type apparatus at SPring-8 BL04B1. Experimental conditions of Ca-Pv and Mg-Pv are 13.8 GPa, 1473 K and 23.0 GPa, 1273 K, respectively. cBN anvils, which was transparent material against X-ray, was used along X-ray path. Two-dimensional X-ray diffraction patterns were taken for 120-180 s using CCD detector. To calculate the stress magnitude from the X-ray diffraction data, we used a model of stress-lattice strain relationship (Singh et al. 1998),

$$d_{hkl}(\psi) = d_{0hkl} [1 + (1 - 3\cos^2\psi) \sigma / 6 G_{hkl}] \quad (1)$$

where  $d_{hkl}$  is the d-spacing measured as a function of azimuth angle  $\psi$ ,  $d_{0hkl}$  is the d-spacing under the hydrostatic pressure,  $G_{hkl}$  is the appropriate shear modulus for a given hkl, and  $\sigma$  is the uniaxial stress. Pressure and stress were estimated using Ca-Pv (110) (200) and Au (111) diffraction in Pressure marker (Au : Fo = 1 : 2 volume ratio) at deformation experiments of Ca-Pv and Mg-Pv, respectively. An X-ray radiograph of the strain markers was taken using an imaging system composed of a YAG crystal and a CCD camera with an exposure time of 60 s.

Uniaxial stress of Ca-Pv at 13.8 GPa, 1473 K and  $\sim 1.2 \times 10^{-5}$  /s and Mg-Pv at 23.0 GPa, 1273 K and  $\sim 1.5 \times 10^{-5}$  /s were estimated as  $\sim 2$  GPa and  $\sim 0.25$  GPa, respectively. Stress of Mg-Pv was significantly smaller than that of Ca-Pv though temperature condition of Mg-Pv was lower than that of Ca-Pv. This fact is doubtful. This reason is thought that stress estimated by Au was much smaller than that of Mg-Pv because of framework made by Ringeoodite, which was polymorphic phase of Fo in pressure marker.

Keywords: In-situ measurements, deformation experiments, Stress, Strain, Perovskite, The Earth's lower mantle

## A new form of the dynamics equation of Maxwellian visco-elastic media

MATSUNO, Taroh<sup>1\*</sup>

<sup>1</sup>Japan Agency for Marine-Earth Science and Technology

Dynamical property of the earth's interior down to the core-mantle boundary has so far been considered to be a Maxwellian visco-elastic medium. It behaves as an elastic body for short time-scale phenomena, while on a very long time-scale it shows fluid-like behavior. So the Navier-Stokes equation for viscous fluids is considered to be appropriate for describing mantle convection, and numerical simulations have been made based on the equation.

As a phenomenon for which both elastic body property and viscous fluid property are essential post-glacial uplift has been discussed based on the constitutive equation proposed by Maxwell. However, so far most of studies apply Laplace transform to expressing time evolution, so it is not possible to treat this problem by use of finite difference method, just like general circulation models of atmosphere and oceans. Thus it is not possible to extend numerical simulation of mantle convection to include elastic property of the plate near the earth's surface.

With intention to overcome this difficulty to enable us to conduct numerical simulations of mantle-plate general circulation, a new formulation of dynamics equations for Maxwellian visco-elastic media is attempted in this study

Keywords: Maxwellian visco-elastic media, visco-elastic medium dynamics, mantle convection, plate-mantle coupling simulation

## Effects of Al content on water partitioning between Opx and Ol: Implications for lithosphere-asthenosphere boundary

SAKURAI, Moe<sup>1\*</sup> ; TSUJINO, Noriyoshi<sup>2</sup> ; SAKUMA, Hiroshi<sup>3</sup> ; KAWAMURA, Katsuyuki<sup>4</sup> ; TAKAHASHI, Eiichi<sup>1</sup>

<sup>1</sup>Earth and Planet. Sci., Tokyo Inst. Tech., <sup>2</sup>ISEI, Okayama, <sup>3</sup>NIMS, <sup>4</sup>Environmental Sci., Okayama Univ.

Most minerals in the Earth's upper mantle contain small amounts of hydrogen (i.e. "water"), structurally bound as hydroxyl. Water has an important influence on the behavior of rock system. This small amount of water has an important influence on the behaviours of rock systems. A large viscosity contrast of more than two orders of magnitude was detected at depths of 70 km to 100 km beneath ocean and was defined as the lithosphere-asthenosphere boundary [1]. The origin of the lithosphere-asthenosphere boundary remains an enigma. The water distribution in the Earth is critical to the nature of the boundary. For example, Mierdel et al. (2007)[2] indicated that a high water solubility in aluminous orthopyroxene among mantle geotherm in the Earth's upper mantle would effectively contribute to a stiffening of the lithosphere. Therefore, precise knowledge on the distribution of water among mantle minerals is very important for understanding the Earth's dynamics. The Earth's uppermost mantle is composed mainly of olivine (Ol), orthopyroxene (Opx), clinopyroxene (Cpx), spinel, and garnet. In particular, Ol accounts for a large proportion (60 vol.%) of the Earth's uppermost mantle. In addition, Opx, which contains significantly more water than does Ol in the mantle xenolith, is the second phase of the Earth's uppermost mantle. The FeO content in mantle Ol shows very limited variation in range, whereas the Al content of Opx in the Earth's upper mantle decreases significantly with increasing pressure [3] Therefore, the variation of Al content in mantle minerals can be important for the solubility of water in mantle minerals.

To investigate the partitioning coefficient of water between Opx and Ol ( $D_{(Opx/Ol)}$ ) under low-water concentrations (3 ~ 387 wt. ppm) similar to the Earth's mantle conditions, high-pressure experiments have been conducted at pressures of 1.5-6 GPa and a temperature of 1573 K. The experiments were performed with Kawai-type multi-anvil and piston-cylinder apparatus by using starting materials of natural Ol and synthetic Opx with various Al contents. The water contents were obtained with a vacuum type Fourier transform infrared spectrometer (Jasco: FT-IR6100, IRT5000). Water content of minerals was calculated based on Paterson's calibration [4]. IR-spectra of Ol and Al-bearing Opx in this study are similar to those obtained by high-pressure experiments [5] and natural rocks [6], respectively. It is believed that broad bands in IR spectra of natural Opx are due to effect of crystal distortion by large Al substitution. On the contrary, IR-spectra of Al-free Opx are not consistent with those reported by Rauch and Keppler (2002) [7] likely because of the large difference of water fugacity.  $D_{(Al-freeOpx/Ol)}$  is  $\sim 1$  at all pressure conditions. However, the water contents of Al-bearing Opx are significantly larger than those of Ol at the same conditions. In addition, the effect of Al concentration in Opx on  $D_{(Opx/Ol)}$  becomes larger with increasing pressure. The high Al content in Opx significantly increases  $D_{(Opx/Ol)}$  and the trend increases with increasing pressure.  $D_{(Opx/Ol)}$  drops sharply at the pressure at which the Al concentration of Opx becomes nearly 0 in the Earth's mantle conditions.

These results imply that viscosity of the upper mantle decreases sharply at depths deeper than those in which orthopyroxene contains no Al. The dramatic change of  $D_{(Opx/Ol)}$  may explain the lithosphere-asthenosphere boundary beneath oceans and continents.

[1] D.L. Anderson, (1989) Blackwell Scientific, Boston [2] K. Mierdel et al. (2007) Science, 315, 364-368 [3] M. Obata, (1976) Am. Mineral., 61, 804-816 [4] M. S. Paterson, (1982) Bull. Mineral., 105, 20-19 [5] Q. Bai and D.L. Kohlsted, (1993) Phys. Chem. Minerals, 19, 460-471 [6] K. Grant et al., (2007) Contrib Mineral Petrol, 154, 15-34 [7] M. Rauch, H. Keppler, (2002) Contrib. Mineral. Petrol., 143, 525-536

Keywords: water partitioning coefficient, olivine, orthopyroxene, viscosity, FT-IR, lithosphereasthenosphere

## Acoustic velocities of MgGeO<sub>3</sub> gel at high pressure by Brillouin scattering

KAWADAI, Tomofumi<sup>1\*</sup> ; MURAKAMI, Motohiko<sup>1</sup> ; OHTANI, Eiji<sup>1</sup>

<sup>1</sup>Tohoku University

Properties of silicate melts are essential for understanding evolution and dynamic behavior of the Earth and terrestrial planets. In the shallow mantle melting processes the density contrast between melts and crystals is well studied, but studies on the deep melting near the core-mantle boundary are still limited due to technical difficulties. The studies of amorphous material, analogs of melt, at high pressure can provide valuable insights about melts in the deep mantle. The Brillouin scattering method is suitable for velocity measurements of amorphous materials. It has been suggested that the change in coordination in the melt or glass structure reflects to the change in acoustic velocity. Thus we conducted sound velocity measurement using the Brillouin scattering method in diamond anvil cell at high pressure. We report in situ high-pressure acoustic velocity measurements of MgGeO<sub>3</sub> gel, an analogue of the MgSiO<sub>3</sub> melt, revealing the gradual coordination change of Ge from four- to six at least up to 80 GPa. We will conduct experiments at higher pressure in order to confirm the possible Ge coordination change in the gel expected to exist in the terrestrial and extraterrestrial planets.

Keywords: sound velocity measurement, high-pressure experiment, mantle dynamics, silicate melts, super-Earth

## Measurement of differential P-wave travel time between two BBOBSs with Correction for crustal reverberation

OBAYASHI, Masayuki<sup>1\*</sup> ; YOSHIMITSU, Junko<sup>1</sup> ; ISHIHARA, Yasushi<sup>1</sup> ; SUETSUGU, Daisuke<sup>1</sup>

<sup>1</sup>JAMSTEC

Seismic observations under the ocean are very important to investigate three-dimensional structure of the whole mantle. However, it is difficult to pick up arrival times of P-waves because noise level of broadband ocean bottom seismometer (BBOBS) is in general high in the period range more than 5 sec. Instead of picking arrival times, differential travel times between two BBOBSs have been measured by cross-correlating the waveforms at a period of around 10 sec or more (e.g. Toomey et al. 1998, Tanaka et al., 2009).

The resolution of P-wave tomography become high effectively by taking dispersion of P-wave travel time into account with the finite frequency theory (e.g. Obayashi et al. 2013 JpGU meeting), and its effect is expected to be significant under the ocean where the observations have been sparse. Obayashi et al. (2004) showed dispersion of PP is generated by interference of crustal reverberations under its bounce point. The reverberation under the station also affects a direct P-wave. Especially the effect of the seawater reverberation is significant.

Obayashi et al. (2013) proposed a method of correction for such reverberations to measure differential travel times between any two stations. In this method a waveform is convolved by the response calculated for the crustal structure under the other station.

We applied this method to the BBOBS array at French Polynesia. In the case of the measurement between a BBOBS and a island station, the waveforms of the two stations become similar each other after the correction, suggesting the correction is effective. We report the characteristics of the observed dispersions and the very first result of P-wave tomography using the new observations.

Keywords: crustal reverberation, broadband ocean bottom seismometer, tomography

## Small shear modulus of cubic CaSiO<sub>3</sub> perovskite

KAWAI, Kenji<sup>1\*</sup>; TSUCHIYA, Taku<sup>2</sup>

<sup>1</sup>Department of Earth and Planetary Sciences, Tokyo Institute of Technology, <sup>2</sup>Geodynamics Research Center, Ehime University

Ca-perovskite (CaPv) is considered to be one of the most abundant minerals in the Earth's lower mantle (LM) and was suggested to have distinctly larger shear modulus than MgPv from static calculations and mean-field theory (Karki and Stixrude 1999; Stixrude et al. 2007). In this study the elasticity of cubic CaPv is reinvestigated using density functional constant-temperature first principles molecular dynamics simulations with strict calculation conditions. First, we computed the stable structure of CaPv and found that the cubic phase is more stable than the tetragonal and orthorhombic in the LM P,T condition. The thermal equation of state of CaPv was analyzed using the MD data set, which indicates its thermal properties including Gruneisen parameter quite similar to those of MgPv. Along the adiabatic temperature, CaPv was found to have higher density than the PREM and 12.5% iron-bearing MgPv. Next, we calculated elastic constants of cubic CaPv. Our new results clearly demonstrate that cubic CaPv does not have anomalously large shear modulus suggested by previous calculations with a small computation cell. This is because the cell applied in the previous studies is too small to allow the rotational phonon motion of SiO<sub>6</sub> octahedra related to the zone boundary optic phonon instability. Acoustic wave velocities were finally determined from the elastic moduli, indicating no significant differences in velocities between CaPv and iron-bearing MgPv.

Keywords: Ca-perovskite, elasticity, lower mantle, first principles

## Seismic Constraints on an Enstatite Chondrite Earth

HOUSER, Christine<sup>1\*</sup> ; GREAU, Steeve<sup>2</sup> ; DU, Wei<sup>2</sup>

<sup>1</sup>Earth-Life Science Institute, Tokyo Tech, <sup>2</sup>Geodynamics Research Center, Ehime University

Recently, Javoy et al., EPSL, 2010 suggested the possibility that Earth had an initial enstatite chondrite composition due to their similar oxygen isotopes. Currently, the calculations of the bulk silicate Earth (BSE) are based on the assumption that the initial Earth began with a composition very close to that of a carbonaceous chondrite. Thus, it is necessary to evaluate whether the 1D seismic properties of the Earth are more consistent with an initial enstatite or chondritic composition. The BSE of an enstatite chondrite Earth (ECE) is different from that of a carbonaceous chondrite since the magnesium/silicon ratio is much lower for the former, resulting in a lower mantle that is almost devoid of Mg. Hence, the primitive lower mantle of an ECE consists mostly of iron-rich perovskite and pure silica. The seismic velocities of these phases are much slower than Mg-perovskite which, by itself, is faster than PREM (the slower MgO phase is necessary to match PREM velocities). However, the present-day lower mantle would be a mix of the primitive upper mantle (ie. pyrolite) and the Mg-depleted lower mantle. The latest mineral physics results are used to calculate possible 1-D seismic profiles of the Earth associated with these two scenarios and to compare with those observed for the Earth today.

## Thermal property modeling of the core-mantle boundary

TSUCHIYA, Taku<sup>1\*</sup> ; DEKURA, Haruhiko<sup>1</sup>

<sup>1</sup>Ehime Univ

Lattice thermal conductivity of minerals under pressure and temperature is a key property to understanding dynamics and evolution of the Earth's interior. We recently established an efficient ab initio technique for calculating the thermal conductivity of silicate minerals with complex structure and chemistry (Dekura, Tsuchiya, Tsuchiya, PRL, 2013). Calculated lattice thermal conductivity of MgSiO<sub>3</sub> perovskite agreed satisfactorily with experimental values at room temperature, and post-perovskite was found to have thermal conductivity quite different from perovskite's, indicating that the D'' discontinuity is not only the phase transition boundary but also the conductivity boundary. Using the obtained results, we determine the effective conductivity of the lower mantle and estimate the energy flow across the core-mantle boundary (CMB). Our results demonstrate that the CMB heat flux could change significantly from place to place by reflecting temperature heterogeneity located atop the core. A large CMB heat flow recently suggested from the outer core side can be reconciled only by considering polycrystalline assemblages yielding high-thermal conductivity.

Keywords: First principles computation, Thermal conductivity, CMB heat flow

## Waveform inversion for localized 3-D seismic velocity structure in the lowermost mantle beneath the Western Pacific

KONISHI, Kensuke<sup>1</sup> ; KAWAI, Kenji<sup>2</sup> ; GELLER, Robert J.<sup>3\*</sup> ; FUJI, Nobuaki<sup>4</sup>

<sup>1</sup>School of Earth and Environmental Sciences, Seoul National University, <sup>2</sup>Department of Earth and Planetary Sciences, Tokyo Institute of Technology, <sup>3</sup>Department of Earth and Planetary Science, Graduate School of Science, University of Tokyo, <sup>4</sup>Institut de Physique du Globe de Paris

We infer 3-D localized shear velocity structure in the lowermost 400 km of the mantle at the western edge of the Pacific large low shear velocity province (LLSVP) by applying waveform inversion to transverse component body-wave waveforms from the F-net seismic array in Japan. Our dataset consists of relatively long period (12.5-200 s) broad-band seismic waveforms of Tonga-Fiji deep focus and intermediate deep earthquakes. We conduct several tests to confirm the robustness of the inversion results. We find two low velocity zones at the bottom of the target region, with a high velocity zone in the middle, and a low velocity zone above the high velocity zone and contiguous with the two deeper low velocity zones at a depth of 200-300 km above the CMB. This supports the idea that the Pacific LLSVP may be an aggregation of small upwelling plumes rather than a single large thermochemical pile.

Keywords: Waveform inversion, Western Pacific, Mantle convection, Lowermost mantle, Plume cluster

## Compressional sound velocity and density measurements of hcp-Fe under core conditions

SAKAMAKI, Tatsuya<sup>1\*</sup> ; OHTANI, Eiji<sup>1</sup> ; FUKUI, Hiroshi<sup>2</sup> ; KAMADA, Seiji<sup>1</sup> ; TAKAHASHI, Suguru<sup>1</sup> ; SAKAIRI, Takanori<sup>1</sup> ; TAKAHATA, Akihiro<sup>1</sup> ; SAKAI, Takeshi<sup>4</sup> ; TSUTSUI, Satoshi<sup>5</sup> ; BARON, Alfred<sup>3</sup>

<sup>1</sup>Tohoku University, <sup>2</sup>University of Hyogo, <sup>3</sup>RIKEN, <sup>4</sup>Ehime University, <sup>5</sup>SPRING-8/JASRI

Sound velocity measurements of Fe and Fe-alloy at high temperature and high pressure are necessary to understand the Earth's inner core. Despite seismological observations providing density-sound velocity data of Earth's core, there are few experimental reports about sound velocity of hcp-Fe at ultrahigh pressure and temperature conditions. In order to push forward with research, we have developed a portable laser-heating system for diamond anvil cell, which is called COMPAT (Fukui et al., 2013). We have succeeded in measuring the sound velocity of hcp-iron up to 160 GPa and 3000 K by inelastic X-ray scattering measurements combining with a laser-heated diamond anvil cell. The obtained pressure and temperature dependence of the sound velocity suggest that compressional sound velocity of hcp-Fe at inner core boundary (330 GPa and 5500 K) is higher than that of Earth's inner core. Thus, we can conclude that the light elements or combination of the light elements and nickel in the inner core decreases both density and compressional sound velocity of hcp-Fe simultaneously under the inner core conditions.

### Reference

Fukui et al., 2013. A compact system for generating extreme pressures and temperatures: An application of laser-heated diamond anvil cell to inelastic X-ray scattering. *Review of Scientific Instruments* 84, 113902; doi: 10.1063/1.4826497.

Keywords: Earth's core, sound velocity, density, high pressure and high temperature, inelastic X-ray scattering, laser-heated diamond anvil cell

## The P-V-T equation of state of liquid pure Fe and Fe-light elements alloys by ab initio molecular dynamics simulations

ICHIKAWA, Hiroki<sup>1\*</sup> ; TSUCHIYA, Taku<sup>1</sup> ; OSUMI, Masanao<sup>2</sup>

<sup>1</sup>GRC, Ehime University and ELSI, Tokyo Institute of Technology, <sup>2</sup>Geodynamics Research Center, Ehime University

The equation of state (EoS) of pure Fe and Fe-light elements alloy liquids were calculated by means of ab initio molecular dynamics simulations at the outer core  $P$ - $T$  conditions. In the outer core, many light elements, such as carbon, nitrogen, oxygen, hydrogen, sulfur, and silicon, have been proposed as possible constituents. The concentrations of these elements have been strongly debated for years. In this study, internally consistent thermodynamic and elastic properties of pure Fe and Fe-light elements alloys, in particular density, adiabatic bulk modulus, and P-wave velocity were analyzed in order to clarify the effect of light elements incorporation on seismically observable data. Then the results were compared with the seismological data of the Earth's outer core to confine the plausible compositions of the outer core. The new EoS model of liquid iron alloys as a function of pressure, temperature and fraction of light elements may serve as fundamental data for the composition model of the Earth's core.

## Simultaneous measurement of liquid Fe-C density and sound velocity at high pressure

SHIMOYAMA, Yuta<sup>1\*</sup> ; TERASAKI, Hidenori<sup>1</sup> ; TAKUBO, Yusaku<sup>1</sup> ; URAKAWA, Satoru<sup>2</sup> ; KUWABARA, Souma<sup>1</sup> ; KATAYAMA, Yoshinori<sup>3</sup>

<sup>1</sup>Graduate School of Science, Osaka University, <sup>2</sup>Department of Earth Sciences, Okayama University, <sup>3</sup>Japan Atomic Energy Agency

The cores of terrestrial planets, such as Mercury, Mars and Moon are considered to contain some light elements. The effect of light elements on density and bulk modulus of liquid iron is necessary for estimating of these core compositions. Sound velocity of liquid iron alloys is also important for identifying light elements in the core by comparison with observed seismic data.

In this study, we have measured density and sound velocity of liquid Fe-C at SPring-8 beamline BL22XU. Density was measured using X-ray absorption method (Katayama et al., 1993) and sound velocity was measured using pulse-echo overlapping method (Higo et al., 2009). Experimental conditions were 1.2-2.9 GPa and 1650-1850 K. Obtained density values of this study were consistent with our previous results (Shimoyama et al., 2013). In sound velocity measurement, we could observe clear sample wave signal. Measured compressional wave velocity of liquid Fe-C was found to increase with pressure.

Keywords: Density, Sound velocity, liquid Fe-C

## Sound velocity and density measurement of liquid FeSi alloy by laser-shock compression

HOSOGI, Ryota<sup>1\*</sup> ; YOKOYAMA, Naoya<sup>1</sup> ; SAKAIYA, Tatsuhiro<sup>1</sup> ; KONDO, Tadashi<sup>1</sup> ; TERASAKI, Hidenori<sup>1</sup> ; SHIGEMORI, Keisuke<sup>2</sup> ; HIRONAKA, Yoichiro<sup>2</sup>

<sup>1</sup>Graduate School of Science, Osaka University, <sup>2</sup>Institute of Laser Engineering, Osaka University

The internal structure of the earth is estimated by observing seismic wave. Comparing seismic wave observations and experimental data of sound velocity of iron(Fe), the composition of the Earth's core is not pure Fe. Several light elements (hydrogen, carbon, oxygen, silicon, sulphur, etc.) have been considered as the candidate of the composition of the Earth's core, but its composition is still unclear. In order to constrain the core composition, it is important to measure the sound velocity of iron alloys because it can be directly compared with the seismic wave. Silicon (Si) has been proposed as a major light element in the inner core [Mao et al., 2012]. So we measured the sound velocity of laser-shocked FeSi alloy in order to investigate the effect of Si for sound velocity of liquid Fe in the outer core condition.

The starting sample was prepared by synthesizing from mixture of Fe (99.98% purity) and Si (99.9% purity) slugs at arc furnace. The compositions of Fe and Si are 66.5 wt.% and 33.5 wt.%, respectively. We measured sound velocities and densities of FeSi at high pressure and high temperature conditions at the large laser facility in Institute of Laser Engineering, Osaka University. The sound velocities were measured by the x-ray radiography [Shigemori et al., 2012].

We obtained the sound velocity and density of FeSi at pressures around 700 GPa. It is seen that Si has the effect of increasing the sound velocity of liquid Fe. Comparing our experimental results and PREM model [Dziewonski and Anderson, 1981], Si may be contained up to 13.1 wt.% at 135 GPa, and up to 5.5 wt.% at 330 GPa in the outer core.

## Effects of hydrous rocks on behaviors of subducting slabs

NAKAO, Atsushi<sup>1\*</sup>; IWAMORI, Hikaru<sup>2</sup>; NAKAKUKI, Tomoeiki<sup>3</sup>

<sup>1</sup>Department of Earth and Planetary Sciences, Tokyo Institute of Technology, <sup>2</sup>Institute for Research on Earth Evolution, JAM-STECC, <sup>3</sup>Department of Earth and Planetary Systems Science, Hiroshima University

**Introduction:** It is widely accepted that Earth's deep mantle contains water in several tens to several hundreds ppm, and that the water causes plate tectonics, volcanoes in subduction zones, deep earthquakes, and large-scale transportation of hydrophilic elements. A number of previous numerical studies on water transportation in the deep mantle are performed. In these simulations, constant plate velocities and/or fixed plate shapes are synthetically imposed. In this study, we systematically investigated water transportation into the deep mantle and how the water changes the spontaneous behavior of the slab using a numerical model of whole mantle convection without external forces.

**Numerical Model:** Based on 2-D fluid mechanics simulation (Tagawa *et al.*, 2007, *EPS*), the motion of mantle rocks is calculated. Advection of hydrous rocks is calculated using a Marker-And-Cell method, and dehydration/hydration reactions are evaluated by experimentally determined phase diagrams of the hydrous basalt and peridotite (Iwamori, 2007, *Chem. Geol.*). Effects of the hydrous rocks are formularized in constitutive laws (*e.g.* Karato and Wu, 1993, *Science*) and a state equation; therefore, the water transportation and the motion of solid phase are interactive. Only two parameters  $r$  ( $= 0, 0.7, 1.0, 1.93$ ) in constitutive laws (viscosity reduction by hydration) and  $\beta$  ( $= 0, 1.0, 2.0$ ) in a state equation (density reduction by hydration) are treated as variable, and other settings are equalized.

**Results and Discussion:** The reaction path ( $p$ - $T$  path) of subducting hydrous rocks in each result is the same as that of southwest Japan (Iwamori, 2007), and a hydrous ultramafic layer along the slab surface ( $\sim 2000$  ppmH<sub>2</sub>O in NAMs) is formed beneath  $\sim 200$ -km depth. Large hydration weakening seems essential for back arc spreading because the subducting slab causes tensile stress within the overlying continental plate, and then the expansive deformation is concentrated on the hydrous weak area. Comparing the results with each other, at large  $r$ , the subduction rate increases. This is because a hydrous layer reduces viscous resistance above the slab. In contrast, at large  $\beta$ , the subduction rate decreases. This is because the positive buoyancy of the hydrous layer partially canceled to the gravitational instability of the slab. The subduction rate significantly controls the velocity field of the corner flow in the mantle wedge. A rapid corner flow causes strong suction force along the slab surface, which determines the angle of subduction. This also causes effective heat advection from the deep mantle to the back arc, and that contributes rapid, sustainable back arc spreading. The analytical discussion enables us to understand why scenarios differ when  $r$  and  $\beta$  are changed. In east Asia, stagnant slabs and back arcs are widely distributed. To realize both, large  $r$  and small  $\beta$  are needed. This is because they require strong corner flow, but  $\beta$  declines it. Thus the slab shapes and the period of back arc spreading may constrain scales of hydrous buoyancy and hydrous weakening in the mantle wedge comparing with those in nature.

Keywords: water transportation, free convection, subduction dynamics, plate velocity, big mantle wedge

## Regional scale variation of splitting intensity observed in Japanese islands by Hi-net II

OGAWA, Naoto<sup>1\*</sup> ; KAWAKATSU, Hitoshi<sup>1</sup> ; TAKEUCHI, Nozomu<sup>1</sup> ; SHIOMI, Katsuhiko<sup>2</sup>

<sup>1</sup>Earthquake Research Institute, the University of Tokyo, <sup>2</sup>National Research Institute for Earth Science and Disaster Prevention

To systematically investigate the spatial variation of seismic anisotropy around the Japanese islands, we measured the splitting intensity (SI) of teleseismic SKS and SKKS phases by Hi-net (Ogawa et al., 2013, SSJ). SI is first introduced by Chevrot (2000) as a method of measuring seismic anisotropy; it is based on cross-correlation of polarized waveforms, and can be modeled like the delay time of seismic tomography considering the effect of finite frequency (e.g., Favier and Chevrot, 2003). In this study, we extend our previous work by measuring SI for a large number of dataset recorded by the dense seismic station network, Hi-net. We use data from tilt-meters of Hi-net from October in 2000 to September in 2013. We have selected the recordings of SKS phases for epicentral distances between 90 and 135 degrees and SKKS beyond 105 degrees, and Mw larger than 6.0, resulting in a total number of events to be 189 that is much larger than the previous case. For the actual analysis, we apply a band-pass filter between 0.05 and 0.125 Hz, and the measurement error of each SI will be carefully estimated using a new formulation, as there appears an error in the Chevrot (2000)'s original treatment. The preliminary analysis indicates regional scale variations of SI patterns that apparently depend on the back azimuth of seismic event, which may be influenced by the subducting slabs.

Keywords: seismic anisotropy, splitting intensity

## Comparison of phase relations in pyrolite, MORB and harzburgite across 660-km discontinuity

ISHII, Takayuki<sup>1\*</sup> ; KOJITANI, Hiroshi<sup>1</sup> ; AKAOGI, Masaki<sup>1</sup>

<sup>1</sup>Department of chemistry, Gakushuin University

Pyrolite is the model rock which composes the average upper mantle. It is accepted that 660-km seismic discontinuity is formed by post-spinel transition of pyrolite. MORB (mid-ocean ridge basalt) and harzburgite in slabs subduct to 660-km seismic discontinuity due to their higher densities than pyrolitic average mantle. It has been considered that the density cross-over between pyrolite and slab materials occurs due to post-spinel transition in pyrolite at the 660-km discontinuity, and MORB and harzburgite are trapped around the depth (e.g. Ringwood and Irifune, 1988). Therefore, the phase transition pressures of these mantle rocks are the important parameters to elucidate the dynamics around 660-km seismic discontinuity. We investigated detailed phase relations of pyrolite, MORB and harzburgite with multi-sample cell technique.

The starting materials were prepared from the oxide mixtures of pyrolite, MORB and harzburgite composition after McDonough and Sun (1995) (excluding MnO, K<sub>2</sub>O and P<sub>2</sub>O<sub>5</sub>), Melson et al. (1976) (P<sub>2</sub>O<sub>5</sub>) and Michael and Bonatti (1975), respectively. High-pressure and high-temperature experiments by quench method were performed at about 20-28 GPa and 1600-2200C for 2-10 hours using a Kawai-type 6-8 multianvil high-pressure apparatus at Gakushuin University. These samples were packed with pressure calibrants (MgSiO<sub>3</sub> or pyrope) in a Re multi-sample capsule with four holes. Temperature was controlled with a LaCrO<sub>3</sub> heater and measured with a W5%Re-W26%Re thermocouple inserted in a Cr<sub>2</sub>O<sub>3</sub>-doped MgO pressure medium. Phases of recovered samples were identified with microfocus-Xray diffractometer and SEM-EDS.

In pyrolite at 1600-2200C, the mineral assemblage of MgSiO<sub>3</sub>-rich perovskite (Mpv) + magnesiowustite (Mw) + garnet (Gt) + CaSiO<sub>3</sub>-perovskite (Cpv) is stable at pressure range of 22-24 GPa, and changes to that of Mpv + Mw + Cpv above 24 GPa. The mineral assemblage of ringwoodite (Rw) + Gt + Cpv at 1600C transforms to that of Rw + Mw + Gt + Cpv due to transition of Rw to Gt + Mw at 1800-2000C, and Rw disappears perfectly above 2200C. In MORB, the mineral assemblage of Gt + stishovite (St) + Cpv changes to that of Mpv + St + Al-rich phase + Cpv with continuous post-garnet transition. In harzburgite at 1600C, the mineral assemblage of akimotoite (Ak) + Rw + Gt changes to that of Mpv + Mw by post-spinel transition after the Ak to Mpv transition. Above 1800C, no Ak was observed.

At 1600C, post-spinel transition in pyrolite occurred by about 0.5 GPa and 2 GPa lower pressure than that of harzburgite and post-garnet transition in MORB, respectively. The Clapeyron slope of post-spinel transition in harzburgite is larger than that of pyrolite, and both boundaries intersect at 2000C. From the comparisons of density profiles at 1600C, MORB and harzburgite have lower densities than pyrolite by post-spinel transition in pyrolite.

Keywords: post-spinel transition, post-garnet transition, 660-km discontinuity, pyrolite, MORB, harzburgite

## Melting experiments in the system Fe-Xe and Earth's missing xenon

MORI, Yuko<sup>1\*</sup> ; HIROSE, Kei<sup>2</sup> ; TATENO, Shigehiko<sup>1</sup> ; OZAWA, Haruka<sup>3</sup> ; OHISHI, Yasuo<sup>4</sup>

<sup>1</sup>Dept. of Earth & Planetary Sciences, Tokyo Institute of Technology, <sup>2</sup>Earth-Life Science Institute, Tokyo Institute of Technology, <sup>3</sup>Japan Agency for Marine-Earth Science and Technology, <sup>4</sup>Japan Synchrotron Radiation Research Institute,

The abundances of noble gases in the Earth's atmosphere should be consistent with those in CI chondrite. However, xenon in the atmosphere is depleted relative to chondritic abundance, while lighter rare gases, Ne, Ar, and Kr, are less depleted. This is the so-called "missing xenon" problem and its reservoir has been discussed for a long time. Since xenon is too heavy to escape toward outer space, the missing xenon (Xe) might be hidden in the deep Earth.

The potential reservoirs are the mantle and core because xenon has a good reactivity under high pressure. Although extensive studies on the reactions of Xe and various mantle materials have been performed, none of those found a Xe reservoir (e.g., Sanloup et al., 2005; 2011; Brock et al., 2011). On the other hand, the alloying of iron with xenon has been expected based on the fact that Xe becomes metallic above 130 GPa (e.g., Eremets et al., 2000). While first-principle calculations suggested that the solubility of xenon in hcp iron is 0.8 mol% at Earth's core conditions (Lee et al., 2006), experimental study showed that the solid Fe-Xe reaction did not occur at least up to 155 GPa and 3000 K (Nishio-Hamane et al., 2010). Here we performed melting experiments in the Fe-Xe system to 86 GPa and 6450 K.

High pressure and temperature (P-T) conditions were generated in a laser-heated diamond-anvil cell. We used pure iron foil as a starting material. Xe was loaded cryogenically. Angle-dispersive X-ray diffraction (XRD) measurements in-situ at high P-T were conducted at BL10XU, SPring-8. The textural and chemical characterizations of recovered samples were made by using a field-emission-type scanning electron-microprobe (FE-SEM) equipped with energy dispersive x-ray spectrometry (EDS). Both cross section and surface of a sample were carefully examined by combining a focused Ga ion beam (FIB) with FE-SEM.

Any evidence for the reaction was not observed at least up to 83 GPa and 3810 K based on both XRD measurements and chemical analyses. On the other hand, chemical analysis on the sample recovered from 86 GPa and 6450 K, the highest P-T condition achieved in this study, showed Fe alloyed with up to ~1.6 wt.% Xe as tiny grains. This sample had a difference in the texture between heated and unheated regions. We calculated the concentration of Xe in the entire molten area by assuming the heated region and the small grains of Fe-Xe alloy as a cylinder and spheres, respectively. The xenon content was estimated to be 0.02 wt. % for the heated area which is high enough to account for the missing xenon problem ( $10^{-10}$  wt.% Xe in the core). The present results could be a clue to solve the "missing xenon" paradox. Since the temperature of the present Earth's core is most likely lower than 6000 K, xenon might be incorporated into the core during Earth's early history at higher temperature.

Keywords: Missing Xe, melting experiments, High pressure and temperature, core

## Whole-mantle P-wave radial anisotropy tomography

KITAGAWA, Hiroki<sup>1\*</sup>; ZHAO, Dapeng<sup>1</sup>; TOYOKUNI, Genti<sup>1</sup>

<sup>1</sup>RCPEVE, Tohoku Univ.

### 1. Introduction

When studying seismic anisotropy, it is generally assumed that the medium under study has a hexagonal symmetry (i.e., transverse isotropy). In most cases, the axis of symmetry is assumed in the vertical direction (i.e., azimuthal anisotropy) or in the horizontal plane (i.e., radial anisotropy). Seismic anisotropy is induced mainly by the lattice-preferred orientation (LPO) of anisotropic minerals, especially for the olivine in the mantle (e.g., Zhang & Karato, 1995; Tommasi et al., 2000; Kaminski & Ribe, 2001). Studying seismic anisotropy is very important for understanding the structure and dynamics of the Earth's interior (e.g., Silver, 1996). Many previous studies have investigated P-wave azimuthal anisotropy tomography for several regions including the Japan Islands. Recently, Wang & Zhao (2013) studied P-wave radial anisotropy tomography of the Kyushu and Tohoku subduction zones. In this work, we have attempted to conduct global tomography to understand 3-D P-wave radial anisotropy in the whole mantle.

### 2. Data and method

In this study we used 12,657 earthquakes recorded by 6765 seismic stations which were selected from the ISC-EHB catalog by Yamamoto & Zhao, 2010. About 1.4 million arrival times of P, pP, PP, PcP and Pdiff waves are used in the tomographic inversion. The method of radial anisotropy tomography by Wang & Zhao (2013) is combined with the flexible-grid global tomography of Zhao et al. (2013) to conduct the whole-mantle tomographic inversion in this work.

### 3. Result

In comparison with the isotropic tomographic model, our anisotropic tomography model results in a smaller root-mean-square travel-time residual, suggesting that the anisotropic tomography model fits the data better. The isotropic component of this model is very consistent with the previous isotropic tomography. In upper mantle, low-velocity anomalies along the Pacific Rim, and high-velocity anomalies under the stable continents are visible. In addition, low-velocity anomalies exist from the surface down to the core-mantle boundary under South Pacific and East Africa, which represent two superplumes. The anisotropic results show that vertical velocity is greater than horizontal velocity under some regions such as South Pacific, which may reflect the mantle upwelling.

### References

- Kaminski & Ribe (2001) A kinematic model for recrystallization and texture development in olivine polycrystals. *Earth Planet. Sci. Lett.* 189, 253-267.
- Silver (1996) Seismic anisotropy beneath the continents: Probing the depths of geology. *Ann. Rev. Earth Planet. Sci.* 24, 385-432.
- Tommasi, Mainprice, Canova & Chastel (2000) Viscoplastic self-consistent and equilibrium-based modeling of olivine lattice preferred orientations: Implications for the upper mantle seismic anisotropy. *J. Geophys. Res.* 105, 7893-7908.
- Wang & Zhao (2013) P-wave tomography for 3-D radial and azimuthal anisotropy of Tohoku and Kyushu subduction zones. *Geophys. J. Int.* 193, 1161-1181.
- Yamamoto & Zhao (2010), Whole-mantle P-wave tomography -Tohoku model-, *Chikyū monthly*, 32, 312-324.
- Zhang & Karato (1995) Lattice preferred orientation of olivine aggregates deformed in simple shear. *Nature* 375, 774-777.
- Zhao, D., Y. Yamamoto, T. Yanada (2013) Global mantle heterogeneity and its influence on teleseismic regional tomography. *Gondwana Res.* 23, 595-616.

Keywords: tomography, mantle, anisotropy tomography

## Melting experiments on the MgO-MgSiO<sub>3</sub> system using double CO<sub>2</sub> lasers heated diamond anvil cell

OHNISHI, Satoka<sup>1\*</sup> ; KIMURA, Tomoaki<sup>1</sup> ; KUWAYAMA, Yasuhiro<sup>1</sup>

<sup>1</sup>Geodynamics Research Center, Ehime University

Seismological studies suggest the presence of ultralow-velocity zones (ULVZ) near the core mantle boundary (CMB). Partial melting of the lower mantle materials has been proposed to explain these zones, but experimental validation at the appropriate temperature and pressure regimes remains challenging. The melting curve of the lower mantle material is a key to constrain the existence of melt at the base of the mantle. A laser heated diamond anvil cell (LHDAC) provides an enabling tool for determination of melting temperatures of materials under high *P-T* conditions. Although YAG, YLF lasers (the wavelengths are about 1  $\mu\text{m}$ ) have been generally used for LHDAC experiments, the use of metal absorber is required to heat silicate materials. However, the thermal absorber may cause a chemical reaction and a temperature gradient in the sample. The accuracy of temperature determination is suffered from the chemical reaction and the temperature gradient. In contrast, the CO<sub>2</sub> laser with the wavelength of about 10  $\mu\text{m}$  can directly heat silicate materials. For the minimization of temperature gradients, double-sided heating system for LHDAC was suggested by Shen *et al.* (1996). This technique using the YAG laser has been widely used to study the behavior of materials under high *P-T* conditions. However, the double CO<sub>2</sub> laser heating system has not been used due to the wavelength of this laser is different from that of visible light.

The requirements for the pressure medium in laser heating experiments are low thermal conductivity and chemical inertness. Ar, which is a noble gas, is one of the suitable pressure mediums. However, loading Ar into the DAC is difficult under room temperature and ambient pressure. Therefore, a simplified method to load Ar into the DAC is required. In this study, I established new experimental technique for the minimization of temperature gradients and chemical reactions and performed melting experiments of the lower mantle materials using LHDAC.

First, a double-sided heating system using CO<sub>2</sub> laser was developed by separating optical elements. This system consists of the heating system using two CO<sub>2</sub> lasers which have the high power (100 W), the observation systems and the temperature measurement system. By using lenses designed for the CO<sub>2</sub> laser wavelength, the laser system is separated from observation and temperature measurement system. Two dimensional images and radiation spectrums are observed by Charge Coupled Device (CCD) camera and spectrometer, respectively.

Second, a simplified method to load Ar into the DAC was developed by the cryogenic technique. In this technique, Ar is cooled using liquefied N<sub>2</sub> until it forms a liquid, and the liquefied Ar is loaded into the sample chamber of the DAC. Cu was used to enhance cooling efficiency.

Finally, I performed melting experiments of the lower mantle materials using the double CO<sub>2</sub> lasers heated diamond anvil cell and Ar as the pressure medium. I used forsterite (Mg<sub>2</sub>SiO<sub>4</sub>) and mixtures of MgO and MgSiO<sub>3</sub> as the starting material. After the complete pressure release, the sample was recovered from the DAC and examined by FE-SEM. From the surface texture of recovered samples, I discussed melting temperatures of the lower mantle materials under high *P-T* conditions.

The double CO<sub>2</sub> laser heating and loading Ar methods developed in this study could powerful tool for determination of melting temperatures of the lower mantle materials.

## Ultra high pressure generation using the double-stage diamond anvil cell

SAKAI, Takeshi<sup>1\*</sup>; YAGI, Takehiko<sup>1</sup>; OHFUJI, Hiroaki<sup>1</sup>; IRIFUNE, Tetsuo<sup>1</sup>; OHISHI, Yasuo<sup>3</sup>; HIRAO, Naohisa<sup>3</sup>; SUZUKI, Yuya<sup>4</sup>; KURODA, Yasushi<sup>4</sup>; ASAKAWA, Takayuki<sup>4</sup>; KANEMURA, Takashi<sup>4</sup>

<sup>1</sup>Geodynamics Research Center, Ehime University, <sup>2</sup>Earth-Life Science Institute, Tokyo Institute of Technology, <sup>3</sup>Japan Synchrotron Radiation Research Institute, <sup>4</sup>HITACHI High-Technologies

1 TPa region is still far frontier for the high pressure physics. The maximum pressure generated by diamond anvil cell is about 400 GPa (Akahama and Kawamura, 2010). On the other hand, recently Dubrovinsky et al. (2012) reported the generation of 640 GPa using double stage diamond anvil cell. This new technique makes 1TPa region a realistic goal for static compression experiments. But there are some technical difficulties such as a second-stage anvil's shape controllability, shift under pressure, and the difficulty of a sample filling. These problems depress the reproducibility of experiment.

In this study, second-stage microanvils were made by focused ion beam system from the nano-polycrystalline diamond (NPD) or single crystal (SC) diamond. Micro manufacturing using focused ion beam system enables us to control anvil shape, process any materials (NPD, SC and also sample), and fill the sample between the second-stage anvil gap precisely. Using this method, we generated up to 340 GPa. This method has a high reproducibility of the experiment. Thus, we can optimize the experimental parameters such as an anvil shape, confining pressure and so on.

Keywords: nano-polycrystalline diamond (NPD), microanvil

## Ab initio molecular dynamics study on a phase separation in liquid Fe-O

OHSUMI, Masanao<sup>1\*</sup> ; TSUCHIYA, Taku<sup>1</sup> ; ICHIKAWA, Hiroki<sup>1</sup>

<sup>1</sup>Geodynamic Research Center, Ehime University

The Earth's outer core is mainly composed of liquid Fe-Ni alloy. The density of the outer core is, however, ~10% smaller than this alloy. The density deficit indicates that substantial amount of light elements are present in the outer core [Birch, 1964]. Recent seismological observations proposed that seismic wave velocity is ~3% slower than PREM below a few hundred kilometers of the CMB [Helffrich and Kaneshima, 2010]. The low-velocity anomaly is considered to be caused by stratification. However, mechanisms of the stratification have not been clarified yet. One possible cause is phase separation into Fe-rich and light element-rich liquid. Oxygen is one of the most important light elements, because an iron-oxygen phase separation was observed experimentally at low-pressure condition [Tsuno et al., 2007]. This immiscible behavior is, however, still unclear at the outer core pressure.

In this study, we calculated liquid Fe-O alloy at the outer core condition by means of *ab initio* molecular dynamics simulations. First, we analyzed local structures of liquid Fe-O alloy to detect signs of phase separation. Second, we evaluated its excess enthalpy. Both indicate that the liquid was well-mixed. Finally, we computed P-wave velocity in liquid Fe-O alloy. P-wave velocity was found to increase with increasing the oxygen concentration. All these results suggest that the simple enrichment process is less suitable to explain the low-velocity anomaly.

Keywords: ab initio molecular dynamics simulation, phase separation, liquid Fe-O alloy

## In situ X-ray observations of phase transitions in MgCr<sub>2</sub>O<sub>4</sub> to 30 GPa using Kawai-type multianvil apparatus

KUNIMOTO, Takehiro<sup>1\*</sup>; IRIFUNE, Tetsuo<sup>1</sup>; FUJINO, Kiyoshi<sup>1</sup>

<sup>1</sup>Ehime University

Phase relations in MgCr<sub>2</sub>O<sub>4</sub> (magnesiochromite) have been studied up to 30 GPa and 1600 °C, using a large volume Kawai-type multianvil apparatus and in situ X-ray diffraction measurements system installed at SPring-8/BL04B1. MgCr<sub>2</sub>O<sub>4</sub> spinel dissociates into Mg<sub>2</sub>Cr<sub>2</sub>O<sub>5</sub> (orthorhombic type) + Cr<sub>2</sub>O<sub>3</sub> (eskolate) at 9 GPa and 1200 °C, and then reunion to higher pressure phase (CaTi<sub>2</sub>O<sub>4</sub> type) at 22 GPa and 1200 °C. Moreover, another high-pressure phase was observed above CaTi<sub>2</sub>O<sub>4</sub> type structure phase, and this phase was unquenchable to ambient condition. In addition, pressure-induced phase transition in MgCr<sub>2</sub>O<sub>4</sub> was confirmed without decomposition under cold compression process. In this cause, Magnesiochromite is directly transformed to high-pressure phase through the mixture of spinel and high-pressure phase. In this study, CaFe<sub>2</sub>O<sub>4</sub> type and ε-phase, which reported in earlier studies in MgAl<sub>2</sub>O<sub>4</sub> were not observed. The Birch-Murnaghan equation of state was used for least-squares fitting of the volume data (assuming  $K_0' = 4$ ). Thus, determined zero-pressure bulk modulus ( $K_0$ ) of the CaTi<sub>2</sub>O<sub>4</sub> type MgCr<sub>2</sub>O<sub>4</sub> was 195 GPa.

In this presentation, we will discuss further details of high-pressure phase relation and physical properties of high-pressure phases in MgCr<sub>2</sub>O<sub>4</sub> series.

Keywords: Magnesiochromite, in situ X-ray diffraction measurement, Kawai-type multianvil apparatus, phase transition

## Sound velocities of laser-shocked Fe-Ni alloys under Earth core conditions

SAKAIYA, Tatsuihiro<sup>1\*</sup> ; YOKOYAMA, Naoya<sup>1</sup> ; HOSOGI, Ryota<sup>1</sup> ; KONDO, Tadashi<sup>1</sup> ; TERASAKI, Hidenori<sup>1</sup> ; SHIGEMORI, Keisuke<sup>2</sup> ; HIRONAKA, Yoichiro<sup>2</sup>

<sup>1</sup>Graduate School of Science, Osaka University, <sup>2</sup>Institute of Laser Engineering, Osaka University

When we consider the structure of Earth's interior, the sound velocity is one of the important physical properties of the interior materials because it can be directly compared with the seismological data (1) which can yield the physical properties of the Earth's interior. Cosmochemical data and the composition of iron meteorites suggest that Earth's core contains mainly Fe-Ni alloy with 5-25 wt.% Ni. Although Lin et al. (2) and Kantor et al. (3) measured compressional sound velocities of Fe-Ni alloys at room temperature by inelastic x-ray scattering (IXS) at diamond anvil cell (DAC), the sound velocity data of liquid Fe-Ni alloys is very few (4).

We performed laser-shock experiments of liquid Fe-Ni alloys at HIPER system of Gekko-XII laser in Institute of Laser Engineering, Osaka University (5). Sound velocities were measured by side-on radiography (6, 7). We obtained sound velocities of Fe-Ni alloys at pressures up to 770 GPa. The sound velocity of Fe-Ni alloy was about 10% lower than that of liquid Fe at inner core boundary (ICB) pressure.

Part of this work was performed under the joint research project of the Institute of Laser Engineering, Osaka University.

### References

1. A.M. Dziewonski, D.L. Anderson, *Phys. Earth Planet. Inter.* 25, 297 (1981).
2. J.F. Lin et al., *Geophys. Res. Lett.* 30, 2112 (2003).
3. A.P. Kantor et al., *Phys. Earth Planet. Inter.* 164, 83 (2007).
4. P.M. Nasch, M.H. Manghnani, *Geophys. Monograph Ser.* 101, 307 (1998).
5. C. Yamanaka et al., *Nucl. Fusion* 27, 19 (1987).
6. K. Shigemori et al., *Rev. Sci. Instrum.* 83, 10E529 (2012).
7. T. Sakaiya et al., *Earth Planet. Sci. Lett.* in press (2014).

Keywords: sound velocity, laser, shock wave, iron alloy, Earth's core, experiment

## 3D imaging of geofluid by wideband magnetotellurics

OGAWA, Yasuo<sup>1\*</sup> ; ICHIKI, Masahiro<sup>2</sup> ; KANDA, Wataru<sup>1</sup>

<sup>1</sup>Volcanic Fluid Research Center, Tokyo Institute of Technology, <sup>2</sup>Graduate School of Science, Tohoku University

Magnetotelluric measurements have been conducted over the five years in the central part of NE Japan arc surrounding the Naruko Volcano with approximately 3km grid. Over 200 sites were used for modeling the crustal resistivity structure in detail. Full impedance tensors for 8 periods were used for inversion. To alleviate the computational load, first four short periods were used to image upper crustal features and the resultant model was used for a prior model for another set of inversions with longer 4 periods.

The obtained model show the crustal conductor underneath the Mukaimachi caldera and Sanzugawa caldera. Seismic tomography shows low S-wave velocity for both, however, the resistivity image show clear low resistivity for Mukaimachi Caldera, but not for Sanzugawa Caldera. This difference may be due to the salinity of the fluids underlying the volcanic regions.

Keywords: geofluid, magnetotellurics, resistivity, 3d

## Three dimensional electrical conductivity model in the subduction zone beneath north-eastern Japan

ICHIKI, Masahiro<sup>1\*</sup> ; OGAWA, Yasuo<sup>2</sup> ; KAIDA, Toshiki<sup>1</sup> ; DEMACHI, Tomotsugu<sup>1</sup> ; HIRAHARA, Satoshi<sup>1</sup> ; HONKURA, Yoshimori<sup>2</sup> ; ICHIHARA, Hiroshi<sup>3</sup> ; KANDA, Wataru<sup>2</sup> ; KONO, Toshio<sup>1</sup> ; KOYAMA, Takao<sup>4</sup> ; MATSUSHIMA, Masaki<sup>5</sup> ; NAKAYAMA, Takashi<sup>1</sup> ; SUZUKI, Shu'ichi<sup>1</sup> ; TOH, Hiroaki<sup>6</sup> ; UYESHIMA, Makoto<sup>4</sup>

<sup>1</sup>Grad. School of Sci., Tohoku University, <sup>2</sup>VFRC, Tokyo Institute of Technology, <sup>3</sup>IFREE, JAMSTEC, <sup>4</sup>ERI, The University of Tokyo, <sup>5</sup>Grad. School of Sci. & Eng., Tokyo Tech, <sup>6</sup>Grad. School of Sci., Kyoto University

Our final goal is to infer a geofluid map (GFM) from both of the seismological (seismic velocity,  $V_p/V_s$ ,  $Q$  etc.) and electrical conductivity structures in the wedge mantle of subduction zone beneath northeastern Japan. While plenty of high-resolution three dimensional (3-D) seismic tomographic images has been revealed there, none of 3-D electrical conductivity distribution model, of which the resolution is comparative to those of seismic tomography, has been proposed in terms of wedge mantle in subduction zones. Here, we show a high-resolution 3-D electrical conductivity distribution model in the wedge mantle beneath northeastern Japan used as input of GFM.

We carried out long-period MT observation using the state-of-the-art equipments, LEMI-417 and NIMS. The total 72 site observation has been completed. To remove tilt changes, baseline steps and drifts of fluxgate magnetometers, we first subtracted magnetic field variations to which a median filter was applied, from raw data. The horizontal coordinate of magnetic field data in each site was rotated before the response calculation such that the declination of the averaged horizontal component should be consistent with the 2010 absolute geomagnetic observation map provided by Geospatial Information Authority of Japan. We used the BIRRP processing code (Chave and Thomson, 2004) to estimate MT responses and have successfully retrieved them up to 61440 seconds in period.

The MT impedance responses were inverted into 3-D electrical conductivity model using WSINV3D (Siripunvaraporn et al, 2005), the data-space Occam inversion method. The all input data error floor was assigned to be 10 percent. We investigated the optimal reference model with trial and errors. The test model was (1) uniform models, (2) layered models and (3) layered models with subducting slab models. The best RMS in each reference model was (1) 2.81, (2) 2.71 and (3) 2.48, respectively. Hence, we adopted the reference model of the layered model with subducting slab.

The conductivity profiles normal to the trench axis in higher latitude than N 39 degrees delineate conductive region on the subducting slab, and the conductive region is raised just beneath the central range of northeastern Japan (Ou-backbone range). This electrical image is well consistent with that obtained by the seismic tomographic model. On the other hand, a profile in lower latitude than N 39 degrees reveals that the conductive region is overturned towards backarc. The top of the overturned conductive body coincides with Gassan Volcano location, one of the outstanding backarc volcanism. However, Chokai Volcano, another distinctive backarc volcanism has no subsurface conductive root originated from deep upper mantle. The overturned mantle convection image is not found in the seismic tomographic image.

## S-wave attenuation on the western side of Nankai subduction zone: implications for geofluid distribution and dynamics

TAKAHASHI, Tsutomu<sup>1\*</sup> ; OBANA, Koichiro<sup>1</sup> ; YAMAMOTO, Yojiro<sup>1</sup> ; NAKANISHI, Ayako<sup>1</sup> ; KODAIRA, Shuichi<sup>1</sup> ; KANEDA, Yoshiyuki<sup>1</sup>

<sup>1</sup>JAMSTEC

One major cause of seismic wave attenuation is the presence of fluid in rocks. In this study, we estimated the attenuation structure in southwestern Japan and western Nankai trough by applying the attenuation tomography that takes account of apparent amplitude attenuation due to multiple forward scattering [Takahashi, 2012]. Because the estimated attenuation  $1/Q$  in our tomographic study was much larger than  $1/Q$  due to wide-angle scattering, our estimated  $1/Q$  is composed mainly the intrinsic  $1/Q$ .

High  $1/Q$  ( $>1/500$  at 4-8 Hz) was imaged beneath the Quaternary volcanoes. The highest attenuation ( $1/Q \sim 1/250$  at 4-8 Hz) distributes beneath the Beppu-Shimabara rift zone at 40-60km depth. Beneath this rift zone,  $1/Q$  becomes larger as depth increases. Random inhomogeneities in this zone are relatively strong at 0-40 km depth; whereas at 40-60 km depth random inhomogeneities are almost comparable to those in non-volcanic area. Meanwhile, in northeastern Japan, uppermost mantle beneath the volcanoes shows strong inhomogeneities and high attenuation. Apparent attenuation at the uppermost mantle beneath the Quaternary volcanoes is high in both study areas, but relative contributions of scattering and intrinsic attenuation differ between northeastern Japan and the Beppu-Shimabara rift zone. If we consider random inhomogeneities and  $1/Q$  in other areas, the weak random inhomogeneities and high  $1/Q$  beneath this rift zone suggest that random inhomogeneities due to the presence of igneous rocks are not significant, and that any magma inclusions are too small to excite S-wave scattering at 4-32 Hz.

At off Shikoku region, moderate  $1/Q$  ( $1/800 \sim 1/1000$  at 4-8 Hz) is imaged at 0-20 km depth. This moderate  $1/Q$  is estimated as  $1/Q(f) \sim 10^{-2.5} f^{-0.5}$ . Similar moderate attenuation can be found beneath the south of Shikoku at 20-40km, beneath the northern edge of Shikoku at 40-60km depth, and beneath Chugoku area at 40-60km depth. From geometry models of subducting Philippine Sea plate, most of the moderate  $1/Q$  zone is located in and around the oceanic crust of subducting Philippine Sea plate except beneath Chugoku region. In this area, Shelly et al. [2006] pointed out fluid existence in the oceanic crust by estimating  $V_p/V_s$  structure. This correspondence implies this moderate  $1/Q$  reflects fluid in the subducting slab. If we suppose that  $1/Q$  of P- and S-wave have the same frequency dependences and that random inhomogeneities of P- and S-wave has the same scale dependences, we can show possible cases of fluid flow induced by the passage of low frequency seismic waves ( $<1$  Hz) by applying a theoretical model of wave attenuation in saturated porous random media [Muller and Gurevich, 2005]. As a phenomenon suggesting such fluid flow by lower frequency seismic wave, triggering of non-volcanic tremors by surface waves passing has been observed [e.g., Miyazawa and Brodsky, 2008]. Even though we further need P-wave studies for detailed examination of this topic, it is likely that random inhomogeneity, intrinsic at 4-32 Hz and triggered tremors can be used to investigate medium properties and fluid dynamics.

## Seismic activity near the Moriyoshi-zan volcano in northeastern Japan: Implications for geofluid migration

KOSUGA, Masahiro<sup>1\*</sup>

<sup>1</sup>Graduate School of Science and Technology

The 2011 Off the Pacific coast of Tohoku (Tohoku-oki) Earthquake caused increased seismicity in many inland areas. A seismic cluster that occurred north of the Moriyoshi-zan volcano in the Akita prefecture of the Tohoku District is of interest in light of contribution of geofluids to seismic activity. We observed a seismic cluster characterized by the migration of seismicity, reflected/scattered phases, and deep low-frequency earthquakes. We relocated hypocenters by using the data of temporal observation and by using the Double-Difference location technique, which increased the depth accuracy. We interpreted the spatiotemporal variation of the hypocenters in the most active cluster by estimating the migration of pore fluid pressure. The hydraulic diffusivity of the cluster was in the range of 0.01-1.0 m<sup>2</sup>/s, and increased with time, implying that the migration of hypocenters accelerated after a pathway for fluids was formed by the fracturing of the wallrock that produced the initial stage of seismic activity. A prominent feature of the seismograms is a reflected/scattered phase observed at stations around the volcano. We have interpreted the phase as S-to-S scattered waves and estimated the location of scatterers using a back-projection method. The scatterers are located about 5 km northwest of the Moriyoshi-zan volcano and at an approximate depth of 13 km. The Moriyoshi-zan area is one of the source areas of deep low-frequency earthquakes that have previously been interpreted as events generated by the migration of geofluids. The depth of scatterers is close to the upper limit of the depth at which low-frequency earthquakes occur. Thus, we regard the observed scatterers to be a reservoir of geofluid that came from the uppermost mantle accompanying contemporaneous low-frequency earthquakes. The geofluid reservoir is the probable source of overpressurized fluid that induces the migration of seismicity in the upper crust. A time delay in seismic activity from the Tohoku-oki Earthquake was considered as the time needed to migrate across a gap between the reservoir and the earthquake cluster with a hydraulic diffusivity comparable to that observed for the initial stage of seismicity, i.e., fracturing of the wallrock.

Keywords: The 2011 Off the Pacific coast of Tohoku Earthquake, triggered seismicity, hypocenter migration, scattering, geofluid

## Is H<sub>2</sub>O-NaCl fluid enough to explain high electrical conductivity in the earth's crust?

SAKUMA, Hiroshi<sup>1\*</sup> ; ICHIKI, Masahiro<sup>2</sup>

<sup>1</sup>National Institute for Materials Science, <sup>2</sup>Tohoku University

Old continental crust has a high electrical conductivity layer at 20 to 30 km in depth [1]. Presence of aqueous fluids is a plausible hypothesis for explaining the high conductivity zone [2]. Therefore the electrical conductivities of aqueous fluids under high pressure ( $P$ ), temperature ( $T$ ) conditions should be investigated in order to evaluate the hypothesis. The phases of water and aqueous NaCl solutions at the  $P$ - $T$  conditions of the Earth's crust correspond from liquid to supercritical states.

Experimental approaches to measure the electrical conductivities at high  $P$ ,  $T$  and salt concentration ( $c$ ) conditions are limited and the data at  $P < 400$  MPa,  $T < 1073$  K and  $c < 0.6$  wt% for aqueous NaCl solutions is only available [3]. Classical molecular dynamics (MD) simulations are useful to obtain the electric conductivities at high  $P$ ,  $T$  and  $c$  conditions and for understanding the underlying mechanism controlling the conductivities.

We used the flexible and induced point charge (FIPC) H<sub>2</sub>O model [4] for MD simulations of aqueous NaCl solution. The technical details of the model and computational methods are explained in the literature [4]. The unit cell contained 2222 H<sub>2</sub>O and 4 NaCl, 2035 H<sub>2</sub>O and 22 NaCl, and 2035 H<sub>2</sub>O and 66 NaCl for  $c = 0.6, 3.4,$  and  $9.6$  wt% NaCl solutions, respectively.

The isotherms indicate that the conductivity increases with increasing pressures and saturated at high pressures. The conductivity decreased with increasing temperature. This behavior may seem to be strange, since the ionic mobility should be high at high temperatures. This can be explained by the mixed effects of the change of (i) the density, (ii) ionic mobility, and (iii) dielectric constant of water as discussed in Quist and Marshall (1968) [3]. We concluded that the change of the conductivity of H<sub>2</sub>O-NaCl fluids along with a geotherm model can explain one order of the increased magnitude at the high conductivity layer in depth, but more change observed by the Magnetotelluric method should be explained by the additional mechanism such as the connectivity of the fluids and the conductivity of H<sub>2</sub>O-CO<sub>2</sub> fluids.

### References

- [1] T. J. Shankland and M. E. Ander (1983) *J. Geophys. Res.* **88** 9475-9484.
- [2] B. E. Nesbitt (1993) *J. Geophys. Res.* **98** 4301-4310.
- [3] A. S. Quist, and W. L. Marshall, (1968) *J. Phys. Chem.* **72** 684-703.
- [4] H. Sakuma, M. Ichiki, K. Kawamura and K. Fuji-ta (2013) *J. Chem. Phys.* **138** 134506.

Keywords: salt water, electrical resistivity, supercritical fluid, molecular dynamics, static dielectric constant

## Connectivity of cracks and pores in a granitic rock

WATANABE, Tohru<sup>1\*</sup> ; HIGUCHI, Akiyoshi<sup>1</sup> ; YONEDA, Akira<sup>2</sup>

<sup>1</sup>Graduate school of science and engineering, University of Toyama, <sup>2</sup>Institute for Study of Earth's Interior, Okayama University

Seismic velocity and electrical conductivity are used to map the fluid distribution in the crust. Seismic velocity reflects the contiguity of solid phases, while electrical conductivity the connectivity of fluid phases. The combination of velocity and conductivity could provide us a strong constraint on the fluid distribution. However, mapping of the fluid distribution has not been successful. The connectivity of fluid phases in rocks is poorly understood. In order to understand the connectivity of fluid phases in rocks, we have made conductivity measurements on a fluid-bearing granitic rock under various confining pressures.

Fine grained (100-500 $\mu$ m) biotite granite (Aji, Kagawa pref., Japan) was used as a rock sample. The sample is composed of 52.8% plagioclase, 36.0% Quartz, 3.0% K-feldspar, 8.2% biotite. The density is 2.66(1) g/cm<sup>3</sup>, and the porosity 0.8(1) %. The porosity was estimated from the mass of the dry and wet samples. Cylindrical samples have dimensions of 25 mm in diameter and 30 mm in length, and saturated with 0.01 mol/l KCl aqueous solution. Simultaneous measurements of elastic wave velocity and electrical conductivity were made using a 200 MPa hydrostatic pressure vessel. The pore-fluid is electrically insulated from the metal work by using plastic devices (Watanabe and Higuchi, 2013). The confining pressure was progressively increased up to 125 MPa, while the pore-fluid pressure was kept at 0.1 MPa. It took five days or longer for the electrical conductivity to become stationary after increasing the confining pressure.

Elastic wave velocities and electrical conductivity showed reproducibly contrasting changes for a small increase in the confining pressure. Elastic wave velocities increased only by 5% as the confining pressure increased from 0.1 MPa to 25 MPa, while electrical conductivity decreased by an order of magnitude. The increase in velocities is caused by the closure of cracks. Most (~80%) of the decrease in electrical conductivity occurred below the confining pressure of 5 MPa. The decrease in electrical conductivity must also be caused by the closure of cracks. The decrease in porosity was only 0.07(1) %. Such a small change in porosity caused a large change in electrical conductivity. The connectivity of fluid was maintained at least up to the confining pressure of 125 MPa. A calculation with the effective medium theory (Kirkpatrick, 1973) suggests that the fluid forms a network with small coordination number (average coordination number=2.3), and that the connectivity at higher pressures is maintained by stiff pores. More cracks are open at lower pressures to link pores, drastically increasing electrical conductivity.

Keywords: pore, crack, connectivity, granitic rock, electrical conductivity

## Geometry of intergranular fluids in the mantle xenoliths: Implications for the physical properties of upper mantle

NAKAMURA, Michihiko<sup>1\*</sup>; OKUMURA, Satoshi<sup>1</sup>; YOSHIDA, Takeyoshi<sup>1</sup>; SASAKI, Osamu<sup>2</sup>; TAKAHASHI, Eiichi<sup>3</sup>

<sup>1</sup>Graduate School of Science, Tohoku University, <sup>2</sup>Tohoku University Museum, <sup>3</sup>Graduate School of Science and Engineering, Tokyo Institute of Technology

Recent magnetotelluric (MT) studies have revealed that crust and uppermost mantle are less resistive than dry rocks in various localities in the world. This suggests that interconnected fluid phases present more ubiquitously than previously realized. Intergranular fluids also decrease seismic wave velocities and changes Vp/Vs ratio, thus interpretation of the seismic tomographic images largely depends on the volume fraction and geometry of the fluid phase. The conventional view on grain-scale fluid distribution is based on dihedral angle between minerals and fluids in isotropic monomineralic rocks (i.e. ideal equilibrium geometry). Natural rocks are, however, composed of anisotropic multiple phases and undergo textural adjustment to minimize interfacial and strain energy such as grain growth and dynamic recrystallization, which results in microstructural complexity. In order to understand real fluid distribution in deep-seated rocks, we conducted an X-ray CT study of xenoliths from the uppermost mantle from various localities.

The mantle xenolith samples investigated were from Ichinomegata (NE Japan), Eifel (W Germany), San Carlos (AZ, USA), Bullen Merri and Shadwell (Victoria, AU), Kilbourne Hole (New Mexico, USA), Longang-hu (NE China), Gi-rona (Spain), Lanzarote (Canary islands), and Moses Rocks (Uta, USA). The micro-focus X-ray CT imaging was performed using Comscantecno ScanXmate-D160TSS105 in Tohoku University Museum with a tube voltage of 100 – 130 kV and current of 90 – 120 mA. The voxel size was typically 43 – 73  $\mu\text{m}^3$ . The 3-D image analysis was carried out with a software package Slice[1].

All the observed spinel lherzolite and Harzburgite xenoliths contained up to a few vol% of intergranular pores, indicating that the rocks were saturated with a free-fluid phase. The imaged pore fluids are typically polyhedral and tens – hundreds of micrometers in scale; this suggests that they were formed via coalescence of smaller pore fluids. The fluids are localized in interphase boundaries (between different mineral phases), while most of the monomineralic triple junctions lack pore fluids. All these characteristics are consistent with the results of grain-growth experiments in a fluid-bearing biminerale system[2]; in other words, the role of interfacial energy anisotropy and grain growth are crucial in determining fluid distribution in nature. In the ellipsoid approximation, the 3-D shape of the intergranular fluids show deformed rugby-ball shape with aspect ratios larger than those of the equilibrium fluid geometry determined by the dihedral angle[3]. The geometry, distribution and thus connectivity of fluids cannot be assessed simply from dihedral angles.

The results of CT imaging suggest that no pervasive grain-scale fluid interconnection is established in the uppermost mantle. To explain the observed low electrical resistivity in the mantle which does not undergo partial melting, concentration (localization) and interconnection of CHO fluids in a larger spacing, such as in meter-scale shear zones should be necessary. Given the observed geometry of the inter-granular fluids, their effects on Vp/Vs ratio is limited.

References: [1] Nakano et al. <http://www-bl20.spring8.or.jp/slice/> (2006). [2] T. Ohuchi and M. Nakamura J. Geophys. Res. 111, B01201, doi: 10.1029/2004JB003340 (2005). [3] Y. Takei JGR 107 (B2) doi:10.1029/2001JB000522 (2002).

Keywords: mantle xenoliths, rock microstructure, elastic wave velocity, electrical resistivity, grain growth

## Ultra-fine textures along grain boundaries in nominally fresh mantle xenoliths

MURATA, Masami<sup>1\*</sup> ; UEMATSU, Katsuyuki<sup>2</sup> ; YAMAMOTO, Takafumi<sup>3</sup> ; TANI, Kenichiro<sup>4</sup> ; SHUKUNO, Hiroshi<sup>5</sup> ; MIZUKAMI, Tomoyuki<sup>1</sup> ; MORISHITA, Tomoaki<sup>1</sup>

<sup>1</sup>Kanazawa Univ., <sup>2</sup>Marine Works Japan LTD., <sup>3</sup>Hiroshima Univ., <sup>4</sup>JAMSTEC, <sup>5</sup>non party

It is important for the evolution of the Earth to understand the role of grain boundaries during melts/fluids migrations in mantle peridotites. There are, however, very limited numbers of studies on grain boundaries in natural samples, although many experimental and theoretical approaches have been carried out (e.g., Drury and Fitz Gerald, *Geophys. Res. Lett.*, 1996; Hiraga et al., *Nature*, 2004).

We focus on nanoscale microstructures of crystal surface (grain boundary) in “ nominally fresh ” peridotite xenoliths from the San Carlos, USA, which is one of the most famous localities of peridotite xenolith in the world. Thin amorphous films along grain boundaries were already reported in some San Carlos xenoliths (Wirth, *Contrib. Mineral. Petrol.*, 1996).

We recovered mineral grains with a selfFrag at the Japan Agency for Marine-Earth Science and Technology (JAMSTEC) in order to minimize mechanical damages during mineral separations. We observed multiple grains of peridotite xenoliths using a high-resolution electron microscope (FE-SEM) at JAMSTEC.

Microstructures of crystal surface of these peridotite xenoliths are classified as follows. (1) over micron scale structures such as moth-eaten structures, vermicular structures, automorphic crystals and etch pits. (2) submicron scale structures. It is interesting to note that (2) submicron scale structures are frequently observed on (1) over micron scale structures. These textures suggest that microstructures were developed by several stages. We analysed on the surface of these textures using a micro-Raman and SEM-EDS techniques. We are also planning to perform transmission electron microscope, combined with chemical analyses in order to identify the surface materials that constrain P-T conditions and fluids for the formation of these textures.

Keywords: peridotite xenolith, Microstructures, TEM, grain boundary, fluids

## Elemental transport under lower-middle crustal condition: example from hydration of basic schist, Sanbagawa belt, Japan

UNO, Masaaki<sup>1\*</sup>; NAKAMURA, Hitomi<sup>2</sup>; IWAMORI, Hikaru<sup>3</sup>

<sup>1</sup>Graduate School of Environmental Studies, Tohoku University, <sup>2</sup>Department of Earth and Planetary Sciences, Tokyo Institute of Technology, <sup>3</sup>Geochemical Evolution Research Program, Japan Agency for Marine-Earth Science and Technology

To constrain the behavior of geofluids under the lower to middle crustal conditions, hydration reactions and trace element and Sr-Nd-Pb isotopic compositions of basic schists in the Cretaceous Sanbagawa metamorphic belt, a typical regional metamorphic belt in the circum-Pacific orogeny, have been investigated based on the observations of thin-sections and outcrops. The basic schists have undergone significant hydration from 0.8 GPa, 550 °C to 0.3 GPa, 400 °C during decompression towards the surface at the final stage of metamorphism. High-field-strength and rare-earth element compositions of the basic schists, as well as the Sr-Nd-Pb isotopic ratios, are different among three mineral zones with different peak P-T metamorphic conditions; the basic schists in the low-grade chlorite zone shows N-MORB-like compositions whereas those in the higher-grades, garnet and oligoclase-biotite zones, show more enriched compositions (E-MORB-like). On the other hand, there is a common feature to all the metamorphic zones; the enrichment degree of some group of elements (e.g., large-ion lithophile elements) relative to high-field-strength and heavy-rare-earth elements is proportional to loss on ignition that approximately measures the bulk rock H<sub>2</sub>O content. This correlation suggests that Li, B, K, Cr, Ni, Rb, Sr, Cs and Ba have been added to the basic schists during hydration. The addition of these elements amounts to as much as 60-80% of the bulk abundance, indicating that significant amounts of elements were transported via pervasive fluid flow, which overprinted the variation in the bulk rock compositions of the protolith. The estimated compositions of hydration fluid show high concentrations in large-ion lithophile elements, lead and light-rare-earth elements (10-100 times denser than primitive mantle, Fig. 1) and are similar to those of the slab-derived fluids<sup>[1]</sup> that induce arc volcanism. These elements (Cs, Rb, Ba, K, La, Ce and Pb) are thought to have been preferentially partitioned into the fluid when it was generated at depth. Such high concentrations indicate a high temperature origin of the hydration fluid, and are consistent with a model of hot slab subduction during exhumation of the Sanbagawa belt.

### References:

[1] Nakamura, H., Iwamori, H., and Kimura, J.-I., 2008 *Nat. Geosci.*, **1**, 380-384

Keywords: geofluid, metamorphism, trace elements, Sr-Nd-Pb isotopes, hydration reaction, Sanbagawa metamorphic belt

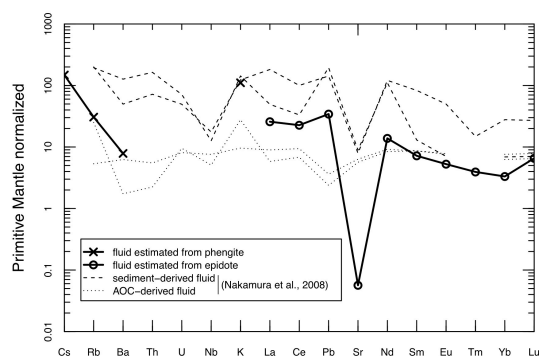


Fig. 1 Estimated compositions of the hydration fluid (solid lines). Compositions of slab-derived fluids estimated for arc volcanism (dotted lines; Nakamura *et al.*, 2008 *Nat. Geosci.*, **1**, 380-384) are shown for comparison. Note that the concentrations of LILE, Pb and LREE in the hydration fluid are in the range of slab-derived fluids.

## Progress of serpentinization in the mantle wedge and its effect on the redox state

KOGISO, Tetsu<sup>1\*</sup> ; MIYOSHI, Akane<sup>2</sup>

<sup>1</sup>Human Environ. Stds., Kyoto Univ., <sup>2</sup>JX Nippon Oil & Energy Corporation

Serpentinization of peridotite in the mantle is a key process that significantly changes the physical properties of the mantle. Serpentinization also produces hydrogen, which is essential not only for the activity of microbial systems in hydrothermal fields on the seafloor, but also for controlling the oxidation state of the mantle in subduction zones. Hydrogen is generated along with the formation of magnetite during serpentinization. However, there still remains controversy about what factors promote the mineralogical reactions responsible for magnetite formation during serpentinization in natural ultramafic rocks. Recent petrologic studies have proposed that serpentinization reactions proceed via a two-stage process involving the early formation of serpentine and brucite and subsequent magnetite formation. Many studies proposed that magnetite forms by the break down of ferrous brucite promoted by the addition of aqueous silica, but others proposed that magnetite forms by the breakdown of ferrous serpentine which releases silica component. To solve this controversy, we examined a number of variably serpentinized harzburgite and dunite samples taken from the Iwanaidake ultramafic body in Kamuikotan belt, Japan (Miyoshi et al. 2014). Petrographic observations of these samples revealed that successive changes in textures, mineral chemistry, whole-rock H<sub>2</sub>O contents, and magnetic susceptibility with the progress of serpentinization of harzburgite involved two stages: replacement of olivine by serpentine and brucite, and subsequent formation of magnetite along with more-magnesian serpentine and brucite. The later reactions occurred concurrently with serpentinization of orthopyroxene, which supplied the silica component. In serpentinized dunite, which doesn't contain orthopyroxene, serpentinization involved replacement of olivine by serpentine and brucite, and the fraction of magnetite did not increase with the progress of serpentinization. These observations, and the fact that the Iwanaidake ultramafic body originated from the forearc mantle of the Northeast Japan arc, suggest that the silica supply from serpentinization of orthopyroxene is an essential factor for the formation of magnetite during serpentinization in mantle wedge.

Our observations imply that serpentinization in the mantle wedge of subduction zone produces H<sub>2</sub> along with magnetite if sufficient amounts of silica component are supplied from subducting slab, which will probably occur because dehydration in subducted sediments can supply silica-rich fluids. Since H<sub>2</sub> is expected to exist as immiscible hydrogen-rich gas phases that coexist with H<sub>2</sub>O fluids in normal subduction zone conditions, it will be rapidly migrate upwards owing to its very low density. Then the remaining serpentinites will become oxidized. Such oxidation associated with serpentinization would occur in the shallow part of the wedge corner where temperatures are lower than ~600 °C, but the oxidized (magnetite-bearing) serpentinite will be dragged downwards in the mantle wedge. Thus serpentinization reactions can be one of the main processes to increase the oxygen fugacity of the mantle wedge. On the other hand, the H<sub>2</sub> gas removed from the wedge corner will produce highly reduced fluid phases, which may result in reducing the shallowest part of the forearc mantle and the lower part of the forearc crust. This could be the cause of rare presence of metal phases in subarc peridotite.

Reference:

A. Miyoshi, T. Kogiso, N. Ishikawa, K. Mibe (2014) *American Mineralogist*, in press.

Keywords: serpentinization, hydrogen, magnetite, subduction zone, redox state

## Evolution of porosity structures in a fracture during quartz vein formation

YAMADA, Ryo<sup>1\*</sup>; OKAMOTO, Atsushi<sup>1</sup>; SAISHU, Hanae<sup>1</sup>; NAKAMURA, Michihiko<sup>2</sup>; OKUMURA, Satoshi<sup>2</sup>; SASAKI, Osamu<sup>3</sup>; TSUCHIYA, Noriyoshi<sup>1</sup>

<sup>1</sup>Tohoku university, <sup>2</sup>Tohoku university, <sup>3</sup>The Tohoku university museum

Ubiquitous occurrences of quartz veins suggest that dissolution/precipitation of silica provides significant effects on the hydrological and mechanical properties within the crust. For example, a model has been proposed that fracture sealing processes control the change of pore fluid pressure and thus earthquake cycle. Previous studies on natural quartz veins have focused on estimates of P-T conditions, stress and strain fields and fluid compositions; however, details of dynamics of fluid flow and how fractures are sealed during vein formation are still unclear. In this study, we synthesized quartz veins by the hydrothermal experiments, and observed the aperture structures by using X-ray CT to clarify how aperture structures evolve during vein formation.

We conducted the hydrothermal flow-through experiments for quartz precipitation from Si-supersaturated solutions under controlled high temperature and high pressure condition. The experimental apparatus consists of two vessels for preparation of the Si-supersaturated solution and for precipitation, respectively. The precipitation vessel has double-structure: the main flow path was the inner alumina tube (diameter=4mm), and the outer SUS tube was filled with static solutions. The advantage of this system is that we can take out the non-destructive sample for the X-ray CT analyses. We conducted two types experiments: first one is precipitation in porous media with alumina balls, the second one is rock slice as analog of a fracture.

In the alumina-ball experiments, we carried out the precipitation experiment at supercritical (430C, 30MPa) and vapor condition (370C, 20MPa). In both experiments, the significant silica precipitation within few days, but showed contrasting porosity structures. Under supercritical condition, amorphous silica was predominantly formed with covering the surfaces of the alumina balls and alumina tube, and discrete quartz crystal (50  $\mu\text{m}$ ) within the amorphous silica layers. The porosity ( $\phi$ ) gradually decreases with minimal porosity ( $\phi = 0.4$ ) at  $\sim 38\text{mm}$  from the inlet. In contrast, under vapor condition, fine-grained quartz grains (0.1-1  $\mu\text{m}$ ) were directly nucleated in solutions using surface of vapor, and immediately settled on the bottom. The porosity rapidly decreases from 18 mm ( $\phi = 0.8$ ) to 25 mm ( $\phi < 0.1$ ) from the inlet. These results suggest that a depressurization of crustal fluids related to fault dilation by earthquakes would cause a formation of fine-grained silica particles, and their mineralogy and transport/deposition properties strongly depend on properties water.

In the experiment with rock slits, we evaluated the effect of rock substrate (amount and distribution quartz in the fracture wall). The P-T conditions and solution chemistry are similar to the previous experiments, but we used granite core with a slit ( $\sim 300 \mu\text{m}$ ). The mineralogy and aperture structures changes systematically along the fluid flow path. From the inlet to 35 mm of fracture, nucleation of quartz and other silica polymorphs predominantly occurred, regardless of vein wall minerals. From  $>35\text{mm}$  low Si concentration, silica precipitates occurred as epitaxial overgrowth from quartz crystal. The wavelength of aperture structures is controlled by distribution and grain size of quartz of the host granite. Accordingly, fractures are not sealed homogeneously, but complex flow pathways are evolved during vein formation. Such a variation in the precipitation mechanism and porosity structures during quartz vein formation may affect the evolutions of permeability and strength of rock fractures in the Earth's crust.

Keywords: Hydrothermal experiments, Quartz, Vein, Fracture, Porosity

## High precision in situ Pb isotope analysis of galena by LAL-ICPMS technique

WAKAKI, Shigeyuki<sup>1\*</sup> ; TANIMIZU, Masaharu<sup>1</sup>

<sup>1</sup>Kochi Institute for Core Sample Research, JAMSTEC

Radiogenic Nd and Pb isotopic compositions of the fluids originated from subducting Pacific and Philippine Sea plates have been characterized from isotopic trends observed among arctic volcanic rocks (Nakamura et al., 2008). Origin and evolution of the fluids that produced hydrothermal ore deposits may now be investigated by radiogenic isotopic compositions of ore deposits. In this study, we analyzed the micro scale isotopic variation of Pb in a hydrothermal galena to shed light on the macro scale dynamics of the fluids. To investigate the possibly small degree of isotopic changes within a galena sample, both high spatial resolution and high precision are required for the isotopic analysis. We employed the combination of laser ablation in liquid (LAL) micro sampling technique (Okabayashi and Hirata, 2011) and solution-based Pb isotopic analysis by MC-ICPMS technique to meet the analytical requirements. In the LAL micro sampling, laser-ablated sample particles are trapped in the liquid that placed above the sampling area. The trapped samples are then dissolved and introduced to the ICPMS as a solution. The advantage of the combined LAL-ICPMS technique over laser ablation (LA) ICPMS technique is the stable ion signals due to solution form, which allows high-precision isotope ratio measurement.

Sample analyzed in this study was a hydrothermal galena from Hosokura mine (Miyagi, Japan). A microscopic texture of the sample was observed in detail with FE-SEM-EDS system (JEOL JSM-6500F) prior to the isotopic analysis. A fs laser (IFRIT, Cyber Laser, Japan) with a wavelength of 780 nm (~200 fs pulse width) was used for the LAL micro sampling. Care was taken to avoid sampling of grain boundaries and inclusions. Typical spatial resolution was 150 micron in diameter and 30 micron in depth. The laser-sampled PbS (300-400ng Pb) trapped in Milli-Q water was dissolved in conc. HNO<sub>3</sub>, and adjusted to 200 ng/mL Pb solution in 0.15 M HNO<sub>3</sub> for Pb isotopic analysis. Pb isotope ratios were determined with a MC-ICPMS, Neptune (Thermo Instruments, Bremen, Germany). An isotopic reference material of Tl (NIST-SRM 997) was added to the final sample solutions for the correction of mass discrimination of Pb in the instrument to have a concentration of 20 ppb Tl.

Galena occurs as discrete layers of ca. 1cm width in between layered CaF<sub>2</sub> as well as sub mm-sized inclusion within thick CaF<sub>2</sub> layer. Galena inclusion and layers were numbered from 1 to 3 according to its precipitation order. Grain size of the galena in each of the layer is several hundred microns to several millimeters. Euhedral quartz with a size of 10-100 micron occurs along the grain boundary of galena and as an inclusion within galena grains.

Small but significant Pb isotopic variation of sub-permil order was observed among and within the 3 galena layers. The analyzed samples clearly form a linear trend in the <sup>208</sup>Pb/<sup>207</sup>Pb vs. <sup>206</sup>Pb/<sup>207</sup>Pb diagram. The observed Pb isotopic trend indicates that the Pb isotopic composition of the fluid that produced the galena has slightly changed during galena precipitation. The Pb isotopic composition of the galena is consistent with mixing of a sediment component of the Pacific plate (Nakamura et al., 2008) with a deep fluid derived from Pacific Ocean plate (Nakamura et al., 2008) and/or the DMM. With the high-precision isotopic analysis as demonstrated in this study, LAL-ICPMS may have an important contribution to high-spatial-resolution geochemical studies in the future.

Keywords: Geofluids, laser ablation in liquid, Pb isotope ratio, galena, in situ isotope analysis

## Origin of saline waters distributed along the Median Tectonic Line in southwest Japan

AMITA, Kazuhiro<sup>1\*</sup> ; OHSAWA, Shinji<sup>2</sup> ; NISHIMURA, Koshi<sup>3</sup> ; YAMADA, Makoto<sup>4</sup> ; MISHIMA, Taketoshi<sup>2</sup> ; KAZAHAYA, Kohei<sup>5</sup> ; MORIKAWA, Noritoshi<sup>5</sup> ; HIRAJIMA, Takao<sup>6</sup>

<sup>1</sup>Department of Earth Science & Technology Faculty of Engineering and Resource Science Akita University, <sup>2</sup>Institute for Geothermal Sciences, Graduate School of Science, Kyoto University, <sup>3</sup>Faculty of Economics, Toyo University, <sup>4</sup>Research Institute for Humanity and Nature, <sup>5</sup>Geological Survey of Japan, AIST, <sup>6</sup>Department of Geology and Mineralogy, Graduate School of Science, Kyoto University

To identify of metamorphic dehydrated fluid as source fluid of hot spring water, we conducted chemical and isotopic analyses of water and accompanied gas samples collected from hot-spring wells along the Median Tectonic Line (MTL) in the forearc region of the southwestern part of Japan. As a result, we found hot spring waters having anomalous dD and d<sup>18</sup>O compositions as compared with modern seawater and shallow groundwater in Wakayama and Shikoku regions. Judging from data in relative B-Li-Cl composition and He isotopic systematics, the source fluid of the hot springs in Shikoku could be identified to be one of diagenetic fluids. On the other hand, the source fluid of the hot springs of Wakayama had different B-Li-Cl composition and higher 3He/4He ratio in comparison with diagenetic dehydrated fluids and then the fluid was thought to be originated from metamorphic dehydrated fluid as well as Oita plain. There was another striking contrast between the source fluid of Wakayama and Oita and that of Shikoku and Miyazaki; accompanied gases by the former were rich in CO<sub>2</sub>, whereas those with the latter were rich in CH<sub>4</sub>, and CO<sub>2</sub> in the accompanied gases of Wakayama and Oita is mostly derived from marine carbonate like volcanic gases in subduction zones. Moreover, the Li-B-Cl compositions of them showed transitive values between the relative composition of diagenetic fluids and those of volcanic thermal waters. Consequently, the source fluid of hot springs in Wakayama and Oita was likely to be dehydrated metamorphic fluids released from the subducting Philippine-Sea plate.

Keywords: hot spring water, dehydrated fluid from subducting plate, Median Tectonic Line

## Distribution of the helium isotope ratios in northeast Japan in terms of geological setting

HORIGUCHI, Keika<sup>1\*</sup> ; KAZAHAYA, Kohei<sup>1</sup> ; TSUKAMOTO, Hitoshi<sup>1</sup> ; MORIKAWA, Noritoshi<sup>1</sup> ; SATO, Tsutomu<sup>1</sup> ; OHWADA, Michiko<sup>1</sup> ; NAKAMA, Atsuko<sup>1</sup>

<sup>1</sup>Geological Survey of Japan, AIST

The distribution of slab fluid defined by high Li/Cl ratios conforms the area of "hot fingers"(Tamura et al., 2002) in Northeast Japan (Kazahaya et al., submitted). Conversely, the high  $^3\text{He}/^4\text{He}$  ratios distribute wider and do not match with slab-derived fluids indicating that some of the mantle-derived helium would not be transported with magmas or slab fluids but directly upwells as mantle-derived fluid. The  $^3\text{He}/^4\text{He}$  ratios vary along the volcanic front showing an areal contrast; such as a low-ratio-area close to volcanoes are observed in the central part of Tohoku. We propose here an extended helium upwell model which can explain the spatial variation of  $^3\text{He}/^4\text{He}$  ratios with the following concept; 1) The most important constraint for mantle helium upwelling is the crustal structure divided by tectonic lines; Hatagawa Tectonic Line (HTL) divides the Kitakami and Abukuma belts. Ryoke belt and north part of Abukuma belt is torn apart by number of faulting events. The rest of parts, Abukuma granitic province and Kitakami province form very large stable blocks which might prohibit helium to upwell from mantle. 2) A view from U-Th content in the crust is important to understand the flat distribution of mantle helium in back-arc region; Low U-Th crust in the back-arc with less crustal  $^4\text{He}$  production is favorable to explain the flat and high  $^3\text{He}/^4\text{He}$  signature, such as oceanic crust might have. Tanakura Tectonic Line (TTL) divides the thick crust of continental margin (sedimentary prism and granite) with Ryoke belt.

Keywords: helium isotope ratio, northeast Japan, areal distribution, geological structure

## The Li-Cl-Br systematics of saline groundwater: A new indicator for slab fluid

KAZAHAYA, Kohei<sup>1\*</sup>; TAKAHASHI, Masaaki<sup>1</sup>; IWAMORI, Hikaru<sup>2</sup>

<sup>1</sup>Geological Survey of Japan, AIST, <sup>2</sup>Geochemical Evolution Research Program, Japan Agency for Marine-Earth Science and Technology

In this study, we propose Br/Cl ratio as a new indicator for slab-derived fluids, which is useful to distinguish their sources between pore water and hydrous minerals in subducting slab. The areal distribution of slab-derived fluids and their sources using Li/Cl and Br/Cl as geochemical evidences will provide a view for water circulation in subduction zones.

Subducting slab contains waters (originally seawater) as pore water and many kinds of hydrous minerals. Hydrous minerals such as opal, clay or mica will decompose to release water during subsiding, and pore water will be released by compaction. Even though such complex process occurs, behavior of halogen ions in the subducting slab may be simple because they are always enriched in aqueous phase (pore water) and the rest are in minerals as a replacement of OH. Some metamorphic fluids in wedge mantle peridotite with Br-enriched signature have been observed and were indicated to be from pore water in the slab. The mineral dehydration process is supposed to be responsible for Br-depletion in slab-derived aqueous fluid. Therefore, halogens are potentially good indicators concerning with the water behavior in subduction processes.

The higher Br/Cl ratios (>0.0035 in wt.) have been observed in fossil seawater and oil field brines due to the addition of Br from organic matters. The very low Br/Cl waters (<0.0025 in wt.) have feature of <sup>18</sup>O-shift to the slab (magmatic) fluid end member, which is quite lower than that in seawater (Br/Cl = 0.0034 in wt.), indicating that these waters originate from dehydration of the slab.

Keywords: Li-Cl-Br, slab-derived fluid, groundwater, subduction process

## Origin of U-Th disequilibrium in subduction zone volcanic rocks

YOKOYAMA, Tetsuya<sup>1\*</sup>; IKEMOTO, Akihiko<sup>1</sup>; IWAMORI, Hikaru<sup>2</sup>; UEKI, Kenta<sup>1</sup>

<sup>1</sup>Department of Earth and Planetary Sciences, Tokyo Institute of Technology, <sup>2</sup>JAMSTEC

Subduction zone magmatism is induced by the addition of slab derived fluids to the mantle wedge [1]. Chemical compositions of subduction zone volcanic rocks are largely controlled by the chemical and physical properties of the slab fluid. The nature of slab fluids have been extensively studied by geochemical approach utilizing trace element abundances and isotope compositions in arc basalts [2]. U-series disequilibrium in arc volcanic rocks is a useful tracer to understand the origin of arc magmas as well as the timescales of fluid/melt migration in subduction zones. However, detail of the process that producing <sup>238</sup>U-<sup>230</sup>Th disequilibrium in primary melts in the mantle wedge is still poorly constrained.

In this study, we determined <sup>238</sup>U-<sup>230</sup>Th disequilibrium in volcanic rocks from the Northeast Japan Arc (Iwate, Akitakoma, Yakeyama, Hachimantai, and Kampu). In addition, we performed a numerical simulation that reproduced (<sup>238</sup>U/<sup>232</sup>Th) and (<sup>230</sup>Th/<sup>232</sup>Th) ratios in primary melts in a subduction zone, by simultaneously calculating mantle dynamics, hydro phase reactions and trace elements transport. To discuss the origin of U-Th disequilibrium in arc volcanic rocks, the new data and previously published U-Th data around Japan were evaluated based on the result of the numerical simulation. The numerical simulation performed in this study

Most of arc volcanic rocks possess <sup>238</sup>U-<sup>230</sup>Th disequilibrium with <sup>238</sup>U excesses, suggesting the addition to the mantle wedge of slab fluid enriched in U relative to Th. The feature of <sup>238</sup>U enrichment is well reproduced by the numerical simulation. Interestingly, the simulation produced two positive trends in the U-Th diagram; the shallow trend matches data from the Izu-Mariana arc, while the steep slope is consistent with data from the Kamchatka arc. This strongly suggests that the positive trend in the U-Th diagram for a single arc samples simply reflects the variation of (<sup>238</sup>U/<sup>232</sup>Th) and (<sup>230</sup>Th/<sup>232</sup>Th) ratios in primary melts produced in the mantle wedge, and the slope does not have any age significance. Thus, as discussed in [3], the decoupling of U-Th and Th-Ra ages for arc samples would be explained by assuming that the slab derived fluid have (<sup>230</sup>Th/<sup>232</sup>Th) ratios higher than the mantle wedge composition.

Although the NEJ frontal-arc lavas (Iwate) possess <sup>238</sup>U-<sup>230</sup>Th disequilibrium with <sup>238</sup>U excesses, the extent of <sup>238</sup>U enrichment is moderate (<10%) compared to the other frontal-arc samples. In addition, Iwate lavas have relatively low (<sup>230</sup>Th/<sup>232</sup>Th) ratios that cannot be explained by the numerical simulation. This implies that the (<sup>230</sup>Th/<sup>232</sup>Th) in mantle wedge beneath Iwate volcano is lower than that in the depleted MORB mantle (DMM), due presumably to ancient mantle metasomatism by Th-enriched fluids derived from sediments.

In contrast to the frontal arc samples, the extent of <sup>238</sup>U enrichment in the NEJ samples decreases as the slab depth increases, and the rear-arc lavas (Kampu) show <sup>230</sup>Th enrichments relative to <sup>238</sup>U (<10%). This generally reflects gradual decrease of the amount of slab derived fluid mixed into the wedge mantle. The <sup>230</sup>Th excesses in rear-arc lavas would be produced by the melting of garnet-bearing upwelling mantle, as reproduced by the simulation. However, our data for Kampu show <sup>230</sup>Th excesses with an extremely low (<sup>230</sup>Th/<sup>232</sup>Th) ratio (~0.8) that plots outside the simulation data. This is explained by assuming the existence of metasomatised mantle beneath the NE Japan as discussed above, although the possibility of direct addition of Th-enriched fluid to the DMM-like mantle cannot be ruled out for the generation of rear-arc magmas.

References: [1] Iwamori (1998) *EPSL* 160, 65. [2] Nakamura et al. (2008) *Nature Geosci.* 1 380. [3] Yokoyama et al. (2003) *JGR* doi: 10.1029/2002JB002103.

Keywords: U-Th disequilibrium, Subduction zone, volcanic rocks, slab derived fluid

## Water transport coupled dynamically with a plate-mantle convection system involving a shallow to deep subduction zone

NAKAKUKI, Tomoeki<sup>1\*</sup>; KANEKO, Takeo<sup>1</sup>; NAKAO, Atsushi<sup>2</sup>; IWAMORI, Hikaru<sup>3</sup>

<sup>1</sup>Dept. Earth and Planetary Systems Science, Hiroshima Univ., <sup>2</sup>Dept. Earth and Planetary Sciences, Tokyo Inst. Technology, <sup>3</sup>Geochemical Evolution Research Program, JAMSTEC

Numerical study for water transport under a volcanic arc revealed dynamics of the water processes inducing melt generation (Iwamori, 1998; 2007). Back-arc and intra-plate volcanisms also indicate water migration from a deeper section of the subduction zone. Aiming to understand geodynamical processes of water derived and transported from the subducted slab in the deep subduction zone, we developed a numerical model of water transport coupled dynamically with plate-mantle convection system with a whole mantle scale. We here focus on the mechanism of dehydration from stagnating or penetrating slab and water transport from the mantle transition zone (MTZ). We also consider water transport to deeper mantle and the effects on the global distribution of water-compatible elements (Iwamori and Nakamura, 2012).

We assume that a viscous fluid in a 2-D rectangular box with an extended Boussinesq approximation represents the mantle convection system with integrated lithospheric plates (Tagawa et al, 2007). We incorporate water transport and hydrous mineral phase diagram (Iwamori, 1998; 2007) into the numerical plate-mantle model. We assume that the water dehydrated from water-saturated minerals migrates upward with porous flow that is much faster than mantle flow. In our model, the emitted water is instantaneously transported only to the upward direction. We introduce reduction of the density and the viscosity due to the hydration into the density and rheology model according to experimental study (karato and Jung, 2003). We also consider viscous weakening of serpentine or chlorite that is important for water transport in shallow subduction zone [6]. A numerical method developed by Tagawa et al. (2007) is used to solve momentum and energy conservation equations for the mantle convection. To solve an equation for water transport advected by the mantle flow in which the diffusion term is negligible, a Marker-And-Cell (MAC) method is employed to avoid artificial diffusion.

A serpentine layer generated by dehydration of the oceanic crust plays a key role to control water transport by the subducted slab shallower than about 150 km (Iwamori, 1998; 2007; Horiuchi, 2013). To continuously generate this layer, coupling between the serpentine layer and the plate boundary fault is essential. After dehydration of serpentine, nominally anhydrous minerals (NAMs) (Iwamori, 1998; 2007) are a main veneer of the water. In this stage, water capacity of NAMs, which depends on the grain boundary storage as well as that of the hydrous minerals, is the primary factor to control the amount of transported water. This is not so large as about 0.4 wt. % to maintain water-filled region under the arc. The water is carried without dehydration above the 660 km boundary. If the water capacity in the lower mantle is as large as that of NAMs in the mantle shallower than 410 km (~0.2 wt. %), the water is entirely transported to the lower mantle. When the lower mantle water capacity is lower than that, the water is expelled at the post-spinel phase transition. While the water ascends with the porous flow, the medium rocks descend with asthenospheric flow dragged by the downwelling slab. The repetition of these processes broadens the hydrous layer at the 660 km boundary. A thin water-saturated layer is formed at the 660 km boundary around the penetrating slab. Because of the buoyancy, this becomes unstable so that hydrous plumes are generated. On the contrary to this, the hydrous plume was not formed from the hydrous NAMs layer over the stagnant slab. At the 410 km boundary, the water is ejected from the hydrous plume as the olivine phase minerals can bear the water much less than MTZ minerals. The ejected water rises with porous flow till the emission is completed. The hydrous plumes fill the water within the mantle wedge from the edge to the 500 to 1000 km distant back-arc area, and those erode to thin the overriding lithosphere.

Keywords: subduction zone, water transport, transition zone, slab, hydrous plume, mantle convection

## An overview of seismic coupling and crustal deformation on the basis of geofluid and shallow slow earthquakes

ARIYOSHI, Keisuke<sup>1\*</sup>; MATSUZAWA, Toru<sup>2</sup>; HINO, Ryota<sup>3</sup>; HASEGAWA, Akira<sup>2</sup>; HORI, Takane<sup>1</sup>; NAKATA, Ryoko<sup>1</sup>; KANEDA, Yoshiyuki<sup>1</sup>

<sup>1</sup>Japan Agency for Marine-Earth Science and Technology (JAMSTEC), <sup>2</sup>Research Center for Prediction of Earthquakes and Volcanic Eruptions, Tohoku University, <sup>3</sup>International Research Institute of Disaster Science, Tohoku University

Due to the use of broadband seafloor seismometers near the trench and dense inland networks of highly sensitive seismic stations, very low-frequency events (VLFs) have been observed in the shallow transition zone near the trench of subduction plate boundaries as well as the deep one. Following the 2004 Sumatra Earthquake, the Japanese government has established the Dense Oceanfloor Network system for Earthquakes and Tsunamis (DONET) along the Nankai Trough. In the Tonankai district, M8-class megathrust earthquakes will probably occur in the near future; DONET-I has now operated since August 2011. In this study, we perform numerical simulations of multiscale earthquake cycles, including a megathrust earthquake and VLFs, on a 3-D subduction plate boundary, in order to understand the change in VLF activity after megathrust earthquakes and hydraulic pressure gauge data.

In our simulation, the motion equation for a subduction plate boundary is described by a quasi-dynamic equilibrium between the shear stress (due to reverse dip-slip on the discretized faults) and the frictional stress based on a rate- and state-dependent friction (RSF) law. To perform multiscale earthquake cycle simulations, we assumed single large asperity and numerous small asperities arranged along the strike direction, where the large asperity generates megathrust earthquakes and a chain reaction of numerous small asperities generate a migration of slow earthquakes along the strike direction.

From our simulation results, we concluded as follows: (i) For a megathrust earthquake in which the coseismic slip penetrates to the trench, plate coupling in the postseismic stage will be strong in the region from the central part of the source region to the shallower part toward the trench, which will cause the shallow VLF after-events to be quiescent or to occur infrequently in isolation. On the outer rim, shallow VLF after-events will be reactivated earlier than they will be in the center because of weak plate coupling. (ii) Since leveling change due to slow earthquakes at DONET is expected to be local and incoherent in the same node because of the short distance between their sources and the (DONET) receiver, it is useful to remove an average from original data in the same node in order to extract a signal.

Keywords: megathrust earthquake, subduction zone, seismic quiescence, high pore pressure, seafloor observation, rate- and state-dependent friction law

## Three-dimensional seismic attenuation structure beneath Kyusyu

SAITA, Hiroto<sup>1\*</sup> ; NAKAJIMA, Junichi<sup>1</sup>

<sup>1</sup>Tohoku University

The Philippine Sea (PHS) plate is subducting beneath Kyusyu and a clear volcanic front is formed through the middle of the arc. Furthermore, there is a volcanic gap between Aso and Kirishima volcanos. Seismic attenuation provides additional insights into subduction-zone dynamics, because higher-temperature environments or the existence of fluids may have different effects on seismic attenuation from on seismic velocity. Therefore the estimate of seismic attenuation is very important to understand arc magmatism and mantle dynamics in subduction zone. This study estimates seismic attenuation structure beneath Kyushu using a large number of high-quality waveform data. Data and method

We used 5195 earthquakes that occurred from April 2003 to December 2013 by applying the method of Nakajima et al. [2013] to waveform data recorded at a nation-wide seismograph network in Japan. We determined the corner frequency of earthquakes by using the spectral ratio method of S-coda waves. Then, we determined a whole-path attenuation term ( $t^*$ ), site-amplification factors and spectrum level simultaneously by a joint inversion. Finally, these  $t^*$  values ( $N= 75207$ ) were inverted to obtain three-dimensional attenuation structure.

The obtained results show several interesting feature. First, the subducting PHS slab is imaged as a low attenuation zone. Second, an inclined high-attenuation zone that is interpreted as mantle upwelling flow is served in the back-arc mantle. However, the inclined high-attenuation zone is less developed in the volcanic gap between Aso and Kirishima volcanos. This correspondence suggests the important role of mantle-wedge processes in the genesis of arc magmas.

Keywords: seismic attenuation structure, Philippine Sea Plate, Kyusyu

### 3D Electrical Resistivity Imaging beneath Kyushu by Geomagnetic transfer function data

HATA, Maki<sup>1\*</sup>; UYESHIMA, Makoto<sup>1</sup>; HANDA, Shun<sup>2</sup>; SHIMOIZUMI, Masashi<sup>3</sup>; TANAKA, Yoshikazu<sup>4</sup>; HASHIMOTO, Takeshi<sup>5</sup>; KAGIYAMA, Tsuneomi<sup>4</sup>; UTADA, Hisashi<sup>1</sup>; MUNEKANE, Hiroshi<sup>6</sup>; ICHIKI, Masahiro<sup>7</sup>; FUJI-TA, Kiyoshi<sup>8</sup>

<sup>1</sup>Earthquake Research Institute, the University of Tokyo, <sup>2</sup>Faculty of Agricultural Science, Saga University, <sup>3</sup>Kyushu Polytechnic College, <sup>4</sup>Graduate School of Science, Kyoto University, <sup>5</sup>Institute of Seismology and Volcanology, Graduate School of Science, Hokkaido University, <sup>6</sup>Geographical Survey Institute, <sup>7</sup>Graduate School of Science, Tohoku University, <sup>8</sup>GSE, Osaka University

The Kyushu island in the Southwest Japan Arc has many Quaternary active volcanoes in relation to the subduction of the Philippine Sea Plate (PSP). The volcanoes exist along the volcanic front of N30°E-S30°W, whereas the volcanoes are densely located in the northern and southern regions of the island. The Kyushu island has a non-volcanic region in the central region of the island between the two volcanic regions. We performed three-dimensional (3D) inversion analyses to obtain a lithospheric-scale electrical resistivity model beneath the entire Kyushu island using the Network-Magnetotelluric (MT) data. The electrical resistivity model, however, has a limited resolution in a horizontal direction because of the sparse Network-MT data in several areas of Kyushu. Thus data of geomagnetic variations are used anew to improve the uncertainty of the electrical resistivity structure in a horizontal direction. Data of geomagnetic variations were obtained at the entire Kyushu island and several islands off the western coast of Kyushu from 1980's to 1990's [e.g., Handa et al., 1992; Shimoizumi et al., 1997; Munekane et al., 1997]. In this study, accessible data of geomagnetic variations around Kyushu are compiled. Geomagnetic transfer functions for the data of geomagnetic variations in the northern Kyushu are re-estimated using the BIRRP code [Chave and Thomson, 2004] in order to enhance the quality of the transfer functions and their error estimation. The transfer functions at about 150 sites, which are 12 periods between 20 and 960 s, are obtained with improving quality at the entire Kyushu island. The induction vector representation [Parkinson, 1962] is generally used to delineate the lateral variation of electrical resistivity structure because the vectors point to current concentration in conductive anomalies. Induction vectors determined using the improved transfer functions have the following specific features. First, the vectors on the northern and central Kyushu do not point to the Pacific ocean off the eastern coast of Kyushu but point to the East China Sea of the shallow sea off the western coast of Kyushu. Second, the induction vectors on the southern Kyushu point to the Pacific ocean in the eastern part and point to the East China Sea in the western part at short period, whereas the vectors are arranged along a direction parallel to a direction of the coast line at longer period (>300 s). These results are consistent with the previous work [Handa et al., 1992; Shimoizumi et al., 1997; Munekane, 2000]. It is considered that the complex behavior of the induction vectors are influenced by conditions of the Earth's mantle relating to the igneous activities. Then we applied three-dimensional (3D) inversion analyses for geomagnetic transfer functions using the WSINV3DMT inversion code [Siripunvaraporn and Egbert, 2009]. The electrical resistivity of a starting model is based on values of the 3D electrical resistivity model estimated by using the Network-MT data. In this presentation, we will mainly describe features of the 3D electrical resistivity structure using the geomagnetic transfer functions and them of the 3D electrical resistivity structure using only the Network-MT data [Hata et al., 2013].

## Influence of confining and pore-fluid pressures on velocity and conductivity of a fluid-saturated rock

SEMA, Fumie<sup>1\*</sup> ; MAKIMURA, Miho<sup>1</sup> ; HIGUCHI, Akiyoshi<sup>1</sup> ; WATANABE, Tohru<sup>1</sup>

<sup>1</sup>Department of Earth Sciences, University of Toyama

Pore-fluid pressure in seismogenic zones can play a key role in the occurrence of an earthquake (e.g., Sibson, 2009). Its evaluation via geophysical observation can lead to a good understanding of seismic activities. It is critical to understand how pore-fluid pressure affects seismic velocity and electrical conductivity. We have studied the influence of pore-fluid pressure on elastic wave velocity and electrical conductivity of water-saturated rocks.

Measurements have been made using a 200 MPa hydrostatic pressure vessel, in which confining and pore-fluid pressures can be separately controlled. An aqueous pore-fluid is electrically insulated from the metal work by using a specially designed device (Watanabe and Higuchi, 2013). Elastic wave velocity was measured with the pulse transmission technique (PZT transducers,  $f=2$  MHz), and electrical conductivity the four-electrode method (Ag-AgCl electrodes,  $f=100$  mHz-100 kHz) to minimize the influence of polarization on electrodes.

Berea sandstone (OH, USA) was used for its high porosity (19.1%) and permeability ( $\sim 10^{-13}$  m<sup>2</sup>). It is mainly composed of subangular quartz grains. Microstructural examinations show clay minerals (e.g., kaolinite) and carbonates (e.g., calcite) fill many gaps between quartz grains. A small amount of feldspar grains are also present. The grain size is 100-200 micrometers. Cylindrical samples have dimensions of 25 mm in diameter and 30 mm in length. Their axes are perpendicular to sedimentation bed. Elastic wave velocity is slightly higher in the direction perpendicular to the axis than in that parallel to the axis.

Confining and pore-fluid pressures work in opposite ways. Increasing confining pressure closes pores, while increasing pore-fluid pressure opens them. For a given pore-fluid pressure, both compressional and shear velocities increase with increasing confining pressure, while electrical conductivity decreases. When confining pressure is fixed, velocity decreases with increasing pore-fluid pressure while conductivity increases. The closure and opening of pores can explain observed changes of velocity and conductivity.

Effective confining pressure is defined by the difference between confining and pore-fluid pressures. Velocity increases with increasing effective confining pressure, while conductivity decreases. However, neither velocity nor conductivity is unique function of the effective confining pressure. For a given effective confining pressure, conductivity significantly increases with increasing confining pressure. Velocity also increases with increasing confining pressure, though it is not so significant. Increasing pore-fluid pressure can compress clay minerals to increase pore space. This might explain observed conductivity change.

Keywords: pore-fluid pressure, seismic velocity, electrical conductivity, geofluid

## A study on grain boundary brine in halite rocks using electrical conductivity measurements

WATANABE, Tohru<sup>1\*</sup> ; KITANO, Motoki<sup>1</sup>

<sup>1</sup>Graduate school of science and engineering, University of Toyama

Intercrystalline fluid can significantly affect rheological and transport properties of rocks. Its influences are strongly dependent on the style of distribution. When a fluid fills grain boundaries in a rock, it will significantly reduce the strength of the rock. The fluid distribution is mainly controlled by the dihedral angle between solid and fluid phases. The grain boundary wetting is expected only when the dihedral angle is 0°. The dihedral angle of the halite-water system was studied through microstructural analyses of quenched materials (Lewis and Holness, 1996). The dihedral angle is 50~70° at  $P < 200$  MPa and  $T < 300$  °C. However, deformation experiments (e.g., Watanabe and Peach, 2002) and cryo-SEM observations (e.g., Schenk et al., 2006) on halite rocks have indicated the coexistence of grain boundary brine with a positive dihedral angle. In order to understand the nature of grain boundary brine, we have conducted electrical impedance measurements on synthetic wet halite rocks over a wide range of pressure and temperature.

Wet halite rock samples (9 mm diameter and 6 mm long) are prepared by cold-pressing ( $P=140$  MPa, 40 min.) of wet NaCl powder and annealing ( $T=180$ °C,  $P=180$  MPa, 160 hours). Grains are polygonal and equidimensional with a mean diameter of 50-100  $\mu$ m. The porosity is less than 1 %. The volume fraction of brine is estimated to be 11.1% by the thermo gravimetric analysis. Microstructural observation shows that most of brine is enclosed inside halite grains. Electrical impedance is measured in the axial direction of a sample by a lock-in-amplifier (SRS, SR830) with a current amplifier (SRS, SR570). The cylindrical surface of a sample is weakly dried and coated with RTV rubber to suppress the contribution of surface conduction. A conventional externally heated, cold-seal vessel (pressure medium: silicone oil) is used to control pressure and temperature.

Electrical conductivity of wet halite rocks is higher than that of NaCl by orders of magnitude even at the conditions of the dihedral angle larger than 60 degrees. The conduction through brine dominates the bulk conduction. This is also supported by the quick conductivity change in response to the change in pressure. Brine is interconnected over a whole range of pressure and temperature.

No remarkable change in conductivity is observed around the condition of the dihedral angle of 60 degrees. Although the interconnection of triple-junction tubes might drastically change at the dihedral angle of 60 degrees, its influence on the bulk conductivity is masked by more conductive paths. A triple-junction tube is so stiff that it cannot give observed conductivity changes in response to changes in pressure. The dominant conduction paths are not triple-junction tubes. Grain boundary brine must be the dominant conduction paths.

Electrical conductivity decreases with increasing pressure. Larger change is observed for lower temperatures. A simple model of fluid tube with elliptical cross-section shows that the thickness of a fluid tube decreases by less than 10%. The observed large change in conductivity suggests that the conductivity of brine is strongly dependent on the fluid thickness. When the thickness is comparable to the molecular size, the mobility of ions must be sensitive to the thickness. The observed large change in conductivity might be caused by the decrease in ionic mobility.

Keywords: salt, grain boundary, water, electrical conductivity

## Estimation of the maximum burial depth of siltstones from the Kazusa Group by laboratory experiments

TAMURA, Yukie<sup>1</sup> ; MARUMO, Haruna<sup>2</sup> ; MITSUHASHI, Shunsuke<sup>1</sup> ; UEHARA, Shin-ichi<sup>1\*</sup>

<sup>1</sup>Faculty of Science, Toho University, <sup>2</sup>Graduate School of Science, Toho University

To evaluate maximum burial depth of sedimentary formations is important for many topics in earth science and engineering such as estimating uplift and erosion of sedimentary basins. As a one of effective methods of the evaluation, a laboratory-based method for determining the maximum effective stress have been proposed. This method is based on a conventional method to evaluate preconsolidation stress (maximum effective stress experienced) of soil. However, this method cannot be necessarily applied to sedimentary rocks in simple ways, because sedimentary rocks have experienced not only mechanical compaction but also other processes such as cementation between grains, which should affect the mechanical properties of the rock. Thus applicability of this method to sedimentary rocks should be examined for several sedimentary basins. We performed laboratory experiments to measure porosity of siltstone specimens collected from several formations of the Kazusa Group, Boso peninsula, Japan, and tried to estimate the maximum burial depth based the results. We then compared the results with differences of burial depth ( $\Delta Depth$ ) among locations of collecting samples which were estimated from geological setting, and examined the applicability of this method for estimation of the maximum burial depth in this site.

We collected rock blocks from Umegase (UMG), Otadai (OTD), Kiwada (KWD), Ohara (OHR), and Katsuura (KTR) Formations (in the descending order of stratigraphic horizon), and prepared cylindrical specimens of approximately 40 mm in diameter and 30 mm in length from these blocks. The porosity of these specimens was measured under different confining pressure (up to 35 MPa) and constant pore pressure (1 MPa) by using an intra-vessel deformation fluid-flow apparatus at Toho University. We used water as a pore fluid, and the measurements were performed at room temperature. Porosity under each effective pressure (the difference between confining pressure and pore pressure) was estimated by measuring volume of water drained from a specimen when confining pressure was loaded. The relation between measured porosity and effective pressure could be bilinear in log-log scale. The maximum effective stress experienced ( $P_{e,B}$ ) of the tested rocks was determined from the intersection point of the two straight lines of the compaction curve. The maximum burial depth ( $D_{max}$ ) was obtained by  $D_{max} = P_{e,B} / [(\rho_r - \rho_w)g]$ , where  $\rho_r$ ,  $\rho_w$  and  $g$  are density of rock, water and gravity acceleration, respectively.

In the case of UMG, OTD and KTR, porosities decrease as the burial depth increases. Porosities of OHR and KWD, however, were relatively high although their burial depth is relatively large. There was a linear correlation between  $D_{max}$  and  $\Delta Depth$  except for OHR, but the slope of the relationship was less than one (approximately 0.27). Therefore, further investigation is necessary to examine the applicability of this methods to this site.  $P_{e,B}$  of OHR was less than that of other specimens, which supports the possibility that pore pressure in this formation was approximately 5 to 12 MPa higher than hydrostatic conditions.

Keywords: porosity, maximum burial depth, maximum effective stress experienced, Kazusa Group, overpressure, laboratory rock experiment

## Experimental constraints on the serpentinization rate under the antigorite-stable P-T condition

NAKATANI, Takayuki<sup>1\*</sup> ; NAKAMURA, Michihiko<sup>1</sup>

<sup>1</sup>Earth and Planet Materials Sci., Tohoku Univ.

Water transport into the Earth's interior can be limited by the rate of serpentinization reaction proceeding at slow spreading ridges and along bending related faults (Iyer et al., 2012). Moreover, the distribution of H<sub>2</sub>O in the mantle wedge may be controlled by the extent of progression of the reaction between the slab-derived fluid and the hanging wall mantle, as suggested by theoretical models (Iwamori, 1998). Previous hydration experiments for kinetic studies have been vigorously conducted at relatively low P-T condition (up to ca. 400 °C and 0.3 GPa) where the low T serpentine variety lizardite or chrysotile is stable. In contrast, antigorite is expected to be the dominant serpentine variety under the higher P-T condition corresponding to the deep oceanic lithosphere and the mantle wedge.

In order to constrain the serpentinization rates of peridotite under the antigorite-stable conditions, we conducted piston-cylinder experiments at 580 °C and 1.3 GPa. Four types of starting materials were prepared from the crushed powder of a San Carlos lherzolite xenolith: 1) olivine (Ol), 2) orthopyroxene (Opx) + clinopyroxene (Cpx), 3) Ol + Opx, and 4) Ol + Opx + Cpx + spinel. These systems were abbreviated as OL, OPX+CPX, OL+OPX, and LHZ, respectively. The starting materials were reacted with 15 wt% distilled water for 4-15 days. The formation of serpentine + talc + magnetite was observed in all the systems except for OL. Based on Raman spectroscopy results and crystal shapes, the synthesized serpentine mineral was identified as lizardite with 6.9 wt% Al<sub>2</sub>O<sub>3</sub>, rather than antigorite. The high Al<sub>2</sub>O<sub>3</sub> content in the system possibly stabilized the aluminous lizardite at the experimental temperatures. Low silica activity precluded olivine reaction in the OL system, whereas olivine reacted with the SiO<sub>2</sub> component in orthopyroxene to form lizardite and talc in the other systems. The reaction progress followed an interface-controlled rate law. The growth rate, *G*, was estimated to be  $2.31 \pm 0.37$ ,  $1.23 \pm 0.20$ , and  $2.78 \pm 0.64$  μm/day in the OPX+CPX, OL+OPX, and LHZ systems, respectively. As an example, we applied the hydration rates of peridotites, which were obtained experimentally, to a reactive-transport model for the convecting mantle wedge hydration. In the case of grain-scale pervasive flow, the mass flux ratio of water fixable in the hanging wall peridotites to that supplied from the dehydrating oceanic lithosphere was calculated to be  $2.7 \times 10^5 - 1.5 \times 10^8$ . This indicates that the water is completely fixable in the convecting mantle wedge and carried down to the stability limit of serpentine as soon as it is supplied from the slab. Aqueous fluid may penetrate all the way through the serpentine stable layer and reach the hot center of the mantle wedge only when the fluid migrates via crack-like pathways with a spacing >270-15000 m, which is not consistent with observations of natural serpentinites.

Keywords: hydration, serpentine, fluid, subduction zone, mantle wedge

## Diffusive kinetic isotope fractionation of water in silicate glasses

KURODA, Minami<sup>1\*</sup>; YAMAMOTO, Daiki<sup>1</sup>; TACHIBANA, Shogo<sup>1</sup>; NAKAMURA, Michihiko<sup>2</sup>; OKUMURA, Satoshi<sup>2</sup>; ASAKI, Miho<sup>2</sup>; ISHIBASHI, Atsuko<sup>1</sup>; SAKAMOTO, Naoya<sup>1</sup>; YURIMOTO, Hisayoshi<sup>1</sup>

<sup>1</sup>Department of Natural History Science, Hokkaido University, <sup>2</sup>Department of Earth Science, Tohoku University

Oversaturation of dissolved volatiles in an ascending magma leads to bubble nucleation and growth, which depend on volatile solubility and diffusivity, and drives explosive volcanic eruptions in the Earth. It is thus important to clarify the behaviors of volatiles in silicate melts in understanding the mechanism and dynamics of volcanic eruptions.

Hydrogen isotopes record the degassing processes of hydrous magmas due to isotopic fractionation between dissolved and exsolved water. The degree of hydrogen isotopic fractionation is correlated with the water content in natural volcanic rock samples; Deuterium is more deficient in water-poor samples, and the degree of D-deficiency increases as the water content decreases. This trend has been interpreted to reflect the transition of degassing model from that in a closed-system to in an open-system. However, these two extreme degassing schemes do not take the diffusive transport of water in magmas into account, which should be included in a realistic degassing model, because the timescale of diffusion is not necessarily negligibly small compared to that of degassing during magma ascent. Moreover, diffusion of water in silicate melts may cause kinetic isotope fractionation between silicate melt and explosive fluid phases because H<sub>2</sub>O is likely to diffuse faster than HDO, of which effect can be overprinted in the D/H ratios of natural samples. The hydrogen isotopic fractionation during water diffusion in silicate melts, however, has not yet been fully determined. In order to determine the isotopic fractionation factor of hydrogen due to water diffusion in silicate melts, we performed diffusion experiments of water in SiO<sub>2</sub> and synthetic rhyolite glasses in a D-enriched system (H/D=10, 5 and 1).

The experiments were performed for SiO<sub>2</sub> and rhyolite glasses at 850 °C and water pressure of 50 bar in sealed silica tubes and at 650 °C and water pressure of 500 and 1000 bar in a hydrothermal furnace developed at Tohoku University. Concentration profiles of H and D in run products were measured with the ion microprobe (Cameca ims-6f at Hokkaido University) to evaluate diffusion coefficients of water (including H<sub>2</sub>O and HDO) in glasses. The obtained diffusivity (a diffusion coefficient divided by a water content) in SiO<sub>2</sub> glass at 650 and 850 °C were consistent with the values reported in previous studies (Davis and Tomozawa, 1995; Berger and Tomozawa, 2003). The D/H ratios along the diffusion profile were also analyzed for SiO<sub>2</sub> glasses with the ion microprobe. The D/H ratio first decreases, but apparently increases along the profile. The decrease of D/H ratio may imply the kinetic isotope fractionation during diffusion. However, the increase of D/H ratio cannot be explained simply by diffusion and may reflect the change of instrumental mass fractionation with water content (Hauri et al., 2006), which should be precisely determined to correct the profile of hydrogen isotopic ratio.

Keywords: eruption dynamics, silicate glass, water, diffusion, hydrogen isotope, isotopic fractionation

## Development of high-precision geobarometer

TAKAHATA, Kohei<sup>1\*</sup> ; TORIMOTO, Junji<sup>2</sup> ; YAMAMOTO, Junji<sup>2</sup>

<sup>1</sup>Earth and Planetary System Science, Hokkaido University, <sup>2</sup>Hokkaido University Museum

Fluid inclusions in mantle-derived minerals can serve as a messenger from deep Earth. If CO<sub>2</sub> is a dominant phase of the fluid, the relationship between intensity ratio and frequency separation of the Fermi diad bands in the Raman spectra of CO<sub>2</sub> can be used for determination of density of the inclusions.

In this study, we installed new Raman spectrometer that was improved spectral resolution. And we also measured its precision of frequency separation ( $\Delta$ ). As a result of this study, we determined that the error of  $\Delta$  is  $\pm 0.003 \text{ cm}^{-1}$  ( $1\sigma$ ). Converted into the error of density, this value is  $\pm 0.0025 \text{ g / cm}^{-3}$ .

Keywords: fluid inclusion, carbon dioxide, Raman spectroscopy, mantle xenolith, geobarometer

## Applications of rapid and precise $^{11}\text{B}/^{10}\text{B}$ isotopic analysis to water and rock samples

TANIMIZU, Masaharu<sup>1\*</sup>; NAGAISHI, Kazuya<sup>2</sup>; ISHIKAWA, Tsuyoshi<sup>1</sup>

<sup>1</sup>Kochi Institute, JAMSTEC, <sup>2</sup>Marine Works Japan Ltd.

Boron isotope ratio is a powerful tracer in the fields of geochemistry, biochemistry, and environmental chemistry. Boron isotope ratios are determined by TIMS or MC-ICP-MS with precisions of better than 0.1 % RSD, but a large inter-lab discrepancy of 0.6 % is still observed for actual carbonate samples (Foster, 2008). Here, we are trying to determine B isotope ratio by MC-ICP-MS with a simple and common analytical techniques using a quartz sample introduction system with a PFA nebulizer, and compared to recently developed precise B isotope ratio analysis techniques by TIMS in positive ion detection mode determined as  $\text{Cs}_2\text{BO}_2^+$  ions with sample amount of  $<100$  ng (Ishikawa and Nagaishi, 2011) and by MC-ICP-MS (Foster, 2008, Louvat et al., 2011).

In this year, our developed B analytical method above for carbonate and water samples are applied to rock samples. Resultant analytical reproducibility (twice standard deviation) was  $\pm 0.04$  % with a consumption of 50 ng B for several geochemical reference rocks issued from GSJ. Their relative differences from the standard were consistent with those determined by the positive TIMS within analytical uncertainty. Current potential B isotopic analysis by MC-ICP-MS will be discussed.

## Water migration with a subducting slab and the dynamic effects on whole mantle convection

KANEKO, Takeo<sup>1\*</sup> ; NAKAKUKI, Tomoeiki<sup>1</sup> ; IWAMORI, Hikaru<sup>2</sup>

<sup>1</sup>Dept. Earth and Planetary Systems Science, Hiroshima Univ, <sup>2</sup>Geochemical Evolution Research Program, JAMSTEC

Existence of liquid water is a characteristic of the earth. The water of interior of the Earths involved with the subducting plate reduces density and viscosity of the crustal and mantle rocks. These effects are essential to emerge the solid Earth activity such as, plate tectonics and island arc volcanism. Although the most of subducted water circulates through upper mantle, there is a possibility that portion of the water penetrates into lower mantle. Where does the water migrate? How much does the water affect mantle dynamics through the rock rheology and property? We performed numerical mantle convection simulation to investigate the water cycle and dynamic effects on the whole mantle convection.

In this study, we use the numerical model based on the model (Tagawa et al., 2007; Nakakuki et al., 2010) including the subducting oceanic plate driven dynamically. This model includes migration of water with the plate motion. We consider influences of reducing density and viscosity due to the water on the mantle flow (Karato and Jung, 2003). The maximum water content in the upper mantle is determined using phase relations of the basalt and the peridotite (Iwamori, 2004; 2007). We use various values of the maximum water content of rocks in the lower mantle, because it has been not clearly defined. We also treated the following physical properties as varying parameters: friction coefficient at the plate boundary, amount of the water injection at the trench, density-water dependence coefficient, and maximum water content in the lower mantle. Addition to we calculated dislocation creep by non-newtonian fluid or newtonian fluid.

A part of subducted water associate with the subducting oceanic plate is absorbed into peridotitic rocks and transported to about 150 km deep mantle. After that, dehydration with the serpentine decomposition occurs, and transported to deeper mantle by hot nominally anhydrous minerals (NAMs). The amount of dehydration at the 660 km phase boundary depends on the maximum water content of lower mantle, when the slab penetrates into lower mantle. The ejected water forms thin and high-water-content layer over the 660 km phase transition. As a result, the buoyancy of this layer induces instability, so that hydrated plumes are generated. We propose that this mechanism is important for the water cycle in the upper mantle. On the other hand, considerable portion of the water is transported into lower mantle with subducting slab, although notable water capacity of the lower mantle much smaller than that of the upper mantle, and reach core-mantle boundary. We have not yet observed notable water influence on mantle convection at lowermost mantle because of the small water concentration. Also, the hydrated materials do not rise to surface with hot plumes generated at the core-mantle boundary.

Keywords: mantle convection, plume, transition zone, water transport

## Microstructural and fabric characteristics of the uppermost mantle peridotites in the Taitao ophiolite, South America

YOSHIDA, Yoshiaki<sup>1\*</sup> ; MICHIBAYASHI, Katsuyoshi<sup>1</sup> ; ANMA, Ryo<sup>2</sup>

<sup>1</sup>Institute of Geosciences, Shizuoka University, <sup>2</sup>Faculty of Life and Environmental Science, University of Tsukuba

The <6Ma young Taitao ophiolite, exposed at the westernmost promontory of the Taitao Peninsula, is located approximately 40 km southeast of the Chile triple junction and consists of a complete sequence of oceanic lithosphere, including ultramafic rocks, gabbros, a dyke complex and volcanoclastic rocks. The ophiolite is surrounded by several contemporaneous granite plutons intruded in between the ophiolite and the Pre-Jurassic metamorphic basement. Several studies have been carried out on the Taitao ophiolite and surrounding granites. Whereas they have focused mostly on petrology and geochemistry, we investigated microstructures and crystal-fabrics of the ultramafic rocks, aiming to understand the origin of the ophiolite. 6 out of 16 ultramafic rocks preserved peridotite textures despite of intense serpentinization and show mostly porphyroclastic textures consisting of pyroxene porphyroclasts with a fine-grained olivine-pyroxene matrix. Their olivine crystal-fabrics shows [100]{0kl} and [100](001) patterns. These indicate that the uppermost mantle section have remarkably been deformed before and/or during the obduction process after their formation beneath the mid-ocean ridge.

Keywords: Taitao ophiolite, mantle section, peridotite, microstructure, olivine fabrics

## Gabbroic petrology of oceanic lithosphere: comparison between Godzilla Megamullion and megamullions in mid-ocean ridges

YAMASHITA, Hiroyuki<sup>1\*</sup> ; OHARA, Yasuhiko<sup>2</sup> ; ARIMA, Makoto<sup>3</sup>

<sup>1</sup>Kanagawa Prefectural Museum of Natural History, <sup>2</sup>Hydrog. & Oceanog. Dept. of Japan, <sup>3</sup>Yokohama National University

Godzilla Megamullion is the largest oceanic core complex on the Earth, with the dimension 125 km (along axis) and 55 km (across axis) (Ohara et al., 2001). Our study has revealed systematic petrological characteristics of the gabbroic rocks from the Godzilla Megamullion. In this contribution, we will report these characteristics and compare the results with those of gabbroic rocks from mid-ocean ridges.

Low modal abundance of olivine and high abundances of amphibole and iron oxide minerals are the prominent feature of the majority of the gabbroic rocks recovered from the Godzilla Megamullion. The studied gabbroic rocks are classified into troctolite, olivine gabbro, gabbro, hornblende pyroxene gabbro, pyroxene hornblende gabbro, hornblende gabbro on the basis of the classification by Streckeisen (1976). The chemical compositions of constituent minerals show systematic variations that are indicative of magmatic differentiation. Anorthite content in plagioclase, XMg (Mg / (Mg + Fe)) value in olivine and clinopyroxene decrease from less differentiated to highly siliceous evolved rocks. The mineral compositions indicate that troctolite is the most primitive variety and that trondhjemite is the most differentiated variety in the Godzilla Megamullion.

Troctolite, olivine gabbro and gabbro were recovered only from the distal parts of the Godzilla Megamullion. An age of ~13 Ma has been reported from this region (Tani *et al.*, 2011). On the other hand, trondhjemite was recovered from the medial and proximal parts of the megamullion, with ages of 11 and 8.7 Ma (Tani *et al.*, 2011), respectively. Gabbroic rocks with relatively primitive composition were recovered from the Neck Peak region (age of 8.4 Ma; Tani *et al.*, 2011). The spatial and temporal distribution of gabbroic rocks in the Godzilla Megamullion suggests the following magmatic model: a robust magmatic activity was predominant in the distal part, a declined magmatic activity in the medial to proximal parts, and a resurgent magmatic activity in the Neck Peak region. This model is consistent to the results obtained independently from petrological analysis on the peridotites from the Godzilla Megamullion (Snow *et al.*, in preparation).

The lithological proportions of the gabbroic rocks in the Godzilla Megamullion are characterized by lower primitive gabbro (troctolite and olivine gabbro) ratio than in the Kane Megamullion in the Mid-Atlantic Ridge and in the Atlantis Bank in the Southwest Indian Ridge.

Keywords: Parece Vela Basin, Godzilla Megamullion, gabbro, Oceanic core complex

## The Po/So waves propagating in the Philippine Sea

SHITO, Azusa<sup>1\*</sup>; SUETSUGU, Daisuke<sup>2</sup>; FURUMURA, Takashi<sup>3</sup>

<sup>1</sup>Institute for Geothermal Science, Kyoto University, <sup>2</sup>JAMSTEC, <sup>3</sup>Earthquake Research Institute, The University of Tokyo

The Po/So waves which have high-frequency content, large amplitude, and long-duration propagate for large distance (up to 3000 km) across the oceanic lithosphere. In our previous study, we analyzed Po/So waves from deep-focus earthquakes occurring in the subducting slab beneath Japan, recorded by broadband ocean bottom seismometers (BBOBSs) at northwestern Pacific [Shito et al., 2013]. We demonstrated that the Po/So waves are developed by multiple forward scattering of P and S waves due to laterally elongated heterogeneities in both the subducting and laterally extending oceanic lithosphere. Following this study, the question when and where do the small-scale heterogeneities form in the oceanic lithosphere comes about. In order to answer this question, the Po/So waves in younger oceanic lithosphere need to be analyzed. Therefore in this study, we investigate the Po/So waves in the Philippine Sea plate (15-60 Ma), which is much younger than the Pacific Plate (130 Ma).

The Philippine Sea is one of the marginal seas of the Pacific Ocean. It is fundamentally divided into two regions bounded by the Kyushu-Palau Ridge. It is thought that these two regions were formed in different episodes of back-arc spreading and that western part (45-60 Ma) is older than eastern part (15-30 Ma) [e.g., Seno and Maruyama, 1984]. The comparison of Po/So waves propagation in the different ages of the oceanic lithosphere is expected to reveal the origin of the small-scale heterogeneities.

Seismological observations using BBOBSs was conducted in the Philippine Sea from 2005 to 2008, and high-quality Po/So waves from earthquakes in subducting Philippine Sea plate were recorded very clearly. The findings from the observed Po/So waves in the Philippine Sea plate are summarized as follows. (1) The Po/So waves propagate much effectively in western part than eastern part of the Philippine Sea. (2) The Po/So waves propagate even in youngest oceanic lithosphere (15 Ma) near the past spreading center of the Shikoku Basin.

In order to reveal the structure of the oceanic lithosphere and propagation efficiency in the Po/So waves, we performed numerical FDM simulations of 2-D seismic wave propagation in a realistic oceanic lithosphere model. The model is developed in the same procedure as the case of the Pacific plate [Shito et al., 2013]. In the oceanic lithosphere, we introduce laterally elongated small-scale heterogeneities, which are described by von Karman type stochastic random distribution function. Because the thickness of the oceanic lithosphere is considered to correlate with the age [e.g., Kawakatsu, et al. 2009], we vary the thickness of the oceanic lithosphere from 80 km to 20 km. To evaluate the fit of the computed waveforms to the data, we use the spatial attenuation of the seismic wave energy along the record section (up to 1500 km). The seismic wave energy is defined as integrated squares of amplitudes in a certain time window (25 s from the Po/So wave onset). The model with the thickness of the oceanic lithosphere of 60 km and 30 km successfully explain the spatial attenuation of the Po/So waves record section observed at western and eastern parts of the Philippine Sea, respectively. The thicknesses are consistent with those obtained by previous studies [Kawakatsu et al., 2009]

This result suggests that the oceanic lithosphere including small-scale heterogeneities grow as it ages and develop large-amplitude and long-duration of high-frequency Po/So waves. The small-scale heterogeneities may form at the bottom of the lithosphere as it cools. They suggest that small-scale melts in the asthenosphere are frozen and attached at the bottom of the lithosphere, which remain even after the lithosphere is subducted into the mantle.

Keywords: Po/So waves, Philippine Sea plate, oceanic lithosphere

## Multi-scale heterogeneity of abyssal peridotite

TAMURA, Akihiro<sup>1\*</sup>; MORISHITA, Tomoaki<sup>1</sup>; ARAI, Shoji<sup>1</sup>

<sup>1</sup>Earth Sciences, Kanazawa University

Petrological studies of peridotite have increasingly revealed the origin of magma as well as materials and processes of Earth interior. Although we now only access to the interior indirectly, we can obtain the mantle-derived material brought by magma transporter or by large tectonic reconstruction of the earth surface. At the ocean floor near the mid-ocean ridge spreading center, where the deep seated rock is exposed along spreading axis or fracture zone, abyssal peridotite is collected. The abyssal peridotite studies significantly contribute not only to understanding of the formation of oceanic lithosphere but also to development of analytical way for the mantle material. In mineralogical and geochemical approaches, chromian spinel is a good indicator for the origin; for example, the spinel Cr# reflects a partial melting degree of the upper mantle material (e.g., Dick and Bullen, 1984; Arai, 1987). Trace-element compositions of clinopyroxene allow us to discuss the melting process quantitatively (e.g., Johnson et al., 1990). Recently, further discussions can be available by using ultra-trace elements and PGE isotopes (e.g., Harvey et al., 2006; Ishikawa, 2012).

Several petrological studies of abyssal peridotite samples have demonstrated "regional-scale" heterogeneity of the upper mantle along Mid-Atlantic Ridge based on their spinel Cr# (e.g., Dick et al, 1984; Michael and Bonatti, 1985). In "Global-scope" differences between Atlantic, Indian and Pacific oceans, Niu and Hekinian (1997) proposed that the spinel Cr# of abyssal peridotite is dependent on spreading rate. Contrasting to such a heterogeneity, Ghose et al. (1996) and Dick et al. (2010) showed that the compositional variation of the abyssal peridotite is controlled by local structures at the mid-ocean ridge: for example, spreading axis, fracture zone, abyssal plane and oceanic core complex. Geochemical heterogeneity of each abyssal peridotite sample is recently discussed in aspects of magmatic event during or after partial melting stage (Tamura et al., 2008; Warren and Shimizu, 2010).

In our presentation, to review petrological characteristics of abyssal peridotite, we will demonstrate our compiling data set focused on relationship between their spinel Cr# and sample localities, such as ocean floor structures at the mid-ocean ridge. The example of abyssal peridotite sample heterogeneity are also discussed. Then, we would like to discuss the factor and significance of compositional variation of abyssal peridotite.

Keywords: abyssal peridotite, spinel, ocean floor

## Heterogeneity from mantle to crust at the central Southwest Indian Ridge (1) -Upper mantle-

MATSUNO, Tetsuo<sup>1\*</sup> ; SEAMA, Nobukazu<sup>2</sup> ; SATO, Hiroshi<sup>3</sup> ; SATO, Taichi<sup>4</sup> ; SENDA, Ryoko<sup>5</sup> ; MACHIDA, Shiki<sup>6</sup> ; NAKAMURA, Kentaro<sup>5</sup> ; MORISHITA, Tomoaki<sup>7</sup> ; MIZUMA, Keiko<sup>2</sup> ; NOGI, Yoshifumi<sup>1</sup> ; OKINO, Kyoko<sup>8</sup>

<sup>1</sup>National Institute of Polar Research, <sup>2</sup>Kobe University, <sup>3</sup>Senshu University, <sup>4</sup>National Institute of Advanced Industrial Science and Technology, <sup>5</sup>Japan Agency for Marine-Earth Science and Technology, <sup>6</sup>Waseda University, <sup>7</sup>Kanazawa University, <sup>8</sup>University of Tokyo

Mantle is heterogeneous in terms of geophysical (e.g., bathymetry, geomagnetics, and gravity) and geological (e.g., petrology and geochemistry) aspects. Because heterogeneity is enhanced at slow spreading ridge, the ultra-slow spreading Southwest Indian Ridge (SWIR) is suitable for understanding the heterogeneity. We conducted geophysical and geological investigations since 2007 at the segment along the central SWIR between 35°E and 40°E, where the ridge segment is close to the Marion hotspot.

Serpentinised mantle peridotites occurring as clasts in the conglomerate were dredged from a topographic high within the Prince Edward fracture zone at 35°E. A marine electromagnetic experiment was conducted along a 110 km transect across a subsegment at 37°E to reveal an electrical resistivity structure of the upper mantle.

The peridotites are considered to have originally been lherzolite based on petrographic and mineral chemical composition analyses. Chemical compositions of spinel (Cr# and Mg#) in the peridotites suggest that the peridotites have undergone moderate partial melting without enhancement of melting by the hotspot regardless of proximity of the dredge site to the Marion hotspot. Light rare earth elements of clinopyroxene are more depleted than were previously reported for SWIR peridotites, suggesting that the peridotites have undergone little to no metasomatism of a melt-mantle interaction. Osmium isotope ratios are highly depleted, resulting in that a model age of rhenium depletion ( $T_{RD}$ ) is 1 billion years. These results suggest that the dredged peridotites have not been enriched after the last melt extraction event 1 billion years ago, preserve their initial depleted compositions without hotspot effects, and show the presence of a refractory mantle domain under the central SWIR.

A preliminary 2-D electrical resistivity structure of the upper mantle down to 200 km depth does not show a remarkable conductive melting region beneath the ridge axis and a more conductive asthenospheric mantle than those observed at other mid-ocean ridges. The resistivity model suggests that the presence of the Marion hotspot does not result in enhancement of melt production beneath the ridge and enrichment of conductors like water in the upper mantle at present.

The result of this study suggests that the source mantle contain ancient, refractory, and depleted portion. This mantle may be a part of the depleted mantle prevailed under the Marion Rise, which was proposed by Zhou and Dick (2013) and may be supported by the absence of slow velocity anomalies around the Marion hotspot in upper mantle seismic tomography images (e.g., Zhao, 2007).

## Heterogeneity from mantle to crust at the central Southwest Indian Ridge (2) -Crust-

SATO, Hiroshi<sup>1\*</sup> ; SATO, Taichi<sup>2</sup> ; MACHIDA, Shiki<sup>3</sup> ; SENDA, Ryoko<sup>4</sup> ; MATSUNO, Tetsuo<sup>8</sup> ; SEAMA, Nobukazu<sup>5</sup> ; NAKAMURA, Kentaro<sup>6</sup> ; MORISHITA, Tomoaki<sup>7</sup> ; NOGI, Yoshifumi<sup>8</sup> ; OKINO, Kyoko<sup>9</sup>

<sup>1</sup>Senshu Univ., <sup>2</sup>AIST, <sup>3</sup>Waseda Univ., <sup>4</sup>JAMSTEC, <sup>5</sup>Kobe Univ., <sup>6</sup>Dept. System Innovation, Univ. of Tokyo, <sup>7</sup>Kanazawa Univ., <sup>8</sup>NIPR, <sup>9</sup>AORI, Univ. of Tokyo

Mantle is heterogeneous in terms of geophysical (e.g., bathymetry, geomagnetics, and gravity) and geological (e.g., petrology and geochemistry) aspects. Because heterogeneity is enhanced at slow spreading ridge, the ultra-slow spreading Southwest Indian ridge is suitable for understanding the heterogeneity. We conducted geophysical and geological investigations since 2007 at the segment along the central Southwest Indian Ridge (SWIR) between 35E and 40E, where the ridge segment is close to the Marion hotspot.

Recent investigations of topography and geophysics along the central Southwest Indian ridge between 35E and 40E (Sato, T. et al., 2013) classify the segment between the Prince Edward and Eric Simpson fracture zones as four subsegments: PE-1, PE-2, PE-3, and PE-4 from west to east. A long oblique axial valley (NTD-1) is recognized between PE-1 and PE-2. Geochemical and isotopic compositions of MORB samples from these subsegments consist with previously reported MORB and/or SWIR basalts. However, small scale geochemical and isotopic heterogeneity are recognized in these samples. Sato, T. et al. (2013) considered that strong melt-focusing could be principle process to produce volcanic and low volcanic subsegment rather than the effect of proximity to the Marion hotspot. Continuous seafloor morphology and isochrons over off-axis areas of segment PE-1 and NTD-1 suggest that PE-1 shortened after the C2An chron, indicating the magmatic process has changed for several million years.

Among MORB from the subsegments, PE-1 and NTD-1, geochemically enriched sample (e.g. those with La/Sm>1) are enriched in isotope (higher Sr and lower Nd), suggesting that enrichment is due to source enrichment rather than smaller degree of melting of the homogeneous source mantle. Although geochemical and isotopic compositions could be explained by the mixture of depleted MORB source and the Marion components, contribution of the Marion component is limited only in the eastern part of PE-1 and NTD-1 subsegments. Therefore, it is reasonable to consider that source mantle beneath eastern part of PE-1 segment contains the enriched Marion components rather than direct contribution from Marion hotspot. Degree of enrichment (i.e. amount of enriched component) is higher beneath the present eastern part of PE-1 subsegment.

Sato, T. et al. (2013) pointed out that the melt supply center (tip of V-shaped bathymetric structure) between segment PE-1 and NTD-1 has migrated westward. It means that the enriched portion in the source mantle beneath PE-1 and NTD-1 subsegments has migrated westward. Melting of enriched, probably preferentially melting, components induced the strong melt-focusing process to form the V-shape bathymetric structure between PE-1 and NTD-1. This constraints the spatial scale and type of enriched component in depleted mantle.

### References

Sato, T., K. Okino, H. Sato, M. Mizuno, T. Hanyu, and N. Seama (2013), Magmatic activities on the Southwest Indian Ridge between 35E and 40E, the closest segment to the Marion hotspot, *Geochem. Geophys. Geosyst.*, 14, 5286?5307, doi:10.1002/2013GC004814.

Keywords: heterogeneity, mantle, crust, MORB, Southwest Indian Ridge

## Origin of Magnetization High at the Yokoniwa Hydrothermal Vent Fields, the Central Indian Ridge

FUJII, Masakazu<sup>1\*</sup> ; OKINO, Kyoko<sup>1</sup> ; SATO, Taichi<sup>2</sup> ; SATO, Hiroshi<sup>3</sup> ; NAKAMURA, Kentaro<sup>4</sup>

<sup>1</sup>AORI, University of Tokyo, <sup>2</sup>Geological survey of Japan, AIST, <sup>3</sup>Senshu University, <sup>4</sup>University of Tokyo

Measurement of near bottom magnetic anomalies is an effective method to reveal the spatial extent of hydrothermal alteration zone and to find buried hydrothermal vent fields because hydrothermal alteration processes can change crustal magnetization by destruction and creation of magnetic minerals. In the Yokoniwa vent field (YVF), which is located at the top of the non-transform offset massif, called the Yokoniwa Rise, in the southernmost part of the Central Indian Ridge, a high magnetization zone was discovered by AUV r2D4 in 2009. Basalts and ultramafic rocks were found around the YVF, however the origin of positive magnetization and the relationships between high magnetization and hydrothermal activity are remains to be investigated.

In order to constrain the origin of magnetic source near the YVF, we conducted deep-sea geological observation and magnetic measurements using submersible Shinkai 6500 during the R/V Yokosuka cruises, YK09-13 and YK13-03. Vector geomagnetic field were successfully obtained along the all dive tracks at an altitude of ~10 m. The distribution of crustal magnetization is estimated by vertical and horizontal components of magnetic anomalies using the 2-dimesional forward modeling technique and frequency analysis.

In the southern slope of the Yokoniwa Rise, serpentized-peridotites were discovered and absolute magnetization shows entirely low (~6 A/m). On the other hand, just around the YVF, hydrothermal sulfide deposits, tiny dead chimneys, shimmering and talc were observed and absolute magnetization shows relatively high (9 A/m). This magnetization contrast between the YVF and the surrounding area may be attributed to the difference in amount of magnetite, controlled by the degree and the temperature of serpentization. One of the serpentized-peridotite recovered during the cruises showed large amount of magnetite and high natural remanent magnetization. However, the highest absolute magnetization (20 A/m) was discovered at pillow basalt area with thin sediment just ~700 m away from the YVF, implying recent off-axis volcanic activity. Therefore basaltic intrusion beneath the YVF is also possible for the origin of high magnetization. In addition, magnetic iron sulfide (pyrrhotite) grown during hydrothermal circulation, which is proposed at the Rainbow hydrothermal vent field, is also possible.

**Consequently, we proposed three possibilities for the origin of high magnetization at the YVF; serpentized peridotites with high temperature hydrothermal alteration, basaltic intrusion bodies, and pyrrhotites concentration. All of these hypotheses are related to hydrothermal activity. For the further inspection, recovering seafloor rocks and inspection of rock magnetic properties are absolutely necessary.**

Keywords: Seafloor hydrothermal activity, Mid-ocean ridge, Ultramafic rock, Deepsea magnetic anomaly, Off-axis volcanism, Oceani lithosphere

## Three-dimensional seismic structure of the Rainbow area, Mid-Atlantic Ridge 36 degree N

ARAI, Ryuta<sup>1\*</sup> ; DUNN, Robert<sup>1</sup> ; CANALES, Pablo<sup>2</sup> ; SOHN, Robert<sup>2</sup>

<sup>1</sup>University of Hawaii, <sup>2</sup>Woods Hole Oceanographic Institution

Oceanic lithosphere formed along slow-spreading mid-ocean ridges is structurally and compositionally heterogeneous due to spatial and temporal variations in tectonic extension, magmatic accretion, and mantle temperature and composition. While mid-ocean ridges with greater magma supply host a greater abundance of hydrothermal systems, the relative roles of magmatic input, heat advection and faulting in controlling ridge structures are still poorly understood. These are particularly important to understanding formation and evolution of oceanic core complexes where ultramafic-hosted lithologies are exhumed at the seafloor by long-lived detachment faulting. The MARINER (Mid-Atlantic Ridge INtegrated Experiments at Rainbow) seismic and geophysical mapping experiment was designed to examine the relationship between tectonic rifting, heat/melt supply, and oceanic core complex formation at a non-transform offset of the Mid-Atlantic Ridge, 36° 14' N, the site of the ultramafic-hosted Rainbow hydrothermal system. Using the seismic refraction data from this experiment, we constructed three-dimensional tomographic images of the crust and upper mantle around the Rainbow area. The seismic velocity images reveal undulations in crustal thickness across the ultramafic Rainbow massif, indicating temporal variations in melt supply, magmatic processes, and crustal construction. Previous studies suggest that a current heat source for the vents, which probably arises from a magmatic body, is required just beneath the hydrothermal vent, but the tomography does not detect a low-velocity anomaly indicating a significant magmatic system or high-temperature region beneath the Rainbow vent site. The only candidate region for high-temperatures and perhaps melt at shallow levels is much further to the south, and located roughly beneath the central valley of the spreading center. At the Rainbow massif, where mantle rocks have been recovered by direct sampling, mantle velocities near the seafloor are significantly reduced to ~ 5 km/s. This velocity reduction implies that an active hydrothermal circulation system altered the mantle via recharge and discharge of seawater.

Keywords: Slow-spreading ridge, Oceanic core complex, Rainbow hydrothermal field, Mantle alteration, Hydrothermal circulation, Seismic tomography

## Thermal structure of old oceanic upper mantle: Constraints from electrical conductivity imaging in the NW Pacific

BABA, Kiyoshi<sup>1\*</sup> ; TADA, Noriko<sup>2</sup> ; LIANG, Pengfei<sup>1</sup> ; ZHANG, Luolei<sup>1</sup> ; SHIMIZU, Hisayoshi<sup>1</sup> ; UTADA, Hisashi<sup>1</sup>

<sup>1</sup>Earthquake Research Institute, The University of Tokyo, <sup>2</sup>Japan Agency for Marine-Earth Science and Technology

Northwestern part of Pacific plate is very old as the crustal age is over 100 Ma. Seafloor subsidence and heat flow change with age for such old ocean have been explained by cooling of a plate with constant thickness (e.g., Parsons & Sclater, 1977; Stein & Stein, 1992). Electrical conductivity of the upper oceanic mantle typically has resistive layer over a conductive zone reflecting the thermal structure. However, our recent results on the electrical conductivity of the upper mantle beneath northwestern Pacific suggest that a simple plate cooling model can not explain the observations.

We have run marine electromagnetic observation in two areas (Areas A and B) of the northwestern Pacific since 2010. Areas A and B locate northwest and southeast of Shatsky Rise, respectively. Although a part of the observation is still going on, we analyzed the data collected by the last year to obtain magnetotelluric responses and one-dimensional (1-D) electrical conductivity structure beneath the observation areas. Here, we compare the results together with a model obtained for the mantle beneath the Pacific ocean off the Bonin Trench (Area C) by a past project. The mean lithospheric ages of Area A, B, and C are about 130, 140, and 147 Ma, respectively. Based on a plate cooling model, the age differences for the thermal structure among the areas are very small. However, the obtained electrical conductivity models show significant difference in the thickness of the resistive layer. The depth the mantle become more conductive than 0.01 S/m are about 80 km for Area A, about 110 km for Area B, and about 200 km for Area C. These differences can not be reconstructed from the age difference of a single plate cooling model.

Our observations revealed that there is large scale lateral heterogeneity in electrical conductivity. We need to consider another factors rather than age difference of the thermal structure to explain such the lateral heterogeneity.

Keywords: oceanic upper mantle, northwestern Pacific, magnetotellurics, electrical conductivity structure, thermal structure

## PGE abundances and Os isotope ratios of troctolites from pacific oceanic lithosphere

SENDA, Ryoko<sup>1\*</sup>; ISHIKAWA, Akira<sup>2</sup>; MORISHITA, Tomoaki<sup>3</sup>; SUZUKI, Katsuhiko<sup>1</sup>; ISHII, Teruaki<sup>4</sup>

<sup>1</sup>JAMSTEC, <sup>2</sup>Department of Earth Science and Astronomy, The University of Tokyo, <sup>3</sup>School of Natural System, College of Science and Technology, Kanazawa University, <sup>4</sup>Fukada Geological Institute

The structure of oceanic lithosphere becomes much clear in these days. Troctolite is a kind of gabbro, mainly consisting of olivine and calcic plagioclase with minor pyroxene, found in oceanic lithosphere. Melt-rock interactions at mantle-crust transition zone are believed to play a main role for troctolite formation. Troctolites are locally found at Atlantis Massif oceanic core complex, Mid Atlantic Ridge 30 iii N (Blackman et al., 2006), at Kane Megamullion, Mid Atlantic Ridge 23N (Dick et al., 2008; 2010), at Uraniwa Hills, Central Indian Ridge (Nakamura et al., 2009), and at Godzilla Megamullion, Parece Vela Basin of the Philippine Sea (Sanfilippo et al., 2013). They also occurred as sections of the oceanic lithosphere in ophiolites and show similarity to lower crust sections from slow and ultra-slow spreading ridges (e.g., Herbert et al., 1989; Sanfilippo and Tribuzio, 2013). The formation process of the troctolites is in debate. From the ophiolite studies, troctolites were formed as cumulates from primitive basalts in a closed system (Bezzi and Piccardo, 1970; 1971; Borghini and Rampone, 2007). Alternatively, troctolites were the results of a substantial amount of mantle olivine incorporated into the lower oceanic crust (Suhr et al., 2008; Drouin et al., 2009; 2010) based on the studies of oceanic core complex.

Troctolites were also found in the drilled core at site 895 of ODP Leg 147 in Hess Deep, located at a triple junction between EPR and Cocos-Nazca plate boundary. Hess Deep is a small rift with intra-rift ridges, where deep-seated rocks probably formed at EPR are exposed (Francheteau et al., 1990; 1992). Ultramafic and related rocks were expected to be found at the site in fast-spreading ridge system and sequences of dunite, harzburgite, troctolite, and gabbro were actually drilled (Allan and Dick, 1996; Dick and Natland, 1996; Arai and Matsukage, 1996). Troctolite appears to be transitional from dunite to olivine gabbro (Arai and Matsukage, 1998).

Major, trace and platinum group element (PGE) abundances and Os isotope ratios of troctolites from Holes 895C, 895D and 895E were newly measured using XRF, ICP-MS, and TIMS. The samples are clearly divided in two groups by Al<sub>2</sub>O<sub>3</sub>, MgO and NiO. Prichard et al. (1996) reported the PGE and trace element abundances of the ultramafic rocks from Holes 895. Their PGE concentrations of the troctolites were in a similar range to harzburgites and dunites from the same sites and Pt and Pd are enriched in some troctolites. They also found platinum-group alloys and base metals in troctolites. New data set with Os isotope ratios possibly make constraints on the forming process of troctolites under the oceanic ridge.

Keywords: troctolite, Os isotope ratio, PGE abundance, oceanic lithosphere

## The origin for the olivine-rich troctolites from the oceanic lithosphere: remnants of a re-active MOHO

SANFILIPPO, Alessio<sup>1\*</sup> ; MORISHITA, Tomoaki<sup>2</sup> ; HARA, Kaori<sup>2</sup> ; TAMURA, Akihiro<sup>2</sup> ; ARAI, Shoji<sup>2</sup>

<sup>1</sup>University of Pavia, Kanazawa University, <sup>2</sup>Kanazawa University

Olivine-rich troctolites are documented since the early 1970s in the lower crust and mantle sections of the Jurassic oceanic lithosphere exposed along the Alpine-Apennine belt (Italy). These rocks were first interpreted to be cumulates formed by precipitation of olivine and accessory spinel from primitive basalts (Bezzi A. and Piccardo G.B., 1971. Mem. Soc. Geol. It.). The founding of olivine-rich troctolites bodies within the gabbroic sections of the Hess Deep (East Pacific Rise) and Atlantis Massif and Kane Megamullion (Mid Atlantic Ridge) called into question this idea, suggesting that they may represent portion of the crust-mantle transition entrapped during the growth of the lower crust (Arai and Matsukage, 1996, Lithos; Suhr et al., 2008, G-cubed). Recently, Japanese scientific cruises found olivine-rich troctolites associated with mantle harzburgites at the Godzilla Megamullion (Philippine Sea) [3] and at the Uraniwa Hills (Central Indian Ridge) (Nakamura et al., 2009, EPSL; Sanfilippo et al., 2013, J. Petrol.). We show that the olivine-rich troctolites from all these occurrences show peculiar structural and compositional features: i) highly variable forsterite, Ni and Co contents of olivine; ii) high Mg/(Mg+Fe), high Cr<sub>2</sub>O<sub>3</sub> contents, and fractionated incompatible element compositions (i.e. Ti/REE and Zr/REE) of clinopyroxene; iii) the occurrence hydrous silicate mineral inclusions in spinels anomalously enriched in TiO<sub>2</sub>. These features agree with the idea that olivine-rich troctolites formed through reactions between a pre-existing olivine-matrix and migrating melts [see also Renna and Tribuzio, 2011, J. Petrol.). In particular, we suggest that these chemical features were acquired at the crust-mantle transition, through interactions between mantle peridotites and melt stagnating at the base of the igneous crust. The occurrence of olivine-rich troctolites both at slow- to intermediate spreading ridges and at back-arc settings suggests that melt-peridotites reaction processes constrain the Moho under the totality of the oceanic plates.

Keywords: Ocean floor, Peridotite, Troctolite, Melt-Mantle reaction, Moho

## Experimental study of anelasticity of a polycrystalline material for seismological application

TAKEI, Yasuko<sup>1\*</sup> ; YAMAUCHI, Hatsuki<sup>1</sup> ; KARASAWA, Fumiya<sup>2</sup>

<sup>1</sup>Earthquake Research Institute, Univ. of Tokyo, <sup>2</sup>Yahoo, Japan

Rock anelasticity causes dispersion and attenuation of seismic waves. Therefore, for the quantitative interpretation of seismic low velocity and/or low Q regions in the upper mantle, understanding of rock anelasticity is necessary. However, due to the difficulty of forced-oscillation experiment under high-temperature ( $>1000^{\circ}\text{C}$ ) and small strain ( $<10^{-6}$ ) conditions, systematic data on rock anelasticity, needed for the understanding of underlying mechanisms, have not been obtained adequately. To address this lack of data, data from rock analogue (polycrystalline organic borneol) will be of merit. Our recent result published in McCarthy et al (2001) has shown that anelasticity of polycrystalline materials is subject to the Maxwell frequency scaling:  $Q = Q(f/f_m)$ . However, the applicability of this scaling to the seismic dispersion and attenuation has not been guaranteed because experimentally testing frequencies normalized to the Maxwell frequency  $f_m$  of the laboratory samples are usually much lower than the seismic range in the upper mantle ( $10^6 < f/f_m < 10^9$ ). In this study, by using borneol as an analogue to mantle rock, we measured anelasticity up to higher normalized frequencies ( $0.1 < f/f_m < 10^8$ ), and examined the applicability of the Maxwell frequency scaling to these new data. The obtained data show that the Maxwell frequency scaling is no more applicable to higher normalized frequencies than  $f/f_m = 10^4$ , where attenuation spectra plotted as functions of  $f/f_m$  scatter significantly by temperature, grain size, and impurity. Especially, a small amount of impurity (diphenylamine) significantly enhanced the anelastic relaxation. The addition of diphenylamine to borneol significantly lowers the melting temperature from  $T_m=477\text{ K}$  to  $T_m=316\text{ K}$ . From these results, we have speculated that the enhancement of anelasticity with impurity and/or temperature might be scaled by  $T/T_m$ . If this speculation is true and can be generalized to the other polycrystalline materials, it will give a crucial insight for the underlying mechanism. Because  $T/T_m$  is close to one in the upper mantle and it is important to investigate the detailed behavior of anelasticity near  $T/T_m=1$ .

Keywords: anelasticity, polycrystalline material

## Seismic structural changes in the incoming oceanic plate beneath the well-developed horst and grabens

FUJIE, Gou<sup>1\*</sup> ; TAKAHASHI, Tsutomu<sup>1</sup> ; KODAIRA, Shuichi<sup>1</sup> ; OBANA, Koichiro<sup>1</sup> ; YAMADA, Tomoaki<sup>2</sup>

<sup>1</sup>JAMSTEC, <sup>2</sup>ERI, Univ. of Tokyo

Recent seismic, electromagnetic, and thermal structure studies in the trench-outer rise region have revealed the structural changes of the incoming plate in the trench-outer rise region. These structural changes are considered to be caused by the plate bending-related faulting and water penetration. However, there are many unresolved questions such as the maximum depth of the structural changes, the mechanisms of the water penetration, and the source of the water.

The northwestern Pacific margin, where extremely old (more than 120Ma) oceanic plate is subducting, is a good place to study structural changes in the incoming plate prior to subduction, because the horst and graben structure, which is caused by the bending-related faulting, is well developed in this region. However, the former seismic survey could not revealed the seismic structure around the trench axis, where seismic structure is expected to be significantly changed, because of the large water depth in the vicinity of the trench axis.

In 2013, we conducted extensive wide-angle seismic reflection and refraction surveys across the Japan trench with use of ultra-deep Ocean Bottom Seismometers (OBSs). Our obtained data enabled us to reveal the seismic structure in the vicinity of the trench axis, and we confirmed that the bending-related structural changes reach to the top of the oceanic crust. In addition, in the record sections obtained at the deep grabens, we observed seismic waves that laterally propagate within the sedimentary layer as well as the phases vertically propagate within the sedimentary layer. These two phases provided us new insights to the sedimentary structure, which implies that the bottom of the sedimentary layer can be the water source to the oceanic crust in the trench-outer rise region.

Keywords: oceanic plate, trench-outer rise region, bending-related faults, seismic structure, water contents, ocean bottom seismometer

## Mafic minerals within a sediment core sampled by ABISMO in Mariana Trench

MICHIBAYASHI, Katsuyoshi<sup>1\*</sup>; TERUMINE, Naonobu<sup>2</sup>; HARIGANE, Yumiko<sup>3</sup>; NUNOURA, Takuro<sup>4</sup>; UEHARA, Shigeki<sup>1</sup>; OHARA, Yasuhiko<sup>5</sup>; MIYAZAKI, Junichi<sup>4</sup>; TAKAI, Ken<sup>4</sup>

<sup>1</sup>Institute of Geosciences, Shizuoka University, <sup>2</sup>Institute of Geosciences, Shizuoka University, <sup>3</sup>AIST/GSJ, <sup>4</sup>JAMSTEC, <sup>5</sup>Hydrographic and Oceanographic Department of Japan

Mariana Trench is one of the deepest oceans in the world more than 10,000 m depth. Although the mantle section outcrops along the land-side slope of the southern Mariana Trench, the studied depth so far is approximately shallower than 7,000 m and therefore few geological information is available for the mantle section deeper than 7,000 m. In 2008, a sediment core has been sampled at 10,350 m in Challenger Deep of Mariana Trench by ABISMO (Automatic Bottom Inspection and Sediment Mobile) during KR08-05 cruise. The sediment core is 161.5 cm in length and contains mafic sandy grains such as olivine and spinel. In this study, we sampled the mafic minerals from the sediment core and analyzed their major element compositions. As a result, the chemical compositions of the mafic sandy grains were compatible with those of mafic minerals within the peridotites along the land-side slope of Mariana Trench shallower than 7,000 m. We will discuss the origin of these sandy grains.

Keywords: ABISMO, Mariana Trench, Challenger Deep, sediment core, spinel, olivine

## High Ni and Mg olivine as a time recorder of chromitite P-T history

MIURA, Makoto<sup>1\*</sup> ; ARAI, Shoji<sup>1</sup> ; YAMAMOTO, Shinji<sup>2</sup> ; SHMELEV, Vladimir<sup>3</sup>

<sup>1</sup>Department of Earth Sciences, Kanazawa University, <sup>2</sup>Department of Earth Science and Astronomy, University of Tokyo,

<sup>3</sup>Institute of Geology and Geochemistry, Ural Branch Russian Academy of Sciences

High Ni and Mg olivines were found in dunites enveloping podiform chromitites from Oman, Ray-Iz and Luobusa ophiolites. These high Ni and Mg olivines occur only in dunite adjacent to chromitite. This characteristic suggests subsolidus Ni and Mg diffusion from the chromites of the chromitite. In the case of dunite enveloping concordant chromitite from Oman ophiolite, olivines show high NiO (up to 0.5 wt %) and Fo (around 92 mol %) contents. This is not the case, however, for the dunite envelope around the discordant chromitite in the Oman ophiolite. On the other hand, olivines in dunite enveloping UHP chromitites from Ray-Iz and Luobusa ophiolites are extraordinarily high in Fo value (94 - 96) and NiO (around 0.5 wt %). Silicate exsolution lamellae in spinel from UHP chromitites and concordant chromitite suggest that these chromitites have experienced substantial cooling, and probably decompression, for a longer period than the discordant chromitite from Oman. According to the well-known Ni and Mg diffusion coefficients in olivine, the high-Ni and -Mg olivine in the dunite envelope may constrain the cooling duration of the chromitite and the history of ophiolite. Podiform chromitites are enigmatic in origin, and their origins should be systematically classified to understand concerning mantle processes. Their temporal relationship is a clue to solve this problem.

Keywords: Olivine, Ni and Mg diffusion, Podiform chromitite, Low pressure chromitite, Ultra-high pressure chromitite, P-T history

## Geochemistry and genetic conditions of primary boninites from the Ogasawara Island Group and Oman ophiolite

KITAMURA, Keitaro<sup>1\*</sup>; KANAYAMA, Kyoko<sup>1</sup>; UMINO, Susumu<sup>1</sup>; ISHIZUKA, Osamu<sup>2</sup>; KUSANO, Yuki<sup>1</sup>

<sup>1</sup>Department of Earth Sciences, Kanazawa University, <sup>2</sup>Geological Survey of Japan/AIST

Subduction initiation and arc crust evolution along oceanic plate boundaries are fundamental processes that modify oceanic lithosphere and promotes the material evolution of the Earth. How subduction of oceanic plates initiates and develops largely depend on the thermochemical structure and mechanical strength of the colliding two plates. The resulting conditions of the wedge mantle can be best represented by the varying geochemistry of primary magmas produced through the subduction initiation. For example, the subduction zone in the Izu-Bonin (Ogasawara)-Mariana (IBM) arc started with an intense high-Si to low-Si boninite magmatism during 48-45 Ma (Ishizuka et al., 2006; Kanayama et al., 2012). By contrast, the subduction stage of the Oman Ophiolite lacked typical boninite and is characterized by the low-Si boninite magmatism (Ishikawa et al., 2002; Kusano et al., 2014). Because of its high Mg#s and andesitic chemistry, boninite is generally considered to be a candidate of a primary magma derived from the hydrous upper mantle, and therefore, its compositional variations reflect various thermochemical conditions of the source mantle. The geochemical and petrological studies on boninite magma genesis can provide crucial information on the evolution of arc and the formation of continental crust. Boninites are distinct from ordinary arc magmas in highly depleted U-shaped and depleted spoon-shaped chondrite-normalized rare earth elements (REE) patterns.

We have investigated melt (glass) inclusions enclosed by boninite-derived chrome spinel grains in beach sand, called “uguisu-zuna” from Ogasawara islands, and in wadi sand from the Oman Ophiolite. We analyzed major- and trace-element compositions of the boninitic melt inclusions by EPMA and LA-ICP-MS (Kanazawa Univ.) and H<sub>2</sub>O by SIMS (Hokkaido Univ. Creative Research Institution). Glass inclusions in spinel have more Mg-rich compositions than aphyric whole rocks, indicating their primitive nature since derivation from the source mantle, which experienced least modification by the processes such as crystal fractionation, and assimilation and contamination by the crust. Volatile measurements of melt inclusions confirmed that they were only slightly degassed and retain primitive contents. Five geochemical types (BIC-1~5) are identified among boninites from the Ogasawara Islands and a single geochemical type from the Oman Ophiolite. Both Ogasawara and Oman low-Si boninites show lower H<sub>2</sub>O contents than high-Si boninites. Assuming that the most magnesium-rich melts of each geochemical type in Ogasawara and Oman boninites coexisted with olivine and orthopyroxene, the P-T conditions of these primary boninite magmas were estimated by using the geothermobarometers of Putirka et al. (2007) and Putirka (2008). High-Si boninites erupted on the Ogasawara Islands during 48-46 Ma were generated at 1400-1440 °C and 0.7-0.9 GPa, whereas the subsequent low-Si boninite at 45 Ma formed at 1380-1400 °C and 0.8-0.95 GPa. This suggest that the geothermal gradient descended from 48 Ma to 45 Ma. On the other hand, low-Si boninite from the Oman Ophiolite was generated at 1320 °C and 0.5 GPa. Hence, it is apparent that the wedge mantle beneath the proto-IBM arc was significantly hotter than that in the Oman paleoarc.

Keywords: subduction initiation, IBM forearc, Oman Ophiolite, high-Si boninite, low-Si boninite, melt inclusion

## Thermo-chemical evolution of mantle wedge during the incipient stage of the Izu-Ogasawara-Mariana subduction zone

KANAYAMA, Kyoko<sup>1\*</sup>; KITAMURA, Keitaro<sup>2</sup>; UMINO, Susumu<sup>1</sup>; ISHIZUKA, Osamu<sup>3</sup>

<sup>1</sup>College of Science and Engineering, Kanazawa University, <sup>2</sup>Graduate School of Natural Science and Technology, Kanazawa University, <sup>3</sup>Geological Survey of Japan/AIST

It is essential to understand the processes of subduction zone initiation and evolution of oceanic arcs which promote the development of Earth's structure and composition. We present the genetic conditions of the Eocene magmas from the Ogasawara (Bonin) Ridge and discuss the thermo-chemical structure of the mantle wedge beneath the Ogasawara region during the incipient stages of the IBM arc. On the Ogasawara Ridge, MORB-like basalt (forearc basalt: FAB) is generated just after the beginning of subduction of the Pacific Plate at 52 Ma, followed by ultra-depleted high-Si boninite activities began at 48Ma. This high-Si boninite magmatism gradually changed through less-depleted low-Si boninite at 45 Ma to arc tholeiite and calc-alkaline magmatism [1, 2].

Major element compositions of high- and low-Si boninites are similar to those of experimentally produced melts of harzburgite [3] and lherzolite [e.g. 4], respectively. Ultra low concentrations in rare earth elements ( $Yb > 0.3$  ppm) of high-Si boninite also indicate a depleted harzburgite source. On the other hand, characteristically high Zr/Ti ratio ( $< 0.04$ ) of boninites from the Ogasawara Islands reflects high contributions of slab melt [2]. FAB is produced by less than 10 % fractional melting of MORB source mantle, leaving residue of moderately depleted lherzolite. This suggests that the residue of FAB cannot be the highly depleted source of high-Si boninite.

P-T conditions at which the most primitive boninitic melts can coexist with harzburgite are 1430 °C and 0.83-0.96 GPa for high-Si boninite ( $MgO=23$ ,  $H_2O=3.2$  wt%) and 1380 °C and 0.86 GPa for low-Si boninite ( $MgO=19$ ,  $H_2O=2.6$  wt%) [5]. Genetic conditions of magmas other than boninite are dry, ~1350 °C and 1.3-1.7 GPa for FAB and water-undersaturated (0-0.5 wt%), 1300-1350 °C and 1-1.2 GPa for arc tholeiitic and calc-alkaline magmas, which were estimated by comparing calculated primitive liquid compositions with experimentally produced liquid compositions of lherzolite melting [e.g.4].

Mantle potential temperatures ( $T_p$ ) calculated based on MgO content of primary magmas are 1500 °C for high-Si boninite and 1450 °C for low-Si boninite, which are higher than the ambient mantle ( $T_p=1300-1400$ ). Especially  $T_p$  for high-Si boninite is comparable to  $T_{ps}$  of mantle plumes [6]. This result is consistent with plume-related magmatism (51-45Ma) in the West Philippine Basin simultaneously with the high-Si boninite magmatism in the Ogasawara Ridge [7]. The ultra-depleted source of high-Si boninite is possibly the residue of the plume-related magmatism.  $T_p$  of FAB and arc tholeiitic and calc-alkaline magmas is 1400 °C, equivalent to the ordinary oceanic mantle.

From the above, the thermo-chemical history of the mantle wedge beneath the Ogasawara Ridge during the incipient stage of the IBM subduction zone is advocated as follows; Spontaneous sinking of old, dense Pacific Plate induced upwelling of asthenosphere which melted to produce FAB in eastern margin of the Philippine Sea Plate at 52 Ma. At 48 Ma, depleted residual harzburgite of plume-related magmatism upwelled from deeper (~3.5 GPa ?) asthenosphere to 1 GPa, suffering flux melting incorporating slab melt to generate the high-Si boninite magma. By 45 Ma, shallow mantle wedge was cooled by the subducted slab and asthenosphere began circulating in the wedge. As a result, magma composition changed from high-Si boninite through low-Si boninite to arc tholeiite and calc-alkaline magmas more fertile than the Quaternary frontal lava. Subsequently the IBM subduction zone changed to a stable arc-trench system.

[1] Ishizuka et al. (2011) EPSL, 306, 229-240. [2] Kanayama et al. (2012) Island Arc, 21, 288-316. [3] Falloon and Danyushevsky (2000) J. Petrol., 41, 257-283. [4] Hirose and Kawamoto (1995) EPSL, 133, 463-473. [5] Kitamura et al. (2014) JPGU. [6] Herzberg and Gazel (2009) Nature, 458, 619-623. [7] Ishizuka et al. (2013) Geology, 41, 1011-1014.

Keywords: Ogasawara (Bonin) Islands, boninite, mantle wedge, IBM arc, mantle potential temperature, subduction zone

## Hot and ephemeral subduction zone magmatisms in the Oman Ophiolite

KUSANO, Yuki<sup>1\*</sup> ; KITAMURA, Keitaro<sup>1</sup> ; ADACHI, Yoshiko<sup>2</sup> ; SHINJO, Ryuichi<sup>3</sup> ; UMINO, Susumu<sup>1</sup> ; MIYASHITA, Sumio<sup>2</sup>

<sup>1</sup>Kanazawa University, <sup>2</sup>Niigata University, <sup>3</sup>University of Ryukyus

Subduction zone is initiated by descending oceanic plate at the plate boundary and a counter flow of the mantle advances growth of the wedge mantle in the Izu-Ogasawara-Mariana arc (e.g. Stern, 2004). But it is questioned that do initial arc always develop a long-survived subduction zone? We present detailed volcanostratigraphy, petrology and geochemistry of short-lived juvenile arc tholeiite and subsequent boninite magmatism from the northern Oman ophiolite.

The Oman ophiolite belonging to the Tethys ophiolite belt is one of the best places to investigate magmatic and volcanic developing processes of an infant arc. The Ophiolite had formed on a spreading axis and followed by subduction stage magmatism at approximately 100 Ma. The V2 sequence was constructed by initial arc magmatism begun <2 m.y. after the spreading ridge stage (e.g. Hacker et al., 1996). Based on the radiolarian fossil age, the V2 volcanism ceased 2-3 m.y. after the ridge stage (Kurihara and Hara, 2012), therefore, it seems to record short-spanned island arc magmatism.

An 1110 m thick V2 sequence is divided into the lower 970 m (LV2) and upper 140 m (UV2) thick subsequences by a 1.0 m thick sedimentary layer in Wadi Bidi. Pahoehoe flows dominate in the lower part of the LV2, while the upper part consists mainly of sheet flows with intervened few pelagic sediments, a fissure vent and a cylindrical plug. In addition to the presence of feeder conduits, the flow-dominant lithofacies with a few thin sedimentary interbeds in the LV2 indicates that the study area was the center of a monogenetic volcano grown in a short period. The LV2 consist of arc tholeiite with orthopyroxene phenocrysts increasing in amount upward. The UV2 is composed of sheet flows overlain by a 2.0 m thick subaqueous pyroclastic fall deposit. They are boninite containing olivine and two-pyroxene phenocrysts with plagioclase in the groundmass. Successive orthopyroxene-bearing arc tholeiitic volcanism in the LV2 followed by a relatively small amount of boninite lavas in the UV2 overlain by thick pelagic sediments suggests that the infant arc volcanism was short lived and terminated long before the ophiolite obduction.

Keywords: High-T subduction zone, Initial arc magmatism, Boninite, Oman Ophiolite

## Fate of high-T subduction zone and the obduction of the Oman Ophiolite

UMINO, Susumu<sup>1\*</sup>; KUSANO, Yuki<sup>1</sup>; KITAMURA, Keitaro<sup>1</sup>; NAGAISHI, Kazuya<sup>2</sup>; ISHIKAWA, Tsuyoshi<sup>3</sup>; KANAYAMA, Kyoko<sup>1</sup>

<sup>1</sup>Department of Earth Sciences, Kanazawa University, <sup>2</sup>Marine Works Japan, <sup>3</sup>JAMSTEC

Obduction of ophiolitic bodies onto continental crust inevitably follows a tectonic event of conversion from divergence to convergence of plates. This is commonly accomplished by the formation of intraoceanic subduction zone near the ridge axis, where lithospheric lid is thinnest and weakest, and accompanies the boninite volcanism [3]. The upper part of the subducted slab is metamorphosed and later thrust over onto a continent with the overlying mantle to become " the metamorphic sole ". Known examples of metamorphic soles record peak T-P of 600~840 °C and ~1 GPa, whereas the thickness of overlying ophiolite sheets are only 10-20 km, yielding too small lithospheric load compared to the metamorphic pressure of the sole [4]. This discrepancy has been explained that the ophiolite sheet and the metamorphic sole formed at discrete places were emplaced and superposed at the same place during the obduction process [3].

However, we have demonstrated by examining the trace element geochemistry of the arc magmas and metamorphic sole of the Oman Ophiolite that fluid liberated from the metamorphic sole triggered flux melting of the overlying depleted mantle peridotite and produced arc tholeiitic basalt magma first, and subsequently low-Si boninite magma. Therefore, the ophiolite and the underlying metamorphic sole did not form independently at distant places, but were formed and transported together as an intact body with the present structural relationship. Genetic conditions estimated for a primitive boninite melt with 16 wt% MgO enclosed by Cr spinel indicate the segregation pressure of 0.5 GPa and 1320 °C from the mantle with the potential T of 1400 °C [1, Kusano et al., this session]. Thus, the boninite magma should have segregated from the mantle at a depth >17 km. Nevertheless, the present ophiolite body has the maximum thickness <15 km.

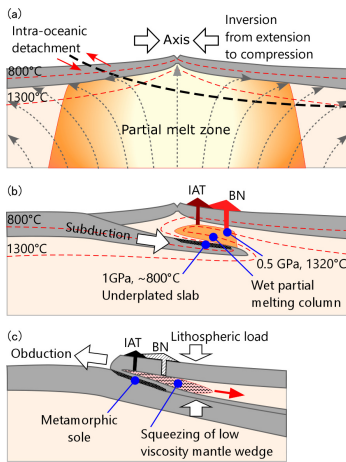
The above lines of evidence urged us to propose the following model; Conversion from spreading to closure of the Tethys resulted in the subduction of young and hot oceanic lithosphere beneath the Tethyan ridge axis. The oceanic crust of the subducted slab was metamorphosed to cpx-bearing amphibolite at a depth of ~35 km and 800 °C. Trace elements and Nd-isotopic evidence indicate fluids and partial melt of subducted sediments liberated from the dehydrated slab migrated upward and formed a partially melted column in the wedge mantle [6, 7]. Primary boninite magmas segregated from the residual harzburgite on the top of the melting column at a depth of ~17 km and at 1320 °C and ascended to form dunite channels and depleted zones through the uppermost lithospheric mantle [8]. Because serpentine and chlorite are unstable >800 °C, the subducted crustal rocks are metamorphosed to amphibolite and the overlying mantle peridotite becomes amphibolite-bearing lherzolite. The lack of mineral phases which could act as lubricant caused large friction and eventual cohesion of the metamorphic slab and hanging wall of the mantle peridotite. Because of the large mechanical strength of the upper crustal and the lower mantle section of the slab, the lower slab of lithospheric mantle are decoupled from the crustal upper slab and continued to subduct without dehydration because the lower slab was virtually anhydrous. This terminated the Oman arc volcanism in a few million years with the production of boninite magma. The strongly coupled upper slab with the overlying wedge mantle obducted together onto the Arabian Peninsula as the metamorphic sole. During the course of thrusting toward the continent, the hot and partially molten asthenospheric mantle in the wedge was squeezed and flattened by the load of the overlying lithosphere, resulted in the present structure of the thin (<15 km) ophiolite sheets underlain by the metamorphic sole formed at a high pressure ~1 GPa.

Keywords: Oman Ophiolite, boninite, high-T subduction zone, metamorphic sole, subduction initiation, obduction

SIT41-19

Room:314

Time:April 28 17:00-17:15



## Magmatic diversity of the ultramafic rock in the oceanic crustal sequence, Oman ophiolite

KANEKO, Ryu<sup>1\*</sup> ; ADACHI, Yoshiko<sup>2</sup> ; MIYASHITA, Sumio<sup>2</sup>

<sup>1</sup>Graduate School of Science and Technology, Niigata University, <sup>2</sup>Niigata University

Although all the wehrlitic intrusions in the Oman Ophiolite are regarded as a single group (e.g. Koepke et al. 2009), there are two different types of wehrlitic intrusions. The first are ordinary wehrlitic intrusions that have similar features to the crustal sequence of V1 (MOR basalt). The second are a depleted type characterized by the appearance of true wehrlite and depleted mineral compositions (Adachi & Miyashita 2003; Yamasaki et al. 2006; Goodenough et al. 2010). The former and latter groups are linked to V1 and V2 magmatism, respectively.

We report the discovery of a new occurrence of the ultramafic rock in the oceanic crustal sequence from the Oman ophiolite, which does not intrude into the crustal sequence. This ultramafic rock is referred to as the Lasail-South complex, and the oldest rock in the study area because of being intruded by sheeted dyke complex. TiO<sub>2</sub> and Na<sub>2</sub>O contents of clinopyroxene from the complex range 0.06-0.59 and 0.09-0.42 wt%, respectively, and are similar to the fractional crystallization trend of oceanic gabbro. Co-variation of Mg values of clinopyroxene and An contents of plagioclase show that most of samples plot in the Oman layered gabbro field. Although mineral compositions of the Lasail-South complex show characteristic of mid-ocean ridge magmatism, the complex mainly comprises plagioclase?hornblende lherzolite, olivine clinopyroxenite and clinopyroxenite. Such rock assemblage of is different from the assemblage of the oceanic crust of the Oman ophiolite. The Lasail-South complex shows intermediate characteristic of mid-ocean ridge and island arc magmatisms, and we attempt to discuss the origin of the complex.

### References

- Adachi and Miyashita, 2003. *Geochemistry Geophysics Geosystems*, **4**(9), doi.org/10.1029/2001GC000272.  
Goodenough et al., 2010. *Arabian Journal of Geosciences*, **3**, 439-458, doi.org/10.1007/s12517-010-0177-3.  
Koepke et al., 2009. *Geochemistry Geophysics Geosystems*, **10**, 10002, doi.org/10.1029/2009GC002488.  
Yamasaki et al., 2006. *Earth and Planetary Science Letters*, **251**, 52-65, doi.org/10.1016/j.epsl.2006.08.027.

Keywords: Oman ophiolite, ultramafic rock, mid-ocean ridge magmatism, island arc magmatism

## Compositionally and genetically distinct domains found in the southernmost Salahi mantle section in the Oman ophiolite

FUJII, Satoru<sup>1\*</sup> ; TAKAZAWA, Eiichi<sup>2</sup>

<sup>1</sup>Graduate school Science and Technology, Niigata University, <sup>2</sup>Faculty of Science, Niigata University

We investigate spatial variability in mineral compositions in the southernmost part of the Salahi mantle section and discuss genetic relationship between highly refractory peridotites and less refractory plagioclase-bearing peridotites in this region. The study separates the study area into two domains based on spinel Cr# such as high Cr# domain in the eastern part that is closer to Moho and low Cr# domain in the central part. Concordant dunites commonly occur in the low Cr# domain whereas discordant dunites are common in the high Cr# domain. Plagioclase-bearing peridotites and wehrlite also occur in the low Cr# region.

Highly refractory dunite with spinel Cr# >0.7 frequently occurs in the high Cr# domain. In the low Cr# domain, spinel Cr# is low and ranges from 0.47 to 0.57. We analyzed clinopyroxene (cpx) in dunites and harzburgite from both domains for REE abundances by LA-ICP-MS. The results show that harzburgite cpxs in the high Cr# domain and low Cr# domain are highly depleted in LREE ([Ce]CH = 0.01~0.02) with [Yb]CH = 2~3. Dunite cpxs in the low Cr# domain have REE abundances similar to the harzburgites in the same outcrop whereas those in the high Cr# domain are enriched in LREE relative to the harzburgite cpxs in the same outcrop. This implies that dunite cpxs in the high Cr# domain were reacted with LREE-enriched fluid infiltrated from the base of the ophiolite.

In the low Cr# domain, plagioclase-bearing dunite, plagioclase-bearing lherzolite vein occur and phlogopite-bearing wehrlite discordantly cuts them. The spinel Cr# of these dunites are in a range from 0.46 to 0.56. Abundances of REE in a melt in equilibrium with cpx in plagioclase-bearing peridotites and associated dunites are similar to those of N-MORB. On other hand, a melt in equilibrium with wehrlite cpx resembles to those of boninitic dikes from the Fizh block in the northern Oman ophiolite (Yamazaki, 2013). From the field occurrence, plagioclase-bearing dunite and plagioclase-bearing lherzolite formed by a reaction with MORB melt beneath spreading ridge whereas cumulative wehrlite was crystallized from a boninitic melt.

## Mafic and ultramafic rocks along the southern Central Indian Ridge close to the Kairei Hydrothermal Field

NISHIMURA, Takuma<sup>1</sup> ; HARIGANE, Yumiko<sup>2</sup> ; MICHIBAYASHI, Katsuyoshi<sup>3\*</sup> ; MORISHITA, Tomoaki<sup>4</sup> ; SATO, Hiroshi<sup>5</sup>

<sup>1</sup>Institute of Geosciences, Shizuoka University, <sup>2</sup>AIST/GSJ, <sup>3</sup>Institute of Geosciences, Shizuoka University, <sup>4</sup>School of Natural System, College of Science and Technology, Kanazawa University, <sup>5</sup>School of Business Administration, Senshu University

The central Indian Ridge (CIR) is situated at the north of the Rodrigues Triple Junction (RTJ) and is a slow- to intermediate-spreading mid-ocean ridge with a spreading rate increasing from 30 mm/year in full rate near the Equator to 49 mm/year in full rate at the RTJ. In the southern CIR near RTJ, the Kairei Hydrothermal Field (KHF) was discovered in August 2000 as the first directly observed hydrothermal vent site in the Indian Ocean. Recently, KH-10-06 cruise aboard R/V Hakuho-maru was organized for understanding the hydrothermal system and geological feature around KHF. In this study, we present the petrography of mafic and ultramafic rocks dredged from the vicinity of the KHF during KH-10-06 cruise. A total of 76 samples have been studied from 9 sites, including 24 ultramafic rocks and 38 mafic rocks and 14 other rocks. Most of them are remarkably altered and hydrated. We classified them into sub-groups based on their textures and mineral assemblies. The ultramafic rocks were classified into 5 sub-groups: 1 peridotite, 2 pyroxenites, 3 serpentized peridotites, 9 olivine-bearing serpentinites and 9 serpentinites. The mafic rocks were classified into 8 sub-groups: 21 Fe-Ti oxide gabbros, 4 gabbros including 2 mylonites, 3 olivine gabbros, 7 gabbroic rocks with various textures and 8 amphibole-rich gabbros. The other rocks consist of 5 aragonites and 9 hydrothermally altered rocks.

Keywords: mafic rock, ultramafic rock, Central Indian Ridge, Kairei Hydrothermal Field

## Upper mantle electrical resistivity structure at the continental margin of East Antarctica

MATSUNO, Tetsuo<sup>1\*</sup> ; NOGI, Yoshifumi<sup>1</sup> ; SEAMA, Nobukazu<sup>2</sup>

<sup>1</sup>National Institute of Polar Research, <sup>2</sup>Kobe University

The breakup of the Gondwana supercontinent is one of targets of the study on the plate tectonics and related mantle dynamics. The crust and the upper mantle structure under the western Cosmonauts Sea at the continental margin of East Antarctica, where a rifting of Gondwana and a subsequent seafloor spreading occurred, are anticipated to reflect the breakup process of Gondwana. We carried out a marine electromagnetic experiment to reveal an electrical resistivity structure at depth of the crust and the upper mantle under the western Cosmonauts Sea. Time variations of the electromagnetic field were acquired at two seafloor sites in the experiment. The time variations data were processed on the basis of the magnetotelluric (MT) method. The MT response function was obtained after considering influence of non-plane magnetic field sources at high geomagnetic co-latitude. The obtained MT response functions and polar diagrams imply that the MT responses involve topographic distortion and/or reflect a higher dimensional resistivity structure under the observational sites. Three dimensional forward modeling was conducted to examine influence on the observed MT responses from the topographic variation around the observational sites and a conductive layer just under the sites, which is mostly regarded as sediment. The results of the forward modeling clearly show that the topographic variation and the surface conductive layer have severe influence on the observed MT responses. A series of 3-D forward modeling with the topographic variation and the surface conductive layer was implemented to examine a resistivity structure at depth of the crust and the upper mantle. The results indicate that the resistivity structure is explained by a two-layer resistivity structure, in which the upper layer is resistive and the lower layer is conductive. The upper resistive and the lower conductive layers likely represent dry and water/melt rich oceanic upper mantle, respectively. The thickness of the upper resistive layer is thinner than that expected for a typical oceanic upper mantle of the seafloor age of the study area. The thin upper resistive layer may require high temperature and high water/melt anomalies that were generated through mantle convection, which was related to the breakup process of Gondwana at the continental margin of East Antarctica.

## Geochemical characteristics of the peridotites from the southern Mariana forearc

SAKUYAMA, Tetsuya<sup>1\*</sup>; ISHII, Teruaki<sup>4</sup>; MICHIBAYASHI, Katsuyoshi<sup>2</sup>; OHARA, Yasuhiko<sup>3</sup>; CHANG, Qing<sup>1</sup>; HARAGUCHI, Satoru<sup>5</sup>; KIMURA, Jun-ichi<sup>1</sup>

<sup>1</sup>JAMSTEC, <sup>2</sup>Shizuoka Univ., <sup>3</sup>Japan Coast Guard, <sup>4</sup>Fukada Geological Institute, <sup>5</sup>Faculty of Engineering, Univ. Tokyo

Dehydration of a subducting oceanic plate and infiltration of the fluid/melt released from the oceanic plate are thought to be the key processes to invoke melting of the wedge mantle. Although a number of studies on volcanic rocks in arcs have been conducted to reveal a material recycling process at subduction zone, understanding of geochemical development process within the wedge mantle is still not as far advanced. The southern Mariana forearc is one of the best locations on the Earth to investigate issues above, since serpentinized peridotites are widely exposed on the inner slope of the Mariana Trench. We have collected peridotite samples obtained by dredging and Shinkai diving from 3000 – 7000 mbsl at the southern Mariana Trench. The dredge and dive points are geographically grouped into three sites: site 1 (KH98-1-D1, KH98-1-D2, and 6K-973), 2 (KH03-3, KH98-1-D3, and 6K-1094), and 3 (6K-1095, 6K-1232, 6K-1233, and 6K-1234) from the east to the west. We conducted EPMA and LA-ICP-MS analyses on minerals in the recovered samples to reveal geochemical development process of the wedge mantle.

Peridotites from the easternmost site 1 consist of olivine (Fo# = 90 – 91), orthopyroxene (Mg# = 90 – 91), spinel (Cr# = 40 – 50), clinopyroxene (Mg# = 89 – 93), tremolite (TiO<sub>2</sub> = 0 – 0.4 wt%), pargasite (TiO<sub>2</sub> = 2.0 – 2.5 wt%), plagioclase, and serpentine. Clinopyroxene and pargasite exhibit LREE-depleted (type C1 and A1, respectively) and orthopyroxene LREE- and MREE-depleted patterns (type O1) in a chondrite-normalized diagram.

Peridotites from the westernmost site 3 consist of olivine (Fo# = 91 – 92.5), orthopyroxene (Mg# = 91 – 93.5), spinel (Cr# = 45 – 75), clinopyroxene (Mg# = 94 – 96), tremolite (TiO<sub>2</sub> = 0 – 0.2 wt%) and serpentine. Some clinopyroxene exhibits LREE-enriched convex upward pattern (type C2), others strong LREE- and MREE-enriched REE pattern (type C3). Tremolite and orthopyroxene exhibit LREE-enriched convex upward (type A3) and weakly LREE-enriched convex upward REE patterns (type O2), respectively. HREE, Ti, and Y abundances of type C3 clinopyroxene are higher and their LREE and Sr abundances lower than those of type C1 clinopyroxene.

Peridotites from the middle site 2 show intermediate characteristics between site 1 and 3. They consist of olivine (Fo# = 90 – 92), orthopyroxene (Mg# = 91 – 92.5), spinel (Cr# = 45 – 52), clinopyroxene (Mg# = ~95), pargasite (TiO<sub>2</sub> = 0.8 – 1.7 wt%), tremolite (TiO<sub>2</sub> = 0 – 0.2 wt%), plagioclase and serpentine. Some clinopyroxene exhibits C1-type REE pattern and coexists with A1-type pargasite, while other clinopyroxene exhibits LREE- and MREE-depleted patterns (type C2) coexisting with LREE- and MREE-depleted tremolite with weak enrichment in LREE (type A2).

Compared to results of high-pressure melting experiments on peridotite, monotonous increase of Mg# of olivine, clinopyroxene, and orthopyroxene as well as Cr# of spinel from site 1 to 3 suggests increase of melting degree of the mantle peridotite from site 1 to 3. Monotonous decrease of HREEs, Ti, Y, Zr, and Hf abundance from C1- to C3-type clinopyroxene, from A1- to A3-type amphibole, and from O1- to O2-type orthopyroxene, is consistent with major element variations above. However, in contrast to the observation above, LREE and LILE abundance increase from C1- to C3-type clinopyroxene, from A1- to A3-type amphibole, and from O1- to O2-type orthopyroxene, suggesting involvement of melt/fluid enriched in such elements.

LREE-enriched clinopyroxene and amphibole have been found from mantle xenoliths and subaerial peridotite complex. Those clinopyroxene and amphibole have been interpreted as a product of melting and melt separation involving infiltration of LREE-enriched melt/fluid into the melting system. Similarity of geochemical characteristics of type C3 clinopyroxene and A3 amphibole to those in xenoliths or peridotite complexes may suggest involvement of LREE-enriched melt/fluid to the mantle beneath the southern Mariana forearc.

Keywords: Mariana Trench, peridotite, pyroxene, amphibole, trace element

## Petrological features of the peridotite xenoliths in the 1991 Pinatubo dacite and mantle metasomatism by subducted ocean

YOSHIKAWA, Masako<sup>1\*</sup>; TAMURA, Akihiro<sup>2</sup>; ARAI, Shoji<sup>2</sup>; KOBAYASHI, Tetsuo<sup>3</sup>; KAWAMOTO, Tatsuhiko<sup>1</sup>; OKUNO, Mitsuru<sup>4</sup>; PAYOT, Betchaida<sup>2</sup>; RIVERA, Danikko<sup>5</sup>; BARISO, Ericson<sup>5</sup>; MIRABUENO MA., Hannah T.<sup>6</sup>

<sup>1</sup>Institute for Geothermal Sciences, Kyoto Univ., <sup>2</sup>Department of Earth Sciences, Kanazawa Univ., <sup>3</sup>Department of Earth and Environmental Sciences, Kagoshima Univ., <sup>4</sup>Department of Earth System Science, Fukuoka Univ., <sup>5</sup>PHIVOLCS, <sup>6</sup>Institute of Volcanology and Seismology, University of the Philippines

We observed peridotite xenoliths in the dacite of the 1991 pyroclastic flow deposit of Pinatubo volcano, which is located at the volcanic front of the Luzon (Bataan) arc, Luzon island, the Philippines. The Luzon arc is associated with eastward subduction of the South China Sea plate along the Manila Trench. We also found olivine xenocrysts and xenoliths of amphibolite and granitic rocks in the dacitic deposits. The largest xenolith was up to 14 cm across among about 200 collected samples. Selvage of hornblendite, up to 5 mm width, is common between the peridotite and the dacite host.

Arai et al. (1996) classified peridotite xenoliths from Iraya volcano, Batan Island, the Philippines, into coarse grained (C) and fine grained (F) types depend in terms of olivine grain size. The C-type xenoliths are equivalent to ordinary mantle xenoliths from various localities and the F-type xenoliths are quite different in texture, its individual grains being hardly visible by the naked eye and the fine-grained ( $\leq 0.1$  mm) part occupying  $>10$  % by volume (Arai and Kida, 2000). They interpreted that the F-type peridotite was possibly formed from the C-type one by recrystallization assisted by  $\text{SiO}_2$ -rich fluid or melt originated from subducting slab. Such peculiar F-type xenoliths can be observed in the peridotite xenoliths from Avacha volcano on the volcanic front of the Kamchatka arc, Russia (Ishimaru et al., 2007) and at Tubaf and Edison volcanos, Tabar-Lihir-Tang-Feni island arc, which occur in the fore-arc region of the New Ireland intra-oceanic island arc, Papua New Guinea (McInnes et al., 2001). According to their definition, the F-type peridotites occupy about 50 % of 40 Pinatubo samples. Almost all of the Pinatubo C-type xenoliths are spinel harzburgites (olivine + orthopyroxene + amphibole + spinel  $\pm$  clinopyroxene  $\pm$  phlogopite) except a wehrlite and a dunite samples.  $\text{CO}_2$ -bearing saline fluid inclusions were observed in all samples (Kawamoto et al., 2013).

The Sr-Nd isotopic compositions of amphibole from the primary C-type xenolith containing least amounts of fine-grained part are consistent with the most depleted values of the range of andesite and dacite ( $^{87}\text{Sr}/^{86}\text{Sr} = 0.70419 - 0.70425$ ,  $^{143}\text{Nd}/^{144}\text{Nd} = 0.512863 - 0.512924$ ; Castillo et al, 1991; Bernard et al, 1991). Their compositional variation is within a range of South China Sea oceanic basalt (Tu et al., 1992). Multi-element chondrite-normalized patterns of the amphiboles show depleted signatures with enrichment of Ba, Rb, U, in Pb. These enriching elements are considered as fluid mobile during dehydration of subducting mantle, oceanic crust and sediment (e.g. Tatsumi et al., 1986; McCulloch & Gamble, 1991). The present Sr-Nd isotopic and geochemical signatures of the amphibole suggest that the Pinatubo C-type mantle xenoliths have also been metasomatized by aqueous fluids released from subducted oceanic crust beneath the volcanic front.

References; Arai et al., Sci. Rep. Kanazawa Univ., 41, 25-45, 1996; Arai & Kida, Is. Arc, 9, 458-471, 2000; Bernard et al, in Newhall & Punongbayan (eds.) Fire and mud: PHILVOLCS, 767-798, 1991; Castillo & Punongbayan, in Newhall & Punongbayan (eds.) Fire and mud, PHILVOLCS, 799-806, 1991; Ishimaru et al., J. Petrol., 48, 395-433, 2007; Kawamoto et al., PNAS, 110, 9663-9668, 2013; McCulloch & Gamble, EPSL, 102, 358-374, 1991; McInnes et al., EPSL, 188, 169-183, 2001; Tu et al., Chem. Geol., 97, 47-63, 1992.

Keywords: amphibole-bearing peridotite xenolith, Pinatubo, mantle metasomatism, mantle wedge

## Petrology of mafic-ultramafic rocks in the East Taiwan Ophiolite, in the Lichi melange, Taiwan

KOMARU, Chihiro<sup>1\*</sup> ; MORISHITA, Tomoaki<sup>1</sup> ; TAMURA, Akihiro<sup>1</sup> ; ARAI, Shoji<sup>1</sup>

<sup>1</sup>Graduate School of Natural Science, Kanazawa University

Taiwan is located on the border between the Philippine Sea Plate and the Eurasia Plate. The blocks of cherts, volcanic rocks, plutonic rocks (mafic-ultramafic rocks) are widely distributed as exotic blocks in the Lichi melange, southeastern Taiwan (Liou et al., 1977). These ophiolite-like rocks (cherts, volcanic rocks, plutonic rocks) are defined as the East Taiwan Ophiolite (Liou, 1977). The origin of the East Taiwan Ophiolite is still in debate. Three possible candidates are (1) Philippine Sea Plate (Liou, 1974), (2) the north extension of the Luzon volcanic arc (Ota and Kaneko, 2010), and (3) the South China Sea (Suppe et al., 1981). In this study, we focus on petrological characteristics of gabbros and peridotites in the East Taiwan Ophiolite.

In this research, we collected mafic-ultramafic rocks to cover a wide range of variations in terms of mineral variations at each outcrop. The gabbros are classified into troctolite, olivine gabbro, hornblende gabbro, and gabbronorite. Most of ultramafic rocks are extensively serpentized, but have equigranular textures based on shape of relic and pseudomorph minerals except for a few serpentine mylonites. The serpentized peridotites are classified into clinopyroxene-bearing harzburgite and dunite. The Cr# (Cr/(Cr+Al) atomic ratio) and Mg# (Mg/(Mg+Fe) atomic ratio) of spinels in the serpentized peridotites are 0.3-0.6 and 0.3-0.5, respectively. It is well characterized that the high-Cr# spinel (>0.6) coupled with the formation of secondary orthopyroxene are commonly observed in ultramafic xenoliths in Luzon arcs (Arai et al., 2004). We conclude that the East Taiwan Ophiolite is similar with abyssal peridotites and gabbros collected from mid-ocean ridges or back arc basins.

## Petrological evidence for arc-metasomatized peridotites beneath mid-ocean ridges

MORISHITA, Tomoaki<sup>1\*</sup> ; SENDA, Ryoko<sup>3</sup> ; SUZUKI, Katsuhiko<sup>3</sup> ; NAKAMURA, Kentaro<sup>3</sup> ; SATO, Hiroshi<sup>2</sup> ; OKINO, Kyoko<sup>4</sup>

<sup>1</sup>Kanazawa University, <sup>2</sup>JAMSTEC, <sup>3</sup>Senshu University, <sup>4</sup>University of Tokyo

Here we report for the first time petrological evidence of recycled subduction-modified mantle materials beneath the Mid-Ocean Ridge. We conducted several cruises with submersible SHINKAI 6500 dives and dredges in the south end of the Central Indian Ridges (Phenix knoll). We recovered orthopyroxene-rich lithologies coupled with peridotites and gabbros from a small knoll along the present mid-ocean ridge. The orthopyroxene-rich lithologies can be formed by magmatic processes beneath the present mid-ocean ridges by crystallization from ultra-depleted primary melts (Sobolev and Shimizu, 1993, Nature) in the Mid-Ocean ridge system. Orthopyroxene-rich peridotites are also commonly observed in peridotite bodies of suprasubduction ophiolites (e.g., Morishita et al., 2011 Lithos) as well as in several sub-arc xenoliths (McInnes et al., 2001 EPSL; Arai and Kida, 2000 Island Arc; Arai et al., 2004 J. Petrol; Shimizu et al., 2004 Trans. Royal Soc. London; Ishimaru et al., 2007 J. Petrol). It is also well known that 30% of continental upper mantle samples are enriched in OPX/olivine relative to residual peridotite from partial melting of the primitive mantle (e.g., Boyd, 1989 EPSL; Kelemen et al., 1998 EPSL). Silica-enrichment in the uppermost mantle section under island-arcs is explained by infiltration of silica-rich hydrous fluids/melts derived from subducting slabs. The Re-Os system also supports subduction-metasomatized peridotite origins for orthopyroxene-rich lithologies. The Re-Os isotope system is used for a tracer of recycled crustal materials because oceanic/continental crust possess high Re/Os (parent/daughter) ratios, and develop radiogenic Os isotope compositions over time, which can be readily traced as recycled material if mixed back into the convective mantle. We examined the Os-isotopic compositions of the representative samples: dunite, one harzburgite and one olivine-orthopyroxenite, without signs of petrological and chemical modifications caused by the formation of gabbroic veins. The orthopyroxenite is characterized by a distinctively high in radiogenic Os ( $^{187}\text{Os}/^{188}\text{Os}$ ) isotope signatures (0.1475-0.1499) with relatively high in Re contents (382-402 ppt) whereas the Os isotope of the harzburgite is slightly lower than the present-day depleted MORB mantle (0.123-0.126). High  $^{187}\text{Os}/^{188}\text{Os}$  ratio coupled with high Os and Re contents of the olivine-orthopyroxenite cannot be accounted for by in situ  $^{187}\text{Re}$  decay after interaction between MORBs and peridotites for a million years. Radiogenic Os isotope compositions have been reported for MORB glass, and attributed to the presence of recycled oceanic crust in the upper mantle. Mixing of depleted mantle with exotic component that have an isotopic component with high  $^{187}\text{Os}/^{188}\text{Os}$  ratios, i.e., radiogenic Os components, are required for the sample. We evaluate the effect of metasomatism of mantle by slab-derived fluids or melts on Os systematics observed in the samples. We conclude that ancient subduction-modified mantle domains, probably formed at continental margin of the Gondwanaland, now exists beneath the Central Indian Ridge.

Keywords: Mid-Ocean Ridge, Mantle, Peridotite, arc, recycling

---

SGL42-01

Room:419

Time:April 29 09:00-09:30

## Why is the IntCal13 special?

NAKAGAWA, Takeshi<sup>1\*</sup> ; SUIGETSU 2006, Project members<sup>1</sup>

<sup>1</sup>Department of Geography, Newcastle University (UK)

Please see Japanese abstract (the presentation will be in Japanese).

Keywords: IntCal13, Radiocarbon dating, Radiocarbon calibration, Varved sediment, Lake Suigetsu, Marine reservoir effect

## An evaluation of the effect on $^{14}\text{C}$ dating (AMS) by alkaline treatment of the ABA method on charcoal sample

ATSUMI, Shin<sup>1\*</sup>

<sup>1</sup>Tokyo University of Sciences

Charcoal treatment by means of the Acid-Base-Acid (ABA) method (or Acid-Alkali-Acid; AAA method) has been widely used for radiocarbon ( $^{14}\text{C}$ ) dating in the Earth Science and Archaeological field. Although the ABA method is a basic charcoal pretreatment method for  $^{14}\text{C}$  dating, the evaluation of processing conditions of the ABA method based on any chemical indicator does exist few until today. This study aims to clarify the error of  $^{14}\text{C}$  dating caused by the alkaline pretreatment which is not studied hitherto. The author performed 3 types of experiments for the purpose. The first experiment was performed for confirmation of the reproducibility of ges. The second experiment was performed for confirmation of optimal treatment time of an alkaline solution. The third experiment was performed for confirmation of the optimal concentration of alkaline solution for the ABA pretreatment.

The first experiment:  $X^2$  test of the results shows  $T=0.45(df=3;5\% \text{ risk rate } T >12.59)$  for the treated samples which means high convergent validity, while  $T=10.74(df=4;5\% \text{ risk rate } T >9.49)$  for the untreated samples which means large scattering and significant variability.

The second experiment: even after the visual judgment of the completion of alkaline extraction, 3-DF detected humic acid in the retrieved NaOH solution, and Atsumi et. al. (2009) showed that radiocarbon ( $^{14}\text{C}$ ) dating was influenced the existence of humic acid. These results suggest that visual observation is inadequate for the judgment of the completion of alkaline extraction, and that 3-DF is more effective for monitoring the presence of dissolved organic contamination.

The third experiment: three charcoal samples from a single archaeological context were split into 8 aliquots respectively, and treated with 8 different concentrations of NaOH solutions ranging from 0.001 to 2.0 mol/l. Dating results and  $X^2$  tests showed minimum convergence at 1.2 mol/l. This is supported by 3-dimensional fluorescent (3-DF) analysis, which clearly shows different leaching characteristics between 2.0-1.0 and 0.5-0.001 mol/l. 0.5-0.001 mol/l NaOH solutions were too weak in humic leaching capacity at low excitation ranges, which is thought to be the phenomenon that generates the scattering of dates. We recommend using from 1.0 to 1.5 mol/l NaOH for radiocarbon pretreatment.

These results show that the  $^{14}\text{C}$  age is affected by difference of the residual of humic acid caused by the difference of chemical conditions of the pretreatment .

Keywords:  $^{14}\text{C}$  dating, ABA pretreatment, 3-D fluorescent spectroscopy, Humic acid, Charcoal sample

## Dating of sea-floor hydrothermal barite collected at the Okinawa Trough by ESR and radioactive disequilibrium

FUJIWARA, Taisei<sup>2\*</sup> ; TOYODA, Shin<sup>1</sup> ; UCHIDA, Ai<sup>2</sup> ; ISHIBASHI, Jun-ichiro<sup>3</sup> ; NAKAI, Shun'ichi<sup>4</sup> ; TAKAMASA, Asako<sup>5</sup>

<sup>1</sup>Faculty of Science, Okayama University of Science, <sup>2</sup>Graduate School of Science, Okayama University of Science, <sup>3</sup>Faculty of Science, Kyushu University, <sup>4</sup>Earthquake Research Institute, University of Tokyo, <sup>5</sup>National Institute of Radiological Sciences

The temporal change of submarine hydrothermal activities has been an important issue in the aspect of the evolution of hydrothermal systems which is related with ore formation (Urabe, 1995) and biological systems sustained by the chemical species arising from hydrothermal activities (Macdonald et al., 1980). Dating methods using disequilibrium between radioisotopes such as U-Th method (e.g. You and Bickle, 1998), <sup>226</sup>Ra-<sup>210</sup>Pb and <sup>228</sup>Ra-<sup>228</sup>Th method (e.g. Noguchi et al., 2011) have been employed for such studies.

Okumura et al., (2010) made the first practical application of ESR (electron spin resonance) dating technique to a sample of submarine hydrothermal barite to obtain preliminary ages, while Kasuya et al. (1991) first pointed out that barite can be used for ESR dating. Toyoda et al. (2011) determined the optimum ESR condition while Sato et al. (2011) confirmed that the signal is thermally stable enough for an age range of several thousand years. Takamasa et al. (2013) obtained U-Th and ESR ages which are roughly consistent with each other.

The samples were taken by research cruises operated by JAMSTEC. Barite (BaSO<sub>4</sub>) was extracted from hydrothermal sulfide chimney samples taken from two sites at the Okinawa Trough. Blocks of sulfide deposits were cut into pieces, and about 2.0g was crushed. The samples were soaked in 12M hydrochloric acid, left for approximately 24 hours. Then, 13M nitric acid was added. Finally, after rinsing in distilled water, the sample was filtered and dried. Impurities were removed by handpicking. An X-ray diffraction study was made to confirm that the grains are pure barite. After gamma-ray irradiation at Takasaki Advanced Radiation Research Institute, Japan Atomic Energy Agency, they were measured at room temperature with an ESR spectrometer (JES-PX2300) with a microwave power of 1mW, and the magnetic field modulation amplitude of 0.1mT. The bulk Ra concentration was measured by the low background pure Ge gamma ray spectrometer. Assuming that Ra is populated only in barite, the dose rate was calculated with the alpha effectiveness of 0.043 (Toyoda et al., 2012), where the decay of Ra (a half life of 1600 years) was also taken into account.

The obtained ages range from 4.1 to 16000 years, being consistent with detection of <sup>228</sup>Ra in younger samples and radioactive equilibrium/disequilibrium between radium and daughter nuclei. The variation of the ages within each sample is mostly within the statistical error range. The relative order of the ages is consistent with the result of <sup>226</sup>Ra-<sup>210</sup>Pb method, where the difference in absolute ages would be explained by several hydrothermal events that form the chimney. It was found that Yoron Hole field is the youngest, then, Daiyon-Yonaguni Knoll field, Hatoma Knoll field, being nearly equal to Iheya North Knoll field, then Izena Hole field, which is consistent with the direct observation from the submersible.

Keywords: barite, hydrothermal activities, electron spin resonance, dating

## Thermoluminescence property of calcite

OGATA, Manabu<sup>1\*</sup> ; HASEBE, Noriko<sup>1</sup> ; FUKUSHI, Keisuke<sup>1</sup> ; FUJII, Naoki<sup>2</sup> ; SATO, Tsutomu<sup>3</sup> ; ITO, Kazumi<sup>4</sup>

<sup>1</sup>Kanazawa University, <sup>2</sup>RWMC, <sup>3</sup>Hokkaido University, <sup>4</sup>AIST

In earth science, the date of past event is very important. To determine accurate age, we have to select suitable dating method for an analyzed sample.

Thermoluminescence dating method calculates a date from equivalent dose estimated by emitted luminescence when mineral is heated. Thermoluminescence dating has been often applied to carbonate minerals because it emits strong luminescence and wider age range applicable than C14 dating method is an advantage of thermoluminescence dating.

However, thermoluminescence dating of calcite is sometimes problematic; e.g., sensitivity change of calcite occurred through repeated heating of samples, possible anomalous fading, difference in characteristics of luminescence response against different kinds of radiation (e.g., gamma-ray, beta-ray, alpha-ray, and x-ray), and so on.

In this study, calcite from Philippine, Mongol, and synthetic calcite are analysed to understand luminescence characteristics of calcite. Mgnesite is also analyzed to see the effect of chemistry. Luminescence was detected by Photon Multiplier (R649, HMA-MATSU) with filter of 600-650nm. Chemical composition, especially impurity concentration was measured by LA-ICP-MS.

First, we evaluate X-ray induced thermoluminescence property of each sample.

Second, we measured luminescence caused by alpha-ray, beta-ray and gamma-ray and compare it to the luminescence induced by the x-ray. .

Finally, the relationship between luminescence characteristics (namely a-x-value, b-x-value and c-x-value) and impurity concentration is examined.

As a result;

1. Most calcites have thermoluminescence peak at 80 and 230 degrees Celsius.
2. In thermoluminescence peak of calcite at 80 degrees Celsius, fading is detected, while at 230 degrees peak is stable.
3. Results show negative or positive relationship between luminescence efficiency factors (a-x-value, b-x-value and c-x-value) and Mg, Mn, Fe and Sr concentrations.
4. The concentration of Fe has a correlation with a luminescence emitting efficiency.

Fe plays an important role for thermoluminescence of calcite. Thermoluminescence property of calcite may be subject to multiple chemical factors (ex; Mg, Mn and Sr), therefore, further analyses on calcites with the variety of impurity is necessary to evaluate a relation between multiple impurity concentration and thermoluminescence properties quantitatively.

Keywords: thermoluminescence, calcite, dating

## Zircon observation by atomic force microscope: Fission track or alpha recoil track?

HASEBE, Noriko<sup>1\*</sup> ; ITO, Kentaro<sup>1</sup> ; OHISHI, Shinnosuke<sup>1</sup> ; HONDA, Chiaki<sup>1</sup> ; MATSUKI, Atsushi<sup>1</sup> ; FUKUMA, Takeshi<sup>1</sup>

<sup>1</sup>Kanazawa University

Fission track (FT) method is a dating technique based on the observation of damage (tracks) by spontaneous fission of <sup>238</sup>U left in a mineral. The number of tracks is counted under an optical microscope after etching (chemical expansion of a track). However, as FT density per unit area rises, it becomes difficult to count the number of tracks. This is due to the fact that FTs overlap one another and are unable to be readily distinguished. The atomic force microscope has a potential to observe FT with high track density after a short time etching. However, when etching time is too short, the number of counted tracks were increased probably due to difficulties in recognizing the FT among structures other than FT (e.g., alpha recoil tracks). In the observation of young zircons collected from modern volcanic product, the surface structures found in old zircons do not exist, and a hole with the depth of ~10nm can be found on the smooth surface. These countable holes may lead us to the alpha recoil track dating.

Keywords: zircon, fission track, alpha recoil track, atomic force microscope

## Excess argon in phengite from the Sanbagawa eclogites: Constraints on argon behavior during subduction zone metamorphism

ITAYA, Tetsumaru<sup>1\*</sup> ; TSUJIMORI, Tatsuki<sup>2</sup>

<sup>1</sup>Okayama University of Science, <sup>2</sup>Okayama University

K-Ar system dating of phengitic mica is a powerful tool to determine cooling ages of HP/UHP metamorphic rocks. However, discordant ages in a same metamorphic unit have been often reported, particularly from rocks in Alpine-Himalayan type collisional metamorphic belts. For example, UHP-metamorphosed continental crust materials of the Dola Maira massif (western Alps, Italy) show the discrepancy due to the existence of excess argon in metamorphic minerals that has been inherited from the precursor rocks with polyphase metamorphic records. Over the last two decades, we have addressed an excess-argon free hypothesis in oceanic petrogenesis of Pacific-type convergent margins. According to the hypothesis, metamorphosed oceanic materials in Pacific-type HP metamorphic belts with only a monophase metamorphic records do not contain significant amount of excess <sup>40</sup>Ar; in other words, the K-Ar system in syn-metamorphic phengitic mica is significantly reset during fluid-induced metamorphic recrystallization at a Pacific-type convergent margin. Well-documented geological examples are of schists from Sanbagawa, Suo and Renge metamorphic belts in SW Japan, and from Otago metamorphic belt in New Zealand. Ar-Ar phengite analyses of HP-UHP metamorphosed oceanic lithologies of the Lago di Cignana (western Alps, Italy) also show negligible excess <sup>40</sup>Ar in eclogite-facies syn-metamorphic phengitic mica.

In the year 2000, as a preparation to guide participants for the IEC Conference in Japan, we have determined K-Ar ages of phengite and paragonite from the eclogite-facies Sanbagawa metamorphic rocks in Shikoku; the twenty-two results were obtained from four localities including Seba (84-89 Ma), Gongen (123-136 Ma) and Western Iratsu (78-80 Ma), and Kotsu/Bizan (82-88 Ma). Excepting for the quartz-rich kyanite eclogite from Gongen (GO), phengite and/or paragonite yields similar cooling-age ranges of metasedimentary rocks of the Sanbagawa metamorphic rocks in central Shikoku. Phengite K-Ar ages of GO eclogites are significantly older than syn-metamorphic zircon U-Pb ages at the same unit. These old ages are interpreted as the presence of excess <sup>40</sup>Ar in phengitic mica. The bulk-rock compositions of GO eclogites suggest a sedimentary protolith such as greywacke. When, where and how has the excess argon been trapped in phengite crystals? Considering the geological fact that the GO eclogites are closely associated with the Higashi-Akaishi (HA) meta-peridotite body, the false age obtained from phengite were likely attributed to an interaction between the meta-sediment (GO eclogite) and the meta-peridotite (HA peridotite) at eclogite-facies depth. We postulate that the fluids exchange between deep-subducted sediments and mantle material enhanced a hydration of peridotite and mantle-derived noble gas (including extreme <sup>40</sup>Ar) was diffused from mantle material to the sediments. During the exhumation of them, the rigid HA peridotite might have prevented a ductile deformation of GO eclogite and consequently mantle-derived argon gained from HA peridotite in GO eclogite might have been inherited by the limited-argon-depletion due to less deformation. This is not only very rare example of false K-Ar age of metamorphosed oceanic materials but also remarkable observation to explain argon behavior during sediments/peridotite interaction at a deep portion of subduction zone environment.

Keywords: Sanbagawa belt, eclogite, phengite, excess argon

## Deciphering early Earth's differentiation using short-lived isotope systematics

IIZUKA, Tsuyoshi<sup>1\*</sup>

<sup>1</sup>Tsuyoshi IIZUKA

Knowledge of the timescale and nature of early Earth's differentiation is central to understanding the evolution of the young Earth. Here I discuss short-lived isotope systematics of terrestrial samples that extended our knowledge of early Earth's differentiation. Recent high-precision W isotopic studies revealed positive  $^{182}\text{W}$  anomalies of up to 0.15 epsilon unit in ca. 3.8 Ga Itsaq rocks from West Greenland and 2.8 Ga Kostomuksha komatiites from Russia. I explored the geologic significance of the  $^{182}\text{W}$  anomalies by combining with trace element and other isotopic data. In this context, the W isotopic data are interpreted to reflect early silicate differentiation events on Earth. Under the assumption that the bulk silicate Earth has a 5% higher Sm/Nd than the chondrite average, the  $^{182}\text{W}$ - $^{142}\text{Nd}$ - $^{143}\text{Nd}$  chronometry constrains the age of the source mantle differentiation for the Itsaq samples to 4.53-4.49 Ga. The age may reflect the timing of silicate differentiation during a sequence of magma ocean solidification.

Keywords: Hadean, early differentiation, extinct radionuclides, non-chondritic Earth

## Formation age of Fengtien Nephrite, Taiwan: Dating low-temperature thin (<20 $\mu\text{m}$ ) zircon rims by NanoSIMS

YUI, Tzen-fu<sup>1</sup> ; USUKI, Tadashi<sup>1\*</sup> ; CHEN, Chun-yen<sup>1</sup> ; ISHIDA, Akizumi<sup>2</sup> ; SANNO, Yuji<sup>2</sup>

<sup>1</sup>Institute of Earth Sciences, Academia Sinica, Taiwan, <sup>2</sup>Atmosphere and Ocean Research Institute, The University of Tokyo

Nephrite in the Fengtien area is associated with serpentinites within the subduction-accretionary complex in eastern part of the Central Mountain Range, Taiwan. In addition to nephrite, there are also other metasomatic rocks, such as diopsidefels and epidotite, present between serpentinites and their country rocks (metapelites and metapsammites). Among these metasomatic rocks, diopsidefels is the most common one observed, while nephrite and epidotite are less frequently present in association with diopsidefels. When all these rocks are present at one outcrop, the common lithologic sequence is serpentinite-nephrite-diopsidefels-epidotite- metasedimentary rocks. Nephrite, diopsidefels and epidotite were interpreted resulting from fluid-rock (serpentinite+country rocks) interactions during subduction metamorphism. Field occurrence and petrographic observations clearly showed that while nephrite and diopsidefels are mainly metasomatic products after serpentinite, epidotite is after metapsammite. The formation temperature has been estimated to be 300 - 400 °C based on regional geology and thermodynamic calculations by previous studies. Timing of these metasomatic processes, however, has not been constrained, although the hosting subduction-accretionary complex was thought to be of late Cretaceous in age due to paleo-Pacific subduction beneath the Eurasia continent and to be correlated with the Sambagawa belt in Japan. Zircons were separated from one epidotite sample in this study. Most of these detrital zircons were shown to have a thin zircon rim, which is less than 15 - 20  $\mu\text{m}$  in thickness. These zircon rims were considered to be newly formed during metasomatic interactions between serpentinite and country rocks, which also led to nephrite/diopsidefels/epidotite formation. The CAMECA NanoSIMS NS50 at AORI, the University of Tokyo was employed to date these low-temperature thin zircon rims with a  $\sim 5$  nA O<sup>-</sup> primary beam confined to a  $\sim 15$   $\mu\text{m}$  diameter. Sample surface was pre-ablated for 5 minutes to remove the surface Au coating and any possible surface contaminants. Data acquisition time was 500 seconds. The resulting  $^{238}\text{U}/^{206}\text{Pb}$ - $^{204}\text{Pb}/^{206}\text{Pb}$  inverse isochron gave a young age of  $3.3 \pm 1.7$  Ma (MSWD = 2.1, n = 5). The date clearly showed that the Fengtien nephrite would have formed during the (initial) exhumation of the subduction-accretionary complex, which should be of late Cenozoic in age related to subduction of the South China Sea plate beneath the Luzon arc. The present study gave a good example that NanoSIMS is able to date zircon rims with a thickness about 15  $\mu\text{m}$  formed under low temperature conditions only a few million years ago. The instrument has a great potential in future studies dating various low-temperature hydrothermal, metasomatic or metamorphic zircon overgrowths.

Keywords: NanoSIMS, zircon, U-Pb dating, Nephrite, Central Mountain Range, Taiwan

## Significance of external morphology and zircon chemistry for precise U-Pb zircon dating

TAKEHARA, Mami<sup>1\*</sup>; HORIE, Kenji<sup>2</sup>; TANI, Kenichiro<sup>3</sup>; YOSHIDA, Takeyoshi<sup>4</sup>; HOKADA, Tomokazu<sup>2</sup>; KIYOKAWA, Shoichi<sup>5</sup>

<sup>1</sup>Department of Earth and Planetary Sciences, Graduate School of Sciences, Kyushu University, <sup>2</sup>National Institute of Polar Research, <sup>3</sup>Institute for Research on Earth Evolution, Japan Agency for Marine-Earth Science and Technology, <sup>4</sup>Institute of Earth Sciences, Graduate School of Science, Tohoku University, <sup>5</sup>Department of Earth and Planetary Sciences, Faculty of Sciences, Kyushu University

Improvement of U-Pb zircon dating by microbeam analysis has been provided opportunity of discussion about more detailed geological events. Recent analytical precision of less than 2% at Paleogene zircon allows us to investigate shorter period events such as crystallization differentiation in magma chamber. However, the highly precise U-Pb age data yield an importance of confirming their accuracy and assaying disturbance of U-Pb system and incorporation of exotic components. In this study, we introduce data processing method of the highly precise ages based on zircon morphology, trace element abundances as well as statistics.

The precise U-Pb zircon dating by using a sensitive high-resolution ion microprobe (SHRIMP II) at National Institute of Polar Research, Japan, was applied to igneous rocks of the Tertiary Ishizuchi Cauldron in the Setouchi volcanic belt of Miocene age in northwestern Shikoku. A primary ion beam of about 10 nA was used to sputter an analytical spot of about 40  $\mu\text{m}$  diameter. A retardation lens system was utilized as a means to increase signal-to-noise ratio, and a secondary ion optics including slits of source and collector was adjusted to maximum transmission of the secondary ion under suitable mass resolution avoiding isobaric interferences on Pb isotopes. The surfaces of grain mounts were carefully washed with diluted HCl and ultra pure water to remove Pb contamination. A correction for common Pb was made on the basis of the measured <sup>204</sup>Pb and the model for common Pb composition.

Weighted mean ages were calculated from <sup>206</sup>Pb/<sup>238</sup>U ratios corrected by <sup>207</sup>Pb. In order to ensure the accuracy of U-Pb age, age known zircon, OD-3, was analyzed together with unknown sample. Concentrations of Hf and rare earth element (REE) in zircons were also measured at the same analytical spot of U-Pb dating by SHRIMP.

Zircon grains from the Bansyodani-biotite-rhyolite were divided to two types based on the external morphology: sharply euhedral type and relatively rounded edge of prism and pyramid type. <sup>206</sup>Pb/<sup>238</sup>U data of whole zircon grains were widely scattered beyond analytical uncertainty and show a weighted mean of  $14.78 \pm 0.18$  Ma (mean square weighted deviation, MSWD: 3.4). On the other hand, the euhedral zircons yielded the weighted mean of  $14.21 \pm 0.19$  Ma (MSWD: 1.0), whereas the relatively rounded zircons were older than the euhedral zircons, which suggests the incorporation of exotic components.

Zircon chemistry supported the classification by the morphology and the U-Pb dating. An average of Hf contents of the euhedral zircons were 9523 ppm ranging from 8883 to 10496 ppm and those of the relatively rounded zircons were 8475 ppm ranging from 7616 to 8803 ppm. Hf contents of the euhedral zircons were higher than those of relatively rounded zircons. C1 chondrite-normalized REE patterns of the euhedral zircons were characterized by a large fractionation between light REE and heavy REE, large positive Ce anomalies and large negative Eu anomalies. In contrast, those of the relatively rounded zircons were enrichment of light REE, weaker anomalies of Ce and Eu. Difference of the zircon chemistry between the euhedral zircons and the relatively rounded zircons reflects source melt composition. Therefore, the external morphology, Hf content, and REE abundance are useful criteria for the data processing of the highly precise U-Pb age data.

## LA-ICP-MS U-Pb dating of Oki Dozen volcano using non-polished zircons

ITO, Hisatoshi<sup>1\*</sup> ; BRENNAN, Marco<sup>2</sup> ; MIURA, Daisuke<sup>1</sup> ; TOSHIDA, Kiyoshi<sup>1</sup> ; NAKADA, Setsuya<sup>2</sup>

<sup>1</sup>CRIEPI, <sup>2</sup>Univ. of Tokyo

LA-ICP-MS U-Pb dating using zircon is now widely used with great success. The normal dating process includes polishing zircons. This process is good in terms of avoiding surface contamination of common Pb and/or Pb loss and is essential for SHRIMP, in which only small fraction (drilling depth of 1-2  $\mu\text{m}$ ) is used for dating. Compared to SHRIMP, LA-ICP-MS ablates a much larger volume (drilling depth of  $>10 \mu\text{m}$ ) of zircon. This means that it is easy to date zircons from the surface to the inner core of the crystal and examine the existence of inherited cores and potentially investigate the timespan of crystallization. Here we dated non-polished zircons for some reference samples (Fish Canyon Tuff and OD-3) and samples from Oki Dozen volcano. Zircons were ablated for 30 seconds using 213 nm Nd-YAG laser with 10 Hz repetition rate and 4-5  $\text{J}/\text{cm}^2$  energy density. Final drilling depth for 5  $\text{J}/\text{cm}^2$  was 27  $\mu\text{m}$  and the  $^{206}\text{Pb}/^{238}\text{U}$  ratio from 9-18  $\mu\text{m}$  depth were used to determine ages. It was found that non-polished zircons yield reliable ages because of agreement with reference ages. The Oki Dozen samples yielded 6-7 Ma ages, in agreement with or slightly older than K-Ar ages of 5.4-7.4 Ma.

Keywords: U-Pb dating, zircon, LA-ICP-MS, Oki Dozen volcano

## Crustal noble gases anomaly associated with fault movement and aftershock the 3.11 Northeast Japan Earthquake

SATO, Keiko<sup>1\*</sup> ; KUMAGAI, Hidenori<sup>2</sup> ; IWATA, Naoyoshi<sup>3</sup> ; HYODO, Hironobu<sup>4</sup> ; SUZUKI, Katsuhiko<sup>2</sup> ; TAKAOKA, Nobuo<sup>5</sup>

<sup>1</sup>JAMSTEC, SRRP, <sup>2</sup>JAMSTEC, IFREE, <sup>3</sup>Faculty of Science, Yamagata University, <sup>4</sup>Okayama University of Science, <sup>5</sup>Faculty of Science, Kyusyu University

Noble gases have unique characteristics that they are rarely combined with other chemicals as their very stable nature. Because its main reservoir is atmosphere, their isotopic composition is well defined and believed to be uniform all over the world insensitive to disturbance from anthropogenic and/or natural emission of geologically trapped noble gases in the earth interior. Based on our preliminary friction experiment, however, detectable amount of noble gases seem to be emitted accompanied with a fault motion (Sato et al., 2009). After the extreme Northeast Japan Earthquake occurred on March 11, 2011, extraordinary increase of seismic activity as numerous aftershocks e.g. over 4000 felt earthquakes in four months, which may be a source of non-atmospheric component preserved in the earth interior. In terms of anthropogenic component, (Nuclear Power Plant) is a potential source, which is frequently monitored by radioactive species of noble gases.

We widely collected atmosphere samples all over Japan from Hokkaido, Honsyu, Chugoku and Kyusyu Is. The atmospheres have been sampled into vacuumed containers, Isotube®, at each sampling site to evaluate time-series changes. The elemental and isotopic compositions of the samples were analyzed mainly by quadrupole residual gas analyzers (RGA-200, SRS Co.) and partly confirmed by sector-type mass spectrometers (GVI-5400, GV instruments). In the duplicated analyses of the selected a few samples, the measured elemental and isotopic compositions were consistent within analytical uncertainties.

The relative elemental abundances were changed at least in heavier noble gases. Argon was enriched to pre-3.11 Earthquake atmospheres associating with a high <sup>40</sup>Ar/<sup>36</sup>Ar ratio. It might be contributed by emission of crustal Ar at aftershock earthquakes, deformation and fault movements. In addition, a frictional melting was occurred in a >M5 earthquake as reported by Kanamori et al. (1998). Further, radioactive Ar isotopes (<sup>42</sup>Ar and <sup>39</sup>Ar) were slightly abundant than those in "pre" 3.11 Earthquake atmospheres. These radioactive Ar isotopes were regarded to be detected limitedly in neutron irradiated geological samples especially in Ar - Ar dating. These altered atmospheric Argon isotopic composition in Eastern Japan area were observed until typhoon season.

Keywords: noble gas, 3.11 Northeast Japan Earthquake, aftershock earthquake, nuclear power plant disaster, Ar Isotope

## Ultra-high-sensitive simultaneous determination of halogens and noble gases by an extension of Ar-Ar and I-Xe methods

SUMINO, Hirochika<sup>1\*</sup> ; KOBAYASHI, Masahiro<sup>1</sup> ; SAITO, Takehiko<sup>1</sup> ; NAGAO, Keisuke<sup>1</sup> ; TOYAMA, Chiaki<sup>2</sup> ; MURAMATSU, Yasuyuki<sup>2</sup>

<sup>1</sup>Geochemical Research Center, Graduate School of Science, University of Tokyo, <sup>2</sup>Department of Chemistry, Gakushuin University

Noble gas isotope ratios in various geochemical components in the Earth are significantly different, making them useful tracers to constrain origin of volatiles in the mantle. The development of noble gas mass spectrometry during the last two decades has enabled us to detect less than 10000 noble gas atoms (e.g., [1]).

An extension of Ar-Ar and I-Xe dating methods allows us to simultaneously determine trace amounts of noble gases, halogens, K, Ca, Ba, and U by use of ultra-high-sensitive noble gas mass spectrometry on neutron-irradiated samples. This method has several advantages: (i) detection limits for halogens are three or four orders of magnitude lower than those of other conventional analytical methods, (ii) several components of different origin can be distinguished based on their relations with specific noble gas isotopes such as mantle-derived <sup>3</sup>He and by using various noble gas extraction methods such as laser microprobe [2], and (iii) in-situ production of radiogenic noble gas isotopes (such as <sup>4</sup>He and <sup>40</sup>Ar) after the entrapment of the noble gas component of interest in the sample can be corrected by the simultaneously determined their parent elements, such as U and K, when the age of the entrapment is known or can be assumed.

We have developed a new noble gas mass spectrometric system for this method based on an Ar-Ar and I-Xe dating system [3]. Accuracy and precision of our method were examined by analyzing GSJ and USGS reference materials, their original rocks, and scapolite standards [4] and by comparing the halogen data with those obtained with ion chromatography and ICP-MS followed by pyrohydrolysis extraction [5].

By using this method, we analyzed halogens and noble gases in exhumed mantle wedge peridotites and eclogites from the Sanbagawa-metamorphic belt, southwest Japan and those in mantle-derived xenoliths from Kamchatka and N. Philippines, in all of which relicts of slab-derived water are contained as hydrous mineral/fluid inclusions. The striking similarities of the observed noble gas and halogen compositions with marine pore fluids [6,7] challenge a popular concept, in which the water flux into the mantle wedge is controlled only by hydrous minerals in altered oceanic crust and sediment (e.g., [8]).

On the other hand, halogen ratios of olivines in lavas from the northern Izu-Ogasawara arc [9] indicate insignificant contribution to the mantle wedge of pore fluid-derived halogens. This implies a relatively small amount of the pore water subduction fluids would be released from the Izu slab at a sub-arc depth resulting in further subduction to great depths in the mantle, possibly resulting in the seawater-like heavy noble gas composition of the convecting mantle [10].

Based on the relation with <sup>129</sup>Xe produced from decay of short-lived nuclide <sup>129</sup>I during stepwise heating noble-gas extraction of the Allende and Shallowater meteorites, intrinsic I and U to the meteorites were distinguished from those of terrestrial contamination origin.

These results demonstrate that simultaneous determinations of noble gases, halogens, K, Ca, Ba, and U in mantle-derived rocks and meteorites provide important information about their origins.

[1] Sumino et al. (2001) *J. Mass Spectrom. Soc. Jpn.* 49, 61-68. [2] Sumino et al. (2008) *J. Volcanol. Geotherm. Res.* 175, 189-207. [3] Ebisawa et al. (2004) *J. Mass Spectrom. Soc. Jpn.* 52, 219-229. [4] Kendrick (2012) *Chem. Geol.* 292-293, 116-126. [5] Muramatsu & Wedepohl (1998) *Chem. Geol.* 147, 201-216. [6] Sumino et al. (2010) *Earth Planet. Sci. Lett.* 294, 163-172. [7] Kobayashi et al. (2013) *Mineral. Mag.* 77, 1484. [8] Schmidt & Poli (1998) *Earth Planet. Sci. Lett.* 163, 361-379. [9] Sumino et al. (2013) *Mineral. Mag.* 77, 2285. [10] Holland & Ballentine (2006) *Nature* 441, 186-191.

Keywords: noble gas, halogen, mass spectrometry, Ar-Ar dating, I-Xe dating

## Unspiked K-Ar dating for lavas from Zao volcano

YAMASAKI, Seiko<sup>1\*</sup> ; OIKAWA, Teruki<sup>1</sup> ; BAN, Masao<sup>2</sup>

<sup>1</sup>Geological Survey of Japan, AIST, <sup>2</sup>Faculty of Science, Yamagata Univ.

Zao volcano is located in the central part on the volcanic front of the NE Japan arc. Previous study revealed that the onset of the volcanic activity is ca. 0.8 Ma, the main edifice-building stage is ca. 0.3-0.1 Ma, and the newest stage is from 0.03 Ma to the present. On this volcano, about 50 K-Ar age data are reported, but not all units are covered and some data contradict the stratigraphy probably because of low-K and/or excess Ar contamination. We report new unspiked K-Ar age data for the lavas collected also from unexplored units, in order to construct the detailed history of the volcano.

Keywords: Zao volcano, K-Ar dating

## Diffusion experiment by stepwise heating and muscovite

HYODO, Hironobu<sup>1\*</sup>

<sup>1</sup>RINS, Okayama Univ. of Sci.

It is generally recognized that diffusion experiment on micas in vacuum during stepwise heating for  $^{40}\text{Ar}/^{39}\text{Ar}$  dating was unsuitable for diffusion studies because of the destruction of crystal structure from dehydration. However, we showed that estimates of closure temperature from single grain biotites during laser heating experiment gives reasonable values. The problem in case of muscovite is that it seems to have structural transition or significant destruction between 600 and 700°C. The recent study using hydrothermal environment reported the activation energy  $E$  of 63 kcal/mole and an estimation of closure temperature exceeding 400°C. The high  $E$  and closure temperature  $T_c$  are derived on the steep slope in Arrhenius plot. Without change in crystal structure, muscovite does not give high  $E$  and  $T_c$ . This is contradictory for samples with high  $E$  and  $T_c$ . It is necessary to separate diffusion phenomena from structural change, and even a hydrothermal experiment at high temperatures in a laboratory may not be suitable for such studies. Muscovite is known to have relatively high  $T_c$  in field. To make a practical estimate for  $T_c$ , it is necessary to consider both laboratory and field setting.

Keywords: diffusion experiment, argon, closure temperature, stepwise heating, muscovite

## Luminescence dating and analysis of environmental change of fine grained sediments from Lake Yogo, Japan

ITO, Kazumi<sup>1\*</sup>

<sup>1</sup>Geological Survey of Japan, AIST

We applied optically stimulated luminescence (OSL), infrared stimulated luminescence (IRSL), post-IR IRSL (pIRIR) and <sup>14</sup>C dating to the sediment core YG11-3 (294cm) from Lake Yogo, Japan. The fine grained quartz and polymineral sample are used for equivalent dose ( $D_e$ ) estimation. As a result of several basic tests, the preheat temperature of 200 °C for 10 s and a cut heat of 160 °C were suitable to all OSL measurements. The accepted aliquots are about 90 % per measurement discs and the range of  $D_e$ s are 0.3 ~3.5 (Gy). The bulk <sup>14</sup>C ages are ca. 300 years older than those of plant residue. After subtracting this age difference from bulk <sup>14</sup>C ages, the corrected ages agree with the OSL ages except the ages of sediments from some depths. Two excepted OSL ages are older than the corrected bulk <sup>14</sup>C ages (YG11-3-245, YG11-3-343) and these layers include a lot of plant residue enough to analyze the plant residue <sup>14</sup>C ages. It seems that these sediments from two layers have been transported quickly in muddy stream based on a temporary environmental event. Additionally, the result of the IRSL<sub>50/225</sub> and pIRIR<sub>225</sub> age confirms the existence of this temporary event. By comparing the OSL ages with <sup>14</sup>C, IRSL and pIRIR ages, the quartz from the small catchment area can be applied to reconstruct the age model of sediment core in Japan.

Keywords: OSL dating, pIRIR dating, lake sediments

## U-Pb dating of Eoarchaeon zircon using a NanoSIMS -implication for the measurement of volatile in the inclusions

ISHIDA, Akizumi<sup>1\*</sup> ; TAKAHATA, Naoto<sup>1</sup> ; SANO, Yuji<sup>1</sup> ; DAVID, Jean<sup>2</sup> ; PINTI L., Daniela<sup>2</sup>

<sup>1</sup>AORI the University of Tokyo, <sup>2</sup>University of Montreal

Volatiles, such as hydrogen or sulfur, trapped in the Eoarchaeon igneous rocks, are one of the most important tracers of the evolution of the interior of the early Earth. Apatite or glass inclusions found in the zircon crystal, are expected to preserve such volatiles. However, because of their scarceness, high-sensitive, high-resolution analytical methods are required for quantify them and reveal their isotopic compositions. Furthermore, discriminating between pristine compositions and later alteration is problematic. We are trying to approach these issues carrying out analyses by NanoSIMS50.

Euhedral to subhedral zircons were separated from a tonalite which was from the Eoarchaeon Nuvvuagittuq supracrustal belt, Superior Craton, Canada. The reported U-Pb age of this tonalite is  $3661 \pm 4$  Ma by using LA-MC-ICP-MS [1]. The size distribution of zircons was from approximately 50 micrometers to 200 micrometers. Some of them have inclusions of apatite and glass whose size were 10 to 30 micrometers in diameter. Dating measurements were done avoiding such inclusions.

We performed  $^{238}\text{U}$ - $^{206}\text{Pb}$  and  $^{207}\text{Pb}$ - $^{206}\text{Pb}$  dating in the same analytical spot of zircon crystals. A 5 nA  $\text{O}^-$  primary beam, with spot size of approximately 10 micrometers in diameter, was used for ionizing the sample surface, and secondary positive ions were collected in a multicollector. The detector system was modified to measure  $^{30}\text{Si}^+$ ,  $^{90}\text{Zr}_2^{16}\text{O}^+$ ,  $^{204}\text{Pb}^+$ ,  $^{206}\text{Pb}^+$ ,  $^{238}\text{U}^{16}\text{O}^+$ , and  $^{238}\text{U}^{16}\text{O}_2^+$  ions simultaneously in  $^{238}\text{U}$ - $^{206}\text{Pb}$  dating session. In  $^{207}\text{Pb}$ - $^{206}\text{Pb}$  dating session,  $^{204}\text{Pb}^+$ ,  $^{206}\text{Pb}^+$ , and  $^{207}\text{Pb}^+$  ions were collected in the same detector by changing the magnetic field. Detailed analytical procedure and standard calibration is described in Takahata et al.(2008) [2].

Measured  $^{206}\text{Pb}/^{238}\text{U}$  ratios range from 0.4932 to 0.7993, and the  $^{207}\text{Pb}/^{206}\text{Pb}$  ratios range from 0.3052 to 0.3443. After the correction of common Pb, those values were plotted on Tera-Wasserburg Concordia diagram, giving a corrected age of  $3633 \pm 35$  Ma, consistent with the previous value obtained by [1]. On the other hand, some samples showed a discordant age. Since such crystals are thought to have suffered metamorphism with subsequent loss of Pb, volatiles in the inclusions might have lost their initial information as well. Now we are proceeding to measure the volatile compositions of inclusions based on the results of U-Pb dating.

[1] David et al., GSA Bulletin, 121, 150-163, 2008.

[2] Takahata et al., Gondwana Res., 14, 587-596, 2008.

Keywords: U-Pb dating, NanoSIMS, zircon, inclusion, Archaean

## Geochronological-geochemical characterization of Proterozoic age, western part of the Napier Complex, East Antarctic

HORIE, Kenji<sup>1\*</sup> ; HOKADA, Tomokazu<sup>1</sup> ; HIROI, Yoshikuni<sup>2</sup> ; MOTOYOSHI, Yoichi<sup>1</sup> ; SHIRAIISHI, Kazuyuki<sup>1</sup>

<sup>1</sup>NIPR, <sup>2</sup>Chiba University

The Napier Complex in East Antarctica has attracted considerable interest from a viewpoint of long Archaean crustal history from 3800 Ma to 2500 Ma (e.g., Harley & Black 1997) and >1000 °C ultrahigh-temperature (UHT) metamorphism in a regional scale (e.g., Sheraton et al., 1987; Harley & Hensen 1990). The timing of ultrahigh-temperature metamorphism is in argument either >2550 Ma or <2480 Ma (Kelly and Harley, 2005). However, some previous works reported relatively younger ages, such as 2380 Ma, ~2200 Ma, and ~1820 Ma (e.g., Grew et al., 2001; Owada et al., 2001; Suzuki et al., 2001, 2006; Carson et al., 2002; Hokada and Motoyoshi, 2006). In addition, Horie et al. (2012) reported similar ages in felsic orthogneiss from Fyfe Hills and quartzite from Mt. Cronus via zircon U-Pb dating. In this study, we try to characterize the "younger ages" in order to interpret thermal history after the UHT metamorphism in the Napier Complex.

A quartzo-feldspathic gneiss, YH05021606A, collected from Fyfe Hills by Y.H. during the field work at the 2004-2005 Japanese Antarctic Research Expedition was analyzed by using a high-resolution ion microprobe (SHRIMP II) at the National Institute of Polar Research, Japan. The zircon U-Pb ages of the YH05021606A sample are already reported in Horie et al. (2012). The sample shows multiple age peaks centered at ca. 3025, 2943, 2883, 2818, 2759, 2674, 2518, and 2437 Ma, and evidence of the "younger ages" has never been reported. In this study, primary ion beam was focused up to 10 μm in order to observe detailed zircon structure. The U-Pb analysis of zircon yielded similar age population to the previous work and revealed the "younger ages" of ca. 2273, 2195, 2106, and 1980 Ma. Distribution of the "younger ages" is consistent with those of a felsic orthogneiss, YH05021603A, in Fyfe Hills and those of a quartzo-feldspathic gneiss, YH05021701A, and a quartzite, YH05021701H, in Mt. Cronus (Horie et al., 2012). The "younger ages" in this sample could be found in overgrowth rim and single grain, which indicates that both of Fyfe Hills and Mt. Cronus had been affected by any geological events after the UHT metamorphism. Previous workers suggested that the ca. 2200 Ma age that they obtained for beryllium syn-metamorphic pegmatites reflects post-emplacement deformation and metamorphism (Grew et al., 2001), and a ca. 1930-1800 Ma U-Pb upper intercept age for zircons were affected by aqueous fluid from Paleozoic pegmatite (Carson et al., 2002). Horie et al. (2012) only suggests that these 2380-820Ma ages represent local fluid infiltration or a local deformation events. We will discuss about character of the "younger ages" zircon with trace element signature.

Keywords: East Antarctica, Napier Complex, zircon, U-Pb dating, rare earth element, metamorphism

## Sr and Nd isotope systematics of metacarbonate rocks as proxies for reconstructing extinct oceans: Mozambique Ocean

OTSUJI, Naho<sup>1\*</sup> ; KAMEI, Atsushi<sup>2</sup> ; TSUCHIYA, Noriyoshi<sup>3</sup> ; G.H., Grantham<sup>4</sup> ; KAWAKAMI, Tetsuo<sup>5</sup> ; ISHIKAWA, Masahiro<sup>6</sup>

<sup>1</sup>Niigata University, <sup>2</sup>Shimane University, <sup>3</sup>Tohoku University, <sup>4</sup>Council for Geoscience, South Africa, <sup>5</sup>Kyoto University, <sup>6</sup>Yokohama National University

Geochemistry of sedimentary rocks is widely used for understanding the depositional environment and tectonic setting, including source rock composition and paleo-ocean signature. In particular, chemically deposited carbonate rocks are directly precipitated from saturated seawater are supposed to hold key information of extinct paleo-oceans. An important geochemical tool that can lead to the identification of contemporaneous seawater is isotopic composition of strontium and neodymium in carbonate rocks, because these elements have distinct residence and mixing time in seawater and also characterized by surrounding continents.

In the Sør Rondane Mountains (SRMs), East Antarctica, metasedimentary rocks including metacarbonate rocks are widely distributed. These rocks were supposed to have formed in the paleo-ocean called as "Mozambique Ocean". SRMs are divided into two terranes, the SW and NE terranes, by the Main Tectonic Boundary (MTB). In the SW terrane, metaigneous rock that were formed at ca. 1000 Ma and metasedimentary rocks occur as main lithological units, which underwent metamorphic evolution along a anticlockwise *P-T* path, whereas the NE terrane is dominated by metasedimentary rocks, with a characteristic clockwise of *P-T* path. Additionally, metapelitic rocks in the SW terrane have similar detrital age population with the nearby metaigneous rocks, in contrast to those in the NE terrane show older detrital ages (~ca. 3300Ma)(Osanai *et al.*, 2013). If it is possible to reveal the relationship between ocean and continents during depositional timing of carbonate rocks in both terranes, we will be able to put forward a model to explain the difference in depositional setting between SW and NE terranes. To achieve this, analyzed detailed study of Sr and Nd isotopic composition of metacarbonate and metamorphosed silicate rocks, such as pelitic, felsic, mafic and ultramafic rocks, from several important outcrops throughout SRMs were carried out. Based on these data, we discuss about the relationship with continent and depositional basin of carbonate sediments before the final amalgamation of Gondwana.

After geochemical screening for post-depositional alteration, using oxygen isotopes, trace elements and REE + Y patterns, strontium isotope chemostratigraphy was applied to the metacarbonate rocks from SRMs and depositional ages of 880-850 Ma and 820-790 Ma (late-Tonian and early-Cryogenian age) were estimated (Otsuji *et al.*, 2013). Metacarbonate rocks in the Bratnippene and Tanngardene regions in the SW terrane are showing typical seawater-rock mixing relationship in a  $\epsilon\text{Sr}$  vs.  $\epsilon\text{Nd}$  cross-plot indicating the deposition of metacarbonate rocks nearby meta-tonalitic and orthogneiss dominated continental arc. By contrast, the Perlebandet region exhibits an extremely different depositional setting of a seamount based on Nd model and depositional age and REE and  $\epsilon\text{Nd}$  compositions. Moreover, the Balchen metacarbonate rocks show a signature of depositional setting surrounding a continent, based on the comparison of metacarbonate rocks with continental and oceanic derived rock units. A comparison of isotopic characteristics of Balchen carbonate rocks with the basement rocks from neighboring Gondwana regions suggested the presence of an ancient continent that is different from Kalahari and Dharwar Craton.

Thus, the Sr and Nd isotopic compositions of carbonate rocks deposited in the Mozambique Ocean have preserved important information about depositional setting of sedimentary rocks and relationship with surrounding basement and continents. In summary, geochemical proxies such as Nd and Sr isotopes of metacarbonate rocks can yield key information not only of paleo-oceans but also about the surrounding rocks during depositional timing, which can lead to a better understanding of oceanic closure during the formation of supercontinents.

Reference cited: Osanai *et al.*, 2013. PR, 234, 8-29. Otsuji *et al.*, 2013. PR, 234, 257-278.

Keywords: Sr and Nd isotope ratios, metacarbonate rocks, the Sor Rondane Mountains, Mozambique Ocean, Gondwana

## Geochemistry of Archaean Banded Iron Formations in the Chitradurga Schist Belt, Dharwar Craton, Southern India

KOINUMA, Kentaro<sup>1\*</sup>; MADHUSOODHAN, Satish-kumar<sup>1</sup>; MISHIMA, Kaoru<sup>2</sup>; UENO, Yuichiro<sup>2</sup>; HOKADA, Tomokazu<sup>3</sup>

<sup>1</sup>Niigata University, <sup>2</sup>Tokyo Institute of Technology, <sup>3</sup>National Institute of Polar Research

Banded iron formations (BIF) are marine chemical sediment rocks precipitated mostly in Archaean and early Paleoproterozoic between 2.7Ga and 2.3Ga. This time interval record profound changes in the redox state of the oceans and atmosphere, such as the Great Oxidation Event (GOE). We present here the geochemical data obtained from 3.0 Ga banded iron formation (BIF) in the Chitradurga Schist Belt, Dharwar Craton, Southern India. This region exposes the Archaean strata predominated by supracrustal greenstone belts, stratigraphically overlying the Peninsular gneiss. Chitradurga schist belt comprises of three important BIF layers distributed in the Bababudan and Chitradurga groups. We present here the salient geochemical characteristics and strontium and neodymium isotope results of the BIFs and discuss the depositional environment.

BIF contain very low content of Al<sub>2</sub>O<sub>3</sub> (<1wt.% except 1 sample) indicating less detrital components. The PAAS-normalized REY patterns shows positive La and Eu anomaly, low concentration of rare earth element, depletion of light rare earth elements (LREEs) relative to heavy rare earth elements (HREEs). These features differ with other Archaean BIFs in terms of lack of positive Y anomaly. The large positive Eu anomalies in Archean BIF of Chitradurga schist belt attribute to high-T hydrothermal fluid fluxes (>250 °C), while the negative Ce anomaly reflects the lack of significant oxidizing agents.

Sr isotopic composition of BIF shows large variations suggesting post depositional alterations, whereas Nd isotope ratios gave consistent information. Most of the samples show  $\epsilon\text{Nd}(3000\text{Ma})$  in the range of +2 to +4 and  $T_{DM}$  model age in accordance with sedimentation age. The  $\epsilon\text{Nd}(3000\text{Ma})$  of depleted mantle is about +4, which suggests that most of the Chitradurga BIFs were deposited in an environment strongly affected by input from a depleted mantle. However samples with different REY pattern show higher  $\epsilon\text{Nd}(3000\text{Ma})$  between +6 and +14 and their  $T_{DM}$  model age are not equal to the sedimentation age. The geochemical results thus suggest that the BIFs in the Chitradurga schist belt were deposited near possible ridges affected by hydrothermal activities.

Keywords: Banded Iron Formations, Dharwar Craton, Archaean, Nd isotope

## Tectonic evolution of Karwar and Coorg blocks, southern India

C, Ishwar-kumar<sup>1\*</sup> ; K, Sajeev<sup>1</sup> ; B.F, Windley<sup>2</sup> ; M, Satish-kumar<sup>3</sup> ; T, Hokada<sup>4</sup> ; K, Horie<sup>4</sup> ; T, Itaya<sup>5</sup>

<sup>1</sup>Centre for Earth Sciences, Indian Institute of Science, Bangalore 560 012, India, <sup>2</sup>Department of Geology, University of Leicester, Leicester LE1 7RH, UK, <sup>3</sup>Department of Geology, Niigata University, 2-8050, Ikarashi, Nishi-ku, Niigata 950-2181, Japan, <sup>4</sup>National Institute of Polar Research, 10-3 Midori-cho, Tachikawa, Tokyo190-8518, Japan, <sup>5</sup>Institute of Natural Sciences, Okayama University of Science, 1-1 Ridai-cho, Kita-ku, Okayama 700-0

The Karwar and Coorg blocks in western India are important terranes in the point of paleogeographic study of India and Madagascar. The c. 1300 Ma Kumta suture separates the Karwar and Dharwar blocks within the western Dharwar craton of India (Ishwar-Kumar et al., 2013a). The major rock types are quartz phengite schist, chlorite schist, fuchsite schist, garnet biotite schist etc. Isochemical phase diagram estimates of the quartz phengite schist suggest peak metamorphic *P-T* conditions were c. 18 kbar and 550° C. Towards the east of the suture Sirsi shelf contains weakly deformed sedimentary rocks, unconformable on high-grade gneisses of the Dharwar craton. The Karwar block to the west of the Kumta suture is mainly composed of undeformed tonalite-trondhjemite-granodiorite (TTG) with minor enclaves of amphibolite cut by later granites. Whole-rock major and trace element data suggest that the TTGs were derived from a volcanic arc, and that the granites have within-plate signatures. Amphibolites have a chemical composition comparable to basalts to basaltic andesites with MORB signatures. The TTGs from Karwar block shows a U-Pb zircon magmatic ages of ca. 3200 Ma (Ishwar-Kumar et al., 2013a). The K-Ar biotite age from the TTGs (1746 Ma and 1796 Ma) and amphibolite (ca. 1697 Ma) represents late-stage c. 1700 Ma uplift event of both TTGs and amphibolites. The Coorg block, which is about 100 km south of Karwar block, contains mainly granulite grade rocks (Chetty et al., 2012; Ishwar-Kumar et al., 2013b; Santosh et al., 2014). Major rocks types are charnockite, mafic granulites, hornblende-biotite gneiss, garnet-hornblende gabbro, anorthosite and granite. The Coorg (Mercara) suture which separates the Coorg block from the Dharwar craton to the east contains garnet-kyanite-sillimanite gneiss, mylonitic gneiss, calc-silicate granulite, mafic granulite, granite and syenite. Pseudosection calculations indicate that the constituent calc-silicate granulite and mafic granulite were re-equilibrated under high-pressure conditions of 15-20 kbar at a temperature of 800-900° C (Ishwar-Kumar et al., 2013b). Santosh et al. (2014) recorded a metamorphic age of c. 1200 Ma from metapelites from the Coorg (Mercara) suture zone. Integration of our structural, geological and geochronological results integrated with published data suggests the presence of a 1300-1200 Ma paleosubduction zone in western India. We propose that the Kumta and Coorg sutures are an eastern extension in western India of the northern and southern parts of the Betsimisaraka suture of north-eastern Madagascar.

Keywords: Karwar block, Coorg block, Kumta suture, Dharwar craton, Southern India, India-Madagascar

## Cambrian tonalite from Horei, Ofunato in southern Kitakami Mountains, Japan

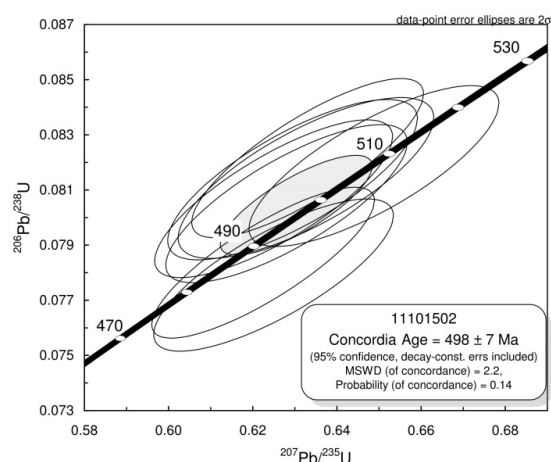
TSUCHIYA, Nobutaka<sup>1\*</sup>; TAKEDA, Tomoyo<sup>1</sup>; SASAKI, Jun<sup>1</sup>; ADACHI, Tatsuro<sup>2</sup>; NAKANO, Nobuhiko<sup>2</sup>; OSANAI, Yasuhito<sup>2</sup>; ADACHI, Yoshiko<sup>3</sup>

<sup>1</sup>Iwate University, <sup>2</sup>Kyushu University, <sup>3</sup>Niigata University

The Lower Cretaceous volcanic rocks of Ofunato Group and plagioclase quartz diorite porphyry dikes are distributed in Ryori district, south Kitakami belt, Japan. The felsic volcanoclastic rocks and tonalite is discovered within the Ofunato Group in Horei, Ofunato, Japan. The felsic volcanoclastic rocks occur as blocks less than 10 m size, and tonalite are found as blocks less than 2 x 1 m in size. The tonalite composed mainly of plagioclase, quartz, biotite, and hornblende and is characterized by poverty of K-feldspar. The tonalite is rich in SiO<sub>2</sub> (73.1–73.4%), and is classified as volcanic arc granite after Pearce et al. (1984). However, it is characterized by low K<sub>2</sub>O (0.72–1.27wt%), Rb (16–32ppm), and Ba (91–97ppm) concentrations. This rock is considered to be derived from arc magmatism in immature oceanic arc setting.

U-Pb dating of zircons were carried out using Agilent 7500cx quadrupole inductively coupled plasma mass spectrometer (ICP-MS) with a New Wave Research UP-213 Nd-YAG UV (213 nm) laser ablation system (LA) installed at the Kyushu University (Adachi et al., 2012). Zircon grains from tonalite concentrate around ca. 500 Ma, 8 analyses from 8 grains define a concordia age of 498 ± 7 Ma. U-Pb zircon age obtained here correspond to latest Cambrian age, and is similar to U-Pb zircon SHRIMP age of the granitic rocks from the Daiouin granite in Hitachi metamorphic rocks (490.8 ± 6.1 Ma) and the Hikawa granite in Higo metamorphic rocks, Kyushu (502.5 ± 9.6 Ma) after Sakashima et al. (2003). In addition, Tagiri et al. (2010) described U-Pb zircon SHRIMP age of metamorphic porphyry (505.1 ± 4.4 Ma) and metamorphic granite clast (499.6 ± 5.6 Ma), and Tagiri et al. (2011) reported U-Pb zircon SHRIMP age of felsic schist (510.0 ± 4.0 Ma) from the Hitachi metamorphic rocks. These rocks are considered to be resulted from Cambrian arc-trench system in proto-Japan (Isozaki et al., 2010). In south Kitakami Mountains, Shimojo et al. (2010) described U-Pb zircon SHRIMP age of trondjemite in Hayachine complex (466 ± 6 Ma), and Sasaki et al. (2013) reported that the solidification age of the Hikami granites is 450 Ma. In addition, Osanai et al. (in press) described U-Pb zircon LA-ICPMS age of granitic rocks in the Kurosegawa tectonic line in Kyushu (446–472 Ma). These data suggests that the granitic activity in early Paleozoic of proto-Japan arc occurs at ca. 500 Ma and ca. 450 Ma.

Keywords: Kitakami, Cambrian, zircon, U-Pb age, tonalite



## U-Pb ages of zircon in plutonic rocks within the southern Abukuma Mountains

TAKAHASHI, Yutaka<sup>1\*</sup> ; MIKOSHIBA, Masumi<sup>1</sup> ; KUBO, Kazuya<sup>1</sup> ; DANHARA, Toru<sup>2</sup> ; IWANO, Hideki<sup>2</sup> ; HIRATA, Takefumi<sup>3</sup>

<sup>1</sup>Geological Survey of Japan, AIST, <sup>2</sup>Kyoto Fission Track Co., Ltd., <sup>3</sup>Kyoto University

Abukuma Plutonic and Metamorphic Rocks are widely distributed in the southern Abukuma Mountains. These rocks had been studied in detail (e.g. Miyashiro, 1958; Research Group of the Abukuma Plateau, 1969; Kano et al., 1974; Maruyama, 1979). Radiometric age datings of the Abukuma Plutonic Rocks were carried out by Kawano and Ueda (1965), Maruyama (1978), Shibata and Uchiumi (1983), Shibata (1987), Shibata and Tanaka (1987) and others. These studies indicated that radiometric ages of the Abukuma Plutonic Rocks are almost 90 to 120 Ma. Recently, Ar-Ar age dating of hornblende (Takagi and Kamei, 2008) and U-Pb age dating of zircon (Kon and Takagi, 2012) for plutonic rocks in northern Abukuma Mountains were carried out. They showed that the ages of gabbro and granitic rocks are similar. On the other hand, U-Pb age dating of zircon for plutonic rocks in southern Abukuma Mountains is not yet performed. Therefore, U-Pb age dating of zircon for major plutons of southern Abukuma Mountains was carried out, result of which is reported and tectonics of the Abukuma Mountains is discussed based on the cooling history of the plutons.

Plutonic rocks in the southern Abukuma Mountains are classified into gabbro and diorite, fine-grained diorite, hornblende-biotite granodiorite (Irishiken Pluton, Kamikimita Pluton, Tabito Pluton, Ishikawa Pluton, Miyamoto Pluton and Samegawa Pluton), biotite granodiorite (Torisone Pluton), biotite granite and fine-grained leucogranite, based on the geological relations. The U-Pb ages of zircon for gabbro are 102.7 $\pm$ 0.8 Ma (Tabito Pluton), 109.0 $\pm$ 1.1 Ma (Hanawa Pluton), 114.2 $\pm$ 0.8 Ma (Miyamoto Pluton). As for the hornblende-biotite granodiorite, U-Pb ages are 105.3 $\pm$ 0.8 Ma (Irishiken Pluton), 105.2 $\pm$ 0.8 Ma (Kamikimita Pluton), 113.8 $\pm$ 0.7 Ma (Tabito Pluton), 104.4 $\pm$ 0.7 Ma (Ishikawa Pluton) and 106.4 $\pm$ 0.8 Ma (Miyamoto Pluton). Also for the biotite granodiorite (Hanawa Pluton), the biotite granite and fine-grained leucogranite U-Pb ages are 105.7 $\pm$ 1.0 Ma, 104.5 $\pm$ 0.5 Ma and 100.2 $\pm$ 0.8 Ma, respectively. These data indicate that the intrusion ages of Gabbro and surrounding granitic rocks are similar to each other. Furthermore, K-Ar ages of biotite and or hornblende, and fission track ages of the same rock samples were measured. Accordingly, it is clear that these rocks had been cooled rapidly to 300 degree C (Ar blocking temperature of biotite) after their intrusion. This implies that the Abukuma Mountains were uplifted rapidly after the intrusion of the Abukuma Plutonic Rocks.

### References

- Kano, H. et al. (1973) Geology of the Takanuki district. Quadrangle series, 1:50,000, Geological Survey of Japan. 115 p.  
Kon Y. and Takagi, T. (2012) Jour. Mineral. Petrol. Sci., vol. 107, 183-191.  
Maruyama, T. (1978) Jour. Min. Coll. Akita Univ., Ser. A, 5, p. 53-102.  
Maruyama, T. (1979) Basement of the Japanese Islands, 523-558.  
Miyashiro, A. (1958) Jour. Fac. Sci., Univ. Tokyo, Sec. C, vol. 8, p. 245-268.  
Research Group of the Abukuma Plateau (1969) Mem. Geol. Soc. Japan, no. 4, 83-97.  
Shibata, K. (1987) Jour. Min. Petrol. Econ. Geol., vol. 82, p. 36-40.  
Shibata, K. and Tanaka, T. (1987) Jour. Min. Petrol. Econ. Geol. vol. 82, p. 433-440.  
Shibata, K. and Uchiumi, S. (1985) Jour. Min. Petrol. Econ. Geol. vol. 82, p. 405-410.  
Takagi, T. and Kamei, A. (2008) Jour. Mineral. Petrol. Sci., vol. 103, p. 307-317.

Keywords: Abukuma Granites, Gabbro, Abukuma Belt, UU-Pb age, zircon

## Structural trends and tectonic inversion in Miocene sedimentary basins in the Tsugawa-Aizu province, Niigata prefecture

NARISAWA, Sayaka<sup>1\*</sup> ; KURITA, Hiroshi<sup>2</sup>

<sup>1</sup>Niigata University, <sup>2</sup>Niigata University

The Tsugawa and Mikawa Sedimentary Basins in the northeastern part of Niigata are composed mainly of Early to Middle Miocene formations that contain so-called "Green Tuff" volcanic sediments. Previous studies emphasized the NW-SE trend in the basement during the genesis of the Tsugawa basin. This outcrop-based study intends to discuss structural trends in the development of the Miocene sedimentary basin in the Mikawa area, Aga Town, Niigata.

The Miocene in this study area are divided into the Kanose, Tsugawa, and Araya/Igashima Formations in ascending order. Sedimentary facies analysis showed that the Kanose and Tsugawa formations filled half graben or graben. N-S to NNE-SSW trending faults of a map-scale limited the extent of the formations. NW-SE trending faults formed minor steps on the basement as well as minor, syn-sedimentary faults in the Miocene. They also affected the dyke intrusion trend. In short, the genesis of the Tsugawa basin involved 2 structural trends in this study area, while more significant is the N-S to NNE-SSW trend.

At present, the extent of the Miocene in this study area is, in many places, limited by thrust faults. Thrust faults locate at the position where rift-border faults are suggested. This indicates that tectonic inversion occurred with reactivation of N-S to NNE-SSW trending faults of the two. The trend of fault reactivation suggests that development of the basin in this study area is influenced by the Shibata-Koide tectonic line.

Keywords: Niigata sedimentary basin, Miocene, rift, structural trend, inversion

## K-Ar whole rock dating of the metamorphic rocks in the Yorii-Ogawa area of the north-eastern part of the Kanto Mountains

ONO, Akira<sup>1\*</sup>

<sup>1</sup>none

Atokura Nappe is widely exposed in the Yorii-Ogawa area. It is mainly composed of Permian granitic rocks, Cretaceous Atokura Formation, Cretaceous pyroclastic rocks, Paleogene Yorii Formation and Paleogene Kiroko greenstone melange (Figure 1). Mid-Cretaceous metamorphic and granitic rocks are also distributed as small tectonic blocks. Kiroko greenstone melange mainly consists of high-pressure-type metamorphic rocks (Kiroko metamorphic rocks), meta-gabbro, meta-tonalite, serpentinite, epidote amphibolite and amphibolite. The Atokura Nappe tectonically overlies on the Mikabu greenstones and Chichibu Complex.

K-Ar whole rock ages of the Kiroko metamorphic rocks were determined on three slates and one mafic rock. The results for the slates are 127Ma, 117Ma and 115Ma. Whereas the K-Ar whole rock age of the mafic rock is 57.4Ma. The older ages of the slates are due to the presence of detrital white mica [1]. Based on the results of the K-Ar ages, the Kiroko metamorphic rocks are regarded as members of Sanbagawa metamorphic rocks. This conclusion reveals that nappe tectonics took place even in the region where Sanbagawa metamorphic rocks were exhumed.

The nappe tectonics occurred at many times in Cretaceous and Paleogene forearcs of Southwest Japan. In the northeastern part of the Kanto Mountains weakly metamorphosed Chichibu complex lie on the Mikabu greenstones by thrust faults [2, 3]. The existence of unconsolidated fault gouges suggests the formation of the thrust faults in a surface part of the crust. The thrust faults were formed by Cretaceous nappe tectonics before the formation of the Atokura Nappe.

Radiometric dating of the metamorphic rocks of the Chichibu and Mikabu belts is lack in the surveyed area. Hence, K-Ar whole rock dating was performed on a muscovite-chlorite schist from the Mikabu belt and a slate from the Chichibu belt. The results are presented on the left side of Figure 1. Locations of the samples are described below and are shown by star signs in the geological map.

The sample Yorii-Mikabu is a pelitic schist of the Mikabu belt exposed near the River Arakawa, Yorii town. The sample Sekisonzan is a weakly metamorphosed slate of the Chichibu belt which was exposed near Mt. Sekisonzan, Ogawa town. The sample Suguro-P2 is a black slate rich in carbonaceous materials and fine white mica. The location of the slate is loc. d of Ref. [1]. It is a member of the Kiroko metamorphic rocks.

Particle sizes of white micas vary considerably for each slate specimen studied. This is an evidence for insufficient recrystallization of white mica during regional metamorphism. Therefore, K-Ar whole rock ages of all the studied slates are older than the assumed metamorphic ages.

[1] A.Ono, 2013, Abs. Japan Geosci. Union Meeting, SMP43-P16.

[2] K.Sudo and K.Matsumaru, 1973, Bull. Chichibu Mus. Nat. History, 17, p.13-24.

[3] T. Kimura, 1977, Abs. Geol. Soc. Japan Meeting, p.104.

Keywords: Kanto Mountains, Yorii-Ogawa area, Mikabu greenstones, Chichibu Complex, K-Ar dating, Nappe

SGL43-P01

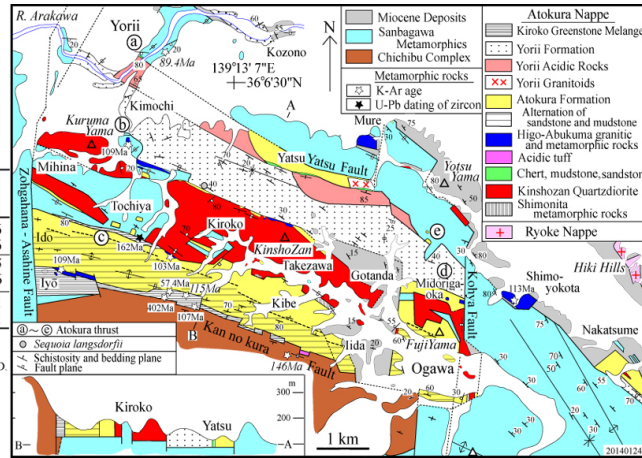
Room:Poster

Time:May 1 18:15-19:30

New K-Ar whole rock ages of metamorphic rocks from the Yorii-Ogawa area

Sample	Age (Ma)	$^{40}\text{Ar rad (scc/g} \times 10^{-5})$	$^{40}\text{Ar rad (%)}$	K (%)
Yorii-Mikabu	89.4 ± 2.2	1.34	95.9	3.76
		1.34	95.1	3.76
Sekisonzan	146 ± 4.0	1.60	95.2	2.75
		1.66	95.4	2.76
Suguro-P2	115 ± 3.0	1.86	97.4	4.01
		1.84	97.9	4.01

$\lambda_{\beta} = 4.962 \times 10^{-10} \text{ yr}^{-1}$ ,  $\lambda_{\epsilon} = 0.581 \times 10^{-10} \text{ yr}^{-1}$   
 $^{40}\text{K}/\text{K} = 0.01167 \text{ atom\%}$  Geospace Science CO.,LTD



## Detrital zircon geochronology of the Tetori Group in the Arimine and Itoshiro areas, central Japan

KAWAGOE, Yuta<sup>1</sup> ; SANO, Shin-ichi<sup>2</sup> ; ORIHASHI, Yuji<sup>3</sup> ; KOUCHI, Yoshikazu<sup>1\*</sup> ; UEDA, Tetsuya<sup>1</sup> ; YAMAMOTO, Koshi<sup>4</sup> ; OTOH, Shigeru<sup>1</sup>

<sup>1</sup>Grad. School Sci. Eng., Univ. Toyama, <sup>2</sup>Fukui Prefectural Dinosaur Museum, <sup>3</sup>ERI, Univ. Tokyo, <sup>4</sup>Grad. School Env. Stu., Nagoya Univ.

**Introduction** Provenance of the Tetori Group in the Arimine (Toyama-Gifu prefs.) and Itoshiro (Fukui Pref.) areas was analyzed using detrital zircon age distribution. In the course of the study, zircon ages of the Hida gneiss and granitoid were also determined.

**Geologic Setting** The Tetori Group consists of Middle Jurassic to Early Cretaceous shallow marine to terrestrial deposits. The group is divided, in ascending order, into the Kuzuryu, Itoshiro, and Akaiwa subgroups in the Itoshiro area (Maeda, 1961), and into the Higashisakamori, Nagatogawa, and Atotsugawa formations in the Arimine area (Kawai & Nozawa, 1958); the lower, middle, and upper units of the two areas have been correlated with each other. The lower members of the Nagatogawa-Atotsugawa formations consist of gravelly deposits of eastward running braided rivers, whereas the upper members consist of sandstone and mudstone of southward running meandering rivers. The U-Pb age of a tuff bed in the upper member of the Atotsugawa Formation is 120.0 +/- 1.2 Ma.

**Zircon ages from surrounding areas** The Hida Gneiss to the west of the Arimine area contains abundant 250-220-Ma zircons (Sano et al., 2000). The Korean Peninsula is mainly occupied by Archean-Paleoproterozoic basements of the Nangnim and Yeongnam massifs, covered with Cambrian-Jurassic deposits and cut by 250-160-Ma granitic rocks (e.g. Zhao et al., 2005). On the other hand, Northeast China between the Jiamusi Massif and the Songliao Basin, famous for " Phanerozoic crustal growth " (Wu et al., 2000), is composed primarily of 250-160-Ma granitic rocks and virtually no Precambrian rocks.

**Samples and method of study** U-Pb ages of zircons from (1) sandstone and sandy siltstone samples from six formations (members) of the Tetori Group from each area, (2) the Shimonomoto, Funatsu and Utsubo bodies of the Hida granite around the Arimine area, and (3) the Hida meta-granite on the north of the Arimine area were determined with laser ablation inductively coupled mass spectrometers (LA-ICP-MS) equipped in the Earthquake Research Institute of the University of Tokyo and Graduate School of Environmental Studies, Nagoya University.

**Results** There was marked difference in the percentage of Precambrian zircons (%Pc) between the Itoshiro-Akaiwa subgroups and the Nagatogawa-Atotsugawa formations: i.e. the %Pc of the former is 80 or more whereas that of the latter is less than 10. The samples of the Itoshiro-Akaiwa subgroups contained abundant 2500-1500-Ma zircons and a couple of Archean zircons. Age peaks of 190-170-Ma and 250-220-Ma were commonly seen for all samples of the Tetori Group. Among them, the peak of 250-220-Ma was higher in the braided river deposits and that of 190-170-Ma was higher in the meandering river deposits in the Arimine area. The Shimonomoto, Funatsu, Utsubo, and meta-granite bodies mainly contained 200-180-Ma, 250-190-Ma, 205-185-Ma, and 280-220-Ma zircons, respectively, and 180-170-Ma zircons were rare in the Hida Belt.

**Discussion** The meandering-river deposits in the Arimine area contain abundant 180-170-Ma zircons, which are virtually absent in the Hida Belt, and very few Precambrian zircons (%Pc <10). The catchment of the meandering rivers must have been occupied by Triassic-Jurassic igneous rocks with narrow exposures of Precambrian rocks. Considering the geology of eastern margin of Asia, the meandering rivers most likely passed through Northeast China (Jiamusi-Songliao). On the other hand, the braided river deposits of the area contain many 250-220 Ma zircons, suggesting that they were likely supplied at the time of uplifting of the Hida gneiss to the west. On the other hand, the Itoshiro-Akaiwa subgroups have abundant Precambrian zircons (%Pc >80). Possible candidates of the Precambrian exposure that could supply the sediments of these subgroups are the Yeongnam-Nangnim massifs. Hence the sediments of the Itoshiro-Akaiwa subgroups were likely carried by rivers that passed through the massifs.

Keywords: U-Pb age, detrital zircon, LA-ICP-MS, Tetori Group, Northeast China, East Asia

## Quaternary Tectonic Environments in North-Central Japan

TAKEUCHI, Akira<sup>1\*</sup>

<sup>1</sup>Graduate school of Science and Engineering for Research, University of Toyama

The present-day central Japan is located at the convergent junction area among four tectonic plates, Amur, Okhotsk, Philippine Sea and Pacific plates. The Toyama Trough - Fossa Magna region is a major tectonic depression bounding the contrasting, tectonic provinces, i.e. the Northeast Japan (NEJ) arc on the Okhotsk plate and the Southwest Japan (SWJ) arc on the Amur plate. The north-central Japan on the Japan Sea side of Honshu Island is characterized by the latest Cenozoic thrust/fold belts, which are considered as the results of a series of inversion/conversion tectonics in relation to the Quaternary changes in relative motion between Eurasia/Amur and Philippine Sea plates.

This paper aims at describing these changes in crustal movements including active tectonics, and evaluates the existing hypotheses on the plate tectonic framework.

At the end of Pliocene in the NEJ arc, typical basin inversion has been occurred along the NE-SW trending, boundary faults of the Miocene sedimentary basins. While, on the side of SWJ arc, boundary faults of the Miocene basins were not reactivated, but other preexisting fractures have been reused to form the reverse fault and strike-slip fault provinces in response to N-S compression due to the Early Pleistocene northward subduction of the Philippine Sea plate, and to E-W compression due to the eastward motion of Amur plate, although the Present tectonic zone of strain concentration is probably related to the subduction of Pacific plate. In order to account for the Quaternary tectonic environment with a widespread stress field of strike-slip faulting in the basement as inferred from focal mechanism solutions, an accommodation mechanism is likely to have been worked in the asthenospheric mantle of the present arc-arc collision zone.

Considering the above neotectonic circumstances from the existence of the tectonic inversion of north-central Japan and stress field of the seismogenic layer, the hypotheses on eastward motion of Amur plate and on the nascent plate-boundary along the eastern margin of Japan Sea were positively evaluated.

Keywords: Amur Plate, Toyama Trough, Fossa Magna, Quaternary, neotectonics, north-central Japan

## Fracture system in the Sawara Granite at the area beside the Hinatatoge-Okasagitoge Fault, northern Kyushu

YUHARA, Masaki<sup>1\*</sup> ; MIYAZAKI, Sotaro<sup>1</sup> ; AIZAWA, Jun<sup>1</sup>

<sup>1</sup>Department of Earth System Science, Faculty of Science, Fukuoka University

The Hinatatoge-Okasagitoge Fault has been identified by recent research. This fault continues to the Maebaru and Itoshima-hanto-oki Faults Group, and forms a single fault zone (Shimoyama et al., 2013). Activity rank of this fault is estimated C class. We recorded fractures in the Sawara Granite at the area beside the Hinatatoge-Okasagitoge Fault, and examined formation history of fracture system.

The fractures in the surveyed area are classified by their orientations into three types: NNW-SSE to NW-SE-oriented high-angle fractures, ENE-WSW-oriented high-angle fractures, and low-angle fractures. The fractures are further divided into three groups: minor faults associated with cataclasite, minor faults associated with fault gouge, and joints.

Based on the crosscut relationships of these fractures and the mineralization along joints, the formation process of the fractures related to activity of the Hinatatoge-Okasagitoge Fault involves five stages.

The minor faults associated with cataclasite were formed at the first stage. The laumontite veins were precipitated in spaces formed by the opening of joints at next stage. At the third stage, the minor faults associated with fault gouge were formed. The stilbite veins were precipitated in spaces formed by the opening of joints at next stage. At the last stage, the minor faults associated with fault gouge were formed.

Keywords: Hinatatoge-Okasagitoge Fault, Sawara Granite, fracture system, hydrothermal activity

## Bouguer gravity anomaly related to Cretaceous volcanic rocks in the Yanahara area, Okayama prefecture, SW Japan

ISHIKAWA, Nobuyo<sup>1\*</sup> ; KOMURO, Hiroaki<sup>1</sup> ; YAMAMOTO, Akihiko<sup>2</sup>

<sup>1</sup>Dept. of Geoscience, Shimane Univ., <sup>2</sup>Dept. of Earth's Evolution Environment, Division of Mathematics, Physics, Earth Science, Ehime Univ.

Cretaceous volcanic rocks (volcanic, pyroclastic and lesser sedimentary rocks) unconformably overlying the basement rocks composed of the Maizuru Group and the Yakuno complex are widely distributed in the region from Okayama to Hyogo Prefectures, central Chugoku, SW Japan. Remarkable low gravity anomalous areas observed in the region of these volcanic rocks suggest some cauldrons. Total 610 observation points including 411 new points and 199 published points (GSJ, 2000; Shichi and Yamamoto, 2001) depict a detailed Bouguer gravity anomaly map of the Yanahara district through the band-pass filter between 1 to 30 km after the terrane and Bouguer corrections with a density of 2670kg/m<sup>3</sup>.

The Bouguer gravity anomaly map reveals low gravity anomalous areas corresponding with the Cretaceous volcanic rocks and the related granitic intrusive rocks; whereas high gravity anomalous areas corresponding with the Maizuru Group and the Yakuno complex.

The low gravity anomalous areas of the Yanahara district are observed in two parts: western and northeastern areas. The western low gravity anomalous area, measuring 20×7km in size, shows a flat-floor type anomaly surrounded with high gradient margins. The relative anomaly value is 8mgal less than that of the peripheral area. This suggests a flat-floor caldera (cauldron) filled up with thick rhyolitic volcanic rocks. This inferred caldera was possibly produced 80Ma, because quartz diorite intruded into this caldera has been dated as 79.8±1.8Ma by biotite K-Ar method.

Another area northeast of Yanahara shows an elongated funnel floor surrounded with high gradient margin. The anomaly value is 7mgal less than that of the peripheral area. This value is nearly equivalent to the gravity anomaly in the above mentioned western area. Accordingly, another lesser cauldron possibly lies in this area.

## Distribution of stratigraphic units of Middle Pleistocene Izumiyatsu Formation and their arsenic concentrations

YOSHIDA, Takeshi<sup>1\*</sup> ; KUSUDA, Takashi<sup>2</sup> ; NIREI, Hisashi<sup>3</sup>

<sup>1</sup>Research Institute of Environmental Geology, Chiba, <sup>2</sup>Former Research Institute of Environmental Geology, Chiba, <sup>3</sup>Institute of medical geology

We identified the strata units of the Pleistocene Izumiyatsu Formation, which extends from the central part of Chiba Prefecture to the northeast, and the distribution of arsenic in these strata. In our summary of the geology, we refer to the Shimofusa Group.

It is possible to divide the facies of the Izumiyatsu Formation, a type locality, into five beds ? a muddy sand layer (facies 1: an estuarine sediment), an interbed of fine sand and mud (facies 2: a tidal flat sediment), a sand layer (facies 3: a tidal channel sediment), a silt layer (facies 4: a freshwater?seawater marsh sediment), and a medium sandy mud layer (facies 5: a inner bay marine sediment). The Izumiyatsu Formation, with changing facies, exhibits the following distribution pattern: facies 1, 2, 3, 4, and 5 in the southwest area, facies 5 only in the central area, and facies 4 and 5 in the northeast area. Only facies 5 is continuously distributed throughout the research areas.

Silt layer(Facies 4), the freshwater?seawater marsh sediment, has lower arsenic concentrations in sediment and in leachate than the other facies. Facies 5, the inner bay sediment, has higher arsenic concentrations in sediment and in than the other facies.

Keywords: Member unit, Groundwater flow, Arsenic

## Chronology of Brunhes-Matuyama geomagnetic polarity transition recorded in sediments and climate change

ODA, Hirokuni<sup>1\*</sup>

<sup>1</sup>National Institute of Advanced Industrial Science and Technology

Channell et al. (2010) suggested that the midpoint of the M-B boundary lies at 773.1 ka, ~7 kyr younger than the previously accepted astrochronological age for this polarity reversal (780-781 ka). Their results are based on the five high-resolution Matuyama-Brunhes polarity transition records from the North Atlantic placed on isotope age models produced by correlation of the  $\delta^{18}O$  record to an ice volume model. They further inferred that the  $^{40}Ar/^{39}Ar$  Fish Canyon sanidine (FCs) standard age that best fits the astrochronological ages is 27.93 Ma, which is younger than the two recently proposed FCs ages of 28.201 ± 0.046 Ma (Kuiper et al., 2008) and 28.305 ± 0.036 Ma (Rene et al., 2010). However, recent study by Ganerod et al. (2011) suggested an age of 28.393 ± 0.194 Ma for FCs based on paired  $^{40}Ar/^{39}Ar$  and  $^{206}Pb$ - $^{238}U$  radiometric dating supporting the calibrations of Kuiper et al. (2008) and Renne et al. (2010). Furthermore, recent study by Rivera et al. (2011) suggested an age of 28.172 ± 0.028 Ma for FCs based on cross-calibration with an astronomically tuned age of A1 tephra sanidines in the studied sequence of Faneromeni section in Crete. The discrepancy is significant that needs to be investigated carefully especially in terms of climate system involved.

On the other hand, the age model for relative paleointensity stack PISO-1500 (Channell et al., 2009) is based on IODP U1308 from North Atlantic. Channell et al. (2008) developed the age model for U1308 by correlating the benthic oxygen isotope curve with LR04 oxygen isotope stack (Lisiecki&Raymo, 2005). LR04 stack is known as oxygen isotope stack for benthic foraminifera, whose age model is dependent on ice volume model with a certain time lag. Caballero-Gill et al. (2012) developed an absolute age model based on U-Th dating for stalagmites from China and correlated the oxygen isotope curve with that on planktonic foraminifera for a deep-sea core from South China Sea. On the basis of the radiometrically calibrated chronology, they estimated that the time constant of the ice sheet is 5.4 kyr at the precession band and 10.4 kyr at the obliquity band. These values are significantly shorter than the single 17 kyr time constant originally estimated by Imbrie et al. (1984), based primarily on the timing of terminations I and II and the 15 kyr time constant used by Lisiecki and Raymo (2005) for LR04 stack.

In the presentation, the chronology of Brunhes-Matuyama geomagnetic polarity transition will be further discussed in relation to the chronology of  $^{10}Be$  records of EPICA Dome C (Dreyfus et al., 2008).

Keywords: Brunhes-Matuyama polarity transition, chronology, sediment, oxygen isotope, ice sheet, astronomical calibration

## SHRIMP U-Pb zircon dating for Byakubi tephra: implication for refined chronology for the Matuyama-Brunhes boundary

SUGANUMA, Yusuke<sup>1\*</sup>; OKADA, Makoto<sup>2</sup>; HORIE, Kenji<sup>1</sup>; KAIDEN, Hiroshi<sup>1</sup>; TAKEHARA, Mami<sup>3</sup>; SENDA, Ryoko<sup>4</sup>; KIMURA, Jun-ichi<sup>4</sup>; KAZAOKA, Osamu<sup>5</sup>

<sup>1</sup>National Institute of Polar Research, <sup>2</sup>Ibaraki University, <sup>3</sup>Kyushu University, <sup>4</sup>JAMSTEC, <sup>5</sup>Research Institute of Environmental Geology, Chiba

Paleomagnetic records from marine sediments have contributed to improved understanding of variations in the Earth's magnetic field and have helped to establish age models for marine sediments. However, lock-in of the paleomagnetic signal at some depth below the sediment-water interface in marine sediments through acquisition of a post-depositional remanent magnetization (PDRM) adds uncertainty to synchronization of marine sedimentary records (e.g., Roberts and 2004; Suganuma et al., 2011; Roberts et al., 2013). Recently, Suganuma et al. (2010) presents clear evidence for a downward offset of the paleointensity minimum relative to the <sup>10</sup>Be flux anomaly at the Matuyama-Brunhes (M-B) geomagnetic polarity boundary, which they interpret to result from a 16 cm PDRM lock-in depth. This indicates that a certain age offset probably occurs when a paleomagnetic record is used for dating marine sediments. This phenomenon also suggests that the accepted ages for the geomagnetic polarity boundaries, including the M-B boundary, should be revised (ca. 10 kyr younger in case of the M-B boundary). Contrary, two recently proposed revisions of the age of the <sup>40</sup>Ar/<sup>39</sup>Ar Fish Canyon sanidine (FCs) standard (Kuiper et al., 2008; Renne et al., 2010) would adjust <sup>40</sup>Ar/<sup>39</sup>Ar ages of the M-B boundary from Maui (Singer et al., 2005) to 781 ± 2 ka and 784 ± 2 ka, respectively.

Plio-Pleistocene marine sedimentary sequences are widely distributed in the Boso and Miura Peninsula, central Japan. Because these sequences have a significantly high sedimentation rate with well-preserved planktonic and benthic foraminifera fossils, it is possible to reconstruct a detailed geomagnetic behavior along the polarity boundaries such as M-B with high resolution oxygen isotope records. In addition, a number of tephra layers are accompanied with these sedimentary sequences, which make it possible to provide absolute age constraints for the boundaries. The Byakubi tephra, located few tens of cm above the M-B boundary, has been investigated based on SHRIMP (Sensitive High Resolution Ion Microprobe) U-Pb dating of single zircon crystals from the tephra. The initial U-Th ratio is also corrected by using ICP-MS (Inductively Coupled Plasma Mass Spectrometer) analysis of volcanic glasses of the tephra. The <sup>206</sup>Pb/<sup>238</sup>U ratio corrected by <sup>207</sup>Pb assuming <sup>206</sup>Pb/<sup>238</sup>U-<sup>207</sup>Pb/<sup>235</sup>U age concordance from 20 grains are equivalent with a weighted mean of 761.1 ± 7.6 ka. Although this M-B boundary age is ~23 kyr younger than previously accepted <sup>40</sup>Ar/<sup>39</sup>Ar ages, this is almost consistent with a younger ice core derived age of 770 ± 6 ka (Dreyfus et al., 2008), marine sediments age of 770 ka based on <sup>10</sup>Be anomaly (Suganuma et al., 2010), and <sup>40</sup>Ar/<sup>39</sup>Ar age of 761 ± 2 ka adjusted by the K-Ar based FCs standard ages (27.5 Ma: Mochizuki et al., 2010).

## Rockmagnetic and Paleomagnetic examinations for the Matuyama-Brunhes polarity transition recorded in the Kazusa Group

OKADA, Makoto<sup>1\*</sup> ; SUGANUMA, Yusuke<sup>2</sup> ; MARUOKA, Toru<sup>1</sup> ; HANEDA, Yuki<sup>1</sup> ; KAZAOKA, Osamu<sup>3</sup>

<sup>1</sup>Ibaraki University, <sup>2</sup>National Institute of Polar Research, <sup>3</sup>Research Institute of Environmental Geology, Chiba Pref.

We report results of rockmagnetic and paleomagnetic examinations for the Matuyama-Brunhes polarity transition recorded a marine sequence of the Kokumoto Formation, Kazusa Group in the Boso Peninsula. We have taken 130 oriented mini-cores from a 13 meters interval of sandy-siltstones spanning across the TNTT bed (Byakubi-ash layer) at the Tabuchi section along to the Yoro River and at the Yanagawa section. Results from thermal magnetic experiments suggested that the samples include iron sulfide, magnetite as a primary remanence carrier and no hematite. Measurements of magnetic hysteresis indicated that a domain state of the samples was PSD. Results of progressive alternating field demagnetization indicated a reversed to normal polarity transition boundary was observed at around 1.5 meter below the TNTT bed as well as previous studies, however the transition boundary was observed at around the TNTT bed in thermal demagnetization results. In the samples showing this discrepancy, a magnetite derived reversed polarity component was observed after a normal polarity component completely demagnetized at around 300-400 °C. This phenomenon would be due to that the magnetite derived primary component was slightly acquired under a weak magnetic field condition just before the M-B boundary, and then chemically yielded iron sulfide magnetic minerals acquired a much stronger normal polarity component under a strong filed condition after the polarity transition. Those results exhibited that the M-B boundary situated at around the TNTT bed where about 1.5 metes above the position reported in previous studies.

Keywords: Matuyama-Brunhes boundary, rockmagnetism, paleomagnetism, L-M Pleistocene boundary, Boso Peninsula, Kazusa Group

## High-resolution magnetostratigraphy across the Matuyama-Brunhes polarity transition from the Chiba Section

HYODO, Masayuki<sup>1\*</sup> ; TAKASAKI, Kenta<sup>2</sup> ; MATSUSHITA, Hayato<sup>2</sup> ; KITABA, Ikuko<sup>1</sup> ; KATOH, Shigehiro<sup>3</sup> ; KITAMURA, Akihisa<sup>4</sup> ; OKADA, Makoto<sup>5</sup>

<sup>1</sup>Research Center for Inland Seas, Kobe University, <sup>2</sup>Department of Earth and Planetary Sciences, Kobe University, <sup>3</sup>Division of Natural History, Hyogo Museum of Nature and Human Activities, <sup>4</sup>Institute of Geosciences, Faculty of Science, Shizuoka University, <sup>5</sup>Department of Earth Sciences, Faculty of Science, Ibaraki University

An oriented 54-m core was collected from the Kokumoto Formation of the Kazusa Group, near the Chiba Section, a candidate for the GSSP of the Early-Middle Pleistocene boundary. The core spans in stratigraphy from a thick sand layer below a mud clast layer up to just below the Ku-2B tuff. A detailed Matuyama-Brunhes (MB) geomagnetic reversal record was obtained, using u-channel samples of 1 m long cut out from 1-m core section. Magnetization components were separated by stepwise alternating field demagnetization (AFD). Low field magnetic susceptibility and anhysteretic remanent magnetization show the core consists of magnetically homogeneous sediments. Magnetizations of discrete samples of 2.2cm x 2.2cm x 2.2cm were also measured, being subjected to progressive thermal demagnetizations (THD) and AFD. The declinations of characteristic remanent magnetization (ChRM) well agree across the boundary of 1m-sections, indicating that orientation of each 1m-core section was successful. Magnetic hysteresis measurements show magnetic grains are of PSD size. THD shows that hematite is included besides magnetite, a main magnetic carrier. Thermomagnetic measurements and THD suggest that the sediments include greigite, ferrimagnetic iron sulfide, which may cause a false reversal due to self-reversal of magnetic minerals. The paleomagnetic results show that the upper boundary of the MB transition lies above the Byakubi volcanic ash layer, which is much higher than the previous result. Our data show normal polarity continues from a depth of about 1m below the Byakubi, but several polarity swings exist above it. From about 70cm above the Byakubi to the top of the core, normal polarity continues. Relative paleointensity data show the lower end of the MB transition lies below the base of the core. The relative paleointensity keeps low values in the lower part below the Byakubi, and gradually increases upward above it, reaching a maximum value at about 39 m above the Byakubi. This linear increase feature is similar to the post-MB reversal intensity pattern observed in the paleointensity stack Sint-2000 (Valet et al., 2005). The low paleointensity kept throughout the basal part suggests the beginning of the MB transition lies much below the base of the core.

Keywords: Matuyama-Brunhes boundary, magnetostratigraphy, Chiba section, oriented core

## Identification of Pleistocene tephra layers in marine sediment core C9001C, offshore Shimokita Peninsula, NE Japan

HASEGAWA, Takeshi<sup>1\*</sup> ; SUGAYA, Manami<sup>1</sup> ; OKADA, Makoto<sup>1</sup> ; MOCHIZUKI, Nobutatsu<sup>2</sup> ; FUJII, Satomu<sup>2</sup> ; SHIBUYA, Hidetoshi<sup>2</sup>

<sup>1</sup>Faculty of Science, Ibaraki University, <sup>2</sup>Kumamoto University

Correlations for Pleistocene tephra layers in marine sediment core C9001C was investigated. The core was obtained from near the Shimokita Peninsula, Japan by the CK06-06 D/V CHIKYU Shakedown Cruise in 2006. The stratigraphy of the Hole C9001C (365 m long) has been well established based on the correlation of the benthic  $\delta^{18}O$  curve with the LR04 stack (Domitsu et al., 2011). Tephra layers, a few millimeters to centimeters in thickness, can be often recognized in this sediment core that is mainly composed of dark olive-gray, diatomaceous silty clay. Two tephra layers at 30.3 mbsf and 54.3 mbsf were already correlated with the Spfa-1 and Aso-4, respectively. In this study, we focus on relatively thick and coarse tephra samples from 20 mbsf to 150 mbsf (30 - 240 ka, LR04 age). As the result, seven tephra layers were newly identified on the basis of tephro-stratigraphy and petrology, such as glass chemistry and mineralogy.

We identified the To-Of (BP1) at 19.6 mbsf, To-GP at 24.8 mbsf, Ko-i at 25.5 mbsf, Toya at 61.4 mbsf, Aso-3 at 73.9 mbsf, Mb-1 at 115.6 mbsf and Tn-C at 145.9 mbsf based on tephra databases (e.g. Okumura, 1991; Machida and Arai, 2003; Aoki and Machida, 2005). Descriptions of each tephra layer are as follows: The tephra layer at 19.6 mbsf is 6 cm thick, medium-sand sized, crystal vitric ash, including Cpx and Opx crystals. Chemical composition of glass shards is  $SiO_2=77.5\%$ ,  $K_2O=1.2\%$  (100% normalized). The tephra layer at 24.6 mbsf is 3 cm thick, medium-sand sized, vitric crystal (Cpx, Opx) ash, showing Low-K glass composition ( $SiO_2=75.4\%$ ,  $K_2O=1.1\%$ ). The tephra at 25.5 mbsf is patchy (5 mm in maximum thickness), fine-sand sized, vitric ash, showing the Medium-K composition ( $SiO_2=76.2\%$ ,  $K_2O=2.1\%$ ). The tephra at 61.4 mbsf is 1.5 m thick, fine-sand sized, vitric ash, containing trace amount of Opx. Glass shards have Medium-K composition ( $SiO_2=79.0\%$ ,  $K_2O=2.7\%$ ). The tephra layer at 73.9 mbsf is 2 cm thick, medium-sand sized, vitric crystal (Cpx, Opx) ash, characteristically showing High-K glass composition ( $SiO_2=70.3\%$ ,  $K_2O=4.6\%$ ). The tephra layer at 115.6 mbsf is 4 cm thick, medium-sand sized, vitric crystal ash, characteristically including Bt, Hb crystals in addition to pyroxenes. The glass chemistry is:  $SiO_2=78.1\%$ ,  $K_2O=3.9\%$ . The tephra layer at 145.9 mbsf is 20 cm thick, medium to coarse-sand sized, vitric crystal (Cpx, Opx) ash, showing relatively Low-K glass composition ( $SiO_2=78.4\%$ ,  $K_2O=1.5\%$ ).

We can re-examine the correlations for tephra layers with marine isotope stages (MIS) based on LR04 age. The To-Of tephra from Towada volcano can be newly correlated with early MIS 2 (<29 ka). The Aso-3 can be correlated with late MIS 6. It is also needed to revise the estimations of eruption volume and distribution of Aso-3. The Tn-C tephra from Osore volcano can be correlated with MIS 7 (<240 ka). Detailed identification of these seven tephra layers and further correlations for other tephra samples are now in progress, and will be presented elsewhere.

Keywords: Shimokita Peninsula, marine sediment core, Pleistocene, tephra, CHIKYU, glass chemistry

## Overview of tephrochronological study on Kazusa Group, the standard Quaternary marine sediments, central Japan

SUZUKI, Takehiko<sup>1\*</sup>

<sup>1</sup>Tokyo Metropolitan University

The author will review tephrochronological study on Kazusa Group, the standard Quaternary marine sediments, central Japan, and will point out issues to study in future. The former will be carried out by referring to previous works by each area such as Boso, Tama Hills, Yokohama, Choshi, and underground of central Kanto Plain. Recent studies have focused on description of characteristic properties of tephras and correlation between areas in Kanto district. Moreover, studies for correlation with proximal tephras around source volcanoes had been carried out.

Keywords: Kazusa Group, Tephrochronology, Quaternary sediments

## The Kazusa Group as a standard tephrostratigraphy of Japanese Lower to Middle Pleistocene formations

SATOGUCHI, Yasufumi<sup>1\*</sup>

<sup>1</sup>Lake Biwa Museum

Tephrostratigraphy of the Pliocene to Pleistocene formations at Kyushu and Honshu Island are established (Satoguchi and Nagahashi, 2012). Establishment of stratigraphy and chronological model needs integrative interpretation of biostratigraphy, paleo-magnetostratigraphy and other stratigraphic and chronological studies. In the early stages of the work like this, decision of standard stratigraphy for is valid. Satoguchi and Nagahashi (2012) adopted the Kazusa Group as a standard formation of the Pleistocene stratigraphy of Japan.

The Kazusa Group, which is composed of marine deposits, is investigated about magnetostratigraphy, biostratigraphy, correlated with MIS and other stratigraphical studies. Many tephra beds in this group have been described, and data of characteristic properties of these tephras for correlations are accumulated (e.g. Satoguchi, 1995). Some of these tephras are examined for correlations with widespread tephras, are revealed about their volcanic source area. For example, the Ss-Pnk, the Ss-Az and the Kb-Ks tephras are from Kyushu Island (Hayashida et al., 1996; Kamata et al., 1994; Kikkawa et al., 1991). The Ho-Kd39, Eb-Fukuda, Om-SK110 tephras are from the Chubu Mountains (Nagahashi et al., 2000). The JA-O18L tephra is from north of the Kanto district (Nakamura and Arai, 1998). The As-Kd8 and the Hkd-Ku tephras are from the Tohoku district (Murata and Suzuki, 2011; Suzuki et al., 2005). The Kazusa Group contains tephras from various areas. This thing is important for being standard tephrostratigraphy. Tephras mentioned above are widespread tephras that are distributed over 500km. Some tephras in this group are revealed that they distributed relatively small area. Volcanic source of the Byakubi tephra, which is intercalated around boundary of the Lower-Middle Pleistocene, is the Older Ontake Volcano (Takeshita et al., 2005). The Ks12 tephra above the Byakubi tephra is also from the Older Ontake Volcano. These tephras are important for investigation of volcanic history about the Older Ontake Volcano. Therefore, the Kazusa Group is important formation for Japanese stratigraphic studies and investigation of explosive volcanism in the Pleistocene.

REFERENCES: Hayashida, A. et al. (1996) Quaternary International 34?36, 89?98.; Kamata, H. et al. (1994) Journal of Geological Society of Japan, 100, 848?866.; Kikkawa, K. et al. (1991) Monthly Chikyu, 13, 228?234.; Murata, M. and Suzuki, T. (2011) Daiyonki-Kenkyu, 50, 49?60. Nagahashi, Y. et al. (2005) Journal of Geological Society of Japan, 106, 51-69.; Nakamura, M. and Arai, F. (1998) Chikyu-Kagaku, 52, 153-157.; Satoguchi, Y. (1995) Journal of Geological Society of Japan, 101, 767-782.; Satoguchi, Y. & Nagahashi, Y. (2012) Island Arc, 149-169.; Suzuki, T. et al. (2005) Island Arc, 14, 666?78.; Takeshita, Y. et al. (2005) Journal of Geological Society of Japan, 111, 417-433.

Keywords: Kazusa Group, widespread tephra, Pleistocene, Byakubi tephra

## Reconstruction of paleogeography of Kanto district about 1.6 Ma based on tephrostratigraphy

NAKAJIMA, Eri<sup>1\*</sup> ; SUZUKI, Takehiko<sup>2</sup>

<sup>1</sup>Graduate student, Tokyo Metropolitan University, <sup>2</sup>Tokyo Metropolitan University

First Horinouchi Tuff (HU<sub>1</sub>) in the Oyamada Formation of the Kazusa Group, erupted about 1.63 Ma, had been found in and around Kanto Plain by previous studies. We examined the correlation of HU<sub>1</sub> and tephtras stratigraphically near to HU<sub>1</sub> to reconstruct paleogeography of Kanto district in Early Pleistocene. The tephtras collected from the river bed of the Tama River (Tachikawa city), the Sayama Hills, the Yokohama area, the Choshi area, Enoki Trench Core, Tachikawa Core, and Higashiyamato Core were analyzed. The tephtras were correlated based on their mineral contents, refractive indices of volcanic glass shards and minerals, chemical compositions of volcanic glass shards and titanomagnetite. As a result, it was newly revealed that three tephtra layers (Sayama Gomashio Volcanic Ash in Sayama Formation, pumice fall deposit in the Tachikawa Core Fujimi of Tachikawa, HY-1.1-HY1-6 in the Higashiyamato Core Narabashi of Higashiyamato) are correlated with HU<sub>1</sub>. Also, We analyzed Tobiratoge Pyroclastic Rocks and Sanjiro Pyroclastic Rocks occurred in the south part of the Utsukushigahara Plateau in order to detect the source volcano of HU<sub>1</sub>. As a result, both Tobiratoge Pyroclastic Rocks and Sanjiro Pyroclastic Rocks are not correlated because of difference refractive indices and chemical compositions of volcanic glass shards and refractive indices of hornblende. Thus, it was revealed that HU<sub>1</sub> has not been erupted from the volcano vicinity of Utsukushigahara Plateau. We estimated the accumulation rates of sedimentation based on correlated tephtras. The accumulation rates of sediments are 46.3 cm/kyr in the Yokohama area, 59.0 cm/kyr at Tachikawa Core, 2.5-10.3 cm/kyr at Haginaka Core, 3.8-6.7 cm/kyr in the Choshi area. These differences of the accumulation rates of sediments reflect the difference of the sedimental environment. Moreover, in Tachikawa Core and Sayama Hills, HU<sub>1</sub> are accumulated thicker than other areas. It is expected that HU<sub>1</sub> had reworked again and again after its primal deposition by the effect of wave action in shallow sea.

Keywords: tephtra, Kazusa Group, First Horinouchi Tuff, paleogeography

## Stratigraphy of the L-M Pleistocene boundary section in the Kokumoto Formation with re-definition of the Byk-TNTT tephra

KAZAOKA, Osamu<sup>1\*</sup>; OKADA, Makoto<sup>2</sup>; KAMEYAMA, Shun<sup>1</sup>; SUGANUMA, Yusuke<sup>3</sup>; AIDA, Nobuyuki<sup>4</sup>; MORISAKI, Masaaki<sup>1</sup>; KAGAWA, Atsushi<sup>1</sup>; KUMAI, Hisao<sup>5</sup>; NIREI, Hisashi<sup>6</sup>

<sup>1</sup>Research Institute of Environmental Geology, Chiba, <sup>2</sup>Ibaraki University, <sup>3</sup>National Institute of Polar Research, <sup>4</sup>Shumei University, <sup>5</sup>Osaka City University, <sup>6</sup>Officer of IUGS-GEM

Detailed stratigraphy of the Kazusa Group was surveyed for development of water-soluble natural gas on many marker tephra in Boso peninsula (Kanehara et al., 1949; Shinada et al., 1951; Mitsunashi et al., 1959; Mitsunashi et al., 1961; Ishiwada et al., 1971; Mitsunashi et al., 1979). Magnetostratigraphy (Nakagawa et al., 1969; Niitsuma, 1976; Okada & Niitsuma, 1989), planktonic foraminifera (Oda, 1977), nannofossils (Takayama, 1967; Sato et al., 1988) and diatom (Cherepanova et al., 2002) were studied on the detailed stratigraphy for international correlation.

The Early-Middle Pleistocene boundary is in the middle part of the Kokumoto Formation in Kazusa Group (Kumai, 1996). Many marker tephra are interbedded in Kiwada F., Otadai F., Umegase F. and Kakinokidai F. Only 5 marker tephra are intercalated in Kokumoto F. Over twenty thin tephra, pumice bed, scoria bed and vitric fine tuff were fined out in the middle silty part of the Kokumoto F. for detailed stratigraphy around the Early-Middle Pleistocene boundary in Yoro river route, type route of the Kazusa G. (WQSB, 1996). Byakubi(Byk) tephra, 1-3cm thick vitric fine tuff under 27m thick from Ku2 distribute in Byakubi district along Yoro river. Matuyama?Brunhes magnetic reversal was fined out in the middle silty part under Ku2 tephra (Nakagawa et al., 1969). Aida(1997) showed that the magnetic reversal distribute just below the Byk tephra. TNTT tephra and the Matuyama?Brunhes magnetic reversal just below the TNTT tephra were fined under Ku2 on Yanagawa route (Niitsuma, 1976). Same tephra and the magnetic reversal were fined on Heizo route and Chonan route (Okada & Niitsuma, 1989). White vitric tephra are interbedded often in the Kazusa G. So marker tephra is necessary tephra association with over 2 tephra. 4 tephra, 3 scoria bed and 1 vitric fine tuff, were fine out just above Byk tephra on Yoro river route for detailed stratigraphy around the magnetic reversal by this study. And same tephra association were recognized just above the TNTT tephra in Yanagawa route, too.

Byk tephra zone is defined as follows. Byk tephra zone is composed of 5 tephra which in ascending order are Byk-E, Byk-D, Byk-C, Byk-B and Byk-A. Byk-B, Byk-C and Byk-D are medium sand grain scoria lenticular beds. Byk-A is 9 cm thick reddish gray vitric fine tuff. Byk-E is 1-3cm thick white vitric fine tuff. Byk-E tephra is correlated with TNTT tephra.

Keywords: L-M Pleistocene boundary, Kokumoto Formation, Kazusa Group, Byakubi tephra, TNTT tephra, Byk tephra zone

## Lower - Middle Pleistocene Boundary at Chiba Section and distribution situation of Byakubi Ash, central Japan

KIMURA, Hideto<sup>1\*</sup> ; KAZAOKA, Osamu<sup>2</sup> ; NIREI, Hisashi<sup>3</sup>

<sup>1</sup>Toho Chisui Co., Ltd. Kanto office, <sup>2</sup>Research Institute of Environmental Geology, Chiba, <sup>3</sup>International Union of Geological Science for Environmental Management(IUGS-GEM)

The Byakubi Ash is distributed over the Ichihara City southern part and is located in the vicinity of a base of the middle-upper member of Kokumoto formation, Kazusa Group. Kokumoto formation is sorted four member by facies, is upper member (sandy alternation), middle-upper member (mussive mud), middle-lower member (sandy alternation) , and lower member (mussive mud). The Matsuyama / Brunhes chron boundary as the Lower - Middle Pleistocene Boundary is attracted by the lower base of the Byakubi Ash, it was confirmed that the Byakubi Ash was distributed from the Yoro River(Tabuchi) , Tabuchi River(Tabuchi), Nishi River(Tsukide), to the Koshikiya River (Koshikiya).

The future follow-up survey comes to need a careful survey, but it is thought that it is to the important clue of the chase because the distribution situation of Ku2(Ku2B' and Ku2B) inserted between the high rank of the Buakubi Ash is considerably confirmed.

Keywords: Byakubi Ash, Kokumoto Formation middle-upper member, Yoro River, Chiba Section

## Tephra of the Kokumoto Formation in the Mobara area

NAKAZATO, Hiroomi<sup>1\*</sup> ; NANAYAMA, Futoshi<sup>2</sup>

<sup>1</sup>NARO, <sup>2</sup>AIST

Authors are examining the tephra stratigraphy of the Kazusa Group as part of the geologic map investigation in 1/50,000 Mobara district. The tephra of Ku0.6-Ku6E were confirmed from the Kokumoto Formation. The TNTT tephra (Niitsuma, 1971) which is just above the B/M boundary is pursued to Obota, Chonan town by Okada and Niitsuma (1989). The TNTT is a fine vitric volcanic ash with abundant hornblende ( $n_2=1.680-1.703$ ) and the pumice type volcanic glass ( $n=1.505-1.510$ ). This tephra was correlated with the tephra from the Older Ontake Volcano (Takeshita et al., 2005). The distribution of the TNTT was confirmed to Baba, Mutsuzawa town in the authors' investigations. Tephra of Ku0.6, Ku0.9 and Ku2.5 were confirmed in Terasaki, Mobara city where is the northeast limit of distribution of the Kokumoto Formation. The TNTT and the B/M boundary horizon are able to trace to this region.

Keywords: tephra, stratigraphy, TNTT

## The source volcano and age of the Byakubi tephra in the Kazusa Group in Boso Peninsula, central Japan

UCHIYAMA, Takashi<sup>1\*</sup>; TAKESHITA, Yoshihiro<sup>2</sup>; KUMAI, Hisao<sup>3</sup>

<sup>1</sup>Yamanashi Institute of Environmental Sciences, <sup>2</sup>Shinshu University, <sup>3</sup>Prof. Emeritus, Osaka City University

### Introduction

The Kazusa Group in the Boso Peninsula, central Japan is composed of Lower- Middle Pleistocene marine sediments that contain numerous tephra layers (Mitsunashi et al.1959; Machida et al. 1980; Satoguchi 1995; Satoguchi 1996 and so on). One of numerous tephra layers, Byakubi tephra (BYK; Takeshita et al. 2005) is intercalated just above Brunhes/ Matuyama (B/M) boundary in middle part of the Kokumoto Formation (Okada and Niitsuma 1989; Aida et al. 1996). BYK was correlated with YUT4 or 5 from the Older Ontake Volcano, which provide a datum plane of the Lower-Middle Pleistocene boundary in central Japan (Takeshita et al. 2005).

### Correlation of the tephra beds in the Kazusa Group with those from the Older Ontake Volcano

Heavy mineral assemblage and chemical compositions of hornblende of nine Lower-Middle Pleistocene tephra beds (Ku6E, Ku5C, BYK, Ka2.4A, Ka2.4B, Ch3, Ch1.5, Ks18, Ks12) from the Kazusa Group, in Boso Peninsula were examined in order to correlate with the tephra from the Older Ontake Volcano in central Japan by Takeshita et al. (2005). Conclusively, hornblende compositions from the nine tephra beds were distinguishable. Two of the nine beds, BYK and Ks12 tephra, were correlated with two tephra from the Older Ontake Volcano, YUT4 or 5 and KZT, respectively. The age of these tephra beds of the Kazusa Group could be inferred from the stratigraphic relationships with 47 dated lava flows on the foot of the Older Ontake Volcano, and from presence of well-known widespread tephra and magnetostratigraphy in the Boso Peninsula. Correlated these two tephra beds became valuable marker tephra for geochronological studies in inland and marine sediments from central Japan. It was also emphasized that the BYK and YUT4 or 5 could provide a datum plane of the Lower-Middle Pleistocene boundary in this region.

Keywords: Lower-Middle Pleistocene Boundary GSSP, Kazusa Group, Byakubi tephra, Ontake Volcano, Boso Peninsula

## Concentration of Elements Related to Redox Evolution in Oceanic Environments

OTAKE, Tsubasa<sup>1\*</sup>

<sup>1</sup>Faculty of Engineering, Hokkaido University

Chemical sedimentary rocks, which are precipitates from ancient seawater, not only concentrate useful elements (e.g., Fe, Mn, Co, Ni, Rare Earth Elements (REEs)), but may also reflect changes in Earth's surface environments (e.g., pH, redox conditions, surface temperature). The temporal distribution of Banded Iron Formations (BIFs), the main economic Fe source, has been proposed to indicate changes in atmospheric and ocean chemistry in early Earth related to the evolution of the biosphere. However, to acquire a better understanding of the surface environments, BIFs deposited in various sedimentary setting need to be investigated. In this study, geological and geochemical investigations of BIFs that were deposited in a shallow ocean in the Archean Barberton Greenstone Belt, South Africa, show that the Cr/Ti and U/Th ratios are higher in the BIFs compared with the underlying and overlying clastic sedimentary rocks. Oxygen isotope compositions in each chromite grain, a host mineral of Cr, were determined by SIMS. The results show the chromite has lower  $\delta^{18}\text{O}$  values compared with igneous and metamorphosed chromites, indicating that they were formed under hydrothermal conditions. The results suggest that dissolved Cr and U species in ocean were coprecipitated with ferric (hydr)oxides during the formation of the BIFs, and that chromite was formed by later hydrothermal alteration. Therefore, the results of the study indicate that enrichments of redox-sensitive elements (e.g., Cr, U) in BIFs have already occurred through chemical processes as early as 3.2 billion years ago due to the oxygenation of a shallow part of the ocean.

Volcanogenic Massive Sulfide (VMS) deposits such as Kuroko deposits in the Hokuroku district, Akita Prefecture were formed by ancient submarine hydrothermal activity, and are also associated with Fe-rich chemical sedimentary rocks. Because VMS deposits are primarily composed of sulfide minerals that are unstable in an oxic environment, such as pyrite and chalcopyrite, an anoxic environment in the Hokuroku basin may play an important role in the preservation of sulfide ores. Therefore, REE patterns and Fe isotope compositions of the Fe-rich chemical sedimentary rocks were investigated since geochemical evidence of such an environment being present in the Hokuroku basin is currently lacking. The results of these analyses show that the  $\delta^{56}\text{Fe}$  values of samples occurring directly on and above Kuroko deposits were -1.5 to 0.5 ‰. These values are largely fractionated from the  $\delta^{56}\text{Fe}$  value of the standard (i.e., 0 ‰), which is similar to that of igneous rocks. The samples that have a large negative value also bears negative Ce anomaly. These signatures indicate that partial oxidation of dissolved ferrous iron occurred by mixing ferrous iron-bearing anoxic water with oxygen-bearing seawater, and therefore that the seafloor of the Hokuroku Basin was anoxic. On the other hand,  $\delta^{56}\text{Fe}$  values of chemical sedimentary rocks formed 2 - 3 Ma after the Kuroko deposits formed ranges from -0.8 to -0.3 ‰. These values are similar to those of dissolved ferrous iron in a modern seafloor hydrothermal fluid. Therefore, the  $\delta^{56}\text{Fe}$  values of the samples indicate near complete oxidation of dissolved ferrous iron in an oxic environment. Therefore, these results suggest that the depositional environment in the Hokuroku basin shifted from anoxic to oxic after the formation of Kuroko deposits.

Keywords: Chemical sedimentary rock, Banded Iron Formation, Barberton Greenstone Belt, Chromium, Volcanogenic Massive Sulfide deposit, Iron isotope

## Os isotope stratigraphy of a ferromanganese crust: Its principles and applications

NOZAKI, Tatsuo<sup>1\*</sup> ; GOTO, Kosuke T.<sup>2</sup> ; TOKUMARU, Ayaka<sup>3</sup> ; TAKAYA, Yutaro<sup>4</sup> ; SUZUKI, Katsuhiko<sup>1</sup> ; CHANG, Qing<sup>1</sup> ; KIMURA, Jun-ichi<sup>1</sup> ; KATO, Yasuhiro<sup>4</sup> ; SHIMODA, Gen<sup>2</sup> ; TOYOFUKU, Takashi<sup>5</sup> ; USUI, Akira<sup>6</sup> ; URABE, Tetsuro<sup>3</sup>

<sup>1</sup>JAMSTEC/IFREE, <sup>2</sup>AIST/GSJ, <sup>3</sup>Univ. of Tokyo, <sup>4</sup>Univ. of Tokyo, <sup>5</sup>JAMSTEC/BIOGEOS, <sup>6</sup>Kochi Univ.

Sedimentation age determination by using an Os isotope stratigraphy is one of the effective dating methods for a ferromanganese crust. This dating method is applicable to the almost whole sedimentation age of a ferromanganese crust from the Late Cretaceous to present. So far, we have applied the Os isotope dating method to various ferromanganese crust samples collected from Northwestern Pacific, South Atlantic Oceans and Philippine Sea. In this presentation, we introduce the principles and applications of the Os isotope dating method, and discuss our recent results especially focusing on the growth hiatus of a ferromanganese crust.

Keywords: ferromanganese crust, Os isotope, geochemistry, growth hiatus, paleoceanography

## Occurrence of hydrothermal alteration minerals at the Jade hydrothermal field, in the Izena Hole, mid-Okinawa Trough

MIYOSHI, Youko<sup>1\*</sup> ; ISHIBASHI, Jun-ichiro<sup>2</sup> ; YOKOYAMA, Yuka<sup>3</sup> ; TAKAHASHI, Yoshio<sup>3</sup>

<sup>1</sup>National Institute of Advanced Industrial Science and Technology (AIST), <sup>2</sup>Department of Earth and Planetary Sciences, Graduate School of Sciences, Kyushu University, <sup>3</sup>Department of Earth and Planetary Systems Science, Graduate School of Science, Hiroshima University

Mineralization at the Jade hydrothermal field, in the Izena Hole, mid-Okinawa Trough, resembles in many aspects the Kuroko type ore mineralization. In the Kuroko type ore deposits, zonal distribution of hydrothermal clay minerals was recognized around the deposit. This study aims to reveal occurrence of hydrothermal clay minerals below the seafloor in the Jade hydrothermal field. We report mineralogy and geochemistry of hydrothermal clay minerals identified in surface sediments in the Jade field and compare with those in the Kuroko type ore deposits.

Surface sediment cores (~30 cmbsf (centimeters below the seafloor)) were collected by an acrylic push corer (MBARI-type corer) attached to remotely operated vehicle (ROV) Hyper-Dolphin. The core sampling was conducted during the NT10-17 cruise of R/V Natsushima (Japan Agency for Marine-Earth Science and Technology (JAMSTEC)) in September 2010. Minerals in the sediment were identified by X-ray diffraction (XRD), at the Department of Earth and Planetary Sciences, Kyushu University. For some sediment samples, clay fractions (<2 $\mu$ m) were collected from suspending particles in the distilled water according to the Stokes' law. Clay minerals in the clay fraction samples were identified by the XRD and analyzed chemically using a transmission electron microscope (TEM) equipped with an energy dispersive spectrometer (EDS) in the Research Laboratory for High Voltage Electron Microscopy (HVEM), Kyushu University.

A surface sediment core collected near the sulfide chimney venting high temperature fluid up to 320°C was characterized by occurrence of kaolinite, with sulfide minerals such as sphalerite and galena. The kaolinite would be related to be formed under acidic condition caused by oxidation and dissolution of the sulfide minerals by penetrating seawater. Surface sediment cores collected near clear hydrothermal fluid venting of about 100°C, which is located in 400 m distant from the sulfide chimney, were characterized by assemblage of chlorite and smectite. The chlorite had chemical composition close to Al-rich chlorite (sudoite) which was found around a few Kuroko type ore deposits. In the Kuroko type ore deposits, sudoite was considered to be stable under acidic condition because of the associated clay minerals. This study revealed occurrence of acidic alteration minerals in surface sediment at the Jade hydrothermal field, in the Izena Hole, mid-Okinawa Trough.

Keywords: clay mineral, hydrothermal alteration, Okinawa Trough

## Geochemistry of hydrothermal fluids collected from submarine volcanoes in the Izu-Bonin Arc

ISHIBASHI, Jun-ichiro<sup>1\*</sup>; NAGATOMI, Kentaro<sup>1</sup>; TAKAHASHI, Minoru<sup>1</sup>; KODAMATANI, Hitoshi<sup>2</sup>; TOMIYASU, Takashi<sup>2</sup>; TAKEUCHI, Akinori<sup>3</sup>; YAMANAKA, Toshiro<sup>4</sup>

<sup>1</sup>Graduate School of Science, Kyushu University, <sup>2</sup>Graduate School of Science and Engineering, Kagoshima University, <sup>3</sup>National Institute for Environmental Studies, <sup>4</sup>Graduate School of Natural Science and Technology, Okayama University

The Izu-Bonin Arc is an intraoceanic arc related to subduction of the Pacific Plate beneath the Philippine Sea Plate. At some submarine volcanoes on the volcanic front, active hydrothermal fields have been located. Hydrothermal fluids were collected from two active fields, the Suiyo Seamount and Myojin Knoll, and analyzed. Geochemical characteristics of hydrothermal fluids collected from the Izu-Bonin Arc hydrothermal fields will be presented, comparing with those of Okinawa Trough hydrothermal fields.

Hydrothermal fluid samples were collected from the Suiyo Seamount during the NT07-08 cruise in 2007, and from the Myojin Knoll during the NT12-10 cruise in 2012. Fluid samples were collected with ROCS (Rotary Clean Seawater Sampler) installed on ROV Hyper Dolphin (JAMSTEC). Temperature monitored during the fluid sampling showed up to 296 degC at the Suiyo Seamount, and 235 degC at the Myojin Knoll.

Fluid chemistry was characterized as 1) Depletion in Mg and SO<sub>4</sub>, 2) Enrichment in K and Ca compared with seawater; especially Ca enrichment is notable, and 3) Low concentration of organic derived species such as NH<sub>4</sub>. The fluid chemistry is explained by high-temperature water-rock interactions. Notable enrichment in Ca would be in accordance with low- and Mid-K series chemical composition of volcanic rocks. Low NH<sub>4</sub> concentration would be related to depletion in organic-rich terrestrial sediment around the volcanoes. Concentration of minor elements including metal elements will be present, to discuss linkage with mineralogy of hydrothermal deposits in these hydrothermal fields.

Keywords: seafloor massive sulfide deposit, Suiyo Seamount, Myojin Knoll, fluid-rock interaction

## Relationship between the formation of mercury deposits and the occurrences of organic minerals in subduction zones

ECHIGO, Takuya<sup>1\*</sup>

<sup>1</sup>Faculty of Education, Shiga University

Karpatite and idrialite occur in mercury deposits in the West Coast in the USA. In addition, organic matter was also found in mercury deposit in Hokkaido. Both mercury deposits are epithermal type and formed in subducting zone. The relationship between organic minerals and mercury deposits in subducting zone will be discussed.

Keywords: Mercury deposits, Organic minerals, Subducting zone, Polycyclic aromatic hydrocarbons

## A pilot magnetotelluric survey for geothermal exploration in northern Thailand

AMATYAKUL, Puwis<sup>1\*</sup> ; RUNG-ARUNWAN, Tawat<sup>1</sup> ; OGAWA, Yasuo<sup>2</sup> ; SIRIPUNVARAPORN, Weerachai<sup>1</sup>

<sup>1</sup>Geophysics Research Group, Department of Physics, Faculty of Science, Mahidol University, <sup>2</sup>Volcanic Fluid Research Center, Tokyo Institute of Technology

One of Thailand's most prominent geothermal field is located in Maechan district, Chiangrai province, along the active Maechan fault which is East-West left-lateral strike-slip fault. Its surface temperature is 99.5 degree Celsius with the flow rate of 3 l/s. Magnetotelluric (MT) survey is proposed to help delineating geothermal fluid and controlling features of the hydrothermal system. In July 2013, 7 magnetotelluric stations were deployed covering the area of Maechan geothermal field. Horizontal magnetic and electric fields ( $H_x$ ,  $H_y$ ,  $E_x$  and  $E_y$ ) were collected with the remote reference site located 70 km away in Fang district, Chiangmai province. To obtain 3-D resistivity model, 18 periods of off-diagonal ( $Z_{xy}$  and  $Z_{yx}$ ) elements ranging from 0.003 to 300 second were applied with WSINV3DMT, a 3-D MT inversion widely used among many authors. The obtained resistivity model shows the shallow conductive zones which their locations coincide with the hot springs manifestation. These conductive zone locates from the surface to not more than 500 m and referred as the reservoir of hot geothermal fluid heated by the deeper resistive batholith granite basement. The resistivity contrast in the obtained model up to 2 km northward is corresponding to the lineament of Maechan fault. This also confirms the hypothesis from previous studies that the hot fluid is being stored in fractures of weathered granite which is the damage zone of Maechan fault and reaches the surface where the springs are located through shallow fractures and faults.

Keywords: magnetotellurics, geothermal field, three-dimensional inversion, electrical resistivity, Maechan fault

## Development of in-situ Cu isotope ratio measurement by femtosecond-LA-MC-ICP-MS and its applications to ore minerals

IKEHATA, Kei<sup>1\*</sup>

<sup>1</sup>Faculty of Life and Environmental Sciences, University of Tsukuba

A new method for determining copper isotope compositions of copper-rich minerals (native copper, cuprite, chalcocite, chalcopyrite, cubanite and malachite) using a femtosecond LA-MC-ICP-MS has been developed. The standard-sample-standard bracketing technique was applied to correct the instrumental mass fractionation. Matrix effects found in chalcocite, chalcopyrite, cubanite and malachite can be corrected using the matrix-matched calibration standard. The analytical precision ( $<0.14\text{ ‰}$ ,  $2\sigma$ ) and accuracy were significantly improved compared with those of previous works using a nanosecond-LA-MC-ICP-MS.

The developed LA-MC-ICP-MS method was applied to the measurements of copper isotope ratios of minute copper ore minerals in igneous rocks (e.g., Horoman peridotite complex) and seafloor hydrothermal deposits (modern: Mariana Trough; ancient: Besshi-type and Kuroko-type volcanogenic massive sulfide deposits) in order to investigate variability of copper isotopic compositions in these samples.

The  $\delta^{65}\text{Cu}$  (where  $\delta^{65}\text{Cu} = [(^{65}\text{Cu}/^{63}\text{Cu})_{\text{sample}} / (^{65}\text{Cu}/^{63}\text{Cu})_{\text{NIST-SRM976-1}}] \times 1000$ ) values of copper-rich sulfide minerals of the active seafloor hydrothermal deposits are significantly large ( $\delta^{65}\text{Cu} = -0.7$  to  $4.0\text{ ‰}$ ) compared to those of the ancient submarine hydrothermal deposits ( $\delta^{65}\text{Cu} = -0.3$  to  $0.4\text{ ‰}$ ) and the igneous rocks ( $\delta^{65}\text{Cu} = -0.3$  to  $0.3\text{ ‰}$ ). These large copper isotope variations in the modern active seafloor hydrothermal deposits are most likely explained in terms of a redox-controlled isotope fractionation during hydrothermal reworking or alteration of precipitated copper-rich minerals. These results also suggest that sub-seafloor and metamorphic recrystallization effects probably have reduced the original range of copper isotopes.

Secondary malachite ( $\delta^{65}\text{Cu} = 2.6$  to  $3.0\text{ ‰}$ ) and native copper ( $\delta^{65}\text{Cu} = 1.4$  to  $1.7\text{ ‰}$ ) in the Besshi-type deposit have heavier copper isotope values compared to precursor copper-rich minerals. These variations are mainly due to isotope fractionation during redox reactions (weathering) at low temperatures involving the preferential incorporation of heavy copper isotope in secondary Cu(II) solutions. Therefore, copper isotope geochemistry could be a useful tool for understanding geochemical processes of copper transport and deposition in ore-forming systems.

Keywords: copper isotope ratio, femtosecond-LA-MC-ICP-MS, ore minerals

## Origin of Heavy-REE-rich apatite in deep-sea mud from Minami-Torishima area, south-eastern Japan

KON, Yoshiaki<sup>1\*</sup> ; SHIN, Ki-cheoul<sup>2</sup> ; HOSHINO, Mihoko<sup>1</sup> ; SANEMATSU, Kenzo<sup>1</sup> ; OKAMOTO, Nobuyuki<sup>3</sup> ; YANO, Nobuhiko<sup>3</sup> ; TANAKA, Mikiya<sup>4</sup> ; TAKAGI, Tetsuichi<sup>1</sup>

<sup>1</sup>Geological Survey of Japan, AIST, <sup>2</sup>Research Institute for Humanity and Nature, <sup>3</sup>JOGMEC, <sup>4</sup>Research Institute for Environmental Management Technology, AIST

We have conducted geochemical and mineralogical investigations of the rare earth and yttrium (REY)-rich mud from Minami-Torishima area in the Pacific in order to clarify the concentration of REY and their host-phase in the mud. X-ray diffraction analysis shows that the mud is mainly composed of phillipsite, fluorapatite, quartz, albite, illite and montmorillonite. Whole-rock CaO, P<sub>2</sub>O<sub>5</sub> and total REY contents of the mud are positively correlated. Relative abundance of apatite is also positively correlated to P<sub>2</sub>O<sub>5</sub> and total REY contents. These correlations suggest that apatite is the main host of the P<sub>2</sub>O<sub>5</sub> and REY in the mud. In order to quantitatively estimate the REY-host phase, we make in-situ compositional analyses of constituent minerals in the REY-mud. The result shows that the apatite is abundant in REY (9300 to 32000 ppm) and characterized by negative Ce-anomaly. In contrast, phillipsite is less abundant in REY (60 to 170 ppm). We conclude that the main REY host phase of the mud is apatite.

Keywords: REE, deep-sea mud, apatite, Minami-Torishima, LA-ICPMS, Nd isotope

## Upgradation of silica rich fluvial sands of Bangladesh: Proposals for alternate uses

RAJIB, Mohammad<sup>1\*</sup>

<sup>1</sup>Bangladesh Atomic Energy Commission / Graduate Student, Grad. Sch. Sc. Eng., Saitama University

Major rivers of Bangladesh are carrying billions of tons of sediments from the Himalayan mountain range from the north, forming bars almost on every river. These bars inundate in floodwater every year, eroding some sediments as well as depositing more. Thus, almost all the rivers are getting filled with the sediment in course of time. The government of Bangladesh has undertaken a mega plan for Capital Dredging, for raising navigability of the main and important rivers across the country. But there is not enough space to keep those dredged materials. Hence, most of the time, the dredged materials are thrown only in the vicinity of dredging area. In course of very short time, those materials eventually return back to river bed with the precipitation and surface runoff. This makes wastage of time and money.

The river sediments are rich in silicate mineral, mainly quartz and feldspar, along with others, like heavy and micaceous minerals. Quartz (SiO<sub>2</sub>) is the raw material for glass production. River sands of Bangladesh also contain some heavy minerals like magnetite, ilmenite, rutile, zircon, garnet, leucosene, pyroxene etc., and some Mica group minerals like muscovite, biotite, chlorite etc. Industrial use of these minerals are widely accepted. Upgradation of river silica by some physical separation procedures like density, magnetic and electric separators, and chemical composition revealed from X-ray fluorescence analysis shows that 60-70% silica of river sediment can be easily enriched up to 94%. Very low amount of Fe, Al, Ca, Mg and absence of Cr and Ti indicates the probable use of this upgraded silica as glass producing sand.

For industrial use, advance research is necessary for potential use of such silica for silicon extraction or other silicon products e.g. silicon chip, if the upgradation can be reached more than 99%. The heavy and magnetic minerals associated with silica also can be used economically as by-products of the process. Mining of this sediment from the rivers will increase the navigability of the rivers. As dredging is a must in almost every river of Bangladesh, the mining will work as alternative work of dredging, saving huge amount of money to be spent for dredging. This will also lessen the risk of dangerous flood problem of the country.

Moreover, since fluvial sands has been used as earth filling materials for long time and is suitable in many technical aspects, potentiality of using such sediments for artificial islands can be thought. Japan has been implementing several artificial islands where materials like solid waste, soil from mountains are mostly used as filling materials which are not always environment friendly. Feasibility study for using bulk fluvial sand from Bangladesh as earth filling materials for future artificial islands of Japan can a better alternative. This will decrease the risk of potential environmental hazards that can be created from solid waste or hill-cutting. Use of dredged materials from Bangladesh will help decreasing environmental hazards like floods too. Economical sustainability can be achieved through such reduction of hazard risk.

Keywords: Fluvial Sand, Bangladesh, Silica, Heavy Minerals, Capital Dredging, Artificial Islands

## Iron isotopic composition of the Palaeoproterozoic Hotazel Formation in the Kalahari Manganese Field, South Africa

ASAKURA, Jun<sup>1\*</sup> ; YAMAOKA, Kyoko<sup>2</sup> ; BORROK, David<sup>3</sup> ; WATANABE, Yasushi<sup>2</sup> ; KAWAHATA, Hodaka<sup>1</sup>

<sup>1</sup>Atmosphere and Ocean Research Institute, The University of Tokyo, <sup>2</sup>National Institute of Advanced Industrial Science and Technology, <sup>3</sup>University of Louisiana

Kalahari manganese deposit in the Palaeoproterozoic Hotazel Formation of Transvaal Supergroup of South Africa is the world's largest layered manganese deposit. It has alternating layers structure of three manganese rich layers and banded iron formation. This banded iron formation and manganese deposits of Hotazel Formation were formed at approximately the same time as Global Oxidation Event, which was the period of explosive growth of oxygen in Earth's atmosphere. In addition, the relevance of the snowball Earth event of Huronian glaciation has also been suggested from its formation age. Iron isotopes are sensitive indicators of the redox state, and it is suitable for estimating the marine environment when the banded iron formation was formed. Although a prior study on the iron isotope analysis of manganese deposits and banded iron formation of Hotazel Formation has been reported by Tsikos et al. in 2010, it is hard to say enough data is gathered.

In this study, drill core that was collected from the Kalahari manganese deposit in South Africa was subjected to iron isotope analysis with MC-ICP-MS and XRD analysis, and the results were compared with those of Tsikos et al.(2010). In isotopic analysis,  $\delta^{56}\text{Fe}$  values of drill core samples for the standard sample IRMM-14 were measured.

From the results, low  $\delta^{56}\text{Fe}$  values (not higher than  $-0.70\text{‰}$ ) throughout the all samples were measured. When limited to manganese-rich layers,  $\delta^{56}\text{Fe}$  values are between  $-1.66$  and  $-2.86\text{‰}$ . Relationship between Fe-Mn ratio and  $\delta^{56}\text{Fe}$  value showed that  $\delta^{56}\text{Fe}$  value have a tendency to drop to a lower value with the increasing abundance ratio of manganese to iron in a formation. This results are consistent with those of Tsikos et al.(2010). In other words, this results support their theory that banded iron formation has a role as a sink of heavy iron isotopes, and manganese are deposited in an environment that was rich in light iron isotopes.

### Reference

Harilaos Tsikos, Alan Matthews, Yigal Erel, John M. Moore, 2010. Iron isotopes constrain biogeochemical redox cycling of iron and manganese in a Palaeoproterozoic stratified basin. *Earth and Planetary Science Letters* 298, 125-134. doi: 10.1016/j.epsl.2010.07.032

Keywords: iron isotope, banded iron formation, Kalahari manganese deposit

## Hydrogen transport into the bottom of the lower mantle by phase H- phase delta solid solution $\text{MgSiO}_2(\text{OH})_2$ - $\text{AlOOH}$

OHTANI, Eiji<sup>1\*</sup> ; AMAIKE, Yohei<sup>1</sup> ; OHIRA, Itaru<sup>1</sup> ; KAMADA, Seiji<sup>1</sup> ; SAKAMAKI, Tatsuya<sup>1</sup> ; HIRAO, Naohisa<sup>2</sup>

<sup>1</sup>Tohoku University, <sup>2</sup>SPring-8

Water circulation in a global scale is a key for understanding dynamics and evolution of the Earth. Subducting slabs transport water into the Earth's deep interior. There are many studies on the stability of hydrous phases under the deep mantle conditions, and several hydrous minerals such as phase D and superhydrous phase B have been reported to be stable to the top of the lower mantle. It has been reported that hydrous phase  $\delta$ - $\text{AlOOH}$  is stable up to the bottom of the lower mantle (Ohtani et al., 2005; Sano et al., 2008). Tsuchiya (2013) theoretically predicted that Phase H,  $\text{MgSiO}_2(\text{OH})_2$ , which is the iso-structure with  $\delta$ - $\text{AlOOH}$ , is stable from 45 GPa to 55 GPa. This phase was experimentally confirmed at around 50 GPa (Nishi et al., 2014). Here, we present our recent results on synthesis experiments of hydrous phase H and a solid solution of phase H and phase  $\delta$  up to the base of the lower mantle along the normal mantle geotherm. The high pressure and high temperature in situ X-ray diffraction experiments were performed by using a double-sided laser heated diamond anvil cell at BL10XU, SPing-8. We observed that the stability field of this new candidate of water reservoir, hydrous phase H, under the lower mantle conditions up to 75 GPa and 2000 K in the  $\text{MgO-SiO}_2\text{-H}_2\text{O}$  system, although the previous studies claimed that phase H is broken down at pressures above 55 GPa. Thus, hydrous phase H is a host phase of water in the lower mantle at least up to the depth of 2000 km along both slab and normal mantle geotherms. Our experiments also revealed that the solid solution of phase H and phase  $\delta$ ,  $\text{AlOOH-MgSiO}_2(\text{OH})_2$ , containing 15 mol % of  $\text{MgSiO}_2(\text{OH})_2$  can coexist with Mg-perovskite and/or Mg-post perovskite up to 135 GPa and 2000 K. If this hydrous phase contacts with the metallic outer core, hydrogen could be dissolved into the core by forming iron hydride, FeH (Terasaki et al., 2012).

Keywords: hydrogen, hydrous phase H, hydrous phase delta,  $\text{MgSiO}_2(\text{OH})_2$ ,  $\text{AlOOH}$ , lower mantle

## Influence of H<sub>2</sub> fluid on the stability of MgSiO<sub>3</sub> enstatite in the upper mantle condition

SHINOZAKI, Ayako<sup>1\*</sup> ; KAGI, Hiroyuki<sup>1</sup> ; HIRAI, Hisako<sup>2</sup> ; OHFUJI, Hiroaki<sup>2</sup> ; OKADA, Taku<sup>3</sup> ; NAKANO, Satoshi<sup>4</sup> ; YAGI, Takehiko<sup>2</sup>

<sup>1</sup>GCRC, The university of Tokyo, <sup>2</sup>GRC, Ehime university, <sup>3</sup>ISSP, The university of Tokyo, <sup>4</sup>NIMS

C-O-H fluids affect the phase relation and melting of silicate minerals in the mantle of the Earth. The mantle is expected to become progressively reduced with increasing depth, so that H<sub>2</sub> fluid is considered to exist in the deep mantle with H<sub>2</sub>O fluids. In this study, influence of H<sub>2</sub> fluid on stability and phase relation of enstatite, which was the secondary most abundant mineral in the upper mantle, was examined using a laser heated diamond anvil cell.

In this presentation, we will report the results of MgSiO<sub>3</sub>-H<sub>2</sub> system, which is non-iron-bearing system. After heating at 3.1-13.8 GPa and about 1500-2000 K, decomposition of enstatite and formation of forsterite (Mg<sub>2</sub>SiO<sub>4</sub>), periclase (MgO) and coesite/stishovite (SiO<sub>2</sub>) were observed from XRD measurements. The presence of H<sub>2</sub> fluid were observed from Raman spectra even after the heating. Since the studied P-T range is in the stability field of orthoenstatite and high pressure clinoenstatite under dry condition, the decomposition reaction observed in the present study was presumably induced by H<sub>2</sub> fluid. Formation process of these silicate phases were evaluated by observation of quench texture of the recovered samples using SEM and TEM.

Keywords: enstatite, H<sub>2</sub> fluid, upper mantle, laser heated diamond anvil cell

## Dehydration boundary and the EoS of chlorite under high pressure and temperature

SUENAMI, Hideki<sup>1</sup> ; INOUE, Toru<sup>1\*</sup> ; KAKIZAWA, Sho<sup>1</sup> ; KIKEGAWA, Takumi<sup>2</sup>

<sup>1</sup>Geodynamics Research Center, Ehime University, <sup>2</sup>High Energy Accelerator Research Organization

Water in hydrous minerals has been transported to deep Earth's interior by subducting slab, which dehydrate at certain pressure and temperature. The existence of deep Earth's water affects the physical properties of Earth's mantle minerals, such as melting point, viscosity, elastic velocity, and so on. Therefore it is important to study the effect of water for the subducting slab materials. Serpentine ((Mg,Fe)<sub>6</sub>Si<sub>4</sub>O<sub>10</sub>(OH)<sub>8</sub>) is major hydrous mineral in subducting slab, and chlorite ((Mg,Fe,Al)<sub>6</sub>(Si,Al)<sub>4</sub>O<sub>10</sub>(OH)<sub>8</sub>) should be also important hydrous mineral in the subducting slab because Al is included in slab materials. In this study, the dehydration reactions of chlorite were determined by time-resolved X-ray diffraction analysis under high pressure and temperature using MAX80, PF-AR, KEK. In addition, P-V-T experiments of chlorite have also been conducted under HPHT. We found that chlorite was quickly dehydrated to forsterite + pyrope + fluid within 1 hour at 3 - 7 GPa when across the phase equilibrium boundary. On the other hand, the kinetic boundary was observed above 7 GPa because of low temperature phase equilibrium boundary, and the dehydration product was Mg-sursassite + unknown + fluid, The result of P-V-T experiments will be also reported.

Keywords: chlorite, hydrous phase, subducting slab, dehydration, equation of state, synchrotron X-ray in-situ experiment

## Composition and nature of melts, supercritical fluids and liquids formed by dehydration of subducted oceanic lithosphere

ULMER, Peter<sup>1\*</sup> ; SCHMIDT, Max W.<sup>1</sup> ; PETTKE, Thomas<sup>2</sup> ; LUGINBUEHL, Stefanie<sup>1</sup>

<sup>1</sup>Department of Earth Sciences, ETH Zurich, <sup>2</sup>Inst. Geol. Sciences, University of Bern

At crustal pressures, phase relations in natural rock-H<sub>2</sub>O systems involve low density aqueous fluids and/or high density hydrous melts. The wide miscibility gap between these two liquid phases leads to a dichotomy of mobile phases with quite distinct major element solubilities and trace element geochemical signatures. With increasing pressure, the fluid-melt miscibility gap closes until the crest of the miscibility gap intersects the fluid-saturated solidus, leaving a single supercritical liquid that has chemical and physical properties continuously evolving with temperature. The question is if the endpoint of the solidus is relevant for natural rock compositions. We have experimentally determined these endpoints in a variety of systems ranging from MOR basalt, to pelitic systems and to the simplified mantle systems MgO-SiO<sub>2</sub>-H<sub>2</sub>O (MSH) using different experimental techniques in the P-T range from 2.0 GPa/700 °C to 13.5 GPa/1300 °C. Supercriticality occurs over a wide range of P-T conditions ranging from 1 GPa/1100 °C for the SiO<sub>2</sub>-H<sub>2</sub>O system to 12-13 GPa in the SiO<sub>2</sub>-poor part of the MSH system.

In the MORB system, major element compositions of the fluid/melt phase evolve from peralkaline, H<sub>2</sub>O-rich, granite-like compositions to metaluminous, andesitic to basaltic compositions with increasing temperature. The endpoint of the fluid-saturated solidus occurs around 5 GPa and 1000 °C; thus, the dichotomy of fluid versus melt ceases to exist in the oceanic crust. Similar conditions were determined for pelitic to greywacke systems representing deep-sea sediments. In the mantle-like system MSH critical endpoints for fluid/melt solvi along the solidus are located between 12 and 13.5 GPa at 1100 °C. Melt compositions buffered by olivine and opx remain enstatite - olivine normative below the critical endpoint; in contrast, fluids below the endpoint become progressively enriched in MgO and are silica undersaturated (Mg/Si ratios >2) at pressures exceeding 6 GPa. Supercritical liquids coexisting with forsterite and enstatite or dense hydrous silicates are strongly silica undersaturated. The P-T evolution of fluids and liquids in the MSH system allows drawing conclusions regarding the effects of Mg-Si metasomatism in the overlying mantle wedge of a subduction system.

The consequences of the various nature of hydrous mobile phases emanating from hydrated subducted oceanic lithosphere were investigated in the MORB system by determining trace element partitioning between cpx, gar, amphibole, epidote, rutile, titanite, staurolite and phengite and liquid, the latter either being an aqueous fluid, a hydrous melt, or a supercritical liquid. Hydrous melts and supercritical liquids have almost identical trace element pattern. Thus, recycling rates of these elements are not indicative of melting, and in the fast and steep circum-pacific subduction zones, they most likely testify for production of a mobile phase from the subducting crust in the supercritical liquid regime (i.e. at pressure in excess of 4-5 GPa).

Modeling of trace element signatures of fluids, melts and supercritical liquids generated in or passing through eclogitic crustal lithologies during their ascent into the overlying mantle wedge indicate that (1) the mode of fluid advection - porous flow or - focused fluid flow - produces rather contrasting trace element signatures and (2) the presence or absence of accessory phases such as epidote, staurolite, rutile/titanite controls to a large extent the concentrations of high field strength, light REE elements and Th, U. Thus, inversion of geochemical compositions of igneous products in arc settings used to constrain the nature and composition of metasomatizing agents released from the subducted oceanic lithosphere is not straightforward and it is unlikely that an unequivocal solution is obtained.

Keywords: hydrous fluid, supercritical liquid, trace element partitioning, fluid metasomatism, high pressure experiments, subducted oceanic lithosphere

## Trace element mass balance in hydrous adiabatic mantle melting: The HAMMS1 model

KIMURA, Jun-ichi<sup>1\*</sup>; KAWABATA, Hiroshi<sup>2</sup>

<sup>1</sup>JAMSTEC, <sup>2</sup>Kochi University

A numerical mass balance calculation model for the adiabatic melting of a hydrous metasomatized peridotite source was programmed in order to simulate trace element compositions of mid ocean ridge basalt, back arc basin basalt, ocean island basalt, and large igneous province basalt. The Excel spreadsheet-based calculator, Hydrous Adiabatic Mantle Melting Simulator ver.1 (HAMMS1) uses: (1) a thermodynamic adiabatic melting model of mantle peridotite; with (2) experimentally parameterized melting relationships in terms of pressure, temperature, water content, and degree of partial melting. The trace element composition of the model basalt is calculated from the accumulated incremental melts within adiabatic melting, with consideration of source mantle depletion. The mineralogic mode in the mantle in adiabat is calculated using experimental parameterization, and is incorporated into the program. Partition coefficients of the residual mantle minerals are from lattice strain model based parameterization tested by the latest compilations of experimental results. The parameters that control the trace element composition in the model are: (1) mantle potential temperature, (2) water content in the source mantle, (3) depth of termination of adiabatic melting, and (4) source mantle depletion. It is possible to obtain the above controlling parameters by using Monte Carlo fitting calculations and comparing the calculated basalt compositions with primary basalt compositions. Additionally, HAMMS1 compares those melting parameters with its major element model. HAMMS1 provides a unique estimate of the source conditions of basalt genesis using an incompatible trace element mass balance.

Keywords: peridotite, water, adiabatic melting, trace element, forward model

## Very Large Intramolecular D-H Partitioning in Hydrated Silicate Melts Synthesized at Upper Mantle P and T

CODY, George<sup>1\*</sup> ; WANG, Ying<sup>1</sup> ; CODY, Samantha<sup>1</sup> ; FOUSTOUKOS, Dionysis<sup>1</sup> ; MYSEN, Bjorn<sup>1</sup> ; LE LOSQ, Charles<sup>1</sup>

<sup>1</sup>Geophysical Laboratory, Carnegie Institution of Washington

Hydrogen isotope fractionation during magmatic processes is key to understanding the deep Earth hydrological cycle and may place constraints on the origin of Earth's oceans. It is well established that the D/H content of water in hydrated nominally anhydrous mantle minerals is systematically lower ( $< -100$  ‰) than the standard mean ocean water (SMOW,  $D/H = 1.5576 \times 10^{-4}$ , defined as 0 ‰). Experiments have revealed significant hydrogen isotope partitioning between melts and fluids or vapors at magmatic temperatures. The origin of such fractionation, given the high temperatures of magmatic processes, is not likely due to classical isotope effects as described by bond energies via statistical mechanics.

It is well known that water has a very high affinity for silicate melts, it both dissolves in the melt as molecular water and hydrolyzes Si-O-Si linkages forming Si-OH. Whereas the molecular forms of water in melts are limited to H<sub>2</sub>O and OH, the variety of environments available for water to reside in the melt structure is surprising large. In order to study water in silicate melts one is restricted to molecular spectroscopy, e.g. Raman spectroscopy in the mid infrared regime, in windowed high pressure devices, e.g. the hydrothermal diamond anvil cell. Alternatively, one can study melts quenched to glass, where the structure of the glass corresponds to the structure of the melt at the glass transition temperature. The advantage of glasses is that one can use Solid State Nuclear Magnetic Resonance (NMR) Spectroscopy. The hydrogen isotopes conveniently provide two stable nuclei with spin, <sup>1</sup>H (H) and <sup>2</sup>H (D), thus we can use D and H solid state NMR to analyze the nature of water in silicate melts quenched to glass. Given that glass transition temperatures for silicate melts are high (500-600 °C), one does not expect H and D to behave differently. D-NMR can, however, be useful in characterizing the molecular dynamics of water in various sites in the glass.

We studied hydrated (with D<sub>2</sub>O and H<sub>2</sub>O) sodium tetrasilicate glasses, quenched from melts at 1400°C and 1.5 GPa, using <sup>1</sup>H, <sup>2</sup>H and <sup>29</sup>Si solid state NMR. Whereas D<sub>2</sub>O and H<sub>2</sub>O depolymerize the silicate melt to similar degrees, as would be expected, we surprisingly find that protium (H) and deuterium (D) intramolecular partitioning between different molecular sites within the glasses is very large and controlled by a strong preferential association of deuterons to sites with short O-D-O distances. This preference is independent of total water content and D/H ratio. Substantial intramolecular D-H partitioning is also observed in a glass with a model hydrous basalt composition. Such large isotope partitioning cannot result from classic fractionation effects because of the high synthesis temperatures. Potential kinetic isotope effects are excluded via a slow quench experiment. The partitioning is likely governed by density/molar volume isotope effects, where deuterium prefers sites with smaller molar volume. Large intramolecular site partitioning in melts could lead to significant D-H partitioning between water saturated melt and exsolved aqueous fluid (where  $D/H_{W,Melt} \neq D/H_{W,Fluid}$ ) during crystallization of Earth's magma ocean, potentially controlling the D/H content of the Earth's oceans.

Keywords: Silicate Melt, D-H fractionation, NMR, Magma Ocean

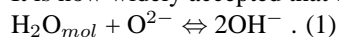
## Chemical dependence of the speciation and structural position of water in silicate melts

LE LOSQ, Charles<sup>1\*</sup> ; CODY, George<sup>1</sup> ; MYSEN, Bjorn<sup>1</sup>

<sup>1</sup>Geophysical Laboratory, Carnegie Institution of Washington

Water is the main volatile component affecting the thermodynamic, structural and rheological properties of magmatic liquids in the Earth's interior resulting in major influence on past history and present magmatic activity of the Earth. Previous experiments and modelling have shown that water can be dissolved as H<sub>2</sub>O molecules (H<sub>2</sub>O<sub>mol</sub>) and OH<sup>-</sup> groups, with the OH<sup>-</sup> groups bonded to the silicate network to form Si-OH or Al-OH bonds and perhaps alkali-OH and alkaline earth-OH complexes. However, important questions remain as to how bulk chemistry governs the link between the different OH groups and the silicate network, and the global H<sub>2</sub>O<sub>mol</sub>/OH ratio.

It is now widely accepted that dissolved water reacts with the O<sup>2-</sup> oxygen composing the silicate network following:



As O<sup>2-</sup> from the silicate network is involved in this reaction, its equilibrium constant must depend on the activities of bridging (BO), non-bridging (NBO), and free oxygen species potentially present in silicate melts, and hence on their global chemistry. Even if Al-OH and Si-OH bonding were the only variables (and, therefore, the Al/Si ratio of a melt), reaction (1) implies that the H<sub>2</sub>O<sub>mol</sub>/OH should depend on silicate melt composition. However, as the activity of NBO species is also affected by the ionic field strength of alkali and alkaline earth cations, we expect the equilibrium of reaction (1) to be affected by those cations.

To test and to quantify the occurrence and the impact of chemical effects on the speciation of water in quenched, hydrous silicate melt (glass), we analysed M<sub>2</sub>Si<sub>4</sub>O<sub>9</sub> glasses (M = Li, Na or K) containing different amounts of water (from 3.3 up to 17.6 mol%) with the help of <sup>1</sup>H and <sup>29</sup>Si MAS NMR, Raman and Infrared spectroscopy. Glasses were formed by temperature quenching (~100 °C/s) at 1.5 GPa. Raman and infrared spectroscopy show three different bands close to 2300, 2800 and 3600 cm<sup>-1</sup>. These are assigned to O-H stretching from OH groups bonded to silicate components and from H<sub>2</sub>O molecules. Correlation of those frequencies with the O ··· O distances in minerals suggest that those three bands arise from OH stretching in two main different environments: one with a mean O ··· O distance close to ~0.26 nm and another one with a ~0.29 nm O ··· O distance. In the <sup>1</sup>H MAS NMR spectra, we retrieved signals near 15 and 5 ppm arising from the ~0.26 and ~0.29 nm environments respectively. Increasing the alkali radius tends to increase the intensities of the 15 ppm <sup>1</sup>H MAS NMR peak and of the 2000-2900 cm<sup>-1</sup> Raman region, indicating an increase of the population of OH groups in the ~0.26 nm environment. In addition, the higher the alkali radius the higher the effect of water on the polymerization degree is, as testified by changes of the <sup>29</sup>Si NMR and Raman signals.

Those NMR and Raman observations suggest that the H<sub>2</sub>O<sub>mol</sub>/OH ratio in quenched hydrous silicate melts decreases in the order Li, Na, K. The greater the radius of alkali, the higher the proportion of OH<sup>-</sup> the smaller the mean O ··· O distance in their environment, and hence the more extensive hydrogen bonding. We propose that this structural evolution arises from a combination of steric hindrance and electron distribution around alkali elements that affects both equilibrium reaction (1), which will decrease in the order K > Na > Li, and the local environment of the formed OH<sup>-</sup> groups. This interplay between the nature of the alkali modifier, the speciation of water and the polymerization of the silicate network must result in non-negligible differences in viscosity of Li, Na and K silicate melts. Therefore, following this study, variation of the concentration of alkali and alkaline-earth elements in natural hydrous magmas, following their origin, will result in changes of their rheological properties, not only because of the different effects of alkali/alkaline earth elements on Si-O bonds, but also because of differences in the water speciation and OH<sup>-</sup> environments.

Keywords: water, silicate glass, Raman spectroscopy, NMR spectroscopy

## Large ion lithophile elements delivered by saline fluids to sub-arc mantle

KAWAMOTO, Tatsuhiko<sup>1\*</sup> ; MIBE, Kenji<sup>2</sup>

<sup>1</sup>Inst Geotherm Sci, Grad School Sci, Kyoto Univ, <sup>2</sup>Earth Research Institute, Univ of Tokyo

Geochemical signatures of arc basalts are explained by addition of aqueous fluids, melts, and/or supercritical fluids from subducting slab to sub-arc mantle. Partitioning of large ion lithophile elements between aqueous fluids and melts is crucial as these two liquid phases are present in the sub-arc pressure-temperature conditions. Using synchrotron x-ray beams, in-situ x-ray fluorescence (XRF) spectra are obtained from aqueous fluids and silicate melts at high-temperature and high-pressure conditions under varied concentrations of (Na, K)Cl (0-25 wt.%). There is a positive correlation between partition coefficients and pressure, as well as partition coefficients and salinity. In the systems with 13-25 wt.% (Na, K)Cl, partition coefficients of Rb, Cs, and Pb are greater than unity, indicating the capacity of such highly saline fluids to effectively transfer those elements. Enrichment of large ion lithophile elements in arc basalts relative to mid oceanic ridge basalts has been attributed to the mantle source fertilization by aqueous fluids from dehydrating oceanic plate. Such aqueous fluids are likely to contain Cl, although their amount remains to be quantified.

Keywords: subduction zone, magma, high temperature and high pressure, mantle wedge, synchrotron X-ray, chlorine

## In-situ characterization of carbon-speciation in silicate-C-O-H fluid and melt with temperature, pressure, and redox con

MYSEN, Bjorn<sup>1\*</sup>

<sup>1</sup>Geophysical Laboratory, CIW, USA

Speciation and partitioning of C-bearing volatiles species in and between silicate-saturated C-O-H fluids and (C-O-H)-saturated melts have been determined in-situ with the samples to pressures and temperatures of ~2GPa and 900°C, respectively. Structural characterization was conducted with vibrational spectroscopy of samples contained in externally-heated, hydrothermal diamond anvil cells. The redox conditions were controlled near that of the Fe+H<sub>2</sub>O=FeO+H<sub>2</sub> (reducing, RED) and Ni+H<sub>2</sub>O=NiO+H<sub>2</sub> (oxidizing, OX) equilibria, respectively. Melts are, therefore saturated in H<sub>2</sub>O, H<sub>2</sub>, and C-bearing species (redox dependent) and coexisting fluids saturated in silicate components. Solubility of volatile and silicate components depend on both temperature and pressure.

The melt/fluid partition coefficients of the C-bearing species vary with redox conditions and temperature with the  $\Delta H_{RED}^{melt/fluid} = 44(7)$  kJ/mol and  $\Delta H_{OX}^{melt/fluid} = -70(32)$  kJ/mol. Pressure is a dependent variable and increases with increasing temperature. It is assumed no pressure effect of the partition coefficients.

The solution equilibria under reducing and oxidizing conditions, respectively, were; (1)  $2CH_3^- + H_2O + Q^{n+1} = 2CH_4 + Q^n$  and (2)  $2CO_3^{2-} + H_2O + 2Q^{n+1} = HCO_3^- + 2Q^n$ , where the superscript, n, in the Q-species denotes number of bridging oxygen in the silicate species (Q-species). In the absence of H<sub>2</sub>O equilibrium (1) changes to  $CH_3^- + Q^n = CH_4 + Q^{n+1}$ . For oxidized carbon, there is an analogous expression expressing equilibrium between molecular CO<sub>2</sub> and structurally bound CO<sub>3</sub><sup>2-</sup>-groups. Under both oxidizing and reducing conditions, the abundance ratios, CH<sub>4</sub>/CH<sub>3</sub><sup>-</sup> and HCO<sub>3</sub><sup>-</sup>/CO<sub>3</sub><sup>2-</sup> increase with temperature. The enthalpy change associated with the species transformation does, however, differ for fluids and melts and also for oxidized and reduced carbon ( $\Delta H_{(1)}^{fluid} = -16(5)$  kJ/mol,  $\Delta H_{(1)}^{melt} = -49(5)$  kJ/mol,  $\Delta H_{(2)}^{fluid} = 81(14)$  kJ/mol). For the exchange equilibrium of CH<sub>4</sub> and CH<sub>3</sub><sup>-</sup> species, the temperature-dependent equilibrium constant yields  $\Delta H = 34(3)$  kJ/mol.

Reactions (1) and (2) involve changes in silicate polymerization where increasing abundance ratios, CH<sub>4</sub>/CH<sub>3</sub><sup>-</sup> and CO<sub>3</sub><sup>2-</sup>/HCO<sub>3</sub><sup>-</sup> lead to increased silicate melt polymerization. As a result of the relations between speciation of C-bearing species and melt and fluid structure, stable isotope (C and H) and element partition coefficients between melts and fluids, which depend on and silicate polymerization and silicate speciation, also vary with speciation of C-bearing species in silicate-C-O-H systems. Pressure, temperature, and redox control on the C-speciation also govern those (and other) properties.

Keywords: COH volatiles, fluid structure, melt structure, high pressure, high temperature, redox conditions

## Effect of CO<sub>2</sub> content on melting phase relations in kimberlite group I at 6.5 GPa and 1200-1600°C

SHATSKIY, Anton<sup>1</sup> ; LITASOV, Konstantin<sup>1\*</sup> ; SHARYGIN, Igor<sup>1</sup> ; OHTANI, Eiji<sup>2</sup>

<sup>1</sup>V.S. Sobolev Institute of Geology and Mineralogy SB RAS, Novosibirsk 630090, Russia, <sup>2</sup>Department of Earth and Planetary Material Science, Graduate School of Science, Tohoku University

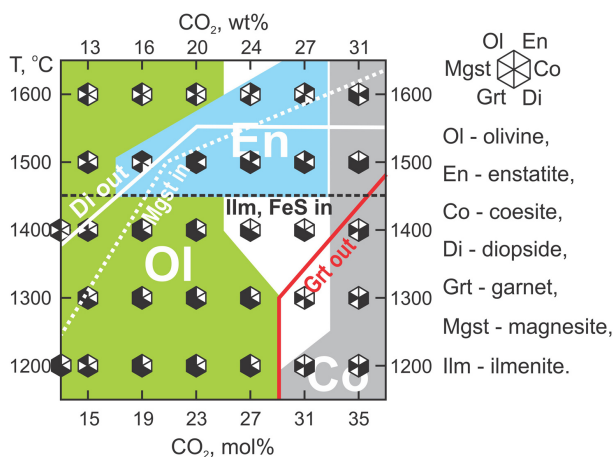
Our understanding of kimberlite petrogenesis is significantly hampered by uncertainty about the compositions of kimberlite magma. It is generally accepted that the last equilibration of kimberlite magma with surrounding mantle (garnet lherzolite) occurred beneath cratons at 6-7 GPa prior its rapid ascent (about 70 km/h) to the surface. This conclusion is based on the following facts. The deepest (170-220 km depths) and hottest (1200-1500°C) xenoliths entrapped by kimberlites are sheared garnet lherzolites originating from the lower part of lithospheric mantle. The preservation of deformation features in sheared lherzolites indicates that the rock was undergoing dynamic recrystallization just before it was picked up by the magma and that it reached the surface after less than a few days or even hours in magma rising by crack propagation (Green and Gueguen, 1983; Meyer, 1985; Sparks et al., 2006). Based on our recent study (Sharygin et al., 2013) of melting phase relations in an exceptionally fresh kimberlite group I from Udachnaya-East kimberlite (UEK) pipe at 3.0-6.5 GPa and 900-1500°C, the kimberlite melt had essentially Na-K-Ca carbonatite composition <15 wt.% SiO<sub>2</sub>, Na<sub>2</sub>O + K<sub>2</sub>O = 5-18 wt%, Na/K = 2, Cl >1.5 wt%, and Ca/(Ca+Mg) >0.5. However, the mineral assemblages obtained in these experiments differ from known mantle parageneses. This may be due to unaccounted CO<sub>2</sub> budget missed at shallow depth as a result of decarbonation reactions at 1.5-2.5 GPa. Therefore, in present study we examined the effect of additional CO<sub>2</sub> on melting phase relations in synthetic UEK kimberlite system at 6.5 GPa and 1200-1600°C.

Based on obtained results mineral assemblage equilibrated with kimberlite partial melt gradually changes from peridotite to eclogite paragenesis with increasing its CO<sub>2</sub> content from 13 to 35 mol %. As can be seen at 6.5 GPa kimberlite partial melt (i.e. Na-K-Ca carbonatite melt) becomes equilibrium with garnet lherzolite (i.e. olivine + enstatite + diopside + garnet + FeS + ilmenite assembly) at 1500°C and 23 mol % (20 wt%) CO<sub>2</sub>. This value is 10 mol% more than natural abundance of CO<sub>2</sub> in the Udachnaya-East kimberlite rock (group I kimberlite). In other words, the kimberlite magma lost almost half of the CO<sub>2</sub> budget during the eruption.

**We greatly thank the Global Center-of-Excellence program at Tohoku University (Sendai, Japan) for the technical and financial support of this study.**

Figure. Melting phase relations in Udachnaya-East kimberlite (kimberlite group I) versus temperature and CO<sub>2</sub> content at 6.5 GPa. 13 mol % CO<sub>2</sub> corresponds to the natural abundance of CO<sub>2</sub> in UEK rock.

Keywords: kimberlite, carbonatite, carbon dioxide, high-pressure experiment, Earth's mantle, melting



## Carbon dioxide in granitic magma under lower crustal conditions

YOSHIMURA, Shumpei<sup>1\*</sup>; NAKAMURA, Michihiko<sup>2</sup>; YURIMOTO, Hisayoshi<sup>3</sup>

<sup>1</sup>Department of Earth and Environmental Sciences, Yamagata University, <sup>2</sup>Department of Earth Science, Tohoku University, <sup>3</sup>Department of Natural History Sciences, Hokkaido University

### <Introduction>

Carbon dioxide is a major volatile component in the crust and mantle. Its solubility and speciation in silicate melts are important in understanding of mechanisms of magmatism and volcanism. However, they are not well constrained under lower-crustal conditions, especially in granitic magma, which is common in the crustal magmatism. In this study, we carried out equilibrium experiments in the CO<sub>2</sub>-H<sub>2</sub>O-granitic melt system to investigate the solubility and speciation of CO<sub>2</sub>.

### <Experimental procedure>

High-PT experiments were performed using a piston cylinder apparatus and a cold-seal pressure vessel. Obsidian flakes of a granitic composition and oxalic acid dehydrate (fluid source) were put in a gold or platinum capsule and run at 1123 and 1473 K and 0.1-1.5 GPa. Oxygen fugacity was estimated to be close to NNO. After quench, volatiles dissolved in the glass were analysed with FTIR spectroscopy. The composition of the coexisting fluid was quantified either by manometric analysis or based on the low-pressure solubility law and volatile contents of the glass.

### <Results>

FTIR spectra showed that both CO<sub>2</sub> molecules (CO<sub>2mol</sub>) and carbonate anions (CO<sub>3</sub><sup>2-</sup>) were present in all of the glass samples. The concentrations of CO<sub>2mol</sub>, CO<sub>3</sub><sup>2-</sup> and total H<sub>2</sub>O increased generally with increasing pressure; they were 9200 ppm, 2100 ppm and 6.1 wt%, respectively, at 1.5 GPa and 1473 K. Here, we used new molar absorption coefficients of 2350 cm<sup>-1</sup> (1192 ± 130 L cm<sup>-1</sup> mol<sup>-1</sup>; CO<sub>2mol</sub>) and 1410 cm<sup>-1</sup> (91 ± 28 L cm<sup>-1</sup> mol<sup>-1</sup>; CO<sub>3</sub><sup>2-</sup>) determined in this study. The fraction of CO<sub>3</sub><sup>2-</sup> to total CO<sub>2</sub> in the granitic melt increased with increasing total CO<sub>2</sub> content, from 0.09 (total CO<sub>2</sub> = 260 ppm) to 0.19 (11300 ppm). The molar fractions of CO<sub>2</sub> in the fluids (X<sub>CO<sub>2</sub></sub><sup>fluid</sup>) were 0.25-0.48 for the cold-seal experiments and 0.73-0.79 for the piston cylinder experiments.

### <Discussion>

We formulated the solubility law of CO<sub>2mol</sub> based on a vapour-liquid equilibrium equation. On the basis of the reaction CO<sub>2</sub> (vapour) ⇌ CO<sub>2mol</sub> (melt), we calculated the partial molar volume of CO<sub>2mol</sub> in the granitic melt and the reaction enthalpy to be 24.9 ± 2.0 cm<sup>3</sup>/mol and -22.2 ± 6.3 kJ/mol, respectively. These values are similar to those in previous experiments carried out at <6.6 kbar (Fogel and Rutherford, 1989; Behrens et al., 2004), indicating that the low-pressure solubility law can be extrapolated to 1.5 GPa. As for the formation of CO<sub>3</sub><sup>2-</sup>, we assumed a reaction CO<sub>2mol</sub> + O<sup>2-</sup> (non-bridging oxygen) ⇌ CO<sub>3</sub><sup>2-</sup>. Possible factors shifting the equilibrium to the right-hand side include the total pressure (e.g., Fine and Stolper, 1985; Guillot and Sator, 2011) and water content (King and Holloway, 1992; Behrens et al., 2004). In this study, it was difficult to evaluate these parameters separately, since the water content increased simultaneously with total pressure. If we assume that the effect of water is small enough to be neglected, the change of the partial molar volume of CO<sub>2</sub> in the melt and the reaction enthalpy can be calculated to be -8.6 ± 6.0 cm<sup>3</sup>/mol and -0.4 ± 3.1 kJ/mol, respectively.

### <Application>

Recently, unusually CO<sub>2</sub>-rich rhyolitic melt inclusions (up to 1.7 wt% total CO<sub>2</sub>) were reported by Blundy et al. (2010). The saturation pressure of this CO<sub>2</sub> content is estimated to be 1.4 GPa when CO<sub>2</sub> dissolved only as CO<sub>2mol</sub> (X<sub>CO<sub>2</sub></sub><sup>fluid</sup> = 1; T=1173 K). If we consider the formation of CO<sub>3</sub><sup>2-</sup>, the saturation pressure is estimated to 1.2 GPa.

Keywords: CO<sub>2</sub>, H<sub>2</sub>O, solubility, granitic melt

## Hydrogen positions in hydrous ringwoodite determined by pulsed neutron powder diffraction

PUREVJAV, Narangoo<sup>1\*</sup>; OKUCHI, Takuo<sup>1</sup>; TOMIOKA, Naotaka<sup>1</sup>; ABE, Jun<sup>2</sup>; HARJO, Stefanus<sup>3</sup>; AIZAWA, Kazuya<sup>3</sup>

<sup>1</sup>Institute for Study of the Earth's Interior, Okayama University, <sup>2</sup>CROSS-Tokai, <sup>3</sup>J-PARC Center, Japan Atomic Energy Agency

The transition zone in the Earth's mantle has been considered potentially large water reservoir. It was experimentally evidenced that its main constituent minerals can uptake significant amount of water as hydroxyl groups in their crystal structures. The ringwoodite  $[(\gamma\text{-Mg,Fe})_2\text{SiO}_4]$  is one of the high pressure polymorph of olivine, which is the most major phase in the lower part of the transition zone, between 525 to 660 km in depth. It was reported that ringwoodite can incorporate up to 2.6 wt.% of water (Kohlstedt et al., 1996). The hydration of ringwoodite strongly affects its physical and chemical properties such as electrical conductivity, compressibility and seismic velocities. However, crystallographic sites of hydrogen and its incorporation mechanism are still unclear mainly due to insensitiveness of X-ray probe for hydrogen. The previous studies of its structure refinement by X-ray diffraction demonstrated that hydrous ringwoodite has cubic spinel structure with  $Fd\text{-}3m$  space group (Kudoh et al., 2000; Smyth et al., 2003). Here we applied neutron diffraction for hydrous ringwoodite for the first time to analyze its hydrogen positions.

Deuterated ringwoodite powder samples were synthesized at 1300 °C and 18 GPa for 5 minutes using a scaled-up Kawai-type multi anvil apparatus. The run products were evaluated by micro-focused X-ray, Raman spectroscopy and powder X-ray diffractometer to confirm their purity.

Neutron powder diffraction patterns were taken at BL-19 (TAKUMI) at Materials and Life Science Experimental Facility, J-PARC. The two representative deuterated ringwoodite samples were with identical composition mixed and measured together in a sample holder made of TiZr "null" alloy. The obtained diffraction pattern has been analyzed by Rietveld refinement using the "Z-Rietveld" code in order to determine positions and site occupancies of deuterium atoms in the ringwoodite structure.

We can propose two possible models for the deuterium atomic positions, 96g and 192i. These refined models were given with almost identical R factors. They also gave similar site occupancies and temperature factors for the elements except for the deuterium. However, in terms of deuterium temperature factor, the 192i model is more preferable than the 96g model. The refinement results also showed that the (Mg+Fe)/Si ratio is lower than the ideal ratio of dry ringwoodite [(Mg+Fe)/Si = 2.0] while Si in T sites are fully occupied, which demonstrates that deuterium only substitutes Mg and Fe in M sites and Si in T sites is not affected.

### References:

- [1] Kohlstedt, et al., Contrib. Mineral. Petrol., 123, 345, 1996.
- [2] Kudoh, et al., Phys.Chem.Minerals., 27, 474, 2000.
- [3] Smyth, et al., Am Mineral., 88, 1402, 2003.

Keywords: ringwoodite, neutron diffraction, Rietveld refinement

## Stability of Hydrous phase H MgSiO<sub>2</sub>(OH)<sub>2</sub> in the lower mantle

AMAIKE, Yohei<sup>1\*</sup> ; OHTANI, Eiji<sup>1</sup> ; KAMADA, Seiji<sup>1</sup> ; SAKAMAKI, Tatsuya<sup>1</sup> ; TAKAHASHI, Suguru<sup>1</sup> ; HIRAO, Naohisa<sup>2</sup> ; OHISHI, Yasuo<sup>2</sup>

<sup>1</sup>Department of Earth and Planetary Materials Science, Graduate School of Science, Tohoku University, <sup>2</sup>Japan Synchrotron Radiation Research Institute

Subducting slabs transport water to Earth's deep interior and its circulation on a global scale is the key to understanding the evolution of the planet. However, it is still a matter of debate how deep water can be transported. Therefore, there are many studies on phase relationships in hydrous minerals or MORB-H<sub>2</sub>O systems. Most dense hydrous magnesium silicates (DHMS) are stable up to 50 GPa (e.g., Komabayashi et al., 2004). Recently, the synthesis of Mg- and Si- bearing  $\delta$ -AlOOH, which is a solid solution between 2AlOOH-MgSiO<sub>2</sub>(OH)<sub>2</sub>, was reported and it might be transported with Mg-perovskite or Mg-post perovskite up to 135 GPa (Ohira et al., 2012, AGU). Tsuchiya (2013) theoretically reported Phase H, the end member of the system, was stable above 45 GPa and up to 55 GPa. And also it was experimentally synthesized at 50 GPa (Nishi et al., 2014). Although the previous studies claimed that Phase H was broken down above 55 GPa, it may be a host phase of water in the deep Earth interior. Here, we report the stability field of a new candidate phase of water reservoir at the lower mantle conditions by investigating the MgO-SiO<sub>2</sub>-H<sub>2</sub>O system up to 75 GPa and 2000 K.

A mixture of quartz and brucite (molar ratio 1 : 1 ) powders were used as starting materials. The high pressure and high temperature experiments were performed by using a double-sided Laser heated diamond anvil cell. A pellet with thickness of about 15  $\mu$ m was made by a cold compression technique. In situ XRD experiments in the MgO-SiO<sub>2</sub>-H<sub>2</sub>O system were performed at BL10XU, SPring-8. In this study we confirmed that hydrous phase H does exist in the MgO-SiO<sub>2</sub>-H<sub>2</sub>O system and its stability fields expands at least up to 75 GPa and above 2000 K in contrary with previous reports (Tsuchiya, 2013; Nishi et al., 2014).

If Phase H exists under high pressure conditions corresponding to the pressure of CMB, it may transport water to CMB and thus the core may contains hydrogen as a light element.

Keywords: hydrous phase, hydrous phase, subduction

## Partitioning of carbon between metallic- and silicate-liquids in carbonaceous chondrite compositions at high pressure

ASAHARA, Yuki<sup>1\*</sup> ; OHTANI, Eiji<sup>1</sup>

<sup>1</sup>Tohoku University

Major volatile elements in the terrestrial planets are oxygen, sulfur, carbon, hydrogen, and nitrogen. They are also candidates for light components in the earth's core which were incorporated into the core at terrestrial magma ocean stage. Partitioning behavior of carbon has not been determined well though it is one of the strong candidates for light elements in the earth's core. We investigated partitioning of carbon with sulfur and oxygen between metallic- and silicate liquids at 6 GPa and 2073 K in carbonaceous chondrite composition (Allende meteorite; CV3). Effect of nitrogen and water as accessory components were also examined. High pressure experiments were conducted with multi-anvil high pressure apparatus. Graphite was used as capsule material. Composition of coexisting metallic- and silicate liquids were measured by electron microprobe with wavelength dispersion type spectrometer except for carbon in silicate liquid. Carbon concentration of bulk recovered sample was measured by elemental analyzer. Then, carbon concentration in silicate liquid was obtained by subtraction of carbon amounts in metallic phase which obtained by electron microprobe and SEM image analyses. Present result suggests that in oxidized carbonaceous chondrite composition, partitioning coefficient of carbon [ $D^{Metallicliquid/Silicateliquid} = C^{Metallicliquid}/C^{Silicateliquid}$ ;  $C$  is concentration of carbon in wt.%] is close to 1, and it may increase with increasing the  $Fe^{metal}/Fe^{oxide}$  ratio in the carbonaceous chondrite composition.

## Microanalysis of H<sub>2</sub>O and CO<sub>2</sub> in silicate melt using laser Raman spectroscopy

YOSHIMURA, Shumpei<sup>1\*</sup>; KAGASHIMA, Shin-ichi<sup>1</sup>; NAKASHIMA, Kazuo<sup>1</sup>

<sup>1</sup>Department of Earth and Environmental Sciences, Yamagata University

### <Introduction>

Water and carbon dioxide are the major volatile components in the crust and mantle. Development of microanalytical techniques of these volatiles has made it possible to investigate mechanisms of igneous and volcanic processes. FTIR has been used as a fundamental tool for this purpose, but its spatial resolution is too large (~30 μm) to analyse small melt inclusions and micro-scale volatile distribution within a high-pressure experimental sample. In this study, we developed a new technique for volatile analysis in silicate glasses with ~1 μm spatial resolution using laser Raman spectroscopy.

### <Experimental and analytical procedure>

Standard glasses were synthesized by using a piston-cylinder apparatus in M. Nakamura's laboratory. Basaltic glass powder was loaded into a platinum-sleeved nickel capsule together with oxalic acid and run at 1473 K and 0.5-1.2 GPa. After quench, the H<sub>2</sub>O and CO<sub>2</sub> (dissolved as CO<sub>3</sub><sup>2-</sup>) contents of the glasses were measured by using FTIR. The same glasses were then analysed with a Thermofisher DXR laser-Raman spectrometer. Wave length, power and diameter of the laser beam were 532 nm, 10 mw and 0.7 μm, respectively. We normalized the Raman spectra by the intensity of a peak at 500 cm<sup>-1</sup> (T-O-T bond) and subtracted the spectrum of the volatile-free glass. The intensities of peaks at 3550 cm<sup>-1</sup> (H<sub>2</sub>O) and 1080 cm<sup>-1</sup> (CO<sub>3</sub><sup>2-</sup>) in the resulting spectra were compared with the H<sub>2</sub>O and CO<sub>2</sub> contents determined by FTIR spectroscopy.

### <Results>

The H<sub>2</sub>O and CO<sub>2</sub> contents were determined to be 0.7-2.1 wt% and 0.05-0.82 wt%, respectively. Raman spectroscopy showed that the intensities of peaks at 3550 and 1080 cm<sup>-1</sup> increased with increasing H<sub>2</sub>O and CO<sub>2</sub> contents, respectively. We fitted a linear equation to the data and obtained H<sub>2</sub>O (wt%) = (3.58±0.14)×I<sub>3550</sub> and CO<sub>2</sub>(wt%) = (4.61±0.21)×I<sub>1080</sub>.

### <Application>

We applied this technique to volatile analysis of an experimentally-produced bubble-bearing basaltic glass. In the experiment, basaltic melt was first equilibrated with H<sub>2</sub>O-CO<sub>2</sub> mixture fluid at 1473 K and 1 GPa, and then decompressed to 0.5 GPa and kept for 10 minutes. After quench, the H<sub>2</sub>O and CO<sub>2</sub> contents around bubbles were measured along the radial direction at 2-μm intervals for a total of 50 μm. The CO<sub>2</sub> contents decreased on moving towards the bubble, indicating that CO<sub>2</sub> was diffusing into the bubble. Fitting the diffusion equation to this profile, we estimated the diffusivity of CO<sub>2</sub> to be 1.2×10<sup>-12</sup> m<sup>2</sup>/s. This value is consistent with that reported by Zhang et al. (2007). In contrast to CO<sub>2</sub>, H<sub>2</sub>O showed a flat profile, suggesting that H<sub>2</sub>O was already equilibrated with the fluid in the bubble. This is because the diffusivity of H<sub>2</sub>O is one order of magnitude greater than that of CO<sub>2</sub>. Such a diffusive fractionation was observed also in rhyolitic melt (Yoshimura and Nakamura, 2010).

Keywords: CO<sub>2</sub>, H<sub>2</sub>O, glass, Raman

## Dynamic and cyclic process of carbon-bearing phases of the terrestrial interior

MIURA, Yasunori<sup>1\*</sup>

<sup>1</sup>In & Out Universities

The results of the present study are summarized as follows:

1) Carbon-bearing mineral phases of the terrestrial interior are discussed to elucidate dynamic change of material states (air, liquid and solid) on active Earth planet.

2) Samples used in this study are diamond (Congo,Africa), limestone (Akiyoshi, Japan), carbonatite (Lengai, Tanzania,Africa and Europe-North America), and shungite (Shunga, Russia) together with carbonate grains of Libyan glass (Africa) to observe micro nano-grains of carbon-bearing materials with the FE analytical SEM etc.

3) The present data indicate that micro carbon-bearing grains are easily changed and remained as the three materials states mainly as solidified glasses by high pressure shock waves of earthquake, volcano and impact events to the surface to the interior.

4) Local fluid-bearing depositions irregularly distributed on the surface and interior of active Earth are based on storages on the interior formed by solidified mixtures of multiple carbon-bearing material states originally triggered by impact process on primordial Earth and ocean floors of evolved Earth.

5) The primordial planet Earth with remained heterogeneous surface by original impact-related process is considered to produce dynamic cyclic system of three material states (air, liquid and solid) of carbon-bearing materials with macro-life activity which is formed by huge production from the interior triggered by huge collision process of the giant impact and followed inner movement of active Earth with complicate local reservoir.

Keywords: carbon, interior, cyclic process, shock wave event, irregular distribution, local deposit

## Placing time constraints on a P-T-D evolution: insights from Lu-Hf garnet and U-Th-Pb monazite dating

SKRZYPEK, Etienne<sup>1\*</sup> ; SZCZEPANSKI, Jacek<sup>2</sup> ; ANCKIEWICZ, Robert<sup>3</sup> ; STIPSKA, Pavla<sup>4</sup> ; KRONER, Alfred<sup>5</sup>

<sup>1</sup>Kyoto University, <sup>2</sup>University of Wroclaw, <sup>3</sup>Polish Academy of Sciences, Krakow, <sup>4</sup>Universite de Strasbourg, <sup>5</sup>Universitat Mainz

The best approach for understanding the tectono-thermal evolution of a crustal level is through reconstructing its pressure-temperature-deformation-time (*P-T-D-t*) evolution. Whereas *P-T-D* paths can be inferred from crystallization-deformation relationships, placing absolute time constraints on such paths remains challenging, especially because a link between major element-bearing index minerals and trace element-bearing geochronometers needs to be established.

We present the example of medium-grade metasedimentary rocks (Orlica-Snieznik Dome, European Variscan Belt) for which results of Lu-Hf garnet and U-Th-Pb monazite dating are linked with prograde and retrograde stages of the *P-T-D* evolution, respectively. On the macroscopic scale, a succession of three metamorphic foliations is recognized: initial subhorizontal S1, intermediate subvertical S2, and late subhorizontal S3. A garnet±staurolite assemblage is ascribed to the S1 foliation, whereas the S2 fabric is associated with staurolite demise producing a garnet-biotite-sillimanite/andalusite assemblage. Post-S2 garnet and cordierite blastesis is followed by chlorite growth during and after the formation of the S3 foliation. Garnet porphyroblasts show a peculiar zoning pattern with a linear Mn-Ca decrease in the allanite-bearing core, an inner rim of alternating Ca-Y- and P-rich annuli, and a Ca-poor outer rim. Monazite is found as subhedral aggregates at garnet rim, and lone matrix grains close to partially resorbed garnet, staurolite or apatite. Textural observations and modelling of the garnet composition suggest that the inner rim with Ca-Y-rich annuli reflects the allanite-to-monazite transition which occurred close to the staurolite isograd. In this inner rim, a Lu oscillatory zoning pattern coincides with the zone of Ca-Y-rich annuli. Since the inner rim dominates the Lu budget of garnet, the associated Lu-Hf garnet-whole-rock isochron age of  $344 \pm 3$  Ma is ascribed to *P-T* conditions of the staurolite isograd, i.e.  $\sim 5$  kbar/575 °C in the S1 fabric. A subsequent temperature increase to peak conditions of  $\sim 5$  kbar/580-625 °C in the S2 fabric is indicated by the Ca-poor garnet outer rim that reflects staurolite breakdown. LA-ICP-MS monazite dating yields <sup>208</sup>Pb/<sup>232</sup>Th ages defining a dominant group at  $313 \pm 2$  Ma and a secondary peak at  $328 \pm 2$  Ma. Based on monazite textures, these relatively young ages are ascribed to fluid influx during retrograde chloritization.

The short time span between prograde garnet growth ( $\sim 344$  Ma) and existing Ar-Ar cooling ages on micas ( $\sim 335$  Ma) points to a tectono-thermal event of about 10 Ma. Assumed high heating and cooling rates during this event are explained by the synchronous intrusion of granitoid sheets. Nevertheless, monazite ages indicate that a low-grade overprint occurred more than 20 Ma after peak conditions.

Keywords: P-T-D-t path, prograde garnet zoning, retrograde monazite

## Microdiamond - bearing UHP chromitite from the Higo Metamorphic Rocks, Central Kyushu, Japan

NISHIYAMA, Tadao<sup>1\*</sup> ; SHIOSAKI, Dai<sup>1</sup> ; EGUCHI, Hibiki<sup>1</sup> ; YOSHIASA, Akira<sup>1</sup>

<sup>1</sup>Graduate School of Science and technology, Kumamoto University

Microdiamond-bearing ultrahigh-pressure (UHP) chromitite was newly found from a spinifex-textured metaperidotite in the Higo Metamorphic Rocks (HMR), Central Kyushu, Japan. This is the first finding of microdiamond from Japanese metamorphic rocks and the second finding in Japan following the first one from a mantle xenolith in a Cenozoic lamprophyre dyke in Shikoku<sup>1</sup>. The HMR represents a low P/T metamorphism of Cretaceous in age, however, the precursor HP or UHP metamorphism of ca. 250Ma has been inferred<sup>2</sup>. A great deal of debate has been done on whether or how the Dabie-Sulu UHP terrane extends eastward to the Korean Peninsula and also to Japan. The HMR is one of the candidates<sup>3</sup> for the eastern extension in Japan, but no definitive evidence has been given yet.

Metaperidotites occur in two localities in the HMR: one at Yamato Town in the biotite zone and the other in Matsubase Town in the garnet-cordierite I zone<sup>4</sup>. The metaperidotites from Matsubase Town show distinct spinifex-texture with decimeter-sized elongated olivine (mostly serpentinized) and enstatite. Those from Yamato Town shows either spinifex-texture or granular texture of finer grains (several mm to 1 cm across), and is strongly serpentinized. The metaperidotite bodies occur in mostly pelitic gneisses as small lenticular bodies about several ten meters in size, which are concordant to the gneissosity. The mineral assemblage of the metaperidotite is olivine (mostly serpentinized) + enstatite with secondary tremolite and antigorite. Talc occurs locally along the cleavage of enstatite. A podiform chromitite occurs in such a strongly serpentinized metaperidotite at Yamato Town as a nodular form of about 10 cm in diameter, in which we found many inclusions of microdiamond 1 to 10  $\mu\text{m}$  in size. We have made four thin sections, polished with colloidal silica, from one chromitite sample, and found many microdiamond inclusions in all thin sections. Microdiamonds occur both in chromite and in nickeline, and they are all monocrystalline. Many euhedral to subhedral grains (mostly 1  $\mu\text{m}$  in size) of microdiamond occurs in chromite, making several lines of aligned grains. Identification of diamond was carried out with an energy dispersive X-ray spectroscopy (EDS) analysis (carbon peak) and Raman spectroscopy with a He-Ne laser. We observed a Raman peak at  $1333.5\text{ cm}^{-1}$ , which is comparable to the peak ( $1332\text{ cm}^{-1}$ ) characteristic of diamond. They show no evidence of partial or total graphitization. The occurrence suggests that the striations represent healed cracks and that microdiamonds precipitated from a reduced C-O-H fluid<sup>5,6</sup>. Our finding presents a convincing evidence for the hypothesis that the Higo Metamorphic Rocks is an eastern extension of the Dabie-Sulu UHP terrane in Japan. The second implication of our finding is on the nature of UHP chromitite. Microdiamonds are found from several UHP metamorphic terranes<sup>5,6,7</sup>, however, microdiamond-bearing UHP chromitite has been found from ophiolites in non-UHP metamorphic terrane<sup>8</sup>, making the occurrence of UHP chromitite as an enigma<sup>9</sup>. The Higo UHP chromitite represents a deep subduction product as indicated by spinifex-texture in the host metaperidotite due to high pressure breakdown of antigorite (serpentine), instead of a product of mantle migration<sup>10</sup>. Therefore the origin of the UHP chromitite requires a specific interpretation in each case.

### References

1. Mizukami, T., et al., *Geology*, 36, 219-222, 2008; 2. Osanai, Y., et al., *Gondwana Res.*, 9, 152-166, 2006; 3. Omori, S., and Isozaki, Y., *J. Geogr.*, 120, 40-51, 2011; 4. Miyazaki, K., *JMG*, 22, 793-809, 2004; 5. Liou J.G., et al., *J. Asian Earth Sci.*, 35, 199-231; 6. Dobrzhinetskaya, L.F., *Gondwana Res.*, 21, 207-223, 2012; 7. Schertle, H-P., and Sobolev, N.V., *J. Asian Earth Sci.*, 63, 5-38, 2013; 8. Yang, J-S., et al., *Geology*, 35, 875-878, 2007; 9. Arai, S., *JMPS*, 105, 280-285, 2010; 10. Yamamoto, S. et al., *Lithos*, 109, 314-322, 2009

Keywords: microdiamond, UHP chromitite, Higo Metamorphic Rocks, Ultrahigh-pressure metamorphic rocks, Spinifex-texture, Dabie-Sulu UHP terrane

## Grain Size Grading of Garnet in the Liesegang Metamorphism

TORIUMI, Mitsuhiro<sup>1\*</sup> ; FUKUYAMA, Mayuko<sup>2</sup>

<sup>1</sup>JAMSTEC, <sup>2</sup>Akita univ.

The very puzzling phenomena is that the grain size of metamorphic garnet shows apparently gradational in both basic and pelitic schists, for bulk chemistries of large grain and small - grain layers are not different with each other and for chemical zonings of large and small grains of garnet display very similar pattern. These facts suggest that the domain structure by diffusion and growth of garnet should be formed in the layer and the spacing of the domain changes gradually across the grain - size layering in the metamorphism.

The layering shows parallel to subparallel against the schistosity plane, suggesting the parameter changes uniaxially along the normal direction against the schistosity. The length scales of the grain size layering ranges from several to several ten cm, being likely to those of the compositional banding derived from metasomatism. Judging from these facts, it seems that the size grading process in the plate boundary metamorphism is governed by the diffusion, reaction and grain growth mechanism, that is the precipitation mechanism in the Liesegang bands. The precipitation in the Liesegang band is considered as the Cahn - Hillert - Cook process (1), which is characterized by the relation of average grain size, size distribution, width of the layer, and spacing distribution among grains.

In this paper, we would like to investigate these relations of the size grading of garnet in the subduction zone metamorphism.

### References

(1), A. DEWIT, 1999, Advances in Chemical Physics, Volume109, Edited by I. Prigogine and Stuart A. Rice ISBN 0-471-32920-7 0 1999 John Wiley & Sons, Inc

Keywords: grain size, grading, Liesegang, metamorphism

## Metamorphism of sodic pyroxene-bearing quartz schists from the Bizan area, Sambagawa belt, eastern Shikoku, Japan

KABIR, Md fazle<sup>1\*</sup> ; TAKASU, Akira<sup>1</sup> ; KAINUMA, Masaaki<sup>1</sup>

<sup>1</sup>Department of Geoscience, Shimane University, Japan

The Bizan area of the Sambagawa metamorphic belt is occurs in easternmost Shikoku, southwest Japan. The Bizan and Kotsu areas are located in the same tectonostratigraphic horizon, i.e. the Kotsu Formation in eastern Shikoku. The Kotsu Formation in the Kotsu-Bizan area is structurally overlying and underlying by the Kawata Formation and the Kawatayama Formation, respectively. The main rock types in the Bizan area include pelitic, basic and siliceous schists, with minor amounts of psammitic and calcareous schists (Iwasaki, 1963). Faure (1983) suggested a melange zone containing tectonic blocks of serpentinite, metagabbro and garnet-amphibolite (garnet-glaucophane schist) occurs along a ductile shear zone between spotted and non-spotted schist zones. Sodic pyroxene-bearing quartz schists consist mainly of quartz and phengite, with minor amounts of amphibole (Fgl, Mrbk, Rbk, Mkt, Wnc, Brs, Fbrs), garnet, Na-Ca pyroxene (hereafter sodic pyroxene) (aegirine, aegirine-augite and omphacite) and albite. Hematite, chlorite, and epidote occur occasionally. A schistosity is defined by preferred orientation of phengite and quartz.

Garnets are spessartine-rich in composition, show a growth zoning with decreasing spessartine ( $X_{Spss}$  0.82-0.35) and increasing almandine ( $X_{Alm}$  0.01-0.41) and pyrope ( $X_{Prp}$  0.03-0.09) from core to the rim and contain inclusions of phengite (6.84 pfu), epidote, hematite and quartz. The garnets are occasionally replaced by chlorite and biotite along cracks and at the rims. Amphiboles occurring as inclusions in porphyroblastic albite are compositionally zoned, with Fbrs and Brs cores and Rbk rims. Matrix amphiboles are Brs and Mkt core, Fgl mantle and Rbk and Mrbk rims, and contain inclusions of phengite (6.50-6.51 pfu), hematite and quartz. Sodic pyroxenes occurring as inclusions in porphyroblastic albite are aegirine, aegirine-augite and omphacite with  $X_{Jd}$  0.08-0.37 contents. Some of them are compositionally zoned, with aegirine-augite and omphacite cores ( $X_{Jd}$  0.34-0.37) to aegirine-augite and aegirine rims ( $X_{Jd}$  0.34-0.21). Matrix sodic pyroxenes are aegirine-augite ( $X_{Jd}$  0.09-0.27), decreasing  $X_{Jd}$  from cores (0.22-0.25) to the rims (0.22-0.17). Some other sodic pyroxenes in the matrix display increasing  $X_{Jd}$  from core to the mantle (0.13-0.19) and decreasing towards the rim (0.19-0.12). They contain inclusions of amphibole (Brs, Fbrs, Rbk), phengite (6.66-6.82 pfu), hematite and quartz, and are partially replaced by chlorite along their cleavages. Porphyroblastic albite crystals up to 2 mm across contain inclusions of garnet, amphibole (Brs, Fbrs, Rbk), sodic pyroxene ( $X_{Jd}$  0.10-0.37), phengite (6.57-6.76 pfu) and quartz. Matrix phengites show relatively higher in Si (6.33-6.98 pfu) contents than inclusions.

According to the occurrence of mineral assemblage the Kwata, Kotsu and Kawatayama Formation probably correlate with the albite-biotite zone of the Besshi area (Enami *et al.*, 1994). Jadeite content in the sodic pyroxenes are significantly higher in sodic pyroxene-bearing quartz schists ( $X_{Jd}$  0.08-0.37) than those of garnet-aegirine augite-alkali amphibole-quartz schist ( $X_{Jd}$  0.30) in the Bizan area (Iwasaki, 1963) and Asemigawa ( $X_{Jd}$  0.15-0.19), Besshi ( $X_{Jd}$  0.14-0.23) and the Sarutagawa area ( $X_{Jd}$  0.17-0.30) in the central Shikoku (Enami *et al.*, 1994). This higher jadeite content in sodic pyroxenes suggests metamorphic conditions in the Bizan sodic pyroxene-bearing quartz schists might be higher in pressure than those of the metamorphic zonation in the albite-biotite zone of the Sambagawa belt central Shikoku by Enami *et al.* (1994).

### References

Enami *et al.* (1994) *Contrib Mineral Petrol*, 116, 182-198. Faure M. (1983) *J Geol Soci Japan* 89, 319-329. Iwasaki, M. (1963) *J Faculty of Science, Univ Tokyo, Section II*, 15, 1-90.

Keywords: Sambagawa (Sanbagawa) metamorphic belt, Bizan area, quartz schist, omphacite, aegirine-augite

## Application of the Raman carbonaceous material thermometer to the Chichibu-Sanbagawa belt in the Kanto Mountains, Japan

KOUKETSU, Yui<sup>1\*</sup> ; SHIMIZU, Ichiko<sup>2</sup>

<sup>1</sup>Geochemical Research Center, Graduate School of Science, The University of Tokyo, <sup>2</sup>Department of Earth and Planetary Science, Graduate School of Science, The University of Tokyo

The structure and tectonic history of the Chichibu-Sanbagawa belt have been investigated by the lithological structure, radiolarian age, radiometric age, deformation microstructural analysis, and X-ray diffraction analysis of carbonaceous material (CM). The structural discontinuities (nappe boundaries) within the Chichibu-Sanbagawa belt are proposed in several studies (e.g., Shimizu 1988, *J.Geol. Soc. Japan*; Isozaki & Maruyama 1991, *J. Geogr.*; Hirajima *et al.* 1992, *J.Geol. Soc. Japan*). However, the boundary between the Chichibu and Sanbagawa belts and their structural relationship are still under debate. In addition, the thermal structure was not well investigated because the geothermometer that can be applied over the temperature range of the Chichibu and Sanbagawa belts was not available. Recently, several studies proposed the geothermometers applying the Raman spectroscopy. Kouketsu *et al.* (2014, *Island Arc*) analyzed the CMs with a wide range of crystallinity, from amorphous carbon to well-crystallized graphite, in sedimentary and metamorphic rocks and proposed a new Raman CM geothermometer. By using this technique, we evaluate the peak temperatures of the rocks in the Chichibu and Sanbagawa belts in the Kanto Mountains, which is the type locality of these belts.

We investigated the mudstone, sandstone, and pelitic schist taken from the Kannagawa, Sanbagawa, and Ayukawa River districts in the Kanto Mountains, Gunma Prefecture. In the studied area, the accretionary complexes of the Northern Chichibu belt are distributed in the south, crystalline schists of the Sanbagawa belt are distributed in the north, and the Mikabu greenstones are exposed between them. The Chichibu belt is divided into three units: Kamiyoshida, Manba, and Kashiwagi units, in descending structural order (Shimizu & Yoshida 2004, *Island Arc*). The Sanbagawa belt is divided into three metamorphic zones: chlorite, garnet, and biotite zones, in order of ascending metamorphic grade (Yano & Tagiri 1998, *J.Geol. Soc. Japan*). The strata gently dip to the north and the metamorphic grade monotonously increases towards the lower structural level.

The Raman spectra of CM in mudstone and sandstone taken from the Chichibu belt include broad peaks that are characteristic of the amorphous carbon structure. The temperatures of most samples estimated by full width and half maximum (FWHM) of the D1-band are around 260-300 °C. Several CMs in the rocks near the Mt. Nishi-Mikabo show the temperature higher than 300 °C.

The intensities of Raman spectra of CM in the Sanbagawa schists are one order weaker than those in the rocks taken from the Chichibu belt. The D4-band, which is the characteristic peak in amorphous carbon, is not observed. Instead, G-band, which is the characteristic peak in well-crystallized graphite, becomes the most prominent peak at higher-grade zone. The metamorphic temperatures are estimated by using the FWHM of D1- and D2-bands and area ratio (R2) of CM Raman spectra. The metamorphic temperatures of the samples are estimated around 360-400 °C, 420-450 °C, and 460-510 °C in the chlorite, garnet, and biotite zones, respectively.

The temperatures estimated from CM show the gap of several tens of degrees or more between the Chichibu and the Sanbagawa belts. Further sampling and analysis will be proceeded.

Keywords: Raman spectroscopy, Carbonaceous material, Geothermometer, Chichibu belt, Sanbagawa belt, Kanto Mountains

## Fission track and U-Pb zircon ages of psammitic rocks from the Harushinai unit of the Kamuikotan belt, Hokkaido

OKAMOTO, Ayumi S.<sup>1\*</sup> ; TAKESHITA, Toru<sup>1</sup> ; IWANO, Hideki<sup>2</sup> ; DANHARA, Tohru<sup>2</sup> ; HIRATA, Takafumi<sup>3</sup> ; NISHIDO, Hirotsugu<sup>4</sup>

<sup>1</sup>Hokkaido University, <sup>2</sup>Kyoto Fission-Track Co., Ltd., <sup>3</sup>Kyoto University, <sup>4</sup>Okayama University of Science

In order to discuss exhumation processes and mechanisms for high-*P/T* type metamorphic rocks, it is necessary to obtain correct informations on pressure-temperature-time paths of these rocks from sedimentation to exhumation through maximum burial. We conducted coupled fission-track (FT) and U-Pb dating on detrital zircon grains in two psammitic rock samples collected from the Harushinai unit of the Kamuikotan metamorphic rocks using a Laser Ablation-Inductively Coupled Plasma-Mass Spectrometry (LA-ICP-MS). The results indicate that the concordant zircon U-Pb ages greatly vary between 1980-90 Ma. Among them, the youngest U-Pb age cluster (*c.* 110-90 Ma) is dominant, yielding the weighted mean ages of Albian ( $100.8 \pm 1.1$  and  $99.3 \pm 1.0$  Ma with  $2\sigma$  errors) for both samples. According to an oscillatory zoning of igneous origin without any overgrown rims in the analyzed zircon, the zircon U-Pb ages were not reset by the high-*P/T* type metamorphism, and hence the youngest U-Pb ages indicate the upper bound of sedimentary ages. On the other hand, the zircon FT data show the spectra with a single peak age at 100-90 Ma, which are comparable with the youngest U-Pb age cluster. The fact indicates that these zircon FT ages were once reset at *c.* 100 Ma due to an intense igneous activity at the provenance, but have not been essentially reset since the sedimentation. The scenario is supported by the temperature conditions slightly less than those of brittle-ductile transition of quartz (*c.* 300 °C, also closure temperature of zircon FT) estimated from the microstructures in deformed quartz detrital grains constituting the psammitic rocks. Combining these results with the previously reported K-Ar ages of white mica, it is inferred that Harushinai unit was deposited after *c.* 100 Ma, dragged down to the maximum depth, and further affected by a localized thermal overprint during exhumation (*c.* 58 Ma).

Keywords: Kamuikotan metamorphic rocks, zircon, U-Pb ages, Fission track ages, deformation microstructure

## Shape evolution of spinel grains in the Horoman Peridotite Complex, Hokkaido

KOIDE, Satoko<sup>1\*</sup> ; SHIBATA, Tomoki<sup>2</sup> ; MICHIBAYASHI, Katsuyoshi<sup>1</sup>

<sup>1</sup>Institute of Geosciences, Shizuoka University, <sup>2</sup>Institute of Geosciences, Shizuoka University

We present the evolution of spinel grains in the Horoman Peridotite Complex, Hokkaido. For deformation under differential stresses at high temperature conditions, both diffusion processes including diffusion creep and annealing process and dislocation creep will affect shape change of a crystal inclusion (Okamoto and Michibayashi, 2005 JGR). Grain size and grain shape are related to the shape change of the crystal with respect to given temperature and differential stress conditions. We applied this theory to spinel grains in the Horoman Peridotite Complex, Hokkaido. As a result, grain shapes of coarser spinel grains more than 100 micron are dominantly controlled by dislocation creep, whereas those of smaller spinel grains less than 100 micron are influenced by both diffusion processes and dislocation creep. Moreover, we found that grain shapes of the smaller spinel grains can be only explained by post-tectonic annealing process after their intense deformation. Our result will provide a new insight to understand the deformation processes in mantle.

Keywords: spinel, grain shape, diffusion process, dislocation creep, Horoman

## Verification of ultra-low strain rate effect from microstructural observation on naturally deformed olivine

YAMAMOTO, Takafumi<sup>1\*</sup> ; ANDO, Jun-ichi<sup>1</sup> ; OHFUJI, Hiroaki<sup>2</sup> ; MORISHITA, Tomoaki<sup>3</sup> ; TOMIOKA, Naotaka<sup>4</sup>

<sup>1</sup>Department of Earth and Planetary Systems Science, Hiroshima University, <sup>2</sup>Geodynamics Research Center, Ehime University, <sup>3</sup>School of Natural System, College of Science and Technology, Kanazawa University, <sup>4</sup>Institute for Study of the Earth's Interior, Okayama University

Kitamura et al. (1986) and Ando et al. (2001) reported Fe concentration on dislocation core in naturally deformed olivine. They suggested that compositional heterogeneity is formed by Cottrell atmosphere of solute atoms. This phenomenon is well known in the realm of metallurgical science, and only occurs during dislocation creep at very low strain rate condition. The presence of Cottrell atmosphere has a pinning effect on dislocations and prohibits their movements. As a consequence, plastic behavior of materials is drastically changed in the presence of Cottrell atmosphere. On the basis of this compositional heterogeneity, they demonstrate that the study of ultra-low strain rate effect on olivine plasticity is very important to understand the dynamics of the upper mantle.

With this background, the purposes of the present research are: (1) to confirm whether the Fe concentration on dislocation core is a common phenomenon in deformed olivine grains of mantle-derived peridotite, (2) to verify the deformation condition at which Fe concentration was occurred, from the microstructural observation of each studied peridotite samples, (3) to clarify the exact mechanism of Fe concentration, namely Cottrell atmosphere or pipe diffusion. The studied peridotite samples are xenoliths from basalt (Takashima, Megata, Kurose and Salt Lake), and alpine rocks (Uenzaru and Horoman). The techniques employed for the present study include optical microscopy, EPMA, SEM-EBSD, TEM and ATEM.

The main results are as follows:

- 1) Fe concentration on dislocation core in all olivine samples is detected, which suggests that it is common phenomenon in mantle peridotite.
- 2) The mechanism of Fe concentration on dislocation core in olivine grains is preferably Cottrell atmosphere than other phenomena such as pipe diffusion. However we need to carry out more careful and detailed observations to confirm it.
- 3) The microstructural observations indicate that the all peridotites preserve the deformation characteristics developed at the upper mantle. This fact suggests strongly that the Fe concentration on dislocation core in olivine grains occurred in the upper mantle condition.

Ando et al. (2001) *Nature*, 414, 893; Kitamura et al. (1986) *Proc. Japan Acad.*, 62, 149.

Keywords: Olivine, Cottrell atmosphere, Dislocation creep

## The relationship between microstructures and metasomatism preserved within coarse granular peridotites derived from Kaap

TOMITA, Daiki<sup>1\*</sup> ; MICHIBAYASHI, Katsuyoshi<sup>1</sup> ; KATAYAMA, Ikuo<sup>2</sup> ; KOMIYA, Tsuyoshi<sup>3</sup>

<sup>1</sup>Institute of Geosciences, Shizuoka University, <sup>2</sup>Department of Earth and Planetary Systems Science, Hiroshima University, <sup>3</sup>Department of Earth Science & Astronomy Graduate School of Arts and Sciences The University of Tokyo

Kimberlite was generated in deep upper mantle (70-250km) beneath craton and subsequently ascended to surface rapidly. Peridotite xenoliths, which were entrained by kimberlite, record composition and texture formed in upper mantle beneath the craton. We studied coarse granular peridotites obtained from Kimberley pipe, South Africa, as they have a few studies in terms of microstructural development, presumably because of very coarser grains. We performed mineral crystal-fabric analyses of the coarse granular peridotites in order to understand the structure of the cratonic lithosphere. The peridotites consist mostly of olivine and orthopyroxene with clinopyroxene, garnet and a minor amount of spinel and phlogopite. The crystallization of clinopyroxene appears to be associated with melt metasomatism, whereas that of phlogopite could be associated with hydration metasomatism. Garnet grains occur commonly with kelyphite consisting of fine-grained orthopyroxene, clinopyroxene and spinel, indicating that these peridotites could have been uplifted above the phase boundary between garnet peridotite and spinel peridotite stability fields. Although both foliation and lineation are not commonly identified because of coarse granular texture, olivine crystal fabrics are characterized by a single maximum of [010] with single maxima or weak girdles of [100] and [001]. We found that the intensities of olivine and orthopyroxene crystal-fabrics are correlated to the modal composition of clinopyroxene and phlogopite. It suggests that the melt metasomatism weakened crystal-fabrics, whereas the hydration metasomatism intensified crystal-fabrics. As a consequence, the metasomatism could result in the development of different types of microstructures in the peridotites and may weaken the craton lithosphere.

Keywords: kimberlite, peridotite, garnet, olivine, craton, crystal-fabrics

## Corona-forming reaction in the Lutzow-Holm Complex, East Antarctica at Ongul Island

SHIMADA, Asami<sup>1\*</sup>; IKEDA, Takeshi<sup>1</sup>

<sup>1</sup>Kyushu University

### [Introduction]

Corona is a microstructure that aggregate of one or several species of mineral surrounds another mineral. This suggests that corona was formed by the reaction between the interior mineral and the matrix minerals (Passchier and Trouw 1996). Estimating this reaction enables us to know which component transferred and how temperature and pressure changed. In this study, we estimated corona-forming reaction by describing the microstructure and chemical composition of a corona in the Lutzow-Holm Complex at Ongul Island.

### [Geological Outline]

In the Lutzow-Holm Complex, metamorphic grade increases from amphibolites facies in the northeast to granulite facies in southwest (Hiroi et al., 2006). The granulite facies metamorphic rocks are widely distributed throughout East Ongul Island. The rock types are mainly garnet gneiss and hornblende gneiss (Shiraishi et al., 1994). Ultramafic rocks occur as thin layers in the garnet gneiss. The ultramafic rocks analyzed in this study are composed mainly of hornblende and porphyroblasts of garnet. Corona structure forms around the garnet.

### [Microstructure]

In the ultramafic rocks, hornblende-rich domain and plagioclase-rich domain occur. Both domains consist of hornblende, plagioclase, brown biotite and orthopyroxene. The corona consists mainly of green biotite and plagioclase, and occurs around the garnet. Plagioclase in the matrix and the corona has twin and chemical zoning. Garnet porphyroblast (about 15mm diameter) shows concavo-convex shape. In the embayed part of garnet, biotite tends to occur with long axis is at right angles to garnet surface.

### [Chemical Composition]

Garnet; Rim shows higher Fe and lower Mg than the interior.

Plagioclase; Ca/(Ca+Na) increases in the order of Pl-rich domain, Hbl-rich domain and corona. Ca/(Ca+Na) in every domain increases from core to rim.

Biotite; Mg/(Fe+Mg) decreases in the order of Hbl-rich domain, Pl-rich domain and corona. Rim in every domain shows lower Al than the core.

Hornblende; Hbl-rich domain shows higher Al and Mg/(Fe+Mg) than Pl-rich domain. The rim of both domains shows higher Al than the core.

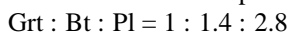
Orthopyroxene; Composition is almost homogeneous within the domain.

### [Discussion]

The compositional difference between core and rim of each mineral in the matrix can be regarded as growth zoning. We used the rim-composition in each domain to estimate the corona-forming reaction. The average of analyses was used for plagioclase and biotite in the corona and for garnet. The corona-forming reaction employing the compositions of Hbl-rich domain was given as follows.



On the other hand, the reaction using the compositions of Pl-rich domain expects garnet as products, which is inconsistent with the observation that garnet was consumed. This suggests that K is supplied from the outside through fluid during corona formation. We also compared volume of left side minerals, that is,



Garnet is minimum in amount. Nevertheless, corona formed around garnet. This suggests that diffusion of component from garnet controlled the rate of the reaction.

Keywords: corona, East Antarctica, Lutzow-Holm Complex

## Possible tectonic models before, during and after mylonitization in the Sor Rondane Mountains, East Antarctica

TOYOSHIMA, Tsuyoshi<sup>1\*</sup>; KANEYA, Akiko<sup>1</sup>; OSANAI, Yasuhito<sup>2</sup>; BABA, Sotaro<sup>3</sup>; HOKADA, Tomokazu<sup>4</sup>; NAKANO, Nobuhiko<sup>2</sup>; ADACHI, Tatsuro<sup>2</sup>

<sup>1</sup>Niigata University, <sup>2</sup>Kyusyu University, <sup>3</sup>University of the Ryukyus, <sup>4</sup>National Institute of Polar Research

The deformational history in the Sor Rondane Mountains (SRMs), eastern Dronning Maud Land (DML), East Antarctica, is divided into 13 stages (D1?D13). The tectonic regime varied frequently from extension (D3?D4) to layer-normal compression and layer-parallel extension (D5), to compression (D6), top-to-the S shearing (D7), top-to-the SE shearing and sinistral strike-slip (D8), compression (D9?D11), and ?nally extension related to dextral shearing (D12?D13). In this paper we discuss change in deformation and P-T conditions before, during and after the D7-D8 mylonitization, using mineral textures, assemblage, compositions and microstructures of D7 and D8 mylonites.

Garnet porphyroclasts of the D7-D8 mylonites include high-Ca mantles and crenulation microfolds defined by sillimanite fibrolites. The high-Ca mantles of garnets and their plagioclase inclusions in the mylonites imply an increase in pressure before the D7-D8 mylonitization. S-tectonites having a dominant planar fabric were formed before the D7-D8 mylonites and after the high-Ca mantles of the garnets. The planar fabric (foliation) of the S-tectonites is produced by fan-shaped arrangement of sillimanite and biotite grains. The sillimanite and biotite grains were formed by breakdown of garnet. Most of the sillimanite and biotite grains have been rotated and folded by the D7-D8 mylonitization. The D7-D8 mylonite foliations are parallel to the planar fabric of the S-tectonites. The S-tectonites indicate a flattening type of strain and resulted from the layer-normal shortening after the increase in pressure and before the D7-D8 mylonitization. kyanite-quartz porphyroblasts and randomly oriented crystals of sillimanite/kyanite and biotite were formed after the D7-D8 mylonitization. The randomly oriented crystals of sillimanite/kyanite and biotite resulted from the breakdown of garnet porphyroclasts of the D7-D8 mylonites. The kyanite-quartz porphyroblasts accompany leucogranite veins cutting the D7-D8 mylonite foliations. The randomly oriented crystals and porphyroblasts imply non-deformational conditions after the D7-D8 mylonitization and D9 folding.

Three possible tectonic models for D7 and D8 mylonite-forming events before the D9 deformation can be considered as follows: extensional tectonic model, positive flower structure model and rotated mylonite model. In the former model, D7 and D8 indicate major extensional tectonic activity in the southern part of the East African and Antarctic Orogen (EAAO) before the Pan-African compressional event, and after the 650-600 Ma peak of metamorphism. In the latter two models, D7 and D8 mylonites may have resulted from the compressional events. In the positive flower structure model, the SRMs are the southern half of the E-trending positive flower structure. The flower structure model needs top-to-the N shear zones to the north of the SRMs. In the rotated mylonite model, the present S-dip of the D7 and D8 mylonites results from the rotation and folding of originally N-dipping reverse (top-to-the S-SE, normal-sinistral shear, present day coordinates) mylonites. The Pan-African compressional event resulted in the formation of upright folds with horizontal axes that curve along the coastline in central to eastern DML during the D9 deformation that took place between 600 and 560 Ma. The coastline-parallel fold axes and subvertical axial-planes correspond to the X-axes and the XY-planes, respectively, of strain ellipsoids that were progressively rotated counterclockwise toward the central parts of a sinistral shear zone. Therefore, the curved fold axes and axial-planes suggest the EAAO acted as a zone of sinistral transpression during the collision of parts of East and West Gondwana.

Keywords: S-tectonite, flattening, mylonitization, Sor Rondane Mountains, Gondwana, East Antarctica

## Significance of multi-stage chloride brine activity- An example from Sor Rondane Mountains, East Antarctica

HIGASHINO, Fumiko<sup>1\*</sup>; KAWAKAMI, Tetsuo<sup>1</sup>; TSUCHIYA, Noriyoshi<sup>2</sup>; MADHUSOODHAN, Satish-kumar<sup>3</sup>; ISHIKAWA, Masahiro<sup>4</sup>; GRANTHAM, Geoffrey H.<sup>5</sup>

<sup>1</sup>Kyoto University, <sup>2</sup>Tohoku University, <sup>3</sup>Niigata University, <sup>4</sup>Yokohama National University, <sup>5</sup>Council for Geoscience, South Africa

It has been gradually recognized chloride brine potentially plays an important role in large-scale mass transfer during high-grade metamorphism without partial melting. This is because brine is a powerful solvent, can coexist with CO<sub>2</sub>-rich fluid under the granulite facies conditions and has low-H<sub>2</sub>O activity (Newton & Manning, 2010; Heinrich et al., 2004). In natural observation, evidence for the presence of brine is often found as fluid inclusions. In metamorphic rocks under granulite facies conditions, however, brine inclusions are only rarely found (Markl & Bucher, 1998). This is partly because brines have a high mobility due to their low viscosity and low wetting angle (Watson & Brenan, 1987; Holness, 1997).

On the other hand, hydrous minerals such as biotite (Bt), hornblende (Hb) and apatite can record the  $f_{H_2O}/f_{HCl}$  of the last equilibrated Cl-rich fluid as their mineral compositions. In order to understand the metamorphic fluid activity using these minerals, *P-T* condition under which these minerals equilibrated with a fluid as well as the crystallographic requirements for these minerals to record the fluid composition should be known (e.g., Makino, 2000). However, there still are a lot of unsolved issues about brines, for example, cations transported in the fluid, *P-T* condition and areal scale of brine activity, and its origin (Newton et al., 1998).

In order to understand the multiple brine activities and the cation composition in brines, two meta-mafic gneisses are studied in detail in Brattnipene, Sor Rondane Mountains (SRM), East Antarctica.

In a Grt-Bt-Hb gneiss, Cl-rich Bt is exclusively included in garnet (Grt). Bt, Hb, and cummingtonite (Cum) in the matrix are Cl-poor. These compositional differences imply that Bt included in the Grt formed under the presence of chloride brine and Cl-poor fluid infiltrated after Grt formation. Grt is enveloped by the gneissosity defined by the arrangement of Cum overgrown by Hb, and Bt. Therefore, chloride brine activity predated or was simultaneous with the penetrative gneissosity formation in this area. After considering the effect of Mg-Cl avoidance rule and compositional change during retrogression, the geothermobarometry (Holdaway, 2000; Wu et al., 2004) gave 650 < *T* < 800 °C and 0.96 GPa for the peak *P-T* condition of this sample. The Cl-rich Bt entrapment was probably predated or simultaneous with the attainment of this *P-T* condition.

In a Grt-Opx-Hb gneiss, ca. 1cm-thick Grt-Hb vein cut the penetrative gneissosity in this area. Cl-content of Hb and Bt, and K-content of Hb decrease with the distance from the vein center and become constant at ca. 1.6 cm from the vein center. Plagioclase present next to the vein has a core (An<sub>55</sub>) and mantle (An<sub>68</sub>) which is sharply overgrown by Na-richer rim (An<sub>51</sub>). Plagioclase in the vein is An<sub>51</sub> without zoning, and development of Na-richer rim gets thinner with a distance from the vein. Therefore, the Grt-Hb vein was probably formed by NaCl-KCl brine infiltration. This is also supported by the isocon analysis of whole-rock chemistry determined for wall rock of the vein. *P-T* condition of the vein formation is estimated as 720 °C and 0.70 GPa (Holdaway, 2000; Wu et al., 2004).

*P-T* conditions of multi-stage chloride brine activity, cation composition of the brine, and outcrop-scale pathways of the brine are constrained in SRM from these two gneisses. From the pelitic gneisses in SRM, Cl-rich fluid or melt activity with a linear distribution over 200 km has been reported (Higashino et al., 2013). Additionally, this study revealed that the brine activity in SRM is not controlled by the lithology or specific deformational stages. It is clear that chloride brine in SRM was not a result of *in situ* fractionation through the selective consumption of H<sub>2</sub>O in the fluid (Kullerud, 1995), but substantial amount of brine was actually moving, and was playing an important role in mass transfer.

Keywords: NaCl-KCl brine, fluid infiltration, continental collision zone, Sor Rondane Mountains

## Rate-limiting process and degree of disequilibrium of garnet-forming reaction

MIYAZAKI, Kazuhiro<sup>1\*</sup>

<sup>1</sup>GSJ AIST

Water released by dehydration reaction in metamorphic rocks will take a major role in rheology, mass transport, and reactivity of metamorphic rocks. Rate-limiting process of the dehydration reaction can be divided into the following three steps, such as reaction at interface, diffusion, and heat-flow. Garnet is one of the common minerals produced by dehydration reaction in metamorphic rocks. The rate-limiting process of garnet-forming reaction is usually assumed to be diffusion-controlled reaction. However, there are few cases where clear evidences for diffusion-controlled reaction were proposed. In addition, degree of disequilibrium of the diffusion-controlled reaction is not well known. Here, I report evidence of diffusion-controlled reaction and estimation of degree of disequilibrium of garnet-forming reaction in the Tsukuba Metamorphic Rocks.

Garnets in the Tsukuba Metamorphic Rocks are formed by the dehydration reaction of biotite + sillimanite + quartz = garnet + cordierite + K-feldspar + water. Biotite-depleted region surround the irregular shaped garnet. The depleted region of reactant is typically expected for diffusion-controlled reaction, but is rare for natural garnet-forming reaction. Irregular shape of garnet is also expected for diffusional instability of growing interface (Mullins & Sekerka, 1963). These sets of observations strongly suggest that the garnets were formed by diffusion-controlled reaction.

Spherical shape of growing particle under diffusion-controlled reaction becomes unstable due to diffusional instability, but interfacial energy will reduce the instability. Using spherical harmonics function, instability of small perturbation from spherical shape can be evaluated. Assuming interfacial energy of garnet, dominant wavelength in unstable regime is predicted with degree of super-saturation under diffusion-limited reaction. Dominant wavelength of the irregular garnet suggests that degree of super-saturation is less than 0.1. This value can be translated to degree of disequilibrium temperature with entropy change of the garnet-forming reaction. The disequilibrium temperature  $\Delta T$  is less than 5 °C, and is very small. This small value of disequilibrium temperature suggests that spherical or euhedral garnets that are more common than irregular garnets, should be produced near equilibrium condition. Otherwise, such common spherical or euhedral garnets should be produced by interface-controlled reaction associated with influent fluid.

Keywords: garnet, dehydration reaction, disequilibrium, metamorphism, metamorphic rock, metamorphic reaction

## FLUID RELATED ORIGIN OF SILLIMANITE VEINS IN POLYMETAMORPHIC ROCKS FROM THE RYOKE BELT, JAPAN

AMANO, Saori<sup>1\*</sup> ; KAWAKAMI, Tetsuo<sup>1</sup>

<sup>1</sup>Graduate School of Science, Kyoto University

In the polymetamorphic area, it is important to distinguish the effect of each metamorphism in order to appreciate the evolution of thermal structure of the area. Some authors have successfully distinguished the regional metamorphism from the postdating contact metamorphism (e.g. Miyake et al., 1992), but studies dealing with a fluid activity during polymetamorphism is not sufficiently available. Veins consisting of fibrous sillimanite (Sil) in a contact metamorphic aureole have been previously interpreted as a result of fluid activity (e.g. Johnson et al., 2003).

In Kasagi area (Kyoto, Japan), Ryoke metamorphic rocks are widely exposed and main lithology is pelitic and psammitic schists and gneisses. Younger Ryoke granites discordantly intrude to the metamorphic rocks and, therefore, the regional metamorphic rocks are overprinted by the heat (Ozaki et al., 2000) and fluid flux from the granites. This area belongs to the Sil zone that is defined by the presence of Sil in the pelitic lithology (Ozaki et al., 2000) whose origin has not been discussed in detail.

However in this area, fibrolite bundles are often observed to cross-cut the gneissosity formed by the regional metamorphism and it seems difficult to explain their formation during the regional metamorphism. In this study, we report the mode of occurrence of Sil veins emanating from the granite into psammitic gneiss and discuss the fluid-related origin of them.

The studied psammitic gneiss containing Sil veins is collected from the Sil zone near the granite intrusion contact. Ryoke granite intrudes discordantly to the gneissosity of this sample, and the Sil vein subparallel to the gneissosity emanate from it. The Sil vein consists of fibrolite and retrograde muscovite (Ms) replacing it. Quartz (Qtz) in the matrix near the vein are coarser-grained and they include fibrolite grains. The amount of fibrolite included in the Qtz decreases as a distance from the Sil vein increases. Fibrolite is present in veins and Qtz grains. Fine, retrograde Ms after fibrolite is present along grain boundaries in the matrix. Although plagioclase (Pl) is a common constituent mineral in the matrix, it is almost completely absent near and in the Sil veins. K-feldspar is absent in the studied sample, but instead, retrograde Ms cutting the schistosity is abundant in the matrix.

Cathodoluminescence (CL) observation of the microstructures around the Sil veins revealed that the brightness of CL signal of Qtz grains increases as the distance from the Sil vein increases. That is, Qtz grains near the vein or including Sil are dark under CL observation. In particular, part of a single Qtz grain including more fibrolite grains appears dark under CL image.

From the observation of microstructural relationships described above, we consider that Sil veins were formed by the fluid released from the Ryoke granite. Formation of fibrous Sil by the action of mobile hydrogen ions on pre-existing minerals has been previously discussed (Vernon, 1979). Moreover, experimental work has shown that Al<sub>2</sub>SiO<sub>5</sub> minerals and Ms can be produced by the action of acidic, aqueous solutions on various common silicate minerals (Burnham, 1967). In this study, fibrolite is present in veins and Qtz grains and the amount of fibrolite crystals included in the Qtz crystals decreases as a distance from the vein increases. Pl is absent in and at the vicinity of the veins. From these pieces of observation, a fluid from the granite would have reacted with the matrix to dissolve Pl and to form coarser-grained Qtz and fibrolite bundles simultaneously. Thermodynamic calculation using SUPCRT92 (Johnson et al. 1992) has revealed that infiltration of the aqueous fluid with low Na<sup>+</sup>/H<sup>+</sup> and K<sup>+</sup>/H<sup>+</sup> ratio can destabilize Pl and stabilize Sil under the presence of Qtz at 3 kbar, 600°C. Therefore, Sil in this study is not regional metamorphic in origin, but is probably a result of fluid infiltration during a contact metamorphism by the Ryoke granite.

Keywords: fibrous sillimanite, Ryoke belt, fluid-related origin, polymetamorphism

## Comparison of UHP chromitites from the Higo and Nishisonogi Metamorphic Rocks, Kyushu, Japan.

SHIOSAKI, Dai<sup>1\*</sup>; MORIBE, Yosuke<sup>1</sup>; EGUCHI, Hibiki<sup>1</sup>; NISHIYAMA, Tadao<sup>1</sup>

<sup>1</sup>Department of Earth and Environmental Sciences, School of Science and Technology Kumamoto University

We have found microdiamond - bearing ultrahigh-pressure (UHP) chromitites from two metamorphic terranes in Kyushu: the Higo (HMR)<sup>1</sup> and Nishisonogi (NMR)<sup>2</sup> Metamorphic Rocks. This paper describes the similarity and difference between the two UHP chromitites. The HMR are located in west-central Kyushu with an E-W trend. They have undergone low P /T metamorphism, however, precursor HP or UHP metamorphism of ca. 250 Ma has been inferred<sup>3</sup>. The protoliths have affinity to continental shelf deposits<sup>4</sup>, consisting mainly of pelitic gneisses and meta-carbonates with minor metabasites and metaperidotites (partly serpentinite). Chromitite occurs very rarely as a nodular form in serpentinitized metaperidotites which shows spinifex-texture. The NMR is located in western Kyushu with a N-S trend. They have undergone high P /T metamorphism of epidote-blueschist subfacies. They consist mainly of pelitic and psammitic schists with minor basic schists and serpentinites, some of which show a character of serpentinite melange<sup>5</sup>. Detrital zircon from the pelitic schists show the age of 89-86 Ma<sup>6</sup>, whereas zircon from jadeitites in a serpentinite melange does 136 -126 Ma in the core and 84 - 80 Ma in the rim<sup>7,8</sup>. Chromitite occurs as a deformed schlieren-like layer in serpentinite with no relic minerals. The P-T condition of the HMR has been estimated to be 200 - 600 MPa and 600 - 800 °C<sup>3,9,10,11,12,13</sup>. Higher pressure and temperature conditions are reported from the following two samples: a sapphirine-bearing granulite<sup>3,10</sup> as a tectonic block in the spinifex-textured metaperidotite (900 MPa and 950 °C) and a calc-silicate granulite<sup>13</sup> (900 MPa and 820 °C) intercalating with garnet - biotite gneiss. We newly estimated the peak P-T condition of Al-spinel and chlorite -bearing metaperidotite as 2.0 GPa and 780 - 990 °C. In the case of the NMR, the peak metamorphic condition of the crystalline schists is 1.4 GPa and 520 °C for a garnet galucophanite<sup>14</sup>. Jadeitites<sup>15</sup> as tectonic blocks in the serpentinite melange shows the peak condition of 1.5 GPa and 500 °C. Chromite from the HMR has the composition  $(\text{Mg}_{0.34}\text{Fe}^{2+}_{0.75}\text{Mn}_{0.02})(\text{Cr}_{0.81}\text{Al}_{0.06}\text{Fe}^{3+}_{0.04}\text{Si}_{0.05})_2\text{O}_4$ , whereas that from the NMR has similar composition  $(\text{Mg}_{0.33}\text{Fe}^{2+}_{0.65}\text{Mn}_{0.03})(\text{Cr}_{0.84}\text{Al}_{0.12}\text{Fe}^{3+}_{0.04})_2\text{O}_4$  in the core and Fe-rich composition  $(\text{Mg}_{0.06}\text{Fe}^{2+}_{0.89}\text{Zn}_{0.02}\text{Mn}_{0.03})(\text{Cr}_{0.85}\text{Al}_{0.12}\text{Fe}^{3+}_{0.04})_2\text{O}_4$  in the rim. Microdiamonds occur as *in situ* inclusions in chromite in both chromitites. They are 1 to 10 μm in size in HMR chromite, and those in NMR chromite is much smaller, mostly <1 μm with small number of larger grains. In both chromitites microdiamonds occur in some cases as numerous aligned grains, making diamond - rich zones. Both microdiamonds are identified with Raman spectra. HMR microdiamonds show a broad peak at 1333 cm<sup>-1</sup>. NMR microdiamond, also shows a broad peak at 1331 cm<sup>-1</sup> with graphite peak at around 1600 cm<sup>-1</sup>, suggesting partial graphitization. Both UHP chromitites will be deep subduction origin. HMR can be an eastern extension of the Dabie-Sulu UHP terrane in China, however, NMR is more problematic. No corresponding UHP terrane of ca. 80Ma is found around Kyushu. Our findings of UHP chromitites require reexamination of micro-tectonics in Kyushu, a peculiar location of an arc-arc junction at the continental margin.

References 1:Nishiyama et al., JpGU Meeting, S-MP46, 2014; 2: Nishiyama et al., JpGU Meeting, S-CG08, 2014; 3: Osanai, et al., Gondwana Res., 9, 152-166, 2006; 4: Omori and Isozaki, J.Geogr., 120, 40-51, 2011; 5: Nishiyama, Mem. Geol. Soc. Japan, 33, 237-257, 1989; 6: Kouchi, Y., J. Geogr., 120, 30-39, 2011; 7: Mori, et al., JMG, 29, 673-684, 2011; 8: Yui, et al., EJM., 24, 263-275, 2011; 9: Obata et al., Lithos, 32, 135-147, 1994; 10: Osanai et al., JMG., 16, 53-66, 1998; 11: Maki et al., JMPS, 99, 1-18, 2004; 12: Miyazaki, JMG., 22, 793-809, 2004; 13: Maki et al., JMG., 27, 107-124, 2009; 14: Moribe, Mc thesis, Kumamoto U.; 15: Shigeno et al., EJM, 24, 289-311, 2012

Keywords: microdiamond, chromitite, UHP, Higo metamorphic rocks, Nishisonogi metamorphic rocks, subduction

## 3D imaging of the Mn-caldera shaped zoning of the garnet found from the Sanbagawa metamorphic belt and its origin.

YOSHIDA, Kenta<sup>1\*</sup> ; HIRAJIMA, Takao<sup>1</sup>

<sup>1</sup>Graduate School of Science, Kyoto University

Garnets with a complex compositional zoning were found from the northern proximal area of the Western Iratsu body of the Sanbagawa metamorphic belt of the Besshi district, southwest Japan. The studied garnet shows incipient Mn-reverse (increasing) zoning part (defined as core) and subsequent Mn-bell shape (decreasing) zoning part (defined as mantle), which is almost identical to the “ Mn-caldera shaped zoning ” described by Banno et al. (2004) in the Asemigawa region of the central Shikoku. In order to describe the chemical characteristic sterically, X-ray chemical mapping were performed by each 0.2-0.3 mm depth step, for one very-coarse-grained garnet with ca. 11 mm in diameter. The result clearly shows that the core/mantle boundary has the highest Mn content with euhedral shape, and that the chemical composition continuously changes through the grain. Internal schistosity defined by sigmoidal inclusion arrays cross-cuts the core/mantle boundary. This fact also suggests the continuous growth of garnet from the central part to the outer part. In the same sample, garnets with Mn-bell shape type zoning are also observed, which are relatively fine-grained up to 5 mm. Raman barometry and thermodynamic modeling suggest the climax *P-T* conditions of the studied sample did not reach the eclogite facies, which are consistent with the conditions of the oligoclase-biotite zone of the Sanbagawa metamorphic belt (610 °C and 1.0 GPa, Enami, 1994).

Contrary to the simple Mn-bell shape type zoning which grown up with progressive regional metamorphism, “ Mn-caldera shaped zoning ” could be generated from the crystal nucleation under oversaturated environment (Matsumoto and Kitamura, 2004). Such oversaturation is expected in a rapid increase of temperature. Recently, Aoya et al. (2013) proposed the eclogite nappe covering the large part of the Besshi district. However, the exact boundary between the eclogite nappe and lower grade surrounding rocks is still under the debate. The conjunction of the eclogite nappe and the lower-grade surrounding rocks are thought to have taken place near the peak metamorphic stage of the surrounding rocks (500-600 °C and ca. 1 GPa, Aoya et al., 2013). Mn-caldera shaped zoning garnet found in the Besshi district (this study; Xu et al., 1994) are both found from the northern proximal of the hypothesized eclogite nappe. Those Mn-caldera shaped zonings are possibly originated from the conjunction of the eclogite nappe and surrounding crystalline schist, and corresponding rapid heating. Such features of garnet can help to determine the boundary of the eclogite nappe in the Besshi district.

Keywords: garnet, Sanbagawa metamorphic belt, compositional zoning, disequilibrium crystal growth

## Widespread analyses of pressure-temperature trajectory and timing in the Altai Range, Mongolia

NAKANO, Nobuhiko<sup>1\*</sup> ; OSANAI, Yasuhito<sup>1</sup> ; OWADA, Masaaki<sup>2</sup> ; SATISH-KUMAR, M.<sup>3</sup> ; ADACHI, Tatsuro<sup>1</sup> ; JARGALAN, Sereenen<sup>4</sup> ; YOSHIMOTO, Aya<sup>1</sup> ; KUNDYZ, Syeryekhan<sup>4</sup> ; BOLDBAATAR, Chimedtseie<sup>5</sup>

<sup>1</sup>Kyushu University, <sup>2</sup>Yamaguchi University, <sup>3</sup>Niigata University, <sup>4</sup>Mongolian University of Science and Technology, <sup>5</sup>Mongolian Exploration Partners, LLC

This study performed large-scale petrographical and geochronological investigation in the Altai Range, Mongolia distributed in the Central Asian Orogenic Belt, which is the typical subduction-accretion-collision orogeny on the Earth. Based on the petrographical observation, clockwise and anti-clockwise pressure-temperature trajectories were identified in whole of the studied area (400 km long). U-Th-Pb monazite dating yields c. 350 Ma and c. 260 Ma. Samples with clockwise pressure-temperature path, containing kyanite in garnet and sillimanite in the matrix, commonly have c. 350 Ma monazite in garnet and c. 260 Ma monazite in the matrix. In contrast, samples with anti-clockwise pressure-temperature path containing sillimanite in garnet and kyanite in the matrix have monazites showing (i) c. 350 Ma both in garnet and the matrix, (ii) c. 260 Ma both in garnet and the matrix, and (iii) c. 350 Ma in garnet and c. 260 Ma in the matrix. Ca zoning pattern in garnet shows either continuous or discontinuous zoning. Samples containing single monazite age cluster (either c. 350 Ma or c. 260 Ma) have continuously zoned garnet, in which samples with anti-clockwise pressure-temperature trajectory at both periods show Ca zoning increasing from core to rim or mantle, whereas some samples with unknown pressure-temperature path at both periods show opposite zoning. These features strongly suggest both clockwise and anti-clockwise evolutions occurred at both periods. Discontinuous Ca zoning in garnet is observed in samples that contain c. 350 Ma monazite inclusions in garnet and c. 260 Ma monazite grains in the matrix, and the zoning patterns show a decrease in Ca at the rim for samples with clockwise paths and an increase in Ca at the rim for those with counterclockwise paths. In some cases, c. 350 Ma monazite grains are included in the large garnet cores but c. 260 Ma monazite grains are found in the garnet rims as well as in the matrix. These rocks might be metamorphosed at c. 350 Ma, whereas they did not exhume to the surface and have remained deep crustal level. Subsequent compression and decompression event formed garnet rim and monazite at c. 260 Ma, which should be caused by same tectonic regime to clockwise and anti-clockwise pressure-temperature path at the period. The presence of the regional-scale clockwise and anti-clockwise trajectories and their repetition during less than 100 My have never reported from any other orogenic belts in the world. Further studies may allow to realize the complex tectonic evolution of the Altai Range.

Keywords: P-T trajectory, U-Th-Pb monazite age, Altai Mountains, Mongolia, Central Asian Orogenic Belt

## Temporal change of modal abundance of minerals during formation of arrested charnockite from Sri Lanka

YAMASAKI, Yukiko<sup>1\*</sup> ; IKEDA, Takeshi<sup>1</sup> ; MOTOYOSHI, Yoichi<sup>2</sup> ; HIROI, Yoshikuni<sup>3</sup> ; PRAME, Bernard<sup>4</sup>

<sup>1</sup>Kyushu University, <sup>2</sup>National Institute of Polar Research, <sup>3</sup>Chiba University, <sup>4</sup>Geological Survey of Sri Lanka

Charnockite occurs as a number of several-decimeters patches in hornblende-biotite gneiss in central Sri Lanka. This type of charnockite has been called arrested charnockite. Local condition of low-H<sub>2</sub>O activity or low-oxygen fugacity could explain the difference of mineral assemblage in local scale. They might be caused by fluid influx and/or partial melting (e.g. Newton et al., 1980; Hiroi et al., 1990; Burton and O'Nions, 1990; Ravindra Kumar, 2004; Endo et al., 2012). The temporal and spatial development of charnockite has been unclear. This study describes variation in modal abundance of hornblende, biotite and orthopyroxene in melanocratic and leucocratic parts from surrounding gneiss to charnockite.

Charnockite and surrounding gneiss have layer structure composed of melanocratic and leucocratic parts. Each part can be traced continuously between the two rock types. Melanocratic parts consist mainly of hornblende and biotite in gneiss, and orthopyroxene added in charnockite. Leucocratic parts are composed of biotite and colorless minerals in gneiss, while biotite is absent in charnockite. Modal abundances of hornblende and biotite have no systematic trend in melanocratic parts of gneiss. Hornblende and biotite decrease drastically and gradually, respectively, while orthopyroxene increases gradually in melanocratic parts of charnockite. Biotite decreases gradually toward charnockite in leucocratic parts in gneiss.

Biotite of leucocratic parts breaks down within gneiss. Orthopyroxene appears in the location of dehydration reaction of biotite and hornblende in melanocratic parts. This suggests that the element released due to break down of biotite in leucocratic layer diffused from leucocratic part to melanocratic part to produce orthopyroxene. It is a possible that hornblende broke down first to produce significant amount of orthopyroxene in melanocratic part. The element released due to break down of biotite in leucocratic part transported to the location of preexisting orthopyroxene in order to grow the crystals. Biotite in leucocratic layers is enriched in Fe as compared with that in melanocratic part. Fe-rich biotite breaks down under lower temperature (or higher activity of H<sub>2</sub>O) than Mg-rich biotite. This could explain the decrease of biotite in leucocratic layer in gneiss.

### Reference

Burton K. W. and O'Nions R. K., The timescale and mechanism of granulite formation at Kurunegala, Sri Lanka, *Contrib. Mineral. Petrol.* 106, 66-89 (1990)

Endo et al., Phase equilibrium modeling of incipient charnockite formation in NKCFMASHTO and MnNCKFMASHTO systems: A case study from Rajapalaiyam, Madurai Block, southern India, *Geoscience Frontiers* 3, 801-811 (2012)

Hiroi Y. et al., Arrested charnockite formation in Sri Lanka: Field and petrographical evidence for low-pressure conditions, *Proc. NIPR Symp. Antarct. Geosci.* 4, 213-230 (1990)

Newton R. C. et al., Carbonic metamorphism, granulites and crustal growth, *Nature* 288, 45-50 (1980)

Ravindra Kumar G. R., Mechanism of arrested charnockite formation at Nemmara, Palghat region, southern India, *Lithos* 75, 331-358 (2004)

Keywords: Sri Lanka, Charnockite, Hornblende-biotite gneiss, modal abundance

## Thermal structure and water transportation in subduction zones: a comparison between NE and SW Japan

ISHII, Kazuhiko<sup>1\*</sup> ; OKUNO, Masashi<sup>1</sup>

<sup>1</sup>Graduate School of Sciences, Osaka Prefecture University

Northeastern and southwestern Japan are considered to be typical examples of cold and hot subduction zones, respectively. The old Pacific plate subducts beneath northeastern Japan at high rate and the young Philippine Sea plate subducts beneath southwestern Japan at low rate. These contrasts in the subduction conditions reveals in several aspects including higher activity of arc volcanism and deeper down dip limit of inter-plate earthquake in northeastern Japan, and deep low-frequency tremors at plate boundary of southwestern Japan. We have investigated thermal structure and geophysical and geochemical processes in these subduction zones using a numerical model. The model includes hydration and dehydration of the slab and mantle wedge, melting and solidification of mantle peridotites, permeable flow of melt and aqueous fluids, and temperature-dependent solid flow of mantle peridotites with water- and melt-induced weakening. We will discuss effects of the subduction conditions on the volcanic and seismic activities through the processes, especially water transportation.

Keywords: subduction zones, NE Japan nad SW Japan

## Stress and strain history during the microboudinage for granite intrusion: Mt. Edger granite complex, East Pilbara

MATUMURA, Taroujirou<sup>1\*</sup> ; KIMURA, Nozomi<sup>2</sup> ; OKAMOTO, Atsushi<sup>3</sup> ; MASUDA, Toshiaki<sup>2</sup>

<sup>1</sup>Graduate school of science and Technology, Shizuoka University, <sup>2</sup>Institute of Geoscience, Shizuoka University, <sup>3</sup>Graduate school of Environmental studies, Tohoku University

Stress and strain analysis is essential to improving the understanding of deformation process. Microboudinaged columnar minerals can be used as an indicator of stress and strain during the microboudinage for quartzose and calcareous metamorphic tectonites. In this presentation, we discuss the stress and strain history during the microboudinage deduced by the microboudin method with a collaboration of the strain reversal method.

We collected samples of metachert from the Archean Warrawoona greenstone belt around Mt. Edger granite complex, East Pilbara, Western Australia, and identified microboudinaged tourmaline grains embedded within quartz matrix in 10 samples. The result revealed that the samples experienced extensional strain at least -0.56 and differential stress in the range from 3.9 to 11.9 MPa. We obtained stress-strain curves which show increase in differential stress with increasing inverse natural strain ( $\varepsilon_{inv}$ ). The frequency distribution of interboudine gaps between separated grains with respect to  $\varepsilon_{inv}$  for boudinaged tourmaline grains shows that end of microboudinage occurred immediately after the peak frequency of fracturing. This occurrence commonly appeared in all the 10 samples. These results provided us with keys to discuss a stress-strain history during the microboudinage in relation to evolution of the granite complex. The spectacular implication would be a drop or relaxation in increased differential stress at the end of the microboudinage.

Keywords: microboudin structure, stress, strain, granite complex, Archean

## Time scale for formation of diffusion zoning in response to breakdown reaction

IKEDA, Takeshi<sup>1\*</sup>

<sup>1</sup>Kyushu University

In high-grade metamorphic rocks, garnet commonly represents an increase in Mn or Fe toward margin. This feature has been interpreted as diffusion zoning owing to garnet-consuming reactions during retrograde metamorphism. In this process, the zoned thickness can be described in terms of distances of internal diffusion and surface retreating. This study preliminarily formulated to express these distances as a function of time and retreating velocity of the surface. Applying the formulation to some high-temperature metamorphic belts yielded that the diffusion zoning with zoned thickness of 0.04 to 0.1 mm was formed by 1 to several million years. This result may be applied to estimate cooling rate provided that the surface equilibrium was maintained during the formation of diffusion zoning.

Keywords: diffusion zoning, duration time, cooling rate

## Integrated radiometric dating of schist clasts from the Eocene and Miocene conglomerates in Shikoku

IZUKA, Ryota<sup>1\*</sup> ; TAKAGI, Hideo<sup>1</sup> ; HONDA, Emi<sup>1</sup> ; IWANO, Hideki<sup>2</sup> ; ISHIDA, Akizumi<sup>3</sup> ; SANNO, Yuji<sup>3</sup>

<sup>1</sup>Waseda University, <sup>2</sup>Kyoto Fission-Track Co. Ltd., <sup>3</sup>AORI, the University of Tokyo

The age that the high P/T type Sanbagawa metamorphic rocks reached at erosion level gives an important constraints for considering exhumation processes of the Sanbagawa metamorphic rocks. It is shown by the oldest age of the conglomerate containing schist clasts derived from the Sanbagawa Belt. Integrated radiometric dating has been carried out for schist clasts from the Paleogene and Neogene conglomerates in Shikoku. The results of K-Ar and fission-track (FT) ages for the schist clasts from the Eocene Hiwadatoge Formation and the Miocene Furuiwaya Formation (Kuma Group) were already reported (Takagi and Sakisaka, 2012; Takagi et al., 2013). We have been doing U-Pb dating of zircon grains from the same clasts for the FT dating using NanoSIMS 50 ion microprobe of AORI. The youngest U-Pb age of zircon grains approximates the sedimentary age of the protoliths of the schist, because the zircon grains in the low-grade metamorphic rocks are detrital origin. The tentative results shown by the youngest peak yield around 110 Ma in all samples. We will report on details of the U-Pb ages at the meeting. FT dating was also carried out for the schist clasts from Eocene Oyamamisaki Formation in the Shimanto Belt where K-Ar ages (78.2-71.4 Ma) of the clasts have been already reported by Yoshikura et al (1991). The FT ages were 67.3 +/- 9.0 Ma and 68.4 +/- 8.2 Ma. From the results of K-Ar phengite ages and FT zircon ages for schist clasts (Table 1), it is suggested that the exhumation rate of the schist eroded at Eocene time is faster than that eroded at Miocene time.

### References :

- Takagi and Sakisaka, 2012, 119th Geol. Soc. Japan Congress, Abstracts, p.93.  
 Takagi et al., 2013, 120th Geol. Soc. Japan Congress, Abstracts, p.49.  
 Yoshikura et al., 1991, 98th Geol. Soc. Japan Congress, Abstracts, p.434.

Keywords: Sanbagawa belt, schist, radiometric dating

Table1. Phengite K-Ar and zircon fission track ages of schist clasts from the Miocene and Eocene strata in Shikoku.

Series	Formation Name	Sample	Phengite K-Ar age (Ma)	Zircon FT age (Ma)
Miocene	Kuma Group Furuiwaya Formation	32204-2 psamm.sch.	81.5 ± 1.3	68.7 ± 6.0
		112101-2 pel.sch.	83.5 ± 1.3	64.9 ± 5.8
Eocene	Hiwadatoge Formation	2003-8 psamm.sch.	86.8 ± 1.3	85.2 ± 7.7
	Oyamamisaki Formation	1-B psamm.sch.	78.2 - 71.4 (Yoshikura et al., 1991)	67.3 ± 9.0
		1-F psamm.sch.		68.4 ± 8.2

## The metamorphic evolution from PrP to LBS facies in a late Paleozoic cold subduction system in Kurosegawa belt

SATO, Eitaro<sup>1\*</sup> ; HIRAJIMA, Takao<sup>1</sup>

<sup>1</sup>Graduate School of Science, Kyoto University

**Introduction:** Recent progress of thermal modeling and thermodynamic calculation can help the general understanding of the thermal structure of subducting plate and the total movement of H<sub>2</sub>O stored in high-pressure type metamorphic rocks from the trench to the upper mantle depth in various subduction settings (e.g., Peacock & Wang, 1999; Hacker et al., 2003). For example, Peacock (2009) indicated that the oceanic plate in the Philippine Sea plate subducting below the Kii Peninsula would suffer the cold HP/LT type metamorphism represented by zeolite facies, prehnite-pumpellyite facies, pumpellyite-actinolite facies, lawsonite-blueschist facies to jadeite-lawsonite-blueschist to 2GPa. However, the natural example recording abovementioned progressive metamorphic evolution has not been recognized yet.

Recently prehnite-pumpellyite facies and lawsonite-blueschist facies units have been recognized in the Otao unit of Kurosegawa belt in Yatsushiro area, Kyushu, Japan (Kamimura et al., 2012). However, the relationship of two metamorphic units has not been verified yet.

In this paper, we propose the progressive change of metamorphic grade from the prehnite-pumpellyite facies to lawsonite-blueschist facies based on petrography and thermodynamic phase analysis in metabasite system.

**Petrography and Mineralogy:** We confirmed that the prehnite-pumpellyite facies assemblage is predominant in the Tobiishi subunit of (Kamimura et al., 2012), but we newly found pumpellyite-actinolite facies from the western end of this subunit.

In the lawsonite-blueschist facies unit, Hakoishi-subunit of (Kamimura et al., 2012), located to the west of the Tobiishi-subunit, following mineral assemblage with excess chlorite, quartz, albite and phengite are systematically distributed from the east to the west in the subunit:

lawsonite + pumpellyite + aegirine-augite, pumpellyite + Na-amphibole, lawsonite + pumpellyite + Na-amphibole, lawsonite + Na-amphibole + aegirine-augite.

The compositions of sodic pyroxene, pumpellyite and Na-amphibole also show the following systematic trend westwards in the subunit; jadeite component of sodic pyroxene generally increases from X<sub>Jd</sub>=0.12 to X<sub>Jd</sub>=0.50 with X<sub>Aeg</sub>= up to 0.5. Al content of pumpellyite increases from 3.7 to 4.6 p.f.u. for O=24.5 Fe<sub>3</sub>/(Al+Fe<sub>3</sub>) in Na-amphibole decreases from 0.8 (riebeckite) to 0.15 (glaucophane).

**Thermodynamic phase analysis:** To evaluate stability relationship among abovementioned mineral assemblages, the phase diagram was constructed in the NCFMASH system with PERPLE\_X software package (Connolly, 2005) for 1-10 kbar and 100-400 C. The considered minerals are stilbite, laumontite, prehnite, pumpellyite, ferro pumpellyite, tremolite, ferro tremolite, diopside, hednbergite, clinocllore, daphnite, lawsonite, glaucophane, ferro glaucophane, clinozoisite and albite with excess, quartz and water. As the first order approximation, solid solution in each mineral was ignored. The newly constructed phase diagram predicts following representative mineral assemblages appear with the increase of the pressure along the high HP/LT path.

lawsonite + pumpellyite + clinopyroxene, pumpellyite + glaucophane, lawsonite + pumpellyite + glaucophane, lawsonite + glaucophane + clinopyroxene.

This metamorphic evolution in the model system is coincident well with the natural observation in the Hakoishi subunits.

**Conclusion:** Mineral assemblages observed in metabasites of the Tobiishi and Hakoishi subunits and the newly constructed petrogenetic grid suggest the metamorphic grade increases from prehnite-pumpellyite facies to lawsonite-blueschist facies westward ca. 20km in the Otao unit of Kurosegawa belt. The westward increase of Al content in pumpellyite, Na-amphibole, and Na-clinopyroxene also suggest the metamorphic grade increases westward. Thus, this area would become a type locality of a cold subduction system as proposed by the Peacock (2009)s thermal modeling.

Keywords: lawsonite, blueschist, HP/LT type metamorphic rocks, Kurosegawa belt, petrogenetic grid, cold subduction system

## Morphological change of zircon under high temperature metamorphism: Example of the Kiso Ryoke metamorphic rocks

IKAWA, Chiaki<sup>1\*</sup> ; MOTOYOSHI, Yoichi<sup>2</sup> ; HOKADA, Tomokazu<sup>2</sup> ; HORIE, Kenji<sup>2</sup>

<sup>1</sup>Department of Polar Science, the Graduate University for Advanced Studies, <sup>2</sup>National Institute of Polar Research

Zircon is an important key mineral to obtain the age of rocks, however zircon newly grew at each metamorphic cycle and its timing of crystallization should have been recorded as U-Pb age. It is not always fully understood how zircon crystal grows at different metamorphic grade. Williams (2001) demonstrated that the behavior of zircon has been changed accompanying with metamorphic grade in Cooma complex, SE Australia. In low grade, there are detrital zircons but in high grade, overgrown or newly formed zircons are observed. Kawakami et al (2013) reported the behavior of zircon in the upper-amphibolite to granulite facies schist/migmatite transition, Aoyama area, Ryoke metamorphic belt. They concluded that the recrystallization of zircon has been controlled by partial melt. Thus, crystal morphology is quite important for understanding the U-Pb age of zircon.

This study reports morphological change of zircon crystal at different metamorphic grades in the Kiso area, Ryoke metamorphic belt in Central Japan, where metamorphic grade continuously increases from non-metamorphic (Mino belt) to migmatite facies, similar with Cooma complex. The district is located in northeastern part of Mt. Kisokomagatake and the study area is about 43km from north to south, and about 22km west to east. In this district, regional metamorphic rocks (metasediments, quartz schist, basic schist, and carbonate rocks, etc.) and non-metamorphic rocks widely occur. Morikiyo (1984) classified the district into nine mineral zones (I to VII) based on the mineral assemblages.

We have studied total 46 samples from all zones. Mineral assembles of the studied samples indicate the following characteristics features: biotite appears in zone II, albite disappears in zone IIIa, chlorite disappears in zone IIIb and sillimanite appears in zone VIa.

On the basis of the optical microscope and SEM observations, morphology of zircon is divided into 3 groups, such as zones I-II, zones IIIa-V and zones VIa-VII.

Zones I-II: Under the optical microscope, each zircon grain shows different color (purple, pale-pink and colourless). Zircon grains are essentially euhedral, and show variable range of grain size (40-220  $\mu\text{m}$ ). In SEM observation, the abrasion and cracks are notable in zircon crystal surface. The above observations are consistent that the zircons in these zones are detrital origin that were derived from a variety of different source rocks.

Zones IIIa-V: Surface of zircon in these zones are irregular and rough with small holes which are likely to reflect resorption during the metamorphism. In contrast with the zircons from zones I-II, zircon crystal surface is relatively rough and shows no abrasion and cracks. But, even in the same zircon grain, both resorption surface and non-resorption surface can also be observed. Non-resorption surface is considered to preserve detrital surface (same with zone I-II), and resorption surface possibly reflects metamorphic dissolution or recrystallization (similar to zone VIa-VII). According to BSE images, no obvious new growth zone can be observed in many of zircon grains, but a few grains show sign of new overgrowth zone. Grain size of newly growing zircon is relatively small about 30 $\mu\text{m}$ .

Zones VIa-VII: Surface of zircon in these zones is relatively smooth, which differs from rough crystal surface in zones IIIa-V. It is assumed that the irregular surface of zone IIIa-V zircons are overgrown and filled by smooth surface as temperature increases to zones VIa-VII. In the highest-grade zone VII, the rough surface is disappeared, and smooth zircon grains are dominated.

Thus in the Ryoke metamorphic rocks from Kiso area, crystal morphology of zircons changes from the dominant detrital signature in the lowest-grade zone through irregular and rough resorption and recrystallization features in the middle-grade zone to the more smooth overgrowth recrystallization in the higher-grade. New zircon grain growth can be found in the middle to higher-grade zone.

Keywords: zircon morphology, regional metamorphism, Ryoke belt

## P-T estimates of a metapelite containig garnet zoning from Mefjell, Sr Rondane Mountain, East Antarctica

TSUBOKAWA, Yumiko<sup>1\*</sup> ; ISHIKAWA, Masahiro<sup>1</sup> ; ICHIKI, Takashi<sup>1</sup> ; KAWAKAMI, Tetsuo<sup>2</sup> ; MADHUSOODHAN, Satishkumar<sup>3</sup> ; TSUCHIYA, Noriyoshi<sup>4</sup> ; GEOFF, Grantham<sup>5</sup>

<sup>1</sup>Yokohama National University, <sup>2</sup>Kyoto University, <sup>3</sup>Niigata University, <sup>4</sup>Tohoku University, <sup>5</sup>Council for geoscience, South Africa

The Sør Rondane Mountains, East Antarctica have been considered to be situated in the Gondwana suture zones. Therefore the mountains have attracted interest as a key area for understanding amalgamation process of the supercontinent. The mountains consist of amphibolite- to granulite-facies metamorphic rocks with granitic intrusions, and the timings of the main metamorphism are interpreted as *c.* 640-600 Ma and *c.* 550-500 Ma. Metamorphic rocks from northern and eastern part of the mountains (Balchenfjella and northern part of Austkampane) record a clockwise *P-T* path, on the other hand, metamorphic rocks from central part of the mountains (Brattnipene and eastern Menipa) record anti-clockwise *P-T* path. This suggests each area records a different *P-T* path. However, pre-peak *P-T* conditions of southwestern part of the mountain such as Mefjell have been still not clear.

In this study, we report a garnet porphyroblast with a prograde zoning in a metapelite from Mefjell. The St-bearing Grt-Sil-Bt gneiss mainly consists of garnet, biotite, sillimanite, quartz and plagioclase, with minor K-feldspar, staurolite, apatite, monazite, ilmenite and magnetite. The garnet grain is 12 mm in diameter, with the change of color from reddish in the core to transparent in the rim. The garnet has core-rim boundary defined by Mn-zoning. The garnet is typically almandine-rich, and shows compositional zoning with decrease in spessartine content from the core (Alm<sub>63</sub>Sps<sub>24</sub>Prp<sub>14</sub>Grs<sub>6</sub>) to the rim (Alm<sub>74</sub>Sps<sub>2</sub>Prp<sub>20</sub>Grs<sub>4</sub>), and spessartine content increase again towards the outer-rim (Alm<sub>73</sub>Sps<sub>11</sub>Prp<sub>20</sub>Grs<sub>6</sub>). The garnet includes staurolite, sillimanite, biotite, chlorite, plagioclase, K-feldspar, quartz, apatite and ilmenite. Garnet-ilmenite and staurolite-garnet geothermometers yield a temperature increase towards rim from 350-400 to 630-700 °C. Garnet-Al<sub>2</sub>SiO<sub>5</sub>-quartz-plagioclase geobarometer applied to rim inclusions yields 7.2kbar±0.9kbar for an assumed temperature of 650 °C.

Keywords: East Antarctica, Sør Rondane Mountain, pressure and temperature conditions

## Syn-metamorphic fluid infiltration and petrogenesis of leucogranites in the MCT zone in Eastern Nepal

KAWAKAMI, Tetsuo<sup>1\*</sup> ; SAKAI, Harutaka<sup>1</sup> ; SATO, Katsushi<sup>1</sup>

<sup>1</sup>Graduate School of Science, Kyoto University

Syn-metamorphic fluid activity in the continental collision zone is of great importance especially for the petrogenesis of leucogranites and mass transfer through the fluid/melt extraction. Tourmaline (Tur) is a common accessory mineral in the crust having a wide stability field [1]. It is the most important sink of B in metapelites [2, 3, 4]. Although B behaves incompatibly under the absence of its sink minerals and is transported in fluid, once the *P-T-X* condition permits, it can be precipitated as Tur and other borosilicates in the site of fluid/rock interaction. Therefore, Tur can be a good tracer of B-bearing fluid [4]. Since Tur is a polar mineral, different concentrations of cations are incorporated at opposite poles of the crystal as a function of temperature up to 650°C, and this inter-polar element partitioning in Tur can be used as a geothermometer [2, 5].

We have investigated the mode of occurrence of Qtz veins and Tur-rich veins in the MCT zone around Dhankuta, Eastern Nepal. In this area, pelitic schists are widely exposed and subordinate amounts of metamorphosed dolostone, quartzite and mafic rocks are intercalated with them. The metamorphic grade decreases from the Ky zone through the St zone to the Grt zone as the distance from the MCT increases toward the south.

Qtz veins are abundant in metapelites of this area. They are mostly deformed by the ductile deformation with top-to-S sense of shear during the activity of the MCT, and are found as lenses. In the Ky zone, Qtz veins contain mm- to cm-sized crystals of Ky and minor Pl. Grt and Ky are coarse-grained only at the vicinity of the Qtz veins, and Ky tends to be formed exclusively around the Qtz veins. This suggests that the fluid activity that formed the Qtz veins took place around the peak metamorphism of the Ky zone, and Si, Al, Na and Ca were mobile in the fluid. Preliminary *P-T* estimate of this fluid activity using Grt-Ky-Pl-Bt-Qtz assemblage gave ca. 8kbar and ca. 600°C. In the St and Grt zones as well, Grt tends to be coarser grained around the Qtz veins. Therefore, these veins are the evidence for the externally derived fluid that infiltrated during the prograde to peak metamorphism of each zone.

Unusually abundant Tur is locally found in metapelites of the MCT zone. It is localized in aluminous, Ms-rich layers and can be formed through the input of external B into the appropriate whole-rock composition for Tur growth. Such a B-bearing fluid infiltration continued from the prograde stage because Grt with prograde chemical zoning includes abundant Tur crystals. B-bearing fluid infiltration continued in the post-peak stage as suggested by the presence of Tur-rich vein cross-cutting the schistosity. Inter-polar Ca/Na partitioning of Tur [5] gives 530-590°C for the temperature of the Tur-rich vein formation. A potential source of external fluid could be lower grade metasediments underlying these metamorphic zones, because syn-metamorphic dehydration reactions of hydrous minerals can supply not only H<sub>2</sub>O but also B in the fluid.

B-bearing fluid infiltration during the prograde to post-peak metamorphism in the MCT zone is important for the petrogenesis of the Higher Himalayan (HH) and North Himalayan leucogranites whose source region and petrogenesis remain highly controversial [6]. Observation in this study supports the fluid-fluxed melting of the MCT zone or Higher Himalayan Crystallines (HHC) [7]. Tur-bearing leucogranite veins in the HHC just above the MCT could be a potential product of such a fluid fluxed partial melting that took place near the MCT.

References: [1] van Hinsberg et al, 2011, *Can Min*, 49, 1-16. [2] Henry & Dutrow, 1996, *Rev Min*, 33, 503-557. [3] Sperlich et al, 1996, *Am Min*, 81, 1222-1236. [4] Kawakami, 2004, *TRSE*, 95, 111-123. [5] van Hinsberg & Schumacher, 2007, *CMP*, 153, 289-301. [6] Guo & Wilson, 2012, *GR*, 22, 360-376. [7] Le Fort, 1981, *JGR*, 86, 10545-10568.

Keywords: fluid, tourmaline, boron, inverted metamorphism, partial melting, continental collision zone

## Geochronology of the metamorphic rocks from the Masora, Antananarivo and Betsimisaraka domains, east-central Madagascar

ICHIKI, Takashi<sup>1\*</sup> ; ISHIKAWA, Masahiro<sup>1</sup> ; OSANAI, Yasuhito<sup>2</sup> ; NAKANO, Nobuhiko<sup>2</sup> ; ADACHI, Tatsuro<sup>2</sup>

<sup>1</sup>Yokohama National University, <sup>2</sup>Kyushu University

In a previous reconstruction of Gondwana supercontinent, Madagascar is located within the interior of the supercontinent (e.g. Jacobs and Thomas, 2004). Therefore, Madagascar is one of the most significant areas to understand the process of Gondwana supercontinent formation. However, it is still controversial whether the central part of Gondwana supercontinent was formed by young arc-arc collision and amalgamation (Stern, 1994), or was reworked of old continent (e.g. Collins and Pisarevsky, 2005; Tucker et al., 2012). In this study we estimated the age of protolith formation by applying LA-ICP-MS zircon dating method to metaigneous rocks and the age of metamorphism by applying EPMA monazite dating method to metasedimentary rocks, to understand the geochronological characteristics of the composed domains in east-central Madagascar.

East-central Madagascar is divided into Masora, Betsimisaraka and Antananarivo domains from east to west based on the geology and geochronology (Tucker et al., 2011). The Masora domain is mainly composed of the felsic metamorphic rocks with subordinate amounts of the metasedimentary rocks. Two metasedimentary rocks gave ages ranging from ca. 520 to 510 Ma. This age range is consistent with the age obtained from the meta-granitoid (ca. 530 to 510 Ma, Smith et al., 2008) and from quartzite (ca. 540 to 520 Ma, De Waele et al., 2011) by U-Pb zircon dating method. The felsic metamorphic rock gave igneous age at ca. 3300 Ma. This age is consistent with the age obtained from the migmatized gneiss (Tucker et al., 2011).

The Antananarivo domain is mainly composed of the felsic metamorphic rocks with subordinate amounts of the metasedimentary rocks. This domain is divided into east and west on the basis of the metamorphic condition and structural geology. The east and west areas are bounded by the low-angle ductile shear zone of top-to-west sense. Monazites from the metasedimentary rock in the east gave ages ranging from ca. 500 to 480 Ma. In the west monazites from the two types of the metasedimentary rocks gave ages ranging from ca. 540 to 500 Ma (Martelat et al., 2000) and ca. 630 to 540 Ma (Jöns and Schenk, 2011) and from the meta-granitoid gave age ranging from ca. 560 to 540 Ma (Grégoire et al., 2009). Therefore, the metamorphic age in the east is relatively younger than in the west. The felsic metamorphic rocks are geochemically classified into two types, which gave individual igneous ages of ca. 2700 Ma in the east and ca. 760 Ma in the west, respectively. The intermediate metamorphic rocks are exposed in the west and gave igneous age at ca. 550 Ma.

The Betsimisaraka domain is mainly composed of the metasedimentary rocks. Monazites from the metasedimentary rocks gave ages of ca. 500 Ma. This age is younger than the ages reported from the quartzite at ca. 550-520 Ma (Tucker et al., 2011) and rim ages from the metasedimentary rock at ca. 550 Ma (Collins et al., 2003) by U-Pb zircon dating method.

As a consequence east-central Madagascar was metamorphosed between ca. 550 and 500 Ma. Both the east of the Antananarivo and Betsimisaraka domains was metamorphosed at the youngest age around ca. 500 Ma. In previously reported geochronological results the oldest igneous activity was at ca. 2500 Ma in the Antananarivo domain (e.g. Kröner et al., 2000). Therefore the ca. 2700 Ma igneous age is new and the oldest igneous age in this domain. The east of the Antananarivo domain was older than the west and the oldest part of this domain. The age transition zone was possibly exposed between the Masora, Betsimisaraka and the west of the Antananarivo domains. The age and geological relationship in Archean domain was recently reported from the Dhawar Craton in southern India (Peucat et al., 2013). The existence of the ca. 2700 Ma igneous activity in the east of the Antananarivo domain could be the significant evidence of the continuity between India and Madagascar since Archean.

Keywords: Gondwana supercontinent, east-central Madagascar, LA-ICP-MS U-Pb zircon dating, EPMA monazite dating

## Deformation microstructures of a Kamila amphibolite mylonite and their formative temperatures

ARAI, Tomoyuki<sup>1\*</sup>; KANAGAWA, Kyuichi<sup>1</sup>; YOSHINO, Takashi<sup>2</sup>

<sup>1</sup>Graduate School of Science, Chiba University, <sup>2</sup>Institute for Study of the Earth's Interior, Okayama University

The Kohistan complex and the Kamila amphibolite belt in the northern Pakistan are considered to represent a Cretaceous island arc crust and a part of its lower crust, respectively. Here we report deformation microstructures of a Kamila amphibolite mylonite sample and their formative temperatures.

The amphibolite mylonite sample studied is composed of 100  $\mu\text{m}$  to 1 mm thick alternating layers of hornblende + pyroxene, plagioclase, and hornblende + plagioclase + quartz, intercalating a 3 mm thick layer of garnet + quartz + plagioclase. Composite planar fabrics of a top-to-south sense of shear are developed in this sample; C plane defined by compositional layering (= foliation), S plane defined by lenticular domains of plagioclase aggregate clockwise oblique to the C plane, and C' plane anticlockwise oblique to the C plane.

Hornblende + pyroxene layers contain pyroxene porphyroclasts of grain sizes  $\approx 200 \mu\text{m}$  scattered in matrix mainly composed of hornblende grains with grain sizes  $\approx 30 \mu\text{m}$ . Hornblende exhibits a strong crystallographic preferred orientation with (100) and [001] subparallel to foliation and lineation, respectively. Orthopyroxene porphyroclasts are elongated subparallel to foliation, and are accompanied by asymmetric tails mainly composed of hornblende indicating a top-to-south sense of shear. In addition, pyroxene porphyroclasts are surrounded by fine-grained ( $\approx 10 \mu\text{m}$ ) hornblende and quartz, suggesting a breakdown reaction of pyroxenes (orthopyroxene + clinopyroxene + H<sub>2</sub>O = hornblende + quartz), which is a retrograde reaction from granulite facies to amphibolite facies.

Plagioclase layers are composed of dynamically recrystallized plagioclase grains of An<sub>47-54</sub> in composition. Lenticular domains of plagioclase are likely porphyroclasts in origin. Plagioclase grains are polygonal in shape, and weakly aligned clockwise oblique to foliation, which also suggests a top-to-south sense of shear. Plagioclase exhibits a distinct crystallographic preferred orientation with {131} and <1-12> clockwise oblique to foliation and lineation, respectively by  $\approx 20$  degrees. But {131} and <1-12> are aligned subparallel to the S plane, suggesting the dominance of {131}<1-12> during the dynamic recrystallization of plagioclase.

We applied three pyroxene geothermometers to the chemical compositions of orthopyroxene and clinopyroxene porphyroclasts, which yielded temperatures around 850 degrees C. We also applied a hornblende-plagioclase geothermometer to the average chemical compositions of hornblende and plagioclase in hornblende + plagioclase + quartz layers, and obtained a temperature of  $\approx 610$  degrees C. Thus, the amphibolite mylonite studied likely experienced a peak metamorphism of granulite facies at  $\approx 850$  degrees C, and subsequently a retrograde metamorphism of amphibolite facies at  $\approx 610$  degrees C, during which it was sheared by top-to-south thrusting.

## The tectonics evolution of metamorphic and igneous rocks embedded in the serpentinite melange from the Kurosegawa Tecton

YOSHIMOTO, Aya<sup>1\*</sup> ; OSANAI, Yasuhito<sup>1</sup> ; NAKANO, Nobuhiko<sup>1</sup> ; ADACHI, Tatsuro<sup>1</sup> ; KITANO, Ippei<sup>1</sup> ; YONEMURA, Kazuhiro<sup>2</sup> ; ISHIZUKA, Hideo<sup>3</sup>

<sup>1</sup>Kyushu Univ., <sup>2</sup>JOGMEC, <sup>3</sup>Kochi Univ.

This study focuses petrology of the Kurosegawa Tectonic Zone, which is characterized by serpentinite melange in the Jurassic Chichibu Belt, in SW Japan. The serpentinite melange contains several blocks including high-pressure/low-temperature metamorphic rocks, high-temperature metamorphic rocks and granites. A small amount of age data obtained in previous study suggests that all rock types were formed before the Jurassic. However, detailed petrological and geochronological works on the blocks have been never performed so far. In this study, we carried out regional-scale geological, geochemical and geochronological analyses on the blocks in serpentinite from the western part of Kyushu to the eastern part of Kii peninsula.

Keywords: Kurosegawa Tectonic Zone, U-Pb zircon age

## Metamorphism of the NE side of the Seba eclogitic basic schist in the Sambagawa metamorphic belt, central Shikoku, Japan

KISHIRA, Naohito<sup>1\*</sup> ; TAKASU, Akira<sup>1</sup> ; KABIR, Md fazle<sup>1</sup>

<sup>1</sup>Department of Geoscience, Shimane University, Japan

The Sebadani area belongs to the albite-biotite zone and is located in the central part of the Besshi district. The Sebadani area is composed of the Sebadani metagabbro mass and surrounding Seba basic schists, pelitic and siliceous schists occur as intercalation within the Seba basic schists (Takasu and Makino, 1980; Takasu, 1984). Eclogitic mineral assemblages are sporadically preserved in both the Sebadani metagabbro and the Seba basic schists (Seba eclogitic basic schists) (e.g. Takasu, 1984; Naohara and Aoya, 1997; Aoya, 2001). The Onodani eclogites preserved within the Seba basic schists have a complex metamorphic history, undergoing three different metamorphic episodes (Kabir and Takasu, 2010). The first and second eclogite facies metamorphism is estimated as 530-590 °C and 19-21 kbar and 630-680 °C and 20-22 kbar, respectively. The second metamorphic event is similar to that of the Seba eclogitic basic schist of Aoya (2001) (610-640 °C and 12-24 kbar). The pelitic schists intercalated within the Seba eclogitic basic schists also underwent eclogite facies metamorphism of 520-550 °C and *c.* 18 kbar (Zaw Win Ko *et al.*, 2005; Kouketsu *et al.*, 2010).

The eclogite in the northeastern part of the Seba eclogitic basic schists consist mainly of garnet, epidote, amphibole (glauco-phane, barroisite, taramite, Mg-taramite, Mg-katophorite, edinite), omphacite ( $X_{Jd}$  0.27-0.41), phengite (Si 6.5-6.9 pfu). Minor amounts of albite, dolomite, rutile, titanite, biotite, chlorite and quartz. The schistosity is defined by preferred orientation of phengite, amphibole and epidote. Garnets are almandine-rich in composition, increasing almandine ( $X_{Alm}$  0.54-0.60), pyrope ( $X_{Prp}$  0.07-0.13) and decreasing spessartine ( $X_{Sprs}$  0.10-0.03) from core to the rim and contain inclusions of epidote, omphacite ( $X_{Jd}$  0.27-0.41), dolomite, quartz and titanite. They also contain inclusions of barroisite/Mg-katophorite and albite symplectite. Amphibole in the matrix are zoned, barroisite/Mg-katophorite cores to edinite rims. Some other amphiboles in the matrix are parallel to the schistosity and occasionally occur as randomly oriented. The cores of these amphiboles are resorbed barroisite, glaucophane in the mantle and barroisite/edenite in the rim.

Based on the mineral paragenesis of the eclogites the metamorphism is divided into three events. The first eclogitic metamorphic event is deduced from symplectites of barroisite/ Mg-katophorite and albite after omphacite inclusions in garnet. The prograde stage of the second eclogitic metamorphic event is represented by the inclusions minerals within the mantle and rim of garnets consisting of epidote, barroisite and dolomite. The peak eclogite facies stage is defined by garnet rim and omphacite inclusions within the garnets with schistosity forming minerals of barroisite, omphacite and phengite. Garnet and omphacite rim-rim pairs yielded 530-570 °C and >11-14 kbar, and garnet and omphacite inclusion within garnet yields 520-560 °C, >11-12 kbar (Ellis & Green, 1979 ; Banno, 1986). THEMOCALC (Holland & Powell, 1998) average *P-T* calculation for garnet + omphacite + barroisite + phengite assemblage obtained 590-610 °C and 19-20 kbar. The retrograde stage is defined by symplectite of barroisite and albite after omphacite. The third metamorphic event is defined by zoned amphibole in the matrix.

The estimated matamorphic temperatures of the eclogites are lower than that of the second high-pressure metamorphic event of the Onodani eclogite and similar to that of the omphacite-bearing metapelites from the NW part of the Seba eclogitic basic schists (Kouketsu *et al.*, 2010). This suggests a metamorphic thermal gradient existed within the Seba eclogitic basic schists.

Keywords: Sambagawa (Sanbagawa) metamorphic belt, Seba basic schist, eclogite, glaucophane, P-T path, thermal gradient

## Metamorphic history of garnet amphibolite from the Neldy Formation, Makbal district in the Kyrgyz Northern Tien-Shan

KASYMBEKOV, Adil<sup>1\*</sup> ; TAKASU, Akira<sup>1</sup> ; KABIR, Md fazle<sup>1</sup> ; BAKIROV, Apas<sup>2</sup> ; SAKIEV, Kadyrbek<sup>2</sup>

<sup>1</sup>Department of Geoscience, Shimane University, Japan, <sup>2</sup>Institute of Geology, Academy of Science, Kyrgyz Republic

The Kyrgyz Tien-Shan Mountains extend from east to west, separating the Kazakhstan plate to the north and the Tarim plate to the south. They are divided into three tectonic units; the Northern Tien-Shan, the Central (or Middle) Tien-Shan and the Southern Tien-Shan. In the Northern Tien-Shan there are two HP and UHP metamorphic complexes, Makbal HP and UHP in the western part, and Aktyuz HP in the eastern part of the complexes. The Makbal complex in the Kyrgyz Northern Tien-Shan is located in the western segment of the CAOB.

The metamorphic rocks exposed in the Makbal district are divided into the Akdzhon and the Scharkyrak Groups based on their metamorphic conditions. The Akdzhon Group contains rocks of the HP and UHP metamorphic conditions, whereas the Scharkyrak Group underwent greenschists facies metamorphism. The Akdzhon Group is divided into two contrasting metamorphic formations, the structurally lower Makbal Formation and the upper Neldy Formation.

The Neldy Formation is mainly composed of garnet-phengite schists and chlorite-carbonate rocks, along with minor metaquartzites and marbles. Amphibolites and garnet amphibolites occur in the garnet-phengite schists as lenses or blocks up to 50 m across. Eclogites preserved in the cores of the garnet amphibolite bodies. Garnet amphibolite consists mainly of amphibole (magnesian hornblende, ferropargasite, ferrotschermakite, tschermakite, barroisite, actinolite), garnet and chlorite, with minor amounts of quartz, epidote and albite. Accessory minerals are paragonite, titanite and calcite. A schistosity is defined by preferred orientation of amphibole.

Garnets in the garnet amphibolite are rich in almandine ( $X_{Alm}$  0.35-0.64), with variable amounts of spessartine ( $X_{Sps}$  0.00-0.20), grossular ( $X_{Grs}$  0.27-0.61) and pyrope ( $X_{Prp}$  0.01-0.07) compositions. Garnet displays a compositional zoning, in which decrease  $X_{Sps}$  (0.20-0.04), increases  $X_{Alm}$  (0.35-0.60),  $X_{Grs}$  (0.31-0.62) and slightly increase  $X_{Prp}$  (0.01-0.03) from the core to the rim and contain inclusion of paragonite, titanite, chlorite, epidote and amphibole (actinolite, magnesian hornblende). The garnets are partly replaced by chlorite and aggregates of amphibole (ferrotschermakite, barroisite), chlorite and quartz along the cracks. Amphiboles in the matrix are zoned with magnesian hornblende and barroisite cores to ferrotschermakite and tschermakite rims and contain inclusions of titanite and quartz.

Based on the texture and mineral composition, we consider that the prograde stage probably stable in the epidote-amphibolite facies condition due to the existing of barroisitic amphibole and epidote along with garnet, paragonite, albite and chlorite. The tschermakitic rim of matrix amphibole suggests that the peak stage probably stable in the amphibolite facies conditions. The expected metamorphic condition of the garnet amphibolite from the Neldy Formation corresponding with peak  $P-T$  conditions of 610-620 °C and 14-16 kbar for the garnet amphibolite from the Makbal complex (Rojas-Agramonte *et al.*, 2013).

### References:

Rojas-Agramonte Y., Herwartz D., Garcia-Gasco A. *et al.*, (2013) *Contrib Mineral Petrol*, 166, 525-543.

Keywords: Garnet amphibolite, metamorphic history, amphibolite facies, Makbal complex, Neldy Formation, Kyrgyz Tien-Shan

## The stress-strain history of metamorphic sole: the case study of Greece, Turkey, Oman and Andaman islands

HOSHINO, Kenta<sup>1\*</sup>

<sup>1</sup>Shizuoka University, Graduate School of Science

Metamorphic sole is formed by intra-oceanic thrusting and is found in some locations around the world. Greece, Turkey, Oman and Andaman islands are Tethys type ophiolite exposed area. The microboudin method, which is palaeostress analysis, is based on the proportion of boudinaged mineral grains with respect to applied differential stress. In this study, we used columnar minerals bearing metacherts from four areas and examined the value of palaeodifferential stress. The microboudin method revealed the value of palaeodifferential stress is 3.3~24.8 MPa and we got stress-strain curve by using strain reversal method. The stress-strain curve indicate the stress history. Palaeodifferential stress increased until the end of deformation in all samples. This result show that peak P-T condition and peak differential stress are not simultaneous.

Keywords: microboudin, metamorphic sole, palaeodifferential stress, Tethys, stress-strain history

## Late Cretaceous and Paleogene nappe tectonics in the forearc regions of Southwest Japan

ONO, Akira<sup>1\*</sup>

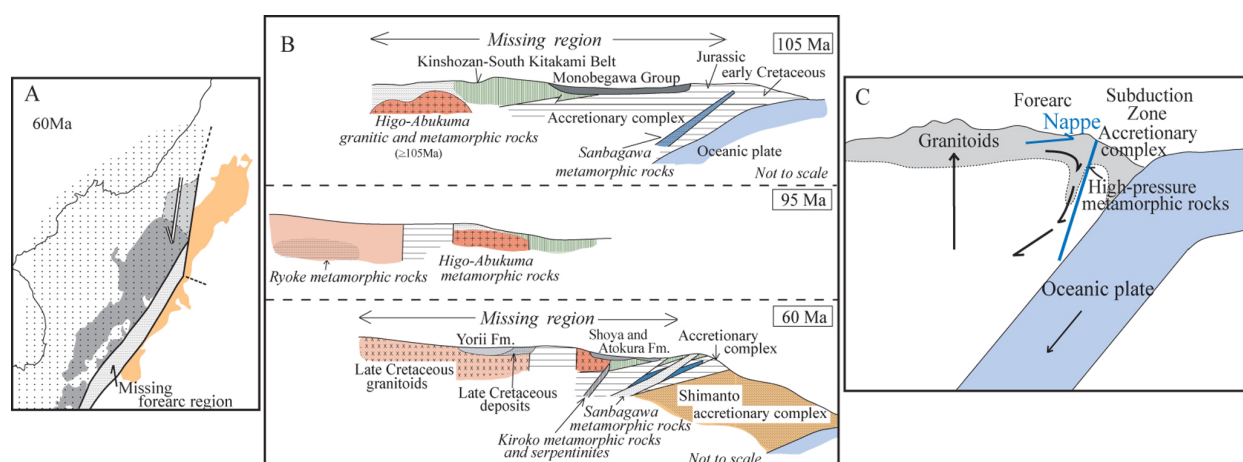
<sup>1</sup>none

Nappe tectonics occurred at many times in the Paleogene and late Cretaceous forearcs of Southwest Japan. Upper parts of the crust moved toward trench by the nappe tectonics (Figures A and B). Actually the Atokura and Ryoke Nappes are observed in the northern margin of the Kanto Mountains although most of the nappes were eroded. The Atokura Nappe is mainly composed of Permian granites, mid-Cretaceous granitic and metamorphic rocks, late Cretaceous Atokura Formation, early Paleogene Yorii Formation and late Cretaceous pyroclastic rocks. The Ryoke Nappe mainly consists of late Cretaceous granitic and metamorphic rocks. The Permian granitoids are geological bodies of the Kinshozan-South Kitakami Belt. The mid-Cretaceous granitic and metamorphic rocks were geological members of the Higo-Abukuma Belt. The late Cretaceous granitic and metamorphic rocks were distributed in or near the Ryoke Belt. These various rocks were located in the early Paleogene forearc (Figure B) and were removed by nappe tectonics (Ono, 2011, Abs. Geol. Soc. Japan, Meeting, p. 196).

It is important to reveal the tectonics of the lower crust when the upper crust of about 5km in thickness was moved as a nappe toward trench. The author postulates that the lower crust moved toward mantle. The surface layer of the crust moves as a nappe and the lower crust flows towards the mantle. A thrust is assumed near the base of the lower crust. Figure C shows directions of the movements of crustal materials. Tectonics like this has been repeated in late Cretaceous and Paleogene and almost all the mid-Cretaceous Higo-Abukuma metamorphic rocks were eliminated. The Ryoke Belt was also partly removed after the nappe tectonics.

The tectonics described above is consistent with the geological structure near the Median tectonic Line where the Ryoke Belt is directly in contact with the Shimanto Belt in the central part of the Kii Mountains. In this context, Ryoke granitic and metamorphic rocks are in contact with Sanbagawa metamorphic rocks from surface to lower crust according to the crustal section of Southwest Japan (Ito and Sato, 2010, Journal of Geography, 119, p.235). It is difficult to find a crustal layer which was situated in the deep parts of the Higo-Abukuma and Kinshozan-South Kitakami Belts in the crustal section.

Keywords: Southwest Japan, Forearc, Late Cretaceous and Paleogene, Nappe tectonics, Lower crust



## First-principles calculations of the structure of MgSiO<sub>3</sub> melt at high temperature and high pressure

MATSUI, Masanori<sup>1\*</sup>

<sup>1</sup>School of Sci., Univ. of Hyogo

Crystals and melts with MgSiO<sub>3</sub> composition are important constituents of the Earth's lower crust and mantle. Therefore an accurate knowledge of their structural and elastic properties at high temperatures and high pressures is crucial to investigate the chemical and physical structures, and the conditions of formation and evolution of the Earth. However, reliable experimental data under geophysically relevant conditions are generally lacking for MgSiO<sub>3</sub> melt, mainly due to the difficulty in obtaining such data at the combined high temperature and high pressure found in the Earth's interior. Here we use the first-principles molecular dynamics (FPMD) method to study the structures and elastic properties of MgSiO<sub>3</sub> melt at high temperatures and high pressures.

All calculations were performed with the Vienna Ab Initio Simulation Package VASP (Kresse and Furthmuller, 1996). The projector-augmented wave (PAW) method was used in the local density approximation (LDA) for the exchange-correlation functional (Blochl, 1994; Kresse and Joubert, 1999). FPMD calculations were carried out in the canonical ensemble (constant temperature  $T$ , constant volume  $V$ , and constant number of atoms  $N$  in the system) using cubic basic cells.  $N$  was taken to be 160 (32 MgSiO<sub>3</sub>) throughout this study. After annealing the system sufficiently at 4000 K, and then 3000 K, we fixed  $V$  at 38.54 cm<sup>3</sup>/mol and  $T$  at 2000 K to calculate the interference function  $S(Q)$ , where  $Q$  is the length of scattering vector, and the radial distribution function (RDF) for each atom pair. We found FPMD calculated  $S(Q)$  compares reasonably well with the observed data from X-ray analyses at 1973 K by Waseda and Toguri(1990). The FPMD predicted average nearest neighbor bond distances  $r(ij)$ , and coordination numbers  $n(ij)$  between atoms  $i$  and  $j$  are also compared well with the data by Waseda and Toguri(1990), except the  $r(\text{MgO})$  distance, in which the FPMD value of 1.97 Å is much shorter than the value [2.12(1) Å] by the X-ray analyses. We further apply the FPMD technique to investigate the temperature and pressure dependencies of the structure of MgSiO<sub>3</sub> melt.

Keywords: MgSiO<sub>3</sub> melt, high temperature, high pressure, first-principles calculation

## Forsterite-MgSiO<sub>3</sub> liquid interface : molecular dynamics perspective

NORITAKE, Fumiya<sup>1\*</sup> ; KAWAMURA, Katsuyuki<sup>1</sup>

<sup>1</sup>Okayama University

Knowledge about the viscosity and permeability of partial molten rocks is important to understand the thermal history of the Earth and volcanisms. For understanding those obtained by experiments and estimating the physical properties at extreme conditions those are difficult to reproduce in laboratory experiments, the knowledge about structure and properties of silicate crystal-liquid interfaces is necessary. The properties of melt as sandwiched thin films are considered as being different with ones in bulk melts by the effect of crystal surface. For instance, lateral self-diffusivity of water to crystal surfaces shows different from bulk one in the case of water-brucite surface (Sakuma et al. 2003), water-muscovite mica surface (Sakuma and Kawamura, 2009). The dynamic property anomalies on solid - liquid surfaces affect properties of bulk rock such as permeability (Ichikawa et al. 2001).

In this study, structure and properties of the forsterite-MgSiO<sub>3</sub> liquid interfaces are investigated by using molecular dynamics simulations. It is essential to know the structure and physical properties of forsterite-MgSiO<sub>3</sub> liquid interfaces since forsterite is the liquidus mineral of primordial magmas.

Molecular dynamics simulations were performed with NPT ensemble using MXDORTO code (Sakuma and Kawamura, 2009). The initial structure is a 21440 atom system in which a sheet of MgSiO<sub>3</sub> liquid consist of 8000 atoms (~5 nm) is sandwiched between (010) surfaces of forsterite(Pbnm) and 43440 atom system in which a sheet of MgSiO<sub>3</sub> liquid consist of 30000 atoms (~20 nm) is sandwiched between (010) surfaces of forsterite. Firstly we calculated equilibrated MgSiO<sub>3</sub> liquid film in vacuum starting with a randomly generated structure and randomly generated velocities of atoms through 0.5 ns (1,000,000 steps) at 1973 K and quench to 300 K. Secondly we calculated a bulk forsterite crystal with 13440 atoms (11\*5\*8 unit cells of forsterite(Pbnm)) starting with a given experimental crystal structure which was obtained by the experiment [5] and with randomly generated velocities of atoms and then cut along (010) surface. Finally we combined forsterite cut along (010) surface and MgSiO<sub>3</sub> liquid film. Under maintaining isobaric and isothermal conditions, we performed the relaxation of 0.5~1.5 ns. Then the statistical averages of the structure and physical properties were obtained from the velocities and coordinates of each atom in the simulations through 500 ps. The function of inter-atomic potential model was same as used in our previous work (Noritake et al. 2012).

By these simulations, characteristic structures in the forsterite-MgSiO<sub>3</sub> liquid interface are observed. The layered structure of alternated crystal surface, Si-rich and Mg-rich layers in the crystal-liquid interface was observed. The layered structure was formed by energy difference between Si-O semi-covalent bonds and Mg-O ionic bonds. Si-O-Si bridging and free oxygen atoms are excessively formed and in the near surface since the energy of Si-O bonding is much lower than that of Mg-O bonding. The difference of layered structure by thickness of MgSiO<sub>3</sub> liquid film might be caused by the difference of the degree of freedom of configuration in liquid film. The two-dimensional diffusivity of oxygen atoms is controlled by two factors. The one is the thickness of liquid film that decreases oxygen diffusivity with decreasing the film thickness because of decrease of degree of freedom of configuration in liquid film. The other is composition of sliced layer where oxygen diffusivity increases with increasing the Mg/Si ratio since Si-O bonding is much stronger than Mg-O ones.

Keywords: Interface, High-Temperature, Silicates, Molecular dynamics simulation

## Phase transitions in $\text{Zn}_2\text{SiO}_4$ : first-principles study

KANZAKI, Masami<sup>1\*</sup>

<sup>1</sup>Inst. Study Earth's Interior, Okayama University

Recent experimental study (Liu et al., *PCM*, 40, 467, 2013) suggested that high-pressure phases of III and IV in  $\text{Zn}_2\text{SiO}_4$  could be retrograde phases transformed during decompression. In order to check stabilities of these phases under pressure, and to find original high-pressure phases, density functional theory total energy calculations of 12 phases at 0 K have been conducted.

Three pressure-induced "phase transitions" during structural optimization were observed: phase II to spinel structure, phase III to a new high-pressure phase, and phase IV to  $\text{Na}_2\text{SO}_4$  III-type structure. Phase III, having tetrahedral olivine structure, exhibited extraordinary high compressibility, which is due to large volume reductions in vacant octahedral sites corresponding M1 and M2 sites in olivine structure. Calculated enthalpies of the phases at 0 K confirmed that phase III and IV are not stable at any pressure. It also suggested that  $\text{Na}_2\text{SO}_4$  III and II phases will be stable phases replacing phase III and IV, respectively.

Keywords:  $\text{Zn}_2\text{SiO}_4$ , phase transition, high pressure phase, first-principles, transition mechanism

## A new high pressure phase of $\text{Fe}_2\text{SiO}_4$ and the relationship between spin and structural transitions

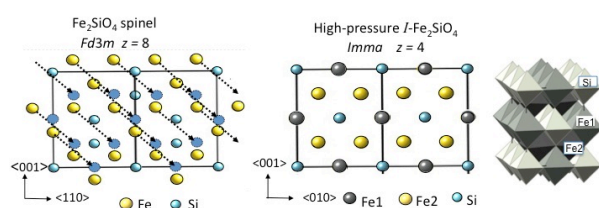
YAMANAKA, Takamitsu<sup>1\*</sup>; KYONO, Atsushi<sup>2</sup>; NAKAMOTO, Yuki<sup>3</sup>; KHARLAMOVA, Svetlana<sup>1</sup>; STRUZKIN, Viktor<sup>1</sup>; MAO, Ho-kwang<sup>1</sup>; HEMLY, Russell<sup>1</sup>

<sup>1</sup>Carnegie Institution of Washington Geophysical Laboratory, <sup>2</sup>Division of Earth Evolution Sciences, Life and Environment Sciences, University of Tsukuba, <sup>3</sup>Center for Quantum Science and Technology Under Extreme Conditions, Osaka University

A structural change in  $\text{Fe}_2\text{SiO}_4$  spinel (ringwoodite) has been found by synchrotron powder diffraction study and the structure of a new high-pressure phase was determined by Monte-Carlo simulation method and Rietveld profile fitting of x-ray diffraction data up to 64 GPa at ambient temperature. A transition from the cubic spinel structure to a body centered orthorhombic phase (I- $\text{Fe}_2\text{SiO}_4$ ) with space group  $Imma$  and  $Z=4$  was observed at approximately 34 GPa. The structure of I- $\text{Fe}_2\text{SiO}_4$  has two crystallographically independent  $\text{FeO}_6$  octahedra. Iron resides in two different sites of six-fold coordination: Fe1 and Fe2, which are arranged in layers parallel to (101) and (011), and very similar to the layers of  $\text{FeO}_6$  octahedra in the spinel structure. Silicon is located in the six-fold coordination in I- $\text{Fe}_2\text{SiO}_4$ . The transformation to the new high-pressure phase is reversible under decompression at ambient temperature. A martensitic transformation of each slab of the spinel structure with transition vector  $\langle 1/8 \ 1/8 \ 1/8 \rangle$  generates the I- $\text{Fe}_2\text{SiO}_4$  structure. Laser heating of I- $\text{Fe}_2\text{SiO}_4$  at 1500 K results in a decomposition of the material to rhombohedral FeO and  $\text{SiO}_2$  stishovite.

Fe K beta x-ray emission measurements at high pressure up to 65GPa show that the transition from a high spin (HS) to an intermediate spin (IS) state begins at 17 GPa in the spinel phase. The IS electron spin state is gradually enhanced with pressure. The  $\text{Fe}^{2+}$  ion at the octahedral site changes the iron radius under compression from 0.78 Å at the high-spin state to 0.61 Å at the low spin, which results in the changes of the lattice parameter and the deformation of the octahedra of the spinel structure. The compression curve of the lattice parameter of the spinel is discontinuous at approximately 20 GPa. The spin transition induces an isostructural change.

Keywords:  $\text{Fe}_2\text{SiO}_4$  spinel, new high-pressure phase, spin transition, X-ray emission, martensitic transition



## Synchrotron Mössbauer spectroscopy on Fe<sub>3</sub>S, FeO and natural almandine

KAMADA, Seiji<sup>1\*</sup>; HIRAO, Naohisa<sup>2</sup>; HAMADA, Maki<sup>3</sup>; SUZUKI, Nanami<sup>1</sup>; OHTANI, Eiji<sup>1</sup>; OHISHI, Yasuo<sup>2</sup>; MASUDA, Ryo<sup>4</sup>; MITSUI, Takaya<sup>5</sup>

<sup>1</sup>Tohoku Univ., <sup>2</sup>JASRI, <sup>3</sup>School of Nature system, College of Science and Engineering, Kanazawa University, <sup>4</sup>Research Reactor Institute, Kyoto Univ., <sup>5</sup>JAEA

The Earth's core is considered to be composed of an iron alloy with light elements since its density is smaller than that of pure iron under core conditions (e.g., Birch, 1964; Dubrovinsky et al., 2000). Although there are many candidates for these elements, such as H, C, O, Si, and S, sulfur in particular has been considered as one of the most plausible candidates. This is because it is depleted in the mantle, suggesting that it exists in the Earth's core (Murthy and Hall, 1970), and iron sulfides are found universally in iron meteorites, i.e., analogues of the Earth's core. Although the content of sulfur in the Earth's core is not known precisely, the sulfur content in the core is estimated to be at least a few wt% based on cosmic element abundances (McDonough, 2003) and high pressure partitioning experiments (e.g., Hillgren et al., 2000).

Since sulfur is one of the most plausible light elements, a compressibility and phase diagram in the Fe-FeS system has been studied (e.g., Campbell et al., 2007; Chen et al., 2007; Fei et al., 2000; Kamada et al., 2010; Li et al., 2001; Seagle et al., 2006). According to previous studies, Fe<sub>3</sub>S is stable from 21 GPa and at least up to 200 GPa. Therefore, Fe<sub>3</sub>S can be one of a candidate of the inner core materials. In addition, a synchrotron Mössbauer spectroscopy (SMS) and X-ray emission spectroscopic studies on Fe<sub>3</sub>S revealed a spin transition and magnetic transition between 20 and 25 GPa (Lin et al., 2004; Shen et al., 2003). It also showed an abnormal evolution of a and c axes with increasing pressure (Chen et al., 2007).

Synchrotron Mössbauer spectroscopy is a good probe of a small sample under high pressure to investigate magnetic properties and electronic states of Fe of core and mantle minerals. An energy domain Mössbauer spectroscopic system has been recently developed at the BL10XU, SPring-8. We have measured Mössbauer spectra from Fe<sub>3</sub>S and FeO under high pressure and a natural almandine at ambient pressure.

A powder mixture was made from <sup>57</sup>Fe (96.63%, ISOFLEX) and FeS (99.9%, RAREMETALLIC co., LTD.) with a ratio of Fe:S=75.0:25.0 (in at%). A foil was made from the mixture by a cold compression using a diamond anvil cell (DAC) and loaded into a sample chamber. <sup>57</sup>Fe enriched Fe<sub>3</sub>S was synthesized from the powder mixture in a DAC at 30 GPa and 1350 K. The synthesis of Fe<sub>3</sub>S was confirmed by X-ray diffraction patterns at BL10XU, SPring-8. <sup>57</sup>FeO was made by reducing from <sup>57</sup>Fe<sub>2</sub>O<sub>3</sub> (ISOFLEX) at ambient pressure and high temperature. A pellet was made from <sup>57</sup>FeO powder and loaded into a sample chamber of a DAC. We also measured Mössbauer spectra of a natural almandine (Py<sub>15.7</sub>Alm<sub>78.6</sub>Gros<sub>4.4</sub>Sp<sub>1.3</sub>, Idaho, USA). The energy of used X-ray for Mössbauer spectroscopy was 14.4125 keV.

We have measured Mössbauer spectra of Fe<sub>3</sub>S during decompression at 5, 15, 20, 25, and 30 GPa and room temperature at BL10XU and BL11XU. At BL10XU, those of FeO and the almandine were obtained at 200 GPa and ambient pressure, respectively. The magnetic transition in Fe<sub>3</sub>S was observed between 20 and 25 GPa, which is consistent with Lin et al. (2004). We observed doublet peaks from FeO. An evidence of Fe<sup>3+</sup> in the almandine was not detected in this study. We will report the results of the Mössbauer spectra based on the newly developed system at BL10XU, SPring-8.

Keywords: Earth's core, Mantle, Mössbauer, Fe<sub>3</sub>S, FeO

## Temperature dependence of Fe<sup>3+</sup>, Al and Ga distributions and local domain structure in synthetic Ca-clinopyroxene

AKASAKA, Masahide<sup>1\*</sup>; HAMADA, Maki<sup>2</sup>; NAGASHIMA, Mariko<sup>3</sup>; EJIMA, Terumi<sup>4</sup>

<sup>1</sup>Dep. Geoscience, Shimane Univ., <sup>2</sup>School of Nature system, Kanazawa Univ., <sup>3</sup>Dept. Earth Sci., Yamaguchi Univ., <sup>4</sup>AIST

Distribution of Fe<sup>3+</sup>, Al<sup>3+</sup> and Ga<sup>3+</sup> among octahedral and tetrahedral sites in synthetic esseneite (CaFeAlSiO<sub>6</sub>)- and (CaFe<sup>3+</sup>GaSiO<sub>6</sub>)<sub>90</sub>(CaGa<sub>2</sub>SiO<sub>6</sub>)<sub>10</sub>-clinopyroxenes at 800 and 1200 °C were investigated using <sup>57</sup>Fe Mössbauer and X-ray Rietveld methods to find a relation between site occupancies of trivalent cations at the octahedral and tetrahedral sites and ionic sizes of trivalent cations. The esseneite was synthesized from oxide mixture using sintering technique at 1200 °C in air. The FeGaTs<sub>90</sub>GaTs<sub>10</sub>-Cpx was crystallized from glass starting material at 1200 °C in air. The Cpxs synthesized and those annealed at 800 °C were analyzed using <sup>57</sup>Fe Mössbauer spectroscopic and X-ray Rietveld methods. In the synthetic esseneite, <sup>VI</sup>Fe<sup>3+</sup>:<sup>IV</sup>Fe<sup>3+</sup>-ratio at 800 °C was determined as 82(1):18(1) by Mössbauer method and 78.2(5):21.8(5) by Rietveld method, whereas, at 1200 °C, 79(1):21(1) by Mössbauer method and 77(1):23(1) by Rietveld analysis. The resulting Fe<sup>3+</sup> populations at octahedral M1 and tetrahedral T sites in the synthetic esseneite are Fe<sup>3+</sup>0.782(5)-0.82(1) apfu and 0.218(5)-0.18(1) apfu, respectively. In the synthetic Fe<sup>3+</sup>-Ga-Cpx, <sup>VI</sup>Fe<sup>3+</sup>:<sup>IV</sup>Fe<sup>3+</sup>-ratio at 800 °C was 74(3):26(2) (Mössbauer analysis data) and 78(1):22(1) (Rietveld analysis data), while, at 1200 °C, 71(3):29(1) (Mössbauer analysis data) and 67(1):33(1) (Rietveld analysis), which results in populations at the octahedral M1 and tetrahedral T sites of [Fe<sup>3+</sup><sub>0.67(1)-0.70(1)</sub>Ga<sub>0.33-0.30</sub>]<sup>M1</sup>[Si<sub>1.0</sub>Fe<sup>3+</sup><sub>0.23-0.20</sub>

Ga<sub>0.77-0.80</sub>]<sup>T</sup> (O = 6) at 800 °C, and [Fe<sup>3+</sup><sub>0.64(1)-0.60(1)</sub>Ga<sub>0.36-0.40</sub>]<sup>M1</sup>[Si<sub>1.0</sub>Fe<sup>3+</sup><sub>0.26-0.30</sub>Ga<sub>0.74-0.70</sub>]<sup>T</sup> at 1200 °C. This result indicates the temperature dependence of Fe<sup>3+</sup>, Al<sup>3+</sup> and Ga<sup>3+</sup> distributions between M1 and T sites. However, it is evident that, even at different temperatures, distributions of Fe<sup>3+</sup>, Al<sup>3+</sup> and Ga<sup>3+</sup> between M1 and T sites are well correlated with the ratio of ionic radius of larger Fe<sup>3+</sup>-cation against smaller Al<sup>3+</sup> and Ga<sup>3+</sup>, as Akasaka et al. (1997) indicated. Another finding in this study is the splitting of a <sup>57</sup>Fe Mössbauer doublet by Fe<sup>3+</sup> at M1 site into two doublets. This indicates existence of short-range domain structure by two kinds of M1 sites with slightly different distortions, which cannot be detected by X-ray diffraction.

Keywords: clinopyroxene, Mossbauer analysis, X-ray structural refinement, Crystal chemistry, ionic distributions, temperature dependence

## Phase Transformation of Zirconium under High P-T Conditions

ONO, Shigeaki<sup>1\*</sup>

<sup>1</sup>JAMSTEC

The behavior of zirconium metal under high pressures is important in the community of the high-pressure study, because changes in resistivity due to the phase transformations of zirconium (Zr) are used as pressure calibration points in the high-pressure experiments. Zirconium metal, which shows the hcp structure at ambient conditions, is known to transform to the bcc structure (beta phase) above 1135 K at ambient pressure. With increasing pressure, phase transformations to a hexagonal structure (omega phase), at the pressure around 5 GPa and to a bcc structure around 30 GPa have been observed at room temperature. The formation of the high-pressure phases is concerned with changes in the electronic structure. Recent investigations for the phase transformation from the hexagonal to the bcc structures at high temperatures (Zhang et al. 2005 and 2007) were inconsistent with previous study at temperatures around the room-T (Xia et al. 1991). Therefore, we reinvestigated the transformation pressure in zirconium metal.

The starting material used in this study was polycrystalline Zr. High-pressure X-ray diffraction experiments were carried out in an external heated diamond anvil cell. The small sample sandwiched between pellets of NaCl powder was loaded into a hole that had predrilled into a rhenium gasket. The heating temperature was up to 800 K, and was recorded using the R-type of thermocouples. The sample was probed using angle-dispersive X-ray diffraction, located on the synchrotron beam lines, at NE1A of the Photon Factory. Details of the synchrotron X-ray experiments have been described elsewhere (e.g., Ono et al. 2005). The angle-dispersive X-ray diffraction patterns were obtained on the imaging plate of an X-ray data collection system (Rigaku, RAXIS). The pressure was calculated from the NaCl unit cell volume using the equation of state (EOS) for NaCl, as developed by Ono (2010).

The boundary from the omega phase to the bcc phase was determined at high temperatures (300 - 800 K). Our results were in good agreement with those reported in previous room-temperature study. The gradient of  $dP/dT$  of the boundary was negative. However, the gradient observed in our experiments was 2-3 times more negative than that reported by previous high-temperature experiments (Zhang et al. 2005 and 2007). Our new data indicated that the difference in the stress conditions of the sample led to the discrepancy of the gradient of  $dP/dT$  slope in previous studies.

Keywords: Zirconium, Phase transition, High pressure and high temperature

## Crystal structure analysis of a new high-pressure strontium silicate

SEKINE, Keisuke<sup>1</sup> ; ISHII, Takayuki<sup>1</sup> ; KOJITANI, Hiroshi<sup>1\*</sup> ; AKAOGI, Masaki<sup>1</sup>

<sup>1</sup>Dept. of Chemistry, Gakushuin University

SrSiO<sub>3</sub> is an analog material to CaSiO<sub>3</sub> which is an important component of the Earth's crust- and mantle-constituting minerals. High-pressure phase relation experiments in SrSiO<sub>3</sub> showed that δ'-SrSiO<sub>3</sub> is stable up to about 10 GPa and decomposes into BaGe<sub>2</sub>O<sub>5</sub>-III -type SrSi<sub>2</sub>O<sub>5</sub> + larnite-type Sr<sub>2</sub>SiO<sub>4</sub> between 14 and 20 GPa (Kojitani et al., 2005). Then, hexagonal perovskite-type SrSiO<sub>3</sub> becomes stable above about 20 GPa (Yusa et al., 2005). However, phases except for larnite-type Sr<sub>2</sub>SiO<sub>4</sub> appearing in the pressure range between 10 and 14 GPa have been unclear. In this study, crystal structure and composition of one of the unknown phases were determined.

A sample for single-crystal structure analysis was synthesized by heating a mixture of pseudowollastonite-type CaSiO<sub>3</sub> and SiO<sub>2</sub> cristobalite (mole ratio of 1:1) with a little amount of water at 12 GPa and 1200 °C for 90 min using a Kawai-type multi-anvil high-pressure apparatus. A single-crystal sample with 120x80x60 μm was used for the single-crystal X-ray diffraction measurement. 953 reflection data were analyzed using the SHELX-97 software. Composition analysis of the high-pressure phase was performed using SEM-EDS.

The composition analysis showed that the new high-pressure phase had a composition of Sr<sub>4</sub>Si<sub>9</sub>O<sub>22</sub>. The single-crystal structure analysis suggests the monoclinic crystal system with the space group of *C2/m*. Lattice parameters were determined to be  $a = 13.3765(4) \text{ \AA}$ ,  $b = 5.2321(2) \text{ \AA}$ ,  $c = 11.6193(6) \text{ \AA}$ ,  $\beta = 113.976(4) \text{ deg}$ . *R* factor was 1.25%. The framework of the obtained crystal structure consists of two layers by corner-sharing single chains of edge-shared SiO<sub>6</sub> octahedra or SiO<sub>5</sub> rhombic pyramid polyhedra and by corner-shared SiO<sub>4</sub> tetrahedra and SiO<sub>6</sub> octahedra. It should be mentioned that this structure includes the SiO<sub>5</sub> rhombic pyramids which are very rare in silicates. Strontium ions in the structure are arranged between the two layers and are coordinated by seven oxygens. The structure of δ'-SrSiO<sub>3</sub> consists of four-membered rings of SiO<sub>4</sub> tetrahedra and strontium ions coordinated by seven oxygens. On the other hand, BaGe<sub>2</sub>O<sub>5</sub>-III type SrSi<sub>2</sub>O<sub>5</sub> has a framework by corner-shared SiO<sub>6</sub> octahedra and SiO<sub>4</sub> octahedra and coordination number of Si<sup>2+</sup> is 12. The crystal structure determined in this study is consistent with the fact that its density would be between those of the lower-pressure and higher-pressure phases.

Keywords: strontium silicate, high-pressure, single-crystal structure analysis, SiO<sub>5</sub> polyhedron

## Heat capacity and entropy measurements by PPMS for high-pressure phases in TiO<sub>2</sub> and MnSiO<sub>3</sub>

AKAOGI, Masaki<sup>1\*</sup> ; KOJIMA, Meiko<sup>1</sup> ; FUKAI, Aya<sup>1</sup> ; KOJITANI, Hiroshi<sup>1</sup>

<sup>1</sup>Dept. of Chemistry, Gakushuin University

Thermodynamic properties of high-pressure minerals are widely used to calculate phase relations at high pressures and high temperatures and to compare with the properties by the first-principles calculations. Standard entropy,  $S_{298.15}$ , is determined by integrating  $C_p/T$  in the temperature range between 0 and 298.15 K, where  $C_p$  is isobaric heat capacity and  $T$  is absolute temperature. To measure  $C_p$  at the temperature range, adiabatic calorimetry has been widely used with the highest precision. However,  $C_p$  of only a few high-pressure minerals have been measured so far, because a sample of more than several gram is required for the adiabatic calorimetry. Recently, low-temperature  $C_p$  measurement with thermal relaxation method using the Physical Properties Measurement System (PPMS) has been developed for samples of about ten milligram quantity. In this method, the sample is cooled with liquid helium and  $C_p$  is measured at about 2-310 K. By measuring the sample temperature change associated with applied heat pulse, thermal relaxation process is analyzed to obtain  $C_p$ . By this method, we measured  $C_p$  and determined  $S_{298.15}$  for Mg<sub>2</sub>SiO<sub>4</sub> wadsleyite and ringwoodite, MgSiO<sub>3</sub> akimotoite and perovskite, and SiO<sub>2</sub> stishovite, in collaboration with Atake-Kawaji laboratory, Tokyo Institute of Technology. Very recently, we have installed the PPMS apparatus in the laboratory in Gakushuin University, and have investigated  $C_p$  and  $S$  of rutile-type and  $\alpha$ -PbO<sub>2</sub>-type TiO<sub>2</sub> and garnet-type MnSiO<sub>3</sub>.

Using a multianvil apparatus, rutile- and  $\alpha$ -PbO<sub>2</sub>-type TiO<sub>2</sub> phases were synthesized at 3 and 8 GPa, respectively, at 600-700 °C, and MnSiO<sub>3</sub> garnet was made at 15 GPa and 1000 °C. All the cylindrical samples were polished and fixed with grease on the stage in the PPMS. The  $C_p$  measurements in this study were performed at 2-308 K using the polycrystalline samples of 10-21 mg. The  $C_p$  measured for  $\alpha$ -Al<sub>2</sub>O<sub>3</sub> (NBS SRM-720) by the PPMS apparatus were consistent within experimental errors with those measured by adiabatic calorimetry by Ditmars et al. (1982).

The measured  $C_p$  of rutile-type TiO<sub>2</sub> were in good agreement with those by previous studies, and the obtained  $S_{298.15}$  was 50.10 J/molK. Our  $C_p$  data of  $\alpha$ -PbO<sub>2</sub>-type TiO<sub>2</sub> were almost consistent with those with PPMS measurement by Yong et al. (2014), but substantially smaller than those with DSC measurement by Manon (2008). The  $S_{298.15}$  of  $\alpha$ -PbO<sub>2</sub>-type TiO<sub>2</sub> was determined as 46.50 J/molK in this study. The  $C_p$  data of MnSiO<sub>3</sub> garnet indicated an anomaly at 15 K probably due to magnetic transition, and  $S_{298.15}$  of 90.92 J/molK. High-pressure phase relations calculated using the above data are also reported.

Keywords: heat capacity, entropy, high-pressure phase, PPMS apparatus

## Mechanisms of phase transitions of methane hydrate under high pressure

KADOBAYASHI, Hirokazu<sup>1\*</sup>; HIRAI, Hisako<sup>1</sup>; HIRAO, Naohisa<sup>2</sup>; OHISHI, Yasuo<sup>2</sup>; OHTAKE, Michika<sup>3</sup>; YAMAMOTO, Yoshitaka<sup>3</sup>; KOJIMA, Yohei<sup>1</sup>

<sup>1</sup>Geodynamics Research Center, Ehime University, <sup>2</sup>Japan Association of Synchrotron Radiation Institute, <sup>3</sup>National Institute of Advanced Industrial Science and Technology

Methane hydrate (MH), called as “ burning ice ”, is expected to be a fruitful natural resource, at the same time, methane is rather effective greenhouse gas than carbon dioxide. It is also thought to be a major constituent of icy bodies in and outside the solar system. MH is composed of hydrogen-bonded host water molecules forming cages or frameworks that include guest methane molecules. Three phases of MH have been known so far. The low-pressure phase, sI, is stable below 0.8 GPa and it transforms into a hexagonal structure, sH, at 0.8 GPa and further transforms to a filled ice Ih (FIIhS) at 1.8 GPa at room temperature. At these phase transitions, release of water content is accompanied. As described above, the existence of phase transitions and the structures of transformed high-pressure phases have been clarified by the previous studies. However, transition mechanisms from the lower-pressure phase to individual high-pressure phases have been unresolved issue. In this study, high-pressure experiments were performed to investigate mechanisms of the phase transitions of MH at high pressures.

Clamp type and lever-spring type diamond anvil cells were used in this study. The pressure and temperature conditions were from 0.2 to 3.0 GPa and 300 K, respectively. Pressure measurements were made via a ruby fluorescence method. The initial samples of MH were prepared by ice-gas interface method. The samples were characterized via time-resolved X-ray diffractometry using synchrotron radiation at BL-10XU, SPring-8, and time-resolved Raman spectroscopy at GRC, Ehime University.

As for sI-sH phase transition, Raman spectroscopy revealed that  $5^{12}$  cages of sI survived during the transition and that the  $5^{12}$  cages remained as same  $5^{12}$  cages of sH structure. And,  $5^{12}6^2$  cages of sI changed to  $4^35^66^3$  and  $5^{12}6^8$  cages of sH. The results suggested that the sI-sH transition may follow a martensitic-like mechanism because of being maintaining  $5^{12}$  cages unchanged in sH structure. On the other hand, at sH-FIIhS transitions, Raman spectroscopy detected abrupt collapse of all constituent cages in sH and release of fluid or solid methane molecules. And then, the framework of FIIhS was gradually reconstructed, absorbing the released methane molecules into the FIIhS structure. The results indicated that the sH-FIIhS transition follows reconstructive mechanism. The explanations may be reasonable, because the former transition is from a cage to another cage structure, and the latter one is from a cage structure to different framework of a filled ice structure.

Keywords: methane hydrate, mechanisms of phase transitions, high-pressure, X-ray diffractometry, Raman spectroscopy

## Incorporation of NaCl into ice VI and ice VII under high pressure.

HIRAI, Hisako<sup>1\*</sup> ; YAMASHITA, Fukunori<sup>1</sup> ; KAGAWA, Shingo<sup>1</sup> ; KADOBAYASHI, Hirokazu<sup>1</sup> ; OHISHI, Yasuo<sup>2</sup> ; YAMAMOTO, Yoshitaka<sup>3</sup>

<sup>1</sup>Geodynamics Research Center, Ehime University, <sup>2</sup>JASRI, <sup>3</sup>AIST

Icy satellites have been thought to contain a large amount of salts besides water ices. Ice exhibits a wide variety of forms consisting of hydrogen-bonded water molecules. More than sixteen stable and metastable forms have been reported so far. Liquid water can dissolve various kinds of solutes. Whereas, in the previous idea, when water crystallizes, the dissolved solutes are excluded, which results in formation of pure water ices. Recently, Frank et al. [1] and Komatsu et al. [2] reported that NaCl or other salts was incorporated into ice VI and/or ice VII. In these studies, however, it has been still unclear which ice can incorporate NaCl, and amount of salts incorporated and states of the salt in the ice structure have not yet been clarified. In this study, in order to understand possible incorporation of salts in to ice VI and VII structures, high-pressure experiments were performed with a system of H<sub>2</sub>O-NaCl, a typical salt, at room temperature.

Lever-and-spring type diamond anvil cell was used. Pressure range examined was from 0.2 to 10 GPa. NaCl aqueous solutions with three concentrations, 1.5, 2.5, and 5.0 w%, were prepared as starting samples. Characterization was made by optical microscopy, X-ray diffractometry (XRD), and Raman spectroscopy.

Similar phase changes were observed for the samples with three different concentrations. The NaCl aqueous solutions finally crystallized to form ice VI above 1.6 GPa, although in case of pure water ice VI is formed at 1.0 GPa at room temperature. At the pressure range from 2.1 to 3.2 GPa, a new high-pressure phase, of which diffraction pattern was not explained by ice VI, ice VII, and solid NaCl, was observed. Above 3.2 GPa, ice VII and solid NaCl appeared. The high-pressure phase observed may correspond to a phase having a modified structure of NaCl-dihydrate reported by Nakayama et al. [3]. Unit cell volumes of ice VII calculated expanded larger than those of pure ice VII. The result was opposite sense to those by Frank et al, where the volumes decreased smaller than those of pure ice VII. The amounts of the volume expansion for 2.5 and 5.0 w% samples were larger than those of 1.5 w% samples. The volume expansions of the former two samples were almost similar. The results suggested that limitation of incorporation into ice VII is less than 2.5 w%. The O-H vibrational modes shifted to higher frequencies by 10 to 20 cm<sup>-1</sup> and 5 to 10 cm<sup>-1</sup> from those of pure ices for ice VI and ice VII, respectively.

All experimental results indicated that NaCl is incorporated both into ice VI and ice VII at room temperature. The amounts of incorporation were estimated to be up to 2.5 w%. Such large amount of incorporation of salt is expected to effect on physical properties of ices, which is important in inferring the interiors of icy bodies.

1. M. R. Frank et al., PEPI 155 (2006) 152; M. R. Frank et al., PEPI 170 (2008) 107; M. R. Frank et al., PEPI 215 (2013) 12.
2. K. Komatsu et al., Abstract of Annual meeting of Jpn. Society High Pressure Tech. (2010).
3. K. Nakayama master thesis (2012).

Keywords: high-pressure ice, NaCl, incorporation, icy satellite

## Structure refinement of legrandite and paradamite : crystal chemistry and hydrogen bonds

JINNOUCHI, Satoshi<sup>1\*</sup> ; YOSHIASA, Akira<sup>1</sup> ; SUGIYAMA, Kazumasa<sup>2</sup> ; ARIMA, Hiroshi<sup>2</sup> ; SHIMURA, Reiko<sup>2</sup> ; MIYAWAKI, Riturou<sup>3</sup>

<sup>1</sup>Graduate School of Science and Technology, Kumamoto University., <sup>2</sup>Institute for Materials Research, Tohoku University,

<sup>3</sup>National Science Museum

Legrandite,  $Zn_2AsO_4(OH)H_2O$  and paradamite,  $Zn_2AsO_4(OH)$ , are zinc arsenate minerals and have a color between pale yellow and yellowish brown. Related minerals of legrandite and paradamite are adamite,  $Zn_2AsO_4(OH)$ , and so on with different structures. We performed the structure refinement of legrandite and paradamite Oujela Mine, Mapimi, Durango, Mexico, by (RAPID) RIGAKU single-crystal structure analysis system. We determined the hydrogen position by difference Fourier method. We revealed the detail hydrogen bond using bond valence calculation and hydrogen positions and compared crystal structures of these. The structure of legrandite is constituted by two  $AsO_4$  tetrahedrons,  $ZnO_6$  octahedron and three  $ZnO_5$  trigonal dipyramids that have large unique distortion.  $AsO_4$  tetrahedron,  $ZnO_5$  trigonal dipyramid and  $ZnO_6$  octahedron constitutes the unique framework. The structure of paradamite is constituted by  $AsO_4$  tetrahedron and two  $ZnO_5$  trigonal dipyramid that have large unique distortion. In legrandite, 5 coordination of trigonal dipyramids have a distance to be expected from ionic radii but interatomic distance of Zn(3)-O(1) has extraordinary distance. Two OH groups bond to Zn1 and Zn2, Zn3 and Zn4 make the  $ZnO_3(H_2O)_2$  trigonal dipyramid that is bonded to two  $H_2O$  group in legrandite. In paradamite, Zn1 and Zn2 make  $ZnO_3(OH)_2$  and  $ZnO_4(OH)$  trigonal dipyramid. Hydrogen atoms make a lot of hydrogen bonding in legrandite and paradamite. Crystal structure of legrandite has a tunnel structure continuous that is only parallel to c axis and similar structure is observed in paradamite only parallel to a axis. There are path of proton-conduction in these direction and we conjecture that these proton-conductivity have large anisotropy of one dimension.

Keywords: structure refinement, legrandite, paradamite, crystal chemistry, hydrogen bonds

## Structure analysis of deuterated brucite at pressures to 3 GPa by pulsed neutron powder diffraction

OKUCHI, Takuo<sup>1\*</sup> ; TOMIOKA, Naotaka<sup>1</sup> ; PUREVJAV, Narangoo<sup>1</sup> ; HARJO, Stefanus<sup>2</sup> ; ABE, Jun<sup>3</sup> ; WU, Gong<sup>2</sup>

<sup>1</sup>Institute for Study of the Earth's Interior, Okayama University, <sup>2</sup>Japan Atomic Energy Agency, <sup>3</sup>CROSS Tokai

Atomic-scale structures around hydrogen atoms in hydrous minerals may significantly change with increasing pressure, which affect thermodynamic stability, optical properties (Raman, IR, etc.), and transport phenomena of the relevant minerals. To directly observe such structure change around hydrogen atoms, we have conducted neutron diffraction experiments of deuterated brucite at high pressures to 2.8 GPa, using a high-resolution neutron powder diffractometer recently installed at J-PARC Materials and Life Science Experimental Facility. To discriminate subtle structure change of deuterium site positions with increasing pressure, the quality of observed diffraction patterns has been considerably improved from the corresponding previous studies by adopting a new-type experimental apparatus and facility. A newly-designed opposed anvil cell apparatus optimized for the pulsed neutron beam (Okuchi et al., *High Pressure Research*, 33, 777, 2013) was effectively coupled with the time of flight diffractometer TAKUMI, which was designed to have the resolution of  $\Delta d / d \sim 0.3\%$  along with moderately-intense beam and low background (Harjo et al., *Materials Science Forum*, 524, 199). We used single crystal diamond anvils with culet diameter of 2 mm for sample compression along with deuterated glycerine pressure medium. The combination gives very high neutron transparency as well as high resolution to enable accurate structure refinements of tiny sample volume of the order of less than 1 mm<sup>3</sup>. Through Rietveld refinements of the observed patterns, tilting of all OD dipoles in the compressed brucite toward one the three nearest-neighbor oxygen anions in the brucite structure was confirmed to be substantial at the observed pressure regime, suggesting the formation of pressure-induced hydrogen bonding. Therefore, at lower crust and mantle wedge conditions, this pressure-induced bonding may play an important role to constrain hydrogen into the relevant hydrous minerals.

Keywords: hydrogen, brucite, high pressure, neutron diffraction

## Factors controlling barite-water distribution of selenium oxyanion

TOKUNAGA, Kouhei<sup>1\*</sup>; YOKOYAMA, Yuka<sup>1</sup>; TAKAHASHI, Yoshio<sup>1</sup>

<sup>1</sup>Department of Earth and Planetary Systems Science, Graduated School of Science, Hiroshima University

Geochemical behavior of trace elements is controlled by their interaction with major minerals through ion exchange, sorption/desorption, and coprecipitation/dissolution processes, which govern the concentrations of trace elements in natural water. Especially, the coprecipitation process with mineral is potentially important because trace elements can be incorporated and immobilized in the crystal lattice at least until the minerals are dissolved. Previous studies showed that the partitioning behaviors of trace elements to minerals were controlled by many complex factors, such as crystal constraints of ion substitution, effects of complexation in the aqueous phase, rate of crystallization, and changes in temperature or pressure. For instance, Yokoyama [2011, 2012] demonstrated that, in the case of arsenic (As) and selenium (Se) incorporation into calcite, arsenate rather than arsenite is selectively incorporated into calcite, whereas selenite (Se(IV)) rather than selenate (Se(VI)) into calcite because of the high stabilities of calcium arsenate and calcium selenate complexes compared with those for arsenite and selenite. In this study, we focused on the distribution behavior of Se into barite to determine the factors controlling the partitioning behaviors of the trace elements to minerals at the molecular scale by X-ray absorption fine structure (XAFS). Our previous results suggested that the distribution behavior of Se into barite was controlled by two factors: the stability of the surface complex between barite and Se species (=chemical affinity) at the initial process and the stability of the ion substitution in the crystal structure (=structural affinity) for the subsequent process. In this presentation, the barite-water distributions of Se controlled by the structural affinity are highlighted.

The coprecipitation experiments were conducted to examine the influence of ion substitution structure on the distribution behavior of Se into barite as a function of the reaction time in term of the variation of barite morphology, total concentration, oxidation states, and coordination structure of Se in barite. The results showed that both total Se concentration and the Se(VI)/Se(IV) ratio in barite increased abruptly within first 24 hour and almost reached equilibrium after 24 hours. EXAFS analysis for the initial and aged samples showed that the coordination number of Se-Ba in the aged sample is larger than that in the initial stage. The results indicates that a larger amount of Se(VI) than Se(IV) was incorporated from adsorption site on the surface into the barite crystal by substituting sulfate site because of their high crystallinity that can excludes Se(IV) to a larger degree than Se(VI) due to the similar structure of sulfate ion and sulfate. Based on these results, it is considered that the Se(VI) was preferentially incorporated into barite due to its high structural affinity than Se(IV), thus, the Se(VI)/Se(IV) ratios in barite relatively increased through crystallization. These results suggest that structural affinity is an important factor for controlling the distribution behavior of Se between barite and water.

Keywords: barite, selenite, selenate, XAFS, distribution behavior, structural affinity

## Mid- and far-infrared spectroscopy for Li-Al-Mg micas

MAKIO, Masato<sup>1\*</sup> ; ISHIDA, Kiyotaka<sup>1</sup>

<sup>1</sup>Graduate School of Social and Cultural Studies

Mica is a one of the major rock forming minerals and widely spread in the earth crust. The hydrothermal synthetic Li-Al-Mg trioctahedral mica series were measured by mid- and far-infrared spectroscopy and X-ray powder diffraction Rietveld refinement: (a)Trilithionite:  $K(Li_{1.5}Al_{1.5})(AlSi_3)O_{10}F_2$ - Phlogopite:  $KMg_3(AlSi_3)O_{10}F_2$ , (b)Polyolithionite:  $K(Li_2Al)Si_4O_{10}F_2$ - Tainiolite:  $K(LiMg_2)Si_4O_{10}F_2$ , (c)Polyolithionite- Eastonite:  $K(Mg_2Al)(Al_2Si_2)O_{10}F_2$  and OD- FMg- Masutomilite:  $K(LiAlMg)AlSi_3O_{10}(F, OD)_2$ .

The Li-Al-Mg micas synthesized hydrothermally at 600- 650 °C and 150- 200MPa in cold-seal externally heated Tuttle-type vessels. The starting materials were mixed and then sealed in Pt/Au capsules with 20 wt % D<sub>2</sub>O (99.9 % in purity). X-ray Rietveld analysis was done using Rietan- 2000 (Izumi and Ikeda 2000). Mid- and far-infrared spectra were measured with JASCO FTIR- 620 spectrometer. Each sample was scanned 256 times in an evacuated sample-chamber.

All samples could refine monoclinic, C2/m (1M polytype). In the 250- 50cm<sup>-1</sup> far-infrared region, three kinds of bands are observed: these bands due to an in- plane tetrahedral torsional band between 170- 150cm<sup>-1</sup>, an interlayer K- O<sub>inner</sub> stretching band between 120- 140 cm<sup>-1</sup> and K- O<sub>outer</sub> stretching band between 90- 100 cm<sup>-1</sup>. With increasing <K- O<sub>inner</sub>>, K- O<sub>inner</sub> stretching band shifts higher frequency, while with increasing <K- O<sub>outer</sub>>, K- O<sub>outer</sub> stretching band shifts lower frequency. In the 650- 250cm<sup>-1</sup> mid- and far-infrared region, two parts of bands are observed. With increasing <sup>[4]</sup>Si→Al, (Si,Al)- O deformational band in the range of 600- 400cm<sup>-1</sup> became broad and merged.

Keywords: Li-Al-Mg mica, hydrothermal synthesis, mid-infrared, far-infrared, Rietveld analysis

## Cesium (Cs) Sorption Experiments into Weathered Biotite in Fukushima

KIKUCHI, Ryosuke<sup>1\*</sup> ; KOGURE, Toshihiro<sup>1</sup>

<sup>1</sup>Earth and Planetary Sci., Univ. Tokyo

After the accident of Fukushima Daiichi nuclear power plant in March 2011, radioactive contamination of the soil around the plant has become an urgent problem in Japan. Previous studies proposed that weathered micaceous minerals present favorable sorption environments for Cs<sup>+</sup>. Because the contaminated areas in Fukushima are mainly covered with weathered granite soil, weathered biotite with hydrated (vermiculite) interlayers is abundant. Hence basic understanding of Cs<sup>+</sup> sorption process into the biotite is important to find the recipe for decontamination of radiation. Some of previous studies reported that Cs<sup>+</sup> is adsorbed mainly at the frayed-edge sites of such micaceous crystals. However, other studies indicated that Cs<sup>+</sup> penetrates deeply inside the crystals, along the interlayer regions by ion-exchange. In this study, we performed Cs<sup>+</sup> sorption experiments using single-crystals of Fukushima weathered biotite with well-regulated edge surfaces, and considered the relationship between the weathering state of biotite and Cs<sup>+</sup> sorption property.

Fresh and two kinds of weathered biotite were collected from granodiolite of Abukuma granite body in Fukushima prefecture. For each sample, cross sections of <1 mm thick perpendicular to the basal planes were prepared. Surface damage formed by the mechanical grinding/polishing was removed by Ar<sup>+</sup> ion sputtering. These sections were immersed in 30 mL of CsCl aqueous solution of 2000 / 200 / 20 / 0 ppm for 24 hours at room temperature to incorporate Cs<sup>+</sup>.

After the reaction, the surfaces of the sections were investigated using scanning electron microscopy (SEM) with energy dispersive X-ray spectroscopy (EDS). SEM-EDS with various acceleration voltage indicated that the concentration of the sorbed Cs<sup>+</sup> does not change in the depth direction of ~several microns range. Cs<sup>+</sup> was apparently sorbed at 2000 ppm but not at 200 ppm for fresh biotite, whereas Cs<sup>+</sup> was sorbed at both concentrations in the weathered biotite. Back-scattered electron (BSE) images and EDS analysis showed preferred sorption of Cs<sup>+</sup> at the regions probably with dense vermiculite interlayers in the weathered biotite. Moreover, some specimens were processed into thin foils using focused ion beam (FIB) and examined using scanning transmission electron microscopy (STEM). High-angle annular dark field (HAADF) imaging in STEM has visualized Cs<sup>+</sup>-incorporated interlayer regions individually in the weathered biotite.

Keywords: Biotite, Vermiculite, Cesium, SEM-EDS, FIB, HAADF-STEM

## Pressure-induced phase transitions of vaterite, a metastable phase of calcium carbonate

MARUYAMA, Koji<sup>1\*</sup>; KOMATSU, Kazuki<sup>1</sup>; KAGI, Hiroyuki<sup>1</sup>; YOSHINO, Toru<sup>2</sup>; NAKANO, Satoshi<sup>3</sup>

<sup>1</sup>Geochemical Research Center, Univ. Tokyo, <sup>2</sup>TIRI, <sup>3</sup>National Institute for Materials Science

### 1. Introduction

Calcium carbonate is one of the most common and ubiquitous minerals on the Earth's surface and plays an important role in global carbon cycle. There are many studies about high-pressure behavior of calcite and aragonite. At ambient temperature, calcite transforms to calcite II at about 1.5 GPa and to calcite III at about 2.0 GPa. The transition from aragonite to post-aragonite phase was observed at about 40 GPa. In contrast, no study has been reported on the high-pressure behavior of vaterite, which is a metastable phase of CaCO<sub>3</sub>, and is known as a precursor material of more stable CaCO<sub>3</sub> polymorphs, calcite and aragonite. In this study, the high-pressure behavior of vaterite was investigated by in situ synchrotron X-ray diffraction (XRD) experiments using a diamond anvil cell.

### 2. Experimental method

In this study, vaterite was synthesized by mixing two aqueous solutions, 60 mM CaCl<sub>2</sub> aq. and 60 mM NaHCO<sub>3</sub> aq., kept at 30 degree C. The mixed solution was sealed in a plastic bottle and stirred for 10 min at 30 degree C, and then filtered using an aspirator, washed by pure water, and dried at about 130oC. The obtained white powder was identified as pure vaterite using powder XRD method.

High-pressure experiments were carried out using a diamond anvil cell (DAC). The synthesized vaterite and several tiny ruby crystals were loaded into a gasket hole together with helium as a pressure transmitting medium. The pressure was changed between 0-14 GPa, which was measured by the ruby fluorescence method. XRD patterns were measured at each pressure at room temperature. X-ray diffraction observations were carried out at room temperature using the synchrotron beam line of BL18C in the Photon Factory, Japan.

### 3. Results and discussion

XRD patterns recorded at pressures lower than 4.7 GPa indicated that the sample consists of vaterite only. At 4.7 GPa, main three peaks of vaterite were split and a peak assignable to calcite III appeared. The discontinuous changes in axial lengths were observed by refinement of lattice constants using a crystal structure model proposed by Le Bail et al. (2011). This change suggests a pressure-induced phase transition from vaterite to a high-pressure form (hereafter vaterite II). Change in the diffraction intensities suggested that vaterite II transformed to calcite III with increasing pressure up to about 9 GPa. At 12.9 GPa, new diffraction spots were observed. These spots were not explainable with the diffraction peaks from any polymorphs of CaCO<sub>3</sub>. This implies that the new spots are derived from another high-pressure phase of vaterite (vaterite III). After decompression, the recovered sample was identified as a mixture of calcite and vaterite. These results indicate that the transition from vaterite II to calcite III is irreversible. In this study, new high-pressure phases of CaCO<sub>3</sub> (vaterite II and III) were discovered by high-pressure experiments of vaterite at ambient temperature.

Keywords: vaterite, phase transition, high-pressure

## Huge plastic deformation of SiO<sub>2</sub> glass at room temperature

WAKABAYASHI, Daisuke<sup>1\*</sup> ; FUNAMORI, Nobumasa<sup>1</sup> ; SATO, Tomoko<sup>2</sup>

<sup>1</sup>Department of Earth and Planetary Science, University of Tokyo, <sup>2</sup>Department of Earth and Planetary Systems Science, Hiroshima University

Covalent solids are known to be hard but brittle. Moreover, glasses do not deform plastically by dislocation movement seen in crystals due to the lack of long-range order. However, SiO<sub>2</sub> glass, a highly covalent glass, has long been known to be densified up to about 20% by applying high pressure. This phenomenon is called permanent densification, which is some kind of phase transformation caused by the reconstruction of the network structure consisting of SiO<sub>4</sub> tetrahedra [e.g., Wakabayashi et al., 2011], and could be considered as plastic deformation in a broad sense. Recently, the differential strain of SiO<sub>2</sub> glass in its intermediate-range structure, corresponding to the first sharp diffraction peak, was measured under uniaxial compression by a radial X-ray diffraction method, in which X-rays irradiate the sample from a direction perpendicular to the compression axis (i.e., from a radial direction) [Sato et al., 2013]. In those measurements, very large differential strains were observed under pressure and surprisingly also after decompression. This residual strain may be attributable to the anisotropic reconstruction of the network structure (i.e., anisotropic permanent densification).

In this study, the change in size of bulk samples was measured for uniaxially-compressed SiO<sub>2</sub> glass to clarify whether SiO<sub>2</sub> glass undergoes plastic deformation in a narrow sense, i.e., without density change. X-ray diffraction measurements were also conducted in a wide Q-range with 50 keV monochromatic X-rays by irradiating the recovered sample from the radial direction to clarify whether a differential strain remains only in the intermediate-range network structure or also in the short-range SiO<sub>4</sub> tetrahedral structure. Pressures were generated by using a diamond-anvil cell. The starting material was in the form of a disk, and was adjusted to have an appropriate initial thickness to be compressed under uniaxial conditions, i.e., pinched directly by the two anvils, above a certain pressure. Three independent experiments were conducted with an argon pressure medium up to 20 GPa in run 1, 12 GPa in run 2, and 6 GPa in run 3. The change in size of sample was measured with an optical microscope. X-ray diffraction measurements were carried out at PF AR-NE1. All the experiments were conducted at room temperature.

In runs 1 and 2, the diameter of sample was found to increase significantly with pressure from 6-8 GPa, where uniaxial conditions were achieved, to the maximum pressure of each run without fracturing, and it became about 15% larger at 20 GPa than at 0 GPa. The macroscopic differential strain was about an order of magnitude larger than the microscopic differential strain reported in the previous study [Sato et al., 2013], suggesting that SiO<sub>2</sub> glass deformed plastically at room temperature. The X-ray diffraction measurements clarified that the recovered samples were in the fully densified state (about 20% densified). It was also revealed that a residual differential strain was observed only in the intermediate-range network structure and its magnitude was consistent with the previous study [Sato et al., 2013]. On the other hand, in run 3, the sample did not deform plastically by uniaxial compression from 2-3 GPa to 6 GPa. The X-ray diffraction pattern of the recovered sample was the same as that of the ordinary SiO<sub>2</sub> glass. Permanent densification is known to begin at about 9 GPa under hydrostatic conditions [e.g., Wakabayashi et al., 2011], and it is suggested that permanently densified SiO<sub>2</sub> glass easily undergoes plastic deformation even at room temperature.

D. Wakabayashi et al., *Phys. Rev. B* **84**, 144103 (2011).

T. Sato et al., *J. Appl. Phys.* **114**, 103509 (2013).

Keywords: SiO<sub>2</sub> glass, plastic deformation, permanent densification, network structure

## Shock compression of synthetic amino acid - silica gel complex modeling for comet nucleus

MURAI, Takuro<sup>1</sup> ; OKUNO, Masayuki<sup>2\*</sup> ; OKUDERA, Hiroki<sup>2</sup> ; ARASUNA, Akane<sup>1</sup> ; MASHIMO, Tsutomu<sup>3</sup> ; CHEN, Liliang<sup>3</sup> ; MIZUKAMI, Tomoyuki<sup>2</sup> ; ARAI, Shoji<sup>2</sup>

<sup>1</sup>Graduate School of Kanazawa University, <sup>2</sup>Kanazawa University, <sup>3</sup>Kumamoto University

Some amino acids were found in comet coma particle and Murchison meteorite [1,2]. These reports may suggest a possibility that basic materials of primitive life on the earth were formed in the space and delivered to the earth.

Greenberg et al. (1997)[3] reported the almost comets are made of organic compounds, silicates and ice. On the other hand, silica gel contains a non crystalline  $\text{SiO}_{4-n}(\text{OH})_n$  framework with water molecules. So, silica gel is a suitable model material for comet. In this study, in order to investigate the stability of amino acid (L-serine) in the comet nucleus during the impact to the earth, synthetic amino L-serine - silica gel complex materials were shock compressed and the structure change of the recovered samples were analyzed by X-ray diffraction measurements, IR and Raman spectroscopies. Shock compression experiments were performed at 8.2, 10.9, 19.7 and 26.9 GPa.

By Raman spectroscopic analyses, it was indicated that synthetic complex materials include two types of L-serine such as crystalline L-serine and hydrated L-serine. Obtained Raman spectra of shocked materials show the L-serine crystal was disappeared and hydrated L-serine molecules survived at 19.7 GPa of shock pressure. Therefore, the sample at 19.7 GPa includes only hydrated L-serine molecules. This may indicate that intermolecular hydrogen bonds of L-serine molecules may be broken by shock compression with water molecule.

The shock pressure of 19.7 GPa is consistent with the estimated impact pressure of about 19% comets to the earth reported by Blank et al. (1999) [4]. This fact may indicate that a possibility for the basic materials of primitive life on the earth were formed in the space and delivered to the earth.

### References

- [1] Elisila J.E., Glavin D.P., Dworkin J.P. (2009) Cometary glycine in samples returned by stardust. *Meteoritics & Planetary Science* 44, 1323-1330
- [2] Cronin J.R. and Pizzarello S. (1983) Amino acid in meteorites. *Advances in space research* 3, 5-18
- [3] Greenberg J.M., Aigen Li (1997) Silicate core-organic refractory mantle articles as interstellar dust and as aggregates in comets and stellar disks. *Advance in space research* 19, 981-990
- [4] Blank J.G., Millar G.H., Michael J.A., Winas R.E. (1999) Experimental shock chemistry of aqueous amino acid solution and cometary delivery of periodic compounds. *Origin of Life and Evolution of the Biosphere* 31, 15-51

Keywords: comet, amino acid, silica gel, shock compression

## Microtexture and formation mechanism of impact diamonds from the Popigai crater, Russia

OHFUJI, Hiroaki<sup>1\*</sup> ; YAMASHITA, Tomoharu<sup>1</sup> ; LITASOV, Konstantin<sup>2</sup> ; AFANASIEV, Valentin<sup>2</sup> ; POKHILENKO, Nikolai<sup>2</sup>

<sup>1</sup>Geodynamics Research Center, Ehime University, <sup>2</sup>Siberian Branch of the Russian Academy of Sciences

Large meteoritic impact occasionally produces an extensive amount of diamond on the surface of the Earth [1, 2]. Popigai crater located in the north central Siberia is a typical example of such diamond-forming shock events and has recently been brought back into the spotlight due to its vast estimated reserves of the impact diamonds [2-4]. Authigenic impact diamonds occur in shocked graphite-bearing garnet-biotite gneisses that are found as inclusions in impact melt rocks, so-called tagamites and suevites. Popigai diamonds occur as irregular to tabular grains of 0.5-2 mm size (up to 10 mm) and usually show yellow, gray or black colors [3]. Electron microscopic (SEM and TEM) observations in previous studies described that they are polycrystalline aggregates of 0.1-1  $\mu\text{m}$  grains and show a distinct preferred orientation along the [111], which is in a coaxial relation to the [001] of the original graphite source [2-4]. This crystallographic feature as well as the occasional coexistence of lonsdaleite, a metastable carbon polymorph, suggest the Martensitic phase transformation for the potential formation process of the impact diamonds from Popigai crater. However, the textural feature of the impact diamonds and its variation has not fully been examined. Here, we present the result of detailed microtextural observations of impact diamonds from the Popigai crater by transmission electron microscopy (TEM) and discuss the formation mechanism and condition in comparison with those of synthetic diamonds obtained by high pressure and high temperature experiments.

In total 10 diamond grains (7 transparent yellowish and 3 black samples) from the Popigai crater were studied. Each sample was first analyzed by a micro-focus XRD equipped with a Mo target and an IP detector. The results showed that transparent samples consist mostly of diamond and occasionally contain lonsdaleite, while black ones are a mixture of graphite, lonsdaleite and diamond, which are all in a coaxial relation as shown by 2D diffraction patterns collected in transmission geometry. Each sample was then transferred to a focused ion beam (FIB) system to cut out TEM foil sections perpendicular to the surface (of the tabular grains). TEM observation revealed that although all the samples commonly possess layered structures and preferred orientation (mostly along [111] of diamond), there are varieties in crystallite (grain) size (down to 10-20 nm) and degree of preferred orientation. Taking into account the similarity in texture and preferred orientation feature between the Popigai diamonds and synthetic diamond, the variation is likely derived from the small difference in crystallinity of the starting graphite sources and perhaps more significantly from the difference in shock temperature.

According to the shock features recorded in the silicate minerals of the diamond-bearing impactites, the threshold pressure for the onset of the graphite-diamond transformation is estimated to be 34-36 GPa [3]. However, our recent experimental synthesis [5] demonstrated that a similar phase assembly (mostly diamond + traces of lonsdaleite) and microtexture can be produced at much lower pressures of 15-25 GPa at  $>2000$  °C. The shock pressure as well as shock- and post-shock temperature accompanied with the formation of the Popigai crater might be needed to be reevaluated carefully to understand the real nature of the giant impact.

- [1] Masaitis V.L. (1998) *Meteoritics & Planetary Science*. 33. 349-359.
- [2] Langenhorst F., Shafranovsky G.I., et al. (1999) *Geology*. 27. 747-750.
- [3] Deutsch A., Masaitis V.L., et al. (2000) *Episodes*. 23. 3-11.
- [4] Koeberl C., Masaitis V.L., et al. (1997) *Geology*. 25. 967-970.
- [5] Isobe F., Ohfuchi H., et al. (2013) *Journal of Nanomaterials*. 2013. 380165.

## Melting and crystal growth textures developed in rapid heating and cooling of olivine fine particles

ISOBE, Hiroshi<sup>1\*</sup> ; GONDO, Takaaki<sup>1</sup>

<sup>1</sup>Grad. Sch. Sci. Tech., Kumamoto Univ.

Olivine is one of the most common mineral in the solid Earth and chondritic meteorites. Olivine crystals show characteristic textures in chondrules depending on heating and cooling histories in chondrule formation processes at the early solar system. In this study, quick heating and cooling experiments of mixed olivine particles were carried out with a fine particles free falling apparatus (Isobe and Gondo, 2013). In the run products, characteristic melting and crystal growth textures controlled by phase relations, diffusion, and nucleation and growth behavior of olivine can be seen.

Starting material is mixed powder of natural olivine (Fo90), fayalite and an artificial olivine (Fo55). The typical diameter of the starting material particles is approximately 100 micron meters. Each particle is single crystal of olivine or mixture of two or three kinds of raw materials. Heating and cooling experiments are carried out in a high temperature furnace with mass flow controllers to regulate oxygen fugacity and total gas flow rate. Particles can be heated to 1400 degrees C within two seconds, are kept over 1400 degrees C approximately one second and quenched within a second. Maximum temperature has negative correlation to diameter of the particles, and cooling rate has positive correlation to the diameter depending on the falling velocity of the particles. Run products show spherical shape when the particles mostly melted, and are crystal fragments when the particles did not melt. The outside shape of the retrieved run products are observed with a scanning electron microscope. Inner textures of the particles are observed on polished section of the particles. Chemical compositions are also analyzed on the sections.

Fayalite grains are completely melted and Fo90 olivine grains are not melted by themselves concordantly with the phase relation of olivine. Internal textures of Fo55 olivine crystals show quick partial melting when the temperature reach solidus temperature. In the mixed olivine particles, relict crystals of Fo90 and Fo55 olivines dissolve to iron-rich melt derived from melting of fayalite. The dissolution of relict crystals produce steep chemical gradient at interface between crystals and melt.

Run products like barred olivine chondrules or melted cosmic spherules are produced from completely melted particles. In the particles including relict crystals, overgrowth textures from the relict crystals can be seen. Dendritic olivine crystals with regulated crystallographic orientation are developed in melted particles. Surface texture of melted particles may be affected by the dendritic olivine crystals. Oriented magnetite dendrites may also occur between olivine crystals when oxygen fugacity was in the magnetite stability field. Melting, nucleation and crystal growth processes in a few seconds can be discussed from the textures in the run products.

Keywords: Olivine, chondrule, nucleation, crystal growth, dendrites, quench texture

## Temperature-dependent thermal expansivities of aluminum-free silicate melts and borosilicate melts

SUGAWARA, Toru<sup>1\*</sup>; KATSUKI, Junki<sup>2</sup>; YOSHIDA, Satoshi<sup>2</sup>; MATSUOKA, Jun<sup>2</sup>; MINAMI, Kazuhiro<sup>3</sup>; OCHI, Eiji<sup>3</sup>

<sup>1</sup>Akita University, <sup>2</sup>The University of Shiga Prefecture, <sup>3</sup>Japan Nuclear Fuel Limited

Thermal expansivities ( $dV/dT$ ) of silicate melts are essential in a thermodynamic calculation of phase equilibria in magmatic system as a function of pressure and temperature and in a numerical simulation of flow and thermal structures in glass melting furnace. Previous studies have been suggested that the  $dV/dT$  of aluminosilicate melts (Lange, 1996; Potuzak et al., 2006) and magmatic silicate melts (Lange, 1997; Ghiorso and Kress, 2004) is a function of composition, but independent of temperature. On the other hand, it has been reported that the  $dV/dT$  of  $SiO_2$ - $TiO_2$ - $Na_2O$  melt (Liu and Lange, 2001) and  $50SiO_2$ - $25CaO$ - $25MgO$  melt (Gottsmann and Dingwell, 2000) decrease with increasing temperature. Recently, we found that simulated-radioactive waste glass melt which has sodium-borosilicate composition also shows negative temperature-dependent  $dV/dT$  (Sugawara et al., 2013). We carried out density measurements for sodium-silicate melts ( $(100-x)SiO_2$ - $xNa_2O$ ,  $x=23$  or  $32.3$  mol%), commercial soda-lime silicate melt ( $71SiO_2$ - $6MgO$ - $9CaO$ - $14Na_2O$ , mol%) and borosilicate melts ( $66.6SiO_2$ - $yB_2O_3$ - $(33.33-y)Na_2O$  where  $y=8.3, 16.6, 25$ ;  $66.6SiO_2$ - $(12.5+z)B_2O_3$ - $(4.2-z)Al_2O_3$ - $zCaO$ - $(16.7-z)Na_2O$  where  $z=0$  or  $4.2$  mol%). The temperature and compositional dependences of the  $dV/dT$  are discussed based on the new density data and the literature data.

The high-temperature density (dHT) measurement has been made by double-bob Archimedean method between 1173K and 1665K. The glass samples were annealed around glass transition temperature ( $T_g$ ) for 6-396 hours and quenched. Then the density of annealed glasses at 298K (d298) and linear thermal expansivity (dL/L) were determined by Archimedean method and TMA, respectively. The densities of supercooled melt around  $T_g$  (dTg) were calculated from the d298 and the dL/L of glasses. Then, molar volume as a function of temperature and the  $dV/dT$  of melts were obtained by combining the dTg and the dHT.

The  $dV/dT$  values of all samples examined in this study show negative temperature dependence. In the sodium silicate melts, the temperature dependence of the  $dV/dT$  is remarkable when the  $SiO_2$  content increases from 50 to 67 mol%, while the  $dV/dT$  becomes close to zero as further increase in the  $SiO_2$  content. The negative temperature-dependent  $dV/dT$  observed in the  $71SiO_2$ - $6MgO$ - $9CaO$ - $14Na_2O$  melt can be reproduced by an additive sum of the  $dV/dT$  of  $67.8SiO_2$ - $32.2Na_2O$ , diopside (Gottsmann and Dingwell, 2000) and wollastonite (Potuzak et al., 2006) melts. High-temperature Raman spectroscopy for the  $SiO_2$ - $Na_2O$  and  $SiO_2$ - $Na_2O$ - $MgO$  melts has been indicated that amount of Q4 species increases with increasing temperature and  $SiO_2$  and  $MgO$  contents (Maehara et al., 2004, 2005). Therefore, the temperature dependent  $dV/dT$  for the sodium-silicate, commercial soda-lime silicate and diopside melts can be rationalized by an increase of rigid Q4 species at high temperature. The temperature dependence of the  $dV/dT$  is most remarkable in the  $66.6SiO_2$ - $8.3B_2O_3$ - $25Na_2O$  melt among the borosilicate melts. The  $dV/dT$  decreases with replacement of  $Na_2O$  by  $B_2O_3$  or  $CaO$  and of  $B_2O_3$  by  $Al_2O_3$ , suggesting that partial molar  $dV/dT$  of  $B_2O_3$  depends on temperature-induced coordination change of boron and their composition dependence (Wu and Stebbins, 2010).

Acknowledgements: This work was a part of the research supported by Japan Nuclear Fuel Limited with Grant-in-Aid by the Ministry of Economy, Trade and Industry.

Keywords: silicate melt, thermal expansivity, densitometry

## Thermodynamic properties of Mg-postperovskite with Fe<sup>3+</sup> and Al<sup>3+</sup> dopant: an internally consistent LSDA+U study

WANG, Xianlong<sup>1\*</sup> ; TSUCHIYA, Taku<sup>1</sup>

<sup>1</sup>GRC, Ehime University and ELSI, Tokyo Institute of Technology

Thermodynamic properties of MgSiO<sub>3</sub> perovskite (Pv) and postperovskite (PPv) with Fe and Al incorporation at high pressure and high temperature are important to understand the Earth's lower mantle (LM). The thermodynamic properties of Fe<sup>2+</sup>, Fe<sup>3+</sup>, and Al<sup>3+</sup>-bearing Pv[1,2,3] and Fe<sup>2+</sup>-bearing PPv[4] have been investigated in our previous works uniformly based on first-principles method combined with the internally consistent LSDA+U method and quasi-harmonic approximation (QHA). However, to date, effects of trivalent ions, Fe<sup>3+</sup> and Al<sup>3+</sup>, on the thermodynamic properties of PPv are still unclear. In this work, by using the same methods with previous works, the structural, electronic, magnetic, and thermodynamic properties of (Mg,Fe<sup>3+</sup>)(Si,Fe<sup>3+</sup>)O<sub>3</sub> and (Mg,Fe<sup>3+</sup>)(Si,Al<sup>3+</sup>)O<sub>3</sub> PPv at several pressures, from 0 GPa to 180 GPa, are investigated. Our results show that for (Mg,Fe<sup>3+</sup>)(Si,Fe<sup>3+</sup>)O<sub>3</sub> PPv, Fe<sup>3+</sup> ions substituted at Mg and Si site respectively have the high and low spin state within the deep LM pressure range, while Fe<sup>3+</sup> in (Mg,Fe<sup>3+</sup>)(Si,Al<sup>3+</sup>)O<sub>3</sub> PPv remains in the high spin state. Furthermore, separated phase between Fe<sub>2</sub>O<sub>3</sub> and Al<sub>2</sub>O<sub>3</sub> in PPv is found unfavorable.

### References:

- [1] Metsue, A. and Tsuchiya, T. (2012) *Geophys. J. Int.* **190**, 310.
- [2] Tsuchiya, T. and Wang, X. (2013) *J. Geophys.* **118**, 83.
- [3] Wang, X. and Tsuchiya, T. To be submitted.
- [4] Metsue, A. and Tsuchiya, T. (2011) *J. Geophys. Res.* **116**, B08207.

Keywords: First-principles method, Internally consistent LSDA+U, Thermodynamic properties, Postperovskite

## Thermal expansion of $\text{Ca}(\text{OD})_2$ at high pressure

NAGAI, Takaya<sup>1\*</sup> ; SANO, Asami<sup>2</sup> ; IIZUKA, Riko<sup>3</sup> ; KAGI, Hiroyuki<sup>3</sup> ; HATTORI, Takanori<sup>4</sup>

<sup>1</sup>Faculty of Science, Hokkaido University, <sup>2</sup>Japan Atomic Energy Agency, <sup>3</sup>Graduate School of Science, The University of Tokyo, <sup>4</sup>Materials and Life Science Division, J-PARC Center

$\text{Ca}(\text{OH})_2$  is one of the important hydrous minerals to understand structural behavior at high pressure and high temperature, because this type of structure is a building unit in more complex hydrous phases such as chondrodite. It is surprising that only a few previous researches can be found on crystallography of  $\text{Ca}(\text{OH})_2$  in the conditions of simultaneously high pressure and high temperature. We gave an oral presentation about some preliminary results in this conference last year. We have continued to analyze the data carefully and will add some new information.

Deuterated samples were prepared via hydrothermal treatment with CaO fine powders and excess  $\text{D}_2\text{O}$  water in a Teflon lined stainless steel autoclave at 493 K for 4 days. After the hydrothermal treatment was completed, precipitates were filtered out, washed with  $\text{D}_2\text{O}$  water, and then dried at 383 K under vacuum for 3 hours. The products were confirmed to have the CdI<sub>2</sub>-type structure by conventional powder X-ray diffraction measurements and were checked to be deuterated by IR absorption spectra. Synchrotron X-ray diffraction experiments were performed at the beamline AR-NE5C, KEK, Japan in order to obtain cell parameters of  $\text{Ca}(\text{OD})_2$  at various P-T conditions from 2-4 GPa and 300-800 K. TOF neutron powder diffraction measurements of  $\text{Ca}(\text{OD})_2$  were carried out from 300 to 773 K at high pressure at the PLANET beamline in J-PARC, Japan. Pressure was estimated by comparing unit cell parameters with those obtained by synchrotron experiments.

All our TOF data obtained include only  $\text{Ca}(\text{OD})_2$  peaks and no peaks from sample surrounding materials such as  $\text{ZrO}_2$  pressure medium, graphite furnace and WC anvils could be detected owing to radial collimators equipped with the 6-ram pressure apparatus (Atsuhime). The detailed structure parameters such as lattice parameters and atomic coordinates could be reasonably refined by the Rietveld method by using a program GSAS. It is an interesting result that thermal expansion along the *c*-axis seems to be suppressed at high pressure comparing to that at ambient pressure. Mechanism of the thermal expansion of  $\text{Ca}(\text{OD})_2$  at high pressure will be discussed.

Keywords: portlandite, thermal expansion, high pressure, synchrotron X-ray diffraction, TOF neutron diffraction

## High-temperature heat capacity of SiO<sub>2</sub>-Al<sub>2</sub>O<sub>3</sub>-RO (R=Mg, Ca, Sr, Ba) melts

SUGAWARA, Toru<sup>1\*</sup>

<sup>1</sup>Akita University

Heat capacity (C<sub>p</sub>) of silicate melts is an important property in consideration of phase equilibria in magmatic system and a numerical simulation of flow and thermal structures in glass melting furnace. Heat capacity of aluminum-free melts can be expressed by an additive function of partial molar heat capacities for components (Richet and Bottinga, 1985). On the other hand, it has been reported that the heat capacities of aluminosilicate melts show complicated dependence on both temperature and composition (Richet and Mysen, 2005). However, they are still poorly understood due to the lack of calorimetric data. This study provides new experimental data for the high-temperature heat capacities of Ca, Sr and Ba-bearing aluminosilicate melts.

Drop calorimetry measurements were performed for 50SiO<sub>2</sub>-25Al<sub>2</sub>O<sub>3</sub>-25CaO (An), 36.5SiO<sub>2</sub>-27Al<sub>2</sub>O<sub>3</sub>-36.5CaO (Ca36.5), 8SiO<sub>2</sub>-30Al<sub>2</sub>O<sub>3</sub>-62CaO (Ca62) and 75SiO<sub>2</sub>-12.5Al<sub>2</sub>O<sub>3</sub>-12.5SrO or 12.5BaO (Sr12.5, Ba12.5) melts between 873K and 1889K using a Bunsen ice calorimeter. Heat capacity of melts was determined from the differential of measured relative enthalpy. The heat capacity of anorthite melt is 1.356+0.0001151T(K) (J/K-g), which is consistent with the value reported by Richet and Bottinga (1985). The heat capacities for Ca36.5, Ca62, Sr12.5 and Ba12.5 are 1.532, 1.508, 1.313 and 1.160 (J/K-g), respectively, and they are independent of temperature.

The temperature and compositional dependence of the C<sub>p</sub> for SiO<sub>2</sub>-Al<sub>2</sub>O<sub>3</sub>-RO (R=Mg, Ca, Sr, Ba) melts are considered by combining new calorimetric data and literature data by drop calorimetry (n=11, Richet and Bottinga, 1984; Courtial and Richet, 1993; Neuville and Richet, 1991; Richet and Neuville, 1992) and by differential scanning calorimetry (n=22, Webb, 2008, 2011). The positive temperature dependence is observed in the SiO<sub>2</sub>-Al<sub>2</sub>O<sub>3</sub>-MgO melts as reported by Courtial and Richet (1993). In the system SiO<sub>2</sub>-Al<sub>2</sub>O<sub>3</sub>-CaO, temperature dependence of the C<sub>p</sub> is only observed at anorthite composition. The heat capacity of alkaline-earth aluminosilicate melts can be expressed by a symmetric solution model. The derived heat capacity of mixing is negative value in all of the systems. At constant temperature and oxide ratio, the heat capacity decreases with decreasing field strength of alkaline-earth elements (Ba < Sr < Ca < Mg), suggesting that configurational freedom is restricted in the cations with lower field strength due to the charge compensation effect of aluminum. Further experimental data for Sr and Ba-bearing melts are required to generalize temperature dependence of the heat capacity.

Keywords: Silicate melt, Heat capacity, Calorimetry

## Viscosity of titanium-bearing silicate melts at high pressure

SUZUKI, Akio<sup>1\*</sup>

<sup>1</sup>Tohoku University

Knowledge about viscosity of silicate melt is valuable for understanding the activity of magma in the planetary interiors. The high-Ti magmas erupted on the lunar surface. These magmas contains TiO<sub>2</sub> up to 16 wt%. Because the viscosity change at high pressure is affected by the structural change of TO<sub>4</sub>-network, it is very interesting to know the influence of Ti on the pressure dependence of viscosity. We performed viscosity measurement of K<sub>2</sub>TiSi<sub>4</sub>O<sub>11</sub> melt as an analogue of the lunar high-Ti magmas. Viscosity was measured by the falling sphere method using an X-ray radiography system. Experiments were performed at the NE7A station of the PF-AR synchrotron radiation facility in KEK, Tsukuba, Japan. We found that the viscosity of K<sub>2</sub>TiSi<sub>4</sub>O<sub>11</sub> melt has a viscosity minimum at 3 GPa. Paris et al. (1994) reported that the coordination number of titanium increases with increasing pressure on the basis of the XANES spectra of glasses synthesized under high pressure. Our results suggest that the viscosity minimum of K<sub>2</sub>TiSi<sub>4</sub>O<sub>11</sub> is strongly related to the coordination change of titanium. The viscosity minimum is also found in the terrestrial MORB magma. Recently, Sakamaki et al. (2013) proposed that the viscosity minimum causes the low velocity zone of seismic wave in the upper mantle. The present study suggests that the high-Ti melt causes an attenuating zone in the deep lunar mantle.

Keywords: magma, viscosity, moon, mantle

## Study of physical properties of Fe-Si alloy at high pressure using synchrotron radiation Mossbauer spectroscopy

SUZUKI, Nanami<sup>1\*</sup> ; OHTANI, Eiji<sup>1</sup> ; HIRAO, Naohisa<sup>2</sup> ; KAMADA, Seiji<sup>1</sup> ; HAMADA, Maki<sup>3</sup> ; SAKAMAKI, Tatsuya<sup>1</sup> ; OHISHI, Yasuo<sup>2</sup> ; MASUDA, Ryo<sup>4</sup> ; MITSUI, Takaya<sup>5</sup>

<sup>1</sup>Department of Earth and planetary materials science, Graduate School of Science, <sup>2</sup>Japan Synchrotron Radiation Research Institute, Hyogo, 679-5198, Japan, <sup>3</sup>School of Natural System, College of Science and Engineering, Kanazawa University, Kanazawa, 920-119, <sup>4</sup>Research Reactor Institute, Kyoto University, Osaka, 590-0494, Japan, <sup>5</sup>Japan Atomic Energy Agency, Hyogo, 679-5148, Japan

The Earth's core is divided into the liquid outer core and solid inner core based on seismological observations. The Earth's core has been geochemically and cosmochemically thought to be mainly composed of Fe. The density of the core is smaller than that of pure iron under the core conditions. Therefore, the core has been considered to contain light elements, such as H, S, Si, C, and O. Si is one of the most important light elements in the core. Although the phase relations and compression behaviors in the Fe-Si alloy have been studied at high pressure and temperature in order to investigate properties of the inner core, magnetic properties of the alloys have not been studied well. In order to clarify the relationship between the magnetic transition and the structural transition of the Fe-Si alloy, we made simultaneous measurements of X-ray diffraction and synchrotron Mössbauer spectroscopy of the Fe-Si alloy up to 40 GPa at room temperature.

The Fe-Si alloy used for the measurements has a composition of Fe<sub>0.95</sub>Si<sub>0.05</sub> enriched with <sup>57</sup>Fe. The starting material was synthesized by melting the mixture of <sup>57</sup>Fe and Fe-Si alloys under the Ar-H<sub>2</sub> atmosphere by laser heating. Mössbauer spectra and XRD patterns were obtained at the beamlines, BL10XU and BL11XU of SPring-8 up to 40 GPa at room temperature. Our Mössbauer data together with X-ray diffraction data revealed that the magnetic transition from magnetic to non-magnetic phase occurs at 18 GPa simultaneously with the bcc to hcp transition. The change in the sound velocity and compression behavior of the Fe-Si alloy has been reported associated with the structural transformation of the alloy from bcc to hcp. The present results imply that the change in these physical properties is caused not only by the structural change but also by the magnetic transition.

## Experimental determination of post-spinel transition boundary in $\text{Fe}_2\text{SiO}_4$

MATSUZAWA, Taisuke<sup>1\*</sup> ; KOJITANI, Hiroshi<sup>1</sup> ; AKAOGI, Masaki<sup>1</sup>

<sup>1</sup>Department of Chemistry, Gakushuin University

It is widely accepted that  $(\text{Mg,Fe})_2\text{SiO}_4$  ringwoodite is the most abundant mineral in the mantle transition zone. Because spinel-type  $\text{Fe}_2\text{SiO}_4$  is the endmember of  $(\text{Mg,Fe})_2\text{SiO}_4$  ringwoodite, many investigators have been studied on phase transitions of  $\text{Fe}_2\text{SiO}_4$  spinel (Kawada 1977, Ohtani 1979, Morooka 1992, Katsura et al. 1998). Spinel-type  $\text{Fe}_2\text{SiO}_4$  decomposes into  $2\text{Fe}_x\text{O} + \text{SiO}_2$  (stishovite) +  $2(1-x)\text{Fe}$  above about 18GPa. However, the dissociation boundary has not yet been established well due in part to difficulty in oxygen fugacity control. In this study, we determined the post-spinel phase boundary in  $\text{Fe}_2\text{SiO}_4$  by high-pressure experiments controlling oxygen fugacity with the Fe-FeO buffer.

A starting material of high-pressure experiments was a mixture of  $\text{Fe}_2\text{SiO}_4$  (fayalite),  $\text{Fe}_x\text{O}$  and Fe with molar ratios of 10:2:1, and it was packed in a Fe capsule. Oxygen fugacity of the sample at high pressure and high temperature was controlled by the Fe-FeO buffer. The high-pressure experiments were performed using a Kawai-type 6-8-type multi-anvil apparatus at 16-20GPa and 1000-1400 °C. The starting samples were heated at the desired conditions for 3-6 hours, and then quenched and decompressed to ambient conditions. Recovered samples were identified by using powder XRD method and SEM-EDS, and then lattice parameters of  $\text{Fe}_x\text{O}$  were determined by using powder XRD. The x values in  $\text{Fe}_x\text{O}$  were estimated from the composition-lattice parameter relationship of  $\text{Fe}_x\text{O}$  by McCammon (1993).

The post-spinel transition boundary in  $\text{Fe}_2\text{SiO}_4$  was determined to be  $P(\text{GPa}) = -0.0021T(^{\circ}\text{C}) + 20.0$  in the temperature range of 1000-1400 °C. The phase boundary has a negative slope. Our boundary is almost consistent with those of Ohtani (1979) and Katsura et al. (1998). Katsura et al. (1998) interpreted that the negative slope of the boundary in the previous studies was apparent which was caused by slow kinetics of spinel decomposition. Because our study indicated that the decomposition of  $\text{Fe}_2\text{SiO}_4$  spinel completed in the runs for 3 hours at 1000 °C and that x values of  $\text{Fe}_x\text{O}$  in the run products for 3 and 6 hours at the 1000 °C were approximately equal, we conclude that heating at 1000 °C for at least 3 hours was enough to reach the equilibrium. Because our transition boundary was determined by the runs for 6 hours at 1000 °C, 3 hours at 1200 °C, and 3 hours at 1400 °C, we suggest that the negative slope of the post-spinel transition boundary in  $\text{Fe}_2\text{SiO}_4$  is not apparent but the essential feature.

Keywords:  $\text{Fe}_2\text{SiO}_4$ , post-spinel, spinel, high-pressure

## Relationship between Raman spectral pattern and crystal orientation of cordierite

ABE, Miyako<sup>1\*</sup> ; MADHUSOODHAN, Satish-kumar<sup>1</sup> ; KAGI, Hiroyuki<sup>2</sup>

<sup>1</sup>Niigata University, <sup>2</sup>Tokyo University

In the crystal structure of cordierite, six-membered rings of (Al, Si) O<sub>4</sub> are stacked along the *c*-axis and form a channel structure. This channel structure can trap volatiles such as H<sub>2</sub>O and CO<sub>2</sub>, and makes cordierite an important mineral for preserving the information of past fluid conditions during metamorphism. Earlier studies have shown that the intensity of CO<sub>2</sub> Raman band represents the contents of CO<sub>2</sub> inside the channel (e.g. Kaindl et al., 2006). Carbon dioxide is aligned linearly along the *a*-axis in the channel (Aines and Rossman, 1984), and therefore the peak intensity of CO<sub>2</sub> at 1383cm<sup>-1</sup> in the Raman spectra varies considerably depending on the crystal orientation of cordierite (Kolesov and Geiger, 2000). Thus, it is necessary to correct the effect of crystal orientation for the determination of true contents of CO<sub>2</sub> in randomly oriented cordierite grains in metamorphic rocks. As a first step to accurately quantify the CO<sub>2</sub> content in cordierite using Raman spectroscopy, we analyzed euhedral crystals of cordierite for revealing the relationship between Raman spectral patterns and crystal orientation.

In this study, euhedral cordierite crystals collected from the volcanic ash deposit in the Takiga swamp, Gunma Prefecture, Japan were examined in detail using micro-Raman spectroscopy. Raman spectra were observed with different conditions for each analytical point to check the effect of polarization and crystal orientation. Mineral chemical analyses of cordierite crystals indicate homogeneity in its composition ( $X_{Mg} = 0.735 \pm 0.14$ ). However, different Raman spectral patterns were obtained for (001) plane and (100) plane; the (001) plane show only one pattern, but the (100) plane showed three different patterns. Peak splitting between 554 and 575 cm<sup>-1</sup>, the peaks of 970 cm<sup>-1</sup> and 1180 cm<sup>-1</sup> changed its intensity drastically, whereas the peak at 670 cm<sup>-1</sup> remained constant. We selected five Raman peaks at 554 cm<sup>-1</sup>, 575 cm<sup>-1</sup>, 670 cm<sup>-1</sup>, 970 cm<sup>-1</sup>, and 1180 cm<sup>-1</sup> attributable to the cordierite (Al, Si)O<sub>4</sub> structure and analyzed the intensity ratio of these five peaks in different orientations. A parameter of  $\Delta$ intensity was defined, where the intensity ratios of (001) plane were concentrated around 0, and those of (100) plane deviates from 0. This parameter can be used to identify the crystal orientation of cordierite. The spectral variations observed in cordierite and its relationship with crystal orientation are interpreted based on the stretching and/or bending vibrations of cordierite unit cell structure

Keywords: Cordierite, Raman spectroscopy, Crystal orientation

References

Aines, R. D. and Rossman, G. R. (1984) The high temperature behavior of water and carbon dioxide in cordierite and beryl. *American Mineralogist*, 69, 319-327

Kaindl, R., Tropper, P. and Deibl, I. (2006) A semi-quantitative technique for determination of CO<sub>2</sub> in cordierite by Raman spectroscopy in thin sections. *European Journal of Mineralogy*, 18, 331-335

Kolesov, B. A. and Geiger, C. A. (2000) Cordierite II: The role of CO<sub>2</sub> and H<sub>2</sub>O. *American Mineralogist*, 85, 1265-1274

Keywords: Cordierite, Raman spectroscopy, Crystal orientation

## The low-temperature Moessbauer spectroscopy of an M3' epidote from Osayama, Okayama prefecture, Japan

YAMAKAWA, Junji<sup>1\*</sup>; KAWASE, Masaya<sup>2</sup>; KUROKUZU, Masayuki<sup>3</sup>; MORIMOTO, Shotaro<sup>4</sup>; SAITO, Tadashi<sup>5</sup>

<sup>1</sup>Graduate School of Natural Science and Technology, Okayama University, <sup>2</sup>Nagahama Institute of Bio-Science and Technology, <sup>3</sup>Research Reactor Institute, Kyoto University, <sup>4</sup>Faculty of Pharmacy, Osaka Ohtani University, <sup>5</sup>Radioisotope Center, Osaka University

Epidote,  $\text{Ca}_2(\text{Al,Fe}^{3+},\text{Fe}^{2+})\text{Al}_2\text{SiO}_4\text{Si}_2\text{O}_7(\text{O,OH})$  is a common rock forming mineral found low-grade metamorphic rocks. The chemical compositions of the epidote vary with the formation conditions and make some complex zoning textures. The distribution of  $\text{Fe}^{2+}$ - $\text{Fe}^{3+}$  ions in the crystal structure will be able to analyze by the Mössbauer spectrometry and the stability/unstability of the sample can be estimated from the distribution.

Moreover, in some sample, the Fe ions are distributed in the characteristic M3' site that can be detected by the Mössbauer spectroscopy. The distribution ratio of the Fe ions in the M3' site can not be estimated by the X-ray structure analysis, so the M3' sites are making a small ordering structures and distribute homogeneously in the crystal. Distribution ratio of Fe in the site of M1/M3/M3' corresponds to the formation conditions of the sample.

In this study, the low-temperature Mössbauer spectrum and Magnetic susceptibility of the M3' epidote sample was measured and the characteristics of the M3' site were analysed.

Keywords: Epidote, Moessbauer spectroscopy, M3' site, Magnetic susceptibility

## Structural change in ikaite ( $\text{CaCO}_3 \cdot 6\text{H}_2\text{O}$ ) near the freezing point temperature of water

TATENO, Natsuki<sup>1</sup> ; KYONO, Atsushi<sup>1\*</sup>

<sup>1</sup>Div of Earth Evolution Sciences, Grad Sch of Life & Environmental Sciences, Univ of Tsukuba

Ikaite, one of the calcium carbonate minerals, is thermodynamically stable only at near-freezing temperature and transformed rapidly into calcite and vaterite at ambient temperature. During the phase transformation with dehydration, its crystal shape is preserved as pseudomorphs, termed glendonite, thinolite, and gennoishi. This study aims to clarify the structure change and dehydration mechanisms by using low-temperature single-crystal X-ray diffraction study. At  $-50$  °C, the crystal structure of ikaite is monoclinic, space group  $C2/c$  with the unit cell parameter  $a = 8.8134$  (1),  $b = 8.3108$  (1),  $c = 11.0183$  (1) Å,  $\beta = 110.418$  (1) °. It is composed of four  $\text{CaCO}_3 \cdot 6\text{H}_2\text{O}$  molecules in the cell. With increasing temperature, the unit cell volume is increased monotonously from 756.3 to 758.0 Å<sup>3</sup> between  $-50$  and  $-20$  °C, and then jumped to 771.0 Å<sup>3</sup> at  $-10$  °C. The unit cell lattice anisotropically expands mainly along the  $c$ -axis, followed by the  $a$ -axis. The intramolecular Ca-O(5) bond distance is drastically elongated at  $-10$  °C, which is associated with elongations of the intermolecular O(2)-O(3), O(2)-O(5), O(4)-O(5) distances. The  $a$  unit cell expansion is directly due to the elongation of the O(2)-O(5) aligned parallel to the  $a$ -axis. The drastic elongation of the Ca-O(5) bond distance gives rise to an initial dehydration of the  $\text{CaCO}_3 \cdot 6\text{H}_2\text{O}$  molecule. The intermolecular Ca-O(3)-O(2) angle is constantly increased with temperature, leading to rotational motion of the  $\text{CaCO}_3 \cdot 6\text{H}_2\text{O}$  molecule along  $b$ -axis. This is responsible for the highest expansion coefficient of the  $c$  lattice parameter.

Keywords: ikaite, vaterite, calcium carbonate, pseudomorph, low-temperature X-ray diffraction study

## Synchrotron powder X-ray diffraction study of the structural thermal properties on hydrogrossular

KATO, Masato<sup>1\*</sup> ; KYONO, Atsushi<sup>2</sup>

<sup>1</sup>Graduate School of Life and Environmental Science, <sup>2</sup>Graduate School of Life and Environmental Science

Synchrotron powder X-ray diffraction study on synthetic Si-free hydrogrossular, katoite  $\text{Ca}_3\text{Al}_2(\text{O}_4\text{H}_4)_3$ , were performed at temperature range from 300 to 10 K. The temperature dependence of structure parameters was refined by Rietveld analysis. Since structural contraction with decreasing temperature would directly cause a phase transition on the hydrogrossular structure, three candidates for space group:  $Ia-3d$  (katoite at ambient),  $I-43d$  (katoite at high pressure), and  $I4_1/acd$  (majorite), were applied to the X-ray diffraction profile fitting collected at 10 K. The final  $R_w$  with the  $Ia-3d$  space group consequently results in the smallest value, which suggests that the katoite structure remains unchanged up to the lowest temperature of 10 K. However, the temperature dependence of the unit cell volume shows two different expansion coefficients at temperatures above and below 100 K. It can be accounted for by the effect of the repulsion between atoms of the same species. Whereas the unit cell of katoite is monotonously contracted with decreasing temperature, the  $\text{O}_4\text{H}_4$  tetrahedron and  $\text{AlO}_6$  octahedron are alternatively expanded and contracted. Compared with the phase transition in katoite under high pressure, moreover, the unit cell volume contraction up to 5 GPa is about eight times larger than that under low temperature. The structural characteristics could therefore explain the reason why no phase transition occurs in katoite at low temperature condition.

Keywords: katoite, synchrotron powder X-ray diffraction, Rietveld analysis,  $\text{O}_4\text{H}_4$  tetrahedron

## Structural study on the phase transformation of natural scolecite with increasing temperature

UCHIDA, Takahiro<sup>1\*</sup>; KURIBAYASHI, Takahiro<sup>1</sup>; NAGASE, Toshiro<sup>2</sup>

<sup>1</sup>Department of Earth Science, graduate school of science, Tohoku University, <sup>2</sup>The Tohoku University Museum, Tohoku University

Scolecite,  $\text{CaAl}_2\text{Si}_3\text{O}_{10}\cdot 3\text{H}_2\text{O}$  is classified to fibrous zeolite group. The sequence of general phase transformation with increasing temperature has been reported for natural scolecite: scolecite  $\rightarrow$  meta-scolecite  $\rightarrow$  amorphous phase and decomposes to An + Qtz (Rykl *et al.* 1986; Gottardi and Galli 1985).

In this study, the high-T evolution of the structure of natural scolecite from Poona, India were studied up to 573 K to reevaluate the dehydration process of scolecite using TG-DTA and in situ single crystal X-ray diffraction experiments.

As the results from structural refinement at room temperature, the lattice constants of the sample are determined as follows :  $a = 18.504(3)\text{Å}$ ,  $b = 18.971(2)\text{Å}$ ,  $c = 6.5262(9)\text{Å}$  and  $\beta = 90.558(5)^\circ$ . The crystal structure of scolecite,  $\text{CaAl}_2\text{Si}_3\text{O}_{10}\cdot 3\text{H}_2\text{O}$ , was refined with the space group  $F1d1$  from 3567 reflections with  $I_o > 2\sigma(I)$ , yielding  $R = 4.62\%$ ,  $wR = 11.41\%$ . At  $\sim 423\text{K}$ , the space group was changed to  $Fd11$  from  $F1d1$ , and scolecite underwent a phase transformation to meta-scolecite phase.

As the results from structural refinement at 523 K, the lattice constants of the sample are determined as follows :  $a = 18.122(3)\text{Å}$ ,  $b = 18.847(3)\text{Å}$ ,  $c = 6.5408(11)\text{Å}$  and  $\alpha = 88.948(7)^\circ$ . The crystal structure of scolecite,  $\text{CaAl}_2\text{Si}_3\text{O}_{10}\cdot 2\text{H}_2\text{O}$ , was refined with the space group  $Fd11$  from 2782 reflections with  $I_o > 2\sigma(I)$ , yielding  $R = 10.72\%$ ,  $wR = 28.85\%$ . When phase transformation occurs, OW2 in scolecite is expelled and then the half of Ca ions move by  $\sim 1/2c$ . At 573 K, the number of observed reflections was decreased dramatically.

Under high-T experiments from 423 to 523 K, two reciprocal lattices were observed, each lattice is corresponding to twin component with the [00-1] twin law. The [00-1] twinning could be associated with the dehydration mechanism. The X-ray diffraction data suggest the possibility of exist of a new  $\text{H}_2\text{O}$  site in meta-scolecite phase. This may be a key to solve the dehydration process of scolecite.

Keywords: scolecite, dehydration, phase transformation, single crystal X-ray diffraction, twin, high temperature

## Near-infrared spectra of ice under high pressure and high temperature

NOGUCHI, Naoki<sup>1\*</sup> ; KOMATSU, Kazuki<sup>2</sup> ; SHINOZAKI, Ayako<sup>2</sup> ; SHINODA, Keiji<sup>3</sup> ; KAGI, Hiroyuki<sup>2</sup>

<sup>1</sup>Graduate School of Engineering, Hiroshima University, <sup>2</sup>Geochemical Laboratory, Graduate School of Science, The University of Tokyo, <sup>3</sup>Department of Geosciences, Faculty of Science, Osaka City University

The physical properties of ice VII under high pressure and high temperature (HP-HT) conditions are important to planetary science. Ice VII is considered a primary constituent of the interior of giant icy satellites and planets (e.g., Podolak et al. 1998). Thus, understanding the physical properties of ice VII will contribute to better knowledge about the structure and dynamics of other satellite and planetary interiors. In particular, the ionic conductivity of ice VII, which affects the magnetic fields of these bodies (Stevenson 2003), is controlled by ionic and rotational defects in the ices (Jaccard 1959); moreover, ionic defects have two types:  $\text{OH}^-$  and  $\text{H}_3\text{O}^+$ . The probability of forming defects in ice VII under the HP - HT conditions that typify the interiors of icy satellites and planets is surely increased by thermal activation.

In the near-infrared (NIR) region, the spectrum of ice VII shows absorption bands of the bending-stretching combination ( $\nu_2 + \nu_3$ ) and stretching overtone ( $2\nu_3$ ) modes of the normal vibration of water molecules (Larsen and Williams 1998). These modes correspond to the high vibrational energy level of the potential well, and provide information regarding the potential barrier along the O...O axis. To determine the probability of forming ionic defects in the ice VII structure at elevated temperatures, the NIR spectra of ice VII must be measured. The aim of this study is to investigate the state of protons in ice VII under HP-HT conditions. Thus, we measured the NIR absorption spectra of water at pressures up to 16 GPa and temperatures up to 368 °C using an external heating diamond anvil cell and synchrotron NIR radiation of BL43IR at SPring-8.

The absorption band of the first OH stretching overtone mode divided into doublet peaks above 5 GPa at room temperature, suggesting that proton tunneling occurs at the overtone level. As the temperature increased, the doublet peaks gradually reduced to a singlet. This result implies that thermally activated protons hop between the two potential minima along the oxygen-oxygen axis. A P-T diagram for the proton state was constructed from the changing band shape of the overtone mode.

Keywords: ice, proton, icy satellite, near-infrared spectroscopy, high pressure and high temperature

## Phase changes of filled ice Ih methane hydrate induced by the orientational ordering of the guest molecules

TANAKA, Takehiko<sup>1\*</sup> ; HIRAI, Hisako<sup>1</sup> ; MATSUOKA, Takahiro<sup>2</sup> ; OHISHI, Yasuo<sup>3</sup> ; YAGI, Takehiko<sup>1</sup> ; OHTAKE, Michika<sup>4</sup> ; YAMAMOTO, Yoshitaka<sup>4</sup> ; NAKANO, Satoshi<sup>5</sup>

<sup>1</sup>Geodynamics Research Center, Ehime University, <sup>2</sup>Gifu University, <sup>3</sup>Japan Synchrotron Radiation Research Institute, <sup>4</sup>The National Institute of Advanced Industrial Science and Technology, <sup>5</sup>National Institute for Materials Science

Oriental ordering of guest methane molecules in a filled ice Ih structure of methane hydrate (MH) was observed above 15 to 20 GPa at room temperature in a previous Raman study. However, the change in the fundamental structure was not observed at the pressure region by X-ray diffractometry. In this study, low-temperature and high-pressure experiments were performed with filled ice Ih structure of methane hydrate under pressure and temperature conditions of 2.0 to 77.0 GPa and 30 to 300 K, respectively, using diamond anvil cells and a helium-refrigeration cryostat. Distinct changes in the axial ratios of the host framework were revealed by In-situ X-ray diffractometry. Splitting in the CH vibration modes of the guest methane molecules, which was previously explained by the orientational ordering of the guest molecules, was observed by Raman spectroscopy. The pressure and temperature conditions at the split of the vibration modes agreed well with those of the axial ratio changes. The results indicated that orientational ordering of the guest methane molecules from orientational disordered-state occurred at high pressures and low temperatures, and that this guest ordering led to the axial ratio changes in the host framework. Existing regions of the guest disordered-phase and the guest ordered-phase were roughly estimated by the X-ray data. In addition, above the pressure of the guest-ordered phase, another high pressure phase was developed at a low-temperature region.

Keywords: Methane Hydrate, X ray diffraction, high pressure, Raman spectroscopy

## Zirconium local structure in tektite and impact-related natural glasses probed by XAFS

TOBASE, Tsubasa<sup>1\*</sup> ; YOSHIASA, Akira<sup>1</sup> ; WANG, Ring<sup>1</sup> ; HIRATOKO, Tatsuya<sup>1</sup>

<sup>1</sup>Graduate School of Science, Kumamoto University, <sup>2</sup>Materials and Structures Laboratory, Tokyo Institute of Technology

The local structures of tektite and natural glasses were studied by Zr K-edge X-ray absorption near edge structure (XANES) and extended X-ray absorption fine structure (EXAFS) in order to provide quantitative data on bonding distances and coordination numbers. The XAFS measurements were performed at the beam line BL-NW10A of the PF-AR in National Laboratory for High Energy Physics (KEK), Tsukuba, Japan. Zr<sup>4+</sup> ion in tektite has different kinds of coordination environment. Various natural glasses are formed under different physical conditions. Impact-related glass, fulgurite and volcanic glasses are typical natural glasses. Glass structure is affected by the pressure and temperature conditions during the glass formation and annealing process. This study indicated that different formation process of natural glasses gives different local structure of zirconium ions.

The Zr K-edge XANES spectra of tektite have the double post-edge peaks with different heights. All tektites are classified in same types. Zr-O distances in tektite are 2.198-2.215 Å and XANES spectra of tektite have similar shape. It indicates that tektites have similar Zr local structure with 7-fold coordination Zr ions. Volcanic glasses are classified same type. Impact-related glasses are classified to different types. Impact glasses are formed under different geological process at impact event and are experienced different physical environments.

Keywords: XAFS, Local structure of Zr, Tektite, Natural glass, XANES, EXAFS

## Light element quantification using electron microprobe and Os surface coating

OHFUJI, Hiroaki<sup>1\*</sup> ; YAMAMOTO, Masashi<sup>1</sup> ; KOJIMA, Yohei<sup>1</sup>

<sup>1</sup>Geodynamics Research Center, Ehime University

Electron microprobe analysis is a non-destructive method widely used for determining the chemical composition of solid materials such as not only minerals and rocks but also industrial and biological materials. Recent advances of solid-state detectors for energy dispersive spectroscopy (EDS) analysis allow us to readily collect precise quantitative data. For SEM and EDS analysis of non-conductive (insulating) materials such as minerals and rocks, surface coating of a thin conductive layer is a prerequisite for sample preparation. For this purpose, carbon and gold are most commonly used; the former with low atomic (Z) number is suitable for microprobe chemical analysis, while the latter is preferable for textural observation of samples with rough, uneven surfaces and/or with high porosity. Recently, osmium coating prepared by chemical vapor deposition (CVD) has been a focus of attention and found to be effective for high-resolution SEM observation of samples with uneven surfaces. In the present study, we applied the sample preparation technique using very thin osmium surface coating for chemical quantification of various mineral samples by EDS.

The SEM-EDS analysis was performed by using FE-SEM (JEOL, JSM-7000F) equipped with a silicon-drift-type EDS detector (Oxford Instruments, X-Max 20). Accelerating voltage and probe current were 15 kV and 1 nA, respectively. Osmium coating of 5 nm thick was carefully made by using a Neoc-ST osmium coater (Meiwafosis). Quantification analyses were conducted on a variety of mineral samples, silicate (including hydrous silicates), carbonate and oxide minerals.

The results showed that the quantification data obtained from samples with osmium coating are as accurate as those from samples with conventional carbon coating for principle elements such as Na, Mg, Al, Si, K, Ca and Fe. With respect to the quantification of light elements such as C, N and O, the results from osmium-coated samples are found to be closer to their stoichiometric values than those from carbon-coated samples. This is likely caused by the absorption correction of the X-rays passing through each coating layer. The thickness of the surface coating layer can be precisely controlled in the case of osmium coating prepared by the CVD technique, but not readily adjusted in carbon coating. As the result, the deviation of the estimated thickness of the coating layer from the actual thickness over/underestimates the effect of X-ray absorption correction, in which low-energy X-rays from light elements are more significantly influenced by the correction. We found that the precise quantification of oxygen as a separate element (not as oxide forms of cations) using osmium surface coating might be helpful and effective in estimation of the valence state of iron in iron-bearing minerals and water (hydrogen) content in hydrous minerals. We also confirmed that the present technique is also useful for precise quantification of carbonate minerals such as CaCO<sub>3</sub>.

## Cathodoluminescence characterization of terrestrial and extraterrestrial alkali-halide minerals

YOSHIDA, Eisuke<sup>1\*</sup>; NISHIDO, Hirotsugu<sup>1</sup>; NINAGAWA, Kiyotaka<sup>1</sup>

<sup>1</sup>Okayama University of Science

Luminescence of natural alkali halides such as halite and sylvite is characterized by structural defects related to F-center (+p) and V-center (+e). On their CL (cathodoluminescence), however, scarcely has been reported so far. Since asteroidal water was discovered as fluid inclusion in halite from H5 chondrite, Monahans (1998), alkali halides in meteorites have been extensively investigated for understandings of aqueous alteration and thermal metamorphism on the parent body. Therefore, luminescence features of halides can provide valuable information on such issues. In this study we have measured CL spectra of terrestrial and extraterrestrial halite samples to clarify luminescence centers in various types of halite.

Halite crystals of terrestrial origin and small halite particles in ureilite meteorites were selected for CL measurements. All samples were prepared using oil while cutting and polishing without water. Also cleavage fragments of terrestrial samples were used for CL spectral measurements after carbon coating.

All samples exhibit weak blue to greenish blue CL with broad band emissions from 350 to 650 nm. CL spectra corrected for total instrumental response were converted into energy units for spectral deconvolution using a Gaussian curve fitting, because Gaussian curve in energy units can be assigned to one specific type of emission center (Stevens-Kalceff, 2009). The deconvoluted components can be assigned to the emission centers related to  $V_k$  (+e), F (+p),  $V_F$  (+e),  $Mn^{2+}$  ( $Na^+$ ) and  $Mn^{2+}$  (interstitial) by referring to Gorobets and Rogojine (2002).

The CL spectra of terrestrial halite at room temperature are consisted of five components at 3.34 eV, 3.05 eV, 2.46 eV, and 2.28 eV and at 2.00 eV. At low temperature the emission of  $Mn^{2+}$  impurity center is enhanced due to an increase in the probability of radiation transition. In the case of high-energy emission, a decrease in sample temperature reduces the intensity of F-center emission, but sensitizes the intensity of  $V_k$ -center emission, suggesting the energy transfer from F-center to  $V_k$ -center. The CL spectral analysis of terrestrial sylvite at room temperature confirms four emission components at 3.32 eV, 2.97 eV, 2.53 eV and 1.89 eV.

Halite in the meteorite of polymict ureilite (Dar al Gani 319) gives a broad emission band in blue region, which is deconvoluted into two components at 2.70 eV for unknown center and at 3.11 eV for F-center. However, no emission in red region associated with Mn impurity center has not recognized in ureilite halite. It implies that high-energy radiation in cosmic space might break up the crystal fields around Mn ions.

## Effects of Mn activator and site occupancy on cathodoluminescence of dolomite

KUSANO, Nobuhiro<sup>1\*</sup>; NISHIDO, Hirotsugu<sup>1</sup>; NINAGAWA, Kiyotaka<sup>1</sup>

<sup>1</sup>Okayama University of Science

Cathodoluminescence (CL) has been widely applied in mineralogical and petrological investigations, especially for carbonates. Dolomite commonly red CL emission related to an impurity center of divalent Mn in Ca-site and Mg-site (Sommer, 1972; Walker et al, 1989). Furthermore, temperature effect on CL efficiency has not been discussed in spite of potentially important function to control CL emission mechanism. In this study we have clarified luminescent mechanism of dolomite in a wide range of temperature using a SEM-CL, and confirmed a temperature quenching of its emissions. The quenching process has been quantitatively evaluated by CL spectral deconvolution method assuming the Mott-Seitz model.

Five dolomite samples from Hase, Japan (D01), Nakase, Japan (D02), Raura, Peru (D03), Binntal, Switzerland (D04), Arizona, USA (D05) were selected for CL measurements after carbon-coating on their polished surfaces. SEM-CL analysis was conducted using an SEM (JEOL:JSM-5410) combined with a grating monochromator (Oxford: Mono CL2) to measure CL spectra ranging from 300 to 800 nm in 1 nm steps with a temperature controlled stage from -190 to 250 °C. The dispersed CL was collected by a photon counting method using a photomultiplier tube (R2228) and converted to digital data. All CL spectra were corrected for the total instrumental response.

CL spectra of all samples at room temperature exhibit almost similar pattern with a broad band at 525-800 nm in a red region. The spectral peaks are sharpened and enhanced at lower temperature due to reduction of thermal lattice vibration and an increase in luminescent efficiency, suggesting high spectral resolution of the emission bands at low temperature. Therefore, a Gaussian fitting was conducted to quantitatively deconvolute spectral data obtained at low temperature in an energy unit. The results confirmed that CL of all samples consist of two emission components at around 1.84 eV (Mg-site) and 2.15 eV (Ca-site) in red region, of which variation might be attributable to crystal field (Mn-ligands distance). In general, luminescence efficiency of the material decreases with a rise in temperature due to an increase in non-radiative transitions. This phenomenon has been recognized in several minerals such as quartz, cristobalite and tridymite as temperature quenching. Furthermore, an increasing temperature makes a shift of the emission peak to a higher wavelength side. The emission intensity varies depending on the samples with different concentrations of activator ( $Mn^{2+}$ ) and quencher ( $Fe^{2+}$ ), and site occupancy of the  $Mn^{2+}$  ion between two cation sites in dolomite structure. The facts suggest that the behavior of the emission intensity with changes in temperature is not explained on the basis of a temperature quenching theory based on an increase in the probability of non-radiative transition with the rise of temperature (Mott-Seitz model). Probably activator ( $Mn^{2+}$ ) concentration affects temperature quenching effect on CL of dolomite considerably.

## Cathodoluminescence of calcite decomposed from dolomite in high-temperature skarn

KUSANO, Nobuhiro<sup>1\*</sup> ; NISHIDO, Hirotsugu<sup>1</sup> ; INOUE, Koichi<sup>1</sup>

<sup>1</sup>Okayama University of Science

Purple luminescent calcite associated with periclase has been found from the high-temperature skarn in Kanehira mine located in the eastern part of Hiroshima Prefecture. Calcite usually emits red to orange in cathodoluminescence (CL), but scarcely purple to blue. In this study we have conducted to clarify the emission center related to purple luminescence by using CL spectral analysis and the origin of the calcite during skarn mineralization.

The specimens collected from the skarn zone in the limestone contacted with intrusive granodiorite in the outcrop of the pit-tunnel. The polished thin sections of the selected samples were employed for optical observation and CL measurements. Color CL images were obtained using a cold-cathode type Luminoscope with a cooled-CCD camera. CL spectroscopy was made by a SEM-CL system, which is comprised of SEM (JEOL: JSM-5410LV) combined with a grating monochromator (OXFORD: Mono CL2). The CL emitted from the samples was dispersed by a grating monochromator (1200 grooves/mm), and recorded by a photon counting method using a photomultiplier tube. All CL spectra were corrected for total instrumental response, which was determined using a calibrated standard lamp.

Color CL imaging reveals two types of CL emission, red and purple, in calcite closely associated with spotted periclase. The CL spectra of both calcite show a broad emission band at 620 nm in a red region, which is assigned to an impurity center derived from an activator of divalent Mn ion substituted for Ca, where the intensity of red CL is higher than that of purple CL. Furthermore, the calcite with purple calcite exhibits a broad emission band at 400-500 nm in a blue region, which might be related to a defect center such as "back-ground blue" found in low-Mn activated calcite.

The calcite with purple CL is accompanied by spotted periclase grains, which is usually found as a component of metamorphosed dolomitic limestone. If the hydrate condition would be presumed during its formation, periclase could easily hydrate and alter to brucite and other magnesium minerals by action of the humidity. According to the results of heating experiments of dolomite, dolomite decomposes to calcite and periclase at around 750 °C, whereas calcite causes its decarbonation above around 850 °C. It implies that the calcite with purple CL might be persisting after the decomposition of dolomite under a dry condition at relatively high-temperature near 800 °C, and leave the defects in the calcite structure during thermal decomposition of dolomite, which can be assigned to the component of an emission band in a blue region.

## Cathodoluminescence characterization of terrestrial and extraterrestrial enstatite

OHGO, Syuhei<sup>1\*</sup> ; MISHIMA, Maki<sup>1</sup> ; NISHIDO, Hirotsugu<sup>1</sup> ; NINAGAWA, Kiyotaka<sup>1</sup>

<sup>1</sup>Okayama University of Science

Enstatite occurred in meteorite shows various cathodoluminescence (CL) emissions, whereas CL emission in terrestrial enstatite has not been reported so far. We have confirmed several luminescent enstatite in terrestrial samples. In this study, we have conducted to clarify the luminescence centers of terrestrial enstatite and comparatively discuss the CL of terrestrial enstatite and extraterrestrial ones in enstatite chondrite (E-chondrite).

Three enstatite with CL emission from Morogoro, Tanzania and Chandrika, SriLanka were selected for CL measurements. The samples were fixed on a brass disk with low-luminescent epoxy resin, and polished with a diamond paste. The polished thin sections of E-chondrite (Dar al Gani 734 and Y-86004) and Aubrite (Al Haggounia 001) were employed for CL examination. Color CL images were obtained using a cold-cathode type Luminoscope with a cooled-CCD camera. CL spectroscopy was made by a SEM-CL system, which is comprised of SEM (JEOL: JSM-5410LV) combined with a grating monochromator (OXFORD: Mono CL2). The CL emitted from the samples was dispersed by a grating (1200 grooves/mm), and recorded by a photon counting method using a photomultiplier tube. All CL spectra were corrected for total instrumental response, which was determined using a calibrated standard lamp.

Color CL imaging reveals various types of CL emissions, red, blue and purple in the both of terrestrial and extraterrestrial samples. The CL spectra of these enstatite show a broad emission band at 670 nm in a red region, which is assigned to an impurity center derived from activated divalent Mn ion substituted for Mg, and a broad emission band at around 400 nm in a blue region, which might be related to a defect center such as "intrinsic defect center" possibly raised during crystal growth.

CL spectra corrected for total instrumental response were converted into energy units for spectral deconvolution using a Gaussian curve fitting, because Gaussian curve in energy units can be assigned to one specific type of emission center (Stevens-Kalceff, 2009). The deconvoluted components can be assigned to the emission centers related to impurity centers of trivalent Cr ion (1.71 eV) and divalent Mn ion (1.87 eV) and to defect centers (3.18 eV). Furthermore, enstatite in Y-86004 E-chondrite gives additional emission component (3.87 eV) in a blue to UV region, which might be characteristic of the enstatite formed under the condition of low-oxygen partial pressure.

## Cathodoluminescence study of metasomatic feldspar in aegirine syenite from Iwaki Island, Ehime Prefecture

MAKI, Seiya<sup>1\*</sup> ; NISHIDO, Hirotugu<sup>1</sup> ; KAYAMA, Masahiro<sup>2</sup>

<sup>1</sup>Okayama University of Science, <sup>2</sup>Hiroshima University

In Iwaki Island, aegirine syenite was emplaced in the Ryoke granite during late Cretaceous time by alkali-rich hydrothermal metasomatism. The syenite and related rocks show various types of petrographic textures in response to the process of hydrothermal alteration, e.g. feldspar minerals. Feldspar exhibits a variety of cathodoluminescence (CL) colors depending on kinds of impurity elements and their concentrations, and defect densities related to Si-Al ordering and other structural disorder. Recently, the deconvolution method of CL spectra enables to assign the luminescence centers characteristic of the feldspar with satisfactory reliability (Kayama et al., 2010). In this study, we have conducted to clarify the metasomatic process through granite to syenite by CL spectral analyses for various types of feldspar.

Polished thin sections of the rock samples collected from granite, altered granite and syenite were employed for petrographic observations under a polarizing light microscope, CL measurements, and electron microprobe analyses (EPMA). Color CL images were obtained using a cold-cathode type Luminoscope with a cooled-CCD camera. CL spectroscopy was made by a SEM-CL system, which is comprised of SEM (JEOL: JSM-5410LV) combined with a grating (OXFORD: Mono CL2). The CL emitted from the samples was dispersed by a grating monochromator (1200 grooves/mm), and recorded by a photon counting method using a photomultiplier tube. All CL spectra were corrected for total instrumental response, which was determined using a calibrated standard lamp.

The feldspar in the unaltered granite shows apple green and blue CL emissions. The former is identified to plagioclase (Ab80, An20) characterized by divalent Mn activator at 556 nm, and the latter to alkali feldspar (Or90, Ab10) by defect center at 417 nm related to Al-O-Al. Altered granite has albite with red CL emission at around 750 nm, and alkali feldspar with inhomogeneous color of red to violet-blue emissions at around 400 nm and 720 nm. These CL emissions in a red region can be assigned to trivalent Fe activator in tetrahedral sites. The feldspar in syenite are mostly altered to albite with enhanced red emission at 748 nm, but minor alkali feldspar as residual after hydrothermal alteration exhibits dull red emission at 722 nm. The results of the spectral deconvolution reveals oxygen defect centers associated with Al-O-Al and Al-O-Ti bridges and impurity centers of trivalent Fe ions substituted for tetrahedral Al sites according to Kayama et al. (2010). Kayama et al. (2010) investigated the peak changes of a blue emission peak at 420 nm in alkali feldspar and they found that the elimination of Al-O-Al defect center was affected by hydrothermal metasomatism possibly at 250 °C. Therefore, the disappearance of blue emission in alkali feldspar in syenite implies that alkali-rich (sodium-rich) hydrothermal metasomatism for the formation of syenite could act at relatively high temperature above 250 °C successively after granitic magmatism.

## Provenance study of quartz grains in aeolian desert sediments using cathodoluminescence method

MASUDA, Risa<sup>1\*</sup> ; SANEYOSHI, Mototaka<sup>1</sup> ; NISHIDO, Hirotsugu<sup>1</sup> ; TSOGTBAATAR, K.<sup>2</sup> ; CHINZORIG, T.<sup>2</sup> ; MAINBAYAR, B.<sup>2</sup>

<sup>1</sup>Okayama University of Science, <sup>2</sup>Mongolian Academy of Sciences, Mongolia

Cathodoluminescence (CL), the emission of light caused by electron irradiation, has been widely applied in earth science, most extensively used in sedimentology. In such studies CL has the advantage that it can reveal characteristics which are invisible using transmitted light, e.g. growth zones of the crystals such as silica and carbonate minerals. In the case of quartz, its CL spectral feature is so complicated to be simply used for the identification of the provenance due to many emission centers related to various types of structural defects. In this study, we have conducted to clarify the luminescence centers in quartz selected from desert sediments using SEM-CL and evaluate quantitative ratios of the emission components of the CL spectra by the deconvolution method.

The quartz grains (#60-80 mesh size) in the aeolian sediments collected from Djadokhta formation (upper Cretaceous) in the Gobi desert were fixed on the slide glass with low-luminescent epoxy resin, of which surfaces were polished with 1 micron diamond paste. Color CL images were obtained using a cold-cathode type Luminoscope with a cooled-CCD camera. CL spectroscopy was made by a SEM-CL system, which is comprised of SEM (JEOL: JSM-5410LV) combined with a grating monochromator (OXFORD: Mono CL2). The CL emitted from the samples was dispersed by a grating monochromator (1200 grooves/mm), and recorded by a photon counting method using a photomultiplier tube. All CL spectra were corrected for total instrumental response, which was determined using a calibrated standard lamp.

All samples show dark blue CL emission, and exhibit two broad bands at 400 nm in a blue region and at 600-650 nm in a red region. CL spectra corrected for total instrumental response were converted into energy units for spectral deconvolution using a Gaussian curve fitting, because Gaussian curve in energy units can be assigned to one specific type of emission center (Stevens-Kalceff, 2009). The deconvoluted components can be assigned to the emission centers related to trivalent Fe at 1.65 eV, NBOHC at 1.89 eV, tetravalent Ti at 2.75 eV and trivalent Al at 3.19 eV by referring to Stevens-Kalceff (2009). We employed 10 grains randomly selected from collected 80 grains for each sample, and determined quantitative ratios of the emission components for these quartz grains using their integral intensities. We discuss variations of characteristic components among the sediments based on the results by a statistical analysis.

## Science and Technology for Geothermal Frontier

TSUCHIYA, Noriyoshi<sup>1\*</sup>

<sup>1</sup>Graduate School of Environmental Studies, Tohoku University

This project should cover multidisciplinary scientific fields such as geology, geochemistry, geophysics, water-rock interactions, rock mechanics, seismology, drilling technology, well logging technologies, reservoir engineering, and environmental science.

(a) Characterization of rock mass in BDT

Preliminary work by the Japanese researchers has revealed some of the behavior of the rock mass in the BDT, such as hydrothermal brecciation and presence of hydrothermally derived fracturing (HDF) (Hirano et al., 2003). However, fundamental understandings of key parameters such as the stress state, lithological structure, mechanical and compositional homogeneity, and thermal characteristics require much additional work. Laboratory tests would be the most effective means to obtain fundamental knowledge on the ductile rock mass in the initial stages of the project combined with analysis of core samples and pore water collected from an experimental borehole. This combination of laboratory and borehole data will generate, new knowledge on the rock mass and provide constraints on, and validation of the laboratory tests.

(b) Creation and control of the reservoirs

The HDF would create a brittle fracture network consisting of very fine fractures at grain boundaries, is created by cooling and depressurization from the borehole in the BDT. If a similar process operates during drilling then cooling of the ductile rock by the drill fluid may be expected to induce a grain-scale fracture network in the near field of the borehole during the drilling phase.

(c) Numerical simulation

To achieve sustainable energy production from EGSs in the BDT, it is essential to design the area of heat exchange between water and rock, and the risk of shortcut flow paths must be carefully evaluated. Simulators with capability to handle T-H-M-C behavior of the rock mass are expected.

Keywords: Geothermal

## Deep seismic reflection profiling in geothermal area: case study of Shirasawa and Shichigashuku calderas

SATO, Hiroshi<sup>1\*</sup> ; ABE, Susumu<sup>2</sup> ; UYESHIMA, Makoto<sup>1</sup>

<sup>1</sup>Earthquake Research Institute, The university of Tokyo, <sup>2</sup>Japex Geoscience Institute, Inc.

Along the Ou Backbone Range, northern Honshu, many piston-cylinder type calderas have been developed in Late Miocene to Pliocene. Recently, such calderas formed in late Miocene are focused as a possible resource of geothermal power plants. To obtain the physical data to estimate the state of deep sited fluids and fractures is significance. Since late 90's, deep seismic reflection profiling was carried out to image the deeper extension of active faults. Some of the seismic lines are crossing such caldera (Sato et al., 2002a Tectonophys., Sato et al., 2002b EPS). Here, we introduce the seismic sections and results of magnetotelluric investigation and discuss possible strategy for future's site survey.

**Shirasawa caldera:** The Shirasawa caldera is a piston-cylinder type caldera with 10-km-diameter and welded tuff and lake deposits are cropping out as caldera fill. By seismic reflection profiling using vibroseis trucks, low frequency strong reflectors are imaged 3 to 5 km beneath the caldera and estimated to be a possible evidence showing fluids. The estimation is well accord to the velocity structure obtained seismic tomography (Nakajima et al., 2006 EPS).

**Shichigashuku caldera:** This caldera is located southern part of Miyagi prefecture and shows piston-cylinder type. Across this caldera, deep seismic reflection profiling was performed in 2013 (Sato et al., 2013: JpGU). Also, magnetotelluric survey is carried out. P-wave velocity structure across the caldera shows low velocity part, which corresponds to the caldera fill, but does not suggest any characteristic feature showing existence of fluids. Magnetotelluric section suggest the distribution of vertical low resistivity zone connected slab to active volcanoes and low resistivity part which located in the md-to upper crust beneath caldera, showing the possibility of existence of fluids.

Significance of integrated geophysical exploration

To understand the physical state and material of deep sited portion beneath caldera, integrated research using several methods, active / passive seismic investigation, MT methods. Seismic reflection survey is not effective for rock unit, which does not have layering. However, it has a potential to evaluate the density of fractures and their pattern.

Keywords: geothermal area, caldera, seismic reflection profiling, magnetotelluric inversion, Shirasawa caldera, Shichigashuku caldera

## Occurrence of rock/mineral fracture under the rapid decompression boiling condition of water

HIRANO, Nobuo<sup>1\*</sup>; AOSHIMA, Satoshi<sup>1</sup>; KASAHARA, Naoya<sup>1</sup>; OKAMOTO, Atsushi<sup>1</sup>; WATANABE, Noriaki<sup>1</sup>; TSUCHIYA, Noriyoshi<sup>1</sup>

<sup>1</sup>Graduate school of Environmental Studies, Tohoku University

In our previous water-rock interaction experiments under the various hydrothermal conditions using granite or artificial quartz samples, clear cracks or fractures in the samples were observed under the specific hydrothermal condition. We have named this phenomenon as "Hydrothermally Derived Fracture (HDF)". Understanding of this fracturing phenomenon may be useful for technological development of geothermal reservoir usage or clarification of vein formation mechanism in the Earth crust. In our previous experimental results, HDF were progressed under the high temperature and low-pressure condition. The result of detailed observation, it was thought that the thermal stress occurred with rapid cooling of rock/mineral sample surface by condensed vapor dew. Similarly, rapid decompression from the high-temperature/pressure state causes, the temperature drop by latent/sensible heat effect. Therefore, when the such rapid decompression was occurred around the rock/mineral samples, HDF may occur under the hydrothermal condition. And so, we attempted rapid decompression experiment from the over 20 MPa / 400°C hydrothermal condition. As a result, the fracturing in the samples was progressed clearly. Therefore, decompression fracturing is possible and the same phenomenon may arise subsurface of near the volcano or hotter and deeper crust with water.

Keywords: Hydrothermally Derived Fracture, Water-Rock Interaction, rapid decompression, granite, fracturing

## Fracturing of granite under pore pressure and evolution of permeability

HAMASAKI, Shohei<sup>1\*</sup> ; KATAYAMA, Ikuo<sup>1</sup>

<sup>1</sup>Department of Earth and Planetary Systems Science, Hiroshima University

Hot Dry Rock (HDR) geothermal power generation, which is included in Enhanced Geothermal System (EGS) is characterized by making artificial geothermal reservoir and this is different from conventional geothermal power generation. This system does not require natural hot water and steam. In this system, artificial reservoir is made by hydraulic fracturing in the basement due to high-pressure water injection, and water circulates in the system. Evolution of permeability is important factor in reservoir assessment. To assess this type of geothermal system, we measured effect of pore pressure compared with permeability during triaxial deformation experiment.

Aji granite was used as experimental sample, which is dense and fine, consists of mainly plagioclase, quartz, and biotite. Permeability was measured by intra-vessel deformation and fluid-flow apparatus (IVA) at Hiroshima University. Aji granite was saturated water before triaxial deformation experiments. Confining pressure ( $P_c$ ) was fixed 20 MPa and pore pressure ( $P_p$ ) was ranged from 0 MPa (undrain condition during triaxial deformation) to 15 MPa by 5 MPa at room temperature in triaxial deformation. The recovered samples after deformation experiments were fixed by resin and observed by polarizing microscopes and scanning electron microscope (SEM). We discussed relation between permeability and pore pressure - fracture strength from triaxial deformation experiments.

In original sample, permeability is  $2.0 \times 10^{-19} \text{ m}^2$  at  $P_c = 20 \text{ MPa}$ . Permeability of fractured samples increased against that of original samples. Permeability proportionally increased from  $2.5 \times 10^{-18} \text{ m}^2$  at  $P_p = 0 \text{ MPa}$  to  $7.0 \times 10^{-17} \text{ m}^2$  at  $P_p = 15 \text{ MPa}$ . Fracture strength decreased with  $P_p$  decreased, from 400 MPa at  $P_p = 0 \text{ MPa}$  to 350 MPa at  $P_p = 15 \text{ MPa}$ . In fractured sample, there are macro fracture surface and microcracks.

The increase of permeability depends on pore pressure suggests that increase of microcrack width and acceleration of crack-connection and propagation in large  $P_p$ . And fracture strength relates crack sharps. Therefore, crack sharp and distribution are important parameter in assessment of permeability. We plan to further experiments which try to reproduce hydraulic fracture and high temperature condition.

Keywords: granite, pore pressure, permeability

## The numerical study for behavior of fracture aperture associated with cold fluid flow

KANETA, Kousuke<sup>1\*</sup> ; MUKUHIRA, Yusuke<sup>1</sup> ; SWENSON, Daniel<sup>2</sup> ; ITO, Takatoshi<sup>1</sup>

<sup>1</sup>Institute of Fluid Science, Tohoku University, Japan, <sup>2</sup>Mechanical and Nuclear Engineering Department, Kansas State University, USA

Power generation of geothermal power plant sometimes decreases due to reduction of reservoir pressure. Reinjection of used geothermal fluid/cold fluid into the reservoir is conducted in several geothermal power plant to keep/recover the reservoir pressure. It is required for recharge of reservoir pressure that appropriate condition of reinjection in terms of injection pressure, amount of injected fluid, and heat balance. On the other hand, it is empirically observed at some of the geothermal field that amount of injected fluid increases when lower temperature fluid is injected. In this research, we investigated relationship between temperatures of cold fluid and fracture aperture, using numerical simulation.

We conducted numerical simulation for the change in fracture aperture when cold fluid flows into the fracture, using 2D FEM code " GEOCRACK2D " (Swenson et al., 1995). We set the condition that cold fluid was injected into a single fracture within high temperature rock mass. In this simulation, cold fluid flowed from center of fracture to edge of fracture. Fluid pressure was 1 MPa at center of fracture and 0 MPa at edge of fracture. This given pressure condition made fluid flow from center of fracture to edge of fracture. Initial temperature of rock mass was 300 °C and that of cold fluid was 100 °C. Initial stress condition was 20 MPa in x direction and y direction.

As a result of simulation, the fracture aperture increased with time although 20 MPa of normal stress worked on the rock mass and fluid pressure was at most 1 MPa. It was also simulated that the rock mass around the fracture was cooled down by cold fluid and cooled area extended with time. Normal stress on the fracture decreased. The area where normal stress decreased extended over time.

These results can be interpreted that cooling of rock mass by cold fluid caused thermal shrinkage of rock mass, which decreased normal stress on the fracture surface. Finally, the fracture aperture became large, suggesting increasing in permeability.

We also conducted the simulation for the effect of difference in initial temperature between rock mass and cold fluid. We compared the change in fracture aperture about four temperature difference conditions. Fluid flow, fluid pressure, temperature of rock mass and initial stress condition were same with first simulation. Temperature of cold fluid was 100 °C, 150 °C, 200 °C and 250 °C.

As a result of simulation, the fracture aperture increased drastically when the temperature difference between rock mass and cold fluid was bigger than 150 °C. The fracture aperture slightly increased when the temperature difference is smaller than 100 °C. The bigger temperature difference was, the earlier fracture aperture opened. The results of simulation suggested that there was the critical value in temperature difference between 100 °C and 150 °C. It was summarized that the fracture aperture increased and that the fracture permeability became large when the temperature difference was bigger than the critical temperature difference.

Keywords: Geothermal reservoir, Fracture, Aperture, Thermal elasticity, Thermal shrinkage, Reinjection

## Slip-able area: New index to evaluate the fault area under critical state based on micro-seismic data at stimulation

MUKUHIRA, Yusuke<sup>1\*</sup>; ASANUMA, Hiroshi<sup>2</sup>; HARING, Markus<sup>3</sup>; ITO, Takatoshi<sup>1</sup>

<sup>1</sup>Institute of Fluid Science, Tohoku University, <sup>2</sup>AIST, <sup>3</sup>Geo Explorer Ltd.

Unexpected occurrence of felt earthquake has been big issue as critical environmental burden associated with geothermal development and other energy extraction. The magnitude of seismic events induced by fluid stimulation is generally small enough to be perceived on the ground. However, at the Basel, Switzerland, some of the events had large magnitude, resulting in the shutdown of engineered geothermal system (EGS) project. Our previous study has revealed the fundamental characteristics and the trigger mechanisms of the large event at Basel. However, we have not reached full understanding of physics of the large events, which enable us to control or manage the magnitude of induced events.

### Concept of Slip-able area

Our previous study suggested that the dynamic behavior of pore pressure especially propagation of pressure at the shut-in correlate the event magnitude because many of large events occurred at the shut-in phase in Basel. The pore pressure gradient should exist from the well head to the pressure front during the stimulation. At the shut-in when pumping is stopped, the pressure source despairs and subsequently the pressure gradient may become small with time. Finally, the pore pressure in the reservoir will go back hydrostatic state uniformly. In the relaxation process of the pore pressure gradient, it can be expected that the pore pressure at the far field from the well might slightly increase to average pore pressure increase in whole reservoir. Pore pressure increase at the front of the stimulated zone may put large part of the fault plane into near critical state. In contrast, only some part of the fault plane may become critical state, when the pore pressure increases with the pressure gradient. This is the expected scenario for occurrence of the large event at the shut-in.

So, in this study, we originally defined new concept of Slip-able area, which describes the summation of fault areas in study area, under critical state during/after the stimulation. The informations used in estimating Slip-able are given by the detailed analysis of microseismic events and stress information. Slip-able area can provide the information of the potential fault area which can have shear slip at semi real time. Slip-able area can be directly converted into the event magnitude, suggesting it is also available to the risk assessment of the large event.

### Methodology of estimation for Slip-able area

We propose the methodology to estimate Slip-able area as follows.

1. Determine the number of the potential fracture within a given rock volume from microseismic data at the first stage of the stimulation.
2. Characterize the size of the fractures from source parameter of microseismic events and their critical pore pressure for shear slip.
3. Divide the reservoir area into a number of the block with the same size of step 1.
4. Determine the stimulated volume in three dimensions by the divided block and information on occurrence of microseismic events.
5. Infer the number of the fracture in a stimulated volume determined in step 4.
6. Estimate maximum increase in pore pressure at given time in each block of stimulated volume.
7. Identify the fault area of the fracture under critical state using the information assumed in step 2.
8. Integrate all fault area of the fractures identified in step 7.

We have to note that the methodology shown above includes some steps with much difficulty or impossible because determination of critical pore pressure is based on the information on orientation of fracture plane and stress information in study area. These informations are not available in many of the geothermal field. Estimation of fault area also required high quality data set of microseismic events. In these cases, it can be valid for simplification to use appropriate constant values like b value as a substitute for characterizing of fault size.

Keywords: Microseismicity, Felt earthquake, Magnitude, Fault area, Risk assessment, Basel

## Hydration of crust through brittle fractures: Example from Sor Rondane Mountains, East Antarctica

UNO, Masaaki<sup>1\*</sup> ; OKAMOTO, Atsushi<sup>1</sup> ; TSUCHIYA, Noriyoshi<sup>1</sup>

<sup>1</sup>Graduate School of Environmental Studies, Tohoku University

Arc lower crust is expected to be amphibolite from its seismic velocity, and such lithology contains abundant hydrous minerals. However, the amount and mechanisms for supply of H<sub>2</sub>O fluid to arc crust are not well constrained. Pervasive flow and channeling flow are the two mechanisms for the transfer of fluid in the crust. As grain boundaries are closed for crustal P-T condition, channeling flow accompanied by brittle fracture is expected. To investigate the role of brittle fracture to the supply of H<sub>2</sub>O fluid for crust, crust-melt hydration reaction was investigated at Sor Rondane Mountains, East Antarctica.

In the survey area, biotite-hornblende-peridotite is intruded by numerous granitic brittle dykes, and reaction zones occur at the boundaries (Fig. 1). The mineral assemblages indicate that the reaction has occurred under lower crustal P-T condition, thus the area is suitable for investigating both mechanical and physical aspects of fluid-rock interactions under the lower crustal condition. Four reaction zones are identified from the granitic dyke to the host rock as follows:

i) granitic dyke

[quartz + plagioclase + K-feldspar + biotite + rutile + zircon ± muscovite]

ii) hornblende-tremolite zone

[hornblende + tremolite ± quartz ± apatite ± biotite]

iii) tremolite-biotite zone

[tremolite + biotite + spinel ± hornblende ± pyroxene]

iv) biotite-hornblende-peridotite

[olivine + orthopyroxene + biotite + hornblende + Cr-spinel ± magnetite ± apatite]

Those reaction zones are product of hydration reactions of host peridotite with H<sub>2</sub>O liberated from granitic melt. From plagioclase in granitic dyke and adjoining hornblende, the temperature of those reactions is estimated<sup>[1]</sup> to be 700 °C.

The amount of H<sub>2</sub>O liberated from the granitic melt will be quantified by the modes of hydrous minerals formed at the reaction zones. Accordingly, the amount of H<sub>2</sub>O supplied through hydrous melts, and the mechanisms for transport of H<sub>2</sub>O and hydration of the crust will be discussed.

Keywords: geofluid, brittle fractures, melt, hydration reaction, fluid-rock interaction, Antarctica



Fig. 1 Biotite-hornblende-peridotite (brown) intruded by granitic dykes (white), Sor Rondane Mountains, East Antarctica. Note that reaction zones occur at the boundary; green or black layers are hornblende-tremolite zone and grey to reddish brown layers are tremolite-biotite zone.

## Composite basaltic andesite lava in Iwanuma (Miyagi, Japan): Differentiation along segregation veins and columnar joints

KIMOTO, Kazuki<sup>2</sup> ; ISHIWATARI, Akira<sup>1\*</sup>

<sup>1</sup>Center for NE Asian Studies, Tohoku Univ., <sup>2</sup>Dept. Earth Sci., Grad. Sch. Sci., Tohoku Univ.

Occurrence of thin (3-5 m) composite lavas with central phenocryst-rich layers was reported by Kuno (1950; JGSJ, 56, 167-172) and others, but we found very thick (>110 m) composite lava comprising a single cooling unit (with penetrating columnar joints) but consisting of some distinct chemical layers with segregation veins at the layer boundaries.

The basaltic andesite lavas of the middle Miocene age (15~13 Ma) occur in Iwanuma City, Miyagi Prefecture, Japan. Thickness of the main lava flow measures more than 110 m. Vertical columnar joints of 1 or 2 m intervals are well developed through the outcrop. This lava flow is a composite lava flow with the lower layer (0~42 m from bottom) having rather felsic composition (SiO<sub>2</sub> 55 wt. %) and the upper layer (45~110 m from bottom) having more mafic compositions (SiO<sub>2</sub> 52~54 wt. %). There are no macroscopic differences between the two layers, but the size of plagioclase in the nearly holocrystalline groundmass of the upper layer is larger (<0.5 mm) than that of the lower layer (<0.3 mm) under the microscope. Red clinker is seen at the bottom of the outcrop, but the top of the flow has been eroded.

Many horizontal segregation veins are observed at the limited portions in the intervals of 6~14 m (lower vein zone), 45~64 m (central vein zone) and 80~95 m (upper vein zone) from bottom. The lower veins are 1 mm in thickness at intervals of 1~10 cm, have glassy structure and contain plagioclase and augite. The central veins are 5~15 mm in thickness at intervals of 10~15 cm at 45 m from bottom and 3~5 mm at intervals of 5~15 cm at 52~64 m from bottom, have crystalline structure and contain plagioclase, pigeonite and subcalcic augite. The upper veins are 3~5 mm in thickness at intervals of 5~7 cm and have similar structure and mineral assemblage to the central veins. The segregated melt of the central veins forms after the approximately 70 % crystallization of the host magma. The segregation veins are apparently formed by the migration of the residual melt into the subhorizontal fractures (platy joints) which resulted from the shear deformation and cooling contraction in the crystallizing lava flow, especially near the bottom of the flow and at the bottom part of the flow and relatively mafic layers in the upper part of the composite lava flow. Rare en echelon segregation veins are the evidence for shear deformation.

The columnar joints always perpendicularly cut segregation veins, and the rocks adjacent to the columnar joint plane show low density and increase of vesicles in comparison with the rocks in the middle of the column. This suggests that columnar joints developed far later than the segregation-filled platy joints, but some melt was still present at that time so as to allow its vesiculation promoted by the columnar joint fracturing.

Keywords: composite lava flow, segregation vein, platy joint, columnar joint, basaltic andesite, crystallization differentiation

## The formation of the permeable-impermeable boundary within the Earth's crust revealed by silica precipitation

SAISHU, Hanae<sup>1\*</sup> ; OKAMOTO, Atsushi<sup>1</sup> ; TSUCHIYA, Noriyoshi<sup>1</sup>

<sup>1</sup>AIST, <sup>2</sup>Tohoku University

Silica is one of the dominant constituents of the Earth's crust. The permeable-impermeable boundary corresponds to the brittle plastic transition at 300-450 C [1]. Ubiquitous occurrence of quartz vein is one of the evidences that the spatial and temporal variations in permeability within the Earth's crust are affected by silica precipitation in aqueous fluids. However, the role of silica-water interaction on fracture permeability is still unclear.

The Kakkonda geothermal field, Japan, has the well WD-1a that penetrated the boundary between the hydrothermal convection zone and the heat conduction zone [2]. Calculation of quartz solubility along the well WD-1a revealed that (1) the depth of a local maximum of quartz solubility correlates with that of the strong reflector in seismic data at 350 C isotherm [3], and that of a maximum of fracture numbers revealed by the logs of FMI [4], and (2) the depth of a local minimum of quartz solubility correlates with that of the permeable-impermeable boundary, in either case of hydrostatic or lithostatic conditions [5]. These results indicate that (1) the preservation of open fractures at the margin of the Kakkonda granite is controlled by dissolution of quartz, and (2) the quartz precipitation could occur from both downwards- and upwards-moving fluids, which could divide the hydrothermal convection zone and the heat conduction zone.

The hydrothermal experiments of temperature dependence of silica precipitation were conducted at 24 and 31 MPa and 170-430 C, by using the solution made by dissolution of granite. The large amount of silica precipitation occurred only in the supercritical conditions of water (>390 C). Strong temperature dependence can be explained by the homogeneous nucleation of quartz in the surface energy of quartz of 130 mJ/m<sup>2</sup> [5].

The results of the calculation of silica solubility at the Kakkonda geothermal field and the hydrothermal experiments of silica precipitation suggest that rapid quartz precipitation via nucleation could occur when fluids are brought to the depth in the supercritical conditions of water. The forming and sustaining the permeable-impermeable boundary within the Earth's crust could be controlled by precipitation of silica minerals.

### References

- [1] Scholz (2002).
- [2] Doi et al. (1998) *Geothermics*, **27**, 663-690.
- [3] Matsushima et al. (2003) *Geothermics*, **32**, 79-99.
- [4] Muraoka et al. (1998) *Geothermics*, **27**, 507-534.
- [5] Saishu et al. (in press) *Terra Nova*.

Keywords: Silica precipitation, Quartz solubility, Permeable-impermeable boundary, Hydrothermal experiment

## Introduction of NANO-EPS

SUZUKI, Yohey<sup>1\*</sup>

<sup>1</sup>Department of Earth & Planetary Science, The University of Tokyo

Nano, a prefix for  $10^{-9}$ , represents vast frontiers for both Earth and Planetary Solid Sciences. Conventional tools such as Electron Probe MicroAnalysis (EPMA) for ppm-level quantification at the micrometer scale and Power X-Ray Diffraction analysis (XRD) for the identification of submicron minerals are being transformed into the next generation instruments. In addition, it is possible to reveal the heterogeneity and oscillation of chemical and isotopic compositions at nano-spatial resolutions. It is becoming more aware that nano-sized solids with extremely large surface areas and distorted structures are ubiquitous in planetary materials and intimately relevant to many issues such as soil and groundwater contamination with metals and radionuclides, mineral resources exploitation, carbon sequestration and so on. In my presentation, nano-frontiers from various fields of Earth and Planetary Sciences and key technological advancements will be overviewed as the introduction of this session.

Keywords: nano

## Properties and depositional process of sub-micron scale manganese oxide minerals in the aqueous surface environment

USUI, Akira<sup>1\*</sup>

<sup>1</sup>Akira Usui

A large variety of minerals form submicron compounds or minerals in the surface aqueous environments (sea waters, rivers, soils, underground waters, organisms etc.) Especially iron and manganese oxide are most mobile elements among others in such environments. The iron and manganese oxides often scavenge numbers of metallic elements and play significant role in material cycling and geochemical cycles. In this paper, we attempt to introduce several types of occurrences of manganese oxide in the diverse environments. For example a phyllo-manganate minerals, nano-scale aggregate are shown in the paper.

Keywords: manganese oxide mineral, manganese crust, manganese nodule, low-temperature hydrothermal activity, phyllo-manganate, redox condition

## Development of PF-STXM and its application to environmental geochemistry

TAKAHASHI, Yoshio<sup>1\*</sup> ; TAKEICHI, Yasuo<sup>2</sup> ; SUGA, Hiroki<sup>1</sup> ; INAMI, Nobuhito<sup>2</sup> ; ONO, Kanta<sup>2</sup>

<sup>1</sup>Graduate School of Science, Hiroshima University, <sup>2</sup>Photon Factory, KEK

Scanning transmission X-ray microscopy (STXM) has been applied to various fields in earth and environmental sciences such as aerosol chemistry, geomicrobiology, soil science, and nanomineral sciences. In particular, the technique has been used in the world because of its great importance in imaging distribution of carbon, or in particular carbon functional group, with about 50 nm spatial resolution. However, STXM that can be used to measure NEXAFS at carbon K-edge has not been in use in Japan. We have constructed STXM in Photon Factory (PF-STXM) from 2012 and started to use it for various topics in earth and environmental sciences.

In the PF-STXM, soft X-rays from the undulator are monochromatized by the grating and focused at the four-way aperture slit. The FZP with the outermost zone width of 30 nm is placed at 1 m distant from the aperture slit. First order diffraction selected through an order sorting aperture (OSA) is focused onto the sample with the focal distance of 0.7-5 mm, and then the transmitted X-rays are detected. The PF-STXM at present is mainly operated at BL-13A in Photon Factor, where the energy range available is from 250 eV to 1600 eV, which covers K-edges of carbon, nitrogen, oxygen, potassium, and aluminum. The beam size of the STXM was around 50 nm focused with Fresnel zone plates (FZP). The intensity of focused X-rays at the sample was expected to be up to  $10^7$  photons/s. Instead of a photomultiplier tube (PMT) which is commonly used in STXM, a silicon avalanche photodiode (APD) is utilized to detect the transmitted X-rays in PF-STXM. Compared with other STXM system in the world, our STXM is made so compact and light that it is easily connected to and removed from the multi-purpose beamlines. The experiments reported below are performed at BL-13A and BL-16A of Photon Factory.

The PF-STXM has been used for various applications. Among them, we would like to present recent results on (i) speciation of calcium in mineral dust with 50 nm spatial resolution, (ii) characterization of carbon adsorbed on particulate matter in river water, and (iii) spatial distribution of rare earth elements in bacterial cell.

Keywords: STXM, PF, Aerosol, Particulate matter, Bacteria

## Nano-scale investigation of the microbe-mineral interaction by scanning transmission X-ray microscopy

MITSUNOBU, Satoshi<sup>1\*</sup> ; SHU, Mei<sup>1</sup> ; TAKAHASHI, Yoshio<sup>2</sup> ; TAKEICHI, Yasuo<sup>3</sup> ; ONO, Kanta<sup>3</sup>

<sup>1</sup>University of Shizuoka, <sup>2</sup>Hiroshima University, <sup>3</sup>KEK-PF

Microorganisms in the environment critically impact global geochemical cycles and redox reactions of various elements. Many geochemically important redox reactions (e.g., sulfate reduction, Fe(II) oxidation) are largely associated with microbial activity. In addition, microbes can mediate both mineral formation (biomineralization) and mineral dissolution (bioleaching). Recent studies suggest a significant relationship between Fe(II)-oxidizing bacteria and ancient Banded Iron Formation, one of the large geochemical events in Earth's history. The general ecological importance of environmental microbial reaction has been well recognized; however, the specific mechanisms of the reactions in the environments such as the reaction rate and spatial dynamics are poorly understood. In the environment such as sediments, microbial reactions and habitability vary locally and form complicated geochemical networks, which makes it difficult to characterize the specific biogenic reactions in detail.

Scanning transmission X-ray microscopy (STXM), which uses near-edge X-ray absorption spectroscopy (NEXAFS) is a powerful new tool that can be applied to hydrated biological materials with high spatial resolution. The STXM provides spatial resolution of better than 50 nm, which is suitable for imaging bacteria and bacterial biofilms.

In the present study, we applied the STXM into the bioleaching of sulfide mineral (pyrite) to determine carbon, oxygen, and iron species in nano-scale. Both metal and biogenic organic materials in pyrite-microbe interface were investigated in the single cell level. Our study shows that the STXM could be a potential technique to provide direct information on specific biogenic reaction microorganism.

Keywords: STXM, pyrite, bioleaching

## In-situ trace element quantification of geological samples using LA-ICPM

KON, Yoshiaki<sup>1\*</sup> ; EJIMA, Terumi<sup>1</sup> ; SUZUKI, Masaya<sup>1</sup> ; HIRATA, Takafumi<sup>2</sup> ; TAKAGI, Tetsuichi<sup>1</sup>

<sup>1</sup>Geological Survey of Japan, AIST, <sup>2</sup>Division of Earth and Planet. Sci., Kyoto Univ.

Laser-Ablation Inductively Coupled Plasma Mass Spectrometry (LA-ICPMS) is a type of mass spectrometry which is capable of in-situ trace element quantification of a solid sample. We introduce an typical application to characterize sub-micron scale particles based on the variation of their geochemical compositions.

Keywords: LA-ICPMS, femtosecond laser, in-situ analyses, trace-element quantification

## Formation rate of iron colloids at pH 2-3

NAGASAKI, Sagakuni<sup>1\*</sup>; YOKOYAMA, Tadashi<sup>2</sup>; HISATOMI, Osamu<sup>2</sup>; NAKASHIMA, Satoru<sup>2</sup>

<sup>1</sup>Department of physics, Osaka University, <sup>2</sup>Department of Earth and Space Science, Graduate School of Science, Osaka University

Various types of iron colloids are widely distributed in the earth's surface conditions, and their formation process, adsorption characteristic, and the material transport mediated by iron colloids are receiving attention. Iron colloids are often formed through several reactions including the dissolution of  $\text{Fe}^{2+}$  and  $\text{Fe}^{3+}$  from minerals, oxidation from  $\text{Fe}^{2+}$  to  $\text{Fe}^{3+}$ , hydrolysis, and crystallization. In the present study, the reaction rate was evaluated focusing on the process in which iron colloids are formed from dissolved  $\text{Fe}^{3+}$ .

A solution of  $\text{Fe}^{3+}$  100 ppm was prepared by dissolving  $\text{FeCl}_3$  into pure water. This solution was reacted at 15, 25, 35, 45, and 55 °C. At 25 °C, pH of the solution was  $\sim 2.7$  at the start of the reaction and decreased to  $\sim 2.2$  as reaction time passed. Such change in pH is known to occur as a result of the following reactions: hydration of  $\text{Fe}^{3+}$  (release of  $\text{H}^+$ )  $\rightarrow$  formation of dissolved  $\text{Fe}(\text{OH})_3 \rightarrow$  formation of solid  $\text{Fe}(\text{OH})_3$  (Grundl and Delwiche, 1993). Therefore, information of the formation rate of iron colloids can be obtained by monitoring the pH of the solution. After the initial period of the reaction in which the rate of the decrease of dissolved  $\text{Fe}(\text{OH})_3$  concentration was slow presumably due to nucleation, the concentration of dissolved  $\text{Fe}(\text{OH})_3$  decreased in a manner like first-order reaction, and the reaction behavior deviated from the first-order reaction at the later stage. By assuming first-order reaction, rate constants of  $3.3\text{E-}5 - 1.1\text{E-}2 \text{ s}^{-1}$  were obtained at 15-55 °C, and good linearity was confirmed in an Arrhenius plot of these rate constants.

In addition to the above experiments in which time variation of the total amount of solid is considered, the time variation of the grain size of iron colloids was evaluated. A solution of  $\text{Fe}^{3+}$  100 ppm was prepared and the change of grain size at 25 °C was continuously measured using a dynamic light scattering apparatus (Zetasizer  $\mu\text{V}$ , Malvern). As a result, enough scattering intensity began to be detected after the mean diameter of iron colloids grew to 10 nm, then the grain size increased. The increase of the grain size almost stopped after 8 hours, and mean diameter at this stage was approximately 30 – 40 nm. By evaluating the number of grains from the total amount of solid and mean grain size, the grain number was estimated to decrease with time.

## Surface complexation modeling for lead adsorption on nano-sized aluminum silicate

USHIYAMA, Tomoki<sup>1\*</sup>; FUKUSHI, Keisuke<sup>2</sup>

<sup>1</sup>Graduate School of Natural Science and Technology, Kanazawa University, <sup>2</sup>Institute of Nature and Environmental Technology, Kanazawa University

There are many abandoned lead-produced mines in Japan. The water pollutions by lead due to the weathering of the mine wastes are environmental concern. The concentrations of lead released from the mine wastes is usually low. Therefore, the adsorption process is expected to dominate the mobility of lead in the affected area. It is well recognized that the materials widely occurred in earth surface conditions are comprised with low-crystalline and/or nano-sized minerals. There are some reports for lead adsorption behavior on crystalline phases such as clay minerals and low-crystalline iron oxides. On the other hand, there are very little reports on nano-sized aluminum silicates which must be dominant phases in surface condition. The quantitative understandings of lead adsorption on nano-sized aluminum silicate is essential for the prediction of lead migration in earth surface conditions. The purpose of the study is to clarify the lead adsorption behavior on nano-sized aluminum silicate under wide range of solution conditions and model the adsorption behavior by means of surface complexation modeling.

Keywords: nano-sized aluminum silicate, lead, adsorption, surface complexation modeling

## Mineralogical study of serpentinite from Akamatsu, Yatsushiro, Kumamoto prefecture.

IWAKI, Yasuyo<sup>1</sup> ; ENJU, Satomi<sup>1\*</sup> ; UEHARA, Seiichiro<sup>1</sup>

<sup>1</sup>Department of Earth and Planetary Sciences, Faculty of Sciences, Kyushu University

Serpentine group minerals are one of the 1:1 layer type sheet silicates and the main component of serpentinite. They are classified into three mineral species chrysotile, lizardite and antigorite. The ideal formula of chrysotile and lizardite is  $Mg_3Si_2O_5(OH)_4$  and that of antigorite is  $Mg_{48}Si_{34}O_{85}(OH)_{62}$ .

In our previous study, we researched serpentinite from a large area in Kyushu Kurosegawa belt (Tanaka et al., 2012), but there are only few reports for each area. So, the purpose of this study is to identify the composition minerals of serpentinite in Akamatsutaro Pass and Tanoura, located in west of Kyushu Kurosegawa belt, and to conduct a detailed study of serpentine.

Mineral species was identified by XRD pattern and serpentinite was classified into three type: antigorite main serpentine (Type AA, 16 specimens), antigorite rich serpentine (Type A, 10 specimens) and antigorite poor serpentine (Type LC, 8 specimens). Antigorite was most abundant. Magnetite, chromite, clinocllore, brucite and hydrotalcite group minerals were identified in specimens from both areas. Only the specimen from Akamatsutaro Pass had andradite, calcite, heazlewoodite ( $Ni_3S_2$ ) and millerite (NiS), while forsterite, hydromagnesite, pyroaurite and awaruite ( $Ni_3Fe$ ) were seen only in Tanoura. The supply of  $H_2S$  in Akamatsutaro Pass can be estimated from the presence of heazlewoodite and millerite. Relict forsterite was observed in serpentinites from Tanoura, indicating the smaller degree of serpentinization compared to Akamatsutaro Pass.

Serpentine contained in massive serpentinite had variable textures such as vein texture, reed shape texture and mesh texture with core and rim, which was formed after serpentinization of olivine. In the specimens of Type LC, mesh texture was often observed, and there were cores with no rim in samples without mesh textures. Also some core texture was replaced by reed shape texture. Chemical compositions obtained by SEM-EDS show some trends for serpentines in each texture. Reed shape texture contains 0.041 (apfu) Al which replaces Mg, while core texture contain 0.07 Al and rim texture contains 0.006 Al, so reed shape texture is rich Al than mesh texture. Reed shape texture contain larger amount of  $SiO_2$  weight percent compared with the ideal formula of chrysotile and lizardite, and resemble that of antigorite.

### Reference

K.Tanaka, T. Inoo and S. Uehara (2012): Microtexture and chemical composition of serpentine minerals from Kurosegawa belt, Kyushu, Japan. The 2nd Asian Clay Conference, Abstract Book.

Keywords: serpentine, antigorite, reed shape texture, mesh texture, Kyushu Kurosegawa belt, Yatsushiro

## The lithium existence form in a lithium ore deposit

SUZUKI, Masaya<sup>1\*</sup> ; KON, Yoshiaki<sup>1</sup> ; EJIMA, Terumi<sup>1</sup> ; HIRABAYASHI, Eri<sup>1</sup> ; SATOU, Takumi<sup>1</sup> ; OOWADA, Akira<sup>1</sup> ; TAKAGI, Tetsuichi<sup>1</sup> ; TSUKIMURA, Katsuhiko<sup>1</sup> ; SAWAKI, Takayuki<sup>1</sup> ; MURAKAMI, Takayoshi<sup>2</sup> ; MOTOORI, Masayuki<sup>2</sup>

<sup>1</sup>AIST, <sup>2</sup>JOGMEC

In the ore deposit containing lithium, Spodumene, Petalite, Lepidolite, etc. are known as a lithium mineral, but these minerals are not contained in the lithium ore deposit examined this time. So, in this research, the result analyzed using XRD and SEM+EDS is released.

In the ore deposit containing lithium in this time, it roughly divides of a white portion and a portion of ashes green. From the result of XRD, it mainly becomes a white portion from Searlesite( $\text{NaBSiO}_5(\text{OH})_2$ ), Calcite( $\text{CaCO}_3$ ), and Orthoclase( $\text{KAlSi}_3\text{O}_8$ ), and the mineral containing lithium is not shown. On the other hand into the portion of ashes green, Calcite( $\text{CaCO}_3$ ), Orthoclase( $\text{KAlSi}_3\text{O}_8$ ), Illite( $\text{K}(\text{Al,Mg,Fe})_2(\text{Si,Al})_4\text{O}_{10}$ ), Rozenite( $\text{FeSO}_4\cdot 4\text{H}_2\text{O}$ ), and Cryolite( $\text{Li}_3\text{Na}_3\text{Al}_2\text{F}_{12}$ ) are contained was obtained. Since the peak of various minerals had appeared, it could not declare that Cryolite existed clearly, but it was suggested that Cryolite may exist as a lithium content mineral.

Next, from the results of SEM+EDS analysis, in the white part, Calcite and Orthoclase were contained at about 10-100 micrometers, and Searlesite existed in it at those circumferences. And in the green gray part, Orthoclase, Calcite, Illite, Rozenite were contained at about 10-30 micrometers, and the particle with a size of 1 micrometer or less existed in those circumferences. Although measurement of Li was not completed in analysis of EDS, it was checked that F is contained in the analysis of these microscopic particles.

From the above result, it was surmised that the lithium content mineral examined this time was Cryolite.

Keywords: lithium, ore deposit, mineral

## The mathematical link between stratigraphic grain size variation of fall deposits and its time variation at the source

IRIYAMA, Yu<sup>1\*</sup> ; TORAMARU, Atsushi<sup>2</sup> ; YAMAMOTO, Tetsuo<sup>3</sup>

<sup>1</sup>Department of Earth and Planetary Sciences, Graduate School of Sciences, Kyushu University, <sup>2</sup>Department of Earth and Planetary Sciences, Faculty of Sciences, Kyushu University, <sup>3</sup>Center for Planetary Science, Kobe University

Pyroclastic fall deposits which are produced by explosive volcanic eruption have various information on the eruption events. The areal distributions of pyroclastic fall deposits such as maximum grain size, median grain size, thickness, mass per unit area, etc. reflect the intensity in a single eruption and the wind conditions. Stratigraphic grain size variations of pyroclastic fall deposits also reflect the temporal behavior of the eruption intensity. For example, normal or reverse grading structures in the pyroclastic fall deposits have been attributed to temporal variation in the volcanic intensity (column height) and/or in the initial grain size distribution at the vent. However, no quantitative methodology has been developed to relate the temporal variation of source characteristics (column height and initial grain size distribution) to stratigraphic variation of grain size distribution at the deposits. In this study, we consider the mathematical description in 1D fall-sedimentation process, which relates the temporal variation of source grain size distribution to stratigraphic variation of grain size distribution.

The number of grains in a size bin must be conserved during sedimentation process and results in the same value at the arrival time on the deposits. The number of a specific-size grains between at the fallout time and at given times is linked by Lagrangian description. The key point is that the grain size and the departure time at the source are mutually related to the grain size and the arrival time at the deposits. As the arrival time corresponds to the stratigraphic location at the deposit, the stratigraphic variation of grain size in the deposit can be connected to the grain size characteristics and departure time at the source using the condition of grain number conservation. As a result, when the time variations of source grain size distribution and of fallout height are given, we obtain the temporal variation of grain size distribution at the sedimentation surface. It means that different sizes of grains which settle at the same arrival time are traced back to the different source time and height. The arrival time on the deposit can be related to the stratigraphic height in the deposit by the differential equation of increasing rate of the thickness, which equals to the volume flux through the sedimentation surface. By using these mathematical descriptions, we develop the mathematical method to link the temporal variation of eruption intensity to the stratigraphic variation of grain size distribution in the fall deposits.

Keywords: pyroclastic fall deposits, grain size distribution, stratigraphic variation, development of eruption

## Color and grainsize of ash samples collected continuously at Sakurajima volcano, Japan

SHIMANO, Taketo<sup>1\*</sup> ; NISHIMURA, Takeshi<sup>2</sup> ; IGUCHI, Masato<sup>3</sup> ; MIKI, Daisuke<sup>3</sup>

<sup>1</sup>Graduate school of Environment and Disaster Research, Tokoha University, <sup>2</sup>Department of Geophysics, Graduate School of Science, Tohoku University, <sup>3</sup>Sakurajima Volcano Research Center, Disaster Prevention Research Institute, Kyoto University

Sakurajima volcano, Southwest Japan, is one of the most active volcano, and one of the leading volcano that are characterized by well-established geophysical observation network and enormous amount of data accumulation. Thus, the changes of magma plumbing system and the explosion processes at Sakurajima are now relatively well-understood for the time scale of years and of several hours, respectively (Iguchi et al., 2013). On the other hand, Sakurajima volcano has experienced several giant explosive eruptions every few hundred years, with some plinian eruptions and with erupted volume in the order of  $>10^8$  m<sup>3</sup>. However, we do not understand the mechanism of phase transition from the recent small eruptions to such bigger ones. Even though we now reached a certain level to recognize that our knowledge of “ vulcanian eruption ” was too simple relative to real one, the fundamental processes that lead to such eruption variety are not yet constrained well enough. As the variety of eruption styles occurs in a time scale of months to days, we have been focusing on the sample acquisition in this time range and collected daily ash samples for years.

We have been succeeded in collecting daily samples by automatic sampling system for more than five years at the site ca 2 km south of Showa crater, Sakurajima volcano (Shimano et al., 2013). We also analyzed matrix glass composition to track chemical evolution of the magma system, and found a shift of FeO\*/MgO in fall of 2009 before the waxing activity toward 2010. On the other hand, we have been searching for some real-time technique of petrological data for the comparison with geophysical data. The development of useful colorimeter and some results of heating experiments of ash resulted in understanding relationship between color of ash and condition of magma at depths (e.g., Yamanoi et al., 2008; Miyagi et al., 2013). So we have made time-series color measurements of ash samples for years. We found L\* value, degree of brightness, decreased broadly during waxing stage in 2009-2010 whereas a\* and b\* values increased broadly at first several months but decrease gradually. These changes can be explained by increase of black fresh lava block particles, increase at the first stage and gradual fluctuating changes of old red oxidized particles in ash sample. We also measured color change of some grain size group and compared with the color of bulk samples. The preliminary results show that the color differs with particle size as Miyagi et al. (2010) reported, but a correlation was found between the color values of bulk sample and those calculated from the weight fraction and each color values.

Keywords: volcanic ash, continuous observation, color change, Sakurajima volcano

## Numerical Simulation of Volcanic Ash Transport for the Eruptions at Mt. Shinmoe-dake during 26-27 January 2011

HASHIMOTO, Akihiro<sup>1\*</sup> ; SUZUKI, Yujiro<sup>2</sup> ; SHIMBORI, Toshiki<sup>1</sup> ; TAKAGI, Akimichi<sup>1</sup>

<sup>1</sup>Meteorological Research Institute, Japan Meteorological Agency, <sup>2</sup>Earthquake Research Institute, The University of Tokyo

The volcanic ash transport associated with the eruptions at Mt. Shinmoe-dake during 26 to 27 January 2011 is simulated using Japan Meteorological Agency Non-Hydrostatic Model (JMA-NHM) to verify the model with satellite observation. In the model, the mixing ratio and number concentration of ash particles are prognosed with the advection, diffusion, sedimentation, and source terms to represent the behavior of ash cloud. Simulation has been performed in the calculation domain covering 2500 km x 2000 km wide area with the horizontal resolution of 5 km.

The model is coupled with one-dimensional eruption column model to define the source term of ash particles, which is simply given as a function of the column height, the level of the release point, and the size of released particle, following Suzuki (1983) and Shimbori et al. (2010). Although the simulated distribution of ash cloud roughly agrees with satellite observation, close examination of the simulation result shows that the model fails to reproduce some of the ash clouds observed by the satellite, which means that much room still remains for improvement in the eruption column model in terms of release point and size spectra of ash particles. Three-dimensional direct numerical simulation has been conducted on a major sub-Plinian eruption during the period at Mt. Shinmoe-dake (Suzuki and Koyaguchi, 2013), in order to make new eruption column model with more realistic function for the source term of ash particles. As a result, it is found that the maximum release rate of the ash particles smaller than 100  $\mu\text{m}$  appears in the height lower than that predicted by the usual eruption column model for same column top height. The authors are developing new eruption column model with realistic profile of release rate, based on this result, so as to improve the reproducibility of the ash transport with JMA-NHM. The sensitivity of the ash transport to altering the new and usual eruption column models will be presented.

### Acknowledgement

This study was supported by the Earthquake Research Institute cooperative research program.

### References

Shimbori, T., Y. Aikawa, K. Fukui, A. Hashimoto, N. Seino, and H. Yamasato, 2010: Quantitative tephra fall prediction with the JMA mesoscale tracer transport model for volcanic ash: A case study of the eruption at Asama volcano in 2009. *Pap. Met. Geophys.*, **61**, 13-29.

Suzuki, T., 1983: A theoretical model for dispersion of tephra. *Arc Volcanism: Physics and Tectonics. TERRAPUB*, 95-113.

Suzuki, Y. and T. Koyaguchi, 2013: 3D numerical simulation of volcanic eruption clouds during the 2011 Shinmoe-dake eruptions. *Earth Planets Space*, **65**, 581-589.

Keywords: volcanic-ash dispersal, Atmospheric Transport Model,, Shinmoe-dake volcano, 2011

## Weather Radar Investigation of Volcanic Smoke for Disaster-Prevention

MAKI, Masayuki<sup>1\*</sup>; IGUCHI, Masato<sup>2</sup>; FUJITA, Eisuke<sup>3</sup>; MAESAKA, Takeshi<sup>3</sup>; SHUSSE, Yukari<sup>4</sup>; KOZONO, Tomofumi<sup>4</sup>; MOMOTANI, Tatsuya<sup>5</sup>; YAMAJI, Akihiko<sup>5</sup>

<sup>1</sup>Kagoshima University, <sup>2</sup>DPRI, Kyoto University., <sup>3</sup>NIED, <sup>4</sup>Tohoku University, <sup>5</sup>Japan Weather Association

Sakurajima volcano has been active since February 2009. The total number of explosive eruptions was 966 in 2011, which was the highest number in recorded history. Corresponding to volcano activities, the ash accumulation in Kagoshima city increased and total ash amount of 3,500g/ m<sup>2</sup> was recorded at Kagoshima local meteorological observatory. Because the volume of volcanic ash in rural area paralyze public ground transportations such as rail road and highway, fast recovery efforts are required to the railroad company and city government. However, no quantitative volcanic ash fall estimation has been established. The present study focuses on utilization of operational weather radar for quantitative ash estimation (QAE), quantitative ash forecasting (QAF), and utilization of crustal movement information for providing ash volume which is necessary for initial conditions of a numerical diffusion model. Although the target volcano of the present study is Sakurajima, the knowledge on volcanic ash and algorithm developed by the present study can be applied to any other volcano which is located in operational weather radar observation area.

Keywords: weather radar, volcanic ash, quantitative ash estimation, Sakurajima, polarimetric radar

## Eruption types determined by the mass flux and volatile component content of ascending magma flow

IDA, Yoshiaki<sup>1\*</sup> ; OIKAWA, Jun<sup>2</sup>

<sup>1</sup>Advance Soft Co., <sup>2</sup>Earthquake Res. Inst., Univ. of Tokyo

Volcanic eruptions include the effusive ones that erupt fluid lava and the explosive ones that emit magma fragments in gassy flows or other forms. Traditionally, explosive eruptions are further classified into Plinian eruptions accompanied by high eruption columns, Pelean eruptions involving abundant pyroclastic flows, Vulcanian eruptions with strong instantaneous explosions, Strombolian eruptions involving periodic lava fountains and so on. Effusive and explosive eruptions are clearly controlled by the efficiency of degassing, but what produces various types of explosive eruptions has not yet been explained quite clearly. In this paper I propose a simple idea about how various explosive eruptions arise depending on the natures of ascending deep magma flow based on a stationary conduit flow model.

The state of erupting magma may be represented by exit velocity and the volatile content that determines the vesicularity of volcanic products. The volatile content is specified by its mass ratio to the fluid magma (including solidified part). On the other hand, it is convenient to represent the deep state of magma flow by the mass flux of fluid magma and the volatile contents before degassing takes place. When the magma flow is in a stationary state the mass flux of fluid magma is constant so that it defines the deep state of magma flow with the initial volatile content independently of the specific depth at which magma ascent starts.

The relation between the surface and deep states of ascending magma is calculated using a stationary conduit flow model. In this calculation the volatile component is assumed to move at the same speed as the fluid magma neglecting relative motions. In bubbly magma horizontal permeable flow of volatile gas is assumed to control the rate of degassing. In this treatment, the pressure gradient that drives the permeable flow is considered to arise from the ascent velocity change from center to side and the resulting difference of relaxation of gas expansion due to decompression (Ida, JVGR, 162, 172-184, 2007). The wall friction is assumed to be proportional to ascent velocity in bubbly flow and to the square of ascent velocity in gassy flow with suitable friction coefficients. The relation for water steam in magma is used for solubility of volatiles in magma.

The integration of conduit flow is executed from the surface to a deep conduit. Namely, the deep state of magma flux and volatile content are calculated for various sets of the exit velocity and volatile content at the surface prescribed with the magma pressure equal to the atmospheric pressure. Compiling the calculation results shows that some groups characterize the relation between the surface and deep conditions. Each group can be interpreted in connection with eruption types in the following way.

Firstly, high-speed gassy flow erupts violently when the deep magma contains sufficiently abundant volatile component. This case may produce a Plinian eruption. In this case the exit velocity and gas content are determined by the deep magma flux alone independently of deep gas content because of adjustment by degassing during the ascent process. Secondly, a stationary conduit flow disappears below the critical value of fluid magma flux with high gas content in a deep conduit. In this case magma flow should be non-stationary and may produce Vulcanian or Strombolian eruptions. Thirdly, a relatively slow magma flow with low vesicularity flows out when volatile component is poor. This case likely results in Pelean eruptions because of difficult acceleration of gassy flow in the air.

Our analysis and interpretation suggest that various eruption types arise from different combinations of ascending magma flux and degassing efficiency. It is non-linearity involved in ascending magma flow with vesiculation and degassing that produces separate groups characterizing eruption types.

Keywords: volcanic eruption type, ascending magma flow, conduit flow model, volatile component content, degassing, computer simulation

## Magma eruption rates, eruption styles, and preeruptive magma viscosity

TOMIYA, Akihiko<sup>1\*</sup> ; KOYAGUCHI, Takehiro<sup>2</sup> ; KOZONO, Tomofumi<sup>3</sup> ; TAKEUCHI, Shingo<sup>4</sup>

<sup>1</sup>Geological Survey of Japan, AIST, <sup>2</sup>Earthquake Research Institute, University of Tokyo, <sup>3</sup>Department of Geophysics, Graduate School of Science, Tohoku University, <sup>4</sup>Civil Engineering Research Laboratory, Central Research Institute of Electric Power Industry

Magma eruption rate is one of the most fundamental parameters for a volcanic eruption (e.g., Pyle, 2000). It is obtained mainly by geophysical or geological observations. We interpret this important parameter from a petrological point of view and also from a fluid dynamic point of view.

We have collected a hundred of data on magma eruption rates, bulk rock chemical compositions, and phenocryst contents for various styles of eruptions (Plinian, sub-Plinian, basaltic Plinian, lava flow, and lava dome). We are compiling these data on the basis of their 'preeruptive magma viscosities', which are important measures of magma eruptibility (Takeuchi, 2011). Preeruptive magma viscosity is the viscosity of magma (melt + crystals) in the magma chamber at the preeruptive conditions. This value can be obtained by the bulk rock chemical composition and phenocryst content, using an empirical formula (Takeuchi, 2010). We have found that eruption styles are closely correlated to preeruptive magma viscosities but poorly correlated to bulk rock compositions.

We have also examined the difference in magma eruption rates between the explosive phase(s) (e.g., Plinian) and the effusive phase (e.g., dome) in a series of eruptions, in order to understand the transition between these two eruption styles (e.g., Kozono and Koyaguchi, 2009a,b). We have found that the difference is positively correlated to preeruptive magma viscosity.

The above results indicate that preeruptive magma viscosities largely control eruption styles and eruption rates. Our results also show that the eruptive magmas are divided into two types, low-viscosity type (basalt to low-phenocryst-content andesite) and high-viscosity type (high-phenocryst-content andesite to rhyolite). The boundary is at about  $10^4$  Pa s. These two types may be closely linked to the magma generation processes (e.g., fractional crystallization and melt segregation from crystal mush).

**Keywords:** magma eruption rates, eruption styles, preeruptive magma viscosity, transition between explosive and effusive eruption, phenocryst content, bulk rock chemical composition

## Conditions for transition from lava dome to explosive eruption

KOZONO, Tomofumi<sup>1\*</sup>; KOYAGUCHI, Takehiro<sup>2</sup>

<sup>1</sup>Department of Geophysics, Graduate School of Science, Tohoku University, <sup>2</sup>Earthquake Research Institute, University of Tokyo

Conduit flow dynamics involving magma vesiculation, gas escape, and crystallization during a lava dome eruption lead to complex processes such as a transition to an explosive eruption. Because the transition from the lava dome to the explosive eruption is accompanied with a drastic increase in eruption intensity, it is important for volcanic hazard mitigation to determine conditions for this transition to occur. In this study, on the basis of a 1-dimensional conduit flow model, we investigated how the conditions for the transition from the lava dome to the explosive eruption depend on magmatic and geological parameters.

In order to systematically investigate the dependence of the transition conditions on the magmatic and geological parameters, we used the relationship between chamber pressure ( $p_{ch}$ ) and mass flow rate ( $q$ ) for steady conduit flow (the  $p_{ch}$ - $q$  relationship). When the slope of the  $p_{ch}$ - $q$  relationship ( $dp_{ch}/dq$ ) has a positive value (positive differential resistance), the steady flow is stable. When  $dp_{ch}/dq$  has a negative value (negative differential resistance), on the other hand, the steady flow is unstable. The negative differential resistance is generated by two positive-feedback mechanisms. First, effective magma viscosity decreases with increasing  $q$  because of delay of crystallization, leading to reduced viscous wall friction (feedback 1). Second, magma porosity increases with increasing  $q$  because of less efficient gas escape, leading to reduced gravitational load (feedback 2). These two feedback mechanisms induce a sigmoidal  $p_{ch}$ - $q$  relationship for some realistic conditions; the positive differential resistance in the low- $q$  and high- $q$  regimes, and the negative differential resistance in the intermediate regime. The analyses of time-dependent conduit flow model indicate that, because of the sigmoidal  $p_{ch}$ - $q$  relationship, as magma supply at depth gradually increases from the low- $q$  regime to the intermediate regime, magma discharge rate abruptly increases from the low- $q$  to high- $q$  regimes. This abrupt increase in magma discharge rate accounts for the transition from a stable lava-dome eruption to an explosive eruption. We, therefore, define the value of  $q$  at the boundary between the low- $q$  and the intermediate regimes as the critical magma supply rate for the transition ( $q_{cr}$ ).

Our results show that  $q_{cr}$  is mainly controlled by the feedback 2 for a wide range of magmatic and geological conditions, whereas it is controlled by the feedback 1 only when phenocryst content is very high. When  $q_{cr}$  is controlled by the feedback 2, the value of  $q_{cr}$  depends on parameters related to gas escape such as the permeability for vertical gas escape and that for lateral gas escape. We found that for a plausible range of vertical permeability which is constrained from permeability measurements of volcanic rocks,  $q_{cr}$  remarkably decreases with decreasing lateral permeability, and it becomes substantially lower than typical magma discharge rates for observed lava-dome eruptions in the limiting case of zero-lateral permeability (i.e. no lateral gas escape). This indicates that the presence of lateral gas escape is a necessary condition for a stable lava-dome eruption to occur. In addition, we found that  $q_{cr}$  strongly depends on conduit radius owing to the effects of the change in the conduit radius on the degree of gas escape. As the conduit radius decreases, the ascent of the liquid is suppressed because of the increase in wall friction force, which promotes vertical gas escape. The decrease in the conduit radius also induces an increase in the ratio of the perimeter to the cross-sectional area of the conduit and a decrease in the length scale of pressure gradient that drives lateral permeable gas flow, which promotes lateral gas escape. These promotions of gas escape lead to an increase in  $q_{cr}$ . The above results suggest that the variation of conduit radius is a key factor for the transition from a lava-dome to an explosive eruption.

Keywords: conduit flow, numerical model, eruption transition, lava dome, explosive eruption, gas escape

## A phreatic explosion model for Mayon volcano, Philippines, inferred from analyses of an explosion earthquake

MAEDA, Yuta<sup>1\*</sup>; KUMAGAI, Hiroyuki<sup>1</sup>; LACSON, Rudy<sup>2</sup>; FIGUEROA, Melquiades<sup>2</sup>; YAMASHINA, Tadashi<sup>3</sup>; OHKURA, Takahiro<sup>4</sup>; BORNAS, Antonia<sup>2</sup>

<sup>1</sup>Nagoya University, <sup>2</sup>PHIVOLCS, <sup>3</sup>Kochi University, <sup>4</sup>Kyoto University

Mayon is one of the most active volcanoes in the Philippines with 49 known historical eruptions from 1616 to 2010. A phreatic explosion took place at Mayon on 7 May 2013 that killed five climbers. In this presentation, we show the results of the waveform inversion for the explosion earthquake and discuss a phreatic explosion model for Mayon.

During the explosion in 2013, a VLP event with a peak frequency of 0.4 Hz was recorded by three broadband seismometers which we had installed in 2011. We performed a frequency-domain waveform inversion in 0.1-0.6 Hz, which pointed to a combination of a subhorizontal tensile crack and a vertical single force at a shallow part beneath the summit crater. Contributions from the crack and force to the waveforms had amplitudes comparable to each other.

The source time functions obtained by the waveform inversion are bandpassed forms (filtered source time functions; FSTFs), which may be different from the source time functions without filters (deconvolved forms of the source time functions; DSTFs). Instead of performing numerically unstable deconvolution operations, we assumed simple step- and impulse-type functions with finite durations as candidates of the DSTFs. We applied the bandpass filter to these functions and compared with the FSTFs. The bandpassed waveforms of the impulse-type functions were similar to the FSTFs for both the crack and force, suggesting that the DSTFs can be approximated by the impulse-type functions. The estimated DSTF for the tensile crack showed an inflation followed by a deflation, whereas that for the single force showed a downward force around the time of the maximum opening of the crack.

The RMS seismic amplitudes, GPS baseline lengths over the volcano, ground surface temperatures around the summit, waveform correlations among the seismic stations, the sulfur dioxide emission, and rainfall did not show clear precursory signals.

Since the analyzed VLP event occurred during the phreatic explosion, the initial inflation in the DSTF for the crack may have been caused by boiling of underground water. This crack is subhorizontal and located at a shallow part, suggesting that the crack may be located on a boundary between permeable and impermeable layers where the water may have accumulated and finally boiled, generating the explosion. The downward force may represent the counter force of the explosion. The deflation of the crack in the latter half of the DSTF may have been caused by outgassing of water vapor during the explosion.

The estimated moment amplitude is explained by a volume change of  $400 \text{ m} \times 400 \text{ m} \times 0.4 \text{ m}$ . A topographic change comparable to this crack size was not observed during the explosion, suggesting that the explosion destroyed only a limited portion of the crack. This crack may repeat the explosion once the fragmented portion of the crack is sealed through the hydrothermal alteration. At Mayon, small ash explosions occurred in 2003, 2004, 2006, and 2009, with intervals of a few days to a few years (mostly longer than one month). These intervals are close to experimentally derived time scales of fracture sealing by the hydrothermal alteration; according to the experiments by Berger et al. (1994, *Geochim. Cosmochim. Acta*), who used basalt samples with chemical compositions similar to magmatic eruption deposits at Mayon, a centimeter-order fracture is sealed in two months for 300 °C and 54 months for 150 °C.

In this model, timings of the explosions are controlled by the sealing of the fracture. Therefore the explosions can occur even with a constant supply of heat and water. This may be the reason why no clear precursory signals were observed before the explosion in 2013. No VLP events other than that associated with the explosion in 2013 have been observed at Mayon since the beginning of the observation in 2011, which may be explained by the sealing of the fracture just prior to the explosion.

**Keywords:** Phreatic explosion, Waveform inversion, Source time function, Hydrothermal alteration

## Magma accumulation process of Izu-Oshima volcano, as revealed from deep LF earthquakes, deformation and CO<sub>2</sub> out-gassing

WATANABE, Hidefumi<sup>1\*</sup>

<sup>1</sup>Disaster Prevention Division, Tokyo Metropolitan Government

In order to make successful mid-term eruption predictions, we need to detect particular precursory processes operating in magma-plumbing system. Since 1989, Izu-Oshima volcano has continued its re-inflation, after the last eruption in 1986, and further repeated deflation-inflation cycles, resulting a net inflation of the volcano. The rate of secular inflation decreased exponentially until 2006, while the amplitudes of the deflation-inflation cycles increased. Since 2007, the rate of secular inflation has kept a constant speed and has also increased the activity of deep low-frequency (LF) earthquakes occurring at the depth range of 30-40 km beneath the volcano. Each episodic LF earthquake activity was preceded by the volcano deflation and accompanied by the inflation. Based on these evidences, we may suppose that the volcano inflation is caused by the supply of magma from a source region at the depth range of 30-40 km beneath the volcano, and that an episodic out-gassing from the shallow magma reservoir triggers each deflation-inflation cycle. To demonstrate the proposed mechanism, we need to combine the data on magma accumulation and out-gassing processes. To monitor the out-gassing of basaltic magma accumulating beneath the volcano, CO<sub>2</sub> is most helpful. In September 2005, we started continuous monitoring of soil CO<sub>2</sub> concentration at the summit of Izu-Oshima volcano, and obtained an evidence for the out-gassing process; the correlated increase of soil CO<sub>2</sub> concentration during the periods of not only accelerated inflation but also deflation of the volcano. Integrating the observational data, we suppose that the rate of magma supply from the upper mantle has increased since 2007 and that the increase in amplitude of deflation-inflation cycles might indicate a volume increase of CO<sub>2</sub> over-saturated region at the upper part of the magma reservoir beneath the volcano.

Keywords: Izu Oshima volcano, eruption prediction, precursors to eruption, volcano deformation, CO<sub>2</sub> out-gassing

## Spatio-temporal characteristics of volcanic tremor during the 2011 Kirishima eruption by seismic wave analysis

NAKAMOTO, Manami<sup>1\*</sup>; MATSUMOTO, Satoshi<sup>1</sup>; YAMANAKA, Yoshiko<sup>2</sup>; SHIMIZU, Hiroshi<sup>1</sup>; NAKAMICHI, Haruhisa<sup>4</sup>; ICHIHARA, Mie<sup>3</sup>; OIKAWA, Jun<sup>3</sup>

<sup>1</sup>SEVO, Kyushu Univ., <sup>2</sup>EVRC, Nagoya Univ., <sup>3</sup>ERI, University of Tokyo, <sup>4</sup>DPRI, Kyoto Univ.

Volcanic tremors are considered as oscillations occurred in magma supply system and provide us important information about condition of the system from magma chamber to crater through a conduit. Therefore, it is important to investigate locations of their source and their characteristics for understanding the condition and process of volcanic activity and modeling the magma supply system. In this study, we reveal features of volcanic tremor using seismic data at Kirishima volcano.

An array observation help us to get information of incident waves on the stations. The two array seismic observations were carried out around Shinmoe-dake during the 2011 Kirishima eruption. One consisted of 25 seismometers located 3 km southwest of the Shinmoe-dake crater (Matsumoto et al., 2013), and the other consisted of 16 seismometers located 5 km northeast of the crater (Nakamichi et al., 2013). The combining data from two arrays enable us to determine the tremor sources. Moreover, we estimated mechanism of the tremor source by using waveforms recorded at temporal seismic station in Kirishima volcanic area and tremor sources obtained by array analysis.

This study focus on the volcanic tremor which occurred on February 2, 2011, and its duration was about 40 minutes. Peak frequencies of the tremor were about 1, 2, 3, and 4 Hz. We investigated temporal variation in the source location of the tremor from the slowness and azimuth of incident wave by MUSIC method. we found that most part of the tremor were radiated around Shinmoe-dake crater. In this part, the tremor that had large slowness and relatively long duration was located in shallow region beneath the crater. In contrast, at some parts of the tremor, source location for waves with short duration were near Ohnami pond, 3.3 km northeast of the crater. Based on amplitude analysis for the seismogram recorded by the seismic network, we also found out difference in radiation patterns of the volcanic tremor among the tremor sources. Assuming single crack model, we found the strike and dip direction of the crack beneath the Shinmoe-dake crater is different from those near Ohnami pond.

Keywords: volcanic tremor, Shinmoedake

## Relationship BH-type earthquake swarms and ground deformations prior to eruptions at Showa crater at Sakurajima volcano

TAMEGURI, Takeshi<sup>1\*</sup> ; IGUCHI, Masato<sup>1</sup>

<sup>1</sup>DPRI, Kyoto University

Vulcanian eruptions have occurred at the Minamidake crater at the summit since 1955 at Sakurajima volcano. Principal eruptive activity shifted to the Showa crater at the eastern flank of the summit in 2006. The eruptions at the crater become active and minor vulcanian eruptions occurred about 1,000 times per year in 2010-2013. Ash plume height of the eruptions sometimes reached to 3000m in 2013. The eruptive activities at the Showa crater gradually increase.

Inflationary strain changes are observed by extensometers a few tens of minutes to several hours prior to the eruptions and are caused by pressure sources located at depths of 0-1.5 km (Iguchi et al., 2013). The inflation rates decrease or sometimes suspend about 30 minutes before the eruptions. Small earthquakes dominated by high frequency components (5-6 Hz) swarm when duration of inflation is longer than 1 hour. The hypocenters of the earthquakes are located at a depth of 0.5 km beneath the crater and are close to depth of the pressure source. The earthquakes begin to occur a half hour to 1 hour after the start of the inflation. The amplitudes and number of the earthquakes further increase when the inflation rates decrease or suspend. And, the occurrences of the earthquakes suddenly stop at the start of the eruptions. The occurrences of the earthquake swarms are related to the decrease of inflation rate and the long inflation.

Seismic energy releases of the precursory earthquakes related to every eruption accelerate before eruptions. There are all kinds of large and small seismic energy releases in the eruptions. The accelerations of the seismic energy releases before eruptions with explosive events tend to be larger than those with non-explosive events. And, the accelerations of the seismic energy releases are rapid in the case of large deflations after eruptions. The precursory earthquakes may be generated by release of excess pressure accumulated by inflation of the pressure source. We might be able to predict eruption types and scales from occurrence patterns of the precursory earthquakes.

Keywords: Sakurajima volcano, precursory earthquake, ground deformation

## Volcanic tremor caused by flow-induced oscillation of a magma-filled dike

SAKURABA, Ataru<sup>1\*</sup>; YAMAUCHI, Hatsuki<sup>2</sup>

<sup>1</sup>Department of Earth and Planetary Science, University of Tokyo, <sup>2</sup>Earthquake Research Institute, University of Tokyo

Volcanic tremor (VT) is known to be long-period and long-duration ground motion generally observed during or before eruptions. Majority of VTs show an emergent onset and, when accompanied with eruptions, an exponentially growing phase in amplitude is typically observed (Konstantinou and Schlindwein 2002; McNutt and Nishimura 2008). This characteristic suggests that VT is manifestation of self-oscillation, in which a persistent steady forcing excites an eigen oscillation of a system and the amplitude exponentially grows until a nonlinear process leads to a limit cycle. In volcanic settings, a steady magma flow through an underground conduit may cause flow-induced self-oscillation of bedrocks, and this is the idea first presented by Julian (1994). In the case of the collapse of Tacoma Narrows bridge, which is known to be caused by flow-induced oscillation, the vibrating bridge can be modeled by an elastic plate placed parallel to an infinite flow. Here we consider a reversed setting: a fluid-flowing thin layer in an infinite elastic body. This system is also unstable if the flow speed is high enough, and may be a generation mechanism of some VTs.

We consider a fluid-flowing plane layer sandwiched between two semi-infinite elastic bodies, expanding Julian's idea to a more general elastodynamic model (for details, see Sakuraba and Yamauchi 2014 to appear in *Earth, Planets and Space*). The eigen oscillation that should be excited in this self-oscillation model is an elastic surface wave. Therefore, we solve the Navier-Stokes equation linearized about a laminar flow with the boundary condition that can maintain a surface wave traveling along the layer. We succeeded in obtaining a complex phase speed of the surface wave as a function of wavenumber (and some parameters) using a shooting method, and found that a relatively slow magma flow could lead to instability in which the imaginary part of the phase speed is positive. Remarkably, the most unstable mode exhibits an antisymmetric (flexural) deformation, which has not been discussed in previous similar studies (Balmforth, Craster and Rust 2005; Dunham and Ogden 2012). The unstable mode is identical to two parallel Rayleigh waves traveling against the basic magma flow. The instability can be understood as acceleration of nearly circular particle motion of the Rayleigh wave due to viscous drag of the main laminar flow. As the critical flow speed giving a neutrally stable state decreases in inversely proportional to wavelength, instability will occur with the largest possible wavelength, which could be several kilometers and produce an oscillation period of around 1 second. In that case, the critical flow speed can be reduced to less than 1 m/s when the magma is basaltic. As the magma flow speed in a dike will not exceed several meters per second, there would be a lower bound in the critical wavelength, producing a period of 0.1 second. Thus our model naturally explains typical periods of 0.1-1 seconds observed on volcanoes. Our model also explains typical timescales of the linearly growing phase in some VTs.

## Magnitude-frequency distribution of volcanic eruptions from an open conduit

NISHIMURA, Takeshi<sup>1\*</sup> ; IGUCHI, Masato<sup>2</sup> ; MUHAMAD, Hendrasto<sup>3</sup> ; AOYAMA, Hiroshi<sup>4</sup>

<sup>1</sup>Science, Tohoku Univ., <sup>2</sup>DPRI, Kyoto Univ., <sup>3</sup>CVGHM, Indonesia, <sup>4</sup>Science, Hokkaido Univ.

Explosive eruptions such as vulcanian, strombolian, or significant gas burst excite seismic waves. Such seismic signals, which are often called as explosion earthquakes or explosion quake, are used to quantitatively evaluate the magnitude of such volcanic explosions. In the present study, we systematically examine magnitude-frequency distributions of explosion earthquakes observed at Sakurajima and Suwanosejima volcanoes in Japan, and Semeru and Lokon volcanoes in Indonesia. We use the long-term catalog data of Sakurajima explosions for the period from 1963 to 2011, which are routinely summarized by Sakurajima Volcano Research Center (SVRC). Also, we measure the amplitudes of explosion earthquakes from continuous seismic records observed at Suwanosejima and Semeru and Lokon volcanoes in Indonesia. We measure the number of earthquakes that exceed a given amplitude, and then plot the cumulative number of earthquakes versus amplitude, as is often done for examining Ishimoto-Iida's relation, which expresses a power law distribution. However, the observed frequencies of earthquakes at the four volcanoes do not seem to fit the Ishimoto-Iida's relation. The cumulative numbers are well explained by exponential functions. This means that the magnitude of explosion earthquake at each volcano is randomly determined with an average scale.

Keywords: Volcanic Explosion, Vulcano, Gas burst, Magnitude-frequency distribution

## Rheological transition of plagioclase-bearing magma: high-temperature uniaxial deformation experiments of sanukite lava

ISHIBASHI, Hidemi<sup>1\*</sup>

<sup>1</sup>Graduate School of Science, Shizuoka University

High-temperature uniaxial compression experiments were done for bubble- and phenocryst-free, plagioclase-bearing lava to investigate the effect of tabular crystals on rheological properties of highly crystalline magma. High-Mg andesite lava from Goshikidai lava plateau, southwest Japan, was used for starting material. The lava is bubble- and phenocryst-free, composed of 60 vol.% rhyolitic glass, 36 vol.% of tabular plagioclase and 4 vol.% of pyroxenes and magnetite and plagioclase crystals are well aligned parallel. High-temperature uniaxial deformation apparatus at Earthquake Research Institute, the University of Tokyo, was used for experiments. The lava was cut to 10 x 10 x 20 mm rectangular solids and deformed under conditions of temperatures of 1238, 1188, and 1138 K and deformation rates from 3.16 to 0.003 mm/min. Run samples were quenched and processed to thin section for textural and compositional analyses by using EPMA.

Phase proportions in all run samples were the same as that of starting material, indicating crystallization did not occur during experiments. The lava behaves as shear thinning fluid under all temperature conditions. Viscosity at strain rate of  $10^{-4} \text{ s}^{-1}$  increases from  $10^{8.7}$  to  $10^{9.4}$  Pas with decreasing temperature. Power law exponent [=  $d(\log \text{ viscosity})/d(\log \text{ strain rate})$ ] is ca. 0.64, which is consistent with extrapolation of previous studies for natural plagioclase-bearing magmas. Relative viscosity [=  $(\text{bulk viscosity})/(\text{melt viscosity})$ ] is ca.  $10^{2.4}$  at strain rate of  $10^{-4} \text{ s}^{-1}$  under all temperatures, indicating that the concept of relative viscosity works well under present experimental condition. The relative viscosity-crystal fraction relation is also consistent with extrapolation of previous studies for natural plagioclase-bearing magmas. Marron-Piece equation well explains the relation with the maximum packing fraction of 0.43. Present results suggest that rheological transition occurs at crystal fraction near 0.43 for plagioclase-bearing natural lava in which plagioclase crystals are well aligned parallel. The value is higher than ca. 0.3 proposed by Picard et al. (2013)'s experiments in which plagioclase orientation is random in starting materials, indicating the first order importance of plagioclase orientation distribution on rheological transition.

Keywords: rheological transition, viscosity, magma, plagioclase, non-Newtonian fluid, sanukite

## Conduit flow of silicic magma: Viscous flow or Frictional sliding?

OKUMURA, Satoshi<sup>1\*</sup> ; UESUGI, Kentaro<sup>2</sup>

<sup>1</sup>Department of Earth Science, Graduate School of Science, Tohoku University, <sup>2</sup>Japan Synchrotron Radiation Research Institute

Outgassing rate and bulk magma viscosity that control the style of volcanic eruptions depend on flow type of magma ascending in a volcanic conduit. When magma behaves as a Newtonian fluid, magma in the conduit experiences shear strain large enough to cause effective outgassing. On the other hand, once shear starts to localize, bulk magma viscosity may decrease due to slip deformation and outgassing rate also decreases in parts other than shear-localized region (Okumura et al., 2013 EPSL). Silicic magma experiences shear-induced brittle fracturing and subsequent frictional sliding along the fracturing zone during its ascent (e.g. Gonnermann and Manga, 2003 Nature; Tuffen et al., 2003 Geology). Therefore, outgassing rate and bulk magma viscosity during the ascent are expected to change dramatically. Previous studies (Tuffen et al., 2003 Geology; Gonnermann and Manga, 2005 EPSL) also proposed that fractured magma can heal during magma ascent and that fracturing and healing processes may control the dynamics of magma ascent. In contrast to this model, some experimental studies (e.g. Okumura et al., 2010) indicated that fractured magma cannot heal as long as the deformation continues. In this study, we perform deformation experiments for fractured magma to investigate flow type of magma in the conduit, i.e. viscous flow or frictional sliding, and controlling factors of the transition from viscous flow to frictional sliding.

The deformation experiments were carried out using a custom-made torsional deformation apparatus which was installed in synchrotron radiation X-ray imaging system (BL20B2) of SPring-8. To simulate fractured silicic magma, we crushed rhyolite obsidian and sorted them into fragments of 75-250  $\mu\text{m}$  in size. The powdered sample was sandwiched by two obsidian discs and they were twisted by rotating a piston attached with a rotational motor. The torsional deformation experiments were performed at temperatures of 800 and 900  $^{\circ}\text{C}$  under 1-10 MPa pressures. The rotational rate was set to be 0.1 to 10 rpm, corresponding to strain rates of  $10^{-2}$  to  $1 \text{ s}^{-1}$  if the sample deforms homogeneously. The deformed samples were observed in situ using an X-ray radiography.

At a temperature of 900  $^{\circ}\text{C}$  and rotational rates of 0.1-1 rpm, homogeneous deformation through a sample was observed under a pressure of 10 MPa, which indicates viscous deformation. In contrast, the sliding at the interface between powdered obsidian and the disc was observed under 1 and 5 MPa pressures. At a temperature of 800  $^{\circ}\text{C}$ , the sliding was found under 1-10 MPa pressures. These results indicate that frictional sliding along fractured zone is flow type of magma in shallow parts of the conduit (<10 MPa).

We assume that flow type is determined by competition of shear stress necessary for viscous flow and frictional sliding. If magma has high viscosity and shear stress to deform a sample viscously is large, the flow type becomes frictional sliding. At a temperature of 900  $^{\circ}\text{C}$ , viscous flow and frictional sliding were found at 10 and 1-5 MPa pressures, respectively. At this condition, magma viscosity is approximately  $10^7 \text{ Pa s}$  (Hess and Dingwell., 1996) and shear stress necessary for viscous deformation is 1 MPa at a strain rate of  $0.1 \text{ s}^{-1}$ . Because the frictional sliding was observed at pressures of 1-5 MPa, the frictional coefficient is estimated to be ca. 0.1. When we use this value and the criterion for shear-induced brittle fracturing proposed by Okumura et al. (2010), the dynamics of magma ascent is controlled by frictional sliding at shallow parts of the conduit. In addition, silicic magma can ascend quickly due to low frictional coefficient of fractured magma.

Keywords: Silicic magma, Volcanic eruption, Viscous flow, Frictional sliding, Synchrotron radiation X-ray

## Mechanism of delayed brittle-like fragmentation of vesicular magma analogue

KAMEDA, Masaharu<sup>1\*</sup> ; SHIDA, Tsukasa<sup>1</sup> ; ICHIHARA, Mie<sup>2</sup> ; TSUGO, Mitsuaki<sup>1</sup> ; OKUMURA, Satoshi<sup>3</sup> ; UESUGI, Kentaro<sup>4</sup>

<sup>1</sup>Mech. Sys. Eng., TUAT, <sup>2</sup>ERI, Univ. of Tokyo, <sup>3</sup>Earth Sci., Tohoku Univ., <sup>4</sup>JASRI

Magma fragmentation is a key phenomenon controlling volcanic eruptions. The fragmentation is classified into two styles: solid-like brittle fragmentation and liquid-like ductile fragmentation. Brittle fragmentation is more hazardous than ductile fragmentation because violent release of pressurized gas in the bubbles contained in the magma may lead to explosive eruptions

The fragmentation of magma, which is a viscoelastic fluid, occurs through a combination of viscoelasticity and rapid deformation. We conducted a rapid decompression experiment over ten years in order to clarify the viscoelastic effect on the fragmentation using a magma analogue, syrup containing gas bubbles (Kameda et al GRL 2008; Kameda et al. JVGR 2013).

Through the experiment we demonstrated the existence of a transitional fragmentation behavior. This transition behavior, which we refer to herein as brittle-like fragmentation, occurred even if the response of material should be in a ductile manner. Comparing the realistic decompression time with the viscoelastic relaxation time for magma, it is more probable that the fragmentation in the real volcanic system occurs in a brittle-like manner.

Observation by high-speed photography using a visible light-source indicated that the onset of brittle-like fragmentation was triggered by the sudden release of a considerable amount of gas from a crack in the specimen. Further observation (Shida et al. IAVCEI 2013) showed that reducing the volume of the specimen suppressed the onset of fragmentation even if their brittleness (Ichihara and Rubin 2010) was close to unity. In our case, the pore distribution of the small samples was more uniform than that of large samples. This observation implies that the crack is initiated from the interior of the specimen due to non-uniform spatial distribution of bubbles.

Then, we observed the interior of the specimen by synchrotron X-ray tomographic microscopy. The X-ray tomographic microscopy was performed at the BL20B2 beamline of the Japan Synchrotron Radiation Research Institute (JASRI, Hyogo, Japan). Initial structure of the specimen was observed by three-dimensional tomographic imaging. High-speed radiography was performed during the decompression. A digital charge-coupled device (CCD) camera was used as the detector whose imaging area is about 16 mm (horizontal) by 5 mm (height) with spatial resolution of 8  $\mu\text{m}/\text{pixel}$ . We took 1800 projections over 180 degrees of rotation for tomographic imaging. The framing rate of radiography is 200 frames per second. We successfully captured a series of images during the brittle-like fragmentation. The reconstructed 3D image of the specimen indicated that the brittle-like fracture was initiated at a notch and a chain of small bubbles in the vicinity of a large bubble.

We propose the following scenario for brittle-like fragmentation: It is initiated from ductile growth of internal cracks by connection of bubbles. The stress concentration and the brittleness at crack tip may exceed the critical level at some moment, which leads to brittle failure of the crack. Rapid decompression due to sudden release of a considerable amount of gas from the crack may increase local brittleness to cause partial fragmentation. Such a sequence from ductile crack growth to partial fragmentation may successively occur in brittle-like fragmentation.

Keywords: Magma, Fragmentation, Viscoelasticity, Decompression, X-ray CT

## Approach by volcanic observation for dynamics of volcanic phenomena

IGUCHI, Masato<sup>1\*</sup>

<sup>1</sup>DPRI, Kyoto University

Dynamics of volcanic activity has been revealed by various kinds of observation. Inflation of volcanic body prior to eruptions corresponds to intrusion of magma to the underground of volcanoes and deflation is accompanied by eruptive activity.

Prior to vulcanian eruptions, minor deflation is detected. This corresponds to leakage of volcanic gas from a gas pocket formed at the uppermost conduit. The minor deflation reflecting minor pressure decrease induces a sudden degassing in oversaturated magma. The sudden degassing corresponds to a volume increase at a deep part in the conduit, as revealed by outward first motions of explosion earthquakes. The volume increase attained at the top of the conduit and the gas pocket overbursts. As the results of collapse of the gas pocket, infrasound of air-shock type is generated with ejection of incandescent bombs followed by ejection of volcanic ash.

Keywords: vulcanian eruption, Sakurajima

## Tephra-Fall Predictions with the JMA Regional Atmospheric Transport Model for the 1914 Eruption at Sakurajima Volcano

SHIMBORI, Toshiki<sup>1\*</sup> ; SHIRATO, Shomei<sup>2</sup> ; HASEGAWA, Yoshihiko<sup>3</sup> ; HASHIMOTO, Akihiro<sup>1</sup> ; TAKAGI, Akimichi<sup>1</sup> ; YAMAMOTO, Tetsuya<sup>1</sup> ; YAMAMOTO, Akira<sup>1</sup>

<sup>1</sup>Meteorological Research Institute, <sup>2</sup>Kagoshima Local Meteorological Office, <sup>3</sup>Japan Meteorological Agency

A hundred years ago, the largest eruption in 20th century Japan, *i.e.* the Sakurajima Taisho Eruption occurred on 12 January 1914. With this eruption, tephra-falls were observed large-area in Japan from Kyushu to Tohoku region (Hasegawa, 1914; Omori, 1916). For such large-scale eruptions, the Meteorological Research Institute (MRI) is going to do new research project of the tephra-fall predictions with the JMA Regional Atmospheric Transport Model (JMA-RATM) from this year. The research will lead to the improvement of the Volcanic Ash Fall Forecasts (VAFFs) of the Japan Meteorological Agency (JMA). For the purpose of investigating the predictability of the current JMA-RATM against large-scale eruptions, predictions of volcanic-ash dispersion and tephra-fall for the Sakurajima Taisho Eruption were carried out. The initial values which are the total volume (ash and pumice) of  $6 \times 10^8 \text{ m}^3$ , the plume height of 3000-18000 m and the eruption duration of 38 hours are assumed based on Yamashina (1999), Yasui *et al.* (2006), Iguchi (2014) and so on. The input GPVs are the JMA Mesoscale Analysis after 28 March 2013. The forecast time by the JMA-RATM is 72 hours from starting time. Results of the calculations indicate that, under the assumption of the ash-density of  $1 \text{ g/cm}^3$ , the predictions of tephra-fall depths are over 1 m in Sakurajima Island for weak-wind weather condition, several 10 cm at Kagoshima City for easterly wind in summertime, and of the order of 0.1-1 mm at Osaka, Nagoya and Tokyo Metropolitan area for southwesterly wind field. In the atmosphere, dispersions of volcanic-ash up to Tohoku and Hokkaido region are also predicted at the same forecast time.

In the presentation, from the results of volcanic-ash dispersion and tephra-fall prediction, the predictability and problems of the current JMA-RATM for large-scale eruptions will be reported.

### References

- Hasegawa, K., 1914: Summary report on the Sakurajima eruption. *Geophys. Rev.*, **170**, Central Meteorological Observatory, Tokyo, 1-16.
- Iguchi, M., 2014: The centennial anniversary of the Taisho Eruption. Lecture note, Ceremony for the Sakurajima Taisho Eruption 100th Anniversary.
- Omori, F., 1916: Accumulation and transportation of ashes thrown out during the Sakura-jima eruptions of 1914: The Sakura-jima eruptions and earthquakes II. *Bull. Imperial Earthq. Invest. Comm.*, **8**, 113-133.
- Yamashina, K., 1999: Volcanic cloud height of the 1914 eruption at Sakurajima volcano - Discussions on documentary records and photographs. *Bull. Volcanol. Soc. Japan*, **44**, 71-82.
- Yasui, M., M. Takahashi, K. Ishihara and D. Miki, 2006: Records on the 1914-1915 eruption of Sakurajima volcano, Japan. *Proc. Inst. Nat. Sci.*, Nihon Univ., **41**, 75-107.

Keywords: Atmospheric Transport Model, volcanic-ash dispersal, tephra fall, Volcanic Ash Fall Forecast, Sakurajima volcano, 1914

## Evaluation of wind data for tephra dispersion simulations

KIYOSUGI, Koji<sup>1\*</sup> ; KOYAGUCHI, Takehiro<sup>1</sup> ; SUZUKI, Yujiro<sup>1</sup>

<sup>1</sup>Earthquake Research Institute, University of Tokyo, Tokyo, Japan

Understanding how pyroclasts disperse from volcanic plumes is a fundamental problem of volcanology to reconstruct eruption conditions from tephra fallout deposits. Tephra dispersion is not only a scientifically interesting but also socially and economically important problem. For this reason, advection-diffusion models for tephra transportation have been developed with simplified assumptions (e.g. TEPHA2, PUFF, FALL3D). Simulation results of these advection-diffusion models are affected by the input wind data. For example, in a case study of the Kirishima 2011 eruption with PUFF, simulation results with finer temporal-spatial resolution wind data (Japan Meteorological Agency Mesoscale Model and ERA Interim) reproduced a more wavy shape of observed eastward extending plume (about 900 km from the vent) than that with coarser temporal-spatial resolution wind data (NCEP/NCAR Reanalysis).

Some wind data are available from Japan Meteorological Agency Mesoscale Model, ERA Interim of the European Center for Medium-Range Weather Forecasts and NCEP/NCAR Reanalysis of the National Oceanic and Atmospheric Administration of the United States. Between these wind data, there are differences in data assimilation methods, forecast models and temporal-spatial resolution. In addition, a finer temporal-spatial resolution wind data can be generated with using weather forecast models, such as the Weather Research and Forecasting (WRF) model. The WRF model is a fully compressible, Euler non-hydrostatic mesoscale forecast model developed by a multiagency collaboration. The WRF model is suitable for use in a broad spectrum of applications across scales ranging from meters to thousands of kilometers.

We are developing a system to generate wind data suitable for simulations of the advection-diffusion models. Such wind data should have a spatial resolution of several hundred meters near the vent, that of several kilometers far from the vent and vertically several tens of layers. In addition, it must be required to reproduce the interaction between ambient atmosphere and volcanic plumes. For this purpose, we are carrying out numerical calculations with the WRF model and the available wind data sets; we attempt to generate wind data with higher temporal-spatial resolution using data assimilation based on the observations from the regions of interest (e.g. volcano locations and downwind area) and other observations (e.g. the radar observations).

Keywords: Tephra dispersion simulation, Weather forecast model

## Classification of infrasound waveforms and analysis of video images at volcano eruption

SATO, Yusuke<sup>1\*</sup> ; YOKOO, Akihiko<sup>1</sup>

<sup>1</sup>Graduate School of Science, Kyoto University

Volcano infrasound is an increasingly useful technique for measuring and analyzing eruptive activity. In order to reveal causes of characteristics of infrasound waveform, we analyzed infrasound records and video images at eruptions that occurred at Yasur Volcano, Vanuatu during an hour at 15:00, 21th September, 2011. Yasur Volcano has three active vents in the summit crater. Infrasound waves are generated every 1-3 minutes at various eruptions with reddish magma, vapor rich gas and ash. Infrasonic waveforms are mostly symmetric with a sharp compressive onset, followed by a small rarefaction phase. In this study, we analyzed infrasound events whose maximum amplitude is more than 50 Pa at one station on the summit crater rim. We conducted cross correlation analysis to 29 wave records and classified them into 3 types; A (13 events), B (12 events) and C (4 events). Time window of the analysis was 5s from a second before the maximum peak time. In contrast to type C, cross correlation coefficient among wave forms of types A and B was very high ( $> \sim 0.75$ ). The compressive ratio and the ratio of positive and negative peak are different between type A and B. On the other hand, we analyzed selected video sequences of these eruptions. We read the RGB and brightness values on horizontal line above each vent until the end of the eruptions from 2s before the ejecta reaches the line. The maximum R and brightness value of type B events was twice as other type eruptions. This result may suggest that type B eruptions release relative much reddish magma and whitish gas compared to those of type A and C.

Keywords: infrasound, volcano eruption

## Numerical treatment of dry bed problem in the model of pyroclastic flows based on the 1-D shallow-water equations

SHIMIZU, Hiroyuki<sup>1\*</sup>; KOYAGUCHI, Takehiro<sup>1</sup>; SUZUKI, Yujiro<sup>1</sup>

<sup>1</sup>Earthquake Research Institute, The University of Tokyo

During explosive volcanic eruptions, a mixture of pyroclasts and volcanic gases is released from the vent. When the mixture loses its upward momentum before the density of the mixture becomes lower than the atmospheric density, the mixture forms a pyroclastic flow. Dynamics of pyroclastic flows can be approximated by that of an inviscid gravity current. The dynamics of inviscid gravity currents are controlled by an inertial-buoyancy balance on the front (e.g., Benjamin, 1968); we refer to this condition as "the front condition". The front condition, and hence, the dynamics of the inviscid gravity currents strongly depends on the density ratio of the current ( $\rho_c$ ) to the ambient ( $\rho_a$ ) (e.g., Ungarish, 2009). When  $\rho_c/\rho_a \sim 1$ , the current is characterized by a high front, whereas a front height does not develop when  $\rho_c/\rho_a \gg 1$ . In pyroclastic flows, because density ratio  $\rho_c/\rho_a$  varies spatially and temporally, the dynamics of pyroclastic flows becomes complicated; the basic features of pyroclastic flows, such as the run-out distance, have not been fully understood. The aim of our study is to develop a unified model of the inviscid gravity currents for various density ratio  $\rho_c/\rho_a$ .

In general, the dynamics of shallow inviscid gravity currents can be described by the shallow-water equations. There are two numerical models to solve the shallow-water equations: "shock front condition model" (SFC model) and "artificial bed-wetting model" (ABW model). SFC model is a model, in which the front condition is applied to the boundary condition (e.g., Ungarish, 2009). The boundary condition is given as a function of  $\rho_c/\rho_a$ . On the other hand, in ABW model, an artificial wet bed with the height of  $\epsilon h_0$  is set on the dry bed in order to express the front condition, where  $h_0$  is a characteristic height scale (e.g., Toro, 2001; Larrieu et al., 2006; Doyle et al., 2007). This model has the only parameter  $\epsilon$  for the front condition. Although the front condition, and hence the appropriate value of  $\epsilon$  must be a function of  $\rho_c/\rho_a$ , the relationship between  $\epsilon$  and  $\rho_c/\rho_a$  has not been studied. In order to resolve these problems, we carried out parameter studies using the two models for solving a simple "one-dimensional (1-D) dam-break problem".

On the basis of systematic comparisons between the results of SFC model and ABW model, we found the relationship between the parameter  $\epsilon$  and  $\rho_c/\rho_a$ :  $\epsilon \sim 8.62 \cdot 10^{-2} \cdot (\rho_c/\rho_a)^{-1.87}$ . We also found that the application of ABW model should be limited to  $15 < \rho_c/\rho_a$ . In the case of  $1 < \rho_c/\rho_a < 15$ , an unphysical shock wave propagates into the artificial bed so that the velocity and height of the current substantially deviate from the solution satisfying the correct front condition.

Keywords: pyroclastic flows, gravity currents, shallow-water equations, numerical simulation, volcanic disaster prevention

## Moment tensor representation of elliptical volume sources

MIZUNO, Naoto<sup>1\*</sup> ; KUSAKABE, Tetsuya<sup>2</sup> ; ICHIHARA, Mie<sup>2</sup> ; KAME, Nobuki<sup>2</sup>

<sup>1</sup>School of Science, The University of Tokyo, <sup>2</sup>Earthquake Research Institute, The University of Tokyo

A moment tensor inversion is a powerful tool to extract source information from seismic and geodetic observations. However, widely-used moment tensor representation for volumetric sources has been limited to a few basic geometries such as a sphere, a flat crack, and a cylinder. These sources give particular diagonal component ratios:  $(M_1:M_2:M_3)=(1:1:1)$  for a sphere,  $(1:1:3)$  for a crack, and  $(2:2:1)$  for a cylinder. When different component ratios are obtained from the inversion analysis, they are interpreted as combination of these simple geometries without considering internal pressure balance.

Although the moment tensor representation for elliptical sources was obtained 30 years ago (Davis, 1986), the solution has been rarely applied in volcanology. We consider two disadvantages of Davis (1986). The one is that the theories to relate the actual volume change to moment tensor have been proposed but not unified, which has caused some confusion. The accompanying paper (Ichihara et al., 2014, this meeting) presents a unified explanation based on the representation theorem and makes a clear link among volume change, geometry, and moment tensor. In this context, we have confirmed the applicability of Davis (1986) to the observed moment tensor.

The other disadvantage is that researchers have to search in the numerical table to find a geometry fitting to the observed moment tensor. Here we develop a facilitative tool that diagnoses the diagonal part of observed moment tensors to given the aspect ratios and the apparent compressibility. In addition, if the density and the compressibility of the internal material are given, the tool estimates mass change inside the source, which is an important parameter in volcanology.

This tool will provide a reference model satisfying pressure balance and help improving the volumetric source modeling beyond the conventional kinematic summation of simple sources.

Keywords: moment tensor, volumetric source, volcano seismology, magma

## Volume source representations: a possible unified explanation based on the representation theorem

ICHIHARA, Mie<sup>1\*</sup> ; KUSAKABE, Tetsuya<sup>1</sup> ; KAME, Nobuki<sup>1</sup> ; MIZUNO, Naoto<sup>2</sup> ; KUMAGAI, Hiroyuki<sup>3</sup>

<sup>1</sup>Earthquake Research Institute, The University of Tokyo, <sup>2</sup>School of Science, The University of Tokyo, <sup>3</sup>Graduate School of Environmental Studies, Nagoya University

The moment tensor inversion is a powerful tool to extract source information from seismic and geodetic observations. A moment tensor for earthquake faulting has been determined and its non-diagonal components give the seismic moment (rigidity  $\times$  slip  $\times$  fault area), which is one of essential source parameters of an earthquake. The sum of the diagonal components (the trace) of a moment tensor represents volumetric change at the source. A moment tensor determined for a volcanic source frequently has non-zero trace. However, it has been failed to uniquely relate the diagonal components to the actual volume change, which remains a critical issue in volcanic seismology (Kazahaya et al., 2011). For example, two different volume changes DV and dV have been proposed for the seismic moment of a spherical source geometry; DV comes from the moment tensor definition of a seismic fault having opening displacements whereas dV is obtained from the equivalence of resultant displacement fields due to the former moment tensor and an isotropically expanding sphere in an elastostatic equilibrium.

The difference between DV and dV has been discussed in the last decade. Muller (2001) considered an open crack of a spherical shell shape and showed that DV is the volume of the opening and dV is only the part opening outward. Aki and Richards (2002) and Richards and Kim (2005) adopted Eshelby's approach which considers virtual operations consisting of cutting, stress-free transformation, elastic straining, and welding, and concluded that the difference is due to whether the volumetric change occurs in an unconfined condition (DV) or in a confined condition (dV). Kumagai et al. (2013) reconsidered this problem and concluded that the displacement field due to a spherical source does not coincide with that due to a three-perpendicular-crack source though they both are represented by isotropic moment tensors. They also extended the insights into sources in a bimaterial medium. It is worth mentioning that the approaches of AR2002 and RK2005 give a conceptual explanation on how to adjust DV to the actual volume change dV for a sphere, but not for arbitrarily shapes. Here we address how to make such adjustments for general geometries on the basis of the representation theorem. Our imaginary operation below gives a unified explanation for the two different volumetric changes and newly proposes a method of estimating dV of the inversion results for arbitrary source geometries.

We start with the representation theorem that gives the displacement field by two terms (without a body force): a surface integration on the source region with convolution of the surface displacement and the gradient of the Green's function normal to the surface (1), and that with convolution of the surface traction and the Green's function (2). Only (1) has been considered for the seismic fault because (2) vanishes due to the balance of the traction at the contacting surfaces of a fault. On the other hand, (2) does not vanish in the case of a volumetric source, and therefore a quantitative adjustment is required to include the effect of (2) into (1). We here demonstrate that such an adjustment, is always realized by introducing an additional imaginary volumetric change, which works as 'displacement glut' in our representation of moment tensor. Our representation is found to be mathematically equivalent to the rather conceptual 'stress glut' representation proposed by Backus and Mulcahy (1976). We present a unified explanation for the existing various representations and propose a method to practically evaluate the moment tensor components from the boundary conditions of the volumetric source. The proposed representation will be useful in connecting dynamical models of volcanic processes and moment tensors.

Keywords: Moment tensor, Volumetric source, Representation theorem, Green's function, Volcano seismology, Explosion source

## X-ray CT observation of delayed fragmentation of vesicular magma analog

SHIDA, Tsukasa<sup>1</sup> ; AOKI, Yamato<sup>1\*</sup> ; KAMEDA, Masaharu<sup>1</sup> ; ICHIHARA, Mie<sup>2</sup> ; OKUMURA, Satoshi<sup>3</sup> ; UESUGI, Kentaro<sup>4</sup>

<sup>1</sup>Mech. Systems Eng., TUAT, <sup>2</sup>ERI, Univ. of Tokyo, <sup>3</sup>Earth Sci., Tohoku Univ., <sup>4</sup>JASRI

A laboratory experiment was performed to understand the mechanism of fragmentation of vesicular magma, which is a trigger of explosive volcanic eruption. From the observation of Shinmoe-dake 2011 eruption, the viscosity of magma is not so high as its response is in solid manner. Thus, we aim to reveal the mechanism of brittle-like fragmentation of the magma which behaves in fluid manner.

Rapid decompression test was conducted using syrup containing oxygen bubbles as a magma analogue. The decompression facility consists of a high-pressure chamber in which the specimen can be placed, and an electromagnetic valve. The pore structure of interior of the specimen was observed by X-ray microscopic tomography. The X-ray tomographic microscopy was performed at the BL20B2 beamline of the Japan Synchrotron Radiation Research Institute (JASRI, Hyogo, Japan). Initial structure of the specimen was observed by three-dimensional tomographic imaging. A digital charge-coupled device (CCD) camera was used as the detector whose imaging area is about 2048 pixels (horizontal) by 644 pixels (height) with spatial resolution of 8  $\mu\text{m}/\text{pixel}$ . We took 1800 projections over 180 degrees of rotation for tomographic imaging. High-speed radiography was performed during the decompression. The framing rate of radiography is 200 frames per second.

The specimen has a semi-spherical shape whose diameter was 20 mm. The initial pressure ( $p_0$ ) was 1.5 MPa, the characteristic time of decompression ( $t_{dec}$ ) was 50 ms, the viscosity of syrup was about  $1 \times 10^8$  Pa s, the initial averaged void fraction  $\phi_0$  was about 10%. We tested nine samples whose pore structure was different to each other.

The fragmentation occurred with two samples in which a 10-mm-diameter bubble was contained, while the fragmentation did not occur using the seven samples whose pore structure was relatively uniform. The onset of fragmentation is 960 ms after the decompression was started. The onset was substantially delayed not only from the characteristic decompression time but also from the relaxation time of Maxwellian viscoelastic material (viscosity/rigidity = 150 ms). Referring to the radiographic images, we found that the fracture was initiated from a chain of small gas bubbles and a notch in the vicinity of the 10-mm (large) bubble. The internal crack may grow in ductile manner when the hoop stress around the large bubble increased due to decompression. At a certain instance the stress concentration and the brittleness at crack tip may exceed the critical level, which leads to brittle failure of the crack.

The experimental result indicates that brittle-like fragmentation can occur in the non-uniform vesicular magma even if the response of magma is in fluid manner.

## Model experiments on magma migration in a viscoelastic host rock : effect of viscosity

TAKEGUCHI, Izumi<sup>1\*</sup> ; SUMITA, Ikuro<sup>1</sup>

<sup>1</sup>Graduate School of Natural Science and Technology, Kanazawa University

Magma generated from partial melting ascends upwards by its buoyancy to the magma chamber, some of which erupt at the Earth's surface. Magma is considered to ascend in the form of diapir in the asthenosphere and transforms to dykes in the lithosphere (Rubin, 1995). These two end member cases have been studied in detail, but the mechanism of magma ascent in the transitional regime is still poorly known. We have been studying the ascent mechanism in the transitional regime by model experiments using a viscoelastic agar (Sumita and Ota, 2011). Here we report the results of experiments which focus on the effect of fluid viscosity on the magma migration in a viscoelastic medium.

We conducted (1) rheology measurement of agar and (2) fluid injection experiments. We inject magma (CsCl solution to which a thickener is added) using a syringe from the top of a cylindrical acrylic tank (height of 250 and 500 mm). The fluid has a volume of 1ml, density difference with the agar of 0.108 g/ml, and is injected at a constant rate of 0.1 ml/s. We vary the agar concentration in the range of 0.04-0.5 wt% and the fluid viscosity in the range of  $10^{-3}$  - 650 Pas. As we increase the agar concentration in this range, we find that the yield stress and the rigidity of the agar increases by 3 orders of magnitude. By shearing the sample under a constant stress (creep test) we find that the agar can be approximated by a Voigt model to which a spring is connected in series. The experiments are recorded using video cameras from two sides and from the bottom of the tank.

From the injection experiments, we find that as the agar rigidity ( $G$ ) decreases, the crack shape transforms from 2D (blade-like) to 3D (having a bulged head). The critical rigidity ( $G_c$ ) of the 2D-3D transformation is around  $G_c=10$  Pa, and this value becomes smaller when a high viscosity fluid is injected. The value of  $G_c$  is consistent with the rigidity estimated from the balance between the elasticity and buoyancy at which the strain becomes 1. The crack consists of a bulged head and a thin sheet-like tail, and the head becomes thinner and smaller as the crack elongates. When a stiff agar is used as the host, or when a high viscosity fluid is injected, the crack propagation stops within a certain distance from the injection point. We find that this propagation distance becomes shorter as we increase the agar yield stress or the viscosity of the injected fluid, and this result can be associated with the transformation of the crack shape to 2D. We fit the time-distance data to a power-law relation, and find that the exponent varies from  $1/3$  to 1. An exponent of  $1/3$  corresponds to the scaling obtained for a 2D crack which thins uniformly as it elongates (Taisne et al, 2011). An exponent larger than  $1/3$  corresponds to the crack shape becoming more 3D. To conclude, we find that the magma viscosity not only slows its migration velocity, but also controls the crack shape, its deceleration, and the propagation distance until it stops.

### References:

- Rubin, A. M., 1995, *Ann. Rev. Earth Planet. Sci.*, 23, 287-336.
- Sumita, I. and Y. Ota, 2011. *Earth Planet. Sci. Lett.*, 304, 337-346.
- Taisne, B. et al., 2011, *Bull. Volcanol.*, 73, 191-204.

Keywords: viscoelasticity, Magma ascent, rheology, crack

## Bubble growth and resorption in magma: insights from dissolved water distributions in volcanic glass

MCINTOSH, Iona<sup>1\*</sup> ; LLEWELLIN, Ed<sup>2</sup> ; HUMPHREYS, Madeleine<sup>2</sup> ; NICHOLS, Alex<sup>1</sup> ; BURGISSER, Alain<sup>3</sup> ; SCHIPPER, C ian<sup>4</sup>

<sup>1</sup>IFREE, JAMSTEC, Japan, <sup>2</sup>Department of Earth Sciences, Durham University, United Kingdom, <sup>3</sup>ISTerre, Universite de Savoie - CNRS, France, <sup>4</sup>SGEES, Victoria University, New Zealand

Volcanic eruptions are driven by the growth of gas bubbles in magma, which grow and shrink as volatile species exsolve from and dissolve back into the melt in response to changes in the local environment, particularly in pressure and temperature. This movement of volatiles, particularly water, is recorded in the glass around vesicles and recent studies have used this record to interpret natural samples. Here we investigate the processes that control bubble growth and resorption in magma, by measuring the distribution of dissolved water in experimentally-vesiculated volcanic glasses. Water concentration profiles obtained using SIMS-calibrated BSEM imaging and water speciation data obtained using FTIR spectroscopy, are interpreted in the context of the known pressure and temperature history of the samples.

Samples are found to have undergone partial bubble resorption during the quench to glass at the end of experiments, as a result of increasing water solubility with decreasing temperature. Analysis of the lengthscale and timing of the resulting water concentration profiles demonstrates that the majority of resorption occurs above the glass transition. This quench resorption is associated with a reduction in bubble volumes that creates characteristic textures, such as buckled melt films between adjacent vesicles and reoriented cracks around resorption halos. Highly disequilibrium water speciation ratios within resorption halos are found to be diagnostic of quench resorption and can preserve evidence of pre-quench bubble growth

Quench resorption can increase sample water concentrations and ratios of molecular to hydroxyl water species, and reduce bubble volumes and sample porosities. Studies based on these parameters must therefore consider the potential impact of quench resorption, which is expected to be greatest for samples with high water concentrations, slow quench and low initial sample porosities. Water speciation data offer a way to investigate these impacts in unconstrained natural samples and could provide a tool for forensic interrogation of their eruptive history.

Keywords: Bubble growth, Bubble resorption, Water speciation, FTIR, SIMS, Backscatter SEM

## Formulation of the 1-D magmatic flow including vesiculation kinetics

TORAMARU, Atsushi<sup>1\*</sup>

<sup>1</sup>Department of Earth and Planetary Sciences, Kyushu University

In most of existing fluid mechanical modeling and numerical calculations, the equilibrium vesiculation has been assumed according to the solubility relation. However, in order to understand the transient behaviors such as triggering of eruptions and shifts of eruption intensity, we need to examine the effect of vesiculation kinetics on the fluid mechanical behaviors in the conduit. In this study, we formulate the governing equations describing the one dimensional fluid mechanics taken into account the vesiculation kinetics, that is, the nucleation and growth of bubbles, assuming the homogeneous flow.

As we adapt the single fluid approximation, we build upon the advantage of the formulation in which the mass conservation equation about density is converted to the pressure equation through the equation of state. We make the similar procedure to obtain pressure equation while in our case the density is a function of not only pressure but also gas phase fraction. The gas phase fraction is calculated by the vesiculation kinetics. As a result we have four equations; 1) pressure equation (mass conservation), 2) equation of motion (momentum conservation), 3) constitutive equations describing vesiculation kinetics. These partial differential equations consisting of pressure, velocity and gas phase fraction, can be solved numerically.

In order to confirm the validity and fundamental characters of the formulation, we numerically solve the shock tube problem, using modified CIP method for advective terms. In the case that the kinetic effect is negligible due to relatively large initial gas fraction in the high pressure region, we obtain the similar solution to that of single fluid, consisting of shock wave in downstream and rarefaction fan in upstream. On the other hand, in the case that kinetics of vesiculation works effectively, we have different behaviors in the high pressure region in which rarefaction front, nucleation pressure front and nucleation event propagate with different velocities, while the behavior in the low pressure region is basically same as the case without the kinetic effect. Each propagation velocity depends on nucleation pressure (liquid/gas interfacial energy), bubble growth rate, initial gas fraction in the high pressure region. The essential difference between two cases, the pressure of bubble formation becomes lower in the case with the kinetic effect than in the case without kinetic effect. If the kinetic effect is dominated, it is expected that the time to the vent from the bubble nucleation is relatively short. On the other hand, in the case that the vesiculation proceeds at equilibrium without the kinetic effect, it needs longer time to the vent, suggesting that the relative motion between gas and liquid, the bubble coalescence and degassing become dominate. Thus, this suggests that the kinetics of vesiculation may control the transition of eruption styles such as explosive and non-explosive eruptions.

Keywords: conduit flow, vesiculation kinetics, bubble nucleation, shock tube

## Pre-eruptive conditions of rhyolitic magma from Kawagodaira Volcano, Izu Peninsula

TAKASHIMA, Jun<sup>1\*</sup> ; ISHIBASHI, Hidemi<sup>1</sup>

<sup>1</sup>Graduate school of science, Shizuoka University

Kawagodaira volcano is a rhyolitic monogenic volcano located in the Higashi-Izu monogenic volcano field at Izu Peninsula. The volcano erupted at ca. 3060~3190. During the eruption, transition of eruption style was occurred from Plinian explosion to obsidian extrusion. Such transition often occurred in silicic magma, and depend on pre-eruptive condition and outgassing during magma ascent in the vent. However, detailed mechanism is still under study. In this study, we collect volcanic products of 3 eruption style which are plinian eruption, pyroclastic flow, and lava flow. We conducted petrography and analysis of chemical compositions of glass and phenocryst minerals for these volcanic products, and we estimated the pre-eruptive condition of temperature and pressure and water content to examine mechanism in transition of eruption style.

All samples in this study include ca. 15 vol. % of phenocrysts chiefly composed of hornblende and plagioclase with minor amount of orthopyroxene and magnetite, and include ca. 85 vol. % of groundmass composed of glass. Hornblende phenocrysts show chemical zoning with obvious gap of Al content near rim. Al content is higher in core part (ca. 1.7 atoms per formula unit (apfu)) than rim part (ca. 1.2 apfu).

The estimated pressure using hornblende Al content geobarometer shows bimodal distribution with ca. 100 MPa and 200-300 MPa in each sample. The former and the latter correspond to the crystallization pressure of rim and core part of hornblende, respectively. The estimated temperature using plagioclase-hornblende geothermometer indicate constant in all samples, and average to be 1132K. The water content is estimated to be 5wt. % by using plagioclase-melt geohydrometer, and this value coincident with H<sub>2</sub>O solubility in rhyolitic melt at 100MPa.

The estimated P-T conditions show that magma decompressed from 200~300MPa to 100MPa without change of magma temperature. This indicates that transition of eruption style occurred less than 100MPa. The coincidence between water content and the H<sub>2</sub>O solubility at 100MPa suggest that bubbles were already formed at this pressure. And, we think that magma stopped at 2.5~3km depth until growth of hornblende and plagioclase phenocrysts finished. During cessation of magma ascent, bubbles rised to upper part of magma chamber, forming bubble zoning in magma chamber. This zoning might relate to transition of eruption style.

Keywords: Higashi-Izu monogenetic volcanic field, rhyolitic magma, eruption style, hornblende

## Hydrothermal system around the Bandaiko hot spring inferred from a 3-D resistivity structure

KANDA, Wataru<sup>1\*</sup>; TAKAKURA, Shinichi<sup>2</sup>; KOYAMA, Takao<sup>3</sup>; OGAWA, Yasuo<sup>1</sup>; SEKI, Kaori<sup>1</sup>; HINO, Yuta<sup>1</sup>; HASE, Hideaki<sup>1</sup>

<sup>1</sup>Tokyo Institute of Technology, <sup>2</sup>The National Institute of Advanced Industrial Science and Technology (AIST), <sup>3</sup>Earthquake Research Institute, University of Tokyo

Bandaiko is a hot spring located in the eastern flank of the Kusatsu-Shirane volcano, 3km west from Kusatsu-Onsen. It was discovered in 1967 during excavation of a sulfur mine, and has been utilized as one of the sources of Kusatsu-onsen since 1976. It is presumed that a gush point is located in 505 m west from a tunnel entrance. The ground temperature above the presumed gash point exceeds 80 degrees. About 10 to 20 percent of the hot spring water is always discharged as vapor, so that existence of a two-phase hydrothermal system in a shallow part of tunnel end is considered to be certain. Moreover, since the chemical nature of hot spring is well investigated, Bandaiko is a suitable field which clarifies the resistivity image of a hydrothermal system.

We investigated the shallow resistivity structure around the Bandaiko hot spring using the AMT (audio-frequency magnetotelluric) method. The measurement was done on Oct.19th through Oct.26th, 2013. Five components of EM fields were measured at 19 sites around the presumed gush point: measurements were carried out during the nighttime at 15 of them with sufficient S/N. Because the measuring frequency was 1-10400Hz, information on the resistivity structure from the vicinity of surface to the depths of 1-2km can be obtained. A site for the remote-reference was not installed. Instead, a local-site-reference was applied each other. The 60 Hz noise as well as the 50 Hz noise caused by the local commercial power was extensively seen, because the survey area is located in close proximity to a prefectural border of Nagano where 60 Hz power is used.

Three-dimensional (3-D) analysis was performed in this study. A 3-D resistivity structure model was estimated from the inversion code of Siripunvaraporn and Egbert (2009) using 15 frequencies of all components of impedance data. The inferred model shows low resistivity near the end and the entrance of tunnel. In this presentation, we will report the up-to-date model of the 3-D resistivity structure and discuss the hydrothermal system around Bandaiko in consideration of the measured values of the electrical conductivity of hot spring water, etc.

This study was supported by the Earthquake Research Institute cooperative research program.

Keywords: resistivity structure, Kusatsu-Shirane volcano, hydrothermal system, Kusatsu-onsen, Bandaiko

## Resistivity structure around the Jigokudani valley, Tateyama volcano, Japan, inferred from AMT

SEKI, Kaori<sup>1\*</sup> ; KANDA, Wataru<sup>2</sup> ; OGAWA, Yasuo<sup>2</sup> ; HASE, Hideaki<sup>2</sup> ; HINO, Yuta<sup>1</sup> ; KOBAYASHI, Tomokazu<sup>3</sup> ; TANBO, Toshiya<sup>4</sup>

<sup>1</sup>Department of Earth and Planetary Sciences , Tokyo Institute of Technology, <sup>2</sup>Volcanic Fluid Research Center, Tokyo Institute of Technology, <sup>3</sup>Geospatial Information Authority of Japan, <sup>4</sup>Tateyama Caldera and Sabo Museum

Midagahara (Tateyama volcano) is situated in the northern part of the Japan Alps, and fumarolic activity occurs in the Jigokudani valley located in the northeast end of the Midagahara Plateau. Jigokudani valley was formed by the periodically repeated vapor explosions. Increase in volcanic activity is a great concern because of recent events such as a sulfur outflow, a composition change of the fumarolic gases and the emergence of high temperature fumaroles. We investigated the distribution of hydrothermal fluid and gas reservoir beneath Jigokudani using the AMT method to image the 2D resistivity structure and checked the position of fumaroles. In this observation, the AMT sites were installed along the ENE-SWS survey line around the Jigokudani Valley. The final model revealed that there is a conductive body beneath the Jigokudani valley, and that a relatively low resistive body extends through between the high resistivities beneath the conductor. Near-surface conductor is divided into slightly conductive upper part and lower part. The upper part is explained by clay sediments and hydrothermal fluids. The lower part indicates the presence of gases and fluids. Because of clay's impermeability, the upper clay sediments play the role as a cap for gases. The deep resistive layer is estimated to be the basement of granites that are widely exposed around the Jigokudani valley. We inferred that the relatively conductive body separating these granites is a path of the magmatic gases. The most active fumarole in the Jigokudani valley is on extension of this path.

## Hydrothermal system at Tatun Volcano Group, northern Taiwan, inferred from resistivity structure

KOMORI, Shogo<sup>1\*</sup>; UTSUGI, Mitsuru<sup>2</sup>; KAGIYAMA, Tsuneomi<sup>2</sup>; INOUE, Hiroyuki<sup>2</sup>; CHEN, Chang-hwa<sup>1</sup>; CHIANG, Hsieh-tang<sup>3</sup>; YOSHIMURA, Ryokei<sup>4</sup>; KANDA, Wataru<sup>5</sup>

<sup>1</sup>Institute for Earth Sciences, Academia Sinica (Taiwan), <sup>2</sup>Aso Volcanological Laboratory, Kyoto University, <sup>3</sup>National Taiwan University, <sup>4</sup>Disaster Prevention Research Institute, Kyoto University, <sup>5</sup>Tokyo Institute of Technology

Tatun Volcano Group is composed of over twenty volcanoes, which were formed within faults at the northern tip of Taiwan. So far, these volcanoes were regarded as extinct because of no historical record of eruption. However, recent studies have found the relatively young ejecta (Chen and Lin, 2002; Belousov et al., 2010), high  $3\text{He}/4\text{He}$  ratio (Yang et al., 1999; Ohba et al., 2010), and hypocenter distribution suggesting the fluid flow and the high temperature condition (Konstantinou et al., 2007); that suggest the presence of potentially eruptive magma beneath TVG. Further, active heat discharge from fumaroles and springs also suggests a large amount of the volcanic fluids released from magma beneath Chishinshan volcano. Focusing on this phenomenon, Utsugi et al. (2012, JPGU) conducted AMT surveys at the volcano for a better understanding of this magma degassing, and showed the preliminary resistivity structure suggesting the low resistivity region at the depths of 1-2km.

On the basis of their work, the authors conducted further AMT surveys around Matsao hot spring and Da-you-keng fumarole areas, about 2 km northeast of the volcano. Time series of the electric and magnetic fields were acquired for about 4 hours at each site. Totally 10 observation sites were configured to cover the areas. After data acquisition, the frequency domains were obtained from the time series, using FFT processing. The impedances were estimated for each frequency. The obtained frequency range was between 1 and 10400 Hz. The authors used not only the data of the present study but also those of Utsugi et al. (2012, JPGU).

This study categorized the study area into two areas, mainly from the characteristics of the main axes of the impedance phase tensor ellipse by the method of Caldwell et al. (2004): 1) Mt. Chishinshan area and 2) Matsao and Da-you-keng areas. In this study, two-dimensional resistivity structure was estimated for each area, using the inversion code of Ogawa and Uchida (1996). By incorporating them with the evidences from geochemistry and geophysics (MRSO, 1969, 1970, 1971, 1973; Ohba et al., 2010; Ohsawa et al., 2013; Murase et al., 2013, IAVCEI), the following features of the hydrothermal system was inferred.

Beneath Mt. Chishinshan two-phase fluids are supplied; which is represented by the extremely-low resistivity column (less than 3 Ohm-m) and the deflation pressure source below 1 km depth. As the fluids ascend, their phase is changed into vapor-phase, leading to low to relatively-low resistivities (6-30 Ohm-m) at the depths of 0.3-1 km. The vapor-rich region is covered by the low-permeability cap represented by the extremely-low resistivity layer near the surface (less than 3 Ohm-m). A portion of the vapors is mixed with shallow groundwater, and flows along a topographical relief to form Matsao hot spring; whose area is represented by resistivities less than 10 Ohm-m.

On the other hand, Da-you-keng area has intense fumaroles; whose vapor-dominated fluids are supplied from the region beneath Cing-tian-gang, represented by the low to low-resistivity region (3-30 Ohm-m) and the inflation pressure source below 1 km depth. This vapor-bearing region is covered by the overlying low-permeability cap represented by the extremely-low resistivity region (less than 3 Ohm-m).

This study estimated the horizontally-extending vapor-rich region beneath Mt. Chishinshan, Da-you-keng, and Cing-tian-gang. Actually, this area has experienced a phreatic eruption ca. 6 Ka (Belousov et al., 2010). These suggest that the vapors have been maintained for at least several thousands years, and that there is still a possibility of phreatic explosions.

Keywords: Tatun Volcano Group, Hydrothermal system, Two-phase region, Vapor-dominated region, Pressure sources

## Conductivity distribution of the surface layer in Aso Caldera

KAGIYAMA, Tsuneomi<sup>1\*</sup> ; YOSHIKAWA, Shin<sup>1</sup> ; UTSUGI, Mitsuru<sup>1</sup>

<sup>1</sup>Graduate School of Science, Kyoto University

Kagiyama and Morita(2008) proposed that volcanism has a wide range of diversity represented by two typical end members controlled by the easiness of magma storage beneath volcano; Eruption dominant (ED) volcanism in difficult condition and Geothermal activity dominant (GD) volcanism in easier condition. In GD volcanoes, magma stagnates beneath volcanoes and maintains geothermal activity. This seems GD volcanoes continue to give much benefit to human society. However, GD volcanoes sometimes have large eruptions after repeated stagnations of magma. This fact suggests it is very important to understand where and why magma stops ascending. Kagiyama and Morita (2008) indicated magma degassing is one of the important factors to control magma ascending. On this aspect, the authors have carried out VLF-MT survey around some active volcanoes in Japan, because electrical conductivity of ground strongly depends on the conductivity of pore water.

Aso Caldera has an acid crater lake in Nakadake, which is one of the post caldera cones, and has many hot springs such as Uchinomaki, Akamizu. Conductivity distribution shows two typical features; caldera floor has almost homogeneous and high conductivity (>10mS/m), while the post caldera cones show wide range.

Most cones such as Kishima-dake and Ohjo-dake have lower conductivity (<3mS/m), except around Naka-dake Craters and western flank of post caldera cones such as Yoshioka, Yunotani and Jogoku-Tarutama (>30mS/m). Kusanenri Volcano, located between Naka-dake and Yoshioka has also rather high conductivity (3-10mS/m). These areas locate along the E-W trend of the major post caldera cones. Most part of the northern flank of the post caldera cones shows low conductivity (<3mS/m). However, higher conductivity was found around Sensuikyo, just north of Nakadake Craters. This suggests down flow of hydrothermal water from Naka-dake Craters to the caldera floor. Similar features are detected in the southern flank; from Nakadake to Shirakawa Hot Spring, from Jigoku-Tarutama Hot Springs to Tochinoki Hot Springs.

Caldera floor has almost homogeneous conductivity. This feature is explained by the fact that the caldera floor was under the lake until 9 ka and is covered by lake deposit. However, extremely high conductivity was found at three areas (>50mS/m). Two of them correspond hot spring areas; Uchinomaki in the north and Akamizu in the west. The third area is distributed around old post caldera cones, Mietsuka. The age of these cones was estimated around 46 ka, and no hot spring is distributed. High conductive zones, Uchinomaki, Mietsuka and Naka-dake are located along the NNW-SSE line. Hydrothermal water may be supplied along this line.

These results suggest that hydrothermal water is supplied along the E-W trend crack from Naka-dake to Yoshioka, mainly supplied beneath Naka-dake, and expanded to the northern caldera floor. The NNW-SSE trend from Naka-dake to Uchinomaki may suggest a tectonic fault. Aso has wide high conductivity area and degassing in Aso might be large to be GD volcano.

Reference: Kagiyama and Morita, First steps in understanding caldera forming eruptions, *J. Disaster Res.*, 3, 270-275, 2008.

Keywords: Electrical conductivity, Geothermal activity, Failed eruption, Aso Caldera

## The thermal expansion model and the Mogi model for volcanic ground deformation

KITSUNEZAKI, Choro<sup>1\*</sup>

<sup>1</sup>none

(1) Basic aspects of the thermal expansion model, which was proposed by the author in this meeting of the last year (Kitsunezaki and Muraoka, 2013), is reorganized in relation to the Mogi model (Mogi, 1958). In the Mogi model, the earth's crust is assumed to be a semi-infinite isotropic homogeneous elastic solid with the horizontal free plane (the ground surface). Displacement of the ground surface caused by a spherical pressure source set up in the earth's crust is evaluated. Gravity change associated with the deformation was estimated by Hagiwara (1977). Basically, the inside of the spherical source of this model is void (or material different from the surroundings). As a special case, we assume that the inside is filled with the same material as the surroundings and that temperature in the inside is raised (keeping the outside temperature constant). Thermal expansion of the sphere behaves as a pressure source, and the Mogi model is transformed to the spherical thermal expansion model (ST model). In this case, as the mass of the sphere does not change, the change in gravity on the ground surface is caused by the free-air effect (FE) due to uplift of the ground surface alone.

(2) The above ST model can be extended to the case in which the temperature-rise region (T region) has arbitrary shape. Let the T region be subdivided into a large number of small cubic cells. Every cell effectively behaves as a spherical thermal element. Its outputs (displacement and gravity change on the ground surface) are given by the ST model. The output of the entire T region is given as a sum of the output of each element. Hence in the T region with any shape, the change in gravity is caused by the FE due to the vertical displacement of ground surface alone.\*

\*[Note] The related description in Kitsunezaki and Muraoka (2013) has been corrected here.

(3) Shallow regions of actual volcanoes may be regarded as porous media. Let's assume that the pores are saturated by water and are in open condition. In the thermal expansion model described in (1) and (2), the earth medium is replaced by such a water-saturated porous medium. In this case, pressure of pore water is kept constant. Hence the solid part (skeleton of the medium) behaves in deformation independently from pore water. Thermal expansion of the solid part causes the displacement of the ground surface and the gravity change due to the FE as described in (2). On the other hand in the T region, the pore water expands freely responding to the temperature-rise (below the boiling point), hence its density decreases. (Thermal expansion coefficient of water is more than ten times larger than that of solid part (rock)). This effect causes negative gravity change, which is added to the FE so as to amplify the total gravity reduction to some degree. This example is numerically demonstrated in gravity variation observed in Akita-Komagatake volcano after the 1970-eruption.

[References]

Hagiwara, Y. (1977): The Mogi model as a possible cause of the crustal uplift in the eastern part of Izu Peninsula and the related

gravity change, Bull. Earthq. Res. Inst., Vol.52, 301-309 (in Japanese).

Kitsunezaki, C., and Muraoka, A. (2013): Gravity variation in Akita-Komagatake volcano and thermal expansion model, Japan Geoscience Union Meeting, SVC52-04.

Mogi, K. (1958): Relations between the eruptions of various volcanoes and the deformations of the ground surfaces around them, Bull. Earthq. Res. Inst., Vol.36, 99-134.

Keywords: thermal expansion model, Mogi model, gravity change, ground deformation, Akita-Komagatake, porous media

## El Cobreloa: A geyser with two distinct eruption styles

NAMIKI, Atsuko<sup>1\*</sup> ; MUNOZ, Carolina<sup>2</sup> ; MANGA, Michael<sup>2</sup>

<sup>1</sup>DEPS, Univ. of Tokyo, <sup>2</sup>UC Berkeley

We performed field measurements at a geyser nicknamed “El Cobreloa”, located in the El Tatio Geyser Field, Northern Andes, Chile. The El Cobreloa geyser has two distinct eruption styles: minor eruptions, and more energetic and long-lived major eruptions. Minor eruptions splash hot water intermittently over an approximately 4 minute time period. A major eruption begins with an eruption style similar to minor eruptions, but then transitions to a voluminous water-dominated eruption, and finally ends with energetic steam discharge that continues for approximately 1 hour. We calculated eruption intervals by visual observations, acoustic measurements, and ground temperature measurements. All measurements consistently show that each eruption style has a regular interval: 4 hours and 40 minutes for major eruptions, and approximately 14 minutes for minor eruptions. We develop a model, in which the geyser reservoir, connected to the surface by a conduit, is recharged by the deep, hot aquifer. More deeply derived magmatic fluids provide the enthalpy to heat the reservoir. Boiling in the reservoir releases steam and hot water to the overlying conduit causing minor eruptions, and heating the water in the conduit. When the conduit becomes warm enough, the water in the conduit is able to boil, leading to a steam-dominated eruption that empties the conduit. The conduit is then recharged by the shallow, colder aquifer, and the eruption cycle begins anew. El Cobreloa provides insight into how small eruptions prepare the geyser system for large eruptions.

Keywords: geyser, El Tatio, geothermal systems, eruption

## Time variation in the chemical composition of fumarolic gases at Hakone volcano, Japan

OHBA, Takeshi<sup>1\*</sup> ; KUNO, Yuki<sup>1</sup> ; SAGOU, Masakazu<sup>1</sup>

<sup>1</sup>Dep. Chem. School Sci. Tokai Univ.

### Introduction

Mt Hakone having the caldera structure is an active volcano located on the western end of Kanagawa prefecture. At the central region of caldera, several volcanic cones are located. On the flank of cones, geothermal areas have been developed. The magmatic activity, which formed the cones, started 50 Ka (Kuno, 1972). The activity is estimated to have continued until 3 Ka (Kobayashi et al., 1997). At the last eruption, the western flank collapsed at one of the central cones, resulting in the formation of dammed Lake Ashi (Ooki and Hakamada, 1975).

At Mt Hakone, volcanic earthquakes have been observed frequently, although no historical eruption is known. Especially in 2001, the occurrence of volcanic earthquake was intense. The seismic activity was accompanied with an inflation of body at the central cones. The inflation was interpreted to be brought by a pressure source at 7 km of depth (Daita et al., 2009).

### Sampling of fumarolic gas

We sampled fumarolic gas at two sites since May 2013 at Owakudani geothermal area developed on the central cones. One of the sites is located 200m far from the Owakudani car parking in the direction of southeast. At the site we had sampled fumarolic gas in previous study. We call the fumarole as the regular fumarole. Another fumarole is located 500m far from Owakudani car parking in the direction of north. The fumarole has been generated recently. Before the generation, the area was forest. Now many large stout trees were killed by the geothermal effect. We call the fumarole as the new fumarole. Both of the fumarolic gases were sampled in the evacuated Giggenbach bottle containing 20 ml of 5M KOH solution.

### Result

The main component of the regular and new fumarole was water vapor (H<sub>2</sub>O). The molar percentage of H<sub>2</sub>O was about 98% for the both fumaroles. Both of the gas contain CO<sub>2</sub> gas as the major component next to H<sub>2</sub>O, the percentage was about 1 to 2%. The regular fumarolic gas contained H<sub>2</sub>S as much as 0.2 to 0.4%. The H<sub>2</sub>S concentration in the new fumarolic gas was only 0.036 to 0.050%, about 1/10 to the regular fumarolic gas.

The CO<sub>2</sub>/H<sub>2</sub>S molar ratio indicated a time variation, a monotonic decrease since May 2013 to Oct 2013. Daita (2013) reported a similar trend based on the observation with detecting tubes. Daita (2013) found an abrupt increase in the CO<sub>2</sub>/H<sub>2</sub>S molar ratio on Jan 2013. The increased ratio had been kept until April then decreased gradually toward Oct 2013. According to the seismic observation by Hot Springs Research Institute of Kanagawa Prefecture, volcanic earthquakes occurred frequently in Jan and Feb 2013. We suppose the change in the CO<sub>2</sub>/H<sub>2</sub>S ratio has been synchronized with the occurrence of volcanic earthquakes.

Keywords: Fumarolic gas, CO<sub>2</sub>, Volcanic activity, Hydrothermal system

## Geochemical characteristics and changes of thermal waters around Tokachidake volcano, Japan

TAKAHASHI, Ryo<sup>1\*</sup> ; SHIBATA, Tomo<sup>1</sup> ; MURAYAMA, Yasuji<sup>1</sup> ; OGINO, Tagiru<sup>1</sup> ; OKAZAKI, Noritoshi<sup>1</sup>

<sup>1</sup>Geological Survey of Hokkaido, HRO

Tokachidake volcano, located in central Hokkaido, caused three magmatic eruptions (AD 1926, 1962 and 1988-89) in the 20<sup>th</sup> century. The seismic and thermal activities at the summit crater area have increased since AD 2010. We have continuously investigated thermal waters around the volcano since AD 1986 in order to understand the volcanic activity. Around the AD 1988-89 eruption, the chemical compositions and temperature of the thermal waters had obviously changed (Murayama et al., 1991). Therefore, we need to reveal the origin and changes of the thermal waters in order to forecast the future volcanic activity.

The thermal waters are discharged in the Nukkakushi crater (Ansei crater) and at its lower reaches, which is located at about 2 km southwest from the summit craters. Each thermal water is acidic with pH <3.2. At the time of AD 1986, all thermal waters were rich in sulfate ion but were scarce in chloride ion. In addition, anion content of the thermal waters decreases in proportion to the distance from the Nukkakushi crater. Therefore, the thermal waters derived from the Nukkakushi crater area flow, while mixing with groundwater, and are discharged at the lower reaches.

At the Fukiage hot spring area (1,000 m a.s.l.), the concentration of chloride and sodium ions in the thermal waters had abruptly increased since AD 1986. The increase of these chemical concentrations had continued until AD 1992, and the concentration of them had decreased since then. Accompanied with the chemical change, the temperature of the thermal waters had also increased more than 20 °C around the AD 1988-89 eruption. Such increase of the chemical compositions and temperature of the thermal waters had occurred related to the increase of the volcanic activity. Thus, these increases can be explained by mixing of highly dense NaCl type thermal water into shallow aquifer, and its mixing ratio changed with the volcanic activity. The chemical and thermal changes of the thermal waters have not occurred at the Okina hot spring (1,060 m a.s.l.). This indicates that the input of highly dense NaCl type thermal water has occurred at the lower reaches of the Okina hot spring.

Based on our investigations, the thermal waters in this area are formed by mixing of three end-members, sulfate ion rich thermal water, dense NaCl type thermal water and groundwater. The effect of the dense NaCl type thermal water is recognized only at the Fukiage hot spring area, and the mixing ratio changes according to the volcanic activity. The concentration of chloride and sodium ions in the thermal waters has begun to increase again since AD 2012. However, the increase is obviously small compared with that before the AD 1988-89 eruption, and the oxygen and hydrogen isotopic compositions of these thermal waters have not shown obvious change yet. Observations of the thermal waters will provide useful information to forecast the future volcanic activity in Tokachidake volcano, and hence we will continue the observations.

Keywords: Tokachidake volcano, thermal water, chemical composition, eruption forecasting

## Case study of the behavior of isotope in several hot-spring field

YANAGISAWA, Norio<sup>1\*</sup>

<sup>1</sup>AIST

### 1. Introduction

The behavior of oxygen and hydrogen isotope in geothermal field suggests the origin of fluids and the water rock interaction in fluid path. And there are various origins of high temperature hot springs in Japan, for example, separation from magma, heating meteoric water in the underground.

In this paper, we show the several samples of the isotopic analysis in high temperature hot spring fields including hot spring binary test field and we discuss the diversity of origin of the hot springs.

### 2. Examples of several hot spring fields

#### (1) Hachijo Island

There is a geothermal power plant (3.3MW) in Hachijo Island. To clarify hydraulic system, we measured oxygen and the hydrogen isotope ratio of the hot spring fluid, underground water as spring and the fluid at geothermal power plant. The isotope ratio of spring is similar as rain in Hachijo Island and the value of  $d$  is about 20 and hydrogen isotope ratio of spring is about -35 ‰. The hot spring fluid in Hachijo Island has two patterns. One is the origin of meteoric water due to similar isotope ratio as spring water. And another is the origin of seawater due to similar isotope ratio as seawater. The isotope ratio of fluid of geothermal plant is higher oxygen ratio than spring and hot spring water and this suggest that the origin of the fluid of geothermal plant is mixture meteoric and magmatic water.

#### (2) Matsunoyama hot spring field

In Matsunoyama hot spring field, the test of binary power plant is carried out using Takanoyu #3 hot spring fluid with about 100 °C and 10,000 mg/l Cl. The hydrogen isotope ratio is about -25 ‰ and oxygen isotope ratio is about 0 ‰ higher than meteoric water. And the isotope ratio of Matsunoyama #4 well with 2,000mg/l shows the mixture of meteoric water and Takanoyu #3. The origin of Takanoyu#3 is fossil salt water with methane gas and geo-pressure structure.

#### (3) Minami-Izu hot spring field

There is high temperature hot spring with about 100 °C and 10,000 mg/l Cl in Minami-Izu hot spring field, too. In this field the temperature and Cl concentration decrease eastern area. The isotope ratios of the several hot springs and underground water exist on the meteoric line. This suggest the origin of hot spring is meteoric water and the reason of temperature and cl concentration decreasing is mixture with low temperature meteoric water.

Keywords: hot spring, geothermal, isotope, meteoric water, fossil salt water

## Fluid geochemistry of hot springs at Kotakara-jima, Tokara Islands

TSUTSUMI, Saki<sup>1\*</sup> ; ISHIBASHI, Jun-ichiro<sup>1</sup> ; KONNO, Uta<sup>2</sup> ; YOKOSE, Hisayoshi<sup>3</sup>

<sup>1</sup>Department of Earth and Planetary Sciences, Graduate School of Sciences, 33 Kyushu University, <sup>2</sup>JAMSTEC, <sup>3</sup>Graduate School of Science and Technology, Kumamoto University

Yokose et al.(2010) proposed giant calderas related to Quaternary volcanic activity, on the seafloor along the Tokara Islands. Kotakarajima is located on the rim of the Takarajima Caldera, which belongs to this caldera chain. A hot spring called as Yutomari-onsen is located at the coastline of the Kotakarajima island, which water temperature reaches higher than 90 degC. Fluid chemistry of this hot spring was studied with the aim of understanding a hydrothermal system associated with the seafloor caldera.

Hot spring water was collected in May, 2013. Temperature, pH, electrical conductivity, and oxidation-reduction potential were measured on site. Fluid samples were filtered with a 0.45 um diskfilter and stored. Major cations and anions were analyzed by ICP-AES and ion chromatography. Alkalinity was determined by HCl titration and Si concentration was determined by colorimetry.

Fluid chemistry of the hot spring water is characterized by high Cl<sup>-</sup> concentration, Na/Cl ratio (=0.75) closed to that of seawater, and isotopic composition similar to seawater, which strongly suggests that it is originated from seawater. Depletion in Mg<sup>2+</sup> and SO<sub>4</sub><sup>2-</sup> and enrichment in K<sup>+</sup> and Ca<sup>2+</sup> compared with seawater, are in accordance with the idea that the fluid experiences seawater-rock interactions. Fluid temperature in the aquifer where interactions attain to equilibrium is estimated as 250-300 degC based on chemical geothermometers.

From these results, the Yutomari-hot spring at the Kotakarajima Island is considered as fluid discharge of a submarine hydrothermal system that is associated with Takarajima Caldera.

Keywords: Giant caldera, hydrothermal system, seawater-rock interaction

## Hydrothermal system beneath Shirahone hot spring, Nagano, Central Japan, revealed by resistivity survey

YAMAYA, Yusuke<sup>1\*</sup> ; MOGI, Toru<sup>2</sup>

<sup>1</sup>GSI, AIST, <sup>2</sup>ISV, Hokkaido Univ.

Shirahone hot spring is one of the most active geothermal area, located in the western part of Nagano prefecture, Japan. A source of hot water has not been clarified, because there are few geophysical exploration and borehole logging. We performed an electrical resistivity exploration employing the magnetotelluric (MT) method in order to identify a hot-water reservoir and whole hydrothermal system providing the Shirahone hot spring. The MT data were measured at six stations along the NNE-SSW line crossing the Shirahone area. The apparent resistivity and impedance phase were inverted to a two-dimensional resistivity section down to 3 km deep with the aid of the code developed by Ogawa and Uchida (1996). The estimated resistivity section generally indicates a range of resistivity 1-3000  $\Omega$ m, including two considerable conductors below 3  $\Omega$ m. These conductors are found at a depth 400-1000 m and deeper than 2000 m beneath the Shirahone hot spring. The upper conductor is interpreted as a hot-water reservoir which acts as a source of the Shirahone hot spring. The hot water would ascend from this reservoir to the discharge area through a fracture zone. The deeper conductor can be a heat source consisting of high temperature intrusive complex. This source might sustainably supply heat to the upper reservoir, which can keep itself a long time. A high resistivity zone is found beneath the Sakaigawa active fault zone. In general, an active fault is identified as a conductive zone due to saturated water into a fractured zone. Conversely, our resistivity section indicates a relatively resistive zone beneath the fault. This implies a locked part of the fracture zone where groundwater had declined after the last active phase of the fault.

Keywords: hydrothermal reservoir, Shirahone hot spring, resistivity, magnetotellurics, geothermal system

## Ground deformation around Ohaaki geothermal field, New Zealand inferred from persistent scatterer SAR interferometry

ISHITSUKA, Kazuya<sup>1\*</sup> ; TSUJI, Takeshi<sup>2</sup> ; MATSUOKA, Toshifumi<sup>1</sup> ; FUJIMITSU, Yasuhiro<sup>3</sup> ; NISHIJIMA, Jun<sup>3</sup>

<sup>1</sup>Graduate School of Engineering, Kyoto University, <sup>2</sup>International Institute for Carbon-Neutral Energy Research (I2CNER), Kyushu University, <sup>3</sup>Faculty of Engineering, Kyushu University

There are several producing geothermal fields in Taupo Volcanic Zone (TVZ), northeast-trending zone of mainly andesitic to rhyolitic arc/back arc volcanism, within the central North Island, New Zealand. It has been reported that ground subsidence with the rate of 30-50 mm/year has occurred at the Wairakei geothermal field, one of the biggest geothermal fields in TVZ [Allis et al., 2009]. Such a research on ground deformation around geothermal field is, however, rarely documented. Thus, it would be important to study deformation pattern at the geothermal field.

In this study, we mapped ground deformation around Ohaaki geothermal field located northeast of TVZ using persistent scatterer SAR interferometry (PS-InSAR). Since the analysis makes use of high quality phase information of the coherent target of SAR image, the estimated deformation is more accurate compared with the standard differential SAR interferometry (DInSAR). We processed 21 ALOS/PALSAR images acquired from January 2007 to January 2011 from an ascending orbit. As a result, we estimated ground deformation opposite to line of sight direction, which may correspond to ground subsidence. Moreover, the deformed area showed sharp boundary which we can be attributed to fault location in the area.

Allis, R., C. Bromley, and S. Currie, Update on subsidence at the Wairakei-Tauhara geothermal system, New Zealand, *Geothermics*, vol. 38, pp.169-180, 2009.

Keywords: ground deformation, persistent scatterer SAR interferometry, Ohaaki geothermal area

## Gravity Monitoring at Takigami Geothermal Area, Oita Prefecture, Japan

PRATIWI, Maryati<sup>1\*</sup>; FUJIMITSU, Yasuhiro<sup>1</sup>; NISHIJIMA, Jun<sup>1</sup>

<sup>1</sup>Kyushu University, Fukuoka, Japan

The gravity monitoring at Takigami geothermal area has been applied since November 1996 (Oka et al., 2011). In this area, the nearest geothermal manifestations are about 1-2 km to north and east of Takigami (Furuya et al., 2000). So, there are no geothermal manifestations at the surface. The geothermal power plant was built at Takigami in August 1991. It was reported that its power plant output was changed from 25,000 kW to 27,500 kW in June 2010 (Kyushu Electric Power Co., Inc., 2010)

We analyzed the gravity data from August 2008 until August 2013. We found that the gravity changes at the northern zone, the western zone, and the southwestern zone of this area are quite stable historically. This result indicates that the recovery state for these zones is almost done. However, the data at the eastern zone shows gravity increasing. It was assumed that the subsurface fluid at Takigami area flows from south, which is the direction Kuju Mountain area. Then, we noted that the fluid from south is filling the faults in eastern area in the beginning before going through to northern area (due to its high permeability (Jalilinasrabad et al., 2011)), thus the recovery state in the eastern zone has not been done.

By using theorem of Gauss, we calculated the mass changes based on the gravity changes from August 2009 to August 2012. This calculation is excluding the northern area as it has different water system, and removed the effects of precipitation and evapotranspiration by Gwater-e program (Kazama, 2011). And, we found that the mass increases as much as 10.12 Mt in the Takigami geothermal area. This mass change is associated with the production and reinjection process of geothermal fluids.

### REFERENCES

- Furuya, S., Aoki, M., Gotoh, H. and Takenaka, T. (2000), " Takigami geothermal system, northeastern Kyushu, Japan, " *Geothermics*, 29. 191-211.
- Jalilinasrabad, S., Itoi, R., Gotoh, H., and Tanaka, T. (2011), " Development of the Optimum Numerical Reservoir Model of the Takigami Geothermal Field, Oita, Japan " *Proc. of 36th Workshop on Geothermal Reservoir Engineering Stanford University, Stanford , California, SGP ? TR ? 191.*
- Kazama, T., K. Yamamoto, and Y. Fukuda (2011), " Hydrological disturbance corrections for relative gravity data observed at Sakurajima Volcano. " *116th Meeting of the Geodetic Society of Japan*, 17 (oral presentation at Gifu).
- Kyushu Electric Power Co., Inc. (2010). " Introduction to Geothermal Power Station of Kyushu Electric Power Co., Inc. " [Company brochure].
- Oka, D., Fujimitsu, Y., Nishijima, J., Fukuda, Y. and Taniguchi, M. (2011), " Geothermal Fluid Flow Monitoring by the Repeat Gravity Measurement at the Takigami Geothermal Field, Japan — Application of Hybrid Gravity Measurement by an Absolute Gravimeter (A10) and Relative Gravimeters (CG-3M and CG-5) —" *Proc. of 36th Workshop on Geothermal Reservoir Engineering Stanford University, Stanford , California, SGP ? TR ? 191.*

Keywords: gravity change, gravity monitoring, mass change, Takigami

## Heat balance technique under the condition that the influence of solar radiation can be negligible

FUJIMITSU, Yasuhiro<sup>1\*</sup> ; NISHIJIMA, Jun<sup>1</sup>

<sup>1</sup>Faculty of Engineering, Kyushu University

The coefficient of geothermal flux is essential for the heat balance technique (Sekioka and Yuhara, 1974), which is one of the methods for measurement of heat discharge rate from geothermal fields, and is determined by micrometeorological data of a target area. In order to comprehend the temporal change of the micrometeorological conditions and the coefficient of geothermal flux, we have manufactured an automated continuous micrometeorological measurement system and measured micrometeorological data at some geothermal fields. And we have discussed about the coefficient of geothermal flux (Fujimitsu et al., 2009; Fujimitsu et al., 2010; Fujimitsu et al., 2011).

In the heat balance technique, a reference temperature is set on a ground surface where there is no geothermal anomaly, and the area that indicates higher ground surface temperature than the reference temperature is regarded as the geothermally anomalous area. However, the influence of solar radiation on the determination of the reference temperature is one of the main factors in accuracy of the estimated heat discharge rate by the heat balance technique. Therefore, we assumed the condition that the influence of solar radiation can be negligible, and conducted the observation experiments during the nights by using an artificial heating element as a heat source in order to improve the accuracy of the heat balance technique by a new analytical method.

For the new analytical method, we considered the heat balance at the ground surface under the condition of no solar radiation, adopted Richardson number for determination of the transfer velocity, and changed the determination procedure of the reciprocal of the Bowen ratio. As a result, the new analytical method estimated the heat discharge rates that are almost the same as the actual heat generation rates from the artificial heating element.

We are grateful to Mr. Shohei Oshikata who had progressed this study.

Fujimitsu, Y., Nishijima, J. and Ehara, S. (2009) Temporal change of the coefficient of geothermal flux used in the heat balance technique. Abstracts of Japan Geoscience Union Meeting 2009, V161-P012.

Fujimitsu, Y., Nishijima, J. and Ehara, S. (2010) Relationship between the coefficient of geothermal flux and ground surface temperature anomaly. Abstracts of Japan Geoscience Union Meeting 2010, SVC061-P03.

Fujimitsu, Y., Nishijima, J. and Ehara, S. (2011) Relationship between the coefficient of geothermal flux for the heat balance technique and micrometeorological data. Abstracts of Japan Geoscience Union Meeting 2011, SVC049-P10.

Sekioka, M. and Yuhara, K. (1974) Heat flux estimation in geothermal areas based on the heat balance of the ground surface. *J. Geophys. Res.*, Vol. 79, No. 14, 2053-2058.

**Keywords:** Heat balance technique, coefficient of geothermal flux, micrometeorology, heat discharge rate, solar radiation, reference temperature

## Simulation of the Daisen-Kurayoshi tephra, in the San-in district, SW Japan, using Tephra2

YAMAMOTO, Takahiro<sup>1\*</sup> ; SUGIYAMA, Minoru<sup>2</sup> ; TAJIMA, Yasuhisa<sup>2</sup>

<sup>1</sup>Geological Survey of Japan, AIST, <sup>2</sup>Nippon Koei Co Ltd

The Daisen-Kurayoshi tephra, which erupted from Daisen volcano at about 53 ka, is one of the most voluminous Plinian fall deposits in Japan. Its apparent volume was estimated as more than 20 km<sup>3</sup>, but quantitative study of this tephra have not be done. So, we try to analyze this tephra using Tephra2 and decide its eruption parameters. In the simulation, we set 5 cases in height of the eruption column from 10 to 18 km, 4 cases in weight of the erupted magma from 1 to 8x10E+18 kg, 4 cases in medium grain size of the ejected materials from 0 to 3 phi, and 5 cases in sorting of the ejected material under the average wind data above Yonago. A total of 400 cases have been calculated. To explain the observed distribution of the tephra, the column height and ejecta weight have to be 18 km and 4 to 8x10E+18 kg (40 to 80 km<sup>3</sup>), respectively.

Keywords: Daisen-Kurayoshi tephra, Tephra2

## Insight into setup of typical meteorological conditions for evaluating volcanic ash hazard

HATTORI, Yasuo<sup>1\*</sup> ; SUTO, Hitoshi<sup>1</sup> ; GO, Yumiko<sup>2</sup> ; TOSHIDA, Kiyoshi<sup>1</sup> ; HIRAKUCHI, Hiromaru<sup>1</sup> ; ISHIHARA, Shuji<sup>2</sup>

<sup>1</sup>Central Research Institute of Electric Power Industry, <sup>2</sup>Denryoku Computing Center

Estimation of ash concentration and deposition is of practical interest in evaluation of volcanic ash risk on critical infrastructure (e.g. Wardman et al. 2012). For estimating ash concentration and deposition, numerical simulations with an ash transport- and deposition-model have become a powerful tool (e.g. Folch 2012). However, the setup of meteorological conditions, which mainly control the ash transport- and deposition- processes in the atmosphere and on the ground, has not been discussed in details.

In the present study, we examine the estimation of ground deposition for a real test case, a volcanic ash hazard in Kanto-area for an eruption at Mt. Fuji, with various meteorological conditions by using an ash transport- and deposition-model, fall3d. The meteorological conditions are generated with the 53 years reanalysis meteorological dataset, CRIEPI-RCM-Era2, which has a temporal- and spatial resolutions of 1 hr and 5 km; the typical and extreme conditions were sampled by using Gumbel plot and an artificial neural network technique.

The ash deposition is invariably limited to the west area of Mt. Fuji, even with the typical wind conditions on summer, while the isopach of ground deposition depicted various distributions, which strongly depends on meteorological conditions. This implies that the concentric circular distribution must not be realistic. Also, a long-term eruption, such as the Hoei eruption during stage3, yields large deposition area due to the diurnal variations of wind direction, suggesting that the attention to the differences between diurnal variation and fluctuations of wind direction on evaluating of volcanic ash risk is vital.

More details will be presented in the presentation, and we believe that our study must be helpful to develop the numerical simulations for evaluation of volcanic ash risk.

Keywords: Ash transport- and deposition-model, Long-term meteorological reanalysis, Extreme value, Artificial neural network, Advection-diffusion, Numerical simulation

## Numerical model of 3D ballistic trajectory for hazard assessments at Upper Te Maari eruption of Tongariro volcano in New

TSUNEMATSU, Kae<sup>1\*</sup> ; FITZGERALD, Rebecca<sup>2</sup> ; KENNEDY, Ben<sup>2</sup>

<sup>1</sup>Graduate School of Environmental Studies, Nagoya University, <sup>2</sup>Department of Geological Sciences, University of Canterbury

Ballistic bombs and blocks are energetic pyroclasts deposited around volcanic craters. Hazard assessments of ballistic projectiles are important for people, buildings, and roads around vent especially in tourist and residential areas. Tongariro volcano, an active volcano in a popular national park in New Zealand, erupted August 6th, 2012 after one hundred years. By combining acoustic signals with eyewitness descriptions, five eruption pulses from fissures around Upper Te Maari crater were characterized and conditions of particle ejection were defined. A distribution of ballistic blocks was mapped from orthophotos and field campaigns. In order to clarify characteristics of ballistics at Tongariro volcano and assess future hazards, a numerical model of ballistics is modified and applied to the 2012 eruption. At first, 3D multiparticle model based on Discrete Event Simulation (DES) method is converted to the model based on semi-Lagrangian method to include an effect of air drag and gas flow around airborne particles. Initial conditions, such as ejection direction and speed, were calibrated to explain both spatial and size distribution of deposit bombs. Finally, an initial particle velocity of 200 m/s and gas flow velocity (constant) of 150 m/s are obtained as conditions of best fit. Furthermore, we applied this model to the assessment of future eruption regarding Tongariro Alpine Crossing, a walking trail in the national park frequented by ~80,000 people each year. Impacts of two extreme eruption cases are simulated by the numerical model. Negligible probabilities of fatality along the TAC are found from a magnitude smaller eruption, similar in size to the November 2012 eruption. However, a magnitude larger eruption could result in higher probabilities in certain areas of the track which it would be unlikely to survive the eruption. Varying the input parameters from the calibrated model allows for the assessment of future ballistic hazard from larger and smaller eruptions of Upper Te Maari Crater. A possibility of applying this model to the assessment of Japanese volcanoes such as Mt. Fuji will be discussed.

Keywords: Ballistics, Hazard map, Numerical model, Volcanic eruptions, Hazard assessment, Tongariro Volcano

## Estimation of locations and migration of debris flows on Izu-Ohshima Island on 16 Oct., 2013 by seismic amplitudes

OGISO, Masashi<sup>1\*</sup> ; YOMOGIDA, Kiyoshi<sup>2</sup>

<sup>1</sup>Matsushiro Seismological Observatory, JMA, <sup>2</sup>Grad. Sch. Sci., Hokkaido Univ.

Typhoon 1326 (Wipha) with heavy rainfall caused severe damage at Izu-Ohshima Island on 16 October 2013 with large-scale debris flow, probably not only a single event but sequence of flows.

Seismic networks on Izu-Ohshima recorded the signals originated from those debris flows. At least five events of large amplitudes are recognized in continuous records of seismographs.

It is hard to estimate the location of such events with conventional methods of epicenter determination because of the difficulty to identify any seismic phase arrivals. We estimate the locations of the five events with spatial distribution of seismic amplitudes (Battaglia and Aki, 2003; Kumagai et al., 2010). In this method, after correcting the site effect of each station, the RMS amplitude of high-frequency seismic waveform is assumed to decay only with geometrical spreading and intrinsic absorption. Although amplitudes depend on radiation pattern of seismic waves, the isotropic distribution of amplitudes could be assumed at high frequencies because of the scattering effect by small scale heterogeneity in the crust (Takemura et al., 2009). The location of each event is derived as the point of the minimum residual between observed and calculated amplitudes of all the seismic stations. Before estimating the locations of the five events, we apply the band pass filter of 5-10Hz to each seismic record. We assume that the filtered waveform is composed of S body waves only, S-wave velocity is 1.44km/s, and  $Q=100$  for intrinsic absorption. We limit the search range of each event only on the surface of the island. Site factors of stations are estimated by amplitudes of coda waves for regional earthquakes.

The estimated locations of all the five events are located in an eastern side of Motomachi district, where huge casualties were suffered, agreeing with the debris flow traces mapped carefully after the disaster occurred. In addition, the location is migrated to the west (i.e., from the volcano flank to the sea coast) within its duration time of 60-80 sec except for one event with small duration time. Such migrations may correspond to the flow of debris, with its speed about few tens km/h. Time series of source amplitudes, that is, the maximum value and duration time of each event show the variability of the debris flows occurred on Izu-Ohshima Island within several hours on that day.

Generally, seismic networks focused on volcanic activities are generally composed of stations of higher density than other seismic networks. The records of such dense seismic networks are useful to analyze not only earthquakes and tremor on volcanoes, but also debris flows or other disastrous events, as shown in this study. The present location method using the spatial distribution of seismic amplitudes is conceptually able to apply in quasi-real time, so it should be useful to early estimation of location and magnitude of various disasters in and around volcanoes.

### Acknowledgements

We analyzed the seismic waveforms recorded in the networks on Izu-Ohshima Island which are operated by Earthquake Research Institute of the University of Tokyo, the National Research Institute for Earth Science and Disaster Prevention, and the Japan Meteorological Agency. We used the digital elevation model and topographical map images of Digital Japan Web System provided by the Geospatial Information Authority of Japan.

Keywords: distribution of seismic amplitudes, locations and migration of debris flows, Izu-Ohshima Island

## G-EVER Next-generation Volcanic Hazard Assessment System

TAKARADA, Shinji<sup>1\*</sup> ; BANDIBAS, Joel<sup>1</sup>

<sup>1</sup>Geological Survey of Japan, AIST

The Asia-Pacific Region Global Earthquake and Volcanic Eruption Risk Management (G-EVER) is a consortium of geohazard research institutes that was established in Asia-Pacific region in 2012. G-EVER aims to formulate strategies to reduce the risks caused by earthquakes, tsunamis and volcanic eruptions worldwide. The G-EVER next-generation volcano hazard assessment working group is developing a useful system for volcanic eruption prediction, risk assessment, and evacuation strategy at various eruption stages. The assessment system is based on volcanic eruption history datasets, eruption database and numerical simulations. Eruption history datasets including precursor phenomena leading to major eruptions are important for the prediction of future volcanic eruptions. A high quality eruption database which contains compilations of eruption dates, volumes, and styles, is important for the next-generation volcano hazard assessment system. Formulating international standards on how to estimate the volume of volcanic materials is important to establish a high quality volcanic eruption database. GIS-based spatial distribution database of volcanic materials (e.g. Tephra and pyroclastic flow distributions) is important for accurate area and volume estimation and risk assessments. The volcanic eruption database is developed based on past eruption results, which only represent a subset of possible future scenarios. Therefore, numerical simulations with controlled parameters are needed for more precise volcanic eruption predictions. The "best-fit" parameters of the past major eruptions in the world have to be estimated and the simulation results database should be made.

The use of the next-generation system should enable the visualization of past volcanic eruptions datasets such as distributions, eruption volumes and eruption rates, on maps and diagrams using timeline and GIS software. Similar volcanic eruption types should be easily searchable from the eruption database. Using the volcano hazard assessment system, prediction of the time and area that would be affected by volcanic eruptions at any location near a volcano should be possible using numerical simulations. The system should be able to estimate volcanic hazard risks by overlaying the distributions of volcanic deposits on major roads, houses and evacuation areas using a GIS enabled systems. The next-generation real-time hazard assessment system will be implemented with user-friendly interface, making the risk assessment system easily usable and accessible online.

Preliminary version of the next-generation volcanic hazard assessment system is available since June 2013. This can run energy cone simulations at any volcano in the world using ASTER Global DEM, and the links to major volcanic databases, such as Smithsonian, VOGRIPA and Quaternary volcanoes. Almost all volcanoes in the world can be evaluated using this volcanic hazard assessment system. Currently, the system covers more than 3200 Quaternary volcanoes worldwide. Links to major volcanic databases in the world are useful to examine eruption history in detail. Using Google and Bing maps as base maps provide more information for hazard evaluations. A hazard evaluation system using Titan2D will be available soon. Hazard assessment system using probabilistic analysis is also being planned in collaboration with INGV in Italy. This hazard assessment system is expected to be used for hazard mapping and risk management planning by government authorities and policy makers.

G-EVER Next-generation Hazard Assessment System URL (<http://volcano.g-ever1.org/vhazard/HazardAssessment/>)

Keywords: volcano, hazard, Asia-Pacific, G-EVER, simulation, database

## An attempt to obtain empirical evidences for petrological assessment of volcanic activity based on magma database

TAKEUCHI, Shingo<sup>1\*</sup> ; TOSHIDA, Kiyoshi<sup>1</sup> ; MIURA, Daisuke<sup>1</sup>

<sup>1</sup>Central Research Institute of Electric Power Industry

For Japanese volcanoes, high-quality databases of volcanic eruptions have been developed, for example Japanese active volcanoes (Kudo and Hoshizumi, 2006-) and one-million years chronology of volcanic eruptions (Hayakawa, 1996-). These databases involve eruptive age, eruption style and eruption magnitude, *M*. In contrast, it is often the case that properties of magma that caused these eruptions remain unrevealed. We have sampled and analyzed eruptive products of ca. 90 eruptions in Japan during the last one hundred thousand years and are constructing a database of magmatic properties (petrological properties), as a magma database. This database involves mainly large scale eruptions with *M*=4-8 and additionally recent small eruption of *M*=1-3. In the magma database, we estimate melt compositions, and phenocryst contents, which are important factors controlling physical properties of magmas, and thus eruption dynamics. Based on the magma database, we have attempted to obtain empirical evidences between these magmatic properties and eruption characteristics (eruption magnitude, eruption style and so on).

Examining relationship between eruption magnitude, *M*, and magmatic properties for ca. 100 eruptions, including 11 eruptions compiled in Takeuchi (2011), some relationships are found.

(1) Rhyolitic melt (>70 wt% SiO<sub>2</sub>)-bearing magmas (andesitic to rhyolitic magmas) caused *M*=4-8 eruptions. In contrast, basaltic to dacitic melt (<70 wt% SiO<sub>2</sub>)-bearing magmas (basaltic to dacitic magmas) caused *M*=1-5 eruptions.

(2) For rhyolitic melt-bearing magma, the maximum eruption magnitudes are correlated with phenocryst content. Phenocryst-poor magmas with 0-20 vol% caused caldera-forming eruption with *M*=8 at the maximum, where phenocryst-rich magmas with 20-50 vol% phenocryst have the maximum eruption magnitude with ca.6.

These empirical evidences suggest that petrological properties, such as melt composition and phenocryst content, are some level of constraint on eruption magnitude. Thus, petrological analysis of eruptive materials in early eruptive stage may contribute to constructing eruption scenario.

Keywords: magma, petrological analysis of volcanic rock, assessment of volcanic activity, database

## Temporal variation (2011-2013) of the amount of CO<sub>2</sub> dissolved in Lake Monoun, Cameroon

OHBA, Takeshi<sup>1\*</sup>; ISSA, I<sup>1</sup>; SASAKI, Yuka<sup>1</sup>; KUSAKABE, Minoru<sup>2</sup>; YOSHIDA, Yutaka<sup>3</sup>; UEDA, Akira<sup>2</sup>; ANAZAWA, Katsuro<sup>4</sup>; SAIKI, Kazuto<sup>5</sup>; KANEKO, Katsuya<sup>6</sup>; MIYABUCHI, Yasuo<sup>7</sup>; AKA, F t<sup>8</sup>; TANYILEKE, G<sup>8</sup>; HELL, J v<sup>8</sup>

<sup>1</sup>Tokai Univ, <sup>2</sup>Univ Toyama, <sup>3</sup>Yoshida Eng Office, <sup>4</sup>Univ Tokyo, <sup>5</sup>Osaka Univ, <sup>6</sup>Kyoto Univ, <sup>7</sup>Kumamoto Univ, <sup>8</sup>IRGM Cameroon

### Introduction

On 15th Aug 1984, the people living Lake Monoun, western Cameroon, heard a loud sound and experienced earth tremors. After the event, a deadly phenomenon occurred as 37 people were asphyxiated by gas that was discharged from the lake. Sigurdsson et al (1987) attributed the cause of the outburst of CO<sub>2</sub> to landslide that plunged into the Lake's depth, which was CO<sub>2</sub>-charged. After a scientific consensus that proceeded from a similar phenomenon at Lake Nyos (100 km NW of Lake Monoun) in 1986, the explosive discharge of CO<sub>2</sub> gas from lakes was named "limnic eruption". In 2001, the concentration of CO<sub>2</sub> dissolved in Lake Monoun approached saturation at the depth of 50 m (Kusakabe et al., 2008), suggesting a possibility of recurrence of the limnic eruption if no preventive measures were taken. To prevent another limnic eruption, a degassing pipe was installed at Lake Monoun in 2003 (Halbwachs et al., 2004), and by 2009, the lake was almost free of dissolved CO<sub>2</sub> and lost its natural gas self-lifting capability through the pipes. Recently we observed that concentration of CO<sub>2</sub> has increased slightly in the bottom water. To avoid gas re-buildup in the lake, in 2013, we installed a solar energy driven system to artificially pump the CO<sub>2</sub>-rich water to the surface.

So far we have employed two methods (MK and CTD) to determine a reliable CO<sub>2</sub> concentration profile in lakes.

The MK method (Kusakabe et al, 2000)

With this method, we determine CO<sub>2</sub> concentration in lake water as follows. A disposable plastic syringe that contains 10 ml of 5M KOH solution is immersed in the lake at a given depth using an MK sampler. After that, we suck 30ml of lake water into the syringe to fix the total dissolved CO<sub>2</sub> (CO<sub>2</sub> dissolved gas, HCO<sub>3</sub><sup>-</sup> and CO<sub>3</sub><sup>-</sup>) as CO<sub>3</sub><sup>-</sup>. Then a volumetric titration with standard HCl solution allows the determination of the total carbonate in the syringe. The results obtained so far indicate that the MK method is accurate and reliable. However, the method gives discrete data in terms of depth.

The CTD method

The CTD (Conductivity, Temperature, Depth) enables us to estimate the CO<sub>2</sub> concentration as a smooth depth profile. The absolute value of CO<sub>2</sub> concentration by the CTD method depends strongly on pH and conductivity values, thus the data from the CTD method need to be carefully examined compared to those from the MK method. We introduced an adjustable parameter  $k$  as defined by  $C\text{-corr}=k \times C$ , where  $C$  is the measured raw conductivity and  $C\text{-corr}$  is the corrected conductivity. Assuming an appropriate molar conductivity for HCO<sub>3</sub><sup>-</sup>, the  $C\text{-corr}$  gives the total CO<sub>2</sub> concentration under the assumption of chemical equilibrium among the dissolved carbon species (CO<sub>2</sub>aq, HCO<sub>3</sub><sup>-</sup> and CO<sub>3</sub><sup>-</sup>). We compared the total CO<sub>2</sub> concentration by MK method and CTD method at the every depth where we have the values by MK method. The difference between the two methods was squared and the summation of squared values was calculated. The summation was minimized with changing the parameter  $k$ .

### Results

As shown in Fig. 1, the thickness of bottom water with CO<sub>2</sub> concentration higher than 20 mmol/L increased significantly in 2012 relative to 2011. This tendency continued in 2013, although CO<sub>2</sub> concentration of the bottom water decreased slightly. The lake water shallower than 30m is affected by inflowing river water contains low concentration of total CO<sub>2</sub>. The total CO<sub>2</sub> profile was integrated between -98m (near bottom) to -30m and estimate of the total amount of CO<sub>2</sub> in the lake were 101, 118 and 119 Mmol in 2011, 2012 and 2013, respectively. Those values are much smaller than 600 Mmol, which was the amount of CO<sub>2</sub> gas in lake just before the degassing pipe started functioning (Kusakabe et al., 2008). However, it should be noted the amount of dissolved CO<sub>2</sub> is gradually increasing, so a regular monitoring of the lake is imperative.

Keywords: Lake Monoun, CO<sub>2</sub>, Limnic eruption, Cameroon, Magma

SVC52-07

Room:416

Time:April 28 11:45-12:00

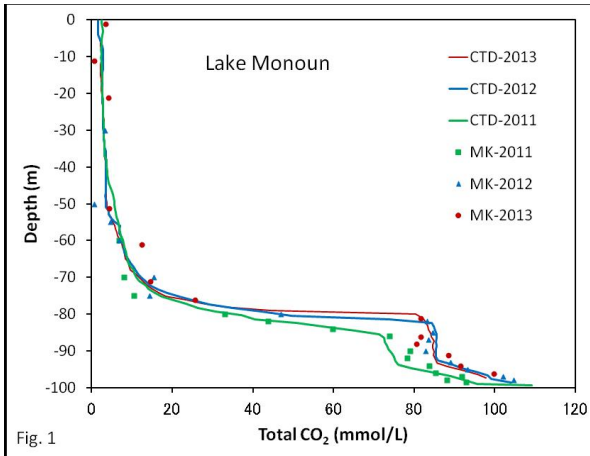


Fig. 1

## Topographical features of Fuji volcano as seen in the polar coordinate system

CHIBA, Tatsuro<sup>1\*</sup>

<sup>1</sup>Asia Air Survey Co., Ltd.

### Introduction

Fuji volcano is the highest mountain in Japan and the most active volcano in past 12 thousand years, in Japan except for the caldera eruption (Miyaji 1988). The inclination is loosely about 300,000 people each year climb to the summit.

As a result of repeated eruption of central vent, volcanic body of a huge cone-shaped with a diameter of 10km high specific 2000m is formed around the crater. Fuji volcano had piled up in stages on Komitake, Old-fuji, and New-fuji. The remaining part of the old edifice also so as to project on the slope. Fuji is seen variety profile from the direction by such features.

### Study range

In this paper, the technique of polar coordinate conversion. Study subjects ranged circular radius 13.5km centered summit. This point is not the highest point, the approximate center of Dainai-in Institute (The latitude is 35.36295 and longitude is 138.73035). The terrain data is base map information 0.4 seconds mesh of the Geographical Survey Institute (about 10m) source, was used in resampled to 50m mesh Japanese orthogonal coordinate system (VIII, system).

### Angle of repose

Slope gradient of the volcano, is determined by the movement mechanism and state of matter that has been brought to the ground from the crater in general, the angle of repose and stable gradient. Looking at the topography of the polar coordinate transformed, it can be seen that the portions to concentrated lateral cone is higher than ambient, and is raised as acne. In particular, it is found that it is concentrated in a direction 315 degrees and 135 degrees direction. It should be noted that the gap of advanced 250 degrees around, under the influence of Tanzawa is protruding from the east, to the south of Gotemba is lower.

### Projected section

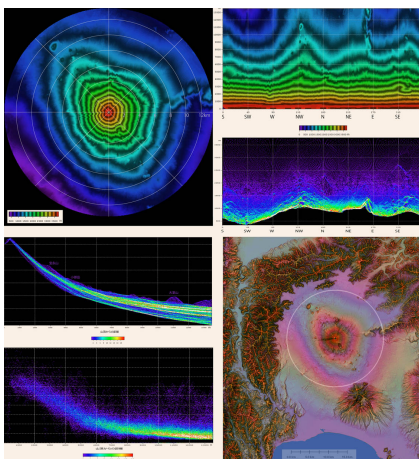
Take the elevation direction from the summit, the Y-axis in X-axis, to prepare a projected section shows the projection section color grid point frequency distribution of 50mDEM. If likened to Mount Fuji skirt, bright line of lower limit corresponds to the height of the perimeter of the flared skirt. According to this chart, it can be seen that the low altitude most Fujinomiya direction of southwest. Then, a Fuji-Yoshida direction Gotemba direction, finally. Design such as bubbling southeast and northwest direction direction can be seen, but it is the effect of mountain body side of the volcano. In addition, over the surface of Lake Yamanaka from Oshino of 250 degrees from 200 degrees azimuth, elevation is significantly higher than at the periphery. In this direction there is a mountain slope body of old Fuji.

### Literature

Tatsuro Chiba (2010) Landform -50mDEM cylindrical coordinate transform analysis, Fujigaku studies, 7, 1, 3-13.

Miyaji Naomichi (1988) Activity history of younger Fuji volcano, Journal of the Geological Society, 94, 6, 433-452.

Keywords: DEM, angle of repose, profile, slush abalanche, lava flow, active fault



## Tool handing down disaster experiences using Geoparks: examples of Unzen Volcanic Area Global Geopark

OHNO, Marekazu<sup>1\*</sup>

<sup>1</sup>Unzen Volcanic Area Geopark Promotion Office

Local inhabitants living in Shimabara peninsula has suffered volcanic disasters of Mt. Unzen repeatedly, which include the worst volcanic disasters occurred in 1792 (Kansei eruption and Shimabara Catastrophe). Nevertheless these conditions, they stay near Mt. Unzen to take good living environments.

Since they continue living in the near active volcano, they are always at risk of the volcanic disasters. If these experiences of disasters pass down to next generations, disaster prevention awareness in local inhabitants and, as the result, risk from disasters should be reduced. However, because of a long eruption interval (a few hundred years) of Mt. Unzen, it is difficult to pass down these experiences to next generations. Furthermore, the information that emphasized a disaster more than required may lead the uneasiness of local inhabitants. The system to overcome these problems is a Geopark.

Education is one of main component of businesses of geoparks. Thus, we have carried out an education program of disaster prevention for local school students as a business of Geopark and promote their awareness of disaster prevention.

Actually, all of 6th grade of elementary school students in Shimabara city visit geosites for a day as a geotour and learn the highlights of the Geopark. Main theme of the geotour is a *Kansei and Heisei eruptions and their disasters*. School students learn what happened at their home town in about 20 years ago through observation of a building of elementary school burned by a fire derived from pyroclastic surge and a memorial park preserved houses buried by lahar. In the tour, I also try to inquire why you stay near the active volcano introducing great landscapes created by big landslides occurred in 1792, spring water sprung out from a head of a lava flow emitted in 1792 and local special foods using local natural environments.

This is not a program to learn disaster prevention directly. However, when local inhabitants (especially children) understand academic value of local resources (e.g. strata, landscapes, human history, culture, and so on) and realize reasons to stay near active volcanoes, their consciousness of disaster prevention must be promoted. I believe the system of Geopark must contribute promotion of volcanic disaster prevention in Japan.

Keywords: Unzen Volcanic Area Global Geopark, Education of disaster prevention, geosites, Heisei eruptopm, Shimabara Catastrophe

## Reproduction of the Eruptive sequence of the 2011 Shinmoedake eruption using the kitchen volcano experiments

IMURA, Ryusuke<sup>1\*</sup> ; TANIYAMA, Hirokazu<sup>2</sup>

<sup>1</sup>Graduate School of Science and Engineering, Kagoshima University, <sup>2</sup>Takaharu Town Office, Miyazaki Prefecture

For elementary and junior high school students, we conducted a program for the reproduction of the eruptive sequence of the 2011 Shinmoedake eruption using the kitchen volcano experiments. Learning about the Shinmoedake eruption in 2011 will lead to disaster prevention. This program plays an important part of education and disaster prevention activities in the Kirishima Geopark.

Keywords: The 2011 Shinmoedake eruption, kitchen volcano experiment

## HOMURA: Development of mobile sensor for volcanic exploration

KANEKO, Katsuya<sup>1\*</sup> ; ITO, Koichi<sup>2</sup> ; ANBE, Yuichi<sup>3</sup> ; IWAHORI, Kodai<sup>4</sup>

<sup>1</sup>Human and Environmental Studies, Kyoto University, <sup>2</sup>Graduate school of Science, Kyoto University, <sup>3</sup>Graduate school of Technology, Kyoto University, <sup>4</sup>Faculty of Science, Kyoto University

Monitoring of phenomena near craters of active volcanoes is important to learn symptoms of volcanic eruptions and to understand eruption dynamics. At present, some devices such as crater camera, volcanic gas sensors, and seismographs that have been installed in a calm period of volcanic activity are monitoring volcanic phenomena near the craters. On the other hand, we cannot approach the crater and cannot install new devices after beginning of a volcanic eruption, even if we want to observe unexpected volcanic phenomena. Therefore, unmanned robots that observe them on an ad hoc basis are needed. Previously some projects have tried to develop robots for volcanic exploration. However, those projects which required large budgets ended before a practical application.

We hope to destroy the status quo and are trying to develop a practical unmanned-ground-vehicle-type robot for volcanic exploration that carries out monitoring near active craters. We named this system "Homura". Homura is controlled by wireless remote control, move in volcanic field, approach an active crater, monitor volcanic phenomena with sensors equipped in the vehicle, and send their data to the base station in real time. In this presentation, we introduce a prototype of Homura and report a test campaign in Mihara-yama volcano, Izu-Oshima.

Guidelines of development of Homura are two: (1) the vehicle does not readily become undrivable in volcanic fields, and (2) assemblage and use of Homura require low costs. We produced the prototype of Homura these guidelines. Homura is a six-wheeled vehicle with a vertically symmetric shape. Its size is 750 length x 430 width x height 310 mm, its weight is about 12 kg. The power source is two-cell lithium polymer battery (7.4 V, about 250 Wh capacity). Some sensors such as camera, GPS, CO<sub>2</sub> gas sensors are installed in the vehicle. Homura communicates with the base station by digital radio communication, and receives and send commands from base stations and data in real time. An installed small computer control all telecommunication, movement, and sensors. Production cost of vehicle is about 200,000 JPY, which is much lower than the robots developed in the previous projects.

Means of stable radio communication are needed for practical missions in volcanic field. Homura can use wireless transceiver modules that directly communicate with another module and Docomo FOMA modem using mobile phone network. The former wireless transceiver modules can be used in any volcanic field but distance between Homura and the base must be less than 1 km. The latter FOMA communication needs cell phone network. If the network is available, we can control Homura in any place.

We carried out a test campaign of Homura around Mihara-yama volcano, Izu-Oshima in November, 2013 to examine remote control with FOMA communication. The base station was placed at Ohshima Spa Hotel which is about 2 km distant from the summit crater. Homura started Ohshima Spa Hotel. We controlled Homura only with information from sensors such as camera, GPS, and gyro. Homura moved on the mountain trail and reached the summit. Then, it climbed down on scoria slope without trail. This campaign result indicate that we can control Homura with remote control in volcanic fields. On the other hand, the radio communication with FOMA was not stable enough in Izu-Oshima. At four areas where lava walls were barriers between Homura and a relay antenna of FOMA, the communication became unstable or disconnected. This indicates that we cannot move Homura to the summit only by remote control in Mihara-yama. When a UGV robot carries out missions in the volcanic field, we must obtain means of stable telecommunication before the missions. There are some cases where temporal stations of relay antenna are needed to use cell phone network.

Keywords: robot, Remote control, Telecommunication by cell phone, Izu-ohshima

## Particle fallout from an eruption column (2) - evaluation of reproducibility

MANNEN, Kazutaka<sup>1\*</sup>

<sup>1</sup>Hot Springs Research Institute of Kanagawa Prefecture

One of the major sources of error in tephra fall simulation is considered to be the source term, which depicts amount of particle release as a function of height in eruption column. The source term has been assumed to be linear or modeled using relationship between particle size and plume velocity (Suzuki function); however, no direct observation of the source term has been reported. The author has tried to obtain source term of the 1986 Izu-Oshima B eruption based on inversion technique using a tephra simulation code named Tephra2. Here the reproducibility of the inversion is evaluated.

In this study, two methods are applied to evaluate reproducibility. One is validation using a dummy source term. In this method, a dummy source term is given and tephra loads on each observation point is calculated using Tephra2. Based on the calculated loads, the source term is inversely calculated and compared with the originally given source term.

The other method is jackknifing. In this method, source terms are calculated using dataset in which a single observation is deleted one by one. The calculated source term is called as pseudo-value and the estimated source term is defined as an average of the pseudo-values. The error of the source term is also defined as a standard deviation of the pseudo-values.

In the 1986 Izu-Oshima B eruption, range of reproducible height changes as a function of grain size; 0-7 km for -3 phi particles and 0-4 km for 0 phi particles. The errors of obtained source parameter was limited; less than 10 % in the most cases.

Keywords: Pyroclastic fall, Tephra2, simulation

## Detection of thermal anomaly associated with volcanic activity from MODIS data

TSUTSUMI, Rika<sup>1\*</sup>

<sup>1</sup>Chiba University

There are a lot of volcanoes in the world. And then, it is difficult to monitor all volcanoes because of costs. But we can monitor efficiently a lot of volcanoes using satellite remote sensing, because a volcanic activity will cause the increase in surface temperature and satellite (whose sensor can observe the surface temperature) remote sensing can cover a large area on surface. Therefore, various approaches have been suggested to monitor volcanic activities using remote-sensing satellite data.

Removing cloud pixel is essential to monitor volcanic activities using remote-sensing satellite data. Therefore, the purpose of this study is to remove cloud accurately and to develop an adequate algorithm continuously to detect thermal anomalies related to volcanic activities (especially lava activity which causes serious damages involve human lives) using MODIS (Moderate Resolution Imaging Spectroradiometer) infrared sensor onboard Aqua satellite.

We investigate spatial-time changes in thermal infrared in the statistical way. In order to detect only hotspots related to lava activities without faints, the developed algorithm investigates the difference temperature behavior between a target point and reference points, and we get spatial difference of brightness temperature (S). The presence of cloud causes large value of S that doesn't related to volcanic activities (Noguchi 2011). Therefore, removing cloud is essential in the proposed algorithm. To remove cloud, we use some BTD (Brightness Temperature Difference) which is sensitive to cloud. And we verified the technique of cloud removal as compared with Lidar data.

Keywords: MODIS, Lidar, Volcanic activity, Shinmoe-dake, lava activity

## Variations of basaltic magmas and their timing of injection into the magma system of Sakurajima volcano since AD 1779

EBIHARA, Kaho<sup>1</sup> ; NAKAGAWA, Mitsuhiro<sup>1\*</sup> ; YOSHIMOTO, Mitsuhiro<sup>1</sup> ; KOBAYASHI, Tetsuo<sup>4</sup>

<sup>1</sup>Earth & Planetary System Sci., Hokkaido Univ., <sup>2</sup>Earth & Planetary System Sci., Hokkaido Univ., <sup>3</sup>Earth & Planetary System Sci., Hokkaido Univ., <sup>4</sup>Earth & Environmental Sci., Kagoshima Univ.

Sakurajima volcano has repeated plinian eruptions three times during the last 600 years and changed the mode of eruptive activity since the AD 1914 plinian eruption. Frequent vulcanian eruptions has continued since AD 1955. Nakagawa et. al(2011) concluded that two-end-member magma mixing of silicic magma(S-magma) and andesite magma(A-magma) occurred in 1471 and 1779, and three-end-member magma mixing of mixed magma(S+A) and basaltic magma(B-magma) since the 20th century. They concluded that the injection of the B magma has frequently occurred since then to change the mode of eruptive activity. Their evidences of the injecting were presence of Olivine and An=90 plagioclase phenocrysts and different mixing trend in SiO<sub>2</sub> variation diagrams between the 20th century and previous products. However, petrological features of AD 1779 submarine eruptive products just after the terrestrial plinian eruption have not been revealed in detail. In this study, newly collected 1779 submarine products are investigated to discuss the magma plumbing system.

The AD 1779 submarine products are banded pumice and slightly vesiculated lavas. These contain plagioclase, orthopyroxene, clinopyroxene and magnetite as phenocryst associated with small amounts of olivine microphenocrysts, which were not recognized in the AD 1779 terrestrial products. These olivine phenocrysts do not have reaction rims of orthopyroxene. Average core compositions of these are about Fo=77. Compositional variations of other phenocrysts, except for magnetite, are nearly the same as those in the AD 1779 terrestrial and 20th eruption products. These olivine phenocrysts are diequilibrium with pyroxenes on the basis of Fe-Mg partitioning, suggesting that the basaltic magma injected into the mixed magma between the S and A magmas, which erupted as the AD 1779 terrestrial products. It should be noted that the injection of the basaltic magma had started just before the submarine eruption. On the other hand, olivine phenocrysts in the 20th century products are composed of two types, with or without reaction rims of orthopyroxene. Average core compositions of those without reaction rims are Fo=81, whereas those with reaction rims are less than Fo=74. These suggest that the 20th century products had been repeatedly injected by the basaltic magmas and that the basaltic magma injecting just before the AD 1779 submarine eruption had olivine phenocrysts with Fo=81. Although the injections of the basaltic magma has occurred just before the AD 1779 submarine eruption, two types of basaltic magma have injected. The basaltic magma in AD 1779 was less magnesian and contained olivine phenocrysts with Fo=77, whereas those in 20th century were magnesian, having olivine phenocrysts with Fo=81. This is consistent with distinct two chemical trends of AD 1779 submarine and 20th century products in SiO<sub>2</sub> variation diagrams, such as P<sub>2</sub>O<sub>5</sub> and MgO. Considering the presence and absence of the relict olivine phenocrysts, with reaction rims, the erupted magma during the 20th century were effected by previous injections of basaltic magmas. After the injection of olivine (Fo=77) in AD 1779, these olivine phenocrysts were reacted with more silicic melt not only to form the reaction rim but also to change their chemical compositions with less magnesian. Just before AD 1914 eruption, voluminous another basaltic magma with more magnesian olivine (Fo=81) had injected just before the AD 1914. The injected magma since AD 1955 has been similar to that of AD 1914, whereas volume of the magma has become smaller. However frequent, small scale of injection has continued to cause number of small, but explosive vulcanian eruptions.

Keywords: Sakurajima volcano, magma system, magma mixing, olivine, volcanic eruption

## Bulk density change of juvenile clasts during the climactic phase of the 2011 Shinmoe-dake eruption

SUZUKI, Yuki<sup>1\*</sup> ; ICHIHARA, Mie<sup>1</sup> ; MAENO, Fukashi<sup>1</sup> ; NAGAI, Masashi<sup>2</sup> ; NAKADA, Setsuya<sup>1</sup>

<sup>1</sup>ERI, Univ. of Tokyo, <sup>2</sup>NIED

In the 2011 eruption of Shinmoe-dake, three sub-Plinian events occurred intermittently between Jan 26 PM and Jan 27 PM (1/26PM, 1/27AM and 1/27PM). This was followed by lava accumulation in the crater (Nakada et al. 2013, EPS). Based on Suzuki et al. (2013a, JVGR) that clarified characteristics and plumbing system of the erupted magmas, we reveal evolution of conduit magma flow during the climactic phase as above, by using groundmass textures. The questions we would like to address are, 1) mechanisms that led to the intermittent sub-Plinian events, including triggering process of each event, 2) timing and condition of syneruptive magma ascent that were responsible for the shifting eruption intensity and style.

As a preliminary result, we here present bulk density data for samples (gray and brown pumices and lava) of the same chemical and storage conditions just prior to ascent from the reservoir. If lithic fragments in sub-Plinian deposit can be judged juvenile (i.e. from the 2011 magma) based on whole rock composition and appearance under the microscopy, they were included in the sample set for the bulk density analysis. Generally, the bulk density data reflect syneruptive ascent condition and resultant degree of syneruptive outgassing. This time, the data allowed us to select representative samples for further textural analyses. The bulk density data also helped us newly define the horizon corresponding to the start of the second sub-Plinian event.

Following the results in Maeno et al. (revised) and Nakada et al. (2013, EPS), the sub-Plinian deposit was collected at locations on dispersal axes and 2-3km from the crater. The following unit numbers are after Nakada et al. (2013). We had no difficulty in identifying the deposit of the third sub-Plinian event (Layer5), because the field survey was in progress at the time of occurrence. The lower units (Layer2, 3 and 4) exhibit reverse grading from layer2 to layer3 and normal grading from layer3 to layer4, as if it was generated in a single event. This occurrence had prevented us from identifying the boundary between the first and second sub-Plinian events. As far as area of the sampling is considered, we believe no deposition during the resting phase between the first and second sub-Plinian events (Jan 26, 19:00 - Jan 27, 2:00). The most likely deposit for the resting phase is ash, if plume height of 3.5km and lower (Shimbori and Fukui, 2012; lower than 6-7km during the sub-Plinian events) is considered. We did not find ash layers between the two of the three layers (layer2, 3 and 4).

The bulk densities of the samples change systematically with the subunits; 1.0-1.7 g/cm<sup>3</sup> from Layer2-low to Layer3-low, 1.0-2.0 g/cm<sup>3</sup> in Layer3-up, and 0.8-1.4 g/cm<sup>3</sup> from Layer4-low to Layer4-up. The average densities for the subunits are 1.25 g/cm<sup>3</sup>, 1.28 g/cm<sup>3</sup>, 1.27 g/cm<sup>3</sup>, 1.44 g/cm<sup>3</sup>, 1.14 g/cm<sup>3</sup>, 1.17 g/cm<sup>3</sup> in order from Layer2-low.

We propose that Layer3-up corresponds to the start of the second sub-Plinian event, based on a judgment that high-density pumices in Layer3-up are from upper-conduit degassed magma that was generated during the resting phase (Jan 26, 19:00 - Jan 27, 2:00). The infrasound and seismic data (Ichihara et al., submitted) recorded no explosion for the resting phase. Therefore, we infer the degassed magma did not block the conduit completely.

We could not know exact time of the Layer4 deposition. However, the lower bulk densities in Layer4, in comparison with those of layer3-up, is consistent with the temporal increase of plume height (e.g. ca. 5km at AM2 of Jan 27 <ca. 7km at AM4 of Jan 27) and mass eruption rate (Ueda et al., 2013) during the second sub-Plinian event. In this model, we however must explain smaller pumice sizes in Layer4 in comparison with those of Layer3-up.

Keywords: Shinmoe-dake, Sub-Plinian eruption, Bulk density, Outgassing, Infrasound, Plume height

## Hypocentral migration associated with magma intrusion in the 2000 Miyakejima eruption

MATSUYAMA, Ryotaro<sup>1\*</sup> ; MORITA, Yuichi<sup>1</sup> ; SAKAI, Shin'ichi<sup>1</sup> ; UEDA, Hideki<sup>2</sup>

<sup>1</sup>ERI, Univ. of Tokyo, <sup>2</sup>NIED

A dike intrusion is a phenomena that large amount of magma emplaces in the shape of vertical plane. It is much controlled by tectonic stress. A dike intrusion process is one of the important key informations to understand the relation between tectonic stress and volcanoes. In the case of the Miyakejima eruption in 2000, it is confirmed that a large scale dike intruded beneath sea floor from the following observations; Hypocenters migrate from inland area of Miyakejima to the area near by Kozushima and Niijima. Large ground inflation is measured by nation-wide GNSS network. However, the detail process in this event has been unsolved because hypocenter locations cannot be estimated precisely. Therefore, we try to relocate hypocenters and to reveal the dike intrusion process of the 2000 Miyakejima eruption in this study.

Because hypocenters migrated to the offshore of Miyakejima, hypocenters could not be located precisely from the data recorded at inland of islands surrounding hypocenter area. Eight days after the initiation of the activity, ocean bottom seismometers(OBSs) were installed just above hypocenters. The hypocenter locations was improved very much using the OBSs data. However, analysis of OBS's data did not cover a whole period of the activity. We try to relocate hypocenters that has no OBS's data (approximately 30,000 events) relative to the reference hypocenters (approximately 3000 events) that are located precisely using OBSs data. In our analysis, we modify Double Difference method to give constraints not to move the reference hypocenters and apply it to all earthquakes occurring during 26 June and 31 August, 2000. We also use the velocity structure that is smoothly varying in the depth because of prevention of artificial hypocenter concentration.

From the relocated hypocenters, we find out the following features in the seismic activity associated with the 2000 Miyakejima eruption. 1) There are two groups in the seismic activity. One is the hypocenters aligned from the summit of Miyakejima to the point around 8km off the coast line (near coast activity), the other is the seismic activity distributed on a sub-vertical plain located beneath sea floor at the area surrounded by Miyakejima, Kozushima and Niijima (main activity). The alignment of the hypocenters match with the direction of the maximum tectonic stress. 2) The near coast activity began with an initiation of the volcanic activity and concluded on July 1st. The seismicity in this area was active only in the first week of the whole volcanic activity, and earthquakes did not occur after the period at all. 3) The main activity lasted during two months, and it was accompanied with gradual ground deformation measured by nation-wide GNSS network that represents a large scale of dyke intruded at hypocentral area. The vertical section of the hypocenters shows that the vertical alignment changes at the depth of 12 km where the structure discontinues is implied from a seismic survey. 4) In the later periods of the activity, there are many earthquakes at the area next to the main activity. Their focal mechanisms were strike slip types that agree with the direction of tectonic stress.

Considering the features of the hypocentral distribution mentioned above and other observational facts, we can conclude that there are two types of the magma flow during the 2000 Miyakejima eruption. One is horizontal emplacement just after an initiation of the volcanic activity and the other is gradual upward migration from deep zone to the main activity. Because the coast activity was inactive after July 1st, we suppose that the two magma flow is independent during almost whole period except at the beginning of the activity. In other words, the magma that generate the main activity is not supplied horizontally from Miyakejima but from just beneath hypocenter area.

Acknowledgments: We are much grateful to JMA, NIED, Tokyo Pref. for permitting to use their seismic data.

Keywords: dike intrusion, 2000 Miyakejima eruption, hypocenter migration, seismic activity, tectonics

## Temporal variation of mineral composition of Hanafusa Formation distributed in the western area of Aso caldera

SUGIYAMA, Fumiko<sup>1\*</sup> ; HASENAKA, Toshiaki<sup>1</sup>

<sup>1</sup>Graduate school of Science and Technology, Kumamoto university

Aso volcano made four large-scale pyroclastic eruptions, with magma composition changing with time, so that hornblende phenocryst appeared in the latest Aso-4 pyroclastic flow deposits (Watanabe, 1979). Hornblende becomes a key mineral to detect the physicochemical change, as it also appeared as microphenocryst in volcanic products of Omine volcano and associated Takayubarū lava flow, which erupted just before Aso-4 event (Kurokawa et al., 2012). Hanafusa Formation is a lake deposit forming 20 km west of Aso caldera just before Aso-4 pyroclastic eruption, thus it is suitable for finding the appearance time of hornblende from the minerals included in the deposits.

Hanafusa Formation consists of silt and sand with thickness of up to 10 m, and formed between Aso-3 and Aso-4 pyroclastic flow events. We collected samples from pumice deposit and overlying sand in Kajisako, Kikuchi city. We also collected samples from silt layer just below the contact with Aso-4 pyroclastic deposit, and from the type locality of Hanafusa Formation in Kikoji, Kikuchi city. We divided silt layer into upper unit and lower unit with boundary at the tephra layer, which we identified as Ata regional tephra by its mineral assemblage and existence of abundant bubble-shape glass and estimated age of 100 ka.

(1) The lower unit contain plagioclase, clinopyroxene and orthopyroxene. Plagioclase crystals indicate euhedral and have the surface which give a dirty impression.

(2) The upper unit contains euhedral hornblende and euhedral plagioclase crystals which are not observed in the lower unit. The upper unit contains clinopyroxene and orthopyroxene crystals. The mineral assemblage and their ratios are the same as observed among Aso-4 pyroclastic flow deposit.

(3) Chemical compositions of pumice fragments in Pumice layer resembled those of all Aso-4 pyroclastic flow deposits. However, in detail, Oyatsu pumice flow deposit, Benri scoria flow deposit and Omine volcanic products show distinct compositional trends from this pumice layer (Kurokawa et al., 2012; Yamasaki et al., 2013).

(4) Observed crystals in sand just above the pumice layer include plagioclase, clinopyroxene, orthopyroxene, opaque minerals and olivine, which is not included in the lower pumice layer.

Our findings suggest that the appearance of hornblende was 10,000 years before Aso-4 pyroclastic eruptions, however their source is unknown, because we did not find obvious tephra layers other than Ata regional tephra.

Keywords: Hanafusa formation, hornblende, Aso-4 tephra, Aso-4 pyroclastic flow

## Estimating composition of primitive magma by using opx, and temporal and spatial change of HMA magmatism in NE Shikoku

MORISATO, Fumitoshi<sup>1\*</sup> ; OZAWA, Kazuhito<sup>1</sup>

<sup>1</sup>School of science, The University of Tokyo, <sup>2</sup>School of science, The University of Tokyo

In the subduction zone, oceanic plates start sinking into the mantle, and continental crusts are generated and eroded. So it is important for understanding the evolution of plate-tectonics. As for the subduction initiation, temporal change of thermal structure and water content of the mantle wedge is mainly estimated by numerical simulations (Iwamori, 2000 *etc.*), but there are few constraints from material informations. Using magma information is a possible method to estimate thermal structure of the Earth (Green, 1981). Although it is necessary to estimate chemical composition of the primitive magma, the effects of crystal differentiation and, especially in subduction zone, crustal process (magma mixing, crustal assimilation, and degassing) should be evaluated. Moreover, the magmatism in subduction zone is assumed to be affected by mantle flow in mantle wedge (Tatsumi *et al.*, 1983; Tamura, 2003). To estimate such upwelling, Sakuyama *et al.* (2009) investigated temporal and spatial change of the magma generation field.

SW Japan is an example of juvenile subduction zone. Shikoku basin initiated to sink 17 Ma ago, and magmatisms migrated from forearc to reararc (Kimura *et al.*, 2005). In the Setouchi volcanic zone, the generation of high-Mg andesite (HMA) has been discussed from the view of thermal structure of the mantle wedge and subducting plate (Tatsumi & Hanyu, 2003 *etc.*), but there remains some questions about magma mixing and degassing, and about temporal and spatial change of magma generation field.

In this study, we suggest a method to estimate the primitive magma composition by using oscillationally-zoned opx, and apply to the HMA in the Setouchi volcanic zone. And we try to estimate the magma generation mechanism by evaluating temporal and spatial change of magmatism in the area.

Firstly, we investigated a HMA in Mt. Kiyama, central part of NE Shikoku, Japan (Sato, 1982 *etc.*). It has the most primitive composition (SiO<sub>2</sub>: 57.3wt%, MgO: 8.56wt%, Mg#: 69.3), and it contains olivine, opx, and cpx as phenocrysts. The olivine phenocrysts are normally-zoned, and their highest Mg# (87.6) is lower than the equilibrium value calculated from whole rock composition of the HMA (88.7). Therefore the olivine phenocrysts are considered to be crystallized in closed system. On the other hand, opx phenocrysts are reversely-zoned, and their composition boundaries are sharp. Moreover they have higher Mg# (up to 91.5) than calculated equilibrium value (88.8). Accordingly, these opx could record the composition of more primitive melts. And zoning pattern among opx is consistent, so they could reflect compositional change of the same melt.

According to Putirka (2005), the composition of primitive magma can be estimated by adding fractionated olivine or opx until the melt's composition become in equilibrium with the opx which has the highest Mg#. But we must remove the effects of magma mixing before it. Kuritani (1998) used the fact that the An content of plagioclase phenocryst can be changed in a magma chamber reflecting the difference of temperature or water content. He investigated the pattern of zoning and quantity ratio of them, and estimated mixing ratio.

We estimated the change of melt composition. (1) Calculating the melt compositions from opx composition by using distribution coefficients. (2) Comparing the change of the melt composition and modeled composition in Rayleigh fractionation or magma mixing. (3) Estimating mixing ratio by evaluating the pattern of zoning in opx and their quantity ratio, and estimating end member of mixing. (4) According to the true fractionation trend, determining primitive magma composition which is in equilibrium with opx having the highest Mg#.

By applying this method to the HMA in Mt. Shichihousan, western part of NE Shikoku (Kawabata & Suto, 2000), we estimated the spatial change of primitive magma composition and magma generation field.

Keywords: subduction, Southwest Japan, primitive magma, magma mixing, High-Mg andesite

## The relation of volcanic stages for the recent 10000 years of Kirisima and Southern Kyushu volcanoes

TAJIMA, Yasuhisa<sup>1\*</sup>

<sup>1</sup>Nippon Koei Co., Ltd.

In this study the eruption ages of tephra and lava generated from Shinmoedake volcano and Ebinokogen volcanic area by <sup>14</sup>C dating were determined. Those ages indicate that the Kirishima volcanoes have three eruptive stages among the recent 10,000 years. The eruptive stage C started from 9.0 to 8.0 cal ka BP with RyD-L from Shinmoedake volcano and Fd-TmA tephra and Fudoike lava from Ebinokogen volcanic area. Old-Takachihono volcano and Takachihonomine volcano grew rapidly in this stage. The eruptive stage B continued from 5.6 to 2.3 cal ka BP growing the Shinmodedake and Nakadake volcanic edifices. Three eruptions at the same time, which were the Miike plinian eruption at 4.6 cal ka BP from Miike maar, Sm-Sy eruption at 4.5 cal ka BP from Shinmoedake volcano and Kn-EbD eruption at 4.3 cal ka BP from Ebinokogen volcanic area in this stage. The time interval between eruptive stage B and eruptive stage A was 2.3 to 1.6 cal ka BP. The youngest eruptive stage A started with Fd-EbC tephra from Ebinokogen volcanic area at 1.6 ka. In this stage, the Ohachi volcano grew from 6th century and Shinmoedake volcano erupted from 18th century. This result indicates that the Kirisima volcanoes repeated a few thousand years of eruptive stages and 500 to 1000 years intervals. The current eruptive stage A lasts about 1600 years. The relation of eruption ages of Kirishima volcanoes and Sakurajima volcano is well.

Keywords: Kirishima Volcano, Volcanic stage, Shinmoedake, Ebinokogen, Long term activity

## Investigation report of rootless cone in Iceland -as an analogue of that of on Mars-

NOGUCHI, Rina<sup>1\*</sup> ; SARUYA, Tomotaka<sup>1</sup> ; SUZUKI, Yuki<sup>1</sup> ; KURITA, Kei<sup>1</sup>

<sup>1</sup>Earthquake Research Institute, the University of Tokyo

Rootless cone is a pyroclastic cone which has a variety of shape. It's formed by lava-water interaction [e.g. Fagents et al., 2002, Hamilton et al., 2010], but details such as formation conditions are still unknown. Since pervasive existence of various types of rootless cones has been clarified on the martian surface, terrestrial rootless cones are key to understand Martian volcanism and strong interests have been paid in the field of planetary science. We surveyed rootless cones in Iceland by RTKGPS (Real-Time Kinematic GPS) with material-scientific investigations on the constituent materials.

We investigated 3 rootless cone fields; Myvatn (northern Iceland), Landbrot (eastern Iceland), and Thjorsardalur (western of Hekla volcano). In this presentation, we will focus on Myvatn area. In Myvatn, rootless cones were formed by lava-lake water interaction. The lava is basaltic, and emanated from the fissure which locates in east of the lake [Thorarinsson, 1951], and flowed into the lake. We mapped more than 500 rootless cones by aerial photo survey. Most of cones locate around the lake, but some cone locates in in the down-flow region (40 km far from the lava source) area. In Myvatn, here exists unique rootless cone which has an inner cone in the summit crater. We named this as double cone. We focus on this type and conducted detailed morphological survey.

We found that slope angle of rootless cone depends on its size. For double cone, inner cone has gentler slope than that of outer cone. In case of single cone (no inner cone), large cones have steeper slope than that of small cones. Also, large cones have constant slope (repose angle: 32-33 degree), despite the slope angle of small cone varies. In case of the double cone, we found that the constituting material of the inner cone differs from that of the outer cone. The component material of the outer cone is lapilli - coarse ash size pyroclast. On the other hand, that of the inner cone is welded pyroclasts or agglutinate. For small cones, the summit part is covered with agglutinate. These differences should indicate different condition of the formation such as the amount of available water/heat supply by magma.

A We measured bulk chemical composition of the lava and the pyroclasts by XRF confirming no significant change along lava flow traveling. We also measured bulk density and size distribution of the pyroclasts of the rootless cones. We found density of the lava concordantly increases with traveling distance, which means bubbles progressively escaped from the lava during traveling while the formation of rootless cone seems not to be influenced by the vesicularity of lava. The size distribution seems to be correlated with the slope value of the cone, which strongly suggests the control of fragmentation on the formation of rootless cone.

Keywords: rootless cone, Iceland, Mars, Myvatn, double cone

## Volume of magma chamber and eruption ratio for caldera collapse

GESHI, Nobuo<sup>1\*</sup>

<sup>1</sup>Geological Survey of Japan, AIST

Mechanism of caldera collapse is modeled with a comparison of a piston-cylinder caldera model and the compiled data of caldera size and eruptive volume in nature.

Collapse caldera is formed by the fracturing and subsidence of the roof of magma chamber with rapid withdrawal of massive magma from a magma chamber. As the fracturing and subsidence of the roof of magma chamber may enhance the additional eruption of magma inside the magma chamber, understanding of the mechanisms of the precursory eruption is crucial to evaluation of the potential eruption from caldera volcanoes.

Collapse calderas are formed only by the largest eruptions of its life, though, in many cases, caldera volcanoes repeat many eruptions with various scales before and after caldera formation. Smaller eruptions have no significant contribution for collapse. Aira caldera in Japan was formed at 29ka eruption during which  $\sim 400 \text{ km}^3$  of magma was erupted. Though many smaller eruptions including Fukuyama pumice eruption ( $10 \text{ km}^3 \text{ DRE}$ ) and Sz-S eruption ( $4 \text{ km}^3 \text{ DRE}$ ) occurred from the Aira caldera, no significant collapse was occurred. During the 29 ka eruption, Osumi pumice fall was erupted prior to the onset of collapse, and the emission of Ito pyroclastic flow followed the collapse. The erupted volume of Osumi pumice fall ( $\sim 40 \text{ km}^3 \text{ DRE}$ ) is larger than those of the eruptions without collapse. This relationship is commonly observed in other caldera volcanoes. The erupted volume during the precursory eruption is in correlation with the size of caldera.

The volume of magma withdrawal to induce collapse is modeled with piston-cylinder model. The driving force of collapse is the decompression in magma chamber by the magma extraction. The friction in the ring fault sustains the roof. Competition between the decompression of magma chamber and the friction controls the onset of collapse. The decompression of magma chamber is in the function of the eruption ratio (volume of magma withdrawal / total volume of magma chamber). This model shows that a larger volume of magma withdrawal is required for the onset of collapse with larger diameter. The critical eruption ratio for collapse is smaller for the larger caldera.

Though this model has potentially large ambiguity from the simplified shape of caldera fault and the assumption of the bulk modulus of magma, this model can give the total volume of magma chamber associating collapse caldera. In the case of Aira caldera, with 15 km in diameter and 6 km to the roof of magma chamber, the total volume of magma chamber before the eruption is estimated as  $600 \text{ km}^3$ . The caldera collapse occurred when the erupted volume reached to 8% of the total magma chamber, and 60 % of magma was erupted as Ito pyroclastic flow after the onset of collapse.

Keywords: large eruption, caldera volcano, magma chamber

## Identification and Geology of Taftan volcano Calderas, Sistan and Baluchestan, Southeast of Iran

BIABANGARD, Habib<sup>1\*</sup>

<sup>1</sup>Department of Geology, Sistan and Baluchestan University of Zahedan, Iran

The Taftan volcano, Sistan and Baluchestan province, SE Iran, is above 4050 m sea level and currently dormant, showing fumarolic activity near the summit. This volcano is located in a structural zone along the subduction of Oman oceanic crust below the Eurasia plate. Large volcanic centers including Chah-Shahe, Bazman and Taftan in Iran and Soltan in Pakistan have been developed during the Quaternary. Anjerk and Tamandan are two calderas from of Taftan volcano that identified for the first time. Theses calderas are mostly composed of pyroclastics, lava flows, ignimbrites and tuffs. Various volcanic eruptions had occurred during these calderas formation. The exposed lava flows and pyroclastics of these calderas mainly consist of andesitic and dacitic in compositions. The geochemical evaluation of the major and trace element compositions indicate the magma erupted from this volcano show a calk-alkaline trend.

Keywords: Taftan Volcano, Makran belt, Anjerk caldera, Tamandan caldera, Geochemical evaluation, Iran

## K-Ar ages of Kelut-Welirang volcano cluster, East Java, Sunda arc: comparison with clusters that hosts large calderas

TOSHIDA, Kiyoshi<sup>1\*</sup> ; TAKADA, Akira<sup>2</sup> ; KITSUKAWA, Takashi<sup>3</sup> ; TAKEUCHI, Shingo<sup>1</sup>

<sup>1</sup>CRIEPI, <sup>2</sup>AIST, GSJ, <sup>3</sup>Ceres, Inc.

Sunda arc, Indonesia, has many active caldera volcanoes and is well suited for studying the evolution of large caldera systems. Volcano groups are distributed in clusters at Sunda arc. Two adjacent volcano clusters in East Java, Semeru-Tengger and Kelut-Welirang, are compared. Semeru-Tengger volcano cluster consist of Semeru and Tengger-Bromo volcano systems. Tengger-Bromo system has formed Ngadisari and Sand Sea calderas. Kelut-Welirang volcano cluster consists of multiple active volcano groups and has comparable footprint and cumulative volume as Tengger-Bromo. However, large-scale eruptions in the order of 10km<sup>3</sup> or greater have not taken place at Kelut-Welirang volcano cluster.

Kelut-Welirang volcano cluster consists of five volcano groups. They are Penanggungan, Arjuno-Welirang, Argowayan, Butak-Kawi-Panderman, and Kelut from northeast to southwest. They are classified as active volcanoes except for Argowayan, and Kelut is currently active. However, their formation ages are not understood.

K-Ar dating is performed in order to determine and compare the long-term activity of the two clusters. Mass fractionation correction method is used for argon measurement, for many of the samples are very young. Samples with crystalline groundmass are selected for dating to obtain precise and reliable age. Groundmass is separated from phenocryst and used for dating.

The active periods and the ages of the volcano groups are identified by K-Ar dating as follows. (a) Argowayan, which consists about half of the volume of Kelut-Welirang cluster, has formed between 1.0-0.8Ma. (b) There was long dormancy in the area of this cluster, and the four volcano groups have formed within the past 0.2 m.y. (c) Kelut has started to form by 0.2Ma, and has repeatedly produced lava domes to present. (d) Much of Butak-Kawi-Panderman has formed around 0.2Ma. The group is considered active, but the long-term eruption rate of the group has decreased substantially since the early stage of edifice building activity at 0.2Ma. (e) Arjuno-Welirang is younger and likely started to form by 0.1Ma. (f) Penanggungan is the youngest volcano group and likely to have formed within the past 0.05 m.y.

The obtained ages allow us to compare Kelut-Welirang and Tengger-Semeru volcano clusters. Although Kelut-Welirang cluster has comparable volume to Tengger-Semeru, it consists of separate volcano groups formed at different ages. The long-term eruption rate for the past 0.2Ma is relatively large, but much of the erupted volume is contributed from new volcano group. In contrast, the volcano edifices of Semeru-Tengger have almost entirely formed from 0.5Ma to present. The eruptive centers are concentrated at Tengger and Semeru, and have repeated active periods.

Keywords: age dating, Quaternary, Indonesia, mass fractionation correction method

## Correlation between petrology and magneto-stratigraphy of Holocene volcanic products from Aso central cones

HIRAKAWA, Yuichiro<sup>1\*</sup> ; HASENAKA, Toshiaki<sup>1</sup> ; MOCHIZUKI, Nobutatsu<sup>2</sup> ; MORI, Yasushi<sup>3</sup>

<sup>1</sup>Grad School Sci & Tech, Kumamoto Univ., <sup>2</sup>Priority Organization for Innovation and Excellence, Kumamoto University, <sup>3</sup>Kitakyushu Museum of Natural History and Human History

We collected samples from 25 sites where Yato et al. (2013) and Miyabuchi et al. (2012) reported magneto-stratigraphy of six different lava flows distributed in the northwestern region of Aso central cones. We conducted petrographic descriptions and chemical analyses of these samples and correlated them with paleomagnetic directions and stratigraphy of Miyabuchi (2009) based on radiocarbon dating.

Kijimadake lava is divided into two lava flow units with different paleomagnetic directions suggesting interval of at least several hundreds of years. They show the same mineral assemblage, but different groundmass texture, modal composition and whole-rock chemical composition. The upper lava flow unit has the same petrological characteristics as Kishimadake scoria, whose estimation age was 4000 y.b.p. from the radiocarbon dating.

Possibility of multiple eruptions has been suggested for Ojodake lava flows, because they are intercalated by soil, and show different paleomagnetic directions. However, no distinction was made in petrographic descriptions and chemical compositions between these lava flows.

Six different lava flows younger than Akahoya tephra have similar appearance and similar petrographic characteristics, however they are distinguishable by chemical compositions. Lava flow units with possible simultaneous eruptions (e.g. old Kijimadake lava and Nakadake younger stage lava, Kamikomezuka scoria and old Ojodake lava) show about 1% difference in SiO<sub>2</sub> content. A series of Holocene lava flows in Aso central cones are possibly derived from a common magma supply system with different conduits.

Keywords: post-caldera central cones of Aso volcano, volcanic products, Holocene, paleomagnetic directions, petrography, chemical compositions

## Magma genesis of Miocene basalts from Ootsu district, Yamaguchi Prefecture, SW Japan arc

HIGASHIYAMA, Yoji<sup>1</sup> ; HASENAKA, Toshiaki<sup>1\*</sup> ; SHIBATA, Tomoyuki<sup>2</sup> ; YOSHIKAWA, Masako<sup>2</sup> ; NAGAO, Takashi<sup>3</sup>

<sup>1</sup>Grad School Sci. & Tech., Kumamoto Univ., <sup>2</sup>Beppu Geothermal Res. Lab., Kyoto Univ., <sup>3</sup>Grad School Sci. & Eng., Yamaguchi Univ.

The geological, petrological and geochemical studies of Miocene Ootsu basalts, distributed in Tsunoshima and Yuyashima islands along the coast of the Japan Sea, revealed the temporal and vertical changes in mantle melting processes. Based on their volcanic stratigraphy and petrological data, Ootsu basalts were grouped into; (1) clinopyroxene-olivine basalt (COB), (2) olivine basalt, magnetite-rich type 1 (MRB1), (3) olivine basalt, magnetite-rich type 2 (MRB2), and (4) olivine basalt, magnetite-poor type (MPB). MRB1 and MRB2 are rich in FeO\* and TiO<sub>2</sub> contents, and MPB is rich in SiO<sub>2</sub> and Al<sub>2</sub>O<sub>3</sub> contents. MRB1, MRB2 and COB are alkalic and MPB is tholeiitic.

Phase diagram and mass balance calculations indicate that these four groups were derived from different primary magmas, and had experienced polybaric crystallization. The compositions of primary magmas for these four groups suggest that MRB1 and MPB were generated at the deepest and shallowest depths, by the lowest and the highest degrees of melting, respectively. Multi trace element plots (normalized by the primitive mantle values) of Ootsu basalts show the strong enrichment of LILE (Rb, Ba, and K), and distinct negative anomaly of Nb and Sm. The compositions of coexisting olivine and spinel (OSMA) suggest that MPB's mantle source is the most fertile among four groups. The different ratios of LREE/HREE among four groups suggest different mantle source and different degree of partial melting. B/Nb ratio of four groups is getting higher with decreasing segregation depth. These systematic differences in B/Nb ratio indicate that the upper mantle beneath Ootsu district is characterized by an increased degree of metasomatism at shallow level.

We concluded that the diversities of chemical composition in Ootsu basalts attribute largely to different segregation depth and heterogeneous mantle source.

Keywords: alkaline rock, tholeiite, boron, rare earth element, mantle

## Rifting- and subduction-related volcanism of the northern Fossa Magna related to the formation of the Sea of Japan

OKAMURA, Satoshi<sup>1\*</sup> ; INABA, Mitsuru<sup>2</sup> ; YOSHIDA, Takanori<sup>3</sup> ; ADACHI, Yoshiko<sup>4</sup> ; SHINJO, Ryuichi<sup>5</sup> ; IKEDA, Yasuo<sup>6</sup>

<sup>1</sup>Sapporo, Hokkaido Educ. Univ., <sup>2</sup>Japan Petroleum Exploration Co., Ltd., <sup>3</sup>Sapporo, Hokkaido Educ. Univ., <sup>4</sup>Faculty of Science. Niigata Univ., <sup>5</sup>Faculty of Science. Univ. Ryukyus, <sup>6</sup>Kushiro, Hokkaido Educ. Univ.

Specific aims of the research are; 1) to characterize the chemical composition of the magmatic sources for the Cenozoic volcanic suite in the Fossa Magna region, a boundary fault zone between north and south Japan, 2) to relate the magmatic evolution to the simultaneous tectonic process of the opening of the Japan Sea, and 3) to assess the role of rifting and subduction processes in the evolution of the continental margin of the northwestern Pacific rim with inferences for the other tectonic zone.

Keywords: Fossa Magna, Yamato Basin, MORB source, Enrich mantle

## The Middle Miocene tectonics and volcanism in the intra-arc and the back-arc region, Northeast Japan

HOSOI, Jun<sup>1\*</sup> ; AMANO, Kazuo<sup>2</sup>

<sup>1</sup>Graduate School of Science and Engineering, Ibaraki University, <sup>2</sup>Faculty of Science, Ibaraki University

In northeast Japan, many submarine volcanic rocks related to opening of the Japan Sea in the Early Miocene are widely distributed. They are very important to consider the evolutionary process of Japan Arc and to elucidate the submarine volcanism. Despite the importance, there were no detailed sedimentological studies of these volcanic rocks, and the detailed sedimentary processes, sedimentary basin formation, paleo-volcanism and tectonics were poorly understood. In this study, we tried to reconstruct the detail volcanic edifices and volcanism based on the facies analysis of volcanics in typical two area; one is Ou Backbone Ranges in Nishiwaga town, Iwate prefecture and the other is Dewa Mountains in Sakata, Yamagata prefecture, that were located in the intra arc and the back arc in the Miocene respectively.

As results, we could elucidate paleo volcanism in each area. Remarkable tectonic change occurred in 15Ma with active volcanism, counterclockwise rotation and rapid subsidence (Hosoi et al., 2013). Regional paleostress around 15 to 12Ma is NW-SE tensional stress (Otsuki, 1989; Hosoi, 2013). This tectonic change happened in 15Ma with opening of Japan Sea, and active bimodal volcanism, rotation movement and tectonic subsidence occurred.

[References]

Hosoi, J., 2013, Research Report for the Fukada Grant-in-Aid in the H24 fiscal year, 9-23.

Hosoi, J. et al., 2013, *Jour. Sediment. Soc. Japan*, 72, 141-146.

Sato, H. and Amano, K., 1991, *Sedimentary Geology*, 74, 323-343.

Keywords: Miocene, tectonics, back-arc, intra-arc, greentuff, Northeast Japan

## Paleostress analysis of dilational fractures using genetic algorithm

YAMAJI, Atsushi<sup>1\*</sup>

<sup>1</sup>Kyoto University

The attitudes of dilational fractures, including dikes and veins, are clues to the paleostresses under which the structures were formed. A software tool for clustering their 3D orientations has been developed in this study. The software fits mixed Bingham distributions to them, and detects girdle, elliptical and circular clusters. In addition, it determines the three principal stress axes, stress ratios and maximum fluid pressure for each of the clusters. Fitting a mixed Bingham distribution is not a well posed problem, because the mathematical inversion is highly non-linear and its object function is multimodal. It is demonstrated that genetic algorithm is more effective than the expectation-maximization algorithm which was used by previous researchers (Yamaji and Sato, 2011).

Keywords: real-coded genetic algorithm, magma pressure, mixed Bingham distribution, dike, vein

## Eruption History and Future Scenario of Sinabung volcano, North Sumatra, Indonesia

YOSHIMOTO, Mitsuhiro<sup>1\*</sup>; NAKADA, Setsuya<sup>2</sup>; ZAENNUDIN, Akhmad<sup>3</sup>; PRAMBADA, Oktory<sup>3</sup>; HOKANISHI, Natsumi<sup>2</sup>; TAKAGI, Natsuko<sup>2</sup>; HENDRASTO, Muhamad<sup>3</sup>; IGUCHI, Masato<sup>4</sup>

<sup>1</sup>Faculty of Science, Hokkaido University, <sup>2</sup>Earthquake Research Institute, University of Tokyo, <sup>3</sup>Center for Volcanology and Geological Hazard Mitigation, Indonesia, <sup>4</sup>Sakurajima Volcano Research Center, Disaster Prevention Research Institute, Kyoto University

Sinabung Volcano is an andesitic stratovolcano located 40 km northwest of Lake Toba, North Sumatra. The activity began after the latest caldera-forming eruption of Toba Lake (ca. 74ka). The eruption history can be divided into two stages (old and young stages) based on topographical and geochemical features. The edifice is characterized by multiple thick lava flows/domes, and their collapsed materials of block-and-ash flow and associated surge deposits. The lava spine is located at the southern end of one of the summit craters which trend in N-S. Pumice-fall deposits by relatively large explosive eruptions, such as plinian-to subplinian types, were not recognized. The last magmatic eruption before 2010 occurred during 9 to 10th century, whose products are mainly pyroclastic-flow deposits, distributed in the SE slope.

The present activities began with phreatic events in August and September 2010. It resumed its activity in September 2013 with phreatic events. After the repeated phreatic to phreatomagmatic events, lava appeared in the summit crater in late December and started its partial collapse on 30 December. Several tens collapses occurred everyday in January 2014. Those pyroclastic flows descended on the SE slope of the volcano and traveled 4.5 km in maximum.

Lavas of the volcano are basaltic andesite to andesite in composition, and andesitic lavas contain hornblende phenocrysts. Although old lava have a SiO<sub>2</sub> range similar to young lavas, the old lava are more enriched in K<sub>2</sub>O than the young lava. The lava spine is highly enriched in SiO<sub>2</sub> and extremely depleted in Na<sub>2</sub>O, a result of high alteration by volcanic gases, suggested by the mineralogical features. Bulk composition of 2010 ash seems to be intermediate between the young lava and the altered lava spine. In contrast, pumice of 2013 eruption has a similar composition of juvenile materials of 9-10th eruption.

Before the 2013-2014 events, highly possible scenario for future eruption have been proposed the similar case of lava-dome eruptions at Unzen, Japan, in 1991-95 and at Soufriere Hills, Montserrat, West Indies, in 1995-present, based on the eruption history. The present eruption at Sinabung follows the proposed scenario of the highest probability.

This work was supported by SATREPS research project (Multi-disciplinary Hazard Reduction from Earthquakes and Volcanoes in Indonesia) and the Indonesian Center for Volcanology and Geological Hazard Mitigation (CVGHM).

Keywords: Indonesia, Sinabung, volcanic eruption, eruption history, Scenario, pyroclastic flow

## Petrological study of monogenetic volcanoes in the fore-arc region of the northern Kamchatka Peninsula

NISHIZAWA, Tatsuji<sup>1\*</sup>; CHURIKOVA, Tatiana<sup>2</sup>; GORDEYCHIK, Boris<sup>3</sup>; ISHIZUKA, Osamu<sup>4</sup>; NAKAMURA, Hitomi<sup>1</sup>; IWAMORI, Hikaru<sup>5</sup>

<sup>1</sup>Department of Earth and Planetary Sciences, Tokyo Institute of Technology, <sup>2</sup>Institute of Volcanology and Seismology Far East Division, Russian Academy, <sup>3</sup>Institute of Experimental Mineralogy, Russian Academy, <sup>4</sup>Research Core for Deep Geological Environments, AIST, <sup>5</sup>Japan Agency for Marine-Earth Science and Technology

The western part of the Pacific Plate is subducting under the Okhotsk Plate along Kuril-Kamchatka Trench, and the northern part of it is subducting under the Bering Sea Plate with high obliquity along the western Aleutians arc. The three plates form the Aleutian-Kamchatka triple junction (Eichelberger *et al.*, 2013). The northern edge of the Pacific Plate is separated from Bering Sea Plate by transform fault, and the mantle edge beneath the Kamchatka Peninsula is thought to be open towards the Bering Sea.

There are at least 29 active volcanoes in the Kamchatka Peninsula. From the east to the west, arc volcanism on the Kamchatka Peninsula forms three zones parallel to the Kamchatka trench: the Eastern Volcanic Front (EVF), the Central Kamchatka Depression (CKD) including Klychevskaya Volcano Group (KVG) where the large volcanoes concentrate, and the Sredinny Ridge (SR) in the back arc side.

Along EVF, the straight volcanic chain is terminated around 55°N (near the Kizimen volcano), and in further north the volcanic chain seems to deflect toward KVG corresponding to deeper depth of subducting slab. However, monogenetic volcanoes on the northward extension of the EVF exist and were studied in 1960s, called 'Kumuroch range' (Fedororenko., 1969). The present-day slab depth beneath the monogenetic volcanoes is about 60km (Gorbatov *et al.*, 1997), and the crustal thickness is about 20-30km (Levin *et al.*, 2002). These volcanic rocks were reported as basalt to andesite, having relatively high MgO content (~11.8 wt. %) and low FeO/MgO ratio (<1.0) (Uspensky and Shapiro., 1984). In summer 2013, we have identified 15 monogenetic volcanoes in this area (hereafter 'East Cone volcanic group', EC) by using stereogram, and had investigated 8 volcanoes by using a helicopter.

In this study, we aim to reveal the origin of the EC lavas. For this purpose, we have first examined mineral assemblages under optical microscope and analyzed the whole rock major element compositions by XRF. All 16 samples are classified as basalt or basaltic andesite, of which the two lavas contain xenoliths, and one sample oxidized to red. The rocks exhibit porphyritic to seriate texture, containing plagioclase, clinopyroxene, olivine, opaque minerals, although, the proportion of minerals varies from sample to sample. The silica contents of all samples are over 50 wt. %, with the FeO/MgO ratio less than 2, indicating relatively undifferentiated characteristics.

In comparison to the typical island arc basalts having a similar silica content, the MgO contents of the EC lavas are higher by ~4 wt. %. Accordingly, the EC lavas are similar to or classified into high-Mg andesite, which is considered to be generated by melting of relatively hydrous mantle (as an example, unsaturated with H<sub>2</sub>O, 1.0GPa, 1100-1250 °C, saturated with H<sub>2</sub>O, 1.5GPa, 1030-1150 °C) (Tatsumi., 1995; 2003).

The EC lavas scarcely include orthopyroxene, on the other hand, volcanic rocks of KG include orthopyroxene (Churikova *et al.*, 2013). Mantle xenoliths from the Bezymianny volcano of KG is reported to be spinel harzburgites (Ionov *et al.*, 2013). Combining these constraints, we discuss a regional variation in mineral assemblage and H<sub>2</sub>O content in source mantle, H<sub>2</sub>O content in the primary magma, and the crystallization temperature and pressure of the magmas.

By comparing the petrological characteristics of the EC lavas with those from other regions (e.g., KG), clear constraints on the relationship between magma genesis and the tectonic setting are expected to be imposed.

Keywords: arc, high-Mg andesite, Kamchatka Peninsula, triple junction

## Geology and petrology of Taisetsu volcano group, Japan; Evolution of magma and long-term time variation of eruption rate

ISHIGE, Kosuke<sup>1\*</sup>; NAKAGAWA, Mitsuhiro<sup>1</sup>; MATSUMOTO, Akikazu<sup>2</sup>

<sup>1</sup>Department of Natural History Sciences, Graduate School of Science, Hokkaido University, <sup>2</sup>Geological Survey of Japan, National Institute of advanced Industrial Science and Technology

Taisetsu volcano group locates at the northern part of the Taisetsu-Tokachi volcanic chain, which is situated at the southern end of Kuril arc. The volcano group started its activity ca. 1 Ma and is composed of andesitic lava domes and stratovolcanoes. Although previous studies (eg., NEDO, 1990; Katsui, 1979) revealed the outline of structure and eruptive history of the group, detail chronological and petrological studies have not been carried out. We have revealed the volcano stratigraphy and petrological features of the whole area of the volcano group. In addition, K-Ar ages of representative samples are also determined. Based on these data, we focus on the temporal change of eruption rate and magma types during 1 My in the volcano group.

According to the stratigraphy, location of eruption centers, mode of eruptive activity and petrological features, the activity of the volcano group can be divided into four major stages, as follows. Stage 1(1.0 ~0.75Ma): Fluidal andesite lava were effused from several eruption centers to form flat-shaped volcanic edifices which are distributed in N-S direction. Their total estimated eruptive volume is 26km<sup>3</sup>(DRE). Stage 2: It can be subdivided into sub-stage 2-1 (0.6Ma) and 2-2 (0.35 ~0.05Ma). Eruptive lavas of the former sub-stage are mostly covered by younger deposits. Detail structure of the edifice and the distribution of deposits have not been clear. The sub-stage 2-2, is further subdivided into central and western group according to the differences in mode of activity and location of eruption centers. The total estimated eruptive volume of stage 2 is 23km<sup>3</sup>. Stage 3(ca. 30 ka): The stage is characterized by most explosive eruptions in the volcano group, resulting to the formation of a plinian column and related pyroclastic flows. These activities formed the Ohachidaira caldera with 2 km in a diameter. The total eruptive volume is estimated to be 13km<sup>3</sup>. Stage 4 (ca. 30 ka - present): Main eruption centers moves to the southwestern part of the caldera to form several stratovolcanoes and lava domes. The total eruptive volume of stage 4 is 10km<sup>3</sup>. Based on the ages and estimated eruptive volume, the magma discharge stepdiagram of the volcano group is created to discuss a temporal change of magma discharge rate. The eruption rate of each stage is as follows; >0.07km<sup>3</sup>/ky for stage 1, >0.01km<sup>3</sup>/ky for stage 2-1, >0.06km<sup>3</sup>/ky for stage 2-2, >0.33km<sup>3</sup>/ky for stage 3, >0.33km<sup>3</sup>/ky for stage 4. According to the stepdiagram, the period from 0.7 to 0.4 Ma could be characterized by extremely low eruption rate and/or the presence of dormant stage.

Petrological features of the ejecta of Taisetsu volcano group can be distinguished among stages. All of the rocks are andesite and dacite, often containing mafic inclusions. These rocks contain plagioclase, clinopyroxene, orthopyroxene and Ti-magnetite as phenocrysts, associated with minor amounts of olivine, and quartz phenocrysts in some rocks. Although the rocks of stage 1 do not contain hornblende phenocrysts, those of stage 2 and 3 usually include hornblende phenocrysts. However, there rarely exist hornblende phenocrysts in the rocks of stage 4. The whole-rock SiO<sub>2</sub> contents range from 56.4 to 69.1 wt.% for host rocks and from 52.7 to 57.4 for the inclusions. Almost all the rocks are defined as medium-K in SiO<sub>2</sub> - K<sub>2</sub>O and CA types in SiO<sub>2</sub>-FeO/MgO diagrams, respectively. The host of the rocks from stage 1 is characterized by high Zr contents, compared with the rocks from other stages, whereas Zr contents in the mafic inclusions in the rocks from stage 1 are the same as those from other stages. Considering Zr contents and occurrence of hornblende phenocryst in andesite, magma type had changed largely during the possible long dormancy from 0.7 to 0.4 Ma. This would be related to the tectonic change at the junction between NE Japan and Kuril arcs.

Keywords: Volcano, Eruption rate, Formation history, Taisetsu, Geology and petrology, Transition of magma

## Reconstruction accuracy of eruptive sequence inferred from the pyroclastic fall deposits of the Asama-Maekake volcano

YASUI, Maya<sup>1\*</sup>

<sup>1</sup>Dept. of geosystem sciences, Nihon University

The pyroclastic fall deposits of the Asama-Maekake volcano, such as A (1783AD), B' and B (12<sup>th</sup> century), and C (4<sup>th</sup> century), are mainly composed of pumice layers. On the other hand, ash fall derived from the recent vulcanian eruptions (e.g., 2004 and 2009 eruptions) is too small in scale to be preserved as a geologic unit. Ash particles from such small-scale eruptions are mainly lithic fragments originating from solidified lava in a shallow level of the conduit. After the 1783 eruption, repeated vulcanian eruptions have formed ash and soil mixtures on the flank of the volcano. Similar ash and soil mixtures are also recognized beneath A, B, C, and D pyroclastic fall deposits, respectively. These ash and soil mixtures contain lithic fragments as the ash component, indicating that vulcanian eruptions occurred repeatedly in the period between large-scale eruptions, similarly to the period after the 1783 eruption. Lithic ash layers are also interbedded with pumice fall layers of B', B, and E pyroclastic fall deposits. There seem to be some cases of intermittent vulcanian and sub-plinian eruptions in the course of the large-scale eruption.

In the case of the 1783 eruption, detailed reconstruction of the eruptive sequence is possible on the basis of correlation between the stratigraphy of the eruptive products and old documents. The large-scale sub-plinian eruption is considered to be associated with the formation of a pyroclastic cone in a proximal area owing to vigorous fountaining. Subsequently, large-scale clastogenic lava flows are generated throughout its climactic eruption. On the other hand, little information is available for eruptions before 1783 because of limited exposure and few old documents. Although the reconstruction accuracy for the eruptions in the 12<sup>th</sup> century is not as good as that for the 1783 eruption, these eruptions might have occurred with a different sequence from the 1783 eruption. Intermittent events of ash and pumice fall occurred in the initial stage of these eruptions. Phreatomagmatic eruption also occurred in the early stage of the 1128 eruption, resulting in a B' pyroclastic fall deposit. The existence of many units of pyroclastic flows in the 1108 eruption indicates that pyroclastic flow occurred on multiple occasions. Since the stratigraphic relationship between the B pyroclastic fall and these pyroclastic flows is unclear, the sequence of the eruption is still in question. Furthermore, little information is available for eruptions predating the 12<sup>th</sup> century.

Comparative study of the distributions of pyroclastic fall deposits using isopach maps reveals that some fall units from B' and B are larger in scale than that of the climactic pyroclastic fall deposit of the 1783 eruption. In addition, the A' pyroclastic fall deposit is estimated to be comparable to or smaller than the preclimactic fall unit of the 1783 eruption. Although the isopach maps of A, B', B, C, and E could be prepared, the accuracy of the isopach maps for the C and E pyroclastic fall deposits is insufficient. The preparation of an accurate map is difficult for deposits of older age. Consequently, at this point, the 1783 eruption is the only example in which the temporal variation in eruptive style and in eruptive volume can be discussed with high accuracy in the history of the Asama-Maekake volcano.

## Polybaric crystallization of H<sub>2</sub>O-saturated island arc low-K tholeiite magmas: A case study of the Izu-Oshima volcano

HAMADA, Morihisa<sup>1\*</sup>; OKAYAMA, Yuko<sup>2</sup>; KANEKO, Takayuki<sup>3</sup>; YASUDA, Atsushi<sup>3</sup>; FUJII, Toshitsugu<sup>4</sup>

<sup>1</sup>Japan Agency for Marine-Earth Science and Technology, <sup>2</sup>National Museum of Emerging Science and Innovation, <sup>3</sup>Earthquake Research Institute, University of Tokyo, <sup>4</sup>Crisis and Environment Management Policy Institute

**Introduction:** The H<sub>2</sub>O concentration of pre-eruptive melts, particularly that of primitive melts, provides information on the *P-T* conditions of their generation, their differentiation pathways, and their potential explosivity of eruptions. Consensus with regard to the H<sub>2</sub>O concentration of island arc low-K tholeiitic magmas (melts) remains elusive. We investigated conditions of their crystallization differentiation, particularly the H<sub>2</sub>O concentration in melts, using geochemical data of volcanic rocks from Izu-Oshima volcano in the Izu arc, along with the results of hydrous melting experiments.

**Geochemistry and petrology of volcanic rocks:** We selected 68 aphyric volcanic rocks which exhibit multiply saturated liquid compositions of the Izu-Oshima volcano. Among them, two magma groups are distinguished by the K/Zr ratio, a lower-K subgroup (K/Zr<60) and a higher-K subgroup (K/Zr≥60). In this study, we focus on the higher-K subgroup liquids. Two endmember trends, referred to here as a higher-Al/Si trend and a lower-Al/Si trend, have been distinguished in the higher-K subgroup liquids. All the liquids are bracketed by these two endmembers, and thus may be mixtures of the two endmembers or may have been derived under intermediate conditions between those responsible for the two endmembers. An experimental study by Hamada and Fujii (2008, *Contrib. Mineral. Petrol.*) suggests that the higher-Al/Si and lower-Al/Si trends can be reproduced by upper crustal crystallization differentiation of primitive basalt under moderately hydrous (~3 wt % H<sub>2</sub>O) and almost dry conditions, respectively.

**Hydrous melting experiments on island arc low-K tholeiite magmas:** Island arc low-K tholeiite magma is characterized by presence of Ca-rich plagioclase (An≥90), with Ca-poor rim (~An75). Hydrous melting experiments on two volcanic rocks from the Izu-Oshima volcano, MA43 and MA44 (MgO~5 wt %), were conducted at 250 MPa to constrain the origin of Ca-rich plagioclase (Hamada and Fujii 2007, *Geochem. J.*). MA43 and MA44 represent less differentiated liquid compositions on the higher-Al/Si and lower-Al/Si trends, respectively. In the melting experiments on MA43, plagioclase crystallized as the liquidus phase at all H<sub>2</sub>O content (1~6 wt % H<sub>2</sub>O), and anorthite content of the plagioclase increased from ~An80 under nearly dry conditions to An≥90 with ≥3 wt % H<sub>2</sub>O in melt. In the melting experiments on MA44, plagioclase crystallized as the liquidus phase under low-H<sub>2</sub>O (≤2 wt %) conditions, but augite replaced plagioclase as the liquidus phase with more H<sub>2</sub>O in melt. Anorthite content of plagioclase increased from about An70 under nearly dry conditions to An80 with ~4 wt% H<sub>2</sub>O in melt. Increases in anorthite content of plagioclase crystallized from the MA44 melt were suppressed compared with plagioclase crystallized from the MA43 melt. In short, Ca-rich plagioclase (An≥90) can be crystallized from melts on the higher-Al/Si trend with ≥3 wt % H<sub>2</sub>O, but cannot be crystallized from melts on the lower-Al/Si trend with any H<sub>2</sub>O. Ca-poor rim (~An75) cannot be crystallized from melts on the higher-Al/Si trend, but can be crystallized from melts on the lower-Al/Si trend.

**Summary:** Geochemical variations in the liquids from the Izu-Oshima volcano are bracketed by two endmember trends, namely, the higher-Al/Si and the lower-Al/Si trends. Origins of the higher-Al/Si and the lower-Al/Si trends can be explained by crystallization differentiation under moderately hydrous conditions (~3 wt% H<sub>2</sub>O) and almost dry conditions, respectively. We propose that polybaric crystallization of H<sub>2</sub>O-saturated melts, at a depth range between the ~4-km-deep magma chamber (~3 wt% H<sub>2</sub>O) and near surface level (nearly dry) beneath the Izu-Oshima volcano, is a ubiquitous feature of island arc low-K tholeiite magmas.

Keywords: Island arc low-K tholeiite, Volcanic front, Ca-rich plagioclase, Izu-Oshima volcano

## The change time from magmatic to phreatomagmatic eruption, in the Hachodaira caldera eruption at Miyakejima Volcano

OIKAWA, Teruki<sup>1\*</sup> ; GESHI, Nobuo<sup>1</sup>

<sup>1</sup>GSI, AIST

The Miyakejima volcano formed the caldera in 2000. This volcano erupted Hachodaira Scoria and Hachodaira Ash at ca.3ka of Hachodaira caldera collapse. Many plant fossils (*Miscanthus* sp.) are recognized in Hachodaira Scoria and Ash. Based on plant fossils in these tephras occurrence, deposition late of soil in the Miyakejima volcano, and form of the boundary of Hachodaira Scoria and Ash, The change time from magmatic eruption (Hachodaira Scoria eruption) to phreatomagmatic eruption (Hachodaira Ash) is under 1 year, probably it is several days or less. Thus, there was no time gap almost between magma eruption and phreatomagmatic eruption. This eruption style change can be explained such as 2000 eruption (Geshi and Oikawa,2008:JVGR) as follows. The altitude of the summit part approached the sea level by caldera collapse; as a result, phreatomagmatic eruption occurred.

Keywords: volcano, caldera, Miyakejima, eruption, *Miscanthus*

## Pumice deposits of the pre-Ofunato stage distributed in northwest of the Miyake-jima volcano, northern Izu-Bonin Arc

NANRI, Shohei<sup>1\*</sup> ; SUZUKI, Takehiko<sup>2</sup>

<sup>1</sup>Graduate student, Tokyo Metropolitan University, <sup>2</sup>Tokyo Metropolitan University

Miyake-jima Island, a volcanic island of the northern Izu-Bonin Arc, is located in the northwestern Pacific Ocean, approximately 180 km south of Tokyo. A pale-orange-tuff layer had been reported by Issiki (1960) on coastal cliff in the northwestern part of the island. The aim of this study is to clarify (i) distribution, (ii) stratigraphic position, (iii) sedimentary structure, (iv) petrological features, and (v) mineralogical features, for this pyroclastic deposit in more detail. The layer was re-defined as "Miyake-jima Ofunato Pumice deposit: OFP". The OFP is distributed from western to northern parts of the island. The OFP exists below the Aira-Tn tephra, erupted at 30 ka. The sedimental facies of OFP deposits suggest it formed as a pyroclastic flow deposit.

The relation between K<sub>2</sub>O and FeO concentrations in the OFP is characterized by higher FeO wt.% and lower K<sub>2</sub>O wt.%. Tsukui et al. (2006) and Saito & Miyairi (2008) showed that the chemical trends in the volcanic products of forearc of Izu-Bonin Arc such as Izu-Oshima and Hachijo-jima are characterized by high FeO wt.% and low K<sub>2</sub>O wt.%, and those of the backarc Izu-Bonin Arc such as Nii-jima and Koju-shima shows low FeO wt.% and high K<sub>2</sub>O wt.%. Consequently, chemistry of the OFP suggests that it was originated from forearc of Izu-Bonin Arc.

This paper concludes that the activities of the Miyake-jima volcano around 30 ka are characterized by a production of pumice by the eruption at the northwestern part of the present island. The current stage of this study, it is not possible to discuss the source vent of the OFP in detail and specify the type of the volcanic eruption produced the OFP. In future, we attempt to find a clue to account for these two problems by the detailed study on the OFP with referring to its facies like a pyroclastic flow deposits.

Keywords: Miyake-jima volcano, Pumice, Miyake-jima Ofunato Pumice deposit, Northern Izu-Bonin Arc

## Formation process of a volcanic island during the 2013-2014 eruption at Nishinoshima, Ogasawara, Japan

MAENO, Fukashi<sup>1\*</sup> ; NAKADA, Setsuya<sup>1</sup> ; KANEKO, Takayuki<sup>1</sup>

<sup>1</sup>Earthquake Research Institute, Univ. Tokyo

New volcanic islets created by submarine eruptions are often observed around Japanese Islands. However, in most cases, such new islets are disappeared by wave erosion in short periods. To make a new volcanic island remaining for a long time, an amount of lava flows must occur and reclaim land from the sea. However, such relatively large-scale lava eruptions rarely occur. Therefore, the very initial stage of the formation process of a volcanic island has been poorly understood.

The submarine eruption off Nishinoshima, Ogasawara, has created a new volcanic islet since Nov 2013. The lava flow eruption continues for more than a few months, and the islet keeps growing. This eruption will give an opportunity to understand the birth and growth of a new volcanic islet. We studied variation of eruptive styles and sequences of this 2013-2014 eruption at Nishinoshima based on airborne observations and publicized aerial and satellite images (taken by JCG, GSI, and JAXA).

Nishinoshima forms a part of summit crater rim of a huge submarine volcano. The 2013-2014 eruption occurred inside the summit crater about 400 m off Nishinoshima with a depth of dozens of meters. In the first stage, Surtseyan eruptions repeated due to seawater entering a main crater of an islet. With the growth of the islet, the main crater was dried up and the eruption style changed to Strombolian with a scoria cone formation and lava flows that continuously effuse from the main crater over a few months. Lava flow front is brecciated by rapid cooling, or auto-brecciated, and eventually reclaimed the foreshore from the sea. The lava flows are then branched many times and extended to almost all directions. The continuous activity of Strombolian with lava flows suggests that magma is stably supplied from the deeper part of conduit.

Based on the change of outline of the islet and bathymetry data before the eruption, volume and discharge rate of lava flows are estimated. For the first 2.5 months by early Feb 2014, the volume of lava flow is estimated at about 6 M m<sup>3</sup>. The discharge rate is estimated at 0.5-1\*10<sup>5</sup> m<sup>3</sup>/day with some fluctuations. This discharge rate is almost the same as that estimated for lava effusion in the 1934-1935 eruption at Showa Iwojima, southern Kyushu (1\*10<sup>5</sup> m<sup>3</sup>/day; Maeno and Taniguchi, 2006), which is one of the youngest remained volcanic islands in Japan. The volume of the 2013-2014 eruption is so far 1/4 of the total volume (24 M m<sup>3</sup>) of the last 1973-1974 eruption, in which the volume of the last eruption was estimated based on bathymetry change before and after the eruption. The eruptive sequence and growth rate of the islet in 2013-2014 is different from the last eruption. This is probably because the eruption began at shallower depth than the last eruption. At the time of early Feb 2014, erosion signatures on lava flows are little, so that the new island is expected to further grow.

Keywords: Nishinoshima, volcanic island, lava flow, Surtseyan eruption, Strombolian eruption

## Petrological characteristics of volcanic materials ejected during 2012-2013 explosive events on Ioto Island

IKEHATA, Kei<sup>1\*</sup> ; TAMURA, Tomoya<sup>2</sup>

<sup>1</sup>Faculty of Life and Environmental Science, University of Tsukuba, <sup>2</sup>Graduate School of Life and Environmental Sciences, University of Tsukuba

Ioto is an active volcanic island (8.5km long in NE-SW and 4.5km wide) located about 1250km south of central Tokyo. Since early February 2012, small explosive eruptions have repeatedly occurred at the Old Crater (Million Dollar Hole) in the western part of the island (JMA, 2013). Four (February 2012, March 2012, February 2013 and April 2013) ejected mud materials collected in the vicinity of the crater consist of free crystals (plagioclase, clinopyroxene, olivine, and Fe-Ti oxides), relatively fresh volcanic glass, altered volcanic glass, lithic fragment, altered lithic fragment and pyrite aggregate (Ikehata and Tamura, 2013). Among the mud samples, there is little difference in component of grains except for high abundance of altered lithic fragment in the mud ejected in February 2012.

Detailed SEM/BSE image observation of the relatively fresh volcanic glasses show that even these fresh glasses have pitted alteration and hydration features. The extent of hydration could be different among volcanic glass shards in geothermal field like Ioto because hydration rate depends on chemical compositions of volcanic glasses and groundwater, and soil temperature. To eliminate such hydration effects, heating (400 °C-12h) is conducted for the relatively fresh volcanic glasses before analyzing. As a result of the chemical analysis, all of these volcanic glasses are trachytic, and their chemical compositions are homogeneous within the analytical error. In conclusion, no juvenile materials existed in the mud samples, suggesting these explosive events were not phreatomagmatic but phreatic eruption.

We would like to thank members of JMSDF Ioto Air Base weather team for sampling around the Old Crater and providing information on the studied area. Ministry of Defense, JMA and NIED are also thanked for their cooperation.

Keywords: Ioto Island, the Old Crater, mud, volcanic glass, phreatic eruption

## Compositions of minerals in volcanic products from pre- and the early stage of Aso-4 large-scale pyroclastic flow

KUROKAWA, Kiyoshi<sup>1</sup> ; YAMASAKI, Hideto<sup>1</sup> ; HASENAKA, Toshiaki<sup>1\*</sup> ; MORI, Yasushi<sup>2</sup>

<sup>1</sup>Grad School Sci. & Tech., Kumamoto Univ., <sup>2</sup>Kitakyushu Museum of Natural and Human History

Formation of Omine scoria cone, Takayubaru lava flow, and Oyatsu pumice flow are a series of volcanic events just before and after the large-scale Aso-4 pyroclastic eruption. Compositions of volcanic products change from 62-66 SiO<sub>2</sub> wt.% for Omine scoria, 63-66 SiO<sub>2</sub> wt.% for Takayubaru lava, to 67-69 SiO<sub>2</sub> wt.% for Oyatsu pumice. The difference between Omine-Takayubaru compositional trend and Oyatsu trend is small but evident (Yamasaki et al., 2013). Common phenocryst assemblage is plagioclase, orthopyroxene, clinopyroxene, and opaque minerals. In addition, Omine scoria and Takayubaru lava contain hornblende microphenocrysts, whereas Oyatsu pumice contains phenocrysts of hornblende. Most plagioclase characteristically shows sieve texture among Omine-Takayubaru samples. Such texture is not so common among Oyatsu pumice samples. We analyzed these minerals using EPMA in order to characterize the change in magma supply system that lead to large-scale pyroclastic eruption.

In response to different compositional trends observed between Omine-Takayubaru and Oyatsu samples, different mineral compositions are also found. Plagioclase phenocrysts in Omine-Takayubaru samples are An50-An60 with uni-modal peak, where as those in Oyatsu samples are An37-An56 with three peaks. Slight difference in Mg# are also found between orthopyroxene, clinopyroxene, and hornblende of Omine-Takayubaru and those of Oyatsu samples.

Estimated temperature for Omine scoria using Wells (1977) pyroxene thermometer is 950 °C, and dry viscosity is 10<sup>5.6</sup> Pa • s. That for Tamaraigawa lava (SiO<sub>2</sub>=61 wt.%) extruded before Aso-2 pyroclastic eruption was reported as 1120 °C and 10<sup>3.9</sup> Pa • s, respectively, by Kobayashi (2013). The difference in viscosity is reflected by different aspect ratio, i.e. 100 m thick and 7 km long for Takayubaru lava flow, and 10 m thick and 10 km long for Tamaraigawa lava flow.

Sieve texture and microphenocrysts in Omine scoria and Takayubaru lava make an important restriction for making models of magma supply system before and after the large-scale pyroclastic eruption. If sieve texture suggests melting process of plagioclase, it indicates temperature ascent and/or water vapor pressure increase. In contrast, growth of hornblende microphenocryst suggests temperature drop and/or water vapor pressure increase. Omine-Takayubaru samples do not contain mafic inclusions and mafic minerals with reverse zoning, thus possibility of magma mixing and temperature ascent is small. The change in physico-chemical condition in Aso-4 magma supply system is yet to be solved.

Keywords: Aso-4 pyroclastic flow, Takayubaru lava, Omine volcano, lava flow

## Forming process of Minamidake stratovolcano, Sakurajima, inferred from paleomagnetic age and volume of lava flows

MIKI, Daisuke<sup>1\*</sup>

<sup>1</sup>DPRI, yoto University

A paleomagnetic measurement was carried out on the Arimura lava, which consists uppermost part of the main body of Minamidake stratovolcano, Sakurajima volcano, Kyushu, Japan. A mean paleomagnetic direction,  $D=4.0^{\circ}$   $E I=40.5^{\circ}$  down, was obtained from the Arimura lava. By comparison between measured paleomagnetic direction and the paleo-secularvariation of geomagnetic field, the age of the Arimura lava was estimated as about 3.1-2.7 ka, moreover the age of the Kannonzaki lava lying beneath the Arimura lava, was thought as about 3 ka. These two lavas are considerable to be formed by a sequence of intermittent eruption during several hundred years at around 3 ka. The volumes of individual lava that extruded in recent 4,000 years were estimated. The main body of Minamidake stratovolcano had grown rapidly at around 3 ka, since estimated lava volume. The volume of the Nagasakihana lava erupted in 764-766 AD was estimated as about  $0.8\text{km}^3$ . The scale of 764-766 AD eruption may be greater than previously thought. The long-term magma effusion rate during historic time, particularly recent 240 years, was estimated as larger than earlier.

## Morphology of microlite -projections of plagioclase microlite-

SANO, Kyohei<sup>1\*</sup> ; TORAMARU, Atsushi<sup>2</sup> ; WADA, Keiji<sup>3</sup>

<sup>1</sup>Department of Earth and Planetary Sciences, Graduate School of Sciences, Kyushu University, <sup>2</sup>Department of Earth and Planetary Sciences, Faculty of Sciences, Kyushu University, <sup>3</sup>Hokkaido University of Education at Asahikawa

At Tokachi-Ishizawa (TI) rhyolite lava, Shirataki, Hokkaido, northern part of Japan, the interior structure transition can be observed, from the outer obsidian layer to the inner rhyolite layer. Thus TI lava is an appropriate target field for correlating textural characteristics with lava interior structure. In order to obtain insights into the magma ascent and outgassing process of viscous magma, we have analyzed oxide microlites of TI rhyolite lava, suggesting that dominant outgassing process is ductile permeable development (Sano et al., 2013 JpGU meeting). However, we have not examined the morphology of microlite. Morphology of crystal is considered to reflect the effective undercooling of the melt and provide the constraint for ascent process and water exsolution processes. In this study, we focused on the morphology of microlites, especially projections of plagioclase microlites. The projections mean localized growth of crystal from plagioclase surface.

In Shirataki, aphyric rhyolite lavas erupted ca. 2.2Ma and composed of 10 flow units. The TI lava is about 50 m in height and stratigraphic sequences from the bottom are a obsidian layer region, a boundary bounded region of obsidian and rhyolite, and rhyolite layer region. The obsidian layer region consists of a single vesicle-free obsidian about 7 m high. The rhyolite layer region consists of rhyolite layers with variable vesicularity, crystallinity and characteristic scales in layer thickness. The boundary banded region, which is located between the obsidian and rhyolite regions, consists of thin obsidian (<10mm in width) and rhyolite. In this study, we define the obsidian and rhyolite based on the differences in appearance of hand specimens and rock texture. Rhyolite has perlitic cracks in the glass and contains some amounts of crystalline materials, namely, spherulite and lithophysae. In boundary banded region, the fraction of obsidian decreases toward rhyolite layer region.

From the examination by scanning electron microscope (SEM) for thin sections from obsidian layer region, boundary banded region and rhyolite layer region, we found the projection texture in all samples. We measured projection length and number density ( $Nv$ ) of plagioclase microlites for obsidian and rhyolite layer regions. The measurement results show that plagioclase microlites in obsidian and rhyolite layer regions indicate the similar number density.  $Nv$  for obsidian layer region is  $1.8 \times 10^{11} - 3.5 \times 10^{11} [m^{-3}]$  and  $8.2 \times 10^{10} - 3.0 \times 10^{11} [m^{-3}]$  for rhyolite layer region, respectively. However, the length of projection is remarkably different between two regions. The mean values are  $2.3 \mu m$  in obsidian layer region, and  $8.7 \mu m$  in rhyolite layer region. The transition of mean length can be observed in boundary layer region.

Since the difference of projection length reflects the growth rate ( $G [m/s]$ ) and growth time ( $t [s]$ ) according to the theory of crystal growth (Keith and Padden, 1963; Lofgren, 1971; Rao, 2002), we can estimate the degree of effective undercooling at the formation time of projections. Under the assumption that  $G$  is constant for the time, the length of projection can be given by  $Gdt$ . Assuming the constant growth rate and growth time, the difference in projection lengths indicate that in growth rate, namely, the undercooling. Using experimental values for growth rate and undercooling, it is found that the rhyolite layer region experiences higher undercooling than obsidian layer region by 30 – 70 K. The projection can be formed after the nucleation of plagioclase microlite, which indicate the similar number density in obsidian and rhyolite layer region. Thus projections reflect the different undercooling after the nucleation of microlites. Based on the quantitative analysis of crystal morphology of microlites, we can obtain the insights into the magma ascent process that rhyolite layer region experienced higher undercooling than obsidian layer region.

Keywords: textural analysis, obsidian, rhyolite, lava, Shirataki

## Differentiation process of arc magmas revealed by principal component analysis on trace element composition

UEKI, Kenta<sup>1\*</sup>

<sup>1</sup>Volcanic Fluid Research Center, Tokyo Institute of Technology

Chemical composition of magma can be used to address state of the magmatic system and the processes during magma generation, ascent and eruption. Various processes from the mantle to the crust in various pressure, temperature and chemical composition modify magma composition. Consequently, bulk chemical composition of erupted magma represents a sum of these processes.

Differentiation in terms of major element composition is controlled by non-linear thermodynamic relation. Major element composition of magma is modified by temperature, pressure and H<sub>2</sub>O content dependent saturation states of mineral phases, and partition between melt phase and mineral phases. In this sense, major element composition can be a proxy of physical state during magma generation and ascent. However, the non-linearity of major element processes and a small degree of freedom in compositional space prevent us from decomposition of processes that have derived compositional variation in terms of major element.

On the other hand, partition of trace elements between melt and mineral phase can be modeled with relatively simple equation, and can be considered as a linear process. Consequently, trace element composition of erupted magma represents a simple sum of a melting and differentiation processes. Trace element can be a tracer of the specific phase or reaction, because partition coefficients between various minerals melt show wide range of variation. Therefore, trace element can be used as a proxy of a specific chemical mass reaction process during magma generation and ascent. In addition, trace element composition shows a large degree of freedom. Therefore, it is expected that nature and the number of processes during magma generation and ascent can be decomposed by analyzing trace element composition of volcanic rock using multivariate statistics.

In this study, principal component analysis is used to analyze compositional variation of volcanic rocks in Northeastern Japan Arc.

Analysis based on a series of volcanic rocks from single volcanic activity has shown that the differentiation process and/or mantle melting process beneath each volcano (crystal fractionation and magma mixing) can be decomposed by using principal component analysis on trace element compositions. Consistent relationship between the trace element principal components, major element composition, and petrological information such as mineral composition is derived from the analysis.

In order to illustrate the differentiation process in terms of large scale spatial and compositional range, 262 samples from 17 different volcanoes in the Sengan region, northeastern Japan are analyzed with principal component analysis. Result of the analysis clearly demonstrates that differentiation processes in the arc crust, are the primary controlling factor to derive compositional variation of arc magmas. Only three principal components account for the compositional variation of 262 samples. It is estimated the three principal components represent magma mixing, relatively high pressure olivine fractionation, and relatively shallower pressure plagioclase differentiation, respectively. No strong mantle signature is identified by the analysis. This result shows intermediate-felsic magmas (SiO<sub>2</sub>>60 wt. %) can only be derived through magma mixing, not by crystal fractionation.

Keywords: volcanic rock, arc magma, crystal fractionation, magma mixing, trace element

## A preliminary estimation of water content of the mantle beneath Changbaishan Volcano, northeast China

KURITANI, Takeshi<sup>1\*</sup>; OKUMURA, Satoshi<sup>2</sup>; YOKOYAMA, Tetsuya<sup>3</sup>; ITO, Yoshinori<sup>2</sup>; NAKAMURA, Michihiko<sup>2</sup>; WEI, Haiquan<sup>4</sup>

<sup>1</sup>Osaka City University, <sup>2</sup>Tohoku University, <sup>3</sup>Tokyo Institute of Technology, <sup>4</sup>China Earthquake Administration

In northeast China, Cenozoic intraplate volcanic products are widely distributed. Geophysical studies have suggested that the underlying mantle transition zone is remarkably hydrous (Kelbert et al., 2009) and contains remnants of the subducted Pacific slab (Fukao et al., 1992); therefore, the Pacific slab stagnation and its relation to observed magmatism has received growing attention (e.g., Ohtani and Zhao, 2009; Richard and Iwamori, 2010). Beneath the Changbaishan volcanic field, a prominent low-velocity anomaly with a plume-like shape has been imaged in the upper mantle by P-wave tomography, which is suggestive of an upwelling of a mantle plume from the mantle transition zone (e.g., Zhao et al., 2009). In this study, to characterize the nature of the transition zone-derived mantle plume, the water content of the source mantle is estimated for basaltic products from the Changbaishan volcano.

Basaltic scoria samples were collected from a cinder cone, located about 20 km to the northeast of Tianchi volcano. One scoria sample was used for preliminary analysis of glass inclusions in some plagioclase phenocrysts. Basaltic lavas, which occur with abundant mantle xenoliths, were also collected from the outcrop near the cinder cone to know the primitive magma composition at the volcano. The MgO contents of the scoria and the lava are 5.1 wt.% and 9.1 wt.%, respectively. Major element compositions of quenched glass inclusions in the scoria sample were analyzed using EPMA, and the water contents were estimated by the difference of the analytical total of the major element analysis from 100 wt.%. Through calibration using an in-house standard glass sample of known water content, the water contents of the glass inclusions were obtained to be 0.15-3.4 wt.%. The FT-IR analysis was also performed for one glass inclusion of the estimated water content of 0.15 wt.% by EPMA, which yields the total water content of 0.2 wt.%.

Given that 3.4 wt.% represents the original water content of the melt without leakage, the H<sub>2</sub>O/K<sub>2</sub>O ratio of the melt of 0.90 is obtained. If we assume that the H<sub>2</sub>O/K<sub>2</sub>O ratio of the melt was not affected significantly by magmatic processes and the ratio is essentially constant in basaltic magmas at Changbaishan volcano, the water content of the primitive magma (2.4 wt.% in K<sub>2</sub>O) is estimated to be 2.2 wt.%. The source mantle for the Changbaishan basalts may contain ~0.5% sediment component (Kuritani et al., 2011), and the Ce content of the source mantle is estimated to be ~1.1 ppm using the Ce content of the sediment component of 57.3 ppm (Plank and Langmuir, 1998) and that of the depleted mantle of 0.77 ppm (Salters and Stracke, 2004). If we assume that Ce and H<sub>2</sub>O behave similarly during mantle melting (e.g., Michael, 1995), the compositions of the primitive basalt lava (Ce: 70 ppm, H<sub>2</sub>O: 2.2 wt.%) yield the water content of the source mantle of ~350 ppm. This estimated water content is significantly higher than that of the normal depleted mantle (~120 ppm; Salters and Stracke, 2004), suggesting that the transition zone-derived mantle plume is hydrous compared with the surrounding ambient upper mantle.

In this preliminary study, we have analyzed only seven glass inclusions in a single sample, and therefore, the water content of ~350 ppm may represent the minimum estimate. It is necessary to increase the number of data by EPMA and FT-IR analyses to more reliably estimate the source water content for the Changbaishan basalts.

Keywords: mantle, water content, China

## Petrological and geochemical variations within an off-axial submarine large lava flow from the Oman Ophiolite

OTSUKA, Ryo<sup>1\*</sup> ; KUSANO, Yuki<sup>1</sup> ; KANAYAMA, Kyoko<sup>1</sup> ; UMINO, Susumu<sup>1</sup>

<sup>1</sup>Department of Earth Sciences, Kanazawa University

Large submarine lava with thicknesses >100 m and volumes exceeding a few cubic kilometers are not uncommon volcanic constructs of mid-ocean ridges and around Hawaii Islands, yet details of the physical processes of eruption of these large lava flows are poorly understood. The V3 flow of the Oman ophiolite extruded at 90 Ma far off the paleospreading axis as thick lava flows with a minimum areal extent of >11 km by 1.5 km and the maximum thickness >270 m, yielding a minimum estimated volume >1.2 cubic kilometers. The V3 flow was fed by a thick feeder dike in the SW of the flow field and buried off-axial fault-bounded basins with a thick sedimentary cover in ~40 days. The upper V3 flow field consists of compound lobes that merge upstream into larger and thicker sheet-like lava, which grew endogenously as a vast sheet lobe.

Low-T hydrothermal alteration and weathering slightly modified the bulk compositions as indicated by moderate albitization of plagioclase and partial replacement of titanomagnetite and clinopyroxene by titanite and chlorite, respectively. However, strong positive correlations among incompatible HFSEs and REEs and relatively good correlations with major elements besides LILEs and Pb show that these elements were less mobile and preserve primary characteristics. FeO and TiO<sub>2</sub> show moderate increases with a decrease in MgO from 8 to 5 wt%, and then decreases with the decrease in MgO down to 4 wt%. 20-50 times enrichment in Th and depleted HREEs compared to primitive mantle of the V3 flow is similar to differentiated EMORBs.

Whole-rock major and trace element variations through a vertical transect at 8.7 km (T-21) from the feeder dike show fractional crystallization of clinopyroxene and plagioclase, the major phases in the groundmass of the lava, at a pressure of the paleowater depth. The stratigraphic variations show a notable enrichment in MgO and depletion in incompatible elements in the lowermost core, consistent with accumulation of olivine phenocrysts. Enrichment in incompatible elements in the uppermost core of the flow is in accordance with the model that the last solidified, residual melt resided in this horizon.

By contrast, samples collected from the basal crust every 0.5-1 km from the feeder dike, and vertical transects at 6.7 km (T-14) from the dike have whole-rock compositions spread over compositional spaces that could be explained by internal mixing of variably differentiated magmas. Interestingly, incompatible elements like Yb and Ti of the basal crust show increases downflow to ~5 km from the feeder dike and decreases further downflow. Because the basal crust is the quenched lava that came to rest first at that place, samples farther away from the feeder were extruded and emplaced later in the eruptive event. The downflow variations show extrusion of differentiated lava in the middle stage of the eruption and less differentiated lava in early and late stages. Meanwhile, the transect at T-14 is differentiated in the upper and lower crust and less differentiated in the core.

These intraflow variations in the bulk geochemistry indicate supply of less differentiated magma in an early stage of the eruption, which was progressively replaced by mixed magmas of variably differentiated and less differentiated ones toward the end of the eruption. The eruptive sequence of less differentiated to differentiated magmas with increasing FeO suggests extrusion from a density stratified magma chamber with less dense and Mg-rich magma underlain by more dense Fe-rich magma. The internal mixing among variably differentiated magmas with the progress of the eruption and the extrusion of less differentiated magma toward the end of the eruption suggest a renewal of magma toward the end of the eruption caused mixing of newly supplied less differentiated magma with the differentiated magma within the conduit and the lava tubes.

Keywords: Oman Ophiolite, obduction, V3, Large Lava Flow, chemical variation geochemistry

## Factors governing fragmentation of submarine lava - mechanism of hyaloclastite formation

UMEZAWA, Yumi<sup>1\*</sup> ; UMINO, Susumu<sup>1</sup> ; KUSANO, Yuki<sup>1</sup> ; KANAYAMA, Kyoko<sup>1</sup> ; KITAMURA, Keitaro<sup>1</sup>

<sup>1</sup>Department of Earth Sciences, Kanazawa University

Hyaloclastite is water-lain volcanic breccia embedded in a matrix of glassy clasts by fragmentation of brittle lava under thermal stress. Fluidal basalt lava tends to form coherent flows like pillow lava and sheet flows. In contrast, viscous lava such as andesite and dacite is more likely to form hyaloclastite. This preference of hyaloclastite on lava composition indicates that mechanical response of solidified lava under stress is strongly dependent on composition. Fracturing of lava occurs when the rate of stress accumulation exceeds the rate of stress relaxation and ultimately reaches the mechanical strength of the lava. The rate of stress relaxation decreases with the increase in lava viscosity. Therefore, hyaloclastite is more common in viscous silicic lava.

However, the occurrences of pillow lava of dacite and rhyolite are known from the Ogasawara Islands, Unalaska Island, Oman Ophiolite, etc. Pillow lava is commonly associated with hyaloclastite of the same compositions. These examples demonstrate that factors other than lava composition determines fragmentation of lava. Then, the problem arises what are the governing factors that control the mechanical response of lava under stress. We will address these issues through comparative study on glass, quenched melt, of pillow lava and hyaloclastite of variable compositions spanning from basaltic andesite to rhyolite from the Eocene submarine volcanic strata in Chichijima, Ogasawara Islands.

Samples of glass from these sites were analyzed by EPMA for major elements and by SIMS for water contents. Eruption temperatures were estimated by clinopyroxene-liquid geothermometer of Putirka (2008). Crystal number densities of groundmass plagioclase and clinopyroxene were determined on COMPO images and modal abundance of constituent minerals were determined on element distribution maps of EPMA. Bulk viscosity of lava was estimated by the methods of Giordano et al. (2008) and Pinkerton and Stevenson (1992).

Dacite has phenocrysts of clinopyroxene, orthopyroxene, plagioclase and magnetite. Groundmass consists of clinopyroxene and plagioclase microlites and magnetite set in glass. In dacite glass, there is little difference in melt composition, eruption temperature, crystal number density between pillow lava and hyaloclastite. However, lower water content in hyaloclastite glass than in pillow margin glass yields higher bulk viscosity.

Andesite has phenocrysts of clinopyroxene, orthopyroxene, plagioclase and magnetite. Groundmass consists of clinopyroxene and plagioclase microlites and magnetite set in glass. Clinoenstatite xenocrysts enclosed by orthopyroxene rim are occasionally present. Hyaloclastite is higher in crystal number density and mode of groundmass plagioclase than associated pillow lava. Hyaloclastite glass is lower in Al<sub>2</sub>O<sub>3</sub> than associated pillow glass, consistent with preferential crystallization of plagioclase. However, the cpx-saturated melt temperatures show little difference between pillow lava and hyaloclastite. Bulk viscosity estimated for the lava to become hyaloclastite is higher than the lava that formed pillows because of the larger crystal number density in hyaloclastite.

The above observations on dacite glass clearly indicate that water played an essential role in formation of hyaloclastite. Degassing either within the conduit or during flowage through lava tubes raised the bulk viscosity of lava and stress relaxation time, resulted in fragmentation of lava to form hyaloclastite. Although water content was not determined for andesite glass, higher crystal number density and modal amount of plagioclase in hyaloclastite with the same temperature as the coexisting pillow lava can be explained by volatile loss which raised the liquidus of plagioclase and its preferential crystallization, resulted in higher bulk viscosity and fragmentation of lava.

Keywords: hyaloclastite, the Bonin Islands Chichijima, viscosity, submarine lava

## Eruption history and petrography of Akanfuji in the Me-akan volcano, eastern Hokkaido, Japan

SATO, Eiichi<sup>1\*</sup> ; WADA, Keiji<sup>2</sup>

<sup>1</sup>Institute for Promotion of Higher Education, Kobe University, <sup>2</sup>Hokkaido University of Education at Asahikawa

Me-akan volcano is located in the Akan volcanic field, eastern Hokkaido, and ~250 km inland from the Kuril trench. The volcanic activity of Me-akan volcano began at least a few tens thousand years ago, and eight volcanic bodies with different peaks have been formed.

Akanfuji (1476 m), which is the newest volcanic body in the Me-akan volcano, started its eruptions about 2.5 ka, and the volcanic activity continued for 1,500 years. The eruption products of Akanfuji are composed of scoria fall deposits and lava flows. The scoria fall deposits are distributed from northeast to south from present vent. We described the scoria fall deposits to interpret the complex depositional sequence. As a result, 17 scoria fall layers were recognized for 1,500 years.

Akanfuji had erupted basalts through its history. Two types of basalts (types I and II) are recognized on the basis of phenocrysts assemblage. Type I is orthopyroxene (opx) bearing olivine (ol)-crynopyroxene (cpx) basalt and Type II is cpx bearing ol-opx basalt. They were formed by mixing between different types of basaltic magmas on the basis of the textural and mineralogical evidences.

Keywords: Me-akan volcano, Akanfuji, Eruption history, basalt, magma mixing

## Evidence of eruption episodes before AD1741 of Oshima-Oshima Volcano, Hokkaido, Japan

YOSHIMOTO, Mitsuhiro<sup>1\*</sup> ; NAKAMURA, Yugo<sup>1</sup> ; FUKUHARA, Genta<sup>2</sup> ; NISHIMURA, Yuichi<sup>1</sup>

<sup>1</sup>Faculty of Science, Hokkaido University, <sup>2</sup>Faculty of Science, Hokkaido University

We newly identified two eruption episodes of Oshima-oshima volcano below eruption products of the AD 1741 eruption at an outcrop on the summit of the volcano. The upper eruption product consists of alternating volcanic lapilli fall and ash fall deposits, and the lower one consists of scoria fall deposits. Tephra from those eruptions have not found in the other area including southern Hokkaido. We also identified two thin tephra layers between three eruption products of Oshima-oshima volcano with intercalating soil layers. They are correlating with well-known wide spread tephra such as Ko-d (AD 1640) from Hokkaido-Komagatake Volcano and B-Tm (ca. AD 940) from Changbaishan Volcano, China-North Korea, based on chemistry of volcanic glass shards. Considering the thickness of soil layers, those eruption episodes would occur at around AD 1450 and BC 600. It suggests that Oshima-Oshima volcano erupted at least 4 times in last 2500 years including 2 historical eruptions in AD 1741-1742 and 1759.

This work was supported by JSPS Grant-in-Aid for Scientific Research C, Grant Number 24540447.

Keywords: Oshima-oshima, eruption history, tephra

## Compositional variation and magmatic differentiation at the northern Kita-Hakkoda volcanic group

KOMATSU, Sho<sup>1\*</sup> ; OHBA, Tsukasa<sup>1</sup>

<sup>1</sup>Akita Univ.

Since 0.6 Ma, magmatic eruptions have occurred several times at Kita-Hakkoda volcanic group. This study focuses on the activity between 0.4 and 0.2 Ma. Magmatic differentiation process is investigated from whole-rock chemistry and mineralogy along with stratigraphy. This area consists of 12 geologic layers: Hakkoda 2nd Stage Pyroclastic Flow Deposit, Northern Kita-Hakkoda Basaltic Andesite Lavas, Lower Kansuisawa Pumice Flow Deposit, Lower Tamoyachi-dake Andesite Lavas, Upper Kansuisawa Pumice Flow deposit, the Upper Tamoyachi-dake Andesite Lavas, the Tashirotai Lacustrine Deposit, Narusawa Debris Flow Deposit, Maedake Lavas, Narusawa-daichi Andesite Lavas, Okuzuresawa Debris Flow Deposit and Okuzuresawa Pyroclastic Flow deposit in stratigraphic order. Temporal variation of chemical composition in stratigraphic order is evaluated. The activity initiated with the effusion of differentiated tholeiitic basaltic magma around 0.4 Ma. After a dormancy the activity resumed around 0.2 Ma with effusion of andesitic magma (60wt% SiO<sub>2</sub>), followed by a fluctuating activity between tholeiitic basalt and low-silica calc-alkaline andesite magmas. Then, the magma composition jumped to high silica (60wt% SiO<sub>2</sub>) calc-alkaline andesite. No evidence for open system process is recorded in phenocrysts in the tholeiitic rocks. Previous studies accounted for the chemical variation of tholeiitic magma by crystallization differentiation, and our new data is consistent with the model. Disequilibrium mineral assemblages in calc-alkaline rocks, e.g., coexistences of magnesian olivine and embayed quartz, and of reversely zoned pyroxenes and normally zoned pyroxenes, implies open system processes. As indicated by linear trends between tholeiitic basalt and the high-silica andesite, magma mixing is a plausible process to produce the series. Stratigraphic chemical variation might be caused by temporal variation in mixing ratios.

Keywords: Magma mixing

## The volcanic history and geological structure of Sanzugawa Caldera, Yuzawa, Akita prefecture

OKI, Fumiya<sup>1\*</sup>; OHBA, Tsukasa<sup>1</sup>

<sup>1</sup>Akita Univ.

Sanzugawa caldera, located in the southern part of Akita prefecture, was formed by collapses after eruptions of voluminous ash flows about >ca. 1 Ma. Torageyama Formation, deposited during the caldera formation, thickly infills the caldera depression. The Formation is divided into two members: Torageyama tuff member and Minasegawa tuff member. Torageyama tuff member consists of welded tuff, lapilli tuff, and alternation of tuffaceous sandstone, mudstone, and conglomerate. Thickness of Torageyama tuff member is approximately 900m. Minasegawa tuff member consists of lapilli tuff, tuff and conglomerate. Thickness of Minasegawa tuff member is about 450m. In this study, on the basis of lithology, Torageyama Formation is divided into 10 layers, including pyroclastic density current deposits (PDC-1 to PDC-8), a debris flow deposit (DF-1) and a lacustrine deposit (LD-1). Stratigraphic order from the bottom is PDC-1, DF-1, LD-1 and PDC-2 to PDC-8. Approximate thicknesses of the layers are 20m, 80m, 140m, 50m, 250m, 200m, 340m, 160m, 90m and 30m, respectively. Pyroclastic density current deposits consist of massive lapilli tuff. The lapilli tuff contains pumice clasts and lithics, and minor amount of wood pieces. Bases of PDC-4 and PDC-6 consist of ground surge deposits. Low-angle cross-laminar and dunes are developed in the ground surge deposits. The ground surge deposit of PDC-6 is further underlied by a ground breccia layer. The ground breccia layer consists of matrix-supported conglomerate, containing lithics with a maximum grain-size of 2.5 m. Lapilli tuff of PDC-1, 3, 4, 8 include welded parts, developing degassing pipes and columnar joints. Welded parts often contain spherulites and exhibit eutaxitic texture. Debris flow deposit (DF-1) consists of clast-supported conglomerate with rounded clasts. The clasts are directed parallel to the bedding plane, showing coarse-tail reverse grading. Lacustrine deposit (LD-1) consists of alternation of tuffaceous sandstone, mudstone, and conglomerate. In mudstone, laminar is well developed. Laminar and bedding are well developed in tuffaceous sandstone. Conglomerate is massive. PDC-2 overlying the lacustrine deposit (LD-1) shows sedimentary structures that imply subaqueous setting. Pyroclastic density current occurred more than eight times, suggested by the number of pyroclastic density current layers. The source of PDC-4 is Takinohara vent, determined from paleocurrent estimated with dunes of a ground surge deposit. Presence of a lacustrine deposit (LD-1) in the middle of the Formation implies that caldera collapsed two times. Half-concentric distribution of strike surrounds Mt. Ishigami and their dips incline outward of the caldera. This structure implies a resurgent dome. This resurgent dome resulted in uplift of Oyasudake area where the center of the caldera. Presence of resurgent dome, thick pyroclastic density current deposits and ring fractures suggests that Sanzugawa caldera is classified as a Valles type caldera.

Keywords: Sanzugawa caldera, Torageyama Formation, Pyroclastic density current deposit, Resurgent dome

## Stratigraphy and chemical compositions of eruption products in Umanose agglutinate activity, Zao volcano

KAWANO, Gen<sup>1\*</sup>; BAN, Masao<sup>2</sup>; OIKAWA, Teruki<sup>3</sup>

<sup>1</sup>Graduate School of Science and Engineering, Yamagata University, <sup>2</sup>Faculty of Science, Yamagata University, <sup>3</sup>Geological Survey of Japan/ AIST

The newest stage of the Zao volcano, central part of NE Japan, began at about 30 ka and the activity has continued to present. The Zao newest stage eruption products are classified into Komakusadaira agglutinate, Umanose agglutinate and Goshikidake pyroclastics. In this study, we examined the stratigraphy of eruption products in the Umanose agglutinate activity (ca. 8-4 ka). Besides, we examined temporal change in chemical compositions of the products.

«Tephra-stratigraphy» We re-examined the tephra-stratigraphy and recognized nine volcanic sand layers (Z-To 5a, 5b, 5c, 5d, 5e, 5, 6, 7, 8) during the Umanose agglutinate activity. The tephra (volcanic sand) layers younger than the Z-To 5e widely distribute around the summit area, while the others are found only in the northern part. Based on <sup>14</sup>C ages on paleosols and fossil leaf samples from the tephra-loam succession coupled with the stratigraphy, ages of Z-To 5a to 8, except for Z-To 5, are estimated to be ca. 8.9, 7.3, 6.0, 5.6, 5.3, 4.7, 3.9, 3.6 ka, respectively.

In addition, we found whitish yellow colored wide-spread tephra layer between Z-To 5e and 5d in the northern and bellow 5e in the southern part of the summit area. This tephra is mainly composed of pumice type volcanic glass. This layer can be correlated to To-Cu (Towada-Chuseri) tephra, based on the major element compositions of the volcanic glass and the stratigraphic horizon.

«Stratigraphy of the proximal layers» The proximal layers are well exposed in the central part of the summit area. In this part, the Umanose agglutinate covers the Komakusadaira agglutinate, which include less-vesiculated volcanic bombs with glassy luster as well as scoria. Overlying products of the Umanose agglutinate are composed of alternation of agglutinate, scoria fall deposit, and pyroclastic surge deposit. More than ten layers are recognized by intercalating loam layers.

«Temporal change in chemical compositions» The eruptive products are olivine +- pyroxene andesite (56.0-59.2% SiO<sub>2</sub>) and belong to medium-K calc-alkaline series. All samples are plotted on same linear trends in SiO<sub>2</sub> variation diagrams. The silica contents increase gradually from the bottom to the middle part. Afterwards, the content drops to the lowest, and gradually increase upwards again.

Keywords: Zao volcano, Umanose agglutinate, tephra stratigraphy, evolution of magma

## Eruptive History of Post-caldera Stage, East-Azuma Volcano -Correlation between ejecta intra-caldera and boring core-

OZAKI, Mamoru<sup>1\*</sup> ; FUJINAWA, Akihiko<sup>2</sup>

<sup>1</sup>Ibaraki Univ., <sup>2</sup>Ibaraki Univ.

### Introduction

Azuma Volcano is one of the Quaternary stratovolcanoes located at the volcanic front of the Northeast Japan arc. The recent 7ka activities of this volcano are characterized by dominant fall out tephra (Yamamoto, 2005). Eruptive history occurred at the Jododaira explosion caldera (Fujinawa and Kamoshida, 1999) is built by comparing boring core of the Jododaira with the ejecta deposited the intra-caldera area.

### Stratigraphy and lithofacies of boring core

Boring site is at about 500m NW from Azuma-Kofuji cone. This core was described most immediately after core-recovery, and stratigraphic sequence was outlined (CCPVE core analysis group, 2011). Layers of andesitic volcanic block and lapilli (11.20m-1.50m in depth) are lithologically correlated to the Azuma-Kofuji volcanic ejecta.

Andesite lava (100.55m-81.07m, sample No.19-17 near the bottom of the core) and welded tuff breccia / lapilli tuff (79.90m-14.20m, No.13-10) are to be the keys to reveal the eruption history. Andesite lava (19-17) is dark-gray in color with dominant plagioclase phenocrysts of 2~3mm in diameter. Inclusions are rarely recognizable. Welded tuff breccia/lapilli tuff (No. 13-10) are characterized by dark-gray, highly deformed and elongated blocks/lapilli at the densely welded part.

### Description of outcrops

3 lava flows and 1 pyroclastic flow deposit were newly found at the outcrops of intra-caldera area.

Lava flow1 (Lf1) does not show distinct lobe topography. This is exposed only at altitudes of 430m along forest road with about 5m thick. Lf1 is massive, dark-gray in color and characterized by dominant plagioclase phenocrysts of 2~3mm in diameter. Rare cognate inclusion is also recognized.

Pyroclastic flow deposit (Pfl) intermittently cropped out around at altitudes of 470m along the route 126, showing a thickness about 2.5m. The Pfl is overlain by unconsolidated talus deposit. The stratigraphy of these deposits was not confirmed in the field observation. This Pfl includes dark-gray lithic fragments in weakly welded light-gray matrix.

Lava flow2 (Lf2) constitutes thick massive spreading widely on the floor of the Jododaira explosion caldera (Fujinawa and Kamoshida, 1999). Judged from topography, the Lf2 stratigraphically overlies the Pfl. At altitudes of 660m along forest road, the Lf2 of over 10m in thick showing an well-developed columnar joint is cropped out. The Lf2 is directly covered by Ak-Lf at this locality (Kamoshida, 1991MS). Lithology of Lf2 is massive, gray in color and pyroxene phenocrysts are discerned easily.

Lava flow3 (Lf3) is distributed in the southern part of the intra-caldera, well foamed and grey tinged with red in color. The Lf3 topographically overlies the Lf2, furthermore, and covered by Ak-Lf. The Lf3 consists of 3~5 flow units, lobes and levees at its surface.

### Comparison of lithofacies

The lava samples of the core (19~17) are lithographically similar to those for the Lf1, but distinguishable to those of the Lf2 or Lf3. The core samples of the welded tuff (13~10) is slightly different from Pfl in the degree of welding, but are similar to each other in terms of including dark-gray lithic fragments in light-gray matrix.

### Eruptive history based on comparison of lithofacies

The welded pyroclastic deposits in boring core are as thick as 20m, suggesting that the deposit is the deposit of an enormous pyroclastic eruption. If such eruption occurs, a sort of depression would often be remained in the supply source area. Judging from topography, the Jododaira explosion caldera is the most plausible candidate. Because the Lf1 (=core 19~17) lie beneath welded Pfl (=core 13~10), this lava is promisingly erupted during pre-caldera activities. Because the Lf2 and Lf3 are topographically come above the Lf1, it is considered that these lavas erupted in the post-caldera stage.

Keywords: Azuma Volcano, Jododaira, eruptive history, boring core, stratigraphy

## Plagioclase phenocrysts and Opx-magnetite symplectite of the Sessho Lava of the Kusatsu-Shirane Volcano

OSHIO, Kazuki<sup>1\*</sup> ; UEKI, Kenta<sup>2</sup> ; KAWANO, Munehiro<sup>3</sup> ; INUI, Mutsuko<sup>3</sup> ; NOGAMI, Kenji<sup>2</sup>

<sup>1</sup>Kokushikan University Graduate School of Engineering, <sup>2</sup>Volcanic Fluid Research Center, Tokyo Institute of Technology, <sup>3</sup>Kokushikan University

Chemical composition and crystal size distribution of plagioclase phenocrysts may represent the cooling rate and chemical heterogeneity of the magma chamber. Therefore, chemical and physical conditions in the magma storage before eruption can be constrained by analyzing the morphology and chemical composition of phenocrysts in lava.

For the purpose, we focused on the Sessho lava, a single lava flow erupted from Kusatsu-Shirane volcano. Kusatsu-Shirane volcano is a quaternary active volcano located in the Central Japan arc. According to Uto *et al.* (1983), the Sessho lava is estimated to have erupted from the Moto Shirane cone during an eruption about 3000 years ago. The Sessho lava shows andesitic composition (Takahashi *et al.*, 2010; Ueki and Terada, 2012). In this study, detailed descriptions in morphologies of phenocryst minerals have been carried out. We determined the modal composition of phenocrysts, and measured the aspect ratio and the crystal size distribution of plagioclase phenocryst. We also carried out the detailed description of opx-magnetite symplectite, which have been observed in several samples.

The phenocrysts assemblage of the Sessho lava is plagioclase, clinopyroxene, orthopyroxene, magnetite, and rare olivine. Groundmass shows glassy structure. Modal composition of phenocrysts shows homogeneous value in a single lava flow; 54.0 to 59.0 vol. % for groundmass, 33.4 to 38.1 vol. % for plagioclase, 2.1 to for 4.2 vol. % for magnetite, 3.0 to 6.4 vol. % for pyroxene. On the other hand, the aspect ratios of plagioclase phenocrysts show wide range of variation in a single lava flow. Fine grained plagioclase shows needle-like morphology whereas coarse grained plagioclase shows tabular morphology. Although the modal composition shows the homogeneous value, sizes of plagioclase phenocrysts show wide range of variation; samples rich in fine-grained phenocrysts and samples rich in coarse-grained phenocrysts are both present in the single lava flow.

Observations and quantitative analysis using EPMA and SEM show that the structure of plagioclase phenocrysts can be classified into following five groups; normal zoning, reverse zoning, oscillatory zoning, patchy zoning, dusty zoning. Plagioclase phenocrysts show a wide range of composition in the single lava flow. An# ranges 55-84 %. Olivine phenocryst is observed in some samples, its Mg# is -83, which is a non-equilibrium composition with its host rock.

Opx-magnetite symplectite have been observed in several samples. The symplectite show oval form. Its diameter ranges 2-4 mm. Magnetite shows lamella structure, and is concentrated at the central part of the symplectite. Orthopyroxene is 75-975  $\mu\text{m}$  in diameter and distributes around the magnetite lamella. Orthopyroxene in the symplectite is characterized by its low birefringence than the typical orthopyroxene phenocrysts of the Sessho lava. This structure is estimated to be formed by the rapid oxidation of olivine, indicating that during the formation of andesite magma of Sessho lava, oxygen fugacity in the magma storage may have rapidly increased.

In conclusion, it is estimated that final temperature was homogeneous in the magma strage of the Sessho lava, because modal contents of phenocrysts in the single lava flow show homogeneous value. On the other hand, several types of the chemical composition and size of plagioclase have been observed in the lava flow, indicating rate of crystallization and cooling had variation in the magma storage of the Sessho lava. Existences of orthopyroxene-magnetite symplectite and non-equilibrium olivine indicate magma mixing and oxidization event had occurred during the formation of andesitic magma of the Kusatsu-Shirane volcano.

### References

- Uto *et al.*, Kusatsu-Shirane volcano geological map, Geological Survey (1983)
- Takahashi *et al.*, Nihon University College of Humanities and Sciences, Research bulletins, 45, 205-254 (2010)
- Ueki & Terada, Volcano 57, 4, 235-251 (2012)

Keywords: Lava flow, Crystal size distribution, Eruption, Andesite, Active volcano, Symplectite

## Boring Core Observation of the Izu Oshima Sembazaki Strain Meter Well.

KAWANABE, Yoshihisa<sup>1\*</sup> ; ONIZAWA, Shin'ya<sup>2</sup> ; KOKUBO, Kazuya<sup>3</sup>

<sup>1</sup>Geol. Surv. Japan, AIST, <sup>2</sup>Meteorological Research Institute, <sup>3</sup>Japan Meteorological Agency

We report the boring core observations of strain gauge well that Japan Meteorological Agency has been installed in the Sembasaki, Izu Oshima. The location of the well is at 34 42' 20.5168 "N, and 139 21' 40.7016"E, and well altitude is 51.2m, and drilling depth is 100m. For deeper than about 70m deep, the core was recovered.

Depth from 70m to 86m is composed of volcanic breccia with thin layers of volcanic ash. Volcanic breccia is solidified and including fragments of various basalt, scoria and altered rocks. Some basalt fragments seems to be the essential with a quench rim. From the surrounding geology, this breccia can be compared to the Senzu Formation that is the product of explosive eruption at shallow sea in the first stage of Izu Oshima volcano.

The core, depth of 86m (below sea level 34.8m) or deeper, is made of fresh aphyric basaltic lava flow. At least 2 flow units can be identified. Both lava flows contain very small amount of plagioclase and clinopyroxene phenocrysts. There is no evidence that is water-cooled to the lava flow.

We performed the whole rock chemical composition analysis for basalt fragment of breccia and lava flows. All specimen have  $\text{SiO}_2 = 49.8 \sim 52.9\text{wt}\%$  and significantly lower  $\text{K}_2\text{O}$  content, about 0.2wt%, than the basalts of Izu Oshima volcano, except for one breccia fragment. The lower  $\text{K}_2\text{O}$  content than that of the rock of Izu Oshima volcano is consistent with the characteristics of the old basement volcanoes such as Fudeshima volcano.

In the sea floor of the west of the Izu Oshima, there are Semba spur accompanied by magnetic anomaly. Oshima et.al.(1987) pointed out that the Semba spur might be the older volcanic body and they named it Semba volcano. The height of the sea cliff is gradually increased from Sembazaki toward the north, and the highest around Tsuwai. The distribution of valleys around Tsuwai also shows the discordant rise in the foot of Izu Oshima volcano, and this discordant may lead to the Semba spur. The basalts from the Semba core indicate that the old basement volcano, Semba volcano, is also present in the Izu-Oshima southwest side.

Keywords: Izu Oshima, boring core, basalt

## Origin and deformation of the clastic flow bands in the Takanoobane rhyolite lava

FURUKAWA, Kuniyuki<sup>1\*</sup> ; KANAMARU, Tatsuo<sup>2</sup> ; UNO, Koji<sup>3</sup>

<sup>1</sup>Faculty of Business Administration, Aichi University, <sup>2</sup>Department of Geosystem Sciences, College of Humanities and Sciences, Nihon University, <sup>3</sup>Graduate School of Education, Okayama University

In this study, we showed that the clastic flow bands, which are developed in the Takanoobane rhyolite lava, were formed by shear fracturing of the high viscous magma within the shallow conduit. The flow bands broke up into the small particle-rich flow lines, which are ubiquitously observed in obsidian lavas.

The Takanoobane rhyolite lava (TR lava) is located at the Aso caldera in the middle of Kyushu Island in SW Japan. The lava is effused at 51±5 ka (Matsumoto et al., 1991). The thickness, estimated volume, and bulk rock chemistry of TR lava are 60-90 m, 0.14 km<sup>3</sup> (Miyabuchi et al., 2004), and 71-72 SiO<sub>2</sub> wt.% (Furukawa, 2006), respectively. In this study, we examined two drill cores (AVL1 and AVL4) provided by the Aso Volcanological Laboratory. Both drill holes penetrated the proximal part of TR lava. TR lava is composed of an inner crystalline part and marginal glassy parts.

The black to dark gray colored flow bands within a few millimeters thick are concentrated around the boundary between crystalline part and basal obsidian. The bands are composed of clastic materials with a diameter below a few mm. The clastic materials are composed of glassy lithics and minerals. Some clasts are rounded and fluidal shapes and show different textural occurrences from the surrounding rhyolite. The chemical compositions of the glassy lithics and those of glassy matrix of the surrounding rhyolite are slightly different. Within the bands, the streak texture, which is defined by difference of clasts and microlite contents, is conspicuous.

The differences in texture and chemical compositions between the clasts in the bands and surrounding rhyolite indicate that the clastic bands were not formed by autobrecciation within the lava. These observations indicate that the clastic bands are likely to be formed by shear fracturing of the high viscous magma within the shallow conduit such as Tuffen et al. (2003). The fractures would become pathway of the volcanic gasses, and the clasts were transported by the gas transport. The streak texture within the bands is interpreted as sedimentary structures, which were formed by gas transportation of clasts through fracture system. The rounded and fluidal shapes of the clasts indicate that the fracturing occurred when the conduit magma was enough hot. The clastic bands consequently break up and disappear. The bands show progressive loosening along the individual streak, where will be the structural weakness. Consequently, the streak develops into the individual thin bands. The small particles, such as glass particles, microlites and lithics, are released from margin of the clastic bands to the surrounding rhyolite. Since the high viscosity of the lava inhibits their homogenization, the particles are likely to be aligned along the flow line. The clastic flow bands, originated from shear fracturing, will thoroughly break up via this process. Our results mean that the clastic flow bands developed within silicic lavas is important for understanding of the shallow conduit system of silicic magma.

Keywords: rhyolite, lava, flow band, conduit, Aso

## Magma chamber processes revealed by textures in plagioclase phenocrysts through Taisho eruptions of Sakurajima volcano

YAMASHITA, Shunsuke<sup>1\*</sup> ; TORAMARU, Atsushi<sup>2</sup>

<sup>1</sup>Department of Earth and Planetary Sciences, Graduate School of Sciences, <sup>2</sup>Department of Earth and Planetary Sciences, Faculty of Sciences

Textures in volcanic products record important information about the origin of the rock. Especially, plagioclase phenocrysts have been studied in order to understand the magma chamber processes because they are commonly included in various types of volcanic rocks. Two types of plagioclase phenocrysts are found in lavas by the 1914-1915 eruption of Sakurajima volcano, Southern Kyushu, Japan: (1) honeycomb plagioclase(H-Pl) with large melt inclusions in cores; and(2) clear plagioclase(C-Pl) without any melt inclusions. In Sakurajima volcano, magma mixing has been suggested by bimodal compositions of plagioclase phenocrysts. However, relationship between textures and chemical compositions has not been reported. In addition, the crystal size distributions (CSDs) also may provide essential information for the production environment of the crystals. Therefore, in order to obtain insights into magma chamber and magma mixing processes, we conduct chemical composition and crystal size distribution (CSD) analyses.

We carried out chemical compositional analysis by FE-SEM. As a result, it is found that H-Pl phenocrysts have heterogeneous mosaic cores with An75-90 and An55-70 and very low An#(An40-55) around melt inclusions. On the other hand, C-Pl phenocrysts are uniform in compositions while the An contents varies from grain to grain. The histogram of An contents in H-Pl cores shows narrow bimodal distributions around An78 and An86, whereas that of C-Pl cores shows the wide bimodal distribution around An62 and An86. We carried out CSD analysis. It is found that H-Pl and C-Pl phenocrysts showed different trends. CSD of C-Pl is strongly convex-downward showing crossover with two different slopes.

We revealed plagioclase are classified into three types: (1) type-H with an An-rich (An74-89) and heterogeneous core containing large melt inclusions; and (2) type-C-1 with an An62 and homogeneous core not containing melt inclusions; and (3) type-C-2 with an An-rich (An85) and homogeneous core not containing melt inclusions. The results of CSD suggest different formation processes between H-Pl and C-Pl, and crossover in the slopes of C-Pl CSDs suggest the mixing of two magmas from which two populations of phenocrysts originate (Higgins, 1996b). In Sakurajima, magma mixing has been suggested, therefore it is important to understand the temperature of magmas. So, we estimated temperature on equilibrium constants by plagioclase- and alkali feldspar-liquid thermobarometers (Putirka, 2008). The results show the temperature on equilibrium constants of the dacitic magma was about 850 °C, and that of the basaltic magma was about 1050 °C. Since the honeycomb plagioclases are generated by the skeletal growth under high supercooling condition, the H-Pl phenocrysts is formed in the basaltic magmas during cooling at mixing events. In summary, type-H is formed by skeletal growth due to the thermal interaction during mixing events in basaltic magma, type-C-1 is formed under magma chamber with mixed homogeneous magma, type-C-2 is formed under magma chamber with the basaltic magma before mixing, respectively.

Keywords: plagioclase phenocryst, honeycomb texture, textural analysis, crystal size distribution, magma mixing, Sakurajima volcano

## Ground Deformation of Active Volcano in Kunashiri and Etorofu Islands using InSAR time series analysis

ANDO, Shinobu<sup>1\*</sup> ; MIURA, Yuji<sup>2</sup> ; MATSUMORI, Toshiyuki<sup>2</sup>

<sup>1</sup>MRI, <sup>2</sup>JMA

ALOS has an L-band SAR (PALSAR), which is not affected by vegetation, and the interference is good even in mountainous areas. So these methods are effective for the crustal deformation observation of volcanic areas.

In previous studies, we have reported the analysis results about all domestic active volcanic areas, using D-InSAR of ALOS since 2007. However, ALOS has suspended the operation in May 2011. Therefore, we did not do D-InSAR analysis for the period thereafter. In recent years, InSAR time series analysis technique called PS-InSAR and SBAS has been developed, a number of cases have been reported.

There are 11 active volcanoes in the Kunashiri and Etorofu island, Southern Kuril Islands. It has still continued an active volcanic activity in the some volcanoes of them. In this report, we have take advantaged of the archive data of ALOS/PALSAR, and tried to analyze the ground deformation of around these 11 active volcanoes using *StaMPS* program was developed by the Stanford Institute of Technology. Note, we analyzed except for the data captured in the winter in order to remove the effect of the snow. Also, besides PS-InSAR and SBAS methods, *StaMPS* program has the analysis methods to merge these results. Therefore, we will also present about the difference of these results.

Some of PALSAR data were prepared by Japan Aerospace Exploration Agency (JAXA) via the Coordinating Committee for the Prediction of Volcanic Eruption (CCPVE) as part of the project "ALOS Domestic Demonstration on Disaster Management Application" of the Volcano Working Group. Also, we used some of PALSAR data that are shared within PALSAR Interferometry Consortium to Study our Evolving Land surface (PIXEL). PALSAR data belongs to Ministry of Economy, Trade and Industry (METI) and JAXA. In the process of the InSAR analysis, we used "the ASTER Global Digital Elevation Model" was developed jointly by METI and the United States National Aeronautics and Space Administration (NASA), and Generic Mapping Tools (P.Wessel and W.H.F.Smith, 1999) to prepare illustrations.

Keywords: InSAR time series analysis, Ground deformation, ALOS/PALSAR, Domestic active volcano

## Preliminary result of resistivity modeling around Ponmachineshiri crater at Meakandake Volcano, Japan

TAKAHASHI, Kosuke<sup>1\*</sup> ; MATSUSHIMA, Nobuo<sup>2</sup> ; TAKAKURA, Shinichi<sup>2</sup> ; YAMAYA, Yusuke<sup>2</sup> ; ARITA, Shin<sup>1</sup> ; NAGAMACHI, Shingo<sup>1</sup> ; OISHI, Masayuki<sup>2</sup> ; KAZAHAYA, Ryunosuke<sup>2</sup> ; FUJII, Ikuko<sup>1</sup>

<sup>1</sup>Kakioka Magnetic Observatory, Japan Meteorological Agency, <sup>2</sup>National Institute of Advanced Industrial Science and Technology

Meakandake Volcano, situated in Eastern Hokkaido, Japan, is an active volcano where a phreatic eruption occurs in every several years. Volcano-tectonic (VT) earthquakes mainly occurred below Ponmachineshiri crater which is one of active craters of the volcano (Japan Meteorological Agency, 2013). A source region of the tremors occurred before the 2008 eruption was estimated beneath the southern slope of the crater (Ogiso and Yomogida, 2012). Significant changes in the geomagnetic field were observed in 2008 and 2009 around the crater. Hashimoto et al. (2009) pointed out that the temporal variations of the geomagnetic field in 2008-2009 were due to the thermal demagnetization of the material beneath the southern slope of the crater.

These VT earthquake, tremor and rock demagnetization events probably associated with the movement of volcanic fluids such as hydrothermal water, gas and melt. Therefore, understanding of a hydrothermal system of the volcano is a key to reveal the mechanism of the tectonic events occurred there.

Resistivity of rock strongly depends on the fluid inclusion. Therefore, an electro-magnetic measurement is an effective method to image the fluid distribution. We conducted audio-frequency magnetotelluric (AMT) surveys in August 2013 on the western slope of the volcano. The objective of the survey is to reveal the resistivity structure around Ponmachineshiri crater and to infer the relationships among the fluid distribution, the seismic focal area, and the demagnetized area around the crater.

Since we have not finished the AMT survey on the eastern slope of the volcano yet, the resistivity structure around the Ponmachineshiri summit crater is not well-constrained. Therefore, we present the two-dimensional resistivity structure beneath the western slope of the volcano as a preliminary result. The characteristics of the resistivity distribution are described as follow.

1) A resistive (more than several hundred  $\Omega$  m) layer locates at the top of the western slope of the volcano. Its thickness varies from 100 to 300 m on the profile. This layer can be regarded as a permeable lava or pyroclastic fall deposits.

2) Below the resistive surface layer, two conductive (less than 10  $\Omega$  m) bodies are found. One is located to the west of Ponmachineshiri crater at depths of 300-1000 m from the surface. This conductor corresponds to a hydrothermal reservoir which relates to the fumarolic activity in the crater. The second conductor is found beneath the western part of the profile at a depth of about 1000 m from the surface. The discharge of hot spring water at the west of our survey region suggests that this conductor can be explained by the presence of the hydrothermal fluid and/or the altered rocks.

3) A resistive area (more than several hundred  $\Omega$  m) exists below the two conductors. Causes of this high resistivity are unknown yet.

Keywords: resistivity structure, Meakandake Volcano, volcanic fluid

## Variation of Geomagnetic Total Intensity at Meakandake Volcano after the Eruptions in 2008

SHIMAMURA, Tetsuya<sup>1\*</sup> ; ARITA, Shin<sup>1</sup> ; MASHIKO, Norimichi<sup>1</sup> ; FUJII, Ikuko<sup>1</sup> ; FUKUI, Keiichi<sup>1</sup> ; OGISO, Masashi<sup>2</sup>

<sup>1</sup>Kakioka Magnetic Observatory, JMA, <sup>2</sup>Matsushiro Seismological Observatory, JMA

This study reports on the geomagnetic total intensity change at Meakandake volcano and its relations with volcanic activity after eruptions in 2008.

Meakandake volcano is located in eastern Hokkaido and is a volcanic complex which consists of eight volcanoes, such as Ponmachineshiri, Nakamachineshiri, Akanfuji and so on. Ponmachineshiri has been active in recent years and minor phreatic eruptions repeatedly occurred in 1988, 1996, 1998, 2006 and 2008.

Kakioka Magnetic Observatory, Japan Meteorological Agency has carried out a repeat observation of the geomagnetic total intensity in one or two times a year since 1992 for the purpose of detecting geomagnetic field changes accompanying the volcanic activity of Meakandake volcano. Twelve repeat stations were installed on the east side of summit craters' edge and south slope of Ponmachineshiri in 1992 and since then we have improved the repeat station network step by step. About thirty stations are used recently. A continuous station of the geomagnetic total intensity (MEA) was installed on the south slope of Ponmachineshiri on October 16, 2003 in order to improve the time resolution of the observation. Then, a new continuous station (ME2) was installed between the 96-1 crater of Ponmachineshiri and MEA on September 28, 2013. The geomagnetic intensities are acquired every 5-minutes at MEA and ME2.

A significant decrease of the geomagnetic total intensity was observed at Meakandake volcano in July, 2013 and continues up to now (January, 2014). The total intensity varied with the eruptive activity in 2008, and no remarkable change of the total intensity was seen for thirty months from January 2011 to June, 2013. There has been no significant variations in volcano-tectonic earthquakes, tremors, volcanic smoke and tectonic deformation at Meakandake volcano since July, 2013 (Volcanic Observations and Information Center, Sapporo District Meteorological Observatory, JMA), which differs from the situation at the 2008 eruptions when significant variations of the total intensity and the other tectonic measurements were observed.

It is assumed that the decrease of the geomagnetic total intensity at Meakandake volcano in 2013 is due to the thermal demagnetization accompanying heating of the inside of the volcanic body. A source of the thermal demagnetization was estimated beneath the southern slope of the 96-1 crater at Ponmachineshiri by using geomagnetic total intensity changes at repeat stations for about 3 months from June to September, 2013. This source location is almost the same as that of the demagnetization in 2008. And it is inside the focal area of migrating volcanic tremors which occurred on November 16, 2008 reported by Ogiso and Yomogida (2012). We used MaGCAP-V (Seismology and Volcanology Research Department, Meteorological Research Institute, JMA, 2013) as a support software for the modelling of the demagnetization source.

It is indicated that the position of the thermal demagnetization source has not changed for last four months, because the difference of the geomagnetic total intensities at two continuous stations (MEA and ME2) has been almost constant since the end of September, 2013.

Only the geomagnetic total intensity detects a possible on-going heating process inside the Ponmachineshiri which commenced in July 2013. This case strongly suggests that the observation of the geomagnetic field is important to monitor heating or cooling of the volcanic body. The observation with two or more continuous stations is effective in order to monitor the source position of the thermal demagnetization. In addition, Hashimoto *et al.* (2009) suggested a possibility of the volcanic eruption prediction at Meakandake volcano, because a decrease of the geomagnetic total intensity was observed two days before the eruption on November 18, 2008 when the amplitude of the volcanic tremors had been increased.

Keywords: Meakandake, geomagnetic total intensity, volcano, eruption, thermal demagnetization

## Recent volcanic deformations observed by campaign GPS on and around Mt.Tokachi and Mt.Meakan

WADA, Sayaka<sup>1\*</sup> ; MORI, Hitoshi, Y.<sup>1</sup> ; OKUYAMA, Satoshi<sup>1</sup>

<sup>1</sup>Hokkaido University, Institute of Seismology and Volcanology

Mt. Tokachi is one of the famous active volcanoes located in the central Hokkaido, Japan. In the recent 100 years, major magmatic eruptions at Mt. Tokachi occurred in 1926, 1962 and 1988-1989. Mt. Meakan sits in the eastern Hokkaido. It is also an active volcano and made phreatic eruptions in 1996, 1998, 2006 and 2008.

In this study, we will discuss the results of the campaign GPS on and around Mt. Tokachi and Mt. Meakan. Each broad area GPS observation had begun at Mt. Tokachi in 2007 and at Mt. Meakan in 2006. The campaign GPS observation for Mt. Tokachi made at 12 sites and that for Mt. Meakan at 8 sites, for several days to weeks in each year.

We used the data of our campaign observations since 2007 for Mt. Tokachi and after the 2008 eruption for Mt. Meakan. For evaluating spatial deformation pattern in more detail, we also used the data of several GPS sites operated by JMA (Japan Meteorological Agency) at the same time. Analyzing these data, annual movements at those stations were estimated. The regional tectonic movement and the coseismic step of Tohoku-oki earthquake on March 11, 2011 are included in those movements. We used the continuous data at GEONET sites by Geospatial Information Authority of Japan (GSI) around the volcanoes to make corrections for non-volcanic deformations. Using the GEONET data from 2007 to 2013, the regional tectonic and the seismic deformations were estimated by linear approximation in space. Seasonal changes should be taken into consideration to study the volcanic deformation. The discussion about deduced volcanic deformations will be made, after the corrections about the regional deformation, the coseismic step and the after slip of 2011 Tohoku-oki earthquake, and the seasonal variations.

### Acknowledgements

In this study, JMA, Sapporo District Meteorological Observatory furnish their observation data to us. We would like to express our gratitude to them. Also, we used the data of GEONET sites of GSI with thanks.

Keywords: Mt. Tokachi, Mt. Meakan, volcanic crustal deformation, GPS

## The Volcanic activity of Tarumaesan Volcano in 2013 and Trial of Application to the Eruption scenario

NAGAYAMA, Hiroaki<sup>1\*</sup> ; MIYAMOTO, Masashi<sup>1</sup> ; FUJIMATSU, Jun<sup>1</sup> ; USUI, Yuji<sup>1</sup> ; FUSHIYA, Yuji<sup>1</sup> ; MIYAMURA, Jun'ichi<sup>1</sup>

<sup>1</sup>Sapporo Regional Headquarters, JMA

Continuous observation network with tiltmeter and strainmeter in Mt.Tarumae, which is located on the southeastern edge of Shikotsu caldera, operated by Japan Meteorological Agency (JMA) and Hokkaido University Institute of Seismology and Volcanology (ISV) detected volcanic ground deformation during June 19 to July 4, 2013. According to the Mogi model (Mogi, 1958), the ground deformation is interpreted as volume increase of about  $10^5 \text{ m}^3$  at about 3-4km in depth beneath sea level around Mt.Kitayama, is located in about 1.5km northwest from Tarumae summit. It is different from the deformation in shallow region (above the sea level) beneath the summit, reported by MRI (2008), the Meteorological Research Institute, and ISV et al.(2011). According to the classification suggested by MRI (2013), it corresponds to slowly accumulation process of magma, as magma chamber or dike intrusion. B-type earthquakes, have been occurred in shallow region (~sea level) beneath the summit, became active slightly in synchronization with the ground deformation. As a result of the process of volcanic fluid, the actual medium is unknown, rise to the volume increase area (depth 3-4km), it is interpreted as an increase in heat flux to shallow region beneath the summit.

Volcano-tectonic earthquake (VT earthquake) activated at a depth of 3-5km surrounding the deformation area in mid-July, after ground deformation, it is still ongoing. The VT seismicity was very active until August and maximum shock was M3.0 in late September. VT earthquakes have occurred in the relative high resistivity layer (50-500 $\Omega\text{m}$ ) of Resistivity imaging by Yamaya et al. (2005, 2012). Whereas, it has not occurred in the deformation area and the path to beneath Tarumae summit, that is relative conductive area.

Order to carry out disaster prevention appropriately and promptly in the eruption, JMA has operated the eruption alert level on 31 volcanoes across the country. It is intended to share the consciousness of the local government by flow assuming the transition of volcanic activity, called the eruption scenario. For operating the level effectively, the eruption scenario, flow chart assuming the progress of the volcanic activity of each volcano, has been shared with the local government. As the lastest magma eruption is in 1909, major volcanic activity had been occurred in the very shallow part around lava dome for a long time. It is unknown what the phenomenon is observed when the magma is supplied to the shallow depth from the deeper. Therefore, the scenario that assumed the magma eruption is supplemented by the general knowledge that was observed at other volcanoes. The mechanism of the deformation and VT-seismicity is not clear. But, it can be considered of the distribution that related to the heat supply system or the geological structure beneath Tarumae. In this study, we tried to apply the interpretation of the ground deformation and VT-seismicity to the eruption scenario. However, our interpretation on the activity is unverifiable evidence so poor at present. In order to improve the eruption scenario certainly, elucidation of the magma supply system in Tarumae is essential, but it is not clear at present. To clarify the magma supply system, it is necessary to more information of geological structures and observed results such as ground deformation and VT-seismicity in this time. However, we are at present able to investigate detection of the high attenuation region used natural earthquake and to estimate fault plane solutions of VT earthquake (P-axes) using P-waves, and would like to approach. In addition, it is necessary to operate new observation system to capture phenomena such as seismic activity and ground deformation more certainly due to magma rising from the deep.

Acknowledgment:In this study, we use the data of ISV, tiltmeter and strainmeter, and the waveform data. Thank you for permission to use data.

Keywords: tarumae, volcanic activity, eruption scenario, ground deformation, VT seismicity

## Volcanic activities of Hakkoda volcano after the 2011 Tohoku-Oki earthquake

YAMAMOTO, Mare<sup>1\*</sup>

<sup>1</sup>Geophysics, Science, Tohoku University

The 2011 Tohoku-Oki earthquake of 11 March 2011 is one of the largest earthquakes in recent times, and it generated large displacements and deformation in and around the Japanese islands. Such large crustal deformation, especially the east-west extension exerted on Tohoku area, raises fear of further disasters including triggered volcanic activities as well as triggered seismicity. To assess the potential risks of triggered volcanic activities, understanding of the behavior of volcanic fluids in the crust and volcanic bodies would be a key. In this presentation, as examples of such possibly triggers volcanic activities, we report the recent seismic activities of Hakkoda volcano, and discuss the relation to the movement of volcanic fluids.

Hakkoda volcano is a group of stratovolcanoes at the northern end of Honshu Island, Japan. There are fumaroles and hot springs around the volcano, and phreatic eruptions from Jigoku-numa on the southwestern flank of Odake volcano, which is the highest peak in the main cones of Northern-Hakkoda volcanic group, were documented in its history. Since just after the occurrence of Tohoku-Oki earthquake, the seismicity around the volcano became higher, and the migration of hypocenters of high-frequency volcano-tectonic (VT) earthquake was observed.

In addition to these VT events, long-period (LP) events started occurring beneath Odake at a depth of about 2-3 km from February, 2013, and subtle crustal deformation caused by deep inflation source was also detected by GEONET GNSS network around the same time. The characteristics of LP events are summarized as follows: (1) The spectra of LP events are common between events irrespective of the magnitude of events, and they have spectral peaks at 6-7 sec, 2-3 sec, 1 sec, and so on. (2) The long-period component of LP events appears as a wave packet of a few cycles, and high-frequency (>1 Hz) signals sometimes overlaps it. (3) LP events sometimes occur like a swarm with an interval of several minutes. These characteristics of LP events at Hakkoda volcano are similar to those of LP events at other active volcanoes and hydrothermal area in the world, where abundant fluids exist. Our further analysis using far-field Rayleigh radiation pattern observed by NIED Hi-net stations reveals that the source of LP events is most likely to be a nearly vertical tensile crack whose strike is almost parallel to the direction connecting Odake summit crater and Jigoku-numa. The number of VLPs gradually decreased after September, 2013, and high-frequency VT earthquakes became more dominant in the seismicity around Hakkoda volcano. However, there were a burst of earthquakes beneath Southern-Hakkoda volcanic group, that includes a few low-frequency earthquakes, at the end of December, 2013.

These results suggest that the extensional stress field generated by the 2011 Tohoku-Oki earthquake causes the upward movement of volcanic fluids and heat from the deep, and results in an activation of hydrothermal activities at the pre-existent fracture zone at Hakkoda volcanic group.

Acknowledgment: We used Hi-net data provided by the National Research Institute for Earth Science and Disaster Prevention.

Keywords: Volcanic earthquakes, Volcanic fluids, Geofluids, Long-period events

## New knowledge of eruptive sequence in Heian eruption of Towada volcano

HIROI, Yoshimi<sup>1\*</sup> ; MIYAMOTO, Tsuyoshi<sup>2</sup>

<sup>1</sup>Grad.Sci.Tohoku Univ., <sup>2</sup>CNEAS.,Tohoku Univ.

### 1. Introduction

Heian eruption is the latest activity at Towada volcano, in Heian period (eruptive episode A : Hayakawa,1985). This eruption has been started from Nakanoumi caldera lake (Kudo,2010) filled with lake water, and repeated magmatic and phreatomagmatic eruption alternately. The details of the eruptive sequence have already been shown by Hiroi and Miyamoto (2010), however, we got and report new knowledge about the activity of first plinian phase and the occurrence mechanism of large pyroclastic flow unit.

### 2. Ash layers within unit OYU-1

The first plinian pumice fall unit OYU-1 has a SW dispersal axis and it achieves 50km farther. OYU-1 in distal shows very well sorting and uniform grain size distribution , but we found plural outcrops that OYU-1 accompanies with fine ash layers within 12km from source vent. Two kinds of ashes are observed, one is a beige colored ash in the lower part of OYU-1. The thickness is about 1-8 cm, and dispersal area is SW-SSE. Others are gray colored ashes and intercalated in the upper part of OYU-1. Their thicknesses are about 1-3 cm, and each dispersal area is SW-SSW.

All of ashes are intercalated in pumice layer, and the boundary between pumice layer and ash one is almost clear. Because OYU-1 without ash layers in distal shows uniform grain size distribution, the extent of these ashes deposit is limited in narrow area if their ash had been accumulated during the plinian column formation. The clear boundaries between pumice and ash suggest that ash layers are not fall deposit accumulated for a long period, but flow deposit piled in a very short time. Ash layers can be found not only a valley, but the little highland such as a mountain ridge line. This feature of distribution shows that they are regarded as surge deposit.

Because the ashes intercalated with pumice layer in OYU-1 indicate the feature of density current, they are intra-plinian flow. As one of their origin these ashes are derived from small-scale density current by the partial column collapse. The dispersal area of the ashes is limited adjacent to source vent and just only the direction of dispersal axis. This tendency of distribution seems that it corresponds with the direction of strong wind of 22[m/s] blew.

On the other hand, the source vent within a caldera lake and the fine grain features of ashes indicate a possibility that ash layers are phreatomagmatic base-surge deposit. In that case the occurrence of magma-water explosion might be caused by satisfying a condition of magma-water ratio partially or temporarily on the surface of eruption column. Unit OYU-2, overlying OYU-1 pumice fall directly, is phreatomagmatic base-surge deposit. Thus these ash layers may be a precursor phenomenon of eruptive style transition.

### 3. Distribution and draining style of KPf

Kemanai Pyroclastic flow is the climax deposit of Heian eruption, the total volume is estimated about 5km<sup>3</sup>(Hayakawa,1985). KPf distributes only the south area of Towada caldera, except for Oirase River to east direction. The Towada caldera rim is lowest at southwest edge (630m above sea level). The highest outcrop of KPf on caldera rim is located in 760m. In spite of adjacent to the source vent KPf cannot be shown on Mt. Akaiwa(785m) on the south caldera rim. These distribution features suggest that KPf flew out over the lower part of caldera rim. KPf deposit has been regarded that it occurred by plinian column collapse of preceded unit OYU-3 (Matsu-ura et al.,2007,etc.). But the column collapse type pyroclastic flow can be accumulated in high-altitude, KPf seems to be piled on only lower portion. Thus KPf is not occurred by column collapse, but derived by currents over the lower caldera wall. This conclusion agrees with the new eruptive sequence by Hiroi and Miyamoto(2010), that the unit just before KPf is not plinian pumice fall OYU-3, but phreatomagmatic base-surge unit OYU-4 without higher eruption column.

Keywords: Towada volcano, Heian eruption, intra-plinian flow, Soufriere-type pyroclastic flow

## Petrological study of northern part of ca. 300-100 ka volcanic edifices in Zao volcano.

TAKANO, Toru<sup>1\*</sup>; INOUE, Tsuyoshi<sup>2</sup>; BAN, Masao<sup>3</sup>; OIKAWA, Teruki<sup>4</sup>; YAMASAKI, Seiko<sup>4</sup>

<sup>1</sup>Graduate School of Department of Earth and Environmental Sciences, Yamagata University, <sup>2</sup>Nippon Koei Co., Ltd., <sup>3</sup> Department of Earth and Environmental Sciences, Faculty of Science, Yamagata University, <sup>4</sup>Institute of Geology and Geoinformation, Geological Survey of Japan, National Institute of Advance

Zao volcano is a Quaternary stratovolcano located in the middle part of the volcanic front of northeast Japan arc. The volcanic activity started at about 800 ka, and has continued to present. During ca. 300 to 100 ka activity of the Zao volcano, several middle sized edifices were formed. These volcanic edifices can be divided into northern and southern parts. We performed petrologic study on eruption products of the northern part to reveal the variation of magma compositions along with the evolutionary history.

Eruption products are divided into 8 units from lower to upper: Yokokurayama lavas, Kanshodaira lavas, Jizosan west lavas, Kumanodake west eruption products, Kumanodake main edifice products, Jizosan east agglutinate and lavas, Kumanodake agglutinate and lavas, Umanose eruption products. Yokokurayama lavas, Kanshodaira lavas, and Jizosan west lavas are composed of andesitic lavas. Kumanodake west eruption products are consisted of andesitic lapilli tuff, tuff breccia, agglomerate, and andesitic lavas. Kumanodake main edifice products are consisted of alternation of andesitic lavas and pyroclastic rocks in the lower part, and andesitic tuff breccia and agglomerate in the upper part. Jizosan east agglutinate and lavas, Kumanodake agglutinate and lavas are consisted of basaltic andesitic agglutinate, agglomerate, and lavas. Umanose eruption products are mainly composed of basaltic andesitic lavas, with subordinate amounts of agglomerate.

The eruption center of the Yokokurayama lavas would be located westward from the main chain of eruption centers. The main eruption centers for the other units were located in between the Kumanodake-Jizosan area. Jizosan east agglutinate and lavas, Kumanodake agglutinate and lavas, Umanose eruption products are characterized by the agglutinate and/or agglomerate distributing near the eruption centers.

All of eruption products belong to medium-K calc-alkaline series. All units other than the Yokokurayama lavas are plotted on same general trends in most of the SiO<sub>2</sub> variation diagrams. The Yokokurayama lavas show a lower trend than the other units in K<sub>2</sub>O diagram. Other than the Yokokura lavas, the lower four units are andesitic, whereas upper three units are basaltic andesitic. Looking at in detail, slight differences in compositions can be observed among units. Among the four andesitic units, Kumanodake main edifice products show higher trends in the Cr, Ni, Zr, Nb diagrams and a lower trend in Rb diagram than the others. The Umanose eruption products are plotted in higher part in Cr and Ni diagrams from the trends of the other products.

Keywords: Zao volcano, stratovolcano, eruption history, evolution of magma

## Characteristics of data observed by multi-component strainmeter installed at Senba, Izu-Oshima

YAMAMOTO, Tetsuya<sup>1\*</sup> ; ANDO, Shinobu<sup>1</sup> ; KOKUBO, Kazuya<sup>2</sup> ; KOBAYASHI, Akio<sup>1</sup> ; KIMURA, Kazuhiro<sup>1</sup>

<sup>1</sup>Meteorological Research Institute, <sup>2</sup>Japan Meteorological Agency

Meteorological Research Institute installed a multi-component borehole strainmeter at Senba Station in Izu-Oshima, one of the most active volcanos in Japan, in February 2013. By the strainmeter, we aim to research on evaluation of volcanic activity by means of crustal deformation and also to monitor the activity of the volcano. In many cases, unavoidable drift were shown in data of strainmeter installed in a borehole from just after the installation for several years. In order to utilize the strainmeter for volcano monitoring effectively, it is important to grasp the drift and noise quantitatively from early stage of observation. We report a result of research about characteristics of the data observed for about a year.

The strainmeter has 4 sensors which measure linear strains in the horizontal plane in every 45 degrees. In data observed by the sensors, tidal variation of about a day or half day period over 500 nano-strains is obvious, as well as a long term variation. Generally only three components are independent in a plane, the strainmeter has redundancy and it makes us possible to evaluate quality of the data. Examining hourly mean values, all strain components look consistent in the period range of a day or half day. It suggests the data of strain are reliable in the period. On the other hand, the long term variation has an inconsistency as much as 4 micro-strains for 6 month. The inconsistency could be caused by only one sensor of the four, it is difficult to conclude what amount of volcanic deformation is observed at the present stage. In the periods shorter than a half day, almost all variation is less than 2-3 nano-strains. It indicates the accuracy of observation for a short interval.

Keywords: Izu-Oshima, Monitoring of active volcano, Strainmeter, Ground deformation

## Gravity changes during magma accumulation period in Izu-Oshima volcano

ONIZAWA, Shin'ya<sup>1\*</sup>; TAKAGI, Akimichi<sup>1</sup>; FUKUI, Keiichi<sup>2</sup>; ANDO, Shinobu<sup>1</sup>

<sup>1</sup>Meteorological Research Institute, JMA, <sup>2</sup>Kakioka Magnetic Observatory, JMA

Since March, 2004, we have been conducting series of campaign gravity measurements, in order to understand magma accumulation process and to detect eruption precursor of Izu-Oshima volcano. Here, we show calibration results of relative scale factors between gravimeters, and characteristics of temporal gravity changes observed in the volcano.

We have been measuring relative gravity changes in the volcano using three instruments; LaCoste & Romberg Type-D #109, Scintrex CG3M #454, and Scintrex CG5 #033. Gravity differences in our campaign network are about 180 mgal in maximum from the coastal sites to the summit sites. Such large differences easily induce systematic deviations between data obtained by different instruments, when gravimeter scales are not calibrated. Further, temporal changes in the scale factor of Scintrex CG3M have been reported by some previous gravity researches.

Since scale calibrations using absolute gravity networks had not conducted until 2012, we cannot absolutely calibrate for past data. However, we can check relative scales between gravimeters and their temporal changes by comparing campaign data obtained simultaneously. The scale factor for CG3M#454 relative to one for D#109 shows clear temporal decrease. One for CG5#033 also shows change at breakdown occurred in 2010. This can be explained by a parameter change done by the maker during repairing processes. Furthermore, we found a non-linear relationship between D#109 and CG5#033, which implies a non-linear scale factor of either instrument. Probably, the non-linearity occurs in LaCoste & Romberg Type-D, and we should calibrate further.

Although calibrations of each instrument are still not sufficient to discuss smaller gravity changes down to c.a. 10 micro-gal, we can find systematic temporal changes in relative gravity by correcting relative scale factors. Gravity increases at higher altitude sites relative to coastal sites are observed during a two-year period from July, 2008 to June, 2010. Temporal changes in relative gravities reaches up to 100 micro-gal in maximum. A spatial pattern of the changes suggests its center is at the northern caldera, which implies some relationship with ground deformation sources inferred by GPS data. However, both the amplitudes and phases of the relative gravity changes can never be explained by the ground deformation observed during the period. The change seems to be related to temporal changes in precipitation. Increase in water content in vadose zone may be one of possible factor of the changes. Apart from these candidates, we tentatively inferred source location and mass increase by assuming single point mass source. The best fit location after grid searches was at depth of 3 km b.s.l. beneath the northern caldera, where approximately coincides with the ground deformation source. However, the estimated mass increase is as much as  $1.8 \times 10^8$  ton, which is equivalent to erupted materials of one large scale eruption of the volcano. It is difficult to accept easily such large amount of mass increase without any another significant signs. To detect signs of magmatic activities and to evaluate volcanic activities appropriately by gravity measurements, it is important to calibrate instruments further and to evaluate effects of environmental factors such as precipitations.

Keywords: Izu-Oshima volcano, gravity change, ground deformation

## Preparation for the practical use of unmanned observation robots in the next Izu-Oshima eruption

SAIKI, Kazuto<sup>1\*</sup> ; ICHIHARA, Mie<sup>2</sup>

<sup>1</sup>Graduate School of Science, Osaka Univ., <sup>2</sup>Earthquake Research Institute, Univ. of Tokyo

In the case of a volcanic eruption, in order to carry out evacuation guidance, it is important to observe the changing situation from just after the eruption to the completion of evacuation. In the 1986 eruption of Izu-Oshima, the explosive eruptions occurred at the unexpected points such as caldera floor and outside of a caldera. Therefore, volcanologists could not approach the vents and the opportunity of observation to gain the precious data for scientific understanding of the eruption phenomenon or disaster mitigation was lost. Moreover, during the evacuation from the island, the situation of the eruption had not been announced correctly to residents, and the mistaken information that the lava flow cut off the traffic between Okada-Motomachi was spread. Today, 20 years or more pass since a previous eruption in Izu-Oshima, and it has become the time to prepare the next eruption. In order to improve the situation at the time of the next eruption, development of the new observation robot which can respond immediately to an eruption and the establishment of an operation framework are required. From such a viewpoint, the author started Izu-Oshima Unmanned Observation Robot Symposium in 2009. This symposium is intended to bring together experts developing unmanned observation robots from different study fields such as volcanology, space engineering, and disaster relief to Izu-Oshima and to provide them the opportunity of field tests and exchange of knowledge to make them accelerate the development of the robots and the establishment of the operation framework. For these four years, many participants gathered to perform field test and to have an active information exchange. 8 UGV and 2 UAV from 9 research groups (2009), 5 UGV and 2 UAV from 5 groups (2010), 13 UGV and 3 UAV from 9 groups (2011), and 13 UGV and 6 UAV from 10 groups (2012) participated in the symposium. In the 2013 fiscal year, Izu-Oshima was hit by the 27th typhoon of the year just before the symposium. While an open lecture meeting was canceled, 5 UGV and 1 UAV from 6 groups performed field tests. In the 2013 fiscal year, we started to obtain an accommodation of the research funds for this activity from the specific joint research B of Earthquake Research Institute of the University of Tokyo. Furthermore, installation of volcano monitor cameras was also begun by inhabitants' cooperation. At the presentation, the results so far and a future view will be shown. For further detail of the symposium in the current fiscal year please refer to the following URL (<http://www.volcano-robot.org/index.html>). Izu-Oshima monitor camera can be accessed by the following URL ([http://www.volcano-robot.org/oshima\\_camera/monitor\\_top.php](http://www.volcano-robot.org/oshima_camera/monitor_top.php)) .

Keywords: Izu-Oshima, unmanned observation robot, robot, Miharayama

## Pressure sources of Miyakejima volcano estimated from crustal deformation

FUKUI, Miyo<sup>1\*</sup> ; MATSUSHIMA, Takeshi<sup>1</sup> ; OIKAWA, Jun<sup>2</sup> ; WATANABE, Atsushi<sup>2</sup> ; OKUDA, Takashi<sup>3</sup> ; OZAWA, Taku<sup>4</sup> ; MIYAGI, Yosuke<sup>4</sup> ; KOHNO, Yuhki<sup>4</sup>

<sup>1</sup>SEVO, Kyushu University, <sup>2</sup>ERI, University of Tokyo, <sup>3</sup>EVRC, Nagoya University, <sup>4</sup>NIED, Japan

Miyakejima volcano had deflated after the 2000 eruption. The deep region of the volcano has inflated since 2006 (JMA, 2013). It suggests magma accumulation for future eruptions. JMA, GSI, JCG and NIED independently observe crustal deformation using GPS. However, the observation networks are not enough to reveal the magma accumulation model.

A dense GPS campaign observation started in Miyakejima from 2011 associate with Kyushu University, University of Tokyo, Nagoya University and NIED. New GPS observation points have been established every year to improve spatial resolution of crustal deformation and estimation of the magma source parameter. In 2013, our observation network are constructed 21 points in total including new two points near summit crater where no observation after the 2000 eruption.

By assembling all the continuous GPS data that has been observed by each institution, and our observation data, integrated processing was made so as to measure the precise crustal deformation on the island for two years in 2011-2013.

As the result, the obtained deformation in this study indicates inflation in the south region of Miyakejima and deflation around the crater. The estimated magma sources are a shallow deflation sill source under the crater, a southern inflation dyke source and a deep inflation spherical source. Ozawa & Ueda (2011) estimated a flat source under the caldera using InSAR technique. The parameters of this model are consistent with our sill model. Further, only deep spherical inflation source estimated in prior studies cannot be described the observed deformation during this period. We think the supply of magma began to new inflation dyke source from deep spherical inflation source. In order to monitor the inflation source, it is necessary to enhance the southern observation network and obtain more detailed geodetic data.

Keywords: GPS, Miyakejima, Crustal deformation, Volcano, Magma chamber

## The products of 2012-2013 mud eruption event at Million Dollar Hole crater, Ioto volcano

NAGAI, Masashi<sup>1\*</sup> ; TANADA, Toshikazu<sup>1</sup> ; UEDA, Hideki<sup>1</sup> ; KOBAYASHI, Tetsuo<sup>2</sup>

<sup>1</sup>National Research Institute for Earth Science and Disaster Prevention, <sup>2</sup>Kagoshima University

Explosive eruptions occurred several times in the period from February 2012 to April 2013 at the Million Dollar Hall crater in Ioto (Iwo Jima) Island. The situation of eruptions and properties of the ejecta are summarized as follows.

At the eruption occurred in the duration from 7 to 9 February 2012, muddy volcanic ash were erupted from vents arranged NNW-SSE direction. The main vents were consist of follows. Vent A that occurred within the existing crater (25m in diameter, approximately 10m deep) at south-southeast side, vent C that was occurred in center of the existing shallow crater (30m in diameter) at north-northwest side, and vent B that was probably newly formed between the two. Thickness of ejecta layer was 30 or 40 cm on rim of each vent. Because isopach contours are irregularly shaped, tephra are estimated that were emitted directionally from each vent. Then, small scale muddy volcanic ash release and steam plume activities was followed.

The eruption on 17 to 18 February 2013 was the largest. Muddy volcanic ash were erupted from the location of vent A and B, and fell on the western side. Thickness of ejecta layer are 1 to 3 meter on vent rim. Cinders and minor man-made Objects there were possibility of ballistic ejecta reached distant point approximately 220m at the maximum from the vents. After the eruption, vent A and B were combined into a single crater (35m in diameter, 17m deep). In addition, the formation of collapse crater about 40m in diameter began at the location of vent C.

The eruption on 11 April 2013 was occurred at the collapse crater (vent C). Muddy volcanic ash deposited on the southern side. The maximum thickness of ejecta layer is 45 centimeter on the vent rim. Ballistic cinders were witnessed at the eruption, but the limit of distribution was not estimated. Vent C was combined with vents A. Therefore, the whole shape of the crater became a cocoon (60m in major axis, 17m deep). Thereafter, the crater has remained in calm state.

Volcanic ash that erupted in the series of eruptions were wet at the ejection and deposition. They are composed mainly of hydrothermal alteration clay consisting of smectite and kaolin minerals and also includes large amount of lithic fragments, free crystals and volcanic glass fragments that are altered varying degree. In addition, pieces of glass and iron piece of man-made weaponry, which is said to have been abandoned after World War II. In addition, pieces of glass and iron which were derived from weapons abandoned immediately after World War II are also included. Ballistic cinders consists of such as tuffaceous sandstone, tuff and altered trachyandesite.

Eruptive volume of each eruption are estimated approximately as follows. The eruption in February 2012 is 800 m<sup>3</sup>, the eruption on 17-18 February 2013 is 11,000 m<sup>3</sup>, and the eruption on April 11, 2013 is 2,000-4,000 m<sup>3</sup>. Total volume is 14,000 to 16,000 m<sup>3</sup> approximately. On the other hand, total amount of subsidence in this peroid is 10,000 to 15,000 m<sup>3</sup>, it is roughly equal to the eruptive volume.

These eruptions are considered phreatic explosion that blew off strongly altered rocks surrounding the hydrothermal reservoir and shallow non- or weakly altered tuffaceous rocks. It indicates that the hydrothermal activity under Million Dollar Hole crater became active in relation to rapid crustal deformation that occurred in Ioto from early 2011 to May 2012.

Keywords: tephra, depositional structure, surface phenomena, eruption record

## 2013 eruption of Nishinoshima volcano, Ogasawara islands, Japan

ITO, Koji<sup>1\*</sup> ; ONO, Tomozo<sup>1</sup> ; SASAHARA, Noboru<sup>1</sup> ; NOGAMI, Kenji<sup>2</sup>

<sup>1</sup>Japan Coast Guard, <sup>2</sup>Volcanic Fluid Research Center, Tokyo Institute of Technology

Nishinoshima volcano is a basaltic to andesitic maritime volcano on the volcanic front of the Izu-Bonin arc. For the first time ever, the submarine eruption including movement of vents and development and disappearance of new islands happened off the southeastern coast of the Nishinoshima island in 1973. The eruption stopped in May 1974 and the Nishinoshima island and the new volcanic islands were joined by sand drift in June. Then geographic changes was continued by erosion and sand drift till 1990s.

The eruption column and new volcanic island were firstly discovered by the airplane of Japan Defensive Force on 20 Nov. 2013. Then Japan Coast Guard found the new volcanic island with violent phreatomagmatic eruption. The following day, 21 Nov. 2013, phreatomagmatic eruption had occurred and volcanic edifice was developing. The eruption style changed into the Strombolian-type and lava started to flow from the vent on the eastern flank of main edifice on 22 Nov. 2013. In succeeding days, lava emerged from the western vent and pyroclastic cone was built up in the large crater in the center of main edifice. The vent of the pyroclastic cone effused blue-white volcanic gas consistently and spatter occasionally. On 24 Dec. 2013, new vent started to produce eruption column at the north of the central vent. These vents are located on the 1973 vents.

The new volcanic island consists of lava flow and water depth around eruption center may be almost constant, so growth rate of the island and magma supply rate should be equal. The growth rate estimated from the air photo is almost constant, hence the magma supply rate may be kept constant.

It is unclear that when did this volcanic activity start. But high temperature anomaly and difference of normalized water-leaving radiance within sea water are shown at the southern sea area in the satellite images published by the Earth Observation Research Center on Nov. 7. The volcanic activity may start on or before Nov. 7.

Future volcanic scenarios are uncertain, but volcanism is still active and shows no sign of end of eruption as of early-February.

**Keywords:** Nishinoshima volcano, volcanic island, Izu-Ogasawara arc, phreatomagmatic eruption, Strombolian eruption, maritime volcano

## The recent volcanic activities of Mt. Asosan

KATO, Koji<sup>1\*</sup> ; NAGATO, Shinya<sup>2</sup> ; MATSUSUE, Shinichi<sup>2</sup> ; HIRAMATSU, Hideyuki<sup>2</sup>

<sup>1</sup>Japan Meteorological Agency, <sup>2</sup>Fukuoka District Meteorological Observatory

Mt. Asosan is one of the most active volcanoes in Japan.

In Mt. Asosan, volcanic tremor amplitude and volcanic earthquakes increased on September 2013. On November 2014, water level of crater lake decreased. On December 2014, volcanic tremor amplitude increased again and the emission rate of the SO<sub>2</sub> increased. On January 2014, Mt. Asosan erupted. We report about recent volcanic activity of Mt. Asosan

## Gravity variation near the crater of Aso volcano and gravity contribution of precipitation

HAYAKAWA, Hideaki<sup>1\*</sup> ; KAGIYAMA, Tsuneomi<sup>1</sup> ; OHKURA, Takahiro<sup>1</sup> ; YOSHIKAWA, Shin<sup>1</sup>

<sup>1</sup>Graduate School of Science, Kyoto University

We investigated the gravity variation continuously measured near the active crater of Aso volcano. At the period of low volcanic activity, the gravity variation is dominated by a contribution of water mass movement arisen from percolation of rain water and discharge in a permeable layer under about 100m.

In this study, it is used a time series measured by a superconducting gravity meter, CT-200, which installed in Hondo tunnel under 30m located in about 1000m southwest of Nakadake first crater. An analysis period is for 3 years from February, 1998 to January, 2001. Aso volcano was quiet low active for this period. The hot lake in Nakadake first crater, Yudamari, which its state is an index of the volcanic activity, had been in high water level. There were no events of drying up and eruption of volcanic ash. The gravity variation removed tide and air response shows large seasonality, increasing 20 - 40  $\mu\text{Gal}$  at July and August after rainy season and decreasing gradually after that. It also has some minor changes in response to precipitation, for example, an increase of about 10  $\mu\text{Gal}$  after autumnal rain.

It is known that precipitation has an affect on gravity. However, the effect near the crater of Aso volcano did not well understand. We computed water flux by percolation into underground and water discharge from a permeable layer using a kind of physical model of storage function method known as tank model. Model input is amount of precipitation measured at Asosan meteorological station by Japan Meteorological Agency. The change of water volume contained in underground is computed from input-output difference of tank model. The gravity contribution is obtained from the corresponding density change in a region of 1400km in north-south and in east-west around the gravity meter with thickness from surface to 200m depth. It assumes that there is no gravity change by volcanic activity. Outflow resistance of a tank and permeable layer depth are decided so that the gravity contribution fits in the measured gravity variation as much as possible.

The gravity contribution of water mass movement by model computation is well coincident with the measured gravity variation in the case that rainwater percolates under 100m in vertically and is discharged horizontally from the permeable layer at 100 - 110 m depth. The model value correlates highly with the measured gravity value in the coefficient of 0.9. The root mean squares (RMS) are 10.5  $\mu\text{Gal}$  for the measured gravity and 11.4  $\mu\text{Gal}$  for the model computation, and 4.8  $\mu\text{Gal}$  for difference between the two. The model computation overestimates to a certain degree. It is considered for a reason of the discrepancy that percolation and ground water flow in general are complicate and non-linear phenomena in contrast to our linear model. However, the model computation represents sufficiently figures of the measured variation and explains it in accuracy of 14.4  $\mu\text{Gal}$  in  $3\sigma$  RMS of the difference. The contribution of water mass movement in shallow underground to 110m depth is inferred to be main component of gravity change near the crater.

The water mass movement can be computed at any period of time. In this study, we obtained the gravity contribution under 30m where the gravity meter located in. Converting it to on ground, the model prediction is available for use in correction of values measured near the crater in the repeated gravity survey at Aso volcano area. A part of discharge from the permeable layer in the computing region is considered as a source of ground water flow into Yudamari. A seasonal peak of precipitation is for about a month from June to July, however the ground water flow continues for several months after rainy season. This is coincident with the seasonal water level change of Yudamari. It is expected to estimate a possible quantity of ground water flow into Yudamari as time variation.

Keywords: Aso volcano, Gravity, Water mass movement, Precipitation, Groundwater, Superconducting gravity meter

## Thermal activities of the Nakadake first crater at Aso volcano, Japan -Unusual heat discharge events in 2012-2014-

TERADA, Akihiko<sup>1\*</sup>

<sup>1</sup>Volcanic Fluid Research Center, Tokyo Institute of Technology

Aso volcano is one of the most active volcanoes in Japan in terms of the persistent release of volatiles and thermal energy from the Nakadake first crater. Throughout most of the calm period, the crater emits significant amounts of volcanic gas, including 200 - 400 tonne/day of SO<sub>2</sub>. The first crater contains a hot crater lake, locally referred to as Yudamari with a diameter greater than 200 m. Applying the model of Ryan et al. (1974), which involves the effects of free and forced convection, Terada et al. (2012) estimated that during the calm period, the heat discharge through the lake surface is almost constant, with a value of approximately 220 MW.

The water level falls rapidly preceding an active period. The disappearance of lake water is followed by the emergence of a red-hot crater bottom or wall and a phreatic-to-phreatomagmatic and strombolian eruption sequence that lasts several months. When the volcanic activity subsides to calm period levels, the lake reforms. These dramatic falls/rises in the lake water level are likely caused by increases/decreases in the input of high-temperature steam to the crater bottom (Terada et al., 2012).

In spring of 2012, an unusual event involving the increase in water temperature and rapid decrease in water level occurred at the Yudamari crater lake. The heat discharge rates approached the figure of 600 MW which is three times higher than the representative figure in a calm period. The computational results based on energy and mass conservation indicate that the event is caused by an increase in temperature and flux of fluid inputs from the lake bottom. Preceding the event, silica content in lake water clearly increased, indicating a rise in temperature of hydrothermal system beneath the Yudamari crater lake. The event was accompanied by slight increase in SO<sub>2</sub> emission rate, but seismicity around the crater did not change significantly.

After September 2013, the lake water of Yudamari almost disappeared. Consequently volcanic fluid emitting from the crater bottom ascended as a buoyant plume into the air without transportation of the heat to the lake water. To estimate the rate of heat discharge from the first crater, we applied the plume rise assumption (Briggs, 1969; Kagiya, 1981). This assumption states that the height  $h$  of a given position in a fumarole increases proportionally with time  $t$  to the power of  $2/3$ . Video records of surveillance camera operated by Japan Meteorological Agency are used to the analysis.

In September, 2013 and December, 2013 - January, 2014, seismicity including earthquake swarms and volcanic tremors were enhanced, which were accompanied by an increase in SO<sub>2</sub> emission rates up to 2,000 tonne/day. During the periods, heat discharge rates are estimated to be 800-1000 MW which is several times higher than the figure measured in a calm period. The ratio of H<sub>2</sub>O/SO<sub>2</sub> has been roughly maintained whereas small amount of volcanic ash including juvenile materials were continuously emitted in January 2014. This may occur as a result of an increase in amount of degassing in the conduit beneath the first crater.

**Acknowledgments:** I would like to thank Yoshihiro Ushiroshoji, Shinya Nagato and the Fukuoka District Meteorological Observatory, Japan Meteorological Agency for sharing their data and for providing permission for the data to be published.

**Keywords:** heat discharge rate, Aso volcano, hot crater lake, eruption

## The temporal changes of the shallower resistivity structure associated with a small eruptions at Aso Volcano, 2014.

UTSUGI, Mitsuru<sup>1\*</sup> ; KAGIYAMA, Tsuneomi<sup>1</sup> ; HAYAKAWA, Hideaki<sup>1</sup> ; INOUE, Hiroyuki<sup>1</sup>

<sup>1</sup>Graduate School of Science, Kyoto Univ.

On Aso volcano, many observations and research have been made to detect the subsurface structure and detailed information about the distribution of the subsurface hydrothermal system have been obtained from previous studies. From the high-density AMT survey, Kanda et al. (2008) found a low resistivity area is localized just beneath the Nakadake first crater. This area is considered as a chamber of the hydrothermal fluid which is formed by a part of the hydrothermal fluid which is supplied from the deeper magma. In recently, the activities of the Nakadake crater were often temporarily increased. Associated with these activities, it is expected that the distribution of the subsurface hydrothermal fluid is changed and subsurface resistivity structure is temporally changed. In order to detect such a temporal change of shallow resistivity structure according to these activities, we carried out the repeated control sourced electromagnetic survey around the Nakadake crater using ACTIVE observation system (Utada et al., 2007). In these observations, we installed electric current transmitter on 1 km NNE from the crater, and magnetic receiver was also installed on the 4 points around crater.

In Aso volcano, a small eruption occurred in January 2014, and this activity has continued after this eruption.

During this activity, we carried out the electromagnetic survey around Nakadake crater of Aso volcano. In our presentation, we will show the observation data and the resistivity structure obtained by the 1-D analysis of our data.

Keywords: resistivity structure, Aso volcano

## Crustal deformation associated with increase in VLP events activity in Aso Volcano

OHKURA, Takahiro<sup>1\*</sup>; YOSHIKAWA, Shin<sup>1</sup>; INOUE, Hiroyuki<sup>1</sup>

<sup>1</sup>AVL, Kyoto Univ.

Aso Volcano, one of the most active volcanoes in Japan, is located in the central part of Kyushu and consists of an elliptical caldera with a diameter of 18km in E-W and 25km in N-S, and of central cones with more than 10 volcanoes aligned in E-W direction. Among central cones, Nakadake volcano is the only active cone and its recent activity is characterized by ash and strombolian eruptions and phreatic or phreatomagmatic explosions. The last strombolian eruptions ended in the beginning of the 1990s and after that, surface activities have been restricted to the fumarolic gas and ash emission from the northernmost crater of the volcano accompanying activity of long period tremors(LPT) or very long period (VLP) events.

Since 1990s, observations using broadband seismometers have revealed that the source of LPT is a crack-like conduit located at depths of 1-1.5 km beneath Nakadake, with a length of 1km and width of 2.5km. It is also revealed that at this depth a pressure was located and caused long-period displacements a few minutes before phreatic eruption which occurred in 1993 and 1994.

The Japan Meteorological Agency (JMA) raised the Volcanic Alert Level from 1 (Normal) to 2 (Do not approach the crater) based on rapid increase in numbers volcanic earthquakes and volcanic gas emission in September 2013, and based on increase in amplitude of volcanic tremors in December 2013, respectively.

Remarkable ground deformation was detected by water-tube tilt meters and super invar-rod extensometers which were installed in a 30m observation tunnel, 1km southwest from the active crater, in September 2013 and January 2014 associated with increase in VLP events activity.

By comparing the calculated deformation assuming a Mogi source and a dyke, is found that observed deformation can be attributed to the expansion of the crack-like conduit. At the beginning of the deformation, the radial component of the extensometer showed dilatation and converted to contraction, which indicates initiation of expansion at the deeper portion of the crack and propagation to the shallower part.

Keywords: Aso Volcano, Crustal deformation, VLP events, Volcanic gas, Conduit

## Remote temperature sensing on fumaroles in active volcanoes using stable isotopes of trace gases in volcanic plume

KOMATSU, Daisuke<sup>1\*</sup> ; TSUNOGAI, Urumu<sup>1</sup> ; NAKAGAWA, Fumiko<sup>2</sup>

<sup>1</sup>Graduate School of Environmental Studies, Nagoya University, <sup>2</sup>Graduate School of Science, Hokkaido University

Molecular hydrogen ( $H_2$ ) in a high-temperature volcanic fumarole ( $>400$  degreeC) reach to the hydrogen isotope exchange equilibrium with coexisting fumarolic  $H_2O$  under the outlet temperature of the fumarole. In this study, we applied this hydrogen isotope exchange equilibrium of fumarolic  $H_2$  as a tracer for the remote temperature sensing on the fumarolic area in the 1<sup>st</sup> crater of Mt. Naka-dake (Aso volcano) where direct measurement on fumaroles was not practical, by deducing the hydrogen isotopic composition (dD value) of fumarolic  $H_2$  remotely from those in volcanic plume. The reciprocal of  $H_2$  concentration in the plume samples showed a good linear relationship with the dD values. The linear relationships suggested that both the concentrations and the dD values of  $H_2$  in the plume samples can be explained by simple mixing between two end-members, both of which can be classified to a single category at least for the dD values of  $H_2$ . By extrapolating the linear relationship between  $1/H_2$  and dD to  $1/H_2=0$  to exclude the contribution of the tropospheric  $H_2$  from the dD value of each sample, we estimated that the dD value of fumarolic  $H_2$  to be  $-172\pm 16$  per mil vs. VSMOW and the apparent equilibrium temperature ( $AET_D$ ) to be  $868\pm 97$  degreeC. Although the estimated temperatures using the IR thermometers were much lower than the  $AET_D$ , we concluded that the  $AET_D$  represented the highest outlet temperature of the fumaroles in Aso volcano and that the dimensions of the fumaroles at surface smaller than the pixel of the IR thermometers was responsible for the temperatures lower than the  $AET_D$ . That is to say, temporal variation in the dimensions of fumaroles at surface, probably due to variation in the emission flux of fumarolic gases, was responsible for the temporal variation in the temperature determined by the IR thermometers, while the actual outlet temperature of the Aso fumaroles keeps the high temperature almost equal to the equilibrium temperature of fumarolic gases.

Keywords: fumarolic gases, carbon dioxide, molecular hydrogen, stable isotopes, isotopic exchange equilibrium, remote temperature sensing

## Strange seismic, infrasonic, and geodetic phenomena observed 3 days before the 2011 eruption of Shinmoe-dake volcano

ICHIHARA, Mie<sup>1\*</sup>; OIKAWA, Jun<sup>1</sup>; TAKEO, Minoru<sup>1</sup>

<sup>1</sup>Earthquake Research Institute, University of Tokyo

Shinmoe-dake volcano started its climatic events on January 26 at 14:49. Some precursory phenomena have been found in petrologic studies. The ash from a phreatic eruption on January 19 contained fresh pumice fragments indicating ascent of new magma to a shallow depth (Miyabuchi et al., 2013; Suzuki et al., 2013). Petrologic analyses of the eruption products from the climatic events showed evidences of magma mixing in two stages before the eruptions; Suzuki et al. (2013) estimated the times of the first and second mixing to the eruption as >14 days and 0.7-15 hours, respectively, while Tomiya et al. (2013) conclusively proposed 0.4-3 days and several hours, respectively, and suggested that the first mixing likely triggered the eruption.

On the other hand, no clear precursory signals have been identified in geophysical observations. Considering the above petrologic studies, we reexamined the seismic, infrasonic, and geodetic data in a few weeks to the eruption, and particularly focused on a sequence of strange phenomena on January 23, three days before the eruption. It was the only notable phenomena recognized in several days to the eruption, but has not been reported elsewhere.

Nakada et al. (2013) referred to the JMA report (2012) that volcanic tremor was first recorded at 01:27 on 19 January and continued from the 19 January afternoon to the morning of 23 January. In fact, the tremor started to be recorded at stations around the summit of Shinmoe-dake at 12:45 on 18 January and increased significantly after the phreatic eruption at 01:27 on the 19th. If there was any sign indicating rise of new magma to the shallow depth before the phreatic eruption, the tremor could be the candidate.

On January 23, there was a clear infrasound signal continuing from 4:11 to 4:53 with an amplitude about 1 Pa and a sharp peak frequency at 1.8 Hz. The events was nearly aseismic and the regional seismic stations recorded infrasound shaking of the ground. The bad weather condition prohibited visual observation to see if any surface activity accompanied. At 6:00, the tremor power increased at stations on the north flank while it decreased at a station on the west flank, indicating some change of the source. The tremor power decreased from 8:00 to 8:30, stayed at the low level until 13:15, and then recovered to the previous level by 14:00. It was more distinct at stations close to the summit of Shinmoe-dake; the power decrease was more than an order of magnitude at the nearest station, SMN, 700 m from the summit. After the recovery the tremor stayed nearly same levels until the small eruptive event on the 26th before the main event. During the quiescent period of the tremor, gradual tilt up toward the summit was detected by a broadband seismometer at station SMN. Although, seismic activity except the tremor was low around the days, the quiescent period had more seismic events including relatively low-frequency ones.

Although causal relations among these events or their relation to the magma mixing are totally unclear, the sequence of phenomena on January 23 is potentially important to understand the processes leading to the climatic events of the Shinmoe-dake eruption.

Keywords: Eruption, Tremor, Infrasound, Precursor, Tilt

## Relationship between Infrasound Signals and Plume Heights by the JMA's Weather Radar, the Shinmoe-dake 2011 Eruption

TAKAGI, Akimichi<sup>1\*</sup> ; SHIMBORI, Toshiki<sup>1</sup> ; YAMAMOTO, Tetsuya<sup>1</sup> ; FUKUI, Keiichi<sup>2</sup>

<sup>1</sup>Meteorological Research Institute, <sup>2</sup>Kakioka Magnetic Observatory

During the continuous sub-plinian eruption of the 2011 Shinmoe-dake eruption, the JMA's weather RADAR detected the sequential echoes from the volcanic plume (Shimbori et al., 2013). We report the brief result of basic analysis for the relationship between the plume heights and infrasound signals.

The eruption cloud echo data observed at the Kagoshima Airport Doppler RADAR (Kagoshima DRAW) were analyzed. While Kagoshima DRAW has the threshold of radar reflectivity factor, its time interval of the volume scan is shorter as 5 minutes. In this study, in order to improve the accuracy of time, the time of the plume top in a volume scan was identified by every scanning time of the antenna.

The relationship between the plume height and discharge rate of magma has the empirical power law, and its power index was estimated to be 0.259 (Sparks, 1997). Assuming that the discharge rate has the proportional relation with the integration of the infrasound signal generated by eruption (Takagi et al., 2013), we estimate the power law between the echo height and infrasound data for this eruption. In the result, the most appropriate power index was estimated to be 0.55, and the delay time and the time window of the infrasound data which make error smaller are 4 minutes and 6 minutes, respectively.

These time delay and window might be subjected to height and velocity of plume top. More advanced analysis for plume heights and infrasound signals would disclose the dynamics of volcanic plume.

### Acknowledgements

We would like to thank Drs. Y. Tanaka, O. Suzuki, H. Yamauchi and E. Sato (MRI, JMA) for the use of their "Draft" radar analysis software.

Keywords: plume height, weather radar, infrasound, Shinmoe-dake

## Long-period seismic waves propagating over Kyushu as associated with the Sakurajima eruption of August 18, 2013

IKEDA, Ayami<sup>1</sup> ; KUGE, Keiko<sup>1\*</sup> ; KAZAMA, Takahito<sup>1</sup> ; MATSUZAWA, Takanori<sup>2</sup>

<sup>1</sup>Dept. Geophysics, Kyoto University, <sup>2</sup>NIED

We found long-period seismic waves propagating over Kyushu after the explosive eruption from Showa crater of Sakurajima volcano at 16:31JST on August 18, 2013. The eruption is one of the most significant ones that Showa crater has experienced since 2006, and the volcanic plume rose approximately 5000 m high. Showa crater is currently very active, causing more than 1000 eruptions a year.

The broadband seismic network F-net recorded the long-period seismic waves traveling in a very wide area covering Amami and the whole Kyushu region. The dominant periods are longer than 5 s. The apparent propagation velocity is approximately 2.75 km/s. In data recorded by Hi-net tilt meters at shorter intervals of around 20 km, the long-period seismic waves arrived earliest at the station AIRH that is the closest to Sakurajima volcano, and propagated with the almost same apparent velocity as observed by F-net. The long-period seismic waves are, therefore, likely to have been radiated from Sakurajima volcano. Assuming that the source is located at Showa crater, we rotated two horizontal components of the F-net and Hi-net data to transverse and radial components. The long-period seismic waves were observed in the radial and transverse components, and the apparent propagation velocity is slightly faster in the transverse component than the radial one. The waves observed in transverse and radial components can be Love and Rayleigh waves, respectively.

For previous eruptions of Sakurajima volcano, we also examined whether or not long-period seismic waves were recorded by F-net. From 5057 eruptions in the period between 2006 and 2013, we selected 43 eruptions that have large amount and height of a volcanic plume as well as large deflation volume. Long-period seismic waves were found for five eruptions including ones from Minami-dake crater. The maximum distances with the observations of long-period seismic waves range from 150 to 331 km, which are much shorter than for the 2013 eruption. Therefore, the 2013 eruption could excite long-period seismic waves more remarkably, compared to the other five eruptions. Observations of long-period seismic waves, on the other hand, did not have clear dependence on the amount and height of a volcanic plume or the deflation volume.

We observed significant transverse components of the long-period seismic waves associated with the 2013 eruption, which are considered Love waves. We also had similar observations for the five eruptions accompanied by long-period seismic waves in F-net data. Eruptions of Sakurajima volcano have been explained by isotropic explosion and contraction of a vertical cylinder (Uhira and Takeo, 1994; Tameguri et al., 2002), and these models cannot excite Love waves. A model for explaining Love waves observed in the present study is to be investigated.

## Comparison between areas of VT earthquakes around Sakurajima Volcano and a 3-D velocity model of the upper crust

YAKIWARA, Hiroshi<sup>1\*</sup> ; HIRANO, Shuichiro<sup>1</sup> ; MIYAMACHI, Hiroki<sup>1</sup> ; TAKAYAMA, Tetsuro<sup>2</sup> ; ICHIKAWA, Nobuo<sup>2</sup> ; TAMEGURI, Takeshi<sup>2</sup>

<sup>1</sup>GSE, Kagoshima Univ., <sup>2</sup>SVRC, DPRI, Kyoto Univ.

Volcano-tectonic (VT) earthquakes associated with volcanic activities of Sakurajima Volcano also occur beneath Kagoshima Bay around the volcano (Hidayati et al., 2007). Not only seismic observations on land but also ones using Ocean Bottom Seismographs (OBSs) are need to detect micro VT earthquakes beneath the bay, and to improve accuracies of the hypocenter locations of the earthquakes. Authors therefore have performed OBS observations five times since 2009. In the present study, we summarize hypocenter distributions of the VT earthquakes obtained by OBS observations. We also compare the hypocenters and a three-dimensional seismic velocity model derived from regional earthquake data in order to extend knowledge for active area of the VT earthquakes.

The areas where the earthquakes occurred are summarized as follows: 1) Shallow VT earthquakes generated beneath Wakamiko Caldera. Most of the earthquakes were located shallower than or equal to 5 km depth. 2) Small number of VT earthquakes were also located at 5-10 km depth off the northeastern coast of the volcano. This activity may be steadily. 3) No earthquake was detected beneath the western half of Aira Caldera.

On the other hand, we also analyzed a three-dimensional seismic velocity model by use of regional earthquake data (Mera et al., 2013) to compare the hypocenter distribution and the velocity model. As a result of the 3-D inversions, we obtained reliable P- and S-wave velocities at the depth range of 5-12km under the area in and around the volcano. At shallower than 6 km depth, the model delineates an area of Low-V<sub>p</sub> (5.3-5.4 km/s) and Low-V<sub>s</sub> (3.0-3.1 km/s) beneath the area of south of Wakamiko Caldera. A peak of the low velocity area tends to close the volcano at the portion deeper than 6 km depth. At 10 km depth, a peak of Low-V<sub>p</sub> (5.4-5.5 km/s) and Low-V<sub>s</sub> (3.1-3.2 km/s) was imaged beneath an area off northeast coast of the volcano (beneath Shin-jima Island). Obviously low velocity areas also spread from the volcano to the area off the south coast of the volcano.

Because several recorder troubles happened among the five OBS observations, we selected the hypocenters of the VT earthquakes which were located using data recorded at common three OBS stations. As a result of the comparison between the hypocenters of the VT earthquakes and the 3-D velocity model, most of the VT earthquakes were located where intermediate velocities were estimated. Furthermore, some of VT earthquakes occurred in close vicinity of the peaks of Low-V<sub>p</sub> and Low-V<sub>s</sub> areas. The former suggests that the strains by crustal deformation hardly accumulate at areas of high and low velocities. The latter may reflect the increase of pore pressures and stress changes generated by existence of volcanic fluids.

Keywords: Sakurajima Volcano, Volcano-tectonic earthquakes, Three-dimensional seismic velocity model

## Repetitive seismic survey 2013 in Sakurajima Volcano.

TSUTSUI, Tomoki<sup>1\*</sup> ; MASATO, Iguchi<sup>2</sup> ; NAKAMICHI, Harushisa<sup>2</sup> ; TAMEGURI, Takeshi<sup>2</sup> ; YAKIWARA, Hiroshi<sup>4</sup> ; OHMINATO, Takao<sup>5</sup> ; SUGAI, Akira<sup>3</sup> ; OSHIMA, Hiromitsu<sup>6</sup> ; MIURA, Satoshi<sup>7</sup> ; YAMAMOTO, Mare<sup>7</sup> ; ICHIKI, Masahiro<sup>7</sup> ; NOGAMI, Kenji<sup>8</sup> ; TAKEO, Minoru<sup>5</sup> ; ICHIHARA, Mie<sup>5</sup> ; OIKAWA, Jun<sup>5</sup> ; YAMANAKA, Yoshiko<sup>9</sup> ; OHKURA, Takahiro<sup>2</sup> ; ABE, Yuki<sup>2</sup> ; SHIMIZU, Hiroshi<sup>10</sup> ; YAMASHITA, Yusuke<sup>10</sup> ; MIYAMACHI, Hiroki<sup>4</sup> ; KOBAYASHI, Reiji<sup>4</sup> ; MIKI, Daisuke<sup>2</sup> ; YAMAMOTO, Keigo<sup>2</sup> ; MAEKAWA, Tokumitsu<sup>6</sup> ; HIRAHARA, Satoshi<sup>7</sup> ; ATSUSHI, Watanabe<sup>5</sup> ; OKUDA, Takashi<sup>9</sup> ; HORIKAWA, Shinichiro<sup>9</sup> ; MATSUHIRO, Kenjiro<sup>9</sup> ; SONODA, Tadaomi<sup>2</sup> ; SEKI, Kenjiro<sup>2</sup> ; YOSHIKAWA, Shin<sup>2</sup> ; HIRANO, Shuichiro<sup>4</sup> ; WATANABE, Yukihiko<sup>3</sup> ; USUI, Yuji<sup>3</sup> ; KOBAYASHI, Tsukasa<sup>3</sup> ; IKEDA, Keiji<sup>3</sup> ; NAGATO, Shinya<sup>3</sup> ; KOEDA, Tomoyuki<sup>3</sup>

<sup>1</sup>Akita University, <sup>2</sup>Kyoto University, <sup>3</sup>Japan Meteorological Agency, <sup>4</sup>Kagoshima University, <sup>5</sup>University of Tokyo, <sup>6</sup>Hokkaido University, <sup>7</sup>Tohoku University, <sup>8</sup>Tokyo Institute of Technology, <sup>9</sup>Nagoya University, <sup>10</sup>Kyushu University

The latest report on structural evolution and on effect of the density reduction in the seismic network will be presented through the sixth round of the repetitive seismic experiment in Sakurajima Volcano. Sakurajima Volcano locates in Kagoshima, south Kyushu, which is one of the most active volcanoes in Japan. The repetitive seismic experiment have been carried out since 2008 in order to detect and research structural evolution along volcanic activity, with using 4.5Hz sensors. This round has carried out as a part of the experiment which presented by Nakamichi et al. in this conference.

The detection and researching the structural evolution approach to magma movement under the ground along volcanic activity and will provide essential measure on development of volcanic activity. Extending its result into evaluation on flux and accumulation will bring significant informations on considering scenario about volcanic activity in progress. And the experiments should be sustainable method because of long time scale of the target.

The latest report about structural evolution will be presented. Details and results of the experiment rounds have been reported in these conferences since 2009. The seismic response along the line in the north flank have changed year by year. Two major sweet spots have been found at 4.9km depth in the northeastern Sakurajima and at 8km depth beneath northern flank of Kitadake, the northern edifice, through these experiments. The changes in seismic response are interpreted as a result of mass movement underground with going volcanic activity. Further change is expected associating with development of volcanic activity.

The effect of density reduction will be also discussed. Though the repetitive seismic experiments with two lines have been done with about 250 stations every December until 2012, the latest experiment with the most sensitive line with 74 stations on the northern flank was carried on December 2013. Discussions on the effect of density reduction in the seismic network is necessary in order to have a style of sustainable execution of the research.

Keywords: Sakurajima Volcano, Reflection seismology, Dynamic structure, Controlled source seismology

## Active source seismic experiment in and around Sakurajima volcano in 2013 and comparison with the experiment in 2008

NAKAMICHI, Haruhisa<sup>1\*</sup>; TSUTSUI, Tomoki<sup>2</sup>; TAMEGURI, Takeshi<sup>1</sup>; IGUCHI, Masato<sup>1</sup>; YAKIWARA, Hiroshi<sup>3</sup>; OHMINATO, Takao<sup>4</sup>; SUGAI, Akira<sup>5</sup>; OSHIMA, Hiromitsu<sup>6</sup>; MIURA, Satoshi<sup>7</sup>; YAMAMOTO, Mare<sup>7</sup>; ICHIKI, Masahiro<sup>7</sup>; NOGAMI, Kenji<sup>8</sup>; TAKEO, Minoru<sup>4</sup>; ICHIHARA, Mie<sup>4</sup>; OIKAWA, Jun<sup>4</sup>; YAMANAKA, Yoshiko<sup>9</sup>; OHKURA, Takahiro<sup>1</sup>; ABE, Yuki<sup>1</sup>; SHIMIZU, Hiroshi<sup>10</sup>; YAMASHITA, Yusuke<sup>10</sup>; MIYAMACHI, Hiroki<sup>3</sup>; KOBAYASHI, Reiji<sup>3</sup>; MIKI, Daisuke<sup>1</sup>; YAMAMOTO, Keigo<sup>1</sup>; MAEKAWA, Tokumitsu<sup>6</sup>; HIRAHARA, Satoshi<sup>7</sup>; WATANABE, Atsushi<sup>4</sup>; OKUDA, Takashi<sup>9</sup>; HORIKAWA, Shinichiro<sup>9</sup>; MATSUHIRO, Kenjiro<sup>9</sup>; SONODA, Tadaomi<sup>1</sup>; SEKI, Kenjiro<sup>1</sup>; YOSHIKAWA, Shin<sup>1</sup>; HIRANO, Shuichiro<sup>3</sup>; WATANABE, Yukihiko<sup>5</sup>; USUI, Yuji<sup>5</sup>; KOBAYASHI, Tsukasa<sup>5</sup>; IKEDA, Keiji<sup>5</sup>; NAGATO, Shinya<sup>5</sup>; KOEDA, Tomoyuki<sup>5</sup>

<sup>1</sup>Kyoto University, <sup>2</sup>Akita University, <sup>3</sup>Kagoshima University, <sup>4</sup>University of Tokyo, <sup>5</sup>Japan Meteorological Agency, <sup>6</sup>Hokkaido University, <sup>7</sup>Tohoku University, <sup>8</sup>Tokyo Institute of Technology, <sup>9</sup>Nagoya University, <sup>10</sup>Kyushu University

We conducted active seismic experiment in and around Sakurajima volcano in December 2013, five years after the similar experiment that was conducted in 2008. We deployed 280 temporary seismic stations, 90% of which were located at the same locations of the experiment in 2008. Six explosive shots with 200 kg or 300 kg charges were detonated in December 5. The 2013 shot locations (S1, S2, S4, S5 and S6) are less than 60 m from the 2008 shot locations except for 1 shot (S3). We successively observed the explosions and volcanic events during nighttime nine hours continuous recording. The continuous records contain not only waveforms excited by the six shots but also by an explosive eruption and volcanic tremor. We evaluate cross-correlations of waveforms at the same station locations that obtained in 2008 and 2013 to detect temporal change of subsurface structure beneath Sakurajima volcano except for S3.

Member organizations of the Research Group of the Seismic Dynamic Structure in Sakurajima Volcano: Graduate School of Science, Hokkaido University, Graduate School of Engineering and Resource Science, Akita University, Graduate School of Science, Tohoku University, Earthquake Research Institute, University of Tokyo, Volcanic Fluid Research Center, Tokyo Institute of Technology, Graduate School of Environmental Studies, Nagoya University, Graduate School of Science, Kyoto University, Disaster Prevention Research Institute, Kyoto University, Graduate School of Science and Engineering, Kagoshima University, and Japan Meteorological Agency

Keywords: active seismic experiment, temporal change, volcanic activity, eruption, Sakurajima volcano, Aira caldera

## Active monitoring by using ACROSS in Sakurajima volcano - observation report 3 -

MIYAMACHI, Hiroki<sup>1\*</sup> ; ARIKADO, Natsumi<sup>1</sup> ; YAKIWARA, Hiroshi<sup>1</sup> ; YAMAOKA, Koshun<sup>2</sup> ; WATANABE, Toshiki<sup>2</sup> ; KUNITOMO, Takahiro<sup>2</sup> ; IGUCHI, Masato<sup>3</sup> ; TAMEGURI, Takeshi<sup>3</sup> ; MIKADA, Hitoshi<sup>3</sup> ; TAKENAKA, Hiroshi<sup>4</sup> ; SHIMIZU, Hiroshi<sup>5</sup> ; IKUTA, Ryoya<sup>6</sup>

<sup>1</sup>Kagoshima University, <sup>2</sup>Nagoya University, <sup>3</sup>Kyoto University, <sup>4</sup>Okayama University, <sup>5</sup>Kyushu University, <sup>6</sup>Shizuoka University

In 2012, in order to realize quantitative monitoring of magma transport process, we deployed the ACROSS (Accurately Controlled Routinely Operated Signal System) vibrator system composed of two vibrators in the site that is 3.6 km apart from the northwest of the Minamidake crater of Sakurajima.

On September 2012, we have started the full-scale operation under synchronized control of two vibrators with a frequency modulation, in which the modulation period is 50 seconds and the frequency range is 5 to 15 Hz, to produce broad frequency range of signal: one vibrator 'SKR1' with a signal frequency range of 7.510Hz +/- 2.50Hz and the other 'SKR2' with the range of 12.505Hz +/- 2.50Hz. The signal from the ACROSS source is routinely monitored with more than 20 permanent seismic stations in and around Sakurajima volcano. Five temporal seismic stations are also deployed to increase the spatial coverage of monitoring. The signals recorded at the seismic stations are deconvoluted with the source function to obtain the transfer function between the source and the receivers.

In this report, we estimated the daily transfer functions for the SKR2 vibrator at each station by every 5 days stacked data during a whole period (400 days from September 19, 2012 to October 23, 2013) of the operation. It is obviously found that these daily transfer functions vary temporally. To detect quantitatively the temporal variation of the transfer functions, we analyzed the variation of the transverse component (Tt) of the transfer functions at 7 seismic stations located in Sakurajima Island as follows:

(1) We analyzed the transfer function obtained at temporal seismic station 'GOMI' located at about 50m apart from the ACROSS source to verify the stability of power of the seismic waves generated by the ACROSS source. According to the result, we rejected the transfer function evaluated during a period of the unstable power condition from a whole period of the operation.

(2) We visually inspected arrival times and amplitudes for the specific phases in the transfer functions at each station during the period of the stable power condition of the ACROSS, and obtained the quantitative temporal variation for the specific phases.

(3) On a simple assumption that the specific phases are SH waves (the transverse component of the transfer functions), we presumed the depth range where each specific phase propagated in the 5 horizontally layered model simplified from the results of the exploration seismic experiment (Miyamachi et al., 2013).

(4) We compared the temporal variation of the specific phases with activity of volcanic eruptions by JMA, the temporal change of the N-S and E-W horizontal distances (GPS data) in Sakurajima Island, and the temporal change of strain at the HAR station measured by Kyoto University.

In the presentation, we will show the observation results in detail. This ACROSS research project in Sakurajima volcano is still in a pioneering stage, and we have plans in the future to continue our project.

Keywords: Sakurajima volcano, ACROSS

## Vertical ground deformation in Sakurajima volcano and around Aira caldera: results of leveling survey in Oct.-Nov. 2013

YAMAMOTO, Keigo<sup>1\*</sup> ; MATSUSHIMA, Takeshi<sup>2</sup> ; YOSHIKAWA, Shin<sup>3</sup> ; OHKURA, Takahiro<sup>3</sup> ; YOKOO, Akihiko<sup>3</sup> ; AIZAWA, Koki<sup>2</sup> ; INOUE, Hiroyuki<sup>3</sup> ; MISHIMA, Taketoshi<sup>3</sup> ; UCHIDA, Kazunari<sup>2</sup> ; SONODA, Tadaomi<sup>1</sup> ; SEKI, Kenjiro<sup>1</sup> ; KOMATSU, Shintaro<sup>1</sup> ; HOTTA, Kohei<sup>3</sup> ; TAKAHASHI, Atsushi<sup>3</sup> ; TOYOFUKU, Takashi<sup>4</sup> ; ASANO, Haruka<sup>4</sup> ; NARITA, Tsugunori<sup>4</sup>

<sup>1</sup>Disaster Prevention Research Institute, Kyoto University, <sup>2</sup>Faculty of Sciences, Kyushu University, <sup>3</sup>Graduate School of Science, Kyoto University, <sup>4</sup>Geospatial Information Authority of Japan

We conducted the precise leveling survey in Sakurajima volcano and around Aira caldera in October and November 2013, following the repeated leveling surveys to evaluate the vertical ground deformation associated with the recent eruptive activity of this volcano. The leveling routes measured in 2013 survey are about 117 km long in total, including Sakurajima coast route, Sakurajima western flank route, Sakurajima northern flank route, Kagoshima Bay western coast route (BM.2469 - BM.2474 - BM.J), Kagoshima Bay eastern coast route (BM.2500 - BM.J.2797) and Soo route (BM.J.2797 - BM.2785). These leveling routes were measured by the joint university team during the period of November 5-22 and by Geospatial Information Authority of Japan (GSI) during the periods from October 25 to November 7 and of November 13-26.

The obtained survey data are compared with those of the previous surveys conducted in October-December 2007 and November-December 2012, resulting in the relative vertical displacements of the bench marks. The resultant displacements show the ground uplift around Aira caldera as well as the ground subsidence near the central part of Sakurajima. From the analysis based on Mogi's model, the inflation and deflation sources are located beneath the center of Aira caldera and beneath the center of Sakurajima, respectively.

These results indicate that the magma storage at the magma reservoir beneath Aira caldera is still progressed. On the other hand, they also suggest the increase of the amount of ejected magma at the magma reservoir beneath the center of Sakurajima volcano, reflecting the recent increase of the eruptive activity at Showa crater.

Keywords: Sakurajima volcano, Aira caldera, precise leveling survey, vertical ground deformation

## Movement of pressure source at Sakurajima volcano after 2006 revealed by continuous GPS observation data

HOTTA, Kohei<sup>1\*</sup> ; IGUCHI, Masato<sup>2</sup> ; OHKURA, Takahiro<sup>1</sup> ; YAMAMOTO, Keigo<sup>2</sup>

<sup>1</sup>Graduate School of Science, Kyoto University, <sup>2</sup>DPRI, Kyoto University

Ground deformation around Sakurajima has been mainly detected by precise leveling, and has been modeled with 2 spherical pressure sources at the center of the Aira caldera (about 10 km depth) and at beneath the summit crater (about 4 km depth) (Eto, 1989, *Annals of DPRI, Kyoto Univ.*). The ground around the Aira caldera turned to uplift since 1993. After continuous GPS observation started at Sakurajima in 1995, explosive activity at summit crater temporally increased at the end of 1999, and Showa crater started eruptive activity at June 2006. Large deformation rate was obtained prior to these eruptive activities, and a pressure source was located at depths 6-8 km near the northern coast of Sakurajima by assuming a spherical source (Hotta et al., 2013, *Annual of DPRI, Kyoto Univ.*). It is thought that both of pressure sources at the center of the Aira caldera and at beneath the summit crater expanded, and a pressure source apparently moved toward northern coast of Sakurajima. Eruptive activity at Showa crater has increased since 2009. In this study, we analyzed GPS data to make clear process of magma movement accompany with eruptive activity of Showa crater.

GPS data observed by SVO (Sakurajima Volcano Observatory) and GEONET data during 2006-2012 were analyzed by using PPP-AR analysis of GIPSY OASIS II ver. 6.1.2. Although no significant deformations are found during 2006-2009, variable deformation rates are found after around 2009.

Here, we focused on the period of the largest deformation rate after eruptive activity at Showa crater started (from October 2011 to March 2012). At first, we searched average positions of pressure sources whole the period by using GA. Pressure sources located at the center of Aira caldera (8.3 km depth; source A) and beneath Sakurajima (2.9 km depth; source B). Next, fixing the position of source A at the average position (because previous studies also obtained pressure source at the center of Aira caldera around this average position), we set a time window with 4 month period, and shifted it by 10 days. Source B moved from around Kitadake toward the northern part of Sakurajima during 1st time window (October 1, 2011-January 31, 2012) to 6th one (November 21, 2011-March 21, 2012), and then moved toward beneath Minamidake at 7th one (December 1, 2011-March 31, 2012). During the period of November 26, 2011-March 25, 2012, which is middle of 6th and 7th time windows, source B located around Kitadake. Deformation pattern of GPS stations at the northern part of Sakurajima changed around the end of December 2011. Moreover, eruptive activity at Showa crater increased from December 2011. These suggest that magma migrated from Aira caldera toward Sakurajima at around December 2011.

Keywords: Sakurajima volcano, Aira caldera, ground deformation, GPS, Mogi's model

## The importance of hydrological disturbance corrections for relative gravity data: A case study at Sakurajima Volcano

KAZAMA, Takahito<sup>1\*</sup> ; YAMAMOTO, Keigo<sup>2</sup> ; FUKUDA, Yoichi<sup>1</sup> ; IGUCHI, Masato<sup>2</sup>

<sup>1</sup>Kyoto Univ., <sup>2</sup>DPRI, Kyoto Univ.

An empirical water balance model was created to correct for hydrological disturbances in relative gravity data repeatedly measured at Sakurajima Volcano, southern Japan. This study aims to quantitatively monitor gravity signals due to magmatic activities of Sakurajima Volcano, and we here present the first applied results of the empirical model. The hydrological disturbances were simply calculated by the product of the instant gravity response to unit precipitation and land water storage, which were estimated using digital topography and observed meteorological data. The calculated hydrological disturbance was consistent with the observed absolute gravity data at Harutayama Station from 2010 to 2011 within 8 micro-gal (1 [micro-gal] = 1 E-8 [m/s<sup>2</sup>]), which was smaller than the typical accuracy of relative gravity measurements (~10 micro-gal). In addition, after we subtracted (i.e., corrected) the calculated disturbances from the measured relative gravity data at Sakurajima Volcano, the average amplitude of the corrected gravity changes during 2007-2009 was reduced by 90 % compared with that of the original gravity data. Since gravity changes have been measured using both absolute and relative gravimeters at volcanic areas these days, hydrological disturbance corrections should be applied to the relative gravity data, not only to the absolute one. By sophisticating the effects of spatiotemporal variations in precipitation, evapotranspiration, and infiltration capacity, this model will enable us to robustly monitor long-period and wide-spread gravity variations associated with volcanic activities.

Keywords: Sakurajima Volcano, gravity change, hydrological disturbance, relative gravity measurement, absolute gravity measurement, infiltration capacity

## Automated sulfur dioxide flux observation at Suwanosejima volcano, Japan, and comparing to seismic data

MORITA, Masaaki<sup>1\*</sup>; MORI, Toshiya<sup>1</sup>; IGUCHI, Masato<sup>2</sup>; NISHIMURA, Takeshi<sup>3</sup>

<sup>1</sup>Geochem. Res. Center, Univ. of Tokyo, <sup>2</sup>DPRI, Kyoto Univ., <sup>3</sup>Dept. Geophys., Tohoku Univ.

Suwanosejima is a remote volcanic island located about 240 km south-southwest of Kagoshima city, Kyushu Island, Japan. This volcano has been erupting very frequently since early-1950s, and is one of the most active volcanoes in Japan. Previous studies on sulfur dioxide (SO<sub>2</sub>) flux measurement of Suwanosejima are very limited and reported that daily average SO<sub>2</sub> flux from this volcano ranged about 5–15 kg/s [Mori et al., 2004; Hirabayashi et al., 2005]. Therefore, we conducted automated SO<sub>2</sub> flux measurement at Suwanosejima volcano to understand SO<sub>2</sub> flux variation with long-term observation at Suwanosejima volcano and to evaluate a relation between SO<sub>2</sub> flux and seismic data.

We developed automated SO<sub>2</sub> flux measurement system to conduct automated observation in such a remote island. The power consumption of the scanning instrument was significantly improved compared to that in the previous studies. The observation was conducted for January 21, 2013–May 7, 2013 (Period I) and November 5, 2013–the present (Period II). The observation system has been working without any trouble for more than 200 days in total showing robustness of the developed system.

SO<sub>2</sub> flux was calculated with a corrected differential optical absorption spectroscopy method for radiative dilution effect [Mori et al., 2006; Kern et al., 2009]. In the observation period of over 200 days, SO<sub>2</sub> flux was calculated for 40 days. The average SO<sub>2</sub> flux in the total observation period was 13.4 kg/s, which ranged from 5.9 kg/s to 34.5 kg/s. The average and the standard deviation in Period I were 16.9 kg/s and 6.2 kg/s, and those in Period II were 14.0 kg/s and 5.7 kg/s, respectively.

Since previously reported SO<sub>2</sub> flux in 2000s [Mori et al., 2004; Hirabayashi et al., 2005] were not corrected for the dilution effect, these values might be significantly underestimated. The average and the standard deviation of uncorrected SO<sub>2</sub> flux for the dilution effect in this study were 9.7 kg/s and 4.3 kg/s. This range was comparable to the range of the previous studies in 2000s. Considering above, SO<sub>2</sub> flux range has been stable since at least 2000s.

Surface and seismic activities in Period I (January 21–May 7, 2013) significantly differed from those in Period II (November 5, 2013–the present). Period I was in a continuous volcanic tremor period (September 2012–July 2013), and Period II was in an intermittent explosions and volcanic tremors period. In contrast to the surface and seismic activities, SO<sub>2</sub> flux variations in Period I and II were almost in the same range. This implies that degassing rate of magma for these two periods were similar. Therefore, the difference of surface and seismic activities which was observed in these periods needs to be explained considering the stable degassing magma rate.

Keywords: Volcanic gas, Sulfur dioxide, Flux, Suwanosejima volcano, Automated observation, Seismic data

## Shallow active magma body beneath Taal Volcano Island, Philippines

KUMAGAI, Hiroyuki<sup>1\*</sup>; LACSON, Rudy<sup>2</sup>; MAEDA, Yuta<sup>1</sup>; FIGUEROA, Melquiades<sup>2</sup>; YAMASHINA, Tadashi<sup>3</sup>; BORNAS, Ma. antonia<sup>2</sup>

<sup>1</sup>Nagoya University, <sup>2</sup>PHIVOLCS, <sup>3</sup>Kochi University

Taal volcano, Philippines, is one the world's most dangerous volcanoes in view of its explosive eruption history and close proximity to populations. Electromagnetic, geodetic, and seismic studies have been extensively conducted at this volcano to reveal its magma system. Recent deployment of a realtime broadband seismic network has detected long-period (LP) and volcano-tectonic (VT) events that occurred beneath Taal. Our source location analysis of VT events using both onset arrival times and high-frequency seismic amplitudes points to the existence of a strong attenuation region with a shear-wave quality factor (Q) of around 10 near the surface at the eastern flank of Volcano Island in Taal Lake. This region is located just beneath the active fumarolic area and LP source and above inflation and deflation pressure sources, and is coincident with a low resistivity region. The attenuation region matches with that inferred from an active seismic survey conducted in 1993 at Taal volcano. These features strongly suggest that the attenuation region represents an active degassing magma body near the surface, which persistently existed for more than 20 years. Our study synthesized with previous studies clarifies the magma system beneath Taal, which further addresses volcanic risk at Volcano Island sitting on a shallow active magma body.

## Waveform analysis on initial phases of explosion earthquakes at Lokon-Empung volcano, Indonesia

TAISHI, Yamada<sup>1\*</sup> ; AOYAMA, Hiroshi<sup>1</sup> ; NISHIMURA, Takeshi<sup>2</sup> ; YAKIWARA, Hiroshi<sup>3</sup> ; NAKAMICHI, Haruhisa<sup>4</sup> ; OIKAWA, Jun<sup>5</sup> ; IGUCHI, Masato<sup>4</sup> ; MUHAMAD, Hendrasto<sup>6</sup> ; YASA, Suparman<sup>6</sup>

<sup>1</sup>Faculty of Sci., Hokkaido Univ., <sup>2</sup>Graduate School of Sci., Tohoku Univ., <sup>3</sup>Faculty of Sci., Kagoshima Univ., <sup>4</sup>DPRI, Kyoto Univ., <sup>5</sup>ERI, Univ. of Tokyo, <sup>6</sup>CVGHM, Indonesia

Excitation mechanism of explosion earthquake that often accompanies explosive Vulcanian eruptions is understood to be macroscopically explained by a downward single force acting in the vent. In the meantime, it is revealed that the excitation of initial phases of explosion earthquake occurs earlier than the explosion at the crater [e.g. Tameguri et al., 2002]. So the excitation of the initial phases of explosion earthquake can be regarded as one of the most important processes to understand the initiation of Vulcanian eruption. However, the researches focusing on the initial phases are not so common in spite of their scientific importance. In this study, we implemented temporary observation of Vulcanian eruption at Lokon-Empung volcano in Indonesia and estimated source parameters of the initial phases of explosion earthquakes to compare them to the previous works at Sakurajima volcano and Suwanosejima volcano.

Lokon-Empung volcano located in the northern part of Sulawesi island is known as one of the very active volcanoes in Indonesia. We deployed seismic and infrasound observation network around Lokon-Empung in September 2012. During about one-year-long observation, 46 events of explosion earthquakes associated with Vulcanian eruptions had been recorded. Seismograms of explosion earthquakes have common features in the initial phases at all stations; the compressional P phase arrives first, and a larger dilatational phase follows it. Comparison between seismic and infrasound record shows that the excitation of the P phase occurs about 1 second earlier than that of infrasound which is thought to be excited by the explosion at the crater. Particle motion analysis reveals that these initial phases consist of P wave and propagate from the direction of the active crater. Since signal to noise ratio of the first compressional wave (P phase) is not good at some distant stations, we focus on the second dilatational phase (D phase). We performed waveform fitting on the D phase using synthetic seismogram to estimate source depth, shape of source time function, contraction mechanism and seismic moment.

For most events, we obtained the best fitting solution with cylindrical contraction source located at 1 km below the crater. We compared the estimated seismic moment of D phase and the amplitude of seismogram and infrasound with those reported in the previous works, and found that the strength of the explosion of Lokon-Empung ranks between those of Sakurajima and Suwanosejima. At Sakurajima volcano, Tameguri et al. (2002) showed that the amplitude of infrasound is independent from the moment of D phase. On the other hand, Hirai (2013) reported a positive correlation between them at Suwanosejima volcano. Estimated focal depths of D phase at these two volcanoes are 2 km and 100 - 400 m, respectively. At Lokon-Empung volcano, we recognized a weak positive correlation between the amplitude of infrasound and the moment of D phase. The comparison suggests that the shallower focal depth of D phase becomes, the stronger the correlation between moment of D phase and strength of infrasound appears. This result we obtained here will provide a new insight into the unrevealed process between the excitation of D phase and the surface explosion.

Keywords: Vulcanian eruption, Explosion earthquake

## Recent eruptive activity at Sinabung Volcano, Northern Sumatra, Indonesia

NAKADA, Setsuya<sup>1\*</sup> ; YOSHIMOTO, Mitsuhiro<sup>2</sup> ; ZAENUDIN, Ahkmad<sup>3</sup> ; SUZUKI, Yuki<sup>1</sup> ; HOKANISHI, Natsumi<sup>1</sup> ; TAKAGI, Natsuko<sup>1</sup> ; HENDRASTO, Mochammad<sup>3</sup> ; IGUCHI, Masato<sup>4</sup> ; OHKURA, Takahiro<sup>5</sup>

<sup>1</sup>ERI, Univ. of Tokyo, <sup>2</sup>Grad. Sch. Sci., Hokkaido Univ., <sup>3</sup>CVGHM, Indonesia, <sup>4</sup>Disaster Res. Inst., Kyoto Univ., <sup>5</sup>Grad. Sch. Sci., Kyoto Univ.

Sinabung in the Northern Sumatra of Indonesia began its eruptive activity with phreatic events in August and September 2010. It resumed its activity in September 2013 with phreatic events. In November 2013, eruption columns stood about 5 km above the volcano. Volcanic ash issued since the middle November contained juvenile particles, and pumice fragments were ejected on to the NE flank of the volcano by the vulcanian event on 23 November 2013. Small-scale pyroclastic flows descended during the events. Though the eruptive activity had declined since early December, occurrence of low-frequency earthquakes replaced high-frequency events common during explosive events. Following partial collapse of the summit crater outer-slope repeated, lava appearance was confirmed in late December. Lava appeared in the summit crater grew as a dome and started its partial collapse on 30 December, generating pyroclastic flows which descended on the SE slope of the volcano. The lava dome grew into a lava flow moving to the SE, repeating its partial collapse. The horizontal length of the lava flow exceeded 1 km in late January 2014.

Several tens collapses occurred everyday in January 2014. Relatively large collapse (pyroclastic flows) generated on 7, 11 and 21 January and 1 February. Pyroclastic flows on 1 February traveled about 4.5 km, according to newspapers, and 15 local people who invaded into the danger zone, 5 km from the summit, were involved in the flows.

The present eruption at Sinabung is close to the eruption of 9 to 10th Century of this volcano in terms of both eruption site and scale. It is also similar to lava-dome eruptions at Unzen, Japan, in 1991-95 and at Soufriere Hills, Montserrat, West Indies, in 1995-present, where lava dome/flow growth associated with pyroclastic-flow events continued for several years.

Based on the chemical analyses of pumice of the Vulcanian event on 23 November 2013 and pebbles included in pyroclastic flow event on 11 January 2014, magma of this eruption (hornblende andesite) is similar to but a little poorer in SiO<sub>2</sub> (58-59%) than the magma of the 9 to 10th Century (59-60%).

Keywords: Indonesia, Sinabung, volcanic eruption, pyroclastic flow, lava flow, hornblende andesite

## Metal-silicate partitioning of U, Th, Nd, Sm at high P-T: Implications for heat and chemical budget in the core

NOMURA, Ryuichi<sup>1\*</sup>; HIROSE, Kei<sup>1</sup>; KIMURA, Jun-ichi<sup>2</sup>; CHANG, Qing<sup>2</sup>

<sup>1</sup>ELSI, Titech, <sup>2</sup>IFREE, JAMSTEC

The excess abundance of siderophile elements in the mantle has been proposed that the core was equilibrated with the mantle at ~3500 K, ~30GPa and  $fO_2 \sim \Delta IW-1$  at the Earth's formation (e.g. Righter, 2011 EPSL). Much more severe condition (>6500 K) is supposed immediately after the moon-forming giant impact based on the study of numerical simulation (e.g. Canup, 2012 Science). The occurrence of high-temperature equilibrium between the core and the mantle evoked that the early core had once incorporated heat-genic radionuclides (U, Th) and rare earth elements (e.g. Nd, Sm), which are known as highly lithophile elements, suggesting profound implications for the thermal history (Nimmo, 2007 Treatise on Geophysics) and early-formed geochemical reservoirs (e.g. sub-chondritic  $^{142}\text{Nd}/^{144}\text{Nd}$ , Boyet and Carlson, 2005 Science).

However, partitioning of these elements between liquid metal and silicate melt has been investigated only up to 20 GPa and 2500 K using multi-anvil apparatus (Malavergne et al., 2007 GCA). Here, we extended pressure and temperature conditions up to 138 GPa and 5200 K at  $\Delta IW-2-1$  using laser-heated diamond cell (LH-DAC) and field emission-type electron probe microanalyzer (FE-EPMA, JXA-8530F, JEOL) and laser-ablation inductively coupled plasma mass spectrometry (LA-ICP-MS, Kimura and Chang, 2012 JAAS). K (4wt%) and trace elements (U, Th, Nd, Sm, Hf, W, Pb) doped pyrolytic gel, and pure iron were used as starting materials. Iron-free pyrolytic gel was used as a thermal insulator. After high P-T experiments using LH-DAC, recovered samples were analyzed by FE-EPMA and LA-ICP-MS for major and trace elements, respectively. Fe and Mg were used as internal standards for metal and silicate, respectively for LA-ICP-MS. The diameter of ablated area was about 10  $\mu\text{m}$ , small enough to measure each (silicate melt/liquid metal) phase.

The results are summarized as follows;

(1) Partition coefficient of U and Th are  $10^{-3}$ - $10^{-2}$  at 3500-4000 K and  $\Delta IW-1$  to -1.5, resulting in 0.02-0.2 ppb (<0.03 TW) U and 0.08-0.8 ppb (<0.04 TW) Th into the core assuming that the abundance of U and Th are 22 and 83 ppb in the Earth's mantle (McDonough and Sun, 1995). Total <0.1 TW (present-day) heat flow in the core has negligible effect on the thermal history of the Earth with <50 K change in the initial temperature at core-mantle boundary (Nimmo, 2007 ToG).

(2) The ratio of partition coefficients,  $D_{Nd}(\text{metal/silicate})/D_{Sm}(\text{metal/silicate})$ , was always unity despite of large temperature dependence for each D, suggesting that the core could not be a candidate for an early-formed (with sub-chondritic  $^{142}\text{Nd}/^{144}\text{Nd}$ ) hidden reservoir.

## Element partitioning between mantle minerals and melt under deep lower mantle condition

TATENO, Shigehiko<sup>1\*</sup>; SAKATA, Shuhei<sup>2</sup>; HIRATA, Takafumi<sup>2</sup>; HIROSE, Kei<sup>3</sup>

<sup>1</sup>Dept. Earth & Planetary Sciences, Tokyo Institute of Technology, <sup>2</sup>Dept. Earth & Planetary Sciences, Kyoto University, <sup>3</sup>Earth-Life Science Institute, Tokyo Institute of Technology

Melting is a primary mechanism of chemical evolution of our planet. Earth's mantle would have been completely molten due to moon-forming giant impact, leading to a global magma ocean. Resultant fractional crystallization by secular cooling progressively induced the chemical evolution of the Earth. As a consequence, remnant silicate melt left at the present day at the base of the mantle is a possible explanation for the seismically observed ultralow-velocity zones (ULVZs). The knowledge of melting phase relations and element partitioning between mantle minerals and partial melt is crucial to understand the chemical evolution in the early Earth and the nature of ULVZs. However, melting experiments under the middle to deep lower mantle conditions are quite limited.

Here we carried out the melting experiments on KLB-1 peridotite and basalt to deep lower mantle conditions up to 179 GPa by a combination of laser-heated diamond-anvil cell experiments and chemical analyses of recovered samples. Textural characterization and chemical analysis on major and minor elements were made by a field-emission-type electron microprobe (FE-EPMA). Trace element abundances were determined by a laser-ablation inductively coupled plasma mass spectrometry (LA-ICP-MS). Typical crater diameter was 2 or 5  $\mu\text{m}$  by using ArF Excimer laser.

Results shows that the liquids phase was  $\text{MgSiO}_3$ -perovskite at least above 34 GPa and further to post-perovskite in KLB-1 peridotite. The Fe-Mg distribution coefficients ( $K_D$ ) between perovskite/post-perovskite and melt decreased considerably with increasing pressure, leading to strong Fe-enrichment in partial melts. It supports dense partial melts in a deep lower mantle, which migrate downward to the core mantle boundary (CMB). Furthermore,  $\text{CaSiO}_3$ -perovskite (CaPv) was found to be a liquids phase under whole lower mantle condition in MORB bulk composition. We then investigated the minor/trace element partitioning between CaPv and melt in basaltic composition. Partition coefficient of alkali elements such as Na and K increases with increasing pressure. In particular, potassium, known as highly incompatible element, become compatible with pressure, whose partition coefficient exceeded the unity at 90 GPa. Although pressure effect on  $D_{Sm}$  and  $D_{Nd}$  was not found even to 80 GPa,  $D_{Sm}/D_{Nd}$  decreases with increasing pressure and will reach to the unity at around 100 GPa. Our results shows that Sm and Nd was equally partitioned to partial melt and residual solids upon fractionation of CaPv from primordial deep magma ocean. This has profound implications for the origin of the super-chondritic  $^{142}\text{Nd}/^{144}\text{Nd}$  for all terrestrial rocks.

## Melting relation on FeO-SiO<sub>2</sub> system at high pressure and the fate of the subducted banded iron formations

KATO, Chie<sup>1\*</sup> ; NOMURA, Ryuichi<sup>1</sup> ; HIROSE, Kei<sup>2</sup> ; MIYAKE, Akira<sup>3</sup> ; OHISHI, Yasuo<sup>4</sup>

<sup>1</sup>Department of Earth and Planetary Sciences, Tokyo Institute of Technology, <sup>2</sup>Earth-Life Science Institute, Tokyo Institute of Technology, <sup>3</sup>Division of Earth and Planetary Sciences, Kyoto University, <sup>4</sup>Japan Synchrotron Radiation Research Institute

Subduction of banded iron formations (BIFs) may have played a significant role on the evolution of the core-mantle boundary (CMB) region and the chemical stratification at the topmost core. Almost all of the BIFs that had been deposited on the seafloor must have been subducted into the mantle and only a small portion was left at the surface today. Because of their high density, BIFs may have fallen down toward the CMB region. The amount of subducted BIFs is estimated to be  $2 \times 10^8$  km<sup>3</sup>, which roughly matches with the total volume of the ultra-low velocity zones (Dobson and Brodholt, 2005, *Nature*). BIFs would be composed mainly of FeO and SiO<sub>2</sub> in the lower mantle because its oxidation state is close to iron-wustite buffer. We have performed melting experiments on FeO-SiO<sub>2</sub> system by laser-heated diamond-anvil cell technique at 25 - 140 GPa. FE-EPMA and FIB-SEM chemical analysis and observation of the texture of the recovered samples revealed that the liquidus phase was SiO<sub>2</sub> when starting from Fe<sub>2</sub>SiO<sub>4</sub> fayalite, and compositions of the quenched melt suggested that the composition of the eutectic point was extremely FeO-rich (<0.6 wt% SiO<sub>2</sub>). The solidus curve was constrained by observing the existence or no-existence of tiny quenched melt pools in each recovered samples. The solidus temperature at CMB pressure was 3,100 to 3,300 K that were lower than the solidus of pyrolite and the geotherm (Nomura et al., 2014, *Science*). These results imply that when the BIFs reach the CMB, they generate FeO-rich liquid that would be mixed with the basal magma ocean (Labrosse et al., 2007, *Nature*). This liquid would form a thin layer spread along CMB and react with the topmost core. Silicon content in liquid iron varies inversely to the oxygen fugacity when equilibrium with silicate melt (Ricolleau et al., 2011 *EPSL*). Assuming silicon-rich bulk core, exchange of silicon and oxygen would occur between the topmost core and FeO-rich silicate melt. This mechanism may account for the seismic wave speed anomaly observed at the topmost core which is thought to be honor to chemical stratification (Helffrich and Kaneshima, 2010 *Nature*; Buffett and Seagle, 2010 *JGR*).

## Standardless determination of Nd isotope ratios in glasses and minerals using LA-MC-ICP-MS

KIMURA, Jun-ichi<sup>1\*</sup>; QING, Chang<sup>1</sup>; KAWABATA, Hiroshi<sup>2</sup>

<sup>1</sup>JAMSTEC, <sup>2</sup>Kochi University

We investigated an appropriate instrumental setup for a laser-ablation multiple-collector inductively coupled plasma mass spectrometer (LA-MC-ICP-MS) and found that a reduced oxide setting allowed accurate and precise analysis of Nd isotope ratios in samples with or without concomitant interfering elements. We used an Aridus II solution/excimer laser dual-intake system. The ICP interface used normal sample and skimmer cones with torch shield switched off and an additional large interface rotary pump. The setting accomplished reduced oxide levels  $\text{NdO}^+/\text{Nd}^+ 0.01\text{--}0.05\%$ , without significant sacrifice of the instrumental sensitivity ( $\sim 70\%$ ). Oxide molecular ions for the lighter elements were negligible and accurate internal mass bias corrections were achieved for both Sm and Nd using isotopic ratios derived from thermal ionization mass spectrometry measurements. This report reveals a novel setup that requires no external mass bias corrections (standardless analysis) for Sm and Nd isotope analyses by both solution- and LA-MC-ICP-MS methods. Solution analysis of La Jolla Nd standard gave a  $^{143}\text{Nd}/^{144}\text{Nd}$  ratio of  $0.511860 \pm 0.000026$ , which is in excellent agreement with the reference value (relative deviation (RD) = +6 ppm). JMC Nd standard solution yielded a  $^{143}\text{Nd}/^{144}\text{Nd}$  ratio of  $0.512216 \pm 0.000044$  (RD = -14 ppm) while a Sm-doped JMC solution showed  $0.512211 \pm 0.000030$  (RD = -23 ppm). For LA analyses, the observed ratios and RDs were  $^{143}\text{Nd}/^{144}\text{Nd} = 0.511921 \pm 0.000013$  (RD = -12 ppm) for NIST SRM 610 glass standard (430 ppm Nd/453 ppm Sm);  $0.512490 \pm 0.000018$  (RD = +14 ppm) for Durango apatite (1121 ppm Nd/147 ppm Sm);  $0.512200 \pm 0.000009$  (RD = -26 ppm) for Fish Canyon Tuff sphene;  $0.512232 \pm 0.000003$  (RD = +65 ppm) for EDR monazite; and  $0.512890 \pm 0.000147$  (RD = +34 ppm) for groundmass of a St. Helena lava (22.7 ppm Nd/ $\sim 5.01$  ppm Sm). All measurements were in good agreement with the reference values. Examinations on Sm/Nd elemental fractionation have also been made and we confirmed that this was originated from the ICP interface region rather than at laser ablation site.

Keywords: LA-MC-ICP-MS, Nd isotope, glasses, minerals

## Grain boundary diffusion of polycrystalline ice I<sub>h</sub> under confining pressure of 100 MPa

NOGUCHI, Naoki<sup>1</sup> ; KUBO, Tomoaki<sup>2\*</sup> ; DURHAM, William<sup>5</sup> ; SHIMIZU, Ichiko<sup>4</sup> ; KAGI, Hiroyuki<sup>3</sup>

<sup>1</sup>Graduate School of Engineering, Hiroshima University, <sup>2</sup>Department of Earth and Planetary Sciences, Faculty of Sciences, Kyushu University, <sup>3</sup>Geochemical Laboratory, Graduate School of Science, University of Tokyo, <sup>4</sup>Department of Earth and Planetary Science, Graduate School of Science, University of Tokyo, <sup>5</sup>Department of Earth, Atmospheric and Planetary Sciences, Massachusetts Institute of Technology

Ice I<sub>h</sub> is a primary constituent of surfaces of the icy Galilean satellites and ice sheets at the Antarctica. Thus understanding rheological behavior of ice I<sub>h</sub> will contribute to better knowledge about the dynamics and tectonics of the surface of the icy satellites and ice sheets. Stress applied by the tidal deformation to the surfaces of the icy satellites was predicted to be very low, ~1 MPa (Sotin and Tobie 2004), and diffusion and grain-size-sensitive creeps probably control the deformation of the surfaces of the ice satellites. The deformation map under such a low stress condition can be constructed, based on two diffusion constants, grain boundary and volume diffusion coefficients, of polycrystalline ice I<sub>h</sub>. The volume diffusion coefficient of ice I<sub>h</sub> was determined from experiments using a single crystal of ice I<sub>h</sub> (Ramseier 1967; Itagaki 1967), while the grain boundary diffusion coefficient has not been determined yet. Thus we carried out experiments to determine directly the grain boundary diffusion coefficient of polycrystalline ice I<sub>h</sub>.

The diffusion couples have been composed of a pair of disks of pore-free polycrystalline H<sub>2</sub>O and D<sub>2</sub>O ices. The glass beads with a diameter of 2 μm were doped in the diffusion couples to prevent the grain growth during diffusion experiments by Zener pinning effect. The volume fraction of the glass beads was approximately 1 %. The diffusion experiments were carried out under the confining pressure of 100 MPa using a gas apparatus surrounded with a cryostat (Durham et al. 2001). Temperatures were set in the range from 235 K to 256 K. After keeping the diffusion couples in the deformation instrument for 20 ~94 hours, we shaved off thin sections from the diffusion couples. Two-dimensional diffusion profiles of the thin section were determined with micro-and imaging- Raman spectroscopes and a cryo-stage. The Raman mapping or Raman imaging measurements were carried out with keeping the thin sections at -90 °C. The concentration of deuterium can be determined from the relative intensity of Raman band of OH stretching mode to that of OD stretching mode using a quantitative curve. The two-dimensional distribution showed enrichment of deuterium at the grain boundaries near the H<sub>2</sub>O/D<sub>2</sub>O boundary. It indicates that grain boundary diffusion of ice I<sub>h</sub> is rapid. The diffusion profiles obtained by the experiments enable to estimate the grain boundary diffusion coefficient of ice I<sub>h</sub>, which is essential to construct the deformation map.

Keywords: ice, diffusion, grain boundary diffusion, hydrogen isotope, Raman spectroscopy, rheology

## Trace elements and Sr-Nd isotopic compositions of the pre-Komitake volcano

SHIBATA, Tomoyuki<sup>1\*</sup> ; YOSHIMOTO, Mitsuhiro<sup>2</sup> ; FUJII, Toshitsugu<sup>3</sup> ; NAKADA, Setsuya<sup>4</sup>

<sup>1</sup>Institute for Geothermal Research, Kyoto University, <sup>2</sup>Faculty of Science, Hokkaido University, <sup>3</sup>Crisis & Environment Management Policy Institute, <sup>4</sup>Earthquake Research Institute, University of Tokyo

The chemical characteristics of magmas from pre-Komitake Volcano, which is a buried and old volcanic body beneath the northeastern flank of Mt. Fuji, show the differences to those of Mt. Fuji (Yoshimoto *et al.*, 2010). According to Yoshimoto *et al.* (2010), incompatible elements of former magmas increase with increasing SiO<sub>2</sub>, whereas those of later magmas increase at nearly constant SiO<sub>2</sub>. They emphasized that those changes of the magma chemistry at this area from 250 ka to recent may have occurred due to a change in regional tectonics around 150 ka, although this remains unproven. To elucidate this problem, geochemical study for the magmas from pre-Komitake is essential. Therefore, we analyzed trace element and Sr-Nd isotopic compositions of those magmas. The samples are selected from the entire group, which are classified by lithology and chemistry (Group 1-3, Yoshimoto *et al.*, 2010), and from 188-412m (core ERI-FJ2) and 426-624m (core ERI-FJ3) in depth. Trace elements are analyzed using by quadrupole inductively coupled plasma mass spectrometer following by the method of Chang *et al.* (2003). Sr-Nd isotopic compositions are measured by thermal ionization mass spectrometer following by the procedure of Shibata *et al.* (2007) and Yoshikawa and Shibata (2003). The enrichments of LILE's, Pb and Sr, which are general characteristics of island arc magma (eg. Wood *et al.*, 1979), are observed from the analyzed samples in the primitive mantle normalized multi-element diagram. High Sr/Y ratios (70 in max.) and the weak positive Eu anomalies ( $Eu^* = [Eu]_N / ([Sm]_N/2 + [Gd]_N/2)$ ; N means chondrite normalized value) are also found from several samples. The Sr and Nd isotope ratios show the variations from 0.703320-0.703476, and 0.512885-0.513087, respectively.

The Sr-Nd isotopic compositions of pre-Komitake volcano show a similar range of Mt. Fuji presented by Nagai *et al.* (2004), indicating that those magmas can be generated from the same source materials. Although the variations of Sr isotope compositions are small, significant differences are found. Most of the samples show similar Nd isotope ratios, whereas few samples show lower significant differences. These observations can be explained by 1) difference of slab derived fluid and 2) different degrees of crustal contaminations. It is unlikely that Nd isotope ratio of slab derived fluid is changed, because it is difficult keeping isotopic heterogeneity during the deep processes. Crustal rocks, which have similar Sr-Nd isotope ratios of Tanzawa tonalities (Kawate, 1996), are the candidate producing the whole isotopic variation of pre-Komitake volcano. Therefore, we prefer the contributions of crustal materials to explain the Sr-Nd isotopic variations of pre-Komitake volcano. The  $Eu^*$  shows positive correlation with Al<sub>2</sub>O<sub>3</sub>. This may indicate the plagioclase accumulation contributed the magma genesis of pre-Komitake volcano, and cause the elevation of Sr/Y ratios.

This study is supported by fund for collaboration from Earthquake Research Institute, The University of Tokyo.

Keywords: pre-Komitake, trace elements, Sr-Nd isotope

## Geochemical connection between HIMU-FOZO-PREMA: link to chemical and water content variation in oceanic crust

SHIMODA, Gen<sup>1\*</sup> ; KOGISO, Tetsu<sup>2</sup>

<sup>1</sup>National Institute of Advanced Industrial Science and Technology, <sup>2</sup>Graduate School of Human and Environmental Studies, Kyoto University, Kyoto

One of fundamental concepts of the geochemistry is an existence of mantle reservoirs. Namely, isotopic composition of the ocean island basalts (OIBs) are explained by mixing of distinct and isolated reservoirs in the Earth (White, 1985; Zindler and Hart, 1986; Hofmann, 1997; Stracke, 2012). In early research on the mantle reservoirs, the isotopic composition of OIBs was mainly explained by the mixing of depleted MORB mantle (DMM) and three enriched reservoirs, those are HIMU (high-u:  $u = 238\text{U}/204\text{Pb}$ ) EM1 (Enriched Mantle 1) and EM2 (Enriched mantle 2) whose isotopic compositions are enriched extremes. In addition to these reservoirs, importance of reservoirs whose isotopic compositions are common and intermediate has been pointed out, these are, FOZO (Focal Zone, Hart et al., 1992), C (common component; Hanan and Graham, 1996), PREMA (Prevalent Mantle, Zindler and Hart, 1986) and PHEM (Primitive Helium Mantle, Farley et al., 1992). Although the existences of these intermediate reservoirs are still in debated, the isotopic compositions of these reservoirs, in particular FOZO, have been frequently used to describe the isotopic distribution of OIBs. Therefore, elucidating the origin of these reservoirs should be important from the perspective of production of mantle heterogeneity (e.g., Hofmann, 1997; Stracke et al. 2005; Stracke, 2012).

To evaluate the origin of high-u (HIMU), focal zone; (FOZO) and Prevalent Mantle (PREMA), geochemical modeling was conducted from the perspective of chemical fractionation at mid-ocean ridges and subduction zones. For the modeling, MORB compositions from the Mid-Atlantic ridge are compiled for seven trace elements (Rb, Sr, Nd, Sm, Pb, Th and U) and used as representatives of oceanic crust compositions. Effect of chemical fractionation at a mid-ocean ridge is estimated based on magnesium number and frequency distribution. The results suggest that the chemical fractionation at a mid-ocean ridge can produce moderately depleted isotopic compositions those are suitable for PREMA if the age of recycled MORBs is 1-2 Ga. It may follow that subduction modification is unnecessary for the production of PREMA, suggesting the importance of recycling of dry MORBs. Dehydration process at a subduction zone can produce FOZO isotopic signatures if degree of dehydration is high (4 %) that may represent maximum amount of dehydrated water. Thus, FOZO-PREMA isotopic array can be explained by mixing between recycled strongly dehydrated and dry MORBs. Consequently, PREMA-FOZO arrays could be produced by mixing between dry and dehydrated MORBs. For the production of HIMU, U and Th enrichment during crystal fractionation at mid-ocean ridge and Pb depletion owing to removal of sulfur during subduction is required in addition to FOZO production condition. As sulfur content in MORBs should be controlled by degassing process at a mid-ocean ridge, key processes that can differentiate HIMU from FOZO may be magma evolution process at mid-ocean ridge.

Keywords: HIMU, FOZO, PREMA, OIBs, recycling, mantle reservoirs

## REY-rich mud deposits around Minamitorishima Island -General overview and future reserach plan-

SUZUKI, Katsuhiko<sup>1\*</sup> ; IIJIMA, Koichi<sup>1</sup> ; KATO, Yasuhiro<sup>2</sup> ; FUJINAGA, Koichiro<sup>2</sup> ; KASHIWABARA, Teruhiko<sup>1</sup> ; NAKA-MURA, Kentaro<sup>2</sup> ; MACHIDA, Shiki<sup>3</sup> ; NOZAKI, Tatsuo<sup>1</sup> ; TAKAYA, Yutaro<sup>2</sup> ; YASUKAWA, Kazutaka<sup>2</sup> ; OTA, Junichiro<sup>2</sup> ; HARAGUCHI, Satoru<sup>2</sup> ; ARAKI, Shuuhei<sup>2</sup> ; LIU, Hanjie<sup>2</sup> ; NISHIO, Yoshiro<sup>1</sup> ; USUI, Yoichi<sup>1</sup>

<sup>1</sup>JAMSTEC, <sup>2</sup>Graduate School of Engineering, Univ. of Tokyo, <sup>3</sup>School Creative Sci. Engineering, Waseda Univ.

We report general overview and future reserach planof REY-rich deposits around Minamitorishima Island.

Keywords: REY rich mud, Minamitorishima Island, chemical composition, research cruise, deep-sea mineral resource

## Distribution and characteristics of REY-rich mud in the Minamitorishima EEZ inferred by sub-bottom profiling

NAKAMURA, Kentaro<sup>1\*</sup>; MACHIDA, Shiki<sup>2</sup>; FUJINAGA, Koichiro<sup>1</sup>; KATO, Yasuhiro<sup>3</sup>; SUZUKI, Katsuhiko<sup>4</sup>; TAKAYA, Yutaro<sup>3</sup>; YASUKAWA, Kazutaka<sup>1</sup>; OTA, Junichiro<sup>1</sup>; HARAGUCHI, Satoru<sup>1</sup>; ARAKI, Shuuhei<sup>1</sup>; LIU, Hanjie<sup>1</sup>; USAMI, Ryo<sup>1</sup>; MAKI, Ryota<sup>1</sup>; IIJIMA, Koichi<sup>4</sup>; NISHIO, Yoshiro<sup>4</sup>; USUI, Yoichi<sup>4</sup>; NOZAKI, Tatsuo<sup>4</sup>; MR13-E02 LEG 2, Cruise members<sup>4</sup>; KR14-02, Cruise members<sup>4</sup>

<sup>1</sup>Sys. Innovation, Univ. of Tokyo, <sup>2</sup>School Creative Sci. Engineering, Waseda Univ., <sup>3</sup>FRCER, Univ. of Tokyo, <sup>4</sup>JAMSTEC

In recent years, particular attention has been paid to the "REY-rich mud" (deep-sea sediment enriched highly in rare-earth and yttrium (REY)), because of its high potential as a REY resource. The REY-rich mud was originally reported from the central Pacific Ocean in 2011 (Kato et al., 2011). In January 2013, during KR-13-02 cruise, the mud was also discovered at southern part of the Minamitorishima within the Japanese exclusive economic zone (EEZ) (Kato et al., 2013; Fujinaga et al., 2013; Suzuki et al., 2013). Then, in the late 2013 and early 2014, we further conducted two more research cruises (MR13-E02 Leg2 and KR14-02 cruises) in the northern and eastern part of the Minamitorishima EEZ. During the cruises, we performed an acoustic survey using sub-bottom profiler (SBP), together with mud sampling by piston coring. In this presentation, we report the distribution and characteristics of the REY-rich mud in the northern and eastern part of Minamitorishima EEZ inferred by the SBP survey.

Keywords: rare-earth elements, REY-rich mud, Minamitorishima, EEZ, sub-bottom profiler

## Geochemical features of rare-earth elements and yttrium-rich mud from north region of Minamitorishima EEZ

FUJINAGA, Koichiro<sup>1\*</sup> ; KATO, Yasuhiro<sup>1</sup> ; NAKAMURA, Kentaro<sup>2</sup> ; SUZUKI, Katsuhiko<sup>3</sup> ; MACHIDA, Shiki<sup>4</sup> ; TAKAYA, Yutaro<sup>1</sup> ; YASUKAWA, Kazutaka<sup>2</sup> ; OTA, Junichiro<sup>2</sup> ; HARAGUCHI, Satoru<sup>1</sup> ; ARAKI, Shuuhei<sup>2</sup> ; LIU, Hanjie<sup>2</sup> ; USAMI, Ryo<sup>2</sup> ; MAKI, Ryota<sup>2</sup> ; IJIMA, Koichi<sup>3</sup> ; NISHIO, Yoshiro<sup>3</sup> ; USUI, Yoichi<sup>3</sup> ; NOZAKI, Tatsuo<sup>3</sup> ; MR13-E02 LEG2, Cruise members<sup>3</sup> ; KR14-02, Cruise members<sup>3</sup>

<sup>1</sup>Frontier Research for Energy and Resources, University of Tokyo, <sup>2</sup>Department of Systems Innovation, University of Tokyo, <sup>3</sup>JAMSTEC, <sup>4</sup>Department of Resources and Environmental Engineering, Waseda University

Recently, deep-sea sediment enriched in rare-earth elements and yttrium (REY) (called REY-rich mud) has been reported from a central part of the Pacific Ocean (Kato et al., 2011). Due to its great potential as a completely new REY resource, the REY-rich mud attracts particular attention from a wide field of scientists and non-scientists. In 2013, we have discovered the deep-sea sediments that are extremely enriched in REY (~6,600 ppm) from the south region of the Minamitorishima within the Japanese exclusive economic zone (EEZ) (Kato et al., 2013; Fujinaga et al., 2013; Suzuki et al., 2013). In 2014, in order to investigate the detailed distribution of REY-rich mud in the EEZ of Minamitorishima, we further conducted research cruises (MR13-E02 Leg. 2 and KR14-02) in the north region of the Minamitorishima. Here, we report the distribution, mineral composition, and geochemical features of the REY-rich mud from the north region of the Minamitorishima EEZ.

Keywords: rare earth elements (REEs), REY-rich mud, Minamitorishima, deep-sea mineral resource

## Independent component analysis to decouple geochemical components of REY-rich mud in the Pacific and Minamitorishima EEZ

YASUKAWA, Kazutaka<sup>1\*</sup> ; TAKAYA, Yutaro<sup>2</sup> ; OTA, Junichiro<sup>1</sup> ; FUJINAGA, Koichiro<sup>1</sup> ; NAKAMURA, Kentaro<sup>1</sup> ; KATO, Yasuhiro<sup>2</sup> ; IWAMORI, Hikaru<sup>3</sup>

<sup>1</sup>Sys. Innovation, Univ. of Tokyo, <sup>2</sup>FR CER, Univ. of Tokyo, <sup>3</sup>JAMSTEC

Rare-earth elements and yttrium (REY) are essential for state-of-the-art devices and green technologies including electric vehicles, fiber optics, smart phones, wind power generation etc. Recently, the deep-sea sediments enriched in REY (termed as "REY-rich mud") have been discovered in the Pacific Ocean, which have great potential as a completely new REY resource (Kato et al., 2011). In 2013, the presence of REY-rich mud was also confirmed within the Japanese exclusive economic zone (EEZ) around Minamitorishima (Fujinaga et al., 2013; Suzuki et al., 2013). The maximum total REY content in the REY-rich mud from Minamitorishima EEZ reaches as high as 6,600 ppm, although typical REY-rich mud in other regions of the Pacific Ocean contains less than 2,230 ppm of total REY.

In order to elucidate a component contributing to REY-enrichment in the sediments, Kato et al. (2011) performed independent component analysis (ICA) on the geochemical data set of Pacific deep-sea sediments. ICA is a relatively new multivariate statistical method established in 1980s, which can extract original independent source signals or factors from observed signals based on an assumption that the observed multivariate data are mutually independent but do not form a multivariate normal (Gaussian) distribution (Hyvärinen et al., 2001).

Four independent components (ICs) were found by Kato et al. (2011): two diluting components corresponding to biogenic carbonate and silica, and two components toward high REY contents with Fe and Al values, respectively. Kato et al. (2011) interpreted that the Fe- and Al-rich ICs that are responsible for the REY-enrichment of the mud correspond to end-member minerals of Fe-oxyhydroxide and phillipsite, respectively. Recently, however, X-ray absorption fine structure (XAFS) analysis and  $\mu$ -XRF elemental mapping using high-energy synchrotron radiation revealed that most of REY are directly bonded to apatite in the REY-rich mud (Toda, 2013; Kashiwabara et al., 2014).

Here, we analyze a new comprehensive geochemical data set of deep-sea sediments from the Pacific Ocean and Minamitorishima EEZ by ICA. In this calculation, we utilize the new chemical composition data of individual crystals of phillipsite and apatite measured by LA-ICP-MS as new end-members for the ICA analysis. We will discuss the results and interpretation of our new analysis.

### – References –

- Fujinaga, K. et al. (2013) *JpGU Meeting 2013*.  
Hyvärinen, A. et al. (2001) *Independent Component Analysis*. John Wiley and Sons.  
Kashiwabara, T. et al. (2014) *Chemistry Letters*, **43**, 199-200.  
Kato, Y. et al. (2011) *Nature Geoscience*, **4**, 535-539.  
Suzuki, K. et al. (2013) *JpGU Meeting 2013*.  
Toda, R. (2013) Master's thesis, Univ. Tokyo.

Keywords: deep-sea sediment, REE, independent component analysis

## Mineralogical features of REY-rich mud in EEZ around Minamitorishima and implications for its genesis

OTA, Junichiro<sup>1\*</sup>; TAKAYA, Yutaro<sup>2</sup>; FUJINAGA, Koichiro<sup>2</sup>; YASUKAWA, Kazutaka<sup>1</sup>; NAKAMURA, Kentaro<sup>1</sup>; MACHIDA, Shiki<sup>3</sup>; HARAGUCHI, Satoru<sup>1</sup>; KATO, Yasuhiro<sup>2</sup>

<sup>1</sup>Department of Systems Innovation, University of Tokyo, <sup>2</sup>Frontier Research Center for Energy and Resources, University of Tokyo, <sup>3</sup>Department of Resources and Environmental Engineering, Waseda University

The KR13-02 cruise was conducted in the southern part of the Minamitorishima to explore rare-earth elements and yttrium-rich mud (REY-rich mud) within Japanese Exclusive Economic Zone (EEZ) on January 2013. During the cruise, seven sediment cores were successfully collected. The results of bulk sediment analyses showed that one of the cores (PC05) has an extremely REY-concentrated layer with 6,596 ppm total REY (Kato et al., 2013; Suzuki et al., 2013) which is three times higher than the maximum concentration in the mud previously reported for the eastern South and central North Pacific Ocean (2,230 ppm; Kato et al., 2011). In addition to REY, P concentration in the layer is also noticeably high (Kato et al., 2013; Suzuki et al., 2013), suggesting that Ca phosphate (apatite) is mainly responsible for the REY-enrichment in the layer, as in the case for the mud presented in other areas (Kashiwabara et al., 2014). However, factors contributing the extreme enrichment of REY, which in turn might provide important insights into the genesis of REY-rich mud, are still uncertain. In the present contribution, we report mineralogical features of Minamitorishima REY-rich mud including the extremely REY-concentrated layer and discuss about its genesis.

Keywords: rare-earth elements (REEs), REY-rich mud, deep-sea mineral resource

## Helium and halogen compositions in MORB vesicles

KAGOSHIMA, Takanori<sup>1\*</sup>; TAKAHATA, Naoto<sup>1</sup>; SANO, Yuji<sup>1</sup>

<sup>1</sup>Atmosphere and Ocean Research Institute, University of Tokyo

Degassing behavior of halogens through submarine volcanism is not well understood. We determined helium and halogen compositions of MORB vesicles to constrain halogen flux at ridges. Samples collected at 8 sites (13oN-17oS on EPR; 15oN-37oN on MAR; 24-25oS on CIR) were crushed in dilute NaOH or NH<sub>3</sub> solution at liquid nitrogen temperature and volatiles were extracted from vesicles. Helium isotope compositions were determined with a VG-5400 MS and F and Cl contents were measured with ICS-2100 ion chromatography. For glass matrix, concentration of F and Cl were determined with a NanoSIMS.

For vesicles, the average <sup>3</sup>He concentration was  $(4.5 \pm 2.1) \times 10^{-15}$  mol/g of sample and the average F/<sup>3</sup>He and Cl/<sup>3</sup>He ratios were  $(1.4 \pm 0.5) \times 10^6$  and  $(2.9 \pm 0.6) \times 10^7$ . This provides F and Cl flux of  $(7.1 \pm 2.8) \times 10^8$  mol/y and  $(1.5 \pm 0.4) \times 10^{10}$  mol/y at ridges calibrating against the known <sup>3</sup>He flux of 530 mol/y. They may be defined as lower limits of MOR flux because F and Cl contents in glass matrix are >7000 and >100 times higher than those in vesicles and dissolution of only a small part of volatiles staying in oceanic crust into the ocean will increase volatile flux significantly. The large difference between F/Cl ratios in vesicles and glass matrix reflects difference in vesicle/glass partition coefficients of these elements, which suggests that they have significantly different degassing behavior at ridges. From the data of the noble gas method on MORB in literature, Br/Cl and I/Cl ratios in vesicles were calculated to be  $(1.8 \pm 0.1) \times 10^{-3}$  and  $(5.4 \pm 0.1) \times 10^{-5}$  which are almost equivalent with those in glass matrix [1], suggesting their vesicle/glass partition coefficients are similar in submarine basaltic magma. Br and I flux at ridges were calculated to be  $(2.7 \pm 0.8) \times 10^7$  mol/y and  $(8.3 \pm 2.4) \times 10^5$  mol/y based on the Cl flux estimated in this study. They are the first estimate of Br and I flux obtained by indirect calibration against <sup>3</sup>He flux and may be lower limits of MOR flux by the same reason as Cl. Combination of the method in this study and the noble gas method on the same sample will give us new insight into degassing behavior and geochemical cycles of halogens.

Reference: [1] Kendrick et al. (2012) GCA 81, 82-93.

Keywords: Mid-ocean ridge basalt, Helium, Halogen, Flux, Geochemical cycle

## Magmatic process of Cretaceous plutonic complex in Ikoma mountains, SW Japan

KOIZUMI, Naoko<sup>1\*</sup> ; OKUDAIRA, Takamoto<sup>1</sup> ; OGAWA, Daisuke<sup>1</sup>

<sup>1</sup>Osaka City University

The Ikoma gabbroic complex is one of the largest Cretaceous mafic pluton in SW Japan are exposed at Ikoma mountains, consisting of mafic rocks (the Ikoma gabbroic rocks) and intermediate to felsic rocks, the Fukihata tonalites and the Kyuanji quartz diorites. These rocks show three modes in whole-rock compositional relation, 1) as Plagioclase (Pl) cumulate, 2) as Hornblende-plagioclase (Hbl-Pl) cumulate and 3) as Hornblende (Hbl) gabbronorite.

The SiO<sub>2</sub> contents of the Ikoma gabbroic complex show 44 to 63 wt.%. Plagioclase cumulate and Hbl-Pl cumulate with SiO<sub>2</sub><50wt.%, their major oxide contents change widely for SiO<sub>2</sub> contents. Hbl gabbronorite are mafic to intermediate with SiO<sub>2</sub>>50wt.%, major oxide contents show linear trends with respect to SiO<sub>2</sub> contents on compositional variation diagrams.

Plagioclase cumulate shows cumulus structure and consists of mainly Ca-rich plagioclase (An<sub>85-90</sub>). On the compositional variation diagrams, plagioclase compositions included in Plagioclase cumulate is located to the end-member on the trend of Plagioclase cumulate. Moreover, their plagioclase mode are shown by a positive trend with respect to the variation of CaO contents. It suggests that Plagioclase cumulates were associated with the accumulation of plagioclase. On the other hand, plagioclase compositions in Hbl-Pl cumulate and Hbl gabbronorite are Ca-poor (An<sub>70-75</sub>). It suggests Hbl-Pl cumulate and Hbl gabbronorite occur after forming Plagioclase cumulate. Whole-rock compositions of the Ikoma gabbroic complex vary linearly with increasing SiO<sub>2</sub> contents, and their <sup>87</sup>Sr/<sup>86</sup>Sr initial ratios at 82 Ma show a positive trend with variation of SiO<sub>2</sub> contents. These characteristics suggest a mixing of mafic magma and felsic materials. The mafic end-member is mafic magma of Ikoma gabbroic complex. Granitoids occurred at the same time of the activity of the Ikoma gabbroic complex are plotted on the extrapolation of the compositional trend of Hbl gabbronorite, but their <sup>87</sup>Sr/<sup>86</sup>Sr initial ratios at 82 Ma is too low as the felsic end-member in a mixing. It is suggesting that the felsic end-member may not be the granitoids, but other crustal materials.

Keywords: Ryoke belt, Magmatic process, cumulate, accumulation

## Volatile compositions of apatite grains from pyroclastic flow deposits of Aso volcano

DOKYU, Marie<sup>1\*</sup> ; KOGISO, Tetsu<sup>1</sup>

<sup>1</sup>Graduate School of Human and Environmental Studies, Kyoto University

Water in the Earth is important for life and mantle dynamics. The amount of water in the early Earth is one of the most essential constraints for revealing the origin of the Earth's water.

An important clue to the water budget in the early Earth is apatite inclusions in ~4.4 Ga zircon from Jack Hills in Australia. Because apatite has volatile components, it is expected to determine the amount of water in the interior of the early Earth from OH composition of the Jack Hills apatite. However, partitioning of OH between apatite and melt is unclear.

We analyzed volatile compositions of apatite grains from pyroclastic flow deposits of Aso volcano in order to reveal the relationship between OH composition of apatite and H<sub>2</sub>O composition of melt. The H<sub>2</sub>O concentrations in the host magma have been estimated from those of melt inclusions in plagioclase phenocrysts. It shows that mafic melt contains more H<sub>2</sub>O than silicic melt does. F concentrations in apatite in each sample show large variations while Cl concentrations are constant, suggesting that F and OH substitute for each other. OH concentration in apatite of mafic sample was larger than that of silicic one, that is, OH concentration in apatite and amount of H<sub>2</sub>O in melt show negative correlation.

The negative correlation would have been caused by difference in Ca content between mafic and silicic samples. It is possible that Ca in melt combines F and affect partitioning F between apatite and melt (Mathez and Webster, 2005). Mafic melt contains more Ca than silicic melt and Ca may disturb partitioning F for apatite and OH concentration can be increase in apatite. Another possibility is that the water compositions of melt inclusions do not represent those in the host melt. The melt inclusions have many bubbles, and the more bubbles they have, the less H<sub>2</sub>O they contain. It means that H<sub>2</sub>O in melt inclusions was lost to the bubbles, resulting in underestimation of water contents in the host melt. Actually another study calculated the amounts of H<sub>2</sub>O in the mafic and silicic melts of the Aso pyroclastic flow and results were 4.1-7.7wt% and 4.1-5.7wt% respectively (Kaneko et al., 2007). If these results are correct, then OH concentration in apatite and the amount of H<sub>2</sub>O in melt are positively correlated.

Range of the amount of F and OH in each sample could mean that melt composition gradually changed by degassing or/and crystallization differentiation. For precise determination of OH partitioning between apatite and melt, it is necessary to reveal the effect of Ca or other components to partitioning behavior of volatile components between apatite and melt.

Keywords: apatite, water, volatile component, the early Earth, magma

## Measuring osmium isotopic composition of natural polycrystalline diamond (carbonado) and implications for its origin

SHIRAISHI, Noriko<sup>1\*</sup> ; SENDA, Ryoko<sup>2</sup> ; KAGI, Hiroyuki<sup>1</sup> ; SUMINO, Hirochika<sup>1</sup> ; SUZUKI, Katsuhiko<sup>2</sup>

<sup>1</sup>Geochemical Research Center, Graduate School of Science, University of Tokyo, <sup>2</sup>Institute for Research on Earth and Evolution, Japan Agency for Marine-Earth Science and Technology

The origin of natural polycrystalline diamond, carbonado, has long been enigmatic. Carbonado is characterized as high porosity, no genetic relations to kimberlites, light carbon isotope ratio, and lack of mantle-derived mineral inclusions. Based on these observations, several hypotheses about the origin of carbonado have been proposed: transformation of subducted organic carbon into diamond in a cold slab (Robinson, 1978); shock metamorphism of organic carbon by meteorite impact (Smith and Dawson, 1985); radiation-induced diamond formation by spontaneous fission of uranium in crustal environment (Ozima *et al.*, 1991); formation in an interstellar environment (Garai *et al.*, 2006); crystallization from C-O-H fluid in cratonic upper mantle (Ishibashi *et al.*, 2012). However, no conclusive evidence has been provided to settle a controversy about the origin of carbonado. In this study, we first tried to measure Os isotopic composition of carbonados collected from placer deposits in the Central African Republic in order to identify its origin.

Natural samples have a wide variety of Os isotopic ratios,  $^{187}\text{Os}/^{188}\text{Os}$ , depending on their origin because  $^{187}\text{Re}$ , the parent nuclide of radiogenic  $^{187}\text{Os}$ , is a mildly incompatible element during mantle melting whereas Os is a strongly compatible element.  $^{187}\text{Os}/^{188}\text{Os}$  ratio of upper continental crust ranges from 1.0 to 1.4 (Peucker-Ehrenbrink and Jahn, 2001), whereas that of primitive upper mantle is about 0.13 (Meisel *et al.*, 1996). Os isotopic ratio of the micro diamond crystal itself can reflect the environment where diamond grains crystallized. Carbonado is a porous aggregate of micrometer-size diamond crystals and original chemical characteristics of the grain boundaries could be heavily altered after the diamond growth.

This study was designed to determine Os isotopic ratios within diamond crystals of carbonados and in the grain boundaries separately. Two-step sample chemical leaching was carried out by Carius tube method (Shirey and Walker, 1995). First, carbonado samples were crushed to submillimeter grains and were sealed in a Carius tube with spike solutions and inverse aqua regia ( $\text{HCl} + 3 \text{HNO}_3$ ). The solution was heated at 220 °C for 24 hours. This procedure was for extract Os in the grain boundaries. Second, the residue of solid samples was heated in a vacuum chamber to convert diamond to graphite. A graphitized sample was decomposed in acid solution in the same way as the first leaching process. The second process was to extract Os within diamond grains. Osmiums in the both solutions were purified with the solvent extraction (Cohen and Waters, 1996) and microdistillation (Roy-Barman, 1993). Osmium isotopic compositions of the samples were determined using thermal ionization mass spectrometry (TIMS). Blank levels of Carius tubes and inverse aqua regia solutions prepared from several chemical reagents were checked. As a result, a quartz glass tube was found to have the lowest blank level compared with other glass tubes made from borosilicate glass.

In the presentation, we will report preliminary results of Os isotopic ratios of the carbonado, which have the potential for a decisive evidence to close the debate on the origin of carbonado.

Keywords: carbonado, TIMS, Os isotope, diamond

## High-pressure high-temperature phase transitions in $\text{ZnTiO}_3$

ABE, Kohei<sup>1\*</sup>; KOJITANI, Hiroshi<sup>1</sup>; AKAOGI, Masaki<sup>1</sup>

<sup>1</sup>Department of Chemistry, Gakushuin University

It is widely accepted that perovskite-type  $\text{MgSiO}_3$  is the most abundant mineral in Earth's lower mantle. Ilmenite-type  $\text{MgSiO}_3$  transforms to perovskite at 23 GPa and 1600 °C. It was reported that ilmenite-type  $\text{ZnTiO}_3$ , an analogue to ilmenite-type  $\text{MgSiO}_3$ , decomposes into  $\text{ZnO}$  and  $\text{TiO}_2$  at about 20-25 GPa (Ito and Matsui, 1979). However, phase relations in  $\text{ZnTiO}_3$  have not been studied yet in detail. Therefore, we investigated the phase relations in  $\text{ZnTiO}_3$  by high-pressure high-temperature experiments.

A starting material of ilmenite-type  $\text{ZnTiO}_3$  was synthesized by heating a mixture of  $\text{ZnO}$  and  $\text{TiO}_2$  with 1:1 mol ratio at 800 °C for 32 hours in air. High-pressure phase relation experiments were made by using a Kawai-type 6-8 multi-anvil apparatus in the pressure and temperature ranges of 13-35 GPa and 1000-1400 °C, respectively. After keeping the starting sample at desired conditions for 1-2 hours, the samples were quenched, and then decompressed to ambient pressure. Recovered samples were identified by using the powder X-ray diffraction method.

We found that the recovered samples which were compressed between 15 and 20 GPa at 1000-1400 °C had the  $\text{LiNbO}_3$ -type (LNO) structure. The ilmenite-LNO phase boundary was determined as  $P(\text{GPa})=19.9-0.0038T(^{\circ}\text{C})$ .  $\text{FeTiO}_3$  ilmenite which is an analogue to ilmenite-type  $\text{MgSiO}_3$  transforms to perovskite above 15 GPa, and the perovskite transforms to the LNO-type structure during decompression (Ming et al., 2006). The ilmenite-perovskite phase boundary in  $\text{FeTiO}_3$  has a negative slope which is caused by a positive entropy change for the transition due to increase of coordination number of divalent cation from 6 to 8. If the LNO-type  $\text{ZnTiO}_3$  is a stable phase, the slope of the boundary should be positive because of no change in the coordination number of the divalent cation. Therefore, the negative slope of the boundary implies that the recovered LNO-type  $\text{ZnTiO}_3$  was originally perovskite-type at 15-20 GPa.

The recovered samples synthesized above 20 GPa were identified to be an assembly of wurtzite-type  $\text{ZnO}$  and  $\alpha\text{-PbO}_2$ -type  $\text{TiO}_2$ . The post-perovskite phase boundary in  $\text{ZnTiO}_3$  is determined as  $P(\text{GPa})=9.5-0.010T(^{\circ}\text{C})$ . Wurtzite-type  $\text{ZnO}$  transforms to NaCl-type at about 6 GPa (Kusaba et al., 1999). Also,  $\alpha\text{-PbO}_2$ -type  $\text{TiO}_2$  transforms to baddeleyite-type at about 17 GPa (Tang and Endo, 1993). Therefore, we suggest that the phase assembly of NaCl-type  $\text{ZnO}$  and baddeleyite-type  $\text{TiO}_2$  is stable above 20 GPa.

Keywords:  $\text{ZnTiO}_3$ , Perovskite,  $\text{LiNbO}_3$ , High pressure

## Quantitative multi-element imaging of geological materials by femto-second LA-ICP-MS

CHANG, Qing<sup>1\*</sup> ; KIMURA, Jun-ichi<sup>1</sup>

<sup>1</sup>Japan Agency for Marine-Earth Science and Technology

Elemental mapping analysis of geological materials using X-ray related methods (EPMA, XRF) or SIMS suffers from insufficient sensitivity and poor quantification. LA-ICP-MS has advantages of high sensitivity and less matrix effect, therefore has been developed for elemental and isotopic imaging analyses over the last decade. However, quantification problem by this method remains unsolved because of the lack of a suitable sampling volume correction method and necessity of matrix-matched standard. This work presents multi-element imaging/mapping analysis of orthopyroxene and plagioclase minerals by femto-second LA-ICP-MS using a novel normalization process. Laser sampling volume is corrected for by analyzing ten major elements (SiO<sub>2</sub>, TiO<sub>2</sub>, Al<sub>2</sub>O<sub>3</sub>, FeO, MnO, MgO, CaO, Na<sub>2</sub>O, K<sub>2</sub>O, and P<sub>2</sub>O<sub>5</sub>) followed by normalization of the analyzed total sum to 100 wt% to obtain correction factor. This correction method is free from any external analysis (e.g., EPMA) for at least one internal standard element (e.g. Ca), and can be applied for both spot and line scanning LA mode. This allows LA-ICP-MS method standalone and liberates from errors inherited from any local heterogeneity of the samples picked up differently by the different analytical techniques used. Use of USGS basalt glass as a standard eliminates matrix effect in the levels less than 10% RD for these silicate minerals. Two-dimensional elemental distribution images of 43 elements were acquired from 4-6 μm depth of the sample surface with a ~40 μm lateral resolution. An area of 500×500 μm can be scanned simultaneously for 43 elements in less than 2.3 hours. Trace elements in silicate minerals can be imaged at sub-ppm concentration level, while major elements were mapped at sub-percent concentration.

Key words: femto-second LA-ICP-MS, elemental mapping, minerals

## Applicability of fictitious domain method in data processing of marine CSEM exploration

KUSUDA, Kei<sup>1\*</sup> ; MIKADA, Hitoshi<sup>1</sup> ; GOTO, Tada-nori<sup>1</sup> ; TAKEKAWA, Junichi<sup>1</sup>

<sup>1</sup>Graduate School of Engineering, Kyoto University

Marine controlled-source electromagnetic (CSEM) survey, one of the electro-magnetic (EM) sounding methods, is considered as a technique in practice for the exploration of hydrocarbon resources including methane hydrate (MH). In the analysis of EM field acquired in CSEM survey, forward modeling is used to model sub-seafloor structure. In the forward modeling, transforming the diffusive Maxwell equation to a fictitious wave domain reduces CPU time (Mittet, 2010). Phase velocities of electromagnetic waves are a function of material properties, i.e., electric conductivity and magnetic permeability. In the fictitious domain, the difference in the phase velocity as a function of materials is exaggerated so that EM field could propagate in the earth with much slower apparent phase velocity compared to the other field propagating through materials above seafloor. However, such character of the fictitious wave domain has not been well exploited for the estimation of subsurface resistivity structure. In the present study, we examine whether the received waveforms in the fictitious wave domain could highlight MH responses better than in the diffusive domain. We conduct numerical simulations using a three-dimensional resistivity model composed of seawater and earth layers, and a thin MH zone of a rectangular shape. Our results show that the sensitivity to the MH response in the received waveform is improved in the fictitious domain. It is mainly due to the separation of EM waves travelling with different phase velocities through the sub-seafloor layers and seawater in the fictitious domain. We then tested to see if the transform from the diffusive domain (e.g., observed EM field) to the fictitious wave domain is possible or not for further utilization of the transform. As a result of the singular value decomposition method to achieve the transform, the transforming EM waves in the fictitious domain indicated that the sensitivity to MH becomes about twice as much than the original EM field in the diffusive domain.

Keywords: CSEM, Fictitious wave domain, methane hydrate

## Subsurface imaging with EM migration of magnetic fields from multiple frequencies

HYODO, Daisuke<sup>1\*</sup> ; GOTO, Tada-nori<sup>1</sup> ; MIKADA, Hitoshi<sup>1</sup> ; TAKEKAWA, Junichi<sup>1</sup>

<sup>1</sup>Kyoto University

These days, the supply of water is facing a crisis due to the dramatic growth of population, industrialization, etc. As a result, the groundwater demand is becoming more and more stronger than before. Electrical prospecting is a method usually attempted for groundwater exploration, but setting the observation equipment in desert regions, where water shortage is a serious problem, causes us difficulty using this method there, since there is nothing that assures electrical contact between electrode and the earth. In these circumstances, some other methods that do not require any contact of electrode are needed. VLF or ULF is the method that satisfies the condition. However, none of these methods could provide information necessary to locate groundwater and it is strongly necessary to locate water head of survey areas. There is some shortcomings in the present processing of these VLF and ULF data. In this study, the phase-shift method, which is used in seismic migration, is applied to the horizontal magnetic components with multiple frequencies in order to image subsurface resistivity structures to locate groundwater. The survey is conducted more easily and shortly, if only the magnetic sensors above the surface are enough for estimating the structures. As in the seismic migration, both upward/downward imaging and the exploding reflector concepts can be applied to the horizontal magnetic components. The synthetic data examples show that the migration method is effective for imaging the conductive anomaly. However, it is necessary to select appropriate frequency bands in order to estimate correct subsurface structures. We conclude that this technique gives an approximate resistivity structures quickly and that the migration of magnetic components is expected to provide information on the subsurface. This method is also useful for geological interpretations and for an initial model of the more complicated inversion method.

Keywords: electromagnetic exploration, migration, apparent resistivity structure

## Application of particle method to forward modeling of marine controlled-source electromagnetic survey

IMAMURA, Naoto<sup>1\*</sup> ; GOTO, Tada-nori<sup>1</sup> ; TAKEKAWA, Junichi<sup>1</sup> ; MIKADA, Hitoshi<sup>1</sup>

<sup>1</sup>Kyoto University, Graduate School of Engineering

A new marine controlled-source electromagnetic (MCSEM) forward simulation is presented in this study. The benefit of the method is the better treatment of complicated seafloor topography and/or buried structures than before. Here, we focused on the moving particle semi-implicit (MPS) method. In our method, the Maxwell's equations are discretized with particle arrangement without grid structure, which is usually used in finite-difference method (FDM). Each particle denotes the three components of electromagnetic fields at each particle. MPS method has some advantages over the other methods such as finite-element method (FEM), FDM, integral method (IE), etc. An obvious advantage of this approach is a numerical model that can flexibly form arbitrary topography shapes. Although FEM is sometimes employed to treat the topographic structure, especially for MCSEM, pre-process for creating grid or mesh structures require a time-consuming procedure especially in three-dimensional cases. A second advantage is that the three components of electric field and electric current as well as magnetic field and source are defined at the same location of every particle, while not at the same location in the case of Yee's grid.

We tested our three dimensional MCSEM forward simulation using the particle method and confirmed that the accuracy of the forward simulation with the simple tilted layered model would be improved. Our forward modeling results show the accuracy sufficient to discuss with the analytical results. The local and arbitrary refinement of particle is conducted to obtain more accurate result using the same model. The local refinement is applied only near the transmitter and receiver dipoles. The accuracy of MPS becomes higher in the local refinement than in the use of isodiametric particles. Our results suggest that the method using MPS with locally refined particles is useful for the forward simulation of electromagnetic field with arbitrary topography in the MCSEM modeling.

Keywords: Marine controlled-source electromagnetic, Forward simulation, Particle method

## Simultaneous inversion of self-potential for estimating hydraulic parameters and streaming current coefficient

OZAKI, Yusuke<sup>1\*</sup> ; MIKADA, Hitoshi<sup>1</sup> ; GOTO, Tada-nori<sup>1</sup> ; TAKEKAWA, Junichi<sup>1</sup>

<sup>1</sup>Graduate School of Engineering, Kyoto University

In this study, we develop an inversion scheme for the simultaneous estimation of hydraulic conductivity, streaming current coefficient and specific storage, using transient self-potential (SP) data. SP is a natural electrical potential, which is thought to be caused by subsurface fluid flow through the electro-kinetic coupling. Recently, several SP measurements are performed during pumping tests to characterize the parameters of the aquifer. Almost of all SP analysis methods are adaptable to the static SP data, but a huge amount of the transient SP data is not used efficiently. Therefore, we develop an inversion scheme for the analysis of transient SP data. The electrical conductivity, streaming current coefficient, hydraulic conductivity and specific storage are parameters effectively influencing the SP profile on the surface, and can be solved in the inversion. The distribution of electrical conductivity structure can be used if the electrical resistivity tomography (ERT) or other EM measurements are performed with the SP measurement. We employ the relationship between hydraulic conductivity and streaming current coefficient to decrease the number of estimating model parameters, and to enable the simultaneous estimation of hydraulic conductivity and streaming current coefficient. First in this study, we check the sensitivities of the hydraulic conductivity and specific storage obtained at different times. The sensitivities of the hydraulic conductivity and specific storage are different with respect to the phase. The simultaneous inversion of hydraulic conductivity and specific storage from the transient SP profile is turned out possible from the difference in phase. Finally, we apply our inversion scheme to a synthetic SP profile, and reconstruct the subsurface structure of hydraulic conductivity, streaming current coefficient and specific storage simultaneously. As a result, our inversion technique allows us to obtain the hydraulic parameters from SP data on the ground surface, although the conventional hydraulic tomography strongly relies on the borehole data.

Keywords: Self potential, Inversion, Time domain, Hydraulic conductivity, Specific storage, Streaming current coefficient

## Numerical study for failure behavior of rock masses including complex free-surfaces using a particle method

TAKEKAWA, Junichi<sup>1\*</sup> ; MIKADA, Hitoshi<sup>1</sup> ; GOTO, Tada-nori<sup>1</sup>

<sup>1</sup>Kyoto Univ.

Failure of rock mass including complex free surfaces is of importance in many engineering and scientific fields. This paper applied an advanced discretization approach to simulate quasi-static failure of rock mass within a Hamiltonian particle method (HPM) framework. In HPM, a free surface is introduced in a simple way, just by removing or ignoring outer particles. This potential can be developed to discretize numerical models including complex free surfaces without the increment of time for pre-processing. In the present study, we developed the numerical simulator based on HPM with a staggered particle technique for simulating brittle failure and AE activities in rock mass with incorporating the elasto-plastic damage model. We, first, conducted uni-axial compressive tests for validating the effectiveness of our approach. Next, we adopted rectangular and circular disc specimens with a hole as complex free surface models. Our numerical results had good agreement with those from laboratory experiments. This suggests that HPM would be a method to simulate failure behavior of rock mass without time-consuming pre-processing.

Keywords: particle method, failure behavior, rock mass

## Forward calculation of Magnetotelluric responses with MPS method

TANI, Masanori<sup>1\*</sup> ; MIKADA, Hitoshi<sup>1</sup> ; GOTO, Tada-nori<sup>1</sup> ; TAKEKAWA, Junichi<sup>1</sup>

<sup>1</sup>Graduate School of Engineering, Kyoto University

In this research, we developed a new 2-D magnetotelluric (MT) forward simulation method based on the MPS (Moving Particle Semi-implicit) method framework. Our final purpose is to calculate MT response with arbitrary three-dimensional topography.

The MPS method is a particle method and was first developed for the simulation of incompressible fluid flow (Koshizuka and Oka, 1996). Recently, the MPS method is used the digital reproduction of failure of materials, for the simulation of elastic wave propagation, etc. We use the MPS method for the simulation of electromagnetic induction.

In our forward calculation, electric and magnetic fields are defined at each particles in a calculation model. MT responses are calculated on the surface of the ground with topography with a horst-graben shape. Our simulation results indicate that MT forward calculation with the MPS method is suitable for free surface like topography, because the MPS method does not require the mesh configuration such as for FDM and FEM, particles in the MPS method could form any shape. The results of MT forward calculation (TE-mode and TM-mode) based on MPS method is reliable enough to calculate MT responses on models with topography. Based on the inherent character of MPS method, the expansion of our code from two-dimension to three-dimension will be easily achieved.

Keywords: Magnetotelluric, MPS, topography

## Fluid-physical simulation of silicate scale formation using lattice Boltzmann method

MIZUSHIMA, Akihiro<sup>1\*</sup>; MIKADA, Hitoshi<sup>1</sup>; GOTO, Tada-nori<sup>1</sup>; TAKEKAWA, Junichi<sup>1</sup>

<sup>1</sup>Graduate School of Engineering, Kyoto University

Scaling behavior has an important role in various geosciences fields. For example, precipitation of silica can cling to pipes and wells, and prevent the geothermal power generation. Silica precipitation strongly affects the circulation of hydrothermal systems by changing the permeability structure, which is related to the nucleation of seafloor massive sulphide. Self-sealing is of importance in the understanding of long-term radionuclide mobility and the safety of deep geological repositories of radioactive waste.

The deposition of amorphous silica is controlled probably by many processes. There have been a number of experimental studies made on the chemical kinetics of silica deposition as a function of the degree of super-saturation. However scaling estimated by the simple chemical precipitations cannot explain the measured features in laboratory and field experiments. On the other hand, a high rate of deposition could be found where fluid flow stagnates. Although it has been empirically observed that the fluid flow structure can influence silica scaling, relatively little research have been conducted to investigate hydrodynamic effect on silica scaling. The aim of this work is to evaluate the importance of both chemical kinetic and hydrodynamic effects on silica scale growth with a method of numerical simulation.

Here using the lattice Boltzmann method, we calculated velocity, temperature and concentration of dissolved silica in the 2D parallel plate channel and predicted the silica deposition of both chemical kinetic and hydrodynamic deposition processes. The laboratory results by Hosoi and Imai (1982) can be as the reference. We also predicted the silica deposition along the channel with sudden expansion of width. For the latter case, the similar field example in the production pipes of the geothermal well was reported (Mercado et al., 1989).

In our numerical simulations, the silica deposition predicted by the kinetic process has the magnitude extremely lower than the amount of laboratory experiment, but shows the similar magnitude if the hydrodynamic process is considered for scaling. In addition, at the another channel model with the sudden expansion scaling predicted by the hydrodynamic process can explain the observed feature at the geothermal well.

It is found that consideration of the simple kinetics process solely is not sufficient for explanation of the real silica deposition. Therefore, we emphasize the importance of hydrodynamic effect on silica scaling. To predict the silica deposition more quantitatively, an advanced-simulation including behaviors of colloid silica particles in flow.

Keywords: scale prediction, silica scaling, kinetics, hydrodynamics, the lattice Boltzmann method

## Distinct element method for solid-fluid coupled interaction in the application of hydraulic fracturing

NAGASO, Masaya<sup>1\*</sup>; MIKADA, Hitoshi<sup>1</sup>; GOTO, Tada-nori<sup>1</sup>; TAKEKAWA, Junichi<sup>1</sup>

<sup>1</sup>Graduate School of Engineering, Kyoto University

The hydraulic fracturing is of great interest in many scientific and engineering fields in hydraulic fracturing, such as the hot dry rock geothermal power(HDR). However, the natural fractures have significant influence on the nucleation and growth of fractures created in hydraulic fracturing. In addition, the viscosity of fluid used in hydraulic fracturing also influences the geometry of hydraulically created fractures. Although the influence of both natural fracture and fluid viscosity has been intensively investigated on the distribution of hydraulic fractures, none of the studies has dealt with natural fractures and fluid viscosity at the same time and the interaction between them has not been revealed yet. We, therefore, performed a series of numerical simulations for hydraulic fracturing in naturally fractured rock using a 2D flow-coupled DEM code to examine the influence of the fluid viscosity on the interaction between hydraulic and natural fractures. In this study, a low viscosity fluid of 0.1 m<sup>2</sup>/s and a high viscosity fluid of 100.0 m<sup>2</sup>/s are used. Our model is a square block with a borehole at the center under a stress field whose maximum and minimum stresses are 10 and 5 MPa, respectively. We apply the hydraulic pressure to the borehole wall, and observe how induced hydraulic fracture would propagate in the presence of a single natural fracture located adjacent to the borehole. The viscosity of fluid and the angle between the maximum stress direction and fracture orientation are the parameters of the numerical simulation. The results show that the lower the oblique intersection angle is, the less linearly the induced fracture crosses the pre-existing fracture. However, when a high viscosity fluid is used, the interruption of natural fractures decreases and the induced fracture tends to go straight along the direction of maximum compression. Our numerical example implies that high viscosity fluid could be used in hydraulic fracturing to reduce the influence of a natural fracture when the hydraulic fracture intersects the pre-existing fracture with certain angles .

Keywords: hydraulic fractureing, viscosity, natural fracture, discrete element method

## Numerical simulation for apparent viscosity change under oscillating boundary condition using lattice Boltzmann method

UEDA, Ryuta<sup>1\*</sup> ; MIKADA, Hitoshi<sup>1</sup> ; GOTO, Tada-nori<sup>1</sup> ; TAKEKAWA, Junichi<sup>1</sup>

<sup>1</sup>Kyoto University

Unsteady fluid dynamics in Newtonian and non-Newtonian fluid is the main concern of aeronautical engineering, mechanical engineering, chemical engineering, resource engineering and civil engineering. It is also true to the oil industry because the amount of oil production in the world is decreasing recently, it is of importance to seek the technological development for enhanced oil recovery (EOR) in place in the subsurface. Recently, many laboratory experiments and field tests have been performed such as water, gas, chemical, or thermal injections to attempt the enhancement of oil production. Seismic stimulation is known as one of the EOR methods and unsteady flow problem. Numerous observations show that seismic stimulation of oil reservoir may improve oil production. However, for effective usage of seismic EOR, we need to understand the characteristics of changing apparent viscosity under oscillating solid-phase. In this study, we attempt to demonstrate the apparent viscous change in laminar flow under oscillating boundary condition with the models of single pore throats and porous media.

We use Lattice Boltzmann method (LBM) describing Boltzmann equation. We use 2-dimensional 9-velocity (2d9v) model to simulate 2-dimensional incompressible viscous flow. We assume that the background pressure difference between inlet and outlet is constant. The flow is generated by a constant pressure difference.

We discuss the apparent viscosity of a single pore throat and porous media.

First, we discuss four characteristics of an incident elastic wave: amplitude, frequency, angle, and pressure disturbance (P wave). The characteristics of amplitude, frequency and angle are largely related with the amount of changing apparent viscosity. The flux increases under cases with large amplitude, high frequency, and large angle (S wave) of incident to the wall. On the other hand, the pressure disturbance (P wave) is not effective for changing apparent viscosity. We then discuss the possibility of changing apparent viscosity in terms of fluid properties. Wall oscillation can cause improving relative permeability. So, if the rock has water wettability, the oil flux largely increase with wall oscillation. After that, we examine the possibility of changing apparent viscosity in terms of pore scales or shapes under the oscillating boundary condition with LBM. The models of single pore throat consists of two half pore and one pore throat. The models of porous media consist of several pore spaces connected by pore throats from one pore to the others. The shapes of single pore throats are also largely related with changing apparent viscosity. The apparent viscosity decreases with increasing length of the pore throats and radius of the pore throats, and with decreasing width of the pore throats and large pore radius. Comparing single pore throat model and porous media model, we find the apparent viscosity change in porous media models cannot be replaced by linear combination of the apparent viscosity changing in single pore throat models.

Our numerical results imply: i) the flow resistance under oscillating condition increases because the velocity difference between the wall and the center of flow is larger than that in steady flow, ii) the effect of the advection term in oscillating boundary condition is larger than that in steady flow, iii) fluid extrusion is generated by partial pressure gradient near the wall and pore throat, and iv) the oscillating boundary may cause improving pressure loss.

Keywords: Lattice Boltzmann method, Unsteady flow, Seismic EOR, Apparent viscosity, Pore throat scale

## Estimation of stress change in ductile part of the crust inferred from seismic scattering

OKAMOTO, Kyosuke<sup>1\*</sup> ; MIKADA, Hitoshi<sup>1</sup> ; GOTO, Tada-nori<sup>1</sup> ; TAKEKAWA, Junichi<sup>1</sup>

<sup>1</sup>Graduate School of Engineering, Kyoto University

In the past, stress field in the subsurface has been measured by various techniques. For example, the borehole-breakout, the stress release method, the hydraulic fracturing, the strain gauge buried in the ground are used to measure the stress field after costly drilling the subsurface. Beside the techniques requiring direct access to the subsurface, the stress field is also measured indirectly. The Electro Distance Meter, the Global Positioning System, etc. are used to measure a surface deformation in time, from which the subsurface stress change is estimated. However, the estimated stress change in the subsurface is largely affected by near-surface inhomogeneities. Thus, information on the stress field should be obtained from other indirect techniques.

Here, we focus on seismic scattering wave, particularly the coda-Q value, to measure spatial and temporal variations of subsurface stress field. The coda-Q, derived from the attenuation of coda envelope, is perceived to be an indicator of the inhomogeneity in the subsurface. Meanwhile, it has been proposed that the coda-Q has a proportional relationship with the magnitude of stress using a numerical simulation. In this study, we hypothesize that the coda-Q, obtained from seismic waves traveling over a wide range of the crust, indicates stress change in a deep subsurface. At first we numerically calculate a relationship between the coda-Q and the magnitude of stress using a homogeneous crustal model, and show that the coda-Q systematically increases against the magnitude of the stress. Then we confirm the relationship using a heterogeneous numerical model, which has a low velocity zone near the surface. It is revealed that the coda-Q indicates the magnitude of the stress change in the deep subsurface, beneath the inhomogeneity, while the surface strain distribution is largely affected by the low velocity zone near the surface. For the next step, using real seismic data acquired at the regions of the 2008 Iwate-Miyagi Nairiku earthquake and the 2004 mid-Niigata prefecture earthquake, we examine whether the coda-Q indicates stress change in the deep subsurface. The stress change estimated from the coda-Q corresponds with the theoretical one in the ductile part, calculated by a fault model acquired by a seismic wave analysis, whereas the estimated stress change dose not correspond with the inferred one from GPS measurement. It means that the coda-Q can indicate stress change in the deep subsurface, which could give more accurate investigation than the GPS measurement.

Keywords: seismic scattering, stress change, ductile, heterogeneity

## 2D simulation of seismic wave propagation for time lapse monitoring of heterogeneous structure and near-surface effects

KAMIMURA, Aya<sup>1\*</sup> ; KASAHARA, Junzo<sup>1</sup> ; MURASE, Kei<sup>1</sup> ; TAZAWA, Oshie<sup>1</sup> ; NISHIYAMA, Eiichiro<sup>1</sup> ; KUBOTA, Ryuji<sup>1</sup> ; FUJIMOTO, Osamu<sup>1</sup> ; OHMURA, Takeshi<sup>1</sup> ; NOGUCHI, Shizuo<sup>1</sup> ; OHNUMA, Hiroshi<sup>1</sup>

<sup>1</sup>Kawasaki Geological Engineering Co.,Ltd.

For the time lapse study in CCS and EOR, we have proposed the method using the seismic ACROSS (Accurately Controlled and Routinely Operated Signal System) and geophone array. However, it is considered that the near-surface effects and their temporal changes caused by water content changes, temperature and surface wave generation, might have very large effects for time lapse estimation, and we would like to evaluate and reduce the near-surface effects by the comparison of surface and borehole geophone records. We have carried out simulation studies to evaluate the effects of near-surface and heterogeneities such as the man-made cavities in the green tuff layers ( $V_p \sim 2.5$  km/s). We also evaluate the near-surface effects by changing geophone depths. The results of the simulations are as follows.

At the simulation of surface hypocenters, seismic waves passed through the man-made cavities attenuated and seismic waves scattered at the man-made cavities. This shows that there will be a heterogeneous structure like man-made cavities when observed seismic waves were attenuated, and the man-made cavities will become a secondary hypocenter.

As the results of simulation of surface hypocenters, the amplitude of scattered waves observed by borehole geophones were larger than that of surface geophones. This means that the borehole geophones are suitable for time lapse monitoring of heterogeneous structures. The amplitude of scattered waves observed by horizontal components of geophones was larger than that of vertical components of geophones. This means that the horizontal components of geophones are suitable for time lapse monitoring of heterogeneous structures.

At the simulations of deep hypocenters (15Hz, 2Hz) as assumed natural earthquakes, seismic waves scattered by the man-made cavities. Observation of natural earthquakes will be helpful to look at the wide seismic structure.

## A time lapse test of seismic waveform changes during several days at the green tuff area in Japan using a seismic vibrator

KASAHARA, Junzo<sup>1\*</sup>; KUBOTA, Ryuji<sup>1</sup>; YUTAKA, Kanai<sup>1</sup>; TAZAWA, Oshie<sup>1</sup>; FUJIMOTO, Osamu<sup>1</sup>; KAMIMURA, Aya<sup>1</sup>; NISHIYAMA, Eiichiro<sup>1</sup>; MURASE, Kei<sup>1</sup>; NOGUCHI, Shizuo<sup>1</sup>; OHMURA, Takeshi<sup>1</sup>; OHMURA, Hiroshi<sup>1</sup>; HASADA, Yoko<sup>2</sup>

<sup>1</sup>Kawasaki Geological Engineering Co. Ltd., <sup>2</sup>Daiwa Exploration and Consulting Co. Ltd., <sup>3</sup>Tokyo University of Marine Science and Technology

In order to estimate the physical property changes in the subsurface, the time-lapse measurement is quite useful for various cases such as CCS (Carbon Capture and Sequestration) zone, EOR, shale gas exploration, and oil production. The authors have carried out the time lapse experiment at the water pumping area in Kingdom of Saudi Arabia using a very accurate and extremely stable seismic source called ACROSS (Accurately Controlled and Routinely Operated Signal System).

Because this seismic ACROSS has been installed semi-permanently at the Saudi test field, it is not easy to bring to any places. Instead, we alternatively used a much conventional electro-magnetic vibrator for this field test in the green tuff area in Japan.

We used the vibrator for 12 hours a day during five days in 2013. We also used 110 geophones and two borehole geophones placed just above the green tuff miming area with 2km x 3km. We used sweep signal from 10 Hz to 50Hz during 100 second.

We repeated 32 sweep during an hour. 32 stacking of waveforms of 100s second time-windows improved the S/N, and we can identify arrivals up to 3 km distance by this one-hour stacked data. If we look the 12 hours waveforms, it is difficult to find the change of those with time.

Using the subtraction of waveforms every day with 12-hour stack data from the first day, we generated residual waveforms. If we use residuals waveforms from the first day, we can clearly identify the change of waveforms with time. In conclusion we can use the time lapse method during five days by the use of residuals waveforms though the period is short. We can use conventional seismic vibrator(s) for the time lapse for several days.

Keywords: time lapse, ACROSS, seismic method, residual waveforms, vibrator source, green tuff

## A Reflectivity Guided Elastic Full Waveform Inversion

JAMALI HONDORI, Ehsan<sup>1\*</sup> ; MIKADA, Hitoshi<sup>2</sup> ; GOTO, Tada-nori<sup>2</sup> ; TAKEKAWA, Junichi<sup>2</sup>

<sup>1</sup>JGI, Inc., <sup>2</sup>Kyoto University

Full Waveform Inversion (FWI) of seismic reflection data has become a common technique for producing subsurface images based on local minimization of least squares misfit between observed data and calculated model. Usually, an initial model that is close to the global solution of the problem is needed to obtain satisfactory results without being trapped in a local minimum of the misfit function. Due to the limitations in quantity of the observed data, e.g. using seismic traces from surface receivers to make an image of earth model, the full waveform inversion problem is ill-posed and underdetermined. The problem becomes even worse when dealing with elastic waveforms which require increased number of model parameters, i.e. P wave velocity, S wave velocity, density etc. In order to overcome this problem, inserting a priori model information in to the inversion process helps the algorithm to converge to a solution in the vicinity of the global minimum. This kind of information could be included in the gradient of the misfit function by adding model terms, when using conjugate gradient method to iteratively update the model parameters.

On the other hand, producing reliable velocity model is a key for successful Pre Stack Depth Migration (PSDM) of seismic data. Assuming an available depth section of seismic reflection data, e.g. by time to depth conversion of time migrated section, we estimate the P wave velocity from seismic section by first extracting reflectivity and then using Gardner equation (Gardner 1974) as stated by Hondori et. al 2013. This will produce a P wave velocity model which is used in full waveform inversion as a priori information. Our frequency domain elastic full waveform inversion is developed using finite difference method and perfectly matched layers are used on the boundaries of the computational area. A preconditioned conjugate gradient method is used together with improved pseudo Hessian matrix for updating the model parameters. At each iteration the gradient is calculated using adjoint state method, and then  $L_2$  norm of the model term is added to the gradient to constrain the inversion. We suggest that this method not only improves the full waveform inversion results, but also resulting FWI models provide a good velocity model for pre stack depth migration of seismic data.

### References

Gardner, G. H. F., Gardner, L. W., and Gregory, A. R., 1974, Formation velocity and density: the diagnostic basics for stratigraphic traps: *Geophysics*, **39**, 770-780.

Hondori, E. J., Mikada, H., Goto, T.N, Takekawa, J., 2013, A random layer-stripping method for seismic reflectivity inversion: *Exploration Geophysics*, **44**, 70-76.

Keywords: Full Waveform Inversion, Frequency Domain, Elastic, Reflectivity

## 3D-FDFD simulation for high resolution eddy-current testing method

SAITO, Takuya<sup>1\*</sup> ; MIKADA, Hitoshi<sup>1</sup> ; GOTO, Tada-nori<sup>1</sup> ; TAKEKAWA, Junichi<sup>1</sup>

<sup>1</sup>Kyoto University

The applicability and the feasibility of eddy-current testing method for the measurement of wall thinning and surface crack of steel structure have been practically confirmed by field and laboratory experiments. Where and how large the cracks would be are roughly understood by this method. However, it is difficult to estimate the exact size and shape of them. For more accurate inspections, there has been a growing demand to quantitatively evaluate the cracks. Therefore, we have developed a numerical simulator for the high accuracy eddy-current method. Eddy-current method measures excitation magnetic and induced magnetic fields, the latter of which is caused by the eddy-current in the inspecting material. In order to calculate induced magnetic field deformed by the cracks, we used three-dimensional finite-difference frequency domain technique to solve Maxwell's equations numerically. As a simulation model, two-layer structure consisting of seawater and steel plate including cracks is used. We simulated a variety of cracks to estimate characteristic of the induced magnetic field, and compared the results in terms of what kind of difference in the induced field would appear. As a result, the effect of surface cracks of steel plate on receiving magnetic field intensity was confirmed as follows: the induced magnetic field intensity increases near the edge of cracks and decays above the cracks with the distance to the edge. The deeper and wider cracks are, the more the magnetic field intensity becomes attenuated. Due to the limitation of our simulation schemes, the response of magnetic field intensity whose detectable scale of cracks was no smaller than mm order. We are introducing a method that could allow us to confirm much finer detectability.

Keywords: NDI, Maxwell's equations, Eddy Current, numerical simulation

## Elastic parameter estimation in full waveform well-to-well tomography

TERANISHI, Keisuke<sup>1\*</sup> ; MIKADA, Hitoshi<sup>1</sup> ; GOTO, Tada-nori<sup>1</sup> ; TAKEKAWA, Junichi<sup>1</sup>

<sup>1</sup>Graduate school of Engineering, Kyoto university

Seismic full-waveform inversion (FWI) method has been used to estimate velocity and density structures in the subsurface. The waveform analysis is a powerful tool to investigate the properties in the areas of interest, and the importance to use the waveform is widely recognized in the seismic explorations. As the wave propagation is influenced by elastic parameters,  $V_p$ ,  $V_s$ , density, it is necessary to include these parameters in FWI (Virieux and Operto 2009). However, there are few previous studies dealing with density as a parameter in the application of elastic FWI. Density is usually estimated using an empirical formula such as Gardner's relationship (Gardner et al., 1974), or is fixed to a constant value. Almost all elastic FWI studies have neglected the influence of approaches how density parameter is estimated. The objective of this study is to investigate how difficult the estimation of density structure is, and propose a new approach to overcome the problem. We employ 2D numerical simulations in order to investigate the important factor in the inversion of density structure. Our results show that it is difficult to estimate density structure because density structure is less sensitive to waveform than  $V_p$  and  $V_s$ . Therefore, we hypothesize that the simultaneous inversion of  $V_p$  and density structures, using a selected dataset can improve the accuracy of the FWI. For testing this hypothesis, various ways for estimation of  $V_p$ ,  $V_s$  and density using different datasets and approaches. We conclude that  $V_p$  and density structures should be estimated simultaneously in the elastic FWI, in which P-wave data separated from the seismic records is used as the input data.

Keywords: full-waveform, tomography, density

## Estimation of fluid contact in terms of attenuation

ISHIKURA, Kazuki<sup>1\*</sup> ; MIKADA, Hitoshi<sup>1</sup> ; GOTO, Tada-nori<sup>1</sup> ; TAKEKAWA, Junichi<sup>1</sup>

<sup>1</sup>Kyoto University graduate school of engineering

Sonic logging has been widely used for many years to acquire physical properties of formations in the vicinity of hydrocarbon reservoirs. When gaseous phase exists in the formation fluid, the compressional waves traveling through the formation could be strongly attenuated due to low bulk modulus of gas in the fluid, while the shear waves are not. For acquiring physical properties of fluid in the formation, Biot physics or poroelastic analysis would be the best method. Among the available technologies, quality factors based on the Biot's equation could be used. Although the Biot's theory considers the viscous attenuation induced at the interface between pore wall and fluids, the intrinsic attenuation caused by the internal friction in the matrix is ignored.

In the present study, adding the intrinsic attenuation we investigate if we take the effect of the viscous attenuation from the acquired quality factor, and then, on the basis of the result, if we estimate the fluid contact (e.g. gas-oil contact and oil-water contact). We employ a 2D finite-difference scheme to simulate seismic wave propagation in a poroelastic medium. The intrinsic attenuation is included in our model using a filter for frequency-independent quality factor (constant-Q). We then achieve the results of compressional and shear wave in our numerical simulations. Our results show that on compressional and shear waves, obtained the quality factors different from each other. We acquire the effect of the viscous attenuation by subtracting the quality factor of shear wave from the quality factor of compressional wave. We conclude that the effect of viscous attenuation is extracted and the gas-oil contact is estimated.

Keywords: Q, attenuation, poroelastic, Biot, sonic logging

## AVO waveform inversion for estimating the fluid contact with fluid transition zone

IWAKI, Yunosuke<sup>1</sup> ; MIKADA, Hitoshi<sup>1\*</sup> ; GOTO, Tada-nori<sup>1</sup> ; TAKEKAWA, Junichi<sup>1</sup>

<sup>1</sup>Graduate School of Engineering, Kyoto University

The fluid distribution in the hydrocarbon reservoir affects waveforms acquired in reflection seismic method. A reflected wave changes its waveform at the transition zone of the interface of two different fluids as a function of volume fraction of the two. AVO is in general used to estimate the difference in the P and S wave velocities for the interfacing two media at the interface without any assumptions on the existence of the transition zone. The consideration of the effect of the volume fraction of a fluid to the other in the waveform could be a key for evaluating the fluid mixture around the fluid contact in the reservoir. Therefore, we try to use the waveform directly to estimate fluid distribution in the transition zone that has not been done in the practice of AVO.

In our research, we consider the effects of the transition zone at a gas-water contact (GWC) in a horizontally stratified medium on seismic waveforms. The numerical simulation reveals that the fluid distribution of transition zone distorts the seismic waveform both in amplitude and in phase. Then we use the difference in amplitude and in phase for estimating some necessary parameters expressing the fluid-mixture. We apply a waveform inversion method to the fluid substitution problems to see if the method is applicable to estimate the fluid contact with the transition zone, while the conventional AVO only utilizes the amplitude derived from observed data. Our numerical approach uses full waveform and the results imply the advantages in the estimation of the parameters including the thickness of the transition zone under that assumption of linear trend in the volume fraction in a contrast porosity condition. We suggest that the phase information should be used simultaneously for the inversion process to get the closer contact image.

## The insulation effects caused by the scattering of electromagnetic waves by fine spheres against insolation heating

HORIE, Jun<sup>1\*</sup> ; MIKADA, Hitoshi<sup>1</sup> ; GOTO, Tada-nori<sup>1</sup> ; TAKEKAWA, Junichi<sup>1</sup> ; TANIGUCHI, Kiyoshi<sup>2</sup> ; ASHIDA, Yuzuru<sup>3</sup>

<sup>1</sup>Kyoto University, <sup>2</sup>West Nippon Expressway, <sup>3</sup>NPO EEFA

The temperature of materials rises when they are exposed to the sunlight (insolation heating). Insolation heating could be suppressed when the materials are coated with paint admixed with fine silica spheres (insulating paint). By coating buildings' walls and roofs with such paint, the temperature in the subjacent rooms could be kept lower than by coating with regular one. The temperature of the former could be enough low so that no air-conditioning becomes necessary even in the mid summer. These phenomena are well known in a practical manner and have been widely utilized. However, the cause of the phenomena has hardly been analyzed theoretically yet. Moreover, micron-scale ceramic spheres have been known as the best commixture than the other metallic commixture of the same size. Theoretical analysis would greatly enhance the effects of the suppression of insolation heating. We focus on the light scattering by fine spheres under the assumption that the scattering of lights, i.e., electromagnetic waves, attributes to suppression of insolation heating and that the imaginary part of scattering coefficients of the spheres is a key to explain the observed phenomena. In this study, we therefore consider commixture sphere materials to be (i)silica, (ii)aluminum and (iii)copper, distributed in a paint layer coating an iron material, and calculate transmission, reflection and absorption coefficient using the Monte Carlo ray tracing method based on the Mie theory. Using these coefficients, the rise in temperature of surface of the iron layer would be estimated. We finally investigate how the structure of the paint attributes to the insulating effects.

We assume three layers: air, paint, and iron, and commixed fine spheres in the paint layer using Distinct Element method (DEM). A number of photons vertically incident to the paint at random position from the air. We then count the number of photons that reaches the iron to estimate the intensity of the transmitted wave, and count the number of photons that are absorbed by spheres to estimate the intensity of the absorbed wave energy. Fresnel Equations are used to identify photons' behavior stochastically using a random number. Moreover, Mie theory is used to calculate the radiation pattern of scattering at each sphere when a photon incident to the sphere. As a result, it is estimated that the transmission coefficient would be less than 0.1 for the commixture material of silica whose radius is smaller than ca. 0.7 micrometers. On the other hand, the transmission coefficient could be much less than 0.1 if we use conductive spheres. However, in the latter case, the absorption coefficient would be approximately 0.5, which could cause the rise in temperature of the spheres and the paint.

We estimate the rise in temperature of iron layer using coefficients calculated above. Near-infrared radiation of the sunlight is assumed to be the incident wave. As a result, whereas the temperature would be 63 degrees Celsius if no paint is coated. On the other hand, the temperature would be suppressed to 39, 59 or 56 degrees Celsius, respectively, if we use silica, aluminum or copper spheres of the same radii of 0.5 micrometers. The metallic commixture could lower the temperature rise but the absorption of the energy seems deteriorate the efficiency of the insulation.

In conclusion, silica is one of ideal material for insulating paint in contrast with conductive ones such as aluminum and copper, mainly due to the absorption phenomena of electromagnetic waves by spheres.

Keywords: mie scattering, monte Carlo Ray-tracing, insulating paint, sphere, electromagnetic scattering

## Three-dimensional joint inversion of gravity and magnetic anomalies using fuzzy c-means clustering

TERANISHI, Yosuke<sup>1\*</sup> ; MIKADA, Hitoshi<sup>1</sup> ; GOTO, Tada-nori<sup>1</sup> ; TAKEKAWA, Junichi<sup>1</sup> ; TADA, Ryohei<sup>2</sup>

<sup>1</sup>Kyoto University, <sup>2</sup>INPEX CORPORATION

The gravity and magnetic surveys have been widely carried out over the years, especially for the exploration of metallic mineral deposits and geothermal resources. These intensity data of gravity and magnetic fields could be acquired in much quicker and simpler ways than the other geophysical or geological surveys. The inversion of such potential field data, however, has been known as a non-uniqueness problem expressed in the Green's equivalent layer theory. Because of this problem, gravity and magnetic data have no inherent resolution in depth. We, therefore, would like to develop a way to make use of high exploration efficiency that takes the advantages of the convenience to conduct gravity and magnetic surveys.

We present a 3D joint inversion method to estimate two physical parameters, density and magnetization of subsurface materials. In the method, we introduce the fuzzy c-means (FCM) clustering technique in our joint inversion algorithm to consider the petrophysical relation between density and magnetization of subsurface materials. The fuzzy c-means clustering technique we introduce does not necessitate any empirical equations but deals with a linear combination of the influence from multiple clusters given a piece of data to belong to plural clusters in the parameter space formed by the petrophysical parameters. Adding the simple FCM clustering scheme, we introduced the smoothness constraint to a weight for membership to each clusters, instead of the conventional smoothness constraint to model parameters. Numerical studies using synthetic data indicate the effectiveness of FCM clustering in the joint inversion: the joint inversion results using gravity and magnetic data sets show higher accuracy and resolution than the individual ones.

As the field example, we focus on submarine volcanoes located at Mozambique Channel, because the world-class gas fields were discovered around that area and it is necessitated to estimate structure of submarine volcanoes near gas fields. We apply our inversion method to the real field gravity and magnetic data of the submarine volcanoes at Mozambique Channel. We conclude that our joint inversion method gives the reliable and detailed density/magnetization structures inside the submarine volcanoes in terms of the gravity and magnetic anomalies.

Keywords: joint inversion, gravity, magnetic, submarine volcano

## Stress field and fracture propagation due to the change of injection pressure

OKUBO, Kurama<sup>1\*</sup> ; MIKADA, Hitoshi<sup>1</sup> ; GOTO, Tada-nori<sup>1</sup> ; TAKEKAWA, Junichi<sup>1</sup>

<sup>1</sup>Kyoto University

Hydraulic fracturing is an indispensable scheme to stimulate fluid production in hydrocarbon reservoir development in conjunction with various well testing methods such as drill stem, buildup tests, etc. In recent years, it is also well known that hydraulic fracturing plays a major role in the development of shale oil or gas reservoirs.

The extension length and the orientation of fractures induced by hydraulic fracturing are strongly influenced by the crustal stress field under which any reservoirs are located. Therefore the propagation of fractures is controlled by the regional stress field. It is, in general, necessary to get some understanding of regional stress field before the application of hydraulic fracturing as well as acquiring the rock physical properties of reservoir formations.

However, hydraulically induced fractures may not be created as planned and could cause some environmental issues such as pollution, induced seismicity, etc. It is, we think, very important to estimate how fractures are induced under various crustal conditions to cope with unexpected behavior of fracture propagation.

We focused the effects of the in-situ stress on the stress field around the pre-existing fracture and the fracture propagation with both steady and non-steady hydraulic pressure conditions. To simulate failures in crustal materials under the complicated stress field, we use an extended finite element method (X-FEM) in this study, which can retrieve the stress distribution affected by fractures effectively and estimate the fracture propagation based on linear elastic fracture mechanics (LEFM). Numerical simulations are conducted for a 2D elastic medium having a borehole and a pre-existing fracture. We put the pre-existing fracture around the borehole initially and simulate the propagation of this fracture by applying the hydraulic pressure. The velocity of fracture propagation and the interval of the stress recovery from the stress drop caused by the propagation are set uniformly for the kinetic simulation.

We first simulate the fracture propagation around the borehole under different steady hydraulic pressures with regional stress field. Then we try to see how the fracture could propagate with the non-steady hydraulic pressure during the propagation.

We confirmed that the orientation of the fracture propagation converges to that of the principal stress. Moreover, the convergence speed could be inversely related to the hydraulic pressure. We also found the time delay of the influence of the hydraulic pressure change to the fracture propagation with non-steady hydraulic pressure condition.

From the results of our numerical simulations, we would like to have two conclusions. First, the curvature of the fracture trace depends on hydraulic pressure, but no matter how the fluid pressure is, the orientation of fracture propagation converges to that of principal stress. Second, the transition of the stress field involves the time delay, which leads to the delayed response of the fracture propagation in the non-steady hydraulic pressure condition.

When we develop a hydrocarbon reservoir using hydraulic fracturing, the orientation of maximum in-situ principal stress and the fluid pressure for fracturing should be quantitatively taken into account for the environmental safety and for the stimulation efficiency. It might be also necessary to consider the time delay of the transition of the stress due to the non-steady hydraulic pressure.

Keywords: Hydraulic fracturing, Fracture propagation, X-FEM, Stress field

## Estimation of the Dispersion Curve for Soil Layers with Lateral Heterogeneity Using Continuous Wavelet Transform

TSAI, Pei-hsun<sup>1\*</sup>

<sup>1</sup>Department of Construction Engineering, Chaoyang University of Technology

The MASW method is the normal method regarding surface wave testing, but it requires 12 or more receivers to measure the phase velocity for statistical redundancy. Therefore, the SASW method has potential for use because only two receivers are required. A time-frequency domain analysis is used to extract a dispersion image of Rayleigh waves and select a dispersion curve from the seismic signals of two receivers during surface wave testing. The signals are transformed by continuous wavelet transform, and the products of the transformed signals of the two receivers are summed at the same slowness over the intercept time to construct a dispersion image. This method is unnecessary empirical judgment in the unwrapping of phases and a significant number of receivers. To examine the applicability of the method on evaluating the dispersion curve for soil layers with lateral heterogeneity, three synthetic examples and an experience example of surface wave testing are discussed. The method is applicable for extracting a dispersion image for lateral heterogeneity soil layers. A high-resolution dispersion image is generated in this study by increasing the interval of the receivers. The result of the experience example was in accordance with that of the borehole data.

Keywords: Dispersion curve, Continuous wavelet transform, Lateral heterogeneity

## Issues and Countermeasures for the Geophysics Investigation of Contaminated with Chlorinated Hydrocarbon

LIU, Hsin-chang<sup>1\*</sup> ; LIN, Chih-ping<sup>1</sup> ; WANG, Tzu-pin<sup>2</sup> ; DONG, Tian-xing<sup>3</sup>

<sup>1</sup>Disaster Prevention and Water Environment Research Center, National Chiao Tung Univ., <sup>2</sup>Chien Hsin University of Science and Technology, <sup>3</sup>APOLLO TECHNOLOGY CO., LTD.

Environmental geophysics survey has the advantages of survey rapidly, high resolution result and less affected by the surface topography and objects. It is suitable to either a wide range of general survey or a small-scale precise survey. Recently, non-invasive technologies such as geophysical technology have been introduced to provide the plane and space information of pollution in subsurface by integrating few bore-hole data. The most common used geophysical technologies are ground-penetrating radar method (GPR) and electrical resistivity tomography (ERT). The electrical resistivity tomography (ERT) is one of the most widely used geophysical methods in geological, hydro-geological, and geo-environmental investigations. This study would first discuss how DNAPL and its soluble-phase components invade into the low permeable layer based on the field observation. Then, the importance of geophysical technology is introduced with comparing to the limitations of bore-hole investigation. Last, the case studies on using geophysical technologies including geophysical well logging are introduced to snapshot the complex profile of DNAPL distribution for improving future application.

Keywords: Geophysical survey, Electrical Resistivity Tomography, Borehole Radar

## Development of a laser strain gradiometer and reduction in its thermal noise.

DEGUCHI, Takehiro<sup>1\*</sup> ; ARAYA, Akito<sup>1</sup>

<sup>1</sup>Earthquake Research Institute, University of Tokyo

An earthquake is essentially a shear slip on a fault. Because the rupture velocity is roughly constant for most earthquakes, the length, the width, and the slip distance of a fault are respectively proportional to the duration of the rupture, and therefore an earthquake follows the scaling law that its seismic moment is proportional to the cube of its duration. In addition to the ordinary earthquakes, slow earthquakes have been discovered recently. Slow earthquakes include short-term and long-term slow slip events, non-volcanic tremors, low-frequency earthquakes, and very low-frequency earthquakes. They are known to be also shear slips but have slower rupture velocity than the ordinary earthquakes (see the reference [Beroza and Ide, 2011]). Ide et al. (2007) proposed that every slow earthquake has the same mechanism with a new scaling law that its seismic moment is proportional to its duration.

However, no middle-term slow earthquakes with duration of 200 s to 1 day have been reported so far. To understand the reason, we conducted analytical calculations including comparisons of expected signals of slow earthquakes and background seismic noise. It was shown that the middle-term slow earthquakes cannot be observed by a single accelerometer, a strainmeter, or a tiltmeter due to the background seismic motion.

AIST's synthetic analysis using the network of strainmeters, tiltmeters, and groundwater pressure gauges [Itaba et al, 2009] detected smaller slow slips.

Let us take the second spatial derivative of displacement, "the strain gradient". Analytical calculations showed that the signals of slow earthquakes with duration of 200 seconds to 1 day can directly be detected from the strain gradient of the ground. The spatial scale of the background ground motion is larger than the typical distance between a hypocenter and an observatory and the typical size of the fault. Taking spatial derivative emphasizes the small-scale crustal deformation, and makes the detection of local slow earthquakes easier. Thus, measuring the strain gradient will be effective to detect them.

We made a prototype instrument of measuring the strain gradient, "strain gradiometer," with laser interferometry. Before installing it on the ground, we measured its instrumental noise in the atmosphere and found the noise following power spectral density of  $10^{-12}[\text{m}^2/\text{s}]$  at  $10^{-5}\text{Hz}$  and tendency of  $1/f^2$  below 0.1Hz. This noise was caused by changes in optical path lengths due to the fluctuation of air pressure. Subsequently, the noise of the interferometer in vacuum was measured; the noise was reduced by 1/10 and had the tendency of  $1/f$  below 0.1Hz. This noise could be reduced by adjusting the optical path difference because it was estimated to be caused by frequency fluctuations of the laser source, which was frequency stabilized by the two-mode method. After the adjustment, there remained noises that had the power spectrum of  $1/f^6$  in the period between 5000s and 20000s and same power in the period longer than 20000s. This noise had similar waveform to temperature in time-domain. This noise was estimated to be caused by thermal expansion of the optical devices and the optical breadboard. Assuming this noise will be reduced in proportion to the square of the baseline length in terms of the strain gradient, the necessary baseline will be more than 300m. In the presentation, analyses of the noise of the interferometer with thermal insulation by ceramics and the future development will be explained.

### References

- Ide, S., Beroza, G. C., Shelly, D. R. and Uchide, T., A scaling law for slow earthquakes, *Nature*, **447**, 76-79, 2007a.  
Beroza, G. C. and Ide, S., Slow earthquakes and nonvolcanic tremor, *Annu. Rev. Earth Planet. Sci.*, **39**, 271-296, 2011.  
Itaba, S., Koizumi, N., Matsumoto, N. and Ohtani, R., Continuous observation of groundwater and crustal deformation for forecasting tonankai and nankai earthquakes in Japan, *Pure Appl. Geophys.*, **167**, 1105-1114, 2010.

Keywords: laser interferometer, strainmeter, strain gradiometer

## Compact Ocean Bottom Cabled Seismic and Tsunami Observation System Using ICT and Installation Plan

SHINOHARA, Masanao<sup>1\*</sup> ; YAMADA, Tomoaki<sup>1</sup> ; SAKAI, Shin'ichi<sup>1</sup> ; SHIOBARA, Hajime<sup>1</sup> ; KANAZAWA, Toshihiko<sup>2</sup>

<sup>1</sup>Earthquake Research Institute, University of Tokyo, <sup>2</sup>National Research Institute for Earth Science and Disaster Prevention

The Pacific plate is subducting below the northeastern Japan islands arc. The 2011 Tohoku earthquake occurred at the plate boundary between the Pacific plate and the landward plate below landward slope of the Japan Trench. In 1996, Earthquake Research Institute (ERI), University of Tokyo had installed seismic and tsunami observation system using seafloor optical fiber in the off-Sanriku area. The continuous real-time observation has been carried out since the installation. The system observed seismic waves and tsunamis generated by the 2011 Tohoku earthquake, and the data from the system are indispensable to estimate accurate position of the source faults and the source process of the 2011 event. However, the landing station of the system was damaged by huge tsunami 30 minutes after the mainshock, and the observation is discontinued. Because the data from the real-time system on seafloor are important, we decide to restore the existing system and install newly developed Ocean Bottom Cabled Seismic and Tsunami (OBCST) observation system off Sanriku for additional observation and/or replacement of the existing system. In this paper, we present a system of the new OBCST in detail, and installation plan.

Until 2010, we had already developed and installed the new compact Ocean Bottom Cabled Seismometer (OBCS) system near Awashima-island in the Japan Sea. After the installation, the OBCS system is being operated continuously and we have continuous seismic data for more than 3 years at the present. The new OBCST system for off-Sanriku area is based on this system, and is characterized by system reliability using TCP/IP technology and down-sizing of an observation node using up-to-date electronics. The new OBCST has three accelerometers as seismic sensors. Signals from accelerometers are 24-bit digitized with a sampling rate of 1 kHz and sent to a landing station using standard TCP/IP data transmission. A precise pressure gauge is also equipped as a tsunami sensor. The tsunami data with a sampling rate of 1ms are also transmitted by TCP/IP protocol. In addition, an observation node can equipped with an external port for additional observation sensor instead of a pressure gauge. Additional sensors on seafloor are supplied the power using Power over Ethernet technology. Clock is delivered from the GPS receiver on a landing station using simple dedicated lines. In addition, clocks in observation nodes can be synchronized through TCP/IP protocol with an accuracy of 200 ns (IEEE 1588). The data will be stored on the landing station and sent to ERI in the real-time. A simple canister for tele-communication seafloor cable is adopted for the observation node, and has diameter of 26cm and length of about 1.3m. This small size of the canister has an advantage for burying the system below seafloor.

At the present, we are producing the observation nodes of the new OBCST. The new system has three observation nodes; two have three-component seismometer and a pressure gauge, one has seismometers and an external port by using the PoE technology. We have a plan to connect a pressure gauge and hydrophone via the PoE external port of the third observation node. Total length of the practical system is approximately 100 km and an interval of the observation node is about 30 km. We have a plan to install the practical system in 2015.

Keywords: Cabled ocean bottom seismometer and tsunami gauge, Sanriku, Japan Trench, seafloor observation

## Long-period duration of the teleseismic events reported to ISC from Syowa Station since 1967

KANAO, Masaki<sup>1\*</sup>

<sup>1</sup>National Institute of Polar Research

Phase identifying procedure for teleseismic events at Syowa Station, East Antarctica have been carried out since 1967 after the International Geophysical Year (1957-1958). From the development of INTELSAT telecommunication link, digital waveform data have been transmitted to the National Institute of Polar Research for utilization of phase identification. Arrival times of teleseismic phases, P, PKP, PP, S, SKS have been reported to the International Seismological Centre (ISC), and published by JARE Data Reports from NIPR. In this paper, hypocentral distribution and time variations for detected earthquakes are demonstrated over the last four decades in 1967-2010. Characteristics of detected events, magnitude dependency, spatial distributions, seasonal variations, together with classification by focal depth are demonstrated. Besides the natural increase in number for occurrence of teleseismic events on the globe, a technical advance in observing system and station infrastructure, as well as the improvement of procedure for reading seismic phases, could be efficiently combined to produce the increase in detection number in last few decades. Variations in teleseismic detectability for longer terms may possibly by associate with meteorological environment and sea-ice spreading area around the Antarctic continent. Recorded teleseismic and local seismic signals have sufficient quality for many analyses on dynamics and structure of the Earth's as viewed from Antarctica. The continuously recorded data are applied not only to lithospheric studies but also to Earths deep interiors, as the significant contribution to the Federation of Digital Seismological Network from high southern latitude.

Keywords: Syowa Station, teleseismic events, detection capability, monitoring observation, global network

## Seismic observation on Greenland Ice Sheet by the Japanese GLISN team (2011-2013), and a plan for the 2014 season

TOYOKUNI, Genti<sup>1\*</sup> ; KANAO, Masaki<sup>2</sup> ; TONO, Yoko<sup>3</sup> ; HIMENO, Tetsuto<sup>4</sup> ; TSUBOI, Seiji<sup>3</sup>

<sup>1</sup>RCPEVE, Tohoku Univ., <sup>2</sup>NIPR, <sup>3</sup>JAMSTEC, <sup>4</sup>Seikei Univ.

Melting of the Greenland ice sheet is now in progress accompanying the global climate change. Recently, a new type of seismic event called "glacial earthquakes", which are generated by the movement of a large mass of ice within the glacial terminus, has been realized as a new way to monitor current ice sheet dynamics. In 2009, the multinational GreenLand Ice Sheet monitoring Network (GLISN), a large broadband seismological network in and around Greenland was initiated to monitor these events.

Japan, a partner country of the GLISN project, has been sending a field team every year since 2011. The joint U.S. and Japanese team first constructed a seismic station (station code: ICESG) on the Greenland ice sheet. In 2012, we serviced two ice sites (ICESG, DY2G) and one rock site (NUUK). In 2013, the same team spent 11 days on ice for maintenance of ICESG and DY2G, and helped logistics for another ice site (NEEM). This presentation summarizes our field activities on the GLISN project for three years, and show a plan for the 2014 season.

Our activity is supported by JSPS KAKENHI 24403006.

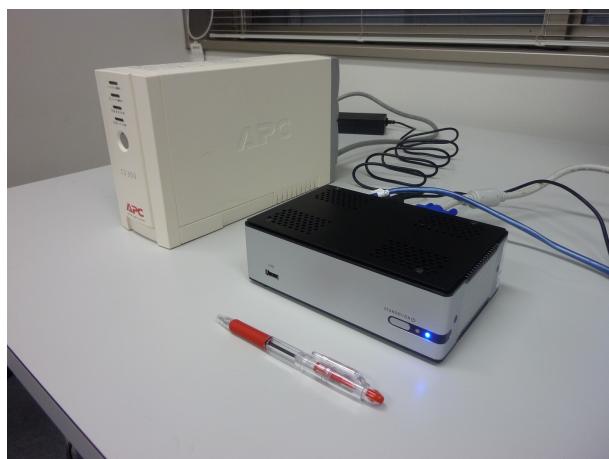
Keywords: Greenland, glacial earthquake, GLISN network

## Development and Operation of Wide-area Observation Monitoring (WONM) System

MURATA, Ken T.<sup>1\*</sup> ; NAGATSUMA, Tsutomu<sup>1</sup> ; YAMAMOTO, Kazunori<sup>1</sup> ; WATANABE, Hidenobu<sup>1</sup> ; UKAWA, Kentaro<sup>2</sup> ; MURANAGA, Kazuya<sup>2</sup> ; YUTAKA, Suzuki<sup>2</sup>

<sup>1</sup>National Institute of Information and Communications Technology, <sup>2</sup>Systems Engineering Consultants Co., LTD.

This paper is devoted to present an operation system to acquire, to transfer and to storage data for world-wide observation networks, which is named as WONM (Wide-area Observation Network Monitoring) system, developed in NICT (National Institute of Information and Communications Technology). This system provides us with easier management of data collection than legacy systems by means of autonomous system recovery, periodical state monitoring, and dynamic warning procedures. We have equipped world-wide observatories for space weather prediction and research works with this system connected with the NICT Science Cloud. Demonstration and discussion will be presented concerning with this challenging system, especially from the viewpoint that we easily operate world-wide observatories on a web application.



## Development of hypocenter location method using envelopes: Application to B-type earthquakes at Miyakejima volcano

UCHIDA, Higashi<sup>1\*</sup> ; NISHIMURA, Takeshi<sup>2</sup> ; NAKAHARA, Hisashi<sup>2</sup> ; YAMASATO, Hitoshi<sup>1</sup> ; FUJITA, Eisuke<sup>3</sup>

<sup>1</sup>Japan Meteorological Agency, <sup>2</sup>Geophysics, Science, Tohoku University, <sup>3</sup>NIED

B-type earthquakes are frequently observed in active volcanoes, but it is difficult to locate them by using traditional phase picking methods because most of B-types show emergent onsets of P- and S-waves. We applied the envelope correlation method of Obara (2002) to B-type earthquakes at Miyakejima volcano, but the located hypocenters shifted towards the south-east by 0.5 - 1 km compared to those determined by phase picking method. Such systematic difference is caused by some assumptions such as that the envelope waveforms at each station are all the same. Actually, the envelope waveform broadens as hypocentral distance increases because of the scattering, or the waveform strongly depends on the site condition. In this study, therefore, we develop a new envelope correlation method in which a small number of the B-type earthquakes whose S-wave arrival times are manually picked are used as reference events. The method estimates S-wave arrival times by taking cross-correlations between envelopes of reference events and that of target event at each station. To find appropriate reference events effectively, we use the similarity of concatenated envelopes: the envelopes of all stations are connected in order keeping the amplitude ratios and time differences of envelopes between stations. The similarity of the concatenated envelopes means that the hypocenters and path effects on the envelope waveform at each station are almost the same with those of the reference events. By applying this method to B-type earthquakes at Miyakejima volcano observed from August 2010 to April 2011, we determine 71 % of the observed ones in an automated way. The B-type earthquakes are located within a 1 km diameter centered on the southern part of the summit caldera, where continuous gas emission occurs. On the other hand, A-type earthquakes, which show clear onsets of P- and S-waves, are distributed from southern part to western part of the summit caldera. To check the reliability, we also compare the result to the hypocenters located by picking P- and S-onset times, and there is no systematic difference between them as seen in the comparison to the result of Obara (2002) method. Our new method is applicable to volcanic earthquakes recorded at other seismic networks that consist of at least several stations surrounding hypocenter regions, which will help us to monitor and understand volcanic activity.

Keywords: hypocenter determination, envelope correlation, Miyakejima volcano

## The annual variation in the teleseismic detection capability at Syowa Station, Antarctica

IWATA, Takaki<sup>1\*</sup> ; KANAOKI, Masaki<sup>2</sup>

<sup>1</sup>The Institute of Statistical Mathematics, <sup>2</sup>National Institute of Polar Research

Kanao et al. [2012a, 2012b] have pointed out the annual variation in the teleseismic detection capability at Syowa Station located in Antarctica. The main cause of the variation is considered to be the increase in area and/or thickness of sea ice in winter, which restrains the generation of sea waves around Antarctica; consequently the noise level in seismic records changes annually [Grob et al., 2011; Kanao et al. 2012c].

This implies that environmental parameters relevant to climate, sea ice, and so forth affect the teleseismic detection capability. To investigate the relationship in detail, a quantitative evaluation of the annual variation in the detection capability is dispensable because the aforementioned studies have revealed the annual variation only qualitatively on the basis of the time history of the minimum magnitude of detected teleseismic events at the station. Therefore, we conducted the following analysis in this study.

The dataset analyzed in this study is the same as the examined one in Kanao [2010] and Kanao et al. [2012]. The data period ranges from 1987 to 2007 and the magnitudes of the events are measured with the body-wave magnitude ( $M_b$ ) scale. The number of analyzed earthquakes of which magnitudes are determined is 19,044. Because the main interest of this study is to quantify the annual variation, the earthquake sequence is divided into periods of one year and these one-year sequences were stacked.

For the quantification of the detection capability, the model representing a magnitude-frequency distribution of earthquake covering the entire range [Ogata & Katsura, 1993] is used with a small modification. In this model, the distribution is assumed to be the product of the Gutenberg-Richter (GR) law [Gutenberg and Richter, 1946] and the detection probability of earthquakes at magnitude  $M$ . As mentioned above, the magnitudes in the examined dataset are given as  $M_b$ , which saturates at its large value. Therefore, instead of the original GR law, we introduced a modified type of the GR law, which is suggested by Utsu [1974], that contains the maximum magnitude of earthquake potentials as a parameter. The detection probability was represented by the cumulative distribution of a normal distribution, following the suggestion of Ringdal [1975] and its accompanied studies [e.g., Ogata & Katsura, 1993; Iwata, 2008, 2012, 2013a, 2013b, 2013c]. This formulation results in the introduction of a parameter  $\mu$ , which corresponds to the magnitude at which 50% of earthquakes are expected to be detected, and this parameter quantifies the quality of the earthquake detection capability.

Then, the annual variation in  $\mu$  was estimated by adopting a Bayesian approach used in Iwata [2013a, 2013b]. In this approach, the annual variation is represented by a piecewise linear approximation of which breaking points were taken at each of the occurrence times of each events. We determined the variation in  $\mu$  with a smoothness constraint.

The result of the estimation is summarized as follows. The significance of the existence of the annual variation was evaluated with ABIC [Akaike, 1980]; the value of ABIC in the case with the annual variation is 54.9 smaller than that in the case without the annual variation, suggesting high significance of the variation. The maximum (i.e., the worst detection capability) and minimum (i.e., the best) values of  $\mu$  appear around the end of December and the middle of August, respectively. The difference between the maximum and minimum values is 0.13. Because the maximum and minimum of the average temperature at Syowa Station also appear in those periods, this result reinforces the relationship between the environmental parameter and teleseismic detection capability.

(The references are listed in the abstract written in Japanese.)

Keywords: earthquake detection capability, annual variation, Antarctica, Syowa Station, Bayesian statistics, statistical seismology

## Towards Detection of Hydraulic Fracturing Induced Earthquakes Using Neural Network

KIM, Ahyi<sup>1\*</sup> ; IIDA, Shuhei<sup>1</sup> ; FUJIHARA, Satoru<sup>2</sup>

<sup>1</sup>Yokohama City University, <sup>2</sup>Itochu Techno-Solutions Corporation

Detection, location and determination of focal mechanism of low frequency and hybrid events such as volcanic and non-volcanic events have been extensively studied. Recently, Das and Zoback (2011) found unusual events which has relatively low frequency in the seismic activity induced during hydraulic fracturing in a gas shale reservoir. Those events were observed in limited frequency band similar to tectonic tremor sequences. It is important to understand the mechanisms of those events for clarifying the fracturing process during the hydraulic stimulation. In this study, we introduce a method to detect the band-limited waveform using neural network. The results of the initial numerical test indicate that the harmonic function waveforms could be identified when they have clear features in shape. As the next step, we will add realistic noise to the synthetic data and perform the synthetic analyses. After we verify the applicability of our method, we will apply the method to real seismic data observed during fluid injection.

Keywords: Neural Network, Waveform detection, Hydraulic fracturing, Low frequency earthquake, Seismic Waveform

## Background noise characteristics of F-net broadband seismograms

KIMURA, Takeshi<sup>1\*</sup> ; MURAKAMI, Hiroshi<sup>2</sup> ; YANO, Tomoko elizabeth<sup>1</sup> ; KIMURA, Hisanori<sup>1</sup> ; KAZAKAMI, Tomoe<sup>1</sup> ; MATSUMOTO, Takumi<sup>1</sup>

<sup>1</sup>NIED, <sup>2</sup>ADEP

National Research Institute for Earth Science and Disaster Prevention (NIED) has operated a broadband seismometer network, F-net. F-net consists of 73 stations in Japan and a broadband seismometer, STS-1/2/2.5 or CMG-1T/3T, has been installed at each station. The seismometers are installed in 30-50 m vault to prevent effects of the temperature and air pressure changes. All the data are openly available on the web, and rapid automated data processing systems, such as AQUA system [Matsumura et al., 2006], have used these data. To evaluate the data quality continually is important for the operation of the observation network, the earthquake monitoring, and the automated analyses. In order to assess the F-net data quality, we investigated the characteristics of their background noise.

To quantify the background noise of F-net waveform data, we used probability density functions (PDFs) of power spectral densities (PSDs) [McNamara & Buland, 2004]. For 1996-2013 continuous waveform data with the interval of 1 sec, PSDs of ground acceleration were computed from overlapping (50 %) 1-day time-windows. Each time-window was divided into 13 time segments (6 hours) overlapping by 75 %, and the 1-day PSD estimate was calculated as the average of the 13 segment PSDs. These 1-day PSDs were gathered by binning periods in 1/8 octave intervals and binning power in one-dB intervals.

We calculated a new noise model for F-net, based on the statistical mode of the obtained PDFs for vertical component of all the F-net stations [McNamara & Buland, 2004]. The noise model was constructed from the minimum PDF mode value among all the stations at each period. The values of the F-net model is ~5 dB higher than ones of the mode noise model of the continental United States [McNamara & Buland, 2004] around periods of 4 sec and 40 sec. The F-net noise model is mainly defined by the STS-1 mode values. The STS-2 values are ~5 dB larger than STS-1 ones at the periods of 200-800 sec, and the CMG-1T/3T are ~15 and ~10 dB larger than STS-1 at 30-2000 sec and 100-2000 sec, respectively.

Recently, we have equipped a styrofoam cover on the broadband sensor for temperature shielding. This cover has reduced the PDF mode values for vertical component of STS-2 by ~5 dB at the periods longer than 500 sec, and is useful to obtain such long-period signals with a good signal/noise ratio.

Keywords: background noise, broadband seismometer, F-net

## Long-term ocean-bottom seismometers in MRI/JMA and some related problems

HIRATA, Kenji<sup>1\*</sup>; TSUSHIMA, Hiroaki<sup>1</sup>; YAMAZAKI, Akira<sup>1</sup>; KATSUMATA, Akio<sup>1</sup>; MAEDA, Kenji<sup>1</sup>; BABA, Hisatoshi<sup>2</sup>; MATSUBARA, Tadayasu<sup>3</sup>; ITOU, Tatsuya<sup>3</sup>; SUGITA, Tomoya<sup>3</sup>; HORI, Katsuhiko<sup>4</sup>; SHIRAKO, Takeshi<sup>4</sup>

<sup>1</sup>Meteorological Research Institute, JMA, <sup>2</sup>School of Marine Science and Technology, Tokai University, <sup>3</sup>Tokyo Sokushin, <sup>4</sup>NiGK Corporation

In 2011 to 2012, seismology and volcanology research department/MRI introduced eight long-term ocean-bottom seismometers (OBSs) by converting existing short-term ones so that we were able to conduct one-year-long, three-component seismographic observation. The conversion was made by changing the control circuit, the AD convert, and the data storage device into low-power consumption ones.

In November 2011, four long-term OBSs were deployed off Boso Peninsula, about 40 km east of Tokyo, to test them and to investigate seismicity in this region that adjoins the southern end of the mainshock rupture area of the March 11, 2011 Tohoku earthquake (Mw9.0). In September 2012, we tried to recover the four long-term OBSs that were deployed in 2011 and re-deploy other four long-term OBSs. However, all transponder units of four long-term OBSs to be newly deployed got out of order soon after the vessel left the port. So we declined to newly deploy other four long-term OBSs. Also, we could not recover two long-term OBSs among four that were deployed. We confirmed that two recovered long-term OBSs recorded ultra-micro earthquake activity successfully.

After the cruise, the OBS transponder units that became out of order were tested in manufacturer's laboratory so that the cause of the trouble was inferred to be (1) possible opening within the housing of transducer unit of OBS transponder due to thermal expansion/contraction thorough high temperature in summer and low temperature in winter, and (2) cavitation in silicon-oil within the housing of transducer unit of OBS transponder due to hull vibration. Countermeasures were devised as follows; (a) overhaul of electric circuits and transducer unit housing filled with silicon oil, (b) use of base-isolation floor-mat on which OBSs should be placed. Both of manufacturer's laboratory tests and actual onboard tests suggest that these countermeasures are effective.

Keywords: long-term, seismographic observation, ocean-bottom seismometer, measure for a glitch

## Value change of ocean bottom pressure gauge (Paroscientific depth sensor) by inclination of the sensor

OGATA, Naoki<sup>1\*</sup> ; SATO, Toshinori<sup>1</sup> ; YAMADA, Tomoaki<sup>2</sup> ; SHINOHARA, Masanao<sup>2</sup>

<sup>1</sup>Graduate School of Science, Chiba Univ., <sup>2</sup>ERI, Univ. Tokyo

### Introduction

Ocean bottom pressure gauges (OBP) using depth sensor of Paroscientific Inc. are used for observation of up-down crustal movement at ocean bottom (e.g. Inazu et al., 2012). Observation error of this sensor is about 0.5 hPa (about 5mm in water) (e.g. Kono et al., 2012). So, this sensor is expected to detect coseismic movements and movements with large slow slip events such as the Boso slow slip events. But, it is known that this sensor shows incorrect values when the sensor is inclined. This suggests the possibility that this sensor can not obtain correct value because OBP itself may be inclined by coseismic crustal deformation. This presentation shows measurements of value change by inclination of the sensor, and discusses limits of inclination based on the observation error.

### Measurements and results

We used an intelligent depth sensor 8CB2000-I, Paroscientific Inc. We set the sensor upright, then incline it, hold it for some time, then return it upright. We measured differences of the values between upright position and inclined position. We found that if we incline the sensor very fast, it shows very large transient values after inclined. So, we need slow inclination (a few ten seconds per 10 degree inclination) of the sensor. After the measurements, we fit the data using a spherical harmonic function.

The observed data show 2 hPa at 10 degree inclination, 6 hPa at 20 degree, and 12 hPa at 30 degree. The data is not symmetrically with respect to the upright position, but symmetrically at a point which is inclined about 15 degree from the upright position. The reproducibility of the values for inclination is within about 0.3 hPa (STD). From this result, inclination limit of OBP is about 5 degree if OBP sits on the ocean bottom flat. If OBP touches down at steeper inclined bottom, the limit become narrower. If OBP is inclined at 20 degree, the limit is about 2 degree.

Keywords: Pressure gauge, inclination correction, Paroscientific Depth Sensor

## Evaluating performance of automatic earthquake detection and location system for the nationwide seismic network(2)

NAKAYAMA, Takashi<sup>1\*</sup> ; HIRAHARA, Satoshi<sup>1</sup> ; KONO, Toshio<sup>1</sup> ; NAKAJIMA, Junichi<sup>1</sup> ; OKADA, Tomomi<sup>1</sup> ; UMINO, Norihito<sup>1</sup> ; HASEGAWA, Akira<sup>1</sup> ; HORIUCHI, Shigeki<sup>2</sup> ; HORIUCHI, Yuko<sup>2</sup>

<sup>1</sup>Graduate School of Science, Tohoku University, <sup>2</sup>Home Seismometer Corporation

The number of seismic stations has tremendously increased by many temporary seismic networks recently deployed in various areas, in addition to dense routine seismic networks such as the nationwide Kiban seismic network. Effective automatic earthquake detection and location system is anticipated, because the ability of data processing is limited. Manually picking P- and S-wave arrival times etc. from a huge amount of seismic waveform data observed by such many seismic stations is considerably time consuming work.

Horiuchi et al. (2012, 2013) have developed such an automatic seismic waveform processing system. This system was set up at Tohoku University on December 2012, and automatic detection and location processing of the nationwide seismic network data has been operating since then. The system can detect and locate many earthquakes which are difficult to be located by the routine processing based on manual pickings. However, sometimes earthquakes cannot be correctly discriminated by the system: for example, when more than two earthquakes occur almost simultaneously. In order to consider the application of automatic earthquake detection and location system to the actual seismic network, we need to know its performance.

Nakayama et al. (2013) tried to evaluate performance of this earthquake detection and location system for the application to the nationwide seismic network. Results showed that the automatic system could detect and locate earthquakes about 1.5 times more than those in the JMA unified catalogue. The automatic system extended the lower limit of the detection capability to much smaller magnitude range than that by the JMA unified catalogue. The evaluation also showed that S-wave arrival times picked by the automatic system were systematically delayed by ~0.05-0.1 sec compared with those by the manual pickings of the unified catalogue. Based on this performance evaluation, Horiuchi et al. (2014 this meeting) have tried to improve the system by developing a new algorithm to better pick S-wave arrivals.

We have evaluated performance of this presently improved automatic processing system by using the waveform data for the same period as those in the previous evaluation. Results show that the systematic delay of S-wave arrivals by the automatic pickings is considerably improved and the difference in S-wave arrivals between the new automatic system and the unified catalogue has become nearly the same as that between the manual pickings by Tohoku University and those in the unified catalogue. This indicates that the S-wave arrival times, as well as P-wave arrival times, picked by the automatic system almost stand comparison with those by the manual picking. Moreover, the evaluation shows that the new system also improved the rate of correct discrimination of earthquakes: the percentage of events that were missed to be correctly located decreased from 19% to 14% (most of these events are those located in and around the Izu-Bonin Islands and the Ryukyu Islands), and the percentage of events that were incorrectly defined as earthquakes decreased from 3.1% to 2.5%. This is because of the improvement of algorithm to correctly discriminate more than two earthquakes that occurred nearly simultaneously.

Keywords: automatic arrival time picking, automatic event detection and location system, performance evaluation

## W-phase analysis with 1Hz GNSS data

UENO, Hiroshi<sup>1\*</sup> ; KATSUMATA, Akio<sup>1</sup> ; KAWAMOTO, Satoshi<sup>2</sup> ; YAHAGI, Toshihiro<sup>2</sup> ; MIYAGAWA, Kohei<sup>2</sup>

<sup>1</sup>Meteorological Research Institute, <sup>2</sup>Geospatial Information Authority of Japan

The Japan Meteorological Agency analyze W-phase inversion solution and CMT solution when big earthquakes occur. Now we can analyze W-phase solution with broadband seismograms in Japan after 6 minutes of earthquake occurrence. These W-phase solution are one of information for performing grade changes or cancel of TSUNAMI warning.

Broadband seismic records is used by integrating for W-phase analysis. Because when big earthquake occur, the waveform data recorded at near site from source area may be unstable, it might be difficult for analyzing W-phase solution. On the other hand, the GNSS data to be recorded directly displacement, it can be used as a stable displacement.

In this study, using 1Hz GNSS data of Geospatial Information Authority of Japan(GSI), we analyzed W-phase solutions of Great Tohoku earthquake in 2011, its aftershock, and Tokachi-oki earthquake in 2003.

Keywords: W-phase analysis, 1Hz GNSS data, Great Tohoku earthquake

## Automated event identification of aftershocks(2)

KATSUMATA, Akio<sup>1\*</sup>

<sup>1</sup>Meteorological Research Institute, JMA

We are developing a seismic event identification technique for a quick grasp of aftershock activities of great earthquakes. For the case of the 2011 off the Pacific coast of Tohoku Earthquake, a number of onsets of aftershocks were not clear due to successive occurrence of aftershocks. Envelops of seismic waves are used to make it possible to estimate source locations of events without clear onsets.

The method is based on peak amplitudes and their times as

- (1)A band pass filter is applied to the seismic waves.
- (2)Envelop of seismic wave is obtained.
- (3)Peak amplitudes and times are checked.
- (4)Possible events are searched for the data of envelop amplitudes and times.

Formerly we tried to estimate source parameters by searching a solution in five-dimensional space of (origin time, latitude, longitude, depth, magnitude) by the shuffled complex evolution (SCE-UA) method. However, good solutions were seldom obtained because a combination of noise data often show a high score.

We changed the source estimation method. At the first, a group with high S/N data is searched for. We select a key data with highest S/N from the group. Then we estimate the best source parameter which is consistent to the selected data. While searching for the source location, the focal depth is fixed and epicentral distance and azimuth are changed. The origin time is obtained from the time of the envelop peak and epicentral distance, and the magnitude is estimated from the peak amplitude and epicentral distance.

Noise is often selected as the key data. Noises are usually rejected because they do not form a group of consistent data. Data of noise and identified events are removed from dataset to be checked. Data search is continued until no candidate is left.

Events are successfully identified and source locations are properly estimated for the events with a number of data. However source locations are not properly estimated for events with a small number of data.

We used seismic data from the National Research Institute for Earth Science and Disaster Prevention, Hokkaido University, Hirosaki University, Tohoku University, University of Tokyo, Nagoya University, Kyoto University, Kochi University, Kyushu University, Kagoshima University, the National Institute of Advanced Industrial Science and Technology, Aomori prefectural government, Tokyo metropolitan government, Shizuoka prefectural government, Kanagawa prefectural government, the City of Yokohama, the Japan Marine Science and Technology Center, and the Japan Meteorological Agency.

Keywords: automated seismic event identification, envelop of seismic wave

## Construction of the seismic observation network around Shimokita Peninsula

SEKINE, Shutaro<sup>1\*</sup> ; SAWADA, Yoshihiro<sup>1</sup> ; KASAHARA, Keiji<sup>1</sup> ; SASAKI, Shunji<sup>1</sup> ; TAZAWA, Yoshihiro<sup>1</sup> ; YAJIMA, Hiroshi<sup>1</sup>

<sup>1</sup>Association for the Development of Earthquake Prediction

### Introduction

Seismic activity in the Shimokita region is not well grasped, because the distribution of the seismic stations is not dense compared with that of Southern Tohoku region. So, it is not enough to estimate the depth of the seismogenic zone. Accordingly, the Association for the Development of Earthquake Prediction (ADEP), determined to newly construct a high-density seismic observation network (AS-net) in the region in question, as a part of its investigation and research into seismic activity in the Shimokita Peninsula. An outline of the observation network is presented below.

### Outline of the network

The AS-net consist 36 seismic observation stations. 20 stations were made before the end of 2013. And the other stations will make in 2014.

The sensors of each station are installed in boreholes at a depth of about 20m. We set the short period three dimensional velocity sensors by Lennartz, and accelerometers by Japan Aviation Electronics Industry ltd. And A/D converter is LS-7000XT made by Hakusan Co.

The data of the each station send to ADEP using with Internet, and relay to other facility for research.

### Future works

It is anticipated that useful data will be obtained regarding detailed velocity and attenuation structures in the area surrounding the seismic observation network, as well as micro earthquake activity in the regions. The number of the earthquakes we estimate in January, is twice as that of JMA.

Keywords: seismic observation network, Shimokita Peninsula

## Regional Airborne Survey for the Evaluation of Geothermal Potential in Japan

SHIMADA, Tadaaki<sup>1\*</sup> ; TAKAI, Katsumi<sup>1</sup> ; MIYAKE, Kazuhiro<sup>1</sup> ; HISATANI, Koichi<sup>1</sup> ; TOSHA, Toshiyuki<sup>1</sup>

<sup>1</sup>Japan Oil, Gas and Metals National Corporation

Japan Oil, Gas and Metals National Corporation (JOGMEC) supports smooth development of geothermal resources in Japan by providing assistance to geological, geophysical, and well-drilling surveys, equity capital or liability guarantees, and information and data on geothermal resources.

As part of them, we planned to conduct evaluation of geothermal potential with airborne technique of gravity gradiometer method and time-domain electromagnetic method.

The gravity gradiometer method measures the differential of gravity, and provides information of much detailed geological structures. The time-domain EM method provides deeper penetration data than the frequency-domain EM method.

Since these methods are state-of-the-art techniques, we demonstrated them first in a couple of area with relatively high geothermal potentials and a lot of surveys conducted.

We carried out airborne survey with the technique of the gravity gradiometer method in the Kuju and the Kirishima areas in 2013. We would like to introduce the result of the airborne survey.

The authors thank local municipalities and related organizations for their understanding and cooperation to conduct the airborne survey.

Keywords: airborne survey, geothermal resources, gravity, gravity survey, electromagnetic survey

## Study on the prediction of the deep catastrophic landslide using the Airborne Electromagnetic Survey

KAWATO, Katsushi<sup>1\*</sup> ; KINOSHITA, Atsuhiko<sup>2</sup> ; TAKAHARA, Teruyoshi<sup>2</sup> ; ISSHIKI, Hiromitsu<sup>2</sup> ; ISHIZUKA, Tadanori<sup>2</sup> ; OKUMURA, Minoru<sup>1</sup> ; UCHIDA, Koichi<sup>1</sup>

<sup>1</sup>Nippon Engineering Consultants Co.,LTD., <sup>2</sup>Public Works Research Institute

Recently, the deep catastrophic landslides were occurred frequently including the disaster of the Kii peninsula by typhoon 12 in 2011. The risk evaluation is demanded to be carried out the measures that we can assume at the both sides of the method constructing sabo dams and evacuation method. Recently, the airborne electromagnetic survey is performed a close-up to evaluate the risk of them. Merits of the airborne electromagnetic survey include that a geological feature border in conjunction with the deep catastrophic landslides having possibilities to become clear, hydrological properties may become clear. On the other hand, there is the uncertain element such as the decision method of the ratio resistance level of the geological feature border and the groundwater not being clear. In this study, we have arranged the results such as in the airborne electromagnetic survey, a geological survey, the hydrological investigations for the points where the deep catastrophic landslides were occurred and where airborne electromagnetic survey was carried out so far. The study areas are Byutano river basin (is about 4.4km<sup>2</sup>), Fujikawa river basin (about 3.7km<sup>2</sup>), Himekawa basin (about 15.2km<sup>2</sup>), and Kumano river basin (about 10.1km<sup>2</sup>). In these areas, in the past, the deep catastrophic landslides were occurred and the airborne electromagnetic surveys were carried out.

First, we have examined ratio resistance properties every area by the airborne electromagnetic survey. The range of the ratio resistance level to appear in the area for showed 1-2400  $\Omega$ -m in 1-1200 $\Omega$ -m, the Kumano river basin in the Himekawa river basin whereas it was 1-400 $\Omega$ -m in Byutano river basin and the Fujikawa river basin, and the distribution of the ratio resistance level knew that there was a difference by a geological feature and an area. And we have found that there were three patterns of the distributions of the resistance when we have paid our attention to the ratio resistance pattern of the plumb directions from the surface of the slope at the point with the fear of the deep catastrophic landslides to the deep part. From this, the depth that a ratio resistance level changes in the plumb direction may become the fundus of the deep catastrophic landslide. Boring investigations were carried out in Byutano river basin, Fujikawa river basin, Himekawa river basin, and a weathering department and the geological feature border of the virginity part are authorized by the observation of the boring core. The ratio resistance level corresponding to this geological feature border indicates 100 $\Omega$ -m in Byutano river basin, 70 $\Omega$ -m in Fujikawa river basin, and in Himekawa river basin indicates 500 $\Omega$ -m, 680 $\Omega$ -m, 1000 $\Omega$ -m.

From these, it was confirmed that the ratio resistance level to correspond to appearance frequency and the geological feature border of the ratio resistance level varied according to an area and a geological feature. Therefore, it is necessary to carry out the risk evaluation of the deep catastrophic landslide after carrying out a boring investigation in addition at a representative point when we carry out the airborne electromagnetic survey, and having arranged a geological feature and the relations of the ratio resistance level.

In addition, at the deep catastrophic landslide point of Kumano river basin, consecutive low ratio resistance zones and the low ratio resistance zone of the plumb direction are common to the valley part from the ridge and are confirmed and agree with the groundwater situation by the hydrological investigation. We need to accumulate data about the ratio resistance structure in conjunction with the deep catastrophic landslide and want to examine the extracting method of the point with the fear of the deep catastrophic landslide, an estimate method of the collapse depth and collapse volume in future.

Keywords: Airborne Electromagnetic Survey, deep catastrophic landslide

## Study on the prediction of the large landslides of the volcanoes using the Airborne Electromagnetic Survey

KINOSHITA, Atsuhiko<sup>1\*</sup> ; TAKAHARA, Teruyoshi<sup>1</sup> ; ISSHIKI, Hiromitsu<sup>1</sup> ; ISHIZUKA, Tadanori<sup>1</sup> ; OODAIRA, Tomohide<sup>2</sup> ; OMORI, Tetsuji<sup>3</sup> ; YAMANE, Hiroyuki<sup>3</sup> ; ARAI, Kenichi<sup>4</sup> ; KIYONO, Koji<sup>5</sup> ; TSUJIOKA, Hideki<sup>6</sup>

<sup>1</sup>Public Works Research Institute, <sup>2</sup>Fukushima River and National Highway Office, <sup>3</sup>Fuji Sabo Office, <sup>4</sup>Asia Air Survey Co., Ltd., <sup>5</sup>Nippon Engineering Consultants Co., Ltd., <sup>6</sup>OYO Corporation

In the lower basins of the active volcanoes, there are always the risks that sediment disasters are occurred. Especially, when large landslides are occurred at the time of heavy rains, the landslide sediment become a debris flow and makes a big damage by the sedimentation and the flooding in a lower basin. In late years, the Airborne Electromagnetic Survey is performed a close-up of as means to predict these large-scale landslides. It is necessary to estimate establishing technique to estimate a collapse side, the water seepage process in the slope to predict the slope where there is possibility of the collapse in at the time of heavy rains, but is the situation that is hard to say to be considered about these enough currently. Therefore, in this study, we have taken Mt. Azuma and Mt. Fuji examples and examined the estimate technique of the collapse side and technique to predict a water seepage process from the result of a geological survey and the quality of the water investigation that we carried out the airborne electromagnetic survey in addition.

First, we performed the documents investigation into the characteristics of the topography, the geological feature, results of the sediment disasters, volcanic activity history there. Next, we performed a field work and confirmed the quality of soil structure in conjunction with the landslides, hydrothermal alteration situation causing the landslides and the hot spring gush situations. We examined areas of the airborne electromagnetic survey in reference to these results. We decided that the top of the mountain body and the representative craters were included and did the investigation object with the area including inclines more than 15 degrees that landslides were possible. The exploration area of Mt. Azuma was about 18km<sup>2</sup> and the exploration area of Mt. Fuji was about 120km<sup>2</sup>. We have arranged them every depth two-dimensionally so that we could recognize the result of the helicopter electromagnetic exploration regionally. And, at the area where sediment disasters were easy to be occurred, there were some craters and water level under the ground were high, we have arranged them every depth two-dimensionally so that we grasped ratio resistance levels of the depth direction for running. We have verified the result of the airborne electromagnetic survey by comparing with the investigation results of the topographic and geological features. In addition, we investigated hydrology and water quality of the water at 10 neighboring streams in Mt. Azuma for the purpose of confirming the result of the airborne electromagnetic survey in detail. The investigation items were water discharge, electric conductivity, pH, water temperature and ion silica concentration. In addition, we have carried out the boring investigation for the purpose of checking the ratio resistance levels by the airborne electromagnetic survey and the relations with the geological feature in Mt. Fuji.

We have found that by using the airborne electromagnetic survey in volcano area we could roughly grasp the geological features and underground water levels. From this, we could roughly predict the slopes that may collapse at the time of a heavy rain by using the airborne electromagnetic survey. On the other hand, we cannot estimate the collapse depth and the collapse volume in detail when it is only the airborne electromagnetic survey. It is necessary to supplement the results of the airborne electromagnetic survey by carrying out other investigations which are the boring investigations and physics explorations on the ground, the water quality and hydrological investigation to estimate these. In the near future, we will carry out the investigations including the airborne electromagnetic survey for models in some volcanoes and want to establish the estimate technology of the collapse dangerous points in the volcano areas, estimate technique of the collapse depths and collapse volume by accumulating data.

Keywords: airborne electromagnetic survey, large landslide, volcano

## Verification of the tunnel geological structure based on the helicopter-borne magnetometry data analysis

OKAZAKI, Kenji<sup>1\*</sup> ; ITO, Yoshihiko<sup>1</sup>

<sup>1</sup>CERI, PWRI

### 1. Introduction

More detailed geological information of tunnel ground is very important for its construction. Especially, geological complicated area, such as accretionary complex, is needed more accurate information for process control and avoidance of risk during construction of tunnels. The authors carried out helicopter-borne magnetic survey to verify its applicability for geotechnical evaluation of a mountainous planned road tunnel in east Hokkaido, Japan. We describe corresponds with the results of the geological profiles estimated from the outcomes of tunnel construction records and its analysis results of magnetic anomalies which was obtained by helicopter-borne magnetometry data.

### 2. Outline

The geology of the study area is mainly consists of greenstone, pyroclastic sedimentary rock and hyaloclastite, and is mixed with pillow lava, chert and limestone. Many faults are formed in the area around the survey site due to tectonic movements at the time of formation of the accretionary complex and after that. Surveyed tunnel is planed to 910 m long and maximum overburden is 150 m. The magnetic intensity was measured from a helicopter at low altitude using a cesium magnetometer, and a magnetic intensity map was compiled based on the scalar volume of the magnetic force after reduction to pole magnetism. The probable geological model of the tunnel profile was analyzed using the magnetic anomaly pattern. The forward modeling process for the magnetic data was conducted using Mag2dc software (Cooper, 2003) based on the Talwani algorithm for calculation anomalies. The forward modeling was carried out according to the type of magnetic anomaly over blocks/steps, dependence of anomaly on width, depth, susceptibility contrast and dip angle. The tunnel geological models that estimated using the magnetic anomaly pattern were verified by the geological properties from tunnel construction records.

### 3. Results of survey

Results of this survey, executed in a mountainous area where accretionary complexes are distributed, are summarized as follows:

1) Helicopter-borne magnetic survey was carried out for a tunnel in northeastern Hokkaido and magnetic intensity map was figured. By the correlation to the other results such as the geological survey or the observation of rock type and fracture shear and conditions in advanced core, high magnetic intensity zone corresponded to the sedimentary rock and the fracture and shear zone of hyaloclastite and massive basalt.

2) Two geological models were made by combining helicopter-borne magnetic survey results with geological survey results and magnetic intensity model. The models were correlated to the detailed data obtained by advanced boring core observation, and these distributions are roughly confirmed by advanced boring core observation.

3) In this case study, helicopter-borne magnetic survey provided useful information for effective interpretation. To analyze geological structure by helicopter-borne magnetic survey is very effective to evaluate potential geotechnical issues when excavating a tunnel.

Keywords: helicopter-borne magnetic survey, magnetic anomalies, accretionary complex, road tunnel

## Magnetic structure of the tsunami inundation area of the 2011 off the Pacific coast of Tohoku Earthquake

OKUMA, Shigeo<sup>1\*</sup> ; UEDA, Takumi<sup>1</sup> ; NAKATSUKA, Tadashi<sup>1</sup> ; MITSUHATA, Yuji<sup>1</sup> ; JINGUUI, Motohara<sup>1</sup> ; UCHIDA, Toshihiro<sup>1</sup>

<sup>1</sup>Geological Survey of Japan, AIST

In June 2012, the Geological Survey of Japan (GSJ) conducted an airborne EM and magnetic survey over the inundation area by the tsunami of the 2011 off the Pacific coast of Tohoku Earthquake, northeast Japan. The purpose of the survey was mainly to map the resistivity of the subsurface structure associated with sea water invasion by the tsunami. Airborne EM data were successful for revealing the subsurface resistivity distribution as an aid for groundwater assessment of the study area.

Aeromagnetic data were also observed by the survey and processed (Okuma et al., 2013). However, it turned out that the magnetic data seem to be contaminated by artificial noise with amount of ~20nT probably caused by the survey helicopter. To mitigate directional errors (Herringbone effect), the generalized mis-tie control method (Nakatsuka and Okuma, 2006) was applied to the observed magnetic data and magnetic anomalies were reduced onto a smoothed observation surface. According to the compiled aeromagnetic anomaly map of the Southern Sendai Plain, magnetic highs lie over the Cretaceous granitic rocks with high magnetic susceptibilities ( $\sim 10^{-2}$  SI; PB-Rock 21) outcropping on the north-trending Wariyama Mountains, which may constrain the groundwater flow system. The magnetic highs also extend NE and reach the Pacific coast, implying the existence of Cretaceous granitic rocks. In a map of the Matsukawaura area, an obvious magnetic high lies over the northern edge of the lagoon without any signatures of magnetic sources on surface. To better understand the subsurface structures of the survey areas, we applied 3D imaging (Nakatsuka and Okuma, 2013) to the observed magnetic anomalies. The preliminary results of the imaging indicate magnetization highs lie below the Wariyama Mountains and coastal regions between the Torinoumi Lagoon and Ushibashi river mouth in the Southern Sendai Plain. An obvious magnetization high is present below the northeastern edge of the Matsukawaura Lagoon, corresponding to granitic rocks with high magnetic susceptibilities ( $\sim 10^{-2}$  SI; PB-Rock 21) at a depth of around 300m below the surface in a hot spring exploration well. The details of the 3D imaging will be shown in the presentation.

Keywords: airborne EM survey, tsunami, groundwater environment, aeromagnetic survey, magnetic structure, basement

## Repeated aeromagnetic surveys in Shinmoedake volcano, Japan, by using an unmanned helicopter

KOYAMA, Takao<sup>1\*</sup> ; KANEKO, Takayuki<sup>1</sup> ; OHMINATO, Takao<sup>1</sup> ; WATANABE, Atsushi<sup>1</sup> ; TAKEO, Minoru<sup>1</sup> ; YANAGISAWA, Takatoshi<sup>2</sup> ; HONDA, Yoshiaki<sup>3</sup>

<sup>1</sup>Earthquake Research Institute, University of Tokyo, <sup>2</sup>Institute for Research on Earth Evolution, Japan Agency for Marine-Earth Science and Technology, <sup>3</sup>Center for Environmental Remote Sensing, Chiba University

After the 2011 eruptions of Shinmoedake volcano in Japan, we conducted three repeated aeromagnetic surveys around this area, by using an autonomously driven unmanned helicopter. Shinmoedake volcano had sub-Plinian eruptions in the end of January 2011 and its vent was filled by uprising intrusive lavas. After that, some Vulcanian eruptions followed, and then volcanic activities were decreasing gradually up to the beginning of April 2011.

After these events, we conducted aeromagnetic surveys in the end of May 2011, the beginning of November 2011, and the end of October 2013. The Yamaha RMAX-G1 unmanned helicopter was used for our surveys, which was usually used to spray the agricultural chemicals to fields, and can make flights following the programmed tracks within about 1 m precision. Availability of precise flights are a great advantage for repeated surveys in order to detect easily the changes of circumstances, such as, geomagnetic changes due to volcanic activities by measuring at the same positions. Almost 85 km flights in total were made in every survey with a flight speed of about 10 m/s. Flight heights above the ground were almost kept in 100 m.

As the result of some data processing, we clearly detected the change of the magnetic fields around the vent of Shinmoedake, which has a kind of a dipolar pattern with positive changes in South and negative changes in North. This indicates a region around the vent got magnetization due to cooling. The intrusive lava is supposed to be the source of magnetization, and  $2.0 \times 10^7$  Am<sup>2</sup> magnetization of lava is evaluated at the second survey (0.5yr) and  $4.8 \times 10^7$  Am<sup>2</sup> is evaluated at the third survey (2.5yr), compared with the first survey. This means the magnetizing rate is almost related to a square root of the elapsed time and it leads to an implication the lava cooling is dominantly made gradually by thermal diffusion, not by other cooling processes such as thermal convection. The common thermal diffusivity of rocks, however, is too small by one order of magnitude to explain this cooling rate, and intrusion of water in lava, say, rainfall water, may play an important role to raise the effective thermal diffusivity to make the lava cool.

## The 3D magnetic imaging using the L1 regularization and variable selection procedure.

UTSUGI, Mitsuru<sup>1\*</sup>

<sup>1</sup>Graduate School of Science, Kyoto Univ.

Recently some new method to obtain 3D subsurface structure from the gravity or geomagnetic data were proposed. Some of them have a goal to obtain a stable and most simple model which reproduce the observed data in high accuracy. This is because, in generally, most of the traditional way of inversion for the potential data provides distorted or unfocused mages of real gravitational or magnetic structures. In this study, we propose a new method introducing a L-1 penalized least square procedure and tried to obtain a simple, and therefor high- resolution model.

Lasso(Tibshirani,1995) is a linear regression and variable selection procedure based on the L1 penalized least square. L1 penalty has a effect of shrinkage the value of regression coefficients which has only weak contributions to be 0. So, the Lasso does both continuous shrinkage and automatic variable selection simultaneously. On the other hand, Lasso has some limitations and restrictions. One of them is, at most Lasso algorithm can select nonzero variables of same number of observed data. So, in the case of  $p \ll n$  problem, i.e. in the case of number of unknown regression coefficients ( $p$ ) is larger than the number of observations( $n$ ), this algorithm cannot be adopted or overly shrinkage model will be obtained.To overcome this limitation, Zou and Hastie (2005) proposed a new L-1 penalized method named Elastic Net.This method is a compromise of the L-1 and L-2 regularization method with two control parameters. Using this method, we can treat  $p \ll n$  problems in the framework of L-1 penalized method.

In our presentation, we will show the results of applying this method to the synthesized and real magnetic data.

Keywords: potential, geomagnetism, magnetic structure, L-1 norm regularization

## Magnetic structure of the north part of Deception Island based on the aeromagnetic survey by a small unmanned airplane

SAKANAKA, Shin'ya<sup>1\*</sup> ; FUNAKI, Minoru<sup>2</sup> ; HIGASHINO, Shin-ichiro<sup>3</sup> ; NAKAMURA, Norihiro<sup>4</sup> ; IWATA, Naoyoshi<sup>5</sup> ; OBARA, Noriaki<sup>6</sup> ; KUWABARA, Mikio<sup>7</sup>

<sup>1</sup>Akita Univ., <sup>2</sup>NIPR, <sup>3</sup>Kyushu Univ., <sup>4</sup>Tohoku Univ., <sup>5</sup>Yamagata Univ., <sup>6</sup>Robotista, <sup>7</sup>RC Service

Aerial magnetic survey was carried out in the part of the flight project of the autonomous unmanned aerial vehicles (UAV). The project was incorporated with National Institute of Polar Research (Japan), Korea Polar Research Institute, Chile Antarctic Institute, Bulgarian Antarctic research and Spanish Antarctic team. Magnetic anomaly data were acquired over the northern part of Deception Island (within South Shetland islands) in Bransfield Strait. It was the first time to succeed to get the geophysical data by a long-flight unmanned aerial vehicle (UAV) in the area of Antarctica as already reported by our team. Due to the severe weather the flight was canceled over the southern half of the Deception Island and its surrounding sea area.

The flight altitude is about 780m averaged. The main survey lines are directed east-west and the intervals of the lines are about 1000m. Longest length of the main survey line is about 18km. Probably due to the unstable attitude of the UAV body by strong wind, some east-west lines are shortcutted regardless of pre-programmed 18km length courses. The flight courses were overlapped on the survey lines along the latitude of 62 degree 53 minute and the longitude of -60 degree 28 minute. On these lines each direction of the flight is opposite. Some unnatural unduration was seen around overlapped lines. These kinds of unduration are occurred due to the difference of the observed magnetic field on each line. These differences have to be corrected, now we have the tolerable data for estimate the structure of the Deception Island.

Outstanding high magnetic anomaly is recognized over the eastern peak of the island. Preparing topographic digital data of the Deception Island and bathymetric data on surrounding sea area, we estimated the distribution and the intensity of magnetization.

Keywords: Antarctica, Deception Island, Unmanned Aerial Vehicle, Magnetic Survey, South Shetland Islands

## Three dimensional inversion for the Grounded Electrical-Source Airborne Transient Electromagnetic (GREATEM) data

ABD ALLAH, Sabry<sup>1\*</sup> ; MOGI, Toru<sup>1</sup> ; KIM, Hee<sup>2</sup> ; FOMENKO, Elena<sup>3</sup>

<sup>1</sup>Institute of Seismology and Volcanology, Hokkaido University, <sup>2</sup>Departments of Environmental Exploration Engineering, Pukyong National University, Busan, Korea, <sup>3</sup>Nova Scotia Community College, Halifax, NV, Canada

Previous studies conducted by the Grounded Electrical-Source Airborne Transient Electromagnetic (GREATEM) have shown that, this system is a promising method for modelling 3D resistivity structures in coastal areas, in addition to inaccessible area such as volcano, mountainous area covered by deep forest. To expand the application of the GREATEM system in the future for studying hazardous wastes, sea water incursion, geothermal exploration and hydrocarbon exploration, a 3D-resistivity modelling that considers large lateral resistivity variations is required in case of large resistivity contrasts between land and sea in surveys of coastal areas where 1D resistivity model that assumes a horizontally layered structure might be inaccurate. In this abstract we present the preparation for developing a consistent three dimensional electromagnetic inversion algorithm to calculate the EM response over arbitrary 3D conductivity structure using GREATEM system. In forward modelling the second order partial differential equations for scalar and vector potential are discretized on a staggered-grid finite difference method (Fomenko and Mogi, 2002, Mogi et al., 2011). In the inversion method the 3D model discretized into a large number of rectangular cells of constant conductivity and the final solution is obtained by minimizing a global objective function composed of the model objective function and data misfit. To deal with a huge number of grids and wide range of frequencies in air borne datasets, a method for approximating sensitivities is introduced for the efficient 3-D inversion. Approximate sensitivities are derived by replacing adjoint secondary electric fields with those computed in the previous iteration. These sensitivities can reduce the computation time, without significant loss of accuracy when constructing a full sensitivity matrix for 3-D inversion, based on the Gauss-Newton method (Han, N. et al., 2008).

Firstly, we started testing the algorithm in the frequency domain electromagnetic response of synthetic model considering a 3D conductor embedded in uniform half space. In the second step we tested more complex synthetic model, considering vertical contact between two different high and low resistivity quarter-spaces and a conductor embedded in a high resistive quarter-space. Frequency-domain computation is executed at frequencies of five equal logarithm spacings in one decade in the frequency range of ( $10^5$ - $10^{-2}$ ) Hz. After the computation, we transformed into time domain using FFT and compared forward value with inverted value. The inverted results in case of the simple model, appear to highlight a conductive zone of potential interest within the resistive region. In addition, in case of two quarter spaces model, it was able to reveal the clear resistivity contrast between the two quarters spaces and highlight a conductive zone within the high resistive quarter space. Both of the forward and inverted models have almost the same EM response which can confirm the accuracy of the inverted method. The next step for preparing this algorithm will be using the field data from previous GREATEM surveys to demonstrate this technique

Keywords: 3D EM inversion, GREATEM, Numerical approximations, Airborne Electromagnetic

## An Advanced Method of Data Analysis for Gravity Exploration System on a Mobile Vehicle

OGURA, Yumiko<sup>1</sup> ; MATSUDA, Shigeo<sup>2</sup> ; YOKOI, Isamu<sup>3</sup> ; SUDA, Haruo<sup>3</sup> ; KIMA, Sadaharu<sup>3</sup> ; MORIKAWA, Hitoshi<sup>1\*</sup> ; SAEKI, Masayuki<sup>4</sup> ; SUZUKI, Takuya<sup>4</sup> ; KOMAZAWA, Masao<sup>5</sup>

<sup>1</sup>Tokyo Institute of Technology, <sup>2</sup>Clover Tech . Inc., <sup>3</sup>Tokyo Sokushin Co.,Ltd., <sup>4</sup>Tokyo University of Science, <sup>5</sup>OYO Corporation

A model of ground structure is very important to estimate earthquake ground motions. Gravity survey is one of exploration methods. We can estimate ground structure by using information of gravity anomaly which comes from heterogeneous density structure of the ground. Generally speaking, there are high correlation between density and velocity structure of the ground. Thus, the gravity survey is comparatively easier than other exploration method to estimate the ground structure, so that it is very suitable for the aspect of the seismic hazard projection.

For gravity survey, spring-type relative gravimeter is usually used. This type of gravimeter can provide accurate data, however, it is very expensive and difficult to handle. Furthermore, it takes much time to obtain adequate data. We, thus, began to develop a simple and inexpensive sensor which can measure gravity anomaly on a moving vehicle, such as air, land, and sea vehicles, that is, airplanes, motor vehicles, and ships. In a case where a gravimeter is used with a moving vehicle, we may survey the gravity over larger area in shorter time than using conventional survey techniques.

Generally, the gravity should be measured with resolution of 10 micro Gal at least for survey to estimate ground structure. However, the signal obtained from sensor is contaminated by various noise such as vibration of a moving vehicle etc. This means that a sensor with high resolution and large dynamic range is required. This is difficult to realize because resolution and dynamic range are conflicting requirement. To solve this problem, we have developed a sensor with a new feedback system, which has high resolution and large dynamic range. The performance of this sensor is examined in this study, and we also propose a technique of data processing based on the combination of second order blind identification (SOBI) and Hilbert Huang transform (HHT) technique. For this two different type of observations are carried out.

First, we set the sensor statically in a tunnel to confirm whether the sensor can respond to the gravitational effects caused by earth tides. From this observation, it is found that the sensor is affected by atmosphere. The effect is can be removed by applying second order blind identification (SOBI).

Second, the ship survey is carried out. Through a technique of data processing based, the observed data provide quite good agreement with theoretical gravity in phase and period of the signal.

Keywords: gravity survey, Hilbert-Huang Transform, Second Order Blind Identification

## DEM accuracy evaluation in mountain area by utilizing topographic corrected products of high-resolution TerraSAR-X data

NONAKA, Takashi<sup>1\*</sup> ; OKAJIMA, Yuki<sup>1</sup> ; TSUKAHARA, Koichi<sup>1</sup>

<sup>1</sup>PASCO CORPORATION

The commercial high-resolution Synthetic Aperture Radar (SAR) sensors have been developed during past few years and became essential source of information in Earth Observation. The production of the maps is examined in the various fields, such as the damaged area caused by disaster, paddy field area, and forest etc. The interpretation of the objects from the images and the positional accuracy of the images are highly important for the map creation and several basic studies for such issues are also conducted by applying high-resolution SAR data.

TerraSAR-X is one of the commercial SAR satellites, and has acquired data worldwide after it was launched in June 2007. Furthermore, TanDEM-X (TerraSAR-X add-on) was launched in 2010. Both satellites are currently acquiring land surface of Earth for creating global and homogeneous Digital Elevation Model (DEM) of very high precision. TerraSAR-X has several processing level products, and the Geocoded Enhanced Ellipsoid Corrected (EEC) is amplitude data projected to the digital elevation model (DEM), which makes possible for users to integrate other optical data and GIS data. Pre-geocoded Single Look Slant Range Complex (SSC) product is complex data with two axes in the azimuth-slant range plane, and used for interferometric and polarimetric analysis.

It was reported that the geometric accuracy of SSC product was better than 1 m in several previous studies, however there are no reports stating details for the validation results of the EEC product using the actual TerraSAR-X data though it is utilized by the most of users. Therefore the authors evaluated the geometric accuracy of the EEC product by performing in-situ experiment using reflectors on the flat area, simultaneously conducted during satellite passed over. The results showed that the accuracy satisfied several meters in case of utilization of SRTM DEM. In the next stage, we developed the model showing the relationships between the geometric accuracy of range direction, DEM accuracy, incidence angle, and it was revealed that the accuracy of the model was about 1 m in the flat area.

The purpose of this study was to evaluate the accuracy of utilized DEM for the topographic correction by applying the model to TerraSAR-X data in the mountain area. The utilized TerraSAR-X data were 2 data sets of high-resolution SpotLight mode (about 2 m resolution) with the different incidence angles, and the DEMs were produced by ASTER with the mesh of 30 m and SRTM with 90 m. We also used the airborne optical data with a geometric accuracy (Digital topographic level of 2,500 scales) for a validation.

Firstly we selected 25 validation points from the intersections and curves of roads easily interpreted both from TerraSAR-X and airborne data. The average, standard deviation, and Root Mean Square Errors (RMSE) value of the difference between TerraSAR-X and reference optical data were evaluated for X-, Y-, and X-Y plane. In the next stage, we examined to apply the model to data in the mountain area. We estimated DEM's errors by assuming that the variation of the differences of the X-direction was corresponded to the errors of the topographic correction since the range direction was almost same for X direction. The results were summarized based on the evaluations of both flat and mountain areas.

Keywords: Geometric accuracy, TerraSAR-X, topographic correction, ASTER, SRTM

## Pi-SAR-L2 observation of the landslide caused by Typhoon Wipha on Izu Oshima island

WATANABE, Manabu<sup>1\*</sup> ; DAN, Risako<sup>2</sup> ; MOTOHKA, Takeshi<sup>1</sup> ; OHKI, Masato<sup>1</sup> ; SHIMADA, Masanobu<sup>1</sup>

<sup>1</sup>Japan Aerospace Exploration Agency, <sup>2</sup>RESTEC

On October 16, 2013, Typhoon Wipha struck Izu Oshima island, and a large-scale landslide was induced by the heavy rain. Six days after the disaster, Pi-SAR-L2 observation was carried out in four different observation directions (L203201?L203204). One Pi-SAR-L observation (L03801) was carried out before the disaster on August 30, 2000 in same observation direction of L203201. The observation data were used to determine which parameters and directions are preferable to detect landslide areas. Several full polarimetric parameters, including Sigma<sub>0</sub>, polarimetric coherence, four-component parameters, and eigenvalue decomposition parameters were obtained using PolSARPro and a self-produced programs. As pointed out by Shimada et al. [1], the change of the land cover from a forest before the disaster to bare soil after the disaster was well detected by the coherence between HH and VV. In addition to this parameter, the eigenvalues and four-component decomposition parameters have the potential to detect landslide areas. The data from observations of the bottom to the top of the landslide detect the landslide well, whereas the observation of the opposite side are not as useful.

Soil from the landslide intruded into the town areas, but none of the full polarimetric parameters show any significant difference between the landslide-affected town areas and the unaffected areas.

[1] Masanobu Shimada, Manabu Watanabe, Noriyuki Kawano, Masato Ohki, Takeshi Motooka, and Yutaka Wada, Detecting Mountainous Landslides by SAR polarimetry: A Comparative Study Using Pi-SAR-L2 and X band SARs, Transactions of the Japan Society for Aeronautical and Space Sciences, Aerospace Technology Japan, 2014, 12, No.ists29, pp. Pn9-Pn15.

Keywords: Full polarimetry, SAR, disaster

## Shoreline change analysis using JERS-1/SAR and ALOS/PALSAR amplitude images

ASAKA, Tomohito<sup>1\*</sup> ; IWASHITA, Keishi<sup>1</sup> ; KUDOU, Katsuteru<sup>1</sup> ; AOYAMA, Sadayoshi<sup>1</sup> ; SUGIMURA, Toshiro<sup>2</sup>

<sup>1</sup>Nihon University, <sup>2</sup>Remote Sensing Technology Center of Japan

Aerial photo analysis and bathymetric survey are commonly conducted to investigate the actual conditions and temporal variation in beach transformation. In recent years, satellite-based optical imagery has been more widely used to evaluate coastal erosion. However, defining shoreline edges using optical imagery is difficult because the sand under seawater near the shoreline can often be seen through clear water. On the other hand, synthetic aperture radar (SAR) imagery can be used to interpret the boundary between a sandy beach and seawater; this is possible because the incident radio waves are not transmitted through water, and SAR images can be compared to trace the shoreline. In this work, we examine the potential of shoreline change analysis by using Japanese Earth Resources Satellite 1 (JERS-1)/SAR and Advanced Land Observing Satellite/Phased Array type L-band Synthetic Aperture Radar (ALOS/PALSAR) amplitude images. We consider Kuji?kurihama beach in Chiba Prefecture as our test site; along this beach, the shoreline is almost perpendicular to the SAR antenna beam orientation for the descending orbit.

We propose a three-step automated shoreline-tracing method to assess the temporal variation of the shoreline in the study area; the HH-polarized JERS-1/SAR amplitude image captured on February 22, 1993, and the HH-polarized ALOS/PALSAR amplitude image captured on May 20, 2010 were used for this purpose. In our method, a shoreline is traced as vector data. In the first step, edge pixels in SAR images are identified by using the Laplacian of a Gaussian filter. In the second step, unwanted edge pixels are masked on the basis of a discriminant analysis in which candidate shoreline edge pixels are estimated by using statistical information within a moving window. The criteria for identifying shoreline edge pixels is decided on the basis of previously gathered data, the backscattering average, and the standard deviation, in the training area (30 by 10 pixels) encompassing the sea, shoreline, and land. In the third step, shoreline vector data are generated from continuous candidate shoreline edge pixels by an automated shoreline-tracing algorithm.

The results were verified in two ways. We first verified the location of the shoreline edge in the SAR amplitude images by overlaying multispectral images acquired on dates close to the acquisition dates of the earlier mentioned JERS-1/SAR data and ALOS/PALSAR data: the JERS-1/Optical Sensor (OPS) color composite image acquired on May 3, 1993, and the ALOS/Advanced Visible and Near Infrared Radiometer type 2 (AVNIR-2) color composite image acquired on January 8, 2011, were used for this analysis. Next, we calculated the statistical information of the backscattering data in the JERS-1/SAR and the ALOS/PALSAR amplitude images for our selected training area. It is noteworthy that the backscattering average and standard deviation in the shoreline training area is a unique than anything training area.

Our proposed method reproduces the temporal variation of the shoreline by using JERS-1/SAR and ALOS/PALSAR amplitude images. However, a part of the shoreline extracted using the JERS-1/SAR amplitude image was inaccurate. The speckle noise in the JERS-1/SAR amplitude image and the low spatial resolution of the raw data may have caused these errors. In our future work, we intend to improve the algorithm for JERS-1/SAR data and accumulate backscattering information of shoreline edge areas using SAR amplitude images.

Keywords: backscattering, beach erosion

## Glacier observations by airbourne synthetic aperture radar, PiSAR2, at Tateyama, Japan

FURUYA, Masato<sup>1\*</sup> ; FUKUI, Kotaro<sup>2</sup> ; SUGIYAMA, Shin<sup>3</sup> ; SAWAGAKI, Takanobu<sup>4</sup>

<sup>1</sup>Hokkaido University, Graduate School of Science, <sup>2</sup>Tateyama Caldera Sabo Museum, <sup>3</sup>Institute of Low Temperature Science, <sup>4</sup>Hokkaido University, Graduate School of Environmental Science

Fukui and Iida (2012) reported that three snowy gorges at Tateyama, Japan, were flowing at a rate of 10-30 cm/month and hence could be identified as glaciers. Fukui and Iida's observations are based on ground-based GPS observations. Because glacier flow velocity data sets are one of the fundamental physical quantities to better understand the dynamics, conventional geodetic techniques have been applied, and the measurement accuracy has significantly improved. However, due to the severe environment and logistic problems, SAR-based velocity mapping has been performed with successful results at large glaciers and ice sheets over the past decades. The velocity mapping technique is so called pixel-offset (or feature) tracking. Thus, applying the same technique to the fore-mentioned newly discovered glaciers, we should also be able to detect the spatial distribution of glacier velocities. However, the presently available satellite-based SAR data set does not have enough spatial resolutions to resolve the velocities. In this regard, the 30-cm resolution of Pi-SAR2 seems promising to perform the pixel-offset tracking. Here we report the first observation images of the Japanese glaciers acquired by Pi-SAR2, and will discuss the preliminary report of velocity mapping.

Keywords: SAR, glacier, Tateyama

## Monitoring of Ice sheet marginal zone using multi-frequency SAR data

YAMANOKUCHI, Tsutomu<sup>1\*</sup> ; DOI, Koichiro<sup>2</sup> ; NAKAMURA, Kazuki<sup>3</sup> ; AOKI, Shigeru<sup>4</sup>

<sup>1</sup>Remote Sensing Technology Center of Japan, <sup>2</sup>National Institute of Polar Research, <sup>3</sup>Nihon University, <sup>4</sup>Institute of Low Temperature Science, Hokkaido University

Environment of Antarctic continent and ice sheet marginal zone is quite important for understanding the mass balance of ice, formation of deep ocean water and other cryospheric phenomena. Previous study showed the usefulness of SAR data to understand what is happen on the boundary area between ice sheet and ice shelf by SAR data analysis, and achieved the mapping of ice sheet surface velocity mapping. In recent, many kinds of satellite equipped SAR sensor plan to launch and these data are available through the scientific Research Announcement (RA) or Announcement of Opportunity (AO).

Based on these facts, this study focuses on the use of multi-frequency SAR data for ice sheet marginal zone monitoring. Especially, we focus on the use of InSAR analysis for grounding line extraction, ice flow velocity mapping by offset tracking, and understanding the image feature difference through the interpretation of X-, C- and L- band SAR data. We use X-band data by TerraSAR-X, C-band data by ENVISAT and ERS-1/2, and L-band data by ALOS/PALSAR data. Then, we will try to describe the applicability and prospectives of ALOS-2 / PALSAR-2 data

TerraSAR-X data were provided by DLRs' AO project (Proposal No. HYD1808), ERS-1/2 and ENVISAT data were provided by ESA Cat-1 AO project, (project CIP.7657) and ALOS/PALSAR data were provided by Research Announcement by JAXA PI project (PI No. P1418002).

Keywords: Ice sheet, multi-frequency, SAR

## Evaluation of surface roughness, magnetic permeability and dielectric permittivity using polarimetric SAR data

KOIKE, Katsuki<sup>1\*</sup> ; MASUDA, Takayuki<sup>1</sup> ; SAEPULOH, Asep<sup>2</sup> ; URAI, Minoru<sup>3</sup> ; OMURA, Makoto<sup>4</sup> ; DOI, Koichiro<sup>5</sup>

<sup>1</sup>Graduate School of Eng., Kyoto Univ., <sup>2</sup>Bandung Institute of Technology, <sup>3</sup>Geological Survey of Japan, AIST, <sup>4</sup>Dept. Cultural Studies, Univ. Kochi, <sup>5</sup>National Institute of Polar Research

Synthetic Aperture Radar (SAR) systems have great advantages of observing the Earth surface regardless of meteorological conditions and detecting crustal deformations by Interferometric processing. Another latest technique, polarimetric SAR has also been widely used through its principle that backscattering intensity differs with polarization mode. However, most applications are limited to image classification. In addition, the evaluation method for surface physical properties has not yet been investigated well. To achieve this evaluation from the viewpoints of geological identification and water-content estimation of soils, this study adopts mdPSAR (**m**agnetic permeability and **d**ielectric permittivity from **P**olarimetric **S**ynthetic **A**perture **R**adar) proposed by Saepuloh *et al.* and tries to evaluate roughness, relative magnetic permeability, and relative dielectric permittivity of the surface materials using the HH, VV, and HV mode SAR data.

As the first step of mdPSAR, the surface roughness is calculated from the backscattering coefficient data at the HV mode and an empirical equation based on an assumption of fractal property of the topography (Campbell and Shepard, 1996). Next, using the Small Perturbation Model (Fung and Chen, 2010) of backscattering coefficient and the Nelder-Mead Simplex method (a method of nonlinear optimization), the relative magnetic permeability and the relative dielectric permittivity are calculated by minimizing the difference between the model and the backscattering coefficient data at the HH and VV modes.

The areas around the Tottori sand dunes were selected as a case study of mdPSAR using two scenes of ALOS PALSAR data acquired on 25 October and 27 April 2009. As the result, the average calculation errors were small as about 1% for both the HH and VV modes and the errors were uniform in general over the scenes. The relative dielectric permittivity values of the Tottori sand dunes were evaluated as 13.4 and 10.6. These values correspond with those of wet sands. It is noted that the value is higher in the scene after raining. Higher values of relative magnetic permeability were evaluated in the sand dunes than the surroundings, which is a reasonable trend because the sands are originated from the weathering of granitic rocks containing magnetite. Consequently, the effectiveness of mdPSAR is demonstrated. However, an improvement is necessary for the surface-roughness estimation of the areas occupied by artificial structures such as buildings. This is because the HH mode intensity becomes strong in them.

Application of mdPSAR to the PARSAR data around Syowa Station, Antarctica is in progress. Its purposes are to clarify distribution of outcrops and snow ice areas, melting state of ices, and development of crevasse topography from the spatio-temporal changes of surface roughness and relative dielectric permittivity.

### References

Campbell, B.A., Shepard, M.K. (1996) Lava flow surface roughness and depolarized radar scattering, *J. Geophys. Res.*, v. 101 (E8), 18941-18951.

Fung, A.K., Chen, K.S. (2010) *Microwave Scattering and Emission Models for Users*, Artech House, Norwood, MA.

Saepuloh, A., Urai, M., Koike, K., Sumantyo, J.T.S.: An advanced technique to identify surface materials on an active volcano by deriving magnetic permeability and dielectric permittivity from polarimetric SAR data, *IEEE Geosci. & Remote Sens. Lett.* (under review)

Keywords: ALOS PALSAR, polarization mode, backscattering coefficient, nonlinear optimization, Tottori sand dunes

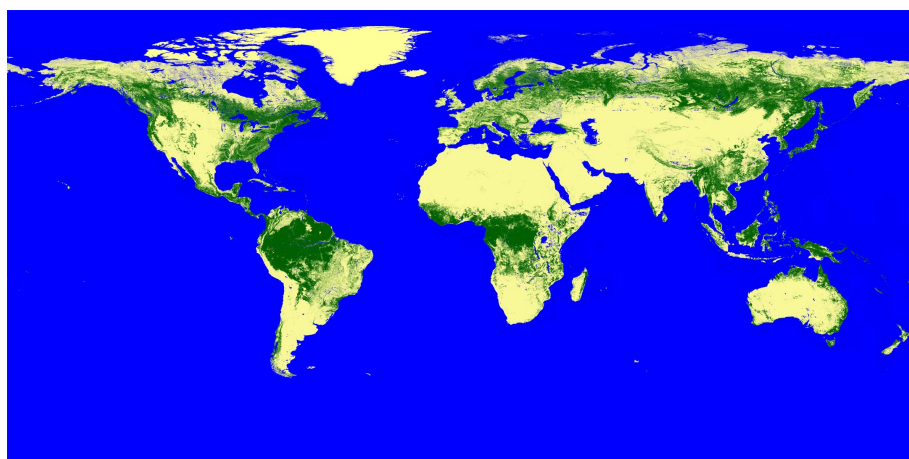
## New Global Forest/Non-Forest Maps from ALOS PALSAR data (2007-2010)

SHIMADA, Masanobu<sup>1\*</sup> ; ITOH, Takuya<sup>2</sup> ; WATANABE, Manabu<sup>1</sup> ; MOTOOKA, Takeshi<sup>1</sup> ; RAJESH, Thapa<sup>1</sup>

<sup>1</sup>Japan Aerospace Exploration Agency, <sup>2</sup>Remote Sensing Technology center of japan

Four global mosaics of Advanced Land Observing Satellite (ALOS) Phased Arrayed L-band Synthetic Aperture Radar (SAR) HH and HV polarization data were generated at 25 m spatial resolution using data acquired annually from 2007 to 2010. Variability in L-band HH and HV gamma-naught for forests was observed between regions, with this attributed to differences in forest structure and vegetation/surface moisture conditions. Region-specific backscatter thresholds were therefore applied to produce from each annual mosaic, a global map of forest and non-forest cover from which maps of forest loss and gain were mapped. Using a combination of Degree Confluence Project (DCP), Forest Resource Assessment (FRA) and Google Earth images as ground data, the overall agreement was 85 %, 91 % and 95 % respectively. Using 2007 as a baseline, decreases of 0.040 and 0.028 dB (with a 0.006 dB confidence level) were observed in the HH and HV gamma-naught respectively suggesting a decrease in forest area and increased smoothing of the global surface at the L-band radar observation. The maps provide a new global resource for documenting the changing extent of forests and contributing to ongoing monitoring through integration with historical (1992-1998) Japanese Earth Resources Satellite (JERS-1) SAR and forthcoming (from 2014) ALOS-2 PALSAR-2 data.

Keywords: SAR, forest/non-forest, SAR mosaic



## Recent progress in InSAR and PolSAR signal processing

HIROSE, Akira<sup>1\*</sup>

<sup>1</sup>The University of Tokyo

This invited talk reviews latest technology in synthetic aperture radar (SAR) signal processing, in particular interferometric SAR (InSAR) and polarimetric SAR (PolSAR), by focusing on the works on adaptive processing made by the author's group. This field attracts more attention because of its usability in solving serious social problems through, e.g., disaster monitoring and mitigation, water resource management, and prevention of global warming. We discuss a radar-physics-based adaptive processing framework, namely complex-valued neural networks, to increase variety of observation functions and/or improve the accuracy. We also introduce a new phase-unwrapping method to discuss its recent progress.

Keywords: synthetic aperture radar, interferometry, polarimetry, complex-valued neural network, phase unwrapping, Singularity-spreading phase unwrapping

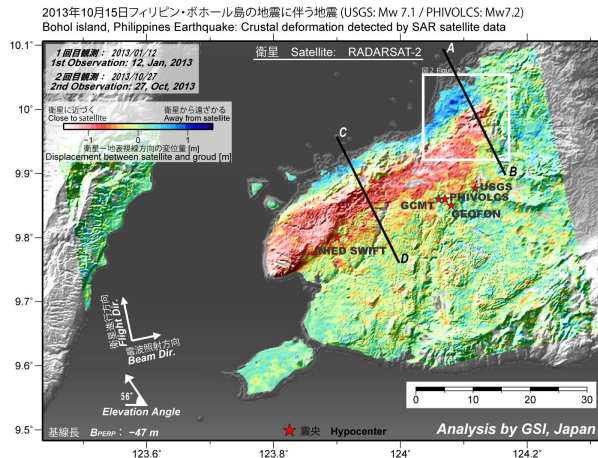
## Uplift and reverse fault rupture of the 2013 Bohol earthquake (Mw 7.2), Philippines, revealed by SAR pixel offset analysis

KOBAYASHI, Tomokazu<sup>1</sup> ; TOBITA, Mikio<sup>1\*</sup>

<sup>1</sup>GSI of Japan

Applying a pixel offset analysis using RADARSAT-2 SAR data to an inland crustal earthquake that occurred in Bohol Island, Philippines on 15 October, 2013, we succeeded in mapping a ground displacement associated with the earthquake. The most concentrated crustal deformation is located in the northwest of the island with ground displacement exceeding 1 m. The crustal deformation is zonally distributed with the length of approximately 50 km in the ENE-WSW direction. The ground in the mountainous area moves toward the satellite, while in the northern coastal zone the ground moves away from the satellite. A clear displacement discontinuity with the length of about 5 km, probably corresponding to earthquake surface faults, can be identified in the northeastern part. Our fault model that consists of two rectangular planes shows nearly pure reverse fault motions on south-southeast-dipping planes with moderate dip angles. A local rupture located in the northeast occurs at shallow depths, causing appearance of surface ruptures. Applying an additive color process using SAR amplitude images, significant changes in the backscatter intensity are detected along the coast from Maribojoc to Loon, suggesting that the seafloor uplifted and the shoreline shifted seaward resultantly. The area showing the shoreline change is in good spatial agreement with the locally-distributed large ground uplift predicted from our fault model. We can identify a good correlation between the ground upheaval produced by the reverse fault motion and the elevation in the mountainous area, consistent with the idea that the historically-repeated reverse faultings have developed the present-day topography.

Keywords: Bohol earthquake, Crustal Deformation, Pixel offset analysis, uplift, SAR, RADARSAT-2



## Estimate of error in ALOS/PALSAR interferograms

HASHIMOTO, Manabu<sup>1\*</sup>

<sup>1</sup>DPRI, Kyoto University

Large deformation is generated by the subduction of the Philippine Sea plate in Shikoku. GNSS observation reveals a WNW ward horizontal motion and a velocity gradient from south to north. This velocity field is suitable for the observation with SAR, which is sensible to the E-W ward displacement field. Based on these facts, we have conducted to derive average velocity in Shikoku using ALOS/PALSAR. We mainly analyzed ascending images acquired during 4 years, but anomalously large displacements (peak-to-peak displacement  $\sim 50$  cm) were often observed possibly due to ionospheric disturbances. We discarded interferograms with such disturbances with visual inspection, and stacked rest of them. However we found E-W velocity gradient in Shikoku that is inconsistent with GNSS observations, when stacked interferograms are superposed from 4 paths. Furthermore, discontinuities between paths are evident in the Chugoku district. Therefore we made error estimate in order to clarify its magnitude and spatial distribution, comparing line-of-sight displacements derived from InSAR and GNSS.

The procedure is as follows:

(1) Calculate displacements of GNSS stations between the acquisitions of master and slave images for a specific pair from the F3 solution of GEONET and convert them to LOS displacements.

(2) Extract LOS displacements at GNSS sites from the interferogram.

(3) Take differences of LOS displacements between interferogram and GNSS.

(4) Examine dependence of latitude, longitude and height, and interpolate differences of LOS displacements with Surface function of GMT.

(5) Add interpolated differences of LOS displacements to the original interferogram.

One typical example is interferogram for the pair of April 11 and May 27, 2010 for the path 419. Since the time difference is 46 days, little motion is expected. However, we observe LOS changes of  $\sim 40$  cm in the E-W direction. We also find a tongue-shaped region of LOS decrease in the Chugoku district. Applying the above procedure, we obtain interpolated differences of LOS displacement with the opposite sign to the original interferogram. The standard error of difference of LOS displacements for 36 GNSS sites is 7.8 cm. However, the dependences of longitude and latitude are obviously different at 34 N. Therefore we use the Surface function instead of a simple linear function for the interpolation. Finally, we obtain a fairly flat interferogram consistent with the GNSS result. There still remain displacements with shorter wavelength than 20 km, however.

Applying to other pairs, we evaluate standard errors. The minimum is 1.2 cm (Jan. 6 - Feb. 21, 2009), while the maximum is 18.9 cm (May 27 - Jul. 12, 2010). In total 24 pairs, 4 is less than 2 cm, 7 for 2  $\sim$  4 cm, 6 for 4  $\sim$  6 cm, 3 for 6  $\sim$  8 cm, 2 for 8  $\sim$  10 cm, and 2 is larger than 10 cm. The median is 4.5 cm. For the neighboring path 418 (30 GNSS sites), the minimum is 1.5 cm, while the maximum is 19.8 cm. The median is 4.7 cm. These estimates may give a rough idea of error of PALSAR interferograms including ionospheric disturbances.

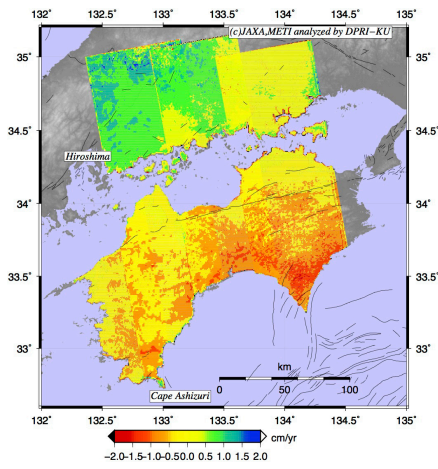
We apply this procedure to other paths (417, 418 and 420) and obtain corrected interferograms that cover the entire Shikoku (Attached figure). This map is fairly consistent with the GNSS velocity field, but there is a discontinuity between the paths 417 and 418. We use interferograms with a rather long perpendicular baseline, which causes decorrelation in mountains. We use only GNSS displacements in plain areas for such interferograms, which results in systematic error.

Keywords: SAR interferometry, PALSAR, ALOS, error, crustal deformation

STT59-10

Room:414

Time:April 29 11:35-11:50



## Persistent scatterer SAR interferometry using multi-polarimetric SAR interferograms

ISHITSUKA, Kazuya<sup>1\*</sup> ; TAMURA, Masayuki<sup>1</sup> ; MATSUOKA, Toshifumi<sup>1</sup>

<sup>1</sup>Graduate School of Engineering, Kyoto University

Persistent scatterer SAR interferometry (PS-InSAR) is a method to estimate surface deformation using a number of SAR interferograms, and has been applied to aseismic fault slip, volcano and land subsidence as a practical monitoring tool. In recent years, more and more satellites that are equipped with SAR, which can acquire multi-polarimetric data has been operated. In this study, we propose a method to processing PS-InSAR analysis using multi-polarimetric SAR interferograms, and show that the estimation accuracy of surface deformation increases.

In this study, we increase estimation accuracy by processing multi-polarimetric SAR interferograms simultaneously. Since, the amount of noise ratio would differ in different multi-polarimetric SAR interferograms depending on the geometry or electromagnetic characteristics of targets, we determine the weighting coefficient between polarimetric SAR interferograms from observed phase based on maximum likelihood method.

We applied the method to ALOS/PALSAR data acquired in multi-polarimetric mode. First, we processed HH-HH and VV-VV interferograms simultaneously. As a result, weighting of HH-HH and VV-VV interferogram was almost identical, suggesting that decorrelation-induced noise in HH-HH and VV-VV interferograms was almost same. In this case, the accuracy of estimated deformation rate would increase twice. On the other hand, when we processed HH-HH and HV-HV interferograms simultaneously, the weighting of HH-HH interferograms are larger than that of HV-HV interferograms, suggesting that HH-HH interferograms has less amount of noise compared with HV-HV interferograms. Nevertheless, we found that the estimation accuracy increases by using both HH-HH and HV-HV interferograms compared with the standard analysis using HH-HH interferograms.

Keywords: persistent scatterer SAR interferometry, surface deformation, polarimetry

## Correction by GNSS data for wide area InSAR analysis

MORISHITA, Yu<sup>1\*</sup>

<sup>1</sup>GSI of Japan

InSAR results include not only deformation signals but also noises caused by orbital inaccuracies, tropospheric delay and ionospheric delay. Orbital inaccuracies yield a residual orbital phase ramp. As spatial wavelengths of tropospheric and ionospheric noise are typically long, the effect is trivial for a small area but it can be significant for a large area.

Tropospheric noise can be mitigated by estimating the amount of tropospheric delay from a numerical weather model. However, the mitigation does not always work because of the limitation of spatial and temporal resolution of the numerical weather model. There is no common and effective technique to correct ionospheric noise so far while several techniques have been proposed. The ionospheric noise remains a big problem because, in particular, L-band is greatly affected by ionospheric noise. A residual orbital phase ramp can be reduced by flattening the phase in an area with no deformation. Another effective correction method is estimating model parameters (e.g. bilinear surface) to fit other deformation data such as GNSS continuous observation (Tobita et al., 2005; Fukushima and Hooper, 2011). This method works even if the deformation extends the entire area (Kobayashi, 2011). However, if the area is wide, a bilinear surface model is not sufficient because of noises with long wavelengths. A spline interpolation method has been proposed to overcome this problem (Fukushima, 2013).

In this presentation, I will report a GNSS correction technique using a natural interpolation method for scattered points. This technique can mitigate not only residual orbital phase ramps but also noises with long wavelength. Adjusting correction steps enables realistic extrapolations while conventional steps sometimes result in outliers in extrapolated areas. The results of wide area time series InSAR analysis using ALOS/PALSAR data show less noise and more apparent phase changes with shorter wavelength than the interval of the GNSS stations.

### References

Tobita, M., H. Munekane, S. Matsuzaka, M. Kato, H. Yarai, M. Murakami, S. Fujiwara, H. Nakagawa and T. Ozawa (2005): Studies on InSAR data processing techniques, Bull. GSI., 106, 37-49 (in Japanese).

Fukushima, Y. and A. Hooper (2011): Crustal deformation after 2004 Niigataken-Chuetsu earthquake, central Japan, investigated by Persistent Scatterer Interferometry, J. Geod. Soc. Japan, 57, 195-214 (in Japanese with English abstract).

Kobayashi, T., M. Tobita, T. Nishimura, A. Suzuki, Y. Noguchi and M. Yamanaka (2011): Crustal deformation map for the 2011 off the Pacific coast of Tohoku Earthquake, detected by InSAR analysis combined with GEONET data, Earth Planets Space, 63, 621-625, 2011.

Fukushima, Y. (2013): Correction of DInSAR noise using GNSS measurements, in proceedings of APSAR 2013, 2013.

Keywords: InSAR, GNSS

## Research on the characteristics of ionospheric disturbance around Japan by GPS-TEC for ionospheric correction to InSAR

NAKAGAWA, Hiroyuki<sup>1\*</sup> ; MUNEKANE, Hiroshi<sup>1</sup> ; KUROISHI, Yuki<sup>1</sup> ; KAMIHARA, Masashi<sup>2</sup>

<sup>1</sup>GSI of Japan, <sup>2</sup>Pascalina Co.,Ltd

In the monitoring surface deformation using SAR interferometry (InSAR), it is a serious problem that the long-wavelength noise caused by ionospheric disturbance degrades accuracy of the detection of deformation. Since 2013, Geospatial Information Authority of Japan (GSI) have conducted a research project on the method for ionospheric correction to satellite InSAR based on TEC information obtained from two-wavelength observation data of GEONET.

For the first step, in order to understand the characteristics of ionospheric disturbance around Japan, we identified ionospheric disturbance of the period between 2000 and 2011 by GPS-TEC of GEONET and estimate characteristic values of each event.

In the manner in Munekane (2013), we first estimate zenith TEC and TEC gradient in north-south and east-west component every thirty second during the period from GEONET thirty-second RINEX data. Then, we adopted high pass filter of 3600s to remove low frequency component.

Next, based on this GPS-TEC time series, we identified ionospheric disturbance event in the period. In this step, we focus rather on revealing overall trend of ionospheric disturbance than inspecting accuracy of the characteristic value of each event.

The process of identification is as follows. First hourly RMS of TEC was calculated every hour, and, if the number of sites which hourly TEC-RMS is over threshold is more than a certain criterion, regard the epoch as a part of ionospheric disturbance event. Then, viewing the "GEONET GPS-TEC maps over Japan" on the web site of NICT, each disturbance event was divided visually into three category according to the pattern of TEC distribution, "traveling ionospheric disturbance (TID)", "plasma bubble" and "other".

After the identification of event category, we decided characteristics such as event start and end time, affected area and its temporal transition based on ten-minute RMS of TEC. Also, we estimate characteristic values associated with event category such as wavelength of a TID or northernmost latitude of a plasma bubble etc. Finally, we derived characteristics of the ionospheric disturbance around Japan statistically.

We identified 8,815 ionospheric disturbance in the period, reaching maximum of 967 events in 2001, decreasing gradually to minimum of 471 in 2007, and having increasing tendency afterwards. This trend is consistent with solar cycle. The occurrence of TID and plasma bubble is found to be consistent with solar cycle, too.

Also, it appears that TID occurs commonly from May to August, in summer season. TID occurrence also concentrates before and after two hours around 22 o'clock in local time. As for plasma bubble, the occurrence is high from the sunset to midnight in local time. These results are consistent with earlier studies.

### References

- Munekane, H., (2013): On ionospheric correction of ALOS/PALSAR interferograms using GEONET data (preliminary report), STT57-09, Japan Geoscience Union Meeting 2013  
National Institute of Information and Communications Technology: GEONET GPS-TEC maps over Japan,  
[http://seg-web.nict.go.jp/GPS/GEONET/index\\_e.html](http://seg-web.nict.go.jp/GPS/GEONET/index_e.html)

Keywords: InSAR, ionospheric disturbance, TEC, GEONET

## APPLICATION OF DINSAR TIME SERIES ANALYSIS USING ALOS PALSAR TO EXTERIOR DEFORMATION MONITORING OF DAMS

HONDA, Kenichi<sup>1\*</sup>; MUSHIAKE, Naruo<sup>1</sup>; SATOH, Wataru<sup>1</sup>; SATOH, Hiroyuki<sup>2</sup>; KOBORI, Toshihide<sup>2</sup>; SASAKI, Takashi<sup>3</sup>; YAMAGUCHI, Yoshikazu<sup>4</sup>; SHIMIZU, Norikazu<sup>5</sup>

<sup>1</sup>Kokusai Kogyo Co., Ltd., <sup>2</sup>Public Works Research Institute, <sup>3</sup>National Institute for Land and Infrastructure Management, <sup>4</sup>Japan Dam Engineering Center, <sup>5</sup>Yamaguchi University

The number of aging civil engineering structures is rapidly increasing in Japan. As for dams, it is estimated that 58% of existing dams in the year 2020 will be 50 years old or over after completion. This situation increasingly requires not only efficient deformation monitoring systems for safety management of civil structures but also safe and rapid methods in case of emergencies such as earthquakes.

Remote sensing techniques, especially Synthetic Aperture Radar (SAR), can play an important role to conduct deformation monitoring of civil structures such as dams. Differential Interferometric SAR (DInSAR) analysis using SAR satellite data can be suitable to deformation monitoring in broad areas.

To investigate the applicability of DInSAR analysis for the deformation monitoring, the Taiho Subdam, which is located in the Okinawa Prefecture, Japan, was selected as a study area because the deformation monitoring using GPS have been rigorously conducted since the completion of the dam from December 2006. In this study area, at maximum 114 mm of deformation was measured from December 2006 to December 2010, which corresponds to the observation period by SAR satellite. ALOS PALSAR data, L-band SAR, was used for DInSAR analysis and the results of deformations calculated by DInSAR analysis were compared with the results of the GPS deformation measurements. 28 scenes of ALOS PALSAR data were used: 14 scenes of descending data from December 6, 2006 to December 17, 2010, and 14 scenes of ascending data from January 12, 2007 to January 23, 2011, respectively.

The values of deformations calculated by DInSAR analysis were about 70 or 80% of those measured by GPS during observation period about four years. Although the DInSAR analysis results were expected to have some errors and were different from the GPS measurement results to some extent, DInSAR deformation monitoring is sufficient enough to monitor few-centimeter deformations. Additionally time series changes by DInSAR analysis can well reproduced the tendency of the settlement of the dam. This indicates a possibility that DInSAR analysis is useful for the deformation monitoring for civil structures.

Keywords: Dam, Exterior deformation monitoring, DInSAR, SBAS, GPS

## Approach for monitoring ground deformation around the active volcanoes in Japan by InSAR time series analysis

MIURA, Yuji<sup>1\*</sup> ; ANDO, Shinobu<sup>2</sup> ; NAKAMURA, Masamichi<sup>1</sup>

<sup>1</sup>Volcanological Division, JMA, <sup>2</sup>MRI

In previous studies, we have reported the analysis results about domestic active volcanic areas using D-InSAR of ALOS since 2007. In recent years, InSAR time series analysis technique has been developed. Therefore various studies have been reported for monitoring ground deformation using InSAR time series analysis. In this study, we have applied this procedure to the analysis of the data of ALOS/PALSAR for monitoring ground deformation of the active volcanoes in Japan.

As a result, we can detect ground deformations associated with volcanic activities of Tokachidake, Azumayama, Izu-Oshima, Miyakejima, Satsuma-Iojima and others. These obtained ground deformations by InSAR time series analysis were basically consistent with the results of GPS.

Keywords: InSAR time series analysis, ground deformation, ALOS/PALSAR, active volcano

## Surface displacement around Hachobaru geothermal field inferred from persistent scatterer SAR interferometry

ISHITSUKA, Kazuya<sup>1\*</sup> ; TSUJI, Takeshi<sup>2</sup> ; MATSUOKA, Toshifumi<sup>1</sup> ; FUJIMITSU, Yasuhiro<sup>3</sup> ; NISHIJIMA, Jun<sup>3</sup>

<sup>1</sup>Graduate School of Engineering, Kyoto University, <sup>2</sup>International Institute for Carbon-Neutral Energy Research (I2CNER), Kyushu University, <sup>3</sup>Faculty of Engineering, Kyushu University

Fluid migration around geothermal field can cause surface displacement. Leveling campaign and GPS measurement has been used to estimate surface displacement and shown the usefulness for reservoir monitoring at geothermal field. Recently, persistent scatterer SAR interferometry (PS-InSAR) analysis has been developed as a practical tool for surface displacement monitoring. By making use of the advantage of wide data coverage of satellite image, the analysis enables us to estimate surface displacement at the whole geothermal field with high spatial density. In this study, we applied PS-InSAR analysis on areas around Hachobaru geothermal field, the largest geothermal field in Japan, located Kyushu Island. For the analysis, we used 18 ALOS/PALSAR images acquired from July 2007 to December 2010 from an ascending orbit.

As a result of the analysis, we estimated secular surface displacement with the maximum rate of 15 mm/year opposite to satellite direction, which can be inferred as ground subsidence. We also found temporally irregular displacement along with the secular displacement. This irregular displacement has occurred all of Mt. Kuju, suggesting that displacement at Mt. Kuju has influenced displacement at the geothermal field. Moreover, we found that the secular displacement has decayed over time and has clear boundaries which possibly correspond to fault locations.

Keywords: surface displacement, persistent scatterer SAR interferometry, Hachobaru geothermal area

## The Steady Crustal Deformation Analysis in Tokai region by InSAR

ANDO, Shinobu<sup>1\*</sup> ; IWAKIRI, Kazuhiro<sup>2</sup> ; AOKI, Gen<sup>2</sup>

<sup>1</sup>MRI, <sup>2</sup>JMA

ALOS has an L-band SAR (PALSAR), which is of help to understand of a ground surface state, and its interferometric coherence is highly effective for the crustal deformation observation.

We analyzed the ALOS/PALSAR data around Omaezaki and Kakegawa cities in Shizuoka Prefecture, and tried to detect steady crustal deformation due to the subduction of the Philippine Sea plate. In this study, in order to obtain steady-state deformation (time series), we subjected to interference processing on the image pairs of a number of different imaging date interval. Then, using a variation of the satellite line-of-sight direction in the interference each images and we were calculated the average variation of the 46 days (stacking process). However, to reduce noise, we analysed except for some interferograms with obvious noise. This method can be expected to improve detection accuracy, because of able to reduce the influence of noise caused by the ionosphere.

We used 23 ascending data acquired from January 2007 to October 2010 and 19 descending data acquired from October 2006 to September 2010. Before solving for the displacement time series, we corrected the atmosphere phase delay by Japan Meteorological Agency nonhydrostatic model (JMA-NHM), and calculated the displacement of the satellite line-of-sight direction of the pair of all. The average displacement of the satellite line-of-sight direction of the 46 days was calculated under the assumption that the variation in the period of each pair is constant. The distance between the imaging date is different for each pair, but we did not weight during the averaging process.

As a result, steady-state deformation was hardly observed in the analysis of the ascending orbit data, but in the analysis of the descending orbit data, were observed the steady-state deformation the away from the satellite in the radar line-of-sight direction. This crustal deformation was significant in Omaezaki area, especially. These results are consistent with the displacement vector by GNSS. In this report, we also reported about InSAR time series analysis using *StaMPS* program was developed by the Stanford Institute of Technology.

Some of PALSAR data were prepared by the Japan Aerospace Exploration Agency (JAXA) via the Geospatial Information Authority of Japan (GSI) as part of the project "ALOS Domestic Demonstration on Disaster Management Application" of the Earth Working Group. Also, we used some of PALSAR data that are shared within PALSAR Interferometry Consortium to Study our Evolving Land surface (PIXEL). PALSAR data belongs to Ministry of Economy Trade and Industry (METI) and JAXA. We would like to thank Dr. Shimada (JAXA) for the use of his *SIGMA-SAR* software. In the process of the InSAR, we used "the digital elevation map 50m-mesh" provided by GSI, and Generic Mapping Tools (P.Wessel and W.H.F.Smith, 1999) to prepare illustrations.

Keywords: InSAR, Ground deformation, ALOS/PALSAR, Tokai region

## Monitoring of Sakurajima Volcano using Cosmo-SkyMed

MIYAGI, Yosuke<sup>1\*</sup> ; OZAWA, Taku<sup>1</sup> ; SHIMADA, Masanobu<sup>2</sup>

<sup>1</sup>National Research Institute for Earth Science and Disaster Prevention, <sup>2</sup>Japan Aerospace Exploration Agency

Sakurajima volcano is located in southwestern part of Japan, and currently a most active volcano in Japan. Eruptive activities from Showa-crater have activated since 2009, and several explosive eruptions occurred in 2012. On July 24, 2012, another large eruption occurred from Minamidake-crater after a lapse of 18 months. To understand current condition and future unrest of Sakurajima, periodic monitoring is required. Although it is generally difficult to make a field observation in dangerous active volcanoes, a satellite remote sensing can make observations of even ongoing volcanoes periodically. Especially, Synthetic Aperture Radar (SAR) sensor is well-suited for monitoring active volcanoes because it can penetrate ash clouds and can observe targets like an active vent. Moreover, SAR data are applicable to use a Differential Interferometric SAR (DInSAR) technique to detect crustal movement associated with the magmatic activities. In this study, we used COSMO-SkyMed data for monitoring Sakurajima volcano and tried DInSAR processing. Monitoring using high-resolution amplitude images revealed changes of backscattering intensity probably due to some kind of surface change within or around the crater. DInSAR processing suffered from low coherence, therefore we acquired quite limited geodetic information.

Keywords: SAR, Sakurajima, Deformation

## Volume Increase of Lava within the Kirishima, Shinmoe-dake Crater, Detected by TerraSAR-X/DInSAR

MIYAGI, Yosuke<sup>1\*</sup> ; OZAWA, Taku<sup>1</sup> ; KOZONO, Tomofumi<sup>2</sup> ; SHIMADA, Masanobu<sup>3</sup>

<sup>1</sup>National Research Institute for Earth Science and Disaster Prevention, <sup>2</sup>Department of Geophysics, Graduate School of Science, Tohoku University, <sup>3</sup>Japan Aerospace Exploration Agency

Shinmoe-dake in the Kirishima volcano group is located in southwestern part of Japan. In January 2011, eruptive activities started from the Shinmoe-dake crater with a rapid accumulation of lava within the crater. The eruption phase ceased by the beginning of September, and the post-eruptive inflation also ceased by November 2011. After the 2011 eruption, monitoring by TerraSAR-X have continued and revealed a continuous shortening of satellite-ground distance even after the end of the main activity. This LOS shortening means uplifts of the lava surface. We estimated the volume increase of the lava after November 2011, using DInSAR processing of TerraSAR-X data, and concluded that the volume increase still continued in January 2014. The volume change rate has exponentially decreased with a small fluctuation as an overall trend. PSInSAR and long-term DInSAR results show LOS elongation including a subsidence in the northeast flank of the crater. It is interpreted that the subsidence is caused by deflation of a shallow deformation source located just beneath the crater. A total amount of effused lava after November 2011 is comparable to a volume decrease of the shallow source estimated from the deflation deformation. This long-term continuous lava extrusion suggests a possibility of an additional injection from the deeper source.

Keywords: SAR, Kirishima, Shinmoe-dake, Deformation

## Crustal deformation in Izu-Oshima Island detected by PS-InSAR analysis and estimation of volcanic deformation source

HASEGAWA, Yuichi<sup>1\*</sup> ; TABELI, Takao<sup>2</sup> ; OZAWA, Taku<sup>3</sup>

<sup>1</sup>Grad. School Int. Arts Sciences, Kochi Univ., <sup>2</sup>Fac. Science, Kochi Univ., <sup>3</sup>National Research Institute for Earth Science and Disaster Prevention

Mt. Mihara in Izu-Oshima Island have erupted 21 times in the last 800 years. The latest eruption occurred in 1986 inside the caldera. Though spatially and temporally dense observation network is desired to continuously monitor volcanic activities, it is not easy to construct such a network in a mountainous region. In this study, we conduct time-series analysis of ALOS/PALSAR images over Izu-Oshima Island using persistent scatter interferometric SAR (PS-InSAR) method to detect volcanic deformation.

From the analysis of 20 images collected from ascending track during the period from October 2007 to February 2011, we detect distance change of about 15 cm extension in the line-of sight (LOS) direction inside the caldera. Similarly the extension of about 14 cm is detected at the same location from the analysis of 18 images from descending track during the period from January 2007 to March 2010. Next we compare the LOS distance changes with those converted from GPS coordinate time-series at four continuous sites in the island. The RMS between them are as large as 1.3-3.2 cm, implying that SAR results are good enough to monitor volcanic deformation over the island.

Combining the LOS distance changes from the ascending and descending tracks, we derive quasi-vertical and quasi-east-west components of the displacement. The most remarkable is the vertical displacement of the caldera where the subsidence of about 16 cm is detected during 2007-2010 with small occasional uplifts. Moreover uplift of about 11 cm is recognized in the eastern coastal area of the island during the same period. Based on the quasi-vertical component of the displacement, we estimate a spherical pressure source model (Mogi, 1958) below the island. We assume two sources with different depth and estimate the optimum model using a grid search method. Horizontal position of the shallower source is fixed to coincide with the location of the caldera and its depth is varied every 0.5 km in a range of 2.0-4.5 km. Horizontal position of the deeper source is varied every 2 km and its depth is checked every 0.5 km in a range of 5.0-10 km. The optimum model shows that the shallower source is located at a depth of 3.0-4.5 km where inflation and deflation are occurring alternatively while the deeper source is located at a depth of 6.0-9.0 km where nearly constant inflation rate of about 8 million m<sup>3</sup> per year is expected. These results can be interpreted that the deeper magma reservoir continues to expand due to magma supply from the mantle while the shallower reservoir is affected by magma supply from the deeper source and gravitational load of lava that spreads within the caldera.

Keywords: PS-InSAR method, time-series analysis, Izu-Oshima Island, crustal deformation, volcanic deformation source

## Flow velocity measurements of ice streams in the southern part of Soya Coast, Antarctica, by DInSAR

SHIRAMIZU, Kaoru<sup>1\*</sup> ; DOI, Koichiro<sup>2</sup> ; AOYAMA, Yuichi<sup>2</sup>

<sup>1</sup>The Graduate University for Advanced Studies, <sup>2</sup>National Institute of Polar Research

Differential Interferometric Synthetic Aperture Radar (DInSAR) is an effective tool to measure flow rate of ice streams on Antarctic continent. In this study, we applied the DInSAR technique to L band (wavelength 23.6cm) SAR data acquired by ALOS/PALSAR, and tried to measure flow velocity around Skallen, in the southern part of Soya Coast, East Antarctica. We used 9 scenes (Path633, Row 571-572), observed during the period from November 23, 2007 through January 13, 2010. In order to remove topographic fringes in the interferograms, we used a digital elevation model ASTER GDEM.

According to the analysis, ice flow rate of up to 3.5cm/day was obtained in the line of sight direction. Although no displacement is expected in areas of outcrops in general, we found displacements up to 37cm in the outcrops of obtained displacement maps. These displacements are considered to be apparent ones and must contain errors induced in the process of analysis. Therefore, it is possible to use apparent changes as a measure of the error contained in ice flow rate estimation.

In this presentation, we will show the results of flow rate estimation of the ice streams, and discuss the errors included in the flow rate estimation.

Keywords: Differential Interferometric SAR, Antarctic ice sheet, ice stream

## Flow measurements of ice sheets in Arctic region by differential SAR interferometry

DOI, Koichiro<sup>1\*</sup> ; YAMANOKUCHI, Tsutomu<sup>3</sup> ; NAKAMURA, Kazuki<sup>4</sup> ; SHIRAMIZU, Kaoru<sup>2</sup>

<sup>1</sup>National Institute of Polar Research, <sup>2</sup>The Graduate University for Advanced Studies (SOKENDAI), <sup>3</sup>RESTEC, <sup>4</sup>Nihon University

Rapid ice sheet mass losses from ice sheets have been found in Greenland and the Canadian Arctic Archipelago on and after 2000 from the observations by the satellite gravity mission GRACE (Svendsen et al. 2012, Gardner et al. 2011). It is considered to be one of the causes that flow rate of ice sheet and ice stream was accelerated and ice mass outflow into the sea increased.

We aim to measure flow rates of ice sheet and ice streams in the Arctic region by applying differential Synthetic Aperture Radar (SAR) interferometry (DInSAR) with a digital elevation model ASTER GDEM to satellite SAR data. In addition, we intend to explore whether changes in the flow rate happen or not.

We obtained displacement maps along line of sight direction for 46 days of three regions in north eastern Greenland and Ellesmere Island of northern Canadian Arctic Archipelago observed by ALOS/PALSAR by applying differential SAR interferometry. We will show the obtained displacement maps in the presentation, and will also intend to discuss changes in the flow rates by applying three or four pass interferometry.

Keywords: Differential SAR interferometry, flow, ice sheet, Arctic region

## Spatial distribution and classification of rock glaciers in Kyrgyz Ala-Too Range, Central Asia

YAMAMURA, Akiko<sup>1\*</sup> ; NARAMA, Chiyuki<sup>1</sup> ; TOMIYAMA, Nobuhiro<sup>2</sup> ; TADONO, Takeo<sup>3</sup>

<sup>1</sup>Niigata University, <sup>2</sup>RESTEC, <sup>3</sup>JAXA

In the arid and semi-arid region of Central Asia, Tien Shan Mountains is known as important water tower in Central Asia. Although the current situation of mountain glaciers and permafrost should be researched for estimate of water resources, mountain permafrost is not clarified in the Tien Shan (Marchenko et al., 2007; Sorg et al., 2012). In recent years, landslides caused by the melting of mountain permafrost in Ak-Shiyrak mountains, show that recent changes of mountain permafrost begin to influence to mountain environment including the disaster. In this study, to clarify mountain permafrost environment, we researched spatial distribution and classification of rock glaciers in Kyrgyz Ala-Too Range, Tien Shan Mountains. In addition, we applied InSAR analysis to the ALOS PALAR data obtained in 2007-2010, to research moving of rock glaciers. We extracted polygon data of rock glaciers based on aerial photo interpretation and ALOS PRISM, using ArcGIS. Rock glaciers were classified an active and inactive-fossil types by NDVI (Normalized Difference Vegetation Index) of ALOS AVNIR-2 and field observation in the summer 2013. The distributions of active rock glaciers show the lower limit of mountain permafrost is 3300m in the northern part and 3500m in the southern part of the Kyrgyz Ala-Too Range. We confirmed moving of some rock glaciers in this mountain area using InSAR analysis. In particularly, the moving of rock glaciers in the southern part of the range is remarkable. The most of these active rock glaciers developed from glacier ice. We report the results in detail in JpGU meeting.

Keywords: mountain permafrost, rock glacier, InSAR, ALOS PALSAR, Tien Shan Mountains

## Development of InSAR processing tools in NIED ?Part3?

OZAWA, Taku<sup>1\*</sup>

<sup>1</sup>National Research Institute for Earth Science and Disaster Prevention

Synthetic aperture radar (SAR) became one of the useful tools for crustal deformation detection. Recently, InSAR processors which can be used freely in scientific research (e.g., ROI\_PAC, GMTSAR, and Doris) were released, and enabled anyone to do crustal deformation detection by InSAR. Especially, algorithm of two-pass differential InSAR analysis matured, and it enabled anyone to obtain almost same results. On the other hand, advanced InSAR analysis methods, e.g., time-series analysis, have been recently used to detect precise crustal deformation. However, many issues to improve remains in such analyses. In order to research on improvements for such analysis, we are developing InSAR processor.

In this InSAR processor, general procedure is adopted. (1) Format conversion of SLC and creation of parameter files. (2) Rough co-registration of two SLCs considering parallel shift only. (3) Estimation of affine transformation coefficients. (4) SLC resampling. (5) Generation of the initial interferogram. (6) Simulation of a SAR intensity image and estimation of translation tables between geodetic and radar coordinates based on DEM. (7) Co-registration between simulated and observed SAR intensity images. (8) Correction of translation tables. (9) Simulation of the orbital and the topographic phase components. (10) Generation of differential interferogram. (11) Applying interferogram filter. (12) Geocoding.

In JPGU meeting 2013, we showed comparison between results from our processor and from GAMMA SAR processor. Although their results were roughly the same, it indicated that many improvement points remained. In 120th meeting of the Geodetic Society of Japan, we presented about improvement of coherence by the spectrum shift filter (Gatelli et al., 1994), improvement of calculation speed, and correspondence to skewed images. After that, this processor corresponded to the InSAR processing with FBS-FBD image pair of ALOS/PALSAR using SLC over-sampling and band-pass filter. We added DEM resampling function by over-sampling method and by the bi-cubic spline interpolation. Furthermore, we are attempting to improvement of the image matching now. After this correspondence, the first step of this development will be finished. In next step, we will attempt more improvements and additions of other advanced algorithms.

Keywords: SAR, InSAR, software, tool

## Creating future of solid Earth science with high performance computing (HPC): Introduction

HORI, Takane<sup>1\*</sup> ; HINO, Ryota<sup>2</sup> ; HONKURA, Yoshimori<sup>3</sup> ; KANEDA, Yoshiyuki<sup>1</sup> ; ARIKAWA, Taro<sup>4</sup> ; ICHIMURA, Tsuyoshi<sup>5</sup> ; TODORIKI, Masaru<sup>5</sup>

<sup>1</sup>JAMSTEC, <sup>2</sup>Tohoku University, <sup>3</sup>Tokyo Institute of Technology, <sup>4</sup>Port and Airport Research Institute, <sup>5</sup>University of Tokyo

In Japan, high performance computing (HPC) had been driven by computer science community (HPC developer). However, recently, computational science community (HPC user) has been expected to contribute to the planning and development of the next generation HPC showing the scientific and/or social issues to be solved for the next 10-20 years using HPC. In various fields of science using HPC, scientists have started to discuss scientific and/or social issues to be solved in each field. Hence, in this session, we aim to examine such issues in solid Earth science, which HPC can contribute to solve. For social issues, we will focus on earthquake and tsunami disaster mitigation. For scientific issues, we would like to discuss construction of the next generation of solid Earth model based on the big data of seismic waves and crustal deformation obtained by high-density observation networks. We will introduce the contents of the "white paper" of the future plans for computer science in various fields including solid Earth science.

Keywords: HPC, hazard mitigation

## The K Computer and Japan Plan for Exascale

HIRAO, Kimihiko<sup>1\*</sup>

<sup>1</sup>AICS RIKEN

At the end of September 2012, official operation of the Kcomputer has started. Already in many areas we see many great results. Users of K are actually very much impressed having experienced using K. The K is Japanese supercomputer jointly developed by Fujitsu and Riken and everything is made in Japan. The K computer won the top position on TOP500 in 2011 achieving a LINPACK benchmark performance of 10 petaflops - becoming the first supercomputer ever to reach this milestone. The K fell behind China and US machines on the latest TOP500. We believe that the K is still one of the most powerful and user-friendly machine in the world. K demonstrates an extraordinary level of stability. K is capable of sustained performance of 1 PF on real applications in a wide range of science. K is the strong science machine.

Computer simulation is becoming more and more important for contemporary science and engineering. Nobel Prizes 2013 in chemistry and physics show how computing is changing every field of research. Particularly simulations performed on the supercomputer will drive progress in science and technology and play an important role in solving difficult problems that we face as a society. There are very critical issues that need to be solved - global warming, alternative energy, disaster mitigation, new materials, healthcare, security, etc. The role of simulations will become increasingly larger, and the results that they provide will undoubtedly greatly affect society. The new frontiers opened up by the K computer will be presented.

The post K project will be lauced from April 2014. MEXT selected RIKEN AICS to develop a new exascale supercomputer by 2020. The post K is 100 times faster than the current K computer. Architecture is hybrid of general-purpose plus accelerator components. We will push the state of the art in power efficiency, scalability & reliability. Power consumption is limited in the range of 30-40MW.Total project cost is ca. JPY140 billion with about JPY 110 billion coming from the government's budget (JPY 1.2 billion for 2014)

Computer simulation will dramatically increase our ability to understand the world around us. With exascale computing, we are reaching a tipping point in predictive science. Its success will have lasting impact on the planet and people all around the world and for generations into the future. With a planned deployment in 2020, the new system is expected to keep Japan at the leading edge of computing science and technology.

## The application of simulation studies using HPC to disaster management: current status and future.

YOKOTA, Takashi<sup>1\*</sup> ; TAIRA, Yutaro<sup>1</sup>

<sup>1</sup>Cabinet Office

In Central Disaster Management Council, estimations of damage by anticipated earthquakes have been conducted to plan measures for disaster management(preparedness, emergency response and recovery). Also, when a large earthquake occurs early assessments of the damage have been carried out immediately to grasp the situation of the disaster and to support decision-making for emergency response operations in central government. These estimations and assessments require high accuracy to develop more effective measures and to decide more appropriate operations.

It is indisputable that the sophistication of forecasting techniques of natural phenomena is necessary to mitigate human damage by encouraging residents to evacuate.

In this presentation, we will introduce our approaches described above, and would like to talk about what to expect from the application of simulation studies using High Performance Computing to the disaster management of earthquakes and tsunamis in particular.

Keywords: disaster managent, damege estimation, HPC

## Development of Integrated Earthquake Simulator on K-computer

ICHIMURA, Tsuyoshi<sup>1\*</sup> ; HORI, Muneeo<sup>1</sup>

<sup>1</sup>Earthquake Research Institute, The University of Tokyo

Earthquake simulation with high-resolution and high-accuracy could have significant contribution on making rational and effective counter measures against earthquake disaster. Such earthquake simulation must consider whole process from a fault rupture to city responses, since each process has significant effects on the resulting responses. We are now developing such earthquake simulation system on K-computer, which is called Integrated Earthquake Simulator (IES). IES combines spatial data and earthquake simulation with a high-fidelity model to simulate the whole process. The target domain of earthquake simulation is typically very large, making it difficult to prepare sufficient data to construct a high-fidelity model. Even if a high-fidelity model can be constructed, it is difficult to resolve the computational expense due to the discretization of such models. Thus, simplified analyses or analytical methods are typically used in earthquake simulation. However, the construction of high-fidelity models has become popular with recent increases in available spatial data, and a considerable volume of data from high-density observation networks is now available for checking their validity. The realization of analyses using high-fidelity models is desirable. Several examples of analyses using such models can currently be found on the K-class supercomputer, although the resolution is not yet adequate. In this presentation, we discuss the following earthquake simulations (parts of IES) on the K computer, together with problems to be solved: non-linear wave simulation with high resolution, crust deformation analysis with island-scale and the seismic response analysis of soil-structures system.

Keywords: earthquake simulation, high performance computing, high fidelity, high resolution and accuracy

## Consideration to the resiliency of protective structures against tsunami by using High Performance Computer

ARIKAWA, Taro<sup>1\*</sup> ; OIE, Takayuki<sup>1</sup> ; TOMITA, Takashi<sup>1</sup>

<sup>1</sup>Port and Airport Research Institute

The Committee for Technical Investigation on Countermeasures for Earthquakes and Tsunami Based on the Lessons Learned from the "Great East Japan Earthquake" (2011) of the Central Disaster Management Council has responded to the Great East Japan Earthquake by proposing that basically, two levels of tsunami must be hypothesized to build future tsunami countermeasures. One is a tsunami hypothesized to build comprehensive disaster prevention countermeasures centered on evacuation of residents. It is set based on a survey of tsunami deposits formed over an ultra-long period and observations of crustal movement, and it is a maximum class tsunami which, although it occurs extremely rarely, causes devastating damage when it does occur. One more is a tsunami which is hypothesized to build coastal protection facilities such as breakwaters and other structures which prevent tsunami from inundating inland regions. It is a tsunami which occurs more often than the maximum class tsunami, and although it is a low type of tsunami, it causes severe damage. At such times, technological development of structures which are capable of resiliently providing effects even under tsunami height which is the object of the design must continue for coastal protection facilities etc. to be improved. So, in this research, the protective effectiveness is considered by using STOC-CADMAS(Arikawa and Tomita, 2005).

## Determination of Earth structure using waveform inversion and Spectral-Element Method

TSUBOI, Seiji<sup>1\*</sup> ; MIYOSHI, Takayuki<sup>1</sup> ; OBAYASHI, Masayuki<sup>1</sup> ; TONO, Yoko<sup>1</sup>

<sup>1</sup>JAMSTEC

Recent progress in large scale computing by using Spectral-Element Method and the Earth Simulator has demonstrated possibilities to perform full-waveform inversion of three dimensional (3D) seismic velocity structure inside the Earth. Specifically Liu and Tromp (2006) have shown that it becomes feasible to compute finite frequency kernel for seismic velocity structure based on adjoint method. We apply their method to obtain 3D velocity structure beneath East Asia. We take one chunk from global mesh of Spectral-Element Method and compute synthetic seismograms with accuracy of about 10 second. We use GAP-P2 mantle tomography model (Obayashi et al., 2009) as an initial 3D model and try to use as many broadband seismic stations available in this region as possible to perform inversion. We then use the time windows for body waves and surface waves to compute adjoint sources and calculate adjoint kernels for seismic velocity structure. We use the earthquakes, which occurred in East Asia since 2001, with magnitude greater than 5.5 and selected 161 events for this inversion. One iteration of the waveform inversion using 256 cores of massively parallel supercomputer, such as K-computer, requires 0.1 million CPU hours. We have performed several iteration and obtained improved 3D velocity structure beneath East Asia. The result demonstrates that waveform misfits between observed and theoretical seismograms improves with the iteration proceeds and it now becomes feasible to perform waveform inversion within practical computational time. We will use much shorter period in our synthetic waveform computation and will try to obtain seismic velocity structure for basin scale model in our future study.

Acknowledgements: We used F-net seismograms of the National Research Institute for Earth Science and Disaster Prevention. This study was supported by the strategic Programs for Innovative Research "Field 3" Advanced prediction Researches for Natural Disaster Prevention and Reduction.

Keywords: Earth structure, Seismic tomography, Synthetic seismogram, Spectral Element Method

## Mantle convection simulations on HPC: past, present and future

KAMEYAMA, Masanori<sup>1\*</sup> ; MIYAGOSHI, Takehiro<sup>2</sup> ; FURUICHI, Mikito<sup>2</sup> ; NAKAGAWA, Takashi<sup>2</sup> ; YANAGISAWA, Takatoshi<sup>2</sup> ; NAKAKUKI, Tomoeiki<sup>3</sup> ; OGAWA, Masaki<sup>4</sup>

<sup>1</sup>GRC, Ehime University, <sup>2</sup>JAMSTEC, <sup>3</sup>Hiroshima University, <sup>4</sup>University of Tokyo

In this presentation, we will discuss (a rather personal view of) the possible directions of the advanced numerical studies of mantle dynamics in concert with the progress of high-performance computing in the next era. We will start with a brief overview of the research targets and outcrops of the numerical modelings of mantle convection to date from a viewpoint of geosciences. Then we will discuss the scientific goals which the mantle dynamics researchers are to tackle with in coming years, together with the technical issues in terms of both software and hardware developments.

Keywords: mantle convection, numerical simulation

## Cloud Services to Release Techniques of Data Assimilation

NAGAO, Hiromichi<sup>1\*</sup> ; HIGUCHI, Tomoyuki<sup>2</sup>

<sup>1</sup>Earthquake Research Institute, The University of Tokyo, <sup>2</sup>The Institute of Statistical Mathematics

Data assimilation (DA) is a fundamental technique to integrate numerical simulations and observation data in the framework of the Bayesian statistics. The purpose of DA is to provide an assimilation model that enables us to predict the future state and/or to determine parameters in the given simulation model. A sequential Bayesian filter, e.g., Kalman filter and particle filter, alternatively estimates probability density functions of one-step-ahead prediction and filtering, which respectively mean the states conditionally given the past observation data and given both past and present observation data. DA seems to be hard to implement due to complex programming of the procedure and needed numerous computation, which essentially requires High Performance Computing (HPC). Cloud service (CS) can be a solution for this through an implementation of the DA procedure on a parallel computing environment.

We have developed and released several CSs related to DA such as CloCK-TiME (Cloud Computing Kernel for Time-series Modeling Engine) and DA system for seismoacoustic waves. CloCK-TiME enables us to carry out a multivariate time-series analysis using the particle filter through the Internet. Users can, via the user interface, construct observation and system models, and specify optional parameters to control the analysis in detail. DA system for seismoacoustic waves enables us to determine hypocentric parameters through DA based on a numerical simulation related to seismoacoustic wave propagation using the normal model summation and observed infrasound data obtained at Shionomisaki and Sugadaira.

We will discuss the importance and availability of CS for DA researches through introduction of CSs we have developed.

Keywords: cloud computing, data assimilation, time-series analysis, seismoacoustic wave, multivariate analysis

## Techniques of Big-Data Processing on the NICT Science Cloud

MURATA, Ken T.<sup>1\*</sup>; WATANABE, Hidenobu<sup>1</sup>; UKAWA, Kentaro<sup>2</sup>; MURANAGA, Kazuya<sup>2</sup>; YUTAKA, Suzuki<sup>2</sup>; TATEBE, Osamu<sup>3</sup>; TANAKA, Masahiro<sup>3</sup>; KIMURA, Eizen<sup>4</sup>

<sup>1</sup>NICT, <sup>2</sup>Systems Engineering Consultants Co., LTD., <sup>3</sup>University of Tsukuba, <sup>4</sup>Ehime University

This paper is to propose a cloud system for science, which has been developed at NICT (National Institute of Information and Communications Technology), Japan. The NICT science cloud is an open cloud system for scientists who are going to carry out their informatics studies for their own science.

The NICT science cloud is not for simple uses. Many functions are expected to the science cloud; such as data standardization, data collection and crawling, large and distributed data storage system, security and reliability, database and meta-database, data stewardship, long-term data preservation, data rescue and preservation, data mining, parallel processing, data publication and provision, semantic web, 3D and 4D visualization, out-reach and in-reach, and capacity buildings.

In the present study, we examine performance of parallelization of I/O on the NICT Science Cloud system. We examine an I/O performance of data file system; distributed file system (Gfarm). The Gfarm file system shows a tremendous fast I/O, as fast as 23 GB/sec using only 30 servers. We should pay attention to this I/O speed (23GB/sec is 184 Gbps) from the viewpoint of network speed. We also discuss that the distributed file system shows high scalability: Parallelization efficiency in the present examination is higher than 90% in case of parallel file system. We finally discuss high-performance data processing on the NICT Science Cloud. We have already archived several examples using our technique for both Earth and Space observation data and simulation data. The speed up of the data processing is more than 60 times for scientific big-data.

## Creating future of solid Earth science with high performance computing (HPC): Discussion

HINO, Ryota<sup>1\*</sup> ; HORI, Takane<sup>2</sup> ; HONKURA, Yoshimori<sup>3</sup> ; KANEDA, Yoshiyuki<sup>2</sup> ; ARIKAWA, Taro<sup>4</sup> ; ICHIMURA, Tsuyoshi<sup>5</sup> ; TODORIKI, Masaru<sup>5</sup>

<sup>1</sup>Tohoku University, <sup>2</sup>JAMSTEC, <sup>3</sup>Tokyo Institute of Technology, <sup>4</sup>Port and Airport Research Institute, <sup>5</sup>University of Tokyo

How the evolution of High Performance Computing (HPC) contributes to progress in earth sciences? We will develop a perspective in the next 10 to 20 years based on comprehensive discussion provided in the session including invited talks. Especially, we will discuss what is necessary for solving the social issues such as improvement of hazard maps, tsunami warning system, long-term forecast, etc. The aim of the concluding discussion is to integrate the opinions of attendees, both speakers and non-speakers, into a proposal for development of next generation HPC as a solution to important problems in terms of scientific breakthrough and social relevance.

## Parallel Performance of Particle Method in Many-Core System

FURUICHI, Mikito<sup>1\*</sup> ; NISHIURA, Daisuke<sup>1</sup>

<sup>1</sup>Japan Agency for Marine-Earth Science and Technology

We present a computational performance of the smoothed particle hydrodynamics (SPH) simulation on three types of current shared-memory parallel computer devices: many integrated core (MIC: Intel Xeon Phi) processor, graphics processing units (GPU: Nvidia Geforce GTX Titan), and multi-core Central Processing Unit (CPU: Intel Xeon E5-2680 and Fujitsu SPARC64 processors). We are especially interested in the efficient shared-memory allocation methods with proper data access patterns on each chipset. We first introduce several parallel implementation techniques of SPH code for shared-memory system. Then they are examined on our target architectures to find the best algorithms for each processor unit. In addition, the computing and the power efficiency, which are increasingly important to compare multi device computer systems, are also examined for SPH calculation. In our bench mark test, GPU is found to mark the best arithmetic performance as the standalone device and the most efficient power consumption. The multi-core CPU shows the best computing efficiency. On the other hand, the computational speed by the MIC on Xeon Phi approached to that by two Xeon CPUs. This indicates that using MIC is attractive choice for the existing SPH codes parallelized by OpenMP to gain the computational acceleration by the many many-core processors.

Keywords: high-performance computing, many core, SPH, Parallel Computing, Performance analysis, Shared memory

## Numerical investigation of efficient parallelization of large scale quasi-dynamic earthquake generation cycle simulation

HYODO, Mamoru<sup>1\*</sup> ; ANDO, Kazuto<sup>1</sup> ; HIYOSHI, Yoshihisa<sup>1</sup> ; HORI, Takane<sup>1</sup>

<sup>1</sup>Japan Agency for Marine-Earth Science and Technology

Recently, Ohtani et al. (2011) applied an efficient compression method of full matrix to the problem of earthquake cycles. Since an original full matrix is approximated by a set of sub-matrices with the hierarchical structure, a compressed full matrix is called as H-matrices. By multiplying H-matrices to a column vector, they found that the required floating-point operation reduces to  $O(N)$ - $O(N \log N)$  where  $N$  means the number of discretization of the model fault, though the original multiplication operation using the full matrix is  $O(N^2)$ . Owing to H-matrices, required memory and computation time are largely reduced for the problems of M8 earthquake cycles with  $N=10^5$ - $10^6$ , and it enables us to execute capability computing consisting of many earthquake scenarios using massively parallel computers like the K computer. However, for more realistic simulation with multi-scale earthquakes and their interactions, we must use 100 times larger  $N$  at least, and capability computing with massively parallel CPUs will be indispensable.

Following Ohtani et al. (2011), we have implemented MPI parallelization of earthquake cycle simulation with H-matrices. First, we applied a 1D division in the row direction to H-matrices. Then, each MPI process took charge of a divided row band region of H-matrices. Since the original H-matrices have a hierarchical structure consisting of many sub-matrices with large variation in size, it is difficult to divide all sub-matrices into MPI processes without overlapping through the 1D row division. Hence, we arrowed the overlapping sub-matrix to be calculated in both adjacent MPI processes for the simplification of parallelization. Then, through the simulation with  $N=3 \times 10^5$ , we confirmed a gradual speed-up with the increase of MPI processes up to about 100. However, further increases of MPI processes caused stagnation of speed-up, because the overlapping operation that is not reduced by the increase of MPI processes became dominant.

Accordingly, for more large-scale simulation with many MPI processes, it is necessary to reconsider the parallelization. At first, based on the current 1D division code, we limit the division number in the row direction so as not to increase the ratio of operations with respect to overlapping sub-matrices to the total operations. Then, each row region is divided into further small sub-regions in the column direction, thus we will apply the 2D division of H-matrices. In dividing a particular row region into further sub-regions, we introduce a reference size for the division,  $B$  (Block size). The column directional division of H-matrices requires data transfers between sub-matrices. Moreover, depending on the value of  $B$ , we also need data transfer inside the large sub-matrix. Though such 2D division increases the data transfers between neighboring MPI processes, the appropriate choices of  $B$  and division number in the column direction will realize the equal load balancing among MPI processes in row bands. Accordingly, parallel implementations with 2D division of H-matrices may overcome the overhead due to the increase of data communications.

As tentative results, for  $N=1.3 \times 10^6$  problem, we implemented parallel calculations with both 1D and 2D divisions. Though the 1D parallelization cannot reduce the computational time with the increase of MPI processes, 2D parallelization successfully achieves speed-up with the increase of the number of parallelization. For the same number of MPI processes (1024 processes), the 2D implementation is more than two times faster than that of 1D.

In the presentation, we will show the more detail of our parallelization algorithm and its dependencies on the values of  $N$ ,  $B$ , and division numbers.

**Acknowledgement:** Part of the results is obtained by using the K computer at the RIKEN Advanced Institute for Computational Science (Proposal number hp120278). We thank the Fujitsu tuning team for helping us to develop the parallelization of simulation codes.

**Keywords:** earthquake cycle, capability computing, parallel computing, H-matrices

## The Van, Turkey Earthquake of October 2011: Seismicity, Mechanism and its Aftershocks

KALAFAT, Dogan<sup>1\*</sup>

<sup>1</sup>Bogazici University Kandilli Observatory and ERI Cengelkoy, Istanbul Turkey

On 23 October 2011, a strong earthquake ( $M_w=7.1$ ) occurred east of Van Lake. The earthquake destroyed damage along the Van Fault Zone. Generally, it is caused significant damage in the city of Van with Ercis town, as well as in many villages. The epicenter of the main shock was located in Tabanlı Village between Van city and Ercis town. Shortly afterwards the November 9, 2011 earthquake ( $M_w=5.6$ ) occurred southeastern part of Van Lake, Edremit town area. The main shock and second shocks caused significant damage and deaths of 644 people.

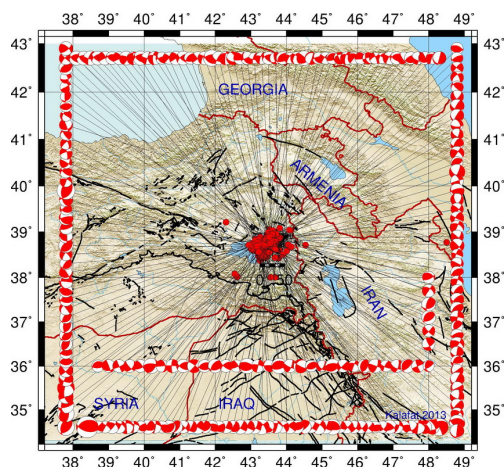
After the main shock 11 important earthquakes ( $5.0 \leq M \leq 6.0$ ) were occurred in the region which has hypo-central distances of 8-38 km. from the main shock location. The main shock triggered mass movement, spreading, and local liquefaction. The important earthquakes and the aftershocks distribution showed that the E-W and NE-SW oriented fault segments caused the earthquake activities. The distribution of the aftershocks supported the presence a rupture of approximately  $70 \pm 10$  km. Aftershocks occurred within an area of approximately 2300 km<sup>2</sup>.

Fault mechanism solution has supported 23 October 2011 Van Earthquake was a reverse fault with a northward dipping fault plane. The fault plane solutions of about 225 important earthquakes ( $M \geq 4.0$ ) were calculated using MT inversion solution technique by this study.

In addition, the stress tensor analysis was completed using the focal mechanism solutions. The stress tensor values of the region were calculated using the azimuth and plunge pairs of P and T axes for 225 earthquakes. The maximum principal stress (P-compressional) of the main shock is aligned in an N-S (NNW/SSE) direction and the tensional axis (T-dilatation) is aligned in an E-W (ENE-WSW) direction. The results of the focal mechanism and stress analysis solutions show that earthquakes have occurred on the reverse faulting and the seismic activity has been continuing under the compressional regime in the region. The Van earthquake activity initiated and caused an increase in seismic activity of the region. This may be explained by the triggering of small faults by the Van Earthquake. The Van earthquake is a good example of compressional deformation and the activity of blind reverse faulting.

This study was supported by Bogazici University Research Projects Commission under SRP/BAP project No. 6671.

Keywords: Van Lake, aftershocks distribution, focal mechanism, stress analysis, reverse faulting



## Microstructural observation of quartz and K-feldspar in quartzo-feldspathic granulite in Sri Lanka

ATHURUPANA, Bhatiya madhura bandara<sup>1\*</sup> ; FUKUDA, Jun-ichi<sup>1</sup> ; MUTO, Jun<sup>1</sup> ; NAGAHAMA, Hiroyuki<sup>1</sup>

<sup>1</sup>Department of Earth Science, Tohoku University, Japan

Sri Lankan basement has been considered as high grade terrains which have suffered poly phase deformation and also upper amphibolite to granulite facies metamorphism during Pan-African amalgamation. In order to illuminate the rheological properties of felsic granulite in deep crustal level associated with high grade metamorphism, microstructural and petrographic observations were conducted.

A quartzofeldspathic gneiss sample (Quartz~40%, K-feldspar~55% and plagioclase <5%) contains highly elongated ribbon quartz which demarcate lineation, in K-feldspar matrix. The sample was collected from the hinge zone of kilometer scale large upright cusped antiform between two large synforms named Dumbara and Huluganga in Sri Lanka. The lineation as maximum elongation direction is N35°W/horizontal. Thin sections were made parallel and perpendicular to the lineation for petrographic and microstructural observations. Based on energy dispersive X-ray spectroscopic (EDS) measurement, most of K-feldspars in the matrix are sanidine [(K<sub>0.59</sub>Na<sub>0.41</sub>)AlSi<sub>3</sub>O<sub>8</sub>] composition. Plagioclase is albite (An 0.1) composition and occurs in clusters and exsolution lamellas in K-feldspar. The grain size of sanidine is from ~50 μm to 2 mm. Large sanidine porphyroclasts are partly recrystallized and show core and mantle structures. Grain boundaries of sanidine are sub polygonal to amoeboid shapes with increasing grain size, while plagioclase grains in clusters show perfect polygonal boundaries with grain size ranging from 50 to 200 μm. Around the plagioclase clusters, scapolite reaction corona exists with crosscutting elongated ribbon quartz. Sericite presents in the same region as very low temperature alteration of plagioclase and scapolite. Most importantly ribbon quartz grains are boudinaged in K-feldspar matrix. Any sign of undulatory extinction or dynamic recrystallization is absent in both boudinaged and large ribbon quartz. Measured average axial ratio of ribbon quartz grains is 21:7:1 with respect to X, Y and Z directions.

The crystallographic orientations of both quartz and sanidine were measured by electron backscattered diffraction (EBSD) method, including large ribbon quartz and boudinaged quartz and also matrix sanidine. The lattice preferred orientation (LPO) patterns of sanidine manifest (010)<001> as a dominant slip system with a minor activation of (010)<100> slip system. The quartz LPO indicates the activations of prism<a> and rhomb<a> slip systems.

According to the presence of K-feldspar as sanidine and their slip systems, we can point out that the sample has prevailed high grade conditions (~550-800°C and ~0.4-0.8 GPa) during deformation [e.g. Menegon et al. 2008]. Scapolitization which occurs at granulite facies could be indicative of peak metamorphism. Also, reaction coronas of scapolite crosscutting ribbon quartz can be interpreted as strong deformation prior to the peak metamorphism. Exsolution of K-feldspar indicates the post dated cooling relative to the strong deformation and the peak metamorphism.

### Reference:

Menegon, L., Pennacchioni G., Spiess R., 2008. Dissolution-precipitation creep of K-feldspar in mid-crustal granite mylonites. *Journal of Structural Geology* 30(5): 565-579

Keywords: Microstructures, Quartz, K-feldspar, Quartz micro boudins

## Multiple events of metamorphism in lenses of eclogite within marbles of Maykhan Tsakhir Formation, Lake Zone, Mongolia

JAVKHLAN, Otgonkhoo<sup>1\*</sup>; TAKASU, Akira<sup>1</sup>; BAT-ULZII, Dash<sup>2</sup>; KABIR, Md fazle<sup>1</sup>

<sup>1</sup>Department of Geoscience, Shimane University, Japan, <sup>2</sup>School of Geology and Petroleum, Mongolian University of Science and Technology, Mongolia

The eclogite-bearing Alag Khadny metamorphic complex in the Lake Zone, SW Mongolia located in the central part of the Central Asian Orogenic Belt, consist mainly of orthogneisses which interleaving with marbles including lenses of garnet-chloritoid schists of Maykhan Tsakhir Formation. Eclogites have two modes of occurrence, i.e. lenses and boudins *eclogite-1* in orthogneisses and *eclogite-2* in marbles. Thermocalc calculations for the peak eclogite facies metamorphism for *eclogite-1* with the assemblage of Grt + Omp + Brs ± Ph ± Ep yielded 570-630 °C and 22-25 kbar (Javkhlan et al., 2013a). In contrast, pressure conditions of the garnet-chloritoid schists (10-11 kbar) are distinctly lower than those of the eclogite-1, whereas temperatures (560-590 °C) are similar (Javkhlan et al., 2013b).

*Eclogite-2* in marbles consists of small grains of garnet (<0.1 mm) and omphacite with minor amounts of amphibole, epidote, paragonite, plagioclase, chlorite, calcite, biotite, quartz, titanite and rutile. The matrix of *eclogite-2* shows a pseudomorphous texture, where small grains of garnet crowd cemented by titanite forming isomorphous round shape. Some of cores of garnet grain contain relics of garnet ( $X_{Ca}=0.32-0.42$ ;  $X_{Mg}=0.06-0.08$ ) indicating previous mineral were larger porphyroblastic garnet. In addition, small grains of omphacite forming rectangular prismatic nature surrounded by garnet grains.

Garnet grains have compositionally zoning with core ( $X_{Ca}=0.08-0.20$ ;  $X_{Mg}=0.10-0.16$ ), mantle ( $X_{Ca}=0.24-0.39$ ;  $X_{Mg}=0.08-0.17$ ), rim ( $X_{Ca}=0.22-0.26$ ;  $X_{Mg}=0.18-0.23$ ) and outer-rim ( $X_{Ca}=0.20-0.22$ ;  $X_{Mg}=0.12-0.18$ ). Few omphacites preserved their core ( $X_{Jd}=0.27-0.31$ ;  $Fe_2O_3=1.34-2.22$  wt%) whereas most of grains have compositional heterogeneity with  $X_{Jd}$  from 0.34 to 0.48 ( $Fe_2O_3=0.04-2.31$ ) and locally with rims of higher  $Fe_2O_3$  (3.79 wt%)-bearing omphacite ( $X_{Jd}=0.32$ ). Omphacites partially replaced by symplectites of Pl (An=15-17), amphibole (Ed, Act, Mg-hbl) and Ep. Three types of amphibole are distinguished by their texture, amphibole (Amp1) [zoned with Act ( $X_{Mg}=0.79-0.81$ ) core, Brs ( $X_{Mg}=0.54-0.69$ ) mantle and rims with Ts, Mg-Trm and Prg in compositions] coexisting with Grt and Omp, poikiloblastic barroisitic amphibole (Amp2) ( $X_{Mg}=0.65-0.75$ ) containing eclogitic minerals of Grt and Omp with their symplectitic assemblage and finally actinolitic amphiboles (Amp3) partially replacing Omp and Grt.

Based on the textures we distinguished two metamorphic events, i.e. eclogite facies metamorphism and poikiloblastic barroisitic amphibole metamorphism. The peak eclogite facies metamorphism characterized by assemblages of Grt (mantle) + Omp + Amp1 (Brs) + Ep + Pg + Rt. Thermocalc calculation yielded  $487 \pm 46$  °C and  $19.7 \pm 2.1$  kbar (sigfit=1.80). Thermocalc calculation of Grt (rim) + Omp (rim) + Amp1 (Mg-Trm) + Ep + Pl yielded  $666 \pm 45$  °C and  $13.7 \pm 1.6$  kbar (sigfit = 2.11) suggesting a decompression stage after the eclogitic metamorphism. The poikiloblastic barroisitic Amp2 shows decreasing Si (7.01-6.69 pfu) and increasing NaB (0.61-0.70 pfu) from core to rim, suggesting that the Amp2 grew after the peak eclogite facies metamorphism, and probably during the second prograde metamorphic event. Approximate P-T conditions of the poikiloblastic barroisitic Amp2 are estimated as 5-7 kbar at c. 450 °C.

<sup>40</sup>Ar/<sup>39</sup>Ar muscovite ages for eclogites ( $543 \pm 3.9$  Ma) in marbles (probably eclogite-2) and the garnet-chloritoid schists ( $537 \pm 2.7$  Ma) were determined (Stipska et al. 2010). K-Ar ages for eclogite-1 [ $603 \pm 15$  Ma,  $602 \pm 15$  Ma (Amp) and  $612 \pm 15$  Ma (Ph)] within orthogneisses have been obtained (Javkhlan et al., 2014). These ages are interpreted as the exhumation ages for the eclogites (-1 and -2) and the garnet-chloritoid schists.

The peak temperature conditions of eclogite-2 considerably lower than eclogite-1 whereas the pressure conditions are similar. The peak P-T conditions garnet-chloritoid schists are correlated with the poikiloblastic Amp2 metamorphism of the eclogite-2.

Keywords: eclogite-2, pseudomorphous texture, garnet-chloritoid schists, Maykhan Tsakhir Formation, Lake Zone, SW Mongolia

## Multiple exhumation episodes recorded in orogenic garnet peridotites from the Bohemian Massif (Czech Republic)

NAEMURA, Kosuke<sup>1\*</sup>; SVOJTKA, Martin<sup>2</sup>; ACKERMAN, Lukas<sup>2</sup>; SHIMIZU, Ichiko<sup>1</sup>; HIRAJIMA, Takao<sup>3</sup>

<sup>1</sup>Department of Earth and Planetary Science, Graduate School of Science, The University of Tokyo, <sup>2</sup>Geologický ústav Akademie, Czech Republic, <sup>3</sup>Department of Geology & Mineralogy, Faculty of Science, Kyoto University

Presence of garnet peridotites in *HP/UHP* metamorphic terranes is taken as evidence for interaction between crust and mantle during orogeny. In order to constrain the timing of interaction, *P-T* paths for both peridotites and crustal rocks have been constrained, which demonstrated that there are significant gaps between peak pressure of peridotites and host continental crust. In this contribution, we will show an evidence for multiple exhumations recorded by clinopyroxene (*Cpx*) megacryst discovered in the garnet peridotite from the Bohemian Massif, and will constrain the timing of crust-mantle interaction in the light of the new data.

The Gföhl Unit experienced the highest metamorphic grade in the Moldanubian zone of the Bohemian Massif, and it mainly consists of quartz-feldspathic garnet-kyanite granulite with peak condition at 2.2-2.3 GPa and 1000 °C (Vrana et al., 2013, *J. Geosci.* **58**, 347-378), although Kotková et al. (2011, *Geology* **39**, 667-670) recently found diamond and coesite from the Saxony-type granulite. Gföhl granulite occurs as tens km-sized isolated blocks and contains garnet peridotites whose peak conditions were estimated as 2-6 GPa and 850-1350 °C (Medaris et al., 2005, *Lithos* **82**, 1-23). We studied *P-T* path for the garnet peridotite at Lom pod Libínem quarry in the Prachatice granulite massif in the south Bohemia. Lom pod Libínem (*LPL*) peridotite generally displays granoblastic texture consisting of mm-sized (0.1-5.0 mm in diameter) garnet, pyroxenes, olivine, and most garnet grains are transformed to kelyphite and are replaced by phlogopite. *LPL* peridotite includes a lot of cm-size *Cpx* megacrysts. Among them, the largest megacryst (3×5 cm) shows a strong chemical zoning consisting of three zones (Fig. 1), namely, core, mantle and rim: (1) the "pale-green core" is poor in Ca-Tschemak (CaTs, ~6 mol.%) and rich in Enstatite (En, ~9 mol.%) (components after Simakov, 2008, *Lithos* **106**, 125-136) and includes phlogopite and orthopyroxene, (2) the "mantle" is lower in CaTs. (4-5 mol.%) and En. (4 mol.%), and includes hornblende, chlorite, apatite, titanite, andradite, olivine, and celsian, and (3) the "rim", rich in CaTs. (7-9 mol.%) and En. (9 mol.%), includes olivine, phlogopite, and hornblende, respectively. The mm-size *Cpx* has identical composition to the megacryst-rim, and (4) the smaller *Cpx* is richer in CaTs. (12 mol.%) and poorer in En. (7 mol.%). Four mineral stages can be identified: **Stage 1** is defined by megacryst-core coexisting with phlogopite, orthopyroxene. Assuming the co-existence with garnet, the equilibrium condition was estimated at ~4 GPa and 1000 °C by use of the single *Cpx* geothermobarometer (Nimis & Taylor, 2000, *Contrib. Mineral. Petrol.* **139**, 541-554), **Stage 2** is defined by the "mantle" coexisting with hornblende, chlorite, orthopyroxene, and andradite, which were equilibrated at ~700 °C, *P*<2.5 GPa. **Stage 3** is defined by the core of mm-size pyroxenes, garnet and olivine that were equilibrated at ~3.0 GPa and 1000 °C in the garnet lherzolite facies. **Stage 4** is defined by the matrix spinel lherzolite assemblage equilibrated at *T*~800 °C at 1-2 GPa.

We envisaged the following juxtaposition mechanism: *LPL* peridotite originally came from the upper mantle (4 GPa) that exhumed to the depth of <2.5 GPa and was partially transformed to chlorite peridotite. Assuming that *LPL* peridotite was entrained in the crust at Stage 2, peridotite and host continental crust could have shared the Variscan *UHP* metamorphism at 3 GPa (Stage 3), followed by final exhumation. Although the peak *P-T* condition of Stage 3 is still higher than that of country granulite (<2.3 GPa), this could reflect different degree of retrogression during the final exhumation. Our study suggests some orogenic peridotites were exotically derived from the *UHP* mantle (>4 GPa), where continental crust have not subducted more than 3 GPa. This will give an another solution to the observed pressure gaps between orogenic peridotites and host continental crust.

Keywords: orogenic peridotite, *UHP* metamorphism, crust-mantle interaction, Bohemian Massif, multiple exhumations

SCG08-04

Room:311

Time:April 29 10:00-10:20

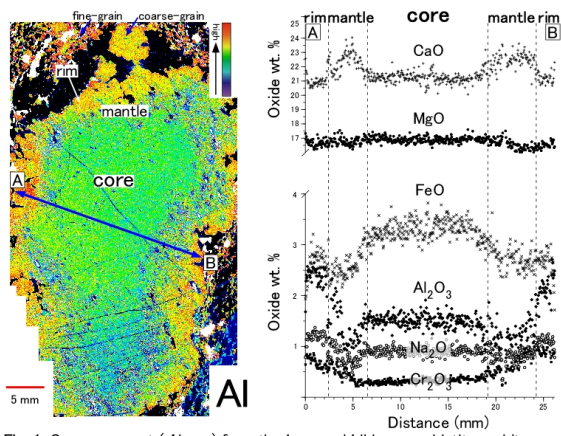


Fig. 1. Cpx megacryst (*Al map*) from the Lom pod Libinem peridotite and its compositions along the line.

## Modelling of the Phase Relations in High- and Ultrahigh-pressure Metabasic Rocks

WEI, Chunjing<sup>1\*</sup>

<sup>1</sup>School of Earth and Space Sciences, Peking University

Pseudosections calculated with THERMOCALC predict that for glaucophane-lawsonite eclogite facies conditions (500-600 °C and 18-28 kbar), MORB compositions in the NCKMnFMASHO system will contain glaucophane, garnet, omphacite, lawsonite, phengite and quartz, with chlorite at lower temperature and talc at higher temperature. In these assemblages, the pyrope contents (X<sub>py</sub>) in garnet is mostly controlled by variations in temperature, grossular content (X<sub>gr</sub>) is strongly controlled by pressure, and the silica content (Si-) in phengite increases linearly with pressure. As the P-T conditions for these given isopleths are only subtly affected by common variations in bulk-rock compositions, the P-T pseudosections potentially present a robust geothermobarometric method for natural glaucophane-bearing eclogites. The maximum X<sub>py</sub> content may define the temperature peak (T<sub>max</sub>) and the minimum X<sub>gr</sub> content constrains the pressure peak (P<sub>max</sub>) conditions. An isothermal decompression of these lawsonite-bearing assemblages would result in epidote-bearing assemblages through dehydration reactions such as lawsonite + omphacite = glaucophane + epidote + H<sub>2</sub>O, releasing a large amount of bound fluid. Thus, most natural HP epidote eclogites may have experienced a metamorphic stage of lawsonite stability.

Under low-T UHP conditions (>28 kb, 550-650 °C), basic rocks are predicted to contain garnet, omphacite, lawsonite, phengite, coesite and talc. In this assemblage, the X<sub>py</sub> contents steadily increase as temperature rises and the Si-in phengite increases linearly with pressure. However, the X<sub>gr</sub> content is very sensitive as pressure changes, showing slowly decrease as pressure rises. The peak P-T conditions for low-T UHP eclogites can be determined using the isopleths of maximum X<sub>py</sub> and Si-in phengite in P-T pseudosections. An isothermal decompression of these low-T UHP eclogites at temperature i.e. 600 °C would result in disappearance of lawsonite and talc in the peak stage, but appearance of glaucophane, epidote and kyanite, forming the mineral assemblages involving garnet + omphacite + glaucophane + epidote + kyanite + quartz/coesite + phengite commonly observed. Moreover, garnet in the low-T UHP eclogites is characteristic of growth zoning with its rims containing lower X<sub>gr</sub> and higher X<sub>py</sub> contents.

Under Medium-T UHP conditions (>28 kb and >650 °C), basic rocks are predicted commonly to contain garnet + omphacite + lawsonite + phengite + coesite. In this assemblage, the X<sub>py</sub> in garnet mostly depends on bulk compositions, whereas the X<sub>gr</sub> in garnet and the Si-contents in phengite regularly increase, respectively, as temperature and as pressure rise, and thus, can provide robust thermobarometric constraints. Decompression of the eclogites with lawsonite in the peak stage is inferred to be dominated by lawsonite dehydration, resulting in increase in the mode of anhydrous minerals, or further eclogitization, and formation of epidote porphyroblasts and kyanite-bearing quartz veins in eclogite. As lawsonite dehydration can facilitate evolution of assemblages under fluid-present conditions, the UHP eclogites with lawsonite are hard to memorize their real peak P-T conditions.

Keywords: HP-UHP eclogites, pseudosection, geothermobarometer, basic rock

## DEHYDRATED FLUID AND SEISMIC DEFORMATION IN DEEP SUBDUCTION ZONE ?constraints from lawsonite eclogite and olivine-opx sp

OKAMOTO, Kazuaki<sup>1\*</sup>

<sup>1</sup>Saitama University, <sup>2</sup>Joint Graduate school, Tokyo Gakugei University

Introduction: It has been considered that there is a correlation between the double seismic zone and metamorphic dehydration reaction in deep slab. The location of the upper limits of the upper seismic plane correspond to metamorphic facies boundary where H<sub>2</sub>O contents change in subducting crust; numerous earthquakes from 60 to 110 km depths in the lawsonite-blueschist facies, many earthquakes in the lower crust of the slab from 110 to 150 km depths in the lawsonite-amphibole eclogite facies and few earthquakes in the lawsonite eclogite facies. It was considered that the dry eclogite is distributed in the area where there is few earthquake [1]. However, ultrahigh pressure experiments and thermodynamic calculation are both demonstrating that the lawsonite eclogite is stable [2] in the area. In order to unravel relation between dehydration and seismic deformation, we have investigated dehydration process of natural metamorphic rocks recording very cold geo-thermal history in the crust and lithosphere in the slab.

Lawsonite eclogite (Alpine Corsica): Alpine Corsica is the best representative field area exhibiting lawsonite eclogite and blueschist as a coherent high pressure, low temperature metamorphic belt. Ophiolite sequence (oceanic plate structure) is also well-preserved, and the pillow structure is clearly recognized in the lawsonite eclogite. Recent petrological researches have revealed that both blueschist (rims of the pillow) and lawsonite eclogite (core of the pillow) are stable in the same pressure and temperature condition [3] because chemical variation including water content creates both lawsonite-amphibole eclogite and lawsonite eclogite in different portion of subducted crust. We carefully observed microtexture of the lawsonite eclogite and blueschist and have found that omphacite vein and lawsonite vein in mylonitized blueschist matrix.

Olivine-opx spinifex in serpentinite (Cerro del Almirez, Nevado complex): Metamorphic olivine after antigorite has been described in Italian Alps and also from the Mt. Shiraga, Japan. However, the olivine was formed with talc and fluid by antigorite breakdown reaction in pressures lower than 1.5 GPa. Spinifex olivine with opx in the Cerro del Almirez, is the product at pressures ( $P > 1.5$  GPa) relevant to the lower seismic plane beneath Northeast Japan. In Cerro del Almirez, olivine-opx rocks underlie antigorite schist by a contact [4]. In the olivine-opx rocks, the blade-like, elongated olivine and opx were grown, representing spinifex texture. It clearly indicates the presence of large amount of water facilitate crystallization of elongated olivine with opx.

Discussion and conclusion: In the lawsonite eclogite in the Alpine Corsica, blueschist and lawsonite coexist together reflecting chemical difference in pillowed structure or lithology. Omphacite and lawsonite veins are observed along the shear band in mylonitized blueschist. It suggests that decomposition of glaucophene caused hydro-fracturing and precipitate omphacite and lawsonite vein. Garnet was grown statically close to the vein.

Olivine-opx spinifex in the serpentinite, Cerro del Almirez, were probably recrystallized in the presence of large amount of water. The estimated dehydration reaction has a negative P-T slope at pressures higher than 1.5 GPa. The reaction is volume reducing reaction and the olivine-opx spinifex texture was formed under volume reducing reaction.

References: [1] S. Kita et al., *Geophys. Res. Lett.*, 33, doi:10.1029/2006GL028239. (2006). [2] K. Okamoto et al., *Geochemistry*, 46 205-215 (2013). [3] A. Vitale Brovarone et al., *J. Met. Geol.*, 29, 583-600, (2011). [4] V. Trommsdorff et al., *CMP*, 132, 139-148 (1998).

Keywords: double-seismic zone, upper seismic plane, Lawsonite eclogite, lower seismic plane, olivine-opx spinifex, dehydrated vein

## Ultrahigh-pressure eclogites: paleo-environment indicators

UR REHMAN, Hafiz<sup>1\*</sup>

<sup>1</sup>Department of Earth and Environmental Sciences, Graduate School of Science and Engineering, Kagoshim

Ultrahigh-pressure (UHP) eclogites generally form by the metamorphism of mafic lithologies (gabbros or basalts) at depths greater than 90 km (minimum stability field of coesite) indicating P-T conditions of >2.7 GPa and 600-800 °C. At such conditions most minerals reequilibrate their chemical elements (e.g. major and trace and even isotopes) and new minerals crystallize or grow at the expense of other minerals formed during the magmatic crystallization. Some chemical elements, considered as relatively less mobile or immobile (e.g. Sm, Nd, Lu, Hf), are widely used for the extraction of past records the rocks have evolved through. Besides those elements, oxygen, the major component of silicates and oxides, impart important information related to protolith formation of rocks and their metamorphism. In general, most basaltic rocks show a narrow range of  $\delta^{18}\text{O}$  (ca.  $+5.7 \pm 0.3$  ‰ relative VSMOW) and values for altered basalts vary from 0 to +12 ‰.

In this paper, I discuss the origin of low or negative  $\delta^{18}\text{O}$  values; recently we found in the Himalayan UHP eclogites of Kaghan Valley and explain the mechanism how these low values were acquired. These eclogites are formed during Eocene by the India-Asia collision and their protoliths were the Panjal Trap basalts which were emplaced in Permian when Indian Plate was part of Gondwana. The  $\delta^{18}\text{O}$  values are as low as  $-2.25$  ‰ in the fresh parts of eclogites and increase towards more positive in the retrogressed or amphibolitized parts. The unusually low  $\delta^{18}\text{O}$  values in eclogites are interpreted to have resulted from the hydrothermal alteration of the protoliths by meteoric water interaction when Greater India was still at southern high latitudes (>65 degrees S) during the Permian indicating glacial paleo-environment. These low  $\delta^{18}\text{O}$  values were frozen-in in the protolith rocks and did not change during subduction-related UHP metamorphism. However retrogressive process, due to infiltration of  $^{18}\text{O}$ -rich fluids during exhumation, shifted these values towards more positive range.

Keywords: Ultrahigh-pressure eclogites, Himalaya, Oxygen isotope, Paleo-environment

## Role of the second continent

KAWAI, Kenji<sup>1\*</sup> ; ICHIKAWA, Hiroki<sup>2</sup> ; YAMAMOTO, Shinji<sup>4</sup> ; TSUCHIYA, Taku<sup>2</sup> ; MARUYAMA, Shigenori<sup>3</sup>

<sup>1</sup>Department of Earth and Planetary Sciences, Tokyo Institute of Technology, <sup>2</sup>Geodynamics Research Center, Ehime University, <sup>3</sup>Earth-Life Science Institute, Tokyo Institute of Technology, <sup>4</sup>Department of Earth and Astronomy, Graduate School of Arts and Sciences, The University of Tokyo

It has been thought that granitic crust, having been formed on the surface, must have survived through the Earth's evolution because of its buoyancy. Recent geological studies have suggested that a significant amount of crustal material has been lost from the surface due to delamination, continental collision, and subduction at oceanic?continental convergent margins (von Huene and Scholl 1991; Yamamoto et al. 2009; Ichikawa et al. 2013a). If so, then the subducted crustal materials are expected to be trapped in the mid-mantle due to the density difference from peridotitic materials induced by the phase transition from coesite to stishovite (Kawai et al. 2013). In order to study the effect of the subducted granitic materials floating around the mantle transition zone, we conducted two-dimensional numerical experiments of mantle convection incorporating a continental drift with a heat source placed around the bottom of the mantle transition zone. We found that the addition of heat source in the mantle transition zone considerably enhances the onset of upwelling plumes in the upper mantle, which further reduces the time scale of continental drift. The heat source also causes massive mechanical mixing, especially in the upper mantle. The results suggest that the heat source floating around the mantle transition zone can be a possible candidate for inducing the supercontinent cycle (Ichikawa et al. 2013b).

Keywords: Second continent, Wilson's cycle, Granite, Tectonic erosion

## Where had the primordial continent gone?

MARUYAMA, Shigenori<sup>1\*</sup>; KAWAI, Kenji<sup>2</sup>; TSUCHIYA, Taku<sup>3</sup>

<sup>1</sup>ELSI Tokyo Institute of Technology, <sup>2</sup>Tokyo Institute of Technology, <sup>3</sup>Ehime University

There are no Hadean rocks on the Earth's surface. This indicates (1) there was no continents on the primordial Earth, or (2) continents were present in the Hadean but lost afterwards. It is well-known that Moon surface was covered by anorthositic continental crust with KREEP basalts with ca. 50-60km thickness. Those rocks are the fractionated final residues of magma ocean after the giant impact at 4.56Ga.

The Earth must have been completely melted if giant impact was correct, but due to 6 times larger gravity, the thickness of anorthositic continents must be 21 km. Moreover, during the consolidation of magma ocean, bulk of anorthositic blobs could be transformed into (1) zoisite+kyanite+quartz, (2) grossular+kyanite+quartz, (3) grossular +kyanite+coesite, (4) grossular +kyanite+stishovite, in 300km depth.

Absence of TTG rocks in the Hadean and nearly absent in early Archean less than 5% among the surface of present continents must be caused by extensive tectonic erosion by subducting slabs which are present even today at trench. Therefore, it is wrong to believe that low-density granite must have accumulated on the surface once formed on the surface of the Earth.

Density calculation of anorthosite, MORB, harzburgite, and pyrolite using first principles calculation showed that anorthosite was heavier if it convected at depth in mantle transition zone. If it turns into lower mantle, it becomes to be heaviest among those as mentioned above, suggesting the stability field at D" layer on the bottom of mantle which is right above CMB.

However, it depends on the geothermal gradient on which phase change of Al<sub>2</sub>O<sub>3</sub> occurs to determine whether or not the heaviest among all rocks at CMB. Depending on cooling the CMB, meta-anorthosite could have been buoyant particularly after the mantle overturn at 2.7-2.6Ga.

Before the overturn, if the basal magma ocean was present in the Archean, the lost primordial continents must have been melted into basal magma ocean where anorthosite-KREEP basalts mixed with FeO-enriched primordial basal magma ocean. The possible bulk chemistry can be estimated, though qualitatively; it must be super-enriched in anorthositic component. It can be expressed in Ca-Pv, Mg-Pv, Ferro-periclase as major components.

When, mantle overturn occurred at 2.7-2.6Ga, low-temperature materials of upper mantle must have cooled down the basal magma ocean to consolidate to crystalize Ca-Pv rock, bi-mineral Ca-Pv + Mg-Pv rock, and the tri-mineral Ca-Pv + Mg-Pv + FM periclase rock. According to the formation of these rocks, those three rocks would have been behaved differently, although depends on not only density but also mass.

Assuming the enough volume of Ca-Pv rocks, those rocks may be floating in mid-depth of lower mantle.

## Subduction origin for UHP chromitite from the Nishisonogi metamorphic rocks, Western Kyushu, Japan

NISHIYAMA, Tadao<sup>1\*</sup>; MORIBE, Yousuke<sup>1</sup>; ISHIMARU, Satoko<sup>1</sup>; ARAI, Shoji<sup>2</sup>; MORI, Yasushi<sup>3</sup>; SHIGENO, Miki<sup>3</sup>

<sup>1</sup>Graduate School of Science and Technology, Kumamoto University, <sup>2</sup>Department of Earth Sciences, Kanazawa University, <sup>3</sup>Kitakyushu Museum of Natural History and Human History

Ultrahigh-pressure (UHP) chromitite from the Luobsa Ophiolite in non UHP terrane has been an enigma because of its peculiar occurrence. We newly found a UHP chromitite from serpentinite in the Nishisonogi metamorphic rocks (NMR), a member of the Nagasaki Metamorphic Rocks, in Western Kyushu, following our finding<sup>1</sup> of it from the Higo Metamorphic Rocks (HMR), Central Kyushu. The UHP chromitite from NMR documents well a fluid-chromite interaction, showing partial graphitization of microdiamond. Such a fluid-chromite interaction is not observed in HMR chromitite. The NMR are high P/T (epidote-glaucophane schist subfacies) metamorphic rocks of Cretaceous in age, mainly consisting of pelitic and psammitic schists intercalating with minor basic schists<sup>2</sup>. The peak metamorphic condition of the crystalline schists is estimated as 1.4 GPa and 520 °C by an assemblage of garnet with inclusions of chloritoid and omphacite, glaucophane, paragonite, and phengite in a garnet galucophanite<sup>3</sup>. Serpentinite and serpentinite melanges occur as elongated bodies or lenses concordant with schistosity trending N-S of the country schists<sup>1</sup>. Jadeitite and omphacite occur as tectonic blocks in the serpentinite melange, showing the peak condition of 1.5 GPa and 500 °C by coexistence of jadeite and quartz<sup>4</sup>. Microdiamond-bearing chromitite was found from serpentinite in a melange at Ooseto Town, Saikai City. Chromitite occurs as a thin layer several cm thick and meter-size long in a serpentinite with numerous magnesite (or ankerite) veins. The layer is strongly deformed to show a schlieren-like structure. The serpentinite consists of fine-grained antigorite with no relics of olivine and pyroxenes. The chromitite consists of an aggregate of rounded and fractured chromite crystals with small amounts of talc and magnesite as a matrix and veins. Microdiamond occurs as aligned crystals in narrow zones ranging from a few μm to several tens of μm in chromite. Chromite is zoned, consisting of Mg-rich core (Mg<sub>0.33</sub>Fe<sup>2+</sup><sub>0.65</sub>Mn<sub>0.03</sub>)(Cr<sub>0.84</sub>Al<sub>0.12</sub>Fe<sup>3+</sup><sub>0.04</sub>)<sub>2</sub>O<sub>4</sub> and Fe-rich rim (Mg<sub>0.06</sub>Fe<sup>2+</sup><sub>0.89</sub>Zn<sub>0.02</sub>Mn<sub>0.03</sub>)(Cr<sub>0.85</sub>Al<sub>0.12</sub>Fe<sup>3+</sup><sub>0.04</sub>)<sub>2</sub>O<sub>4</sub>. The microdiamond-bearing zones are conspicuously richer in Fe<sub>2</sub>O<sub>3</sub> [(Mg<sub>0.03</sub>Fe<sup>2+</sup><sub>0.94</sub>Mn<sub>0.04</sub>Zn<sub>0.01</sub>)(Cr<sub>0.67</sub>Ti<sub>0.01</sub>Fe<sup>3+</sup><sub>0.31</sub>O)<sub>2</sub>O<sub>4</sub>], observed as a brighter zone in a BSE image, than other part of chromite in the same grain. The network-like distribution of the zones clearly indicates fluid infiltration associated with the following exchange reaction of trivalent cations between chromite and the fluid: Cr<sup>3+</sup> + Al<sup>3+</sup>(in chromite) = Fe<sup>3+</sup>(in fluid)

Microdiamond occurs either as polyhedral or as platy crystals, 1 to several μm across. Identification of diamond was carried out with an energy dispersive X-ray spectroscopy (EDS) analysis (carbon peak) and Raman spectroscopy with a He-Ne laser. We observed a broad Raman peak at 1331 cm<sup>-1</sup>, which is comparable to the peak (1332 cm<sup>-1</sup>) characteristic of diamond. Graphite peak at about 1600 cm<sup>-1</sup> is also observed, showing partial graphitization of microdiamond. These lines of evidence show that the fluid infiltration may have occurred after inclusion of microdiamond.

It is quite astonishing that microdiamond is preserved in such a completely serpentinitized ultramafic rock. Chromite can be a good container of microdiamond to prevent graphitization during geologically long duration of exhumation and serpentinitization. Our finding suggests the subduction origin of UHP chromitite from NMR rather than mantle migration origin<sup>5</sup> in the case of the Luobusa Ophiolite.

### References

1. Nishiyama, T., Shiosaki, D., Eguchi, H., and Yoshiasa, A. JpGU Meeting, S-MP46 (2014);
2. Nishiyama, T. Mem. Geol. Soc. Japan 33, 237-257 (1989);
3. Moribe, Y. unpublished Mc thesis, Kumamoto University (2014);
4. Shigeno, M., Mori, Y., Shimada, K., and Nishiyama, T. Eur. J. Mineral., 24, 289-311 (2012);
5. Arai, S. J. Mineral. Petrol. Sci., 105, 280-285 (2010)

Keywords: microdiamond, UHP chromitite, subduction zone, Nishisonogi metamorphic rocks, ultrahigh-pressure metamorphic rocks

## Melt-Peridotite Reactions In The Upper Mantle: Geochemistry Of Peridotite And Pyroxenite From The Beni-Bousera Massif

CHETOUANI, Kamar<sup>1\*</sup> ; AMRI, Isma<sup>1</sup> ; TARGUISTI, Kamal<sup>1</sup>

<sup>1</sup>departement de geologie, Faculte des sciences de Tetouan. Maroc

The Beni-Bousera massif contains ubiquitous pyroxenites of various types, organized into conspicuous layers ranging from 0.5 to 100 cm in thickness, hosted by peridotites. Integrated field features, petrographic observations, and geochemical analyses from 92 samples (whole rock major and trace elements data: 55 samples, microprobe data for minerals: 48 samples, and mineral trace elements data: 30 samples) from pyroxenites provide information to classify the rock types into four different groups typified as: (1) garnet pyroxenites, (2) spinel-garnet websterites, (3) spinel websterites, and (4) spinel chromium websterites. Type 1 rocks, occurring at the base of the massif, are considered as the most primitive type, garnet pyroxenites layers represent the vestiges of an old veined subcontinental lithosphere. They generally indicate temperatures <970°C (based on two-pyroxene thermometry) and a low to very low Mg# (<76%). Trace element contents show enrichment in heavy and middle rare earth elements but strong depletion in light rare earth elements (LREE). Paradoxically, the host peridotites show enrichment in LREE, which give new insights into their genesis history. Based on our field observations and geochemical results, we suggest that garnet-pyroxenite layers metasomatised the host peridotite successively by the partial melting as a consequence of subsequent heating phase(s) of the lithosphere. The magmatic event that led to the diversity and zoning of mafic layers was caused by melting of the base of thinned subcontinental lithosphere by upwelling asthenosphere, followed by infiltration of asthenospheric melts. The different groups of mafic layers record several stages of this event.

Keywords: Geochemistry, Beni Bousera, Pyroxenite, Peridotites

## Petrology and geochemistry of the ultramafic metamorphic rocks from the Masora domain, east-central Madagascar

ICHIKI, Takashi<sup>1\*</sup> ; ISHIKAWA, Masahiro<sup>1</sup> ; KIMURA, Jun-ichi<sup>2</sup> ; SENDA, Ryoko<sup>2</sup>

<sup>1</sup>Yokohama National University, <sup>2</sup>JAMSTEC IFREE

Madagascar is located within the interior of the Neoproterozoic East African Orogen (Jacobs and Thomas, 2004) that marks the join between East and West Gondwana. In the east Madagascar, the Paleo-Mesoarchean Antongil-Masora domains are exposed (Collins, 2006; Tucker et al., 2011). In this study we report the petrological and whole rock and REE geochemical characteristics of the ultramafic metamorphic rocks exposed within the Masora domain and we discuss their origin and tectonic settings. The Masora domain is mainly composed of the Paleo-Mesoarchean felsic metamorphic rocks with subordinate amounts of metasedimentary rocks (e.g. Randriamananjara, 2008; Tucker et al., 2011). This domain was intruded by Neoproterozoic granitoids and mafic-ultramafic rocks (e.g. Smith et al., 2008).

The ultramafic metamorphic rocks are exposed in the north and south Masora domain. Three types of ultramafic metamorphic rocks are identified in the north: peridotite, pyroxenite and hornblendite. The peridotite is mainly composed of olivine and anthophyllite with subordinate amounts of serpentine, magnesite and magnetite. The pyroxenite is mainly composed of clinopyroxene and hornblende with subordinate amount of magnesite and magnetite. The hornblendite is mainly composed of hornblende with subordinate amount of actinolite and magnetite. Some of the hornblendite has spinel. An ultramafic metamorphic rock body occurs as a lens within metasedimentary rock in the south. This metasedimentary rock is kyanite+biotite+muscovite schist. The mineral assemblage of the ultramafic lens differs between core and rim. It is mainly composed of olivine, tremolite, actinolite and chlorite with subordinate amounts of serpentine, magnetite and altered minerals in the core. The rim is mainly composed of tremolite, actinolite and chlorite with subordinate amount of magnetite and ilmenite.

The ultramafic metamorphic rocks except for the hornblendites have  $\text{SiO}_2 = 42.7\text{-}51.7$  wt.%,  $\text{Al}_2\text{O}_3 = 1.5\text{-}7.5$  wt.%,  $\text{MgO} = 19.8\text{-}35.4$  wt.%, and  $\text{CaO} = 3.5\text{-}16.5$  wt.%. They have high Mg# (molar ratio of  $\text{Mg}^{2+}/(\text{Mg}^{2+} + \text{Fe}^{2+})$ ) of 0.76-0.83. On the basis of bulk rock CIPW normative Ol-Cpx-Opx composition, the ultramafic metamorphic rocks except for the hornblendites plot in the field of the lherzolite, olivine websterite and websterite (Streckeisen, 1976). Compared with the geochemical characteristics of abyssal peridotites (Niu, 2004), the ultramafic metamorphic rocks shows lower MgO, higher  $\text{TiO}_2$  and CaO than those in the abyssal peridotites. On the MgO-Ni diagram (Pfeifer, 1990 in Katzir et al., 1999) one of the samples plot in the typical abyssal lherzolite field whereas the others plot in higher-Ni (orogenic) field. Chondrite normalized REE patterns of the ultramafic metamorphic rocks show flat HREE with variable LREE patterns. One of the samples shows enriched LREE pattern and the others show depleted LREE patterns. The depleted LREE samples have flat HREE with about twice amount of chondritic HREE abundances. This is typical characteristic of an orogenic lherzolite such as Ronda massif in the southern Spain and Lanzo lherzolites in the Italian Alps (Bodinier and Godard, 2003). Enriched LREE pattern is also a typical characteristic of pyroxenites occurring in orogenic peridotites (Bodinier and Godard, 2003). On the basis of petrological and geochemical characteristics, their protoliths are orogenic lherzolite, websterite and pyroxenite.

Keywords: Gondwana supercontinent, east-central Madagascar, geochemistry, Masora domain, ultramafic metamorphic rocks

## Zircon Nano-SIMS U-Pb dating from the country gneiss beside Horoman peridotite, Hokkaido, Japan

SUZUKI, Ryosuke<sup>1</sup> ; OKAMOTO, Kazuaki<sup>1\*</sup>

<sup>1</sup>Saitama university, Japan

Hidaka Metamorphic Belt, Hokkaido, Japan includes the youngest granulites and the Horoman peridotite complex in the highest grade zone. Age of the Hidaka gneiss and amphibolite have been determined by various methods (e.g. K-Ar, U-Pb, Rb-Sr and etc). However, the age of Horoman peridotite complex has not been determined yet. Only Yoshikawa et al (1993) reported the cooling age of the complex as 23 Ma based on whole rock Rb-Sr isochron method. This study performed U-Pb dating of zircons from the paragneiss surrounding the Horoman peridotite complex in order to determine the intrusive age of the Horoman peridotite complex from the upper mantle into the lower crustal conditions. The zircons have detrital cores and thin rims (<20 microns). Therefore we used Nano-SIMS because it is possible to focus the secondary beam diameters down to submicrons for the analysis. As a result of this measurement, rim ages of the zircons show that <sup>238</sup>U-<sup>206</sup>Pb age are 7-11Ma (n=7) and detrital core ages show 25.6 Ma, 34-35 Ma, 78 Ma and 150 Ma (n=8). The rim ages are the youngest in Hidaka metamorphic rocks and there is a discrepancy with zircon rim ages (19Ma) from the granulite (Kemp et al. 2007; Usuki et al. 2006). The present rim ages (7-11 Ma) fit well with the tectonic scenario of the collision process of Hokkaido Island proposed by Yamamoto et al. (2010). It is considered that the Horoman peridotite complex was juxtaposed onto the Hidaka metamorphic belt at 7-11Ma by the subducting Pacific plate after the collision between North American and Eurasian plates.

Keywords: Zircon, U-Pb, Nano-SIMS, Horoman peridotite, country gneiss, juxtaposition age

### 3 types of Ca-Amp found from Nove Dvory UHP eclogites and their origin, Moldanubian Zone of the Bohemian Massif

YASUMOTO, Atsushi<sup>1\*</sup>; HIRAJIMA, Takao<sup>1</sup>

<sup>1</sup>Department of Geology and Mineralogy, Graduate School of Science, Kyoto University

The upper-stability limit of Ca/Na amphibole (Amp) in meta-mafic rocks are considered to be around 2-3 GPa in pressures (Schmidt & Poli, 1998). Thus, most Ca-Amp in (ultra)-high pressure metamorphic rocks have been considered as retrograde products. The peak metamorphic conditions of Nové Dvory eclogites are estimated to be 4.5-4.9 GPa and 1050-1150°C. However, some Ca-Amp inclusions in Grt are likely to be interpreted as prograde relicts survived the ultra-high pressure metamorphism. This paper reports the mode of occurrence and the chemical compositions of Ca-Amp and the coexisting minerals in Nové Dvory eclogite, and discusses when Ca-Amp crystallized. Investigated two eclogite samples, ND0107 and ND120, collected from the same outcrop, are composed mainly of garnet (Grt) and Omphacite (Omp) with minor amounts of apatite (Apt) and rutile (Rt) at the UHP stage, and suffered hydration reactions, represented by Ca-Amp and plagioclase (Pl) formation, with various degree during the exhumation stage.

Ca-Amp in studied eclogite can be classified into 3 types based on their modes of occurrence; Type 1 Amp occurs in sporadic euhedral shaped polyphase mineral aggregates (PMAs) in Grt along with Omp, Rt, and Apt. Type 1 Amp is identified only from ND0107, and is classified as pargasite (Prg) or kaersutite (Krs). Omp inclusions associated with Type 1 Amp are homogeneous and have high  $X_{Jd}$  of 40-45, suggesting that the associated Omp did not suffer retrogressive reactions. On ACF diagram, Type 1 Amp is plotted between the associated Omp and host Grt. It suggests that Type 1 Amp could be a relict of the following reaction,  $Amp = Omp + Grt + W$ , during the subduction stage. Type 2 Amp is identified as a member of PMAs in Grt along with spinel (Spl) and diopside (Di). Those PMAs with Type 2 Amp show unidiomorphic shapes and straight alignment in Grt. They are classified as Prg or magnesio-hastingsite (Mg-Hs). Type 3 Amp is a member of the symplectite along with Omp, Di, Spl, and Pl developed at Grt rim. These facts suggest that Type 2/3 Amp were formed during the exhumation stage reacted with infiltrated fluids to the host eclogite.

The different stage origins of Type 1/2 Amp mentioned above is supported by F and Cl contents in them. Type 1 Prg contains 0.21-0.30 wt% of F, but is almost free from Cl (<0.01wt%). Type 2 Prg contains 0.43-1.17wt% of Cl. Type 2 Prg in ND0107 with Type 1 Amp contains 0.05-0.29wt% of F. On the other hand, Type 2 Prg in ND120, which is free from Type 1 Amp, is scarce in F (<0.05wt%). Type 3 Amp is free from Cl.

It is generally considered that Ca-Amp enriched in  $(Na+K)^A$ ,  $^{IV}Al$ , and  $^{VI}Fe^{2+}$  can incorporate more Cl (Makino, 2000). However, Type 1/2 Amp have a similar major element compositions such as  $(Na+K)^A = 0.79-0.95$  pfu (for  $O+OH+F+Cl=24$  basis),  $^{IV}Al = 2.01-2.45$  pfu, and  $^{VI}Fe^{2+} = 0.56-0.97$  pfu, in spite of a scarce but significant difference in Cl content among them. Cl-free Type 3 Amp contains similar amount of  $(Na+K)^A$  (0.75-0.96 pfu) and  $^{IV}Al$  (1.95-2.38 pfu), but less in  $^{VI}Fe^{2+}$  content (<0.47pfu) compared with those of Type 1/2 Amp.

As a present stage conclusion, Type 1 Amp crystallized under F-bearing and Cl-poor environment during the prograde stage, and Type 2/3 Amp crystallized during the retrograde stage along with supply of Cl from outside of the rock. F identified in Type 2 Amp in ND0107 with F-bearing Type 1 Amp could be supplied from the Type 1 Amp through the retrogressive reactions.

Keywords: Eclogite, Amphibole, Ultra-high pressure metamorphism, Bohemian Massif, Fluorine, Chlorine

## carbon and helium in faulted-seismogenic areas

SANO, Yuji<sup>1\*</sup>

<sup>1</sup>Atmosphere and Ocean Research Institute, University of Tokyo

Carbon and helium have been discharging for a long time from the Earth's mantle to the atmosphere through volcanic and hydrothermal activity. In addition they are derived from faulted-seismogenic areas. It is obvious that volcanic fluxes are originated in magma source even though they may be partly contaminated by crustal material. In contrast, it is difficult to estimate how deep they are derived in non-volcanic and tectonically active regions. Irwin & Barnes [1] reported that CO<sub>2</sub>-rich springs occur worldwide along major zones of seismicity. They further suggested that much of the CO<sub>2</sub> is derived from the mantle and that other important sources are the metamorphism of marine carbonate-bearing sedimentary rocks and the degradation of organic material. Carbon isotopes may provide information of the origin. When the delta13C value of spring gas in faulted-seismogenic area shows -6permil, it is explained by either mantle carbon or a mixing of marine carbonate (0permil) and sedimentary organic matter (-30permil). Thus it is difficult to estimate the origin of carbon. If the data are combined with helium isotopes, however, we can deconvolve the mantle contribution quantitatively [2]. There are several evidences of mantle carbon and helium degassing from active fault. Kennedy et al. [3] suggested the mantle helium flux in the San Andreas fault system located at boundary between the Pacific and North American plate. The bottom may extend the upper mantle. Significant CO<sub>2</sub> discharges were observed at the same time. A part of CO<sub>2</sub>, up to 3.3% may be derived from the mantle [4]. Similar discharges have been observed in the North and East Anatolian fault zones [5,6]. These are examples of steady-state degassing from active fault. Non steady-state, catastrophic degassing of carbon and helium were reported in the 1995 Kobe earthquake, even though they are originated in shallow crust [7,8]. On the other hand, increase of helium isotopes in bottom seawater in the trench region after the 2011 Tohoku-oki earthquake suggested substantial input of mantle helium [9]. There may be a fluid flow induced by the earthquake, which would carry helium and methane from the mantle wedge to the trench through the entire plate boundary.

Reference [1] Irwin & Barnes, 1980. *JGR* **85**, 3115-3121. [2] Sano & Marty, 1995. *Chem Geol* **119**, 265-274. [3] Kennedy et al., 1997. *Science* **278**, 1278-1281. [4] Kulongoski et al., 2013. *Chem Geol* **339**, 92-102 [5] de Leeuw et al., 2010. *App Geochem* **25**, 524-539. [6] Italiano et al., 2013. *Chem Geol* **339**, 103-114. [7] Sano et al., 1998. *Chem Geol* **150**, 171-179. [8] Famin et al., 2008. *EPSL* **265**, 487-497. [9] Sano et al., 2014. *Nature Commun* **5**, 3084.

Keywords: Helium, Carbon, Origin, Flux, Fault

## Volatiles in kimberlites:an indicator of possible deep mantle origin

KANEOKA, Ichiro<sup>1\*</sup>

<sup>1</sup>Earthquake Research Institute, University of Tokyo

Kimberlites are well known to bear diamonds and their magmas are regarded to have been derived from a depth of at least more than 150km. They are found only in old continental areas and the exposed areas at the surface are quite limited to a diameter of less than 2km in most cases. Although their distributions are quite sparse, they have quite unique characteristics in their chemical and isotope compositions.

In spite of ultrabasic properties, they bear abundant volatiles such as H<sub>2</sub>O, CO<sub>2</sub>, halogens, sulfur and they also contain relatively abundant LIL elements. On the other hand, they show more abundant concentrations of Os and Ir compared to those of other kinds of lavas such as MORBs (mid-oceanic ridge basalts) and OIBs (oceanic island basalts). Their magmas are generally regarded to have been produced in relatively less oxidized environments compared to MORBs, OIBs and IABs (island arc basalts). Hence, it is a quite significant issue to clarify the origin of volatiles in kimberlite magmas, which might be related to the chemical circumstances of deep mantle.

Based on Sr-Nd isotope systematics, kimberlites are classified in two groups (Smith, 1983). In the <sup>87</sup>Sr/<sup>86</sup>Sr-<sup>143</sup>Nd/<sup>144</sup>Nd diagram, Group I kimberlites are relatively concentrated in an area which is close to the Bulk Earth value. In contrast, Group II kimberlites are located in an area of typical enriched character and widely scattered. Most kimberlites are regarded to belong to Group I. Since Group II kimberlite magmas show the effect of recycled materials with an enriched character, volatiles in Group II kimberlites might have been also affected from them.

On the other hand, distribution of data of Group I kimberlites on the Sr-Nd isotope diagram implies that the magma source of Group I kimberlites is less fractionated from the assumed Bulk Earth material than those of MORBs. Further, Ne isotopes in kimberlites from Russia indicates that its magma source is similar to those of OIBs isotopically and different from those of MORBs (Sumino et al. 2006). Noble gas signatures of OIBs indicate the occurrence primordial components in the OIB source (e.g.Kaneoka, 2008). The magma source of MORBs has been generally assigned to be located in the upper mantle, while those of OIBs are located at a deeper part than those of MORBs. These signatures suggest that volatiles in Group I kimberlites would probably reflect those of the deep mantle. In effect, some diamonds are regarded to have been derived from the upper part of the lower mantle. Thus, at least Group I kimberlites might contain volatiles including carbon of the lower mantle origin which has not always been recycled.

Further, kimberlite magmas are conjectured to have been erupted directly from a magma reservoir located below the thick continental lithosphere within a few hours so that captured diamonds might not be decomposed during the rise of a kimberlite magma. Hence, it is inferred that chemical contamination for a kimberlite magma might be less compared to that for a OIB magma which would take much longer time to be transported to the surface from a magma reservoir. If so, Group I kimberlites might keep more primary information on the chemical state of the lower mantle compared to OIBs.

### References

- Kaneoka, I. (2008) *Geochem. J.*42, 3-20.
- Smith, C.B. (1983)*Nature*304,51-54.
- Sumino, H. et al.(2006) *Geophys. Res. Lett.*L16318.

Keywords: volatiles, kimberlite, deep mantle, OIBs, isotopes, diamond

## Carbon isotope systematics during carbonated silicate melting under upper mantle conditions

MADHUSOODHAN, Satish-kumar<sup>1\*</sup> ; MIZUTANI, Shogo<sup>2</sup> ; YOSHINO, Takashi<sup>3</sup>

<sup>1</sup>Niigata University, <sup>2</sup>Shizuoka University, <sup>3</sup>Okayama University

Carbon isotope fractionation between graphite and carbonated silicate melt was determined at 5 GPa and in the temperature range between 1400 and 1900 °C. High pressure experiments were carried out in the carbon-saturated model harzbergite system (Enstatite-Magnesite-Olivine-Graphite), where carbonated silicate melt and graphite were the two stable carbon-bearing phases in the run products. Carbonated silicate melting resulted in an isotopic fractionation between graphite and carbon in the silicate melt, where the carbon in the melt is <sup>13</sup>C enriched than co-existing graphite (Mizutani et al., 2014). <sup>13</sup>C enrichment in carbonate melt were further confirmed in experiments where redox melting between olivine and graphite produced carbonate melt as well as carbonate reduction experiments to form graphite.

According to the results of carbon isotope fractionation obtained in this study between graphite and carbonated silicate melt, heavier carbon will be selectively partitioned to the melt and graphite will be lighter than the melt in the order of 1 to 2 permil. If locally oxidative or reductive domains are present or melt extraction and a Rayleigh fractionation process dominate in the upper mantle, then carbonate silicate melt-graphite carbon isotope partitioning at upper mantle conditions will have larger effect on carbon isotopic composition. It is possible that carbonate melt will progressively enrich in carbon isotopes, which corresponds to the primary igneous carbonatite values (-5 to -8 permil) and even rare carbonatites having the more enriched <sup>13</sup>C (-2 to -5 permil) may be explainable in term of the existence of more reductive environment. Conversely, the graphite coexisting with such melts will have delta13C values corresponding to main mantle carbon reservoir. Recent experiments have shown that carbonate melts can be a medium for the efficient crystallization of diamonds in Earths mantle. Therefore, redox reaction at lower upper mantle is likely to yield the range of carbon isotope variation of mantle derived diamond. Moreover, carbonated mantle melting according to redox melting at upwelling mantle can be an alternative explanation for the formation of <sup>12</sup>C enriched diamonds in the deep mantle

Mizutani, S., Satish-Kumar, M. and Yoshino, T., (2014) Experimental determination of carbon isotope fractionation between graphite and carbonated silicate melt under upper mantle conditions, Earth and Planetary Science Letters (in press).

Keywords: carbonated mantle melting, carbon isotopes, graphite, fractionation

## **$^3\text{He}/^4\text{He}$ distributions near the Tancheng-Lujiang faults zones, at Liaoning, NE China**

ZHENG, Guodong<sup>1\*</sup> ; XU, Sheng<sup>1</sup> ; NAKAI, Shun'ichi<sup>2</sup> ; WAKITA, Hiroshi<sup>3</sup> ; WANG, Xianbin<sup>1</sup>

<sup>1</sup>Institute of Geology and Geophysics, Chinese Academy of Sciences, <sup>2</sup>Earthquake Research Institute, The University of Tokyo,

<sup>3</sup>Faculty of Science, The University of Tokyo

Chemical and isotopic compositions have been measured for natural gases near the NNE trending Tancheng-Lujiang Fault Zones (TLFZ) at Liaoning Province, NE China, including hydrocarbon-rich natural gases from Liaohe basin (121°E-124°E, 40.5°N-42°N) and nitrogen-rich geothermal gases from the eastern Liaoning Mountains. Observed  $^3\text{He}/^4\text{He}$  ratios show two orders of magnitude variability from 0.04 RA to 3.5 RA where RA is atmospheric  $^3\text{He}/^4\text{He}$  ratio  $1.4 \times 10^{-6}$ . The following geochemical observations are noted: (1) at Liaohe basin and the adjacent geothermal fields,  $^3\text{He}/^4\text{He}$  ratios show positive correlations with He contents; (2) in Liaohe basin, the  $^3\text{He}/^4\text{He}$  ratios are largely variable (0.04-3.5 RA), generally high in the eastern depress and low in the western depress; (3) in the eastern Liaoning mountains, geothermal  $^3\text{He}/^4\text{He}$  ratios are generally low (0.2-0.7 RA) but have closed relationship with distribution of seismic activity and heat flow; and (4) overall there is a spatial distribution pattern that  $^3\text{He}/^4\text{He}$  ratios gradually decrease from the TLFZ eastwards and westwards. Such a  $^3\text{He}/^4\text{He}$  distribution feature shows strong evidence that the TLFZ played an important role on mantle-derived helium transform from mantle upwards and groundwater circulation along the deep major faults.

Keywords: helium, fault, china, isotopes

## Heterogeneous carbon reservoir in sublithospheric mantle: variations of carbon isotopic composition in diamonds from Sao-

ZEDGENIZOV, Dmitriy<sup>1\*</sup>; KAGI, Hiroyuki<sup>2</sup>; SHATSKY, Vladislav<sup>3</sup>; RAGOZIN, Alexey<sup>2</sup>

<sup>1</sup>V.S.Sobolev Institute of Geology and Mineralogy, Novosibirsk, Russia, <sup>2</sup>University of Tokyo, Tokyo, Japan,, <sup>3</sup>A.V.Vinogradov Institute of Geochemistry, Irkutsk, Russia

The Juina kimberlite field in Brazil is a well-known source of alluvial sublithospheric diamonds as identified by their properties and mineral inclusions. Taking advantage of the rather common occurrence of superdeep mineral inclusion assemblages in diamonds from Sao-Luis river alluvial deposits (Juina, Brazil), we carried out a study of variations of C isotope in diamonds from this locality.

Diamonds from Sao-Luis are characterized by rough morphologies and have complex growth histories. Episodic growth, plastic deformation and breakages are visible in these crystals and most diamonds have experienced a final episode of resorption before exhumation. Total nitrogen content in studied diamonds reach 1200 ppm and more. Only several studied diamonds are nitrogen-free (type IIa). Some diamonds consist of domains that are also nitrogen-free but other parts may contain nitrogen. Many diamonds have very low (>10 ppm) but still detectable nitrogen impurity. Extremely high nitrogen aggregation state and overall platelet degradation detected in the majority diamonds from Sao-Luis are suggested they have stored at considerably higher temperatures that are typical for continental lithosphere.

Syngenetic inclusions in 59 diamonds from Sao-Luis were represented by phases of superdeep paragenesis as it was described previously. The dominated inclusions are majoritic garnets, ferropericlases, CaSi- and CaSiTi-perovskites, MgSi-perovskites, TAPP, SiO<sub>2</sub> phases, kyanites, AlSi-phases, olivines and Fe-sulfides. Rare inclusions of clinopyroxenes, KFsp (K-hollandite?), CF, NAL, grossular, native iron, magnesite, CaCO<sub>3</sub>+CaMgSi<sub>2</sub>O<sub>6</sub> (composite inclusions) have been found in separate diamonds. All majoritic garnets we found are of metabasic affinity and in some cases associated with omphacitic clinopyroxenes.

The studied diamonds from Sao-Luis display wide variations of carbon isotopic compositions ( $\delta^{13}\text{C}$ ) ranging from 2.7 to -25.3 ‰. The diamonds with inclusions of ferropericlase have very narrow range of  $\delta^{13}\text{C}$  values from -2.1 to -7.7 ‰, which are closely similar to the normal mantle values [Cartigny, 2005; Stachel et al., 2009]. From this observation, it may be suggested that their formation may proceed from isotopically homogeneous mantle reservoir that do not support the model of large primordial isotopic variability of carbon isotopes in primitive Earth's mantle with a predicted pyrolite composition. Diamonds with inclusions of majoritic garnet and CaSi- and CaSiTi-perovskites in many cases show marked differences from the expected normal mantle values of  $\delta^{13}\text{C}$  values. Low  $\delta^{13}\text{C}$  values (-10 to -25 ‰) have been observed exclusively in a series of superdeep diamonds with calcic-majorite garnets, Ca-silicates, aluminous silicates and SiO<sub>2</sub> from Sao-Luis.

The  $\delta^{13}\text{C}$  measurements in core to rim traverses within some individual crystals varied substantially, indicating multi-stage growth histories. The variations in  $\delta^{13}\text{C}$  within individual diamonds may be attributed to either different source of carbon or fractionation effect during diamond growth. No correlation of carbon isotope composition and nitrogen content has been found in individual diamonds. It therefore appears that the cores and rims of the Sao-Luis diamonds precipitated from different fluids/melts with variable N/C ratios and/or under different growth conditions. The highly negative  $\delta^{13}\text{C}$  values in the core (-20 to -25 ‰) potentially represent organic matter in sediments or altered basalts, and the lower  $\delta^{13}\text{C}$  values may represent mixing trends towards normal mantle compositions [Schulze et al., 2004; Harte, 2011]. In this study, we have also described a series of diamonds which show opposite trend of change carbon source from primordial mantle to subducted/crustal (either biotic or abiotic carbon).

Keywords: carbon, diamond, sublithospheric mantle, subduction

## Chemical composition of nano-inclusions in super-deep diamonds and implications to the growth condition

KAGI, Hiroyuki<sup>1\*</sup> ; ISHIBASHI, Hidemi<sup>2</sup> ; OHFUJI, Hiroaki<sup>3</sup> ; ZEDGENIZOV, Dmitry<sup>4</sup> ; SHATSKY, Vladislav<sup>4</sup> ; RAGOZIN, Alex<sup>4</sup>

<sup>1</sup>Graduate School of Science, University of Tokyo, <sup>2</sup>Graduate School of Science, Shizuoka University, <sup>3</sup>Geodynamic Research Center, Ehime University, <sup>4</sup>Russian Academy of Science

Superdeep diamonds originating from the mantle transition zone and the lower mantle were found from alluvial deposits of Sao-Luis river (Juina, Brazil). We investigated carbon isotopic variations and chemical compositions of nano-inclusions in the superdeep diamonds which can give a clue for the growth condition.

We found syngenetic inclusions of superdeep paragenesis from 59 diamond samples from Sao-Luis. The dominant inclusions in diamonds from studied here are CaSi-perovskite and AlSi-phases. MgSi- and CaTi-perovskites, ferropericlase, native iron, coesite and zircon have also been found. Our SIMS analysis showed the wide variations of carbon isotopic compositions ranging from 2.7 to -25.3 ‰ in  $\delta^{13}\text{C}$ . The details on the carbon isotopic analysis will be reported by Zefgenizov et al. in this session.

Some samples contained microinclusions and FTIR analyses showed that water and carbonates were not major components of these tiny inclusions. To identify the microinclusions, TEM observations were carried out on a foil of carbonado (0.1 micron thick) made from a polished diamond specimen after Au-coating. The foil was fabricated with a Ga ion beam using a focused ion beam (FIB) instrument (JEOL JEM-9310FIB). The foil was observed with a TEM (JEOL JEM-2010) under an accelerating voltage of 200 kV. We found that the microinclusions were euhedral inclusions of several tens nanometers in size. The TEM observations revealed that the nano-inclusions have a negative crystal shape suggesting the syngenetic origin directly related to the diamond growth. In this study, chemical composition of the nano-inclusions were conducted by synchrotron X-ray fluorescence analysis using X-ray micro-beam as an incident light at BL-4A, Photon Factory, KEK. The obtained results clarified that the nano-inclusions contain S, Cr, Mn, Fe, Co, Ni, Cu Zn, and so on. The present study suggests that the growth media of the superdeep diamonds are composed of sulfide melt.

Keywords: diamond, nano inclusion, X-ray fluorescence analysis, super deep diamonds

## High-pressure melting experiments on magma genesis in Hawaiian plume: effect of volatiles

GAO, Shan<sup>1\*</sup>; TAKAHASHI, Eiichi<sup>1</sup>; IMAI, Takamasa<sup>1</sup>; SUZUKI, Toshihiro<sup>1</sup>

<sup>1</sup>Earth and Planetary Sciences, Tokyo Institute of Technology

**Introduction:** Compared with OIB, Hawaiian tholeiitic basalt is thought to be relatively drier (about 0.5 wt.% H<sub>2</sub>O content; Muenow, 1979). In front of the plume core, overlying mantle is metasomatized by hydrous partial melts derived from the Hawaiian plume. Downstream from the plume core, lavas tap a depleted source region similar to enriched Pacific mid-ocean ridge basalt (Dixon & Clague, 2001). Magma genesis model has been proposed by some authors (Hauri, 1996; Takahashi & Nakajima; 2002; Sobolev et al., 2007) that magma produced near the axis of the plume head may be mixtures of two types of melts 1) basaltic andesite melt formed by melting of eclogite and 2) picritic melts formed by the reactive melting of eclogite and peridotite. A series of high temperature high pressure experiments were conducted to explore the genesis of tholeiitic magma from Hawaiian plume and investigate the role of volatiles in magma genesis.

**Experiments:** A series of experiments were conducted under dry and slightly hydrous conditions at 2.85GPa for 1, 3 to 9 hours and from 1460 to 1520C with a piston cylinder by making basalt peridotite sandwich which using MgO-rich CRB72-180 (Takahashi et al 1998) and a fertile peridotite KLB-1 (Takahashi 1986) as starting materials.

**Results:** Three factors that might affect melting progress and chemical reaction among minerals – temperature, duration and water content – were examined, respectively.

1) Temperature: (1460~1520C and every 20C as an interval.)

Basalt went partial molten at 1460C and completely molten when temperature went above 1500C. Orthopyroxene reaction rim formed on the border area due to the reaction between high Si-rich melt and olivine in the peridotite matrix. The opx film becomes more visible and thicker with the increasing of temperature. Partial melting degree of peridotite is also related to the increasing of temperature but the change is not very sensitive when 20C as an interval. The higher temperature, the more peridotite molten. The area of the peridotite near the opx film has a higher degree of partially melting than areas away from the boundary.

2) Duration: (1, 3 and 9 hours.)

Longer time do accelerate the speed of chemical reaction between basalt and peridotite in this study. Basalt molten completely as the running time longer than 3 hours. The orthopyroxene reaction rim on the boundary between peridotite and basalt becomes thicker. Large clinopyroxene crystals formed on the border (the minerals on the border from melt to peridotite are cpx, opx, garnet) momentarily yet faded away as the chemical reaction went on with time. Partial melting of peridotite is also positively related to duration. When the melt of peridotite is too much and unable to support the weight of basalt and it would get rid of the crack and finally went to the basalt side and mixed with the basalt melt.

3) Water content

Basalt layer melted completely, and large orthopyroxene crystallized in the basalt side. Peridotite layer also melted considerably at the same time than its anhydrous counterparts owing to the reason that the join of water could lower the peridotite liquidus line and finally made it more partial melted than in hydrous condition.

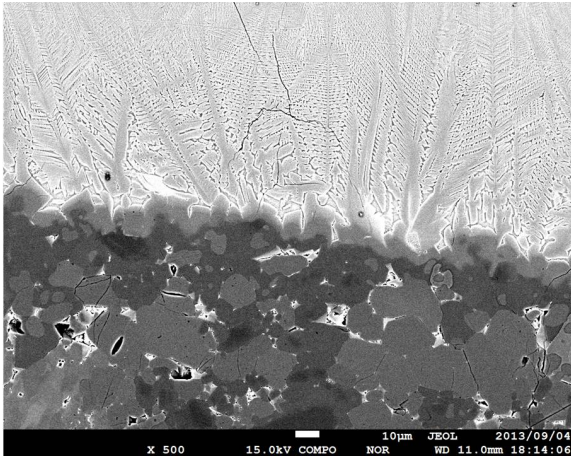
**Discussion:** Under dry conditions below peridotite solidus, melting is limited in eclogite layers and chemical reactions with ambient peridotite is hindered by opx film. On the other hand, under slightly wet conditions, water could accelerate the melting process of both eclogite and peridotite layer. As a result, melts formed under wet conditions are saturated with oliv+opx whereas those formed under dry conditions could be saturated with only opx. Changing nature of Hawaiian magma during the shield building stage will be discussed in the light of present melting experiments.

**Keywords:** Hawaiian plume, high-pressure, magma, volatiles

SCG09-07

Room:315

Time:April 28 15:06-15:21



## Partitioning of carbon between metallic- and silicate-liquids in magma ocean of differentiated planetesimals

ASAHARA, Yuki<sup>1\*</sup> ; OHTANI, Eiji<sup>1</sup>

<sup>1</sup>Tohoku University

Partitioning behavior of carbon has not been determined well though it is one of the strong candidates for light element in the earth's core. We investigated partitioning of carbon with sulfur and oxygen between metallic- and silicate liquids at 6 GPa and 2073 K in carbonaceous chondrite composition (Allende meteorite; CV3). High pressure experiments were conducted with multi-anvil high pressure apparatus. Graphite was used as capsule material. Composition of coexisting metallic- and silicate liquids were measured by electron microprobe with wavelength dispersion type spectrometer except for carbon in silicate liquid. To estimate carbon concentration in silicate liquid, carbon concentration of bulk recovered sample was measured by elemental analyzer. Present result suggests that in oxidized carbonaceous chondrite composition, partitioning coefficient of carbon [ $D_{\text{Metallicliquid/Silicateliquid}} = C_{\text{Metallicliquid}} / C_{\text{Silicateliquid}}$ ;  $C$  is concentration of carbon in wt.%] is close to 1, and it increases with increasing the  $\text{Fe}^{\text{metal}}/\text{Fe}^{\text{oxide}}$  ratio of the bulk carbonaceous chondrite composition.

## Experimental study of Group-I kimberlite: evidences for carbonatite primary melt and implication to mantle plumes

LITASOV, Konstantin<sup>1\*</sup> ; SHARYGIN, Igor<sup>2</sup> ; SHATSKIY, Anton<sup>2</sup> ; OHTANI, Eiji<sup>3</sup>

<sup>1</sup>Novosibirsk State University, Novosibirsk, Russia, <sup>2</sup>V.S. Sobolev Institute of Geology and Mineralogy SB RAS, Novosibirsk, Russia, <sup>3</sup>Department of Earth and Planetary Materials Science, Tohoku University, Sendai, Japan

The experiments on the origin of Udachnaya-East kimberlite (UEK) have been performed using a Kawai-type multianvil apparatus at 2-6.5 GPa and 900-1500 °C. The studied composition represented exceptionally fresh Group-I kimberlite containing (wt.%): SiO<sub>2</sub> = 25.9, TiO<sub>2</sub> = 1.8, Al<sub>2</sub>O<sub>3</sub> = 2.8, FeO = 9.0, MgO = 30.1, CaO = 12.7, Na<sub>2</sub>O = 3.4, K<sub>2</sub>O = 1.3, P<sub>2</sub>O<sub>5</sub> = 1.0, Cl = 0.9, CO<sub>2</sub> = 9.9, and H<sub>2</sub>O = 0.5. Super-solidus assemblage consists of olivine (Ol), Ca-rich garnet (Gt), Al-spinel (Sp), perovskite (Pv), CaCO<sub>3</sub> (calcite or aragonite), and apatite at 4-6.5 GPa with an addition of clinopyroxene at 3-4 GPa and Na-Ca carbonate with molar ratio of (Na+K)/Ca ~ 0.44 at 6.5 GPa and 900 °C. The apparent solidus was established between 900 and 1000 °C at 6.5 GPa. In the studied P-T range, melt has Ca-carbonatite composition (Ca/(Ca+Mg) = 0.6-0.8) with high alkali and Cl contents (2.8-6.7 wt.% K<sub>2</sub>O, 7.3-11.6 wt.% Na<sub>2</sub>O, 1.2-3.7 wt.% Cl). The K, Na and Cl contents and Ca/(Ca+Mg) value decrease with temperature. It is argued, that the primary kimberlite melt at depth >200 km was essentially carbonatitic (<5 wt.% SiO<sub>2</sub>), however, evolved toward carbonate-silicate composition (with 15-20 wt.% SiO<sub>2</sub>) during ascent. The absence of orthopyroxene among the run products indicates that xenogenic orthopyroxene was preferentially dissolved into kimberlite melt. The obtained subliquidus phase assemblage (Ol + Gt + Sp + Pv) at P-T condition of UEK source region differs from lherzolite lithology of this source. Both petrological observations and experiments indicate that kimberlite magma lost substantial amount of CO<sub>2</sub> at shallow depths.

Our study combined with earlier experiments on carbonate-silicate systems at pressures to 30 GPa implies that liquid phase of thermo-chemical plume generated at the core-mantle boundary is represented by alkali-carbonatite melt. This conclusion has broad geodynamic implication providing insight into fluid regime of mantle melting under hotspots along margins of African large low-shear-wave-velocity province. We conclude that the long term activity of rising hot mantle plume and associated carbonatite melt (i.e. proto-kimberlite melt) causes thermo-mechanical erosion of the subcontinental lithosphere mantle (SCLM) roots and creates hot, oxidized, and deformed metasomatic layer at lower parts of initially depleted SCLM, which corresponds to depths constrained from the sheared Gt-lherzolites. The sheared Gt-lherzolites undoubtedly represent the samples from this layer.

Keywords: mantle, kimberlite, carbonatite, plume, melting

## Gas geochemistry and soil CO<sub>2</sub> flux in active volcanic areas, China

WEN, Hsinyi<sup>1\*</sup>; YANG, Tsanyao frank<sup>1</sup>; GUO, Zhengfu<sup>2</sup>; FU, Chingchou<sup>1</sup>; CHEN, Aiti<sup>1</sup>; ZHANG, Maoliang<sup>2</sup>

<sup>1</sup>Department of Geosciences, National Taiwan University, <sup>2</sup>Institute of Geology and Geophysics, Chinese Academy of Sciences

Changbaishan intra-plate volcano and Tengchong hydrothermal area are two of the active volcanic areas in China. In order to better understand current status of magma/hydrothermal activities of the Changbaishan intra-plate volcano and Tengchong hydrothermal area, we have conducted the soil gas survey and bubbling gas sampling from hot springs around the Tianchi crater lake and Rehai geothermal area.

In Changbaishan volcano, the results show that CO<sub>2</sub> is the major component gas for most samples. The maximum value of helium isotopic ratio of 5.8 R<sub>A</sub> (where R<sub>A</sub> = <sup>3</sup>He/<sup>4</sup>He in air) implies more than 60% of helium is contributed by mantle component, while carbon isotope values fall in the range of -5.8 to -2.0 ‰ (vs. PDB), indicating magmatic source signatures as well. Nitrogen dominated samples, 18Dawgo, have helium isotopic ratio of 0.7 R<sub>A</sub> and carbon isotope value of -11.4 ‰, implying the gas source might be associated with regional crustal components beneath 18Dawgo. The first-time systematic soil CO<sub>2</sub> flux measurements indicate the flux is ca. 22.8 g m<sup>-2</sup> day<sup>-1</sup> and 6.8 g m<sup>-2</sup> day<sup>-1</sup> at the western and southern flank of Changbaishan, which is at the same level as the background value in the Tatun Volcano Group (24.6 g m<sup>-2</sup> day<sup>-1</sup>), implying that Changbaishan may not be as active as TVG.

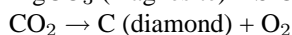
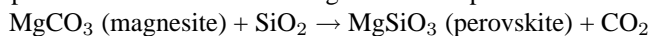
In Tengchong hydrothermal area, the preliminary results show that CO<sub>2</sub> is the major component gas for most samples. The helium and carbon isotopic ratio fall in the range of 0.5 R<sub>A</sub> to 3.5 R<sub>A</sub> and -4.7 to -1.6 ‰ (vs. PDB), respectively. We also analyzed the hot springs water. The δD and δ<sup>18</sup>O values fall in the range from -59.8 to 84.6 ‰ and -6.20 to -12.38 ‰ (vs. SMOW), respectively. Rehai has the highest helium isotopic ratio of 3.5 R<sub>A</sub>, which implies ca. 40% of helium is mantle-derived. The δD and δ<sup>18</sup>O results implied the water in this area was affected by primary magmatic water. Nevertheless, samples from Banglazhang and Shihchiang hydrothermal areas show much lower helium isotopic ratio of 0.8 R<sub>A</sub> and 0.5 R<sub>A</sub>, respectively. It suggests that the local tectonic setting plays an important role for the gas degassing in this area.

## The reaction between $\text{MgCO}_3$ and $\text{SiO}_2$ at high pressure and temperature and genesis of ultra-deep diamonds

MAEDA, Fumiya<sup>1\*</sup> ; OHTANI, Eiji<sup>1</sup> ; KAMADA, Seiji<sup>1</sup> ; SAKAMAKI, Tatsuya<sup>1</sup> ; TAKAHASHI, Suguru<sup>1</sup> ; TAKAHATA, Akihiro<sup>1</sup> ; OHISHI, Yasuo<sup>2</sup> ; HIRAO, Naohisa<sup>2</sup>

<sup>1</sup>Department of Earth and Planetary Materials Science, Graduate School of Science, Tohoku University, <sup>2</sup>Japan Synchrotron Radiation Research Institute

Carbon, one of the important light elements for the Earth science, is reserved in the deep part of the Earth. The evidence of the deep carbon is found in ultra-deep diamonds or estimations of carbon fluxes between the surface and interior of the Earth. Subducting slabs are considered as an important C-source of the Earth. Following reactions of  $\text{MgCO}_3$  and  $\text{SiO}_2$  are potentially important in the slabs descending into the deep mantle:



These reactions can play a fundamental role in the deep carbon cycle.

In this work, we investigated the reaction between  $\text{MgCO}_3$  and  $\text{SiO}_2$  up to about 80 GPa and 3000 K using a laser-heated diamond anvil cell combined with in-situ synchrotron X-ray diffraction (XRD) technique and Raman spectroscopy. The starting material is the powered 1:1 (in mole fraction) mixture of natural magnesite (Brazil, Bahia) and reagent  $\alpha$ -quartz. 5 wt.% platinum powder was added to the sample mixture in order to absorb laser and estimate the pressure in the sample chamber. NaCl, KCl or  $\text{SiO}_2$  glass powder was stuffed into the sample chamber as pressure media. XRD patterns of high P-T samples and recovered samples were acquired at beamline BL10XU of SPring-8. Raman spectroscopy was carried out to high-pressure conditions. Raman spectroscopy was also conducted for the recovered samples.

In the present results made at about 70 GPa, diamond and  $\text{MgSiO}_3$  perovskite are detected at temperatures greater than 1750 K. The high P-T XRD patterns in the experiments at 50-60 GPa and 2000-3000 K show the appearance of a small amount of  $\text{MgSiO}_3$  perovskite. Our study demonstrated that formation of diamonds was confirmed in the range of 1300-1500 km depth of the lower mantle in subducting slabs due to the reaction of  $\text{MgCO}_3$  with  $\text{SiO}_2$  and the breakdown of  $\text{CO}_2$ . This phase relations have a possibility to explain one of the origins of diamonds from the lower mantle.

## Microcracks preceding ruptures: insights gained from laboratory acoustic emission study

LEI, Xinglin<sup>1\*</sup>

<sup>1</sup>Geological Survey of Japan, AIST, Japan

Earthquakes in the crust are caused by the rapid shear fracture of a fault. Thus, understanding the source processes of earthquakes relies on the understanding of shear fracturing in rocks. Abundant experimental evidence shows that macroscopic shear fracturing within rocks and other brittle materials does not occur by the growth of a single shear crack in its own plane. Rather, it is preceded by a very complex pervasive evolution of some pre-failure damage. Therefore, studies focusing on both fracture dynamics and pre-failure damage are a subject of interest in seismology. Fracturing dynamics and the pre-failure damage can be inferred from AE statistics as the number of AE events is proportional to the number of growing cracks, and the AE amplitudes are proportional to the length of crack growth increments in the rock. Therefore, the AE technique, which monitors the spatiotemporal distribution of AE events, is applied to the analysis of the micro-cracking activity inside the sample space, and it can be performed under an artificially controlled pressure, which is very important for the simulation of underground conditions.

The fracture of intact rocks as well as rocks containing natural structures (joints, faults, foliations) under constant stress rate loading or creep conditions is generally characterized by typical stages with different underlying physics. Through an integrated analysis of several AE statistics obtained from AE data collected with the high-speed AE waveform recording system, a three-phase pre-failure-damage model has been proposed and further enforced with new data. The primary phase reflects the initial rupture of pre-existing microcrack population in the sample or in the fault zone. Sub-critical growth dominates the secondary phase. The third phases termed nucleation phase corresponds to the initiation and accelerated growth of the ultimate fracture. In earthquake seismology, researchers have a special interest with the nucleation phase since faulting nucleation governs the predictability of earthquakes.

Lithology, density and size distribution of pre-existing cracks, meso-scale and macro-scale heterogeneities all have an overall role in AEs. There are some cases in which some phases are not clear. In general, homogeneous (both fine-grained and coarse-grained) rocks with pre-existing cracks likely show all phases. Heterogeneous or weak rocks such S-C cataclasite normally show a lack of the primary phase. Samples with few pre-existing cracks and samples containing optimally oriented weak structures, likely show an unpredictable fracturing behaviour as well as a lack of primary and secondary phases, in addition the nucleation phase has a small number of AEs.

Rules obtained at the laboratory scale are helpful for understanding natural earthquakes on a significantly larger scale. However, we cannot simply bridge laboratory scale to a scale several orders larger. At every step up from a smaller scale to a larger scale, we encountered something different. The difference could be small for each step but, after many steps, we could see something quite different. Studies on all scales are important. Quantitative investigation of rock fracture using AE techniques is still an interesting field for the future. On one hand, it may shed some light on earthquake seismology. On the other hand, it may provide a fundamental technical background promoting applications including: enhanced geothermal systems (EGS), extraction of shale gas and core bed gas, and CO<sub>2</sub> geological storage. The latter of which involves fluids being intensively pumped into the deep Earth under high pressure; injection-induced earthquakes would be a problem that must be well-addressed.

Keywords: Acoustic emission (AE), Microfracture, Pre-failure damage, Fault nucleation

## Radio wave emission in friction or collision of various materials

TAKANO, Tadashi<sup>1\*</sup>; HANAWA, Rikuya<sup>1</sup>; SAEGUSA, Saegusa<sup>1</sup>

<sup>1</sup>Nihon University

### 1. Introduction

In fracture of rock, radio wave emission was found experimentally [1]. This phenomenon could be used to detect a rock fracture during an earthquake or a volcanic activity [2] [3]. The cause of the radio wave is expected to be micro-discharges, which are generated by an inhomogeneous potential distribution around micro-cracks [4]. However, the theory of emission is not completely understood yet.

In order to clarify the cause of radio wave emission, we carried out experiments to detect the emission in the cases of friction or collision of various materials. This paper describes the experimental results, and a brief explanation of physical process.

### 2. Tested systems and experimental results

We tested the following systems using the manufactured measuring system at 1 MHz, 300 MHz, 2.0 GHz, and 18.8 GHz [5].

#### (1) A lighter using piezoelectricity

This device makes sparkles by knocking a mineral with piezoelectricity. Due to discharges, strong radio wave is emitted, and detected in our measuring system.

#### (2) A lighter using friction of OL metal

Formerly, this type of a lighter was widely used for igniting cigarettes. The alloy metal of cerium and iron rubs a revolving drum so that sparkles are made changing the friction power to thermal energy. Despite significant sparkles, radio wave could not be detected in this case.

#### (3) Igniter using a flint stone

A flint stone is struck against iron pyrites so that small flakes of iron are scattered being made hot. The flint stone is mostly chert in Europe, and quartz, sanukite, or obsidian in Japan. Sparkles cannot be made by striking two bulks of flint each other. Radio wave is not emitted in this case.

#### (4) Striking a steel lump with a steel hammer

Radio wave is emitted in this case. Probably, the kinetic energy is converted not to thermal energy but to the excitation of electrons or atoms so that inhomogeneous potential distribution is realized.

### 3. Conclusions

In general, sparks are not the origin of radio wave emission. This emission is esteemed a non-thermal phenomenon. An inhomogeneous potential distribution makes micro-discharges that emit radio waves. In some cases, the cause of an inhomogeneous potential distribution makes the sparks.

Further study is needed to clarify the mechanism of the energy transfer to electron excitation.

### References

- [1] Ken-ichiro Maki, Tadashi Takano, Eriko Soma, Kentaro Ishii, Shingo Yoshida and Masao Nakatani, "An experimental study of microwave emission from compression failure of rocks" (in Japanese), Jour. of the Seismological Society of Japan, vol.58, no.4, pp.375-384, 2006.
- [2] Tadashi Takano, Takashi Maeda and Shingo Yoshida, "Experiment and Theoretical Study of Earthquake Detection Capability by Means of Microwave Passive Sensors on a Satellite", IEEE Trans. Geoscience And Remote Sensing, Vol.6, No.1, pp.107-111, 2009.
- [3] T. Maeda and T. Takano, "Discrimination of Local and Faint Changes from Satellite-borne Microwave Radiometer Data", IEEE Trans. on Geoscience and Remote Sensing, vol 46, issue 9, pp. 2684-2691, 2008.
- [4] K. Maki and T. Takano, "Analysis of the microwave radiation field from the discharge due to an impact destruction", National Convention of the Institute of Electrical Engineers of Japan (IEEJ), 1-081, p.87, March 2004.
- [5] T. Takano, J. Kato, M. Hirashima and K. Saegusa, "Radio wave emission from 1 MHz to 18 GHz due to rock fracture and the estimation of the emitted energy", EEIS'12, 978-1-4673-0335-4/12/IEEE, pp.300-303, Cape Town, September 2012.

Keywords: radio wave, friction or collision, various materials, electrical discharge, micro-crack, non-thermal phenomenon

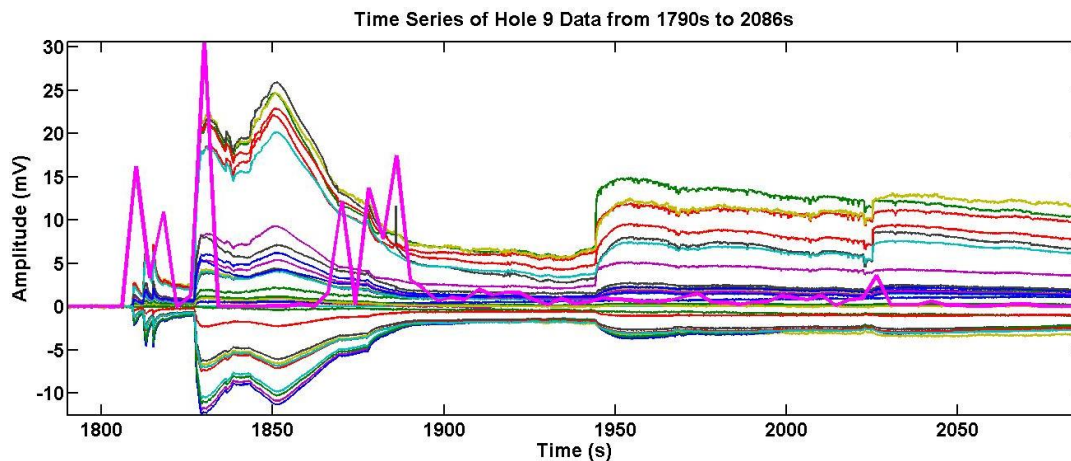
## Seismoelectric phenomena of electrokinetic nature associated with the formation of cracks in porous media

REVIL, Andre<sup>1\*</sup>

<sup>1</sup>Colorado School of Mines, department of Geophysics

I will describe the physics of the generation of electromagnetic disturbances associated with the formation of cracks in porous media. The mechanism is electrokinetic in nature (i.e., associated with the flow of the pore water with respect to the solid phase of a porous material). I will describe the occurrence of these electromagnetic signals and how they can be inverted jointly with seismic signals to determine the position of the hydromechanical disturbance and its moment tensor. I will also demonstrate that electrical fields of electrokinetic nature are associated with the formation of crack through a set of laboratory experiments (see figure below showing the fluctuation in the electrical potential on the surface of the block and the amount of recorded acoustic emissions). The associated electrical field fluctuations can be remotely monitored and the resulting signals used to localize their causative source. The technique is similar to what is performed in electroencephalography (in the medical world) in which an electrical field (associated with the opening of ionic channels at the synapses between the neurons) can be measured on the scalp of a patient and inverted to localize and monitor brain activity. A laboratory experiment shows how these electrical fields can be recorded at the surface of a cement block during the fracking of the block. The measurements are performed with a research-grade medical electroencephalograph and inverted using the genetic algorithm to localize the causative source of electrical current and therefore localize the evolution of the crack. Two snapshots of electrical signals are used to show how the breakage evolves over time. A second experiment is performed to see if we could localize a pulse water injection from a shallow well in field conditions and in the case of a heterogeneous subsurface.

Keywords: electrokinetic, streaming current, self-potential, moment tensor, source localization, electromagnetic phenomena



## Waveform analysis of seismo-magnetic signals in Boso, Japan

HAN, Peng<sup>1\*</sup> ; HATTORI, Katsumi<sup>1</sup> ; FEBTY, Febriani<sup>1</sup> ; HIROKI, Yamaguchi<sup>1</sup> ; CHIE, Yoshino<sup>1</sup>

<sup>1</sup>Graduate School of Science, Chiba University

To clarify the seismo-magnetic phenomena, it is essential to establish theoretical models to explain how the phenomena come out. A reliable model should coincide with field observations. Thus, the fundamental part is to find out what are the signals associated with earthquakes. Therefore, in this study we have checked detailed waveform of seismo-magnetic signals observed in Boso, Japan. Our preliminary results indicate that there are mainly two kinds of seismo-magnetic signals: one is noise-like signals; the other is transient/quasi-rectangular signals. The former are mainly detected before the 2005 M6.1 Boso earthquake; the latter is observed mainly during slow slip events.

Keywords: ULF seismo-magnetic phenomena, waveform analysis, slow slip events

## Quantitative evidence of the coupling between seismic and electromagnetic signals

HUANG, Qinghua<sup>1\*</sup>

<sup>1</sup>Peking University

There are some reports of the coupling between seismic and electromagnetic signals from both the natural earthquakes and the active field experiments. Such coupling effect may provide some useful information of earthquake process and/or oil exploration. Although the coupling mechanisms are not well understood at the current stage, there are some candidate mechanisms, such as the electrokinetic effect and piezoelectric effect. We focused this study on seismic and electromagnetic coupling for the data observed during earthquakes or synthesized from our numerical simulation method based on electrokinetic effect and earthquake models. We presented a quantitative analysis method of the correlation between seismic and electromagnetic signals. As an example of the field data, we investigated the data recorded during the Ms5.7 Ningqiang earthquake, China. The results indicated that there is a clear coupling between seismic and electromagnetic signals. As a further example of the synthetic data of seismic and electromagnetic signals, we obtained the synthetic seismic and electromagnetic signals using our numerical simulation method and confirmed the existence of coupling between the seismic and electromagnetic signals in the synthetic data.

This study is supported by the National Natural Science Foundation of China (41025014, 41274075).

Keywords: Co-seismic electromagnetic signals, Rupture model, Source time function, Electrokinetic effect

## The Development of self-potential tomography to estimate the ground water condition

OTSUBO, Hiroshi<sup>1</sup> ; HATTORI, Katsumi<sup>1</sup> ; YMAZAKI, Tomohiro<sup>1\*</sup>

<sup>1</sup>Graduate school of science, Chiba University

Landslides are one of the most severe natural disasters in the world and there are two types; rainfall induced landslides and landslides triggered by an earthquake. In this research, basic study on early warning system for landslides will be performed to understand rainfall-induced landslide process by hydrological and electromagnetic changes. The final goal of this research is to develop a simple technology for landslide monitoring/forecasting using self potential method. The advantages of this method are lower cost and easier to set up than the hydrological approaches using pore pressure sensors. The laboratory experiments show that the self-potential variation has relationship with the water and soil displacements. But, we can not estimate the ground water condition by self-potential yet. So, in this study, we developed self-potential tomography to estimate the ground water condition.

Measured self-potential value under the ground and charge distribution to estimate is given by the Coulomb's law. Therefore, this is inverse problem. To solve the inverse problem, we adapt Phillips-Tikhonov regularization with Generalized Cross Validation (GCV). To evaluate the reconstructed charge distribution and investigate the relationship with the ground water condition, computational simulations and applications to practical data by using the sandbox experiment has been examined.

It is found that the developed algorithm is effective through numerical simulations. Results of application to sandbox experiments show good performance but there are some problems to solve.

The details will be given in our presentation.

Keywords: landslide, self-potential

## Induced seismicity due to fluid injection at a deep well in Youngstown, Ohio, USA

KIM, Won-young<sup>1\*</sup>

<sup>1</sup>Lamont-Doherty Earth Observatory, Columbia University, <sup>2</sup>Earthquake Research Institute, University of Tokyo

Over 100 small earthquakes (Mw 0.4-3.9) were detected during January 2011- February 2012 in the Youngstown, Ohio, USA area, where there were no known earthquakes in the past. These shocks were apparently close to a deep fluid injection well, and hence, were immediately suspected as induced by the fluid injection. This 14-months seismicity included a half-dozen felt earthquakes and culminated with a Mw 3.9 shock on 31 December 2011, about 24 hours after the fluid injection ceased in the deep well in Youngstown. Among the 109 shocks, 12 events greater than Mw 1.8 were detected by regional network, whereas 97 small earthquakes ( $0.4 < Mw < 1.8$ ) were only detected by using the waveform correlation detector.

Among these shocks, 21 earthquakes were accurately located by using the local portable station data. All of the accurately located earthquakes were distributed along a set of subsurface faults striking N265 (due East-west) and dipping steeply to the north – consistent with the focal mechanism of Mw 3.9 mainshock on 31 December 2011. All of the well-located earthquakes have occurred at depths ranging from 3.5 to 4.0 km in the Precambrian crystalline basement.

We conclude that the recent earthquakes which occurred during 2011 - 2012 in Youngstown, Ohio were indeed induced by the waste fluid injection at a deep injection well due to increased pore pressure along the preexisting East-west trending faults located close to the wellbore in the Precambrian basement. We found that the earthquakes are located along a 1.2 km-long, East-west trending subsurface en echelon fault, and that the seismicity initiated at the eastern end of the subsurface fault – close to the injection point, and migrated toward the west – away from the wellbore, indicating that the expanding high fluid pressure front increased the pore pressure along its East-west trending path and progressively triggered the earthquakes. Further, we observe that the occurrence of these earthquakes is generally correlated to the total daily injection volume and that several sharp peaks in the daily injection volume correlate with the occurrence of earthquakes. We observed that several periods of quiescence of seismicity follow gaps in surface injection volumes and pressure (sudden drops in injection pressure followed by prolonged low pressure), which may indicate that the earthquakes were directly caused by the pressure buildup in the fractured Precambrian basement and stopped when pressure dropped. Geohydrologic properties of the Youngstown, Ohio area behaved as a fractured Precambrian rock similar to the Rocky Mountain Arsenal, Colorado, USA site of induced earthquakes during 1960s.

Keywords: Induced seismicity, Fluid pore pressure, Shale gas extraction, Space and time migration of earthquakes

## Characteristics of Microcracks in the Nucleation Stage of Natural Earthquake

FUJINAWA, Yukio<sup>1\*</sup>; NODA, Yoichi<sup>2</sup>; TAKAHASHI, Kozo<sup>3</sup>

<sup>1</sup>MierukaBosai Inc., <sup>2</sup>Tierra Tecnica Ltd., <sup>3</sup>(former) Communication Research Laboratory

At the last JpGU meeting we reported that a deep underground electric field measurement using special antenna could detect micro-cracks appearing in the nucleation stage of the Tohoku Earthquake (Fujinawa et al., 2013). Here we report several results of further analysis on the characteristic pulse-like phenomena.

### 1) Detection Distance:

Some events of B-type variation have clear first and second phases (Figure 1). The S-P time is 25ms corresponding to about 180m of the epicentral distance. Majority of events have no apparent P phases due to the small strength of the P phase and/or large dissipation. The detection distance of P phase is about 200m. On the other hand the S phase of the frequency of some 100Hz and amplitude of 2mV suggests detection distance of some 10km, much larger than that of the acoustic emission signal of order several hundred meters by elastic observation.

The characteristic electric field variation induced by crack through electro-kinetic mechanism have been discussed by systematic formulations ( Pride, 1994; Revil and Leroy, 2004). As to the wave mode, there are four kinds of wave, slow P and fast P wave (ordinary p wave), S-wave (ordinary S wave) and electromagnetic wave (EM). Events containing P phase have occasionally small forerunners at about the origin time possibly corresponding to (see Fig.1).

### 2) Correspondence to main shock:

The seismological approaches (e.g., Kato et al., 2012) showed that there were two slow seismic slip events from mid-February to the Tohoku Earthquake and microearthquake activities around the foreshocks and mainshocks. Those activities were whole around the epicentral zone, about 300 km northeast from the observation site. The detection distance of the electric field change by the borehole antenna is at most 100 kilometer. Our observational evidence including temporal evolution of the microcrack activity and b value of 0.7 suggest that the micro-cracks of B-type are related to the nucleation process of the main shock, though they occurred at the edge of the giant rupture area. We propose that the nucleation process is not limited at around the asperity, but extends to whole rupture zone. More extensive monitoring of the microcrack of magnitude less than -5 can provide clue to this question.

### 3) Intermittent Criticality

There appeared undulation of microcrack activity after the most active period around 9th March, 2011. The undulation has been suggested to reflect the intermittent criticality indicating another phase of nucleation (Sornette and Sammis, 1995; Kapiris et al., 2005). As approaching to the main shock there appeared two kinds of events. One kind is a superposition of several smaller events. It is interpreted that small events substantially increased with the result of picking up more smaller events in the time interval of data length of 100ms. The second kind is like a long chain of small events. These feature suggest that microcrack activity has changed at the last stage of nucleation stage.

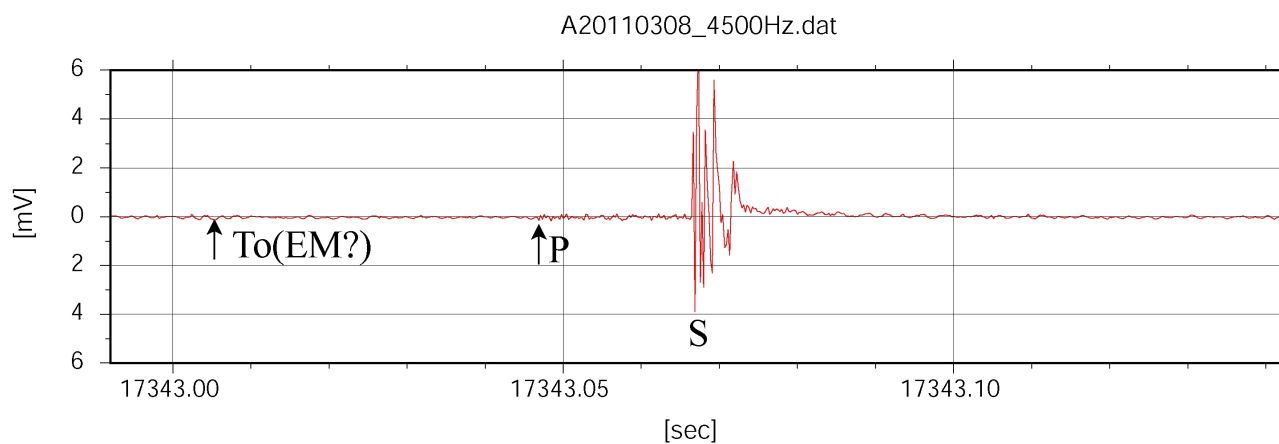
4) It is well known that the crust of the earth is elastic-porous medium filled with fluid as water. The research on the rupture of such kind of medium had a remarkable development in early 1990 contributing to interpret the mysterious seismo-electric phenomena associated earthquakes enabling systematic treatment and suggesting new method of geophysical prospecting. The formulation of Pride and Revil have been used to interpret the phase of faster propagation of EM signal with velocity much larger than the p-wave speed (Fujinawa et al., 2011), the ULF band anomalies associated the slow-slip (Han, 2013). And, our electromagnetic method has been suggested to detect micro-cracks preceding natural earthquakes to identify the nucleation stage providing a break-through for the short term prediction method. The converted electromagnetic mode at the material contrast from elastic seismic wave has been proved to be profitable means to survey for oil and gas.

Keywords: Microcrack, Earthquake Prediction, Nucleation Stage, Seismo-electric- signal, Electrokinetic effect, Tohoku Earthquake

SCG10-08

Room:313

Time:May 2 11:30-11:45



## Electromagnetic emissions from fracture of semiconductor pyrite

OZAWA, Mitsuyuki<sup>1\*</sup> ; MUTO, Jun<sup>1</sup> ; NAGAHAMA, Hiroyuki<sup>1</sup> ; NAGASE, Toshiro<sup>2</sup>

<sup>1</sup>Department of Geoenvironmental Sciences, Graduate School of Science, Tohoku University, <sup>2</sup>The Tohoku University Museum

### Introduction

When elastic waves propagate in orebodies composed of semiconductor minerals, electromagnetic (EM) radiation with radio frequency occurs. Its frequencies were 10-100 times higher than those of the elastic waves. They were observed by geophysical exploration surveys and laboratory experiments. These previous studies suggested that generation of radio waves is closely related to the rectifying property of orebodies which is attributed to semiconductor minerals. Semiconductor minerals are divided into p- or n-type conductivity by its charge carrier. When p- and n-type are joined, the resulting junction (p-n junction) has the rectifying property. Because many p-n junctions of semiconductor minerals exist as which connect in parallel and in series in the orebody, they also show rectifying property. Previous research measured only large scale rectifying property of orebody to understand the generation mechanism of radio wave. However, due to the lack of the measurement of rectifying properties of each micro p-n junction in semiconductor minerals, quantities evaluation was difficult.

Composition of semiconductor minerals is heterogeneous due to the presence of impurities and lattice defects. Because rectifying property depends crucially on the composition, clarifying the composition at each micro region is needed. In this research, we measured the composition and rectifying property of semiconductor pyrite to discuss the possibility of EM emission from the ore bodies.

### Methods

Semiconductor pyrite sample was obtained from Waga-Sennin mine, Akita prefecture, Japan. It was cut into slabs with a thickness of about 0.38 cm and an area of 1.4 cm<sup>2</sup>.

We obtained composition of the sample surface by electroetching method and SEM-EDS. Thermal probing method allowed us to discriminate between p- and n-type conductivity. By electrical probing, we quantified the rectifying properties.

### Results

After the electrolytic etching, heterogeneity of composition in the sample surface was emerged as the difference in solubility. The difference of solubility caused etching figure and zonal structures. Thermal probe method revealed that the differences of p-n type regions corresponded to the difference in solubility of each region. P-types regions showed a higher solubility than n-type regions. According to the SEM-EDS analysis, about 1.0 wt.% of Pb inclusions were precipitated parallel to crystallographic planes in the p-type regions.

In the electrical probing method, rectifying effects were observed at p-n junctions. We obtained the current and voltage characteristic of p-n junction. The reverse and forward breakdown voltages were estimated to be 1.5 V and 0.3 V, respectively.

### Discussion and conclusion

When two types of rocks make contact, electrons move between the surfaces of rocks, producing the potential difference between them. This electrification becomes a possible source of EM radiations during separating rocks. If we regard p- and n-type semiconductor minerals as the two types of rocks, the contact potential is given by the forward breakdown voltage of p-n junction. When the junction is split into two pieces, separated surface can be regarded as capacitance plates. If the surface charge density of plates reaches the Paschen's minimum charge density of breakdown (e.g. air  $5.0 \times 10^{-5}$  C/m<sup>2</sup>), corona discharge occurs. We estimated the charge density of separated plates at p-n junction to be  $2.7 \times 10^{-4}$  C/m<sup>2</sup>. Given the effect of charge relaxation, we must take into account separation velocity of plates. In this case the critical separation velocity to cause corona discharge is estimated to be 2.0 km/s. Therefore, it is expected that the pyrite fractured by propagation speed higher than 2.0 km/s can cause corona discharge.

In conclusion, the fracturing of pyrite becomes a possible source of EM radiations. Further investigation is needed to clarify the properties (e.g. frequency) of EM radiations from the orebodies.

Keywords: Seismic electromagnetic signals, Semiconductor minerals, Radio wave, P-n junction

## Pulsed granitic crust formation revealed by comprehensive SHRIMP zircon dating of the SW Japan granitoids

TANI, Kenichiro<sup>1\*</sup> ; HORIE, Kenji<sup>2</sup> ; DUNKLEY, Daniel<sup>3</sup> ; ISHIHARA, Shunso<sup>4</sup>

<sup>1</sup>Japan Agency for Marine-Earth Science and Technology, <sup>2</sup>National Institute of Polar Research, <sup>3</sup>Curtin University, <sup>4</sup>Geological Survey of Japan/AIST

The origin of continental crust is a fundamental question in Earth's evolution. Granitoids, its volcanic equivalents, and metamorphic and sedimentary rocks with granitic compositions, are the main components of the upper continental crust. It is therefore important to understand the geodynamic settings in which juvenile granitic magma is generated from mantle-derived sources. Convergent plate margins, such as the Mesozoic circum-Pacific orogenic belts, are regarded as one of the plausible candidates for the post-Archean continental crust formation, as they are associated with abundant calc-alkaline I-type batholiths. However, the fundamental tectonic processes that triggered these voluminous granitic crust formations in the Mesozoic have remained largely unresolved due to the lack of precise temporal constraints on the granitic magmatism. We are currently undertaking a comprehensive geochronological study of the granitic batholith exposed in the Southwest Japan Arc, which is typical of the Mesozoic circum-Pacific orogenic belts utilizing high-precision zircon U/Pb geochronology.

In order to precisely determine the space-time distribution of the granitic magmatism that occurred in the SW Japan Arc during the Mesozoic, we have used the zircon U/Pb method to date a comprehensive suite of granitic rocks from the Chugoku Region in the SW Japan. Contrary to the results previously obtained using conventional geochronological methods, which suggested that the magmatism occurred gradually from ~100 to ~50 Ma, with the plutons forming over long time intervals, the newly obtained zircon ages reveal three clear pulses of granitic crust formation at 85, 60 and 35 Ma separated by 25 million year intervals. The 85 Ma magmatism was the most voluminous and was distributed in a broad zone that extends ~120 km across-strike, whereas the magmatism at 60 and 35 Ma were focused on the northern margin of the SW Japan Arc. Furthermore, the granitic magmatism at 85 Ma involved sediment-incorporated, ilmenite series granitic rocks, while the magmatism at 60 and 35 Ma involved more juvenile, mantle-derived, magnetite series rocks. Thus, not only did the granitic magmatism in SW Japan occur in pulses, there was also a spatial and compositional transition in the magmatism through time. This can be best explained by enhanced subduction zone magmatism during the Mesozoic, rather than the previously proposed model in which it was suggested that the granitic crust was formed by the subduction of a mid-ocean ridge on the Pacific Plate during the Middle Cretaceous.

## Petrology and zircon geochronology of the Hikami Granitic Rocks in south Kitakami Mountains, Japan

SASAKI, Jun<sup>1\*</sup> ; TSUCHIYA, Nobutaka<sup>1</sup> ; ADACHI, Tatsuro<sup>2</sup> ; NAKANO, Nobuhiko<sup>2</sup> ; OSANAI, Yasuhito<sup>2</sup> ; ADACHI, Yoshiko<sup>3</sup>

<sup>1</sup>IwateUniversity, <sup>2</sup>KyushuUniversity, <sup>3</sup>NiigataUniversity

The Hikami Granites, pre-Cretaceous older granitic complex of the South Kitakami Terrane, has long been controversial on their age of intrusion. Since unconformable relationship between the granites and the Silurian formation was shown by Murata et al. (1974). However CHIME age determination for the granites (Adachi et al., 1994), indicates Silurian to Permian age. We examined the zircon U-Pb ages of 13 samples from the Hikami Granitic Rocks, and solidification age of around 450 Ma were obtained.

Bulk rock chemical compositions of the Hikami granites were compared with Paleozoic granitic rocks in Japan. Petrochemical similarity between Hikami Granitic Rocks and the granitic rocks in the Kurosegawa Belt is consistent with the correlation between the South Kitakami and Kurosegawa Belts.

Keywords: Hikami Granites, zircon, U-Pb age, Petrochemistry

## Sr-Nd-Pb-Hf isotopic variations of Cretaceous to Paleogene granitic rocks from northeast Japan

TSUCHIYA, Nobutaka<sup>1\*</sup> ; KAGASHIMA, Shin-ichi<sup>2</sup> ; HIRAHARA, Yuka<sup>3</sup> ; TAKAHASHI, Toshiro<sup>3</sup> ; SENDA, Ryoko<sup>3</sup> ; CHANG, Qing<sup>3</sup> ; KIMURA, Jun-ichi<sup>3</sup>

<sup>1</sup>Iwate University, <sup>2</sup>Yamagata University, <sup>3</sup>JAMSTEC

The Japanese Islands represent a segment of a 500 Ma old subduction related orogen developed along the western Pacific convergent margin, and most tectonic units are composed of late Paleozoic to Cenozoic accretionary complexes and their high P/T metamorphic equivalents (e.g., Maruyama, 1997; Isozaki et al., 2010). Maruyama (1997) described the formation of the Japanese Islands has been taken as the standard model for an accretionary orogeny. He also stated that the most important cause of the orogeny is the subduction of an oceanic ridge, by which the continental mass increases through the transfer of granitic melt from the subducting oceanic crust to the orogenic belt. On the other hand, Jahn (2010) described that the subduction-accretion complexes consisting of granitic and sedimentary rocks in southwest Japan are composed mainly of recycled old continental crust. Kagami et al. (1999) described that the Honshu Arc can be divided into three groups based on their Sr-Nd isotope characteristics: the Kitakami, North (Abukuma belt), and South (Ashio/Mino belts) Zones, in order of increasing Sr isotopic enrichment, with Nd isotopic depletion from NE to SW. We present Sr-Nd-Pb-Hf isotopic ratios for granitic rocks in northeast Japan.

Sr-Nd-Pb-Hf isotopic study are made for granitic rocks from the Kitakami belts (Kitakami Mountains), the Abukuma belts (Shirakami Mountains, Obonai area, Taihei Mountain, Sekiryō Mountains, and Abukuma Mountains), and the Ashio/Mino belts (Okutone area, Tadami area, Okutadami area, Taisyaku Mountains, and Ashio Mountains). Newly isotopic data from these granitic rocks show increasing enrichment of crustal component in order of the Kitakami, Abukuma, and Ashio/Mino belts. Multi-isotope plots of these rocks indicate that the trend in variation could result from the mixing of depleted and enriched components. The depleted component is likely to originate from the magmatic flux related to the Lower Cretaceous ridge subduction. On the other hand, the mixing model of subducted sediments and depleted mantle cannot explain the variation of Nd-Hf isotopic compositions of granitic rocks. The enriched component requires existence of a reservoir with low Hf initial isotope ratio, which is considered to be zircon-rich sediment derived from old continental protolith (Chauvel et al., 2008). In addition, the granitic rocks in Kitakami zone shows rather different trend from the granitic rocks in other districts. It can be explained by the hypothesis that the granitic rocks in the Kitakami zone were derived from the mixing of mantle component with enriched end member of lower Hf initial isotope ratio. This model is consistent with the fact that the Kitakami zone is characterized by the occurrence of adakitic rocks related to Lower Cretaceous ridge subduction.

Keywords: Northeast Japan, granite, Sr-Nd-Pb-Hf isotope, petrochemistry

## Garnet-bearing acidic igneous bodies in Mt. Kenashi-yama area, Fujikawaguchiko-machi, Yamanashi, Japan

NAGAHATA, Hiromi<sup>1\*</sup> ; ISHII, Teruaki<sup>2</sup>

<sup>1</sup>Graduate school, Open University of Japan, <sup>2</sup>Fukada Geological Institute

**Introduction** The garnet-bearing quartz porphyrite body in Mt. Kenashi-yama area Fujikawaguchiko-machi, Yamanashi, Prefecture was described by Katada (1956). On the other hand, there are many reports on garnet-bearing boulders in this area (Togawa et al., 1996; Togawa et al., 1997; Matsubara et al., 2008; Tamura et al., 2010).

On the detailed field works, we recognized three groups of garnet-bearing acidic igneous bodies in this area.

**Geology** The studied area is in the northern end of Izu-Bonin Arc, and is located east side of Misaka group, middle to late Miocene.

**Lithology** Three garnet-bearing acidic igneous bodies are recognized, which are named A, B and C groups.

[A group (lava flow(?))] This group exists in 1,100m to 1,200m above sea level, and is located from WSW to ENE over 2km long. The rock consists of quartz (10%-20%, md : maximum diameter = 5mm), feldspar (10%-25%, md = 4mm), garnet (1%, md = 3mm) and groundmass(60%-65%). The rock of A group shows high dense appearance.

[B group (volcanic ash(?))] This group exists at 1,200m, and this group may be exist along above the A group. This group can be assumed as garnet-bearing volcanic ash, because this group contains volcanic glasses (at under microscope) and rock fragments (If B group is not volcanic ash, this group may be the weathered zoon of A group). The B group consists of quartz (10%, md = 5mm), garnet (1%, md = 3mm) and clay matter 80%.

[C group (dike)] This group exists in 1,300m to 1,400m, and is located from WSW to ENE, over 3km long. The rock is little fragile, and consist of quartz (3%-20%, md = 4mm), feldspar (3%-20%, md = 3mm), garnet (0.1%, md = 3mm), hornblende (1%, maximum length = 9mm) and groundmass (65%-85%).

**Chemical analysis** Representative samples of each groups are analyzed by X-ray fluorescent analysis on 10 major elements. The SiO<sub>2</sub> contents of three groups are 72wt%-76wt%. It mean that these rocks are classified into rhyolite according to alkali-SiO<sub>2</sub> diagram (Le Bas, et al., 1986). There are slightly high in Na<sub>2</sub>O, and slightly low P<sub>2</sub>O<sub>5</sub> than Tanzawa Hosokawadani rhyolite (Yamashita, 1997).

**Discussion and Consideration** It can be assumed that three groups of garnet bearing acidic igneous bodies are recognized in Mt. Kenashi-yama area. They are located along WSW-ENE direction 2-3km long. A, B and C groups are possibly lava flow, volcanic ash and intrusive rock, respectively. All of them may be classified into garnet-bearing rhyolite.

Keywords: garnet, quartz, feldspar, rhyolite, Mt. Kenashi-yama, Fujikawaguchiko-machi

## Two types of websterite from the Ust'-Belaya ophiolite, Far East Russia: Origins and implications

MACHI, Sumiaki<sup>1\*</sup> ; ISHIWATARI, Akira<sup>2</sup> ; MORISHITA, Tomoaki<sup>1</sup> ; HAYASAKA, Yasutaka<sup>3</sup> ; ARAI, Shoji<sup>1</sup> ; TAMURA, Akihiro<sup>1</sup>

<sup>1</sup>Natural Sci & Tec., Kanazawa Univ., <sup>2</sup>NE Asia Center, Tohoku Univ., <sup>3</sup>Earth & Planet. Sys. Sci., Hiroshima Univ.

The Ust'-Belaya ophiolite is located in the Koryak Mountains, Far East Russia. We report two types of websterite in the mantle section of the ophiolite.

The lithology of the mantle peridotites from the ophiolite is variable from very fertile lherzolite to moderately depleted harzburgite. The mineral chemistry of the very fertile lherzolite shows similar signature to those of the subcontinental peridotite. The two types of websterite (type1 and type2) occur in them as dikes/veins. Type1 is composed of brownish colored cpx, opx and Al-spinel. On the other hand, type2 is composed of green colored cpx, opx and Cr-spinel.

Type2 websterite is similar to those reported from many other ophiolites. Websterites, which are characterized by extremely aluminous spinel similar to the type1 websterite, are never found in ophiolitic peridotites but are described in passive margin peridotites (e.g. Zabargad Island in Red Sea and Iberia Abyssal plain peridotites). These websterites are generally interpreted as high-pressure cumulates and the host peridotites are considered as fragments of subcontinental mantle.

The mantle section of the Ust'-Belaya ophiolite represents, at least partly, fragments of subcontinental mantle. The two types of websterite might be related to two different magmatisms in two different tectonic settings; type1 is formed former subcontinental to oceanic environment and then type2 is formed later oceanic to arc environment.

Keywords: Ust'-Belaya ophiolite, websterite, subcontinental mantle

## Field geological considerations on the formation mechanism of platy joints in lava flows

SATO, Kei<sup>1\*</sup> ; ISHIWATARI, Akira<sup>2</sup>

<sup>1</sup>Grad. School Sci., Tohoku Univ., <sup>2</sup>CNEAS, Tohoku Univ.

Columnar jointing and platy jointing are characteristic types of jointing in volcanic rocks. The origin of columnar joints has been discussed for centuries, and at the present day it is considered that they are the result of cooling and contraction of lava (Aydin and DeGraff, 1988). However, platy joints have far less attracted researchers than columnar joints and their formation mechanism is still controversial. Platy joints can develop in thick (>100 m) and voluminous lava flows which have glassy margins such as "flood andesite" in Kyushu, Japan (Nagao et al., 1995) and ridge-forming lava flows at Mount Rainier (Lescinsky and Sisson, 1998), probably reflecting stress distribution or physical property within solidifying lava. Previous studies attributed formation of platy joints (sheeting joints) to late stage shear of lava flow and/or microlite orientation (Lescinsky and Fink, 2000), deflation of flow (Spörl and Rowland, 2006) or both flowage and shrinkage of lava (Bonnichsen and Kauffman, 1987). Although absolute evidence for the origin of platy jointing has not been found, restraining of internal lava by solidified flow margin would be an important factor in any case and density (volume ratio of crystals to glass) difference between flow margin and interior would be also important when we consider thermal contraction. It is also a problem when platy joints form, especially in the case that columnar and platy joints intersect without terminating each other. Occasionally platy joints are filled with tridymite and/or mica mineral with or without andesitic to dacitic melt, which might be segregated from the crystallizing lava body, suggesting that platy joints start to form at early stage of cooling of lava.

### References:

- Aydin and DeGraff, 1988, *Science*, 239, 471-476.
- Bonnichsen and Kauffman, 1987, *GSA Special Papers*, 212, 119-145.
- Lescinsky and Fink, 2000, *J. Geophys. Res.*, 105, 23711-23726.
- Lescinsky and Sisson, 1998, *Geology*, 26, 351-354.
- Nagao et al., 1995, *Mem. Geol. Soc. Japan*, 44, 155-164 (in Japanese with English abstract).
- Spörl and Rowland, 2006, *J. Volcanol. Geotherm. Res.*, 157, 294-310.

Keywords: platy joints, flood andesite, internal flowage, thermal contraction, segregation vein

## Oxidation states of Fe within constituent minerals in spinel-lherzolite xenolith from Tariat Depression, Mongolia: Signif

EJIMA, Terumi<sup>1\*</sup>; OSANAI, Yasuhito<sup>2</sup>; OHFUJI, Hiroaki<sup>3</sup>

<sup>1</sup>National Institute of Advanced Industrial Science and Technology, <sup>2</sup>Kyushu Univ., <sup>3</sup>Ehime Univ.

The Tariat depression is one of the most famous areas of deep-seated megacrystic xenoliths and mantle-derived xenoliths in the Baikal-Mongolia rift. Spinel-garnet-bearing websterite, garnet lherzolite and spinel lherzolite have been found in this area (Osanai et al. 2010). In this study, oxidation state of Fe in olivine (Ol), orthopyroxene, clinopyroxene and spinel in fresh spinel-lherzolite xenolith, and olivine in host basalt in Tariat depression were investigated using Mossbauer spectroscopy, X-ray FeL $\alpha$ /FeL $\beta$ -intensity ratio analysis (EPMA method) and transmission electron microscopy (TEM).

Olivine, clinopyroxene, orthopyroxene and spinel have homogeneous chemical compositions. Olivine is forsterite with average composition of Fo<sub>90</sub>Fa<sub>10</sub>, Clinopyroxene is Na-bearing diopside [(Na<sub>0.17</sub>Ca<sub>0.71</sub>Mg<sub>0.81</sub>Fe<sub>0.09</sub>Al<sub>0.20</sub>)<sub>2</sub>O<sub>0</sub>(Si<sub>1.89</sub>Al<sub>0.11</sub>)<sub>2</sub>O<sub>6</sub>], and have symplektite consisting of diopside and glass on the rim with the width of ~50  $\mu$ m. The chemical composition of the glass is similar to that of feldspar with compositions of An. Orthopyroxene is [(Mg<sub>0.85</sub>Fe<sub>0.09</sub>Al<sub>0.04</sub>Ca<sub>0.02</sub>)(Si<sub>0.94</sub>Al<sub>0.06</sub>)O<sub>3</sub>]. Spinel is [(Mg<sub>0.81</sub>Fe<sub>2+0.22</sub>)<sub>1.03</sub>(Al<sub>1.80</sub>Cr<sub>0.17</sub>)<sub>1.97</sub>O<sub>4</sub>].

The Fe<sup>2+</sup>: Fe<sup>3+</sup> ratios of forsterite, orthopyroxene, clinopyroxene and spinel determined by Mossbauer analysis are 97(1):3(1); 85(8):15(1); 74(4):26(3); 66(8):34(5), respectively. Fe<sup>3+</sup> in olivine is not attributed to any precipitates nor minute inclusions, which was confirmed by TEM observation, and, thus, exists in olivine structure. Fe of olivine phenocrysts from host basalt lava is only Fe<sup>2+</sup> which was proved by EPMA method.

Fe<sup>3+</sup>-bearing forsterite in spinel-lherzolite xenolith is considered to have been stable under mantle condition.

Keywords: olivine, oxidation state of Fe, spinel-lherzolite xenolith, Mossbauer methods, Mongolia

## Al/Si disordered anorthite in anorthite megacryst from Miyake-jima: effect of non-stoichiometry on Al/Si distribution

ECHIGO, Takuya<sup>1\*</sup>; HOSHINO, Mihoko<sup>2</sup>; KIMATA, Mitsuyoshi<sup>3</sup>; SHIMIZU, Masahiro<sup>3</sup>; MATSUI, Tomoaki<sup>4</sup>; NISHIDA, Norimasa<sup>5</sup>

<sup>1</sup>Faculty of Education, Shiga University, <sup>2</sup>Mineral Resources Research Group, AIST, <sup>3</sup>Earth Evolution Sciences, University of Tsukuba, <sup>4</sup>Faculty of Education, Kagoshima University, <sup>5</sup>Research Facility Center for Science and Technology, University of Tsukuba

The crystal chemistry of anorthite with the low content of albite (An<sub>92.0</sub>Ab<sub>3.4</sub>), part of a rapid cooled, anorthite megacryst occurring in 1940 ejecta from Miyake-jima volcano, Japan, has been investigated using single-crystal X-ray diffractometer and electron microprobe analyzer with wavelength dispersive X-ray spectroscopy (EMPA-WDS). The structure was refined in space group P-1 and cell parameters,  $a = 8.182(6) \text{ \AA}$ ,  $b = 12.883(4) \text{ \AA}$ ,  $c = 7.092(4) \text{ \AA}$ ,  $\alpha = 93.19(4)^\circ$ ,  $\beta = 115.91(4)^\circ$ ,  $\gamma = 91.18(4)^\circ$ . The final weighted R-factor is 3.77 % for 1549 reflections. Averaged T-O distances are 1.681  $\text{\AA}$  for T1(0), 1.674  $\text{\AA}$  for T1(m), 1.677  $\text{\AA}$  for T2(0) and 1.680  $\text{\AA}$  for T2(m), indicating each Al occupancy of 0.501, 0.453, 0.472, and 0.496, respectively. These results suggest that the Al/Si-distribution in the tetrahedral framework is highly disordered (QOD = 0.06), which results in having the c-axis in half along that determined in Al/Si ordered anorthites ( $c \sim 14 \text{ \AA}$ ).

Keywords: Anorthite, Al/Si order-disorder, Anorthite megacryst, Structural heterogeneity

## Formation temperature of perlite and its texture by heating experiments of obsidians from Hokkaido

IKEYAUCHI, Ryo<sup>1</sup> ; WADA, Keiji<sup>1\*</sup> ; SAITO, Takeaki<sup>1</sup>

<sup>1</sup>Hokkaido University of Education at Asahikawa

The obsidians from Hokkaido were heated in electric furnaces to transform the perlite in a form like pumice in vitreosity, because remained water in obsidians becomes the gas and makes air bubbles by heating.

We examined foaming temperature of the obsidians from 13 samples in 7 Hokkaido sources, and the relations with its foaming temperature and the water content of the obsidians. In addition, we changed a heating temperature and a condition of the heating time and examined the difference in foaming form of the perlite.

Finally, we considered a relations with foaming process of the obsidians and the internal structure of the perlite through the microscopy of the perlite.

Keywords: obsidian, heating experiment, perlite, vesiculation, glass

## Estimation of intracrystalline distribution coefficient of Mg-Fe ions in olivine using Cs-corrected STEM

MIYAKE, Akira<sup>1\*</sup> ; TOH, Shoichi<sup>2</sup> ; FUKUNAGA, Keiichi<sup>3</sup> ; KURIBAYASHI, Takahiro<sup>4</sup>

<sup>1</sup>Kyoto Univ., Sci., <sup>2</sup>Fukuoka Univ., Sci., <sup>3</sup>JFCC, <sup>4</sup>Tohoku Univ., Sci.

Intracrystalline distribution coefficient of Mg-Fe ions between the two types of the octahedral sites (M1, M2-site) of olivine,  $(\text{Mg,Fe})_2\text{SiO}_4$ , have been estimated using X-ray or neutron diffraction studies. Recently, the high angle annular dark field (HAADF) method using scanning transmission electron microscopy with the correction of spherical aberration (Cs-corrected STEM) visualizes the element column sites in crystalline samples. In the present study, the intracrystalline distribution coefficient of Mg-Fe ions in olivine were tried to estimate using HAADF-STEM. And furthermore, Crystal Structure Analysis of same sample was carried out using a four-circle X-ray diffractometer. We used the synthetic forsterite and the natural olivine from San Carlos, Sri Lanka and Miyake-jima. HAADF-STEM images parallel to a-axis show the Mg / Fe atom columns and the columns which alternately formed of Si and O atoms. Intracrystalline distribution coefficients estimated from the brightness in M1/M2-sites for synthetic forsterite, the olivines from San Carlos and SriLanka are good agreement with those estimated from X-ray method. On the other hand, that obtained from Miyake-jima is different with that obtained from X-ray method.

Keywords: STEM, olivine, intracrystalline distribution coefficient

## A Novel Approach for the Classification of Mineral Ore Particles by A Statistical Raman Spectroscopic Method

SASAKURA, Daisuke<sup>1\*</sup> ; HAYAUCHI, Aiko<sup>1</sup>

<sup>1</sup>Malvern Instruments Division of Spectris Japan

### [Introduction]

Mineral ores extracted by mining go through a milling process before ore dressing. An important factor in both milling and ore dressing operations is the determination of the particle size distribution of the materials being processed, commonly referred to as particle size analysis. An elemental analysis technique such as X-Ray fluorescence and destructive wet chemical analysis can determine the quantity of mineral species present in the ore, however, these chemical analysis methods do not allow the study of the composition of individual particles of different size and shape. The statistical Raman spectroscopic method is a novel approach which can resolve this problem. Using this method the Raman spectra of several hundred particles is determined after size and shape classification of each individual particle by automated particle image analysis. Raman spectroscopy can be used to acquire the spectra of any inorganic compounds such as metal oxides and nitrides which are Raman active. Many mineral resources are mined as inorganic compounds. Therefore, Raman spectroscopy can be used for the identification of the chemical composition of mineral ores. Using the statistical Raman spectroscopic method described herein, it is possible to calculate the particle size distribution and proportion by mass or volume of each chemical component or mineral species based on Raman spectroscopic information. This study will report and discuss the capability of the statistical Raman spectroscopic method using iron ore as a model material.

### [Material and Method]

Iron ore samples were purchased from a vendor. These samples had been through the ore dressing process. Statistical Raman analysis was carried out using a Morphologi G3SE-ID instrument (Malvern Instruments, UK) equipped with a dry powder sample dispersion unit (SDU) and Raman module. The laser wavelength of Raman excitation was 785nm the laser power was less than 5mW and the irradiation time was 5 sec. The particle image measurements were made in diascopic mode with a total magnification 250x. Iron ore dry powder samples were dispersed using the SDU using a short duration pulse of compressed air. Measurements were made automatically using Standard Operating Procedures (SOPs) which define the software and hardware settings used. Measurement sample was dispersed on to glass plate as sample carrier which was minimized environmental exposure by the enclosed sample chamber unit. Particle identification by Raman analysis used the spectrum correlation coefficient approach.

### [Results and Discussion]

A Total of 66,436 particles of iron ore were measured by image analysis. The circle equivalent diameter particle size distribution by volume (VCED) exhibited a monomodal distribution with size distribution percentiles as follows: 8.62 $\mu$ m (d10), 21.83 $\mu$ m (d50), 51.29 $\mu$ m (d90). A subset of 700 particles were selected and the Raman spectra were measured. Particles over 20 micron in size were selected randomly from the image analysis data and Raman spectra were acquired. The spectra enabled identification of 4 components (Fig.1). The relative proportion of each component by volume or number of particles is shown in Table 1. Component (A) comprised approximately 90% of the sample. This component exhibited a Raman spectrum typical of  $\alpha$ -Fe<sub>2</sub>O<sub>3</sub> [1]. It is assumed that components (B) and (C) are polymorphs based on the ratio of the intensities at 221cm<sup>-1</sup> and 245cm<sup>-1</sup>. Component (D) exhibited a spectrum typical of  $\alpha$ -FeOOH and composed less than 3% of the sample. This result does show that the statistical Raman analysis approach can detect components present at quite low concentrations.

### [Summary]

This report illustrated the application and capability of statistical Raman analysis for the characterization of mineral ores using a new approach based on combining chemical and particle size / shape information.

SCG61-11

Room:311

Time:May 2 11:45-12:00

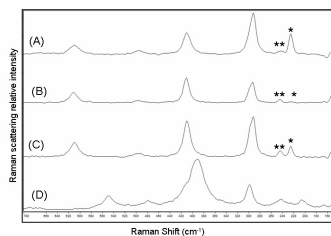


Fig 1. Raman Spectrums of iron ore.  
 (\* : 221cm<sup>-1</sup>, \*\* : 245cm<sup>-1</sup>)

Table 1.  
 Ratio of each component based on Raman spectrum

Component	Number (%)	Volume(%)
A	87.6	90.2
B	2.5	2.1
C	7.2	6.3
D	2.7	1.4

## Assessment of Nakhile porphyry Cu mineralization potential using geological, geochemical and statistical studies: a case

BOOMERI, Mohammad<sup>1\*</sup> ; NAKASHIMA, Kazuo<sup>2</sup> ; F, Yavari<sup>1</sup>

<sup>1</sup>Univ. of Sistan and Baluchestan, <sup>2</sup>Yamagata Univ.

The Nakhile Cu mineralization is located in 145 km northwest of Zahedan in Sistan and Baluchestan province of Iran. This area is geologically located in boundary part of Lut block and flysch zone of east Iran. Geology of the study area consists of Cretaceous to Eocene andesitic lavas and tuffs that were intruded by a dioritic to quartz-dioritic stock. The intrusive rocks are mainly altered and mineralized. Based on the petrography and XRD studies, main mineral in all types of the igneous rocks is plagioclase and the main texture is porphyry. Other minerals are clinopyroxene, amphibole, biotite, quartz, and secondary minerals that vary in the igneous rocks. A large part of the intrusive rocks is rich in pyrite. The pyrite occurs as veins, veinlets and disseminated in the stock. Cu mineralization occurs as vein and can be divided into hypogene and supergene mineralization. Hypogene mineralization is characterized by chalcopyrite and pyrite while supergene mineralization is characterized by malachite, azurite, jarosite, goethite, hematite and limonite. The propylitic alteration is dominant feature of the intrusive rocks as a wide outer zone. Potassic, phyllic and argillic alterations are also important in the area. The potassic alteration is probably important in the center part of the stock in depth. phyllic and argillic alterations are mainly formed by supergene processes.

The samples that were collected from the least altered and altered rocks in the study area were analyzed by ICP were processed by convenient software such as EXCEL and SPSS to obtain statistic parameters of: skewness, maximum, minimum and standard deviation. Then, the histograms for the amount of Cu, Au and related elements were drawn and their correlation coefficients were calculated. There are remarkable positive correlations between Cu, Au and Ag indicating their similar origin. The highest content of Cu is 7000 ppm in the study samples. The Cu anomalies are mainly observed in central and eastern parts of the area. The highest content of Au is 6000 ppb. The Au anomalies are mainly observed in western parts of the area. The higher contents of Pb, Zn and Ag are observed more away from the intrusive rocks.

The outcrops in the area are mainly similar as propylitic alteration zone of porphyry Cu deposits that is characterized by secondary hydrothermal epidote and chlorite and pyrite. The Cu porphyry mineralization and other alteration zones specially potassic probably occur in depth in the area.

## A leucogranite stock rich in high field strength elements, Kanamaru-Oguni area on the Niigata-Yamagata border, NE Japan

KAMEI, Atsushi<sup>1\*</sup> ; NAITO, Kazuki<sup>2</sup> ; TAKAMURA, Sayaka<sup>3</sup> ; KAGASHIMA, Shin-ichi<sup>4</sup> ; OKUZAWA, Koichi<sup>5</sup> ; SEKI, Yoji<sup>6</sup> ; WATANABE, Yoshio<sup>2</sup>

<sup>1</sup>Department of Geoscience, Shimane University, <sup>2</sup>Geological Survey of Japan/ AIST, <sup>3</sup>Ricoh Japan Corporation, <sup>4</sup>Department of Earth and Environmental Sciences, Yamagata University, <sup>5</sup>Technical Research Institute, Obayashi Corporation, <sup>6</sup>Faculty of Science and Technology, Tokyo University of Science

A small stock of leucocratic Grt-two mica granite enriched in high field strength elements (HFSEs) has recently been found in the Kanamaru-Oguni district of the Asahi-Iide mountains in the Ashio Belt of the NE Japan arc. The granite has a high-K peraluminous composition, and is categorized as an A-type within-plate granitoid, according to several geochemical discriminants based on HFSEs. However, total Zr+Nb+Ce+Y contents are lower (166-192 ppm) and Rb/Ba ratios are higher (19-48) than those typical of A-type granitoids ( $Zr+Nb+Ce+Y > 350$ ,  $Rb/Ba < 10$ ). This suggests that this stock is in fact a highly fractionated granite, rather than an A-type intrusive. The stock solidified at shallow depth (about 3 - 6 km) from a silicic granitic magma, under moderately water-rich conditions. Geochemical modeling shows that the petrogenesis of the granite can be explained by partial melting of crustal rocks, leaving abundant plagioclase as a residual phase, with subsequent active fractional crystallization of plagioclase + alkali-feldspar. Many other small stocks composed of Grt-two mica granite occur in the Asahi and Iide mountains. The granitic activity ranges from Late Cretaceous (ca 90 Ma) to Paleogene in age. Although most of these stocks were derived from melting of various crustal rocks, some are highly differentiated, and have HFSE concentrations similar to the Kanamaru-Oguni stock studied here.

HFSE-rich granitoids also occur sporadically within the other Japanese geological units, but they are restricted in the southwestern Japan. The granitoids in the Inner and Outer Zones of SW Japan differ in composition. The HFSE-rich granitoids in the Inner Zone originated from middle to lower crustal materials, and were then strongly differentiated before emplacement. This is similar genesis to the granite in the Kanamaru-Oguni district. In contrast, the solitary HFSE-rich granitoid in the Outer Zone crops out at Cape Ashizuri. This occurrence is the only classic A-type intrusion in Japan, and is considered to have formed by a low degree of partial melting of the upper mantle or mafic lower crust. Although the HFSE-rich granitoids within the SW Japan arc may be similar geochemically to within-plate or ocean-ridge granites, they are in fact volcanic arc granites produced within the subduction zone by specific activities.

Keywords: Granite, HFS elements, Niigata-Yamagata, NE Japan

## Rare earth element compositions of the Kitahata body in the Fukae granite, northern part of Kyushu

KAWANO, Yoshinobu<sup>1\*</sup>

<sup>1</sup>Department of Environment Systems, Faculty of Geo-environmental Science, Rissho University

Cretaceous granitic rocks are widely distributed in northern part of Kyushu (Karakida, 1985), and Fukae granite is located in Kitahata district, Karatsu city, Saga Prefecture. The Fukae granite in this area (hereinafter, Kitahata body) consists of granite, aplite and felsic inclusion. The felsic inclusion is an oval figure about 50 cm in diameter, and is gradually changing from the surrounding granite. Main constituent minerals of the Kitahata body are quartz, k-feldspar, plagioclase and biotite, with apatite, zircon, opaque minerals as accessories. K-Ar biotite age of the body is 95.8 $\pm$ 2.4 Ma (Kitahata village history compilation committee, 2008). Rare earth element compositions are analyzed about ten samples, for comparison with estimated result of Kawano (2013).

In chondrite normalized REE patterns, values of LREE of the Kitahata body are the highest, and, aplite and felsic inclusion are lower than them. Normalized La/Lu ratios of the Kitahata body are also higher than those of the aplite and the felsic inclusion. Although the negative abnormalities of Eu are not observed in the Kitahata body and the felsic inclusion, it is clearly observed in the aplite. That is, Eu/Eu\* ratio of the aplite is low and the Kitahata body and the felsic inclusion show a similar value. SiO<sub>2</sub> contents increase from the Kitahata body to the felsic inclusion and the aplite. The values of LREE and La/Lu ratio of the felsic inclusion and the aplite which are rich in SiO<sub>2</sub> are lower than those of the Kitahata body, and it is suggested that they have the different origin from the Kitahata body. Although aluminum saturation index of the Kitahata body is larger than 1.0, it of the felsic inclusion is less than 0.9 and shows the character of meta-aluminous. The origin of the felsic inclusion not be considered to be a sedimentary rock, but it may originate in different felsic magma.

Keywords: Kyushu, Fukae granite, Kitahata, rare earth element

## Petrographic and geochemical studies of granitoids from the Inbi intrusives, Inner Zone of Southwest Japan

SATO, Kei<sup>1\*</sup>; KAMEI, Atsushi<sup>2</sup>; MINAMI, Masayo<sup>1</sup>; ASAHARA, Yoshihiro<sup>3</sup>; KATO, Takenori<sup>1</sup>

<sup>1</sup>Center for Chronological Research, Nagoya University, <sup>2</sup>Department of Geoscience, Shimane University, <sup>3</sup>Department of Earth and Planetary Sciences, Nagoya University

We report a data set of whole rock compositions of seven granitoids from the early Paleogene Inbi intrusives and a granitoid from the mid Paleogene Namariyama intrusives, Inner Zone of Southwest Japan. The Inner Zone where voluminous granitic plutons occur is subdivided from the north to the south into three areas in terms of mineralogical and petrological characteristics of granitoids: the San-in Belt, the San-yo Belt, and the Ryoke Belt. The examined Paleogene intrusives, which belong to the San-in Belt, show volcano-plutonic association on the eastern side of younger Daisen volcano at the southern part of Tottori Prefecture and the northern part of Okayama Prefecture [e.g. 1-5].

Seven early Paleogene granitoids were collected from three plutons of the Inbi intrusives: Tottori granite, Ningyo Toge granite, and Sangenya granite [4]. Minerals in polished thin sections were first described under microscope. All of the granitoids from the Inbi intrusives contain quartz, feldspars, biotite and iron oxide. Most of them except for Tottori granite contain amphibole. Spinel is found as accessory mineral in some thin sections.

Each mixture of lithium tetraborate and powdered rock was put into a platinum crucible, and then ignited in a furnace at 1000 degree-C and cooled for preparing a glass bead. And then, major and trace elements were measured using XRF analyzer. To prepare sample solutions for measuring trace elements including REEs, the powdered rocks were first digested in a PTFE beaker with HF/HClO<sub>4</sub> mixture on a hotplate at 120-140 degree-C, and then residue probably including heavy minerals such as zircon was dissolved in sealed high-pressure container with HF/HCl mixture at 180 degree-C. The first step decomposed fraction and residual one were well-mixed, and then this mixture was split into two aliquots: one was separated from other elements using a quartz column filled with cation exchange resin for measuring REEs, and the other aliquot was for analysis of trace elements except for REEs. These solutions were analyzed using ICP-MS.

Chemical analyses for whole rock compositions of seven Inbi granitoids yielded the following results. Molecular Al<sub>2</sub>O<sub>3</sub>/(CaO+Na<sub>2</sub>O+K<sub>2</sub>O) values are given as I-type with a range from 0.96 to 1.10. Relationship of Na<sub>2</sub>O+K<sub>2</sub>O vs. total FeO vs. MgO shows calc-alkaline series on AFM diagram. SiO<sub>2</sub> content ranges from 65.7 wt% to 73.4 wt%, and relationship between Si and other major elements gives clear differentiation trend on Harker variation diagrams. Five samples of the granitoids are categorized as high-K series. Many granitoids in this area suffer weathering. The resulting in weathering yields a decrease of CaO (from 2.5 wt% to 1.7 wt%) and Na<sub>2</sub>O (from 4.1 wt% to 3.6 wt%) for Ningyo Toge granites. Whereas Sangenya and Ningyo Toge granites contain about 200 to 360 ppm Sr, Tottori granite contains only 90 ppm Sr. The values of Ti normalized by the mean MORB composition [6] against seven granitoids yield a trend of depletion in Ti. Those of REEs normalized by the MORB composition are given as enriched LREE pattern, negative Eu anomaly, and relatively flat MREE and HREE patterns. All of these normalized patterns have characteristics as volcanic arc granites [e.g. 7].

### References:

[1] Shibata, H. and Saruyama (1959) Paper. ITSR, Okayama Univ., 25, 1-12 (in Japanese with English abstract); [2] Shibata, K. and Yamada (1965) Bull. Geol. Surv. Japan, 16, 437-442; [3] Kawano and Ueda (1966) Jour. Mineral. Petrol. Econom. Geol., 56, 191-211 (in Japanese with English abstract); [4] Sasada et al. (1979) Memoir. Geol. Soc. Japan, 17, 19-34 (in Japanese with English abstract); [5] Shibata, K. (1979) Memoir. Geol. Soc. Japan, 17, 69-72 (in Japanese with English abstract); [6] Albaredo (2005) Geophys. Monogr. R.D. van der Hilst, J. Bass, J. Matas and J. Trampert. Washington D.C., Amer. Geophys. Union, 160, 27-46; [7] Imaoka et al. (2011) Jour. Asian Earth Sci., 40, 509-533.

Keywords: granitoid, San-in Belt, XRF, ICP-MS, trace element, REE

## Petrology of ultramafic rocks in the Gosaisho series, northeastern Japan: Is the Gosaisho series the SSZ ophiolite?

SATO, Yuki<sup>1\*</sup> ; ISHIWATARI, Akira<sup>2</sup>

<sup>1</sup>Dept. Earth Sci., Grad. Sch. Sci., Tohoku Univ., <sup>2</sup>Center for NE Asian Studies, Tohoku Univ.

The Abukuma plateau, which extends ~180km in N-S and ~50km in E-W directions, is located along the Pacific coast of northeastern Japan. This plateau is composed mainly of Cretaceous granitic rocks and regional metamorphic rocks. In the Gosaisho-Takanuki district that is located in the central part of the plateau, the Gosaisho metamorphic rock series in the east overthrust onto the Takanuki metamorphic rock series in the west (e.g. Umemura, 1979). The Gosaisho series is mostly composed of mafic and siliceous rocks, and the Takanuki series is mainly composed of pelitic-psammitic rocks. In the Gosaisho series, many small ultramafic bodies are present in the areas adjacent to the Takanuki series. Metamorphic rocks in the Abukuma Plateau have been well studied since the late 19th century, excepting these ultramafic rocks.

The ultramafic rocks in the Gosaisho-Takanuki district are affected by contact metamorphism of the Cretaceous granitic rocks in various degrees, but their protoliths are judged as mantle peridotites and ultramafic cumulates based on their bulk rock chemistry. The ultramafic cumulates are sometimes accompanied by metagabbros. In an ultramafic body called Mount Ohtsube, mantle peridotites are distributed at the foot of the mountain and cumulates occupy its top part. It is likely that the ultramafic bodies in this area are the fragments of the lower part of an ophiolite. We also note that cordierites and associated gabbroic rocks are present in this area. They are always contained in granitic bodies, and it is likely that intrusion of cordierites coincided with the Cretaceous felsic magmatism.

The bulk rock chemistry of the peridotite is poor in Ca and Al contents (CaO <0.6 wt. %, Al<sub>2</sub>O<sub>3</sub> <1.6 wt. %). This suggests that they are highly depleted mantle peridotite. On the one hand, Cr# of spinel in the peridotite, which supposedly correspond to the degree of mantle depletion, show a wide range (14 - 87) from place to place. The spinel is poor in Ti content (TiO<sub>2</sub> <0.2 wt. %). These characteristic features of spinel suggest that the mantle section was of arc origin (Arai et al., 2011). This is consistent with the bulk rock chemistry of the associated metagabbro which is rich in Ca and Al, and poor in Ti contents (CaO = 11.6 - 17.0 wt. %, Al<sub>2</sub>O<sub>3</sub> = 13.8 - 18.5 wt. %, TiO<sub>2</sub> = 0.06 - 1.06 wt. %). It is also noteworthy that some ultramafic cumulates are very rich in Fe (up to Fo = 73).

In the Gosaisho series, siliceous rock contain early Jurassic radiolarian fossils (Hiroi et al., 1987). In addition, some low-grade metamorphic rocks show original pillow structure (Nohara and Hiroi, 1989). Hiroi et al. (1998) argued that the Gosaisho Series represents the mid-ocean ridge origin oceanic crust which overthrust onto the terrigenous Takanuki Series. However, in some places, there are calc-alkaline intrusions which have experienced regional metamorphism with the country rocks (Umemura, 1970). This is consistent with our idea that the ultramafic rocks are of arc origin. Therefore, it is suggested that the Gosaisho Series is the arc-related, supra-subduction zone ophiolite which thrust onto the Takanuki Series in the Jurassic period. However, it is also possible that the early Paleozoic Hayachine-Miyamori ophiolite (e.g. Machida and Ishiwatari, 2013). Comprehensive study of mafic and ultramafic rocks in the Gosaisho series is needed to solve this problem.

Keywords: supra-subduction zone ophiolite, ultramafic rock, Abukuma metamorphic rocks

## Experimental petrology of Goseong volcanoes, Korea

FUJINAGA, Nozomi<sup>1\*</sup> ; SANO, Takashi<sup>2</sup>

<sup>1</sup>Graduate School of Geo-environmental Science, Rissho University, <sup>2</sup>Department of Geology and Paleontology, National Museum of Nature and Science

Genozoic volcanoes with composition of alkali basalts are widely distributed in Southwest Japan, Korea, and East China. On the basis of geochemical studies, several models to explain magma origin of the alkali basalts were proposed (e.g., upwelling of hot asthenosphere, melting of stagnant slab, and so on). However, little is known about differentiation processes for the alkali basalts based on petrological studies. We therefore performed a series of experimental determinations of melting relation in alkali basalts on Goseong volcanic field, Goseong-do, Korea. Goseong volcanic field consists of seven volcanic plugs, and some of them are accompanied by lava flows. We have carried out petrological studies on alkali basalts from all the seven plugs. The alkali basalts have phenocrysts of olivine and augite and microphenocryst of spinel. Whole rock compositions show that the alkali basalts are relatively primitive ( $\text{FeO/MgO} < 0$  and  $\text{MgO} > 11$  wt %), and mineral chemistry supports this (Forsterite content in olivine  $> 87$ ). The most primitive rock was selected for melting experiments at 1110-1220 °C and 1 bar under the oxygen fugacity along the fayalite-magnetite-quartz buffer. The experimental results show that mineral assemblage (olivine, spinel, and plagioclase) is different from natural one (olivine, spinel, and augite), indicating that crystallization pressures were probably higher than the melting pressure (1 bar). Thus, we will conduct melting experiments at high pressures in future work.

## Metamorphic evolution of garnet-sillimanite gneiss from Ambatofotsy region, Antananarivo domain, east-central Madagascar

ICHIKI, Takashi<sup>1\*</sup> ; ISHIKAWA, Masahiro<sup>1</sup>

<sup>1</sup>Yokohama National University

Madagascar is situated within the central part of the Neoproterozoic East African Orogen (EAAO: Jacobs and Thomas, 2004) that marks the join between East and West Gondwana. Therefore, Madagascar is one of the most significant areas to understand the process of Orogen formation. In this study we report the newly found inclusion of kyanite + staurolite + muscovite + rutile in garnet and the mode of occurrence and discuss the metamorphic evolution of the garnet-sillimanite on the basis of estimated results by using various geothermobarometers and phase equilibrium by constructing pseudosection.

The Antananarivo domain is mainly composed of the felsic metamorphic rocks with subordinate amounts of the metasedimentary rocks (Tucker et al., 2012). There exposed magnetite-orthopyroxene-quartz gneiss (metamorphosed banded iron formation), garnet-orthopyroxene rock and garnet-hornblende-biotite gneiss around the garnet-sillimanite gneiss in the eastern part of the domain. The garnet-sillimanite gneiss is mainly composed of garnet, sillimanite, k-feldspar, plagioclase, and quartz with subordinate amounts of biotite, muscovite, monazite, zircon, rutile and graphite. Sillimanite is present in the matrix and as inclusion in garnet. Kyanite is only present as inclusion in garnet. Garnet ( $X_{Mg}=0.17-0.18$ ) also contains spinel and abundant quartz and monazite inclusions. Spinel shows Mg poor ( $X_{Mg}=0.21-0.22$ ) and Zn rich (ZnO = 18.4-19.0 wt.%) compositions. We newly found kyanite + staurolite + muscovite + rutile in the garnet. This staurolite shows Mg poor ( $X_{Mg}=0.12$ ) and Zn rich (ZnO=3.1 wt.%) composition. Garnet is replaced rim of grain by radial aggregate of biotite ( $X_{Mg}=0.58$ ) + sillimanite.

As a result of the petrographic observation, the metamorphic condition of the garnet-sillimanite gneiss was increased from the stability field from staurolite + quartz to garnet + kyanite (Spear and Cheney, 1989). Garnet + sillimanite + spinel + quartz was stable during the peak metamorphic condition. The estimated peak pressure and temperature condition is ca. 800 °C at 0.9 GPa by using garnet-sillimanite-plagioclase-quartz geobarometer (Spear, 1993) and garnet-sillimanite-spinel-quartz geothermobarometer (Nichols et al., 1982) with garnet activities calculated after Berman (1990). Garnet is replaced rim of grain by radial aggregate of biotite ( $X_{Mg} = 0.58$ ) with sillimanite. This reaction is hydrous reaction from garnet + k-feldspar + H<sub>2</sub>O to biotite + sillimanite + quartz with decreasing temperature (Le Breton and Thompson, 1988). This retrograde metamorphic condition is almost consistent with the estimated P-T condition from the garnet-hornblende-biotite gneiss. The estimated pressure and temperature condition is ca. 700 °C at 0.6 GPa by using garnet-hornblende geothermometer (Graham and Powell, 1984), hornblende-plagioclase geothermometer (Holland and Blundy, 1994) and garnet-hornblende-plagioclase-quartz geobarometer (Kohn and Spear, 1990). In summary we newly identified the clockwise P-T path from the garnet-sillimanite gneiss exposed in Ambatofoty region, eastern part of the Antananarivo domain.

Keywords: Gondwana supercontinent, east-central Madagascar, Antananarivo domain, Garnet-sillimanite gneiss, Clockwise P-T path

## Petrogenesis of garnet-clinopyroxene rocks from the Gondwana collisional orogeny

TAKAMURA, Yusuke<sup>1\*</sup>; TSUNOGAE, Toshiaki<sup>1</sup>; IINUMA, Minako<sup>1</sup>; KOIZUMI, Tatsuya<sup>1</sup>; SANTOSH, M.<sup>2</sup>; MALAVIARACHCHI, Sanjeeva<sup>3</sup>

<sup>1</sup>Univ. Tsukuba, <sup>2</sup>China University of Geosciences Beijing, <sup>3</sup>Univ. Peradeniya

Madagascar - Southern India - Sri Lanka - East Antarctica region, which is regarded as a part of the East African - Antarctic Orogenic Belt formed by complex subduction-accretion-continent tectonic events related to the amalgamation of Gondwana Supercontinent during Neoproterozoic, is characterized by the presence of major suture zones (e.g. Palghat-Cauvery Suture Zone in southern India) which correspond to paleo-plate boundaries formed by the closure of Mozambique Ocean at ca. 530-550 Ma. The dominant lithologies of the suture zones are felsic to intermediate orthogneiss, metasediments, and mafic-ultramafic suites. Particularly, the occurrence of mafic-ultramafic suites (ophiolite or layered intrusion) is a unique character of the suture zones compared to surrounding granulite blocks and cratons. Here, we report new petrological and geochemical data of metagabbroic garnet-clinopyroxene rocks from Sri Lanka and discuss its petrological implications. Mineral assemblages of the rocks are garnet + clinopyroxene + orthopyroxene + ilmenite + hornblende + plagioclase (type 1), and garnet + plagioclase + clinopyroxene + orthopyroxene + quartz + ilmenite (type 2). Type 2 rock shows a decompression texture of orthopyroxene + plagioclase symplectite formed by a reaction: garnet + quartz => orthopyroxene + plagioclase. Similar rocks and textures have been reported from the Palghat-Cauvery Suture Zone in South India (Nishimiya et al., 2008; Sajeew et al., 2009; Saitoh et al., 2011), Highland Complex in Sri Lanka (Osanai et al., 2006), and Lutzow-Holm Complex in East Antarctica (Saitoh et al., 2012). Temperature and pressure conditions inferred for the type-1 Sri Lankan metagabbro based on pseudosection analysis in NCFMASHTO system is 970-1040C and 8-10.5 kbar, which is significantly lower in pressure than the results of Osanai et al. (2006) (>18 kbar, >1000C). Recent petrological and geochemical studies of the Palghat-Cauvery suture zone in southern India suggest that similar metagabbros and related mafic-ultramafic suites occur as various blocks within ortho- and paragneisses as melange. Similar occurrences and P-T evolution of metagabbro bodies in several Gondwana fragments suggest that the Palghat-Cauvery Suture Zone might continue to the Lutzow-Holm Complex (East Antarctica) through Highland Complex (Sri Lanka).

Keywords: granulite, Gondwana, suture zone, pseudosection

## Neoproterozoic and Middle Neoproterozoic bimodal magmatism in the Gondwana orogeny, South India

KOBAYASHI, Airi<sup>1\*</sup> ; TSUNOGAE, Toshiaki<sup>1</sup> ; KOIZUMI, Tatsuya<sup>1</sup>

<sup>1</sup>Univ. Tsukuba

Detailed petrological investigations for bimodal association of basaltic and rhyolitic magmas, which is regarded to have formed at subduction or rift zones, provides important information to investigate magma petrogenesis and tectonic evolution in a convergent or divergent margin settings. Here, we report first preliminary petrological and geochemical data of the Neoproterozoic charnockite-mafic granulite association in the Madras Block and Middle Neoproterozoic granite-amphibolite association in the Mesoarchean Coorg Block, southern India. Irregular-shaped mafic granulite (basaltic andesite) occurs as blocks of about tens of centimeter within charnockite (dacitic) in the Madras Block, while amphibolite (basaltic trachy-andesite) blocks in the Coorg Block are surrounded by sub-alkaline granite. Although there is no obvious texture of magma mixing in the Madras samples probably due to post-magmatic high-grade metamorphism and complete recrystallization, plagioclase in the contact zone between mafic enclave and host granite from the Coorg Block shows oscillatory and dusty zonings, which might suggest bimodal magmatism in Middle Neoproterozoic divergent margin in southern India.

## Infiltration of CO<sub>2</sub>-H<sub>2</sub>O binary fluid and formation of patchy charnockite from Southern India

ENDO, Takahiro<sup>1\*</sup> ; TSUNOGAE, Toshiaki<sup>1</sup> ; M., Santosh<sup>2</sup>

<sup>1</sup>Univ. Tsukuba, <sup>2</sup>China University of Geosciences Beijing

Since the first discovery of patches, veins and ladders of coarse-grained orthopyroxene-bearing felsic granulite (incipient charnockite) within foliated amphibolite-facies gneiss from Kabbal in Karnataka, southern India, by Pichamuthu (1960), the origin and petrogenesis of charnockite and its implications for granulite processes in lower crust have been the focus of many petrologists. According to previous studies, charnockite formation in the SGT is considered to have resulted by the infiltration of CO<sub>2</sub>-rich anhydrous fluids along structural pathways within upper amphibolite-facies gneisses, resulting in the lowering of water activity and stabilization of orthopyroxene through breakdown of biotite (e.g. Janardhan et al., 1979; Newton et al., 1980; Hansen et al., 1987; Santosh et al., 1990; Newton, 1992; among others).

This study presents new petrological data of 'incipient' charnockite developed within garnet-biotite (Grt-Bt) gneiss from Kakkod with the western Trivandrum Granulite Block (TGB), India. In this locality, bulk rock compositions of charnockite and the host Grt-Bt gneiss are almost equivalent. The result of conventional geothermobarometry using Grt-Opx-Pl-Qtz assemblage shows the peak metamorphic condition of 860-960 °C and 6.9-8.4 kbar, which is consistent with the results of mineral equilibrium modeling. The metamorphic condition certainly corresponds to granulite-facies event, and it is higher than those reported from other incipient charnockite localities in the TGB and adjacent Nagercoil Block. Furthermore, the estimated metamorphic condition is too high for the stability of the host Grt-Bt gneiss that contains a mineral assemblage formed at amphibolite-facies condition. In addition, although pseudosecondary fluid inclusions are composed of pure CO<sub>2</sub>, secondary fluid inclusions contain CO<sub>2</sub>-H<sub>2</sub>O binary fluid. Therefore, patchy charnockite in Kakkod from the TGB is considered to have formed by infiltration of CO<sub>2</sub>-H<sub>2</sub>O binary fluid during a retrograde stage. The petrogenetic model of incipient charnockite formation proposed in this study is therefore different from reported petrogenesis from other localities.

Keywords: incipient charnockite, metamorphic fluid, pseudosection, geothermobarometry, Trivandrum Granulite Block, southern India

## Relationship of zeolites and host rocks

SHIMIZU, Kouhei<sup>1\*</sup> ; YASUI, Mana<sup>2</sup>

<sup>1</sup>Department of Natural Sciences, Faculty of Knowledge Engineering, Tokyo City University, <sup>2</sup>Department of Resources and Environmental Engineering, Waseda University

Natural zeolites occur in various rocks, such as igneous rocks, sedimentary rocks, and metamorphic rocks, at surface and shallow zone of upper crust.

In this research, the relationship between chemical composition of the host rocks and zeolite species are discussed in terms of the basis of chemical analysis of samples from Izu Peninsula and the Chichijima of Ogasawara (Bonin) Islands.

Although origin relations between the microscopic zeolite species and host rock compositions are seen under the conditions of low water/rock ratio, like a burial diagenesis, low degree regional metamorphism, and contact metamorphism, it has reported that macroscopic crystals occur in veins and geodes, not controlled by host rock composition, as they produced under the conditions of high water/rock ratio of hydrothermal alteration, in a previous work. (Utada 1995)

### Result and discussion

The identification of the zeolites species are characterized by X-ray diffractometry and bulk rock chemical composition of host rocks are analyzed by X-ray fluorescence.

To research 10 points of Chichijima (Ogasawara islands) and 2 points of Izu Peninsula, eight kinds of zeolite ( Heulandite, Analcime, Chabazite, Mordenite, Erionite, Phillipsite, Stilbite and Yugawalite) were able to be identified.

Samples from Chichijima, Stilbite was detected on Miyanohama, Hatsuneura north side, Hatsuneura south side, Suzaki, Buta seashore, and Kin-shi beach.. Stilbite did not occur on the samples from other 4 points

As a results Si/Al ratio of the host rocks are clearly different between the points of Stilbite occurred and not occurred, Si/Al ratio of former rocks were 5.248~7.672, the latter rocks were 4.230~4.768. The boundary of Stilbite occurrence Si/Al ratio of host rock seems to be around 5. . In the Chichijima (Ogasawara islands), correlation was found between host rocks and formed zeolites.

Keywords: zeolites, host rocks, Chichijima, Ogasawara islands

## Three pyroxene andesite (pigeonite-augite-hypersthen andesite) from Hakone volcano

ISHII, Teruaki<sup>1\*</sup>

<sup>1</sup>Fukada Geological Institute

Pigeonite phenocryst bearing volcanic rock is very rare in the world. Pigeonite-augite-hypersthen andesite (= three pyroxene andesite or pigeonite andesite ) from Hakone volcano is very famous according to the detailed studies on the pyroxenes using microscope by the late professor Kuno (Kuno 1935, Kuno 1936). On the bases of the detailed EPMA analyses of the pyroxene crystallization sequences as well as estimated magmatic temperatures using pyroxene geothermometer, for the pigeonite andesite, the author suggests the following working hypothesis, i.e. the pigeonite andesite was induced by magma mixing between three pyroxenes andesite magma (about 1070 degree C) originated from the primitive high temperature hydrous tholeiitic magma within secondary magma reservoir opened for water, and the high temperature magma (about 1110 degree C) in the secondary magma reservoir. The key concept is that cocrystallization of three pyroxene phenocrysts under open system for water in the secondary magma reservoir.

Keywords: Hakone volcano, pyroxene geothermometer, pigeonite, magma mixing, three pyroxene andesite, magmatic temperature

## The structural water in hydrothermally synthesized monazite

ABE, Takeyasu<sup>1\*</sup> ; NAKAMURA, Michihiko<sup>1</sup>

<sup>1</sup>Department of Earth Sciences, Tohoku University

**Introduction:** The U-Th-Pb dating of accessory minerals such as zircon and monazite is widely applied for various types of rocks [1,2,3]. There has been proposed another method to obtain geochronological information from these minerals: quantifying the degree of metamictization (destruction of crystal structure by radioactive components). It is reported for zircon that the water content (up to 10 wt%) is in proportion to the degree of metamictization, thus to the concentration of radioactive nuclei and geological age[4]. Monazite on the other hand usually undergoes much less metamictization than zircon due to the higher bond strength of P and O compared to that of Si and O; this results in the lower water content in the metamictized monazite. Determination of the structural water content in monazite without radioactive damage is thus necessary to constrain the "initial" water content prior to hydration. The water content bears significance also for better understanding the crystal chemistry of monazite. In this study, we synthesized monazite single crystals at hydrothermal condition and determined the content of structural water as a function of pressure.

**Experimental method:** The hydrothermal synthesis of monazite was conducted at a temperature of 800 degC and pressures of 1.5, 10 and 15 kbar using a cold-seal pressure vessel and a piston cylinder apparatus. The CePO<sub>4</sub> reagent was encapsulated with H<sub>2</sub>O or H<sub>2</sub>O-NaCl solution and run for ca. 100 hours. The FT-IR analyses of the obtained monazite single crystals were conducted to determine the concentration of structural OH on the basis of Lambert-Beer's Law. The molar absorption coefficient was estimated by linear calibration curve against the OH stretching vibration wavenumber [5].

**Results and Discussion:**The broad absorption band was observed at 3100-3600 cm<sup>-1</sup> in the crystals synthesized in all the experimental conditions. The water content of synthesized monazite was estimated approximately to be 20-70 ppm, showing no large pressure dependence. FT-IR analyses of pleochroic absorption are on-going to determine the OH dipole orientation within the crystal structure.

**References:** [1]J. M. Langille, M. J. Jessup, J. M. Cottle, G. Lederer, T. Ahmad, *Journal of Metamorphic Geology*, 30, 769-791 (2012)

[2]E. Janots, A. Berger, E. Gnos, M. Whitehouse, E. Lewin, T. Pettke, *Chemical Geology*, 326-327, 61-71 (2012)

[3]T. Imayama, K. Suzuki, *American Mineralogist*, 98, 1393-1406 (2013)

[4]M. Zhang, E. K. H. Salje, R. C. Ewing, *Journal of Physics: Condensed Matter*, 14, 3333-3352 (2002)

[5]M. S. Paterson, *Bulletin de Mineralogie*, 105, 20-29 (1982)

**Keywords:** hydrothermal synthesis, accessory mineral, monazite dating, metamictization, nominally anhydrous minerals, FT-IR

## Phase relation in ternary feldspar system at high temperature

KODAMA, Yu<sup>1\*</sup>; MIYAKE, Akira<sup>1</sup>; HOKADA, Tomokazu<sup>2</sup>; KAWASAKI, Toshisuke<sup>3</sup>

<sup>1</sup>Kyoto Univ., Sci., <sup>2</sup>National Institute of Polar Research, <sup>3</sup>Ehime Univ., Sci.

During cooling of rocks or by change of chemical composition of feldspar, feldspar transforms to other polymorphs and forms various micro-textures. Observing micro-textures of feldspar is a useful approach to give a constraint to the thermal history of the rock. It has been known that the feldspars in ultrahigh-temperature (UHT) metamorphic rocks have ternary feldspar (Tfs) composition and those have the various and complex microtextures. However, the occurrence and the formation process of micro-textures in Tfs had not been studied in detail and they could not be interpreted by the widely used phase diagram with 2nd-order C2/m-C-1 phase transition at high temperature. And furthermore, although many experimental studies were performed, with respect to the phase relation on the plagioclase feldspar and alkali feldspar systems, the detailed experiments for the phase relations in the An-Ab-Or ternary feldspar system were restricted and its phase relations still remain ambiguous. Due to the high crystallization temperature of ternary feldspar (Tfs), Tfs would preserve the information about thermal history in more detail than those recorded on alkali feldspars and plagioclase feldspars. Previous thermodynamic studies on the C2/m - C-1 phase transition (Kroll et al., 1980; Salje et al. 1985, Carpenter, 1988) were carried out using the in situ powder X-ray experiments on pure Ab compositions. Due to the spatial resolution of analytical instruments, they missed the formation of the micro-texture on C2/m - C-1 phase transition. In this study, high temperature and high pressure experiments were carried out to decide the phase relation at high temperature including the phase relation between the C2/m and the C-1 in the An-Ab-Or ternary feldspar system at 1100 - 1300C and 10 kbar. We reveal the formation process of complex micro-textures of Tfs in UHT metamorphic rock by the present phase diagram.

We employed mixture of powdered lamellae-free oligoclase and sanidine crystal as starting materials. Bulk composition of starting materials was prepared by varying ratio of oligoclase and sanidine. We focused whether micro-textures derived from the C2/m - C-1 phase transition were formed or not. Experimental products were observed using field emission scanning electron microscopy (FE-SEM, JEOL JSM-7001F) and annular dark-field scanning transmission electron microscopy (ADF-STEM, JEOL JEM-2100F) to observe micro-textures.

Exsolution lamellae by a compositional gap between the C2/m and the C-1 which has near (010) interface, were observed in the run products synthesized at 1100 - 1200C. This result strongly suggests that the C2/m - C-1 transition is the first order phase transition. Moreover, the glass phase was observed in run products synthesized at 1250 - 1300C. From these experimental results, we propose the phase diagram on the Olg (An<sub>25</sub>Ab<sub>75</sub>) -Or pseudo-binary.

Napier Complex in northern Enderby Land, East Antarctica is one of the most famous regional ultrahigh-temperature (UHT) metamorphic terranes in the world. Although Tfs in Napier Complex has the complex microtextures (e.g., Harley 1985; Sheraton et al. 1987; Hokada, 2001), the occurrence and the formation process of micro-textures in Tfs have not been understood in detail. By the phase diagram obtained in the study, the formation process of Tfs in the felsic gneiss and the micro-texture in Tfs were revealed as following process. At first heterogeneous distribution of Olg, Tfs, and myrmekite-like textures were result of melting of the felsic gneiss and following crystallization. And then, the peak metamorphic temperature is estimated to be at least 1200 - 1250C. At the cooling process, the complex exsolution textures of Tfs are composed of (010) coarse lamellae derived from C2/m - C-1 first order phase transition and (-901) fine lamellae derived from spinodal decomposition.

Keywords: ternary feldspar, phase relation, high temperature experiment

## Quantitative Analysis of Rock Samples by ICP-Quadrupole Mass Spectrometer (QMS)

AJIRO, Takuya<sup>1\*</sup> ; OOKI, Seigo<sup>2</sup> ; CHAKO TCHAMABE, Boris<sup>3</sup> ; OHBA, Takeshi<sup>2</sup>

<sup>1</sup>Course of Chemistry, Graduate School of Science, Tokai University, <sup>2</sup>Department of chemistry, School of Science, Tokia University, <sup>3</sup>School of Science and Technology, Tokai University

ICP-Quadrupole Mass Spectrometers (QMS) can analyze multi-element quickly with high sensitivity. One problem is the interference by polyatomic molecules. For example, polyatomic molecules, such as ArO and ArCl, obstruct the analysis of Fe and As, respectively. In order to remove polyatomic molecules, ICP-QMSs using the collision gas was developed. For collision gas, generally inert gas such as He gas has been used. In this study, we try to analyze major and trace elements of standard rocks and volcanic rocks of Cameroon Volcanic Line by a ICP-QMS with He collision cell.

The iCAP-Q (ThermoScientific Inc) was selected for study. The plasma was operated at 1.7 kW and 27 MHz. The flux of Ar was about 16 L/min. The sampling cone can be removed easily without any tools and cleaning procedure is simple. The plasma gas, which is injected to vacuum system, is bended to 90 degree by an ion lens and reach to He Collision Cell. Neutral molecules are removed efficiently by the ion lens. Helium collision cell has a function as small QMS, removing interfering ions lighter than target element. The polyatomic molecules are also removed due to the reduction of their kinetic energy with He collision. The ions passing He collision cell go to the main QMS and their signals are detected by analog or pulse detections.

We used three standard rocks (JA-2, JB-2, and JB-3) and volcanic rocks at Borombi Mbo Volcano, Cameroon. The 50 mg of rock powder was put into 100 mL Teflon digestion vessel with 2.0 mL of 35 wt% HCl, 1.0 mL of 60 wt% HClO<sub>4</sub>, and 0.5mL of 50 wt% HF. The vessel was set in microwave heating system (Multiwave 3000, Parkin Elmer Inc.). The microwave power was increased to 500 W by 50 W/min and kept over 60 min. After heating, the digestion vessel was cooled down to 50 °C. In the cooled vessel, 2.5 mL of saturated H<sub>3</sub>BO<sub>3</sub> water and 2.5 mL of pure water were added, and the vessel was heated by microwave heating system again. The micro wave power was increased to 1400W by 280 W/min and kept for 20 min. After cooling, pure water was added to the sample solution and total volume was adjusted to 50 mL.

Yields of major elements in standard rocks, except for Si, were almost more than 70 %. In case most of trace elements, those were also more than 70%. Furthermore, there was no significant difference in the yield of most elements when we analyzed several times for a common sample. It is found that major elements, except Si, and most of trace elements of volcanic rocks can be analyzed by using a single ICP-QMS. In case of volcanic rock samples of Cameroon, type of these samples were identified to be an alkali basalt based on Nb/Y versus Zr/TiO<sub>2</sub> diagram. This result is consistent to the previous study on Cameroon Volcanic Line (A. Marizoli et al., 2000).

Keywords: ICP-QMS, microwave digestion, volcanic rock, quantitative analysis, Cameroon

## Validation of mass attenuation coefficients in quantitative electron probe microanalysis (EPMA)

KATO, Takenori<sup>1\*</sup> ; JEEN, Mi-jung<sup>2</sup> ; CHO, Deung-lyong<sup>3</sup> ; SATO, Kei<sup>1</sup>

<sup>1</sup>Center for Chronological Research, Nagoya University, <sup>2</sup>Center for Research Facilities, Pusan National University, <sup>3</sup>Geological Mapping Department, Korea Institute of Geoscience and Mineral Resources

Mass attenuation coefficients (m.a.c.s) are important factors of accuracy in quantitative electron probe microanalysis (EPMA). New m.a.c.s are calculated from the latest version of two datasets[1][2] for  $Z = 1 - 92$ . The combination of two datasets solves the problems within them, such as spurious discontinuity and unnatural increase at high-energy sides of absorption edges. New m.a.c.s improve accuracy including geological applications.

[1] Henke B.L., Gullikson, E.M. and Davis, J.C. (1993) *At. Data Nucl. Data Tables*, 54, 181 - 342.

[2] Hubbel J.H. and Seltzer S.M. (1995) *NISTIR*, 5632, pp. 116.

Keywords: electron probe microanalysis (EPMA), quantitative analysis, mass attenuation coefficients, matrix correction

## SEM-EDS Automated Particle Analysis of Mineral Compositions of Rocks

MUTOU, Hitomi<sup>1\*</sup>; SHIMADA, Aiko<sup>2</sup>; ONODERA, Hiroshi<sup>3</sup>

<sup>1</sup>JEOL Ltd.SM APPLICATION DEPARTMENT SM BUSINESS UNIT, <sup>2</sup>JEOL RESONANCE Inc. SM APPLICATION DEPARTMENT, <sup>3</sup>JEOL Ltd.SA APPLICATION DEPARTMENT SA BUSINESS UNIT

Rocks consist of various kinds of minerals depending on their localities and formation processes. Mineral compositions of rocks are very important to study their sources and formation processes. X-ray fluorescence analysis (XRF) is commonly needed for mineral composition analysis. The XRF analysis provides the average composition of elements in a rock. Analysis of mineral particles in a rock is sometimes more important to find features of a rock. However, the analysis of a large number of mineral particles in a rock one by one requires a great deal of time. In recent years, the automated particle analysis combined with a scanning electron microscope (SEM) on energy dispersive X-ray spectrometer (EDS), which is called SEM-EDS automated particle analysis has rapidly been advancing. This method enables fast analysis of a large number of particles one by one directly.

In this report, analysis of the mineral compositions of two rocks -the Koujaku granite and the Hakkoda second-stage pyroclastic flow deposition (Ht2) - was carried out with SEM (JSM-IT300LA, JEOL)-EDS (JED2300, JEOL) automated particle analysis. The samples for this analysis were prepared as follows: rocks were crushed separately and each crushed rock embedded in resin was polished. More than a few thousand particles of the rocks were analyzed. In the Koujaku granite, quartz was a dominant constituent. K-feldspar and alkali feldspar were contained in a higher concentration than plagioclase. In addition, some colored minerals were contained. In the Ht2, pumice was a dominant constituent. In addition, quartz, feldspar and some colored minerals were contained. Additionally, many particles in the Ht2 consisted of multiple minerals unlike in the Koujaku granite. In the presentation, we will give more detailed descriptions of minerals and their components of the rocks.

Keywords: Mineral, Particles Analysis, SEM-EDS

## Dependence of water concentration distribution of columnar joints formation in analogue experiments

HAMADA, Ai<sup>1\*</sup> ; TORAMARU, Atsushi<sup>2</sup>

<sup>1</sup>Earth and Planet. Sci., Kyushu Univ., <sup>2</sup>Earth and Planet. Sci., Kyushu Univ.

Columnar joints of igneous rocks and ignimbrites have various morphological patterns. As their unit structure, column structure can be classified in terms of straight or curved. Columnar joint is formed by volume contraction due to cooling and tensile stress accumulated inner the volume is released as sequentially cracks according to the temperature gradient during cooling. Basic research to explain how curved columns are formed has not been conducted. In this study, we report the results of reproducing curved structure in analogue experiments by drying starch and water mixture. We put the mixture into a cylindrical container and light a lamp (60W) 1.5cm above the surface of mixture. We take images with X-ray CT of the specimen before drying perfectly and observe the spatial distribution of water concentration of the mixture on the way to form columnar joints. As a result, we recognize that water concentration distribution at a depth in mixture increases with the horizontal distance from just below the lamp. The direction of crack developing from the surface of the mixture to inner is almost perpendicular to the contour of water concentration. We confirm that the effect of heat from the lamp on the surface of the mixture differs with the distance from the lamp and it suggests inhomogeneous water concentration in mixture is caused by the difference of drying rate depending on the distance from the lamp. We also report the relationship between the direction of crack advance and the change of water concentration distribution with time.

Keywords: columnar joint, analogue experiment, crack formation, Micro-focus X-ray CT, concentration distribution

## Slab-fluids contain chlorine

KAWAMOTO, Tatsuhiko<sup>1\*</sup>

<sup>1</sup>Institute for Geothermal Sciences, Kyoto University

We found that the fluid inclusions of sub-arc mantle peridotites have 5.1 wt. % NaCl beneath the Pinatubo, a frontal volcano (Kawamoto et al., 2013 PNAS) and 3.7 wt. % NaCl beneath the Ichino-megata, a rear-arc volcano (Kumagai et al., under review). Based on these observations, we suggest that the slab-derived fluids are saline fluids.

In order to understand the effects of salinity on the arc-magma chemistry, two series of elemental partitioning experiments between silicate melts and aqueous fluids have been carried out with and without Cl in synchrotron facilities. The experiments show that highly saline fluids can transfer Pb, Rb, and Cs more effectively than Sr and Ba from subducting oceanic lithosphere to the mantle wedge. As suggested by Keppler (1996, *Nature*), saline fluids can be an important agent to transfer large ion lithophile elements. Geochemical studies have suggested that three chemical components are involved in the formation of arc-basalts: the depleted mantle, aqueous fluid, and melt components (Pearce et al., 2005 *G-cube*). If supercritical fluids contain Cl and then subsequently separate into aqueous fluids and melts (Kawamoto et al., 2012, PNAS), then it follows that such aqueous fluids will inherit much of the Cl and also some of the large ion lithophile elements to explain qualitatively the geochemical features of Mariana arc basalts. In contrast, Cl-free aqueous fluids may not be able to transfer Pb to the magma source. Our partitioning experiments were conducted using highly saline fluids (12-25 wt % (Na, K)Cl). Based on the geochemical features, slab-fluids are likely to contain Cl, although their amount remains to be quantified.

### References

Kawamoto T., Kanzaki M., Mibe K., Matsukage K.N., Ono S. (2012) Separation of supercritical slab-fluids to form aqueous fluid and melt components in subduction zone magmatism. *Proc. Nat. Acad. Sci. USA* 109, 18695-18700.

Kawamoto T., Yoshikawa M., Kumagai Y., Mirabueno M.H.T., Okuno M., Kobayashi T. (2013) Mantle wedge infiltrated with saline fluids from dehydration and decarbonation of subducting slab. *Proc. Nat. Acad. Sci. USA* 110, 9663-9668.

Keppler H. (1996) Constraints from partitioning experiments on the composition of subduction-zone fluids. *Nature* 380, 237 - 240.

Pearce J.A., Stern R.J., Bloomer S.H., Fryer P. (2005) Geochemical mapping of the Mariana arc-basin system: Implications for the nature and distribution of subduction components. *Geochem. Geophys. Geosys.* 6, Q07006.

Keywords: subduction zone, H<sub>2</sub>O, fluid inclusion, mantle wedge, synchrotron X-ray, magma

## Numerical modeling of water-rock reaction with a focus on the earth's surface environment

YOKOYAMA, Tadashi<sup>1\*</sup>

<sup>1</sup>Osaka University, Graduate School of Science, Department of Earth and Space Science

Water-rock interaction proceeds by the interplay between dissolution/precipitation, diffusion of ions, and water flow in rock pores. The reaction-transport process in rock is quantitatively described by:

$$\phi(\partial c/\partial t) = D_e(\partial^2 c/\partial x^2) - v\phi(\partial c/\partial x) + Ar_0f(c)$$

This equation is an example of the one-dimensional reaction-transport equation, and  $c$  is the solute concentration (mol/cm<sup>3</sup>),  $t$  is the time (s),  $x$  is the distance (cm),  $\phi$  is the porosity (dimensionless),  $D_e$  is the effective diffusion coefficient (cm<sup>2</sup>/s),  $v$  is the flow rate in pores (cm/s),  $A$  is the surface area per unit volume of rock (cm<sup>2</sup>/cm<sup>3</sup>),  $r_0$  is the rate constant (mol/cm<sup>2</sup>/s).  $f(c)$  is the function that expresses the concentration dependence of the dissolution rate (mol/cm<sup>2</sup>/s), and for quartz,  $f(c) = (1 - c/c_{eq})$  ( $c/c_{eq}$  is the equilibrium Si concentration) (Scott et al., 2009). By solving the reaction-transport equation, we can know how the distributions of the solute concentration and dissolution rate and the amounts of primary and secondary minerals change with time. Such analysis is called the reactive transport modeling and has been applied to the studies of various processes including soil formation (Maher et al., 2009) and the reactions associated with geologic storage of CO<sub>2</sub> (Xu et al., 2010).

The parameters used in the reaction-transport equation can be estimated by direct measurement in the field, laboratory experiment, and fitting in the modeling. To reproduce natural process accurately, we need to estimate each parameter as precisely as possible. However, it is difficult to evaluate what value is most proper. For example, the reactive surface area  $A$  is often determined by measuring the volume of gas adsorbed on the mineral or by approximating the geometry of the mineral. However, the proportion at which the reactive surface area determined by these processes contributes to actual reaction is often unclear. In addition, there are cases where various  $f(c)$  have been proposed for a specific mineral and the dissolution rate varies with time (White and Brantely, 2003). In such case it is unclear what equation should be used. Therefore, the way of setting appropriate parameter is one of the main subjects of research.

In water-rock reaction on the earth's surface environment, evaluation of the effect of water saturation is important because water saturation changes dynamically as a result of the occurrence of intermittent drying and infiltration. It has been reported that both the hydraulic conductivity and effective diffusion coefficient in rock decrease with decreasing water saturation and this significantly affects the result of the reactive transport modeling (Yokoyama, 2013). In addition, how water saturation affects the reactive surface area has been revealed recently (Nishiyama and Yokoyama, 2013).

Keywords: Reactive transport modeling, Water-rock reaction

## Kinetics of overall silica precipitation within the Earth's crust

SAISHU, Hanae<sup>1\*</sup>; OKAMOTO, Atsushi<sup>2</sup>; TSUCHIYA, Noriyoshi<sup>2</sup>

<sup>1</sup>AIST, <sup>2</sup>Tohoku University

The kinetics of dissolution and precipitation of silica minerals is important to reveal the geochemical reaction and to estimate how long silica deposits forms in the Earth's crust. The present kinetic equation for silica-water reactions was determined at 0-300 C and in the low Si saturated solution, where quartz growth on quartz surfaces occurs than that of nucleation of silica polymorphs [1]. However, the precipitation experiments of the high Si supersaturated solution showed that the co-precipitation of silica polymorphs via nucleation could occur [2], and the euhedral quartz crystals precipitates without precursor of silica polymorphs from the solution with minor components (Al and Na) [3].

In this study, the overall precipitation rate of silica minerals, which includes surface reaction of quartz (first term) and nucleation of silica polymorphs (second term), is derived empirically to estimate the total amount of silica precipitation within the Earth's crust. The previous kinetic equation of surface reaction [1] is applied as the first term. Based on the precipitation experiments of flow rate, the nucleation-controlled precipitation of silica minerals is expressed in a first order rate equation in the second term. The applicability of the nucleation term determined as the nucleation parameter is only in the conditions that precipitation occurs: in the solution supersaturated with respect to quartz, and in the supercritical conditions of water. The rate constant of nucleation is derived as a function of Al concentration in the solution based on the experiments of silica precipitation [3].

By using the new kinetic equation, silica-water interaction was simulated at the well WD-1a of the Kakkonda geothermal field, Japan, which penetrated the boundary of the hydrothermal convection and heat conduction zones [4]. Amount of dissolution and precipitation of silica minerals increases with decreasing of the fracture permeability. The largest amount of silica precipitation occurs in the downflow fluid at the permeable-impermeable boundary regardless of the fracture permeability.

The equilibrium consideration [5] and the kinetic results indicate that, if open fractures forms at the depth of the permeable-impermeable boundary, the impermeable zone could be reproduced by precipitation of silica minerals, which cause the sustainable division between the permeable zone and the impermeable zone in the Earth's crust.

### References

- [1] Rimstidt and Barnes (1980) *Geochim. Cosmochim. Acta*, **44**, 1683-1699.
- [2] Okamoto et al. (2010) *Geochim. Cosmochim. Acta*, **74**, 3692-3706.
- [3] Saishu et al. (2012) *Am. Min.*, **97**, 2060-2063.
- [4] Doi et al. (1998) *Geothermics*, **27**, 663-690.
- [5] Saishu et al. (in press) *Terra Nova*.

Keywords: Silica precipitation, Hydrothermal experiment, Kinetic equation, Nucleation, Permeable-impermeable boundary

## Sedimentary pore-fluid origin of H<sub>2</sub>O-rich fluid in mantle wedge revealed by halogens and noble gases

KOBAYASHI, Masahiro<sup>1\*</sup>; SUMINO, Hirochika<sup>1</sup>; NAGAO, Keisuke<sup>1</sup>; ISHIMARU, Satoko<sup>2</sup>; ARAI, Shoji<sup>3</sup>; YOSHIKAWA, Masako<sup>4</sup>; KAWAMOTO, Tatsuhiko<sup>4</sup>; KUMAGAI, Yoshitaka<sup>4</sup>; KOBAYASHI, Tetsuo<sup>5</sup>

<sup>1</sup>GCRC, Univ. Tokyo, <sup>2</sup>Dept. Earth Environ. Sci., Kumamoto Univ., <sup>3</sup>Dept. Earth Sci., Kanazawa Univ., <sup>4</sup>Inst. Geothermal Sci., Kyoto Univ., <sup>5</sup>Dept. Earth Environ. Sci., Kagoshima Univ.

H<sub>2</sub>O plays an important role in mantle processes in subduction zones. Yet its subducting processes to the mantle remain unknown because of scarcity of direct observations of H<sub>2</sub>O in mantle-derived materials. Since halogen and noble gas are strongly partitioned into fluids and they show distinct elemental and/or isotopic ratios depending on their origins, their compositions in mantle rocks can provide complementary constraints on the behavior and origin of H<sub>2</sub>O in the mantle. Although only few researches have been conducted, the subduction of halogens and noble gases derived from sedimentary pore fluids (seawater trapped in pores of deep-sea sediments) has been suggested. Pore fluid-like halogens and noble gases were found in mantle wedge peridotites which captured H<sub>2</sub>O-rich fluids just above a subducting slab [1]. H<sub>2</sub>O-rich fluid inclusions whose salinity is similar to that of pore fluids (salinity of pore fluids is the same level as that of seawater [2]) are found in a mantle xenolith from a subduction zone [3]. We investigated halogen and noble gas compositions of mantle wedge peridotites from subduction zones to better constrain how far the influence of subducted sedimentary pore fluids extends into the mantle.

The samples studied are harzburgitic xenoliths from the Avacha volcano in Kamchatka and the Pinatubo volcano in the Philippines, and alpine-type peridotite from the Horoman massif in Japan. H<sub>2</sub>O-rich fluid inclusions have been found in olivine of those mantle peridotites [3,4,5].

We applied the noble gas method, in which halogens (Cl, Br, and I) are converted to corresponding isotopes of Ar, Kr, and Xe by neutron irradiation in a nuclear reactor and then the concentrations of noble gas isotopes are determined by noble gas mass spectrometry. Halogen detection limits of this method are from two to five orders of magnitude lower than conventional method, which enable to determine the low halogen abundances in mantle-derived materials. By crushing samples under ultra-high vacuum, noble gases are selectively extracted from H<sub>2</sub>O-rich fluid inclusions. Unirradiated peridotites were also analyzed to obtain precise noble gas isotope compositions.

The halogens of all peridotites are heavily enriched in I, although the halogen ratios are distinctive in each locality. These high I/Cl ratios show a strong contribution of sedimentary pore fluids [2]. The noble gases except for He have the elemental and isotopic ratios similar to elementally fractionated atmospheric noble gases dissolved in seawater, which is probably equivalent to those dissolved in sedimentary pore fluids. The <sup>3</sup>He/<sup>4</sup>He ratios are similar to that of the mantle and distinctly higher than the atmospheric ratio. This indicates that the fluids derived from subducting slabs acquired He from the ambient mantle, where He is much more enriched than in seawater.

These pore fluid-like halogen and noble gas signatures are strong evidence that the H<sub>2</sub>O-rich fluids in the studied peridotites are derived from sedimentary pore fluids and transported to the mantle.

References: [1] Sumino *et al.* (2010) *EPSL* **294**, 163. [2] *e.g.* Muramatsu *et al.* (2007) *Appl. Geochem.* **22**, 534. [3] Kawamoto *et al.* (2013) *PNAS* **110**, 9663. [4] Ishimaru *et al.* (2007) *J. Petrol.* **48**, 395. [5] Arai & Hirai (1985) *Nature* **318**, 276.

Keywords: water, halogen, noble gas, subduction zone, mantle, peridotite

## Relations among temperature, dehydration of the PHS plate, and a large earthquake, a SSE, and LFEs in the Tokai district

SUENAGA, Nobuaki<sup>1\*</sup> ; YOSHIOKA, Shoichi<sup>2</sup> ; MATSUMOTO, Takumi<sup>3</sup>

<sup>1</sup>Graduate School of Science, Kobe Univ., <sup>2</sup>RCUSS, Graduate School of Science, Kobe Univ., <sup>3</sup>NIED

In this study, we performed numerical simulations of temperature distribution at the plate boundary and estimated the dehydration process of hydrous mid ocean ridge basalt (MORB) in the oceanic crust in the Tokai district, central Japan. We discuss the relationships among temperature, dehydration, and a future megathrust earthquake, deep low-frequency earthquakes (LFEs), and a slow slip event (SSE). Our results identified a strongly coupled region for an expected megathrust Tokai earthquake based on temperature conditions at the plate boundary. The depth range of the plate boundary where the megathrust earthquake may occur is 9~21 km, narrowing toward the east. An SSE is estimated to have occurred in the transition zone between unstable and stable sliding. Hypocentral depths of LFEs deviating from the isodepth contours of the Philippine Sea plate toward the east may be explained by differences in the dehydration process associated with phase transformations in hydrous MORB.

Keywords: 2-D thermal modeling, megathrust earthquake, low-frequency earthquake (LFE), slow slip event (SSE), temperature, dehydration from hydrous MORB

## The regional and single-vein scale distribution of the CO<sub>2</sub> fluids in the Shimanto accretionary complex, Muroto area, SW

MUSHA, Michimasa<sup>1\*</sup>; TSUCHIYA, Noriyoshi<sup>1</sup>; OKAMOTO, Atsushi<sup>1</sup>

<sup>1</sup>Environmental Studies of Tohoku University

Carbon dioxide and methane are major carbonic components of the fluids in the crust. The crustal fluids generally have composition of C-H-O system, mainly composed of H<sub>2</sub>O, CO<sub>2</sub>, and CH<sub>4</sub>, and they may be carried down into Earth's interior at subduction zones. Many studies have examined fluid components in various accretionary prisms under low-grade metamorphic conditions, and CH<sub>4</sub> is showed as the only carbonic species. Therefore, there is little information on the variation of the components of C-H-O fluids in subduction zones.

The Tertiary (Paleogene and Neogene system) Shimanto belt, southwest in Japan, is one of the best-studied ancient accretionary complexes. The Muroto Peninsula belongs to the Tertiary Shimanto belt, and it is mainly composed of sandstones, mudstones and conglomerates with small amount of basalt. Mineral veins were mainly composed of quartz, with small amount of calcite near the vein walls, while many studies have showed CH<sub>4</sub> is the only carbonic component in the Shimanto belt, therefore it is unclear why calcite precipitated in the veins in absence of CO<sub>2</sub>. Lewis (2000) reported the fluid inclusions of CH<sub>4</sub> and CO<sub>2</sub> mixture at one area in the Muroto Peninsula, but the extensive distribution of CO<sub>2</sub> fluids in the whole peninsula is not clear. In this study, we examined the distribution of C-H-O fluids from the Muroto Peninsula, as fluid inclusions in the mineral veins, using microthermometry and Laser Raman spectroscopy, in regional scale and single vein scale.

Fluid inclusions from quartz in the veins are composed of one-phase carbonic inclusions (only CH<sub>4</sub>) and two-phase aqueous inclusions (carbonic vapor and H<sub>2</sub>O liquid). Carbonic components of the vapor phase in the two-phase inclusions are gradually transitioned from CH<sub>4</sub>-dominant in the north area of the belt to a CO<sub>2</sub>?CH<sub>4</sub> mixture in the south; the CO<sub>2</sub>/(CO<sub>2</sub> + CH<sub>4</sub>) ratio in mole fraction ( $X_{CO_2}$ ) vary from 0 ~0.3 in the north area to 0 ~0.9 in the south.

In single vein scale, we examined single CO<sub>2</sub>-bearing vein from the south area of the Peninsula, where  $X_{CO_2}$  is 0 ~0.8. The CO<sub>2</sub> ratio in the carbonic species is decreased from the vein wall ( $X_{CO_2} = 0.5$ ?0.8) to the vein center, in which carbonic species in the fluids is only CH<sub>4</sub> ( $X_{CO_2} = 0$ ). The existence of CO<sub>2</sub> only near the vein walls is in good agreement of the precipitation of calcite near the vein walls. The homogenization temperature increases from ~180 °C to 240?250 °C, indicating the transition of the carbonic species from CO<sub>2</sub>?CH<sub>4</sub> to CH<sub>4</sub> during vein formation.

The dominant species of carbonic species in most accretionary prisms is CH<sub>4</sub> under low-grade metamorphic conditions, and thermodynamic calculation about equilibrium in the C-H-O fluids also shows that CH<sub>4</sub> is dominant carbonic species in the equilibrium with graphite under the P?T conditions of formation of the CO<sub>2</sub>-bearing veins (235?245 °C, 165?200 MPa). The CO<sub>2</sub>-fluids are preferentially distributed close to an out-of-sequence thrust that brings the Muroto sub-belt into contact with the late Oligocene?early Miocene Nabae sub-belt with its many volcanic lavas and intrusive rocks. Therefore, the CO<sub>2</sub>-fluids were considered to be magmatic-origin, and that the fluids were injected and mixed with the CH<sub>4</sub>-pore-fluids of the sediments in the accretionary prism in the timing of formation of CO<sub>2</sub>-bearing veins.

Keywords: fluid inclusions, accretionary complexes, calcite, mineral veins, C-H-O fluid, Shimanto belt

## Visualization of deep-seated fluid flow in Tokusa Basin, Yamaguchi Prefecture

NISHIYAMA, Nariaki<sup>1\*</sup>; TANAKA, Kazuhiro<sup>2</sup>; SUZUKI, Koichi<sup>3</sup>

<sup>1</sup>Yamaguchi University, <sup>2</sup>Yamaguchi University, <sup>3</sup>Central Research Institute of Electric Power Industry

It is known that highly saline fluids spout out in spite of inland area in Japan (Sakai et al. 1978). These fluids spout out not only at the surface of the ground surface but also at the flowing borehole. However, the erupted region of ascending fluid from flowing borehole and its relationship to the geological structure is not identified. Electromagnetic surveys applying Controlled Source Audio-frequency Magneto-Telluric Method was carried out in the Tokusa basin, Yamaguchi Prefecture to obtain the two dimensional distribution of resistivity to clarify the geological structure and the distribution of deep-seated fluid.

The study area is consisted of the Late Cretaceous welded tuff, rhyolitic lava, and the Holocene sediments. Low resistivity zone continuously is distributed along the Tokusa-Jifuku fault (Sagawa et al, 2008) in bedrock more than 2.5km long and is distributed in north side of the fault in sediments like a tongue shape. Resistivity of erupted highly saline water corresponds to that obtained by CSAMT. Groundwater of the shallow wells drilled in the sediments shows the NaCl type. Therefore, low resistivity zone in the sediments corresponds to the highly saline water diluted by surface groundwater. As a result, deep-seated fluid in the Tokusa basin rises along the Tokusa-Jifuku fault in the basement rock and then flows to river subjected to the dilution by surface groundwater.

Keywords: Deep-seated fluid, CSAMT method, Tokusa-Jifuku fault, Groundwater flow

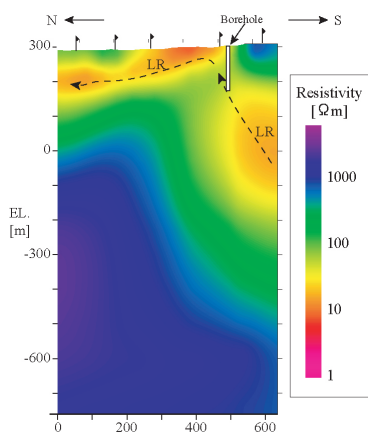


Fig.1 The resistivity profile by the CSAMT survey.

## Can clay minerals account for the non-asperity on the subducting plate interface?

KATAYAMA, Ikuo<sup>1\*</sup> ; KUBO, Tatsuro<sup>1</sup> ; SAKUMA, Hiroshi<sup>2</sup> ; KAWAI, Kenji<sup>3</sup>

<sup>1</sup>Department of Earth and Planetary Systems Science, Hiroshima University, <sup>2</sup>National Institute for Materials Science, <sup>3</sup>Department of Earth and Planetary Sciences, Tokyo Institute of Technology

Seismicity along the subducting plate interface shows a regional variation, in which large earthquakes occur repeatedly at the strongly coupled patches that are surrounded by weakly coupled regions. This model suggests that the subduction plate interface is heterogeneous in terms of frictional properties; however, mechanism making the difference in strong and weak coupling is still not well understood. We consider this difference to relate to the alternation of plate interface due to aqueous fluids that result in the spatial distribution of clay minerals. In this study, we measured the frictional healing of clay minerals and discuss whether the frictional properties of clays can account for the weakly coupled non-asperity regions in the subducting plate interface.

We carried out a series of slide-hold-slide frictional experiments to examine the time-dependent frictional restrengthening of the simulated fault gouge. In the experiments, the axial loading was interrupted for periods ranging 10 to 3000 s after steady-state friction, and we measured the difference between the steady-state friction and the peak friction after each holding period. Mechanical data were recorded continuously with a sampling rate of 10 Hz and the frictional coefficient was calculated from the shear force divided by the normal force assuming zero cohesion.

The preliminary results show that the frictional strength of clay minerals (smectite and chlorite) slightly increases with holding time; however, the healing rate is significantly smaller than that of dry silicates such as quartz. Similar weak healing rate has been reported in the serpentized simulated faults (Katayama et al., 2013). These experimental results suggest that the recovery of fault strength is different in materials, in which clay minerals show weak and slow recovery whereas dry materials show relatively quick and thereby strong coupling on the fault surface. Aqueous fluids that are released from the descending plate may change the mineralogy on the plate interface where clay minerals become dominant at the channel of fluid flow surrounding the unaltered dry patches that potentially act as a seismic asperity. Thus, the heterogeneous fluid pathway and spatial distribution of clay minerals may play a key role for the formation of asperity and non-asperity on the subducting plate interface.

Keywords: Interplate earthquake, Asperity, Clay minerals, Frictional experiment, Frictional healing

## Oxidation state of arc primary magma-inferred from sulfur speciation of melt inclusions

SHIMIZU, Kenji<sup>1\*</sup>; KASHIWABARA, Teruhiko<sup>1</sup>; TAMENORI, Yusuke<sup>2</sup>

<sup>1</sup>JAMSTEC, <sup>2</sup>JASRI, SPring-8

Oxidation state of arc magmas highly influences the chemical behaviors of redox sensitive elements such as chalcophile and some siderophile elements in subduction zone. Therefore, Oxidation state of arc magmas is essential to understand arc magma geneses and evolutions of ore deposits. It has been suggested that sub-arc mantle is oxidized by subducted materials such as fluid, sediments and oceanic crust. However, recent studies contradicted that the oxidation state of primary arc magma (sub-arc mantle) is similar to the average upper mantle and oxidation is caused by differentiation associated with crystallization and interaction within preexisting crust (e.g. Lee et al., 2012, Science, v336, p64).

In order to constrain oxidation state of primary arc magmas at an immature subduction zone, we have analyzed  $S_{6+}/\Sigma S$  of boninitic and tholeiitic melt inclusions within Cr-spinel from Bonin Islands and Guam by soft X-ray microbeam at SPring-8/BL27SU. Boninite in Bonin Islands uniquely formed at the early stage of subduction formation (~50 Ma) by melting of highly depleted hydrous mantle and 0-7 myrs later, related arc tholeiites erupted in southern Bonin Islands and Guam by melting of depleted mantle (Ishizuka et al., 2011, EPSL, v306, p229). Compositions of melt inclusions fully cover compositional ranges of whole-rocks and some boninitic melt inclusions have MgO higher than 20 wt%, showing that they are very primitive magmas.  $S_{6+}/\Sigma S$  of boninitic and tholeiitic melt inclusions are 0.57 to 0.78 and 0.47 to 1, respectively;  $S_{6+}/\Sigma S$  of all high-MgO (7 to 12 wt%) tholeiitic melt inclusions are >0.9. Oxygen fugacities of primary boninite and tholeiite are estimated to be  $\Delta FMQ >+1$  and  $>+1.5$ , respectively by experimental results of Jugo et al. (2010, GCA, v74 p5926), indicating that sub-arc mantle is oxidized even at an early stage of subduction zone. Between the period of eruption of boninite and tholeiite, not only mantle sources but also the subducting component in term of oxidation state of sub-arc mantle may have changed.

Keywords: melt inclusion, boninite, arc, sulfur

## Evaluating slab-fluid contribution into inhomogeneous mantle source: geochemical variation of Central and East Java arc

HANDINI, Esti<sup>1\*</sup> ; HASENAKA, Toshiaki<sup>1</sup> ; WIBOWO, Haryo edi<sup>2</sup> ; SHIBATA, Tomoyuki<sup>3</sup> ; MORI, Yasushi<sup>4</sup> ; HARIJOKO, Agung<sup>2</sup>

<sup>1</sup>Graduate School of Science and Technology, Kumamoto University, <sup>2</sup>Geological Engineering, Gadjah Mada University, <sup>3</sup>Institute for Geothermal Sciences, Kyoto University, <sup>4</sup>Kitakyushu Museum of Natural History and Human History

The spatial distribution of the volcanoes in Central and East sections of Java arc denotes the widest and the narrowest of Java Island. Central Java section corresponds to the largest range and depth of Wadati-Benioff Zone along the island (180-360 km), whereas East Java section shows the narrowest range (190-220 km). However, both sections equally show wide geochemical variation with the function of slab-depth. Both also mark the appearance of the rear-arc alkaline suites in a different slab depth (360 km for Central Java, and 220 km for East Java). Geochemical datasets of basalt to basaltic andesite (further screened on Zr/Nb basis) from these sections were compiled to evaluate the contributions of slab-derived fluid to the mantle sources, and to assess the possible mantle sources of these magmas.

We group the lavas of the Central and East Java into two series: (1) the volcanic front series (VF), calc-alkaline suites of frontal- and middle-arc region volcanoes of Central and East Java, and (2) the rear-arc series (RA) consists of alkaline suites from Central and East Java (Muria, and Ringgit-Beser and Lurus, respectively). The VF series consistently shows typical island arc geochemistry, with strong LILE enrichment (Sr, Ba, Pb, and Rb) relative to HFSE. The RA series, mainly Muria, indicate stronger enrichment of LILE than other volcanoes closer to the trench. Ringgit-Beser and Lurus, the rear-arc lavas of East Java, behave differently in LILE enrichment. Ringgit-Beser lavas shows stronger LILE enrichment than that of lavas from Lurus, within the same enrichment range of Muria lavas. In the other hand, Lurus lavas are showing obvious HFSE depletion compared to OIB. The decreasing trend of LILE/HFSE and LILE/LREE (e.g. Ba/Nb, Ba/La, Pb/Ce, Pb/Nb) is observed across both Central and East Java sections. These ratios become lower toward the rear-arc of both sections, and the lowest in the rear-arc of Central Java. In various normalized plots (such as Nb vs. Ba/Nb), the VF series are plotted within the range of typical island arc basalts (IAB). Muria lavas, the rear-arc alkaline suite of the Central Java, resemble OIB and other non-arc type alkaline rock characteristics, but with positive indications of being island arc, such as negative Nb and Ti anomalies. Ringgit-Beser and Lurus alkaline lavas of East Java, however, are associated with other arc-type alkaline rock characteristics, with stronger signature of island arc than Muria.

Our analyzed samples show that lavas from East Java are closer in compositions to primitive magmas compared to Central Java's. The thicker overriding crust beneath Central Java than East Java possibly acts as the magma retainer that allows extensive fractionation. Across-arc variation of slab-derived fluid in both sections are observed as shown by decreasing LILE/HFSE and LILE/LREE toward rear-arc, suggesting the decreasing amount of slab-fluid added to the great slab-depth. The slab-fluid added to the volcanic front of East Java is slightly higher than that of Central Java, which may be controlled by the narrow range of slab dehydration area in the former that allows more fluid to concentrate. The low ratio of these trace elements in the rear-arc of both sections suggests that these parts have also been affected by dehydration of subducted slab. The stronger slab-fluid contributions in the rear-arc alkaline lavas of East Java than that of Central Java may reflect the role of shallower slab depth. Different mantle characteristics between the rear-arc of Central and East Java may reflect several possibilities: (1) the inhomogeneous mantle plume (E-type/EMI) beneath both sections, or (2) stronger EMI-type mantle contribution to Central Java than to East Java, or (3) the combination of both.

**Keywords:** Sunda arc, slab-derived fluid, across- and along-arc variations, trace elements

## Reaction progress and porosity change in hydrothermal alternation at Olivine/Quartz boundary

OYANAGI, Ryosuke<sup>1\*</sup>; OKAMOTO, Atsushi<sup>1</sup>; TSUCHIYA, Noriyoshi<sup>1</sup>

<sup>1</sup>Graduate School of Environmental Studies, Tohoku University

Serpentinization in oceanic lithosphere is a fundamental process to bring water into deep earth's interior. It is known that silica activity controls the reaction paths during the hydrothermal alternation of peridotites [e.g. 1,2], however the detailed reaction mechanism induced by silica transport is poorly understood. In this study, we conducted hydrothermal experiments in olivine (Ol)-quartz (Qtz)-H<sub>2</sub>O system for investigating the mechanism of silica metasomatism at crust/mantle boundary.

Composite powders, which was composed of Qtz zone and Ol zone was set in inner tubes, with diameters of 1.7 mm and heights of 50 mm, and then loaded into autoclave with alkaline solution (NaOH, aq, pH = 13.8 at 25 °C). Temperature and pressure are 250 °C and vapor-saturated pressure (= 3.98 MPa), respectively. After the experiments, the inner tube was cut into ten segments to evaluate the reaction progress as a function of the distance from Ol/Qtz boundary (hereafter denoted X), by Thermogravimetry and XRD. In order to evaluate the spatial variation of the reactions, the area of each minerals (olivine and reaction products) and pore was measured from the back-scattered electron (BSE) images of the thin section.

After 46 days, the H<sub>2</sub>O content near the Ol/Qtz boundary is lower (3.9 wt.% H<sub>2</sub>O) than that in (12 wt.%) at the margin of the reaction tube. The reaction products after olivine changed systematically as away from Ol/Qtz boundary from smectite+serpentine zone to the serpentine+brucite zones. In the smectite+ serpentine zone, the (Mg+Fe)/Si ratio of the products increases from 0.5 to 1.5, indicating that proportion of serpentine with respect to smectite increased away from the boundary. With increasing time, the smectite+ serpentine zone was enlarged, where as the serpentine+brucite zones was retreated.

Based on the combined analyzes of BSE images, TG and SEM-EDS, we obtained the reaction progresses of individual elementary reactions between 25 and 46 days as follows:

(1) In the smectite+ serpentine zone, smectite was formed via hydration of olivine and dehydration of serpentine by supply of silica. As the result, overall reaction has a variation in the smectite+ serpentine zone;  $\Delta mH_2O$  is negative (hydration) at X=0-4 mm, it is positive (dehydration) at X=4-10 mm. Volume expansion factor (V/V<sub>0</sub>) is much higher (=1.4) at Ol/Qtz boundary than other zones (=1.1), mainly due to Si-metasomatic reaction.

(2) Far from the Ol/Qtz boundary (X = 20-40 mm), there is no influence of silica supply, indicating that silica was completely consumed in the smectite+ serpentine zone. In these area, serpentinization proceeds as the typical olivine hydration reaction to produce brucite and serpentine with constant Srp/Brc ratio.

(3) In the transient zone, serpentine was formed by two ways: hydration of olivine and dehydration of brucite by supply of silica. These two serpentine forming reaction resulted in a large amount of serpentine in this area, and high volume expansion factor (=1.4).

Due to these two volume expansion reactions, low porosity (~5%) area developed locally, never-theless porosity of other area is 30%. The amount of silica ( $\Delta mSiO_2$ , aq), which consumed from 25 to 46days, is largest at Ol/Qtz boundary, and monotonically decreases with increasing distance. If excess silica are available, the zones affected by silica will increase gradually with increasing time during hydrothermal alteration around mantle/crust boundary. In contrast, the porosity has a minimum around X = 15 mm in the transition zone, because Ol-hydration and Brc-dehydration reaction proceed with large volume expansion. Such volume expansion reaction and mineral changes causes the mechanical strength of boundary.

### References:

- [1] Frost, B. R., & Beard, J. S. (2007). *Journal of Petrology*, 48(7), 1351-1368.
- [2] Ogasawara, Y., Okamoto, A., Hirano, N., & Tsuchiya, N. (2013). *Geochimica et Cosmochimica Acta*, 119, 212-230.

Keywords: serpentinization, ultramafic rock, Si-metasomatism, Hydrothermal alternation

## Distribution and transportation of melt in subduction zones

ISHII, Kazuhiko<sup>1\*</sup>

<sup>1</sup>Graduate School of Sciences, Osaka Prefecture University

Volcanic and seismic activities in subduction zones are the result of complex interaction of geophysical and geochemical processes. I have investigated the hydration and dehydration and the generation and transportation of melt in subducting slab and adjacent mantle wedge using a numerical model. The model includes hydration and dehydration of the slab and mantle wedge, melting and solidification of mantle peridotites, permeable flow of melt and aqueous fluids, and solid flow of mantle peridotites with water- and melt-induced weakening. The model shows the melt distribution in the mantle wedge beneath the volcanic front and extending sub-parallel with the subducting slab. The detailed geometry of the melt distribution is strongly dependent on the parameters including water solubility of peridotites and permeable flow velocities of melt and aqueous fluids. I will discuss the effect of these parameters on the melt distribution and the interdependence among the geodynamic processes in the subduction system.

Keywords: subduction zones, melt, distribution and transportation

## Effects of mineral grain size variation on fluid migration in the mantle wedge

WADA, Ikuko<sup>1\*</sup> ; BEHN, Mark D.<sup>2</sup>

<sup>1</sup>IRIDeS, Tohoku University, <sup>2</sup>Woods Hole Oceanographic Institution, USA

In this study, we investigate the effect of mineral grain size on the migration paths of aqueous fluids in the mantle wedge. Grain size is an important parameter that controls the grain-scale permeability of the mantle; in general, the smaller the grain size, the less permeable the mantle is, provided that the pores between grains are connected. The migration paths of aqueous fluids are therefore dependent on the grain size distribution, influencing the location and the degree of hydrous melting in the mantle wedge and the location of arc volcanism. We develop a 2-D fluid migration model with generic subduction zone geometry. In the model, we adopt grain size distributions calculated by coupling a subduction zone thermal model with a laboratory-derived grain size evolution model for a range of subduction parameters (Wada et al., 2011). The fluid migration model also includes the effects of mantle flow velocities and mantle-flow-induced pressure gradients, both of which are also calculated from the thermal model. The calculated grain size immediately above the slab is on the order of 10<sup>2</sup>-100 micrometers beneath the forearc region, depending on the slab thermal structure, and it increases down-dip to a few cm beneath the arc region. Our preliminary modeling results with a simplified fluid influx pattern indicate that the aqueous fluids tend to become trapped in the down-going mantle due to low permeability and dragged down-dip until permeability becomes high enough for the fluids to migrate upward. Grain size above a colder slab tends to be smaller than that above a warmer slab, and therefore fluids become dragged down-dip further in a cold-slab subduction zone than in a warm slab subduction zone. A colder slab also tends to release fluids at deeper depths than a warmer slab, influencing the pattern of fluid influx into the mantle wedge. In this study, we calculate the fluid influx along the base of the mantle wedge, using the thermal modeling results and thermodynamic calculations based on *Perple\_X*, and quantify fluid migration in the mantle wedge with the grain size and fluid influx distributions that are consistent with a given slab thermal structure.

Keywords: subduction zone, mantle wedge, aqueous fluid migration, grain size, slab dehydration, arc volcanism

## Temperature dependence of seismic velocities in a antigorite serpentinite at 1 GPa

SHIRAI, Ryo<sup>1\*</sup> ; WATANABE, Tohru<sup>1</sup> ; YONEDA, Akira<sup>2</sup> ; MICHIBAYASHI, Katsuyoshi<sup>3</sup>

<sup>1</sup>Department of Earth Sciences, Faculty of Science, University of Toyama, <sup>2</sup>Institute for Study of Earth's Interior, Okayama University, <sup>3</sup>Institute of Geosciences, Shizuoka University

Serpentines play key roles in subduction zone processes including water transport, seismogenesis, exhumation of high-pressure rocks, etc. Geophysical mapping of serpentized regions in the mantle wedge leads to further understanding of these processes. Seismic properties of serpentized peridotites are critical to interpretation of seismological observations. Antigorite is a major form of serpentine, which is stable to higher temperatures. The single-crystal elastic properties were recently revealed via Brillouin scattering technique (Bezacier et al., 2010; 2013). However, the temperature dependence of elastic properties is still poorly understood. We have measured elastic wave velocities in a antigorite serpentinite at high temperature and pressure conditions.

A black massive antigorite serpentinite was collected from the Nagasaki metamorphic rocks, western Japan. It is composed of antigorite (98.0 vol.%), diopside (1.5 vol.%) and magnetite (0.5 vol.%). Microstructural observation reveals an interpenetrating texture characterized by randomly oriented antigorite blades. Antigorite CPO data shows weak concentration of antigorite axes. Elastic wave velocities measured at 180 MPa shows very weak anisotropy in elasticity. Cylindrical samples (D=L=6mm) were made with ultrasonic machining.

Measurements were made at the pressure of 1 GPa and the temperature of up to 550 C, by using a piston-cylinder type high pressure apparatus at ISEI, Okayama University. The pulse reflection technique was employed for velocity measurement. One LiNbO<sub>3</sub> transducer with the resonant frequency of 5 MHz was used to transmit and receive ultrasonic signals. The length of the sample at high pressure and temperature conditions was estimated from the length of the recovered sample.

Both compressional and shear wave velocities linearly decrease with increasing temperature. The temperature derivatives are  $-3.6 \times 10^{-4}$  (km/s/K) and  $-2.7 \times 10^{-4}$  (km/s/K) for compressional and shear wave velocities, respectively. The temperature derivative of compressional wave velocity is close to that observed in the direction subparallel to antigorite *c*-axis (Yano et al., in prep.). The temperature dependence of *c*<sub>33</sub> might dominate that of the effective elastic constants of a randomly oriented polycrystalline aggregate. Applications to seismological observations will also be discussed in this presentation.

Keywords: seismic velocity, serpentinites, antigorite, subduction zone, fluid

## Detection of structured water on quartz interface by Raman-FTIR spectroscopy and its evaluation by molecular dynamics

ISHIKAWA, Satoru<sup>1\*</sup> ; SAKUMA, Hiroshi<sup>2</sup> ; TSUCHIYA, Noriyoshi<sup>1</sup>

<sup>1</sup>Graduate School of Environmental Studies, Tohoku University, <sup>2</sup>National Institute for Materials Science

Molecular structure of water in thin film shows different characteristics compared with that of free water. Thin film water was observed at mineral grain boundaries, and its structure might be influenced by mineral surface.

High temperature-pressure cell for micro-Raman and Fourier-transform infrared (FT-IR) spectroscopy have been developed to investigate molecular structure of thin film water at high temperature and pressure conditions. As a result of micro-Raman and FT-IR spectroscopic measurements of water, the broad peak around  $3400\text{ cm}^{-1}$ , attributed to OH stretching vibration mode of water molecular, was observed at ambient temperature and pressure. The broad peak shifted to higher wavenumber with increasing temperature on metal reflector. Compared with the result of IR properties of water on metal reflector, IR properties of water on artificial quartz surface exhibit different trend: the broad peak contained the peak component of the lower wavenumber (around  $3200\text{ cm}^{-1}$ ), even at high temperature.

In addition, molecular dynamics simulations were performed under the conditions of the experiment using MXDORTO. In the simulation, the water of a few nanometers of quartz near the surface was structured. The distribution of water density was different from the free water. These properties are discussed in the hydrogen bond between water molecular and silanol (Si-OH) of quartz.

Keywords: Raman spectroscopy, IR spectroscopy, interfacial water, subcritical, quartz, molecular dynamics

## Generation process of brecciated marble at Hiraodai karst, Kyushu, Japan

ISHIYAMA, Saya<sup>1\*</sup> ; ANDO, Jun-ichi<sup>1</sup> ; NAKAI, Shun'ichi<sup>2</sup> ; OTA, Yasuhiro<sup>3</sup> ; DAS, Kaushik<sup>1</sup>

<sup>1</sup>Department of Earth and Planetary Systems Science, Hiroshima University, <sup>2</sup>Earthquake Research Institute, the University of Tokyo, <sup>3</sup>Kitakyushu Museum of Natural history & Human history

Geofluid is believed to be closely related to the seismic and volcanic activities. However, the detail relationship of geofluids with seismicity and volcanic activity is not studied properly through geological observations. We have found recently the brecciated marble widely distributed at Hiraodai karst plateau, Fukuoka Pref. This brecciated marble offers unique opportunity to study the relationship between geofluid and seismicity. Here, we shall explore the generation process of this brecciated marble through geological, microstructural and geochemical methods using polarization microscope, SEM, TEM, EPMA, microthermometric and MC-ICP-MS techniques.

The marble in Hiraodai karst plateau was thermally metamorphosed due to Cretaceous Hirao granodiorite intrusion. The brecciated marble occupies about 0.7 km x 1km of area in the central part of the karst. The main results of the present study are as follows.

- 1) The brecciated marble is composed of the rock fragments with variety of sizes ranging from millimeter to meter scale, and having angular to rounded shapes.
- 2) Numerous fluid inclusions are observed in the thin section of the brecciated marble.
- 3) TEM observation shows that the dense tangled dislocations are formed in calcite grains of the brecciated marble.
- 4) The homogenization and freezing temperatures of the fluid inclusions are about 240 deg C and 0 deg C, respectively.
- 5) The whole-rock and mineral separates (biotite and plagioclase) of Hirao granodiorite yields Rb-Sr isochron age of 129.4 +/- 2.4 Ma. Interestingly, Rb-Sr data of the fluid inclusions also lie on the Rb-Sr isochron of Hirao granodiorite.

The above-mentioned results of 1) and 2) suggest that the brecciation occurred by fluid infiltration and that the fragments were moved and rotated at very high speed. The result 3) demonstrates that the calcite grains of the brecciated marble experienced high stress. These three results together indicate that the brecciation process might generate seismic wave. On the other hand, the results of 4) and 5) suggest that the possible origin of the fluid inclusion is the released fluid from the Hirao granodiorite magma. Therefore, the brecciation of marble distributed at Hiraodai karst plateau was probably generated by magmatic fluid from Hirao granodiorite under high stress condition at 129.4 +/- 2.4 Ma ago.

Keywords: Brecciated rock, Hiraodai karst, Hirao granodiorite, Fluid inclusion, Rb-Sr isotope

## Equation of state of topaz-OH in the subducted sediment under high pressure and high temperature

NIIZATO, Mizuki<sup>1\*</sup>; INOUE, Toru<sup>2</sup>; CAI, Nao<sup>2</sup>; SUENAMI, Hideki<sup>2</sup>; KAKIZAWA, Sho<sup>2</sup>

<sup>1</sup>Department of Earth Sciences, Ehime University, <sup>2</sup>Geodynamics Research Center, Ehime University

Dehydration reactions of hydrous minerals in the subducted sediment produce a H<sub>2</sub>O-rich fluid which causes generations of magma, decreases of melting temperature of sediment, and variations of magma compositions. Topaz-OH [Al<sub>2</sub>SiO<sub>4</sub>(OH)<sub>2</sub>], which is one of hydrous minerals, is considered to be existed in the sediment of the subducting slab. Topaz-OH is the end-member of natural topaz [Al<sub>2</sub>SiO<sub>4</sub>(OH,F)<sub>2</sub>]. The stability field of topaz-OH extends to 1500 degree C at 5-10 GPa (Wunder *et al.*, 1993; Ono, 1998; Schmidt *et al.*, 1998). The equation of state (EoS) for the natural topaz has been also estimated (Komatsu *et al.*, 2003; Gatta *et al.*, 2003). However, the EoS of the end-member topaz-OH has not been performed yet. In this study, we performed *in situ* X-ray diffraction (XRD) experiments under high pressure and high temperature for determining the thermal elastic properties of topaz-OH.

The starting material of topaz-OH was synthesized at 10 GPa and ~1000 degree C from the quench experiment using multi-anvil apparatus. The high pressure (3-8 GPa) and high temperature (up to 800 degree C) *in situ* XRD experiments were carried out using MAX80 installed at beam-line NE5C at PF-AR, KEK, Japan. These XRD patterns were collected by the energy dispersive method. Thermal elastic properties were calculated from EoS fit v5.2 software (Angel, 2000) using 3rd order Birch-Murnaghan EoS.

From *in situ* XRD experiments, we successfully determined thermal elastic properties using all-data for fixed K'=4 as below: V<sub>0</sub>=354.7(1) Å<sup>3</sup>, K<sub>0</sub>=169.8(22)GPa, (dK<sub>T</sub>/dT)<sub>P</sub>=-0.013(7) GPaK<sup>-1</sup>, a<sub>0</sub>=1.61(23)×10<sup>-5</sup>K<sup>-1</sup>, b<sub>0</sub>=1.36(41)×10<sup>-8</sup>K<sup>-2</sup>. From the detailed analysis of compression data, we found the change of the compression properties near 7 GPa. This change was also seen in a- and b-axis. Therefore we re-calculated the thermal elastic properties using two data sets: (I) below 7 GPa (II) above 7 GPa at room temperature. These calculation results from low pressure data show V<sub>0</sub>=355.2(1) Å<sup>3</sup>, K<sub>0</sub>=160.1(2)GPa, however those from the high pressure data show V<sub>0</sub>=356.5(9) Å<sup>3</sup>, K<sub>0</sub>=153.1(89) GPa (K'=4 fixed). Compared to the natural topaz, topaz-OH shows relatively large volume and bulk modulus. This shows that the volume and bulk modulus increase with increasing OH content. Compared bulk modulus with density, topaz-OH locates near the line for Birch's law and indicates large bulk modulus and density as same as Phase D [Mg<sub>2</sub>SiO<sub>4</sub>(OH)<sub>2</sub>]. We suggest that high density topaz-OH enhances the slab subduction and transports water to deeper earth's interior.

Keywords: topaz-OH, high pressure hydrous phase, subducting slab, equation of state, synchrotron X-ray in-situ experiment

## Water content in arc basaltic magma in northeast Japan and Izu-Mariana arc estimated from melt inclusions in olivine and

USHIODA, Masashi<sup>1\*</sup>; IKEGUCHI, Naoki<sup>1</sup>; TAKAHASHI, Eiichi<sup>1</sup>

<sup>1</sup>Dept. Earth and Planetary Sciences, Tokyo Institute of Technology

Primitive arc basalt magma is generated by partial melting of sub-arc mantle with adding aqueous fluid which was derived from dehydration of subducting slab. Aqueous fluid has profound effects on melting temperature of the mantle, crystallization pathways of generated magmas, and explosivity of magmas. Precise estimation of H<sub>2</sub>O content in arc basalt magma is important to evaluate the effect of water on generation, differentiation, and eruption of magmas in subduction zones. We estimated variation of water content of arc basaltic magmas in the northeast Japan arc and the Izu-Mariana arc using a simple plagioclase phenocryst hygrometer and melt inclusion analysis of olivine phenocrysts.

A simple plagioclase phenocryst hygrometer was constructed by high-pressure and high temperature experiments using internally heated pressure vessels: SMC-2000 and SMC-5000 installed at the Magma Factory, Tokyo Tech (Ushioda et al., 2013, VSJ fall meeting). High-pressure and high-temperature experiments were conducted for relatively primitive basalt from Miyakejima volcano under hydrous conditions. OFS (Ofunato scoria: Tsukui et al., 2001; Niihori et al., 2003) is one of the most primitive basalt in the last 10,000 years. All experiments were conducted near the liquidus of plagioclase ( $\pm$ magnetite) and therefore the composition of melt is essentially the same as the starting material. H<sub>2</sub>O content of melt was calculated by weight ratio of melt using mass balance calculation of all phases assuming that water was concentrated only in melt. Partition coefficient  $K_D^{pl-melt} C_{a-Na}$  is proportional to H<sub>2</sub>O content in melt. In the experimental conditions, both pressure and temperature effects are negligible.

We then chose geochemical data sets of relatively primitive basaltic rocks (with no evidence of magma mixing) and most frequent Ca-rich plagioclase phenocrysts from 15 arc basaltic volcanoes, which includes both frontal arc volcanoes and rear-arc volcanoes from literature. In 15 volcanoes, plagioclase phenocrysts of high anorthite content (An>90) are commonly observed, whereas plagioclase phenocrysts in rear arc volcanoes usually have lower anorthite content (90>An>80). Estimated H<sub>2</sub>O content of basaltic magma is 3 wt.% H<sub>2</sub>O or higher.

We also analyzed H<sub>2</sub>O content of melt inclusions in olivine phenocrysts using FTIR micro reflectance measurement (Yasuda, 2011) and FTIR micro transmission measurement (absorption coefficient: Yamashita et al., 1996) in order to compare H<sub>2</sub>O content between melt inclusion analysis and this simple plagioclase phenocryst hygrometer. For example, melt inclusions of olivine phenocrysts in scoria from Ko-Fuji volcano had up to 3.7 wt.% H<sub>2</sub>O which was consistent with estimate from our simple plagioclase phenocrysts hygrometer. In Miyakejima volcano, melt inclusions of olivine phenocrysts from OFS contained up to 3.3wt.% H<sub>2</sub>O although H<sub>2</sub>O content was 5.2 wt.% estimated from this hygrometer. In either case, basaltic magmas in volcanic front have 3 wt.% H<sub>2</sub>O or higher.

Keywords: water in magma, melt inclusion, equilibrium between plagioclase and melt

## DEM simulation on fracturing induced by hydration and dehydration reactions

OKAMOTO, Atsushi<sup>1\*</sup> ; SHIMIZU, Hiroyuki<sup>2</sup>

<sup>1</sup>Graduate School of environmental Studies, Tohoku University, <sup>2</sup>Institute of Fluid Science, Tohoku University

Dehydration and hydration reactions play significant roles on the global water circulation in the solid Earth, and cause drastic change in the mechanical properties of the subduction zone interface. Progress of both reactions requires an effective transport of water (release or supply) between the reaction sites and outer system, and are commonly characterized by large changes in solid volume, porosity, and fluid pressure. Reaction textures with fracturing are commonly observed both in hydration and dehydration hydration reactions. However, the dynamic relationship among reactions, fluid transport and deformation (fracturing, plastic deformation) is too complicated to be understood solely by observations of natural occurrences.

In the present study, we carried out numerical simulations on fracturing induced by hydration or dehydration reactions by using distinct element method (DEM). At first, we consider a dehydration reaction like a dehydration of serpentine. In the model, the following factors are introduced: (1) pressure dependence of reaction rate, (2) grain boundary as weak and water-saturated region, and that (3) mineral grains become permeable after fracturing or reacted. In this model, reaction rate drastically decreases with progress of dehydration reaction, when fluid cannot escape from the system.

We examined two rock systems; one is composed of reactive minerals (uniform-reactive system) and the other one is composed of reactive minerals embedded in unreactive matrix minerals (reactive minerals in matrix system). In both systems, one is drain-boundary, whereas all the others are undrain-boundary. The spatial variation in fractures and progress of reactions are contrasting between the two systems. In the uniform-reactive system, fracturing does not occur and reactions uniformly occur from the drain-boundary, because fluid effectively escapes through newly-produced pore-network. In contrast, the reactive-mineral-in-matrix-system, the fracture network is produced among the reactive grains, and heterogeneous distributions of reaction progress was produced in the rocks. We will further discuss the key parameters to controls the fracture patterns and difference between hydration and dehydration reactions.

Keywords: hydration, dehydration, fracturing, distinct element method

## Investigation on the temporal change in attenuation within ruptured fault zone of the 1999 Chi-Chi, Taiwan earthquake

MA, Kuo-fong<sup>1\*</sup> ; WANG, Yu-ju<sup>1</sup>

<sup>1</sup>Department of Earth Sciences, National Central University

Attenuation, noted as  $1/Q$ , had been considered as a geophysical parameter related to the fluid content, temperature and fracture of the medium. The attenuation parameter related to S-wave named as  $Q_s$  has more significant indication to the factors indicated above. The damage zone of a large earthquake was often considered as a fracture zone, especially the hanging wall of a thrust faulting earthquake, which suggests a zone with possible high attenuation (decrease in  $Q$ ). Earlier  $Q_p$  and  $Q_s$  tomography studies revealed the feature with high attenuation on the hanging wall of the ruptured Chelungpu fault of the 1999 Chi-Chi earthquake. To examine the attenuation character in the rupture fault, we further investigate the temporal variation of the attenuation, specifically in  $Q_s$ , within the hanging wall before, following and after the earthquake. We observed a decreasing in  $Q_s$  within the fault rupture zone two years following the 1999 Chi-Chi earthquake by  $Q_s$  tomography images and an analysis of single-path  $Q_s$  near the Chelungpu fault. The synthetic and sensitivity tests of the  $Q_s$  determination were carried out accordingly to justify the temporal variation. A  $Q_s$  value within the hanging wall above the hypocenter was determined to be 157 two years following the Chi-Chi earthquake, which is significantly lower than the values of 238 and 289 prior to and two years after the main shock, respectively, from the  $Q_s$  tomography. Similar values using a signal-path  $Q_s$  analysis, from events within the ruptured fault zone to stations along the fault were obtained. The corresponding  $Q_s$  values were 247 prior to the Chi-Chi earthquake. After the earthquake, we obtained the  $Q_s$  values of 158 and 318 for the time, two years following and two years after the earthquake, respectively. Considering the two independent methods in determination of  $Q_s$ , the reduction in  $Q_s$  of 89 two years following the Chi-Chi earthquake in both method is significant. Along with 1%  $V_s$  reduction revealed by the analysis of repeating earthquakes, our studies suggested possible reduction both in  $V_s$  and  $Q_s$  within the fault zone after the Chi-Chi earthquake. The observation of temporal changes in  $Q_s$  after the Chi-Chi earthquake implies variations of pore fluid saturation in the ruptured fault zone. The reduction in  $Q_s$  two years following the Chi-Chi earthquake might indicate high pore-fluid saturation within fractured fault zone rocks due to post-seismic redistribution of the fluid.

Keywords: attenuation, fault zone, temporal variation, earthquake rupture

## Chemical characteristics of hot springs in Southwestern part of Taiwan

SUGAI, Shuto<sup>1\*</sup> ; TANAKA, Hidemi<sup>1</sup> ; TERUSAWA, Shuji<sup>1</sup> ; TSUNOMORI, Fumiaki<sup>2</sup> ; MURAKAMI, Masaki<sup>3</sup> ; KAWABATA, Kuniyo<sup>2</sup>

<sup>1</sup>School of Science, The University of Tokyo, <sup>2</sup>Geochemical Research Center, Graduate School of Science, The University of Tokyo, <sup>3</sup>OYO Corporation

Taiwan is located at the junction of the Ryukyu Trough and the Manila Trench which are the boundaries of the Philippine Sea Plate and the Eurasian plate. While the Philippine Sea plate is subducting beneath the Eurasian plate at the offshore of eastern Taiwan, the Eurasian plate is subducting beneath the Philippine Sea plate at Manila Trench at the south offshore of western Taiwan. The plate boundary is riding on the Taiwan Island in the vicinity of Kaohsiung, southern Taiwan, and the plate boundary appears as active faults to the north. Many faults striking NE - SW have been developed, and there are some hot springs and mud volcanoes (Hamada et al., 2009) along those faults.

We focused on the hot springs around Chiayi and Tainan, southwestern Taiwan in this study. These hot springs show temperature around 34 - 70 °C which are distributed about 20 km apart from the active faults to the east, arranging from north to south. We have conducted chemical analyses for the hot spring water taken from these springs and report the results of these analyses in this presentation.

Keywords: Taiwan, hot springs

## Estimate of isotopic composition and flux of Arima type fluid

TANAKA, Hidemi<sup>1\*</sup> ; TERUSAWA, Shuji<sup>1</sup> ; SUGAI, Shuto<sup>1</sup> ; TSUNOMORI, Fumiaki<sup>2</sup> ; MURAKAMI, Masaki<sup>3</sup> ; KAWABATA, Kuniyo<sup>2</sup>

<sup>1</sup>School of Science, University of Tokyo, <sup>2</sup>Geochemical Research Center, Graduate School of Science, University of Tokyo, <sup>3</sup>OYO Corporation

It has been well known that change in chemical compositions of ground water is associated with crustal activities including large earthquakes. Research for change in chemical compositions of fluids associated with earthquakes is still continuing all over the world. However, reasons to choose the location of wells to measure the chemical and isotopic compositions of the fluids, and to choose particular chemical and isotopic compositions for measurements have not been unambiguous so far.

Because no deterministic theory has been established to predict large earthquake from anomalous chemical precursor signals so far, and fluid-monitoring research to explore earthquake precursor is significantly declined in the community, it would be less meaning to collect more chemical precursors of the earthquakes by repeating procedure in future.

Instead, there are some meaning if observed chemical change can be explained by physical and chemical process in the crust associated with crustal activities. At present, following three subjects are especially important. First, establishing the reliable basis to choose proper fluids and wells, second, designing and constructing the mass-spectrometer which has sufficient performance for fluid continuous monitoring at on-site close to the fault zone, and finally, establishing and improvement of diagnostic theory of fault zone fluid.

Based on the idea mentioned above, the results of examination of fluid of hot springs at Arima area are presented. There are several hot spring sources which are flown out continuously to the surface. After hot spring drillings at the 1940 to 1950's constant amounts and quality of these hot springs are maintained by branch of coal government office of Kobe City. Many researches have been done for the hot springs so far, including surface geology, shallow underground structure, source of fluids and fluids paths. Fluid paths are inferred to be fracture zones of particular fault zones by results of geological survey and resistivity analysis. It is important to recognize these kinds of fluids as "fault zone fluids", since identification whether monitored fluids flow through fault zone or not is important issue to examine the crustal activities from the chemical and isotopic compositions of the fluids. It is also well known that fluids from Arima hot springs show specific isotopic compositions which is inferred to be very deep origin. In this presentation, we discuss about quantity of flux of deep source fluids of Arima hot spring which is important issue to answer the question why we need to observe the fluids for crustal activities and where? and compare the results between this and previous studies.

Keywords: crustal fluids, Arima type Hot spring, fluid flux, saline water, isotopic composition

## Basic experiments for continuous monitoring of CH<sub>3</sub> in the field by Mass spectrometer

KAWABATA, Kuniyo<sup>1\*</sup> ; TSUNOMORI, Fumiaki<sup>1</sup> ; MURAKAMI, Masaki<sup>3</sup> ; TANAKA, Hidemi<sup>2</sup>

<sup>1</sup>Geochemical Research Center, Graduate School of Science, The University of Tokyo, <sup>2</sup>Department of Earth and Planetary Science, Graduate School of Science, The University of Tokyo, <sup>3</sup>OYO Corporation

Continuous gas monitoring in the field is important issue for various purposes such as for heat trapping gas monitoring, poisonous gas monitoring and scientific objective. In order to analyze the gas in the field, small-sized gas analyzer using mass spectrometer have been developed in our group. In the field, identifying the location of the emitted gas is needed. To detect gas-emission in distant places from the analyzer, we made basic laboratory experiments using methane gas. In this presentation, we introduce the results of the experiment.

Keywords: Mass spectrometer, methane, monitoring, in the field

## Geophysical Research of Tachikawa Fault Zone by Rn-222 and Cl- Concentration in Groundwater

SHIMODATE, Tomoya<sup>1\*</sup> ; TSUNOMORI, Fumiaki<sup>2</sup> ; YASUHARA, Masaya<sup>3</sup> ; HAYASHI, Takeshi<sup>4</sup>

<sup>1</sup>International Christian University, <sup>2</sup>The University of Tokyo, <sup>3</sup>AIST, <sup>4</sup>Akita University

The 2011 off the Pacific coast of Tohoku Earthquake enhanced the probability of earthquake in Tachikawa Fault Zone. To evaluate the physical condition of Tachikawa fault zone, we researched Rn-222 concentration in groundwater, which is known as a precursory anomaly of earthquake. Additionally, we focused on the connection between the concentration of chloride ion in groundwater and fault damage zone and measured chloride ion in groundwater as well. Our purpose in this paper is to detect suitable groundwater for continuous measurement: (1) The depth of aquifer is deep enough to reach the bedrock. (2) Water contains much enough radon to monitor. (3) Water contains chloride ion whose concentration is controlled by the condition of fault damage zone.

Radon concentration in confined aquifer is supplied by alpha decay of radium in the surface of the grain. If the specific surface area of the grain changes according to physical condition of fault, radon concentration in the groundwater would change. The upper edge of bedrocks, main source of radon, has a depth of under 2,000 m around Tachikawa Fault Zone and it deepens in the west.

We focus on the distribution of chloride ion around Ayasegawa Fault is similar to one around Tachikawa Fault Zone. Low concentration of chloride ion in groundwater around Ayasegawa Fault is affected by fault damage zone, and we expect that groundwater around Tachikawa Fault Zone also shows low concentration of chloride ion due to fault damage zone. We use RTM1688(SARAD) for radon measurement, and ion chromatography for chloride ion measurement.

As a result, samples around the fault show high concentration of radon and low chloride ion. This suggests that the well around fault reach the bedrock and contain low concentration of chloride ion due to fault damage zone. These samples would show concentration change according to earthquake.

Keywords: radon, chloride ion, Tachikawa Fault Zone, spring water

## Precursory Change of Radon Concentration in Groundwater before 2011 Tohoku Earthquake

TSUNOMORI, Fumiaki<sup>1\*</sup>

<sup>1</sup>Graduate School of Science, University of Tokyo

We will report characteristics of radon concentration changes in groundwater at the Nakaizu observatory around the Tohoku earthquake, 2011.

Radon concentration in groundwater sometimes responds to crustal deformation before the earthquakes. The phenomenon was well known in 1980, and many scientists tried to detect such anomalous signals in order to find a chemical indicator of earthquakes. However few researches have studied a mechanism of the phenomenon. Nonetheless a lot of anomalies of the radon concentration relating to earthquakes are reported every year, thus it is important to clarify the fundamental process of radon concentration change in an aquifer. We would like to report the characteristics of radon concentration change around the 2011 Tohoku earthquake, and to discuss a fundamental model of the radon concentration change in an aquifer.

An anomalous increase in radon concentration was measured at the Nakaizu observatory on the Izu Peninsula prior to the 2011 Tohoku earthquake using a custom-made radon counter. Since the increase was more than three times the standard deviation of radon concentration variations over 35 years of recorded data, it is considered likely that it is a precursor to the earthquake. Following the earthquake, the radon concentration decreased exponentially to the background level. The anomalous increase is explained using a modified volatilization model containing three important aquifer parameters: the groundwater saturation ratio, the fracture surface area per unit volume, and the porosity. The modified model can also explain the radon concentration behavior prior to the 1978 Izu-Oshima-Kinkai earthquake.

Keywords: Radon, Groundwater

## Cooling history of a fracture zone in the Kojyaku granite, Tsuruga area: Constraints from multi-system thermochronology

SUEOKA, Shigeru<sup>1\*</sup> ; YASUE, Ken-ichi<sup>1</sup> ; NIWA, Masakazu<sup>1</sup> ; SHIMADA, Koji<sup>1</sup> ; ISHIMARU, Tsuneari<sup>1</sup> ; UMEDA, Koji<sup>1</sup> ; YAMADA, Ryuji<sup>2</sup> ; DANHARA, Tohru<sup>3</sup> ; IWANO, Hideki<sup>3</sup> ; GOUZU, Chitaro<sup>4</sup>

<sup>1</sup>Japan Atomic Energy Agency, <sup>2</sup>National Research Institute for Earth Science and Disaster Prevention, <sup>3</sup>Kyoto Fission-Track Co., Ltd., <sup>4</sup>Hiruzen Institute for Geology and Chronology Co., Ltd.

Ages of faulting are generally estimated from ages of displaced geomorphic markers, e.g., terrace surfaces, alluvial deposits, or artificial structures. However, these markers are not always available, such as for faults in basement rocks. Such faults have been attempted to date by detecting chronological anomalies (e.g., Ikeya et al., 1982; Murakami and Tagami, 2004; Yamada et al., 2013; Gansawa et al., 2013) or dating hydrothermal veins or clay minerals formed after faulting (e.g., Zwingmann et al., 2004; Watanabe et al., 2008; Siebel et al., 2009; Yamasaki et al., 2013). However, definitive procedures to determine faulting ages based on such geochronological methods have not been established because thermogenesis and mass transport along fault zones are not simple. More basic and case studies are desirable to improve these methods.

We introduce an attempt to date a fracture zone observed in the northwestern part of the Tsuruga peninsula, southwest Japan, by constraining its cooling history from fission-track (FT), K-Ar, and U-Pb thermochronometries. In the northern part of the Kinki Triangle, including the Kohoku and Tsuruga bay areas, NE-SW or NW-SE strike-slip faults such as the Kohokusanchi and Nosaka-Shufukuji fault zones, are dominant (e.g., The Headquarters for Earthquake Research Promotion, 2003a, b). Strike-slip faults in mountainous areas are generally difficult to date by using geomorphic markers. The fault we study is a strike-slip fault formed in the Tsuruga body of the Kojyaku granite (Kurimoto et al., 1999), along which no geomorphic marker is available. We dated 1) the fault gauge, 2) uncrushed host granitic rock, and 3) dolerite intruding within a few meters from the fault. The dispersions between zircon U-Pb ages and zircon fission-track ages of 1) and 2) are not significant at 2 sigma level and both of the zircon fission-track lengths are not shortened, implying 1) and 2) shared the cooling histories between closure temperatures of zircon U-Pb (>900 deg. C) and zircon fission-track methods (210-350 deg. C). On the other hand, apatite fission-track ages of 50.8 +/- 18.5 Ma for 2) and 28.4 +/- 13.6 Ma for 1) may be interpreted to be reflections of different cooling histories below 90-120 deg. C, closure temperature of apatite fission track method. Although the younger age of a) is attributable to the faulting during the Neogene/Quaternary or intrusion of the dolerite at 19.1-18.8 Ma inferred from plagioclase and whole-rock K-Ar ages, definitive conclusions are difficult to be drawn because of the wide error bars of the apatite FT ages and lack of apatite fission-track length data. In this presentation, we are going to give more precise discussions based on apatite fission-track length analyses.

Keywords: dating of a fault, fission-track thermochronology, K-Ar dating method, U-Pb dating method, Kojyaku granite

## Chemical and isotopic examinations of Arima-type high saline hot spring water in southwest Japan

TANAKA, Hidemi<sup>1\*</sup> ; TERUSAWA, Shuji<sup>1</sup> ; SUGAI, Shuto<sup>1</sup> ; TSUNOMORI, Fumiaki<sup>2</sup> ; MURAKAMI, Masaki<sup>3</sup> ; KAWABATA, Kuniyo<sup>2</sup>

<sup>1</sup>School of Science, University of Tokyo, <sup>2</sup>Geochemical Research Center, Graduate School of Science, University of Tokyo, <sup>3</sup>OYO Corporation

Many researches have been conducted to explore component source, heat source and water source of hot spring in Japan. Matshubaya et al.,(1974) classified hot springs into four types by isotopic ratio of hydrogen and oxygen in water and geology (1) volcanic type, (2) Arima type, (3) coastal type, (4)Green tough type. Of these, Arima type is said to have deep origin source because hydrogen and oxygen isotope ratios suggests that the origin is mixture of meteoric water and magmatic water, and dissolving gas have abnormally high He isotopic ratio.

Sugimoto (2012) selected 180 hot springs that seem to be classified as Arima type from 6058 hot springs in Japan, using Li/Cl and Br/Cl values. Li/Cl is used as index of temperature of water was experienced (You et al., 1996). Br/Cl expresses influence from sea water and biological effect (Hurwitz et al., 2005; Uemura et al., 1988). He selected hot springs which have more Li/Cl and less Br/Cl as Arima type. But, his discussion was only about dissolving ion and not discussed hydrogen and oxygen isotope ratios used in the definition of Arima type.

So, we reselected 185 hot springs that seems to Arima type by Sugimoto (2012) method from 9887 hot springs in Japan and sampled 67 hot springs for isotopic analysis and ion analysis. As a result, the hot spring with the isotope shift in the same way as Arima hot spring is found along Median Tectonic Line (MTL) at Kinki, Western Shikoku and Central Japan (Kashio) districts. All mixing lines are converged to one point. Thus, we refer the fluid with this isotopic composition as origin water of Arima type. Since they converge to one point in the relationship of the hydrogen isotope ratio of the chloride ion concentration, the composition of the original water is as  $\delta D = -35\text{‰}$ ,  $\delta^{18}O = 5\text{‰}$ ,  $Cl^- = 42\text{g/l}$ . The method to determine the isotopic composition and the resultant value of  $\delta D$  and  $\delta^{18}O$  is more convincing than those from previous results. Because shift lines from several regions are coincided at one point.

Keywords: Arima hot spring, Oxygen Isotope, Hydrogen Isotope, Brine fluids, original composition

## Spatial and temporal evolution of slip and seismicity during the 2013-2014 Boso slow slip event

FUKUDA, Jun'ichi<sup>1\*</sup> ; KATO, Aitaro<sup>1</sup> ; OBARA, Kazushige<sup>1</sup> ; MIURA, Satoshi<sup>2</sup>

<sup>1</sup>Earthquake Research Institute, University of Tokyo, <sup>2</sup>Graduate School of Science, Tohoku University

GPS time series data show that transient crustal deformation has been occurring in the Boso peninsula, central Japan, since December 2013. Observed spatial and temporal patterns of surface displacements suggest the occurrence of transient aseismic slip on the subducting Philippine Sea plate. In addition, an increased rate of seismicity was observed from 31 December 2013 to 9 January 2014 off the east coast of the Boso peninsula. The location of the increased seismicity partly overlaps with the areas of seismic activity during the past Boso slow slip events.

To estimate spatial and temporal evolution of aseismic slip, we use GPS data from 71 stations of the GEONET in the Kanto region and data from 6 stations located along the east coast of the Boso peninsula, which are operated by Earthquake Research Institute of University of Tokyo and Tohoku University. The data are analyzed with GIPSY-OASIS II software to obtain daily coordinate time series at the 77 stations. Secular velocities, seasonal variations, and postseismic deformation following the 2011 Tohoku-oki earthquake are removed from the time series. We use a modified version of the Network Inversion Filter to estimate spatial and temporal evolution of daily cumulative slip and slip rate on the Philippine Sea plate. Slip slowly started around 20 December 2013 off the east coast of the Boso peninsula and then slip rapidly accelerated around 28 December and propagated to the west. Slip continued to accelerate until 3 January and then rapidly decelerated until 9 January.

To investigate spatial and temporal correlation of slip and seismicity, we use a matched-filter technique to detect earthquakes in the area of increased seismic activity. The detected earthquakes are located along the northern edge of the large aseismic slip and migrated from east to west during the period of rapid aseismic slip (31 December to 9 January). This migration pattern is consistent with the propagation of rapid aseismic slip, suggesting that the earthquakes are triggered by stress loading due to the propagation of aseismic slip. We do not identify significant seismic activity before 28 December, indicating that the slow slip event started well before the initiation of the seismic activity.

Keywords: slow slip event, seismic activity, GPS

## A slow slip event near the Boso Peninsula immediately triggered by the 2011 Tohoku-Oki earthquake

KATO, Aitaro<sup>1\*</sup> ; IGARASHI, Toshihiro<sup>1</sup> ; OBARA, Kazushige<sup>1</sup>

<sup>1</sup>ERI University of Tokyo

It has been recognized that a series of slow slip events, accompanying with ordinary earthquakes, take place with recurrence intervals from 5 to 7 years near the Boso Peninsula along the plate interface of the subducting Philippine Sea plate [e.g., Hirose et al., 2012]. Immediately after the 2011 Tohoku-oki earthquake, intensive afterslip have been detected to start along the plate interface of the Pacific plate from off Tohoku region to southward Kanto region [e.g., Munekane et al., 2012; Fukuda et al., 2013]. It is well known that both the Pacific and the Philippine Sea plates are subducting beneath the Kanto region, and interacting with each other. Therefore, it is expected that the Philippine Sea plate might be dragged by the speeding Pacific plate during the intensive afterslip. We hypothesize that the dragging of the Philippine Sea plate by the Pacific plate leads to triggering of a slow slip event near the Boso Peninsula immediately after the Tohoku-Oki earthquake.

In order to verify the above hypothesis, we analyzed the seismicity including small repeating earthquakes, applying the matched filter technique to continuous waveforms. We used all available earthquakes associated with three sequences of slow slip events in 2007, 2011, and 2014 as template events. Then, we searched for events those have similar waveforms to ones of each template event from continuous waveforms. Based on the new earthquake catalog, we found out an abrupt increase in the swarm-like seismicity at the slow slip source area from March 12 to 14, 2011. In addition, some repeating earthquakes were extracted in the swarm, indicating aseismic slip transient. We, thus, interpret that the seismic swarm were linked to a newly detected slow slip event, which has not been previously recognized. However, based on the amount of aseismic slip deduced from the repeating earthquakes, moment released by the slow slip event is estimated to be smaller than by previously recognized slow slip events. We thus conclude that a small slow slip event might be triggered through the dragging of the Philippine Sea plate by the Pacific plate immediately after the Tohoku-Oki earthquake.

## Tidal correlations of earthquake swarms associated with slow slip events off Boso Peninsula

TANAKA, Sachiko<sup>1\*</sup>

<sup>1</sup>NIED

We investigated statistical correlations between Earth tides and earthquakes in the four swarms associated with slow slip events (SSEs) off Boso Peninsula in 2002, 2007, 2011, and 2014. Following Hirose et al. (2012), we selected the SSE-related events from the Hi-net earthquake catalog. For each event, we assigned the tidal phase angle at the origin time by theoretically calculating tidal Coulomb failure stresses with a frictional coefficient of 0.2. For the fault plane, we assumed a landward-dipping reverse fault from the F-net moment tensor solution of the largest earthquake (Mw 4.9) in the 2014 swarm. Based on the distribution of tidal phase angles, we statistically tested whether they concentrate near some particular angle or not by using the Schuster test. In this test, the result is evaluated by p-value, which represents the significance level to reject the null hypothesis that the earthquakes occur randomly irrespective of the tidal phase angle. The result of analysis shows the 2014 swarm was strongly correlated with tidally-induced stresses ( $p = 0.01\%$ ). The distribution of tidal phase angles exhibited a peak near the angle 0, which corresponds to the time of the maximum tidal stress promoting fault slip. We suggest that tidal stress fluctuations can trigger earthquakes when superimposed on stress buildup caused by nearby slow slip. On the other hand, the other three swarms show insignificant correlations with tides. The resultant p-values are 87%, 16%, and 14% for the 2002, 2007, and 2011 activities, respectively. Geodetic observations indicate larger slow slip in these three episodes than in 2014 (Hirose et al., 2013; Kimura, 2014). It is highly likely that the swarm earthquakes in those activities were fully triggered by stress perturbations imparted by large slow slip. Tides appear to have exerted little or no influence on triggering in that case.

Keywords: Boso Peninsula slow slip events, Earth tides, earthquake triggering

## Interplate coupling and SSE in the Tokai region after 1981 using leveling data

OCHI, Tadafumi<sup>1\*</sup>

<sup>1</sup>AIST

The long-term SSE in the Tokai region, central Japan, from mid-2000 to mid-2005 [Suito and Ozawa (2009)], had continued five years, which was much longer than other SSEs around the world [e.g. Schwartz and Rokosky (2007)]. After the termination of the SSE in 2005, no obvious long-term SSE has been detected and that makes difficult to discuss a recurrence interval of the events. In order to reveal whether the event repeats or not, and if it repeats, in order to clarify the interval and a temporal and spatial change of the interplate coupling and the slow slip, I analyzed a leveling data before the era of GEONET.

Various types of geodetic observations have been conducted in the Tokai region and there are some previous works about the temporal change of the crustal deformation using the data of these observations. For example, Kimata and Yamauchi (1998) analyzed EDM data and Kobayashi and Yoshida (2004) analyzed tidal data to detect irregular feature in the crustal deformation. In this study, I analyzed leveling data in the Tokai region from 1981 to 1999 and reveal spatially the temporal change of the vertical deformation velocity. Leveling observations have been conducted four times a year along the route from Kakegawa City to the Omaezaki Cape and once a year along the others around the Omaezaki Cape. I used all the data from these observations and inferred two-year-averaged vertical deformation rate using the time-dependent network adjustment [Fujii (1991)]. The estimated error of the rate is about 2 mm/yr, which is twice as much as the error of GNSS vertical data in this region [Ochi and Kato (2013)]. Comparing with the other geodetic data, the biggest advantage of the leveling data is that it can produce a spatial view of the crustal deformation with small error.

From the results of the analysis, two patterns of the crustal deformation that may correspond to existence and non-existence of the SSE appear alternately. The pattern that resembles that of in the 2000-05 was detected around 1982-83, 1988-90 and 1997. The duration of the event in 1982-83 is shorter than that of 1988-90, which is again shorter than that of 2000. Summing up these results, it is clear that there are various durations in the SSEs. In addition, if the small event in 1997 is taken into account, small and large events occur alternately and the intervals after the large event may tend to get longer. However, as the 1997 event is temporally close to the large long-term SSE after 2000, the SSE would affect the analysis of 1997 data and it should be considered further.

I also inferred the temporal change of the interplate coupling and slow slip using the results. In order to overcome the lack of temporal resolution, I fixed the distribution center of the slow slip to the same place by the results by Ochi and Kato (2013), the northwestern part of the Lake Hamana with the depth around 30-40 km. According to the forward modeling, the pattern of the crustal deformation in the 1982-83 and 1988-90 require somewhat smaller amount of SSE. On the other hand, the interplate coupling beneath the Omaezaki Cape constantly continues whether the SSE occurs or not.

Keywords: leveling data, interplate coupling, slow slip event, the Tokai region

## A shallow slow-slip-event in northern Hokkaido in 2012-2013: An event triggered by seismic waves.

IKEDA, Shohei<sup>1\*</sup> ; HEKI, Kosuke<sup>2</sup>

<sup>1</sup>Graduate School of Science, Hokkaido University, <sup>2</sup>Department of Natural History Sciences, Faculty of Science, Hokkaido University

GNSS (Global Navigation Satellite System), as represented by GPS (Global Positioning System), enabled us to study SSE (Slow Slip Event), slow displacement of fault without exciting seismic waves. In this study, we report that baseline length between the Horonobe and the Nakatombetsu GNSS stations (part of the GEONET, GNSS Earth Observation Network) in Northern Hokkaido, shortened by ~2 cm over 4-5 months period from 2012 summer to the early 2013. We assumed that an SSE is responsible for this change, and inferred fault parameters of this unique SSE. There have been lots of reports on repeating SSE at plate boundaries, e.g. off the Boso Peninsula, the Nankai Trough, and the Ryukyu Trench. In the Northern Hokkaido, a block boundary is considered to run north-south (Loveless and Meade, 2010) with the convergence rate of about 1 cm/year. This shallow SSE we report here is considered to have occurred at this boundary.

At first, we analyzed time series of the distance change between Horonobe and Nakatombetsu, together with a few additional GNSS stations nearby and estimated the fault parameters of this SSE by grid searches. The estimated slip was about 10 cm ( $M_w$  was ~5.9), which suggests that a similar SSE recurs every decade. However, these GNSS stations started in 2002, and we do not have information on the previous SSE. We modeled the time series using lines with two breaks, and we constrained the onset time and the ending time of the SSE by minimizing the root-mean-square of the post-fit residuals. The optimal onset and termination was 2012.64 and 2013.08, respectively. Around the onset time, there was a deep earthquake beneath Sakhalin ( $M7.7$ ) on August 14, 2012, and there were four  $M4$  class earthquakes close to the Horonobe station in July, 2012. Seismic waves generated by these earthquakes may have triggered this SSE. At the termination time, there was an  $M4.8$  earthquake on 3 Jan. 2013 at the depth of 24 km on the westward extension of the SSE fault. From mechanical point of view, it is difficult to consider that this earthquake encouraged the termination of SSE.

Keywords: GPS, Slow Slip Event, Northern Hokkaido, seismic waves

## Seismicity and pressure changes observed around DONET at the same time

SUZUKI, Kensuke<sup>1\*</sup> ; TAKAHASHI, Narumi<sup>1</sup> ; HORI, Takane<sup>1</sup> ; KAMIYA, Shin'ichiro<sup>1</sup> ; NAKANO, Masaru<sup>1</sup> ; KANEDA, Yoshiyuki<sup>1</sup>

<sup>1</sup>JAMSTEC

The Philippine Sea plate is subducting to northwest below the Eurasian plate along the Nankai trough in southwestern Japan at a convergence rate of about 65 mm/year. In this region mega-thrust earthquakes have repeatedly occurred along the Nankai trough and caused serious and widespread damages in central and western Japan. The Japan Agency for Marine-Earth Science and Technology (JAMSTEC) installed permanent ocean bottom observation stations named as Dense Oceanfloor Network System for Earthquakes and Tsunamis (DONET) off the Kii Peninsula to monitor earthquakes and tsunamis and to decrease damage due to those. Because several kinds of continuous data have sent to JAMSTEC in real time, we can discuss continuous seismicity and other seismic/geodetic information. It is important for considering occurrence of large earthquakes to judge seismicity of small earthquake and to monitor crustal deformation.

Suzuki et al. (2013) has reported that quiescence of seismicity and ocean bottom pressure changes around DONET have occurred almost at same time from Feb. 2013 to Sep. 2013. In this study we extended observational period until Jan. 2014. As a result of investigation by using similar method with Suzuki et al. (2013), these changes seem to have continued after Sep. 2013. Quiescence of seismicity has not finished yet; seismicity is lower than one predicted from ETAS model (Ogata, 1989) represented by five parameters fitted by using data between 2012. Although pressure changes have been observed at only three stations (KMB05, KMB06 and KMB07) on Sep. 2013, pressure change at KMB08 was also observed on extended time series in addition to the three stations. We will try to estimate fault slip model that can cause these pressure changes and investigate how that fault slip influence to seismicity.

Keywords: seismicity, ocean bottom pressure gauge, DONET, ETAS model

## Detection of short-term slow slip events along the Nankai Trough by observations of groundwater level or pressure

KITAGAWA, Yuichi<sup>1</sup> ; KOIZUMI, Naoji<sup>1\*</sup>

<sup>1</sup>Geological Survey of Japan, AIST

Non-volcanic deep low-frequency (DLF) tremors are detected on plate boundaries along many subduction zones around the world [Obara,2002; Ide, 2012]. Short-term slow slip events (S-SSEs), which cause small crustal deformation with no usual seismic waves, are also detected in subduction zones [Rogers and Dragert, 2003; Schwartz and Rokosky, 2007; Sekine et al., 2010]. There is a close spatial and temporal correlation between DLF tremors and S-SSEs. However, S-SSEs do not always occur in areas where DLF tremors occur and vice versa. Therefore, it is important to clarify the detailed spatial and temporal correlations in order to know what occurs on the plate boundaries along subduction zones. In general, detecting S-SSEs via crustal deformation is more difficult than with DLF tremors when using a seismograph. One major reason for this is that the decay of crustal deformation by distance is much larger than that of seismic waves. Therefore, it is necessary to develop new tools or techniques to detect S-SSEs. For this purpose, we attempted to detect S-SSEs in the Nankai Trough, Japan by conducting groundwater pressure observations at ANO station in Mie Prefecture, Japan. The ANO is a groundwater observation station operated by the Geological Survey of Japan, AIST, for earthquake prediction research. The groundwater pressures changed due to six S-SSEs that occurred near ANO from June 2011 to April in 2013. The fault models of these S-SSEs, which were estimated mainly by observing the crustal strains and tilts, explained the changes in the groundwater pressures. We also considered the conditions for detecting S-SSEs via groundwater observations. The volumetric strain changes caused by the S-SSEs along the Nankai Trough were 10-20 nstrain/day at most [Kobayashi et al., 2006], where nstrain means  $10^{-9}$  strain. Therefore, the strain-converted noise level should be 5 nstrain/day or smaller to detect the S-SSEs. Taking the actual conditions of groundwater observation into consideration, it is necessary that the noise level should be smaller than 50 mm/day and that the strain sensitivity of the groundwater pressure or level should be larger than 1 mm/nstrain for the required strain-converted noise level.

Keywords: Slow slip event, Deep low-frequency tremor, Groundwater, Poroelastic theory, Strain, Earthquake forecast

## Time evolution of non-volcanic tremor episode

OBARA, Kazushige<sup>1\*</sup> ; MATSUZAWA, Takanori<sup>2</sup> ; TANAKA, Sachiko<sup>2</sup> ; MAEDA, Takuto<sup>1</sup>

<sup>1</sup>Earthquake Research Institute, Univ. of Tokyo, <sup>2</sup>NIED

Non-volcanic tremor in subduction zones like as Nankai is one of slow earthquake phenomena in the transition zone between the seismogenic zone and the stable sliding zone on the subducting plate interface (Obara, 2002). Major tremor episodes with duration longer than several days are always accompanied by short-term slow slip events (SSEs). The space-time correlation of tremor and SSE suggests that the time evolution of tremor episode reflects the rupture process of SSE. Based on the similarity, studying the mechanism of slow earthquakes is important to understand the activity style of megathrust earthquake. Therefore, we investigate the time evolution of tremor episode based on the clustering catalog (Maeda and Obara, 2009, Obara et al., 2010) because the tremor is well-detected compared to other slow earthquakes.

Tremor belt-like zone is divided into some segments based on their spatial extent and recurrence interval (Obara, 2010). Each segment includes some sub-segment as units of tremor activity (Obara et al., 2013). Tremor episode usually initiates from the deeper part of the tremor belt-like zone. If the episode reaches to the updip part of the tremor zone, it becomes a major episode associated with detectable SSE (Obara et al., 2011). We sometimes observe major episodes initiated from the shallower part. The time evolution of tremor energy at the beginning stage of the tremor episode depends on the location of initiation point. If the episode starts from the deeper part, the evolution velocity is small for a while then increases rapidly after the tremor migration front reaches to the updip edge. On the other hand, the evolution velocity is high if the episode starts from the shallower part. This suggests that the tremor patches radiating high energy concentrate at the updip side. The time evolution of tremor energy at the beginning stage of each episode is not related to the final size of the episode. The size of episode may be controlled by the strain energy accumulation at each portion on the way of migration. This is the same for along-strike evolution of tremor episode. The propagation of tremor episode depends on the slip deficit in each sub-segment ahead of the rupturing sub-segment. We observed temporal deceleration of migration speed in front of the small gap as the sub-segment boundary. On the other hand, we detect acceleration of the migration speed at a common spot during passage of the major tremor episode several times. This spot is considered as a sweet spot where tiny tremor activity continuously occurs in the shallower part of the tremor zone. This spot frequently generates tremor episodes and is considered to be strongly inhomogeneous. Such variation on the plate interface may control the rupture process of SSE.

Keywords: non-volcanic tremor, slow earthquake, source migration, segmentation

## Fundamental properties of non-volcanic low frequency tremor catalogues

TAKEDA, Naoto<sup>1\*</sup> ; KOIZUMI, Naoji<sup>1</sup> ; MATSUZAWA, Takanori<sup>2</sup> ; TANAKA, Sachiko<sup>2</sup> ; OBARA, Kazushige<sup>3</sup> ; MAEDA, Takuto<sup>3</sup>

<sup>1</sup>GSJ, AIST, <sup>2</sup>NIED, <sup>3</sup>ERI, Univ. of Tokyo

Since a discovery of non-volcanic low frequency tremor (NVT) in the subduction zone of southwest Japan (Obara, Science, 2002), the NVT has been found in various subduction zones or bottom of faults all over the world, and has been studied by many researchers. In these studies, an envelope cross-correlation technique for NVT detection and making a catalogue of NVT is important to discuss spatial and temporal activity of NVTs (e.g.; Maeda & Obara, JGR, 2009; Ide, Nature, 2010; Nakata et al., Nature Geoscience, 2008; Imanishi et al., GRL, 2011). There are some differences in NVT catalogues in the same region, since each study developed an original program for NVT catalogue. Furthermore, in some cases, even if they use a same program, parameters to detect NVT in the program were changed depending on a scope of the study. Consequently, there are some different features of NVT activity between the catalogues. In this report, we compare three catalogues, made by Japan Meteorological Agency (JMA), National Research Institute for Earth Science and Disaster Prevention (NIED) and Geological Survey of Japan, National Institute of Advanced Industrial Science and Technology (AIST), regarding a resolution of location and a NVT scale-sensitivity property as fundamental properties of the NVT catalogue.

Based on the method to estimate the resolution of location from a standard deviation of relative location (Ide, Nature, 2010), we calculated the resolution of location in each catalogue using several standard deviations of relative location. The estimated epicentral resolutions in three catalogues are almost 2-3km.

The NVT scale-sensitivity was estimated by a ratio of NVT counts in catalogues. For example, the sensitivity of the NIED catalogue for magnitude (M) based on the JMA catalogue was defined as  $N_{nied-jma}(M)/N_{jma}(M)$ . Here,  $N_{jma}(M)$  is total counts of low frequency earthquakes (LFEs) with M listed in the JMA catalogue, and  $N_{nied-jma}(M)$  is total counts of NVT in the NIED catalogue which is also listed in the JMA catalogue. To examine the relationship between the scale and the sensitivity in the catalogues, we used magnitude and NVT energy as the scale in the JMA and the other catalogues, respectively. By comparison of the NVT scale-sensitivity properties, it is found that these catalogues have characteristic scales in the sensitivity. Furthermore, the sensitivities of all catalogues decrease for large scale NVT. This is attributed to the increase of lost counts due to complex waveforms of highly active NVT. In our presentation, we show some examples of different features of NVT activities arising from different scale-sensitivity properties.

We conclude that these fundamental properties are useful not only for a comparison of catalogues, but also for an optimization of parameters in the programs of NVT detection.

Acknowledgments: We use the earthquake catalogue reported by JMA, and seismic waveform data provided by NIED (Hi-net), AIST, JMA, University of Tokyo, Kyoto University, Kyushu University, Kochi University, and Nagoya University.

Keywords: non-volcanic low frequency tremor, catalogue, position resolution, NVT scale-sensitivity property

## Determination of focal mechanisms of non-volcanic tremors using S-wave polarization: Correction for shear wave splitting

IMANISHI, Kazutoshi<sup>1\*</sup> ; UCHIDE, Takahiko<sup>1</sup> ; TAKEDA, Naoto<sup>1</sup>

<sup>1</sup>Geological Survey of Japan, AIST

Non-volcanic tremors (NVTs) have been found at various plate boundaries during the last decade. Focal mechanisms of NVTs are important for better understanding physical mechanisms of tremor generation. Stacking of many similar event waveforms greatly enhances the signal to noise ratio of tremor signals, which enables us to use conventional focal mechanism determination methods based on P-wave first motion polarities and/or waveforms (Ide et al., 2007; Bostok et al., 2013). However, the stacking approach cannot resolve spatio-temporal variations of focal mechanisms, so a new method is needed.

Imanishi and Takeda (2010) conducted a polarization analysis to continuous seismic data and showed that the scatter in the particle motion directions becomes small in accordance with a period of NVT activity. The same conclusion was reported for Cascadia tremors by Bostock and Christensen (2012). Because NVTs are primarily composed of shear waves (e.g., Obara, 2002), our observed particle motions contain information regarding focal mechanisms. However, the shear wave particle motion should be treated in caution, since shear-wave splitting may distort the particle motion excited by a seismic source (e.g., Zhang and Schwartz, 1994).

In this study, we first explored the existence of seismic anisotropy using tremor signals. A standard shear-wave splitting analysis (Silver and Chan, 1991) was used to determine the fast polarization direction (LSPD) and the lag time between fast and slow shear waves (DT). The analysis detected clear split arrivals separated by about 0.1 s, indicating the need of the correction for splitting effects to recover radiation pattern of S-wave. The LSPD shows two major directions which are normal or subparallel to the strike of the plate margin. These results are consistent with previous studies using regular earthquakes (e.g., Saiga et al., 2011), demonstrating that tremor signals are also available to investigate seismic anisotropy.

We then determined focal mechanisms of NVTs by correcting for splitting effects on particle motions. The actual procedure is as follows:

- (1) We rotate two horizontal seismograms to the fast and slow directions, advance the slow wave by the lag time, and rotate back to NS and EW directions.
- (2) A polarization analysis is subject to 1 minute windows to determine S-wave polarization angles.
- (3) Average and standard deviation of polarization angles are calculated at each hour.
- (4) A grid search approach is performed at each hour to determine the best double-couple solution using polarization angles of multiple stations. Here the epicenter is determined by an average of locations using our ECM catalogue. The depth is assumed to be 35 km.
- (5) Uncertainty is estimated based on a bootstrap approach.

We applied the above method to a tremor sequence at northern Mie prefecture that occurred at the beginning of April 2013. Most solutions show NW-dipping low-angle planes or SE-dipping high-angle planes. Because of 180 degrees ambiguity in polarization angles, the present study alone cannot distinguish compressional quadrant from dilatational one. Together with the observation of very long frequency earthquakes near the present study area (Ito et al., 2007), however, it is reasonable to consider that they represent shear slip on low-angle thrust faults. It is also noted that some of focal mechanism solutions contain large strike-slip component. We will present the spatial and temporal characteristics of focal mechanism solutions based on the analysis of more tremor sequences.

Acknowledgements: Seismograph stations used in this study include permanent stations operated by NIED (Hi-net), JMA, and Earthquake Research Institute. This work was supported by JSPS KAKENHI Grant Number 24540463.

Keywords: Non-volcanic tremors, Focal mechanism, Polarization analysis, Shear wave splitting

## Improved estimation of seismic energy radiation from deep low-frequency tremor

ANNOURA, Satoshi<sup>1\*</sup> ; OBARA, Kazushige<sup>1</sup> ; MAEDA, Takuto<sup>1</sup>

<sup>1</sup>Earthquake Research Institute, the University of Tokyo

Deep low-frequency tremor occurs associated with slow slip event on the subducting plate interface at the downdip part of the megathrust seismogenic zone. Studying these phenomena is considered to play an important role to understand the mechanism of the megathrust earthquake. Until now, spatio-temporal distribution of tremor has been well investigated to get a whole picture of tremor activity. In this paper, we proposed a method for assessing energy radiation of tremor more quantitatively.

The Hybrid Method (HM) [Maeda and Obara, 2009] is a technique which determines epicenter and seismic energy of tremor simultaneously by using relative arrival time and amplitude distribution of the tremor envelope. To avoid false event detection, the “ HM selected catalog ” constructed with a threshold of a high Variance Reduction ( $VR > 90$ ) has been used for tremor study. However, when tremor activity is very high, envelope correlation between stations is relatively poor because of complicated waveforms. Then the VR generally becomes low and some parts of tremor during the active stage are not included in the HM selected catalog [Takeda et al., 2014]. Therefore, in order to investigate the energy release of tremor activity precisely, we have to re-evaluate it by using the waveform data.

Here, we developed a method for estimation of tremor energy by using measurement of tremor duration time from envelope waveform and the HM catalog. We started to search the duration around an origin time of tremor in the HM selected catalog. Then we determined the tremor duration when the amplitude is higher than noise level at each station simultaneously. At each tremor duration, we determined epicenter using centroid location of hypocenters of HM selected catalog within corresponding time and determined energy radiation by summing up of energy of tremor epicenters with VR of larger than 60.

As a result, we found characteristic spatial distribution of energy. It has been already known that there are two peaks of the number of tremors in the dip direction [Obara et al., 2010]. In this study, we found that high-energy region is distributed in the shallower part of the source area of tremor along the strike of the subducting Philippine Sea plate. This biased distribution of high-energy radiation suggests that the shallower part is more brittle in the brittle-ductile transition zone where tremor occurs. This brittle part may radiate higher seismic energy when shear slip occurs. This research will lead to quantitative assessment of the role of tremor in the stress relaxation process in the subduction zone.

Keywords: tremor, Nankai trough, slow earthquake

## The role of tectonic tremor in slow earthquake

YABE, Suguru<sup>1\*</sup> ; IDE, Satoshi<sup>1</sup>

<sup>1</sup>Dept. EPS, The University of Tokyo

Since the discovery of the slow earthquake, tectonic tremors, very low frequency earthquakes (VLFs), and slow slip events (SSEs) are thought to have close relation. Although the tremor activity is often regarded as a proxy of SSEs, the degree of proximity is yet unclear due to the lack of detailed quantitative comparison between them, especially for tectonic tremors. Here, we develop a method to estimate the seismic energy of tremors and apply it to tremors in four subduction zones (Nankai, Japan; Cascadia, USA-Canada; Jalisco, Mexico; South Chile). This method estimates the seismic energy of tremors, after evaluating the regionally averaged seismic attenuation and the site amplification factors, which has not been considered enough in previous studies estimating the seismic energy of tectonic tremors. Then the catalog of the energy rate, which is the seismic energy divided by the tremor duration, is compared with some characteristics of tremors, VLFs, and SSEs.

We have observed three types of spatial distributions in terms of energy rate; heterogeneous, homogeneous, and isolated. In regions where the energy rate is heterogeneously distributed on the plate interface, such as Nankai and northern Cascadia, tremor activities almost always initiate from where the energy rate is low. Sometimes the initial tremors trigger more energetic tremors nearby, which are further followed by a long-distance tremor migration along the strike of the subducting plate. These energetic tremors tend to have longer recurrence intervals, and seem to control the onset of a large-scale tremor migration, which probably corresponds to a SSE. In Nankai, the energy rate of tremors estimated between 2-8 Hz is large where VLFs have been detected in the frequency range of 0.02-0.05 Hz. These observations suggest that the characteristics of tremors are regionally various, but similar in different frequency ranges. In the region where tremor activities are isolated, such as East Shikoku, Jalisco and South Chile, each tremor activity has occurred independently, and the relations between the energy rate and the recurrence intervals cannot be seen. In the region where the energy rate is homogeneously distributed on the plate interface, such as a part of southern Cascadia, tremor activities have occurred spontaneously in the entire tremor zone.

Our observation suggests a possibility that the spatial distribution of the energy rate of tectonic tremors might control the behavior of slow earthquakes in the region. When the energy rate is distributed heterogeneously, some energetic tremors seem to control the activity of SSEs, as a switch that ignites a large-scale migration. When tremor patches are isolated, they are passively controlled by the tectonic loading. When it is homogeneously distributed, minor tremor activities, which rupture the only part of the tremor zone, cannot occur.

Keywords: Slow Earthquake, Tectonic Tremors, Seismic wave energy

## Effect of long-term SSE and megathrust earthquake on tremor activity

IDO, Miki<sup>1\*</sup> ; SUDA, Naoki<sup>1</sup>

<sup>1</sup>Graduate school of Science, Hiroshima University

Tremor activity migrates with a velocity of  $\sim 10$  km/day along the strike of subducting plate boundary. Recently it has been shown that migration front draws a parabolic pattern in spatio-temporal distribution of tremors, indicating that tremor migration is diffusional process [Ide 2010]. We analyzed activities from 2001 to 2013 in western Shikoku, and obtained diffusion coefficients on the order of  $10^4$  m<sup>2</sup>/s for all the activities. Relatively large values ( $>1.5 \times 10^4$  m<sup>2</sup>/s) were obtained for the activities during long-term slow slip events (SSEs) in the Bungo Channel region or just after the 2011 Tohoku earthquake (SSJ2013). In this study we investigate the relation between these activities and external stress perturbations.

To evaluate perturbations due to these events, we calculated Coulomb stress changes ( $\Delta CFF$ ) using Coulomb 3.3 [Toda et al. 2011]. The long-term SSEs in 2003 and 2010 produced  $\Delta CFF$  of 28.7 and 5.4 kPa, respectively. These values are large enough to affect tremor occurrences because they are on the same order of magnitude as the tidal effect, which modulates tremor occurrences. The Tohoku earthquake produced  $\Delta CFF$  of 0.4 kPa. Although it is smaller than the tidal effect by an order, a long-time stress change due to possible viscoelastic response would give some effect on tremor occurrences. Since such a stress perturbation is widespread on the plate interface, it could accelerate tremor migration observed as high diffusion coefficient. We also compare tremor activities with the seismicity calculated with a rate- and state-dependent friction law.

**Keywords:** deep non-volcanic tremor, tremor migration, Coulomb stress change, long-term slow slip event, megathrust earthquake, subduction zone

## Improvement of tectonic tremor detecting and locating methods: Case study in Shikoku and Kanto

CHAO, Kevin<sup>1\*</sup> ; OBARA, Kazushige<sup>1</sup>

<sup>1</sup>ERI, the University of Tokyo

Obtaining accurate tremor sources in time and space is important because it provides essential information that reveals the mechanism of tremor activity. Recent findings of triggered tectonic tremor in recently discovered regions in Hokkaido (Obara, GRL, 2012), Kyushu, and Kanto (Chao and Obara, AGU Meeting, 2012) provide an ideal dataset with which we can test the clock-advanced model, which predicts the occurrence of triggered tremor in regions where ambient tremor occurs. In this study, we improve upon two existing tremor detecting and locating methods: 1) the WECC (Waveform Envelope Correlation and Clustering) auto-detecting algorithm (Wech and Creager, GRL, 2008), which auto-detects tremor episodes, and 2) the improved conventional envelope cross-correlation technique (Obara, Science, 2002; Chao et al., BSSA, 2013), which accurately pinpoints the locations of short duration tremor sources in space. Using WECC, we detected tremor episodes in western Shikoku and compared the results with existing NIED tremor catalogs (Maeda and Obara, JGR 2009; Obara et al., GRL, 2010). Our preliminary results indicate that during testing period (i.e., tremor episodes between 2012/05/25 and 2012/06/02), the WECC was able to successfully auto-detect the same ambient tremor episodes listed in the NIED tremor catalogs. The tremor detections by WECC show similar tremor migrations pattern as the features from the NIED tremor catalog. In addition, the WECC is able to capture more small tremor episodes that are not included in the NIED catalog. Our next step will be to apply the WECC to the entire dataset to determine whether it can successfully detect all tremor episodes while minimizing noise. Using the modified envelope cross-correlation technique, we plan to conduct a 3D grid search to locate accurate triggered tremor sources in Kanto following several teleseismic earthquakes. This modified technique has been used to locate micro-earthquakes ( $M \leq 0.5$ ) in western Shikoku, and a comparison of the hypocenter of these micro-earthquakes with those from the JMA earthquake catalog showed that they were located within 5km of one another.

Keywords: ambient tremor, Shikoku, Kanto, tremor auto-detection technique

## Volcanic Deep Low-Frequency Earthquakes and Cooling Magma

ASO, Naofumi<sup>1\*</sup> ; TSAI, Victor<sup>2</sup> ; IDE, Satoshi<sup>1</sup>

<sup>1</sup>Graduate School of Science, The University of Tokyo, <sup>2</sup>Seismological Laboratory, California Institute of Technology

Deep low-frequency earthquakes (LFEs) are deep earthquakes that radiate low-frequency seismic waves. While tectonic LFEs on plate boundaries are thought to be slip events, the physical mechanism of volcanic LFEs around the Moho beneath volcanoes is not well understood. For initial brittle failure to be produced at these temperature-pressure conditions, high strain rates should exist there.

Since an ascending magma diapir tends to stagnate near the Moho, where there is a density discontinuity, we suspect its thermal contraction acts as a driving force of volcanic LFEs. In the present study, we estimated thermal strain rates caused by a cooling magma near the Moho beneath volcanoes.

We calculated thermal evolution after an initial perturbation of 400K uniformly within planar and cylindrical magma intrusions. Then, we estimated thermal strain rates within the region of  $\delta T < 200\text{K}$ , where the medium can be treated as a Poissonian elastic body. We assume a thermal diffusivity of  $6 \times 10^{-7} \text{m}^2/\text{s}$  and a thermal expansion coefficient of  $2 \times 10^{-5}/\text{K}$ , taking into account latent heat release and the density change caused by a phase change of partially molten material.

As a result, strain rates larger than the effect of tectonic loading ( $> 5 \times 10^{-14}/\text{s}$ ) is observed for planar magmas of width of  $< 200\text{m}$  and cylindrical magmas of radius of  $< 160\text{m}$ . Even if the initial crack were not observed because of small amplitude and high attenuation, an excited larger-scale deformation such as a resonance would be observed as an LFE.

The orientation of produced strain rates differs between planar intrusions and cylindrical intrusions. Assuming that magma shape and strain rate correspond to source distribution and source mechanism, respectively, we expect a correlation between source distribution and source mechanism for volcanic LFEs. Although a part of this relationship has been recognized for the LFEs in eastern Shimane in western Japan [Aso and Ide, 2014], more mechanism analyses are needed to verify our model.

Keywords: volcanic low-frequency earthquakes, cooling magma, CLVD

## Spatiotemporal Distribution of Shallow Very Low Frequency Earthquakes along the Nankai Trough and the Ryukyu Trench

ASANO, Youichi<sup>1\*</sup> ; MATSUZAWA, Takanori<sup>1</sup> ; OBARA, Kazushige<sup>2</sup>

<sup>1</sup>National Research Institute for Earth Science and Disaster Prevention, <sup>2</sup>Earthquake Research Institute, The University of Tokyo

We have investigated spatiotemporal distribution of shallow very low frequency earthquakes (sVLFs) along the Nankai trough and the Ryukyu trench. Three component seismograms recorded at 40 broadband stations of the NIED F-net were analyzed by using waveform-correlation and back-projection techniques after processing a band-pass filter (0.02 to 0.05 Hz). Here we used known 6 sVLFs and 17 regular interplate earthquakes near the trench axis as template events. Time series of cross-correlation function (CC) at each station was calculated from continuous waveform data and triggered seismograms of template events. Assuming surface wave propagation, CCs are back-propagated onto possible origin times and horizontal locations. We obtained sVLF epicenters by performing a grid search in time and space domains to maximize the averaged CCs from all stations under the condition of high signal to noise ratios that was defined as amplitude ratios between two time windows before and after the surface wave arrivals from the epicenters. As the result of this analysis for the last decade, we detected infrequent activity of sVLF episodes at a few clusters adjacent to the locked zone related to the megathrust earthquakes along Nankai trough: in 2004 and 2009 of Kii peninsula, in 2003 and 2009 off cape Muroto, and in 2003 and 2010 off cape Ashizuri. On the other hand, sVLF episodes in Hyuga-nada and areas along the Ryukyu trench are frequent. Such a variation of seismicity of sVLFs revealed from this study based on the same detection capability may suggest the difference of the plate coupling in the seismogenic zone.

Keywords: Very Low Frequency Earthquakes, Nankai Trough, Ryukyu Trench

## Relationship between very low frequency earthquakes and repeating slow slip events in the south Ryukyu Trench

NAKAMURA, Mamoru<sup>1\*</sup> ; SUNAGAWA, Naoya<sup>1</sup>

<sup>1</sup>Faculty of Science, Univ. Ryukyus

The repeating slow slip events (SSEs) occur on the upper interface of subducted Philippine Sea plate at the depth from 30 to 50 km in the south Ryukyu Trench region (Heki & Kataoka, 2008). The afterslip of the March 2002 earthquake ( $M_w=7.2$ ) is distributed at the west of the fault of the repeating SSEs. This afterslip continued from March 2002 to 2005 (Nakamura, 2009).

Recently, very low frequency earthquakes, which occurred continuously along the Ryukyu Trench, were detected (Ando et al., 2012). The occurrences of SSEs, afterslip, and very low frequency earthquakes reflect the state of slip in the plate interface.

Then we investigated the relation between the SSEs with very low frequency earthquakes.

We employed the broad-band seismometer network of NIED (F-NET) and IRIS. We used the station of Ryukyu Islands, Kyusyu, SSE (Shanghai), and TATO (Taipei). We used the waveforms of vertical component for the analysis. The period we used are from January 1, 2002 to September 30, 2013. We filtered the band-pass range of 0.02-0.05 Hz to the waveforms, and detected the low-frequency events and picked the arrival times of surface waves manually. The local and teleseismic earthquakes were eliminated using the earthquake catalogue. The local events were also eliminated with checking the high-pass filtered record. Then we determined the location of low frequency events assuming that the observed waves were Raleigh waves.

We determined the 6299 low frequency events for 12 years. Almost events are distributed along the Ryukyu Trench axis. The low frequency events are clustering at the south Iriomote Island, south of Okinawa Island, and near Amami Island. The events are also distributed near the Okinawa Trough. However, the events in the Okinawa Trough would be the apparent distribution by miss-location of hypocenter determination which is caused by the linear distribution of seismic stations along the Ryukyu Arc.

Next we investigated the cumulative number of low frequency earthquakes in the clusters. The activity of the low frequency events at the cluster of the south of Iriomote Island decreased from 2005 to 2010, and increased since late of 2011. The activation of very low frequency events occurred after the occurrence of repeating SSEs. The 24 SSEs had occurred since 2002, and the 14 activation of the low frequency events occurred after the SSEs. The occurrence rates of the VLFs during the SSEs increased about 2-3 times than the averaged ones. However, the activation of usual earthquakes during the SSEs occurred only two times. These suggest that the SSEs would trigger the VLFs.

Keywords: very low frequency earthquake, slow slip event, Ryukyu Trench

## Activity characteristics of deep very low frequency earthquake and asperity structure

NIZATO, Taro<sup>1</sup> ; SUDA, Naoki<sup>1\*</sup> ; MATSUZAWA, Takanori<sup>2</sup>

<sup>1</sup>Hiroshima Univ., <sup>2</sup>NIED

Deep very low frequency earthquake (VLF) and deep nonvolcanic tremor (NVT) concurrently occur with short-time slow slip event (SSE) in the Nankai subduction zone. Among them VLF is least known since seismic records are usually noisy at dominant periods of VLF signals (20-50 sec). We have developed a new grid-based method for monitoring VLF activity in the Nankai subduction zone. In this method we assume that VLF occurs at equally-spaced grids on model plate boundary, and that VLF at each grid has a fixed source mechanism predetermined from plate boundary model and observed plate convergence direction. Previous studies have used the grid moment-tensor method in which depth and source mechanism are freely determined. These parameters are predetermined in the present method, so that it is expected that small VLFs can be detected even from low S/N records.

As a preliminary study we analyzed Hi-net accelerometer records for two activities in western Shikoku in September 2006 and March 2007. We detected a large number of VLFs compared with previous studies, and observed the following characteristics: (1) Some VLF occurrences were rapidly activated than NVT occurrences, and VLF activity highs were sometimes delayed relative to NVT activity high, (2) There was an NVT cluster with or without VLF depending on activity, (3) Rapid tremor reversals are associated with VLFs, (4) Clusters with maximum moment release were different between VLF and NVT, (5) The cluster of maximum VLF moment release was located in the updip portion next to the region of maximum SSE moment release. Some of these characteristics can be explained by a nested or fractal asperity model, in which small NVT asperities are contained in a VLF asperity.

Keywords: Nankai subduction zone, slow earthquake, very low frequency earthquake, nonvolcanic tremor, automatic detection, asperity

## Preseismic behaviors involving slow slip in rate-state earthquake sequence models with a hierarchical asperity concept

NODA, Hiroyuki<sup>1\*</sup> ; NAKATANI, Masao<sup>2</sup> ; HORI, Takane<sup>1</sup>

<sup>1</sup>JAMSTEC, IFREE, <sup>2</sup>The University of Tokyo, ERI

Understanding preseismic phenomena before large earthquakes is of critical importance in assessing possibility of disaster mitigation by detecting and recognizing them. The 2011 Tohoku-Oki earthquake has long recorded geophysical data for tens of years prior to it. Since the earthquake, multiple studies have reported potentially important phenomena involving slow slip which may be particular to ripe asperities. It is our mission for modelers to see if they are consistent with, or appear naturally without fine tuning of numerical models of earthquake sequences accounting for interseismic processes, as well as earthquake ruptures.

The off-Miyagi to off-Fukushima region was locked at least from Apr. 1995 to Mar. 2002 [Nishimura et al. 2004], with the shallower region not being able to be constrained by on-land GPS stations [Loveless and Mead, 2011]. The region started creeping from 2005 [Ozawa et al., 2012]. Recently, Katsumata [2013, JpGU] pointed out that seismic quiescence [Katsumata, 2011] correlates with the locked period, and inferred that this region may have been creeping at least from 1980 to 1988. In the shallower region near the hypocenter of the Tohoku-Oki earthquake, a couple of slow slip events were reported by Ito et al. [2013], one in Nov. 2008 and the other in Feb. 2011. This interval is much shorter than that for the larger scale events inferred by Katsumata [2013].

Suito et al. [2011] reported that M7-class earthquakes along the Japan Trench after 2005, including the Mw 7.3 preshock 2 days before the Tohoku-Oki earthquake, had unusually large amount of afterslips. The postseismic moment releases are comparable to or even larger than the coseismic ones, with the centroid being located close to the epicenters, not deeper than them.

In the present talk, we present that qualitatively similar behaviors to those observations are recognized in numerical models reported by Noda et al. [2013, JGR]. They presented rate-state earthquake sequence simulations accounting for a hierarchical asperity concept [Ide and Aochi, 2005]; a large tough patch has a small fragile patch in it. Importantly, those simulations were not meant to mimic the Tohoku-Oki earthquake through fine tuning of the model, and are representing general behaviors characteristic to the rate-state (aging law) earthquake sequence with a certain kind of heterogeneity in the parameter distribution.

In those simulations, interseismic penetration of a creep front into a locked velocity-weakening patch often becomes non-steady and accompanied by aseismic transients before nucleation. This is because the critical length scale for impossibility of coherent steady-state slip [Rice et al., 2001] can be smaller than the nucleation size [Rubin and Ampuero, 2005]. In the simulation, the transients take place both in the large tough patch and in the small fragile patch when a creep front penetrates inwards to a certain extent. A transient does not necessarily, but may lead to nucleation. In addition, such an elevated aseismic slip rate in the large patch seems to be a necessary condition for cascade-up rupture growth from the small patch if it is smaller than the nucleation size of the large patch.

A small event which only ruptures the small patch is sometimes followed by a large event before the afterslip smearing out. Such small events are classified as precursory events, since clear causality is recognized between them and the following large ones; the large ones are initiated either by delayed cascade-up or by large nucleation hosted by the afterslip. The precursory small events tend to have larger afterslip than non-precursory ones.

In the rate- and state-dependent friction law, logarithmic slip rate is, by definition, proportional to stress minus strength which correlates with fracture energy. Therefore temporal changes in the aseismic slip rate in a so-called asperity, if detectable, could be used to infer the ripeness of it.

Keywords: Earthquake sequence, Preseismic phenomena, Hierarchical asperity, Numerical simulation

## Numerical simulation of slow slip events before the 2011 Tohoku-Oki Earthquake

NAKATA, Ryoko<sup>1\*</sup> ; ARIYOSHI, Keisuke<sup>1</sup> ; HYODO, Mamoru<sup>1</sup> ; HORI, Takane<sup>1</sup>

<sup>1</sup>JAMSTEC

In the Japan Trench, the M9.0 great interplate earthquake occurred on 11 March 2011, off the coast of Tohoku, Japan. Before this earthquake, two slow slip events (SSEs) were observed on 2008 and 2011. The second SSE occurred on February 2011 at the downdip end of the huge-coseismic-slip region, and it continued at least until the occurrence of the M7.3 largest foreshock on March 9 [Ito et al., 2013]. In addition, following the largest foreshock, postseismic slip propagated to the location of the mainshock hypocenter and triggered the dynamic rupture there [Ando & Imanishi, 2011].

In this study, we numerically simulated cycles for occurrences of seismic and aseismic events along the Japan Trench with the 3D geometry of the Pacific plate. We model the M9 2011 Tohoku-Oki Earthquake, the largest foreshock of the M9 earthquake, and the SSE before the foreshock using the slowness law, which is a type of rate- and state-dependent friction law. We set frictional properties at source area of earthquakes and SSEs to satisfy a condition of unstable slip and slow slip, respectively. We evaluated simulation results achieved using different values of frictional parameters with respect to characteristics such as the slip history leading to the 2011 Tohoku-Oki earthquake and crustal deformation before and after the Tohoku-Oki earthquake.

As a result, we quantitatively reproduced the observed scenario. Temporal characteristics of the resultant scenario were sensitive to both sizes and locations of the circular fault patches. Now, we are improving our model to reproduce various characteristics qualitatively. Based on some of the reasonable results achieved, we will discuss frictional conditions for the pre-seismic process of the 2011 Tohoku-Oki earthquake.

## Deep Triggered Non-Volcanic Tremor in the Slow Earthquake Active Regions in South Chile and Ecuador

CHAO, Kevin<sup>1\*</sup> ; OBARA, Kazushige<sup>1</sup>

<sup>1</sup>ERI, the University of Tokyo

Deep non-volcanic tremor has been observed at many major plate-boundary faults and intraplate faulting systems. Recent studies have shown that the tremor triggered by surface waves of teleseismic earthquake occurs on the same fault patches as the spontaneously occurring ambient tremor. The observations suggest that the triggered tremor can be used as a proxy to estimate the background tremor activity. Here we search for tremor triggered by teleseismic earthquakes in south Chile and Ecuador where the ambient tremor and slow slip event have been observed respectively. In south Chile, we analyzed a temporal array data between 2004 and 2006 and observed clear triggered tremor following the 2004 Mw9.0 Sumatra, 2005 Mw8.6 Nias, and 2006 Tonga earthquakes. Triggered tremor sources are located at the central of the ambient tremor zone. The results indicate both Love and Rayleigh waves promote the tremor triggering potential. The tremor triggering threshold is around 2 kPa, similar to which in Parkfield. In Ecuador, we can only use single station to infer the existence of triggered tremor due to lack of seismic stations in this region. During the period between 2004 and 2012, we observed triggered tremor following the 2010 Mw8.8 Chile and 2007 Mw8.0 Peru earthquakes. Since there is no other station within 500 km near that station, we roughly estimate that the triggered tremor sources are located within 50 km from the station based on the attenuation of tremor from previous studies and the estimation of the time difference between P- and S-waves of triggered tremor. We infer that the triggered tremor source might be located at the region where the slow slip event has been observed. The apparent tremor triggering threshold in Ecuador is about 40 kPa. The high threshold infer a low background tremor rate or simply due to the network capability.

Keywords: non-volcanic tremor, triggered tremor, south America

## Shallow low-frequency tremor activity in the Hyuga-nada, revealed by ocean bottom seismographic observation

YAMASHITA, Yusuke<sup>1\*</sup> ; YAKIWARA, Hiroshi<sup>2</sup> ; UCHIDA, Kazunari<sup>1</sup> ; SHIMIZU, Hiroshi<sup>1</sup> ; HIRANO, Shuichiro<sup>2</sup> ; MIYAMACHI, Hiroki<sup>2</sup> ; UMAKOSHI, Kodo<sup>3</sup> ; YAMADA, Tomoaki<sup>4</sup> ; NAKAMOTO, Manami<sup>1</sup> ; FUKUI, Miyo<sup>1</sup> ; KAMIZONO, Megumi<sup>1</sup>

<sup>1</sup>Institute of Seismology and Volcanology, Kyushu Univ., <sup>2</sup>Nansei-Toko Observatory for Earthquakes and Volcanoes, Kagoshima Univ., <sup>3</sup>Graduate School of Fisheries Science and Environmental Studies, Nagasaki Univ., <sup>4</sup>Earthquake Research Institute, Univ. of Tokyo

In order to reveal the detail of microseismicity from the shallower part of the plate boundary to seismogenic zone in the Hyuga-nada region, we have conducted Ocean Bottom Seismographic observation from May 19 until July 6, 2013. We used 12 Ocean Bottom Seismometers (OBSs) with a three-component short-period seismometer. During this observation, we observed many low-frequency tremors (SLFT) which mainly occurred from end of May to end of July 2013 [Yamashita *et al.*, 2013 AGU fall meeting]. We report the detail of SLFT activity in the Hyuga-nada region based on the semi-automatically analysis using envelope correlation method (ECM)[Obara, 2002].

The differential arrival times between OBS stations using ECM were obtained from the lag times with maximum cross-correlation coefficient between the pair of the root mean square (RMS) envelopes which were converted from composite horizontal components waveform with applying a 2-8 Hz bandpass filter. RMS envelopes were smoothed by using 5 s window and performed down-sampling with a 20Hz. The length of RMS envelopes for calculating of cross-correlation coefficients was set for 150 s. If the maximum cross-correlation coefficient for a pair was larger than 0.85, and more than or equal to 6 pairs, we searched minimum RMS residual position by a grid search algorithm. These processing were performed automatically for the continuous RMS envelope records every 75 s (i.e., overlapping two moving window for 75 s). After the calculation, we carefully examined the candidate tremor events to distinguish "regular" earthquakes, T-phase signals, or background noise.

Based on the result of SLFT location by ECM, we identify two migration episode of the SLFT: 1st episode started in east off Tanegashima Island from end of May, 2013, migrated northward along strike of subducting plate, veered away to the north-west in the around S08 station, then reached under the S06 station on July 12 - 14. 2nd episode started in the south of S08 station on July 17, migrated northward and veered away to the north-west in the around S08 station, reached around the S07 station, veered away to the east, reached around the S09 station.

These migration episodes suggest that undetected short-term slow-slip event may have occurred at the same time in the shallow part of the Hyuga-nada region. Around the focal area of SLFT, the Kyushu-Palau ridge is subducting: the SLFT activity was only found on the south side (i.e., Ryukyu arc side). In particular, the depth of plate boundary around the S08 station is southwestward deepening down to 10 km depth [Park *et al.*, 2009]. Therefore, the episodic slow-slip extended to northward with SLFT activity, and shifted to northwest-ward caused by the Kyushu-Palau ridge which act a segment boundary to control the interplate slip phenomena.

Acknowledgements: We thank the crews of T/S Nagasakimaru (Faculty of Fishers, Nagasaki University) for OBS observation.

Keywords: Shallow low-frequency tremor, Ocean Bottom Seismographic observation, Hyuga-nada

## The Slow Slip Event off the Boso Peninsula on January 2014 and the associated earthquake swarm

KIMURA, Hisanori<sup>1\*</sup>

<sup>1</sup>National Research Institute for Earth Science and Disaster Prevention (NIED)

### Introduction

Off the Boso Peninsula, at the southeastern Kanto, central Japan, slow slip events (SSE) accompanied with earthquake swarms recurs with time interval of 4-7 years. SSEs have occurred in 1983, 1990, 1996, 2002, 2007, and 2011 and the latest SSE recurred from Dec. 2013 to Jan. 2014 with interval of 2 years and 2 months. In this study, detailed activity of the earthquake swarm and a fault model of the Boso SSE were determined.

### Data and Methods

High precision hypocenter distribution was determined for earthquakes shallower than 30 km off the Boso Peninsula, from Jan. 1, 2005 by Double Difference method incorporating waveform correlation analysis. Hypocentral parameters determined by NIED Hi-net (automated hypocenters were partly included) were used as initial hypocenters.

A rectangular fault model with uniform slip was determined using genetic algorithm inversion for fault location and geometry and the weighted least squares method for slip amounts, following a method of Obara *et al.* (2004) based on tilt data recorded by high sensitivity accelerometer co-installed in NIED Hi-net station. In this analysis, slip direction was fixed to the direction of relative plate motion.

### Results

Most earthquakes occurred around the northern edge of the seismic region where seismic swarms associated with the previous Boso SSEs occurred. Seismic swarms first occurred at the eastern offshore area and then migrated to the western onshore area. Migration from offshore to onshore regions is common feature among the previous Boso SSEs. Distribution of earthquake swarms is similar to that of the 2007 SSE, although spatial distribution and number of events are slightly smaller than the 2007 SSE.

The maximum crustal tilting of about  $0.4 \mu$  radian with northwestward direction was observed at KT2H station and the fault model was determined to be located off the Boso Peninsula with size of  $M_W$ 6.1. Location of SSE slip overlaps with locations of the 2007 (Sekine *et al.*, 2007) and initial stage of the 2011 (Hirose *et al.*, 2012) SSEs. Tilting direction is similar to tilting direction of the 2007 SSE, however, its amount is about a half of the 2007 SSE ( $M_W$ 6.4) and the SSE size is also smaller. Smaller number of earthquakes is likely to reflect smaller size of the SSE. In the 2011 SSE, west-northwestward tilting of about  $0.3 \mu$  radian was observed for the first two and a half days and size for this period was estimated as  $M_W$ 6.2. Its direction and amount are similar to those of the 2014 SSE and the SSE size is also close.

### Discussion

Recurrence interval of the 2014 SSE was shortest for the last about 30 years. The size of the 2011 SSE was estimated to be comparable to previous SSEs and a possibility that the 2011 SSE was hastened by the stress increase caused by the 2011 Off Tohoku Earthquake and its afterslip has been proposed (Hirose *et al.*, 2012). On the contrary, size of the 2014 SSE is likely to be smaller than previous SSEs. This result infers that the SSE slip is smaller supposing the same source area and the SSE recurred with shorter interval with smaller stress accumulation. Further analysis is necessary to reveal the detailed source process of the Boso SSE for monitoring of the stress accumulation.

### Acknowledgements:

In this study, seismic data obtained by Earthquake Research Institute (ERI) and Japan Meteorological Agency (JMA) were used.

Keywords: Slow Slip Event, plate boundary, earthquake swarm, Kanto region

## A long-term slow slip event in central Shikoku in 2013

KOBAYASHI, Akio<sup>1\*</sup>

<sup>1</sup>Meteorological Research Institute

A long-term slow slip event in central Shikoku is investigated using the GEONET GNSS data. We estimated the steady deformation rate at each GNSS station from the daily coordinates for the period from January to December 2012. Then the steady deformation rates were subtracted from all the coordinate data. The artificial offsets of the coordinate were corrected using data set shown on the web site of the Geospatial Information Authority of Japan. We can see south-eastern displacements less than 1 cm at GNSS stations in central Shikoku for one year from October 2012. These unsteady displacements are also seen in the time series of the baseline lengths between central Shikoku and Chugoku district.

We estimated slip distribution on the plate boundary, assuming the unsteady displacements were caused by a slip on the plate boundary. The estimated slip is distributed in central Shikoku. Center of the slip is located slightly southeast of the belt of deep low-frequency earthquakes. The size of the slip is equivalent to Mw 6.2, which is smaller than other long-term SSEs along the Nankai Trough.

Keywords: long-term slow slip, GNSS, crustal deformation, central Shikoku

## Rate and state simulation of Yaeyama slow slip events in the southwestern part of the Ryukyu Arc, Japan

OKUDA, Ryosuke<sup>1\*</sup> ; HIRAHARA, Kazuro<sup>1</sup> ; MIYAZAKI, Shinichi<sup>1</sup> ; KANO, Masayuki<sup>1</sup> ; OHTANI, Makiko<sup>1</sup>

<sup>1</sup>Graduate School of Science, Kyoto University

Slow slip events (SSEs) are recurring on the plate interface beneath the source regions of the interplate large earthquakes. It has been proposed that the activity of SSE possibly changes before the occurrence of large interplate earthquakes. Hence, it is essential to know the frictional properties for producing SSEs to predict the occurrence of large earthquakes. Our final goal is to optimize frictional parameters on the fault related to SSE through a data assimilation method which combines the observational data and the forecast ones derived from a simulation model, and then to give information on the occurrence of large interplate earthquakes. In this paper, as a first step of such a data assimilation, we construct a simulation model reproducing the observed spatio-temporal slip evolution of SSE.

In this paper, we consider the Yaeyama SSEs. Around the Yaeyama islands in the southwestern part of the Ryukyu Arc, Japan, GPS observations have caught the frequent recurrence of SSE activity. Around there have occurred almost no large earthquakes that affect the SSE activities during the observational period, which leads to a relatively simple simulation model of SSE. Those are the reasons that we select SSE on this area.

Heki and Kataoka(2008) reported the following features of Yaeyama SSEs; 1) SSEs recur on a plate interface at depths of 20-40km, 2) the average recurrence interval is 6.3 months, 3) its standard deviation is 1.2 months, 4) the slip rate released by SSEs is 11.0 cm/yr, in spite of the estimated convergence rate of 12.5 cm/yr.

We construct a simulation model which reproduces the above mentioned features of SSE. We set a dipping fault embedded in a homogeneous elastic half space. The friction on the fault is assumed to obey a rate- and state-dependent friction law, and the slowness law of state evolution (Dietrich, 1979). To simulate SSE, following Kato(2003), we set an asperity at depths of 20-40 km on a stable sliding plate interface, whose frictional properties are characterized by frictional parameters A, B and L. The asperity has the rate weakening frictional property of  $A-B < 0$  and its radius is nearly equal to or less than the nucleation radius determined by frictional parameters. We also consider the possible presence of a locked zone, namely an asperity, at the shallow portion of the plate boundary close to the Ryukyu Trench, which might cause the 1771 Meiwa tsunami (Nakamura, 2009). Dating of tsunami stones suggests a possible recurrence of 150-400 years of large tsunami (Araoka et al., 2013), and the large tsunami events close to the Ryukyu Trench might have recurred in several hundred years.

It is found that the interval of SSE can be adjustable by changing the friction parameters. For example, if a single asperity with the size of 80 km has frictional parameters of  $A=50$  kPa,  $B=56$  kPa, and  $L=2.2$  mm, the interval is about 6 months. Further, if we add another asperity with 40 % slip deficit rate of the convergent rate of 12.5 cm/yr just above the SSE asperity zone, the slip rate released by SSEs reduces to the observed rate of 11.0 cm/yr. The released slip rate depends on the location, size and assigned slip deficit rate of the shallow asperity. The locking state at the shallow portion is important to give information on the occurrence of possible tsunami earthquake, and we need the further investigation. For reproducing the observed fluctuation of recurrence intervals of SSE, we need to consider the interaction among multiple asperities or the hierarchical asperity model where a large asperity has small asperities with different properties inside itself.

Keywords: slow slip events, Yaeyama, a rate- and state-dependent friction law

## Array observation of short span strainmeter in the Kii peninsula

KANO, Yasuyuki<sup>1\*</sup> ; HOSO, Yoshinobu<sup>1</sup> ; ONOUE, Kensuke<sup>1</sup>

<sup>1</sup>DPRI, Kyoto Univ.

Crustal deformations have been observed associated with deep low-frequency tremors occurring below the Kii peninsula and Shikoku. Strain measurements by an extensometer at Kishu operated by DPRI, for example, show that the sources with epicentral distance of 30 - 40 km causes strain changes of  $10^{-9}$  to  $10^{-8}$  occurring within several days. Although the traditional extensometer observations can detect these strain changes, it is difficult to make detailed analyses because of the limited number of stations. We designed a short-span extensometer with 1.5 m-long standard measure. Strong coupling of the instrument to the ground is important for stable observations, so three anchor bolts fixed to the base of the instrument are cemented into a 50-cm-deep hole. We observed crustal deformation associated with deep low-frequency tremors by the short-span extensometer installed at Nakaheji. We detected strain change associated with low frequency events occurred on March 2013. We are preparing another sites for installation of the strainmeter around the western Kii Peninsula to construct array of strainmeters. The array observation contributes to improve the detection capability of crustal deformation by eliminating noise caused by weather disturbance and to have better understanding of slow slip events such as slip distribution.

Keywords: strainmeter, slow earthquakes, array observation

## Reconstruction of paleostress states in the Walanae fault zone in South Sulawesi using the multiple inverse method with

NISHIKAWA, Osamu<sup>1\*</sup>

<sup>1</sup>Akita University

Paleostress analysis using the multiple inverse method with calcite twin data was performed in the East Walanae fault (EWF) zone in South Sulawesi, Indonesia. The geomorphic trace of the EWF can be recognised as a distinct line between the Bone Mountains and the Walanae Depression, around which an intensive deformation zone characterised by various scales of faults and folds are developed. Carbonate rocks with numerous calcite twins and mesoscale faults are ubiquitous around the EWF trace. Therefore EWF zone is a useful location for testing the inclusion of calcite twin data in the multiple inverse technique to determine paleostress states. One to three poles of differently oriented twin lamellae and c-axis orientation were measured for each grain from three mutually perpendicular thin sections for 11 samples using a U-Stage optical microscope. The data set for multiple inverse method consists of the attitude of the e-plane, gliding direction and sense of shear of e-twinning. We prepared data files not only for twinned e-planes but also for the remaining untwinned e-planes in a grain with one or two twin sets. We incorporated the untwinned e-plane data for determining stress states with the multiple inverse method using calcite twins. In the analysis, the identified stress states by twinned e-plane data were tested calculating misfit angle  $\beta$ , the angle on the untwinned e-plane between the calculated maximum shear stress direction for every identified stress state and the observed potential gliding direction. It is possible to say that the sampled rocks had never experienced stress states to activate any of the untwinned e-planes. Therefore, if most untwinned e-plane data (95% or more in this study) are incompatible ( $\beta > 30$  degree) with the stress state identified from twinned plane data, then the stress state is viable for both the twinned and untwinned e-planes.

The analysis using calcite twin yielded reliable paleostress states similar and consistent with those from fault-slip data throughout the study area. Dominant and common stress states are characterized by NE-SW-to-E-W-trending  $\sigma_1$  and vertically to moderately-south-plunging  $\sigma_3$  with generally small values of stress ratio  $\phi$ . These stress states were most likely caused by collision of eastern Sulawesi with the Australian fragments since the Pliocene, and they could have activated the EWF as a reverse fault with a dextral shear component, accounting for the contraction deformation structures and landforms along the trace of the fault. Calcite twin and mesoscale faults were activated predominantly during the fold tightening stage and subordinately before folding.

Keywords: multiple inverse method, calcite twin, Walanae fault zone

## Capability of calcite twin for estimating stress magnitudes and orientations

YAMAJI, Atsushi<sup>1\*</sup>

<sup>1</sup>Kyoto University

Calcite has three e-twin planes, each of which has a critical resolved shear stress at  $\sim 10$  MPa along the twin gliding direction; and the planes and direction have certain crystallographic orientations (e.g., Lacombe, 2010). We quantified the tightness of the constraints from twin and untwin data on stress conditions. It is shown that twin and untwin data place tight constraints if differential stress is low and large, respectively. Their tightness converges to the same value with increasing differential stress. The constraint from a calcite grain becomes tighter with increasing number of twin sets in the grain. It is also shown to be important to cope with sampling bias to utilize untwin data: The number of twin data compared to the total of twin and untwin ones tend to be underestimated by  $\sim 25\%$ . It is found that calcite e-twin loses resolution in determining stress magnitudes and orientations if differential stress is greater than  $\sim 200$  MPa.

Keywords: twin, calcite aggregate, stress

## Enhanced detectability of stress tensor inversion from heterogeneous fault-slip data with preferred orientations

SATO, Katsushi<sup>1\*</sup>

<sup>1</sup>Div. Earth Planet. Sci., Kyoto Univ.

Fault planes occasionally have preferred orientations according to the slip tendency (e.g., Lisle and Srivastava, 2004), which is defined as the ratio between normal and shear stresses (Morris et al., 1996). In contrast, most stress tensor inversion methods calculate crustal stress states from fault-slip data on the assumption that faults slip along the resolved shear stress vectors on their surfaces. This assumption called Wallace-Bott (W-B) hypothesis allows low values of slip tendency on "misoriented" faults so as to consider faulting along pre-existing weak surfaces in rock masses. However, the weak assumption causes the loose constraint on stress. For example, when a set of conjugate faults is observed, one usually determines principal stress axes as bisectors of fault planes. On the contrary, W-B hypothesis permits only to constrain the axes within the angle between fault planes. Such a disadvantage severely lowers the detectability of multiple stress conditions from heterogeneous fault-slip data. To avoid this problem, this study proposes a new method of stress tensor inversion by combining the W-B hypothesis and the slip tendency.

This study employed a stress tensor inversion method called HIM (Yamaji et al., 2006; Sato 2006) which maximize the fitness between observed slip directions and shear stress vectors. The fitness value is modified to be the product of the conventional fitness and the slip tendency. Artificial fault-slip data are analyzed to examine the performance of the new method. The data set includes 200 faults compatible with N-S compressional stress and 50 faults compatible with E-W tensional stress. The former has random orientations of fault planes and the latter has a preferred orientation so that they have large values of slip tendency. As the result, the conventional HIM could not detect the latter stress, while the new method could detect both stresses.

The new method is applied to fault-slip data from Late Miocene Awa Group in eastern Boso Peninsula. Mesoscale faults in this area have at least two different origins; reverse-faulting stress and normal-faulting one (e.g., Angelier and Huchon, 1987). The new method successfully detected both stresses without a priori classification of faults into subsets.

### References

- Angelier, J. and Huchon, P. 1987, *Earth Planet. Sci. Lett.*, 81, 397-408.
- Morris, A., Ferrill, D.A. and Henderson, D.B., 1996, *Geology*, 24, 275-278.
- Lisle, R.J. and Srivastava, D.C., 2004, *Geology*, 32, 569-572.
- Sato, K., 2006, *Tectonophys.*, 421, 319-330.
- Yamaji, A., Otsubo, M. and Sato, K., 2006, *Journal of Structural Geology*, 28, 980-990.

Keywords: stress tensor inversion, heterogeneous fault-slip data, slip tendency, orientation distribution

## Reconstruction of absolute stress based on a condition of aftershock occurrence

IMANISHI, Kazutoshi<sup>1\*</sup>; UCHIDE, Takahiko<sup>1</sup>

<sup>1</sup>Geological Survey of Japan, AIST

Absolute crustal stress is essential to understand the earthquake generation process. If focal mechanisms both before and after an earthquake together with the fault slip model of the earthquake are available, the magnitude of absolute stress can be constrained (e.g., Hardebeck and Hauksson, 2001; Wesson and Boyd, 2007; Yang et al., 2013). However the application of those methods is inherently limited, because background seismicity is generally low. In this study, we propose a method to reconstruct an absolute stress field incorporating a condition of aftershock occurrence, which is applicable to areas without enough pre-mainshock focal mechanisms.

We suppose that there are pre-existing weak planes represented by aftershock focal mechanisms. Because these planes were locked before the mainshock but afterwards activated, it is reasonable to expect that the slip-tendency, defined by the ratio of shear to normal stress acting on a given plane (Morris et al., 1996), increases after the occurrence of the mainshock. On the basis of this consideration, we search the best absolute stress field as follows.

(1) We assume a pre-mainshock homogeneous absolute stress field (**B**) in the study area. We then compute a post-mainshock stress field (**A**) at each aftershock location by combining the stress change due to the mainshock and the aforementioned pre-shock stress field.

(2) For the fault plane of each aftershock, we compute a pre- and a post-mainshock slip-tendency ( $T_s^b$  and  $T_s^a$ , respectively) based on the pre- and post-mainshock stress fields, **B** and **A**, respectively. Regarding the computation of  $T_s^a$ , we adopt the component of stress acting in the slip direction on a fault instead of the shear stress itself. Therefore,  $T_s^a$  can have a negative value.

(3) We compute the summation of  $T_s^a$  of aftershocks that satisfy the condition of  $T_s^a > T_s^b$ . If both nodal planes satisfy the condition, the larger  $T_s^a$  is used for the summation.

(4) We repeat the procedure (1) to (3) by changing the initial stress field **B**, and search a stress field that has the largest sum of  $T_s^a$ .

Numerical tests of this method work well. It is noted that multiple candidates of stress fields were inferred, if we did not incorporate the condition of  $T_s^a > T_s^b$ , suggesting that the condition is important in the situation without pre-mainshock focal mechanisms. We then applied the method to the 2013 M6.3 Awaji Island earthquake. Focal mechanisms of 115 aftershocks were determined from P-wave polarity data as well as body wave amplitude. A finite fault slip model of the mainshock was derived from slip inversion analysis (see Uchide and Ide, 2007) of KiK-net strong-motion data. A preliminary analysis shows that the pre-mainshock stress field is characterized by a reverse-faulting regime with a WSW-ENE oriented maximum compression and the differential stress of 200-300 MPa.

Acknowledgements: Seismograph stations used in this study include permanent stations operated by NIED (Hi-net, KiK-net), JMA, ERI, and DPRI. We modified a program coded by Satoshi Ide to estimate the focal mechanism solutions. We thank Yoshimitsu Okada for the use of his code in our stress change computation.

Keywords: absolute stress field, aftershock, focal mechanism, 2013 Awaji Island earthquake, slip-tendency

## Motions after rainfall in borehole tiltmeters and the azimuth of crustal stress before and after 2011 Tohoku Earthquake

SHIMADA, Seiichi<sup>1\*</sup> ; KIMURA, Takeshi<sup>1</sup>

<sup>1</sup>NIED

Shimada (1987) has revealed that in borehole telemeter generally the tilt motions after rainfall are tilting to a certain azimuth which is named 'rainfall component', and the perpendicular azimuth is named 'rainfall-free (RFF) component'. In the time series of the RFF component, very little motions are seen after rainfall. From the observations of tiltmeters in NIED Kanto-Tokai network, Shimada (1987, 1989) has found that the azimuths of the RFF component are generally coincided with the azimuth of the crustal maximum compressive stress obtained from the experiments of hydrofracturing and the mechanisms of middle or large scale earthquakes. This is interpreted that the azimuth of the strike of the nearby open crack of the borehole is generally coincided with the azimuth of the crustal maximum compressive stress.

In this study, we examine the azimuth of tilt motions after rainfall for Hi-net borehole high-sensitivity accelerometer (tiltmeter) in the periods from April to December in 2010, 2011, and 2012 before and after the 2011 Great Tohoku Earthquake in the region of the border of Ibaraki and Fukushima prefectures, and the time variations of the azimuth of the maximum principal crustal stress.

The left figure shows the azimuth of the RFF component of the seven borehole tiltmeters in this area obtained from the time series from April to December 2010. In IWEH site, the azimuth of the RFF component is almost N-S direction, suggesting in the nearby area of this site the maximum compressive stress was not E-W direction even before the 2011 Great Tohoku Earthquake. Among the sites south of IWEH site, in the sites near IWEH site and coastal sites the RFF components are generally almost NE-SW direction, suggesting in the area the maximum compressive stress does not coincide with E-W direction which is seen widely in NE Japan before the 2011 Great Tohoku Earthquake.

The right figure shows the azimuth of the RFF component of the same seven borehole tiltmeters obtained from the time series from April to December 2011 or 2012. In this period, there occurs many offsets and large drifts after those offsets arose by the induced earthquakes and aftershocks of the 2011 Great Tohoku Earthquake, and it is not so easy to detect the detections of the motions after rainfall and the azimuth of the RFF components comparing with the period in 2010. In HTAH and YBKH sites, there seems very little time variations in the azimuth of the RFF component. Also in IWEH site, the time variation of the azimuth of the RFF component is only 10 degree. In IWWH site, the azimuth of the RFF component changes significantly, and almost N-S direction. In DGOH site also the azimuth of the RFF component changes from the NE-SW direction before the earthquake to the NNE-SSW direction. In THGH sites, there are very large noises in N-S component in 2012, which is probably mechanical faults, and there seems very little time variations in the azimuth in 2011 compared with that in 2010. In JUOH site, very little tile motions are seen after rainfall, suggesting the closing of the crack opened in 2010 because of the time variations of the azimuth of crustal stress.

Estimating from the tilt motions after rainfall before and after the 2011 Great Tohoku Earthquake in the Hi-net sites in the area of the border of Ibaraki and Fukushima prefectures, it is suggesting that the area with the N-S direction maximum compressive stress is exist near the IWEH site even before the earthquake, and that mainly in the area west of IWEH site the maximum compress stress shifts near N-S direction after the earthquake.

Keywords: borehole tiltmeter, tilt motions after rainfall, azimuth of crustal stress, 2011 Great Tohoku Earthquake



## Evaluation of faults in the site of power plants and stress analyses

SHIGEMATSU, Norio<sup>1\*</sup>

<sup>1</sup>Active Fault and Earthquake Research Center, AIST

The expert meeting on the investigation of fracture zones in the site of the Ohi power station of NRA (Nuclear Regulation Authority) concluded that the F-6 fault in the site is not an active fault. Stress tensor inversion was a key technique to make the conclusion during the discussion. In this talk, I will explain how stress tensor inversion was used to evaluate the faults.

It is difficult to evaluate faults based on paleoseismological techniques in the site of many of the power plants, due to the lack of young sediments and tectonic landforms. For the evaluation of the safety of the power plants, it is important to evaluate if the faults in the site are active. Degree of the activity of the faults is not always important. Stress tensor inversion based on the fault slip data is useful because the phenomenon is relatively clear.

There are two concepts to evaluate if the faults are active or not using stress analyses. One is to compare the structures in the fault with the present stress such as slip tendency. The other is that stress tensor inversion is used as a tool to construct the tectonic histories. The former concept may have a problem concerning the stability of stress, especially after large earthquakes. The later concept used stress tensor inversion to determine the sequence of tectonic stages. Tectonic stage is the period during which faults had repeated to move due to the control of similar stress condition. Once the structures in faults at different places were identified to be controlled by the same stress condition, those structures were formed during the same tectonic stage. The comparison of the result of this analysis with the result of fault trenching enables us to evaluate if the faults are active or not.

Keywords: power plant, fracture zones in the site, stress tensor inversion, tectonic stage

## Stress rate dependency and effect of volatile element on seismicity of volcano-tectonic earthquakes

MORITA, Yuichi<sup>1\*</sup>

<sup>1</sup>ERI, Univ. of Tokyo

Even in a quiescent period, magma is charged and discharged intermittently beneath volcanoes, and volcano-tectonic earthquakes often occur with ground inflation that is caused by upward migration of magma. Moreover, an increasing volatile element sometimes leads an increasing seismicity. Therefore, it is well known that the seismicity around a volcano is one of the well-established indicators of volcanic activities. Many evidences show that increasing seismicity is followed by volcanic eruptions or magma intrusions because magma migration makes large stress change. On the other hand, the increasing seismicity does not always result in volcanic eruptions. We need to evaluate seismicity quantitatively and discriminate some kinds of effects that generate earthquakes. At present, research in this field has not been established well. It is partly because we cannot propose the model that express temporal variation of seismicity quantitatively, and we do not have enough observation data except some volcanoes where dense observation networks are installed multi-disciplinary.

We proposed to apply the Rate and State Friction (RSF) law to the seismicity occurring at Izu Oshima volcano where dense GPS network as well as seismic one are installed. At the volcano, stress rate changes are observed every 1 to 2 years because of the intermittent magma charging and discharging processes. We presented in last fall meeting of volcanological and seismological society that a simple RSF law model cannot reproduce the observed seismicity fully. We try to revise the model and get remarkable improvement. Aim of this presentation is to reveal the effect of stress rate as well as the other effect, such as volatile element emitted from magma that affect the seismicity around volcanoes, and demonstrate that the seismicity has large potential to monitor the condition not only in the stress rate but also in the volatile density beneath volcanoes.

In Izu-Oshima volcano, seismicity is well correlated with stress rate caused by magma accumulation except the period after the long-term inflation is weakened in 2011. In several volcanoes, increasing volatile component causes decreasing normal stress at fault plane in seismogenic zone and earthquakes are generated intensely (e.g. Northern Volcanic Rift zone in Iceland, La Fossa volcano in Italy). The weakened inflation means that fresh magma is less supplied and emission of volatile decreases in Izu-Oshima volcano. Therefore, we added the effect of the increasing and decreasing volatile element in the previously proposed RSF law, and revised the model. Finally, we can complete successfully the revised model that realize the observed seismicity for all analyzed period.

In conclusion, temporal variation in seismic activity around volcano is mainly due to changes in stress field generated by the magma accumulation and partly caused by effect of volatile element that affects the confining pressure of the fault surface at seismogenic zone. The effect of the stress field is well modeled by ordinary RSF law, and its parameters can be estimated from the data in quiescent period. If observed seismicity exceeds the level that estimated from the model, the volatile element much emitted from magma and it may be precursor to the volcanic eruptions. Therefore, the difference between observed seismicity and the calculated one based on the RSF law is one of the powerful indicator to forecast volcanic eruptions. We propose that there are two kinds of earthquake generating mechanisms around the volcano. Further study at other volcanoes will be helpful to understand the volcano-tectonic earthquake systematically. In future, we should examine the model from direct observation of volcanic gas at volcanoes.

Acknowledgements: We are much grateful to GSI for providing GNSS data.

Keywords: volcano-tectonic earthquakes, seismicity, stress rate change, ground deformation, volatile element

## Investigation into stress field and strength at hypocenters at South African gold mines

OGASAWARA, Hiroshi<sup>1\*</sup> ; KATO, Harumi<sup>2</sup> ; HOFMANN, Gerhard<sup>3</sup> ; ROBERTS, Dave<sup>3</sup> ; CLEMENTS, Trevor<sup>4</sup> ; PIPER, Phil<sup>4</sup> ; YABE, Yasuo<sup>5</sup> ; NAKATANI, Masao<sup>6</sup> ; NAOI, Makoto<sup>6</sup>

<sup>1</sup>Ritsumeikan University, <sup>2</sup>3DGeoscience Inc., <sup>3</sup>Anglogold Ashanti Ltd., <sup>4</sup>Groundwork Ltd., <sup>5</sup>Tohoku University, <sup>6</sup>The university of Tokyo

We report on in-situ stress measurements at seven sites at South African gold mines. The depth ranged from 1.0 to 3.4 km (deepest level in the world where mining is in progress). The measured maximum stress ranged from to 146MPa. In the ranges of stress above 100 MPa have not been able to be measured before we introduced a downsized Compact Conical-ended Borehole Overcoring technique (CCBO; ISRM suggested) in South African gold mines, which has several advantages over the methods widely used in South Africa.

The in situ measurements were carried out at the sites with minimal disturbance by mining or geological features at depths of 3.3 and 3.4 km at Tau Tona and Mponeng mines, respectively, both allowing confirmation that the virgin stress assumptions in the mine were acceptable with slight modification. With the modified virgin stress assumptions, the loading conditions for seven seismic events (ML >2.9) over a 9-year period at Tau Tona mine were back-analyzed with an elastic boundary element method that allows non-linear ride and closure on displacement discontinuity elements (Map3D Fault-SlipR), successfully constraining the stress or the strength on the source faults. At the Pink and Green dykes at 116L at Mponeng mine, the rupture plane of a ML2.1 event was finely delineated by the Japanese-German acoustic emission (AE) network with eight AE sensors deployed within several tens of meters from the rupture plane. It was confirmed that, with the virgin stress assumption and the strength, Map3D was able to reproduce an area of ride consistent with the rupture plane delineated by the AE network. A hole of about 90m length was drilled to intersect the ML2.1 rupture plane to constrain stress by analyzing borehole breakout and core discing. The stress thus constrained was consistent with those estimated with Map3D although the former is a little bit larger than the latter. In situ stress measurements were carried out near seismic damage caused by a ML1.5 event, which took place in the area that a Map3D model with simplest geology structure could not predict high stress. The measured stress state was comparable to that evaluated at the above-mentioned seismic sources.

Seismicity is high at a shaft pillar at 1.0 km depth at Ezulwini mine, where BX CCBO stress measurement was carried out. The measured maximum principal stress was significantly higher than the stress at sites at 3.4km depth with no mining activities.

Keywords: SA gold mines, Seismogenic areas, Stress, Strength, In-situ observation

## Comparison of stress modeling with in-situ strain monitoring at seismogenic area in South African gold mines

OGASAWARA, Hiroshi<sup>1\*</sup> ; KATSURA, Taishi<sup>2</sup> ; HOFMANN, Gerhard<sup>3</sup> ; NAKATANI, Masao<sup>4</sup> ; YABE, Yasuo<sup>5</sup> ; ISHII, Hiroshi<sup>6</sup> ; NAKAO, Shigeru<sup>7</sup> ; OKUBO, Makoto<sup>6</sup> ; ANTHONY, Ward<sup>8</sup> ; JERRY, Wienand<sup>9</sup> ; PATRICK, Lenegan<sup>9</sup> ; KAWAKATA, Hironori<sup>1</sup> ; MURAKAMI, Osamu<sup>1</sup> ; UCHIURA, Taka<sup>1</sup>

<sup>1</sup>Ritsumeikan University, <sup>2</sup>Hitachi Solutions, Ltd., <sup>3</sup>Anglogold Ashanti Ltd., <sup>4</sup>The university of Tokyo, <sup>5</sup>Tohoku University, <sup>6</sup>Tono Research Institute of Earthquake, <sup>7</sup>Kagoshima University, <sup>8</sup>Seismogen CC, <sup>9</sup>Sibanye Gold Ltd.

Compared with continuous in-situ strain monitoring in other mines, we discussed the time evolution of stress in rock mass at a depth of 3.3km for a ~1.5-year period 90m beneath a dip pillar at Mponeng mine. The pillar contained a 30m-thick dyke which a ML2.1 seismic event obliquely bisected. We analyzed the recordings of two multi-component Ishii borehole strainmeters which had been already installed nine months prior to the ML2.1 event. One of the strainmeters was installed in the dyke (gabbros) and the other in the host rock (quartzite) near the dyke contact, both being within a few tens of meters from the ML2.1 rupture plane.

The magnitudes and directions of the principal strain changes were similar for both strainmeters in the period prior to the ML2.1 event. This suggested that the increase in stress in the dyke was significantly larger because the dyke was significantly stiffer than the host rock.

After the ML2.1 event, associated with the start of mining on the eastern side of the strainmeters, the pattern of deformation changed between the two strainmeters.

The above-mentioned characteristics of deformation were compared with numerically modelled deformation by an elastic boundary element method using Map3D Fault-Slip. The magnitude of the Map3D strain changes were, however, several times smaller than the observed strain changes both prior to and after the ML2.1 event. The rock mass just around a stope in deep tabular mining is fractured and behaves time-dependently and non-linearly. Whatever the inelastic deformation, the stress field in an elastic area can be reproduced within reason provided that the boundary condition (deformation, force or stress) is appropriately specified on the elastic-inelastic boundary. Because it is well known that time-dependent inelastic stope closure is much larger than instantaneous elastic stope closure, as a trial, we analyzed a response to an additional forced stope closure using Map3Di (Seismic Integrator version). It was then found that the forced additional stope closure better accounted for both the magnitude and the deformation pattern observed by in situ strain monitoring. We concluded that the effect of inelastic deformation around the stope was significantly larger than the elastic effect induced by the advance of mining faces, and the direct effect of the very close ML2.1 event was not so significant.

A great amount of better maintained data sets of strain are now being accumulated in four gold mines, which will allow us to discuss in further depth.

Keywords: SA gold mines, Seismogenic areas, In-situ strain continuous monitoring, Stress time evolution

## Distribution of fault plane solutions of smaller events associated with the motion of Kuril forearc sliver

HIRATSUKA, Shinya<sup>1\*</sup> ; SATO, Tamao<sup>2</sup> ; SUGAWARA, Sou<sup>3</sup> ; IMANISHI, Kazutoshi<sup>4</sup>

<sup>1</sup>ISV, Faculty of Science, Hokkaido Univ., <sup>2</sup>Sci. and Tech., Hirosaki Univ., <sup>3</sup>JGI, Inc., <sup>4</sup>AIST

In order to find the direct evidence of motion of fore-arc sliver along the Kuril trench, we investigated the distribution of fault plane solutions along the estimated boundary of Kuril fore-arc sliver in Hokkaido. Using the P-wave polarity data as well as P- and SH-wave amplitudes, we determined the fault plane solutions of smaller events ( $2.0 < M < 3.5$ ) with the number of P-wave polarity data are 10 or greater. The result is summarized as follows. Along the volcanic front in eastern Hokkaido, strike-slip fault type of events with WNW-ESE trending P-axes are distributed, which is consistent with the motion of Kuril fore-arc sliver along the volcanic front. In the western side of Hidaka Mountains, reverse fault type of events with P-axes sub-parallel to the trench are widely distributed, which is consistent with ongoing process of collision of Kuril fore-arc sliver with northeastern Japan arc. In more detail, we found that reverse fault type of events with NE-SW trending P-axes, which rotates counterclockwise from trench parallel direction are concentrated near the epicenter of 1982 Urakawa-oki earthquake (M7.1). The P-wave velocity perturbation derived from tomography study for the lower portion of the overriding plate show a good correlation with the distribution of events with NE-SW trending P-axes. The seismic tomography study suggests that the lower half of the delaminated lower crust extends to the source region of the 1982 Urakawa-oki earthquake, which may cause counterclockwise rotation of P-axes near the epicenter of 1982 Urakawa-oki earthquake (M7.1).

## Permeable fractures detected by geophysical loggings and their relation to in-situ stress

KIGUCHI, Tsutomu<sup>1\*</sup> ; KUWAHARA, Yasuto<sup>1</sup> ; SATOH, Takashi<sup>1</sup> ; KOIZUMI, Naoji<sup>1</sup>

<sup>1</sup>GSI, AIST

We examine a relation between the orientation of permeable fractures and the state of in-situ stress by using several logging data measured in 16 boreholes at hard rock sites. Geological Survey of Japan, AIST has constructed 16 integrated borehole observation stations in and around the Kii Peninsula and the Shikoku Island since 2006. Three boreholes with different depths of about 600, 200, 30 m were drilled at each site and various kinds of geophysical loggings were conducted. We obtained the values of strike and dip angle of all fractures including the permeable ones from the borehole wall images of borehole televiewer/camera. Permeable fractures intersecting the borehole were detected by analyzing the logging data of fluid electric conductivity, sonic and temperature. The magnitude and orientation of horizontal principal stress were estimated from hydraulic fracturing stress measurements at 6 sites and the orientation of maximum horizontal stress (SHmax) were evaluated at 11 sites from the images of borehole breakout and/or induced tensile fracture.

The preliminary results from the 6 hydraulic fracturing sites are as follows: The total numbers of all fractures and the permeable ones at each site are in ranges from about 2,000 to 5,000 and from about 20 to 30, respectively. The distribution of the orientation of all fractures at each site shows various values of strike and dip angle. We classify the fractures in three types: tensile fracture (Mode I fracture), shear one and others among the distribution by considering the in-situ state of stress at each site. The tensile type has orientations parallel to SHmax and relatively high dip angles. The shear fracture is optimally oriented for shear failure in the current stress field. It is difficult at any sites to say that characteristics of the distribution of the orientation of all fractures are described only with tensile or shear failure types. Next, an examination of the permeable fracture orientation shows that large number of the permeable ones at the Niihama site have strike orientations almost parallel to SHmax and high dip angles. This feature is different from that for all types of fractures at this site. This suggests that the current stress field controls the existence of the permeable fractures at Niihama site. On the other hand, the distributions of the orientations of permeable fractures at other 5 sites have different characters from the Niihama case: The orientations of permeable fractures have the same tendency with all fractures including non-permeable fractures.

Keywords: permeable fracture, geophysical logging, in-situ state of stress, tensile fracture, shear fracture

## Change in paleostress in offscraped accretionary complex, Kayo formation, the Shimanto Belt, Okinawa island

HASHIMOTO, Yoshitaka<sup>1\*</sup>; MOTOMIYA, Yuhei<sup>1</sup>; UJIE, Kohtaro<sup>2</sup>

<sup>1</sup>Kochi University, <sup>2</sup>Tsukuba University

It is important to understand a stress state of subduction zone because it is strongly related to development of accretionary complex, strength of fault, geometry of subduction zone and earthquake process. The purpose of this study is to examine paleo-stress in a off-scraped accretionary complex in Shimanto Belt, Okinawa island.

The study area is Kayo formation in the northeastern coast of Okinawa island. The Kayo formation consists mainly of coherent turbidites, and it was highly deformed by folds and thrusts. Those geological structures of the formation represent characteristics of fold-thrust belt in forearc area[Ujii,1998].

Flexural slip associated with folding is commonly observed. In addition, many micro-faults cutting bedding are also observed. On the slip surfaces both of flexural slip surfaces and micro-faults, slicken lines and slicken steps are identified. From the structures, slip data (strike and dip of fault plane, slip direction and slip sense) was obtained.

The number of slip data for micro-fault is 153 in ~2 km wide of study area. Using the slip data, we conducted micro-fault inversion analysis to examine the stress orientation and stress ratio. The stress ratio is defined as  $\phi=(\sigma_2-\sigma_3)/(\sigma_1-\sigma_3)$ . We used software MIM (Yamaji,2000) for stress analysis and K-means clustering (Ostubo et al, 2007) for automated picking of center of cluster. After the stress analysis, we combined the stress data with stress polygon to examine stress magnitude semi-quantitatively. The stress polygon is based on Anderson's theory. We assumed the vertical stress is always gravity force, which is converted from assumed depth.

As a result of analysis, 4 stress solution (KY1-KY4) were obtained. KY1) NE-SW horizontal compression with high stress ratio, ( $\phi=0.88$ ), KY2) KY3) NW-SE high angle compression with low to intermediate stress ratio ( $\phi=0.22,0.45$ ), and KY4) NW-SE horizontal compression with intermediate stress ratio ( $\phi=0.65$ ).

We picked up the micro-fault with misfit angle less than 40° for each stress. Misfit angle is the angle between calculated slip direction and observed slip direction on the micro-fault surface. Reverse faults are dominant in KY1 and KY4 and normal faults are dominant in KY2 and KY3.

The stresses are projected to horizontal surface and to Shmax (perpendicular to fold axis), Shmin (parallel to fold axis), and Sv. Using stress ratio and stress projection above, linear functions in Shmax and Shmin space are obtained. We can examine the semi-quantitative Shmax and Shmin value for the stresses in overlapping area between the linear functions and stress polygon.

Magnitudes of shear stresses for KY2, KY3, KY1 and KY4 on the horizontal decollement were also estimated as  $\tau_2=39.2\sim54.7$ [MPa],  $\tau_3=52.1\sim64.2$ [MPa] and  $\tau_1=79.0\sim112.3$ [MPa],  $\tau_4=48.0\sim137.7$ [MPa]. The shear stress for reverse fault (KY1, KY4) is bigger than the shear stress for normal fault (KY2, KY3). If the differences in stress represent the stress change in seismic cycle, the differences in shear stress indicate stress drop as  $-16.2\sim173.1$ [MPa]. Stress drop in general earthquake ranges  $0.03\sim30$ [MPa]. The obtained stress drop in this study includes the range of general stress drop.

Keywords: Stress, micro-fault inversion, Shimanto Belt, Okinawa

## Development of heterogeneous rheological model of the Tohoku Island arc-trench system

MUTO, Jun<sup>1\*</sup> ; SHIBAZAKI, Bunichiro<sup>2</sup>

<sup>1</sup>Dept. Earth Sci., Tohoku Univ., <sup>2</sup>Building Res. Inst.

Subduction zone earthquake cycles can be characterized by various deformation processes taking place around the plate boundary and surrounding area. For example, after slip, viscoelastic relaxation and locking of the plate boundary are three primary processes among them. In order to illuminate the recovery of plate coupling after the Mw 9.0 Tohoku-Oki earthquake and strain budgets of island arc during cycles, the detailed viscoelastic structure of the Tohoku region is developed using seismologically determined subsurface structures and densely measured geothermal gradient data. The model is oriented perpendicular to the Japan Trench and also transects an area of large coseismic slip of the 2011 Tohoku Oki earthquake. Petrological model proposed by the laboratory measurement of seismic velocity of various rocks [Nishimoto et al., 2005] was utilized to infer rheologically major minerals from seismic velocity structures. We used geothermal gradient data from the inland Hi-net borehole [Matsumoto, 2007], as well as geothermal gradient data compiled from around Japan [Tanaka et al., 2004]. The strain-rate-dependent, steady state effective viscosity was calculated using constitutive laws of various rocks under the assumption of homogeneous geologic shortening rate [Sato, 1989]. The calculated viscosity structures show lateral viscosity gradients both parallel and normal to the trench axis. Moreover, the minimum viscosities are predicted to be  $10^{19}$  Pa s in the mantle wedge and  $10^{20}$  Pa s in the oceanic mantle. The values are consistent with previous estimates obtained by postseismic deformation analysis of subduction zone earthquakes with similar magnitudes ( $M_w \sim 9$ ). However those minimum values only appear in depths of 30-100 km in the upper mantle and the viscosity increases further with depths because of the pressure hardening effect. Taking the high values of viscosities in shallower part of the lithosphere, the thickness of high viscous layers found to have lateral variations implying the heterogeneous elastic layer thickness. Model viscosity structures of the Tohoku region utilizing realistic temperature and rheological properties of rocks can be used to evaluate the effect of rheological heterogeneity in the postseismic deformation field of the Tohoku-Oki earthquake observed by dense network of geodetic observations. In the presentation, we will mention the detailed information on the choice of the flow law parameters, and physical and ambient conditions for NE Japan to calculate the viscosity structures. We also show how these heterogeneities affect the crustal deformation of the NE Japan during subduction zone earthquake cycles.

Keywords: rheology, Tohoku, viscoelastic relaxation, earthquake cycle, Tohoku oki earthquake

## Detailed seismic attenuation structures beneath the Hokkaido corner, northern Japan (3)

KITA, Saeko<sup>1\*</sup>; NAKAJIMA, Junichi<sup>2</sup>; HASEGAWA, Akira<sup>2</sup>; UCHIDA, Naoki<sup>2</sup>; OKADA, Tomomi<sup>2</sup>; KATSUMATA, Kei<sup>3</sup>; ASANO, Youichi<sup>1</sup>; KIMURA, Takeshi<sup>1</sup>

<sup>1</sup>NIED, <sup>2</sup>RCPEV, Graduate School of Science, Tohoku University, <sup>3</sup>ISV, Hokkaido University

### 1. Introduction

In the Hokkaido corner, the Kuril fore-arc sliver collides with the northeastern Japan arc. Using travel-time data compiled from the nationwide Kiban seismic network and a dense temporary seismic network [Katsumata et al, 2002], Kita et al. [2012] determined high-resolution 3D seismic velocity structure beneath this area for deeper understanding of the collision process of the two fore-arcs. In this study, we merged waveform data from the Kiban-network and from the temporary network, and estimated the seismic attenuation structure to understand seismotectonics and collision process beneath Hokkaido.

### 2. Data and method

We estimated corner frequency for each earthquake by the spectral ratio method of coda waves [e.g. Mayeda et al., 2007]. Then, we simultaneously determined values of  $t^*$  and the amplitude level at low frequencies from the observed spectra after correcting for the source spectrum. Seismic attenuation ( $Q^{-1}$  value) structure was obtained, inverting  $t^*$  values and employing the 3-D ray-tracing technique of Zhao et al. [1992]. The study region covers an area of 41-45N, 140.5-146E, and a depth range of 0-300 km. We obtained 154,293  $t^*$  at 316 stations from 6,196 events ( $M_j > 2.0$ ) that occurred during the period from Aug. 1999 to Dec. 2012. Horizontal and vertical grid nodes were set with spacing of 0.1-0.3 degrees and 10-30 km, respectively.

### 3. Results

The calculated stress drops are distributed from 0.1 to 100 MPa. Stress drops of intraslab earthquakes increase with focal depth. The values of stress drops of events in the slab mantle tend to be larger than those in the slab crust at depths of 80 to 170 km, which might contribute to understanding of the physical nature of intraslab earthquakes.

Seismic attenuation structure is imaged for the region above the subducting Pacific slab at depths down to ~80 km. For the forearc side of the eastern and western parts of Hokkaido, high- $Q_p$  zones are generally imaged at depths of 10 to 80 km in both the crust and mantle wedge above the Pacific slab. In contrast, low- $Q_p$  zones are clearly imaged in the mantle wedge of the backarc side. They are distributed in deeper parts and reach the Moho beneath the volcanic front. Locations of these low- $Q_p$  zones correspond to the low- $V_p$  and low- $V_s$  zones imaged by Zhao et al. [2012]. These suggest that the upper head of the mantle-wedge upwelling flow is detected beneath Hokkaido also by our seismic attenuation imaging.

In the Hokkaido corner, to the west of the Hidaka main thrust a broad low- $Q_p$  zone is imaged at depths of 0-60 km. Location of this broad low- $Q_p$  zone almost corresponds to that of the low- $V$  zone in the collision zone found by Kita et al. [2012]. Fault planes of the 1970 M6.7 and 1982 M7.1 earthquakes are located at the edges of a broad low- $Q_p$  zone, being in contact with a high- $Q_p$  zone at 10 to 35 km. These results suggest that the occurrence of these anomalously deep and large inland earthquakes is related to the presence of hydrous minerals or fluids.

The subducting oceanic crust beneath the Hidaka region is imaged as a low- $Q$  zone whose location corresponds to the low- $V_p$  and low- $V_s$  zone of Kita et al. [2012], suggesting the existence of hydrated materials at the top of the slab. Just above the slab surface, moderately low- $Q$  zones are imaged at depths of 90 to 100 km beneath eastern and southern Hokkaido and at depths of 110 to 130 km beneath the corner, which are located at depths deeper than the upper plane seismic belt. These observations suggest the existence of the hydrated mantle wedge by the aqueous fluids supplied from the oceanic crust right below.

**Keywords:** Seismic attenuation structure, Seismotectonics, arc-arc collision process, Stress drops of intraslab earthquakes

## Crustal deformation in the Mid-Niigata area and its implication for strain concentration

SAGIYA, Takeshi<sup>1\*</sup> ; MENESES, Angela<sup>1</sup>

<sup>1</sup>Nagoya University

The Mid-Niigata area is located within the concentrated strain belt along the eastern margin of the Japan Sea. This area suffered from two large earthquakes, the 2004 Chuetsu and the 2007 Chuetsu-oki earthquakes. Based on GPS velocity data calculated from daily coordinate time series of GEONET, we identified significant time dependence of the interseismic crustal deformation patterns before, between, and after these two earthquakes. Modeling results of the deformation pattern changes are summarized as follows. 1) Contraction before 2004 occurred between the source regions of the two earthquakes and it was attributed to aseismic faulting across almost the whole elastic layer, implying that the observed strain was largely inelastic. This interpretation is also supported from a fact that the historical seismic energy release in this area is much smaller than that expected from geodetic strain accumulation. 2) After two earthquakes, aseismic faulting seems to have continued without explicit time decay. The aseismic faulting is estimated close the source fault of the main shocks, implying that postseismic strength recovery did not occur on the main shock fault or a nearby parallel fault was activated to accommodate regional contraction. This is consistent with an idea that the upper crust in this area is segmented to smaller blocks and the mechanical behavior is very sensitive to external stress changes.

**Keywords:** Strain concentration, Niigata-Kobe Tectonic Zone, 2004 Chuetsu earthquake, 2007 Chuetsu-oki earthquake, aseismic faulting, inelastic deformation

## Tectonic stress fields in subduction zones governed by frictional strength of plate interfaces

MATSU'URA, Mitsuhiro<sup>1\*</sup> ; NODA, Akemi<sup>2</sup> ; TERAOKAWA, Toshiko<sup>3</sup> ; FUKAHATA, Yukitoshi<sup>4</sup>

<sup>1</sup>Institute of Statistical Mathematics, <sup>2</sup>Kozo Keikaku Engineering Inc., <sup>3</sup>Nagoya University, <sup>4</sup>Kyoto University

Tectonic crustal motion in plate convergence zones varies from mountain building (e.g., Himalaya) to back-arc spreading (e.g., Mariana) [1, 2, 3]. Such difference in tectonic crustal motion reflects the diversity of tectonic stress fields. So our question is what causes the diversity of tectonic stress fields in plate convergence zones. Recently, from a theoretical study [4], we revealed that the tectonic stress field consists of basically two different sorts of stress fields; one of which is a horizontally compressional stress field due to frictional resistance at plate interfaces, and another is a horizontally tensile stress field due to steady plate subduction. On a geological timescale, the former can be regarded as constant in time, but the latter increases with time. So, if the earth's crust were infinitely strong, tectonic stress fields in plate convergence zones would become tensile in time everywhere. Actually, the earth's crust includes a number of defects with low strength, over which inelastic deformation (brittle fracture and/or plastic flow) occurs so as to release the tectonic stress caused by mechanical interaction at plate interfaces. From these considerations, we may conclude as follows. When the plate interface is very weak in comparison with the earth's crust, a horizontally tensile stress field becomes dominant, which causes back-arc spreading as in the case of Mariana. When the plate interface is very strong, a horizontal compressional stress field becomes dominant, which causes mountain building as in the case of Himalaya. Tectonic stress fields in most subduction zones, where the strength of plate interfaces are comparable to that of the earth's crust, are between these two extreme cases.

### References

- [1] Takada, Y. and M. Matsu'ura, 2004. A unified interpretation of vertical movement in Himalaya and horizontal deformation in Tibet on the basis of elastic and viscoelastic dislocation theory, *Tectonophysics*, 383, 105-131.
- [2] Hashimoto, C. and M. Matsu'ura, 2006. 3-D simulation of tectonic loading at convergent plate boundary zones: Internal stress fields in northeast Japan, *Pure Appl. Geophys.*, 163, 1803-1817.
- [3] Hashima, A., Y. Fukahata, and M. Matsu'ura, 2008. 3-D simulation of tectonic evolution of the Mariana arc-back-arc system with a coupled model of plate subduction and back-arc spreading, *Tectonophysics*, 458, 127-136.
- [4] Matsu'ura, M., A. Noda, and T. Terakawa, 2013. Strength of plate interfaces and tectonic stress fields in subduction zones, *Seismological Society of Japan 2013 Annual Meeting*, D22-08, Yokohama.

Keywords: subduction zone, tectonic stress field, plate interface, frictional strength, mountain building, back-arc spreading

## Sequential inversion of GPS time series data to estimate spatiotemporal change in interplate coupling

NODA, Akemi<sup>1\*</sup> ; MATSU'URA, Mitsuhiro<sup>2</sup>

<sup>1</sup>Kozo Keikaku Engineering Inc., <sup>2</sup>Institute of Statistical Mathematics

To estimate steady increase rates of slip deficits at plate interfaces, first, we obtain linear trends of the time series of GPS daily coordinate data by removing seasonal variations and coseismic and postseismic changes due to episodic events. Then, we invert the linear trends (surface displacement rates at GPS stations) into steady slip-deficit rate distribution on a plate interface with completely relaxed slip-response functions for an elastic-viscoelastic layered half-space model under gravity (Noda et al., 2013, GJI). Noda et al. (SSJ 2012 Annual Meeting) demonstrated that this method is applicable to GPS time series data in northeast Japan for the interseismic period (March 1997-February 2008) before the 2008 Ibaraki-oki (Mw6.8) and Fukushima-oki (Mw6.9) earthquakes. After these events, the trends of GPS time series data gradually change with time (Suito et al., 2011, EPS), indicating spatiotemporal change in interplate coupling preceding the 2011 Tohoku-oki mega-thrust earthquake.

The change in slip-deficit rate distribution disturbs a steady stress state in the asthenosphere, and so we need to use the viscoelastic transient slip-response functions for the analysis of GPS time series data after the 2008 events (Noda et al., 2013, GJI). An exact treatment of the viscoelastic inverse problem to estimate cyclic slip processes at a plate interface has been given by Fukahata et al. (2004, GJI), but it is not applicable to the present problem because the change in slip-deficit rate distribution is not a cyclic but transient process. So, we propose a simple inversion technique, called sequential inversion of GPS time series data, to estimate spatiotemporal changes in slip-deficit rates at plate interfaces. A similar sequential inversion technique has been used by Lubis et al. (2013, GJI) for the analysis of afterslip distribution following the 2007 southern Sumatra earthquake (Mw8.5) on the assumption that the asthenosphere has been in a steady stress state until the 2007 event.

In the present study, we estimate the spatiotemporal change in interplate coupling by applying the sequential inversion technique to GPS time series data for March 2008-February 2011, and reveal the slip history at the North American-Pacific plate interface off Tohoku during the 14 years before the 2011 Tohoku-oki mega-thrust earthquake.

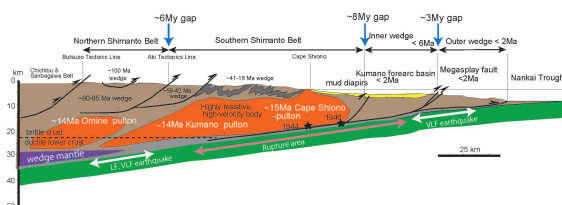
**Keywords:** GPS time series data, sequential inversion, viscoelastic transient response, change in interplate coupling, the 2011 Tohoku-oki earthquake

## Middle Miocene swift migration of the TTT triple junction and rapid crustal growth in SW Japan

KIMURA, Gaku<sup>1\*</sup> ; HASHIMOTO, Yoshitaka<sup>2</sup> ; KITAMURA, Yujin<sup>3</sup> ; YAMAGUCHI, Asuka<sup>4</sup> ; KOGE, Hiroaki<sup>1</sup>

<sup>1</sup>Dept. Earth and Planetary Science, The University of Tokyo, <sup>2</sup>Kochi University, <sup>3</sup>Kagoshima University, <sup>4</sup>Atmosphere and Ocean Research Institute, The University of Tokyo

We review recent progress in geological and geophysical investigation in SW Japan, the Nankai Trough and the Philippine Sea Plate (PSP), and propose a comprehensive hypothesis for the Miocene tectonics of the Nankai Trough. New interpretations are as follows: Near-trench magmatism in the outer zone of SW Japan might have various reasons. The possibility of an arc-arc collision in particular should be examined, in addition to the previous model of an oceanic ridge and hot PSP subduction. The indentation structure at Capes Ashizuri, Muroto in Shikoku, and Shiono on the Kii Peninsula may be explained by the collision of the active arc or topographic peaks such as seamounts, contrary to the previous "kink-folding" model due to recent E-W compression. This inference is drawn from comparison between the many modern examples of seamount collision and sandbox analogue experiments. Crustal components of SW Japan might consist mainly of igneous plutonic rocks, in contrast to the previous inference of Cretaceous to Tertiary accretionary complexes. This is especially the case in the outer zone to the north of Capes Ashizuri, Muroto and Shiono. This is inferred from geophysical observation of gravity anomalies, velocity and resistivity, together with geological estimations of caldera age and the size of its root pluton. Episodic crustal growth due to intrusion of igneous rock and subduction of the PSP may have stopped after ~11 Ma and restarted at ~7-8 Ma. New accretionary prism was again developed after ~6 Ma. This inference is suggested by recently conducted ocean drilling program.



## Spatial relationship between the volcanic chain and high gravity anomalies in subduction zones

FUKAHATA, Yukitoshi<sup>1\*</sup>

<sup>1</sup>DPRI, Kyoto University

The most conspicuous features of arc-trench systems are active seismicity, characteristic topography and gravity anomalies, and volcanism. The topography and gravity anomalies are low in the trench and high in the arc, which can be theoretically explained by mechanical interaction between the subducting oceanic plate and the overriding plate (Sato & Matsu'ura, 1993, GJI; Hashimoto et al, 2004, PAGEOPH). Because the topography is more complicated to be understood, free-air gravity anomaly is more suitable to be compared to the theoretical model. Free-air gravity anomalies with long wave length basically represent the effect of tectonic force, which disturbs gravity equilibrium.

Volcanoes align along the volcanic front in most arcs. Since both of the high free-air gravity anomalies and volcanic front have a subparallel strike to the trench, it should be possible to classify arc-trench systems according to the spatial relationship between them. Based on such an idea, Fukahata (2008, JPGU meeting) classified arc-trench systems, but there was a problem that the recognition of the location of high gravity anomalies was quite subjective. So, in this study, I improved this process.; the location of high gravity anomalies were more quantitatively recognized. As a result, the location of high gravity anomalies relative to the volcanic front did not change for most arcs, but I found that it was difficult to define its location in some arcs (mostly tensile). Using the result, I discuss the spatial relationship between the volcanic chain and high gravity anomalies in subduction zones and consider causes of topographic evolution of island arcs.

Keywords: island arc, subduction zone, gravity anomaly, volcanic front

## Uplift and denudation history of the Yoro-Suzuka-Nunobiki Mountains: Constraints from apatite FT thermochronology

SUEOKA, Shigeru<sup>1\*</sup>; TSUTSUMI, Hiroyuki<sup>2</sup>; TAGAMI, Takahiro<sup>2</sup>; HASEBE, Noriko<sup>3</sup>; TAMURA, Akihiro<sup>3</sup>; ARAI, Shoji<sup>3</sup>; SHIBATA, Kenji<sup>1</sup>

<sup>1</sup>Japan Atomic Energy Agency, <sup>2</sup>Kyoto University, <sup>3</sup>Kanazawa University

The Yoro-Suzuka-Nunobiki Mountains are fault block mountains distributed along the Isewan-Tsurugawan Tectonic Line, a tectonic boundary between the Kinki and Chubu districts. The Kinki district on the west of the mountains is characterized by predominance of reverse faults and alternation of N-S trending mountain ranges and basins (Kinki Triangle; Huzita, 1962), whereas the Chubu district on the east of the mountains has predominance of strike-slip faults and westerly tilting landforms (Chubu tilting block; Kuwahara, 1968). Miyoshi & Ishibashi (2008) mentioned that the Philippine Sea Plate slab beneath the region around the Yoro-Suzuka-Nunobiki Mountains has shallow subduction angle and form a convex shape (Isewan-Kohoku slab) and proposed this shallow slab resulted in the tectonic boundary between the Kinki and Chubu districts in the region. On the eastern and western sides of the Yoro-Suzuka-Nunobiki Mountains, two major subsidence areas have formed and moved northward since the end of the Miocene as recorded by deposition of the Tokai group and Kobiwako group (e.g., Yokoyama, 1995; Yoshida, 1990). On the other hand, there is some debate over the formation process and mechanism of the Yoro-Suzuka-Nunobiki Mountains; Okada (2004) speculated the mountains have uplifted from south to north generally corresponding to the northward moving of the subsidence areas, whereas Ohta and Takemura (2004) proposed the formation of the mountains were still later and independent from the formation of the subsidence areas.

We are attempting revealing uplift and denudation history of the Yoro-Suzuka-Nunobiki Mountains in the past few million years by using apatite fission-track (AFT) thermochronology. We have obtained AFT ages and length distribution data in one site for the Yoro Mountains, eight sites for the Suzuka Range, and one site for the Nunobiki Mountains. Highlights of the results are as below: 1) the AFT ages range 47-30 Ma, 2) the ages were youngest in the middle to south parts of the Suzuka Range and get older to the north and south, 3) thermal histories calculated from the AFT ages and length distributions indicate rapid cooling events in the past few million years in the middle to south parts of Suzuka Range, but not in the Yoro and Nunobiki Mountains and the north part of the Suzuka Range, 4) the rapid cooling events in the past few million years are attributable to the uplift of the Suzuka Range since ~1.3 Ma (Yokoyama, 1995). We are conducting additional AFT analyses in seven sites of the Nunobiki Mountains to expand our results to the south. In this presentation, we are planning to provide progressed discussions containing the results of the additional data.

**Keywords:** Yoro-Suzuka-Nunobiki Mountains, apatite fission-track thermochronology, denudation, eastern margin of the Kinki Triangle

## Self-affinities for Amplitude and Wavelength of Folds

KIKUCHI, Kazuhei<sup>1\*</sup> ; NAGAHAMA, Hiroyuki<sup>1</sup>

<sup>1</sup>Department of Earth Science, Graduate School of Science, Tohoku University

In general, many folds are apparently curved or jagged on a wide range of scales, so that their geometries appear to be similar when viewed at different magnifications. By Matsushita and Ouchi (1989a, b)'s method, we also analyzed the self-affinities of folds in the North Honshu Arc, Japan (Kikuchi et al., 2013). Based on this analysis, geometries were found to be self-affine and can be differently scaled in different directions. We recognize the self-affinities for the amplitude and the wavelength of folds and a crossover from local to global altitude (vertical) variation of the geometries of folds in the Northeast Honshu Arc.

Buckingham's Pi-theorem is sufficient to the first problems of fold systems (Shimamoto, 1974). However, the complete similarity cannot give us the self-affinities of folds. A general renormalization-group argument is proposed to the applicability of the incomplete self-similarity theory (Barenblatt, 1979). Based on the general renormalization-group argument, we derive the self-affinities for the wavelength ( $L$ ) and the amplitude ( $a$ ) of folds:

$$L^{(1-d)} \propto a.$$

The relationship between Hurst exponents  $H$  of fold (Kikuchi et al., 2013) and  $d$  are equation:

$$1-d=H,$$

where  $H$  is index of the continuity of a given fold curve and obtained by the ratio between horizontal scaling exponent and vertical scaling exponent.  $d$  is an exponent of a given incomplete self-similarity theorem.

In  $d \neq 0$  case, the Hurst exponent  $H \neq 1$  indicates self-affinities for the given fold curve. In this case, scale invariance of the fold might be affected by a variety of tectonic processes under the anisotropic stress field. In  $d = 0$  particular case, the Hurst exponent  $H = 1$  indicates self-similarity for the given fold curve. In this case, scale invariance of the fold might not be affected by a variety of tectonic processes under the anisotropic stress field. These results imply that anisotropic stress fields by gravitation and tectonic stresses might cause self-affinities of folds. Self-similarity and self-affinities of the fold might be affected and by a variety of tectonic processes under the isotropy or anisotropic stress field.

### Reference

- Barenblatt, G.I. (1979) *Consultants Bureau*, New York.  
Kikuchi, K., K. Abiko, H. Nagahama, H. Kitazato, and J. Muto (2013) *Acta Geophysica*, **61**, 6, pp. 1642-1658.  
Matsushita, M. and S. Ouchi (1989a) *Physica D*, **38**, 1, pp. 246-251.  
Matsushita, M. and S. Ouchi (1989b) *Journal of the Physical Society of Japan*, **58**, 5, pp. 1489-1492.

Keywords: Fold, Self-affinity, Buckingham's Pi-theorem, Incomplete self-similarity theory

## Reason for strange appearance of Mt. Hakone, and Reason why the Boso Triple Junction has moved to the west most

MASE, Hirofumi<sup>1\*</sup>

<sup>1</sup>none

(Refer to the chart)

Mt. Fuji penetrates through the north end of the Philippine Sea Plate (PHSP), and is the front of land side plate incision, and is the starting point of Suruga and Sagami Trough (1). Mt. Hakone and Mt. Mihara have decided the position of Sagami Trough.

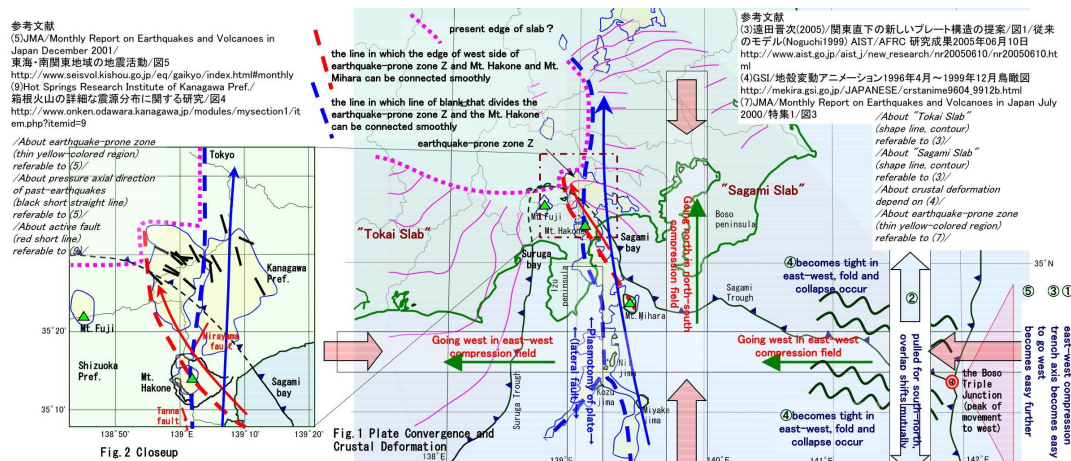
"Tokai Slab" seems to stop beneath the north side of Mt. Fuji. On the other hand, "Sagami Slab" seems to sink and reach the interior of Kanto. (3) It is unnatural as one board. Though the crustal deformation that GPS caught shows that the Izu Peninsula moves to the west, tendencies of Izu islands and Southern part of Kanto to move to the north are strong (4). In 135-140° east, it has been understood that the section of especially 140° meets the requirement of the temperature structure that the power to make the Pacific Ocean's side go north is generated. In a word, I think that only the side of "Sagami Slab" sank greatly in PHSP in the past and the current situation was caused.

Then, where is the crack (lateral fault) that becomes a boundary? There is the earthquake-prone zone that symbolizes subducting of Slab on the north side of the Mt. Hakone (5). If the edge of west side within the range of that distribution is traced, the Mt. Hakone and Mt. Mihara can be connected in a smooth line (red broken line). The line of blank for south-north, that divides the earthquake-prone zone to the east and the west, passes the Mt. Hakone (blue broken line). Because there was no fault in the south from Mt. Mihara, I think the slipping fault shifted to the fault shown in blue broken line though there was an age that the fault shown in red broken line slipped. The Mt. Hakone has the meaning of the west edge of PHSP in the Izu-islands-east and of the starting point of subducting.

On the other hand, why has the trench axis around the Boso Triple Junction moved to the west most? Pacific Plate that goes west compresses land side Plate and PHSP that get on on it into the direction of east-west. And, pulls them for south-north. The Part where land side Plate and PHSP overlap shifts mutually and the overlap becomes shallow. The upper plates expand for south-north to Pacific Plate. As a result, the trench axis becomes easy to go west by the east-west compression. Land side Plate and PHSP and Pacific Plate become tight in the direction of east-west. And, fold and collapse occur in them. As a result, the trench axis becomes easy to go west further. Because usual stresses are absorbed to the fold and collapsing, the trench axis is not easy to return east even if a massive earthquake occurs. This is the cause that the trench axis moves to the west.

### Reference literature

- (1) Hirofumi MASE (2009) / SSJ2009/P3-64 / [http://jglobal.jst.go.jp/detail.php?JGLOBAL\\_ID=200902239527416838](http://jglobal.jst.go.jp/detail.php?JGLOBAL_ID=200902239527416838)
- (3) Shinji TODA (2005) / A new image of plate configuration and seismotectonics of the triple junction beneath the Kanto region / Fig. 1 (Noguchi 1999) / AFRC.AIST/release06/10/2005 / [http://www.aist.go.jp/aist-j/new\\_research/nr20050610/nr20050610.html](http://www.aist.go.jp/aist-j/new_research/nr20050610/nr20050610.html)
- (4) GSI / Animation of Crustal Deformation in Japan / <http://mekira.gsi.go.jp/ENGLISH/crstanime.html>
- (5) JMA / Monthly Report on Earthquakes and Volcanoes in Japan December 2001 / Tokai and South-Kanto / Fig. 5 / <http://www.seisvol.kishou.go.jp/>



## The Ocean Floor was Expanded by Increasing Seawater

MADO, Shinichiro<sup>1\*</sup>

<sup>1</sup>MAROSA

### Introduction

I wrote this paper in order to present the negation of a hypothesis which supports the plate tectonics. The hypothesis is 'Spreading Oceanic Floor Hypothesis'. This negation is based upon a new fact that has been revealed recently. I concluded the negation by such facts and my original reasoning. I already presented another fact negating the hypothesis of 'Spreading Oceanic Floor'. The abstract titled 'it was not switching global geo-magnetic fields that created the alternating anomalies over oceanic ridges' was presented at the Japan Geoscience Union Meeting 2013. Therefore, one of reasons that support the hypothesis of spreading oceanic floor was already denied. In this paper I will deny another reason of the hypothesis, which says that the plates of the oceanic floors are spreading.

### What is the question

The Hypothesis of Plate tectonics was evolved from Wegener's 'Continental Drift Hypothesis' and based upon 'The Hypothesis of Spreading Oceanic Floor'. However, the hypothesis of spreading oceanic floor is denied as far as it means the spreading plate of oceanic floor. It is denied by the fact that the oceanic floors spread not because the oceanic plates themselves spread but merely because the seawater increased. Therefore, the hypothesis of plate tectonics lost one of its evidences.

### The Expanding Oceanic Floor

The hypothesis of plate tectonics is supported by the hypothesis of spreading oceanic floor. The rapidity of the movement of the plate was estimated by the switching pattern of geo-magnetic anomaly near the ridges. The farther and farther it comes from the ridges, the older and older the dates of the basalts and fossils become. The estimated dates fit well the dates estimated from the pattern of geo-magnetic anomalies. It was proved that the rapidity was estimated 2cm per one year for the Pacific Ocean<sup>[1],[2]</sup>.

### Rising Sea Level Caused by Increasing Seawater

However, the hypothesis of spreading oceanic floor neglected the fact that the sea level increased greatly. The sea level increased more than 6000m after the creation of oceanic plates. That fact was revealed by the remaining river valleys on the oceanic floors. For instance the Kushiro River reaches more than 6000m in depth<sup>[Fig1-B]</sup>. The Itoi River reaches about 3500m in depth<sup>[Fig1-A]</sup>.

These facts revealed that the seawater increased greatly after the creation of the oceanic plates. It takes very long time to raise sea level to recent level. Gradually the amount of seawater is increasing even now.

Probably the increase of seawater is caused by crustal movements squeezing water from the rocks of the crust. The squeezed water becomes hot springs.

The date of the fossils near the ridges are newer because those places are higher and newly became under the sea level.

### Conclusion

The oceanic floors spread not because the oceanic plates spread but because the seawater increased largely after the creation of the oceanic floor plates.

Therefore, it has no relation between the dates of the oceanic plates and the date of fossils contained in upper layers. Therefore, one of evidences of plate tectonics was lost.

### References

[1] Maxwell, A. & Von Herzen, R. et al. 'Deep Sea Drilling in the South Atlantic', SCIENCE, Volume 168, pp.1047-1059, 29 May 1970.

[2] Dietz, R. 'Continent and Ocean Basin Evolution by Spreading of of the Sea Floor', NATURE, Volume 190, pp.854-857, June 3, 1861.

[3] Shinichiro Mado, 'It was not switching global geo-magnetic fields that created the alternating anomalies over oceanic ridges', ABSTRACT of Japan Geoscience Union Meeting, SEM36-P01, 2013.

SCG67-01

Room:414

Time:May 1 14:15-14:30

Keywords: Dating the Ocean Floor, Rise in the Sea Level, Increase of Seawater, Expansion of the Ocean Floor

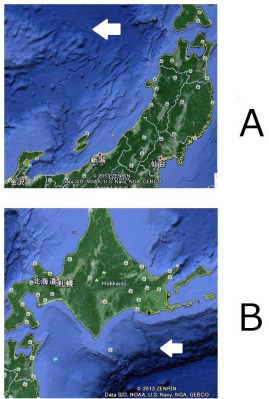


Fig 1

## Noble gas evidence of deep plume origin of the Louisville hotspot

HANYU, Takeshi<sup>1\*</sup>

<sup>1</sup>Japan Agency for Marine-Earth Science and Technology

Louisville seamount chain has been considered to be one of the long-lived hotspot tracks on the Pacific plate, but its magmatic source has not been well understood. I report noble gas compositions of the drill cores from four of the five seamounts drilled during IODP Expedition 330. Because the samples are aged (50-74 Ma), a stepwise crushing test for noble gas extraction from olivine phenocrysts and submarine glasses was made to assess contamination of post-eruption radiogenic nuclides. This test confirmed extraction of magmatic noble gases with minimal release of post-eruption radiogenic nuclides from the olivine samples; however, this was not always the case for the glass samples. The  $^3\text{He}/^4\text{He}$  ratios in the olivine phenocrysts range from a value similar to those of mid-ocean ridge basalts (MORB) to slightly elevated ratios up to 10.6 Ra. Although these ratios are not as high as those observed in other ocean island basalts, two Louisville seamount basalts exhibit a primordial Ne isotopic signature that can be clearly discriminated from MORB Ne. The He and Ne isotopic compositions of the Louisville seamount basalts can be explained by the mixing of less degassed mantle and depleted upper mantle with different He/Ne ratios. The presence of the less degassed mantle component in the source of the Louisville seamounts documents the deep origin of the mantle plume.

One of the major objectives of the IODP Expedition 330 was to test the geodynamic model that predicts lateral advection of mantle plumes in the convecting mantle [Koppers et al., *G-cubed*, 2004; Steinberger and Antretter, *G-cubed*, 2006]. This model assumes a primary mantle plume that is rooted deep in the mantle, and the trajectory of a plume conduit is influenced by the overall mantle flow, which can be monitored by the hotspot drift on the Earth's surface [Tarduno et al., *Science*, 2009]. The paleomagnetic and dating results from IODP Expedition 330 verified the geodynamic modeling predictions for the Louisville seamount chain together with the Hawaiian-Emperor seamount chain [Koppers et al., *Nat. Geosci.*, 2012]. The present noble gas data gives a guarantee for the deep-rooted Louisville plume assumed in the geodynamic model.

Keywords: Louisville seamount, mantle plume, deep mantle, noble gases, IODP

## Preliminary result of the oceanic mantle structure revealed by "Normal Oceanic Mantle Project"

ISSE, Takehi<sup>1\*</sup>; SHIOBARA, Hajime<sup>1</sup>; SUGIOKA, Hiroko<sup>2</sup>; ITO, Aki<sup>2</sup>; TAKEO, Akiko<sup>1</sup>; UTADA, Hisashi<sup>1</sup>; KAWAKATSU, Hitoshi<sup>1</sup>; TONEGAWA, Takashi<sup>2</sup>; TANAKA, Satoru<sup>2</sup>

<sup>1</sup>ERI, Univ. of Tokyo, <sup>2</sup>Institute for Research on Earth Evolution, Japan Agency for Marine-Earth Science and Technology

The oceanic mantle is an important region to understand the Earth system, because more than 2/3 of the surface is covered by oceanic area. Since 1990s, we have operated several seafloor observations by using newly developed long-term broadband ocean bottom seismometers (BBOBSs) in the northwest and central part of the Pacific Ocean. These observations have revealed the structures in and around the subduction zone in the Pacific Ocean and in the Pacific superswells, respectively. However, we have no observation and result in the normal oceanic regions. To reveal the normal oceanic mantle structure from observational approach, we conduct a long-term observation called "Normal Oceanic Mantle Project" (NOMan project) from 2010, deploying ocean bottom geophysical (seismic and electromagnetic) instruments in the northwestern Pacific Ocean. We conduct two arrays in that region. One is northwest side of the Shatsky Rise (Area A) and the other is southeast side of the Shatsky Rise (Area B). Sea floor age of Area A is 125 - 135 Ma, that of Area B is 135 - 145 Ma, so that the shear wave structures of those area should be similar.

By using seismograms of the NOMan project, other BBOBS observations, and permanent broadband seismic stations on land, we have determined the three-dimensional shear wave velocity structure of the upper mantle in the northwestern Pacific Ocean to reveal this area to be really normal. We used a surface wave tomography technique in which multimode phase speed of the surface wave are measured and inverted for a 3-D shear wave velocity structure by incorporating the effects of finite frequency and ray bending.

Our obtained model shows that lateral heterogeneity of each area is not strong and that average structures are different in two areas. Area A is consistent with previous models, whereas Area B is faster than previous models. We think for the present that Area A seems to be normal oceanic mantle, though Area B is not. We will recover all BBOBSs in this year. These BBOBS's data enable us to obtain more reliable mantle structures.

Keywords: upper mantle, BBOBS, surface wave, tomography

## Seismic anisotropy in the oceanic lithosphere/asthenosphere system estimated by the broadband ocean bottom seismology

TAKEO, Akiko<sup>1\*</sup> ; ISSE, Takehi<sup>1</sup> ; NISHIDA, Kiwamu<sup>1</sup> ; KAWAKATSU, Hitoshi<sup>1</sup> ; SHIOBARA, Hajime<sup>1</sup> ; SUGIOKA, Hiroko<sup>2</sup> ; ITO, Aki<sup>2</sup> ; UTADA, Hisashi<sup>1</sup>

<sup>1</sup>Earthquake Research Institute, University of Tokyo, <sup>2</sup>IFREE, JAMSTEC

The uppermost mantle structure beneath the oceanic basins is essential to discuss the oceanic lithosphere/asthenosphere system, the most simple and representative system of the theory of plate tectonics. Seismic anisotropy within the oceanic lithosphere and asthenosphere is especially important, as it reflects the flow and deformation in the uppermost mantle. Previous structural studies have been, however, limited in terms of the depth range: the top of lithosphere at depths of ~10-20 km by refraction surveys, and the structure deeper than ~30 km by surface-wave tomography studies. There has been no discussion from the top of the lithosphere continuously to the asthenosphere, which needs the broadband analysis of surface waves at periods of 3-100 s. In addition, there has been limited discussion about the intensity of seismic anisotropy because of the difficulty of estimating the absolute value of seismic anisotropy by surface-wave tomography studies.

We have developed a new multi-band method to analyze surface waves in broadband array records of ocean bottom seismometers for determining seismic anisotropy structure at depths of ~10-100 km quantitatively (Takeo et al 2013 JGR, submitted to GJI). The method uses the ambient noise cross-correlation method for analyzing surface waves at periods of 3-30 s and to determine structure at depths shallower than ~50 km, as well as the array analysis method of teleseismic waveforms at longer periods for determining deeper structures.

In previous studies, we have applied the multi-band method to records obtained in three oceanic regions: the Shikoku Basin region (Takeo et al. 2013 JGR), the southwestern region of the Shatsky Rise (Takeo et al. submitted to GJI) and the French Polynesia region (Takeo et al. 2012 SSJ Fall Meeting). In this study, we applied the same method to the records of broadband ocean bottom seismometers obtained by the normal oceanic mantle (NOMan) project at two oceanic regions (northwestern and southeastern regions of the Shatsky Rise) from 2010 to 2013. By combining the results for five oceanic regions with different seafloor ages between 20 and 155 Ma, we can discuss the seismic structure and its anisotropy in the oceanic lithosphere and asthenosphere, and the deformation of mantle related to plate motions.

The results for five oceanic regions can be summarized into five points: (i) the high-velocity lid and the low velocity zone corresponds to the oceanic lithosphere and asthenosphere, (ii) the transition from the lithosphere to the asthenosphere occurs at depths of 40-90 km, (iii) the average intensity of S-wave radial anisotropy is 3-6 % at depths of 10-150 km with the velocity of horizontally propagating and vertically polarized S-wave slower than the horizontally polarized S-wave, (iv) the intensity of S-wave azimuthal anisotropy at depths of 10-100 km is weaker than that of S-wave radial anisotropy and weakens with depths, and (v) the azimuth of maximum S-wave velocity is not perpendicular to ancient spreading axis in general. These results indicate complex deformation system in the present and ancient oceanic asthenosphere related to the presence of partial melting, the unusual fabric of olivine and so on. We will summarize these results and discussions, and will also present the potential of the broadband ocean bottom seismology to elucidate structure and deformation in the oceanic lithosphere/asthenosphere system and in other oceanic systems such as hotspots, mid-ocean ridges and subduction zones.

Keywords: surface wave, ambient noise, anisotropy, plate tectonics

## Locality and cause of the characteristics of high-frequency Po/So wave propagating in heterogeneous oceanic lithosphere

FURUMURA, Takashi<sup>1\*</sup> ; KENNETT, Brian<sup>2</sup>

<sup>1</sup>Earthquake Research Institute, The University of Tokyo, <sup>2</sup>Research Schoole of Earth Sciences, The Australian National University

In our previous study (Kennett & Furumura 2013; *Geophys. J. Int.*) we described the characteristics of the propagation of the high-frequency mantle phases Po and So. These oceanic Pn and Sn phases can be observed after propagation over many thousands of kilometres from the source, retaining high frequencies but acquiring a long and complex coda. This study concentrated on the way in which these characteristics can be sustained by fine-scale heterogeneity in the oceanic lithosphere that reinforces the influence of multiple P reverberations in the ocean and sediments as recognized by Sereno & Orcutt (1985; 1987). A form of quasi-laminar heterogeneity with horizontal correlation lengths around 10 km and vertical correlation lengths of about 0.5 km provides a good representation of the Po and So wavefield as also noted by Shito et al. (2013). This class of heterogeneity creates a strong scattering environment within the lithosphere that helps to sustain the Po and So phases over long distances. Propagation of So is most effective in thick old lithosphere, e.g., in the northwest Pacific Plate. Amplitudes of So are reduced significantly by propagation through thinner lithosphere in the Philippine Plate.

In this study we look at the entire Pacific basin and map out the propagation patterns for Po and So, which have the general characteristic of much more efficient propagation in the western sector than in the east that is much less well sampled. There are stronger changes in the nature of So than Po. For the same frequency S waves have a shorter wavelength than P waves, and so the So phase is more sensitive to the effects of both lateral variations in lithospheric structure and seismic attenuation.

We explore the relation of the nature of the observations of Po and So and the age of the lithosphere, based on 2-D FDM simulation seismic wave propagation for examining the influence of changes in lithospheric structure across fracture zones and similar features. The strong diffuse scattering field created in the oceanic lithosphere is hard to destroy and it is quite difficult to explain situations where So is very much weaker than Po, except by introducing enhanced seismic attenuation for younger lithosphere and the warmer asthenosphere in the neighborhood of spreading centers.

## Distribution of petit-spot volcanoes in relation to deformation and structures on a subducting plate

HIRANO, Naoto<sup>1\*</sup> ; NAKANISHI, Masao<sup>2</sup>

<sup>1</sup>Center for Northeast Asian Studies, Tohoku University, <sup>2</sup>Graduate School of Science and Technology, Chiba University

Tiny submarine volcanoes, known as petit-spots, occur in regions of plate flexure prior to subduction and seamount-loading (Hirano *et al.*, 2006, 2013). The surface morphology and distribution of petit-spot monogenetic volcanoes are influenced by the stress field in the lithosphere. The magmas produced by the accumulation of melt originating from asthenosphere just below the site of plate-flexure, are able to rapidly ascend to the surface from the base of the lithosphere (Hirano *et al.*, 2006; 2011; Valentine & Hirano, 2011). As monogenetic petit-spot volcanoes are too small to be detected by satellite altimetry, their study requires a research vessel equipped for shipboard acoustic multibeam surveys. Although previously surveyed areas are limited to the regions off the Japan Trench, the eruption ages of petit-spot volcanoes in this region represent monogenetic eruptions over a period of >9 Myr over a large area, and the eruptions are related to the outer rise bathymetry. Such tiny volcanoes are ubiquitous in regions of plate flexure worldwide, and have been recently reported from the Tonga Trench (Hirano *et al.*, 2008), the Basin and Range province (Valentine & Hirano, 2010), south of Greenland (Uenzelmann-Neben *et al.*, 2012), the Chile Trench (Hirano *et al.*, 2013), an accretionary complex in Costa Rica (Buchs *et al.*, 2013), and submarine French Polynesia (Hirano *et al.*, submitted).

The spatial distribution of submarine petit-spot volcanoes remains poorly constrained because shipboard bathymetry has not covered the entire northwestern Pacific Plate. If petit-spot volcanoes occur only in regions of plate flexure, then tiny submarine volcanoes should appear homogeneously on the submarine surface of outer rises. However, areas devoid of volcanoes and lava have been found surrounding areas of petit-spot volcanoes (i.e., sites A-C in Hirano *et al.*, 2006), indicating that the local characteristics of the lithosphere, in addition to plate flexure, control the occurrence of petit-spot volcanoes. Here we report that the distribution of petit-spot volcanoes is controlled by the tectonic structure of the seafloor. We conducted submersible dives along the linearly distributed petit-spot knolls by JAMSTEC *Shinkai6500* in April 2014. Areas with tectonic fabrics appear on the subducting Pacific Plate off the Japan Trench, including a ridge-perpendicular fabric zone (RPPFZ), ridge-parallel abyssal hills (RPRAH), and subducting 'horst and graven' structures (HAGS) (Nakanishi *et al.*, 2011). At Site C, which is a trench-oceanward slope offshore from Soma City, Fukushima Prefecture, the trend of the Japan Trench changes from N-S in the north to NE-SW in the south, where two areas of trench-parallel HAGSs are intersecting in a complex manner (Nakanishi *et al.*, 2011). The distribution of young volcanic cones of more than 80 petit-spots, reported from Site C by Hirano *et al.* (2008), seems to be controlled by the fabrics of RPPFZ and RPRAH, the trends of which are continuous with the HAGS to the north and south along the trench-oceanward slope, respectively. Although the RPPFZ is not recognized as a fracture zone, its trend is sub-parallel to that of the neighboring Nosappu and Kashima fracture zones (Nakanishi, 1993). As the RPPFZ and RPRAH that control the petit-spot distribution are clearly original structures of the lithosphere (in contrast to HAGS), the occurrence of petit-spot eruptions is possibly related to lithospheric structures.

Keywords: petit-spot, alkali-basalt, Pacific plate, outer rise, lithosphere

## Magnetic Anomalies in the Southern Indian Ocean Revisited

NOGI, Yoshifumi<sup>1\*</sup>; SATO, Taichi<sup>2</sup>; HANYU, Tomoko<sup>3</sup>

<sup>1</sup>National Institute of Polar Research, <sup>2</sup>National Institute of Advanced Industrial Science and Technology, <sup>3</sup>Graduate University for Advanced Studies

Magnetic anomalies in the Southern Indian Ocean are vital to understanding initial breakup process of Gondwana. However, seafloor age estimated from magnetic anomalies still remain less well-defined because of the sparse observations in this area. To understand the seafloor spreading history related to the initial breakup process of Gondwana, vector magnetic anomaly data as well as total intensity magnetic anomaly data obtained in the Enderby Basin, Southern Indian Ocean, are used. The strikes of magnetic structures are deduced from the vector magnetic anomalies.

Magnetic anomaly signals, most likely indicating Mesozoic magnetic anomaly sequence, are obtained almost parallel to WNW-ESE trending lineaments just to the south of Conrad Rise inferred from satellite gravity anomalies. Most of the strikes of magnetic structures indicate NNE-SSW trends, and are almost perpendicular to the WNW-ESE trending lineaments. Mesozoic sequence magnetic anomalies with mostly WNW-ESE strikes are also observed along the NNE-SSW trending lineaments between the south of the Conrad Rise and Gunnerus Ridge. Magnetic anomalies originated from Cretaceous normal polarity superchron are found in these profiles, although magnetic anomaly C34 has been identified just to the north of the Conrad Rise. However, Mesozoic sequence magnetic anomalies are only observed in the west side of the WNW-ESE trending lineaments just to the south of Conrad Rise and not detected to the east of Cretaceous normal superchron signals. These results show that counter part of Mesozoic sequence magnetic anomalies in the south of Conrad Rise would be found in the East Enderby Basin, off East Antarctica. NNE-SSW trending magnetic structures, which are similar to those obtained just to the south of Conrad Rise, are found off East Antarctica in the East Enderby Basin. However, some of the strikes show almost E-W orientations.

Moreover, the thickness of the crust increase just to the north of the Conrad Rise and clear magnetic anomaly signals considered to be magnetic anomaly C34 in this region may indicate continental-ocean boundaries while taking dredged continental origin rock samples at the Ob seamount into account. Therefore, magnetic anomaly C34 identified in the Indian Ocean must be reconsidered. These suggest complicated ridge reorganization occurred during initial breakup of Gondwana in the Indian Ocean.

Keywords: magnetic anomaly, Indian Ocean, Gondwana, continental crust

## Origin of the Palau Basin and a revised spreading model of the West Philippine Basin deduced from three-component magnet

SASAKI, Tomohiro<sup>1</sup> ; YAMAZAKI, Toshitsugu<sup>2\*</sup> ; ISHIZUKA, Osamu<sup>3</sup>

<sup>1</sup>University of Tsukuba, <sup>2</sup>AORI, University of Tokyo, <sup>3</sup>GSJ, AIST

The western part of the Philippine Sea (PHS) plate was occupied by the West Philippine Basin (WPB) in the north and the Palau Basin (PB) in the south. The WPB is generally considered to have opened from about 50 to 30 Ma, but the details are still unclear; in particular the origin and age of the PB was unknown. Studying the history of the WPB is important for understanding better the initiation and evolution of the IBM Arc. Here we discuss the spreading history of the WPB using new data on three-component magnetic anomaly and swath bathymetry acquired in the PB as well as those obtained previously by JAMSTEC fleets in the southern WPB. NS-trending magnetic boundaries and seafloor fabrics occur in the PB, indicating the formation by EW seafloor spreading. With a constraint from a  $^{40}\text{Ar}/^{39}\text{Ar}$  age of 40.4 Ma obtained from the northernmost part of the PB, we interpret that the observed magnetic anomalies correspond to polarity reversals from C16n1r to C18n/C18r (35.6 to 38/39 Ma). Previous models of WPB spreading incorporated a spreading-rate decrease around 40 Ma from about 4.4 to 1.8 cm/year. Our study in the southern WPB, however, suggests that the decrease is unnecessary for correlating observed three-component anomalies to the GPTS. A typical profile along 130E corresponds to C16r to C21 (36.3 to 45.3 Ma). The cessation age of the spreading in our interpretation, about 35 to 37 Ma, is older than the previous estimation (about 30 to 33 Ma). It was difficult to constrain rotation of the PHS plate from the magnetic anomaly skewness.

Keywords: Philippine Sea plate, West Philippine Basin, Palau Basin, magnetic anomaly, seafloor spreading

## The composition of back-arc basin basalts in the West Philippine Basin and association with mantle dynamics

HARAGUCHI, Satoru<sup>1</sup> ; ISHII, Teruaki<sup>2\*</sup>

<sup>1</sup>(Faculty of Engineering, University of Tokyo, <sup>2</sup>Fukuda Geological Institute

The Philippine Sea Plate was expanded by multiple extensions of backarc basins. Ishizuka et al. (2011) and Haraguchi et al. (2012) pointed out that the enriched mantle was flowed from backarc side during the spreading of the Shikoku Basin from 25 to 15 Ma (Okino et al., 1994, 1999). Haraguchi et al. (Meeting of the Volcanological Society of Japan, 2013) considered that the process of flowing of the enriched mantle estimated by the composition of the backarc basin basalts (BABB) recovered by the drilling of the Deep Sea Drilling Project (DSDP), Ocean Drilling Program (ODP) and Integrated Ocean Drilling Program (IODP). In this study, we attend the BABB of the West Philippine Basin, precede backarc spreading of the Shikoku Basin, and consider mantle dynamics by geochemical characteristics of BABB.

The first drillings in the West Philippine Basin by the Deep Sea Drilling Project are the Leg 31 same as the Shikoku Basin, and following operations are Leg 59 and the Ocean Drilling Program (ODP) Leg 195. And the diving of the R/V *Shinkai 6500* during the Y9611 cruise by R/V *Yokosuka* and dredges during the KR9801 cruise by R/V *Kairei* at the spreading axis (e.g. Fujioka et al., 1999). In this study, we discuss the new analyzed data of the basements of DSDP Leg 58 Site 446 and ODP Leg 195 Site 1201, and compare the data of the former studies.

Site 1201 is located in the west of the West Philippine basin, about 500km north from the Central Basin fault, axis of the spreading center. The main purpose of this site is the set up of the borehole site WP-1. Thickness of covered sediments at this site is more than 500m. The chemical characteristics of basements at this site are the typical BABB, not find the island arc characteristics. SiO<sub>2</sub> and MgO contents of these basalts are 49-53 and 5-8 wt%, respectively, and are similar to the basalts from the DSDP Leg 58 Site 442~444 in the Shikoku Basin. The TiO<sub>2</sub> contents of these basalts are 0.9~1.0 wt%, lower than those of the Shikoku Basin. The alkali elements are 1.5-2.8 wt% of Na<sub>2</sub>O and 0.1-1.6 wt% of K<sub>2</sub>O, similar K<sub>2</sub>O and lower Na<sub>2</sub>O contents to Shikoku Basin BABB. The trace elements are 320-420 ppm of Cr, higher than Shikoku Basin BABB, and lower Sr, Y and Zr. The Zr/Y and Nb/Zr ratio are also lower than Shikoku Basin BABB. We consider that these characteristics are the existence of the depleted parent mantle before the spreading of the Shikoku Basin pointed by Ishizuka et al. (2011) and Haraguchi et al. (2012).

Site 446 ate located in the Minami Daito Basin between the Daito and the Oki Daito Ridges. Thickness of covered sediments is about 350m. These volcanic rocks are considered to the intrusion in the sediment layer, different from the basement. The chemical characteristics of this volcanics are classified into alkali basalts, and prominent enrichment of TiO<sub>2</sub>, more than 4 to 5 wt%. This extremely enrichment of TiO<sub>2</sub> is not found from other inner plate volcanism in the Philippine Sea Plate. Therefore, we assume that the different inner plate volcanism from the mantle plume in the West Philippine Basin about 40 Ma (Deschamps and Lallemand 2002) were more active in the other Philippine Sea region.

We discuss these analyzed data and former data of the basements in the Philippine Sea Region, and consider parental material composition and magma dynamics before 30 Ma.

Keywords: Backarc basin basalts, Incompatible element ratio, Parent material of magma, Mantle dynamics

## Long-distance magma transport from oceanic island arc volcanoes

ISHIZUKA, Osamu<sup>1\*</sup> ; GESHI, Nobuo<sup>1</sup> ; KAWANABE, Yoshihisa<sup>1</sup> ; OGITSU, Itaru<sup>1</sup> ; TUZINO, Taqumi<sup>1</sup> ; SAKAMOTO, Izumi<sup>2</sup> ; TAYLOR, Rex<sup>3</sup> ; ARAI, Kohsaku<sup>1</sup> ; NAKANO, Shun<sup>1</sup>

<sup>1</sup>Geological Survey of Japan/AIST, <sup>2</sup>Tokai University, <sup>3</sup>University of Southampton

Long-distance lateral magma transport away from volcanic centers is emerging as a common phenomenon where the regional stress regime is favorable. It should also be recognized as an important factor in the construction and growth of island arcs, and a potential trigger for devastating eruptions. In this contribution, we report on recent investigations into the magma dynamics of Izu-Oshima volcano: an active basaltic volcano with an extensive fissure system.

Geophysical observations in the Izu-Bonin intra-oceanic island arc indicate that magma periodically is moved away from the main basaltic composite volcanoes. When Miyakejima erupted in 2000, seismic activity migrated about 30km northwestward from the volcanic centre (Geshi et al., 2002). This event is interpreted to reflect magma injection and dike propagation at a depth range between 12 and 20km (Kodaira et al., 2002). Long-distance lateral magma transport has also been identified at the Nishiyama volcano on Hachijojima Island using petrological, geochemical and structural studies of satellite vents (Ishizuka et al., 2008). Nishiyama has provided evidence for two types of magma transport: Primitive magma moving laterally for >20km in the middle to lower crust (10-20km deep) and short distance transport (<5km) from shallow, differentiated magma reservoirs. Of these the long-distance transport seems to be controlled by a regional extensional stress regime, while short distance transport may be controlled by the local stress regime resulting from the load of the main volcanic edifice.

Izu-Oshima is flanked by numerous, subparallel NW-SE trending submarine ridges extending up to 22 km to the NW and SE from the center of the volcano. During a recent diving survey we have identified that these ridges are fissures which erupted basaltic spatter and lava flows. Furthermore, lavas are petrographically similar along each ridge, while there are noticeable differences between ridges. The subparallel ridges are observed to transect a series of knolls, the Izu-Tobu monogenetic volcanoes (ITMV), which are dispersed across this area of the rear-arc. However, there is a consistent petrographic difference between these seamounts and the ridges.

We have found similar, and in some cases a matching, geochemistry between the submarine ridges and subaerial ridges of eruptions found ascending the flanks of Izu-Oshima. This implies that the subaerial ridges and submarine ridges together represent the track of a magma transport episode away from the storage system beneath the central volcano.

ITMV and the transecting ridges are found to have quite distinct geochemical characteristics, indicative of different magma sources. Yet, they are essentially found interspersed in outcrop. The most appropriate scenario for their development is one where ITMV are fed by an "in-situ" underlying source, while the NW-SE ridges are fed by lateral magma transport from Izu-Oshima. Unlike Nishiyama volcano, Izu-Oshima does not show a compositional variation along the length of the ridges, and has no evidence of primitive magmas. Hence, the magma transport is likely to be derived from a crustal chamber where crystal fractionation and plagioclase accumulation has taken place.

## Seafloor geodetic observation along the Nankai Trough - Progress report after the 2011 Tohoku-oki earthquake -

SATO, Mariko<sup>1\*</sup> ; WATANABE, Shun-ichi<sup>1</sup> ; YOKOTA, Yusuke<sup>1</sup> ; UJIHARA, Naoto<sup>1</sup> ; ISHIKAWA, Tadashi<sup>2</sup> ; MOCHIZUKI, Masashi<sup>3</sup> ; ASADA, Akira<sup>3</sup>

<sup>1</sup>Hydrogr. and Oceanogr. Dept. of Japan, <sup>2</sup>Japan Coast Guard Academy, <sup>3</sup>IIS, Univ. of Tokyo

We have been carrying out GPS/acoustic seafloor geodetic observation on the landward slope of the major trenches around Japan, such as the Japan Trench and the Nankai Trough. From the past observations, we detected intraplate deformation caused by the subduction of oceanic plates and coseismic displacements associated with large earthquakes.

Along the Nankai Trough, we deployed six seafloor reference points in the sea area from off-Omae-zaki through off-Muroto in 2002-2004 and had been carrying out campaign observations. From the observations conducted before the 2011 Tohoku-oki earthquake, we obtained the intraplate velocities of 2-5 cm/year toward WNW, which were generally consistent with those detected by on-land GPS measurements. A closer look gives us the differences of the velocities by sea areas.

Furthermore, to monitor seafloor movement spatially in the whole expected focal regions along the Nankai Trough, we deployed nine new seafloor reference points mainly off Shikoku in January 2012. If we obtain crustal velocities at all the site, it is expected that a spatial variation of interplate coupling will be revealed in the sea area along the Nankai Trough. It has been two years after the expansion of seafloor reference points and seafloor movements westward and northward are being observed at most of the sites.

In this report, we present a progress report on seafloor geodetic observation along the Nankai Trough after the 2011 Tohoku-oki earthquake.

Keywords: Seafloor geodetic observation, Seafloor geodesy, Nankai Trough

## Postseismic seafloor movements following the 2011 Tohoku-oki earthquake detected by GPS/acoustic positioning

WATANABE, Shun-ichi<sup>1\*</sup> ; SATO, Mariko<sup>1</sup> ; YOKOTA, Yusuke<sup>1</sup> ; UJIHARA, Naoto<sup>1</sup> ; ISHIKAWA, Tadashi<sup>2</sup> ; MOCHIZUKI, Masashi<sup>3</sup> ; ASADA, Akira<sup>3</sup>

<sup>1</sup>Hydrographic and Oceanographic Department, Japan Coast Guard, <sup>2</sup>Japan Coast Guard Academy, <sup>3</sup>Institute of Industrial Science, University of Tokyo

The Hydrographic and Oceanographic Department, Japan Coast Guard, have been developing precise seafloor positioning systems using the GPS/acoustic combination technique and carrying out campaign observations along the major trenches in the Pacific Ocean, such as the Japan Trench and the Nankai Trough. For example, after the 2011 Tohoku-oki earthquake (Mw = 9.0), we detected a huge coseismic displacement of 24 m toward ESE at MYGI which is located above the epicenter. We have been continued the geodetic observations along the Japan Trench in order to detect postseismic deformation.

The results of the observations show that the displacements vary with the sites even in the directions. MYGI and KAMS had moved toward west-northwest at constant rate. MYGW had moved toward south-southeast. KAMN had moved toward northwest. FUKU and CHOS had moved toward east-southeast. In addition, the displacements at FUKU and CHOS decay with time. For vertical component, significant subsidence was detected at all sites except CHOS where no vertical displacement was detected within the accuracy range.

In this presentation, we will report and discuss the latest results of the seafloor geodetic observation along the Japan Trench.

Keywords: seafloor geodetic observation, the 2011 Tohoku Earthquake

## A summary of the achievement in the project for advanced GPS/acoustic survey

KIDO, Motoyuki<sup>1\*</sup>; FUJIMOTO, Hiromi<sup>1</sup>; HINO, Ryota<sup>1</sup>; OHTA, Yusaku<sup>2</sup>; OSADA, Yukihiro<sup>1</sup>; IINUMA, Takeshi<sup>1</sup>; AZUMA, Ryosuke<sup>1</sup>; WADA, Ikuko<sup>1</sup>; SUZUKI, Syuichi<sup>2</sup>; TOMITA, Fumiaki<sup>3</sup>; IMANO, Misae<sup>3</sup>

<sup>1</sup>IRIDeS, Tohoku Univ., <sup>2</sup>RCPEV, Tohoku Univ., <sup>3</sup>Sci., Tohoku Univ.

GPS/acoustic survey is known as a most probable way to measure the crustal deformation of seafloor far from the coasts, where dense GPS network is not available. We, Tohoku University, together with Nagoya University and Japan Coast Guard dedicated in GPS/acoustic survey for more than decade. MEXT has been strongly promotes our activities though financially support as governmental project. We summarize individual topics in the project.

For the moored buoy, collaborating with JAMSTEC and JAXA, we have started long-term continuous and realtime seafloor geodetic survey at Kumano-nada. At the early stage of the project, we employed a small buoy, which can be also used as towing survey, at off-Miyagi site. Because the size of battery is limited, sea-trials was lasting only for two days. However, using this platform, we developed an automatic ranging system and simple on-demand operation technique via UHF communication. In 2012, we have started developing a automatic ranging system in a realistic working condition using a time-proven platform, m-TRITON buoy, operated by JAMSTEC. Together with JAMSTEC and JAXA, satellite communication part and GPS positioning part have been shared for multi-purpose. Tohoku University group concentrate acoustic ranging part and onsite data processing to compute precise traveltimes. Using a limited onsite resource in the buoy, we have eliminated unnecessary and redundant procedure and data as possible. The first sea-trial took place in 2013 for four months and the ongoing second trial has started in 2014 for six months. In the second trial, acoustic ranging data has been successfully transmitted to onshore station every week and we can monitor it from our laboratory.

For the Autonomous Surface Vehicle (ASV) system, we aimed to develop an automatic survey system, which can also be used simultaneous measurements from other platform, such as a research vessel, for improve the ranging accuracy with multi-acoustic-paths. In our system, vehicle is like an unmanned boat (2.4m long and 400kg in weight), whose propulsion system is driven by electric power from onboard diesel generator lasting for a week. As the ASV system demonstrates sufficient performance for our use in GPS/acoustic survey, it can be a candidate of multi surface platform for simultaneous ranging to achieve high accuracy GPS/acoustic measurement taking the spatial sound speed variation into account.

After the Tohoku-Oki earthquake in 2011, the project has an extra mission that significantly enhance the survey framework, especially in deep seafloor (>5000m) near the trench axis. In this extra mission, we have developed a new type of seafloor transponder that works at over 5000m depth and its acoustic communication range is greater than 15km. We made 86 transponders in total and constructed 20 new GPS/acoustic station along the Japan Trench in 2012. In addition, we chartered a research ship for about 50 days per year to construct and observe the new stations. At present we have carried out four times of campaign surveys during 2012-2013. At these new stations, we conducted both moving and stationary surveys, the former generally took several hours and the latter 12 hours for each station. We found a problem in acoustic property in the new transponders, which can be corrected with post-processing shown in Azuma et al. (2014, JpGU). Campaign surveys ranges only about one year, but we have observed post-seismic movement at selected stations. These results are reported in Tomita et al. (2014, JpGU). The new transponders are hybrid type so that Japan Coast Guard has started to make measurements with their own system at several stations above.

This work has been supported by MEXT project for advanced GPS/acoustic survey. Staffs in RCPEV and IRIDeS, Tohoku University gave dedicated support and collaborative operation in the onboard and GPS surveys. The construction and surveys in the new stations were collaboration with Nagoya University.

Keywords: GPS/acoustic, moored buoy, autonomous surface vehicle, Japan trench

## Detection of post-seismic movement after Tohoku-oki Earthquake using GPS/Acoustic technique

TOMITA, Fumiaki<sup>1\*</sup> ; KIDO, Motoyuki<sup>2</sup> ; OSADA, Yukihito<sup>2</sup> ; AZUMA, Ryosuke<sup>2</sup> ; FUJIMOTO, Hiromi<sup>2</sup> ; HINO, Ryota<sup>2</sup> ; IINUMA, Takeshi<sup>2</sup> ; OHTA, Yusaku<sup>1</sup> ; WADA, Ikuko<sup>2</sup>

<sup>1</sup>Graduate School of Science, Tohoku University, <sup>2</sup>International Research Institute of Disaster Science, Tohoku University

Using GPS/Acoustic seafloor geodetic observation (GPS/A observation), we can directly measure seafloor movements, which cannot be obtained from on-land geodetic observation. For example, Kido et al. (2011) and Sato et al. (2011) detected huge co-seismic displacements associated with 2011 off Pacific coast of Tohoku Earthquake near the Japan Trench, 150km distant from the coast.

After the occurrence of the Tohoku-oki Earthquake, we deployed new seafloor benchmarks at 20 sites along the Japan Trench from Ibaraki-oki to Sanriku-oki. Including three sites installed before 2011, we totally have 23 sites to monitor the post-seismic movement for the Tohoku-oki Earthquake. We have conducted four GPS/Acoustic surveys at present (09/2012, 11/2012, 07/2013, 10/2013) at these sites.

The surveys consists of two types of observations; they are moving survey to locate the position of individual seafloor transponders that make up each geodetic site and point survey to determine the precise location of the center of the transponder array. The displacement at each site is estimated from the temporal change of the array center position. However, we identified two dominant factors that influence the precision of the array center positioning in our observation.

The first factor is the instability in the waveforms of acoustic signals. In GPS/A analysis, we calculate cross-correlation waveform between received and transmitted signals, and determine the timing of maximum peak as round trip travel time. However, multiple peaks separated by 0.3-0.5ms each other are found in a cross correlation waveform, whose relative amplitudes are influenced by the relative position between the hydrophone on the research ship and the seafloor transponder. We have developed an algorithm that can automatically picks up the first peak from the multiples and reduces the error in determining round trip travel time. The detail of this problem and the algorithm will be reported by Azuma et al. (2014, JpGU).

The second factor is uncertainty in the position of the hydrophone equipped on the research ship with respect to three GPS antennas at the top of the ship for attitude determination. In our observations, it is difficult to directly measure the relative position of the three GPS antennas and the hydrophone attached at the end of the pole mounted on the ship's side; the provisional position based on the drawing has about 1m offset. The horizontal component of the offset causes systematic deviation in the apparent position of the transponders depend on ship's heading. Taking this behavior into account, we can correct for the horizontal offset with about 5cm in accuracy. The vertical offset is thought to have less influence on the estimation of the array center position because the sound speed correction intrinsically includes the vertical offset. However, accuracy of offset estimation is still insufficient, hence the estimation technique must be refined further.

After these correction, we have succeeded to obtain preliminary movements at 10 sites using the data in two of the four surveys (09/2012 and 07/2013) at present. These preliminary results generally indicate eastward seafloor movements at the northern Sanriku-oki sites and westward movements at off-Miyagi sites. In this talk, we introduce outline of the analysis and up-to-date results of evaluation of the post-seismic movement incorporating the data in 11/2012 and 10/2013.

Keywords: seafloor geodesy, Tohoku-oki Earthquake, Japan Trench, post-seismic movement

## Understanding recoupling process using a seafloor geodesy in megathrust earthquake zone

OSADA, Yukihiro<sup>1\*</sup> ; ITO, Yoshihiro<sup>2</sup> ; KIDO, Motoyuki<sup>1</sup> ; HINO, Ryota<sup>1</sup> ; IINUMA, Takeshi<sup>1</sup>

<sup>1</sup>IRiDes, Tohoku University, <sup>2</sup>DPRI, Kyoto University

The 11 March 2011 Tohoku-Oki earthquake ruptured the interplate boundary off the eastern shore Honshu, generated a devastating tsunami that swept the coastal area along the northeastern Japan. The seafloor geodesy brought important results that show that the large slip was near the Japan Trench and suggested the heterogeneity of the coseismic slip distribution in the plate interface. The maximum displacement region for interplate earthquake is mainly located offshore region. Therefore it is important to monitor the postseismic displacement and the stress accumulation process using seafloor geodesy. And if we can observe the postseismic displacement near the Japan Trench, we contribute to understand the coupling condition of plate boundary. There is a seafloor acoustic ranging system for direct observation of horizontal displacement on seafloor. We improve this system that adapted for the axis of Japan Trench. The system is designed to measure distances of up to 3 km and to adapt the pressure vessel of 9000m water-depth. We deployed the seafloor acoustic ranging system between 2013 May and 2013 Sep. We observed across the Trench baseline (about 7km), baseline between the bottom of Trench to the seaward side of Japan Trench (about 3.6km). We get data both baseline results for 4 month. We report this results on this presentation.

Keywords: seafloor crustal movement, Japan Trench

## Sea trial of tsunami and crustal movement observation buoy system in real-time under environment with high speed sea cur

TAKAHASHI, Narumi<sup>1\*</sup> ; ISHIHARA, Yasuhisa<sup>1</sup> ; FUKUDA, Tatsuya<sup>1</sup> ; OCHI, Hiroshi<sup>1</sup> ; TAHARA, Jun'ichiro<sup>1</sup> ; MORI, Takahito<sup>1</sup> ; KIDO, Motoyuki<sup>2</sup> ; OHTA, Yusaku<sup>2</sup> ; HINO, Ryota<sup>2</sup> ; MUTOH, Katsuhiko<sup>2</sup> ; HASHIMOTO, Gosei<sup>3</sup> ; MOTOHASHI, Osamu<sup>3</sup> ; KANEDA, Yoshiyuki<sup>1</sup>

<sup>1</sup>Japan Agency for for Marine-Earth Science and Technology, <sup>2</sup>Tohoku University, <sup>3</sup>Japan Aerospace Exploration Agency

Japan Agency for Marine-Earth Science and Technology (JAMSTEC), Tohoku University and Japan Aerospace Exploration Agency (JAXA) have developed real-time observation system for tsunami and crustal movement using a buoy since 2011. Although observation interval of crustal movement is generally sparse, because the timing depends on availability of observation ship, we aim to construct to observe tsunami in real-time and crustal movement when it is necessary. Because Japan is surrounded by seismogenic zones with large earthquakes and such large event brought huge damages on coastal region people, early detection is needed to reduce the severe damage. Although online cable system is best for it, the cost for the construction and implementation is huge. Therefore, we point use of the buoy as the removable temporal early detection system. The system is composed of a pressure seafloor unit with pressure sensor and acoustic transmission unit, six seafloor transponders and buoy station incorporating some loggers, transducers to communicate with seafloor systems and data transmission system to land. The seismogenic zones, however, are under the environment of high speed sea current like the Kuroshio. Therefore, we use the slack mooring on our system, but the some technical development is needed for adoption of the mooring. For example, low consumption electricity due to high power acoustic signals for the data transmission and We tried sea trial for three months in last year, and confirmed to fully resistance for high speed sea current over 5.3 knots. On the other hand, the issued to be resolved are clarified, which are on acoustic transmission between the pressure seafloor unit and the buoy, the resistance for the fishery activities and so on. We took measures for above issues and deploy the revised system at off the Kumano Basin. The observation period of the second sea trial is six months. In addition to the measures, we implement tsunami mode. In normal case, we obtain tsunami data with an interval of 15 minutes, but, it is switched to be 15 seconds in tsunami mode. The tsunami mode is triggered when a ratio of average for short period of time (STA) and that of long one (LTA) exceed the threshold level. And, we move the timing of the STA and LTA and try to detect the first arrivals of tsunami. Now, we obtain real-time tsunami and crustal movement data via iridium transmission and introduce it in this presentation.

## Study for improving efficiency in seafloor geodetic observation by means of multi acoustic ranging

YOKOTA, Yusuke<sup>1\*</sup> ; SATO, Mariko<sup>1</sup> ; WATANABE, Shun-ichi<sup>1</sup> ; ISHIKAWA, Tadashi<sup>2</sup>

<sup>1</sup>Hydrographic and Oceanographic Department, Japan Coast Guard, <sup>2</sup>Japan Coast Guard Academy

Japan Hydrographic and Oceanographic Department (JHOD) and the Institute of Industrial Science, University of Tokyo, have been developing a system for precise seafloor geodetic observation with the GPS/Acoustic combination technique. In this observation, the movements of the seafloor reference points are measured with 2 - 3 centimeters precision. JHOD has been carrying out seafloor geodetic observations 2 - 4 times a year for each station and reported the inter-seismic deformation before and after the 2005 Miyagi-oki earthquake and the co- and post-seismic deformations of the 2005 Miyagi-oki earthquake and the 2011 Tohoku-oki earthquake and so on.

After the 2011 Tohoku-oki earthquake, this observation is expected to be broadened and densely-arranged with the objective of large-scale earthquake disaster prevention. In order to expand further seafloor geodetic observation, shortening of observation time, which is about one day for one campaign, is required. Therefore, we are considering a new acoustic ranging method. In this new method, we conduct the acoustic ranging for multi seafloor transponders not individually but sequentially. We report the details of this new multi acoustic ranging method and discuss how much efficiency will be improved by the introduction of the new method.

Keywords: seafloor geodetic observation, acoustic ranging

## Hydrothermal heat mining due to the aquifer thickening toward the trench axis: A model for the Japan Trench

KAWADA, Yoshifumi<sup>1\*</sup> ; YAMANO, Makoto<sup>1</sup> ; SEAMA, Nobukazu<sup>2</sup>

<sup>1</sup>ERI, Univ of Tokyo, <sup>2</sup>Kobe University

**Observation:** At the Japan Trench, a 135-Myr-old Pacific plate is subducting beneath the Japan Island. Heat flow on such an old oceanic plate is expected to be 50m W/m<sup>2</sup> by a thermal model of the oceanic plate. However, observed heat flow values range from 50 to 120 mW/m<sup>2</sup> and the averaged value is 70 mW/m<sup>2</sup> (Yamano et al., 2008, Int. J. Earth Sci.). In the area of high heat-flow anomalies, a high  $V_p/V_s$  layer (highly porous, and probably highly permeable) is observed within the uppermost part of the oceanic plate (Fujie et al., 2013, JpGU Meeting). The layer thickness is observed to increase toward the trench axis.

**Hypothesis:** Permeability within the uppermost several hundred meters of oceanic plate is measured to be high for fluid to convect; this layer is called an aquifer. We assume that thickening of the observed high  $V_p/V_s$  layer is a consequence of thickening of this highly permeable layer. Accordingly, we construct a numerical model including hydrothermal circulation within an aquifer being thickened with time, and calculate the resulted heat flow anomalies.

**Results:** Calculations show that heat flow is increased as the aquifer thickness begins to increase. With typical parameter values for the Japan Trench, the result accounts for the observed high heat-flow anomaly of 20 mW/m<sup>2</sup>. This high heat-flow arises due to the mining of heat from the base of the thickening aquifer. Downward thickening of the aquifer invades the high-temperature region, and incorporates the heat into convection. As a result, this heat is transported upwards through sediments above the aquifer, and heat flow is increased.

Keywords: hydrothermal circulation, heat flow, the Japan Trench, seismogenic zone

## Seismic structure and seismicity survey at the Kairei hydrothermal vent field in the Indian Ocean

SATO, Toshinori<sup>1\*</sup> ; TAKATA, Hiroyoshi<sup>1</sup> ; IMAI, Yuki<sup>2</sup> ; NOGUCHI, Yui<sup>1</sup> ; KOUNO, Akihiro<sup>1</sup> ; YAMADA, Tomoaki<sup>3</sup> ; SHINOHARA, Masanao<sup>3</sup>

<sup>1</sup>Graduate School of Science, Chiba Univ., <sup>2</sup>Dep. Science, Chiba Univ., <sup>3</sup>ERI, Univ. Tokyo

### 1. Introduction

In the first segment of the central Indian Ridge from the Rodriguez triple junction, the Kairei hydrothermal vent field exists and extrudes hydrothermal fluid with richer hydrogen content compared to other hydrothermal vents in the world. Around the Kairei hydrothermal field, serpentinized peridotite and troctolites, and gabbroic rocks were discovered. These deep-seated rocks exposed around the Kairei field may cause the enrichment of H<sub>2</sub> in the Kairei fluids. At the Kairei field, a hydrogen-based subsurface microbial ecosystem and various hydrothermal vent macrofauna were found. In the TAIGA Project (Trans-crustal Advection and In situ reaction of Global sub-seafloor Aquifer), this area is a representative field of TAIGA of hydrogen. To investigate how the deep-seated rocks (originally situated at several kilometers below seafloor) are uplifted and exposed onto seafloor, and the hydrothermal fluids circulate in subsurface, we conducted a seismic refraction/reflection survey and seismicity observation with ocean bottom seismometers (OBSs).

### 2. Observation

We conducted a seismic survey around the Kairei hydrothermal field from January 27 to March 19 in 2013 using S/V Yokosuka of Jamstec. We used 21 OBSs, an air gun (GI gun) and a single channel streamer cable. Deployed intervals of OBSs are about 7.5 km, and 2 km near the Kairei field. Survey lines are 5 lines NNW-SSE direction parallel to the ridge axis, 5 lines E-W direction, and 5 lines NNE-SSW direction. Line lengths are from 7 km to 30 km. In addition, we conducted other 5 lines pass around the point just above the Kairei hydrothermal field and the Yokoniwa Rise. The air gun was a GI gun with 355 cu. in. (5.5 l), and the shot interval was 40 s (about 100 m).

### 3. Results

From seismicity observation, we found many micro earthquakes in this area. A swarm of micro earthquakes exists at a location about 1 km northwest of the Kairei field. The swarm has a NNW-SSE strike, parallel to the ridge axis. The depth of the swarm is very shallow (~4 km from seafloor). This swarm may be related to the hydrothermal activities of the Kairei field. At the first segment of the central Indian Ridge, many micro earthquakes occurred. The depth of these events is deeper than that of the swarm near the Kairei field.

### Acknowledgements

We thank the captain and the crew of S/V Yokosuka of Jamstec for their support. This work was supported by Grant-in-Aid for Scientific Research on Innovative Areas of the Ministry of Education, Culture, Sports, Science and Technology (Grant Number 20109002, TAIGA project).

Keywords: TAIGA, hydrothermal area, seismicity, Triple junction in the Indian Ocean

## Origin of boron in Okinawa Trough hydrothermal fluids using B isotope as a tracer

TOKI, Tomohiro<sup>1\*</sup>; EBINA, Naoya<sup>1</sup>; SHINJO, Ryuichi<sup>1</sup>; ISHIBASHI, Jun-ichiro<sup>2</sup>

<sup>1</sup>University of the Ryukyus, <sup>2</sup>Kyushu University

The Okinawa Trough is a back-arc basin located around the Ryukyu Arc, where several hydrothermal systems have been discovered. The Okinawa Trough has a very thick sedimentary cover, and the chemistry of the hydrothermal fluids appeared to be influenced by interaction with the sediment. However, the temperature environments below the seafloor have not been clarified yet in detail. In this study, we investigated B isotope ratios ( $\delta^{11}\text{B}$ ) in hydrothermal fluids from Okinawa Trough, and discussed the origin of the boron and the reaction temperature.

The hydrothermal fluid samples were collected by WHATS with Hyper Dolphin and *Shinkai 6500* from Iheya North Knoll, Izena Caldron, Hatoma Knoll, and Yonaguni Knoll IV. The sample was filtered and acidified by  $\text{HNO}_3$ . B was isolated by micro-sublimation, and  $\delta^{11}\text{B}$  measurement was carried out using a MC-ICP-MS (Neptune plus). The precision was within 0.3%. All values reported in this study are presented in delta notation relative to NBS SRM 951.

The concentrations of B in the hydrothermal fluids from Okinawa Trough were higher than those from sediment-starved MOR, and the  $\delta^{11}\text{B}$  showed  $^{10}\text{B}$  enrichments. A difference of  $\delta^{11}\text{B}$  among Okinawa Trough hydrothermal fields was found; Yonaguni IV < Izena Caldron < Iheya North < Hatoma Knoll. The  $\delta^{11}\text{B}$  in the hydrothermal fluids showed the strong correlation with the carbon isotopic ratios of methane ( $\delta^{13}\text{C}\text{-CH}_4$ ) in the hydrothermal fluids, suggesting the factor controlling the variation of  $\delta^{11}\text{B}$  in the hydrothermal fluids is identical with the one controlling the variation of  $\delta^{13}\text{C}\text{-CH}_4$  in the hydrothermal fluids. The controlling factor for the variation of  $\delta^{13}\text{C}\text{-CH}_4$  in the hydrothermal fluids is a mixing ratio between thermogenic methane and microbial methane, implying the controlling factor for the variation of  $\delta^{11}\text{B}$  would be a mixing ratio between B derived from sediment at higher temperature and lower temperature.

We calculated the reaction temperature based on the correlated equation of reaction temperature with  $\delta^{11}\text{B}$  fractionation between solid phase and aqueous phase. For  $\delta^{11}\text{B}$  of the solid phase, reported  $\delta^{11}\text{B}$  of surface sediment from Okinawa Trough ( $-5.4$  and  $-2.2$  ‰) was used. However, all observed  $\delta^{11}\text{B}$  in the hydrothermal fluids could not be explained. Instead,  $\delta^{11}\text{B}$  of solid phase was estimated between 50 and 400 °C; the lowest temperature of leaching B from sediment is 50 °C and the highest temperature of sub-critical water is 400 °C.  $\delta^{11}\text{B}$  of sediment involved in B leaching was estimated to be from  $-20$  to  $-10$  ‰, which are lower than the  $\delta^{11}\text{B}$  in surface sediment from Okinawa Trough. Hydrothermal alteration lowered  $\delta^{11}\text{B}$  in sediment, suggesting the origin of the B in Okinawa Trough hydrothermal fluids would be altered sediment. For the reaction temperature, the lowest value among Okinawa Trough hydrothermal fluids was obtained in Hatoma hydrothermal fluids, following Iheya North, Izena, and Yonaguni IV, suggesting a large amount of sediment is distributed in recharge zone in Hatoma Knoll, and the B would be derived from the sediment at relatively low temperature. On the other hand, sediment is distributed in reaction zone beneath Yonaguni IV, and the B would be derived from the sediment at relatively high temperature.

Keywords: hydrothermal fluid, Okinawa Trough, boron isotope

## The structure of iron- and silica-rich mounds at hydrothermal environment in shallow marine, Satsuma Iwo-Jima

KURATOMI, Takashi<sup>1\*</sup>; KIYOKAWA, Shoichi<sup>1</sup>; IKEHARA, Minoru<sup>2</sup>; GOTO, Shusaku<sup>3</sup>; HOSHINO, Tatsuhiko<sup>4</sup>; IKEGAMI, Fumihiko<sup>1</sup>; MINOWA, Yuto<sup>1</sup>

<sup>1</sup>Kyushu University, <sup>2</sup>Center for Advanced Marine Core Research, Kochi University, <sup>3</sup>Geological Survey of Japan, AIST, <sup>4</sup>Japan Agency for Marine-Earth Science and Technology

Satsuma Iwo-Jima Island, located 38km south of Kyusyu, Japan, is a volcanic island in the northwestern rim of Kikai caldera. Iron- and silica-rich mounds develop with hydrothermal activity (pH=5.5, 50-60 degree Celsius) in Nagahama bay located south-western part of the island. The brownish seawater at the bay is due to mixing of the hot spring water with seawater (Shikaura and Tazaki, 2001). Very high deposition rate (33 cm per year) of iron-rich sediments was observed in the bay (Kiyokawa et al., 2012). In this study, we analyzed samples (20-30 cm long) recovered from mounds at the seafloor of Nagahama bay by the observation with X-ray CT scan, FE-SEM, and the thin-sectioned sample, and the chemical analysis with EDS, XRF, XRD and DNA, and found that the structure of mounds has unique information.

Visual observation indicated that the samples were made from two layer: black high-density hard layer and brownish low-density soft layer. X-ray CT scan observation shows that the inside of samples is constructed from the aggregation of convex structure (3-4 cm). Soft layer is covered by a hard layer as a rim. The soft layer has many pipe-like structures (typical radius: 1 mm). Petrographic observations indicate that soft and hard layers have filament-like forms, and the form in soft layer is perpendicular to that in the hard layer. The number of small particles (about 20  $\mu\text{m}$ ) observed on filament-like forms in soft layer increases toward hard layer. FE-SEM observation shows that filament-like form in hard layer consists of aggregation of bacillus-like form as the chain of particle (about 2  $\mu\text{m}$ ). At soft layer, on the other hand, bacteria-like form with smaller particles (<0.5  $\mu\text{m}$ ) is observed. Bacteria-like form could be classified into 3 types (helix, ribbon-like, twisted). Furthermore, the result of XRD and XRF show that hard layer consists of ferrihydrite and opal-A (Si: 26.8%, Fe: 56.0%) and soft one is composed by ferrihydrite, opal-A, quartz, cristobalite and tridimite (Si: 36.5%, Fe: 43.5%). DNA analysis indicated predominance of *Mariiprofundus ferrooxydans* that is known as iron-oxidizing bacteria belonging to Zeta-proteobacteria.

The forming process of the mounds at Nagahama bay is that firstly chemical and biological reaction made soft layer. During occurrence of the reaction, volcanic ash originating from Iwo-dake was contained as silica in the soft layer. Bacteria-like form in soft layer is considered to be the stalk made by iron-oxidizing bacteria according to the result of DNA analysis. Such neutrophilic iron-oxidizing bacteria prefers an environment of redox interface between hydrothermal water and seawater (Chan et al., 2011), and their activity made hard rim at outer soft layer. Inside of hard rim, the keeping of both reaction resulted in relative iron-rich layer and layering at hard rim. Because such process occurred repeatedly, the mounds at Nagahama bay had the aggregation of convex structure with many pipes as the hydrothermal vent. The high depositional rate of iron hydroxides is likely to be influenced by the activity of bacteria.

Keywords: hydrothermal activity, iron-hydroxide, iron-oxidizing bacteria, shallow marine

## GPS/acoustic measurement using a multi-purpose moored buoy system

IMANO, Misae<sup>1\*</sup> ; KIDO, Motoyuki<sup>2</sup> ; OHTA, Yusaku<sup>1</sup> ; FUKUDA, Tatsuya<sup>3</sup> ; OCHI, Hiroshi<sup>3</sup> ; TAKAHASHI, Narumi<sup>3</sup>

<sup>1</sup>Graduate School of Science, Tohoku University, <sup>2</sup>IRIDeS, Tohoku University, <sup>3</sup>Japan Agency for Marine-Earth Science and Technology

For monitoring crustal deformation and tsunami occurrence in the source region of the upcoming Nankai and Tonankai earthquake, JAMSTEC, JAXA, and Tohoku University have jointly developed a realtime continuous observation system using a moored buoy, called m-TRITON, and have started its sea-trial. The system consists of a seafloor pressure sensor for monitoring tsunamis and vertical crustal deformation, a GPS system for monitoring sea-level and position/attitude of the buoy, and a GPS/acoustic system for monitoring horizontal crustal deformation. Measured data are transmitted to onshore station via satellite communication so that they can be monitored in realtime. The first sea-trial was carried out in Kumano-nada in 2013, and the second trial has been started in 2014 after improvement of the system. In this presentation, we focus on the issues particular to acoustic ranging of GPS/acoustic measurement for the purpose to remedy the system based on the data acquired in 2013, and report new data being acquired in the ongoing second trial in 2014.

The GPS/acoustic system measures horizontal movement of a seafloor benchmark, which consists of six transponders by combining GPS analysis of the buoy and acoustic ranging between the buoy and seafloor transponders. Considering bit-rate of the satellite communication, it is not realistic to send full acoustic waveform. So, it is required to send only the result processed on the buoy. In order to proceed acoustic wave with a low-powered device on the buoy, it is necessary (1) to cut out recorded waveform to the minimum requirement and (2) to send the processed data containing minimum but sufficient information. As for (1), in the current system recorded acoustic waveform is cut out by a window of  $\pm 20$  ms centered at synthetic traveltime calculated from provisional position of the buoy and each seafloor transponder. After that, cross-correlation waveform between the transmitted signal and the received signal is calculated to obtain an accurate observed traveltime. Then (2) send the correlogram only a 1 ms window centered at the maximum correlation peak, which is sufficient to include the sidelobe. Since correlation wave is represented in 8 bit and the sampling rate is in 100 kHz, the size-per-single wave to be transmitted can be reduced only to 101 byte.

As a result of considering the fluctuating range for the uncertainty of provisional position obtained by the NMEA output of the GPS ( $\sim 10$  m at most) and the average sound speed variation ( $\sim 2$  m/s) that affect the synthetic traveltime, the window width of  $\pm 20$ ms employed in (1) is a minimum requirement. In order to certainly cut out maximum correlation peak for all acoustic ranging, it is desirable to set the width to  $\pm 30$  ms. As for correlogram to be sent to onshore station, since the envelope of the correlation peak is within the 1 ms, current width is reasonable. However, apparent maximum correlation peak often known to appears due to multiples at sea surface. In that case, it is not possible to achieve proper adjustment only by the width. Therefore the development of an algorithm to detect the true correlation peak is required. We verified based on actual data about the condition that the multiple occurs, and found that it is explained by the incident angle of the sound wave and the directivity of transducer. We are developing an algorithm that automatically detects the true correlation peak based on this hypothesis.

Keywords: crustal deformation, moored buoy

## Inversion analysis for slip deficit rate along the Nankai Trough using on- and offshore crustal velocities

WATANABE, Tsuyoshi<sup>1\*</sup> ; TADOKORO, Keiichi<sup>1</sup> ; YASUDA, Kenji<sup>1</sup> ; FUJII, Cosumo<sup>1</sup> ; IKUTA, Ryoya<sup>2</sup> ; OKUDA, Takashi<sup>1</sup> ; KUNO, Masahiro<sup>3</sup>

<sup>1</sup>Graduate School of Environmental Studies, Nagoya University, <sup>2</sup>Department of Geosciences, Shizuoka University, <sup>3</sup>Mie Prefecture Fisheries Research Institute

Along the Nankai Trough, megathrust earthquakes occur every 100-150 years. A nationwide continuous GPS observation network in Japan has measured precise crustal deformation in this area for the past decade. However, the sources of these earthquakes are located offshore where slip resolution is generally poor. Since the early 2000s, seafloor geodetic observations using GPS/Acoustic techniques have been conducted against such a background in Japan. Today, seafloor geodetic observations are recognized as an effective and essential procedure for understanding the source process of earthquakes that occur in offshore areas. In this study, we show the result of seafloor geodetic observations using GPS/Acoustic techniques from 2004 to 2012 and estimate slip deficit rates along the Nankai Trough using both onshore GPS velocities and offshore crustal velocities derived from seafloor geodetic observations. We conducted inversion analysis with a priori information, and then, a high slip deficit rate of more than 50 mm/yr was detected off the Shikoku district. This decreases to approximately 30-50 mm/yr off the Kii Peninsula, and then it falls to approximately 10-30 mm/yr around the Suruga Trough relative to the Amurian plate, except for slip deficit rate of nearly 40 mm/yr which was detected at a fault segment beside the seafloor benchmark at the Suruga Bay. In addition, we investigated slip resolution by adding new established seafloor benchmarks off Shikoku district. As a result, we found that slip resolution was still poorer in offshore areas such as off the Ashizuri Cape, the Muroto Cape, and the Kii Peninsula near the trench axis than in onshore areas. Thus, it is important to conduct seafloor geodetic observations in areas with poor slip resolution.

Keywords: GPS/Acoustic, Nankai Trough, crustal deformation, slip deficit rate, slip resolution

## Development and examination of new methods for traveltine detection in GPS/A geodetic data to high-precise and automatic

AZUMA, Ryosuke<sup>1\*</sup> ; TOMITA, Fumiaki<sup>2</sup> ; IINUMA, Takeshi<sup>1</sup> ; HINO, Ryota<sup>1</sup> ; KIDO, Motoyuki<sup>1</sup> ; FUJIMOTO, Hiromi<sup>1</sup> ; OSADA, Yukihito<sup>1</sup> ; OHTA, Yusaku<sup>3</sup> ; WADA, Ikuko<sup>1</sup>

<sup>1</sup>IRIDeS, Tohoku Univ., <sup>2</sup>Graduate School of Science, Tohoku Univ., <sup>3</sup>RCPEVE, Tohoku Univ.

The development of a technique for GPS-acoustic (GPS/A) geodetic observations has enabled us to understand the slip distribution of the 2011 Tohoku-oki earthquake. However, there remains an issue with the precision of GPS/A measurement is still lower by two orders of magnitude than that of on-land GPS measurement due to problems in observations and data processing methods. In this study, we focus on the problem for determination of traveltimes of acoustic signals obtained from GPS/A measurement.

The conventional approach for determining the two-way traveltine of observed acoustic signals is to determine the maximum peak of the cross-correlation waveforms between the transmitted and returned signals. However, the maximum peak often differs from the true peak due to the distortion in the correlation waveform which depends on the relative spatial geometry of the ship and station. These misread traveltimes have been re-read manually so far. Such procedure is no longer applicable for processing vast array of data obtained at newly installed over 20 GPS/A stations after the 2011 Tohoku-oki earthquake. The aim of this study is to develop fully automated algorithms for analyzing GPS/A data with high precision. We introduce here two algorithms.

1) We read the maximum peak in the observed correlogram and then deconvolve it by the synthetic correlogram. Then, we apply the same operation to the deconvolved waveform. This procedure is iterated until the correlation coefficient decreases lower than a pre-defined threshold. A true traveltine is defined as the fastest traveltine during the iterations.

2) We classify the observed correlograms into several groups based on their similarity through cluster analyses and choose a master waveform in each group. Then evaluate the traveltine residual between the maximum peak and the true peak in the observed correlogram. Thus obtained residual is applied as the correction value of each clustered group.

We also use a seismic data analysis tool to visually inspect whether above algorithms work properly. We confirmed that the both new methods properly correct for misreadings in the current method, which sometimes amount to several hundred microseconds. This corresponds roughly to a 0.3-m difference in the slant range. Therefore, with the new algorithms, significant improvement in the estimation of the station location is expected. However, both methods have to be assigned an arbitrary value as a threshold. Further analyses are needed to determine arbitrary threshold values and to construct fully automated algorithms.

Keywords: ocean bottom geodetic observation

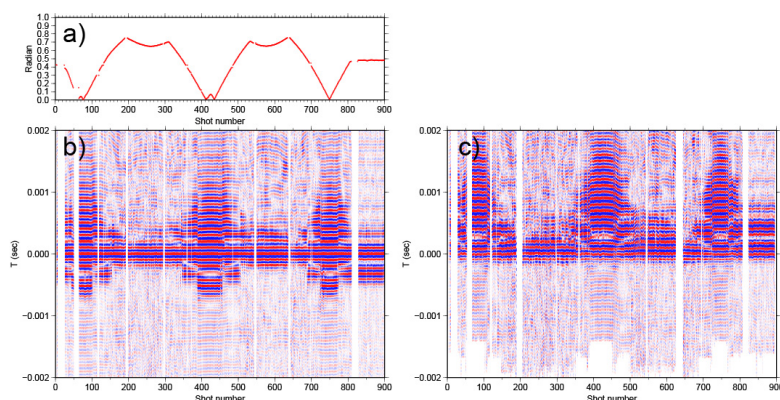


Fig. Incident angle of transmitted signals (a). Pasted correlation waveforms analyzed by reading maximum peak (b) and reading iteratively-deconvolved peak (c). Each trace was moved out by the observed traveltine.

## A NaI spectrometer for long-term radon measurement at the sea floor

NINAGAWA, Kiyotaka<sup>1\*</sup> ; TOYODA, Shin<sup>1</sup> ; FUJIWARA, Taisei<sup>1</sup> ; NAKAGAWA, Masuo<sup>1</sup> ; YAMAMOTO, Isao<sup>1</sup> ; KUMAGAI, Hidenori<sup>2</sup> ; KINOSHITA, Masataka<sup>2</sup> ; KUBO, Shin<sup>3</sup>

<sup>1</sup>Okayama University of Science, <sup>2</sup>Japan Agency for Marine-Earth Science and Technology, <sup>3</sup>CLEAR-PULSE

In the Japanese Islands, the Tokai, Tonankai and Nankai earthquakes are expected within a few decades. It is a very important scientific issue to understand the physicochemical process occurring in the earthquake occurrence belt and the mechanism of earthquakes near the oceanic trench for damage mitigation of human lives and social basis. Increases of the radon concentration in atmosphere and in groundwater before earthquake are reported in the Southern Hyogo Prefecture Earthquake in 1995. In this research, gamma rays from radon daughter radionuclides at the sea floor will be continuously measured on the Kumanonada offing, where is the epicentral area of the expected Tonankai earthquake. The correlation between micro earthquakes and radon concentrations is also investigated to contribute the fundamental research on the response of the fluid in the crust corresponding to change of the crust.

Investigation on the gamma ray at the sea floor has been made only in a certain limited duration up to several hours while the submersible stays at the site for measurement. This time, a time variation of the gamma ray for several months is planned in order to investigate correlation between earthquakes and radon concentration. A battery drive type NaI spectrometer, which will be set on sea floor and can automatically record gamma ray, was designed. In this January it is almost constructed. A preliminary measurement is scheduled in February. After improvements of software and hardware, it will be set on spring water area of the Kumanonada offing from April to September, and will measure for more than about 4.6 months.

Specification of the NaI spectrometer for long-term radon measurement at the sea floor is as follows;

Name: Low consumed power type gamma-ray spectrometer for deep sea

PMT High-voltage : programmable (+1000V max)

Amplifier: Charge sensitive Memory Capacity: 1Gbit (NOR Flash)

Connection: RS-232C 921,600 bps Current: 110mA (on), 10mA (off)

Operation:

1. After initial setting with PC, measurement starts automatically, and records gamma-ray spectra.
2. It has the intermittent mode for electric power saving.
3. Battery Power Supply 30 AA alkaline batteries, 6 series, 9V
4. When the battery power supply voltage falls to 6V or spectral data is over memory capacity, measurement is suspended automatically and the battery power supply is disconnected.
5. It can connect with PC after measurement, and transfer the recorded spectra to PC.

Keywords: Radon, sea floor, long-term measurement, NaI

## Time stamp experiment of MEMS-gyro for the observation of seafloor crustal deformation using multi-buoy system

MUKAIYAMA, Haruka<sup>1\*</sup> ; IKUTA, Ryoya<sup>1</sup> ; TADOKORO, Keiichi<sup>2</sup> ; NAGAI, Satoru<sup>2</sup> ; WATANABE, Tsuyoshi<sup>2</sup>

<sup>1</sup>Graduate school of science , Shizuoka University, <sup>2</sup>Earthquake research center, Graduate school of environmental study, Nagoya University

We are developing a new method for the observation of seafloor crustal deformation using multi-buoy system. The system measures seafloor crustal deformation by determining position of benchmarks on the seafloor using multi-buoy which link-up GPS and acoustic signals. Acoustic ranging is used to measure distance between the buoys and seafloor benchmarks. And kinematic GPS is used to locate the multi-buoy every 0.2 seconds. Now we have deployed 4 seafloor benchmark units at Suruga Bay and 4 units at Kumano Basin. At each survey site, three seafloor transponders are settled to define a benchmark unit. In November 2012, first observation of seafloor crustal deformation using the buoys was held in Suruga Bay. Analyzing observed data, errors of traveltime 's residual were about 0.2ms(Mukaiyama et al 2012JPGU). These errors were too large. From approximate calculation, it is predicted that these errors of 0.16ms at maximum can be removed by introduction of a gyro compass. So, we introduced MEMS-gyro to multi-buoy observation to monitor the attitude of the buoys at Suruga Bay at November 2013. The MEMS-gyro was NAV440CA by Crossbow Co.. For the attitude monitoring of the observation of seafloor crustal deformation, time stamp is important. Although the gyro introduces time stamp provided by its GPS processor, its accuracy was not evaluated. In this study, we conducted rotation experiments to evaluate the accuracy of its time stamp. In the experiment, we used another GPS antenna system as a time reference. The GPS antenna and the gyro were deployed on a rotation table to synchronize their motions and the time stamp of the rotated gyro was checked with reference to the GPS time. Timing between their motions was evaluated by cross correlation between GPS circular trajectory and the rotation angle of the gyro. Specifically, we rotated the table for 3 min every 1 hour. This subset was repeated 3 times. As a result, delay times in first two sets were about -38ms. But third set was -58ms. The delay became lager. Offset of the average angle between GPS and gyro was also deferent from first two sets to third set. This deference might be caused by that of rotation speed between three subsets. We tried additional experiment with different parameter settings of MEMS-gyro under controlled rotation speed. We will also report the result of this additional experiment.

Keywords: Seafloor crustal deformation, buoy, GPS, MEMS-gyro, Time stamp, Rotation experiment

## Three year observations of ocean infragravity waves by broadband seismometers and pressure gauges of Japanese seafloor network

TONO, Yoko<sup>1\*</sup> ; NISHIDA, Kiwamu<sup>2</sup> ; FUKAO, Yoshio<sup>1</sup> ; TO, Akiko<sup>1</sup> ; TAKAHASHI, Narumi<sup>1</sup>

<sup>1</sup>JAMSTEC, <sup>2</sup>ERI

Ocean infragravity (IG) waves are sea-surface gravity waves with periods of several minutes and wavelengths up to tens of kilometers. We used a slant-stack technique to detect IG waves from the three-year period records (2011-2013) of the vertical component broadband seismograms and pressure gauges of the seafloor network deployed in the Nankai Trough region (DONET). IG signals show good match in waveform between the seafloor displacement and pressure with propagation speeds consistent with the seafloor depths of 2000 m. The signal intensities are strongly azimuth-dependent. Except for the days with extreme weather, waves incoming from the SE direction (from the deep ocean to the coast across the Nankai Trough) are by far dominant. The incoming direction sharply splits into two, SSE and ESE. Waves from the deeper ocean in the SSE direction are more dominated in longer-period components than those from the shallower ocean in the ESE direction. Amplitudes of these waves clearly show a seasonal variation, high in winter and low in summer. The effect of typhoon is to generate IG waves incoming from the source direction and those incoming from the NE-ESE direction through the corridor between the coast and the Nankai trough. The latter is often stronger than the former.

Keywords: Infragravity wave, Nankai Trough, DONET

## Evaluation of resolution and estimation error of vessel-based seafloor displacement observation using AUV bathymetry

FUJIWARA, Toshiya<sup>1\*</sup> ; MASAKI, Yuka<sup>1</sup> ; YAMAMOTO, Fujio<sup>1</sup>

<sup>1</sup>JAMSTEC

Bathymetry is basic information for any kind of seafloor observation, and therefore vessel-based multi-narrow beam bathymetric surveys are conducted quite often. In recent years, previous bathymetric data exist in most scientifically-important areas. A repeated bathymetric survey reveals seafloor displacement related to geodynamics [e.g. Fujiwara et al., Science 2011]. However, the spatial resolution and estimation error of the seafloor displacement observation from the vessel-based bathymetric survey are not exactly known. Because the observation compares a pair of limited-resolution bathymetric data. Water depth (distance from the vessel's echo sounder to the seafloor) degrades the spatial resolution and precision of depth measurement from the vessel-based survey. While on the other hand, a near-seafloor Autonomous Underwater Vehicle (AUV)-based survey enables us to obtain high-resolution bathymetric data. In this paper, we evaluated the spatial resolution and estimation error of the seafloor displacement observation from vessel-based bathymetric survey. In this evaluation, bathymetric data from vessel-based and AUV-based surveys in the Iheya-North knoll of the Okinawa Trough were used.

AUV Urashima bathymetric survey was conducted in YK07-07 cruise aboard the R/V Yokosuka in May 2007 [Yamamoto et al., 21st Mtg, Japan Society for Marine Surveys and Technology 2009]. The applied multi-narrow beam echo sounder was a SEABAT 7125. R/V Yokosuka bathymetric survey was performed using a SeaBeam 2112 echo sounder in YK06-09 cruise from 18 to 24 July 2006 [Masaki et al., JAMSTEC R&D 2011]. The vessel passed over the survey area six times with each constant speeds and obtained bathymetric data. One survey track was treated as one's independent survey in this evaluation. The beam angle (angle formed by the vertical line and a narrow sounding beam) was within 40° in the survey area.

AUV bathymetry shows hills (the shallowest depth ~870 m) in the western side and basins (the deepest ~1070 m) in the eastern side. The average/median depth is 1010 m. Hydrothermal chimney mounds ~30 m in diameter and ~10-20 m in height were found on the hillside in the high-resolution bathymetry. Vessel-based bathymetry is spatially-smoothed as a function of the footprint (area of the narrow sounding beam projected onto the seafloor) size. The footprint size of the Yokosuka survey at a depth of 1000 m is ~35×35 m-43×55 m (~5% of water depth). In the vessel bathymetry, geographical features smaller than the footprint size, such as the hydrothermal chimney mounds, cannot be recognized. And seafloor morphology is slightly different from each other track surveys due to distribution of sounding points and measuring error. Standard deviations of depth differences between the AUV- and the vessel-based data were 2.67-3.08 m. The AUV bathymetry are assumed to be the "true" bathymetry, and therefore the precision of the vessel-based depth measurement (standard deviation of measuring error) is considered to be ~0.2-0.3 % of water depth.

Simulated vessel-based bathymetric data "before and after" the seafloor displacement were made using AUV-based bathymetric data. The displacement was verified by comparing these simulated data using the analysis conditions that neither depth accuracy variation within the area nor locational errors of beam sounding points are allowed. We used the method of Fujiwara et al. [2011] to estimate horizontal displacement. As a result, we found that estimation error of the seafloor horizontal displacement depends on the precision of the depth measurement and is ~0.2-0.3 % of water depth. As for the seafloor vertical displacement, the smallest displacement that can be detected occurs when the horizontal extent of the deformation is larger than several times the size of the footprint, and in the situation that the amplitude of the depth difference is greater than the precision of depth measurement.

Keywords: Multi-narrow beam bathymetry, seafloor displacement, Iheya-North knoll, AUV Urashima, R/V Yokosuka

## Bathymetric survey and discovery of hydrothermal plume in the Daiichi-Amami Knoll using autonomous underwater vehicle

MINAMI, Hiroki<sup>1\*</sup> ; OHARA, Yasuhiko<sup>2</sup>

<sup>1</sup>Hydrographic Surveys Division, Hydrographic and Oceanographic Department, Japan Coast Guard, <sup>2</sup>Ocean Research Office, Hydrographic and Oceanographic Department, Japan Coast Guard

Many submarine volcanoes exist along the volcanic front in the Ryuku Arc. The Daiichi-Amami Knoll, which is located about 70 km off Amami Oshima Island, is one of those submarine volcanoes. Detailed bathymetric survey of this knoll has not been done before, therefore its shape and size have not been known. Japan Coast Guard conducted a high resolution bathymetric mapping of the knoll using survey vessel and autonomous underwater vehicle (AUV) and discovered hydrothermal plumes which are rising from the seafloor, indicating that the presence of hydrothermal activities in the Daiichi-Amami Knoll.

### 1. Method

The survey was conducted in August and September, 2013 using survey vessel Takuyo and AUV Gondo. The knoll was surveyed with multibeam echo sounder (MBES) installed on S/V Takuyo. Then the detailed survey was done with MBES on AUV Gondo.

### 2. Bathymetry

The bathymetry of the Daiichi-Amami Knoll indicates that the knoll is a volcanic high. The knoll has flat areas, a caldera with a diameter of 1.6 km and some volcanic cones at its summit. The knoll also has two small depressions near to the volcanic cones and they are deeper about 40 m than the surrounding areas. The relative high of the knoll is about 500 to 700 m and the shallowest depth of the knoll is 245 m.

### 3. Hydrothermal plume

Water column data acquired by MBES on S/V Takuyo detected the clear hydrothermal plumes in the two depressions. The plumes were especially clear at the rim of the depression. Some plumes were observed to rise from the seafloor of 350 m depth to near sea surface (although no discolored water was visually observed on the sea surface). Plumes were also detected at the slope areas of the volcanic cones. AUV Gondo dived to the depressions at the altitude 40-50 m above seafloor and conducted a detailed survey. The high resolution bathymetric map shows a presence of a numerous small depressions near the plume points. The side scan image by AUV Gondo also shows the plumes acoustically at its nadir.

### 4. Water temperature

AUV Gondo observed the water temperature at the altitude 40-50 m in the depressions, but distinguished temperature increases were not observed. Temperature profile observation, which was conducted using expendable bathythermograph launched from S/V Takuyo, showed over 2 degrees temperature increase near the seafloor in the depression. This observation along with the presence of plumes indicate the presence of hydrothermal activity in the Daiichi-Amami Knoll.

### 5. Importance of this survey result

The detailed bathymetry and the presence of plumes in the Daiichi-Amami Knoll were revealed by the survey using survey vessel and AUV. The discovery of plumes suggests the presence of hydrothermal deposits and chemosynthetic community, therefore being important in terms of seafloor resources. The high resolution bathymetric map acquired by AUV is fundamental information which is useful for scientific research and mineral exploration. This result is a first step for further survey to understand the geological history of the knoll and to secure new seafloor resources.

Keywords: Daiichi-Amami Knoll, submarine volcano, plume, AUV, bathymetry

## Topography, geology, tectonics and ore deposit of the Bayonnaise knoll caldera, Izu-Ogasawara arc

HONSHO, Chie<sup>1\*</sup> ; URA, Tamaki<sup>1</sup> ; ASADA, Akira<sup>3</sup> ; KIM, Kangsoo<sup>3</sup> ; NAGAHASHI, Kenji<sup>3</sup>

<sup>1</sup>Atmosphere and Ocean Research Institute, The University of Tokyo, <sup>2</sup>Center for Socio-Robotic Synthesis, Kyushu Institute of Technology, <sup>3</sup>Underwater Technology Research Center, Institute of Industrial Science, The University of Tokyo

Several hydrothermal sites have been discovered in the volcanic front of the Izu-Ogasawara arc: Myojin knoll caldera, Myojinsho caldera, Smith caldera, Suiyo seamount, and Kaikata seamount. The Hakurei hydrothermal site in the Bayonnaise knoll caldera is the only hydrothermal site discovered in the rift zone of the arc. We analyzed deep-sea multibeam and side scan sonar data obtained using autonomous underwater vehicle Urashima in the caldera and discussed the topography, geology, tectonics, and ore deposit of the caldera.

The survey area ~3 km x ~2 km wide covers the southern half circle of the caldera. Major geomorphic elements are, from the outside to the inside, the knoll slope, the steep caldera wall, the flat caldera floor, the central cone with three peaks, and the central depression surrounded by the peaks. The high-resolution bathymetric map shows that large slope failures occurred in the southeastern caldera wall and that the Hakurei deposit is distributed over the failure area. Slope failure is also going on in the southwestern wall and a large collapse may shortly occur. The eastern hill, the main part of the central cone, seems to be a lava dome: it has a small flat surface on the top, convex slopes in the upper part, and rectilinear to concave slopes near the base. The northeastern slope of the dome is relatively flat from top to bottom, indicating that a slope failure occurred there. A series of depressions lying in a NW-SE direction in the western caldera floor would be a crater row, seeing that the terrain gently slopes down from the rim of the depressions. The direction of the crater row suggests that the caldera is under the extension stress in a NE-SW direction.

Morphological and textural characteristics of the Hakurei site were determined by three kinds of analyses. The gray-level co-occurrence matrix was used to describe the texture of the side scan sonar image and to classify the seafloor using cluster analysis. The Hakurei area was distinctly classified to a group that was characterized by high entropy and low homogeneity, and a broad area from the top to the northeast slope of the eastern lava dome was also classified to the group. Some areas belonging to the group were distributed around the top of the southern central cone, in the eastern caldera wall northeast of the Hakurei site, in the southwestern caldera wall, and around the crater row. A band-pass filtered topography was used to determine areas where short-wavelength topographic features like chimneys and mounds observed in the Hakurei site dominate. The band-pass filtering was also performed on the multibeam backscattering intensity data to detect similar patterns to numerous spots of strong backscattering from chimneys observed in the Hakurei area. These results commonly show that areas of similar characteristics to the Hakurei site are distributed in a zone crossing the caldera in a NW-SE direction, from the Hakurei site to the crater row through the central cone.

The Izu-Ogasawara rift zone is separated to many segments ranging in a N-S direction. The Bayonnaise knoll caldera is located on the northeastern margin of an oval depression called the North Myojin rift, which has a longer N-S axis of ~20 km. It appears that the direction of the crater row, the distributions of hydrothermal or volcanic features, and the distribution of slope failures are along the rim of the North Myojin rift going through the caldera. The North Myojin rift is surrounded by seven knolls including the Bayonnaise knoll. Although hydrothermal activity has been discovered only in the Bayonnaise knoll so far, the geological settings that volcanoes of acidic rocks lying along a circular fault of a depression host ore deposits closely resembles that of the Hokuroku Kuroko region in northern Akita. It is suggested that the Hakurei site is the present field of the Kuroko ore formation.

Keywords: hydrothermal deposit, Izu-Ogasawara rift, multibeam sonar, side scan sonar, GLCM, Kuroko deposit

## Electrical resistivity structure of the Snail site at the Southern Mariana Trough spreading center

MATSUNO, Tetsuo<sup>1\*</sup> ; KIMURA, Maho<sup>2</sup> ; SEAMA, Nobukazu<sup>2</sup>

<sup>1</sup>National Institute of Polar Research, <sup>2</sup>Kobe University

The electrical resistivity of the oceanic crust is sensitive to the porosity of the crust and the fluid temperature within crustal fractures and pores. The spatial variation of the crustal porosity and the fluid temperature that is related to a hydrothermal circulation can be deduced by revealing an electrical resistivity structure of the oceanic crust involving a hydrothermal site. We carried out a magnetometric resistivity experiment using an active source to reveal an electrical resistivity structure of the oceanic crust at the Snail site on the ridge crest of the Southern Mariana Trough. Active source electric currents were transmitted along and across the ridge axis in a 4000 m<sup>2</sup> area including the Snail site. Five ocean bottom magnetometers were deployed around the Snail site as receivers to measure the magnetic field induced by the transmission of the active source electric currents. The amplitude of the induced magnetic field was calculated by maximizing data density and the signal to error ratio in the data, and locations of the transmissions were determined using several types of calibration data. An optimal 1-D resistivity structure of the oceanic crust, averaged over the experimental area, was deduced by least squares from the data of the amplitude of the magnetic field and the location of the transmission. After calculating magnetic field anomalies, which are deviations of the observed amplitude from the prediction of the optimal 1-D resistivity model, an optimal 3-D resistivity structure was deduced from the magnetic field anomalies through trial and error 3-D forward modeling. The optimal 1-D resistivity structure is a two-layer model, which consists of a 5.6 Ω-m upper layer having a 1500 m thickness and a 0.1 Ω-m underlying half-space. Using Archie's law and porosity profiles of the oceanic crust, the resistivity of 5.6 Ω-m at depths ranging from 800 to 1500 m suggests the presence of high-temperature fluid related to the hydrothermal circulation. The resistivity of 0.1 Ω-m below 1500 m depth may represent a magma mush that is a heat source for the hydrothermal circulation. The optimal 3-D resistivity structure includes a conductive anomaly (0.56 Ω-m in approximately 300 m<sup>2</sup> area down to 400 m depth) just below the Snail site, two resistive anomalies (56 Ω-m with slightly larger volumes than the conductive anomaly) adjacent to the conductive anomaly on the across-ridge side, and three conductive anomalies away from the Snail site. The conductive anomaly just below the Snail site suggests hydrothermal fluid, and the adjacent resistive anomalies suggest areas of low porosity. The size and distribution of the conductive and resistive anomalies near the Snail site constrains the size and style of the hydrothermal circulation.

Keywords: electrical resistivity structure, temperature and porosity, oceanic crust, hydrothermal circulation, magnetometric resistivity method

## Crustal Imaging of initial structure in Izu-Ogasawara forearc region obtained by seismic reflection survey

YAMASHITA, Mikiya<sup>1\*</sup> ; NO, Tetsuo<sup>1</sup> ; SATO, Takeshi<sup>1</sup> ; KODAIRA, Shuichi<sup>1</sup> ; TAKAHASHI, Narumi<sup>1</sup> ; MIURA, Seiichi<sup>1</sup> ; ISHIZUKA, Osamu<sup>1</sup>

<sup>1</sup>JAMSTEC

The Izu-Bonin (Ogasawara)-Mariana (IBM) arc is known to be the typical oceanic island arc, and it is the most suitable area to understand the growth process of island arc. The existence of two paleo arcs which consist of Oligocene and Eocene paleo arcs is known in the IBM forearc region by geological and geophysical studies. The Ogasawara ridge is also known to locate the initial structure of arc evolution from geologic sampling of research submersible. In this region, IODP drilling site: IBM-2 is proposed in order to understand the temporal and spatial change in arc crust composition from 50 to 40 Ma magmatism. Site IBM-2 consists of two offset drilling holes (BON-1, BON-2). BON-1 is designed to first encounter forearc basalt and will reach the sheeted dykes. BON-2 will start in boninites and finish in fore arc basalts. The purpose of these drillings is sampling the full volcanic stratigraphy from gabbro to boninite. This drilling project is already scheduled in 2014. The survey lines along the proposed sites, however, there are no crossing seismic data around BON-1 and BON-2. Therefore, it is needed to conduct the MCS survey until 2013 for the evaluation of proposed site.

Japan Agency for Marine-Earth Science and Technology (JAMSTEC) newly carried out multi-channel seismic reflection (MCS) survey using 7,800 cu.in. air gun, 5 km streamer with 444 ch hydrophones in April, 2013. We obtained two seismic reflection profiles of lines IBr11n and IBr11 across from Shikoku Basin and current volcanic front to the paleo arc. The preliminary results show the distribution of volcanic sediments and basement. We also identified the block type structure associated with the uplift in northern side of Kinyo seamount. We will discuss about the characteristics between backarc and forearc from north to south.

Keywords: MCS survey, IBM forearc, initial arc structure

## Across-arc geochemical variation of Quaternary Basalts dredged from central part of Izu-arc

YOSHIDA, Takanori<sup>1\*</sup> ; OKAMURA, Satoshi<sup>1</sup> ; SAKAMOTO, Izumi<sup>2</sup> ; ADACHI, Yoshiko<sup>3</sup> ; IKEDA, Yasuo<sup>4</sup> ; SHINJO, Ryuichi<sup>5</sup> ; SUGAWARA, Makoto<sup>6</sup>

<sup>1</sup>Hokkaido University of Education Sapporo, <sup>2</sup>Tokai University, <sup>3</sup>Niigata University, <sup>4</sup>Hokkaido University of Education Kushiro, <sup>5</sup>Ryukyu University, <sup>6</sup>Mitsubishi Materials Techno Corporation

The Izu-Bonin arc located western margin of the Philippine sea plate extend to ca. 1200 km south from central Honshu of Japan with ca. 400 km width. The Izu-Bonin arc is a match for NE Honshu arc (Nishimura and Yuasa, 1991). Although volcano lying on the volcanic front (VF) of northern part of this arc expose above the sea level (e.g. Izu Oshima, Miyakejima), almost this arc sink down to sea surface. Active rifts (AR) exist just behind VF with 20-30 km width. These are parallel to the VF and Izu-Bonin Trench and enclosed with escarpment. Ishizuka et al. (2003b) reported Ar-Ar age of igneous rocks dredged from central part of Izu-Bonin arc. According to these age data, recent volcanism (<1Ma) occurred only VF and AR. In this study, we report geochemical data of basalt dredged from Myojin volcano, Myojin rift and Aogashima rift. Basalts exhibit evident across-arc variations. Ba/La ratio, Sr, Nd and Hf isotopic ratios decrease correspondingly distance from Izu-Bonin trench toward rear-arc. Whereas (La/Sm)<sub>N</sub> increase correspondingly distance from Izu-Bonin trench. Based on ratios of trace elements and each isotopic feature, we conclude that VF basalts generated from flux melting of mantle due to adding aqueous fluid to wedge mantle from subducting slab. On the other hand, genesis of AR basalt is to supply supercritical melt (e.g. Kessel et al. 2005) of slab to wedge mantle. Chromian spinel composition, Cr# of inferred chromian spine equilibrated with mantle is 0.75, held in olivine of VF basalt suggest that residual mantle equilibrated with VF primary magma is dunite. Degree of partial melt of AR basalt decrease correspondingly distance from Izu-Bonin trench toward rear-arc. Tollstrup et al. (2010) interpreted magma genesis of basalt after cessation of Shikoku back-arc basin. They proposed that basalts of western seamount chain (WS) and back-arc knolls (BAK) derived from partial melting of mantle due to adding supercritical melt to mantle wedge from subducting slab, whereas aqueous fluid contributed to partial melting of mantle beneath AR and VF. In their discussion, activity age and activity region are not considered. According to their conclusions, supercritical melt related to genesis of basalts from WS and BAK is not contribute to partial melting of mantle wedge recent volcanism (<1Ma). Bryant et al. (2003) revealed that VF basalt volcanism has continued since 15Ma. Moreover, Ishizuka et al. (2003b) reported volcanism has traveled eastward with time in the central Izu-Bonin arc. It means Izu-Bonin arc volcanism has become narrow range with time. Distinct slab flux between VF and AR in this study suggest that occurrence of supercritical melt is traveling with time toward VF side due to change subducting angle of slab into more steep angle since 15Ma to 3Ma (Honda et al., 2007). Therefore supercritical melt related to genesis of basalt from WS and BAK at predate volcanism contribute to AR recent volcanism.

Keywords: basalt, Izu-Bonin arc, geochemical across-arc variation, Myojin seamount, Aogashima rift, Myojin rift

## The variety of silicic rocks around the Myojin volcano, central Izu-Bonin arc

YOSHIDA, Takanori<sup>1\*</sup>; OKAMURA, Satoshi<sup>1</sup>; SAKAMOTO, Izumi<sup>2</sup>; ADACHI, Yoshiko<sup>3</sup>; IKEDA, Yasuo<sup>4</sup>; SHINJO, Ryuichi<sup>5</sup>; SUGAWARA, Makoto<sup>6</sup>

<sup>1</sup>Hokkaido University of Education Sapporo, <sup>2</sup>Toukai University, <sup>3</sup>Niigata University, <sup>4</sup>Hokkaido University of Education Kushiro, <sup>5</sup>Ryukyu University, <sup>6</sup>Mitsubishi Materials Techno Corporation

The Izu-Bonin arc located western margin of the Philippine sea plate (PSP) extend to ca. 1200 km south from central Honshu of Japan with ca. 400 km width. The Izu-Bonin arc is a match for NE Honshu arc (Nishimura and Yuasa, 1991). Active rifts (AR) exist just behind volcanic front (VF) with 20-30 km width. These are parallel to the VF and Izu-Bonin Trench and enclosed with escarpment. Generally primitive basalts possibly erupted at oceanic arc volcano without any process in the oceanic crust due to be thinner than continental crust. Although it is well known that Izu-Oshima and Miyakejima, located on VF, erupted basalts, Kouzushima, Niijima and Myojin reef are represented volcanoes which provide mostly felsic products exist on the Izu-Bonin arc VF (Tamura et al., 2009). Nowadays extensive seismic experiments in the Izu-Bonin arc have documented the occurrence of middle crust with P-wave velocity of 6.0-7.0km/s (e.g. Suyehiro et al., 1996). Because of the rock, with P-wave velocity of 6.0-7.0km/s, correspond to tonalite exposed Tanzawa complex Izu collision zone and tonalitic xenoliths in the volcanic rocks sampled VF, inferred middle crust of Izu-Bonin arc composed of tonalitic igneous rocks (Suyehiro et al., 1996). In this study, our aim is to understand mechanism of felsic volcanism contribute to making continental crust. Therefore we consider about felsic rocks dredged from Myojin volcano, Myojin rift and Aogashima rift.

Felsic rocks in this study are divided into three suites (type 1, type 2, type 3) on the basis of Zr/Y versus Zr diagram. Type 1 is lowest Zr/Y ratio trend, type 3 exhibit highest Zr/Y ratio and type 2 have intermediate Zr/Y ratio. Type 1 occur mainly VF, and small amount of type 1 appear AR. Type 2 collected overall from VF to AR. Type 3 occurs only AR.

Although Sr and Nd isotopic compositions of type 1 is similar to the basalt from the VF, Hf isotopic compositions of type 1 differ from VF basalt, and Hf isotopic compositions of type 1 is same as mafic xenoliths in VF lava rather than VF basalt. Isotopic features of type 2 are distinguished from lavas erupted normal-arc magmatism after cessation of Shikoku basin. And isotopic features of type 2 dredged from more AR-side have higher Nd, Hf isotope ratios. Although Sr and Nd isotopic compositions of type 3 is similar to the basalt from the AR, Hf isotopic compositions of type 3 differ from AR basalt, and isotopic compositions of type 3 is different from lavas erupted normal-arc magmatism after cessation of Shikoku basin and tephra data from ODP boring (Straub et al., 2010).

On the basis of Na<sub>2</sub>O vs ASI diagram, three type felsic rocks in this study agree with compositions of experimental liquids which derived from basaltic source materials (e.g. Sission et al., 2005). There is possibility that felsic rocks derived from associated basalt. But because of Hf isotope ratio, all felsic rocks are not derived from associated basalt. Therefore all felsic rocks, provided by recent volcanism, are rejuvenated products of old arc crust.

Because of isotopic compositions of type 1 are similar to mafic xenoliths in VF lava, type 1 derived from remelting of arc crust which have postdate VF basalt composition (Bryant et al., 2003). Although There is possibility that type 2 derived from remelting of Oligocene mafic arc crust, type 2 dredged from more AR-side have higher Nd, Hf isotope ratios. It suggests that AR-side type 2 is possibly affected by PSP. Geochemical data which is similar to type 3 have been found out in previous ODP boring data, and it is possible exist crustal material which is peculiar to AR. We long for IODP projects which start at this year to accumulate new AR crustal material data to consider source of type 3. We propose heterogeneous crust model. It have made by underplating or intrusion of mafic magma derived from mantle into PSP for 50Ma.

Keywords: acidic rock, Izu-Bonin arc, Myojin volcano, Myojin rift, Aogashima rift

## General remarks of velocity structures of the Ogasawara Plateau, revealed by the Continental Shelf Survey of Japan

KANEDA, Kentaro<sup>1</sup> ; NISHIZAWA, Azusa<sup>1\*</sup> ; OIKAWA, Mitsuhiro<sup>1</sup> ; MORISHITA, Taisei<sup>1</sup>

<sup>1</sup>JHOD

Japan Coast Guard conducted seismic refraction surveys with OBSs and multi-channel seismic surveys over more than 10 survey lines on the Ogasawara Plateau which is located on the Pacific Plate, close to a plate boundary to the Philippine Sea Plate. Analysis of these seismic data in 2006-2007 revealed that 1)the Ogasawara Plateau collide and partly accreted with the Philippine Sea Plate, 2)crustal thickness of the Ogasawara Plateau is approximately 25 km, close to that of the Izu-Ogasawara Arc, and 3)low velocity structure in lower crust extends below flat seafloor to the south-east to the plateau.

Recently, re-analyzing of the data by utilizing various later phases and MCS profiles revealed more detailed velocity structure of 1')plate boundary between the Pacific Plate and the Philippine Sea Plate, 2')under plating below the Ogasawara Plateau and 3')low velocity structure distributing around the plateau.

Keywords: velocity structure, Ogasawara Plateau, seismic experiment

## Acoustic characterization of abyssal plain, northwestern Pacific region

OKINO, Kyoko<sup>1\*</sup> ; HONSHO, Chie<sup>1</sup> ; MACHIDA, Shiki<sup>2</sup> ; OIKAWA, Mitsuhiro<sup>3</sup> ; NAKAMURA, Kentaro<sup>4</sup>

<sup>1</sup>AORI, The University of Tokyo, <sup>2</sup>School of Creative Science and Engineering, Waseda University, <sup>3</sup>Hydrographic and Oceanographic Department, Japan Coast Guard, <sup>4</sup>School of Engineering, The University of Tokyo

The old seafloor covered by pelagic sediment has not attracted large scientific attention and remained untouched for many years, however, the recent studies on intra-plate volcanism as well as the increasing interest in deep-sea natural resources focus spotlight on the abyssal plains. We analyzed the multi-beam bathymetry, beam intensity, and side-scan images of abyssal plain in the northwestern Pacific, around the Minami-Torishima (Marcus) Island. The data were collected by Japan Coast Guard as part of Japanese EEZ survey and by R/V Yokosuka for decades. The beam intensity data from multi-beam echo sounder were processed to create a backscatter mosaic without geometric distortion. The mosaic shows a large variation of acoustic characteristics in whole study area. The high backscattering areas at the foot of large seamounts likely reflect the distribution of volcanoclastic sediments and debris. We can also recognize another type of high backscattering areas in flat seafloor, where neither remarkable seamounts nor knolls exist. The latter type partly corresponds to the area where the high concentration of rare-earth elements were reported and may suggest a thin cover of uppermost soft sediment layer. We try to integrate the backscattering mosaics and the statistic analysis of bathymetry and to establish a new method of acoustic characterization of abyssal plain. We also plan to compare our results with piston core samples as ground references and to discuss the sedimentation process and the relationship with intra-plate volcanism on old seafloor.

Keywords: marine acoustics, muti-beam echo sounder, backscattering intensity, abyssal plain

## Spreading stability at the mid-ocean ridges derived from 3D magnetic survey

MATSUMOTO, Takeshi<sup>1\*</sup> ; SATOH, Yukitaka<sup>1</sup> ; NOGI, Yoshifumi<sup>2</sup>

<sup>1</sup>University of the Ryukyus, <sup>2</sup>National Institute of Polar Research

The Shipboard Three Component Magnetometer (STCM) has provided vector data of the geomagnetic field provided detailed information more than total magnetic force measurement. Previous study shows the results about relationship with ocean floor topography and standard deviation of magnetic boundary strike (MBS) calculated from Intensity of the Differential Vectors (ISDV) in Southeast Indian Ridge (SEIR) classified intermediate spreading rate. In this study, the standard deviation of MBS and half spreading rate were analyzed from STCM data in East Pacific Rise (EPR) of fast spreading ridge, Explorer Ridge (ER) and Southeast Indian Ridge (SEIR) classified intermediate spreading ridge and Mid Atlantic Ridge (MAR) categorized as slow spreading ridge. In EPR existing axial high, the results shows that standard deviation and half spreading rate are stable in west of EPR whereas standard deviation and half spreading rate are variability in east of EPR. However standard deviation is low and spreading rate is stable on both sides in MAR developed axial valley. Thus there is no relationship with topographic features and spreading of stability. Additionally, standard deviation of MBS is the low although half spreading rate has variability in ER. The results show differential MBS at the same position in SEIR. As a result, dispersion of MBS is caused by inaccurate measurements of magnetic anomaly. In addition, there is no clear relationship though the simulation was run about plate reconstruction. Therefore spreading stability is controlled by the balance among plate reconstruction, slab pull and magma provided from mantle.

Keywords: mid-ocean ridge, spreading rate, 3D magnetometry

## Detailed bathymetry and magnetic anomaly in Central Ryukyu: Implications on westward shift of volcanic front after 2.1Ma

SATO, Taichi<sup>1\*</sup> ; ODA, Hirokuni<sup>1</sup> ; ISHIZUKA, Osamu<sup>1</sup> ; ARAI, Kohsaku<sup>1</sup>

<sup>1</sup>Institute of Geology and Geoinformation, Geological Survey of Japan, AIST

Detailed bathymetry and magnetic anomaly were obtained by GH12 cruise in 2012 using R/V Hakurei, in the southern part of Central Ryukyu. Volcanic structures such as caldera were observed on the southwestward extension of the present-day volcanic front, implying recent volcanic front of the Ryukyu arc. Furthermore, bathymetric highs which are sub-parallel to the recent volcanic front were observed and is located ~20 km east. These are accompanied by spotted magnetic anomalies, which continue to Kume-jima via Aguni-jima Islands to the south, suggesting an existence of an ancient volcanic front. The ages of volcanic rocks from these Islands suggest that the magmatic activity along the ancient volcanic front had been active at least until ~2.1 Ma. The magmatic anomalies connecting two volcanic fronts suggest that a volcanic front have moved gradually westward. This shift would be explained by the termination of asthenospheric upwelling and/or rapid retreat of Ryukyu Trench.

Keywords: Ryukyu arc, Volcanic front, Okinawa Trough, magnetic anomaly, seafloor bathymetry

## Evolution of depositional basin accompanied by recurring caldera collapses in Kikai caldera, southern-off Kyushu, Japan

IKEGAMI, Fumihiko<sup>1\*</sup> ; MINOWA, Yuto<sup>1</sup> ; KURATOMI, Takashi<sup>1</sup> ; KIYOKAWA, Shoichi<sup>2</sup> ; OIWANE, Hisashi<sup>3</sup> ; NAKAMURA, Yasuyuki<sup>4</sup> ; KAMEO, Katsura<sup>5</sup>

<sup>1</sup>Department of Earth and Planetary Sciences, Kyushu University, <sup>2</sup>Faculty of Sciences, Kyushu University, <sup>3</sup>Mishima-mura, <sup>4</sup>JAMSTEC, <sup>5</sup>Atmosphere and Ocean Research Institute, Tokyo University

Kikai caldera (Matsumoto, 1943) is a mostly submerged highly active caldera volcano located in 40 km off Kyushu Island. The caldera is recognized as the product of 7300 cal. BP super-colossal eruption with Akahoya tephra (Machida and Arai, 1978; Fukuzawa, 1995) which is widely distributed along the western part of Japan. Previous studies for near-vent onshore geology strongly suggests such a large eruption was not occurred only once, but multiple times in the Kikai caldera (Ono et al., 1982).

In Kikai caldera, 24 lines of multi-channeled seismic reflection surveys were held in two survey cruises (KT-10-18 and KT-11-11) in 2010 and 2011 using R/V Tansai-maru of JAMSTEC (Japan Agency for Marine-Earth Science and Technology). The acquired seismic data for subseafloor structures spotted thick sedimentary basin at the eastern margin of the caldera. The basin covers 70 square km of the 20 km-wide caldera and is next to caldera rim fault. The infill of the basin is characterized by the group of onlapping stratified deposits named B which maximum thickness is more than 600 m. The B-sequence has two major depositional discontinuities in the middle and the top. The lower one is paraconformity and the upper one is disconformity though, the both of them are associated with similar deformation of the basin itself. The deformation is characterized by 1. Dragged-up reflectors along the caldera rim fault, and 2. Slight outward rotation of the deposits. Both characteristics intensify along the depth, which means lower deposits were experienced much more deformation.

The both two types of the deformation suggest the basin was experienced at least two major subsidence event. The former dragged-up structure is interpreted as the incomplete slip of the caldera rim fault for the relief of the subsidence, while the latter rotation shows the slippages were slightly listric. The displacements of the subsidence events could be estimated from the top and bottom of the dragged-up structures, as more than 100 m in the lower-older event and more than 50 m in the upper-newer event. The subsidence would be an abrupt event, as the paraconformity was formed in the lower-older event. The most likely candidate for such a significant subsidence is caldera collapse. As therefore, the basin might be the one of the pre-caldera structure, and it has been experienced multiple caldera collapse events in the past.

Keywords: caldera, seismic reflection survey, Kikai caldera, Akahoya

## Estimates on fluid migration and material recycling via offshore mud volcanoes

KIOKA, Arata<sup>1\*</sup> ; ASHI, Juichiro<sup>1</sup>

<sup>1</sup>Atmos. Ocean Res. Inst., U. Tokyo

About 300-400 offshore mud volcanoes are currently confirmed and the double is inferred. Mud volcanism can be viewed as a tectonic window to understand geological frameworks at much greater depth, since mud volcanoes bring up deep substances and fluids to seafloor and are consequently good tools to explore their migration mechanism. Herein we present a global catalog of offshore mud volcanoes and estimate their contributions to subsurface fluid migration and material recycling.

Keywords: Submarine mud volcanoes, fluid migration, material recycling, overpressure

## New Marine Sediment Core Database "COEDO"

NAKANO, Yukihiko<sup>1\*</sup>; ICHIYAMA, Yuji<sup>1</sup>; HORIKAWA, Hiroki<sup>1</sup>; TOMIYAMA, Takayuki<sup>1</sup>; SATO, Yusuke<sup>2</sup>; KANESHI, Toko<sup>2</sup>; OGIDO, Eriko<sup>2</sup>; TAKAESU, Yuki<sup>2</sup>; NAGAYAMA, Anri<sup>2</sup>; OSHIRO, Satoshi<sup>2</sup>

<sup>1</sup>Japan Agency for Marine-Earth Science and Technology, <sup>2</sup>Marine Works Japan Ltd.

Japan Agency for Marine-Earth Science and Technology (JAMSTEC) established basic policies on the handling of data and samples ([http://www.jamstec.go.jp/e/database/data\\_policy.html](http://www.jamstec.go.jp/e/database/data_policy.html)). On the basis of the policies, JAMSTEC provides data and samples in an easily accessible manner. Data and sample information of geological sediment core has been published at "JAMSTEC Core Data Site" since 2008. In order to improve quality and usability, we reconstructed and released new database in January 2014.

Details of the new database are shown below:

<Name>

**COre Electronic Database of Ocean floor (COEDO)**

<URL>

<http://www.godac.jamstec.go.jp/coedo/e/>

<Search Method>

Multiple-filter search using interactive map and basic information filters (Cruise ID, date, location etc.)

In the previous version of the database, users have to take longer steps to reach sample information, because only one of two methods (map search for general users and Cruise ID list menu for science parties) were available. In COEDO, all users can search samples by multiple filters in a single step on a single window.

<On-line accessible data>

Basic information of sediment core (Cruise ID, date of collect, chief scientist, ship name, position, depth), core photo, scanned image, visual core description, X-ray photo, X-ray scanned image, physical property data, literature, link for geochemical data.

We are planning further updates to improve the usability, as follows:

1. Acquiring information of sedimentary ages of core, and making them easily accessible on the database as numerically searchable information.
2. Integration with sample inventory information of JAMSTEC core sample collection, which is currently available at the Kochi Institute for Core Sample Research.
3. Publishing other data, which have not been incorporated into the database yet.

We aim not only improving services to current users, but also making effort to propagate the user community. JpGU and Yokohama city government have a special geological training course for junior/senior high school students at Keio University High School in Yokohama city on April 13. JAMSTEC cooperates with the training course, and provides lecture and practices using actual database and real core samples. In the training course, trainers give lectures on how to obtain marine sediment core onboard and how to study core sample data in COEDO, then trainees observe the actual core samples for which they have just pick up the associated data on the database. The course stimulates trainees' interest and curiosity on the geological study, and we can nurture the new generation. As a result of this cooperation, we can hopefully increase educational users of JAMSTEC core samples.

Keywords: JAMSTEC, marine sediment core, database, ocean floor, piston corer, geology

## Geological Annotation for the Deep-Sea Images

IREI, Kazuhiro<sup>1\*</sup> ; OGIDO, Moritaka<sup>1</sup> ; KAYO, Makino<sup>1</sup> ; NAKAMURA, Makoto<sup>1</sup> ; TANAKA, Katsuhiko<sup>2</sup> ; KITAYAMA, Tomoaki<sup>2</sup> ; SAITO, Hideaki<sup>2</sup> ; HANAFUSA, Yasunori<sup>2</sup>

<sup>1</sup>Marine Works Japan LTD., <sup>2</sup>JAMSTEC

The Global Oceanographic Data Center (GODAC) of the Japan Agency for Marine-Earth Science and Technology (JAMSTEC) has been collecting, archiving and disseminating videos and photos acquired by deep-sea research programs using submersibles and remotely operated vehicles owned by JAMSTEC. We register those videos and photos to our database with annotations (keywords), which are names of geological features or organisms, and enable users to search for images of their interest. Those videos and photos with annotations are distributed from the data site called, " JAMSTEC E-library of Deep-sea Images (J-EDI)\*1 " on the Internet.

Researchers of deep-sea can use the videos and photos distributed by J-EDI as materials for their research or lecture, and also for planning of research cruises or dives, etc. Through the database for marine biodiversity, " Biological Information System for Marine Life (BISMaL)\*2 " , biological annotations are used to visualize the distribution of organisms or to accumulate the observation record of them, since those videos and photos of deep-sea organisms are not only valuable data, but also indicate the proof of existence of organisms at those points.

We put annotations which can be recognized from the images itself by clicking icons from the prefixed palette or selecting classification name from hierarchical tree. The videos and photos with annotations concerning to the ocean floor geoscience are 41,000 with 95 different kinds of terms out of approximately total 120,000 videos.

To promote the use of deep-sea videos and photos especially in the solid earth science we tried to register more detailed annotations by using scientific papers, reports or documents about research dives and we found that registration of precise annotations takes considerable time. In order to progress the annotating work efficiently we think it necessary to select contents of annotations that lead to an efficient expansion of its use.

In this presentation, we introduce the current status of annotating work for the geological features of the deep-sea and we also show our approach to expand its use.

\*1 <http://www.godac.jamstec.go.jp/jedi/>

\*2 <http://www.godac.jamstec.go.jp/bismal/>

Keywords: deep-sea video and photo, geological environments, annotation

## Vp/Vs ratio in the southernmost Japan Basin and its transition area, Japan Sea deduced from the seismic survey

SATO, Takeshi<sup>1\*</sup> ; NO, Tetsuo<sup>1</sup> ; KODAIRA, Shuichi<sup>1</sup> ; TAKAHASHI, Narumi<sup>1</sup> ; KANEDA, Yoshiyuki<sup>1</sup>

<sup>1</sup>JAMSTEC

The Japan Sea is one of very well studied back-arc basins in the northwestern Pacific. To clarify the formation process of the back-arc basin in the Japan Sea, many seismic surveys using ocean bottom seismographs (OBSs) and control sources have been conducted in the sea. The Japan Basin, which located in the northern to eastern Japan Sea, has an oceanic crust formed by seafloor spreading (Hirata et al., 1992; No et al., submitted). On the other hand, the ocean-continent transition area between the Japan Basin and the continental shelf in the eastern margin of this sea may have a thick oceanic crust (No et al., submitted). However, it is unknown the origin and the nature of this thick oceanic crust, due to the lack of the information about lithology in the transition area. To understand the origin and the nature of this thick oceanic crust, it is necessary to obtain the information lithology in the crust of the transition and the basin areas. For this study, we will present the Vp/Vs ratio of the crust from the southernmost Japan Basin to its transition area.

From the southernmost Japan Basin to the continental shelf off the west of Aomori and the northern Oga Peninsula, seismic surveys using OBSs and an air-gun array were undertaken. In vertical record sections of several OBSs, not only the first arrived phases but also later phases reflected from interfaces in the crust and uppermost mantle are visible. Moreover, in horizontal record sections of several OBSs, converted phases from P- to S-waves are apparent. In this study, we have obtained the S-wave velocity structure using travel times of these converted phases. Then, we have obtained the Vp/Vs ratio in the crust from the southernmost Japan Basin to its transition area using the obtained P- and S-wave velocity structures.

In the southernmost Japan Basin off west of Aomori, the Vp/Vs ratio in the sedimentary layer of shows 4 to 8 and has a lateral variation. The Vp/Vs ratios in the crustal upper and lower parts show around 1.85 and 1.8, respectively. On the other hand, in the transition area, the Vp/Vs ratio in the crustal upper part is similar to that in the southernmost Japan basin. This Vp/Vs ratio may show that the nature of the whole crust in the basin area and of the crustal upper part in the marginal area has an oceanic origin. Therefore, the crusts in southernmost Japan Basin and in its transition area are suggested as an oceanic crust and a thick oceanic crust, respectively. The oceanic crust formed by the opening of the Japan Sea may extend to the transition area of the southernmost Japan Basin.

## Crustal structure study of the Sea of Japan: Recent results and future perspectives

NO, Tetsuo<sup>1\*</sup> ; SATO, Takeshi<sup>1</sup> ; KODAIRA, Shuichi<sup>1</sup> ; ISHIYAMA, Tatsuya<sup>2</sup> ; SATO, Hiroshi<sup>2</sup> ; TAKAHASHI, Narumi<sup>1</sup> ; OIKAWA, Nobutaka<sup>1</sup> ; KANEDA, Yoshiyuki<sup>1</sup>

<sup>1</sup>JAMSTEC, <sup>2</sup>ERI, Univ. of Tokyo

In recent years, crustal structure study of the Sea of Japan has advanced. Various new seismic data have been obtained in the Sea of Japan; for example, the two ship seismic surveys study (Sato et al. 2007) and onshore-offshore seismic survey (Earthquake Research Institute, 2013) conducted by the University of Tokyo, and 2D/3D seismic reflection survey conducted by R/V SHIGEN (JOGMEC, 2013).

From 2007 to 2012, we conducted marine seismic surveys using the multichannel seismic reflection system and ocean bottom seismometers; the surveys covered the area between the Japanese coast of the Sea of Japan and the Yamato and Japan Basins. Based on the results, the crustal structure of the eastern margin of the Sea of Japan was classified into three types: island arc crust, thick oceanic crust, and oceanic crust (Sato et al. 2014; No et al. submitted). In addition, our studies found that the contractive deformation zones of the eastern margin of the Sea of Japan are associated with the crustal structure distribution. Further, seismic data suggests that the crustal structure in the south (off Yamagata to Niigata) differs from that of the north (off Akita to Nishi-tsugaru). These differences are critical in understanding the relation between the spatial distributions of the seismogenic and contractive deformation zones (JAMSTEC, 2013). These results can contribute to the review of long-term evaluations of earthquake occurrence potentials and the discussion of the seismogenic study in the eastern margin of the Sea of Japan.

In 2013, new projects have been observing and studying earthquakes and tsunamis in the Sea of Japan. *Integrated Research Project on Seis* scheduled in 2014 in order to conduct a seismic survey in the blind areas of the existing observations, which are in the southwest region of the Sea of Japan and off western Hokkaido. The addition of new observation data will advance the study of crustal structure in the Sea of Japan. In this study, we aim to improve the accuracy of the position and size of the source faults in the Sea of Japan. In addition, we investigate the relation among tectonic history, crustal structure, and factors that form source faults in the Sea of Japan. In the future, we aim to clarify the seismogenic zone of the Sea of Japan using new seismic data.

Keywords: the Sea of Japan, crustal structure, MCS, OBS

## Results of 2013 Off-Joetsu and Hokuriku survey for the integrated research project on seismic and tsunami hazards around

SATO, Hiroshi<sup>1\*</sup> ; ISHIYAMA, Tatsuya<sup>1</sup> ; SHIRAIISHI, Kazuya<sup>2</sup> ; ABE, Susumu<sup>2</sup> ; KATO, Naoko<sup>1</sup> ; KURASHIMO, Eiji<sup>1</sup> ; TAKEDA, Tetsuya<sup>3</sup>

<sup>1</sup>Earthquake Research Institute, Univ. Tokyo, <sup>2</sup>JGI. Inc., <sup>3</sup>NIED

An obvious convergent plate boundary cannot be recognized in the Sea of Japan, and convergence accommodates in defused wide area of the back arc. To estimate Tsunami and seismic hazards along the coastal area of Sea of Japan, more detailed survey to identify source faults are needed. A new research project funded by MEXT named "the integrated research project on seismic and tsunami hazards around the Sea of Japan" began in FY 2013. To obtain the information of source faults, we performed deep seismic reflection profiling off-Joetsu and Hokuriku area in the central part of Honshu, Japan. We used two vessels; a gun-ship with 3020 cu. inch air-gun and a cable-ship with a 2-km-long, streamer cable with 156 channels and 480 cu. inch air-gun. Common-mid point reflection data were acquired along 9 seismic lines with total 715 km in length. The seismic profiles portray the structure of failed rift basins, such as Toyama trough and Sado strait, bounded by rift axis reverse faults with rift axis vergence, which represents reactivation of boundary faults between mafic intrusion and pre-rift basement. Noto Peninsula is marked by syn-rift normal faults and their reactivation by shortening deformation. The back arc side of the SW-Japan arc experienced NS trending shortening deformation in the latest Miocene. From the Noto peninsula, undeformed Pliocene sediments covers folded Miocene. Some normal faults reactivated as active strike-slip and reverse faults. The survey results contributed to construct source faults models of Tsunami and seismic hazards estimation.

Keywords: Sea of Japan, source fault, crustal structure, seismic reflection profiling, Off-Joetsu, off-Hokuriku

## Lithospheric Structure of the Hidaka Collision Zone, Hokkaido, from Reanalysis of 1998-2000 Hokkaido Transect Data IV

IWASAKI, Takaya<sup>1\*</sup>; TSUMURA, Noriko<sup>2</sup>; ITO, Taniao<sup>3</sup>; SATO, Hiroshi<sup>1</sup>; KURASHIMO, Eiji<sup>1</sup>; HIRATA, Naoshi<sup>1</sup>; ARITA, Kazunori<sup>4</sup>; NODA, Katsuya<sup>5</sup>; FUJIWARA, Akira<sup>5</sup>; ABE, Susumu<sup>5</sup>; KIKUCHI, Shinsuke<sup>6</sup>; SUZUKI, Kazuko<sup>7</sup>

<sup>1</sup>Earthquake Research Institute, the University of Tokyo, <sup>2</sup>Chiba University, <sup>3</sup>Teikyo Heisei University, <sup>4</sup>Hokkaido University, <sup>5</sup>JGI. Inc., <sup>6</sup>JAPEX, <sup>7</sup>Schlumberger Ltd.

The Hidaka region in the central part of Hokkaido Island, Japan, is known as an arc-arc collision zone ongoing from the middle Miocene. In 2012, we started reinterpretation for a series of seismic reflection/refraction surveys from 1994 to 2000 in this collision zone. In this analysis, we used integrated and sophisticated processing and analysis techniques, including CRS/MDRS method for seismic reflection data and refraction tomography both very dense arrival time data from both the reflection and refraction/wide-angle reflection data. The most important finding so far obtained is a clear image of the NE Japan Arc subducting eastward under the northern part of the collision zone. However, the following problems are remained unsolved.

(1) Shallow structure beneath the Hidaka Collision zone is still unsolved. Particularly, the structure just east of the Hidaka Main Thrust is not sufficiently evaluated from our seismic data.

(2) Delamination of the Hidaka crust as in the southern part of this collision zone is not unclear. Our CRS/MDRS processing for the reflection data provided no positive evidence for the delamination.

(3) Deeper collision structure of the NE Japan Arc and the Kuril Arc is still not constrained. It is necessary to elucidate the subducting structure of the NE Japan Arc from amplitude data as well as travel time data.

In this paper, we focus the items (1) and (3) from seismic refraction/wide-angle reflection approach. Previous refraction tomography elucidated a thick (4-5 km) undulated sediments in the hinterland, the outcrop of crystalline crust beneath the Hidaka Metamorphic Belt with higher  $V_p$  and  $V_p/V_s$  and an enormously thick (>8-10 km) sedimentary package beneath the foreland. In order to obtain the more reliable structure model, we intensively revised the travel time data obtained both from seismic reflection/wide-angle reflection line and reflection lines. The seismic tomography using these revised data sets indicate a clearer high velocity (>6.1 km/s) anomaly just east of the HMT. We also recognized some wide-angle reflections around 5-10 km depth beneath the HMT, from which we expect to determine the finer structure at the collision front. Our present analysis indicates the wide-angle reflection data sample a part of the lower crust of the subducting NE Japan Arc beneath the fold-and-thrust belt. According to the preliminary result, its velocity is ranging from 6.5-7.0 km/s. By combining the amplitude analysis, we expect to estimate the more reliable Moho depth of the NE Japan Arc than in the previous analyses.

Keywords: active source seismic experiment, collision, arc, crustal structure, lithosphere

## Seismic crustal structure beneath the southeastern part of northeast Japan by dense seismic array observation

KURASHIMO, Eiji<sup>1\*</sup> ; SATO, Hiroshi<sup>1</sup> ; ISHIYAMA, Tatsuya<sup>1</sup> ; HIGASHINAKA, Motonori<sup>2</sup> ; ABE, Susumu<sup>2</sup> ; IWASAKI, Takaya<sup>1</sup>

<sup>1</sup>ERI, Univ. Tokyo, <sup>2</sup>JGI, Inc.

The 2011 Tohoku-Oki Earthquake (Mw9.0), that occurred on the Japan Trench off the eastern shore of northern Honshu, Japan, generated enormous crustal deformations. Seismic activity in northeastern Japan increased significantly after the 2011 Tohoku-Oki Earthquake. Detailed crustal structure and deep geometry of the active fault is important to constrain the process of earthquake occurrence. Active and passive seismic experiments were conducted to obtain a structural image beneath the southeastern part of NE Japan (Sato et al., 2013). The geometry of the active faults have been revealed by seismic reflection profiling (Sato et al., 2013). Natural earthquake data set is useful to obtain a deep structural image. Forty portable seismographs were deployed along a 70-km-long line between Souma and Takahata during the period from August 16, 2012 to December 24, 2012. Each seismograph consisted of a 1-Hz 3-component seismometer and off-line data recorder (Shinohara et al., 1997). Waveforms were continuously recorded at a sampling rate of 200 Hz. In the area of the present study, deep seismic reflection profiling was conducted using vibrators (Sato et al., 2013). The off-line recorders observed the controlled seismic signals as well as natural earthquakes. During the seismic array observation, the JMA located 2956 earthquakes in a latitude range of 37.2-38.5 N and a longitude range of 139.6-141.3 E. We selected 200 earthquakes, all of which occurred near the survey line. In order to obtain a high-resolution velocity model, a well-controlled hypocenter is essential. Due to this, we combined the seismic array data with permanent seismic station data. The arrival times for the first P- and S waves obtained from local earthquakes and Vibrator shots were used in a joint inversion for earthquake locations and three-dimensional Vp and Vp/Vs structures, using the iterative damped least-squares algorithm, simul2000 (Thurber and Eberhart-Phillips, 1999). Permanent seismic stations observed the controlled seismic signals as well as natural earthquakes. We added the arrival time data of these controlled sources into the dataset to improve the shallow velocity structure. The depth section of Vp structure along the survey line shows that lateral variation of the Vp value at a shallow depth. This lateral variation correlates with the surface geology along the profile.

Keywords: dense seismic array observation, seismic tomography, the 2011 Tohoku-Oki Earthquake

## Shallow geologic structure around the northern part of the Futaba Fault, northeast Japan, based on gravity survey

KOSHIYA, Shin<sup>1\*</sup> ; TERUI, Kyoko<sup>2</sup> ; YONEZAWA, Kenta<sup>1</sup> ; SATO, Hiroshi<sup>3</sup> ; KATO, Naoko<sup>3</sup> ; ABE, Susumu<sup>4</sup> ; HIGASHINAKA, Motonori<sup>4</sup>

<sup>1</sup>Faculty of Engineering, Iwate Univ., <sup>2</sup>Graduate School of Engineering, Iwate Univ., <sup>3</sup>ERI, Univ. of Tokyo, <sup>4</sup>JGI, Inc.

The Futaba Fault, bounding the eastern margin of the Abukuma Mountains, is known as a left lateral fault in the Cretaceous and Paleogene period with a remarkable fracture zone of a few hundreds meter width. It trends NNW-SSE and divides into two branches between which the Wareyama horst develops. During early to middle Miocene, E-W extensional stress field caused large normal displacement along the western fault to form a half graben filled with sediments including breccia. In late Miocene, it had been a right lateral fault. In present, the eastern fault is active, along which left lateral offsets with western upheaval ingredient are geo-morphologically observed. Thus the Futaba Fault has experienced the complicated history of development. In this study, we modeled two dimensional shallow geological structure across the faults mainly based on gravity survey. The gravity survey was conducted across the faults with a G-type gravity meter (G827; LaCoste and Romberg Inc.) along two E-W survey lines, one of which is ca. 12 km long, (line 1), and the other of which is ca. 13km long (line 2). Each interval of observation sites is about 200 m. The elevation of observation sites was surveyed with a electric level and a RTK-GPS. Acquired gravity data was processed to obtain Bouguer anomaly mostly according to the methodology of Geological Survey of Japan, AIST (2004). We assumed that the density for Bouguer and terrain corrections were 2.2 g/cm<sup>3</sup>. In each survey line, Bouguer anomalies after trend correction show the highest value around the Wareyama horst consisting of pre-Paleogene basement rocks and a few maxima in the western side of the horst. We assume four layers in our model, which have densities of 2.00 g/cm<sup>3</sup> (layer 1), 2.2 g/cm<sup>3</sup> (layer 2), 2.55 g/cm<sup>3</sup> (layer 3), and 2.67 g/cm<sup>3</sup> (layer 4), respectively. The interpretation of the model is as follows. Layer 1 is correlated to the surface covers and Pliocene sedimentary rocks, layer 2 lower to middle Miocene sedimentary rocks, layer 3 Miocene breccia and layer 4 basement rocks. We will discuss the shallow structure across the faults in detail.

Keywords: Futaba fault, gravity anomaly, active fault

## Structural characters of active faults, crustal architecture, and permanent deformation of the Hokuriku region

ISHIYAMA, Tatsuya<sup>1\*</sup> ; SATO, Hiroshi<sup>1</sup> ; KATO, Naoko<sup>1</sup> ; TAKEDA, Tetsuya<sup>2</sup> ; KURASHIMO, Eiji<sup>1</sup>

<sup>1</sup>Eathquake Research Institute, University of Tokyo, <sup>2</sup>NIED

We discuss in this study about characters of crustal architectures around the Toyama trough revealed by new seismic reflection and refraction profiles and seismic tomography, and active structures based on Neogene geology and tectonic geomorphology. As revealed by onshore offshore deep seismic reflection profiling across the Toyama trough funded by MEXT named as The Integrated Research Project on Seismic and Tsunami Hazards around the Sea of Japan since 2013, crustal architectures across the Toyama trough is characterized by three domains: (1) crustal thrust wedge comprising the northwestern flanks of the Hida Mountains, (2) Neogene sedimentary basin near the axis of the Toyama trough, and (3) reactivated normal faults as thrust (or obliquely slipping) faults beneath the Noto peninsula, comprising structural higher domain west of the Toyama trough. These structural patterns and permanent, late Quaternary crustal deformation recorded by tectonic geomorphology are quite similar to adjacent Neogene sedimentary basins in the backarc failed rifts in the Sea of Japan, including northern Fossa Magna, Niigata, and Akita.

## Phase changes and temperature of the subducted crust of Philippine Sea slab beneath Kanto, Japan

ISHIKAWA, Masahiro<sup>1\*</sup> ; NAKAGAWA, Shigeki<sup>2</sup> ; SAKAI, Shin'ichi<sup>2</sup> ; HIRATA, Naoshi<sup>2</sup> ; SATO, Hiroshi<sup>2</sup> ; KASAHARA, Keiji<sup>3</sup>

<sup>1</sup>Graduate School of Environment Information Sciences, Yokohama National University, <sup>2</sup>Earthquake Research Institute, The University of Tokyo, <sup>3</sup>Association for the Development of Earthquake Prediction

The Philippine Sea plate subducts beneath the Greater Tokyo Area of Japan. Devastating M8-class earthquakes occurred on the upper surface of the Philippine Sea plate, examples of which are the Genroku earthquake of 1703 (magnitude M8.0) and the Kanto earthquake of 1923 (M7.9). A M7 or greater (M7) earthquake in this region may occur either on the upper surface or intra slab of Philippine Sea plate. To evaluate seismic hazard in the Greater Tokyo Area of Japan we need to clarify the lithological properties of Philippine Sea slab. This study presents an interpretation of the crustal and mantle structure of the Philippine Sea slab beneath Kanto based on recent MeSO-net seismic tomography data. The seismic tomography reveals that P wave velocity of the subducted crust of the Philippine Sea slab increases stepwise at 30 km and 40 km depths beneath the Kanto area. The cause of these two stepwise increases in P wave velocity of subducted crust is expected to correspond to metamorphic phase changes. Mineralogical assemblages of forearc basalt composition of the Izu arc was calculated by Theriak-Domino software, and the phase diagram shows that phase changes to garnet amphibolite and eclogite can account for these two stepwise increase in P wave velocity of the subducted crust of the Philippine Sea slab.

Keywords: slab, phase change, slab temperature, Kanto, Philippine Sea Plate, crust

## Geologic structure in and around the Beppu Bay estimated by gravity analysis

YAMAKITA, Satoshi<sup>1\*</sup> ; KUDO, Takeshi<sup>2</sup> ; ITO, Tanio<sup>3</sup>

<sup>1</sup>University of Miyazaki, <sup>2</sup>Chubu University, <sup>3</sup>Teikyo-Heisei University

Seismic profiling in the Beppu Bay and the Bungo Strait performed by Kyoto University and JGI inc. from 1988 to 1990 (Yusa et al., 1992) raised new progresses of studies on the geologic structure of the Median Tectonic Line (MTL) in Kyushu and the development of the Beppu Bay Sedimentary Basin (BSB) accompanying it (Yamakita et al., 1995; Ito et al., 1996). The P-wave velocity assumed by Yusa et al. (1992) for the rocks in Ryoke Belt, however, was too low for granitic and metamorphic rocks constituting this Belt, and it is likely that the dip of the MTL beneath it was underestimated. Besides, the structure of the basin in the innermost part of the Beppu Bay has remained uncertain because this part is located in the terminal part of the seismic lines. On the other hand, there are plenty of gravity data in and around the Beppu Bay (Yusa et al., 1992; GSJ, 2000; Gravity Research Group in Southwest Japan, 2001). It can be expected that these gravity data clarify the structure of BSB, combined with correct seismic profiles. Fortunately, a profile reprocessed with re-estimated P-wave velocity along the Bungo straight (J-line) was presented last year (Abe et al., 2013). Using this reprocessed profile and gravity data, we tried to determine the subsurface structure along the G-line of Yusa et al. (1992), trending N70E, 35 km long, from on-land area, across the Asamigawa fault (AF) and the Beppu Bay Central Fault (BCF), to the mouth of the Beppu Bay (Fig. A), occupied by Sanbagawa metamorphic rocks (Sm,  $\rho=3.0\text{g/cm}^3$ ), Ryoke granitic and metamorphic rocks (Rk,  $\rho=2.8\text{g/cm}^3$ ), lower (Bl,  $\rho=2.6\text{g/cm}^3$ ) and upper (Bu,  $\rho=2.4\text{g/cm}^3$ ) sediments of BSB. Assuming only the depth and form of the MTL estimated from the reprocessed profile of J-line and geologic constraints, and the position of the AF on the surface, we determine other subsurface structures to fit with the gravity data through trial and error (Fig. B). In this profile, the upper surface of the Ryoke basement almost coincides with that in the Yusa et al. (1992)'s profile. This fact suggests high reliability of this profile. We concluded the structure of BSB from this and Yusa et al.(1992)'s profiles as follows.

1. The innermost part of the BSB was formed by two listric normal fault systems, NE-dipping Asamigawa Fault System (AFS) and SW-dipping Beppu Bay Central Fault System (BCFS). Both systems formed roll-over structure in the sediments of BSB.
2. The AFS consists of three faults (I, II, III), which converge to the MTL. It is uncertain whether the fault AFS-II reaches the uppermost part of the sediments. The total amount of the vertical displacement of ASF may be up to 3000m, although it depends on the thickness of sediment in the SW-side on AF and the amount of erosion of Ryoke basement
3. Two faults BCFS-I and BCFS-II vertically displaced the bottom of the Bu in 250m and 150m respectively and reach the uppermost part of it, although it is difficult to recognize in this figure because of its highly reduced scale. Both, however, did not displace the bottom of the Bl (= the upper surface of the Ryoke basement).
4. BSB is inferred to be formed and developed by eastward movements of the hanging wall (Ryoke basement), strike-slip on the MTL and downward on the AF. The BCFS was secondarily formed in eastward moving sediments.

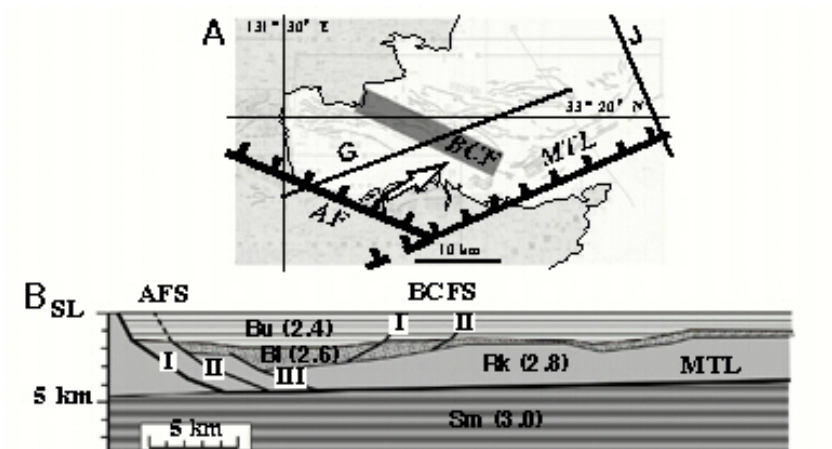
These results are almost concordant with the model of a strike-slip basin proposed by Yamakita and Ito (1999), which assume a not vertical but moderately dipping strike-slip fault with a releasing bend. This model ignored the effects of secondary listric normal faults in sediments, dipping toward the main oblique normal fault forming the oblique ramp, but they contributed to the development of BSB to some extent. Their effects, however, are rather small as indicated by the fact that they did not displace the basement.

Keywords: Gravity analysis, Beppu Bay, MTL, Asamigawa Fault, Beppu Bay Central Fault

SCG68-09

Room:502

Time:April 30 11:15-11:30



## Structure and evolution of the lower crust constrained from alkaline basalts and xenoliths in southwest Japan

IGATA, Eri<sup>1\*</sup> ; OMORI, Soichi<sup>2</sup> ; IWAMORI, Hikaru<sup>3</sup>

<sup>1</sup>Department of Earth and Planetary Sciences, Tokyo institute of technology, <sup>2</sup>The open university of Japan, <sup>3</sup>Japan Agency for Marine-Earth and Technology

The continental crust is unique to the Earth and, in spite of its small mass, is geochemically an important reservoir, concentrating about half of the radiogenic heat producing elements. In order to understand the differentiation history of the Earth, it is essential to decipher how and when the continental crust has been formed.

In contrast to the upper continental crust, which has been well surveyed with direct means, the lower continental crust is largely unknown in terms of composition, mineralogy and age distribution of formation. In this study, we investigate the xenoliths that have been derived possibly from the lower crust, in terms of petrology (mineral assemblages and their composition, modal abundances and bulk composition) and geochronology (zircon U-Pb age dating of both the xenoliths and the host basalt). Study area is located on the Kibi Plateau in southwest Japan. The xenoliths are classified into 4 types by petrography and EPMA analysis; Type 1, pyroxenite; Type 2, eclogitic gabbro; Type 3, anorthosite; Type 4, kyanite/garnet-bearing felsic granulite. Pseudosection and mineral stability analyses were performed by a thermodynamic program "Perplex". These analyses have revealed that pyroxenite is stable beneath the Moho and its seismic velocity estimated from pseudosection ranges from 7.23 to 7.65 km/s. Therefore pyroxenite corresponds to the olivine-pyroxenite layer under the Moho. Gabbro was formed at 8-10 kbar and 873-940 K and its velocity is higher than pyroxenite. Granulite is stable at 7.5- kbar and about 1000 K and its velocity is very low. In spite of the density gap between the eclogitic gabbro and granulite (3900 and 2740 kg/m<sup>3</sup>), the analysis suggests that the felsic granulite exhibits a higher equilibration pressure and may even underlay the eclogitic gabbro. Moreover, composition of the lower crust becomes more felsic than previously thought.

Ages of the eclogitic gabbro xenolith and the host basalt coincide, showing 70 Ma. It is argued that the subducted sediments (now appear as felsic granulites) were subducted and underplated to the bottom of the lower crust during the last 30 million years or so. If such a mechanism operates worldwide, then the continental crust may have an intermediate to felsic composition even without a hypothetical process of lower crustal delimitation.

The authors thank T. Hirata, K. Tani, JI. Kimura and Q. Chang for U-Pb zircon age dating.

## Three-dimensional seismic velocity structure beneath East Asia using adjoint tomography

MIYOSHI, Takayuki<sup>1\*</sup> ; OBAYASHI, Masayuki<sup>1</sup> ; TONO, Yoko<sup>1</sup> ; TSUBOI, Seiji<sup>1</sup>

<sup>1</sup>JAMSTEC

East Asia is the complicated region where tectonic plates meet. In many studies, travel-time tomography based on ray theory has clarified three-dimensional (3D) velocity structure of the Earth. On the other hand, the recent studies show waveform inversion based on wave theory can construct realistic 3D structure (e.g. Obayashi et al., 2010 SSJ; Miyoshi et al., 2013 SSJ). In the present study, we have inferred 3D heterogeneous structure precisely beneath the eastern Asia region by using adjoint tomography method. We selected 161 earthquakes ( $M > 5.5$ , half duration  $< 5$  second) occurred in the region based on Global CMT catalog. Displacement seismograms used in this study were recorded at broadband seismic stations in the region. The average number of stations used in inversion is about 180. Theoretical waveforms were calculated using the spectral-element method (Komatitsch and Tromp, 2001). We used GAP-P2 mantle tomography model (Obayashi et al., 2009) as an initial 3D model of inversion. Both observed and theoretical waveforms were filtered between 12.5 and 100 second to extract time windows of P- and S-waves, and between 30 and 150 second to extract time windows of surface waves. We applied adjoint method (Liu and Tromp, 2006) for calculating the misfit kernel, which is related to velocities, and performed inversion by using the steepest descent method. The parallel computing of theoretical waveforms and misfit kernels were used 256 CPU cores of supercomputers, such as K computer at Riken. The computing time was required 0.1 million CPU hours in each iteration. We have iterated four times on inversion. The VR value was improved about 10% by using the revised model. The  $V_p$  and  $V_s$  of improved model showed a few percent slower than the initial model. The ratios of the velocity perturbation show slightly large value than the initial model at a depth of 100 km in a wide area of the eastern Asia region. Acknowledgements: We used F-net seismograms of the National Research Institute for Earth Science and Disaster Prevention. This study was supported by the strategic Programs for Innovative Research "Field 3" Advanced prediction Researches for Natural Disaster Prevention and Reduction.

Keywords: adjoint method, tomography, velocity structure, East Asia

## Seismological evidence for a transition from "hydrous" oceanic crust to typical oceanic crust in the Lau back-arc basin

ARAI, Ryuta<sup>1\*</sup> ; DUNN, Robert<sup>1</sup>

<sup>1</sup>University of Hawaii

The Lau back-arc basin, associated with subduction of the Pacific plate beneath the Indo-Australian plate at the Tonga Trench, provides a superb study area to understand the interaction between plate subduction and back-arc spreading: Subducting oceanic lithosphere induces mantle corner flow within the mantle wedge above the subducting plate and releases a large amount of water and other elements into this wedge, producing heterogeneous chemical compositions and fluid gradients beneath the back-arc basin. While petrological studies suggest that the heterogeneity in the mantle source composition, mainly caused by slab-derived fluids, plays an important role for melt supply to the back-arc ridges, variations in thickness and internal structure of crust formed along back-arc ridges are poorly documented. On the basis of seismic tomography analyses, we present a structural model of crust formed along the Eastern Lau Spreading Center within the Lau back-arc basin as evidence for a transition from a "hydrous" type of oceanic crust to a more typical oceanic crust. The seismic data indicate that as the back-arc spreading center moved away from the active arc, the crust thinned from 8-9 km to ~7 km, the lower crust changed from high P wave velocity values (7.2-7.4 km/s) to typical values for oceanic crust (7.0-7.2 km/s), and the upper-crustal volcanic layer changed from a thick low-velocity layer to a thinner layer with more typical wave speeds. The seismic results, in combination with other geophysical and geochemical data, suggest that crustal formation along the ELSC is strongly controlled by the influence of slab water: When a spreading center is near the active arc, water from the downgoing slab is entrained in the melting zone beneath the back-arc ridges where it enhances melting. Thereafter, the water enhances crustal differentiation within sub-ridge magma chambers. This creates an anomalous "hydrous" form of oceanic crust with a thick felsic volcanic layer and a mafic/ultramafic lower crust - features that are not typically observed in crust formed at mid-ocean ridges. The Lau basin has a zoned structure with an abrupt transition from this type of oceanic crust to more typical oceanic crust, which resulted from a rapid change in the influence of slab water as the ridge moved away from the arc. The unique geodynamic setting of the Lau basin, such as proximity of the back-arc ridges to the volcanic arc (<100 km), the relatively low subduction angle of the slab (~45 degrees), and the fast subduction rate at the Tonga trench (>20 cm/yr), probably operate to effectively deliver slab-derived water far beyond the volcanic arc to the back-arc ridges and produce this "hydrous" oceanic crust in the back-arc basin. The abundance and high rate of production of the "hydrous" crust suggests that such crust may make up a significant proportion of the arc-like crust that forms continents.

Keywords: Back-arc basin, Crustal differentiation, Oceanic crust, Slab water, Seismic tomography, Eastern Lau Spreading Center

## Tectonic province of the northern Fossa Magna region based on the crustal movement and seismic activity

IMAI, Yuki<sup>1\*</sup> ; TAKEUCHI, Akira<sup>2</sup>

<sup>1</sup>Graduate school of Science and Engineering for Education, University of Toyama, <sup>2</sup>Graduate school of Science and Engineering for Research, University of Toyama

The northern Fossa Magna region is located in an area where the Niigata-Kobe tectonic zone (Sagiya *et al.*, 2000) and geological strain concentration zone along the eastern margin of the Japan Sea (Okamura, 2002) is duplicated. In the past, inland crustal earthquakes, such as the Zenkoji earthquake in 1847 (M7.4) and the Niigata-ken Chuetsu earthquake in 2004 (M6.8), have occurred in this region. In order to discuss the current tectonics of the northern Fossa Magna region that has active crustal movement and seismic activity, it is necessary to clarify the characteristics of "tectonic province". The purpose of this paper is to reveal a detailed three-dimensional tectonic province model from the crustal movement and seismic activity of this region in the recent years. In order to clarify the characteristics of crustal movement and seismic activity, we have analyzed the GEONET observation data (from October 2007 to March 2011) using the GAMIT 10.4 software, and made the E-W cross-sectional view of the JMA hypocenter data.

The horizontal strain distribution for three and a half years just before the 2011 Tohoku-Oki earthquake shows that strain concentration zone with NW-SE directional contraction extends from the Niigata plain to the Matsumoto basin continuously. Moreover, the eastern margin of this zone corresponds roughly to the position of the Shibata-Koide tectonic line (Yamashita, 1970) running NNE-SSW direction in the eastern margin of the Niigata plain. The strain rate in the Echigo mountain range is smaller than in the Niigata plain. Takeuchi (1999) showed tectonic province based on the activity and characteristics of active faults. The strain distribution revealed from GPS data corresponds approximately to active faults provinces. The large and small strain region corresponds approximately to the reverse fault province (Shin'etsu ~Niigata sedimentary basin) and strike-slip faults province (Central upheaval zone and Echigo mountain range) respectively. Focusing on the depth distribution of the seismogenic layer in the E-W cross-section, the depth of the lower limit of seismogenic layer is shallow ( $D = 10-15$  km) in the strike-slip province but is deeper ( $D = 20-30$  km) in the reverse fault province. The seismogenic layer is located beneath the low P-wave velocity zone corresponding to the thick sediments layer in the sedimentary basin.

According to the above results, there is obvious spatial variation of the depth of seismogenic layer and strain distribution at the boundary of the sedimentary basin and Central upheaval zone. It is conceivable that two different tectonic provinces are adjacent along the tectonic boundary where characteristics of the crustal activity are changing greatly. The moderate-large crustal earthquakes around the northern Fossa Magna, such as the Zenkoji earthquake in 1847, the Niigata-ken Chuetsu earthquake in 2004 and the Nagano-ken Hokubu earthquake in 2011, have occurred on or near the tectonic boundary. Stress concentration is likely to occur due to large changing of the physical properties in the tectonic province boundary, and a large crustal earthquake tend to occur at the tectonic province boundary than at the inside province.

Keywords: tectonic province, northern Fossa Magna, crustal movement, seismic activity, seismogenic layer

## Results of 2013 Off-Kanazawa and Noto peninsula survey for the integrated research project on seismic and tsunami hazard

SATO, Hiroshi<sup>1\*</sup> ; ISHIYAMA, Tatsuya<sup>1</sup> ; SHIRAISHI, Kazuya<sup>2</sup> ; ABE, Susumu<sup>1</sup> ; KATO, Naoko<sup>1</sup> ; IWASAKI, Takaya<sup>1</sup>

<sup>1</sup>Earthquake Research Institute, Univ. Tokyo, <sup>2</sup>JGI. Inc.

To estimate Tsunami and seismic hazards along the coastal area of Sea of Japan, more detailed survey to identify source faults are needed. A new research project funded by MEXT named "the integrated research project on seismic and tsunami hazards around the Sea of Japan" began in FY 2013. To obtain the information of source faults, we performed deep seismic reflection profiling off-Kanazawa and Noto area in the central part of Honshu, Japan. The source faults were estimated together with the results of seismic sections in the epicentral area of the 2007 Noto peninsula earthquake (Sato et al., 2007, BERI). We used two vessels; a gun-ship with 3020 cu. inch air-gun and a cable-ship with a 2-km-long, streamer cable with 156 channels and 480 cu. inch air-gun. Common-mid point reflection data were acquired along 4 seismic lines with total 245 km in length. The seismic profiles portray the reactivation of normal faults, which formed during syn-rift periods, associated with the opening of the Sea of Japan. 2007 Noto peninsula earthquake occurred by the oblique motion on source fault dipping 60 degrees, which is favorable normal faulting. The back arc side of the SW-Japan arc experienced NS trending shortening deformation in the latest Miocene. From the Noto peninsula to the west, undeformed Pliocene sediments covers folded Miocene. Some normal faults reactivated as active strike-slip and reverse faults in Quaternary. The survey results contributed to construct source faults models of Tsunami and seismic hazards estimation.

Keywords: Sea of Japan, source fault, crustal structure, seismic reflection profiling, Off-Kanazawa, Off-Noto Peninsula

## Results of 2013 Off-Joetsu survey for the research project on seismic and tsunami hazards around the Sea of Japan

KATO, Naoko<sup>1\*</sup> ; SATO, Hiroshi<sup>1</sup> ; ISHIYAMA, Tatsuya<sup>1</sup> ; SHIRAIISHI, Kazuya<sup>2</sup> ; ABE, Susumu<sup>2</sup> ; KURASHIMO, Eiji<sup>1</sup>

<sup>1</sup>Earthquake Research Institute, Univ. of Tokyo, <sup>2</sup>JGI. Inc.

To estimate Tsunami and seismic hazards along the coastal area of Sea of Japan, more detailed survey to identify source faults are needed. A new research project funded by MEXT named "the integrated research project on seismic and tsunami hazards around the Sea of Japan" began in FY 2013. To obtain the information of source faults, we performed deep seismic reflection profiling off-Joetsu area in the central part of Honshu, Japan. The seismic lines were located in the offshore extension previous onshore seismic lines forming onshore-offshore integrated seismic lines. We used two vessels; a gun-ship with 3020 cu. inch air-gun and a cable-ship with a 2-km-long, streamer cable with 156 channels and 480 cu. inch air-gun. Common-mid point reflection data were acquired along 3 seismic lines. Two offshore seismic lines are connected to the onshore seismic sections. The survey area consists of stretched continental crust, such as Noto peninsula and Sado island, and failed rift area with large amount of large mafic intrusive rocks, such as Sado strait and Toyama trough. Stretched continental area is marked by densely distributed syn-rift normal faults. On the other hand, in the Sado strait and Toyama trough, fault-related folds were developed, which show small amount of vertical displacement. Along the boundary between continental crust area and oceanic crust, thrusts with rift axis vergent well imaged by seismic reflection profiles. The survey results contributed to construct source faults models of Tsunami and seismic hazards estimation.

## Onshore offshore, deep seismic survey across the Toyama trough

ISHIYAMA, Tatsuya<sup>1\*</sup> ; KATO, Naoko<sup>1</sup> ; SATO, Hiroshi<sup>1</sup> ; SHIRAIISHI, Kazuya<sup>2</sup> ; ABE, Susumu<sup>2</sup> ; TAKEDA, Tetsuya<sup>3</sup> ; KURASHIMO, Eiji<sup>1</sup>

<sup>1</sup>Earthquake Research Institute, University of Tokyo, <sup>2</sup>R&D Department, JGI, Inc, <sup>3</sup>NIED

To estimate Tsunami and seismic hazards along the coastal area of Sea of Japan, more detailed survey to identify source faults are needed. A new research project funded by MEXT named “ the integrated research project on seismic and tsunami hazards around the Sea of Japan ” began in FY 2013. To obtain the information of source faults, we performed onshore offshore deep seismic reflection profiling across the Toyama trough. The seismic line extends from Unazuki at the foot hill of the Hida mountains to the shoreline for 15 km and connected with bay cable of 3 km in length. Seismic signals produced by four vibroseis trucks were recorded by onshore receivers and bay cable. For offshore, we used two vessels; a gun-ship with 3020 cu. inch air-gun and a cable-ship with a 2-km-long, streamer cable with 156 channels and 480 cu. inch air-gun. The P-wave velocity profile by refraction tomography, suggests that the upper surface of Vp 5 km/sec is located 5 km below the mean sea level at the Toyama trough. Vertical offset of Vp 5 km/sec layer is about 8 km. Trough fill sediments beneath the Kurobe alluvial fan show northward dipping. Beneath the apex of this fan, velocity profile and reflection profile suggest the existence of south dipping thrust at 4 km in depth. This fault extends northward as a blind thrust. The seismic section suggests the reverse fault at the northern edge of Toyama trough. Based on the distribution of 5e coastal terraces along the southern part of Noto peninsula, the reverse fault played a significant role for the uplift of Noto peninsula. Such basin structure is analogous to the Niigata sedimentary basin, and northern Fossa magna basin. The survey results contributed to construct source faults models of Tsunami and seismic hazards estimation.

## Structure analysis of the Ryukyu arc by the receiver function

ARASHIRO, Yasuhisa<sup>1\*</sup> ; NAKAMURA, Mamoru<sup>1</sup>

<sup>1</sup>Graduate School of Science,Ryukyu University

The Ryukyu arc have converted plate boundary and back arc basin. The volcanic front in Tokara Islands is the main volcanism. Moreover, The activity of shaped Trough is supposed (Kimura, 1985). In addition, by the survey of igneous activity, the Okinawa Trough have upper flow mantle. Analyzed by receiver function in the Ryukyu arc, McCormack et al., (2013) ware anisotropy structure of slab beneath F-net station.

The Ryukyu arc have converted plate boundary and back arc basin. The volcanic front in Tokara Islands is the main volcanism. Moreover, The activity of shaped Trough is supposed (Kimura, 1985). In addition, by the survey of igneous activity, the Okinawa Trough have upper flow mantle. Analyzed by receiver function in the Ryukyu arc, McCormack *et al.*, (2013) ware anisotropy structure of slab beneath F-net station.

However, it was unknown how changed the structure in the slab and wedge mantle structure changed in the subducting direction. Therefore we clarified I sank by making a receiver functional analysis section at right angles to an errand, the trench including a seismometer record in addition to F-net broadband seismometer record in a short period of the Japan Meteorological Agency,(JMA) and how a Slavic angle changed into the direction.

In the receiver function analysis, we use 8 of short-period seismograph by JMA and 3 of broadband seismometers by NIED F-NET established in central Ryukyu . An analysis period is 2002 to 2013. and used 113 remote earthquake events more than M6.0 for analysis.

In receiver functional analysis, the discontinuity imaging depth is as same as JMA , in Okinawa-honto beneath 40km.

Keywords: receiver function, Ryukyu arc, mantle wedge